

Advances in Experimental Medicine and Biology 723

Matthew M. LaVail · John D. Ash
Robert E. Anderson · Joe G. Hollyfield
Christian Grimm *Editors*

Retinal Degenerative Diseases

 Springer

ADVANCES IN EXPERIMENTAL MEDICINE AND BIOLOGY

Editorial Board:

NATHAN BACK, *State University of New York at Buffalo*

IRUN R. COHEN, *The Weizmann Institute of Science*

ABEL LAJTHA, *N. S. Kline Institute for Psychiatric Research*

JOHN D. LAMBRIS, *University of Pennsylvania*

RODOLFO PAOLETTI, *University of Milan*

For further volumes:

<http://www.springer.com/series/5584>

Matthew M. LaVail • John D. Ash
Robert E. Anderson • Joe G. Hollyfield
Christian Grimm
Editors

Retinal Degenerative Diseases

 Springer

Editors

Matthew M. LaVail
Anatomy and Ophthalmology
University of California
San Francisco School of Medicine
San Francisco, CA, USA
matthew.lavail@ucsf.edu

John D. Ash
Ophthalmology
College of Medicine
University of Oklahoma
Health Sciences Center
Oklahoma City, OK, USA
John-Ash@ouhsc.edu

Robert E. Anderson
Ophthalmology and Cell Biology
Dean A. McGee Eye Institute
University of Oklahoma
Health Sciences Center
Oklahoma City, OK, USA
Robert-Anderson@ouhsc.edu

Joe G. Hollyfield
Ophthalmology
Cole Eye Institute at the Cleveland Clinic
Cleveland, OH, USA
hollyfj@ccf.org

Christian Grimm
Experimental Ophthalmology
University of Zurich
Zurich, Switzerland
cgrimm@opht.uzh.ch

ISSN 0065-2598

ISBN 978-1-4614-0630-3

e-ISBN 978-1-4614-0631-0

DOI 10.1007/978-1-4614-0631-0

Springer New York Dordrecht Heidelberg London

Library of Congress Control Number: 2011941578

© Springer Science+Business Media, LLC 2012

All rights reserved. This work may not be translated or copied in whole or in part without the written permission of the publisher (Springer Science+Business Media, LLC, 233 Spring Street, New York, NY 10013, USA), except for brief excerpts in connection with reviews or scholarly analysis. Use in connection with any form of information storage and retrieval, electronic adaptation, computer software, or by similar or dissimilar methodology now known or hereafter developed is forbidden.

The use in this publication of trade names, trademarks, service marks, and similar terms, even if they are not identified as such, is not to be taken as an expression of opinion as to whether or not they are subject to proprietary rights.

Printed on acid-free paper

Springer is part of Springer Science+Business Media (www.springer.com)



Michael Danciger, Ph.D.
1943–2010

Michael Danciger was a pioneer in the identification of modifier genes of complex genetic disorders that lead to blindness. The impact of his research and collaborations continues to be felt and expanded. Equally important was his delightful personal quality of leaving an indelible mark on everyone he met and with whom he worked. Michael was a long-time supporter of the RD Symposia. He is missed, and we are honored to dedicate this proceedings volume to him.



Robert B. Barlow, Jr., Ph.D.
1939–2009

Robert “Bob” Barlow was an extremely energetic man who contributed to many areas of research in vision and neurobiological science and held many responsible positions that influenced numerous investigators. He was a long-time supporter of the RD Symposia, as was his wife, Pat, pictured here together at the RD2004 meeting in Australia. He is missed, and we are honored to dedicate this proceedings volume to him.

Preface

The International Symposia on Retinal Degeneration have been held in conjunction with the biennial International Congress of Eye Research (ICER) since 1984. These RD Symposia have allowed basic and clinician scientists from around the world to convene and present their new research findings. They have been organized to allow sufficient time for discussions and one-on-one interactions in a relaxed atmosphere, where international friendships and collaborations can be fostered.

The XIV International Symposium on Retinal Degeneration (also known as RD2010) was held from July 13–17, 2010 at the Fairmont Tremblant Hotel in the resort village of Mont-Tremblant, Quebec, Canada. The meeting brought together 232 basic and clinician scientists, retinal specialists in ophthalmology, and trainees in the field from all parts of the world. In the course of the meeting, 38 platform and 134 poster presentations were given, and a majority of these are presented in this proceedings volume. New discoveries and state-of-the-art findings from most research areas in the field of retinal degenerations were presented. This was the largest of all of the RD Symposia, with the greatest number of attendees and presentations.

The RD2010 meeting was highlighted by three special plenary lectures. The first was given by *Elise Héon*, MD, of the University of Toronto Hospital for Sick Children, Toronto, Ontario, Canada. Dr. Heon discussed “What Bardet-Biedl Syndrome teaches us about ciliopathies.” The second was given by *Gregory Hageman*, PhD, of the John Moran Eye Center, University of Utah, Salt Lake City, UT. Dr. Hageman described a “New era in the understanding of age-related macular degeneration.” The third plenary lecture was given by *Jayakrishna Ambati*, MD, of the University of Kentucky, Lexington, KY. Dr. Ambati discussed “Age-related macular degeneration and the other double helix.”

We thank the outstanding management and staff of the beautiful Fairmont Tremblant Hotel for all of their assistance in making this an exceptionally smooth-running conference and a truly memorable experience for all of the attendees. These included, in particular, *Isabelle Gilbert*, *Émilie Normandeau*, and *Patrick Skelly*. We also thank *Jonathan Marier* of AVW-TELAV for providing audio/visual equipment and services that resulted in a flawless flow of platform presentations. Lastly, we thank *Steven LeFort* and, particularly, *Marie-Chantal Thibault* of JPdL Tremblant

for their planning and implementing transportation of most of the attendees to and from Montreal and the meeting venue in Mont-Tremblant, as well as all aspects of the end-of-meeting Gala at the beautiful “Summit” overlooking Mont-Tremblant and the majestic Laurentian mountains, with a truly Canadian meal, music, and festivities.

The Symposium received international financial support from a number of organizations. We are particularly pleased to thank The Foundation Fighting Blindness, Columbia, Maryland, for its continuing support of this and all previous biennial Symposia, without which we could not have held these important meetings. In addition, for the fifth time, the National Eye Institute of the National Institutes of Health contributed in a major way to the meeting. In the past, funds from these two organizations allowed us to provide 25–35 Travel Awards to young investigators and trainees working in the field of retinal degenerations. However, the response to the Travel Awards program was extraordinary, with 94 applicants, many more than in the past. For this reason, we sought additional support for the Travel Awards program. The Foundation Fighting Blindness-Canada/Institute of Genetics was a major contributor, and for the first time, we turned to industry sponsors and received generous contributions from Novartis Pharma AG, Alcon, Genentech, Inspire Pharmaceuticals, Pfizer, Inc., Genzyme and Bioptigen, Inc. In total, we were able to fund 42 Travel Awards, the largest number ever for these Symposia. Many of the contributing foundations and industry sponsors sent one to several members of their organization to attend the meeting. Their participation and comments in the scientific sessions were instructive to many, offering new perspectives to some of the problems being discussed.

There were two additional “firsts” for the RD Symposia at RD2010. For the first time, there was a commercial exhibitor at the Symposium, Bioptigen, which demonstrated its Spectral Domain Ophthalmic Imaging System (OCT) for small laboratory animals; this was highly instructive for many of the attendees. Second, the world-famous Tremblant International Blues Festival (17th Edition) was held during the RD2010 meeting, immediately adjacent to the Fairmont Tremblant venue. With almost continuous free performances every evening of the Symposium, many groups of attendees enjoyed these together after dinner.

We also acknowledge the diligent and outstanding efforts of Ms. *Holly Whiteside*, who carried out most of the administrative aspects of the RD2010 Symposium, designed and maintained the meeting website, and participated in the production of this volume. Holly is the Administrative Manager of Dr. Anderson’s laboratory at the University of Oklahoma Health Sciences Center, and she has become the permanent Coordinator for the Retinal Degeneration Symposia. Her dedicated efforts with the Symposia since RD2000 have provided continuity not available previously, and we are deeply indebted to her. Also, Dr. *Michael Matthes* in Dr. LaVail’s laboratory played a major role in all aspects in the production of this volume, along with the assistance of Ms. *Kelly Ahern*, in Dr. LaVail’s laboratory.

Recognizing the need to bring younger individuals into the organizational structure of the RD Symposia, at the RD2008 meeting, we invited Drs. *John Ash* and *Christian Grimm* to become members of the organizing committee. Thus, instead of

the rotating head organizer working mostly with Holly Whiteside to organize the meeting and prepare the proceedings volume, Dr. Ash assumed equal responsibility with Dr. LaVail for both efforts for RD2010. Dr. *Anderson* continued in his role as financial administrator for each of the Symposia, working through the Dean McGee Eye Institute, which generously provides the financial responsibility for the meetings and the mechanism for registration of participants. We were pleased to announce at the Gala at RD2010 that our third new member of the organizing committee is Dr. *Cathy Bowes Rickman*. Dr. Grimm will work closely with Dr. Hollyfield for the RD2012 meeting to be held in Germany.

Finally, we honor the memory of two colleagues who died during the preparation of the RD2010 meeting in 2009 and 2010. *Michael Danciger* was a great friend to most who attend our RD meetings. *Robert Barlow*, likewise, was a long-time attendee of the RD Symposia. Both were outstanding scientists and are missed. We dedicate this volume to Michael and Bob.

San Francisco, CA, USA
Oklahoma City, OK, USA
Oklahoma City, OK, USA
Cleveland, OH, USA
Zurich, Switzerland

Matthew M. LaVail
John D. Ash
Robert E. Anderson
Joe G. Hollyfield
Christian Grimm

About the Editors

Matthew M. LaVail, PhD, is Professor of Anatomy and Ophthalmology at the University of California, San Francisco School of Medicine. He received his Ph.D. degree in Anatomy (1969) from the University of Texas Medical Branch in Galveston and was subsequently a postdoctoral fellow at Harvard Medical School. Dr. LaVail was appointed Assistant Professor of Neurology-Neuropathology at Harvard Medical School in 1973. In 1976, he moved to UCSF, where he was appointed Associate Professor of Anatomy. He was appointed to his current position in 1982, and in 1988, he also became Director of the Retinitis Pigmentosa Research Center at UCSF, later named the Kearn Family Center for the Study of Retinal Degeneration. Dr. LaVail has published extensively in the research areas of photoreceptor-retinal pigment epithelial cell interactions, retinal development, circadian events in the retina, genetics of pigmentation and ocular abnormalities, inherited retinal degenerations, light-induced retinal degeneration, and neuroprotective and gene therapy for retinal degenerative diseases. He has identified several naturally occurring murine models of human retinal degenerations and has developed transgenic mouse and rat models of others. He is the author of more than 160 research publications and has edited 14 books on inherited and environmentally induced retinal degenerations. Dr. LaVail has received the Fight for Sight Citation (1976); the Sundial Award from the Retina Foundation (1976); the Friedenwald Award from the Association for Research in Vision and Ophthalmology (ARVO, 1981); two Senior Scientific Investigators Awards from Research to Prevent Blindness (1988 and 1998); a MERIT Award from the National Eye Institute (1989); an Award for Outstanding Contributions to Vision Research from the Alcon Research Institute (1990); the Award of Merit from the Retina Research Foundation (1990); the first John A. Moran Prize for Vision Research from the University of Utah (1997); the first Trustee Award from The Foundation Fighting Blindness (1998); the fourth Llura Liggett Gund Award from the Foundation Fighting Blindness (2007); and he has received the Distinguished Alumnus Award from both his university (University of North Texas) and his graduate school (University of Texas Medical Branch). He has served on the editorial boards of *Investigative Ophthalmology* and *Visual Science and Experimental Eye Research*. Dr. LaVail has been an active participant in the

program committee of ARVO and has served as a Trustee (Retinal Cell Biology Section) of ARVO. In 2009, he was appointed an inaugural ARVO Fellow, Gold, of the 12,000-member organization. Dr. LaVail has been a member of the program committee and a Vice President of the International Society for Eye research. He has also served on the Scientific Advisory Board of the Foundation Fighting Blindness since 1973.

John D. Ash, PhD, is Associate Professor of Ophthalmology in the College of Medicine at the University of Oklahoma Health Sciences Center. He is also an adjunct Associate Professor in the Department of Cell Biology, a member of the Oklahoma Center for Neuroscience, and a faculty member of the Dean A. McGee Eye Institute. In 1994, he received his PhD from the Ohio State University Biochemistry Program, and then accepted a postdoctoral fellowship in the Cell Biology Department, Baylor College of Medicine, in Houston, Texas. In 1999, he became Assistant Professor of Ophthalmology at the University of Oklahoma Health Sciences Center, and was promoted to Associate professor in 2006. Dr Ash is also a Visiting Professor of the Dalian Medical University, Dalian China. Dr. Ash has written and published 40 manuscripts including research articles, book chapters and invited reviews related to vision research. He is currently an Executive Editor for Experimental Eye Research, and an Associate Editor of the Journal of Angiogenesis Research. Dr Ash is an active reviewer for Molecular Vision, Investigative Ophthalmology & Visual Science, Experimental Eye Research and Diabetes. In 2009, Dr. Ash received a research award from Hope for Vision, and in 2010 he received a Lew R. Wasserman Merit award from Research to Prevent Blindness, Inc. Dr. Ash has received grants from the National Institutes of Health, the Foundation Fighting Blindness, Research to Prevent Blindness, Inc, Hope for Vision, and the American Diabetes Association. Dr. Ash is currently serving on the Program Committee of the Association for Research in Vision and Ophthalmology. Dr Ash has served on the scientific review panel for Fight For Sight (2005-2008), and is currently serving on the Scientific Advisory Board of the Foundation Fighting Blindness (Columbia, MD) where he chairs the review committee on Novel Medical Therapies Program. He also serves on the scientific review panel for the Macular Degeneration program of the American Health Assistance Foundation (Clarksburg, MD).

Robert E. Anderson, MD, PhD, is George Lynn Cross Research Professor, Dean A. McGee Professor of Ophthalmology, Professor of Cell Biology, and Adjunct Professor of Biochemistry & Molecular Biology and Geriatric Medicine at The University of Oklahoma Health Sciences Center in Oklahoma City, Oklahoma. He is also Director of Research at the Dean A. McGee Eye Institute. He received his Ph.D. in Biochemistry (1968) from Texas A&M University and his M.D. from Baylor College of Medicine in 1975. In 1968, he was a postdoctoral fellow at Oak Ridge Associated Universities. At Baylor, he was appointed Assistant Professor in 1969, Associate Professor in 1976, and Professor in 1981. He joined the faculty of the University of Oklahoma Health Sciences Center in January of 1995. Dr. Anderson served as director of the Oklahoma Center for Neuroscience (1995-1999) and chairman of the Department of Cell Biology (1998-2007). He has received several honorary appointments including Visiting Professor, West China School of Medicine,

Sichuan University, Chengdu, China; Honorary Professorship, Xi'an Jiaotong University, Xi'an, China; and Honorary Professor of Sichuan Medical Science Academy, Sichuan Provincial People's Hospital, Sichuan, China. Dr. Anderson has received the Sam and Bertha Brochstein Award for Outstanding Achievement in Retina Research from the Retina Research Foundation (1980), and the Dolly Green Award (1982) and two Senior Scientific Investigator Awards (1990 and 1997) from Research to Prevent Blindness, Inc. He received an Award for Outstanding Contributions to Vision Research from the Alcon Research Institute (1985), and the Marjorie Margolin Prize (1994). He has served on the editorial boards of *Investigative Ophthalmology and Visual Science*, *Journal of Neuroscience Research*, *Neurochemistry International*, *Current Eye Research*, and *Experimental Eye Research*. Dr. Anderson has published extensively in the areas of lipid metabolism in the retina and biochemistry of retinal degenerations. He has edited 15 books, 14 on retinal degenerations and one on the biochemistry of the eye. Dr. Anderson has received grants from the National Institutes of Health, The Retina Research Foundation, the Foundation Fighting Blindness, and Research to Prevent Blindness, Inc. He has been an active participant in the program committees of the Association for Research in Vision and Ophthalmology (ARVO) and was a trustee representing the Biochemistry and Molecular Biology section. He was named a Gold Fellow by ARVO in 2009 and was awarded the Proctor Medal from ARVO in 2011. He has served on the Vision Research Program Committee and Board of Scientific Counselors of the National Eye Institute and the Board of the Basic and Clinical Science Series of The American Academy of Ophthalmology. Dr. Anderson is a past Councilor, Treasurer, and President of the International Society for Eye Research.

Joe G. Hollyfield, PhD, is Chairman of Ophthalmic Research and the Llura and Gordon Gund Professor of Ophthalmology Research in the Cole Eye Institute at the Cleveland Clinic, Cleveland, Ohio. He received a Ph.D. from the University of Texas at Austin and did postdoctoral work at the Hubrecht Laboratory in Utrecht, The Netherlands. He has held faculty positions at Columbia University College of Physicians and Surgeons in New York City and at Baylor College of Medicine in Houston, Texas. He was Director of the Retinitis Pigmentosa Research Center in The Cullen Eye Institute at Baylor from 1978 until his move to The Cleveland Clinic Foundation in 1995. He is currently Director of the Foundation Fighting Blindness Research Center at the Cleveland Clinic. Dr. Hollyfield has published over 200 papers in the area of cell and developmental biology of the retina and retinal pigment epithelium in both normal and retinal degenerative tissue. He has edited 15 books, 14 on retinal degenerations and one on the structure of the eye. Dr. Hollyfield received the Marjorie W. Margolin Prize (1981, 1994), the Sam and Bertha Brochstein Award (1985) and the Award of Merit in Retina Research (1998) from the Retina Research Foundation; the Olga Keith Weiss Distinguished Scholars' Award (1981) and two Senior Scientific Investigator Awards (1988, 1994) from Research to Prevent Blindness, Inc.; an award for Outstanding Contributions to Vision Research from the Alcon Research Institute (1987); the Distinguished Alumnus Award (1991) from Hendrix College, Conway, Arkansas; the Endre A. Balazs Prize (1994) from the International Society for Eye Research (ISER), and

the Proctor Medal (2009) from the Association for Research in Vision and Ophthalmology (ARVO). His Proctor lecture was selected for the 2009 Cless “Best of the Best” Award, given by the University of Illinois Eye and Ear Infirmary. He was named an inaugural Gold Fellow by ARVO in 2009. Since 1991 he has been Editor-in-Chief of the journal, *Experimental Eye Research*, published by Elsevier. Dr. Hollyfield has been active in ARVO, serving on the Program Committee (1976), as Trustee (Retinal Cell Biology, 1989-94), as President (1993-94) and as Immediate Past President (1994-95). He was also President (1988-91) and Secretary (1984-87) of the International Society of Eye Research. He is Chairman of the scientific review panel for the Macular Degeneration program of the American Health Assistance Foundation (Clarksburg, MD), serves on the scientific advisory boards of the Foundation Fighting Blindness (Owings Mills, MD), the Knights Templar Eye Research Foundation (Chicago, IL), the Helen Keller Eye Research Foundation (Birmingham, AL), the South Africa Retinitis Pigmentosa Foundation (Johannesburg, South Africa), and is Co-Chairman of the Medical and Scientific Advisory Board of Retina International (Zurich, Switzerland).

Christian Grimm, PhD, is Professor for Experimental Ophthalmology at the University of Zurich, Switzerland. He received his Ph.D. degree at the Institute for General Microbiology at the University of Berne in 1990. After an initial postdoctoral position in the field of snRNP maturation, Dr. Grimm conducted research at the University of Wisconsin in Madison, WI, where he studied nucleo-cytoplasmic transport of small RNAs. In 1997 Dr. Grimm moved back to Switzerland where he joined the Lab for Retinal Cell Biology in the department of Ophthalmology at the University of Zurich. Dr. Grimm has led the Lab for Retinal Cell Biology since 2006, and was appointed Professor for Experimental Ophthalmology and joined the medical faculty in 2008. Dr. Grimm has published more than 85 original research and review articles, more than 75 in the field of retinal degeneration. His research focuses on molecular mechanisms of photoreceptor cell death and neuroprotection. Dr. Grimm has received the Alfred Vogt Award (2000), the Retinitis Pigmentosa Award of Pro Retina Germany (2003) and the Pfizer Research Award in Neuroscience (2004). He serves on the Editorial Board of *Current Eye Research* and *Experimental Eye Research*, and as a Scientific Review Associate for the *European Journal of Neuroscience*. Dr. Grimm has received research grants from the Swiss National Science Foundation, the European Union, the University of Zurich and several private funding organizations. He serves on the Scientific Advisory Board of the Foundation Fighting Blindness and is Vice Chairman of the Center for Integrative Human Physiology, a priority research program of the University of Zurich.

Contents

Part I AMD: Basic Mechanisms, Inflammation and Immunity

1	A Window to Innate Neuroimmunity: Toll-Like Receptor-Mediated Cell Responses in the Retina	3
	Mark E. Kleinman and Jayakrishna Ambati	
2	Autoimmune Biomarkers in Age-Related Macular Degeneration: A Possible Role Player in Disease Development and Progression	11
	Alessandro Iannaccone, Indira Neeli, Pratheebha Krishnamurthy, Nataliya I. Lenchik, Haibao Wan, Ivan C. Gerling, Dominic M. Desiderio, and Marko Z. Radic	
3	Local Vs. Systemic Mononuclear Phagocytes in Age-Related Macular Degeneration and Their Regulation by <i>CCL2-CCR2</i> and <i>CX3CL1-CX3CR1</i> Chemokine Signalling	17
	Ulrich F.O. Luhmann and Robin R. Ali	
4	Sublytic Membrane-Attack-Complex Activation and VEGF Secretion in Retinal Pigment Epithelial Cells	23
	Kannan Kunchithapautham, Mausumi Bandyopadhyay, Mohammad Dahrouj, Joshua M. Thurman, and Bärbel Rohrer	
5	Complement Activation in Retinal Degeneration	31
	Matt Rutar, Riccardo Natoli, Jan Provis, and Krisztina Valter	
6	Microglia in the Outer Retina and Their Relevance to Pathogenesis of Age-Related Macular Degeneration	37
	Wenxin Ma, Lian Zhao, and Wai T. Wong	

7 Lutein or Zeaxanthin Supplementation Suppresses Inflammatory Responses in Retinal Pigment Epithelial Cells and Macrophages..... 43
 Qingning Bian, Tingyu Qin, Zhihong Ren, Dayong Wu, and Fu Shang

8 Exploring the Potential Role of the Oxidant-Activated Transcription Factor Aryl Hydrocarbon Receptor in the Pathogenesis of AMD 51
 Goldis Malek, Mary Dwyer, and Donald McDonnell

9 Common Mechanisms for Separate Maculopathies? 61
 Elod Kortvely and Marius Ueffing

10 The Role of Amyloid-β in Retinal Degeneration 67
 Julien Bruban, Virginie Dinet, and Frédéric Mascarelli

11 Molecule-Specific Imaging and Quantitation of A2E in the RPE 75
 Zsolt Ablonczy, Danielle B. Gutierrez, Angus C. Grey, Kevin L. Schey, and Rosalie K. Crouch

12 Autophagy in the Retina: A Potential Role in Age-Related Macular Degeneration 83
 Sayak K. Mitter, Haripriya Vittal Rao, Xiaoping Qi, Jun Cai, Andrew Sugrue, William A. Dunn Jr., Maria B. Grant, and Michael E. Boulton

Part II Neuroprotection, Drugs and Novel Protective Therapies

13 Regeneration of Cone Outer Segments Induced by CNTF 93
 Rong Wen, Weng Tao, Lingyu Luo, Deqiang Huang, Konrad Kauper, Paul Stabila, Matthew M. LaVail, Alan M. Laties, and Yiwen Li

14 Glucocorticoid-Dependent Mechanisms in Photoreceptor Survival 101
 Marisa A. Cubilla, Mauricio M. Castañeda, Tomás P. Bachor, and Angela M. Suburo

15 HDAC Inhibition Prevents *Rd1* Mouse Photoreceptor Degeneration..... 107
 Javier Sancho-Pelluz and François Paquet-Durand

16 Neuroprotective Dose Response in RCS Rats Implanted with Microphotodiode Arrays..... 115
 Mabelle T. Pardue, Moon K. Kim, Tiffany A. Walker, Amanda E. Faulkner, Alan Y. Chow, and Vincent T. Ciavatta

17	Treatment with 670-nm Light Protects the Cone Photoreceptors from White Light-Induced Degeneration	121
	Rizalyn S. Albarracin and Krisztina Valter	
18	Dark-Rearing the <i>rd10</i> Mouse: Implications for Therapy	129
	Therese Cronin, Arkady Lyubarsky, and Jean Bennett	
19	Intravitreal Injection of Erythropoietin Glycosylation Analogs Does Not Protect Rod Photoreceptor Cells from Light-Induced Damage	137
	Masaki Tanito, Feng Li, and Robert E. Anderson	
20	Relieving Bottlenecks in RNA Drug Discovery for Retinal Diseases	145
	Jack M. Sullivan, Edwin H. Yau, R. Thomas Taggart, Mark C. Butler, and Tiffany A. Kolniak	
21	On Further Development of Barrier Modulation as a Technique for Systemic Ocular Drug Delivery	155
	Finnian Hanrahan, Matthew Campbell, Anh T. Nguyen, Mayu Suzuki, Anna-Sophia Kiang, Lawrence C. Tam, Oliviero L. Gobbo, Sorcha Ní Dhubhghaill, Marian M. Humphries, Paul F. Kenna, and Pete Humphries	
22	An Application for Mammalian Optic Nerve Repair by Fish Regeneration-Associated Genes	161
	Yoshiki Koriyama, Kayo Sugitani, Toru Matsukawa, and Satoru Kato	
23	The Mechanism of Fenretinide (4-HPR) Inhibition of β-carotene Monooxygenase 1. New Suspect for the Visual Side Effects of Fenretinide	167
	Eugenia Poliakov, Alexander Gubin, James Laird, Susan Gentleman, Robert G. Salomon, and T. Michael Redmond	
 Part III Gene Therapy		
24	Gene Augmentation Trials Using the Rpe65-Deficient Dog: Contributions Towards Development and Refinement of Human Clinical Trials	177
	Simon M. Petersen-Jones, Matthew J. Annear, Joshua T. Bartoe, Freya M. Mowat, Susie E. Barker, Alexander J. Smith, James W. Bainbridge, and Robin R. Ali	
25	Gene Therapy Restores Missing Cone-Mediated Vision in the CNGA3^{-/-} Mouse Model of Achromatopsia	183
	Stylios Michalakis, Regine Mühlfriedel, Naoyuki Tanimoto, Vidhyasankar Krishnamoorthy, Susanne Koch, M. Dominik Fischer, Elvir Becirovic, Lin Bai, Gesine Huber, Susanne C. Beck, Edda Fahl, Hildegard Büning, Jennifer Schmidt, Xiangang Zong, Tim Gollisch, Martin Biel, and Mathias W. Seeliger	

26 Functional Rescue of P23H Rhodopsin Photoreceptors by Gene Delivery 191
 Marina S. Gorbatyuk, Oleg S. Gorbatyuk, Matthew M. LaVail, Jonathan H. Lin, William W. Hauswirth, and Alfred S. Lewin

27 Gene Delivery of Wild-Type Rhodopsin Rescues Retinal Function in an Autosomal Dominant Retinitis Pigmentosa Mouse Model 199
 Haoyu Mao, Marina S. Gorbatyuk, William W. Hauswirth, and Alfred S. Lewin

28 Retinal Degeneration and Cellular Suicide 207
 Wai Gin Fong and Catherine Tsilfidis

29 Suppression of *rd5* Expression by siRNA and Gene Replacement Strategies for Gene Therapy Using rAAV Vector 215
 Hilda Petrs-Silva, Douglas Yasumura, Michael T. Matthes, Matthew M. LaVail, Alfred S. Lewin, and William W. Hauswirth

30 Silencing the Expression of *CTRP5/C1QTNF5* and *ELOVL4* Genes by Small Interfering RNA..... 225
 Venkata Ramana Murthy Chavali, Vidyullatha Vasireddy, and Radha Ayyagari

31 Gene Therapy Strategies for Usher Syndrome Type 1B..... 235
 David S. Williams and Vanda S. Lopes

Part IV Blood Vessels, Angiogenesis, and Neovascularization

32 Neovascularization: Ocular Diseases, Animal Models and Therapies 245
 Xue Cai, Steven A. Sezate, and James F. McGinnis

33 Retinal Neovascular Disorders: Mouse Models for Drug Development Studies..... 253
 Rosanne M. Yetemian and Cheryl M. Craft

34 A Review and Update on the Molecular Basis of Pathogenesis of Sorsby Fundus Dystrophy..... 261
 Heidi Stöhr and Bela Anand-Apte

35 The Importance of Hypoxia-Regulated, RPE-Targeted Gene Therapy for Choroidal Neovascularization 269
 George W. Smith, C. Kathleen Dorey, Howard Prentice, and Janet Blanks

36 What Is the Role of CCR3 in Choroidal Neovascularization?..... 279
 Yiwen Li, Deqiang Huang, Xin Xia, Zhengying Wang, Lingyu Luo, and Rong Wen

37 Intermittent But Not Constant High Glucose Induces ER Stress and Inflammation in Human Retinal Pericytes..... 285
 Yimin Zhong, Joshua J. Wang, and Sarah X. Zhang

38 Regulation of Retinal Vascular Permeability by Betacellulin..... 293
 Masahiko Sugimoto, Alecia Cutler, Gregory Grossman, and Bela Anand-Apte

39 Presence of RPE-Produced VEGF in a Timely Manner Is Critical to Choroidal Vascular Development 299
 Meili Zhu, Yanyan Bai, Lixin Zheng, and Yun-Zheng Le

40 Vasohibin-1 and Retinal Pigment Epithelium 305
 Yumi Ishikawa, Nobuhiro Nagai, Hideyuki Onami, Norihiro Kumasaka, Ryosuke Wakusawa, Hikaru Sonoda, Yasufumi Sato, and Toshiaki Abe

Part V Genotype/Phenotype

41 Polymorphic Variation of RPGRIP1L and IQCB1 as Modifiers of X-Linked Retinitis Pigmentosa Caused by Mutations in RPGR..... 313
 Abigail T. Fahim, Sara J. Bowne, Lori S. Sullivan, Kaylie D. Webb, Jessica T. Williams, Dianna K. Wheaton, David G. Birch, and Stephen P. Daiger

42 RPGRIP1 and Cone-Rod Dystrophy in Dogs..... 321
 Tatyana Kuznetsova, Barbara Zangerl, and Gustavo D. Aguirre

43 High-Throughput Approaches for the Genetic Diagnosis of Retinal Dystrophies 329
 Esther Pomares, Gemma Marfany, and Roser González-Duarte

44 Genes and Mutations in Autosomal Dominant Cone and Cone-Rod Dystrophy 337
 Susanne Kohl, Veronique Kitiratschky, Monika Papke, Simone Schaich, Alexandra Sauer, and Bernd Wissinger

45 The Power of Homozygosity Mapping: Discovery of New Genetic Defects in Patients with Retinal Dystrophy 345
 Karin W. Littink, Anneke I. den Hollander, Frans P.M. Cremers, and Rob W.J. Collin

46 Development and Validation of a Canine-Specific Profiling Array to Examine Expression of Pro-apoptotic and Pro-survival Genes in Retinal Degenerative Diseases..... 353
 Sem Genini, William A. Beltran, and Gustavo D. Aguirre

47 The Chromosome 10q26 Susceptibility Locus in Age-Related Macular Degeneration 365
 Chloe M. Stanton, Kevin J. Chalmers, and Alan F. Wright

48 Congenital Stationary Night Blindness: Mutation Update and Clinical Variability..... 371
 Nidhi Lodha, Catrina M. Loucks, Chandree Beaulieu, Jillian S. Parboosingh, and N. Torben Bech-Hansen

49 Serum Biomarkers and Trafficking Defects in Peripheral Tissues Reflect the Severity of Retinopathy in Three Brothers Affected by Choroideremia 381
 Natalia Strunnikova, Wadih M. Zein, Chris Silvin, and Ian M. MacDonald

Part VI New Animal Models of Retinal Degeneration

50 Translational Vision Research Models Program..... 391
 Jungyeon Won, Lan Ying Shi, Wanda Hicks, Jieping Wang, Juergen K. Naggert, and Patsy M. Nishina

51 Zebrafish: A Model System for the Investigation of Novel Treatments for Retinal Disease 399
 Cheryl Y. Gregory-Evans

52 Retinal Degeneration in the Fly 407
 Nansi Jo Colley

53 Looking into Eyes: Rhodopsin Pathologies in *Drosophila*..... 415
 Ana Griciuc, Liviu Aron, and Marius Ueffing

54 Müller Glia as a Source of Neuronal Progenitor Cells to Regenerate the Damaged Zebrafish Retina..... 425
 Craig M. Nelson and David R. Hyde

55 The Genetics of Outer Segment Morphogenesis in Zebrafish 431
 Alison L. Reynolds, Oliver E. Blacque, and Breandán N. Kennedy

56 Factor XIIIa Induction in the Retina and Optic Nerve After Optic Nerve Lesion in Goldfish..... 443
 Kayo Sugitani, Kazuhiro Oogai, Hiroshi Nakashima, and Satoru Kato

Part VII Analysis of Retinal Degeneration by Imaging and Functional Testing

57 Imaging the Photoreceptor Mosaic with Adaptive Optics: Beyond Counting Cones 451
 Pooja Godara, Melissa Wagner-Schuman, Jungtae Rha, Thomas B. Connor Jr., Kimberly E. Stepien, and Joseph Carroll

58 Baseline Imaging Reveals Preexisting Retinal Abnormalities in Mice 459
 Brent A. Bell, Charles Kaul, Mary E. Rayborn, and Joe G. Hollyfield

59 Correlation Between Spectral Domain OCT Retinal Nerve Fibre Layer Thickness and Multifocal Pattern Electroretinogram in Advanced Retinitis Pigmentosa 471
 Ieva Sliesoraityte, Eric Troeger, Antje Bernd, Anne Kurtenbach, and Eberhart Zrenner

60 Imaging Human Postmortem Eyes with SLO and OCT 479
 Nika Bagheri, Brent A. Bell, Vera L. Bonilha, and Joe G. Hollyfield

61 In Vivo Assessment of Rodent Retinal Structure Using Spectral Domain Optical Coherence Tomography 489
 M. Dominik Fischer, Gesine Huber, Francois Paquet-Durand, Peter Humphries, T. Michael Redmond, Christian Grimm, and Mathias W. Seeliger

62 Rod Photoreceptor Temporal Properties in Retinal Degenerative Diseases 495
 Yuquan Wen, Kirsten G. Locke, Donald C. Hood, and David G. Birch

63 ERG Critical Flicker Frequency Assessment in Humans 503
 Kristen E. Bowles and Timothy W. Kraft

Part VIII Mechanisms of Retinal Degeneration

64 Biology of Retinoschisin 513
 Camasamudram Vijayasarathy, Lucia Ziccardi, and Paul A. Sieving

65 Transcriptome Analyses to Investigate the Pathogenesis of RNA Splicing Factor Retinitis Pigmentosa 519
 Michael H. Farkas, Greg R. Grant, and Eric A. Pierce

66 The Role of the X-linked Retinitis Pigmentosa Protein RP2 in Vesicle Traffic and Cilia Function 527
 Nele Schwarz, Alison J. Hardcastle, and Michael E. Cheetham

67 *Caenorhabditis elegans* as a Model Organism for Ciliopathies and Related Forms of Photoreceptor Degeneration 533
 Calvin A. Mok and Elise Héon

68 Towards a Pathological Mechanism for IMPDH1-Linked Retinitis Pigmentosa 539
 Dharia A. McGrew and Lizbeth Hedstrom

69 Calpain and Photoreceptor Apoptosis..... 547
 Anh T.H. Nguyen, Matthew Campbell, Paul F. Kenna,
 Anna-Sophia Kiang, Lawrence Tam, Marian M. Humphries,
 and Peter Humphries

70 Ceramide Signaling in Retinal Degeneration..... 553
 Hui Chen, Julie-Thu A. Tran, Richard S. Brush, Anisse Saadi,
 Abul K. Rahman, Man Yu, Douglas Yasumura, Michael T. Matthes,
 Kelly Ahern, Haidong Yang, Matthew M. LaVail,
 and Md Nawajes A. Mandal

**71 Endoplasmic Reticulum-Associated Degradation (ERAD)
 of Misfolded Glycoproteins and Mutant P23H Rhodopsin
 in Photoreceptor Cells** 559
 Heike Kroeger, Wei-Chieh Chiang, and Jonathan H. Lin

**72 Protein Misfolding and Potential Therapeutic Treatments
 in Inherited Retinopathies**..... 567
 Lawrence C.S. Tam, Anna-Sophia Kiang, Matthew Campbell,
 James Keane, G. Jane Farrar, Marian M. Humphries,
 Paul F. Kenna, and Pete Humphries

**73 Development of a Cellular Model of Rod Opsin
 Retinitis Pigmentosa** 573
 Matthew Adamowicz, Antonius Song, Samuel Wadsworth,
 Abraham Scaria, and Catherine O’Riordan

**74 A Brief Account of Rho GTPases in Retinal Physiology
 and Pathophysiology**..... 581
 Severin Reinhard Heynen, Omolara O. Ogunshola,
 and Christian Grimm

75 Molecular Clues to Bothnia-Type Retinal Dystrophy..... 589
 Xiaoqin He, Joel Lobsiger, and Achim Stocker

**76 A Novel Missense Mutation in Both *OPNILW* and *OPNIMW*
 Cone Opsin Genes Causes X-Linked Cone
 Dystrophy (*XL COD5*)**..... 595
 Jessica C. Gardner, Tom R. Webb, Naheed Kanuga,
 Anthony G. Robson, Graham E. Holder, Andrew Stockman,
 Caterina Ripamonti, Neil D. Ebenezer, Olufunmilola Ogun,
 Sophie Devery, Genevieve A. Wright, Eamonn R. Maher,
 Michael E. Cheetham, Anthony T. Moore, Michel Michaelides,
 and Alison J. Hardcastle

77 A Potential Cytosolic Function of Bestrophin-1 603
 Olaf Strauß, Rudgar Neussert, Claudia Müller,
 and Vladimir M. Milenkovic

78 Modeling the Structural Consequences of *BEST1* Missense Mutations 611
 Karina E. Guziewicz, Gustavo D. Aguirre, and Barbara Zanger

79 Microglial Activation and Transcriptomic Changes in the Blue Light-Exposed Mouse Retina 619
 Stefanie Ebert, Yana Walczak, Charlotte Remé, and Thomas Langmann

80 Overexpression of ROM-1 in the Cone-Dominant Retina 633
 Dibyendu Chakraborty, Shannon M. Conley, Zack Nash, Xi-Qin Ding, and Muna I. Naash

81 Analysis of the RPE Sheet in the rd10 Retinal Degeneration Model 641
 Micah A. Chrenek, Nupur Dalal, Christopher Gardner, Hans Grossniklaus, Yi Jiang, Jeffrey H. Boatright, and John M. Nickerson

82 Networks Modulating the Retinal Response to Injury: Insights from Microarrays, Expression Genetics, and Bioinformatics 649
 Félix R. Vázquez-Chona and Eldon E. Geisert

83 Mislocalization of Oligomerization-Incompetent RDS is Associated with Mislocalization of Cone Opsins and Cone Transducin 657
 Shannon M. Conley, Dibyendu Chakraborty, and Muna I. Naash

84 HSP70 Gene Expression in the Zebrafish Retina After Optic Nerve Injury: A Comparative Study Under Heat Shock Stresses 663
 Chieko Fujikawa, Mikiko Nagashima, Kazuhiro Mawatari, and Satoru Kato

Part IX Retinal Development, Physiology, Cell and Molecular Biology

85 Restoration of Retinal Development in *Vsx2* Deficient Mice by Reduction of *Gdf11* Levels 671
 Rosaysela Santos, Jeffry Wu, Jason A. Hamilton, Rita Pinter, Robert Hindges, and Anne L. Calof

86 The Different Functions of Norrin 679
 Barbara M. Braunger and Ernst R. Tamm

87 Roles of Homeobox Genes in Retinal Ganglion Cell Differentiation and Axonal Guidance 685
 Qi Zhang and David D. Eisenstat

88	Unraveling the Molecular Mystery of Retinal Pigment Epithelium Phagocytosis	693
	Nora B. Caberoy and Wei Li	
89	Isolating Photoreceptor Compartment-Specific Protein Complexes for Subsequent Proteomic Analysis	701
	Gregory H. Grossman, Gayle J.T. Pauer, George Hoppe, and Stephanie A. Hagstrom	
90	Expression of the Integrin Coreceptor Transglutaminase-2 in the RPE In Vivo and in Culture	709
	Linda Ruggiero and Silvia C. Finnemann	
91	On Your Marks... Get Bound... Internalize!	717
	Ah-Lai Law and Emeline F. Nandrot	
92	Endo-Lysosome Function in the Retinal Pigment Epithelium in Health and Disease	723
	Aparna Lakkaraju	
93	$\alpha\beta 5$ Integrin-Dependent Diurnal Phagocytosis of Shed Photoreceptor Outer Segments by RPE Cells Is Independent of the Integrin Coreceptor Transglutaminase-2	731
	Linda Ruggiero, Zsolt Sarang, Zsuzsa Szondy, and Silvia C. Finnemann	
94	Trafficking of Presynaptic PMCA Signaling Complexes in Mouse Photoreceptors Requires Cav1.4 α_1 Subunits	739
	Wei Xing, Abram Akopian, and David Križaj	
95	Roles for AMP-Activated Protein Kinase in RPE Cell Function	745
	Suofu Qin	
96	Genome-Wide Occupancy Analysis by ChIP-chip and ChIP-Seq	753
	Hong Hao	
97	The Bisretinoids of RPE Lipofuscin: A Complex Mixture	761
	Janet R. Sparrow and Kazunori Yamamoto	
98	Biochemical Characterization of Cone Cyclic Nucleotide-Gated (CNG) Channel Using the Infrared Fluorescence Detection System	769
	Xi-Qin Ding, Alexander Matveev, Anil Singh, Naoka Komori, and Hiroyuki Matsumoto	
99	Ras-Associating Domain Proteins: A New Class of Cyclic Nucleotide-Gated Channel Modulators	777
	Vivek K. Gupta, Ammaji Rajala, and Raju V.S. Rajala	

100 Tulp1 Is Involved in Specific Photoreceptor Protein Transport Pathways..... 783
 Stephanie A. Hagstrom, Rao F. Watson, Gayle J.T. Pauer, and Gregory H. Grossman

101 Potential Cellular Functions of *N*-Ethylmaleimide Sensitive Factor in the Photoreceptor 791
 Shun-Ping Huang and Cheryl M. Craft

102 Identification of Pigment Epithelium-Derived Factor Receptor (PEDF-R) Antibody Epitopes..... 799
 Preeti Subramanian, Matthew Rapp, and S. Patricia Becerra

103 HCN1 Channels Significantly Shape Retinal Photoresponses 807
 Naoyuki Tanimoto, Arne Brombas, Frank Müller, and Mathias W. Seeliger

104 The Role of the P2X7 Receptor in the Retina: Cell Signalling and Dysfunction 813
 Kirstan A. Vessey, Andrew I. Jobling, Ursula Greferath, and Erica L. Fletcher

105 A Tale of Two Kinases in Rods and Cones 821
 Shoji Osawa and Ellen R. Weiss

106 Protein Tyrosine Phosphatase 1B: A Novel Molecular Target for Retinal Degenerative Diseases 829
 Devaraj K. Basavarajappa, Vivek K. Gupta, and Raju V.S. Rajala

107 Protein Tyrosine-*O*-Sulfation in Bovine Ocular Tissues..... 835
 Yogita Kanan, Robert A. Hamilton, Kevin L. Moore, and Muayyad R. Al-Ubaidi

Erratum..... E1

Index 843

Contributors

Toshiaki Abe Division of Clinical Cell Therapy, United Center for Advanced Research and Translational Medicine (ART), Tohoku University Graduate School of Medicine, 1-1 Seiryomachi Aobaku Sendai, Miyagi, Japan
toshi@oph.med.tohoku.ac.jp

Zsolt Ablonczy Department of Ophthalmology, Medical University of South Carolina, Charleston, SC 29425, USA
ablonczy@musc.edu

Matthew Adamowicz Genzyme Corporation, 49 New York Avenue, Framingham, MA 01701, USA
Matthew.Adamowicz@genzyme.com

Gustavo D. Aguirre Department of Clinical Studies, Section of Ophthalmology, School of Veterinary Medicine, University of Pennsylvania, Philadelphia, PA 19104, USA
gda@vet.upenn.edu

Kelly Ahern Beckman Vision Center, University of California, San Francisco, CA 94143, USA
kelly.ahern@ucsf.edu

Abram Akopian Department of Physiology and Neuroscience, New York University Medical Center, New York, NY 10016, USA
aa3@nyu.edu

Rizalyn S. Albarracin Research School of Biology and ARC Centre of Excellence for Vision Sciences, The Australian National University, Canberra, ACT 0200, Australia
rizalyn.albarracin@anu.edu.au

Robin R. Ali Department of Genetics, UCL Institute of Ophthalmology, London, EC1V 9EL, UK
r.ali@ucl.ac.uk

Muayyad R. Al-Ubaidi Department of Cell Biology, University of Oklahoma Health Sciences Center, 940 Stanton L. Young Boulevard, BMSB 781, Oklahoma City, OK 73104, USA
Muayyad-Al-ubaidi@ouhsc.edu

Jayakrishna Ambati Department of Ophthalmology and Visual Sciences, University of Kentucky College of Medicine, Lexington, KY 40536, USA
jamba2@email.uky.edu

Bela Anand-Apte Department of Ophthalmology, Cole Eye Institute, Cleveland Clinic Lerner College of Medicine at Case Western Reserve University, Cleveland, OH, USA
anandab@ccf.org

Robert E. Anderson Department of Ophthalmology, University of Oklahoma Health Sciences Center, Oklahoma City, OK, USA
Dean A. McGee Eye Institute, Oklahoma City, OK, USA
Department of Cell Biology, University of Oklahoma Health Sciences Center, Oklahoma City, OK, USA
Robert-Anderson@ouhsc.edu

Matthew J. Annear Department of Small Animal Clinical Sciences, Michigan State University, East Lansing, MI 48824, USA
annear@cvm.msu.edu

Liviu Aron Department of Pathology, Harvard Medical School, Boston, MA 02115, USA
liviu@hms.harvard.edu

Radha Ayyagari Department of Ophthalmology, Shiley Eye Center, University of California San Diego, La Jolla, CA 92037, USA
rayyagari@ucsd.edu

Tomás P. Bachor Facultad de Ciencias Biomédicas, Universidad Austral, Pilar 1629AHJ, Buenos Aires, Argentina
tomasbachor@gmail.com

Nika Bagheri Department of Ophthalmology, Cole Eye Institute (i31), Cleveland Clinic Lerner College of Medicine, Cleveland, OH 44195, USA
baghern@ccf.org

Lin Bai Department of Pharmacy, Center for Integrated Protein Science Munich (CIPSM), Center for Drug Research, Ludwig-Maximilians-Universität München, Munich, Germany
lin.bai@cup.uni-muenchen.de

Yanyan Bai Department of Medicine Endocrinology and Harold Hamm Oklahoma Diabetes Center, University of Oklahoma Health Sciences Center, Oklahoma City, OK 73104, USA
yy_bai@yahoo.com

James W. Bainbridge Department of Genetics, UCL Institute of Ophthalmology, London, EC1V 9EL, UK
j.bainbridge@ucl.ac.uk

Mausumi Bandyopadhyay Department of Ophthalmology, Medical University of South Carolina, Charleston, SC 29425, USA
bandyopm@musc.edu

Susie E. Barker Department of Genetics, UCL Institute of Ophthalmology, London, EC1V 9EL, UK
S.barker@ucl.ac.uk

Joshua T. Bartoe Department of Small Animal Clinical Sciences, Michigan State University, East Lansing, MI 48824, USA
bartoejo@cvm.msu.edu

Devaraj K. Basavarajappa Department of Ophthalmology, Dean A. McGee Eye Institute, University of Oklahoma Health Sciences Center, 608 Stanton L. Young Boulevard, Oklahoma City, OK 73104, USA
devaraj-basavarajappa@ouhsc.edu

Chandree Beaulieu Department of Medical Genetics, University of Calgary, Calgary, AB, Canada
Alberta Children's Hospital Research Institute, University of Calgary, Calgary, AB, Canada
chandree.beaulieu@albertahealthservices.ca

S. Patricia Becerra National Eye Institute, National Institutes of Health, Building 6, Room 134, 6 Center Drive, MSC 0608, Bethesda, MD 20892-0608, USA
becerrap@nei.nih.gov

N. Torben Bech-Hansen Department of Medical Genetics, University of Calgary, Heritage Medical Research Building, Room No 258, Calgary, AB, Canada
Alberta Children's Hospital Research Institute, University of Calgary, Calgary, AB, Canada
ntbech@ucalgary.ca

Elvir Becirovic Department of Pharmacy, Center for Integrated Protein Science Munich (CIPSM), Center for Drug Research, Ludwig-Maximilians-Universität München, Munich, Germany
elvir.becirovic@cup.uni-muenchen.de

Susanne C. Beck Division of Ocular Neurodegeneration, Centre for Ophthalmology, Institute for Ophthalmic Research, Eberhard Karls-Universität, Tübingen, Germany

Brent A. Bell Department of Ophthalmology, Cole Eye Institute (i31), Cleveland Clinic Lerner College of Medicine, Cleveland, OH 44195, USA
bellb3@ccf.org

William A. Beltran Department of Clinical Studies, University of Pennsylvania, Section of Ophthalmology, School of Veterinary Medicine, 3900 Delancey Street, Philadelphia, PA 19104, USA
wbeltran@vet.upenn.edu

Jean Bennett F.M. Kirby Center for Molecular Ophthalmology, University of Pennsylvania, Philadelphia, PA 19104, USA
jebennet@mail.med.upenn.edu

Antje M. Bernd Centre for Ophthalmology, Institute for Ophthalmic Research, University of Tuebingen, Schleichstr. 12-16, 72076 Tuebingen, Germany
antje.bernd@med.uni-tuebingen.de

Qingning Bian Jean Mayer USDA Human Nutrition Research Center on Aging, Tufts University, Boston, MA 02111, USA
qiningning.bian@tufts.edu

Martin Biel Department of Pharmacy, Center for Integrated Protein Science Munich (CIPSM), Center for Drug Research, Ludwig-Maximilians-Universität München, Munich, Germany
martin.biel@cup.uni-muenchen.de

David G. Birch Retina Foundation of the Southwest, Dallas, TX 75231, USA
Department of Ophthalmology, University of Texas Southwestern Medical Center, Dallas, TX 75390, USA
dbirch@retinafoundation.org

Oliver E. Blacque UCD Conway Institute and UCD School of Biomolecular and Biomedical Sciences, University College Dublin, Belfield, Dublin 4, Ireland
oliver.blacque@ucd.ie

Janet Blanks Department of Biomedical Science, Florida Atlantic University, Boca Raton, FL, USA
Center for Complex Systems and Brain Science, Florida Atlantic University, Boca Raton, FL, USA
blanks@fau.edu

Jeffrey H. Boatright Department of Ophthalmology, Emory University, 1365B Clifton Road NE, TEC-B5602, Atlanta, GA 30322, USA
litjn@emory.edu

Vera L. Bonilha Department of Ophthalmology, Cole Eye Institute (i31), Cleveland Clinic Lerner College of Medicine, Cleveland, OH 44195, USA
bonilhav@ccf.org

Michael E. Boulton Department of Anatomy and Cell Biology, University of Florida, Gainesville, FL, USA
meboulton@ufl.edu

Kristen E. Bowles Department of Vision Sciences, University of Alabama at Birmingham, Birmingham, AL 35223, USA
keb2009@gmail.com

Sara J. Bowne Human Genetics Center, School of Public Health, University of Texas Health Science Center at Houston, Houston, TX 77030, USA
sara.j.bowne@uth.tmc.edu

Barbara M. Braunger Institute of Human Anatomy and Embryology, University of Regensburg, Universitätsstr. 31, Regensburg D-93053, Germany
Barbara.Braunger@vkl.uni-regensburg.de

Arne Brombas Institut für Strukturbiologie und Biophysik (ISB-1), Forschungszentrum Jülich, Jülich, Germany
a.brombas@fz-juelich.de

Julien Bruban Centre de Recherche des Cordeliers, Université Pierre et Marie Curie – Paris 6, UMRS 872, Paris, France
Université Paris Descartes, UMRS 872, Paris, France
INSERM, UMRS872, Paris, France
julien.bruban@exchange.mssm.edu

Richard S. Brush Department of Ophthalmology, OUHSC, Oklahoma City, OK 73104, USA
Dean A. McGee Eye Institute, 608 S. L. Young Boulevard, DMEI 414, Oklahoma City, OK 73104, USA
Richard-Brush@ouhsc.edu

Hildegard Büning Department I of Internal Medicine and Center for Molecular Medicine Cologne, University of Cologne, 50931 Cologne, Germany
hildegard.buening@uk-koeln.de

Mark C. Butler Department of Ophthalmology, University at Buffalo, State University of New York (SUNY), SUNY Eye Institute, Buffalo, NY 14209, USA
mcbutler@buffalo.edu

Nora B. Caberoy Bascom Palmer Eye Institute, Department of Ophthalmology, University of Miami Miller School of Medicine, 1638 NW 10th Avenue, Miami, FL 33136, USA
ncaberoy@med.miami.edu

Jun Cai Departments of Anatomy and Cell Biology, University of Florida, Gainesville, FL 32610, USA
jucai@ufl.edu

Xue Cai Department of Ophthalmology and Dean A. McGee Eye Institute, University of Oklahoma Health Sciences Center, Oklahoma City, OK 73104, USA
xue-cai@ouhsc.edu

Anne L. Calof Department of Anatomy and Neurobiology
and Center for Complex Biological Systems, University of California,
Irvine, CA 92697-1275, USA
alcalof@uci.edu

Matthew Campbell Ocular Genetics Unit, Smurfit Institute of Genetics,
Trinity College Dublin, Dublin 2, Ireland
campbem2@tcd.ie

Joseph Carroll Departments of Ophthalmology, Biophysics,
and Cell Biology, Neurobiology, and Anatomy, Medical College of Wisconsin,
Milwaukee, WI 53226, USA
jcarroll@mcw.edu

Mauricio M. Castañeda Facultad de Ciencias Biomédicas, Universidad Austral,
Pilar 1629AHJ, Buenos Aires, Argentina
mcastaned@cas.austral.edu.ar

Dibyendu Chakraborty Department of Cell Biology, University of Oklahoma
Health Sciences Center, 940 Stanton L. Young Blvd. BMS 781, Oklahoma City,
OK 73104, USA
Dibyendu-chakraborty@ouhsc.edu

Kevin J. Chalmers MRC Human Genetics Unit, Institute of Genetics
and Molecular Medicine, Western General Hospital, Crewe Road,
Edinburgh EH4 2XU, UK

Venkata Ramana Murthy Chavali Department of Ophthalmology,
Shiley Eye Center, University of California, 9415 Campus point Drive,
Jacobs Retina Center, Room 228, San Diego, CA 92037, USA
vchavali@ucsd.edu

Michael E. Cheetham UCL Institute of Ophthalmology,
11-43 Bath Street, London EC1V 9EL, UK
michael.cheetham@ucl.ac.uk

Hui Chen Department of Ophthalmology and Dean A. McGee Eye Institute,
University of Oklahoma Health Sciences Center, Oklahoma City,
OK 73104, USA

Ophthalmology Department of Sichuan Academy of Medical Sciences
and Sichuan Provincial People's Hospital, Chengdu City,
Sichuan Province 610072, China
Hui-Chen@ouhsc.edu

Wei-Chieh Chiang Department of Pathology, University of California,
San Diego, CA 92093-0612, USA
wcchiang@ucsd.edu

Alan Y. Chow Optobionics Corporation, Naperville, IL, USA
AlanYKC@aol.com

Micah A. Chrenek Department of Ophthalmology, Emory University,
1365B Clifton Road NE, TEC-B5602, Atlanta, GA 30322, USA
micah.chrenek@emory.edu

Vincent T. Ciavatta Rehabilitation Research and Development
Center of Excellence, Atlanta VA Medical Center,
1670 Clairmont Rd, Decatur, GA 30033, USA
Department of Ophthalmology, Emory University, Atlanta, GA 30322, USA
vciavat@emory.edu

Nansi Jo Colley Department of Ophthalmology and Visual Sciences
and Department of Genetics, and UW-Eye Research Institute,
University of Wisconsin, Madison, WI 53792, USA
njcolley@wisc.edu

Rob W.J. Collin Department of Human Genetics, Radboud University Nijmegen
Medical Centre, route 855, PO Box 9101, 6500 HB, Nijmegen, The Netherlands
Department of Ophthalmology, Radboud University Nijmegen Medical Centre,
route 400, PO Box 9101, 6500 HB Nijmegen, The Netherlands
Nijmegen Centre for Molecular Life Sciences, Radboud University Nijmegen
Medical Centre, PO Box 9101, 6500 HB Nijmegen, The Netherlands
R.Collin@antrg.umcn.nl

Shannon M. Conley Department of Cell Biology, University of Oklahoma
Health Sciences Center, 940 Stanton L. Young Blvd. BMS 781, Oklahoma City,
OK 73104, USA
Shannon-conley@ouhsc.edu

Thomas B. Connor Department of Ophthalmology, Medical College
of Wisconsin, Milwaukee, WI 53226, USA
tconnor@mcw.edu

Cheryl M. Craft Mary D. Allen Laboratory for Vision Research,
Doheny Eye Institute, Keck School of Medicine of the University
of Southern California, Los Angeles, CA 90033-9224, USA
Department of Ophthalmology, Keck School of Medicine of the University
of Southern California, Los Angeles, CA 90033-9224, USA
Department of Cell and Neurobiology, Keck School of Medicine of the University
of Southern California, Los Angeles, CA 90033-9224, USA
ccraft@usc.edu

Frans P.M. Cremers Department of Human Genetics, Radboud University
Nijmegen Medical Centre, route 855, PO Box 9101, 6500 HB, Nijmegen,
The Netherlands
Department of Human Genetics, Nijmegen Centre for Molecular Life Sciences,
Radboud University Nijmegen Medical Centre, PO Box 9101, 6500 HB
Nijmegen, The Netherlands
F.Cremers@antrg.umcn.nl

Thérèse Cronin F.M. Kirby Center for Molecular Ophthalmology,
University of Pennsylvania, Philadelphia, PA 19104, USA
theresec@mail.med.upenn.edu

Rosalie K. Crouch Department of Ophthalmology, Medical University
of South Carolina, Charleston, SC, USA
crouchrk@musc.edu

Marisa A. Cubilla Facultad de Ciencias Biomédicas, Universidad Austral,
Pilar 1629AHJ, Buenos Aires, Argentina
mcubilla@cas.austral.edu.ar

Paul G. Curran Center for Statistical Consulting,
Michigan State University, East Lansing, MI 48824, USA
curranp1@msu.edu

Alecia Cutler Department of Ophthalmology, Cole Eye Institute,
Cleveland Clinic Lerner College of Medicine at Case Western Reserve University,
Cleveland, OH, USA
cutlera@ccf.org

Mohammad Dahrouj Department of Ophthalmology, Medical University
of South Carolina, Charleston, SC 29425, USA
dahrouj@musc.edu

Stephen P. Daiger Human Genetics Center, School of Public Health,
University of Texas Health Science Center at Houston,
Houston, TX 77030, USA

Nupur Dalal Department of Ophthalmology, Emory University,
Atlanta, GA 30322, USA
ndalal@lsuhsc.edu

Dominic M. Desiderio Department of Neurology, Stout Mass Spectrometry
Laboratory, University of Tennessee Health Science Center, Memphis,
TN 38163, USA
ddesiderio@uthsc.edu

Sophie Devery Moorfields Eye Hospital, City Road, London EC1V 2PD, UK
Sophie.Devery@moorfields.nhs.uk

Sorcha Ní Dhubhghaill Ocular Genetics Unit, Smurfit Institute of Genetics,
Trinity College Dublin, Dublin 2, Ireland
nidhubs@tcd.ie

Virginie Dinet Centre de Recherche des Cordeliers, Université Pierre et Marie
Curie – Paris 6, UMRS 872, 15 rue de l'École de Médecine, Paris 75006, France
Université Paris Descartes, UMRS 872, Paris 75006, France
INSERM, UMRS872, Paris 75006, France
virginie.dinet@inserm.fr

Xi-Qin Ding Department of Cell Biology, University of Oklahoma Health Sciences Center, 940 Stanton L. Young Blvd. BMS 781, Oklahoma City, OK 73104, USA
xding@ouhsc.edu

C. Kathleen Dorey Department of Medicine, Virginia Tech Carilion School of Medicine, Roanoke, VA 24016, USA
ckdorey@carilionclinic.org

William A. Dunn Jr. Department of Anatomy and Cell Biology, University of Florida, 1600 SW Archer Road, PO Box 100235, Gainesville, FL 32610, USA
dunn@ufl.edu

Francois Paquet-Durand Division for Experimental Ophthalmology, Institute for Ophthalmic Research, Centre for Ophthalmology, 72076 Tuebingen, Germany
Francois.Paquet-Durand@med.uni-tuebingen.de

Mary Dwyer Department of Pharmacology and Cancer Biology, Duke University, Durham, NC 27701, USA

Neil D. Ebenezer UCL Institute of Ophthalmology, 11-43 Bath Street London EC1V 9EL, UK

Stefanie Ebert Institute of Human Genetics, University of Regensburg, Franz Josef Strauss Allee 11, 93053 Regensburg, Germany
stefanie.ebert@klinik.uni-regensburg.de

David D. Eisenstat Departments of Human Anatomy and Cell Science, Manitoba Institute of Cell Biology, Pediatrics and Child Health, Biochemistry and Medical Genetics, and Ophthalmology, University of Manitoba, Winnipeg, MB, Canada R3E 0V9
eisensta@cc.umanitoba.ca

Abigail T. Fahim Human Genetics Center, School of Public Health, University of Texas Health Science Center at Houston, Houston, TX 77030, USA
abigail.t.fahim@uth.tmc.edu

Edda Fahl Division of Ocular Neurodegeneration, Centre for Ophthalmology, Institute for Ophthalmic Research, Eberhard Karls-Universität Tübingen, 72076 Tübingen, Germany
edda.fahl@med.uni-tuebingen.de

Michael Farkas Ocular Genomics Institute, Berman Gund Laboratory, Department of Ophthalmology, Massachusetts Eye and Ear Infirmary, 243 Charles St., Boston, MA 02114, USA
mfarkas@mail.med.upenn.edu

G. Jane Farrar Department of Genetics, The Ocular Genetics Unit, Trinity College Dublin, Dublin 2, Ireland
gjfarrar@tcd.ie

Amanda E. Faulkner Rehabilitation Research and Development
Center of Excellence, Atlanta VA Medical Center,
1670 Clairmont Rd, Decatur, GA 30033, USA
iqq2@cdc.gov

Silvia C. Finnemann Department of Biological Sciences,
Fordham University, Bronx, NY 10458, USA
finnemann@fordham.edu

M. Dominik Fischer Division of Ocular Neurodegeneration,
Institute for Ophthalmic Research, Centre for Ophthalmology,
72076 Tübingen, Germany
Dominik.Fischer@med.uni-tuebingen.de

Erica L. Fletcher Department of Anatomy and Cell Biology,
The University of Melbourne, Level 7, Medical Building,
Grattan Street, Melbourne, VIC 3010, Australia
elf@unimelb.edu.au

Wai Gin Fong Ottawa Hospital Research Institute, Ottawa General Hospital,
Ottawa, ON, Canada K1H 8L6
wfong@ohri.ca

Chieko Fujikawa Division of Health Sciences, Kanazawa University,
13-1 Takara-machi, Kanazawa, Ishikawa, 920-8640 Japan
orange@stu.kanazawa-u.ac.jp

Christopher Gardner Department of Ophthalmology, Emory University,
Atlanta, GA 30322, USA
christopher.gardner@emory.edu

Jessica C. Gardner UCL Institute of Ophthalmology,
11-43 Bath Street, London EC1V 9EL, UK
jessica.gardner@ucl.ac.uk

Eldon E. Geisert Department of Ophthalmology, University of TN Health
Science Center, 930 Madison Avenue, Suite 731 Memphis, TN 38163, USA
egeisert@uthsc.edu

Sem Genini Department of Clinical Studies, Section of Ophthalmology,
School of Veterinary Medicine, University of Pennsylvania,
Philadelphia, PA 19104, USA
geninis@vet.upenn.edu

Susan Gentleman LRCMB, National Eye Institute, NIH,
Bethesda, MD 20892, USA
sgman@helix.nih.gov

Ivan C. Gerling Department of Internal Medicine, University of Tennessee
Health Science Center, Memphis, TN 38163, USA
igerling@uthsc.edu

Oliviero L. Gobbo School of Pharmacy and Pharmaceutical Sciences,
Trinity College Dublin, Dublin 2, Ireland
ogobbo@tcd.ie

Pooja Godara Department of Ophthalmology, Medical College of Wisconsin,
Milwaukee, WI 53226, USA
poojagodara145@gmail.com

Tim Gollisch Visual Coding Group, Max Planck Institute of Neurobiology,
82152 Martinsried, Germany
gollisch@neuro.mpg.de

Roser Gonzàlez-Duarte Departament de Genètica, Universitat de Barcelona,
Barcelona 08028, Spain
Institut de Biomedicina, Universitat de Barcelona, Barcelona 08028, Spain
CIBERER, Instituto de Salud Carlos III, Barcelona, Spain
rgonzalez@ub.edu

Marina S. Gorbatyuk Department of Cell Biology and Anatomy,
University of North Texas Health Science Center, Fort Worth, TX 76107, USA
Marina.Gorbatyuk@unthsc.edu

Oleg S. Gorbatyuk Department of Molecular Genetics and Microbiology,
University of Florida, Gainesville, FL 32610, USA
olegor@ufl.edu

Greg R. Grant Penn Center for Bioinformatics, University of Pennsylvania,
Philadelphia, PA 19104, USA
ggrant@grant.org

Maria B. Grant Departments of Pharmacology and Therapeutics,
University of Florida, Gainesville, FL 32610, USA
grantma@ufl.edu

Ursula Greferath Department of Anatomy and Cell Biology,
The University of Melbourne, Level 7, Medical Building, Grattan Street,
Melbourne, VIC 3010, Australia
u.greferath@unimelb.edu.au

Cheryl Y. Gregory-Evans Department of Ophthalmology,
University of British Columbia, Vancouver, BC, Canada
cge30@eyecarecentre.org

Angus C. Grey Department of Optometry and Vision Science,
University of Auckland, Grafton 1023, New Zealand
ac.grey@auckland.ac.nz

Ana Griciuc Department of Protein Science, Helmholtz Zentrum Muenchen – German Research Centre for Environmental Health, 85764, Neuherberg, Germany

Institute for Ophthalmic Research, Centre for Ophthalmology, University of Tuebingen, 72076 Tuebingen, Germany
ana.griciuc@helmholtz-muenchen.de

Christian Grimm Department of Ophthalmology, Laboratory of Retinal Cell Biology, University of Zurich, Sternwartstrasse 148091, Zurich, Switzerland

Gregory H. Grossman Department of Ophthalmic Research, Cole Eye Institute, Cleveland Clinic, Cleveland, OH, USA
grossmg@ccf.org

Hans Grossniklaus Department of Ophthalmology, Emory University, Atlanta, GA 30322, USA
ophtheg@emory.edu

Alexander Gubin LRCMB, National Eye Institute, NIH, Bethesda, MD 20892, USA
gubina@csr.nih.gov

Vivek K. Gupta Department of Ophthalmology, Dean A. McGee Eye Institute, University of Oklahoma Health Sciences Center, 608 Stanton L. Young Blvd, Oklahoma City, OK 73104, USA
vivek-gupta@ouhsc.edu

Danielle B. Gutierrez Laboratory of Retinal Cell and Molecular Biology, National Eye Institute, Bethesda, MD 20892, USA
danielle.gutierrez@nih.gov

Karina E. Guziewicz Department of Clinical Studies, Section of Ophthalmology, University of Pennsylvania, School of Veterinary Medicine, 3900 Delancey Street, Philadelphia, PA 19104, USA
karinag@vet.upenn.edu

Stephanie A. Hagstrom Department of Ophthalmic Research, Cole Eye Institute, Cleveland Clinic, Cleveland, OH, USA

Department of Ophthalmology, Cleveland Clinic Lerner College of Medicine of Case Western Reserve University, Cleveland, OH, USA
hagstrs@ccf.org

Jason A. Hamilton Department of Regenerative Medicine, Athersys Inc, 3021 Carnegie Avenue, Cleveland, OH 44115-2634, USA
jhamilton@athersys.com

Robert A. Hamilton Department of Cell Biology, University of Oklahoma Health Sciences Center, 940 Stanton L. Young Boulevard, BMSB 781, Oklahoma City, OK 73104, USA
Robert-hamilton@ouhsc.edu

Finnian Hanrahan Ocular Genetics Unit, Smurfit Institute of Genetics,
Trinity College Dublin, Dublin 2, Ireland
hanrahfe@tcd.ie

Hong Hao Neurobiology-Neurodegeneration and Repair Laboratory,
National Eye Institute, National Institutes of Health, Bethesda, MD 20892, USA
haoh@mail.nih.gov

Alison J. Hardcastle UCL Institute of Ophthalmology,
11-43 Bath Street, London, EC1V 9EL, UK
a.hardcastle@ucl.ac.uk

William W. Hauswirth Department of Ophthalmology, University of Florida,
Gainesville, FL 32610, USA
hauswrth@ufl.edu

Xiaoqin He Department of Chemistry and Biochemistry, University of Bern,
Bern, Switzerland
xiaoqin.he@ibc.unibe.ch

Lizbeth Hedstrom Departments of Biology and Chemistry, Brandeis University,
Waltham, MA 02453, USA
hedstrom@brandeis.edu

Elise Héon The Hospital for Sick Children, 555 University Avenue,
Toronto, Canada ON M5G 1X8
elise.heon@sickkids.ca

Severin R. Heynen Laboratory of Retinal Cell Biology,
Department of Ophthalmology, University of Zurich,
Wagistrasse 14, 8952, Schlieren, Switzerland
Zurich Center for Integrative Human Physiology, Zurich, Switzerland
severin.heynen@usz.ch

Wanda Hicks The Jackson Laboratory, Bar Harbor, ME 04609, USA
wanda.jordan@jax.org

Robert Hindges MRC Center for Developmental Neurobiology, Kings College,
London, SE1 1UL, UK
Robert.Hindges@kcl.ac.uk

Graham E. Holder Moorfields Eye Hospital, City Road, London
EC1V 2PD, UK
Graham.Holder@ Moorfields.nhs.uk

Anneke I.den Hollander Department of Human Genetics, Radboud University
Nijmegen Medical Centre, route 855, PO Box 9101, 6500 HB Nijmegen,
The Netherlands
Department of Ophthalmology, Radboud University Nijmegen Medical Centre,
Route 400, PO Box 9101, 6500 HB, Nijmegen,
The Netherlands

Nijmegen Centre for Molecular Life Sciences, Radboud University Nijmegen
Medical Centre, PO Box 9101, 6500 HB Nijmegen, The Netherlands
A.denHollander@antrg.umcn.nl

Joe G. Hollyfield Department of Ophthalmology, Cole Eye Institute (i31),
Cleveland Clinic Lerner College of Medicine, Cleveland, OH 44195, USA
hollyfj@ccf.org

Donald C. Hood Department of Psychology and Ophthalmology,
450 Riverside Drive New York, NY 10027, USA
dch3@columbia.edu

George Hoppe Department of Ophthalmic Research (i31), Cole Eye Institute,
Cleveland Clinic, 9500 Euclid Avenue Cleveland, OH 44195, USA
hoppeg@ccf.org

Hu-Deqiang Huang Bascom Palmer Eye Institute,
Miller School of Medicine, University of Miami, Miami, FL 33136, USA
dhuang2@med.miami.edu

Shun-Ping Huang Mary D. Allen Laboratory for Vision Research,
Doheny Eye Institute, Keck School of Medicine of the University of Southern
California, Los Angeles, CA 90033-9224, USA

Department of Ophthalmology, Keck School of Medicine of the University
of Southern California, Los Angeles, CA 90033-9224, USA
sphophdoc1688@gmail.com

Gesine Huber Division of Ocular Neurodegeneration,
Centre for Ophthalmology, Institute for Ophthalmic Research,
Eberhard Karls-Universität Tübingen, 72076 Tübingen, Germany
gesine.huber@med.uni-tuebingen.de

Marian M. Humphries Ocular Genetics Unit, Smurfit Institute of Genetics,
Trinity College Dublin, Dublin 2, Ireland
mhumphri@tcd.ie

Pete Humphries Ocular Genetics Unit, Smurfit Institute of Genetics,
Trinity College Dublin, Dublin 2, Ireland
Pete.Humphries@tcd.ie

David R. Hyde Department of Biological Sciences and the Center for
Zebrafish Research, University of Notre Dame, Notre Dame, IN 46556, USA
dhyde@nd.edu

Alessandro Iannaccone Department of Ophthalmology, Hamilton Eye Institute,
University of Tennessee Health Science Center, Memphis, TN 38163, USA
aiannacc@uthsc.edu

Yumi Ishikawa Division of Clinical Cell Therapy, United Center for Advanced
Research and Translational Medicine (ART), Tohoku University
Graduate School of Medicine, Miyagi, Japan
jagariko@med.tohoku.ac.jp

Yi Jiang Theoretical Division, Los Alamos National Laboratory,
Los Alamos, NM 87545, USA
jiang@lanl.gov

Andrew I. Jobling Department of Anatomy and Cell Biology,
The University of Melbourne, Level 7, Medical Building,
Grattan Street, Melbourne, VIC 3010, Australia
aij@unimelb.edu.au

Yogita Kanan Department of Cell Biology, University of Oklahoma
Health Sciences Center, 940 Stanton L. Young Boulevard, BMSB 781,
Oklahoma City, OK 73104, USA
ykanan@ouhsc.edu

Naheed Kanuga UCL Institute of Ophthalmology, 11-43 Bath Street,
London EC1V 9EL, UK
n.kanuga@ucl.ac.uk

Satoru Kato Department of Molecular Neurobiology, Graduate School
of Medicine, Kanazawa University, 13-1 Takara-machi, Kanazawa,
Ishikawa 920-8640, Japan
satoru@med.kanazawa-u.ac.jp

Charles Kaul Department of Ophthalmology, Cole Eye Institute (i31),
Cleveland Clinic Lerner College of Medicine, Cleveland, OH 44195, USA

Konrad Kauper Neurotech USA, Lincoln, RI 02865, USA
k.kauper@neurotechusa.com

James Keaney Department of Genetics, The Ocular Genetics Unit,
Trinity College Dublin, Dublin 2, Ireland jkeaney@tcd.ie

Paul F. Kenna Ocular Genetics Unit, Smurfit Institute of Genetics,
Trinity College Dublin, Dublin 2, Ireland
pfkenna@tcd.ie

Breandán N. Kennedy UCD Conway Institute and UCD School of Biomolecular
and Biomedical Sciences, University College Dublin, Belfield, Dublin 4, Ireland
brendan.kennedy@ucd.ie

Anna-Sophia Kiang Ocular Genetics Unit, Smurfit Institute of Genetics,
Trinity College Dublin, Dublin 2, Ireland
skiang@tcd.ie

Moon K. Kim Rehabilitation Research and Development Center of Excellence,
Atlanta VA Medical Center, Decatur, GA 30033, USA
zlalunar@gmail.com

Veronique Kitiratschky veronique.kitiratschky@med.uni-tuebingen.de
Department for Ophthalmology, Molecular Genetics Laboratory,
Institute for Ophthalmic Research, University Tuebingen, Roentgenweg 11,
S Tuebingen 72076, Germany

Mark E. Kleinman Department of Ophthalmology and Visual Sciences, University of Kentucky College of Medicine, Lexington, KY 40536, USA
mark.kleinman@uky.edu

Susanne Koch Department of Pharmacy, Center for Integrated Protein Science Munich (CIPSM), Center for Drug Research, Ludwig-Maximilians-Universität München, 81377 Munich, Germany
susanne.koch@cup.uni-muenchen.de

Susanne Kohl Department for Ophthalmology, Molecular Genetics Laboratory, Institute for Ophthalmic Research, University Tuebingen, Roentgenweg 11, Tuebingen 72076, Germany
susanne.kohl@uni-tuebingen.de

Tiffany A. Kolniak Department of Ophthalmology and Department of Neuroscience Program, (Ross Eye Institute), School of Medicine and Biomedical Sciences, University at Buffalo, State University of New York (SUNY), SUNY Eye Institute, Buffalo, NY 14209, USA

Naoka Komori Department of Biochemistry and Molecular Biology, University of Oklahoma Health Sciences Center, Oklahoma City, OK 73104, USA
naoka-komori@ouhsc.edu

Yoshiki Koriyama Department of Molecular Neurobiology, Kanazawa University, Kanazawa 920-8640, Japan
koriyama@med.kanazawa-u.ac.jp

Eloed Kortvely Division of Experimental Ophthalmology, University of Tuebingen, Roentgenweg 11, Tuebingen, 72076, Germany
eloed.koertvely@uni-tuebingen.de

Timothy W. Kraft Department of Vision Sciences, University of Alabama at Birmingham, Birmingham, AL 35223, USA
twkraft@uab.edu

Vidhyasankar Krishnamoorthy Visual Coding Group, Max Planck Institute of Neurobiology, 82152 Martinsried, Germany
vidhya@neuro.mpg.de

Pratheebha Krishnamurthy Department of Ophthalmology, Hamilton Eye Institute, University of Tennessee Health Science Center, Memphis, TN 38163, USA
pkrishn5@uthsc.edu

David Krizaj Departments of Ophthalmology and Visual Sciences, Moran Eye Center, and Physiology, University of Utah School of Medicine, Salt Lake City, UT 84132, USA

The Brain Institute, University of Utah, Salt Lake City, UT 84112, USA
david.krizaj@hsc.utah.edu

Heike Kroeger Department of Pathology, University of California,
San Diego, CA 92093-0612, USA
hkroeger@ucsd.edu

Norihiro Kumasaka Division of Clinical Cell Therapy, United Center
for Advanced Research and Translational Medicine (ART), Tohoku University,
Graduate School of Medicine, Miyagi, Japan
a9mm5010@s.tohoku.ac.jp

Kannan Kunchithapautham Department of Neurosciences,
Division of Research, Medical University of South Carolina,
Charleston, SC 29425, USA
kunchit@musc.edu

Anne Kurtenbach Centre for Ophthalmology, Institute for Ophthalmic Research,
University of Tuebingen, Schleichstr. 12-16, 72076 Tuebingen, Germany
anne.kurtenbach@uni-tuebingen.de

Tatyana Kuznetsova Department of Clinical Studies,
Section of Ophthalmology, School of Veterinary Medicine,
University of Pennsylvania, Philadelphia, PA, USA
tatyanak@vet.upenn.edu

James Laird Department of Chemistry, Case Western Reserve University,
Cleveland, OH, USA
jxl122@case.edu

Aparna Lakkaraju Department of Ophthalmology and Visual Sciences,
School of Medicine and Public Health, University of Wisconsin-Madison,
1300 University Avenue, MSC 3385, Madison, WI 53706, USA
lakkaraju@wisc.edu

Thomas Langmann Institute of Human Genetics, University of Regensburg,
Franz Josef Strauss Allee 11, 93053 Regensburg, Germany
thomas.langmann@klinik.uni-regensburg.de

Alan M. Laties Department of Ophthalmology, School of Medicine,
University of Pennsylvania, Philadelphia, PA, USA
laties@mail.med.upenn.edu

Matthew M. LaVail Beckman Vision Center, University of California,
San Francisco, CA 94143, USA
matthew.lavail@ucsf.edu

Ah-Lai Law INSERM, U968, Paris 75012, France
Genetics Department, UPMC Univ Paris 06, UMR_S 968, Institut de la Vision,
Paris 75012, France
CNRS, UMR_7210, 17 rue Moreau, Paris 75012, France
ah-lai.law@inserm.fr

Yun-Zheng Le Departments of Medicine Endocrinology and Cell Biology and Ophthalmology, Harold Hamm Oklahoma Diabetes Center, Dean A. McGee Eye Institute, University of Oklahoma Health Sciences Center, Oklahoma City, OK 73104, USA
yun-le@ouhsc.edu

Nataliya I. Lenchik Department of Internal Medicine, University of Tennessee Health Science Center, Memphis, TN 38163, USA
nlenchik@uthsc.edu

Alfred S. Lewin Department of Molecular Genetics and Microbiology and Ophthalmology, University of Florida, Gainesville, FL 32610, USA
lewin@ufl.edu

Feng Li Department of Ophthalmology and Dean A. McGee Eye Institute, University of Oklahoma Health Sciences Center, Oklahoma City, OK 73104, USA
Feng-Li@ouhsc.edu

Wei Li Bascom Palmer Eye Institute, Department of Ophthalmology, University of Miami Miller School of Medicine, 1638 NW 10th Avenue, Miami, FL 33136, USA
wli@med.miami.edu

Yiwen Li Bascom Palmer Eye Institute, University of Miami, Miller School of Medicine, Miami, FL 33136, USA
yli2@med.miami.edu

Jonathan H. Lin Department of Pathology, University of California at San Diego, La Jolla, CA 92093, USA
jlin@ucsd.edu

Karin W. Littink The Rotterdam Eye Hospital, PO Box 70030, 3000 LM Rotterdam, The Netherlands
Department of Human Genetics, Radboud University Nijmegen Medical Centre, route 855, PO Box 9101, 6500 HB Nijmegen, The Netherlands
K.Littink@oogziekenhuis.nl

Joel Lobsiger Institute for Molecular Biology and Biophysics, ETH, Zürich, Switzerland

Kirsten G. Locke Retina Foundation of the Southwest, 9900 N Central Expressway, Suite 400, Dallas, TX 75231, USA
kglocke@retinafoundation.org

Nidhi Lodha Department of Medical Genetics, University of Calgary, Heritage, Calgary, AB, Canada
Alberta Children's Hospital Research Institute, University of Calgary, Calgary, AB, Canada
nlodha@ucalgary.ca

Vanda S. Lopes Departments of Ophthalmology and Neurobiology,
UCLA School of Medicine, Los Angeles, CA 90095, USA
vslopes@ucla.edu

Catrina M. Loucks Department of Medical Genetics, University of Calgary,
Calgary, AB, Canada

Alberta Children's Hospital Research Institute, University of Calgary,
Calgary, AB, Canada
cmloucks@ucalgary.ca

Ulrich F.O. Luhmann Department of Genetics, UCL Institute of Ophthalmology,
11-43 Bath Street, London EC1V 9EL, UK
u.luhmann@ucl.ac.uk

Lingyu Luo Bascom Palmer Eye Institute, Miller School of Medicine,
University of Miami, Miami, FL 33136, USA
lluo@med.miami.edu

Arkady Lyubarsky F.M. Kirby Center for Molecular Ophthalmology,
University of Pennsylvania, Philadelphia, PA 19104, USA
arkady@mail.med.upenn.edu

Wenxin Ma Unit on Neuron–Glia Interactions in Retinal Disease, National Eye
Institute, 6 Center Drive, Building 6, Room 215, Bethesda, MD 20892, USA
mawenxin@nei.nih.gov

Ian M. MacDonald Department of Ophthalmology,
University of Alberta, Edmonton AB 10240, Canada
Ian.M.Macdonald@albertahealthservices.ca

Eamonn R. Maher West Midlands Regional Genetics Service,
Birmingham Women's Hospital, Birmingham, UK
e.r.maher@bham.ac.uk

Goldis Malek Department of Ophthalmology, Duke University,
Durham, NC 27701, USA
gmalek@duke.edu

Md Nawajes A. Mandal Department of Ophthalmology and Dean A. McGee
Eye Institute, University of Oklahoma Health Sciences Center, Oklahoma City,
OK 73104, USA
mmandal@ouhsc.edu

Haoyu Mao Department of Molecular Genetics and Microbiology,
University of Florida, Gainesville, FL 32610-0266, USA
maohaoyu@ufl.edu

Gemma Marfany Departament de Genètica, Universitat de Barcelona,
Barcelona 08028, Spain

Institut de Biomedicina, Universitat de Barcelona, Barcelona 08028, Spain
CIBERER, Instituto de Salud Carlos III, Barcelona, Spain
gmarfany@ub.edu

Frédéric Mascarelli Centre de Recherche des Cordeliers, Université Pierre et Marie Curie – Paris 6, UMRS 872, 15 rue de l'École de Médecine, Paris 75006, France
Université Paris Descartes, UMRS 872, Paris 75006, France
INSERM, UMRS872, Paris 75006, France
frederic.mascarelli@inserm.fr

Toru Matsukawa Department of Molecular Neurobiology,
Kanazawa University, Kanazawa 920-8640, Japan
makken@med.kanazawa-u.ac.jp

Hiroyuki Matsumoto Department of Biochemistry and Molecular Biology,
University of Oklahoma Health Sciences Center, Oklahoma City, OK 73104, USA
hiroyuki-matsumoto@ouhsc.edu

Michael T. Matthes Beckman Vision Center, University of California,
San Francisco, CA 94143, USA
Michael.matthes@ucsf.edu

Alexander Matveev Department of Cell Biology, University of Oklahoma
Health Sciences Center, Oklahoma City, OK 73104, USA
alexander-matveev@ouhsc.edu

Kazuhiro Mawatari Division of Health Sciences, Kanazawa University,
13-1 Takara-machi Kanazawa, Ishikawa 920-8640, Japan

Donald McDonnell Department of Pharmacology and Cancer Biology,
Duke University, Durham, NC 27701, USA
Donald.mcdonnell@duke.edu

James F. McGinnis Departments of Cell Biology and Ophthalmology,
Dean A. McGee Eye Institute, Oklahoma Center for Neuroscience, University
of Oklahoma Health Sciences Center, Oklahoma City, OK 73104, USA
james-mcginnis@ouhsc.edu

Dharia A. McGrew Department of Biology, Brandeis University,
Waltham, MA 02453, USA
dharia@brandeis.edu

Michel Michaelides UCL Institute of Ophthalmology, 11-43 Bath Street,
London EC1V 9EL, UK
Moorfields Eye Hospital, City Road, London EC1V 2PD, UK
michel.michaelides@ucl.ac.uk

Stylianos Michalakis Department of Pharmacy, Center for Integrated Protein
Science Munich (CIPSM), Center for Drug Research,
Ludwig-Maximilians-Universität München, 81377 Munich, Germany
michalakis@lmu.de

Vladimir M. Milenkovic Experimental Ophthalmology, Eye Hospital, University Health Center Regensburg, Regensburg, Germany
vlada@arcor.de

Sayak K. Mitter Department of Anatomy and Cell Biology, University of Florida, 1600 SW Archer Road, PO Box 100235, Gainesville, FL 32610, USA
mitter29@ufl.edu

Calvin A. Mok The Program in Genetics and Genome Biology, The Hospital for Sick Children, 555 University Avenue, Toronto, ON, Canada, M5G 1X8
Samuel Lunenfeld Research Institute, Mount Sinai Hospital, Toronto, ON, Canada, M5G 1X5
calvin.mok@utoroto.ca

Anthony T. Moore UCL Institute of Ophthalmology, 11-43 Bath Street, London EC1V 9EL, UK
Moorfields Eye Hospital, City Road, London EC1V 2PD, UK
tony.moore@ucl.ac.uk

Kevin L. Moore Cardiovascular Biology Research Program, Oklahoma Medical Research Foundation, Oklahoma City, OK 73104, USA
Kevin-Moore@omrf.org

Freya M. Mowat Department of Small Animal Clinical Sciences, Michigan State University, East Lansing, MI 48824, USA

Regine Mühlfriedel Division of Ocular Neurodegeneration, Centre for Ophthalmology, Institute for Ophthalmic Research, Eberhard Karls-Universität Tübingen, 72076 Tübingen, Germany
regine.muehlfriedel@med.uni-tuebingen.de

Claudia Müller Experimental Ophthalmology, Eye Hospital, University Health Center Regensburg, Regensburg, Germany
mueller@eye-regensburg.de

Frank Müller Institut für Strukturbiologie und Biophysik (ISB-1), Forschungszentrum Jülich, 52425 Jülich, Germany
f.mueller@fz-juelich.de

Muna I. Naash Department of Cell Biology, University of Oklahoma Health Sciences Center, 940 Stanton L. Young Blvd. BMS 781, Oklahoma City, OK 73104, USA
muna-naash@ouhsc.edu

Zack Naash Department of Cell Biology, University of Oklahoma Health Sciences Center, 940 Stanton L. Young Blvd. BMS 781, Oklahoma City, OK 73104, USA
zack.nash@att.net

Nobuhiro Nagai Division of Clinical Cell Therapy, United Center for Advanced Research and Translational Medicine (ART),

Tohoku University Graduate School of Medicine, Miyagi, Japan
nagai@med.tohoku.ac.jp

Mikiko Nagashima Department of Molecular Neurobiology and Division of Health Sciences, Kanazawa University, 13-1 Takara-machi, Kanazawa, Ishikawa 920-8640, Japan
nagai@med.tohoku.ac.jp

Juergen K. Naggert The Jackson Laboratory, Bar Harbor, ME 04609, USA
juergen.naggert@jax.org

Hiroshi Nakashima Division of Health Sciences, Graduate School of Medicine, Kanazawa University, 5-11-80 Kodatsuno, Kanazawa 920-0942, Japan
naka@kenroku.kanazawa-u.ac.jp

Emeline F. Nandrot Genetics Department, Institut de la Vision, INSERM UMR_S968, UPMC Univ Paris 06, CNRS UMR_7210, 17 rue Moreau, 75012 Paris, France
emeline.nandrot@inserm.fr

Riccardo Natoli ANU Medical School, The Australian National University, Canberra, ACT 0200, Australia
riccardo.natoli@anu.edu.au

Indira Neeli Department of Ophthalmology and Molecular Sciences, Hamilton Eye Institute, University of Tennessee Health Science Center, Memphis, TN 38163, USA
ineeli@uthsc.edu

Craig M. Nelson Department of Biological Sciences and the Center for Zebrafish Research, University of Notre Dame, Notre Dame, IN 46556, USA
Craig.M.Nelson.124@nd.edu

Rudgar Neussert Experimental Ophthalmology, Eye Hospital, University Hospital Hamburg-Eppendorf, Hamburg, Germany
Rudgar@gmx.de

Anh T.H. Nguyen Ocular Genetics Unit, Smurfit Institute of Genetics, Trinity College Dublin, Dublin 2, Ireland
nguyenat@tcd.ie

John M. Nickerson Department of Ophthalmology, Emory University, 1365B Clifton Road NE, TEC-B5602, Atlanta, GA 30322, USA
litjn@emory.edu

Patsy M. Nishina The Jackson Laboratory, Bar Harbor, ME 04609, USA
patsy.nishina@jax.org

Olufunmilola Ogun UCL Institute of Ophthalmology, 11-43 Bath Street, London EC1V 9EL, UK
skgtoao@ucl.ac.uk

Omolara O. Ogunshola Zurich Center for Integrative Human Physiology,
Zurich, Switzerland

Institute of Veterinary Physiology, University of Zurich, Winterthurerstrasse 260,
8057, Zurich, Switzerland
laraao@access.uzh.ch

Xiaoping Qi Department of Anatomy and Cell Biology, University of Florida,
1600 SW Archer Road, PO Box 100235, Gainesville, FL 32610, USA
xqi@ufl.edu

Hideyuki Onami Division of Clinical Cell Therapy, United Center
for Advanced Research and Translational Medicine (ART),
Tohoku University Graduate School of Medicine, Miyagi, Japan
honami@oph.med.tohoku.ac.jp

Kazuhiro Oogai Division of Health Sciences, Kanazawa University, Kanazawa
920-0942, Japan
kazu0208@stu.kanazawa-u.ac.jp

Catherine O’Riordan Genzyme Corporation, 49 New York Avenue,
Framingham, MA 01701, USA
Catherine.Oriordan@genzyme.com

Shoji Osawa Department of Cell and Developmental Biology,
The University of North Carolina at Chapel Hill, 108 Taylor Hall,
Chapel Hill, NC 27599-7090, USA
shoosawa@med.unc.edu

Monika Papke Department for Ophthalmology, Molecular Genetics Laboratory,
Institute for Ophthalmic Research, University Tuebingen, Roentgenweg 11,
S Tuebingen 72076, Germany
monika.papke@yahoo.de

François Paquet-Durand Division of Experimental Ophthalmology,
Institute for Ophthalmic Research, University of Tübingen,
Tübingen 72076, Germany
francois.paquet-durand@klinikum.uni-tuebingen.de

Jillian S. Parboosingh Department of Medical Genetics, University of Calgary,
Calgary, AB, Canada

Alberta Children’s Hospital Research Institute, University of Calgary,
Calgary, AB, Canada
jillian.parboosingh@calgaryhealthregion.ca

Machelle T. Pardue Rehabilitation Research and Development
Center of Excellence, Atlanta VA Medical Center,
Decatur, GA 30033, USA

Department of Ophthalmology, Emory University, Atlanta, GA 30322, USA
mpardue@emory.edu

Gayle J.T. Pauer Department of Ophthalmic Research (i31), Cole Eye Institute, Cleveland Clinic, 9500 Euclid Avenue, Cleveland, OH 44195, USA
pauerg@ccf.org

Simon M. Petersen-Jones Department of Small Animal Clinical Sciences, Michigan State University, East Lansing, MI 48824, USA
peter315@cvm.msu.edu

Hilda Petrs-Silva Departments of Ophthalmology, Institute of Biophysics, CCS, UFRJ, Rio de Janeiro 21941-902, Brazil

Eric A. Pierce Ocular Genomics Institute, Berman Gund Laboratory, Department of Ophthalmology, Massachusetts Eye and Ear Infirmary, 243 Charles St., Boston, MA 02114, USA
eric_pierce@meei.harvard.edu

Rita Pinter MRC Centre for Developmental Neurobiology, Kings College, London, SE1 1UL, UK

Akron Molecules GmbH, Campus Vienna Biocenter 5, Vienna, 1030, Austria
rita.pinter@akron-molecules.com

Eugenia Poliakov LRCMB, National Eye Institute, NIH, Bethesda, MD 20892, USA
poliakove@nei.nih.gov

Esther Pomares Departament de Genètica, Universitat de Barcelona, Barcelona 08028, Spain
Institut de Biomedicina, Universitat de Barcelona, Barcelona 08028, Spain
CIBERER, Instituto de Salud Carlos III, Barcelona, Spain
estherpomares@ub.edu

Howard Prentice Department of Biomedical Science, Florida Atlantic University, Boca Raton, FL 33431, USA
hprentic@fau.edu

Jan Provis Departments of Research School of Biology, ARC Centre of Excellence in Vision Science, and ANU Medical School, The Australian National University, Canberra, ACT 0200, Australia
jan.provis@anu.edu.au

Suofu Qin Department of Biological Sciences, Retinal Disease Research, Allergan, Inc, 2525 Dupont Drive, Irvine, CA 92612-1599, USA
qin_suofu@allergan.com

Tingyu Qin Jean Mayer USDA Human Nutrition Research Center on Aging, Tufts University, 711 Washington Street, Boston, MA 02111, USA
tingyuqin@126.com

Marko Z. Radic Department of Molecular Sciences, University of Tennessee Health Science Center, Memphis, TN 38163, USA
mradic@uthsc.edu

Abul K. Rahman Department of Ophthalmology and Dean A. McGee Eye Institute, University of Oklahoma Health Sciences Center, Oklahoma City, OK 73104, USA
drshefa@hotmail.com

Ammaji Rajala Department of Ophthalmology, Dean A. McGee Eye Institute, University of Oklahoma Health Sciences Center, 608 Stanton L. Young Blvd, Oklahoma City, OK 73104, USA
ammaji-rajala@ouhsc.edu

Raju V.S. Rajala Departments of Ophthalmology and Cell Biology, Dean A. McGee Eye Institute, University of Oklahoma Health Sciences Center, 608 Stanton L. Young Blvd, Oklahoma City, OK 73104, USA
raju-rajala@ouhsc.edu

Haripriya Vittal Rao Department of Anatomy and Cell Biology, University of Florida, 1600 SW Archer Road, PO Box 100235, Gainesville, FL 32610, USA
hvittalrao@ufl.edu

Matthew Rapp University of Maryland Baltimore County, Baltimore, MD 21250, USA
rappm1@umbc.edu

Mary R. Rayborn Department of Ophthalmology, Cole Eye Institute (i31), Cleveland Clinic Lerner College of Medicine, Cleveland, OH 44195, USA
RAYBORM@ccf.org

T. Michael Redmond LRCMB, National Eye Institute, NIH, Bethesda, MD 20892, USA
Redmond@helix.nih.gov

Charlotte Remé University of Zurich, Restelbergstrasse 53, 8044 Zürich, Switzerland
chreme@opht.uzh.ch

Zhihong Ren Jean Mayer USDA Human Nutrition Research Center on Aging, Tufts University, 711 Washington Street, Boston, MA 02111, USA
zhihong.ren@tufts.edu

Alison L. Reynolds UCD Conway Institute and UCD School of Biomolecular and Biomedical Sciences, University College Dublin, Belfield, Dublin 4, Ireland
alison.reynolds@ucd.ie

Jungate Rha Department of Ophthalmology, Medical College of Wisconsin, Milwaukee, WI 53226, USA
jrha@mcw.edu

Caterina Ripamonti UCL Institute of Ophthalmology, 11-43 Bath Street,
London EC1V 9EL, UK
c.ripamonti@ucl.ac.uk

Anthony G. Robson UCL Institute of Ophthalmology, 11-43 Bath Street,
London EC1V 9EL, UK
Moorfields Eye Hospital, City Road, London EC1V 2PD, UK
Anthony.Robson@moorfields.nhs.uk

Bärbel Rohrer Departments of Ophthalmology and Neurosciences,
Division of Research, Medical University
of South Carolina, Charleston, SC 29425, USA
rohrer@musc.edu

Linda Ruggiero Department of Biological Sciences,
Fordham University, Bronx, NY 10458, USA
lruggiero6@fordham.edu

Matt Rutar Departments of Research School of Biology, ARC Centre
of Excellence in Vision Science, The Australian National University,
RN Robertson Bldg, Sullivan's Creek Rd, Canberra, ACT 0200, Australia
ARC Centre of Excellence in Vision Science, The Australian National University,
Canberra, ACT 0200, Australia
matt.rutar@rsbs.anu.edu.au

Anisse Saadi Department of Ophthalmology and Dean A. McGee Eye Institute,
University of Oklahoma Health Sciences Center, Oklahoma City, OK 73104, USA
anisse7@hotmail.com

Robert G. Salomon Department of Chemistry, Case Western Reserve University,
Cleveland, OH, USA
rgs@case.edu

Javier Sancho-Pelluz Department of Ophthalmology, Columbia University,
New York, NY 10032, USA
fjs2115@columbia.edu

Rosaysela Santos Department of Anatomy & Neurobiology, Center for Complex
Biological Systems, University of California, Irvine, CA 92697-1275, USA
santosr@uci.edu

Zsolt Sarang Department of Biochemistry and Molecular Biology,
Apoptosis and Genomics Research Group, Hungarian Academy of Sciences,
University of Debrecen, Debrecen, Hungary
sarang@dote.hu

Yasufumi Sato Department of Vascular Biology, Institute of Development,
Aging, and Cancer, Tohoku University, Miyagi, Japan
y-sato@idac.tohoku.ac.jp

Alexandra Sauer Department for Ophthalmology, Molecular Genetics Laboratory, Institute for Ophthalmic Research, University Tuebingen, Röntgenweg 11, S Tubingen 72076, Germany
alexandra.sauer@med.uni-tuebingen.de

Abraham Scaria Genzyme Corporation, 49 New York Avenue, Framingham, MA 01701, USA
Abraham.Scaria@genzyme.com

Simone Schaich Department for Ophthalmology, Molecular Genetics Laboratory, Institute for Ophthalmic Research, University Tuebingen, Röntgenweg 11, S Tubingen 72076, Germany
simone.schaichl@med.uni-tuebingen.de

Kevin L. Schey Department of Biochemistry, Vanderbilt University, Nashville, TN 37240, USA
k.schey@Vanderbilt.edu

Jennifer Schmidt Department of Pharmacy, Center for Integrated Protein Science Munich (CIPSM), Center for Drug Research, Ludwig-Maximilians-Universität München, 81377 Munich, Germany
jennifer.schmidt@cup.uni-muenchen.de

Nele Schwarz UCL Institute of Ophthalmology, 11-43 Bath Street, London EC1V 9EL, UK
n.schwarz@ucl.ac.uk

Mathias W. Seeliger Division of Ocular Neurodegeneration, Institute for Ophthalmic Research, Centre for Ophthalmology, Schleichstrasse 12-16, Tuebingen 72076, Germany
see@uni-tuebingen.de

Steve A. Sezate Department of Ophthalmology and Dean A. McGee Eye Institute, University of Oklahoma Health Sciences Center, Oklahoma City, OK 73104, USA
steven-sezate@ouhsc.edu

Fu Shang Jean Mayer USDA Human Nutrition Research Center on Aging, Tufts University, 711 Washington Street, Boston, MA 02111, USA
fu.shang@tufts.edu

Lan Ying Shi The Jackson Laboratory, Bar Harbor, ME 04609, USA
lanying.shi@jax.org

Paul A. Sieving National Eye Institute at National Institutes of Health, Bethesda, MD 20892, USA
paulsieving@nei.nih.gov

Chris Silvin Genetics and Molecular Biology Branch, National Human Genome Research Institute NIH, Bethesda, MD 20892, USA
csilvin@mail.nih.gov

Anil Singh Department of Biochemistry and Molecular Biology,
University of Oklahoma Health Sciences Center, Oklahoma City, OK 73104, USA
anil-singh@ouhsc.edu

Ieva Sliesoraityte Centre for Ophthalmology, Institute for Ophthalmic Research,
University of Tuebingen, Schleichstr. 12-16, 72076 Tuebingen, Germany
sliesoraityte@yahoo.com

Alexander J. Smith Department of Genetics, UCL Institute of Ophthalmology,
London, EC1V 9EL, UK
alexander.smith@ucl.ac.uk

George W. Smith Department of Ophthalmology, John A. Moran
Eye Center, University of Utah, Salt Lake City, UT, 84132, USA
tyler.smith@hsc.utah.edu

Antonius Song Genzyme Corporation, 49 New York Avenue,
Framingham, MA 01701, USA
Antonius.Song@genzyme.com

Hikaru Sonoda Discovery Research Laboratories, Shionogi and Co. Ltd,
Osaka, Japan
hikaru.sonoda@shionogi.co.jp

Janet R. Sparrow Departments of Ophthalmology and Pathology
and Cell Biology, Columbia University, 630 West 168th Street,
New York, NY 10032, USA
jrs88@columbia.edu

Paul Stabila Neurotech USA, Lincoln, RI 02865, USA
p.stabila@neurotechusa.com

Chloe M. Stanton MRC Human Genetics Unit, Institute of Genetics
and Molecular Medicine, Western General Hospital, Edinburgh EH4 2XU, UK
chloe.stanton@hgu.mrc.ac.uk

Kimberly E. Stepien Department of Ophthalmology, Medical College
of Wisconsin, Milwaukee, WI 53226, USA
kstepien@mcw.edu

Achim Stocker Department of Chemistry and Biochemistry,
University of Bern, Freiestrasse 3, CH-3012 Bern, Switzerland
achim.stocker@ibc.unibe.ch

Andrew Stockman UCL Institute of Ophthalmology, 11-43 Bath Street,
London EC1V 9EL, UK
a.stockman@ucl.ac.uk

Heidi Stöhr Institute of Human Genetics, University Regensburg,
Franz-Josef-Strauss-Allee 11, 93053 Regensburg, Germany
heidi.stoehr@klinik.uni-regensburg.de

Olaf Strauß Experimental Ophthalmology, Eye Hospital, University Health Center Regensburg, Regensburg, Germany
strauss@eye-regensburg.de

Natalia Strunnikova Ophthalmic Genetics and Visual Function Branch, National Eye Inst/NIH, Bethesda, MD 20892, USA
strunnikovan@nei.nih.gov

Preeti Subramanian National Eye Institute, National Institutes of Health, Building 6, Room 134, 6 Center Drive, MSC 0608, Bethesda, MD 20892-0608, USA
subramanianp@nei.nih.gov

Angela M. Suburo Cell and Molecular Medicine, School of Biomedical Sciences, Universidad Austral, Pilar B1629AHJ, Buenos Aires, Argentina
amsuburo@cas.austral.edu.ar

Masahiko Sugimoto Department of Ophthalmology, Cole Eye Institute, Cleveland Clinic Lerner College of Medicine at Case Western Reserve University, Cleveland, OH, USA
sugimom@ccf.org

Kayo Sugitani Division of Health Sciences, Kanazawa University, Kanazawa 920-8640, Japan
sugitani@kenroku.kanazawa-u.ac.jp

Andrew Sugrue Departments of Anatomy and Cell Biology, University of Florida, Gainesville, FL 32610, USA
andysug@gmail.com

Jack M. Sullivan Department of Ophthalmology (Ross Eye Institute), Departments of Pharmacology/Toxicology, Physiology/Biophysics and Neuroscience Program, University at Buffalo, State University of New York (SUNY), School of Medicine and Biomedical Sciences, SUNY Eye Institute, Buffalo, NY 14209, USA

VA Western New York Healthcare System, Buffalo, NY 14215, USA
jackmsullivanmdphd@yahoo.com

Lori S. Sullivan Human Genetics Center, School of Public Health, University of Texas Health Science Center at Houston, Houston, TX 77030, USA
lori.s.sullivan@uth.tmc.edu

Mayu Suzuki Ocular Genetics Unit, Smurfit Institute of Genetics, Trinity College Dublin, Dublin 2, Ireland
suzukim@tcd.ie

Zsuzsa Szondy Department of Biochemistry and Molecular Biology, Apoptosis and Genomics Research Group, Hungarian Academy of Sciences, University of Debrecen, Debrecen, Hungary
szondy@indi.biochem.dote.hu

R. Thomas Taggart Department of Ophthalmology (Ross Eye Institute), University at Buffalo, State University of New York (SUNY), SUNY Eye Institute School of Medicine and Biomedical Sciences, Buffalo, NY 14209, USA
rthomastag@aol.com

Lawrence Tam Department of Genetics, The Ocular Genetics Unit, Trinity College Dublin, Dublin 2, Ireland
lawrenct@tcd.ie

Ernst R. Tamm Institute of Human Anatomy and Embryology, University of Regensburg, Universitätsstr. 31, Regensburg D-93053, Germany
ernst.tamm@vkl.uni-regensburg.de

Naoyuki Tanimoto Division of Ocular Neurodegeneration, Centre for Ophthalmology, Institute for Ophthalmic Research, Eberhard Karls-University of Tübingen, 72076 Tübingen, Germany
naoyuki.tanimoto@med.uni-tuebingen.de

Masaki Tanito Department of Ophthalmology, University of Oklahoma Health Sciences Center, Oklahoma City, OK, USA

Dean A. McGee Eye Institute, Oklahoma City, OK, USA

Department of Ophthalmology, Shimane University Faculty of Medicine, Izumo, Shimane, Japan
tanito-oph@umin.ac.jp

Weng Tao Neurotech USA, Lincoln, RI 02865, USA
w.tao@neurotechusa.com

Joshua M. Thurman Department of Medicine, Denver School of Medicine, University of Colorado, Denver, CO 80045, USA
joshua.thurman@uchsc.edu

Julie-Thu A. Tran Department of Ophthalmology and Dean A. McGee Eye Institute, University of Oklahoma Health Sciences Center, Oklahoma City, OK 73104, USA
Julie-Tran@ouhsc.edu

Eric Troeger Centre for Ophthalmology, Institute for Ophthalmic Research, University of Tuebingen, Schleichstr. 12-16, 72076 Tuebingen, Germany
eric.troeger@med.uni-tuebingen.de

Catherine Tsilfidis Ottawa Hospital Research Institute, Ottawa General Hospital 501 Smyth Road, Ottawa, ON, Canada K1H 8L6
ctsilfidis@ohri.ca

Marius Ueffing Division of Experimental Ophthalmology, University of Tuebingen, Roentgenweg 11, Tuebingen, 72076, Germany
marius.ueffing@uni-tuebingen.de

Krisztina Valter Departments of Research School of Biology, and ARC Centre of Excellence in Vision Science, The Australian National University, Canberra, ACT 0200, Australia

krisztina.valter-kocsi@anu.edu.au

Vidyullatha Vasireddy Department of Ophthalmology, Shiley Eye Center, University of California San Diego, La Jolla, CA 92037, USA

vvasireddy@ucsd.edu

Félix R. Vázquez-Chona Department of Ophthalmology, University of Utah, 65 Mario Capecchi Dr, Salt Lake City, UT 84132, USA

felix.vazquez@utah.edu

Kirstan A. Vessey Department of Anatomy and Cell Biology, The University of Melbourne, Level 7, Medical Building, Grattan Street, Melbourne, VIC 3010, Australia

k.vessey@unimelb.edu.au

Camasamudram Vijayarathy Section for Translation Research in Retinal and Macular Degeneration, NIDCD at National Institutes of Health, Bethesda, MD 20892, USA

camasamv@nidcd.nih.gov

Samuel Wadsworth Genzyme Corporation, 49 New York Avenue, Framingham, MA 01701, USA

Samuel.Wadsworth@genzyme.com

Melissa Wagner-Schuman Departments of Ophthalmology and Biophysics, Medical College of Wisconsin, Milwaukee, WI 53226, USA

mwagner@mcw.edu

Ryosuke Wakusawa Division of Clinical Cell Therapy, United Center for Advanced Research and Translational Medicine (ART), Tohoku University Graduate School of Medicine, Miyagi, Japan

ckd19390@rio.odn.ne.jp

Yana Walczak Institute of Human Genetics, University of Regensburg, Franz Josef Strauss Allee 11, 93053 Regensburg, Germany

stefanie.ebert@klinik.uni-regensburg.de

Tiffany A. Walker Rehabilitation Research and Development Center of Excellence, Atlanta VA Medical Center,

1670 Clairmont Rd, Decatur, GA 30033, USA

TWALK25@emory.edu

Haibao Wan Department of Neurology, Stout Mass Spectrometry Laboratory, University of Tennessee Health Science Center, Memphis, TN 38163, USA

wanhb@yahoo.com

Jieping Wang The Jackson Laboratory, Bar Harbor, ME 04609, USA

jjeping.wang@jax.org

Joshua J. Wang Department of Medicine, Endocrinology and Diabetes, Harold Hamm Oklahoma Diabetes Center, University of Oklahoma Health Sciences Center, Oklahoma City, OK 73104, USA
jianxin-wang@ouhsc.edu

Zhengying Wang Bascom Palmer Eye Institute, University of Miami, Miller School of Medicine, Miami, FL 33136, USA
zwang@med.miami.edu

Rao F. Watson Department of Ophthalmic Research (i31), Cole Eye Institute, Cleveland Clinic, 9500 Euclid Avenue, Cleveland, OH 44195, USA
fur@ccf.org

Kaylie D. Webb Retina Foundation of the Southwest, Dallas, TX 75231, USA
kclark@retinafoundation.org

Tom R. Webb UCL Institute of Ophthalmology, 11-43 Bath Street, London EC1V 9EL, UK
t.r.webb@ucl.ac.uk

Ellen R. Weiss Department of Cell and Developmental Biology, Lineberger Comprehensive Cancer Center, The University of North Carolina at Chapel Hill, Chapel Hill, NC 27599-7090, USA
erweiss@med.unc.edu

Rong Wen Bascom Palmer Eye Institute, Miller School of Medicine, University of Miami, Miami, FL 33136, USA
rwen@med.miami.edu

Yuquan Wen Rose-Silverthorne Retinal Degenerations Laboratory, Retina Foundation of the Southwest, 9900 N Central Expressway, Suite 400, Dallas, TX 75231, USA
ywen@retinafoundation.org

Dianna K. Wheaton Retina Foundation of the Southwest, Dallas, TX 75231, USA
Department of Ophthalmology, University of Texas Southwestern Medical Center, Dallas, TX 75390, USA
dwheaton@retinafoundation.org

David S. Williams Departments of Ophthalmology and Neurobiology, UCLA, School of Medicine, Los Angeles, CA 90095, USA
dswilliams@ucla.edu

Jessica T. Williams Human Genetics Center, School of Public Health, University of Texas Health Science Center at Houston, Houston, TX 77030, USA
jessica.t.williams@uth.tmc.edu

Bernd Wissinger Department for Ophthalmology, Molecular Genetics Laboratory, Institute for Ophthalmic Research, University Tuebingen, Roentgenweg 11, 72076 Tuebingen, Germany
wissinger@uni-tuebingen.de

Jungyeon Won The Jackson Laboratory, Bar Harbor, ME 04609, USA
jungyeon.won@jax.org

Wai T. Wong Unit on Neuron–Glia Interactions in Retinal Disease, National Eye Institute, 6 Center Drive, Building 6, Room 215, Bethesda, MD 20892, USA
wongw@nei.nih.gov

Alan F. Wright MRC Human Genetics Unit, Institute of Genetics and Molecular Medicine, Western General Hospital, Edinburgh EH4 2XU, UK
alan.wright@hgu.mrc.ac.uk

Genevieve A. Wright Moorfields Eye Hospital, City Road, London EC1V 2PD, UK
genevieve.wright@ucl.ac.uk

Dayong Wu Jean Mayer USDA Human Nutrition Research Center on Aging, Tufts University, Boston, MA 02111, USA
dayong.wu@tufts.edu

Jeffry Wu Department of Anatomy & Neurobiology, Center for Complex Biological Systems, University of California, Irvine, CA 92697-1275, USA
BOOPT-School of Optometry, University of California, Berkeley, CA 94720-2284, USA
jeffryw@berkeley.edu

Xin Xia Bascom Palmer Eye Institute, University of Miami, Miller School of Medicine, Miami, FL 33136, USA
xxia2@med.miami.edu

Wei Xing Department of Ophthalmology and Visual Sciences, Moran Eye Center, University of Utah School of Medicine, Salt Lake City, UT 84132, USA
wei.xing@hsc.utah.edu

Kazunori Yamamoto Department of Ophthalmology, Columbia University, New York, NY 10032, USA
yk2428@columbia.edu

Haidong Yang Beckman Vision Center, University of California, San Francisco, CA 94143, USA
Haidong.yang@ucsf.edu

Douglas Yasumura Beckman Vision Center, University of California, San Francisco, CA 94143, USA
douglas.yasumura@ucsf.edu

Edwin H. Yau Department of Ophthalmology (Ross Eye Institute), Department of Pharmacology/Toxicology, University at Buffalo, State University of New York (SUNY), School of Medicine and Biomedical Sciences, Buffalo, NY 14209, USA
edwinyau@buffalo.edu

Rosanne M. Yetemian Mary D. Allen Laboratory for Vision Research, Doheny Eye Institute, Keck School of Medicine, University of Southern California, Los Angeles, CA 90033-9224, USA
yetemian@gmail.com

Department of Ophthalmology, Keck School of Medicine of the University of Southern California, Los Angeles, CA 90033-9224, USA
Regulatory Affairs, Abbott Medical Optics, Inc., Santa Ana, CA 92705, USA

Man Yu Department of Ophthalmology and Dean A. McGee Eye Institute, University of Oklahoma Health Sciences Center, Oklahoma City, OK 73104, USA
Mann-Yu@ouhsc.edu

Barbara Zangerl Section of Ophthalmology, Department of Clinical Studies, School of Veterinary Medicine, University of Pennsylvania, Ryan Veterinary Hospital, Philadelphia, PA 19104, USA
bzangerl@vet.upenn.edu

Wadiah M. Zein Ophthalmic Genetics and Visual Function Branch, National Eye Inst/NIH, Bethesda, MD 20892, USA
zeinw@nei.nih.gov

Qi Zhang Department of Human Anatomy and Cell Science, Manitoba Institute of Cell Biology, University of Manitoba, 5015-675 McDermot Avenue, Winnipeg, MB, Canada R3E 0V9
umzha287@cc.umanitoba.ca

Sarah X. Zhang Department of Medicine, Endocrinology and Diabetes, Harold Hamm Oklahoma Diabetes Center, University of Oklahoma Health Sciences Center, Oklahoma City, OK 73104, USA
xin-zhang@ouhsc.edu

Lian Zhao Unit on Neuron–Glia Interactions in Retinal Disease, National Eye Institute, 6 Center Drive, Building 6, Room 215, Bethesda, MD 20892, USA
zhaolia@nei.nih.gov

Lixin Zheng Department of Ophthalmology and Dean A. McGee Eye Institute, University of Oklahoma Health Sciences Center, Oklahoma City, OK 73104, USA
zhenglixin70@gmail.com

Yimin Zhong Department of Medicine, Endocrinology and Diabetes,
Harold Hamm Oklahoma Diabetes Center, University of Oklahoma Health
Sciences Center, Oklahoma City, OK 73104, USA

State Key Laboratory of Ophthalmology, Zhongshan Ophthalmic Center,
Sun Yat-sen University, Guangzhou 510060, China
Yimin-zhong@ouhsc.edu

Meili Zhu Department of Medicine Endocrinology and Harold Hamm Oklahoma
Diabetes Center, University of Oklahoma Health Sciences Center,
Oklahoma City, OK 73104, USA
Meili-Zhu@ouhsc.edu

Lucia Ziccardi Neurophthalmology Unit, Fondazione “G.B. Bietti” IRCCS,
Via Livenza, 300198 Rome, Italy
lucia.ziccardi@nih.gov

Xiangang Zong Department of Pharmacy, Center for Integrated Protein
Science Munich (CIPSM), Center for Drug Research,
Ludwig-Maximilians-Universität München, 81377 Munich, Germany
xiangang.zong@cup.uni-muenchen.de

Eberhart Zrenner Centre for Ophthalmology, Institute for Ophthalmic Research,
University of Tuebingen, Schleichstr. 12-16, 72076, Tuebingen, Germany
erzenner@uni-tuebingen.de

Travel Awards

We gratefully acknowledge The Foundation Fighting Blindness, the National Eye Institute, The Foundation Fighting Blindness-Canada/Institute of Genetics, Novartis Pharma AG, Alcon, Genentech, Inspire Pharmaceuticals, Pfizer, Inc., Genzyme and Bioptigen, Inc. for their generous support of 42 Travel Awards to attend this meeting. The travel awardees are listed below. Each awardee submitted a chapter to this proceedings volume.

Barbara Maria Braunger
Julien Bruban
Nora Bianca Caberoy
Yingming (Amy) Chen
Therese Cronin
Stefanie Ebert
Abigail Fahim
Michael Farkas
Wai Gin Fong
Ana Griciuc
Vivek Kumar Gupta
Finnian Hanrahan
Hong Hao
Xiaoqin He
Severin Heynen
Shun-Ping Huang
Mark E. Kleinman
Elöd Kortvely
Tatyana Kuznetsova
Aparna Lakkaraju
Karin Littink
Vanda Sofia Lopes
Ulrich Luhmann

Dharia McGrew
Calvin Mok
Anh Thi Hong Nguyen
Francisco Javier Sancho-Pelluz
Rosaysela Santos
Simone Schimpf-Linzenbold
Hilda Petrs Silva
George Wesley Smith
Chloe Stanton
Masahiko Sugimoto
Naoyuki Tanimoto
Félix Vázquez-Chona
Kirstan Vessey
Ajoy Vincent
Yuquan Wen
Wai Wong
Rosanne Yetemian
Qi Zhang
Sarah Zhang

Part I
AMD: Basic Mechanisms, Inflammation
and Immunity

Chapter 1

A Window to Innate Neuroimmunity: Toll-Like Receptor-Mediated Cell Responses in the Retina

Mark E. Kleinman and Jayakrishna Ambati

Keywords Macular degeneration • Innate immunity • Toll-like receptor • Apoptosis • Double-stranded RNA • Short interfering RNA • Angiogenesis • Choroidal neovascularization • Caspase

1.1 Introduction

Since the controversial yet groundbreaking experiments by John Olney on glutamate-induced excitotoxicity, the retina has prevailed as a useful model to address significant questions in neurobiology. The retina which is derived from neural ectoderm, and its surrounding structures which are derived from the neural crest, are essential for vision. Given the vital nature of these specialized tissues, a multi-checkpoint blood-barrier has evolved to prohibit the entry of proinflammatory immune cells into the parenchyma. However, like the central nervous system, the retina remains under constant immune surveillance by its resident cells, including microglia, astrocytes, ganglion cells, pigmented epithelium, and endothelium capable of triggering innate immune response via Toll-like receptors (TLRs).

1.2 TLRs and Neuroimmunity

TLRs are type I transmembrane proteins that recognize pathogen-associated molecular patterns (PAMP) resulting in the initiation of the innate immune response pathways (Medzhitov and Janeway 2000). To date, 13 TLRs have been identified in humans

M.E. Kleinman • J. Ambati (✉)
Department of Ophthalmology and Visual Sciences,
University of Kentucky College of Medicine, Lexington, KY 40536, USA
e-mail: jamba2@email.uky.edu

and mice that bind with specific PAMP (Oda and Kitano 2006). TLRs are critical signal transducers for PAMP detection and are required to activate the intracellular interferon (IFN) mediated immune pathways. Viral double-stranded RNA (dsRNA) has long been known to induce type I IFN genes, although it is only recently that this mechanism was shown to be partly mediated by specific recognition of dsRNA through TLR3 (Alexopoulou et al. 2001). Signal translation is achieved via coupling with various cytosolic adaptor molecules that contain a Toll/IL-1 receptor (TIR) domain. One such adaptor, myeloid differentiation factor 88 (MyD88) was thought to be ubiquitous among TLRs, but data on TLR3 activation by dsRNA suggested the critical involvement of another adaptor called Toll/IL-1 domain-containing adapter inducing IFN- β (TRIF) (Yamamoto et al. 2003). TRIF relays TLR3 signaling through a kinase cascade resulting in nuclear translocation of NF- κ B and IFN regulatory factor-3 (IRF-3), induction of IFN-related genes, and subsequent expression of inflammatory cytokines and pro-apoptotic mediators (Hoebe et al. 2003; Meylan et al. 2004). In addition to TLR3, known dsRNA receptors include the RNA-binding protein kinase (PKR) and retinoic acid inducible gene I (RIG-I) (Sledz et al. 2003).

In many neurodegenerative pathologies including Parkinson's, Alzheimer's, and age-related macular degeneration (AMD), viruses have been speculated to play a key role in disease onset and progression (Margolis et al. 2004; Ringheim and Conant 2004). Several TLRs, including TLR 2–9, are expressed on microglia and astrocytes (Jack et al. 2005), and a multitude of neurocytotoxic effects have been observed with TLR3 activation including neurite growth cone collapse (Cameron et al. 2007), exacerbation of chronic neurodegeneration (Field et al. 2010), and negative regulation of neural progenitor cell proliferation (Lathia et al. 2008). In our studies, we observed TLR3 induced neurodegeneration in the retina which has generated considerable interest in targeting this pathway for the treatment of AMD.

1.3 TLRs and Age-Related Macular Degeneration

The natural history of the AMD is uniquely characterized by advancement to either geographic atrophy (GA) of the macula or choroidal neovascularization (CNV). While the pathogenesis of CNV has been well studied in a surrogate laser injury animal model leading to the development of clinically proven therapeutics, there is a paucity of data on the cellular events leading to GA due to the lack of a suitable animal model. In a world-wide collaboration, a genetic association between GA and a hypomorphic single nucleotide polymorphism in the TLR3 gene called L412F was recently identified (Yang et al. 2008). The study suggested that carriers of the mutation are protected from the development of GA suggesting that TLR3 activation may be deleterious to the macula. In order to evaluate the functionality pathway in vivo, intraocular injections of a potent TLR3 agonist, poly (I:C), were performed in wild-type and TLR3-deficient mice. Serial retinal imaging over a 2-week period demonstrated a progressive accumulation of discrete areas of hypopigmentation in

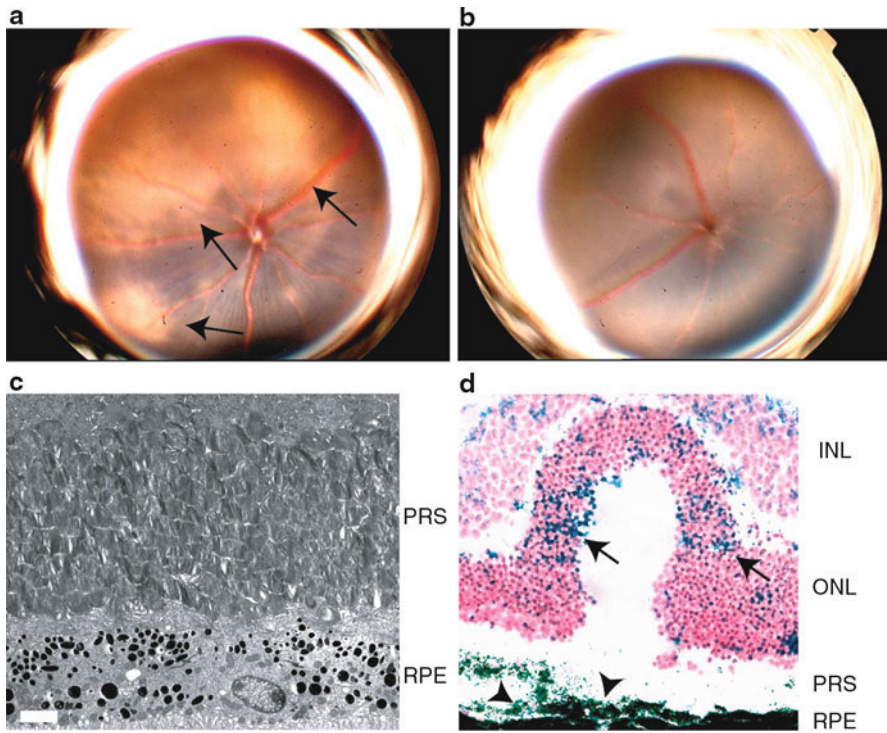


Fig. 1.1 Dilated fundoscopic examination of wild-type mice (a) 2 weeks after treatment with intraocular poly (I:C) (2 μ g) revealed confluent areas of hypo- and complete depigmentation (arrows) suggestive of RPE loss whereas TLR3-deficient mice did not (b). Ultrastructural analysis showed disorganized photoreceptor segments (PRS) and vacuolization of the RPE layer, a sign of autophagy that occurs during cell death (c) (scale bar=2 μ m). Forty-eight hours after treatment, severe disturbances in retinal morphology are evident along with significantly increased apoptotic nuclei (TUNEL+blue, nuclei in red) in the RPE (arrowheads) and nuclear layers (INL, ONL) (arrows) of wild-type treated retinas (d) (scale bar=10 μ m)

wild-type mice similar to the appearance of retinal pigment epithelium (RPE) loss associated with GA (Fig. 1.1). In agreement with a previous study (Kumar et al. 2004), we found abundant TLR3 expression in RPE cells in both human and mouse suggesting that this cell may be directly activated by dsRNA. Moreover, in our most recent unpublished studies, we observed increased concentrations of dsRNA in GA eyes compared to age-matched controls and are currently performing sequencing studies to determine its origin.

On histologic and ultrastructural analyses, photoreceptor arrays and the RPE monolayer were severely disrupted. RPE cell analyses over a 72-h period after poly (I:C) injection revealed a precipitous drop in viable cell numbers in wild-type mice compared to TLR3-deficient mice. Given that TLR3 activation may act through Fas-associated death domains (FADD) to induce caspase-dependent apoptosis (Balachandran et al. 2004), we evaluated the extent of TLR3-induced apoptosis in

our model. At 48 h after treatment in wild-type mice, almost 40% of cells in the RPE and neural retina were undergoing apoptosis as measured by TUNEL, and a fraction of those were also positive for cleaved caspase-3 signifying some level of dependence on this pathway. In vitro, primary human RPE isolates exhibited over a fivefold reduction in survival in the treated cells at 48 h, whereas RPE cells genotyped for the hypomorphic TLR3 variant, L412F, were protected from this cytotoxicity. However, we were surprised that subsequent genetic association studies were unable to corroborate the initial data demonstrating a protective effect of L412F on GA (Cho et al. 2009b; Klein et al. 2010). Nonetheless, we have pursued TLR3 as a potentially critical signaling pathway in dry AMD progression given that functional biology often contradicts hypotheses generated with genetic association data as has occurred with sequencing investigations into VEGF-A polymorphisms and CNV (Richardson et al. 2007). Our functional in vivo and correlate in situ data suggest that TLR3 activation is an important factor in retinal cell health and may provide a critical pathway for the development of targeted therapeutics for GA.

1.4 Short Interfering RNA-Based Drugs Activate TLR3 Pathways

While potent TLR3 activation occurs with long dsRNA of 30 nucleotides (nt) or more, short interfering RNAs (siRNA), commonly designed as 19-nt RNA duplexes with 2-nt overhangs, may also serve as ligands for this highly evolved dsRNA recognition system at concentrations currently used in molecular biology protocols (Kariko et al. 2004). While this initial finding was concerning, we were fascinated that 21-nt siRNAs were being used nearly ubiquitously in molecular biology investigations and that several siRNA-based drugs were undergoing rapid development for clinical deployment with no evidence of unanticipated side effects. In fact, the pioneering clinical trials utilizing siRNA-based therapeutics were designed to test compounds targeting *Vegfa* and *Vegfr1* for the treatment of neovascular AMD. While these initial trials were ongoing, we began studies evaluating siRNAs targeting critical angiogenic factors in the laser injury mouse model of CNV. We were surprised to find that nontargeted control siRNAs equally suppressed vascular growth when compared to siRNAs targeting *Vegfa* in this model. Furthermore, siRNA that was chemically modified to prevent incorporation into the RNAi silencing complex, RISC, also inhibited CNV strongly suggesting that this vascular effect was not due to RNAi but likely linked to an innate immune activation pathway.

In all of these studies, we employed unmodified “naked” siRNAs that cannot cross cell membranes due to their large molecular weight (~14 kDa) and polyanionic structure; therefore, we hypothesized that interaction with an extracellular receptor may be required for this angio-inhibitory effect. Our studies revealed that cell surface TLR3, which is expressed on human and mouse choroidal endothelial cells, is activated by 21-nt siRNA in a sequence- and target-independent fashion leading to downstream IFN-related gene expression and subsequent neovascular

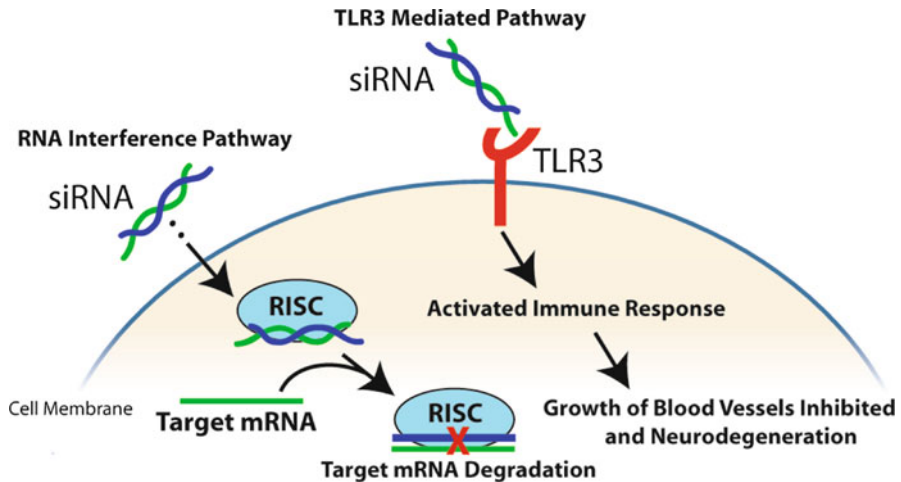


Fig. 1.2 RNA interference may occur through the traditional intracellular pathway mediated by RISC. However, siRNA (≥ 21 nt) bind to and activate TLR3 leading to an angio-inhibitory class effect that is mediated through the upregulation of IFN- γ , interleukin-12, and apoptosis

suppression (Kleinman et al. 2008) (Fig. 1.2). Similar angio-inhibition in the laser-injury CNV model was observed with the synthetic TLR3 agonist, poly I:C. Our initial data have been reproduced with control and targeted siRNAs synthesized by several different commercial sources and in two separate reports from independent laboratories (Ashikari et al. 2010; Gu et al. 2010). In further support of our findings, another laboratory recently observed parallel results of angiogenic suppression with control siRNAs in mouse hepatocellular carcinoma tumor models via IFN- γ upregulation and endothelial cell apoptosis (Berge et al. 2010).

Importantly, TLR3 was expressed on the surface of endothelial cells from all human peripheral tissues tested including lung, aorta, and lymphatics (Cho et al. 2009a) suggesting that this innate response is likely global. These findings are a cause for alarm given that many other diseases are currently being approached with pharmacologic intentions of systemically delivering siRNA-based drugs. Future directions for the development of siRNA therapies should include rational chemical engineering of siRNA molecules that evade TLR3 detection. A Korean group has already reported that an asymmetric 16-nt siRNA design is able to achieve efficient gene-targeted suppression without TLR3 activation (Chang et al. 2009). Collectively, these studies signal a paradigm shift in understanding the role of the innate immune system in the pathogenesis of neurodegenerative diseases, directly address unanticipated immune side effects of siRNA-based drugs, and open new avenues of research into TLR-mediated cellular effects in the retina and brain.

Acknowledgments J.A. was supported by NEI/NIH, the Doris Duke Distinguished Clinical Scientist Award, the Burroughs Wellcome Fund Clinical Scientist Award in Translational Research, the Dr. E. Vernon Smith and Eloise C. Smith Macular Degeneration Endowed Chair, the Senior

Scientist Investigator Award (RPB), the American Health Assistance Foundation, and a departmental unrestricted grant from the RPB. M.E.K. by the International Retinal Research Foundation and NIH T32 grant.

References

- Alexopoulou L, Holt AC, Medzhitov R et al (2001) Recognition of double-stranded RNA and activation of NF-kappaB by Toll-like receptor 3. *Nature* 413:732–738
- Ashikari M, Tokoro M, Itaya M et al (2010) Suppression of laser-induced choroidal neovascularization by nontargeted siRNA. *Invest Ophthalmol Vis Sci* 51:3820–3824
- Balachandran S, Thomas E, Barber GN (2004) A FADD-dependent innate immune mechanism in mammalian cells. *Nature* 432:401–405
- Berge M, Bonnin P, Sulpice E et al (2010) Small Interfering RNAs Induce Target-Independent Inhibition of Tumor Growth and Vasculature Remodeling in a Mouse Model of Hepatocellular Carcinoma. *Am J Pathol*
- Cameron JS, Alexopoulou L, Sloane JA et al (2007) Toll-like receptor 3 is a potent negative regulator of axonal growth in mammals. *J Neurosci* 27:13033–13041
- Chang CI, Yoo JW, Hong SW et al (2009) Asymmetric shorter-duplex siRNA structures trigger efficient gene silencing with reduced nonspecific effects. *Mol Ther* 17:725–732
- Cho WG, Albuquerque RJ, Kleinman ME et al (2009a) Small interfering RNA-induced TLR3 activation inhibits blood and lymphatic vessel growth. *Proc Natl Acad Sci U S A* 106:7137–7142
- Cho Y, Wang JJ, Chew EY et al (2009b) Toll-like receptor polymorphisms and age-related macular degeneration: replication in three case-control samples. *Invest Ophthalmol Vis Sci* 50:5614–5618
- Field R, Campion S, Warren C et al (2010) Systemic challenge with the TLR3 agonist poly I:C induces amplified IFNalpha/beta and IL-1beta responses in the diseased brain and exacerbates chronic neurodegeneration. *Brain Behav Immun* 24:996–1007
- Gu L, Chen H, Tuo J et al (2010) Inhibition of experimental choroidal neovascularization in mice by anti-VEGFA/VEGFR2 or non-specific siRNA. *Exp Eye Res* 91:433–439
- Hoebe K, Janssen EM, Kim SO et al (2003) Upregulation of costimulatory molecules induced by lipopolysaccharide and double-stranded RNA occurs by Trif-dependent and Trif-independent pathways. *Nat Immunol* 4:1223–1229
- Jack CS, Arbour N, Manusow J et al (2005) TLR signaling tailors innate immune responses in human microglia and astrocytes. *J Immunol* 175:4320–4330
- Kariko K, Bhuyan P, Capodici J et al (2004) Small interfering RNAs mediate sequence-independent gene suppression and induce immune activation by signaling through toll-like receptor 3. *J Immunol* 172:6545–6549
- Klein ML, Ferris FL, 3rd, Francis PJ et al (2010) Progression of geographic atrophy and genotype in age-related macular degeneration. *Ophthalmology* 117:1554–1559, 1559 e1551
- Kleinman ME, Yamada K, Takeda A et al (2008) Sequence- and target-independent angiogenesis suppression by siRNA via TLR3. *Nature* 452:591–597
- Kumar MV, Nagineni CN, Chin MS et al (2004) Innate immunity in the retina: Toll-like receptor (TLR) signaling in human retinal pigment epithelial cells. *J Neuroimmunol* 153:7–15
- Lathia JD, Okun E, Tang SC et al (2008) Toll-like receptor 3 is a negative regulator of embryonic neural progenitor cell proliferation. *J Neurosci* 28:13978–13984
- Margolis TP, Lietman T, Strauss E (2004) Infectious agents and ARMD: a connection? *Am J Ophthalmol* 138:468–470
- Medzhitov R, Janeway C, Jr. (2000) The Toll receptor family and microbial recognition. *Trends Microbiol* 8:452–456

- Meylan E, Burns K, Hofmann K et al (2004) RIP1 is an essential mediator of Toll-like receptor 3-induced NF-kappa B activation. *Nat Immunol* 5:503–507
- Oda K, Kitano H (2006) A comprehensive map of the toll-like receptor signaling network. *Mol Syst Biol* 2:2006 0015
- Richardson AJ, Islam FM, Guymer RH et al (2007) A tag-single nucleotide polymorphisms approach to the vascular endothelial growth factor-A gene in age-related macular degeneration. *Mol Vis* 13:2148–2152
- Ringheim GE, Conant K (2004) Neurodegenerative disease and the neuroimmune axis (Alzheimer's and Parkinson's disease, and viral infections). *Journal of Neuroimmunology* 147:43–49
- Sledz CA, Holko M, de Veer MJ et al (2003) Activation of the interferon system by short-interfering RNAs. *Nat Cell Biol* 5:834–839
- Yamamoto M, Sato S, Hemmi H et al (2003) Role of adaptor TRIF in the MyD88-independent toll-like receptor signaling pathway. *Science* 301:640–643
- Yang Z, Stratton C, Francis PJ et al (2008) Toll-like receptor 3 and geographic atrophy in age-related macular degeneration. *N Engl J Med* 359:1456–1463

Chapter 2

Autoimmune Biomarkers in Age-Related Macular Degeneration: A Possible Role Player in Disease Development and Progression

Alessandro Iannaccone, Indira Neeli, Pratheebha Krishnamurthy, Nataliya I. Lenchik, Haibao Wan, Ivan C. Gerling, Dominic M. Desiderio, and Marko Z. Radic

Keywords Age-related macular degeneration • Autoimmunity • Inflammation • Biomarkers • Pathogenesis

2.1 Introduction

Protein modifications have the potential to alter the function and immunogenicity of proteins. The immune system learns to ignore self-proteins through tolerance. However, covalent modifications of proteins alter recognition by the adaptive immune system causing a protein to break tolerance and induce active immunity.

A. Iannaccone (✉) • P. Krishnamurthy
Department of Ophthalmology, Hamilton Eye Institute,
University of Tennessee Health Science Center, Memphis, TN 38163, USA
e-mail: aiannacc@uthsc.edu

I. Neeli
Department of Ophthalmology, Hamilton Eye Institute,
University of Tennessee Health Science Center, Memphis, TN 38163, USA

Department of Molecular Sciences, University of Tennessee
Health Science Center, Memphis, TN 38163, USA

N.I. Lenchik • I.C. Gerling
Department of Internal Medicine, University of Tennessee
Health Science Center, Memphis, TN 38163, USA

H. Wan • D.M. Desiderio
Department of Neurology, Stout Mass Spectrometry Laboratory,
University of Tennessee Health Science Center, Memphis, TN 38163, USA

M.Z. Radic
Department of Molecular Sciences, University of Tennessee
Health Science Center, Memphis, TN 38163, USA

Repair of damaged proteins may become less efficient in aging, causing accumulation of altered proteins in tissues, thus leading to autoimmunity. Evidence suggests that one example of such a process may be age-related macular degeneration (AMD).

AMD is a multifactorial, polygenic complex disease, in which drusen accumulate between the Bruch's membrane (BM) and the RPE (Hageman et al. 2001), and retinal pigment epithelium (RPE) changes occur. Early AMD affects 14% of people 75–79-year old and 23.6% of people ≥ 80 -year old, with minimal vision loss. Advanced AMD affects 3.2% of 75–79-year-old people and 11.8% of people ≥ 80 -year old (Hawkins et al. 1999; Friedman et al. 2004), leading to vision loss. Identification of factors and mechanisms that favor the progression from early to advanced AMD would prove invaluable in mitigating the impact of AMD on the elderly.

It is now accepted that inflammation and the immune system play a direct role in AMD. Here, we briefly review over 30 years of literature highlighting the importance of inflammatory and autoimmune phenomena in the pathogenesis of AMD and one of its hallmarks, drusen deposition, we summarize some of our previous and ongoing research in the field, and we illustrate our overall working hypothesis.

2.2 Evidence in Favor of a Role for Autoimmunity in AMD Pathogenesis

Histopathologic evidence of the involvement of leukocytes, macrophages, and giant cells in association with AMD was found since the late 1970s (Grindle and Marshall 1978) and confirmed subsequently (Killingsworth and Sarks 1982; Penfold et al. 1985, 1986; Killingsworth et al. 1990). There is also evidence that the RPE suffer Ab-mediated complement attack, accumulate immune complexes, degenerate, and contribute to drusen formation (Johnson et al. 2000; Hageman et al. 2001). Dendritic cells (DCs) infiltrate the BM, project processes inside drusen cores, and break the blood–retinal barrier (Hageman et al. 2001), which exposes the RPE to direct inflammatory load, damage, and loss. Drusen may act as a reservoir of autoantigens that may be presented by DCs and drive an autoimmune attack to the macula.

Consistent with these findings, SNPs in genes that play a role in inflammation have emerged as clearly associated with greatly increased (or decreased) odds of having AMD (as reviewed in (Gehrs et al. 2006; Swaroop et al. 2007; Anderson et al. 2010)), whereby AMD can be now largely thought of as a congenital predisposition to defective modulation of inflammatory phenomena.

The hypothesis that autoimmunity may play a role in AMD was put forth by Penfold et al. (1985, 1986), who found anti-retinal auto-Abs in AMD patient sera (Penfold et al. 1990; Gurne et al. 1991). These findings have recently been reappraised (Gu et al. 2003b, 2009, 2010; Patel et al. 2005; Cherepanoff et al. 2006). Studies on murine tissues (Patel et al. 2005) indicate that, in AMD, auto-Abs develop not only against the neuroretina (nRet), but also RPE and choroid/Bruch's membrane

(Ch/BM). The identity of most of the auto-Ab targets is not yet known, and these studies have not been replicated on human tissues.

Highly specific and sensitive auto-Abs against carboxy-ethyl-pyrrole (CEP)-modified adducts have been found in AMD sera (Gu et al. 2003b, 2009, 2010). CEP is pro-angiogenic (Ebrahim et al. 2006) and CEP-modified adducts develop from oxidation of DHA, which is very abundant in photoreceptor outer segments. Immunization of mice against CEP leads to the development of AMD-like lesions (Hollyfield et al. 2008), and CEP serum levels and genetic markers together are highly predictive of the likelihood of having exudative AMD (Gu et al. 2009, 2010). We propose that further studies aimed at discovering additional markers can prove useful in understanding other AMD manifestations. In addition, since free CEP is highly unstable (Gu et al. 2003a) and the identity of CEP-binding proteins in AMD is not yet known, identifying them is likely to reveal other molecular targets that incite autoreactivity in AMD or that could be modified to prevent CEP binding.

2.3 Preliminary Results from Our Research Support the Role of Autoimmunity in AMD

We are analyzing a repository of serum samples from subjects ≥ 70 -year old with and without AMD. Sera are being screened for auto-Abs against nRet, RPE, and BM/Ch human donor tissue homogenates. Multiple auto-Abs occur more commonly/intensely or uniquely in AMD samples than in control samples against various macular tissues (Fig. 2.1). We have also tentatively identified a candidate protein that is approximately fivefold more common in AMD than in controls. Studies are in progress to ascertain in full the identity of this protein, confirm its more common reactivity in AMD samples, and test the possibility that it may act as a CEP-binding protein.

In addition, we have shown that vasoactive intestinal polypeptide (VIP)-positive submacular choroidal nerve fibers from human donor eyes decline with age (Jablonski et al. 2007) and that, while donor eyes age 70–94 have, on average, 8.8% blood vessel VIP fiber coverage, early AMD has 1.6% coverage, and advanced AMD has about 0.5% fiber coverage (unpublished observation). VIP is both a potent vasodilator and a key local anti-inflammatory and immunomodulatory agent (Gonzalez-Rey and Delgado 2005; Pozo et al. 2007; Smalley et al. 2009). These findings help explain choroidal blood flow loss in AMD (Grunwald et al. 1998, 2005), which could result in poor macular nutrition and impaired clearance of inflammatory debris. In addition, VIP fiber loss may compromise anti-inflammatory and immunomodulatory activity in the submacular choroid, thereby facilitating AMD pathogenesis further.

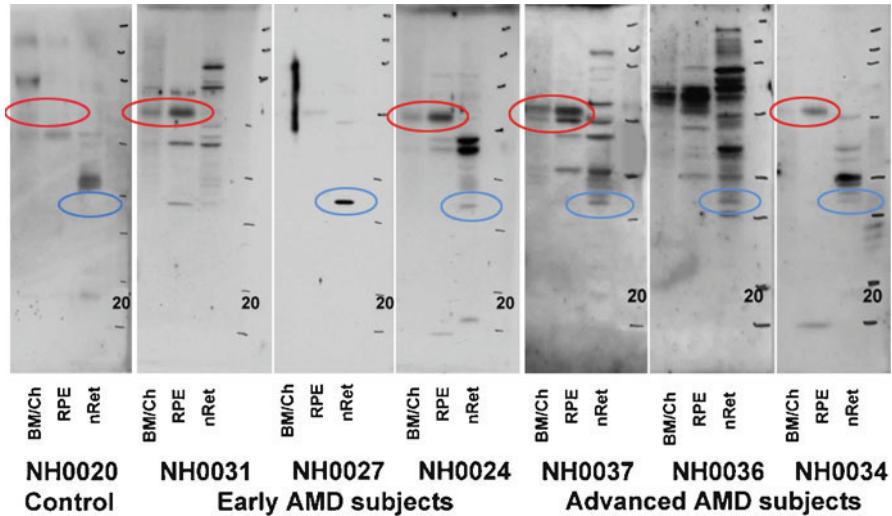


Fig. 2.1 Examples of western blots (control sample, three early and three advanced AMD). Note the recurrent presence of some specific bands for BM/Ch and RPE homogenates (*red ellipses*) and anti-nRet reactivity (*blue ellipses*) in AMD samples not present in the control sample. Note also the marked anti-nRet poly-reactivity in most advanced AMD samples typically not seen in controls and less prominent in early AMD

2.4 Experimental Framework and Future Directions

The role of inflammation and of the immune system in the pathogenesis of AMD is no longer seen simply as a secondary, “after-the-fact” phenomenon. In this proinflammatory context that underlies AMD (that is largely but by no means exclusively genetically driven) we hypothesize that the following chain of events (Fig. 2.2) leads to the formation of auto-Abs that contribute to AMD pathogenesis: Proinflammatory factors (1) known to be AMD risk factors are depicted as inciting agents leading to (2) a build-up in oxidative stress and chronic, low-grade inflammation in the submacular microenvironment. This self-reinforcing cycle leads to (3) progressive inflammatory damage to the choroid, the BM, and the RPE, which in turn (4) recruits to the site of inflammatory damage resident immunocompetent cells (DCs and monocytes, MC). The activation of these cells leads to (5) deposition of immune-mediated and inflammatory effectors. At this stage, drusen begin to develop and infiltration of DCs in drusen cores is seen. This step reinforces step 3 and leads to progressive exposure of Ch, BM, RPE, and nRet antigens (6). Auto-antigens are processed and (7) presented to T-helper lymphocytes (T_H), which in turn leads to (8) activation of B lymphocytes, their differentiation into plasma cells (PCs), and production of auto-Abs (9). These auto-Abs can promote step 3 further and likely feed also back into step 2.

Characterization of proteins involved in this secondary autoreactivity can allow the identification of novel therapeutic targets and prognostic biomarkers for AMD.

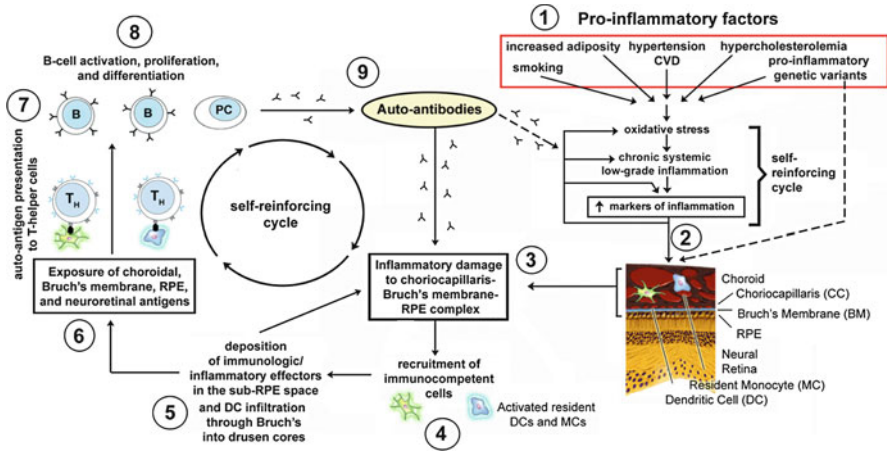


Fig. 2.2 Proposed chain of events leading to formation of auto-Abs in AMD

One can envision a not too distant future in which AMD diagnostics and care may be approached via high-throughput AMD “immunomics.” Much like in the seminal studies by Gu et al. (Gu et al. 2003b, 2009), panels of auto-Abs could be developed to measure levels of autoimmune reaction toward macular antigens in AMD patients and used together with molecular genetics to gauge the “proinflammatory status” of individual AMD patients, counsel them and treat them better either through earlier intervention/more aggressive management in subjects with greater risk profiles, or via treatments that interfered actively with the autoreactivity of AMD patients.

Acknowledgments Supported by the International Retinal Research Foundation, NIH grants K23 EY000409 and R21 EY018416, and an unrestricted grant from Research to Prevent Blindness.

References

- Anderson DH, Radeke MJ, Gallo NB et al (2010) The pivotal role of the complement system in aging and age-related macular degeneration: hypothesis re-visited. *Prog Retin Eye Res* 29:95–112
- Cherepanoff S, Mitchell P, Wang JJ et al (2006) Retinal autoantibody profile in early age-related macular degeneration: preliminary findings from the Blue Mountains Eye Study. *Clin Experiment Ophthalmol* 34:590–595
- Ebrahem Q, Renganathan K, Sears J et al (2006) Carboxyethylpyrrole oxidative protein modifications stimulate neovascularization: Implications for age-related macular degeneration. *Proc Natl Acad Sci U S A* 103:13480–13484
- Friedman DS, O’Colmain BJ, Munoz B et al (2004) Prevalence of age-related macular degeneration in the United States. *Arch Ophthalmol* 122:564–572
- Gehrs KM, Anderson DH, Johnson LV et al (2006) Age-related macular degeneration—emerging pathogenetic and therapeutic concepts. *Ann Med* 38:450–471

- Gonzalez-Rey E, Delgado M (2005) Role of vasoactive intestinal peptide in inflammation and autoimmunity. *Curr Opin Investig Drugs* 6:1116–1123
- Grindle CFJ, Marshall J (1978) Ageing changes in Bruch's membrane and their functional implications. *Trans Ophthalmol Soc UK* 98:172–175
- Grunwald JE, Metelitsina TI, Dupont JC et al (2005) Reduced foveolar choroidal blood flow in eyes with increasing AMD severity. *Invest Ophthalmol Vis Sci* 46:1033–1038
- Grunwald JE, Hariprasad SM, DuPont J et al (1998) Foveolar choroidal blood flow in age-related macular degeneration. *Invest Ophthalmol Vis Sci* 39:385–390
- Gu J, Pauer GJ, Yue X et al (2009) Assessing susceptibility to age-related macular degeneration with proteomic and genomic biomarkers. *Mol Cell Proteomics* 8:1338–1349
- Gu J, Pauer GJ, Yue X et al (2010) Proteomic and Genomic Biomarkers for Age-Related Macular Degeneration. *Adv Exp Med Biol* 664:411–417
- Gu X, Sun M, Gugiu B et al (2003a) Oxidatively truncated docosahexaenoate phospholipids: total synthesis, generation, and peptide adduction chemistry. *J Org Chem* 68:3749–3761
- Gu X, Meer SG, Miyagi M et al (2003b) Carboxyethylpyrrole protein adducts and autoantibodies, biomarkers for age-related macular degeneration. *J Biol Chem* 278:42027–42035
- Grune DH, Tso MO, Edward DP et al (1991) Antiretinal antibodies in serum of patients with age-related macular degeneration. *Ophthalmology* 98:602–607
- Hageman GS, Luthert PJ, Victor Chong NH et al (2001) An integrated hypothesis that considers drusen as biomarkers of immune-mediated processes at the RPE-Bruch's membrane interface in aging and age-related macular degeneration. *Prog Retin Eye Res* 20:705–732
- Hawkins B, Bird A, Klein R et al (1999) Epidemiology of age-related macular degeneration. *Mol Vis* 5:26
- Hollyfield JG, Bonilha VL, Rayborn ME et al (2008) Oxidative damage-induced inflammation initiates age-related macular degeneration. *Nat Med* 14:194–198
- Jablonski MM, Iannaccone A, Reynolds DH et al (2007) Age-Related Decline in VIP-Positive Parasympathetic Nerve Fibers in the Human Submacular Choroid. *Invest Ophthalmol Vis Sci* 48:479–485
- Johnson LV, Ozaki S, Staples MK et al (2000) A potential role for immune complex pathogenesis in drusen formation. *Exp Eye Res* 70:441–449
- Killingsworth MC, Sarks SH (1982) Giant cells in disciform macular degeneration of the human eye. *Micron* 13:359–360
- Killingsworth MC, Sarks JP, Sarks SH (1990) Macrophages related to Bruch's Membrane in Age-Related Macular Degeneration. *Eye* 4:613–621
- Patel N, Ohbayashi M, Nugent AK et al (2005) Circulating anti-retinal antibodies as immune markers in age-related macular degeneration. *Immunology* 115:422–430
- Penfold PL, Killingsworth MC, Sarks SH (1985) Senile macular degeneration: the involvement of immunocompetent cells. *Graefes Arch Clin Exp Ophthalmol* 223:69–76
- Penfold PL, Killingsworth MC, Sarks SH (1986) Senile macular degeneration. The involvement of giant cells in atrophy of the retinal pigment epithelium. *Invest Ophthalmol Vis Sci* 27:364–371
- Penfold PL, Provis JM, Furby JH et al (1990) Autoantibodies to retinal astrocytes associated with age-related macular degeneration. *Graefes Arch Clin Exp Ophthalmol* 228:270–274
- Pozo D, Gonzalez-Rey E, Chorny A et al (2007) Tuning immune tolerance with vasoactive intestinal peptide: a new therapeutic approach for immune disorders. *Peptides* 28:1833–1846
- Smalley SG, Barrow PA, Foster N (2009) Immunomodulation of innate immune responses by vasoactive intestinal peptide (VIP): its therapeutic potential in inflammatory disease. *Clin Exp Immunol* 157:225–234
- Swaroop A, Branham KE, Chen W et al (2007) Genetic susceptibility to age-related macular degeneration: a paradigm for dissecting complex disease traits. *Hum Mol Genet* 16 Spec No. 2:R174-182

Chapter 3

Local Vs. Systemic Mononuclear Phagocytes in Age-Related Macular Degeneration and Their Regulation by *CCL2–CCR2* and *CX3CL1–CX3CR1* Chemokine Signalling

Ulrich F.O. Luhmann and Robin R. Ali

Keywords Mononuclear phagocytes • Age-related macular degeneration • Chemokine signalling • *CCL2* knockout mouse • *CX3CR1* knockout mouse

3.1 Introduction

Age-related macular degeneration (AMD) is the most common cause of vision loss in the elderly of industrialized countries. The early clinical hallmark of AMD is drusen which are extracellular lipid and protein deposits between the basal lamina of the retinal pigment epithelium (RPE) and Bruch's membrane (BM). AMD slowly progresses towards two advanced stages that are responsible for vision loss. Geographic atrophy ("dry" AMD) is characterized by a loss of choriocapillaris and adjacent RPE and photoreceptor cells, while exudative ("wet") AMD is characterized by choroidal neovascularisation (CNV) with subsequent haemorrhages and acute photoreceptor and RPE cell loss. Over the last 2 decades, it has become clear that age, smoking and family history are the major risk factors for the onset of AMD. The recent identification of several complement genes (*CFH*, *C3*, *C2/CFB*), the *ARMS2/HTRA1* locus and the CX3C chemokine receptor 1 (*CX3CR1*) as genetic risk factors for AMD suggests that innate immunity and local chronic inflammation in combination with environmental factors play major roles in pathogenesis of AMD (de Jong 2006).

U.F.O. Luhmann (✉) • R.R. Ali
Department of Genetics, UCL Institute of Ophthalmology,
11-43 Bath Street, London EC1V 9EL, UK
e-mail: u.luhmann@ucl.ac.uk

3.2 Mononuclear Phagocytes Comprise a Heterogeneous Population of Systemic and Local Innate Immune Cells

Monocytes, dendritic cells, macrophages and microglia are all effector cells of the innate immune system and represent heterogeneous cells of the mononuclear phagocytic system that is capable to adapt to certain challenges in specific microenvironments of the body. Peripheral blood monocytes consist first of inflammatory monocytes that migrate to injured and infected sites and second of “resting” monocytes that show surveillance and patrolling behaviour of normal tissue and are recruited to sites of inflammation to participate in the resolution of inflammatory processes (Geissmann et al. 2003). Resident dendritic cells, macrophages and microglia are differentiated tissue mononuclear phagocytes within the tissues and are important for local immune surveillance and tissue homeostasis. Retinal microglia are located throughout the neural parenchyma (parenchymal microglia cells) or surrounding blood vessels (perivascular microglia cells) and are normally located in the inner retina, while the outer retina is free of myeloid cells. After focal injury microglia polarise and change from ramified into an amoeboid morphology and may start migrating towards the insult (Liang et al. 2009). Such myeloid cell activation has been observed, e.g. during physiological ageing, in models of retinal degenerations and during chronic light exposure (Xu et al. 2009). But it remains unclear to which extent local activation of microglia and/or recruitment of blood-derived macrophages contribute to disease or are protective.

3.3 Activation of Mononuclear Phagocytes Is Controlled by Signals from the Microenvironment

Dependent on the inflammatory stimulus in the microenvironment, the tissue responds to the damage with the local production of specific cytokines, chemokines and adhesion molecules. The thereby initiated cellular response and effector functions of these cells are classified as either classical or alternative activation. They represent extremes of a continuum of heterogeneous and plastic responses that range from the pro-inflammatory, classical activation state to the two alternative activation states with either tissue repair and anti-inflammatory or immune suppressive and phagocytic effector functions. Dependent on activation state of the cells they regulated innate and subsequent adaptive immune functions by secretion of specific cytokines (Colton 2009). The chemokines are a very important superfamily of structurally related chemotactic cytokines that are classified based on their amino acid sequence and are subdivided into four subfamilies, the C-, the CC-, the CXC- and the CX3C-chemokines. They bind to members of the corresponding class of G-protein-coupled receptors, which are differentially expressed on the surface of target cells (Mantovani et al. 2004). This chemokine signalling system regulates innate immune responses under homeostatic and diseased conditions and thus will also coordinate innate immunity in AMD.

3.4 Evidence of the Involvement of Myeloid Cells in the Pathophysiology of AMD

A role of myeloid cells in AMD has been suggested previously by the identification of macrophage chemoattractant molecules and elevated levels of inflammatory mediators in drusen isolated from AMD patients (Mullins et al. 2000). Ultrastructural examination of specimens from patients with early, intermediate and late stage of AMD also showed an increasing numbers of immune cells in the choroidal stroma (Penfold et al. 1985). These choroidal mononuclear phagocytes are associated with the outer surface of Bruch's membrane and are particularly common in areas of drusen and basal laminar deposits. In geographic atrophy, myeloid cells surround atrophic lesions, but are much higher in number in eyes with CNV. In CNV, the cells are particularly associated with breaks in Bruch's membrane or are found in close vicinity to newly formed vessels. Interestingly, while the Bruch's membrane macrophages from exudative AMD eyes do not express iNOS, a marker of classical activation, the vessel-associated activated macrophages do, suggesting that different activation states of mononuclear phagocytes have distinct roles in the disease process (Cherepanoff et al. 2009). Also in the retina, local microglia become activated and are found to be associated with early RPE lesions and dying photoreceptors in the subretinal space (Gupta et al. 2003). Furthermore, systemic activation of macrophages has also been suggested in AMD as patients with exudative AMD seem to be more likely to have activated macrophages in their circulation that produce high amounts of the pro-inflammatory cytokine TNF α than patients with dry AMD (Cousins et al. 2004).

3.5 The Identification of the Chemokine Receptor CX3CR1 as a Risk Factor for AMD

These described findings so far have not clarified, whether myeloid cells are primarily involved in disease pathology of AMD or respond secondarily to the disease process. But the recent identification of CX3CR1 as a genetic risk factor for AMD and the functional effect of the M280 risk variant of CX3CR1 on monocyte migration support the hypothesis of a more primary role of this chemokine signalling pathway in the pathogenesis of AMD (Tuo et al. 2004; Combadiere et al. 2007).

3.6 CCR2 and CX3CR1 Signalling Contribute Differentially to the Recruitment of Monocyte Subsets to the Retina and Also Control Local Microglia Responses

Both the CX3CL1–CX3CR1 pathway and the CCL2–CCR2 pathway control and coordinate the recruitment, migration and emigration of specific monocyte subsets from the circulation to inflamed tissue. While CCL2–CCR2 signalling recruits

pro-inflammatory monocytes, CX3CL1–CX3CR1 signalling affects “resident” monocyte trafficking and limits microglia-mediated neurotoxicity (Boring et al. 1997; Cardona et al. 2006). Both chemokine pathways become activated by the inducible expression of the two chemokine ligands CCL2 or CX3CL1 in several cell types including retinal and choroidal endothelial cells, Muller glia, microglia and RPE. There are distinct differences in the expression of the two receptors on different mononuclear phagocytes. Systemically, pro-inflammatory monocytes express low level of CX3CR1, but high level of CCR2, while “resident” monocytes express high level of CX3CR1 but no CCR2 (Tacke and Randolph 2006). Locally, CCR2 shows a very limited degree of expression on perivascular microglia and is absent on parenchymal, quiescent microglia, while CX3CR1 is expressed on tissue macrophages, dendritic cells and microglia (Jung et al. 2000). Recent work in the model of endotoxin-induced autoimmune uveitis (EAU) suggested that recruitment of pro-inflammatory (CCR2 high, CX3CR1 low) monocytes to the inflamed outer retina induces local photoreceptor loss at the peak of the disease, which is attenuated in CCR2-deficient but unaffected in *Cx3cr1*-deficient mice (Xu et al. 2005; Kezic and McMenamin 2010). By contrast, in the context of ageing, *Ccl2* deficiency and *Cx3cr1* deficiency both lead to a slow age-related accumulation of subretinal macrophages/microglia, but only the *Cx3cr1*-deficient mice show an additional marked, progressive age-related retinal degeneration. While there is still some debate about the degree of age-related retinal degeneration associated with the lack of *Ccl2* or *Ccr2* in different mouse lines (Ambati et al. 2003; Luhmann et al. 2009), it is clear that lack of either of the genes results in a reduced response to laser-induced CNV, while *Cx3cr1* deficiency increases this response (Luhmann et al. 2009; Combadiere et al. 2007; Tsutsumi et al. 2003). These findings suggest that *Cx3cl1*–*Cx3cr1* and *Ccl2*–*Ccr2* chemokine signalling both affect activation and migration of mononuclear phagocytes in almost opposite ways and that defects in this fine signalling balance might cause defective activation of local and systemic innate immune cells which in turn might contribute to AMD pathology in early and in both late stages, geographic atrophy and CNV.

3.7 Future Directions

Further studies using the different chemokine mouse models are needed to address how the two signalling pathways are coordinated during the different phases of inflammation and how this correlates with local and systemic myeloid cell activation and recruitment to the eye in the context of ageing, environmental stress (e.g. photooxidative stress) or other AMD-related factors. Interestingly, a synergistic interaction of defects in both signalling pathways has been suggested by the much accelerated and more severe, early onset phenotype in mice lacking both, *Ccl2* and *Cx3cr1*, although this phenotype was initially of variable penetrance and thus requires further investigation (Tuo et al. 2007). However, all the mentioned chemokine knockout mouse models show with age an increased subretinal accumulation of

bloated macrophages and thus raise the question, whether the recently discovered drusenoid deposits in the subretinal space of AMD eyes (also called reticular drusen) (Arnold et al. 1995) might be a consequence of an analogous chemokine signalling defect in AMD patients that might lead to subretinal accumulation of microglia/macrophages in the human disease or whether a similar process occurs in the choroid and might contribute to drusen development as an early pathogenic event in AMD. Analysing the contribution of aberrant chemokine signalling and defective myeloid cell activation to early pathogenesis of AMD and its contribution to the transition from early to late stage disease might in the future help to develop more targeted therapeutic approaches that focus on the cellular innate immune system and might attenuate disease progression of AMD.

References

- Ambati J, Anand A, Fernandez S et al (2003) An animal model of age-related macular degeneration in senescent Ccl-2- or Ccr-2-deficient mice. *Nat Med* 9:1390–1397
- Arnold JJ, Sarks SH, Killingsworth MC, Sarks JP (1995) Reticular pseudodrusen. A risk factor in age-related maculopathy. *Retina* 15:183–191
- Boring L, Gosling J, Chensue SW et al (1997) Impaired monocyte migration and reduced type 1 (Th1) cytokine responses in C-C chemokine receptor 2 knockout mice. *J Clin Invest* 100:2552–2561
- Cardona AE, Pioro EP, Sasse ME et al (2006) Control of microglial neurotoxicity by the fractalkine receptor. *Nat Neurosci* 9:917–924
- Cherepanoff S, McMenamin PG, Gillies MC, Kettle E, Sarks SH (2009) Bruch's membrane and choroidal macrophages in early and advanced age-related macular degeneration. *Br J Ophthalmol*
- Colton C (2009) Heterogeneity of Microglial Activation in the Innate Immune Response in the Brain. *Journal of Neuroimmune Pharmacology* 4:399–418
- Combadiere C, Feumi C, Raoul W et al (2007) CX3CR1-dependent subretinal microglia cell accumulation is associated with cardinal features of age-related macular degeneration. *J Clin Invest* 117:2920–2928
- Cousins SW, Espinosa-Heidmann DG, Csaky KG (2004) Monocyte activation in patients with age-related macular degeneration: a biomarker of risk for choroidal neovascularization? *Arch Ophthalmol.* 2004;122:1013–1018
- de Jong PTVM (2006) Age-Related Macular Degeneration. *N Engl J Med* 355:1474–1485
- Geissmann F, Jung S, Littman DR (2003) Blood Monocytes Consist of Two Principal Subsets with Distinct Migratory Properties. *Immunity* 19:71–82
- Gupta N, Brown KE, Milam AH (2003) Activated microglia in human retinitis pigmentosa, late-onset retinal degeneration, and age-related macular degeneration. *Experimental Eye Research* 76:463–471
- Jung S, Aliberti J, Graemmel P et al (2000) Analysis of Fractalkine Receptor CX3CR1 Function by Targeted Deletion and Green Fluorescent Protein Reporter Gene Insertion. *Mol Cell Biol* 20:4106–4114
- Kezic J, McMenamin PG (2010) The Monocyte Chemokine Receptor CX3CR1 Does Not Play a Significant Role in the Pathogenesis of Experimental Autoimmune Uveoretinitis. *Invest Ophthalmol Vis Sci* 51:5121–5127
- Liang KJ, Lee JE, Wang YD et al (2009) Regulation of Dynamic Behavior of Retinal Microglia by CX3CR1 Signaling. *Invest Ophthalmol Vis Sci* 50:4444–4451
- Luhmann UFO, Robbie S, Munro PM et al (2009) The drusen-like phenotype in aging Ccl2 knockout mice is caused by an accelerated accumulation of swollen autofluorescent subretinal macrophages. *Invest Ophthalmol Vis Sci* 50:5934–5943

- Mantovani A, Sica A, Sozzani S, Allavena P, Vecchi A, Locati M (2004) The chemokine system in diverse forms of macrophage activation and polarization. *Trends in Immunology* 25:677–686
- Mullins RF, Russell SR, Anderson DH, Hageman GS (2000) Drusen associated with aging and age-related macular degeneration contain proteins common to extracellular deposits associated with atherosclerosis, elastosis, amyloidosis, and dense deposit disease. *FASEB J* 14:835–846
- Penfold PL, Killingsworth MC, Sarks SH (1985) Senile macular degeneration: the involvement of immunocompetent cells. *Graefes Arch Clin Exp Ophthalmol* 223:69–76
- Tacke F, Randolph GJ (2006) Migratory fate and differentiation of blood monocyte subsets. *Immunobiology* 211:609–618
- Tsutsumi C, Sonoda KH, Egashira K et al (2003) The critical role of ocular-infiltrating macrophages in the development of choroidal neovascularization. *J Leukoc Biol* 74:25–32
- Tuo J, Bojanowski CM, Zhou M et al (2007) Murine Ccl2/Cx3cr1 Deficiency Results in Retinal Lesions Mimicking Human Age-Related Macular Degeneration. *Invest Ophthalmol Vis Sci* 48:3827–3836
- Tuo J, Smith BC, Bojanowski CM et al (2004) The involvement of sequence variation and expression of CX3CR1 in the pathogenesis of age-related macular degeneration. *FASEB J* 18:1862fj
- Xu H, Chen M, Forrester JV (2009) Para-inflammation in the ageing retina. *Progress in Retinal and Eye Research* 28:348–368
- Xu H, Manivannan A, Dawson R et al (2005) Differentiation to the CCR2+ Inflammatory Phenotype In Vivo Is a Constitutive, Time-Limited Property of Blood Monocytes and Is Independent of Local Inflammatory Mediators. *J Immunol* 175:6915–6923

Chapter 4

Sublytic Membrane-Attack-Complex Activation and VEGF Secretion in Retinal Pigment Epithelial Cells

Kannan Kunchithapautham, Mausumi Bandyopadhyay,
Mohammad Dahrouj, Joshua M. Thurman, and Bärbel Rohrer

Keywords RPE monolayer • VEGF • Complement system • Sublytic activation
• Age-related macular degeneration • Transepithelial resistance

4.1 Introduction

Age-related macular degeneration (AMD) is characterized by progressive loss of central vision resulting from damage to the photoreceptor cells in the central area of the retina, the macula. AMD occurs in two forms: wet and dry; with the dry form making up 80–90% of total cases (Pangburn 2000; Brown et al. 2005). Both forms are associated with pathology at the RPE/choroid interface, which leads to subsequent loss of photoreceptors.

AMD is a complex multifactorial disease and may actually represent a family of diseases that affect the macula (see <http://Retnet.org> for genes associated with autosomal dominant, autosomal recessive, or X-linked macular degeneration). The disease process appears to be influenced by a number of environmental insults making

B. Rohrer (✉)

Departments of Ophthalmology and Neurosciences, Division of Research,
Medical University of South Carolina, Charleston, SC 29425, USA
e-mail: rohrer@musc.edu

K. Kunchithapautham

Department of Neurosciences, Division of Research, Medical University of South Carolina,
Charleston, SC 29425, USA

M. Bandyopadhyay • M. Dahrouj

Department of Ophthalmology, Medical University of South Carolina,
Charleston, SC 29425, USA

J.M. Thurman

Department of Medicine, Denver School of Medicine,
University of Colorado, Denver, CO 80045, USA

it difficult to identify one central cause. Indeed, the genetics of macular degeneration and other forms of retinal degeneration point to multiple targets and multiple causes, each of which may be involved in a subset of patients, and ultimately lead to the common endpoint of failed central vision. The primary risk factor for AMD is aging. The only environmental agent unequivocally linked to AMD is nicotine (Schmidt et al. 2006), presumably by generating oxidative stress. Overall, oxidative stress is thought to be an important risk factor, presumably impacting RPE function (Snodderly 1995). Additional agents thought to be associated with AMD include A2E, a major component of lipofuscin formed as a byproduct of the bleached chromophore 11-*cis* retinal (Sparrow et al. 2003) and iron (Wong et al. 2007). Both nicotine and oxidative stress enhance choroidal neovascularization (CNV) in mice (Suner et al. 2004; Dong et al. 2009); A2E accumulation is associated with Stargardt-like disease pathology in the ABCR4^{+/-} mouse (Mata et al. 2001); and impairment of iron homeostasis leads to retinal degeneration (Hadziahmetovic et al. 2008). Finally, genetic studies have demonstrated that polymorphisms in different complement proteins each increase the risk for developing AMD (Hageman et al. 2005; Haines et al. 2005; Klein et al. 2005; Edwards et al. 2008; McKay et al. 2009; Lee et al. 2010). There are three pathways of complement activation (classical (CP), alternative (AP), and lectin (LP)), which all activate a final common pathway. The proteins encoded by the risk genes participate in the AP, CP/LP, or in the final common pathway. Overall, it has been hypothesized that inadequate control of complement-driven inflammation may be a major factor in disease pathogenesis in AMD. While no effective treatment is available for dry AMD, therapies blocking VEGF ameliorate wet AMD (e.g., van Wijngaarden and Qureshi 2008).

We have used RPE monolayers to elucidate the mechanism of RPE injury caused by the complement- and VEGF-mediated pathways. Results from these studies have led us to propose a central role for the alternative pathway of complement in mediating the pathological increase in VEGF secretion in AMD.

4.2 Results

To examine the effects of complement activation on RPE cells, we used RPE monolayers. For this purpose, we have established RPE cell monolayer systems (ARPE-19 cells; and primary human embryonic and adult RPE cells). RPE cells were initially plated on permeable membrane inserts in the presence of 10% serum; after the cells attached, serum was reduced to 1%. Under these conditions, RPE cells form tight monolayers, which are polarized and stained for markers of tight and adherens junctions (Bailey et al. 2004). These monolayers exhibit stable transepithelial resistance (TER), which can be monitored with an epithelial volt-ohm meter equipped with an STX2 electrode. Absolute TER values are dependent upon the type of RPE culture, but reach maximum levels within 2–3 weeks after reaching confluency (ARPE-19 cells: 40–45 Ωcm^2 ; primary human embryonic and adult RPE: 300–350 Ωcm^2).

ARPE-19 cells when grown as monolayers are resistant to oxidative damage. Importantly, while ARPE-19 (or primary RPE cells) grown in monolayers show no

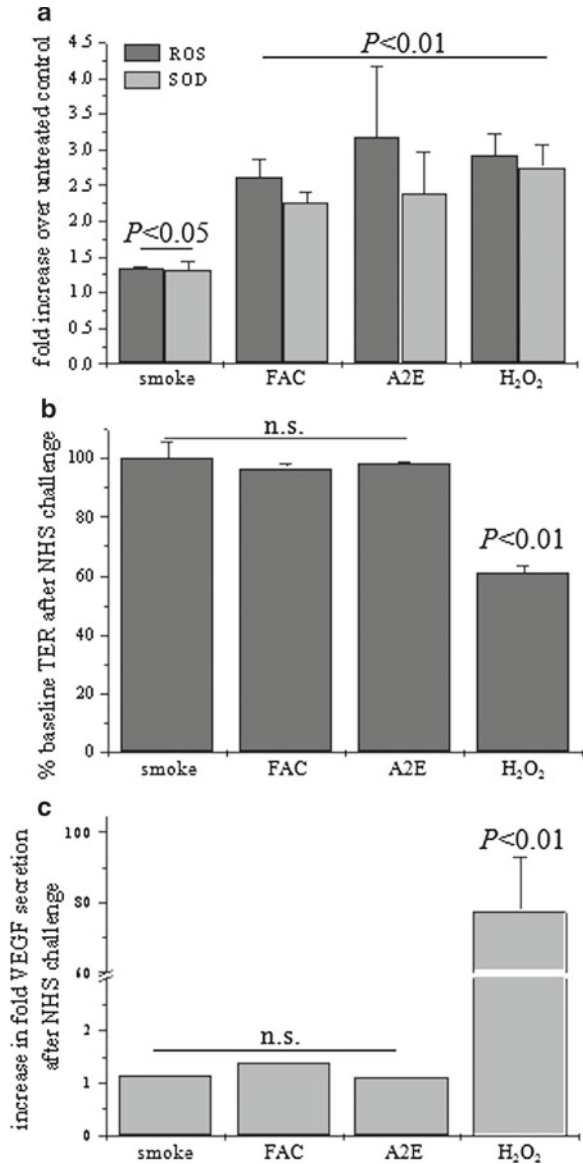
sign of damage up to 0.5 mM of H_2O_2 (Bailey et al. 2004; Thurman et al. 2009) and data not shown), subconfluent ARPE-19 cells exposed to concentrations ≥ 0.1 mM undergo apoptosis (Choudhary et al. 2005). One of the earliest signs of damage occurring with H_2O_2 concentrations ≥ 1 mM is a loss of barrier function or a reduction of TER. Since the RPE in vivo is continuously exposed to low levels of oxidative stress, we asked whether a concentration that did not affect the epithelial integrity (0.5 mM H_2O_2) sensitized the cells to complement attack (Thurman et al. 2009). Oxidative stress was found to decrease the level of alternative pathway inhibition in RPE cells by two known mechanisms: first, expression of the membrane-bound complement inhibitors CD55 and CD59 was significantly reduced upon exposure to H_2O_2 ; and second, AP inhibition at the cell surface by Factor H present within the serum was impaired. Together, these changes sensitized the RPE to complement attack; while exposure of control cells to 25% complement-sufficient normal human serum (NHS) had no effect on TER, oxidatively stressed monolayers exhibited a rapid reduction in TER by $\sim 50\%$ in ARPE-19 cells (Thurman et al. 2009) and $\sim 25\%$ in primary human RPE cells (unpublished data). TER reduction by H_2O_2 and NHS was MAC-dependent (i.e., it could be eliminated by removing an essential component of MAC assembly, C7, from the serum) and required AP activation (i.e., the addition of an AP inhibitor, such as CR2-fH, to the stimulated cells prevented TER reduction). Finally, the reduction in TER involved VEGF secretion from the apical and basolateral surfaces of the RPE, and could be inhibited by blocking VEGF type 2 receptors localized on the apical side of the RPE cells (Ablonczy and Crosson 2007).

Here, we asked whether other factors known to be associated with AMD, such as smoking, iron, and A2E, similarly sensitize the RPE to complement attack (i.e., result in loss of TER in response to NHS). We used published methods to expose ARPE-19 cell monolayers to these compounds. At the onset of treatment, all the media was replaced with fresh media containing the compound of choice. If longer treatments were required (i.e., for A2E and smoke exposure), media with agents was replaced daily. Specifically, ARPE-19 cells were exposed to 2% smoke extract for 5 days (Mulligan et al. 2009), treated with 100 μ M ferric ammonium citrate (FAC) for 24 h (Voloboueva et al. 2007), preloaded with 10 μ M of A2E for 5 days (Finnemann et al. 2002), or exposed to 0.5 mM H_2O_2 for 4 h (Thurman et al. 2009) at which time the cells were challenged with 25% NHS. All four treatments alone, prior to NHS challenge, resulted in significant increase in oxidative stress as shown by reactive oxygen species and superoxide measurements (Fig. 4.1a). However, NHS challenge only resulted in a decrease in TER in H_2O_2 -exposed, but not smoke-extract-, FAC-, or A2E-treated cells (Fig. 4.1b). Concomitantly, only H_2O_2 -exposed cells showed a significant increase in VEGF secretion into the apical (Fig. 4.1c) or basal compartment (data not shown) upon NHS challenge.

4.3 Discussion

We have previously reported in both the animal model of wet AMD and in RPE monolayers that complement activation is upstream of vascular endothelial cell expression (Rohrer et al. 2009; Thurman et al. 2009). In particular, we have argued

Fig. 4.1 Smoke-extract, ferric ammonium citrate, A2E, and H₂O₂ were compared for their ability to result in oxidative stress (a), to sensitize cells to complement attack (b), and to result in VEGF secretion (c). While all agents resulted in oxidative stress, only H₂O₂ resulted in loss of TER and increased VEGF secretion. Results in (a) were normalized to untreated controls; in (b) and (c) to their respective controls (i.e., smoke+NHS normalized to smoke, etc.)



that oxidative stress reduces the levels of membrane-bound complement inhibitors CD55 and CD59 and reduces the inhibitory effect of the soluble inhibitor CFH, which sensitizes the RPE to complement attack. Sublytic MAC activation then results in VEGF release, whereby VEGF, acting through VEGF-R2 receptors, impairs RPE function resulting in TER breakdown. The impairment of the RPE barrier function in the presence of continued VEGF secretion then facilitates CNV.

In the current study, we report that oxidative stress induced by other AMD-associated compounds of the ARPE-19 cells does not have a similar effect. Indeed,

exposure to A2E, FAC, and smoke-extract did not result in loss of TER or a release of VEGF. We initially hypothesized that all forms of oxidative stress might sensitize epithelial cells to complement attack, resulting in the release of VEGF. Our current results, however, suggest that RPE cells respond differently to specific cellular stressors. A2E at the concentration used (10 μ M) has been shown by others to affect RPE cell physiology in monolayers (Finnemann et al. 2002; Lakkaraju et al. 2007; Vives-Bauza et al. 2008), and induce apoptosis in subconfluent cells (Suter et al. 2000). In a model of dry AMD (the *Rdh8^{-/-} Abca4^{-/-}* mouse) which shows a significant increase in A2E, spontaneous CNV, and elevated VEGF levels, rapamycin (an immunosuppressive agent with anti-VEGF activity) was found to reduce A2E accumulation and prevent CNV without affecting VEGF levels. Similarly, exposure of subconfluent ARPE-19 cells to iron impaired their phagocytosis activity (Chen et al. 2009) while iron overload in vivo resulted in oxidative stress, and complement activation and morphological changes in the RPE (Hadziahmetovic et al. 2008). However, no relationship between iron overload and VEGF has yet been established. Finally, components of smoke have been shown to affect RPE cells. Hydroquinone (HQ), which is a pro-oxidant in cigarette smoke, has been shown to produce membrane blebbing in RPE cells, resulting in sub-RPE deposits in mice (Espinosa-Heidmann et al. 2006). Similarly, Benzo(a)Pyrene (B(a)P) impairs RPE physiology in cultured subconfluent RPE cells (Wang et al. 2009). In vivo smoke exposure resulted in mitochondrial defects and complement deposition in mice (Wang et al. 2009), and both nicotine (Suter et al. 2004) and dioxin increased CNV in mice (Takeuchi et al. 2009). While dioxin increased VEGF expression, it has not yet been confirmed that the dioxin effect on CNV is mediated through VEGF. In our original study, we have shown that oxidative stress induced by H_2O_2 reduces the ability of RPE cells to regulate complement on their cell surface (Thurman et al. 2009). We will examine in future experiments the surface levels of CD55 and CD59, as well as the ability of CFH to function as a complement inhibitor in smoke-extract-, FAC-, or A2E-treated cells. However, it appears that RPE cells respond differently to stressors. Similar to these findings here, we reported previously that chemical hypoxia, generated by Antimycin A treatment of the ARPE-19 cells, did not reduce surface levels of CD55, whereas H_2O_2 did (Thurman et al. 2010). In future experiments, it will be essential to examine phagocytic function, mitochondrial metabolism, and other readouts that have been shown to be affected by A2E, FAC, and smoke-extract, in the context of complement activation.

Current therapy for dry AMD is directed at reducing oxidative stress. Subjects at risk for AMD and those with early AMD benefited from supplements containing high levels of antioxidants and zinc (Bartlett and Eperjesi 2003). However, no further treatments targeting the pathology of early AMD (e.g., drusen accumulation, RPE damage, complement activation, etc) are currently available. Also, no treatment is available for the late form of AMD, geographic atrophy. The only pathological target that can be treated is neovascularization of the choroid. To this end, therapies have focused on either physically or pharmacologically interrupting blood vessel growth (summarized in Augustin et al. 2009). Since blood vessel growth is dependent upon the presence of angiogenic factors such as VEGF, the field borrowed from the cancer therapies, starving blood vessels for VEGF. Currently, three anti-angiogenic

drugs (VEGF-inhibitors) are available to treat CNV: Pegaptanib sodium, a 28-base anti-VEGF aptamer; Ranibizumab, a Fab fragment; and Bevacizumab, a full-length monoclonal antibody against VEGF. While the effects are promising (i.e., resulting in regression of CNV, including halting of vision loss or significant improvement of vision (van Wijngaarden and Qureshi 2008)), one must proceed with care. VEGF is an important trophic factor for retina (Saint-Geniez et al. 2008), RPE (Saint-Geniez et al. 2008), and choroidal health (Alon et al. 1995). Thus, depriving these tissues of normal levels of growth factor long-term might lead to complications.

In summary, we have found that RPE cells respond differently to stressors known to be associated with AMD. Overall, no correlation between oxidative stress and susceptibility to complement attack has been established. However, a direct correlation exists between loss of TER and VEGF secretion; stressors that resulted in little VEGF secretion showed little change in TER and vice versa. Since complement activation has been found to be upstream of VEGF in both the CNV model of wet AMD and in RPE monolayers; since complement deposition has been found to be associated with all forms of AMD; and since many stressors have been shown to be associated with complement deposition in cell culture and animal models of AMD, targeting excessive complement activation might be a logical target.

Acknowledgments This work was supported in part by National Institutes of Health Grants DK077661 and DK076690 (JMT), the Foundation Fighting Blindness (BR), and an unrestricted grant to MUSC from Research to Prevent Blindness, Inc., New York, NY. BR is a Research to Prevent Blindness Olga Keith Wiess Scholar. The authors declare the following disclosures. JMT and BR are consultants for Taligen Therapeutics, Inc. The authors thank Luanna Bartholomew for editorial assistance.

References

- Ablonczy Z, Crosson CE (2007) VEGF modulation of retinal pigment epithelium resistance. *Exp Eye Res* 85:762–771
- Alon T, Hemo I, Itin A et al (1995) Vascular endothelial growth factor acts as a survival factor for newly formed retinal vessels and has implications for retinopathy of prematurity. *Nat Med* 1:1024–1028
- Augustin AJ, Scholl S, Kirchhof J (2009) Treatment of neovascular age-related macular degeneration: Current therapies. *Clin Ophthalmol* 3:175–182
- Bailey TA, Kanuga N, Romero IA et al (2004) Oxidative stress affects the junctional integrity of retinal pigment epithelial cells. *Invest Ophthalmol Vis Sci* 45:675–684
- Bartlett H, Eperjesi F (2003) Age-related macular degeneration and nutritional supplementation: a review of randomised controlled trials. *Ophthalmic Physiol Opt* 23:383–399
- Brown MM, Brown GC, Stein JD et al (2005) Age-related macular degeneration: economic burden and value-based medicine analysis. *Can J Ophthalmol* 40:277–287
- Chen H, Lukas TJ, Du Net al (2009) Dysfunction of the retinal pigment epithelium with age: increased iron decreases phagocytosis and lysosomal activity. *Invest Ophthalmol Vis Sci* 50:1895–1902
- Choudhary S, Xiao T, Srivastava S et al (2005) Toxicity and detoxification of lipid-derived aldehydes in cultured retinal pigmented epithelial cells. *Toxicol Appl Pharmacol* 204:122–134

- Dong A, Xie B, Shen J et al (2009) Oxidative stress promotes ocular neovascularization. *J Cell Physiol* 219:544–552
- Edwards AO, Fridley BL, James KM et al (2008) Evaluation of clustering and genotype distribution for replication in genome wide association studies: the age-related eye disease study. *PLoS ONE* 3:e3813. <doi:10.1371/journal.pone.0003813>
- Espinosa-Heidmann DG, Suner IJ, Catanuto P et al (2006) Cigarette smoke-related oxidants and the development of sub-RPE deposits in an experimental animal model of dry AMD. *Invest Ophthalmol Vis Sci* 47:729–737
- Finnemann SC, Leung LW, Rodriguez-Boulan E (2002) The lipofuscin component A2E selectively inhibits phagolysosomal degradation of photoreceptor phospholipid by the retinal pigment epithelium. *Proc Natl Acad Sci U S A* 99:3842–3847
- Hadziahmetovic M, Dentchev T, Song Y et al (2008) Ceruloplasmin/hephaestin knockout mice model morphologic and molecular features of AMD. *Invest Ophthalmol Vis Sci* 49:2728–2736
- Hageman GS, Anderson DH, Johnson LV, et al (2005) A common haplotype in the complement regulatory gene factor H (HF1/CFH) predisposes individuals to age-related macular degeneration. *Proc Natl Acad Sci U S A* 102:7227–7232
- Haines JL, Hauser MA, Schmidt S et al (2005) Complement factor H variant increases the risk of age-related macular degeneration. *Science* 308:419–421
- Klein RJ, Zeiss C, Chew EY et al (2005) Complement factor H polymorphism in age-related macular degeneration. *Science* 308:385–389
- Lakkaraju A, Finnemann SC, Rodriguez-Boulan E (2007) The lipofuscin fluorophore A2E perturbs cholesterol metabolism in retinal pigment epithelial cells. *Proc Natl Acad Sci USA* 104:11026–11031
- Lee AY, Kulkarni M, Fang AM et al (2010) The effect of genetic variants in SERPING1 on the risk of neovascular age-related macular degeneration. *Br J Ophthalmol* 94:915–917
- Mata NL, Tzekov RT, Liu X et al (2001) Delayed dark-adaptation and lipofuscin accumulation in *abcr+/-* mice: implications for involvement of ABCR in age-related macular degeneration. *Invest Ophthalmol Vis Sci* 42:1685–1690
- McKay GJ, Silvestri G, Patterson CC et al (2009) Further assessment of the complement component 2 and factor B region associated with age-related macular degeneration. *Invest Ophthalmol Vis Sci* 50:533–539
- Mulligan RM, Atkinson C, Vertegel AA et al (2009) Cigarette smoke extract stimulates interleukin-8 production in human airway epithelium and is attenuated by superoxide dismutase in vitro. *Am J Rhinol Allergy* 23:1–4
- Pangburn MK (2000) Host recognition and target differentiation by factor H, a regulator of the alternative pathway of complement. *Immunopharmacology* 49:149–157
- Rohrer B, Long Q, Coughlin B et al (2009) A Targeted Inhibitor of the Alternative Complement Pathway Reduces Angiogenesis in a Mouse Model of Age-related Macular Degeneration. *Invest Ophthalmol Vis Sci* 50:3056–3064
- Saint-Geniez M, Maharaj AS, Walshe TE et al (2008) Endogenous VEGF is required for visual function: evidence for a survival role on Muller cells and photoreceptors. *PLoS ONE* 3:e3554
- Schmidt S, Hauser MA, Scott WK et al (2006) Cigarette smoking strongly modifies the association of LOC387715 and age-related macular degeneration. *Am J Hum Genet* 78:852–864
- Snodderly DM (1995) Evidence for protection against age-related macular degeneration by carotenoids and antioxidant vitamins. *Am J Clin Nutr* 62:1448S–1461S
- Sparrow JR, Fishkin N, Zhou J et al (2003) A2E, a byproduct of the visual cycle. *Vision Res* 43:2983–2990
- Suner IJ, Espinosa-Heidmann DG, Marin-Castano ME et al (2004) Nicotine increases size and severity of experimental choroidal neovascularization. *Invest Ophthalmol Vis Sci* 45:311–317
- Suter M, Reme C, Grimm C et al (2000) Age-related macular degeneration. The lipofuscin component N-retinyl-N-retinylidene ethanolamine detaches proapoptotic proteins from mitochondria and induces apoptosis in mammalian retinal pigment epithelial cells. *J Biol Chem* 275:39625–39630

- Takeuchi A, Takeuchi M, Oikawa K et al (2009) Effects of dioxin on vascular endothelial growth factor (VEGF) production in the retina associated with choroidal neovascularization. *Invest Ophthalmol Vis Sci* 50:3410–3416
- Thurman JM, Renner B, Kunchithapautham K et al (2010) Aseptic injury to epithelial cells alters cell surface complement regulation in a tissue specific fashion. *Adv Exp Med Biol* 664:151–158
- Thurman JM, Renner B, Kunchithapautham K et al (2009) Oxidative Stress Renders Retinal Pigment Epithelial Cells Susceptible to Complement-mediated Injury. *J Biol Chem* 284:16939–16947
- van Wijngaarden P, Qureshi SH (2008) Inhibitors of vascular endothelial growth factor (VEGF) in the management of neovascular age-related macular degeneration: a review of current practice. *Clin Exp Optom* 91:427–437
- Vives-Bauza C, Anand M, Shirazi AK et al (2008) The age lipid A2E and mitochondrial dysfunction synergistically impair phagocytosis by retinal pigment epithelial cells. *J Biol Chem* 283:24770–24780
- Voloboueva LA, Killilea DW, Atamna H et al (2007) N-tert-butyl hydroxylamine, a mitochondrial antioxidant, protects human retinal pigment epithelial cells from iron overload: relevance to macular degeneration. *FASEB J* 21:4077–4086
- Wang AL, Lukas TJ, Yuan M et al (2009) Changes in retinal pigment epithelium related to cigarette smoke: possible relevance to smoking as a risk factor for age-related macular degeneration. *PLoS ONE* 4:e5304. <doi:10.1371/journal.pone.0005304>
- Wong RW, Richa DC, Hahn P et al (2007) Iron toxicity as a potential factor in AMD. *Retina* 27:997–1003

Chapter 5

Complement Activation in Retinal Degeneration

Matt Rutar, Riccardo Natoli, Jan Provis, and Krisztina Valter

Keywords Retina • Retinal degeneration • Inflammation • Complement system • Light damage • Hyperoxia • P23H

5.1 Introduction

The complement system is a component of the innate arm of the immune response which provides a rapid host defence against a range of immunological challenges. Through a cascade of enzymatic cleavages culminating chiefly in the deposition of complement component 3 (C3) on activating surfaces, the activity of complement enhances the ability of the host to initiate defence against infection, and clear immune complexes, apoptotic cells and other noxious substances (Gasque 2004).

M. Rutar (✉) • K. Valter

Departments of Research School of Biology, ARC Centre of Excellence in Vision Science, The Australian National University, RN Robertson Bldg, Sullivan's Creek Rd, Canberra, ACT 0200, Australia

ARC Centre of Excellence in Vision Science, The Australian National University, Canberra, ACT 0200, Australia
e-mail: matt.rutar@rsbs.anu.edu.au

R. Natoli

ANU Medical School, The Australian National University, Canberra, ACT 0200, Australia

J. Provis

Departments of Research School of Biology, ARC Centre of Excellence in Vision Science, The Australian National University, RN Robertson Bldg, Sullivan's Creek Rd, Canberra, ACT 0200, Australia

ARC Centre of Excellence in Vision Science, The Australian National University, Canberra, ACT 0200, Australia

ANU Medical School, The Australian National University, Canberra, ACT 0200, Australia

If activated in an exaggerated and inappropriate manner, however, complement also has the capacity to destroy host tissue. Indeed, pathogenic complement activation is directly implicated in neuronal damage following intracerebral haemorrhage (Yang et al. 2006), and post-ischemic cerebral injury (Figueroa et al. 2005). Recently, complement activation has been found to play a role in age-related macular degeneration (AMD), a retinal disease affecting central vision and a leading cause of blindness in the western world. Gene association studies have identified a number of polymorphisms in complement genes, including CFH (Klein et al. 2005), CFB (Jakobsdottir et al. 2008), C2 (Jakobsdottir et al. 2008) and C3 (Yates et al. 2007; Despret et al. 2009), which are strongly associated with the incidence of AMD.

We aimed to investigate whether a common role of complement in retinal dystrophy exists, by comparing the expression of the central component C3 in conjunction with cell death in a range of mechanistically distinct degenerative models. These include acute degeneration induced through either excessive light or hyperoxia, and chronic degeneration using the retinitis pigmentosa-mimicking P23H-3 rodent strain.

5.2 Methods

In the light damage model, young adult albino Sprague Dawley (SD) rats were exposed to a light intensity of 1,000 lx for a period of up to 24 h, after which some animals were kept in dim light (5 lx) to recover. At specific time points during (1, 3, 6, 12, 17 and 24 h) and after exposure (3, and 7 days), animals were euthanized and retinas extracted for analysis of C3 mRNA expression, and for counts of apoptotic cells in the outer nuclear layer (ONL) using the TUNEL technique. In the hyperoxia model, adult C57 mice were subjected to 75% oxygen for up to 14 days. Animals were euthanized after 3, 7 and 14 days, whereby retinas were dissected for the analysis of C3 mRNA expression, and TUNEL. In the P23H model, animals from line 3 of this transgenic strain were born and reared until postnatal day 50–130. Age-matched, non-degenerative SD rodents served as the control tissue. At this time, animals were euthanized and retinas extracted for analysis of C3 mRNA expression and TUNEL. C3 mRNA expression levels were determined by quantitative PCR (qPCR), where the assessment of the relative fold change was determined using the $\Delta\Delta C^q$, with GAPDH serving as the reference gene.

5.3 Results

In light-induced degeneration, qPCR results show that expression levels of complement C3 in the retina (Fig. 5.1) increased significantly over the course of 24 h bright light and continued to increase robustly into the post-exposure period to reach a peak differential expression of 1,038% compared to dim-reared animals. Photoreceptor death (TUNEL) dramatically increased by 24 h bright light exposure,

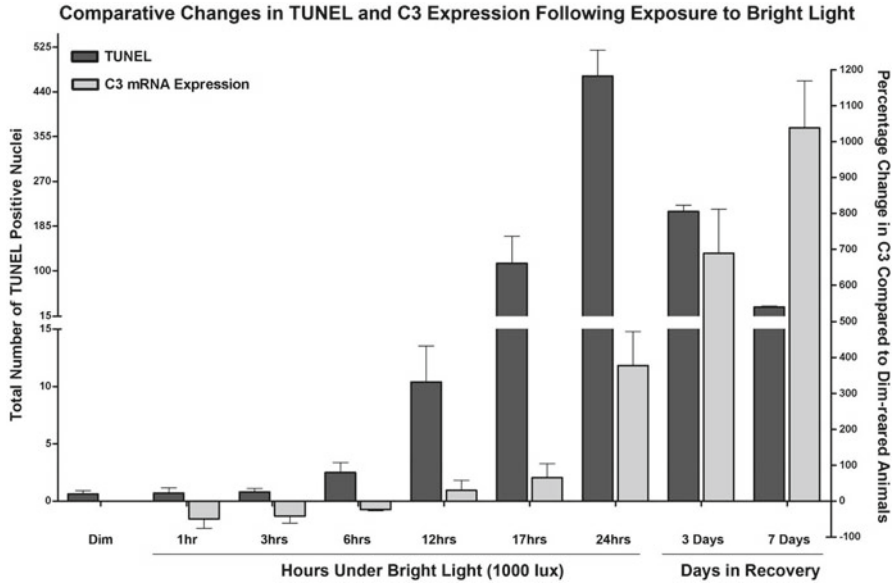


Fig. 5.1 C3 mRNA expression and TUNEL frequency during and following exposure to 1000 lx light. C3 expression during light damage showed a marked up-regulation by 24 h of exposure, which increased further in the ensuing post-exposure period. The number of TUNEL positive nuclei increased dramatically after 24 h of exposure, coinciding with the increase in C3 expression. In the post exposure period, cell death tapered off rapidly though persisted at a relatively low level after 7 days

consistent with the onset of C3 upregulation over the same period (Fig. 5.1). During exposure to hyperoxia, the expression of C3 did not increase after 3 and 7 days (Fig. 5.2). By 14 days, however, C3 expression increased to 180% compared to control animals. The number of TUNEL-positive photoreceptors increased moderately after 7 days hyperoxia, followed by a dramatic increase by 14 days (Fig. 5.2); coinciding with the upregulation of C3. In the retinas of P23H rats, an increase of 80% in C3 expression compared to SD rats was observed, while photoreceptor death was found to be higher in the P23H strain than the SD (Fig. 5.3).

5.4 Discussion

Our results indicate that while the degenerative stimuli in these models differ, an increased expression of C3 mRNA – which fuels the complement cascade – occurs in close association with substantial increases in photoreceptor cell death. Correspondingly, we provide evidence for a common pathway in retinal degeneration involving the activation of complement in response to the induction of photoreceptor injury and death. Our data are consistent with the implication of the

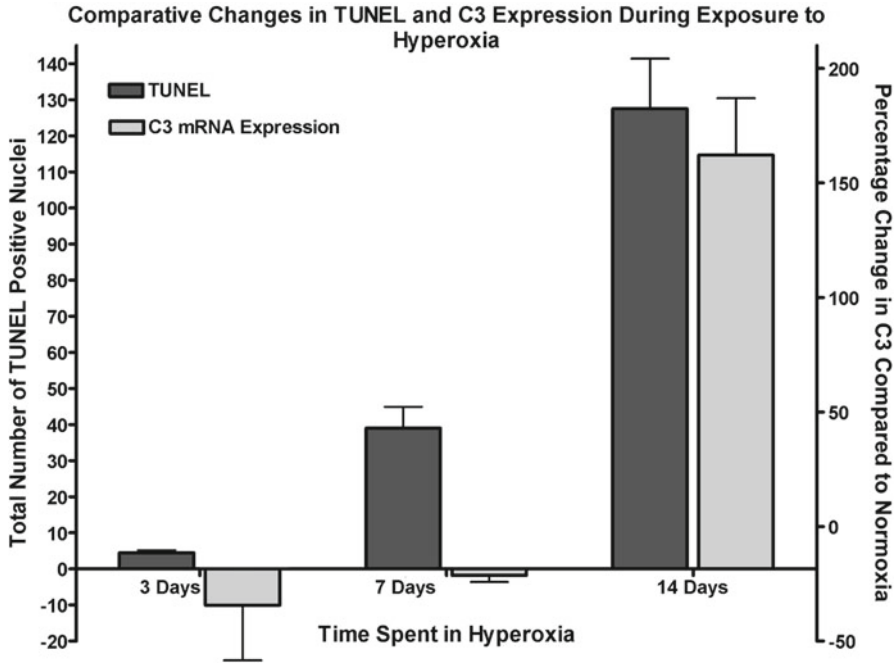


Fig. 5.2 C3 mRNA expression and TUNEL frequency in retinas during exposure to hyperoxia. No increase in C3 expression was evident during the early phases of hyperoxia, although this progressed to a substantial up-regulation by 14 days. A steady increase in TUNEL positive cells was apparent over the 14-day time course, reaching a peak at 14 days hyperoxia

complement system in the clearance of noxious substances, such as apoptotic cells (Gasque 2004; Trouw et al. 2008); which suggests that complement activation is geared toward a beneficial role in the maintenance of retinal homeostasis. This is at odds, however, with the association of complement with the incidence of AMD (Anderson et al. 2010). One explanation is that while complement may be activated to necessitate the efficient clearance of noxious substances, its exaggerated activation in the injured retina – aided by an abundance of apoptotic cells and other activating surfaces – induces further retinal degeneration through propagating an inappropriate inflammatory response (Walport 2001). Indeed, a recent investigation by Rohrer and colleagues has shown that complement activation exacerbates photoreceptor death in light-induced retinal degeneration (Rohrer et al. 2007). While direct evidence for complement-induced pathology in hyperoxia and the degenerative P23H strain are currently lacking, increased synthesis in C3 expression in both models following degeneration – consistent with light damage – supports the existence of a common detrimental role of complement activation in retinal degeneration. Consequently, anticomplement strategies may have a broad therapeutic potential in the treatment of various forms of retinal degeneration.

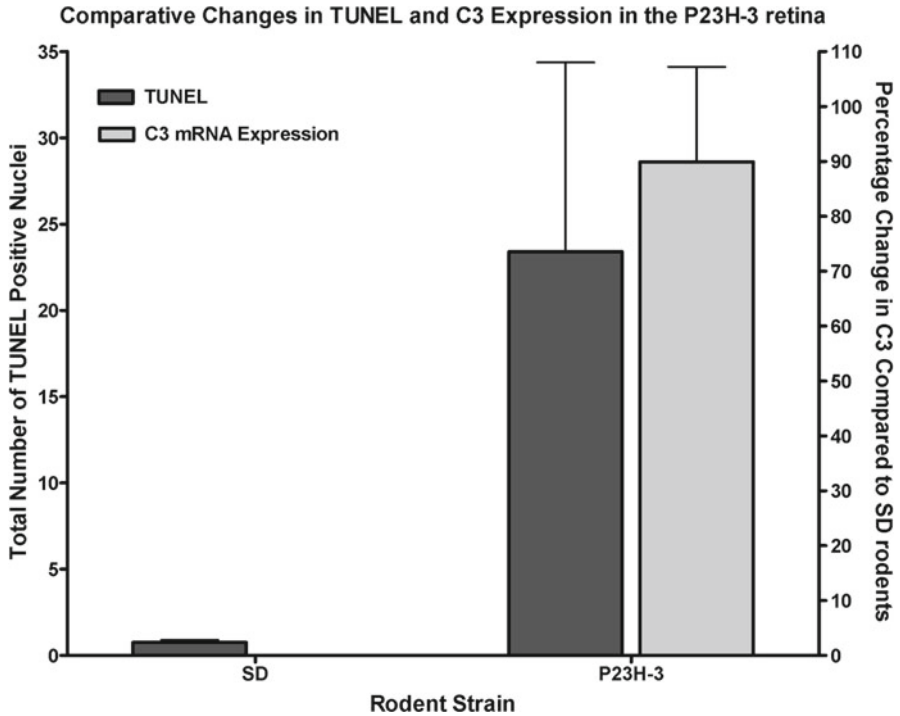


Fig. 5.3 C3 mRNA expression and TUNEL frequency in retinas from SD and degenerative P23H-3 rodents. C3 expression was elevated in retinas from P23H-3 animals compared to those of the SD strain. TUNEL analysis indicated an increase photoreceptor apoptosis in the P23H-3 retina compared to the SD – as expected for this degenerative strain

References

- Anderson DH, Radeke MJ, Gallo NB et al (2010) The pivotal role of the complement system in aging and age-related macular degeneration: Hypothesis re-visited. *Prog Retin Eye Res* 29:95–112
- Despriet DD, van Duijn CM, Oostra BA, et al (2009) Complement component C3 and risk of age-related macular degeneration. *Ophthalmology* 116:474–480 e472
- Figueroa E, Gordon LE, Feldhoff PW et al (2005) The administration of cobra venom factor reduces post-ischemic cerebral injury in adult and neonatal rats. *Neurosci Lett* 380:48–53
- Gasque P (2004) Complement: a unique innate immune sensor for danger signals. *Mol Immunol* 41:1089–1098
- Jakobsdottir J, Conley YP, Weeks DE et al (2008) C2 and CFB genes in age-related maculopathy and joint action with CFH and LOC387715 genes. *PLoS One* 3:e2199.
- Klein RJ, Zeiss C, Chew EY et al (2005) Complement factor H polymorphism in age-related macular degeneration. *Science* 308:385–389
- Rohrer B, Guo Y, Kunchithapautham K et al (2007) Eliminating complement Factor D reduces photoreceptor susceptibility to light-induced damage. *Invest Ophthalmol Vis Sci* 48: 5282–5289

- Trouw LA, Blom AM, Gasque P (2008) Role of complement and complement regulators in the removal of apoptotic cells. *Mol Immunol* 45:1199–1207
- Walport MJ (2001) Complement: Second of two parts. *N Eng J Med* 344:1140–1144
- Yang S, Nakamura T, Hua Y et al (2006) The role of complement C3 in intracerebral hemorrhage-induced brain injury. *J Cereb Blood Flow Metab* 26:1490–1495
- Yates JR, Sepp T, Matharu BK et al (2007) Complement C3 variant and the risk of age-related macular degeneration. *N Engl J Med* 357:553–561

Chapter 6

Microglia in the Outer Retina and Their Relevance to Pathogenesis of Age-Related Macular Degeneration

Wenxin Ma, Lian Zhao, and Wai T. Wong

Keywords Microglia • Retinal pigment epithelium • Age-related macular degeneration • Inflammation • Cell–cell interactions • Angiogenesis • Cytokines • Chemokines

6.1 Introduction

Age-related macular degeneration (AMD), the leading cause of legal blindness in the elderly in the industrialized world (Klein et al. 1997; Friedman et al. 2004), is a disease whose pathogenesis remains unclear (Zarbin 2004). Although multiple mechanisms are likely to contribute to the onset and progression of AMD, the role of inflammation has been given much consideration in the etiology of AMD (Donoso et al. 2006; Augustin and Kirchhof 2009). However, the nature of the immune cell interactions that drive cellular and tissue changes in AMD remain incompletely understood.

Retinal microglia are the primary immune cell type in the retina and comprise a population of resident cells normally present in the retina (Provis et al. 1996). Distributed in a regular array throughout the inner retina, retinal microglia, through their dynamic process movements, carry out constant and dynamic immune surveillance of the extracellular environment (Lee et al. 2008), and can respond rapidly to tissue injury by altering their activation state, acquiring capabilities of migration and proliferation, and secreting inflammatory mediators and neurotrophic agents (Hanisch and Kettenmann 2007). Found throughout the CNS, microglia are capable of carrying out diverse sets of housekeeping functions under normal conditions and

W. Ma • L. Zhao • W.T. Wong (✉)

Unit on Neuron–Glia Interactions in Retinal Disease, National Eye Institute,
6 Center Drive, Building 6, Room 215, Bethesda, MD 20892, USA
e-mail: wongw@nei.nih.gov

also executing adaptive functions under conditions of tissue injury (Ransohoff and Perry 2009). However, maladaptive inflammatory responses of microglia have been implicated in the progression of various chronic neurodegenerative diseases including Alzheimer's disease and Parkinson's disease (Brown 2009; Lucin and Wyss-Coray 2009). In the retina, how microglia may contribute to the pathogenesis of AMD is a subject of interest and an area of investigation in our laboratory.

6.2 AMD Pathology in the Retinochoroidal Interface

It has been well established that the locus of AMD is situated in the outer retina, in particular the retinochoroidal interface. The hallmarks of early and intermediate AMD include drusen, which are located between Bruch's membrane and the retinal pigment epithelial (RPE) layer (Green and Key 1977), and pigmentary changes, which are composed of RPE hyperplasia and atrophy (Green 1999). The lesions of advanced AMD are also in the same locus; the atrophic form of advanced AMD (or geographic atrophy) is defined by photoreceptor and RPE atrophy (Sarks et al. 1988), while the exudative (or "wet") form involves choroidal neovascularization (CNV) which extends through Bruch's membrane into the sub-RPE and subretinal space (Green 1999). Recent studies have also highlighted the presence of drusenoid deposits located within the subretinal space adjacent to the apical surface of RPE cells (Rudolf et al. 2008). These deposits, which form part of early/intermediate AMD, are clinically visible as reticular drusen (Zweifel et al. 2010a) and may be associated with advancement of AMD (Cohen et al. 2007; Zweifel et al. 2010b). The location of these AMD-associated lesions indicates that cellular interactions that drive their formation and progression are also likely to be located in the region of the RPE, subretinal space, and sub-RPE space.

In the young healthy retina, microglia are found distributed in regular horizontal arrays in the inner retina, with their ramified processes concentrated in the inner plexiform layer (IPL) and the outer plexiform layer (OPL) (Provis et al. 1996; Santos et al. 2008). Interestingly, retinal microglia are notably excluded from the outer nuclear layer and subretinal space, indicating that the outer retina may be distinguished as a specialized zone of particular immune privilege (Streilein et al. 2002). Under normal conditions, the outer retina, for reasons that are unclear, appears to be exempt from direct immune surveillance by resident microglia, which occupy the inner retina and much of the entire CNS. How this peculiar microglia-free zone is maintained in the outer retina, and what functional implication this entails are unknown but are likely to be important in the processes of neuroimmune regulation required by the specialized environment of the retinochoroidal interface.

The normal distribution of retinal microglia is, however, perturbed under conditions of advanced age and pathology. In the aged retina, microglia are found to be displaced in increasing numbers into the subretinal space, acquiring morphological and immunohistochemical features of activation (Xu et al. 2008, 2009). In histopathological specimens of AMD, retinal microglia have also been found in contact

with drusenoid deposits (unpublished data) and in association with advanced AMD lesions (Gupta et al. 2003). Also, in genetic mouse models of AMD, in which chemokine ligands/receptors, CX3CR1 and/or CCL2 have been genetically ablated, activated microglia have also been found to accumulate in the subretinal space and become associated with drusen-like accumulations, RPE degeneration, photoreceptor atrophy, and CNV (Combadiere et al. 2007; Tuo et al. 2007). The age-related accumulation of microglia in the outer retina and the association between AMD-associated lesions and displaced microglia in both mouse models and human disease give rise to the hypothesis that altered microglial distribution in the outer retina perturbs tissue homeostasis and promotes chronic neuroinflammation, leading eventually to alterations that constitute AMD advancement.

6.3 Microglia–RPE Interactions in the Outer Retina

We hypothesize that the presence of displaced and activated microglia in the outer retina results in altered cellular interactions that help drive AMD pathogenesis and progression. In addressing this hypothesis, we have investigated in particular the nature of microglia–RPE cell interactions in this context. RPE cells and microglia are normally found in anatomically disparate locations but become uniquely juxtaposed in senescent and pathological situations. Although epithelial in nature, RPE cells play significant immune regulatory roles (Holtkamp et al. 2001) and alterations in RPE structure constitute hallmark lesions in both early and advanced AMD. Thus, contact between microglia and RPE cells in pathological situations may result in cell–cell interactions relevant to the inflammatory etiology of AMD.

We explored the nature of microglia-induced effects on RPE cells by using: (1) an *in vitro* co-culture model in which cultured murine retinal microglia, before and after activation with lipopolysaccharide (LPS), were co-cultured with primary murine RPE cells, and (2) an *in vivo* model of microglia transplantation in which cultured activated murine retinal microglia were transplanted into the subretinal space, adjacent to the RPE layer. We found that activated retinal microglia induced multiple structural and functional alterations in primary RPE cells. RPE cells upon exposure to activated microglia decreased their expression levels of the visual cycle protein, RPE65, and also tight-junctional proteins (ZO-1 and claudin-1) (Ma et al. 2009). In both *in vitro* and *in vivo* models, RPE cells, under the influence of activated microglia, also exhibited a loss of tight-junction contacts, becoming more disorganized and haphazard in distribution. These RPE changes may be analogous to alterations seen in early/intermediate AMD, where RPE hypertrophy and disorganization in the form of pigment clumping are described, and constitute a separate risk factor for AMD advancement (Ferris et al. 2005).

We observed that on exposure to activated microglia, RPE cells *in vitro* altered their gene expression in significant ways (Ma et al. 2009). RPE cell expression levels of chemotactic cytokines (CCL2, CCL5, SDF-1), which are capable of attracting immune cells, and adhesion molecules (VCAM-1 and ICAM-1), which are capable

of retaining immune cells, were both increased. Functionally, supernatants from exposed RPE cultures were capable of inducing increased microglia migration in *in vitro* assays compared to controls. *In vivo*, activated microglia transplanted into the subretinal space were also associated with the displacement of endogenous microglia from the inner retina to the outer retina. These data suggested the possibility of a positive feedback mechanism in which subretinal microglia induces changes in RPE cell gene expression which in turn produces a more chemoattractive environment in the outer retina for the attraction and retention of additional microglia that can further influence RPE cells. This progressive accumulation of subretinal microglia may incrementally abrogate the immune privileged environment of the outer retina, promoting processes of chronic neuroinflammation relevant for AMD pathogenesis.

Lastly, RPE cells under the influence of activated microglia also expressed higher levels of proinflammatory cytokines (IL-1 β , TNF- α , IL-6) and pro-angiogenic molecules such as VEGF and metalloproteinases (MMP-1, -2, -9). Supernatants from exposed RPE cultures were found to promote higher levels of angiogenesis in several *in vitro* assays (endothelial proliferation assay, endothelial migration assay, and aortic ring assay) compared to controls. Significantly, transplantation of activated microglia into the subretinal space also markedly promoted the growth of choroidal vessels into the area of subretinal microglial transplantation in the form of CNV. These results indicated that RPE cells, under the inductive influence of subretinal microglia, may be altered significantly in both function and structure so as to promote a more pro-inflammatory, pro-angiogenic environment in the outer retina that encourages that formation of CNV, a hallmark lesion of advanced “wet” AMD.

6.4 Therapeutic Perspectives

Advancements in the treatment of AMD have occurred in recent years but many therapeutic challenges remain. Comprehensive prevention measures for early and advanced AMD are lacking, and there is still no proven treatment for advanced atrophic AMD. Current anti-VEGF therapies for advanced “wet” AMD have markedly improved visual outcomes but are not without their limitations (Mousa and Mousa 2010a, b). While multiple molecules and mechanisms have been implicated in AMD pathogenesis (Zarbin and Rosenfeld 2010), the cellular mechanisms at play in the locus of AMD disease are still incompletely understood. We posit that microglia-induced influences in the retinochoroidal interface may be of pathogenic significance and the inhibition of these influences represents a potential therapeutic strategy. A more comprehensive understanding of the factors that influence (1) the initial displacement of microglia into the outer retina, (2) the activation of microglia in the outer retina, (3) the increasing recruitment of microglia with age and disease, and (4) the cellular interactions that microglia have with photoreceptors and RPE cells, will be helpful in elucidation of the retinal cell biology underlying AMD and in the design of future treatments.

References

- Augustin AJ, Kirchhof J (2009) Inflammation and the pathogenesis of age-related macular degeneration. *Expert Opin Ther Targets* 13:641–651
- Brown DR (2009) Role of microglia in age-related changes to the nervous system. *ScientificWorld Journal* 9:1061–1071
- Cohen SY, Dubois L, Tadayoni R et al (2007) Prevalence of reticular pseudodrusen in age-related macular degeneration with newly diagnosed choroidal neovascularisation. *Br J Ophthalmol* 91:354–359
- Combadiere C, Feumi C, Raoul W et al (2007) CX3CR1-dependent subretinal microglia cell accumulation is associated with cardinal features of age-related macular degeneration. *J Clin Invest* 117:2920–2928
- Donoso LA, Kim D, Frost A et al (2006) The role of inflammation in the pathogenesis of age-related macular degeneration. *Surv Ophthalmol* 51:137–152
- Ferris FL, Davis MD, Clemons TE et al (2005) A simplified severity scale for age-related macular degeneration: AREDS Report No. 18. *Arch Ophthalmol* 123:1570–1574
- Friedman DS, O'Colmain BJ, Munoz B et al (2004) Prevalence of age-related macular degeneration in the United States. *Arch Ophthalmol* 122:564–572
- Green WR (1999) Histopathology of age-related macular degeneration. *Mol Vis* 5:27
- Green WR, Key SN, 3rd (1977) Senile macular degeneration: a histopathologic study. *Trans Am Ophthalmol Soc* 75:180–254
- Gupta N, Brown KE, Milam AH (2003) Activated microglia in human retinitis pigmentosa, late-onset retinal degeneration, and age-related macular degeneration. *Exp Eye Res* 76:463–471
- Hanisch UK, Kettenmann H (2007) Microglia: active sensor and versatile effector cells in the normal and pathologic brain. *Nat Neurosci* 10:1387–1394
- Holtkamp GM, Kijlstra A, Peek R et al (2001) Retinal pigment epithelium-immune system interactions: cytokine production and cytokine-induced changes. *Prog Retin Eye Res* 20:29–48
- Klein R, Klein BE, Jensen SC et al (1997) The five-year incidence and progression of age-related maculopathy: the Beaver Dam Eye Study. *Ophthalmology* 104:7–21
- Lee JE, Liang KJ, Fariss RN et al (2008) Ex vivo dynamic imaging of retinal microglia using time-lapse confocal microscopy. *Invest Ophthalmol Vis Sci* 49:4169–4176
- Lucin KM, Wyss-Coray T (2009) Immune activation in brain aging and neurodegeneration: too much or too little? *Neuron* 64:110–122
- Ma W, Zhao L, Fontainhas AM et al (2009) Microglia in the mouse retina alter the structure and function of retinal pigmented epithelial cells: a potential cellular interaction relevant to AMD. *PLoS One* 4:e7945
- Mousa SA, Mousa SS (2010) Current status of vascular endothelial growth factor inhibition in age-related macular degeneration. *BioDrugs* 24:183–194
- Provis JM, Diaz CM, Penfold PL (1996) Microglia in human retina: a heterogeneous population with distinct ontogenies. *Perspect Dev Neurobiol* 3:213–222
- Ransohoff RM, Perry VH (2009) Microglial physiology: unique stimuli, specialized responses. *Annu Rev Immunol* 27:119–145
- Rudolf M, Malek G, Messinger JD et al (2008) Sub-retinal drusenoid deposits in human retina: organization and composition. *Exp Eye Res* 87:402–408
- Santos AM, Calvente R, Tassi M et al (2008) Embryonic and postnatal development of microglial cells in the mouse retina. *J Comp Neurol* 506:224–239
- Sarks JP, Sarks SH, Killingsworth MC (1988) Evolution of geographic atrophy of the retinal pigment epithelium. *Eye* 2 (Pt 5):552–577
- Streilein JW, Ma N, Wenkel H et al (2002) Immunobiology and privilege of neuronal retina and pigment epithelium transplants. *Vision Res* 42:487–495
- Tuo J, Bojanowski CM, Zhou M et al (2007) Murine *ccl2/cx3cr1* deficiency results in retinal lesions mimicking human age-related macular degeneration. *Invest Ophthalmol Vis Sci* 48:3827–3836

- Xu H, Chen M, Forrester JV (2009) Para-inflammation in the aging retina. *Prog Retin Eye Res* 28:348–368
- Xu H, Chen M, Manivannan A et al (2008) Age-dependent accumulation of lipofuscin in perivascular and subretinal microglia in experimental mice. *Aging Cell* 7:58–68
- Zarbin MA (2004) Current concepts in the pathogenesis of age-related macular degeneration. *Arch Ophthalmol* 122:598–614
- Zarbin MA, Rosenfeld PJ (2010) Pathway-based therapies for age-related macular degeneration: an integrated survey of emerging treatment alternatives. *Retina* 30:1350–1367
- Zweifel SA, Spaide RF, Curcio CA et al (2010a) Reticular pseudodrusen are subretinal drusenoid deposits. *Ophthalmology* 117:303–312 e301
- Zweifel SA, Imamura Y, Spaide TC et al (2010b) Prevalence and significance of subretinal drusenoid deposits (reticular pseudodrusen) in age-related macular degeneration. *Ophthalmology* 117:1775–1781

Chapter 7

Lutein or Zeaxanthin Supplementation Suppresses Inflammatory Responses in Retinal Pigment Epithelial Cells and Macrophages

Qingning Bian, Tingyu Qin, Zhihong Ren, Dayong Wu, and Fu Shang

Keywords Lutein • Zeaxanthin • IL-6 • IL-8 • TNF α • Inflammation • RPE • Macrophage

7.1 Introduction

Age-related macular degeneration (AMD) is a multifactorial disease and the leading cause of blindness in industrialized countries. In addition to aging, genetic background and cigarette smoking, dietary factors also contribute to the onset and progression of AMD (Bernstein 2009). A growing number of studies indicate that dietary lutein and zeaxanthin play significant protective roles against visual loss from AMD. The epidemiological evidence for the protective effect of lutein and zeaxanthin was first obtained from a large case-control study, which showed that individuals with high dietary intakes and high serum levels of lutein and zeaxanthin have a much lower rate of exudative AMD (Seddon et al. 1994). Results from many, but not all, subsequent epidemiologic and case-control studies support the conclusion that the risk for onset and progression of AMD is inversely related to lutein and zeaxanthin concentrations in the diet, plasma, and macular pigment. In typical American diets, the content of lutein is ~5 times that of zeaxanthin. The ratio of lutein to zeaxanthin in human blood is similar to that found in typical American diets, indicating that lutein and zeaxanthin are equally absorbed by humans. However, it appears that zeaxanthin preferentially accumulates in the retina, particularly in the macular region (Snodderly 1995).

Oxidative stress, particularly lipofuscin-mediated photooxidative damage, contributes to the onset and progress of AMD (Sparrow and Boulton 2005). It is thought

Q. Bian • T. Qin • Z. Ren • D. Wu • F. Shang (✉)
Jean Mayer USDA Human Nutrition Research Center on Aging,
Tufts University, 711 Washington Street, Boston, MA 02111, USA
e-mail: fu.shang@tufts.edu

that lutein and zeaxanthin in the retina may protect against AMD by two different mechanisms, as a blue light blocker and antioxidant. Both lutein and zeaxanthin absorb blue light, the most phototoxic light to which the retina is routinely exposed. Studies in quail provide direct evidence that long-term zeaxanthin supplementation results in an increase in retinal zeaxanthin concentrations and provides a protective effect against light-induced photoreceptor death (Thomson et al. 2002a, b). Lutein and zeaxanthin are also efficient quenchers of singlet oxygen and related reactive oxygen species (Yeum et al. 2003; Li et al. 2010). The high concentration of lutein and zeaxanthin in the retina may protect retina and RPE against photooxidative damage by blocking blue light and/or by quenching singlet oxygen produced by photoreactions.

Recent studies indicate that innate immunity and inflammation play a role in AMD pathogenesis (Anderson et al. 2010; Patel and Chan 2008). The evidence for the involvement of innate immunity and inflammation in AMD pathogenesis includes accumulation of immunoglobulin and complement components in drusen, the association between genetic variants of complement factor H, factor B, C2, C3, factor I and risk for AMD, and elevated serum CRP levels in AMD patients. Emerging evidence indicates dietary lutein plays a role in controlling inflammatory responses, including a reduction of serum levels of CRP and SICAM (van Herpen-Broekmans et al. 2004; Koutsof et al. 2006; Seddon et al. 2006; Hozawa et al. 2007). Based on this information, we propose that lutein and zeaxanthin may reduce the risk for AMD via suppression of ocular or systemic inflammation. To begin to test this hypothesis, we investigated the effects of lutein and zeaxanthin supplementation on expression of pro-inflammatory cytokines in cultured RPE and macrophages.

7.2 Materials and Methods

7.2.1 Materials

Lutein for dietary supplementation (5% lutein beadlet) was obtained from Kemin (Des Moines, IA, USA). Zeaxanthin for dietary supplementation (5% zeaxanthin beadlet) was obtained from ZeaVision (Chesterfield, MO, USA). Pure lutein and zeaxanthin for cell culture experiments were obtained from kemin or purchased from Sigma Aldrich (St. Louis, MO, USA), respectively. Cell culture supplies were obtained from Invitrogen (Carlsbad, CA, USA). The DuoSet ELISA kits for human IL-6, human IL-8, mouse IL-6, and mouse TNF α were obtained from R&D Systems (Minneapolis, MN, USA).

7.2.2 Experiments with Animals

All animal procedures were performed according to the guidelines of the ARVO statement for the “Use of Animals in Ophthalmic and Vision Research” and were approved by the Institutional Animal Care and Use Committee. C57BL mice at

3 months of age, the mice were divided into five groups, six mice in each group. Group 1 was fed a semi-purified diet (AIN-93M) which contains no detectable amount of lutein or zeaxanthin but with the same amounts of beadlets. Groups 2 and 3 were fed the AIN-93M diet containing 0.02 and 0.1% lutein, respectively. Groups 4 and 5 were fed the AIN-93M diet containing 0.02 and 0.1% zeaxanthin, respectively. After 3 months on these diets, the mice were killed and macrophages were isolated by peritoneal lavage as described previously (Wu et al. 2003).

7.2.3 Cell Culture and Treatments

Confluent ARPE-19 cells were first incubated with 0, 1, and 10 μM lutein or zeaxanthin for 3 days. Then the cells were stimulated with 0.5 $\mu\text{g}/\text{mL}$ LPS for 8 h in fresh DMEM supplemented with 10% FBS. The media were collected to measure levels of IL-6 and IL-8. Primary mouse macrophages were cultured in the presence or absence of the indicated concentrations of lutein or zeaxanthin in RPMI 1640 medium overnight and then stimulated with 5 $\mu\text{g}/\text{mL}$ LPS in fresh medium for 8 h, and the medium was collected to measure levels of IL-6 and TNF α . Levels of IL-6, IL-8, and TNF α in the medium were determined by ELISA using the DuoSet ELISA kits obtained from R&D Systems. All ELISA were performed according to the manufacturer's instructions.

7.3 Results

7.3.1 Supplementation with Lutein or Zeaxanthin to RPE Reduces Basal Level and LPS-Induced Secretion of IL-6 and IL-8

Recent studies indicate that ocular or systemic inflammation may play a role in the pathogenesis of AMD. To explore the potential mechanism by which dietary lutein and zeaxanthin may protect the retina and RPE via modulating ocular inflammation, we evaluated the effects of lutein or zeaxanthin supplementation on secretion of pro-inflammatory cytokines in cultured RPE. As shown in Fig. 7.1, cultured RPE secrete significant levels of IL-6 and IL-8 even under resting conditions. Stimulation with LPS increased the production of IL-6 and IL-8 tenfold. Supplementation with lutein to cultured RPE cells reduced the basal and LPS-induced production of IL-6 and IL-8 in a dose-dependent manner (Fig. 7.1). In contrast, supplementation with zeaxanthin to cultured RPE did not suppress the production of IL-6 (Fig. 7.2a). In fact, supplementation with lower levels of zeaxanthin (1 μM) to RPE enhanced the production of IL-6 under experimental condition. However, supplementation with zeaxanthin to cultured RPE reduced the secretion of IL-8 (Fig. 7.2b). These data

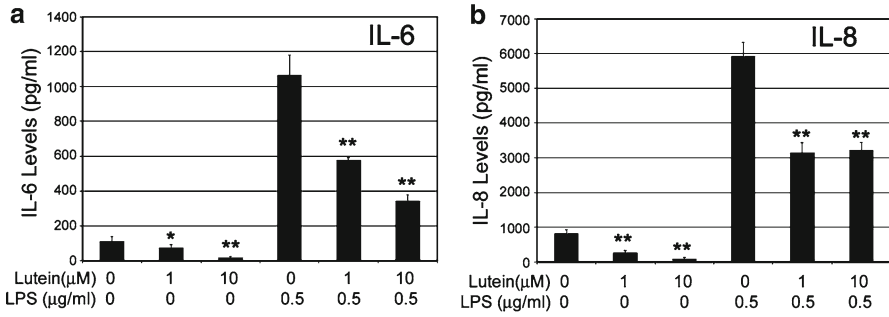


Fig. 7.1 Supplementation of lutein to cultured RPE reduces the production of IL-6 and IL-8. panel **a**: IL-6; panel **b**: IL-8; Data presented are means ± SD of 3 independent experiments. * $p < 0.05$; ** $p < 0.01$ as compared to controls

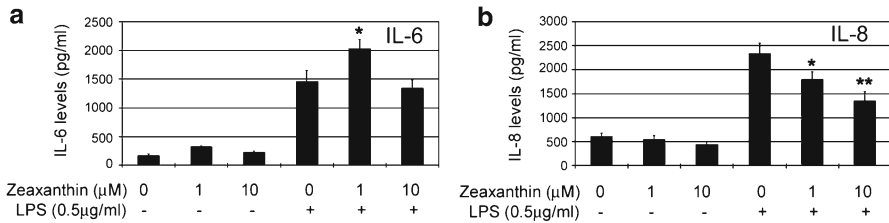


Fig. 7.2 Supplementation of zeaxanthin to cultured RPE reduces the production of IL-8 but not IL-6. panel **a**: IL-6; panel **b**: IL-8; Data presented are means ± SD of 3 independent experiments. * $p < 0.05$; ** $p < 0.01$ as compared to controls

indicate that both lutein and zeaxanthin suppress the production of IL-8 by cultured RPE, but only lutein suppressed the expression of IL-6, indicating that the production of IL-6 and IL-8 by RPE is differentially regulated.

7.3.2 Lutein Supplementation to Primary Macrophage Cultures Suppresses LPS-Induced Secretion of IL-6 and TNFα

To explore role of lutein and zeaxanthin in modulating systemic inflammation, we investigated the effects of lutein and zeaxanthin supplementation on the production of IL-6 and TNFα by primary murine macrophages. Primary macrophages produced very low levels of IL-6 and TNFα in the absence of stimuli. Supplementation with lutein and zeaxanthin had no detectable effects on IL-6 and TNFα secretion by resting macrophages (data not shown). After stimulation with LPS for 8 h, a large quantity of IL-6 and TNFα were produced. Similar to that observed in cultured RPE, supplementation of macrophages with lutein reduced LPS-induced production

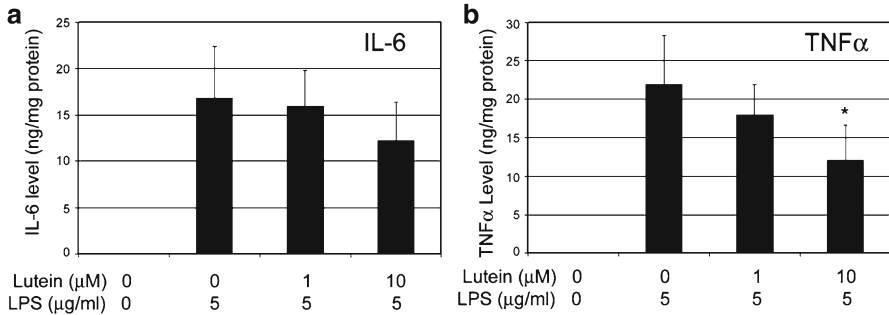


Fig. 7.3 Supplementation of lutein to primary murine macrophages reduces LPS-induced production of IL-6 and TNF α . panel **a**: IL-6; panel **b**: TNF α . Data presented are means \pm SD of six independent experiments. * p < 0.05 as compared to controls

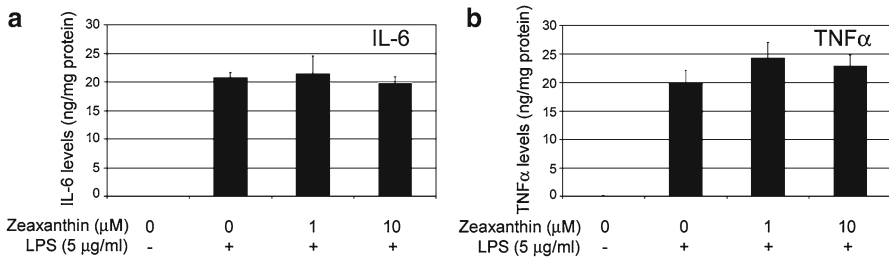


Fig. 7.4 Supplementation of zeaxanthin to primary murine macrophages has no effects on LPS-induced production of IL-6 and TNF α . Panel **a**: IL-6; panel **b**: TNF α . Data presented are means \pm SD of six independent experiments

of IL-6, but the reduction was not statistically significant (Fig. 7.3a). Supplementation with lutein suppressed the LPS-induced production of TNF α in a dose-dependent manner (Fig. 7.3b). However, supplementation of macrophages with zeaxanthin had no detectable effects on LPS-induced secretion of IL-6 and TNF α (Fig. 7.4).

7.3.3 Macrophages Isolated from Lutein or Zeaxanthin Supplemented Mice Produce Less IL-6 and TNF α upon LPS Stimulation

To test the effects of dietary lutein and zeaxanthin supplementation on systemic inflammation *in vivo*, C57BL mice were fed diets containing 0, 0.02, and 0.1% of lutein or zeaxanthin for 3 months. Macrophages were isolated by peritoneal lavage and cultured in the presence of 5 μ g/mL LPS for 16 h. Levels of IL-6 and TNF α in

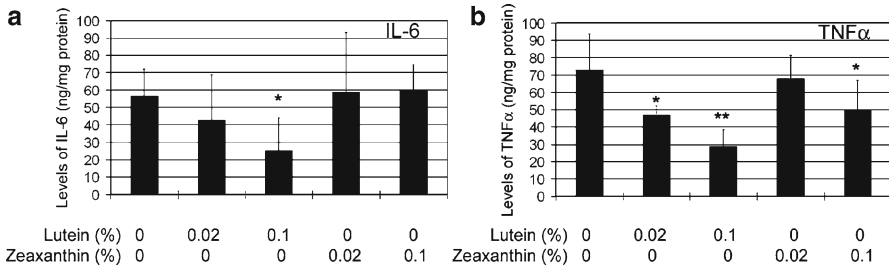


Fig. 7.5 Dietary lutein and zeaxanthin supplementation reduces LPS-induced expression of IL-6 and TNF α by macrophages. Panel **a**: IL-6; panel **b**: TNF α . The data are mean \pm SD of the results from five mice in each group. * $p < 0.05$; ** $p < 0.01$ as compared the control

the medium were determined. As shown in Fig. 7.5, macrophages isolated from control mice secreted the highest amount of IL-6 and TNF α . Macrophages isolated from lutein supplemented mice secreted significantly less IL-6 (Fig. 7.5a) and TNF α (Fig. 7.5b) as compared to the controls. Similar to the results of the in vitro supplementation experiments, the effects of lutein on IL-6 and TNF α secretion were dose dependent (Fig. 7.5). Although dietary zeaxanthin had no detectable effect on IL-6 secretion by macrophages (Fig. 7.5a), the levels of TNF α secreted by macrophages were reduced by dietary zeaxanthin supplementation (Fig. 7.5b).

7.4 Discussion

As in many other age-related diseases, the pathogenesis of AMD is closely related to systemic or local inflammation. Our previous study showed that RPE secretes various pro-inflammatory cytokines in response to inflammatory stimuli or oxidative stress (Fernandes et al. 2006; 2008, 2009), suggesting that RPE is a source of inflammation mediators. It is known that macrophage is a major source of pro-inflammatory cytokines. Data from this study suggest that lutein or zeaxanthin supplementation suppress ocular or systemic inflammation via reducing the production of pro-inflammatory cytokines by RPE and macrophages. We found that supplementation of lutein to cultured RPE suppressed the secretion of both IL-6 and IL-8 (Fig. 7.1). However, supplementation of zeaxanthin to cultured RPE only suppressed the secretion of IL-8, but not IL-6 (Fig. 7.2). Supplementation of the lutein to primary cultured macrophages also reduced the secretion of IL-6 and TNF α (Fig. 7.3), but supplementation of the same levels of zeaxanthin to macrophages had no detectable effects on IL-6 and TNF α secretion. Dietary supplementation of the lutein also reduced the production of IL-6 and TNF α by macrophages upon LPS-stimulation (Fig. 7.5). However, dietary zeaxanthin supplementation only suppressed the production of TNF α , not IL-6, by macrophages. Together, these data suggest that both

lutein and zeaxanthin suppress secretion of pro-inflammatory cytokines by RPE or macrophages in response to inflammatory stimuli although their effects on different cytokine are not the same.

Acknowledgments We thank Kemin Industries and ZeaVison for providing lutein and zeaxanthin for dietary supplementation experiments. This work is supported by USDA AFRI Award 2009-35200-05014, NIH grant EY 011717, USDA contract 1950-510000-060-01A, and Dennis L. Gierhart Charitable Gift.

References

- Anderson DH, Radeke MJ, Gallo NB et al (2010) The pivotal role of the complement system in aging and age-related macular degeneration: hypothesis re-visited. *Prog Retin Eye Res* 29:95–112
- Bernstein PS (2009) Nutritional Interventions against Age-Related Macular Degeneration. *Acta Hort* 841:103–112
- Fernandes AF, Bian Q, Jiang JK et al (2009) Proteasome inactivation promotes p38 mitogen-activated protein kinase-dependent phosphatidylinositol 3-kinase activation and increases interleukin-8 production in retinal pigment epithelial cells. *Mol Biol Cell* 20:3690–3699
- Fernandes AF, Guo W, Zhang X et al (2006) Proteasome-dependent regulation of signal transduction in retinal pigment epithelial cells. *Exp Eye Res*
- Fernandes AF, Zhou J, Zhang X et al (2008) Oxidative inactivation of the proteasome in retinal pigment epithelial cells. A potential link between oxidative stress and up-regulation of interleukin-8. *J Biol Chem* 283:20745–20753
- Hozawa A, Jacobs DR, Jr., Steffes MW et al (2007) Relationships of circulating carotenoid concentrations with several markers of inflammation, oxidative stress, and endothelial dysfunction: the Coronary Artery Risk Development in Young Adults (CARDIA)/Young Adult Longitudinal Trends in Antioxidants (YALTA) study. *Clin Chem* 53:447–455
- Koutsos EA, Garcia Lopez JC, Klasing KC (2006) Carotenoids from in ovo or dietary sources blunt systemic indices of the inflammatory response in growing chicks (*Gallus gallus domesticus*). *J Nutr* 136:1027–1031
- Li B, Ahmed F, Bernstein PS (2010) Studies on the singlet oxygen scavenging mechanism of human macular pigment. *Arch Biochem Biophys* 504:56–60
- Patel M, Chan CC (2008) Immunopathological aspects of age-related macular degeneration. *Semin Immunopathol* 30:97–110
- Seddon JM, Gensler G, Klein ML et al (2006) C-reactive protein and homocysteine are associated with dietary and behavioral risk factors for age-related macular degeneration. *Nutrition* 22:441–443
- Seddon JM, Ajani UA, Sperduto RD et al (1994) Dietary carotenoids, vitamins A, C, and E, and advanced age-related macular degeneration. Eye Disease Case-Control Study Group. *JAMA* 272:1413–1420
- Snodderly DM (1995) Evidence for protection against age-related macular degeneration by carotenoids and antioxidant vitamins. *Am J Clin Nutr* 62:1448 S-1461 S
- Sparrow JR, Boulton M (2005) RPE lipofuscin and its role in retinal pathobiology. *Exp Eye Res* 80:595–606
- Thomson LR, Toyoda Y, Delori FC et al (2002a) Long term dietary supplementation with zeaxanthin reduces photoreceptor death in light-damaged Japanese quail. *Exp Eye Res* 75:529–542
- Thomson LR, Toyoda Y, Langner A et al (2002b) Elevated retinal zeaxanthin and prevention of light-induced photoreceptor cell death in quail. *Invest Ophthalmol Vis Sci* 43:3538–3549

- van Herpen-Broekmans WM, Klopping-Ketelaars IA, Bots ML et al (2004) Serum carotenoids and vitamins in relation to markers of endothelial function and inflammation. *Eur J Epidemiol* 19:915–921
- Wu D, Marko M, Claycombe K et al (2003) Ceramide-induced and age-associated increase in macrophage COX-2 expression is mediated through up-regulation of NF-kappa B activity. *J Biol Chem* 278:10983–10992
- Yeum KJ, Aldini G, Chung HY et al (2003) The activities of antioxidant nutrients in human plasma depend on the localization of attacking radical species. *J Nutr* 133:2688–2691

Chapter 8

Exploring the Potential Role of the Oxidant-Activated Transcription Factor Aryl Hydrocarbon Receptor in the Pathogenesis of AMD

Goldis Malek, Mary Dwyer, and Donald McDonnell

Keywords Age-related macular degeneration • Oxidative stress • Retinal pigment epithelium • Mitochondria • Aryl hydrocarbon receptor

8.1 Introduction

Age-related macular degeneration (AMD) is the leading cause of central vision loss in the elderly population in industrialized nations (Ambati et al. 2003). The fundamental abnormalities occurring in the retinal pigment epithelial (RPE) cells leading to their progressive dysfunction and eventually atrophy in AMD is not known. Approximately 90% of patients with AMD have the early or dry subtype for which, currently, there are no treatment options available (Friedman et al. 2004; Klein et al. 2007; Ciulla and Rosenfeld 2009). Successful future treatments are dependent, in part, on understanding the molecular and biological mechanisms that contribute to RPE dysfunction.

AMD is a complex disease and much of what we know regarding its pathogenesis stems from morphological analysis of human tissue, genetic and epidemiologic studies highlighting risk factors associated with the disease. Morphologically, in early AMD lipid- and protein-rich extracellular deposits accumulate under the RPE, while geographic atrophy is characterized by large areas of RPE atrophy, and wet or exudative AMD is typified by endothelial invasion and pathological neovascularization under the retina (Bird et al. 1995). Genetic linkage and genome-wide association studies have identified polymorphisms in complement, mitochondrial

G. Malek (✉)

Department of Ophthalmology, Duke University, Durham, NC 27701, USA
e-mail: gmalek@duke.edu

M. Dwyer • D. McDonnell

Department of Pharmacology and Cancer Biology, Duke University, Durham, NC 27701, USA

and apolipoprotein E genes associated with AMD, just to name a few (Schmidt et al. 2002; Edwards et al. 2005; Fiotti et al. 2005; Hageman et al. 2005; Haines et al. 2005; Klein et al. 2005; Dewan et al. 2006; Yang et al. 2006; Ross et al. 2007; Canter et al. 2008). Most strikingly, among environmental risk factors, smoking is the single greatest environmental risk factor most consistently associated with incidence and prevalence of AMD (Coleman et al. 2008; Jager et al. 2008; Klein et al. 2008).

8.2 Oxidant Injury of RPE Cells Due to Cigarette Smoke

Cigarette smoke contains numerous cytotoxic substances including 2,3,7,8-tetrachlorodibenzo-p-dioxin (TCDD) and hydroquinone (Pryor 1997). Quinones, of which hydroquinone is the most abundant, are derivatives of (poly)aromatic phenols another major source of oxidants in cigarette smoke (Niki et al. 1993; Winston et al. 1993; Bolton et al. 2000). They are detectable in blood of smokers and are prominent chemical contaminants in automobile exhaust, industrial pollution, and the production of plastics. They have been identified as factors associated with and responsible for oxidative injury to the liver, blood vessels, and other target organs, and as such are reasonable surrogates for the actions of cigarette oxidants. In fact experimental studies investigating the effect of hydroquinone treatment of RPE cells have shown induction of cell blebbing (microvesicles containing actin, oxidative phosphorylation, and extracellular matrix regulating proteins (Alcazar et al. 2009)) and dysregulation of extracellular matrix production in vitro and sub-RPE deposit formation in vivo (Espinosa-Heidmann et al. 2006; Marin-Castano et al. 2006). Further evidence for the potential pathogenic role of cigarette smoking and oxidative stress in onset, progression, and severity of AMD stems from substantiating evidence in several epidemiological cohorts and animal model studies (Schmidt et al. 2005; Seddon et al. 2006; Jia et al. 2007). Though the pathogenic mechanisms through which oxidants compromise RPE function, contribute to deposit formation, and eventually result in RPE atrophy, are not fully elucidated, the effects of oxidant injury at the cellular level have been under investigation and points to a key role for mitochondrial dysfunction and reactive oxygen species (ROS) generation in RPE cells.

8.3 RPE Cellular Response to Oxidant Injury

The “response to injury hypothesis,” one pathogenic paradigm put forth for AMD biology, proposes that RPE cells are targets for specific injury stimuli, resulting in cellular responses including RPE mitochondrial damage and structural alterations implicated in deposit accumulation such as extracellular matrix dysregulation (Jarrett et al. 2008). That injury of mitochondria may create a vicious cycle promoting

disease is not surprising as they are the major source of endogenous ROS, converted from an estimated 1–2% of oxygen consumed (Chomyn and Attardi 2003; Cadenas and Davies 2000), causing oxidative damage to proteins, nucleic acids, and lipids in cells (Jarrett et al. 2008). The resulting superoxide and hydrogen peroxide can damage mitochondrial protein resulting in nuclear and mitochondrial genotoxicity and ultimately apoptosis (Lenaz 1998; Polster and Fiskum 2004). TCDD has been shown to damage mouse liver mitochondria and cause oxidative stress (Senft et al. 2002). The dioxin-mediated oxidative stress response includes increased ROS and hydrogen peroxide production, decreased mitochondrial membrane potential and activities of the antioxidant enzymes superoxide dismutase, catalase, glutathione peroxidase, and reductase, as well as a decrease in mitochondrial respiratory chain complexes II and IV activities (Aly and Domenech 2009), further supporting mitochondria as source of the oxidative stress response.

Evidence for mitochondrial dysfunction in AMD comes from genetic studies identifying a strong association between ARMS2 (AMD susceptibility 2), expressed in mitochondria, and AMD (Fritsche et al. 2008). Also, morphological studies show decreased mitochondrial density, loss of cristae, and changes in matrix density of RPE mitochondria in AMD samples (Feher et al. 2006). These mitochondrial alterations correlate with changes in redox proteins, proteins involved in mitochondrial trafficking and respiration, increased DNA damage, and decreased repair (Liang and Godley 2003; Godley et al. 2005). Finally, *in vivo* mitochondrial superoxide dismutase-2 knockdown results in focal sub-RPE deposits (Kasahara et al. 2005; Imamura et al. 2006) while overexpression protects against oxygen-induced apoptosis in RPE and retinal cells.

In our search for oxidant-activating signaling pathways that may drive dysregulation of mitochondrial function and cell metabolic pathways resulting in RPE injury, we identified the aryl hydrocarbon receptor (AhR) also referred to as the dioxin (TCDD) receptor.

8.4 Aryl Hydrocarbon Receptor

Nuclear receptors and transcription factors are important mediators of many systemic and age-related diseases (Landreth et al. 2008; Wang and Wan 2008; Robinson and Grieve 2009). The AhR is a ligand-activated member of the basic helix-loop-helix family of transcription factors that binds with high affinity to environmental toxins such as polycyclic aromatic hydrocarbons (PAH) including TCDD (Hankinson 1995). Most of the diverse biochemical, biological, and toxicological responses caused by exposure to PAHs are mediated, in part by AhRs. Upon binding and activation, AhR translocates from the cytoplasm to the nucleus, heterodimerizes with AhR nuclear translocator (ARNT), and activates the transcription of carcinogen- and estrogen-metabolism target genes such as members of the cytochrome P450s 1 family (CYP1), through xenobiotic response elements (Hankinson 1995). The CYP1 family including CYP1A and CYP1B is highly

active epoxigenases for oxidants as well as membrane lipids such as arachidonic acid and oxLDL, indicating that they may exert their biologic effects via the metabolism of both endogenous and foreign chemicals (Diani-Moore et al. 2006; Rifkind 2006). AhR activation has been shown to increase oxidative stress, mitochondrial respiration-dependent ROS (Senft et al. 2002). Furthermore, its activity is coupled with inflammation and apoptosis, matrix metabolism, and CD36 fatty acid metabolism, mechanisms also active in AMD biology. Overall, AhR functions can be classified into: (1) an *adaptive response* which results in the detoxification of toxicants by increased expression of toxin metabolizing enzymes which catalyze biotransformation and elimination of toxins within cells and (2) a *toxic response* through the induction of genes involved in metabolic activation of toxicants, resulting in formation of toxic metabolites and aberrant global changes in gene transcription within the cell.

8.4.1 AhR Regulates Cellular Oxidative Stress Response

AhR activation shifts the cellular redox state of cells toward oxidizing conditions, mediated in part by the induction of cytochrome P450 that exhibit loose coupling between oxygen and NADPH utilization and substrate oxidation (Dalton et al. 2002; Aly and Domenech 2009). Mitochondrial ROS production has been shown to be dependent on the AhR. AhR ligands such as TCDD can induce hepatic and extrahepatic oxidative stress and increase mitochondrial respiration-dependent ROS production. In AhR, CYP1A1 and CYP1B1 knockout mice following intraperitoneal treatment with dioxin, the level of H₂O₂ production was decreased by 75% compared to wild-type mice, independent of decreased levels of Mn²⁺ superoxide dismutase-2 or high levels of glutathione peroxidase, supporting that the supposition that induced mitochondrial reactive oxygen production is associated with a function of the AhR. Additionally, overexpression of superoxide dismutase and/or catalase in in vitro cultures exposed to BAP results in an increase in AhR protein, increase in AhR binding to the cytochrome p450 promoter, and decrease in BAP reactive intermediates (Wang et al. 2009).

8.4.2 AhR Regulates Proteosomal Degradation

The transcriptional regulatory system and the ubiquitin-proteasome system are two major target-selective systems that control intracellular protein levels. This target selectivity depends on the recognition of specific DNA elements by sequence-specific transcription factors and the recognition of degradation substrates by E3 ubiquitin ligases (Hershko and Ciechanover 1998). Recent reports have demonstrated that the AhR protein is rapidly downregulated (degraded)

following ligand binding. This downregulation is ubiquitin mediated and occurs via the 26S proteasome pathway following nuclear export of AhR (Pollenz 2002), further demonstrating that the proteolytic degradation of AhR is an important and established mechanism of regulating signal transduction pathways (Ohtake et al. 2007). A consequence of blocking AhR degradation in cell culture appears to be an increase in both the magnitude and duration of gene regulation by the AhR–ARNT complex. Therefore, it is plausible that part of the upregulation of AhR and its activity during the *toxic response* occurs due to impaired proteasomal degradation of the receptor. Furthermore, alterations in AhR’s ability to target proteins for proteosomal degradation through its ubiquitin ligase activity may be another mechanism by which AhR activation regulates lipid and protein deposit accumulation characteristic of dry AMD.

8.5 Potential Role for AhR in AMD Pathogenesis?

We have begun to investigate the AhR signaling pathway in ARPE19 cells. Recently, we showed that the AhR and its partner ARNT are expressed at high levels in three commonly used models for RPE including RPE isolated from adult human donor eyes (older than 65 years), primary RPE cells cultured from donor eyes, and ARPE19 cells (Fig. 8.1). Using a luciferase-based reporter assay (AhR.TR.luc and pCMV-pCMV- β -galactosidase normalization plasmids) (Karchner et al. 2009), we measured transcriptional activity of AhR following a 24-h treatment with toxicants found in cigarette smoke including TCDD, hydroquinone, nicotine, BAP, as well as β -naphthoflavone (β NF) a known pharmacological ligand for AhR. We found that cigarette toxicants increased activity of AhR significantly (Fig. 8.2a). β NF is an AhR antagonist and decreased AhR activity. We also saw significant upregulation of

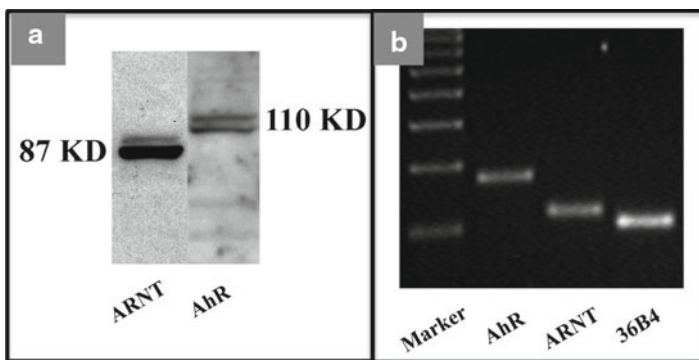


Fig. 8.1 ARPE19 cells express both AhR and its binding partner ARNT (a, protein, b, mRNA)

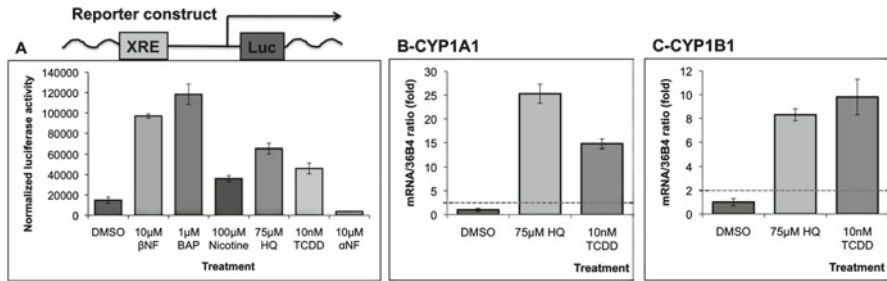


Fig. 8.2 AhR activation following treatment with cigarette smoke toxicants (BAP, nicotine, HQ, and TCDD), β NF an AhR agonist, and α NF an AhR antagonist (a) and AhR target gene expression of CYP1A1 (b) and CYP1B1 (c) in RPE cells treated with cigarette smoke toxicants. Data are \pm SEM, $n=4$

AhR target genes, toxin-metabolizing enzymes including CYP1A1, CYP1B1 (Fig. 8.2b, c), CYP2S1, and IL8 (not shown) supporting cigarette toxins as a relevant AhR ligands in RPE cells. Finally, silencing of AhR confirmed that treatment with toxins decreased target gene expression (not shown). Concentrations of oxidants used in our studies were sublethal and determined based on initial dose–response experiments. Selected doses did not change morphology or membrane permeability of RPE cells as determined by evaluating the tight junction marker, zonula occludens-1 immunocytochemistry and using lactate dehydrogenase assay (not shown). Although AhR is most well known for initiating the detoxifying response to dioxin and other environmental pollutants, this receptor regulates many other processes relevant to the biology of AMD. Our future studies will tease out the role of AhR in processes including matrix metabolism, energy metabolism, and fatty acid metabolism.

Acknowledgments This work was supported by a grant from the American Health Assistance Foundation (GM) and Research to Prevent Blindness.

References

- Alcazar O, Hawkrigde AM, Collier TS et al (2009) Proteomic characterization of cell membrane blebs in human retinal pigment epithelium cells. *Mol Cell Proteomics*
- Aly HA, Domenech O (2009) Cytotoxicity and mitochondrial dysfunction of 2,3,7,8-tetrachlorodibenzo-p-dioxin (TCDD) in isolated rat hepatocytes. *Toxicol Lett* 191:79–87
- Ambati J, Ambati BK, Yoo SH, Ianchulev S, Adamis AP (2003) Age-related macular degeneration: etiology, pathogenesis, and therapeutic strategies. *Surv Ophthalmol* 48:257–293
- Bird AC, Bressler NM, Bressler SB et al (1995) An international classification and grading system for age-related maculopathy and age-related macular degeneration. The International ARM Epidemiological Study Group. *Surv Ophthalmol* 39:367–374

- Bolton JL, Trush MA, Penning TM, Dryhurst G, Monks TJ (2000) Role of quinones in toxicology. *Chem Res Toxicol* 13:135–160
- Cadenas E, Davies KJ (2000) Mitochondrial free radical generation, oxidative stress, and aging. *Free Radic Biol Med* 29:222–230
- Canter JA, Olson LM, Spencer K et al (2008) Mitochondrial DNA polymorphism A4917G is independently associated with age-related macular degeneration. *PLoS ONE* 3:e2091
- Chomyn A, Attardi G (2003) MtDNA mutations in aging and apoptosis. *Biochem Biophys Res Commun* 304:519–529
- Ciulla TA, Rosenfeld PJ (2009) Antivasular endothelial growth factor therapy for neovascular age-related macular degeneration. *Curr Opin Ophthalmol* 20:158–165
- Coleman HR, Chan CC, Ferris FL, 3 rd, Chew EY (2008) Age-related macular degeneration. *Lancet* 372:1835–1845
- Dalton TP, Puga A, Shertzer HG (2002) Induction of cellular oxidative stress by aryl hydrocarbon receptor activation. *Chem Biol Interact* 141:77–95
- Dewan A, Liu M, Hartman S et al (2006) HTRA1 promoter polymorphism in wet age-related macular degeneration. *Science* 314:989–992
- Diani-Moore S, Papachristou F, Labitzke E, Rifkind AB (2006) Induction of CYP1A and cyp2-mediated arachidonic acid epoxygenation and suppression of 20-hydroxyeicosatetraenoic acid by imidazole derivatives including the aromatase inhibitor vorozole. *Drug Metab Dispos* 34:1376–1385
- Edwards AO, Ritter R, 3 rd, Abel KJ, Manning A, Panhuysen C, Farrer LA (2005) Complement factor H polymorphism and age-related macular degeneration. *Science* 308:421–424
- Espinosa-Heidmann DG, Suner JJ, Catanuto P et al (2006) Cigarette smoke-related oxidants and the development of sub-RPE deposits in an experimental animal model of dry AMD. *Invest Ophthalmol Vis Sci* 47:729–737
- Feher J, Kovacs I, Artico M et al (2006) Mitochondrial alterations of retinal pigment epithelium in age-related macular degeneration. *Neurobiol Aging* 27:983–993
- Fiotti N, Pedio M, Battaglia Parodi M et al (2005) MMP-9 microsatellite polymorphism and susceptibility to exudative form of age-related macular degeneration. *Genet Med* 7:272–277
- Friedman DS, O'Colmain BJ, Munoz B et al (2004) Prevalence of age-related macular degeneration in the United States. *Arch Ophthalmol* 122:564–572
- Fritsche LG, Loenhardt T, Janssen A et al (2008) Age-related macular degeneration is associated with an unstable ARMS2 (LOC387715) mRNA. *Nat Genet* 40:892–896
- Godley BF, Shamsi FA, Liang FQ et al (2005) Blue light induces mitochondrial DNA damage and free radical production in epithelial cells. *J Biol Chem* 280:21061–21066
- Hageman GS et al (2005) A common haplotype in the complement regulatory gene factor H (HF1/CFH) predisposes individuals to age-related macular degeneration. *Proc Natl Acad Sci U S A* 102:7227–7232
- Haines JL, Hauser MA, Schmidt S et al (2005) Complement factor H variant increases the risk of age-related macular degeneration. *Science* 308:419–421
- Hankinson O (1995) The aryl hydrocarbon receptor complex. *Annu Rev Pharmacol Toxicol* 35:307–340
- Hershko A, Ciechanover A (1998) The ubiquitin system. *Annu Rev Biochem* 67:425–479
- Imamura Y, Noda S, Hashizume K et al (2006) Drusen, choroidal neovascularization, and retinal pigment epithelium dysfunction in SOD1-deficient mice: a model of age-related macular degeneration. *Proc Natl Acad Sci U S A* 103:11282–11287
- Jager RD, Mieler WF, Miller JW (2008) Age-related macular degeneration. *N Engl J Med* 358:2606–2617
- Jarrett S, Lin H, Godley B, Boulton M (2008) Mitochondrial DNA damage and its potential role in retinal degeneration. *Prog Retin Eye Res* 27:596–607
- Jia L, Liu Z, Sun L et al (2007) Acrolein, a toxicant in cigarette smoke, causes oxidative damage and mitochondrial dysfunction in RPE cells: protection by (R)-alpha-lipoic acid. *Invest Ophthalmol Vis Sci* 48:339–348

- Karchner SI, Jenny MJ, Tarrant AM et al (2009) The active form of human aryl hydrocarbon receptor (AHR) repressor lacks exon 8, and its Pro 185 and Ala 185 variants repress both AHR and hypoxia-inducible factor. *Mol Cell Biol* 29:3465–3477
- Kasahara E, Lin LR, Ho YS, Reddy VN (2005) SOD2 protects against oxidation-induced apoptosis in mouse retinal pigment epithelium: implications for age-related macular degeneration. *Invest Ophthalmol Vis Sci* 46:3426–3434
- Klein R, Knudtson MD, Cruickshanks KJ, Klein BE (2008) Further observations on the association between smoking and the long-term incidence and progression of age-related macular degeneration: the Beaver Dam Eye Study. *Arch Ophthalmol* 126:115–121
- Klein R, Klein BE, Knudtson MD et al (2007) Fifteen-year cumulative incidence of age-related macular degeneration: the Beaver Dam Eye Study. *Ophthalmology* 114:253–262
- Klein RJ, Zeiss C, Chew EY et al (2005) Complement factor H polymorphism in age-related macular degeneration. *Science* 308:385–389
- Landreth G, Jiang Q, Mandrekar S, Heneka M (2008) PPAR γ agonists as therapeutics for the treatment of Alzheimer's disease. *Neurotherapeutics* 5:481–489
- Lenaz G (1998) Role of mitochondria in oxidative stress and ageing. *Biochim Biophys Acta* 1366:53–67
- Liang FQ, Godley BF (2003) Oxidative stress-induced mitochondrial DNA damage in human retinal pigment epithelial cells: a possible mechanism for RPE aging and age-related macular degeneration. *Exp Eye Res* 76:397–403
- Marin-Castano ME, Striker GE, Alcazar O, Catanuto P, Espinosa-Heidmann DG, Cousins SW (2006) Repetitive nonlethal oxidant injury to retinal pigment epithelium decreased extracellular matrix turnover in vitro and induced sub-RPE deposits in vivo. *Invest Ophthalmol Vis Sci* 47:4098–4112
- Niki E, Minamisawa S, Oikawa M, Komuro E (1993) Membrane damage from lipid oxidation induced by free radicals and cigarette smoke. *Ann N Y Acad Sci* 686:29–37. discussion 37–28
- Ohtake F, Baba A, Takada I et al (2007) Dioxin receptor is a ligand-dependent E3 ubiquitin ligase. *Nature* 446:562–566
- Pollenz RS (2002) The mechanism of AH receptor protein down-regulation (degradation) and its impact on AH receptor-mediated gene regulation. *Chem Biol Interact* 141:41–61
- Polster BM, Fiskum G (2004) Mitochondrial mechanisms of neural cell apoptosis. *J Neurochem* 90:1281–1289
- Pryor WA (1997) Cigarette smoke radicals and the role of free radicals in chemical carcinogenicity. *Environ Health Perspect* 105 Suppl 4:875–882
- Rifkind AB (2006) CYP1A in TCDD toxicity and in physiology—with particular reference to CYP dependent arachidonic acid metabolism and other endogenous substrates. *Drug Metab Rev* 38:291–335
- Robinson E, Grieve DJ (2009) Significance of peroxisome proliferator-activated receptors in the cardiovascular system in health and disease. *Pharmacol Ther* 122:246–263
- Ross RJ, Bojanowski CM, Wang JJ et al (2007) The LOC387715 polymorphism and age-related macular degeneration: replication in three case-control samples. *Invest Ophthalmol Vis Sci* 48:1128–1132
- Schmidt S, Haines JL, Postel EA et al (2005) Joint effects of smoking history and APOE genotypes in age-related macular degeneration. *Mol Vis* 11:941–949
- Schmidt S et al (2002) A pooled case-control study of the apolipoprotein E (APOE) gene in age-related maculopathy. *Ophthalmic Genet* 23:209–223
- Seddon JM, George S, Rosner B (2006) Cigarette smoking, fish consumption, omega-3 fatty acid intake, and associations with age-related macular degeneration: the US Twin Study of Age-Related Macular Degeneration. *Arch Ophthalmol* 124:995–1001
- Senft AP, Dalton TP, Nebert DW et al (2002) Mitochondrial reactive oxygen production is dependent on the aromatic hydrocarbon receptor. *Free Radic Biol Med* 33:1268–1278
- Wang K, Wan YJ (2008) Nuclear receptors and inflammatory diseases. *Exp Biol Med* (Maywood) 233:496–506

- Wang Z, Yang H, Ramesh A et al (2009) Overexpression of Cu/Zn-superoxide dismutase and/or catalase accelerates benzo(a)pyrene detoxification by upregulation of the aryl hydrocarbon receptor in mouse endothelial cells. *Free Radic Biol Med* 47:1221–1229
- Winston GW, Church DF, Cueto R, Pryor WA (1993) Oxygen consumption and oxyradical production from microsomal reduction of aqueous extracts of cigarette tar. *Arch Biochem Biophys* 304: 371–378
- Yang Z, Camp NJ, Sun H et al (2006) A variant of the HTRA1 gene increases susceptibility to age-related macular degeneration. *Science* 314:992–993

Chapter 9

Common Mechanisms for Separate Maculopathies?

Elod Kortvely and Marius Ueffing

Keywords Maculopathy • Maculopathies • AMD • Familial • Sporadic • Lipid metabolism • Extracellular matrix • ECM • Complement • CFH • Risk factors

9.1 Introduction

The macula lutea is the most specialized and central part of the primate eye responsible for high acuity vision (Provis et al. 2005). It is characterized by high density of cone photoreceptors, reaching a peak concentration in the very center of the visual axis (foveola). The distinctive yellow coloration observed within this region is due to the presence of carotenoid pigments, which are thought to specifically provide protection to macular photoreceptors against high energy radiation (blue and UV light) and reactive oxygen species. In spite of high metabolic activity, retinal blood supply is restricted in the macular region, which implies that neurons populating this area rely on oxygen and nutrients delivered from remote choriocapillaris. Thus, the permeability of the blood-retinal barrier (including the capillaries) is a key factor ensuring proper metabolic support of the macula. The blockade of these conduits leads to starvation of photoreceptors and compromised clearance of waste products. Conversely, abnormal high flow rates can result in leaky capillaries that manifest as macular edema. Hence, the unique anatomical construction of the macula (i.e., the absence of capillaries on the visual axis) represents a tradeoff between outstanding performance and extreme vulnerability. Continuous perturbations in membrane permeability, protein and lipid turnover, and metabolic balance can lead to abnormal accumulation of extracellular debris, atrophy of retinal pigment epithelium (RPE) and photoreceptor cells, and gradual loss of central vision which hallmark maculopathies.

E. Kortvely (✉) • M. Ueffing
Division of Experimental Ophthalmology, University of Tuebingen,
Roentgenweg 11, Tuebingen, 72076, Germany
e-mail: eloed.koertvely@uni-tuebingen.de

9.2 Shared Protein Networks in Common and Rare Maculopathies

Recent results indicate the existence of a common underlying etiology connecting sporadic and familial (Mendelian) maculopathies (Kortvely et al. 2010). The resulting hypothesis of overlapping associated pathways and mechanisms was recently substantiated with the discovery that *TIMP-3* gene variants associate with AMD (Chen et al. 2010). Mutations in *TIMP-3* genes had previously been identified as causal for a rare autosomal dominant maculopathy called Sorsby's fundus dystrophy (Weber et al. 1994), demonstrating a clear connection between rare and frequent maculopathies. Understanding the context specific function of genes and pathways involved in rare macular disorders may thus provide clues to the molecular pathology of the far more common AMD. The aim here is to hypothesize and discuss putative common molecular mechanisms of diverse maculopathies, in order to improve and refine the current terminology and classification (Table 9.1).

Genetic analyses of maculopathies implicate more than 20 genes in the underlying pathomechanisms (Fig. 9.1). Strikingly, almost all of these proteins enter the secretory pathway, either as genuine-secreted proteins or as transmembrane proteins. Based on their functions, these proteins can be roughly divided into three major categories: (1) proteins involved in lipid metabolism, (2) extracellular matrix (ECM) proteins, and (3) components of the complement system. Accordingly, these findings suggest that three major pathways featuring extracellular elements contribute to the etiology of maculopathies.

Table 9.1 Different maculopathies may have overlapping pathogenesis. Some characteristic features are listed here

	Macular deposition	CNV	Onset	Inheritance
AMD	Large soft drusen (dry, wet)	present (wet)	>60	GP
PCV	Drusen may occur	peculiar	>50 (more women)	GP
SD	Drusen similar to AMD	scarring	>6 (may differ)	AR, AD
HJMD	Dystrophic drusen	absent	>20	AR
VMD	"Egg yolk" and "scrambled egg" drusen	may occur	varies	AD
SFD	Drusen, lipofuscin	may occur	>40	AD
DHRD	Drusen (honeycomb pattern)	may occur	>40	AD
L-ORMD	Drusen-like dots	may occur	>40	AD

AMD is often categorized into dry and wet forms based on the presence of choroidal neovascularization (CNV). The dry form is more prevalent among Caucasians, and it can be transformed to the more severe wet form. Interestingly, affected individuals in Asian populations often develop the wet form directly, without having the dry form first (Dewan et al. 2006). This manifestation is similar to that of "drusenless" PCV, and PCV and AMD were indeed found to share risk alleles (Imamura et al. 2010)

AMD age-related macular degeneration; *PCV* polypoidal choroidal vasculopathy; *SD* Stargardt disease; *HJMD* hypotrichosis with juvenile macular dystrophy; *VMD* vitelliform macular dystrophy (including Best disease); *SFD* Sorsby's fundus dystrophy; *DHRD* Doyne honeycomb retinal dystrophy; *L-ORMD* late-onset retinal macular degeneration; *GP* genetic predisposition; *AR* autosomal recessive; *AD* autosomal dominant

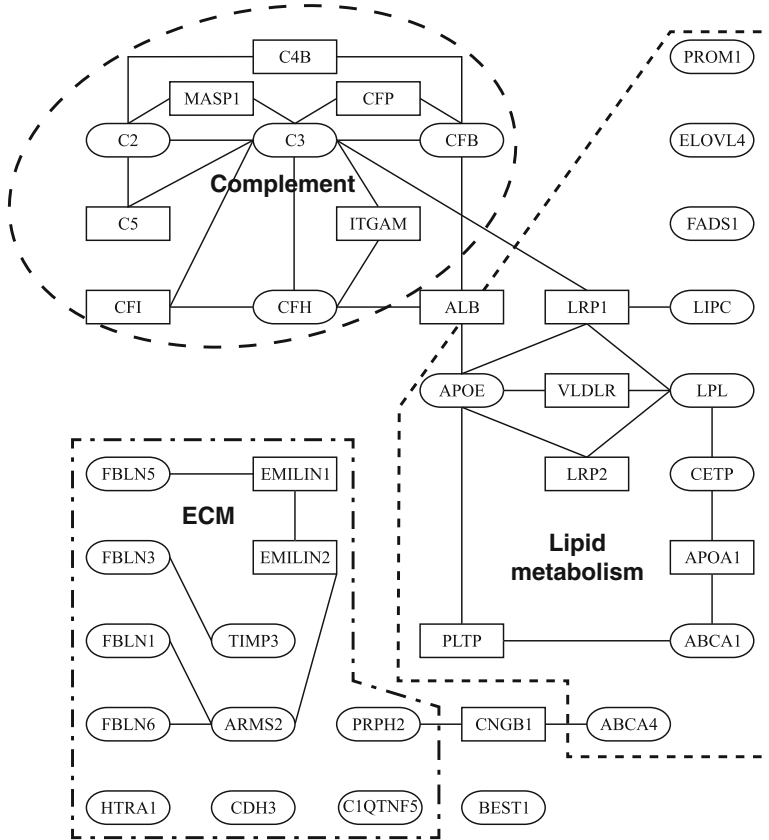


Fig. 9.1 Proteins implicated in maculopathies are in rounded corner boxes. Protein–protein interactions were analyzed using the POINeT tool (<http://poinet.bioinformatics.tw>). Dashed lines delineate three major functional categories. *ABCA1* and *4* ATP-binding cassette, subfamily A, member 1 and 4; *ALB* albumin; *APOA1* apolipoprotein A-I; *APOE* apolipoprotein E; *ARMS2* age-related maculopathy susceptibility 2; *BEST1* bestrophin 1; *C1QTNF5* C1q and tumor necrosis factor-related protein 5; *C2*, *C3*, *C4B*, *C5* complement components 2, 3, 4B, 5, respectively; *CDH3* cadherin 3, type 1, P-cadherin (placental); *CETP* cholesteryl ester transfer protein, plasma; *CFB*, *CFH*, *CFI* complement factor B, H, and I; *CFP* complement factor properdin; *CNGB1* cyclic nucleotide gated channel beta 1; *EFEMP1* (FBLN3) EGF-containing fibulin-like extracellular matrix protein 1; *ELOVL4* elongation of very long chain fatty acids (FEN1/Elo2, SUR4/Elo3, yeast)-like 4; *EMILIN1*, *2* elastin microfibril interfacer 1 and 2; *FADS1* fatty acid desaturase 1; *FBLN5* fibulin 5; *LIPC* lipase, hepatic; *HMCN1* (*FBLN6*) hemicentin 1; *HTRA1* HtrA serine peptidase 1; *ITGAM* integrin, alpha M (complement component 3 receptor 3 subunit); *LPL* lipoprotein lipase; *LRP1* and *2* low-density lipoprotein receptor-related protein 1 and 2; *PLTP* phospholipid transfer protein; *PROM1* prominin 1; *PRPH2* peripherin 2 (retinal degeneration, slow); *TIMP3* TIMP metalloproteinase inhibitor 3; *VLDLR* very low-density lipoprotein receptor

9.3 Pathomechanisms of Maculopathies, Modifiable Risk Factors

Although penetrance can be complete in certain Mendelian maculopathies (e.g., in L-ORMD, (Shu et al. 2006)), symptom development typically varies significantly among individuals carrying the same mutation or risk variant. Furthermore, the two eyes of the same person may be affected differentially, as is often seen in Best disease (Nordstrom and Thorburn 1980). This variability can be explained, at least in part, by different exposure to environmental risk factors. High body mass index (or serum cholesterol level) is a well-established modifiable risk factor for AMD (Reynolds et al. 2010). This observation can be easily fit into the “lipid branch” of the risk factors, as can the fact that drusen are very rich in lipids – further emphasizing the importance of lipid metabolism in the pathomechanism of various maculopathies (Curcio et al. 2010).

The best-studied environmental risk factor of AMD, however, is smoking, which is regarded as a general accelerator of aging (Bernhard et al. 2007). As elastic fibers seem to be the major target of smoke components (Just et al. 2007), smoking could be hypothesized as feeding into the “ECM branch.” In addition, smoking may exert its deleterious effects through an elevated level of oxidative stress. While oxidative stress is considered of primary importance in driving the aging process, recent results showed that antioxidant treatment does not result in extended lifespan (Perez et al. 2009). Specific vulnerability of the macula to reactive oxygen species would suggest that dysfunction of the corresponding radical scavenger system would principally damage this area. Instead, mutations in superoxide dismutase, an enzyme responsible for the elimination of reactive oxygen species, cause familial amyotrophic lateral sclerosis without affecting the macula. Furthermore, loss of function mutation of catalase (acatalasia), an enzyme catalyzing the decomposition of hydrogen peroxide, increases the prevalence of periodontal infection, but does not affect the visual system.

Are genetic and environmental risks interrelated? If any environmental risk would target or effect a sensitive and at the same time important physiological context, this combination of risks may multiply the impact of a single risk factor. In fact, proteins found to be associated with maculopathies can hint to the detrimental action of tobacco smoking as an agent accelerating elastolysis. Elastolysis caused by smoking affects tissue integrity also by reducing the elastic scaffold of the ECM. Looking at skin elasticity, continuous smoking can be seen with the naked eye. With Bruch’s membrane, the resultant wear and tear of the elastic components would lead to more subtle alterations in its microstructure and cause its physiological decay over time. This hypothesis is supported by two primary observations. First, smoking was found to promote the generation of elastin fragments (also called elastokines) in lung (Antonicelli et al. 2007). These fragments (1) display proangiogenic activity as potent as VEGF, and (2) initiate chronic inflammation through monocytes recruitment. Second, a large proportion of proteins implicated in maculopathies are known to associate with basement membranes and elastic fibers (Fig. 9.1). Taken together,

our hypothesis would associate the risk of smoking primarily to the “ECM branch” of maculopathy risk factors.

9.4 The Role of the Extracellular Matrix in the Pathomechanism of Maculopathies

We propose here a prominent role of ECM in the etiology of maculopathies. This hypothesis is supported by the following observations: (1) drusen, being a hallmark for many maculopathies, are extracellular structures, and (2) the Bruch’s membrane has a peculiar composition within the macular region, missing the middle elastic layer (Chong et al. 2005), and this thinning may pose yet unknown additional risks/benefits. The three fibulins found to be associated with different familial macular disorders (Fig. 9.1) suggest that this protein family is tightly linked to a joined pathomechanism of maculopathies. Fibulins contain nine members (Segade 2010). They are primarily known for their association with basement membranes and elastic fibers and play a role in elastogenesis and matrix–cell interaction (Yanagisawa and Davis 2010). In addition, compromised elastic fiber function becomes increasingly prevalent with age and contributes significantly to the burden of human morbidity and mortality (Robert et al. 2008).

ECM architecture and composition can determine the sites where lipid deposition can occur. Local concentrations of unstructured “amyloidogenic” monomers on membrane lattices are of primary importance for the initiation of cerebral neurodegenerative diseases (e.g., Alzheimer’s and Parkinson’s diseases, Fantini and Yahi 2010). Once disease progresses, membrane-bound monomers undergo a series of lipid-dependent conformational changes, leading to the formation of toxic oligomers. In age-related cerebral neurodegenerative diseases, compromised lipid metabolism contributes to disease. This is also true for several maculopathies. In fact, mutations in the *ABCA1* gene coding for the major cholesterol transporter are associated both with Alzheimer’s disease (Koldamova et al. 2010) and AMD (Chen et al. 2010). Deposited complement factors are present in drusen, as well as in senile plaques (Timmer et al. 2010), and CFH implicated in AMD (see below) is simultaneously a plasma biomarker for Alzheimer’s disease (Le Fur et al. 2010).

In fact, the association of CFH was the first genetic risk factor linked to sporadic AMD (Edwards et al. 2005). Under normal conditions, CFH is primarily involved in preventing complement activation, wherever endogenous membrane-bound complement regulators are absent (Kavanagh et al. 2008). Accordingly, cell-sparse structures (like the back of the retina) rely on the protection against complement cascade damage provided solely by CFH. This mechanism may establish a functional link between ECM and the complement system.

In summary, we hypothesize that compromised ECM at the macular region is the common denominator for various maculopathies: as a highly sensitive membrane for nutrient flow affected by aging and smoking, as a critical matrix site for lipid and protein turnover and deposition, and as a prime effector site of the complement system.

References

- Antonicevich F, Bellon G, DeBelle L et al (2007) Elastin-elastases and inflamm-aging. *Curr Top Dev Biol* 79:99–155
- Bernhard D, Moser C, Backovic A et al (2007) Cigarette smoke--an aging accelerator? *Exp Gerontol* 42:160–165
- Chen W, Stambolian D, Edwards AO et al (2010) Genetic variants near TIMP3 and high-density lipoprotein-associated loci influence susceptibility to age-related macular degeneration. *Proc Natl Acad Sci U S A* 107:7401–7406
- Chong NH, Keonin J, Luthert PJ et al (2005) Decreased thickness and integrity of the macular elastic layer of Bruch's membrane correspond to the distribution of lesions associated with age-related macular degeneration. *Am J Pathol* 166:241–251
- Curcio CA, Johnson M, Huang JD et al (2010) Apolipoprotein B-containing lipoproteins in retinal aging and age-related macular degeneration. *J Lipid Res* 51:451–467
- Dewan A, Liu M, Hartman S et al (2006) HTRA1 promoter polymorphism in wet age-related macular degeneration. *Science* 314:989–992
- Edwards AO, Ritter R, 3rd, Abel KJ et al (2005) Complement factor H polymorphism and age-related macular degeneration. *Science* 308:421–424
- Fantini J, Yahi N (2010) Molecular insights into amyloid regulation by membrane cholesterol and sphingolipids: common mechanisms in neurodegenerative diseases. *Expert Rev Mol Med* 12:e27
- Imamura Y, Engelbert M, Iida T et al (2010) Polypoidal choroidal vasculopathy: a review. *Surv Ophthalmol* 55:501–515
- Just M, Ribera M, Monso E et al (2007) Effect of smoking on skin elastic fibres: morphometric and immunohistochemical analysis. *Br J Dermatol* 156:85–91
- Kavanagh D, Richards A, Atkinson J (2008) Complement regulatory genes and hemolytic uremic syndromes. *Annu Rev Med* 59:293–309
- Koldamova R, Fitz NF, Lefterov I (2010) The role of ATP-binding cassette transporter A1 in Alzheimer's disease and neurodegeneration. *Biochim Biophys Acta* 1801:824–830
- Kortvely E, Hauck SM, Duetsch G et al (2010) ARMS2 is a constituent of the extracellular matrix providing a link between familial and sporadic age-related macular degenerations. *Invest Ophthalmol Vis Sci* 51:79–88
- Le Fur I, Laumet G, Richard F et al (2010) Association study of the CFH Y402H polymorphism with Alzheimer's disease. *Neurobiol Aging* 31:165–166
- Nordstrom S, Thorburn W (1980) Dominantly inherited macular degeneration (Best's disease) in a homozygous father with 11 children. *Clin Genet* 18:211–216
- Perez VI, Van Remmen H, Bokov A et al (2009) The overexpression of major antioxidant enzymes does not extend the lifespan of mice. *Aging Cell* 8:73–75
- Provis JM, Penfold PL, Cornish EE et al (2005) Anatomy and development of the macula: specialisation and the vulnerability to macular degeneration. *Clin Exp Optom* 88:269–281
- Reynolds R, Rosner B, Seddon JM (2010) Serum lipid biomarkers and hepatic lipase gene associations with age-related macular degeneration. *Ophthalmology* 117:1989–1995
- Robert L, Robert AM, Fulop T (2008) Rapid increase in human life expectancy: will it soon be limited by the aging of elastin? *Biogerontology* 9:119–133
- Segade F (2010) Molecular evolution of the fibulins: implications on the functionality of the elastic fibulins. *Gene* 464:17–31
- Shu X, Tulloch B, Lennon A et al (2006) Disease mechanisms in late-onset retinal macular degeneration associated with mutation in C1QTNF5. *Hum Mol Genet* 15:1680–1689
- Timmer NM, Kuiperij HB, de Waal RM et al (2010) Do Amyloid-beta-Associated Factors Co-deposit with Abeta in Mouse Models for Alzheimer's Disease? *J Alzheimers Dis*
- Weber BH, Vogt G, Pruett RC et al (1994) Mutations in the tissue inhibitor of metalloproteinases-3 (TIMP3) in patients with Sorsby's fundus dystrophy. *Nat Genet* 8:352–356
- Yanagisawa H, Davis EC (2010) Unraveling the mechanism of elastic fiber assembly: The roles of short fibulins. *Int J Biochem Cell Biol* 42:1084–1093

Chapter 10

The Role of Amyloid- β in Retinal Degeneration

Julien Bruban, Virginie Dinet, and Frédéric Mascarelli

Keywords AMD • Amyloid- β • Retina • Inflammation • Degeneration • Drusen • RPE • Cytotoxicity • Complement

10.1 Physiopathology of Age-Related Macular Degeneration

Age-related macular degeneration (AMD) is a retinal degenerative disease and the leading cause of irreversible vision loss in western countries (Klein et al. 2004). AMD is characterized by the increased formation of drusen, which are extracellular deposits located between the retinal pigment epithelium (RPE) and Bruch's membrane, subsequent disruption of the choroidal blood-eye barrier, and degeneration of photoreceptors. As AMD progresses, drusen typically increase in number and size, eventually compromising function of the RPE monolayer, which is considered to be the prime target of early-stage AMD. Late AMD has dry (atrophic) and wet (neovascular) forms. It has been hypothesized that the progressive loss of vision associated with the dry form is attributable to drusen accumulation (Green 1999). The first sign of wet AMD is serous or hemorrhagic fluid that causes the neuroretina or the RPE to detach from Bruch's membrane. AMD is a complex disease involving many genetic and environmental factors that may confound one another. Although the mechanisms of AMD are not yet clearly understood, several pathogenic pathways have been proposed, including RPE cell dysfunction, inflammatory processes, and oxidative stress (Ding et al. 2009). Though drusen are associated with the

J. Bruban (✉) • V. Dinet • F. Mascarelli
Centre de Recherche des Cordeliers, Université Pierre et Marie Curie – Paris 6,
UMRS 872, 15 rue de l'École de Médecine, Paris 75006, France
Université Paris Descartes, UMR872, Paris 75006, France
INSERM, UMR872, Paris 75006, France
e-mail: julien.bruban@exchange.mssm.edu

disorganization of the RPE and the reduction in photoreceptor cell densities, the relationship between drusen and retina degeneration remains elusive (Johnson et al. 2003).

10.2 Amyloid- β Is a Component of Drusen

Amyloid-beta ($A\beta$) peptides are formed after sequential cleavage of the amyloid precursor protein (APP). $A\beta$ is the main constituent of amyloid plaques in the brains of Alzheimer's disease (AD) patients, the most common form of dementia in the elderly and a progressive neurodegenerative disorder characterized by a decline in cognitive function (Selkoe 2001).

Several lines of evidence suggest that $A\beta$ is a potential trigger peptide for retinal degeneration. The observation of $A\beta$ within RPE cells and drusen in AMD patients is consistent with the hypothesis that the disease is mediated by oxidative/inflammatory stress (Mullins et al. 2000). $A\beta$ is associated with vesicular structures within drusen and the presence of $A\beta$ seems to be specific of drusen from retina of AMD patients (Johnson et al. 2002; Dentchev et al. 2003). Additionally, the number of amyloid assemblies within drusen seems to be positively correlated with confluence of these deposits in retina of AMD patients (Anderson et al. 2004). Nevertheless, these data are controversial since recent works by Luibl et al. albeit using a smaller sample of human donor eyes showed that $A\beta$ was found in the retina of AMD patients and healthy older people (Luibl et al. 2006). In that study, the authors also identified the drusen-associated amyloidogenic proteins as oligomers. Soluble amyloid oligomers may be the primary pathogenic structure in many age-related degenerative diseases (Glabe and Kaye 2006), yet the amyloid hypothesis of AD states that a build-up of $A\beta$ oligomers in the central nervous system is toxic and that $A\beta$ deposition contributes to neuronal apoptosis (Lambert et al. 1998). However, another recent study identified the drusen-associated amyloidogenic proteins as part of a wide spectrum of amyloid structures, including soluble mature fibrils (Isas et al. 2010). Importantly, the nature and the form of $A\beta$ in drusen have not been characterized in either the retina of healthy elderly or in the retina of patients with AMD.

10.3 Amyloid- β Impairs RPE Cell Structure and Function

Neprilysin (NEP) is the dominant $A\beta$ peptide-degrading enzyme in the brain (Iwata et al. 2000). In NEP gene-disrupted mice, the accumulation beneath the RPE layer of $A\beta$ -containing subepithelial deposits that resemble drusen accompanies some characteristic features of AMD, including RPE atrophy and disruption of RPE cell tight junctions. This suggests that $A\beta$ may be responsible for these features (Yoshida et al. 2005). In this study, the authors showed that the $A\beta(1-40)$ upregulates the expression of the proangiogenic vascular endothelial growth factor (VEGF)

and decreases the expression of the anti-angiogenic pigment epithelium-derived factor (PEDF) and the visual cycle protein cellular retinaldehyde-binding protein (CRALBP) in RPE cultures. That increase in VEGF expression is to compare with increased expression of VEGF-immunoreactivity after intravitreal injection of A β (1–42) in rat retina (Anderson et al. 2008). Moreover, ER (endoplasmic reticulum) stress induced by calcium disruption in RPE cells leads to an increased production of A β , which is associated to an increased production of VEGF, PEDF, and the proinflammatory cytokine TNF α (Koyama et al. 2008). These findings suggest that A β plays a role in the pathogenesis of AMD, a hypothesis reinforced by the study of Luibl et al. (2006), which showed that the soluble oligomeric form of A β (1–40) reduces the viability of RPE cells in cultures. Recently, we demonstrated that oxidative stress-induced premature senescence of RPE cells produces these features (Glotin et al. 2008). A particularly striking one is amyloidogenesis, which involves overexpression of APP and β -secretase 1, and oversecretion of A β (1–42). More recently, we showed that the oligomeric form of A β (1–42) increased the production of reactive oxygen species in RPE cells, induced a disorganization of the actin cytoskeleton, and abolished the selective transepithelial permeability of RPE cell cultures (Bruban et al. 2009). Moreover, subretinal injection of the oligomeric form of A β (1–42) induces RPE atrophy and disorganization of actin cytoskeleton in mice, accompanied by decreased expression of the tight junction proteins occludin and zonula occludens 1 and of the visual cycle proteins CRALBP and RPE65 (Bruban et al. 2009). Altogether, these studies show that A β alters the structure and functions of RPE cells and thus strongly suggest that A β present in drusen may play an important role in retinal degeneration through impairment of RPE cells.

10.4 Amyloid- β Is Cytotoxic for the Neural Retina

As AMD progresses, drusen typically increase in number and size and drusen width is associated with a reduction in photoreceptor cell densities, suggesting that these deposits may exert degenerative effects on photoreceptors (Anderson et al. 2004). The presence of TUNEL-positive rods near the edges of RPE atrophy is consistent with rod death involving an apoptotic process (Dunaief et al. 2002). Interestingly, intravitreal injection of the oligomeric form of A β (1–42) induced apoptosis in cells throughout the inner nuclear layer as well as the outer nuclear layers (Guo et al. 2007; Walsh et al. 2002, 2005). Moreover, intravitreal injection of A β (1–42) induces a pronounced reduction in the number of large retinal ganglion cells (RGC) (Walsh et al. 2002, 2005, Anderson et al. 2008). In contrast, subretinal injection of the oligomeric form of A β (1–42) induced a loss of photoreceptor cells (Bruban et al. 2009), indicating a site-of-injection polarity in the response of retinal cells to A β . Altogether, these studies suggest that A β has direct cytotoxic effects on retinal neurons.

Recently, the presence of A β plaques was reported in retinas of postmortem eyes from AD patients (Koronyo-Hamaoui et al. 2010). AD patients commonly exhibit visual abnormalities including retinal dysfunctions and loss of RGC (Blanks et al. 1991).

A β deposits in the nerve fiber layer associated with apoptosis in the ganglion cells were observed in a mouse model of AD (Ning et al. 2008). Moreover, electroretinogram (ERG) recordings revealed visual dysfunction and suggest that A β deposition disrupts retinal structure and may contribute to the visual deficit in another study using a mouse model of AD (Perez et al. 2009). Therefore, these studies using mouse models of AD demonstrate that endogenous production of A β may lead to morphological and functional impairment or neuronal degeneration in the retina.

There is accumulative evidence that increased A β deposits are implicated in other ocular pathologies, including glaucoma. In the DBA/2J glaucomatous mouse model, an age-dependent immunoreactivity against A β is observed in RGC, likely being a contributing factor of apoptotic ganglion cell loss (Goldblum et al. 2007). Moreover, in an experimental rat model of glaucoma, A β was shown to colocalize with apoptotic cells in the RGC layer and targeting the production of endogenous A β significantly reduced the level of retinal ganglion cell loss (Guo et al. 2007). Treatment with A β (25–35) induces cell death of human RGC in cultures (Tsuruma et al. 2010), confirming the direct lethal effects of A β on these cells. Altogether, these studies show that both exogenous and endogenous A β induce retinal cell death and confirm the potential implication of the A β in the degeneration of the retina.

A study based on A β -immunotherapy in ApoE ϵ 4-overexpressing mice exposed to a high-fat, cholesterol-enriched diet strengthens the potential role of the peptide in AMD pathogenesis. In that study, the intraperitoneal injection of anti-A β (33–40) antibody induces a decrease in A β levels within subepithelial deposits and a reduction in visual deficits detected by ERG (Ding et al. 2008). Unfortunately, the interest of this promising immunotherapy against A β in retinal degeneration is reduced by the recent study of Liu et al. These authors show that A β -immunization induces a marked increase in retinal microvascular A β deposition as well as local neuroinflammation in the Tg2576 mouse model of AD (Liu et al. 2009).

10.5 Amyloid- β Is Proinflammatory in the Retina

Many lines of evidence support a role for inflammation in the development of AMD. Drusen composition exhibits several inflammatory proteins, such as complement cascade components, immunoglobulins, and major histocompatibility class (MHC) antigens (Crabb et al. 2002; Seth et al. 2008). Moreover, although AMD is not an inflammatory pathology, macrophages/microglial cells were detected in areas of Bruch's membrane thinning, RPE atrophy, and choroidal neovascularization in AMD eyes (Coleman et al. 2008). However, the role of these inflammatory cells in AMD remains to be determined.

A β within drusen colocalizes with activated complement components C3 and C5, thereby identified as potential primary sites of complement activation (Johnson et al. 2000). Their presence has fueled speculation that drusen biogenesis involves chronic inflammatory processes that can trigger complement activation (Johnson et al. 2001). High expression levels of complement factor H (CFH), a regulatory

protein of the complement alternative pathway, have been also detected in drusen (Hageman et al. 2005). Several studies underlined that the Y402H single nucleotide polymorphism in the gene encoding for CFH was associated with an enhanced risk to develop AMD (Edwards et al. 2005; Hageman et al. 2005; Klein et al. 2005; Haines et al. 2005). This is consistent with the accumulation of C3 in the neural retina and subretinal deposits in CFH-deficient mice, associated with alterations of photoreceptors and RPE cells (Coffey et al. 2007). In that context, polymorphisms of complement factor B (CFB), C2, and C3 are likely to be associated with AMD (Gold et al. 2006; Yates et al. 2007). Altogether, these data support the hypothesis of an inflammatory process in the pathogenesis of AMD, bringing into play the complement alternative pathway. A recent report showed that A β (1–40) can indirectly modulate expression of CFB in RPE cells through an increased production of chemokine monocyte chemoattractant protein-1 (MCP-1) and production of the proinflammatory cytokines IL-1 β and TNF- α in macrophages. Subsequently, that cytokines production correlates with the overexpression of CFB in RPE cells (Wang et al. 2009). Moreover, A β (1–40) binds CFI in human primary RPE cells to prevent the cleavage of C3b in inactive C3b (iC3b) (Wang et al. 2008). The hypothesis of a proinflammatory role of A β through the overexpression of proinflammatory cytokines and components of the complement cascade in the retina is reinforced by recent data showing that A β (1–40) upregulates the expression of IL-1 β and IL-8 and CFI in RPE cells (Kurji et al. 2010). Besides, an age-dependent increase within the RPE of healthy elderly retinas in both APP expression and the number of CD11b-positive macrophages is associated at the Bruch's membrane level with that of C5b-9, a protein of the membrane attack complex (Seth et al. 2008).

In addition, several studies suggested that intravitreal or subretinal injection of A β induces a cytotoxic effect on retinal neurons and an activation of microglial cells (Walsh et al. 2005; Anderson et al. 2008; Bruban et al. 2011). Moreover, recent reports showed A β deposition associated with activation of resident microglial cells in retinas of APP-overexpressing mouse models of AD (Ning et al. 2008; Perez et al. 2009). Altogether, these studies strongly suggest that A β induces inflammation in the retina by regulating the complement pathway and stimulating proinflammatory cytokines and chemokines.

10.6 Conclusions

The mechanisms leading to AMD remain poorly understood. In particular, our understanding of the critical steps in the clinical evolution of the pathology and the role of oxidative stress and inflammation in its development remains elusive. However, several studies over the past decade indicate that A β could participate in the pathogenesis of AMD. First, A β production/accumulation in the retina is common to different degenerative retinal pathologies in human and in murine models, and second, A β induces *in vitro* and *in vivo* characteristic features resembling to those observed in these retinal degenerative pathologies.

Although there is a need to further explore the role of A β in retinal degeneration, the current evidence available provides exciting ways of research outlining retinal dysfunctions, cell death pathways, or retinal inflammation.

References

- Anderson DH, Talaga KC, Rivest AJ et al (2004) Characterization of beta amyloid assemblies in drusen: the deposits associated with aging and age-related macular degeneration. *Exp Eye Res* 78:243–256
- Anderson PJ, Watts H, Hille C et al (2008) Glial and endothelial blood-retinal barrier responses to amyloid-beta in the neural retina of the rat. *Clin Ophthalmol*. 2:801–816
- Blanks JC, Torigoe Y, Hinton DR et al (1991). Retinal degeneration in the macula of patients with Alzheimer's disease. *Ann N Y Acad Sci*. 640:44–46
- Bruban J, Glotin AL, Dinot V et al (2009) Amyloid-beta(1–42) alters structure and function of retinal pigmented epithelial cells. *Aging Cell*. 8:162–177
- Bruban J, Maoui A, Chalour N et al (2011) CCR2/CCL2-mediated inflammation protects photoreceptor cells from amyloid- β -induced apoptosis. *Neurobiol Dis*. 42:55–72
- Coffey PJ, Gias C, McDermott et al (2007) Complement factor H deficiency in aged mice causes retinal abnormalities and visual dysfunction. *Proc Natl Acad Sci U S A*. 104:16651–16656
- Coleman HR, Chan CC, Ferris FL et al (2008) Age-related macular degeneration. *Lancet*. 372:1835–1845
- Crabb JW, Miyagi M, Gu X et al (2002) Drusen proteome analysis: an approach to the etiology of age-related macular degeneration. *Proc Natl Acad Sci U S A*. 99:14682–14687
- Dentchev T, Milam AH, Lee VM et al (2003) Amyloid-beta is found in drusen from some age-related macular degeneration retinas, but not in drusen from normal retinas. *Mol Vis* 9:184–190
- Ding JD, Lin J, Mace BE et al (2008) Targeting age-related macular degeneration with Alzheimer's disease based immunotherapies: anti-amyloid-beta antibody attenuates pathologies in an age-related macular degeneration mouse model. *Vision Res*. 48:339–345
- Ding X, Patel M and Chan CC (2009) Molecular pathology of age-related macular degeneration. *Prog Retin Eye Res*. 28:1–18
- Dunaief JL, Dentchev T, Ying GS et al (2002) The role of apoptosis in age-related macular degeneration. *Arch Ophthalmol* 120:1435–1442
- Edwards AO, Ritter R 3rd, Abel KJ et al (2005) Complement factor H polymorphism and age-related macular degeneration. *Science*. 308:421–424
- Green WR (1999) Histopathology of age-related macular degeneration. *Mol Vis*. 5:27
- Glabe CG and Kaye R (2006) Common structure and toxic function of amyloid oligomers implies a common mechanism of pathogenesis. *Neurology*. 66:S74–78
- Glotin AL, Debacq-Chainiaux F, Brossas Y et al (2008) Prematurely senescent ARPE-19 cells display features of age-related macular degeneration. *Free Radic Biol Med*. 44:1348–1361
- Gold B, Merriam JE, Zernant J et al (2006) Variation in factor B (BF) and complement component 2 (C2) genes is associated with age-related macular degeneration. *Nat Genet*. 38:458–462
- Goldblum D, Kipfer-Kauer A, Sarra GM et al (2007) Distribution of amyloid precursor protein and amyloid-beta immunoreactivity in DBA/2 J glaucomatous mouse retinas. *Invest Ophthalmol Vis Sci*. 48:5085–5090
- Guo L, Salt TE, Luong V et al (2007) Targeting amyloid-beta in glaucoma treatment. *Proc Natl Acad Sci U S A*. 104:13444–13449
- Hageman GS, Anderson DH, Johnson LV et al (2005) A common haplotype in the complement regulatory gene factor H (HF1/CFH) predisposes individuals to age-related macular degeneration. *Proc Natl Acad Sci U S A* 102:7227–7232
- Haines JL, Hauser MA, Schmidt S et al (2005) Complement factor H variant increases the risk of age-related macular degeneration. *Science*. 308:419–421

- Isas JM, Luibl V, Johnson LV et al (2010) Soluble and mature amyloid fibrils in drusen deposits. *Invest Ophthalmol Vis Sci.* 51:1304–1310
- Iwata N, Tsubuki S, Takaki Y et al (2000) Identification of the major Abeta1-42-degrading catabolic pathway in brain parenchyma: suppression leads to biochemical and pathological deposition. *Nat Med.* 6:143–150
- Johnson LV, Leitner WP, Rivest AJ et al (2002) The Alzheimer's Abeta peptide is deposited at sites of complement activation in pathologic deposits associated with aging and age-related macular degeneration. *Proc Natl Acad Sci U S A.* 99:11830–11835
- Johnson LV, Leitner WP, Staples MK et al (2001) Complement activation and inflammatory processes in Drusen formation and age related macular degeneration. *Exp Eye Res.* 73:887–896
- Johnson LV, Ozaki S, Staples MK et al (2000) A potential role for immune complex pathogenesis in drusen formation. *Exp Eye Res.* 70:441–449
- Johnson PT, Lewis GP, Talaga KC et al (2003) Drusen-associated degeneration in the retina. *Invest Ophthalmol Vis Sci.* 44:4481–4488
- Klein R, Peto T, Bird A et al (2004) The epidemiology of age-related macular degeneration *Am J Ophthalmol.* 137:486–495
- Klein RJ, Zeiss C, Chew EY et al (2005) Complement factor H polymorphism in age-related macular degeneration. *Science.* 308:385–389
- Koronyo-Hamaoui M, Koronyo Y, Ljubimov AV et al (2010) Identification of amyloid plaques in retinas from Alzheimer's patients and noninvasive in vivo optical imaging of retinal plaques in a mouse model. *Neuroimage*
- Koyama Y, Matsuzaki S, Gomi F et al (2008) Induction of amyloid beta accumulation by ER calcium disruption and resultant upregulation of angiogenic factors in ARPE19 cells. *Invest Ophthalmol Vis Sci.* 49:2376–2383
- Kurji KH, Cui JZ, Lin T et al (2010) Microarray analysis identifies changes in inflammatory gene expression in response to amyloid-beta stimulation of cultured human retinal pigment epithelial cells. *Invest Ophthalmol Vis Sci.* 51:1151–1163
- Lambert MP, Barlow AK, Chromy BA et al (1998) Diffusible, nonfibrillar ligands derived from Abeta1-42 are potent central nervous system neurotoxins. *Proc Natl Acad Sci U S A.* 95:6448–6453
- Liu B, Rasool S, Yang Z et al (2009) Amyloid-peptide vaccinations reduce {beta}-amyloid plaques but exacerbate vascular deposition and inflammation in the retina of Alzheimer's transgenic mice. *Am J Pathol.* 175:2099–2110
- Luibl V, Isas JM, Kaye R et al (2006) Drusen deposits associated with aging and age-related macular degeneration contain nonfibrillar amyloid oligomers. *J Clin Invest.* 116:378–385
- Mullins RF, Russell SR, Anderson, DH et al (2000) Drusen associated with aging and age-related macular degeneration contain proteins common to extracellular deposits associated with atherosclerosis, elastosis, amyloidosis, and dense deposit disease. *Faseb J* 14:835–846
- Ning A, Cui J, To E et al (2008). Amyloid-beta deposits lead to retinal degeneration in a mouse model of Alzheimer disease. *Invest Ophthalmol Vis Sci.* 49:5136–5143
- Perez SE, Lumayag S, Kovacs B et al (2009) Beta-amyloid deposition and functional impairment in the retina of the APPswe/PS1DeltaE9 transgenic mouse model of Alzheimer's disease. *Invest Ophthalmol Vis Sci.* 50:793–800
- Selkoe DJ (2001) Alzheimer's disease: genes, proteins, and therapy. *Physiol Rev.* 81:741–766
- Seth A, Cui J, To E, et al (2008) Complement-associated deposits in the human retina. *Invest Ophthalmol Vis Sci.* 49:743–750
- Tsuruma K, Tanaka Y, Shimazawa M et al (2010) Induction of amyloid precursor protein by the neurotoxic peptide, amyloid-beta 25–35, causes retinal ganglion cell death. *Neurochem.* 113:1545–1554
- Walsh DT, Bresciani L, Saunders D et al (2005) Amyloid beta peptide causes chronic glial cell activation and neuro-degeneration after intravitreal injection. *Neuropathol Appl Neurobiol.* 31:491–502
- Walsh DT, Monteiro RM, Bresciani LG et al (2002) Amyloid-beta peptide is toxic to neurons in vivo via indirect mechanisms. *Neurobiol Dis.* 10:20–27

- Wang J, Ohno-Matsui K, Yoshida T et al (2009) Amyloid-beta up-regulates complement factor B in retinal pigment epithelial cells through cytokines released from recruited macrophages/microglia. *J Cell Physiol.* 220:119–128
- Wang, J, Ohno-Matsui K., Yoshida T et al (2008) Altered function of factor I caused by amyloid beta: implication for pathogenesis of age-related macular degeneration from Drusen. *J Immunol.* 181:712–720.
- Yates JR, Sepp T, Matharu BK et al (2007) Complement C3 variant and the risk of age-related macular degeneration. *N Engl J Med.* 357:553–561
- Yoshida T, Ohno-Matsui K, Ichinose, S et al (2005) The potential role of amyloid beta in the pathogenesis of age-related macular degeneration. *J Clin Invest* 115:2793–2800

Chapter 11

Molecule-Specific Imaging and Quantitation of A2E in the RPE

Zsolt Ablonczy, Danielle B. Gutierrez, Angus C. Grey, Kevin L. Schey, and Rosalie K. Crouch

Keywords A2E • Lipofuscin • Retinal pigment epithelium • Mass spectrometry • MALDI imaging • Quantitation • Stargardt disease • Age-related macular degeneration

11.1 Introduction

Lipofuscin accumulates with age in the lysosomal storage bodies of the RPE and has been implicated in progressive RPE toxicity, which can eventually lead to retinal degeneration (Winkler et al. 1999). Chemically, lipofuscin is a complex mixture of partially degraded molecules characterized by orange fluorescence (Delori et al. 1995). The *bis*-retinoid A2E was identified from organic extracts of lipofuscin (Sakai et al. 1996). In vivo, *bis*-retinoid precursors form in the photoreceptor outer segments when the all-*trans* retinal to retinol conversion is delayed. A2E is generated from these precursors in the RPE after outer segment phagocytosis. The *bis*-retinoids have received considerable attention, as A2E (and especially its oxides) has been shown to produce RPE damage (Eldred and Lasky 1993).

Z. Ablonczy (✉) • R.K. Crouch
Department of Ophthalmology, Medical University of South Carolina,
Charleston, SC 29425, USA
e-mail: ablonczy@musc.edu

D.B. Gutierrez
Laboratory of Retinal Cell and Molecular Biology, National Eye Institute,
Bethesda, MD 20892, USA

A.C. Grey
Department of Optometry and Vision Science,
University of Auckland, Grafton 1023, New Zealand

K.L. Schey
Department of Biochemistry, Vanderbilt University, Nashville, TN 37240, USA

However, a direct correlation of A2E with lipofuscin has not been possible because fluorescence is not specific enough, and immunolocalization techniques are not applicable for *bis*-retinoids. To understand the spatial localization of lipofuscin components, we utilized matrix-assisted laser desorption/ionization (MALDI) imaging (Caprioli et al. 1997). In this technique, mass information is collected systematically over the surface of a matrix-coated tissue section, and the resulting images represent intensity distributions of molecular signals across the observed surface. With this technique, we analyzed *Abca4*^{-/-} (a model for Stargardt disease with high levels of both A2E and lipofuscin), *Rpe65*^{-/-} (a model for blocked visual cycle, where A2E is not formed), and *wt* mice. The collected MALDI imaging data were utilized to identify *bis*-retinoid components of lipofuscin and to determine their spatial distributions. To further understand the accumulation of A2E, we employed an LC-MS/MS method for the highly sensitive (femtomoles) absolute quantitation of *bis*-retinoids from RPE extracts (Gutierrez et al. 2010). Taken together, these experiments provide a new, molecule-specific understanding of *bis*-retinoids and potentially other retinoid metabolites of the visual cycle.

11.2 Materials and Methods

11.2.1 RPE Tissue Preparation

Abca4^{-/-} and *Rpe65*^{-/-} mice were bred from pairs generously provided by Gabriel Travis (UCLA) and Michael Redmond (NEI). *C57bl6* (*wt*) mice were obtained commercially (Harlan, Indianapolis, IN). Six-month-old mice ($n=4$ each strain, maintained under regular cyclic light) were used. RPE tissue was prepared as described previously for MALDI imaging (Grey et al. 2010) and for absolute quantitation (Gutierrez et al. 2010).

11.2.2 MALDI Imaging

Imaging samples were coated using a thin-layer-chromatography sprayer with 10 mg/mL 3-(4-hydroxy-3,5-dimethoxyphenyl)prop-2-enoic acid (Sigma, St Louis, MO) in 10 mL 70:30 ethanol:water (Thermo Fisher, Fair Lawn, NJ). Data were collected in a MALDI-TOF mass spectrometer (Autoflex III; Bruker Daltonics, Billerica, MA). Further details are described elsewhere (Grey et al. 2010).

11.2.3 Quantitation of A2E

For quantitative analysis, dried RPE extracts were diluted to obtain approximately 10 fmol/ μ L solutions in 85% MeOH, 0.1% TFA and injected for LC-MS/MS analysis. Further details followed previous procedures (Gutierrez et al. 2010).

11.3 Results

11.3.1 Spatial Localization of A2E in Murine RPE

The MALDI mass spectra from *Abca4*^{-/-} RPE tissues were dominated by an abundant mass signal at *m/z* 592. The identity of this signal as A2E was confirmed by tandem mass spectrometry (MS/MS): the observed fragmentation pattern collected from the tissue was consistent with expected A2E fragmentation. In addition to A2E, numerous less abundant components were present in the spectra. In this work, we focused our attention to A2E and its oxides.

MALDI images of A2E were generated by plotting the relative intensities of the *m/z* 592 signal over the entire RPE surface (Fig. 11.1). A2E distributions were determined in *wt* (Fig. 11.1a) and *Abca4*^{-/-} (Fig. 11.1b) mice (no A2E was present in the *Rpe65*^{-/-} model, not shown). In both *Abca4*^{-/-} and *wt* mice, A2E accumulated uniformly and in a concentric manner. However, the abundance of A2E was much higher in the *Abca4*^{-/-} model, where A2E occupied a larger concentric area. In the same MALDI imaging datasets, up to three oxidations on A2E were also detected. Figure 11.1c shows the distribution of singly oxidized A2E (*m/z* 608) in a 6-month-old *Abca4*^{-/-} RPE. The distributions of the three oxidized products closely followed A2E.

11.3.2 Quantitation of A2E

The primary information displayed in the MALDI images is qualitative. To quantitate A2E, an LC-MS/MS-based approach was utilized, which (in comparison with traditional absorption spectroscopic quantitation) is molecularly specific (Gutierrez et al. 2010). This method relies on a standard curve calculated from various amounts

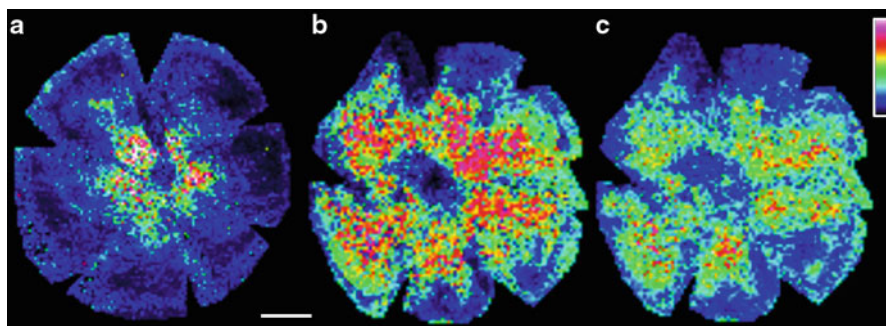
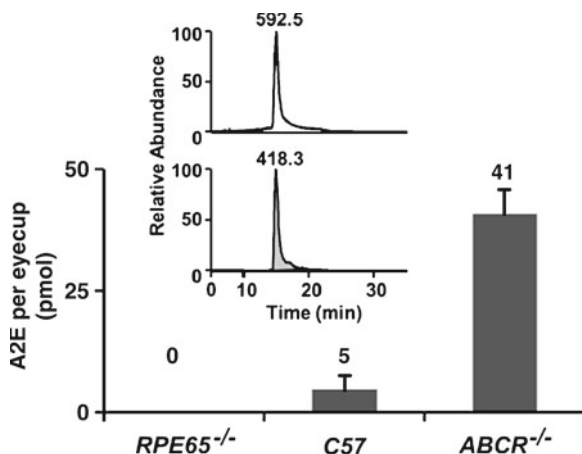


Fig. 11.1 Spatial localization of A2E from murine eyecups. MALDI images of A2E (*m/z* 592) are shown in RPE tissue from a 6-month-old *wt* (a) and *Abca4*^{-/-} (b) animal. (c) MALDI image of singly oxidized A2E (*m/z* 608) from a 6-month-old *Abca4*^{-/-} animal. Bar = 1 mm

Fig. 11.2 Quantitative analysis of A2E via mass spectrometry. Quantitation of A2E is shown for *Rpe65*^{-/-}, *wt*, and *Abca4*^{-/-} mice, all of age 6 months. The inset illustrates the method of quantitation. AUC (shown shaded) was determined for the most intense fragment ion (*m/z* 418, inset bottom), of the intact A2E (*m/z* 592, inset top) in an *Abca4*^{-/-} animal



of synthetic A2E. With this method, low femtomole quantities of A2E can be detected, and amounts of A2E from a single *wt* mouse RPE can routinely be quantitated.

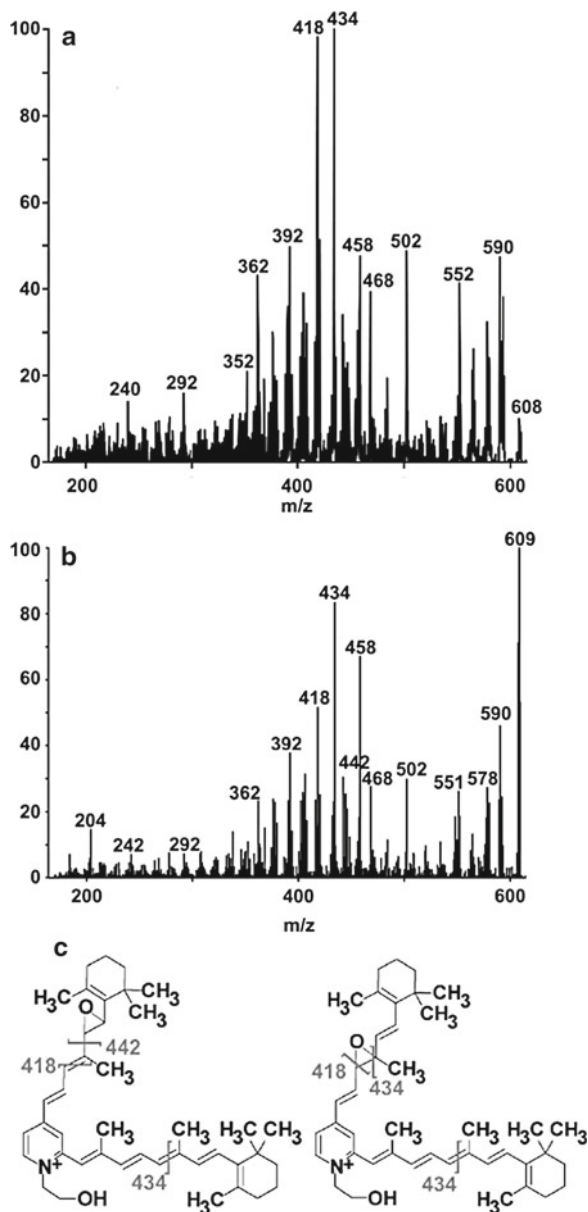
Figure 11.2 summarizes the results of A2E quantitation in *Rpe65*^{-/-}, *wt*, and *Abca4*^{-/-} mice. The inset shows two selected ion chromatograms for A2E from a 6-month-old *Abca4*^{-/-} animal representing 30 min of the elution gradient. The upper trace is based on the intact molecular weight (*m/z* 592), while the lower trace indicates the most prominent MS/MS ion (*m/z* 418). The quantitation is based on the area under the lower trace (shaded), as the instrument is more sensitive in MS/MS mode. As seen in the bar graph, there was no A2E in *Rpe65*^{-/-} animals, while compared to *wt* controls (5 ± 3 pmol) the quantity of A2E was elevated in the *Abca4*^{-/-} mice (41 ± 7 pmol).

11.3.3 A2E Oxidation Sites

A major advantage of MALDI imaging is that tracing any molecule within the targeted range does not require a separate experiment. However, the identification of these molecules requires a second MS/MS experiment. The signals of singly (*m/z* 608) and doubly (*m/z* 624) oxidized A2E were confirmed by MS/MS. Figure 11.3a shows a MS/MS spectrum of singly oxidized A2E from an *Abca4*^{-/-} animal. To see whether the detected oxidation site depends on the utilized sample preparation/instrumentation technique, we also collected MS/MS spectra of oxidized A2E from organic extracts of the RPE (Fig. 11.3b).

There was remarkable agreement between the spectra collected by the two analytical methods. However, they both differed slightly from the published fragmentation patterns for extracted A2E from human eyecups (Avalle et al. 2004),

Fig. 11.3 Oxidation of A2E. MS/MS spectra of singly oxidized A2E (m/z 608) obtained directly from tissue used for MALDI imaging (a) and from organic extracts used for LC-MS/MS analysis (b). (c) The MS/MS spectra support a mixture of one oxygen in either the 7, 8/7', 8' position (left) or 9, 10/9', 10' position (right)



indicating a possible additional site of oxidation in *Abca4*^{-/-} mice. The oxygen can be localized either to the 7, 8/7', 8'-epoxide position (Fig. 11.3c, left) or to the 9, 10/9', 10'-epoxide position (Fig. 11.3c, right).

11.4 Discussion

Lipofuscin accumulation in the RPE is implicated in the development of age-related retino- and maculopathies. The analysis of its components typically requires organic extraction, HPLC separation, and subsequent analysis, which completely preclude spatial localization. A2E is a major component of the chloroform–methanol extract of the RPE. However, without the ability to spatially identify A2E, it is not possible to justify that lipofuscin toxicity is indeed due to A2E accumulation. Because immunohistochemistry cannot be used, it is highly advantageous to utilize the molecularly selective and sensitive MALDI imaging method. With this technique, many compounds can be imaged in a single experiment. In this report, we have focused on A2E and its oxides, but the technique is easily amenable to other *bis*-retinoids and retinoid metabolites.

We have detected A2E and its oxides at 50 μm resolution in 6-month-old native murine RPE tissue. As expected, there was no A2E present in *Rpe65*^{-/-} animals (which do not produce 11-*cis* retinal), confirming that the visual cycle is required for A2E generation (Katz and Redmond 2001). In the *wt* retina, A2E was mainly localized to the center of the RPE, while in the *Abca4*^{-/-} RPE the distribution became more uniform across the entire RPE. These observations reinforce the rapid accumulation of A2E in the *Abca4*^{-/-} model, and that A2E becomes uniform across the RPE as it accumulates. Thus, the data agree with the hypothesis that A2E and lipofuscin correlate spatially.

Although with an internal standard MALDI data can be utilized for relative quantitation, comparing images between different tissues and strains is rather qualitative. On the other hand, our LC-MS/MS-based method allows absolute quantitation of subfemtomole amounts of synthetic A2E. The information obtained through our quantitative analysis reinforced the semiquantitative imaging observations (that is, no A2E in the *Rpe65*^{-/-} animals and higher A2E in *Abca4*^{-/-} animals, than in *wt* mice). Moreover, these experiments provided quantitative data not possible by other current methodologies (such as, the level of A2E in 6-month-old *Abca4*^{-/-} mouse RPE is 8-fold over that in the same age *wt* RPE).

In vitro, up to nine oxygens have been identified on A2E; however, we could detect only two oxidation states in most tissues, and no more than three oxidations in all tissues with two fundamentally different analytical methods. The spatial distribution of oxidized A2E followed closely that of A2E, indicating that oxidized forms of A2E remain in the vicinity of their parent molecule. The sites of oxidation detected with the two techniques were identical. In the literature, A2E mono-oxidation has been reported on the 7, 8/7', 8'-epoxide or the 5, 8/5', 8'-furanoid position (Avalle et al. 2004; Jang et al. 2005). However, in the *Abca4*^{-/-} strain, we found that A2E can be mono-oxidized on a mixture of the 7, 8/7', 8'-, and the 9, 10/9', 10'-epoxide positions, indicating the possibility of two native mono-oxidation sites in vivo.

In conclusion, we have recently developed two new methods for the analysis of A2E and other *bis*-retinoids in RPE tissue from models of retinal degenerations: a MALDI-based technique for multiplex and molecularly specific imaging; and an

LC-MS/MS-based technique for sensitive quantitation. Each method has its own advantages, therefore utilizing both approaches has a great potential for addressing disease pathogenesis in models of retinal degenerations. Together, they will provide valuable new information on distinct spatial regions in normal and diseased tissues.

Acknowledgments The study was supported by NIH grants EY004939 (RKC), EY020661 (ZA/RKC), and an unrestricted award from Research to Prevent Blindness (RPB). RKC is an RPB Senior Scientific Investigator. The work was performed in the MUSC mass spectrometry facility. Experimental animals were housed in a facility constructed with support from NIH grant C06 RR015455.

References

- Avalle LB, Wang Z, Dillon JP et al (2004) Observation of A2E oxidation products in human retinal lipofuscin. *Exp Eye Res* 78:895–898
- Caprioli RM, Farmer TB, Gile J (1997) Molecular imaging of biological samples: localization of peptides and proteins using MALDI-TOF MS. *Anal Chem* 69:4751–4760
- Delori FC, Dorey CK, Staurengli G et al (1995) In vivo fluorescence of the ocular fundus exhibits retinal pigment epithelium lipofuscin characteristics. *Invest Ophthalmol Vis Sci* 36:718–729
- Eldred GE, Lasky MR (1993) Retinal age pigments generated by self-assembling lysomotropic detergents. *Nature* 361:724–726
- Grey AC, Crouch RK, Koutalos Y et al (2010) Spatial localization of A2E in the retinal pigment epithelium. *Invest Ophthalmol Vis Sci* 52:3926–3933
- Gutierrez DB, Blakeley L, Goletz PW et al (2010) Mass spectrometry provides accurate and sensitive quantitation of A2E. *Photochem Photobiol Sci* 9:1513–1519
- Jang YP, Matsuda H, Itagaki Y et al (2005) Characterization of peroxy-A2E and furan-A2E photo-oxidation products and detection in human and mouse retinal pigment epithelial cell lipofuscin. *J Biol Chem* 280:39732–39739
- Katz ML, Redmond TM (2001) Effect of Rpe65 knockout on accumulation of lipofuscin fluorophores in the retinal pigment epithelium. *Invest Ophthalmol Vis Sci* 42:3023–3030
- Sakai N, Decatur J, Nakanishi K et al (1996) Ocular age pigment “A2E”: an unprecedented pyridinium *bis*-retinoid. *J Am Chem Soc* 118:1559–1560
- Winkler BS, Boulton ME, Gottsch JD et al (1999) Oxidative damage and age-related macular degeneration. *Mol Vis* 5:32 <<http://www.molvis.org/molvis/v5/p32/>>

Chapter 12

Autophagy in the Retina: A Potential Role in Age-Related Macular Degeneration*

Sayak K. Mitter, Haripriya Vittal Rao, Xiaoping Qi, Jun Cai, Andrew Sugrue, William A. Dunn Jr., Maria B. Grant, and Michael E. Boulton

Keywords Autophagy • Retinal pigment epithelium • Age-related macular degeneration • Retina • Mitochondria • Lipofuscin • Oxidative damage

12.1 Introduction

The significance of autophagy in health and disease has only become fully appreciated in the last decade. Under normal conditions, autophagy operates constitutively and serves as a housekeeping process through which cytoplasmic proteins and damaged cellular organelles, such as dysfunctional mitochondria, are removed (Marino et al. 2010). Of the three autophagic pathways (chaperone-mediated, micro-, and macroautophagy) that deliver cellular components of varying sizes to lysosomes, macroautophagy is the primary route for sequestration of organelles or large aggregates and their delivery to the lysosome (Cuervo 2008; Lieberthal 2008). It is evident that autophagy plays a key role in cellular homeostasis and that this process can be stimulated to cope with excessive organelle damage, aggregate removal, and pathogen defense (Cuervo 2008).

*Haripriya Vittal Rao and Sayak K. Mitter contributed equally to this work.

S.K. Mitter • H.V. Rao • X. Qi • J. Cai • A. Sugrue • W.A. Dunn Jr. • M.E. Boulton (✉)
Department of Anatomy and Cell Biology, University of Florida, 1600 SW Archer Road,
PO Box 100235, Gainesville, FL 32610, USA
e-mail: meboulton@ufl.edu

M.B. Grant
Department of Pharmacology and Therapeutics, University of Florida,
1600 SW Archer Road, PO Box 100267, Gainesville, FL 32610, USA

12.2 Molecular Events in the Autophagy Process

Since accumulation of proteins and damaged organelles are a general observation in the aging RPE as well as in AMD, it is postulated that a breakdown in the recycling capacity of autophagy may have a strong association. The process of autophagy is outlined in Fig. 12.1 and involves over 30 autophagy-related proteins (Atg) which regulate different stages of the autophagic pathway. The autophagic process begins with the formation of an isolation membrane, also referred to as the phagophore

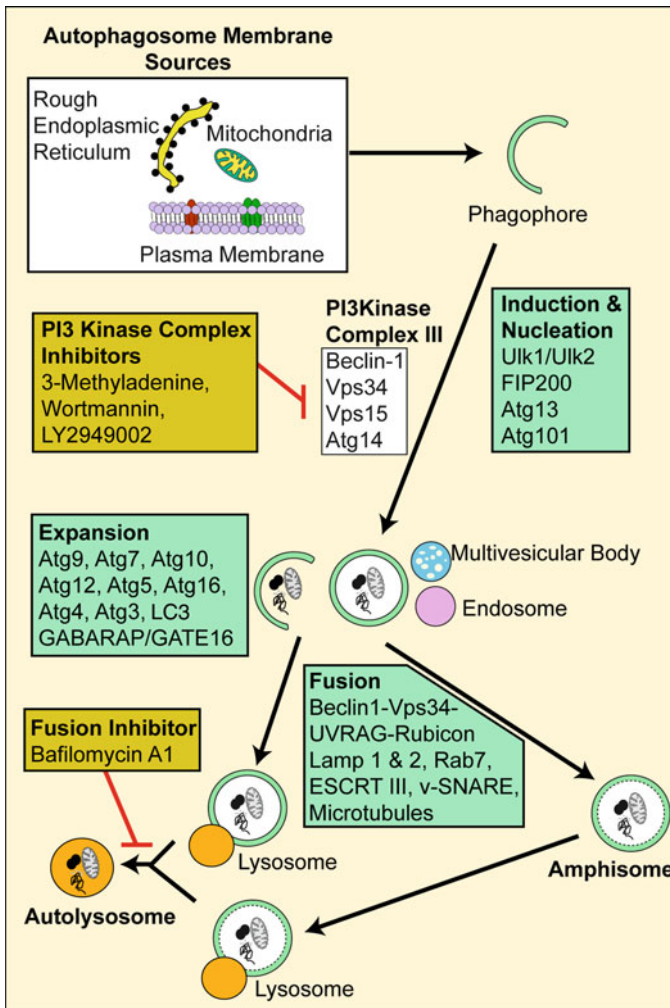


Fig. 12.1 A schematic showing the basic steps of mammalian macroautophagy, the common autophagic molecules involved, and pharmacological inhibitors used to block autophagy at different steps

(Yorimitsu and Klionsky 2005) that is shown to originate primarily from the endoplasmic reticulum (Dunn 1990; Hamasaki and Yoshimori 2010). The phagophore gradually expands to engulf the cargo (e.g., mitochondria) to form a closed double-membrane structure termed an early autophagosome. Autophagosome maturation depends on two ubiquitin-like-conjugation systems namely the Atg12–Atg5–Atg16 complex and the LC3 conjugation system. Both the systems are regulated by the Atg7 molecule (Geng and Klionsky 2008). The mature autophagosome fuses with either the lysosome, late endosome, or the multivesicular body to form the amphisome or late autophagosome which subsequently matures into the autolysosome. Lysosomes contain potent hydrolytic enzymes which then degrade the engulfed contents and the indigestible residual body, formed as an endpoint of lysosomal digestion, may subsequently be removed by exocytosis or may contribute to lipofuscin (Luzio et al. 2007; Settembre et al. 2008). A critical property of the lysosome that facilitates the fusion of the autophagosome to the lysosome and the digestive activity of the lysosomal enzymes is its pH which typically is acidic at around 4.5 (Kawai et al. 2007).

12.3 Signaling Mechanisms in Autophagy

The mTOR kinase complexes have been widely studied as the central signaling molecules of autophagy and can sense regulating conditions such as nutrient abundance, energy state, and growth factor levels (Ravikumar et al. 2004; Nobukuni et al. 2005). Interaction of Beclin1 with the antiapoptotic BH3 proteins such as Bcl-X_L and Bcl-2 is also a critical aspect of autophagy regulation and could influence autophagy even independent of mTOR (Pattingre et al. 2005). However, it is likely that several other mTOR-independent mechanisms of autophagy activation may also exist.

While starvation has been used as an inducer of autophagy in most studies, oxidative stress has also been acknowledged as a positive regulator of autophagy, at least in acute phases (Kiffin et al. 2006). However, it is now becoming evident that the pathways regulating baseline autophagy, starvation-induced autophagy, and stress-induced autophagy have fundamental differences. It has been observed that autophagic-deficient cells tend to accumulate p62-rich aggregates, which in turn cause Nrf2 to be activated after separation from its interacting partner Keap1 which allows Nrf2 to mount an antioxidant response (Komatsu et al. 2010).

12.4 Autophagy in the Neural Retina

We have demonstrated by immunohistochemistry that the autophagy proteins Atg9 and LC3 are strongly expressed in the ganglion cell layer, a subpopulation of cells in the inner nuclear layer, the outer nuclear layer, and the RPE in normal mouse retina (Fig. 12.2). Interestingly, these represent cell layers with high metabolic demand and a propensity for mitochondrial damage (Jarrett et al. 2010).

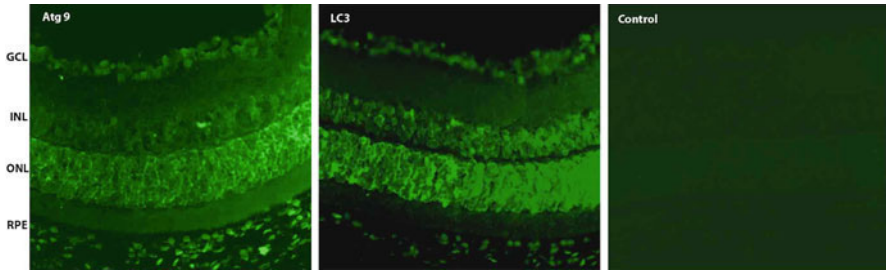


Fig. 12.2 Immunolocalization of autophagy proteins (*green*) in normal mouse retina. Atg9 and LC3 were strongly expressed in the ganglion cell layer, retinal vessels, a subpopulation of the inner nuclear layer, the outer nuclear layer of rods and cones, and the RPE

Autophagy in photoreceptor cells was first documented in 1977 (Reme and Young 1977). Autophagy in photoreceptor inner segments shows circadian rhythmicity (Reme and Wirz-Justice 1985) and is associated with lipofuscin accumulation in rod and cone photoreceptors (Iwasaki and Inomata 1988). Autophagic cell death in the retina has been reported to occur in a variety of retinal cells under oxidative stress (Kunchithapautham and Rohrer 2007) and autophagy occurs prior to programmed necrotic cell death of retinal neurons following ischemia (Rosenbaum et al. 2010). However, it has yet to be shown whether the autophagic response to ischemia is protective or detrimental to the neurons. Autophagy has been shown to induce axonal degeneration of retinal ganglion cells after crush lesion (Knofler et al. 2010), while it can be protective to retinal ganglion cells following optic nerve transection (Kim et al. 2008). Stimulation of the insulin/mTOR pathway protects cone photoreceptors in a mouse model of retinitis pigmentosa (Punzo et al. 2009) and upregulation of the autophagy protein Apg3 guards the retina from severe ischemic injury (Wu et al. 2006).

12.5 Autophagy in the RPE

There is now considerable evidence that the RPE, like most other cells, maintains a basal autophagy for cellular homeostasis and that this changes with both age and disease. We and others have shown that autophagy proteins are strongly expressed in the RPE (Fig. 12.2) (Wang et al. 2009a, b; Krohne et al. 2010; Viiri et al. 2010). Furthermore, RPE cells can accumulate lipofuscin even in the absence of a photoreceptor substrate strongly suggesting that autophagy is involved (Boulton et al. 1989; Burke and Skumatz 1998; Kurz et al. 2009). The autophagy and phagocytic pathways are interdependent and both culminate in lysosomal degradation of the substrate (Fig. 12.3). Thus, autophagy flux in the RPE is likely to be highly susceptible to changes in lysosomal pH or the accumulation of lipofuscin as both will impede the fusion of autophagosomes with lysosomes. Despite the paucity of corroborative data, it does appear that autophagy proteins and flux show an age-related increase within mouse and human RPE (Wang et al. 2009c).

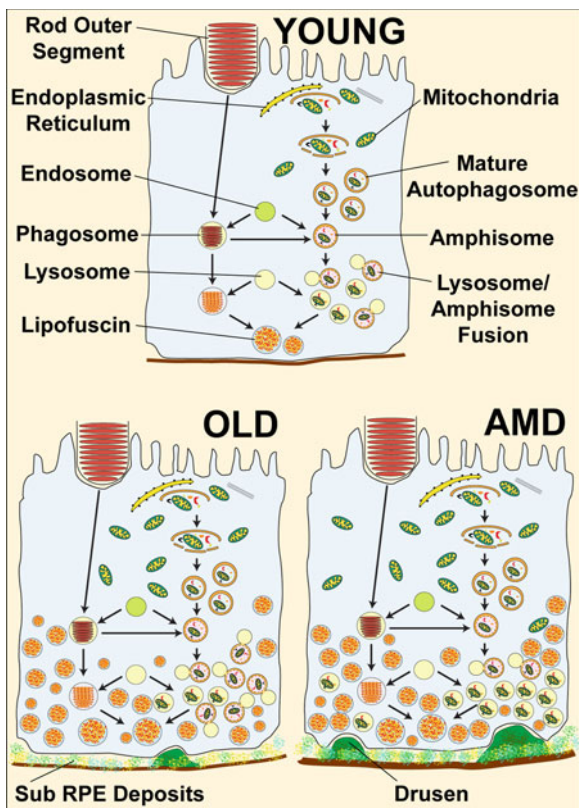


Fig. 12.3 Hypothetical schematic showing possible outcomes for aging and AMD on autophagy in RPE cells. *Young*: Autophagy will occur at a basal level and remove dysfunctional organelles and aggregates. Formation of autophagosomes, fusion of these with lysosomes and clearance are all balanced. Lipofuscin in residual bodies is minimally present. Sub-RPE drusen is absent. *Old*: Autophagy is increased in the old RPE cells compared to young, in line with the increased accumulation of aggregates and damaged organelles with age that need to be cleared. Levels of lipofuscin in residual bodies are increased and drusen are present. *AMD*: autophagy is dysfunctional in the RPE of AMD patients. Although autophagosome formation may be equivalent to an old RPE cell, fusion with the lysosomes and degradation of the engulfed material may be greatly impaired leading to an accumulation of autophagosomes. The cell is laden with secondary lysosomes containing partially degraded material, there are high levels of lipofuscin, and sub-RPE drusen are prominent

12.6 The Association Between Autophagy and AMD

Many of the important pathogenic features of the RPE in AMD, e.g., lipofuscin accumulation, susceptibility to oxidative stress, mitochondrial damage, and lysosomal dysregulation, have an association with autophagy. However, it remains to be determined whether changes in autophagy flux are a cause or consequence of disease and whether autophagy changes reflect alterations in the formation or

elimination of autophagosomes. A recent study by Wang et al suggest that drusen, a feature of early AMD, may reflect an increase in both mitochondrial damage and autophagy (Wang et al. 2009a). Using cultured RPE cells and *ex vivo* AMD donor tissue, they observed that (a) under conditions of increased mtDNA damage, autophagy markers and exosome markers were upregulated and (b) that drusen in AMD donor eyes contain markers for autophagy and exosomes. They speculated that increased autophagy and the release of intracellular proteins via exosomes by the aged RPE may contribute to the formation of drusen. The occupation of lysosomal volume by lipofuscin may alone be sufficient to impair autophagosome–lysosome fusion, while alternatively an increase in lysosomal pH may be responsible. A2E, a component of lipofuscin, (Boulton 2009) has been reported to inhibit the lysosomal ATP-driven proton pump resulting in an increase of the lysosomal pH (Bergmann et al. 2004). Furthermore, lipid peroxidation products reduce autophagy flux and increase lipofuscin accumulation in the RPE (Krohne et al. 2010). Interestingly, the effect of A2E on lysosomal pH can be reversed through reacidification (Liu et al. 2008).

There is substantial cross-talk between autophagy and proteasomal degradation pathways (Kaarniranta et al. 2009; Ryhanen et al. 2009; Kaarniranta 2010). HSP70, proteasomes, and macroautophagy combine to regulate protein turnover in human RPE cells (Ryhanen et al. 2009). The p62/sequestosome 1 links the proteasomal and lysosomal clearance systems (Korolchuk et al. 2009) and, via association with LC3, directs aggregates to the lysosome for autophagic degradation (Seibenhener et al. 2007; Kirkin et al. 2009). Proteasome inhibition in RPE cells evoked the accumulation of perinuclear aggregates that strongly colocalized with p62 and HSP70 and the silencing of p62, rather than HSP70, evoked suppression of autophagy (Viiri et al. 2010).

12.7 Conclusion

It is evident that autophagy plays a significant role as a housekeeping pathway in the retina and that autophagy flux is less effective with aging. Figure 12.3 provides a hypothetical schematic showing possible outcomes for aging and AMD on autophagy in RPE cells. Furthermore, the interactive role between autophagy, phagocytosis, lysosomal function, and the proteasomal system, all of which are dysregulated in AMD, requires further study. Autophagy modulation may offer a treatment regime for various ocular diseases including AMD.

Acknowledgments This work was funded by NIH grant EY019688 and AHAF grant M2009024.

References

- Bergmann M, Schutt F, Holz FG et al (2004) Inhibition of the ATP-driven proton pump in RPE lysosomes by the major lipofuscin fluorophore A2-E may contribute to the pathogenesis of age-related macular degeneration. *FASEB J* 18:562–564
- Boulton M, McKechnie NM, Breda J et al (1989) The formation of autofluorescent granules in cultured human RPE. *Invest Ophthalmol Vis Sci* 30:82–89
- Boulton ME (2009) Lipofuscin of the RPE. In: *Fundus Autofluorescence* (Lois M, Forrester J, eds), pp 14–26 Philadelphia: Lipincott; Williams and Wilkins
- Burke JM, Skumatz CM (1998) Autofluorescent inclusions in long-term postconfluent cultures of retinal pigment epithelium. *Invest Ophthalmol Vis Sci* 39:1478–1486
- Cuervo AM (2008) Autophagy and aging: keeping that old broom working. *Trends Genet* 24:604–612
- Dunn WA, Jr. (1990) Studies on the mechanisms of autophagy: formation of the autophagic vacuole. *J Cell Biol* 110:1923–1933
- Geng J, Klionsky DJ (2008) The Atg8 and Atg12 ubiquitin-like conjugation systems in macroautophagy. 'Protein modifications: beyond the usual suspects' review series. *EMBO Rep* 9:859–864
- Hamasaki M, Yoshimori T (2010) Where do they come from? Insights into autophagosome formation. *FEBS Lett* 584:1296–1301
- Iwasaki M, Inomata H (1988) Lipofuscin granules in human photoreceptor cells. *Invest Ophthalmol Vis Sci* 29:671–679
- Jarrett SG, Lewin AS, Boulton ME (2010) The importance of mitochondria in age-related and inherited eye disorders. *Ophthalmic Res* 44:179–190
- Kaarniranta K (2010) Autophagy--hot topic in AMD. *Acta Ophthalmol* 88:387–388
- Kaarniranta K, Salminen A, Eskelinen EL et al (2009) Heat shock proteins as gatekeepers of proteolytic pathways-Implications for age-related macular degeneration (AMD). *Ageing Res Rev* 8:128–139
- Kawai A, Uchiyama H, Takano S et al (2007) Autophagosome-lysosome fusion depends on the pH in acidic compartments in CHO cells. *Autophagy* 3:154–157
- Kiffin R, Bandyopadhyay U, Cuervo AM (2006) Oxidative stress and autophagy. *Antioxid Redox Signal* 8:152–162
- Kim SH, Munemasa Y, Kwong JM et al (2008) Activation of autophagy in retinal ganglion cells. *J Neurosci Res* 86:2943–2951
- Kirkin V, McEwan DG, Novak I et al (2009) A role for ubiquitin in selective autophagy. *Mol Cell* 34:259–269
- Knoferle J, Koch JC, Ostendorf T et al (2010) Mechanisms of acute axonal degeneration in the optic nerve in vivo. *Proc Natl Acad Sci U S A* 107:6064–6069
- Komatsu M, Kurokawa H, Waguri S et al (2010) The selective autophagy substrate p62 activates the stress responsive transcription factor Nrf2 through inactivation of Keap1. *Nat Cell Biol* 12:213–223
- Korolchuk VI, Mansilla A, Menzies FM et al (2009) Autophagy inhibition compromises degradation of ubiquitin-proteasome pathway substrates. *Mol Cell* 33:517–527
- Krohne TU, Stratmann NK, Kopitz J et al (2010) Effects of lipid peroxidation products on lipofuscinogenesis and autophagy in human retinal pigment epithelial cells. *Exp Eye Res* 90:465–471
- Kunchithapatham K, Rohrer B (2007) Apoptosis and autophagy in photoreceptors exposed to oxidative stress. *Autophagy* 3:433–441
- Kurz T, Karlsson M, Brunk UT et al (2009) ARPE-19 retinal pigment epithelial cells are highly resistant to oxidative stress and exercise strict control over their lysosomal redox-active iron. *Autophagy* 5:494–501
- Lieberthal W (2008) Macroautophagy: a mechanism for mediating cell death or for promoting cell survival? *Kidney Int* 74:555–557

- Liu J, Lu W, Reigada D et al (2008) Restoration of lysosomal pH in RPE cells from cultured human and ABCA4(-/-) mice: pharmacologic approaches and functional recovery. *Invest Ophthalmol Vis Sci* 49:772–780
- Luzio JP, Pryor PR, Bright NA (2007) Lysosomes: fusion and function. *Nat Rev Mol Cell Biol* 8:622–632
- Marino G, Madeo F, Kroemer G (2010) Autophagy for tissue homeostasis and neuroprotection. *Curr Opin Cell Biol*
- Nobukuni T, Joaquin M, Roccio M et al (2005) Amino acids mediate mTOR/raptor signaling through activation of class 3 phosphatidylinositol 3OH-kinase. *Proc Natl Acad Sci U S A* 102:14238–14243
- Pattingre S, Tassa A, Qu X et al (2005) Bcl-2 antiapoptotic proteins inhibit Beclin 1-dependent autophagy. *Cell* 122:927–939
- Punzo C, Kornacker K, Cepko CL (2009) Stimulation of the insulin/mTOR pathway delays cone death in a mouse model of retinitis pigmentosa. *Nat Neurosci* 12:44–52
- Ravikumar B, Vacher C, Berger Z et al (2004) Inhibition of mTOR induces autophagy and reduces toxicity of polyglutamine expansions in fly and mouse models of Huntington disease. *Nat Genet* 36:585–595
- Reme C, Wirz-Justice A (1985) [Circadian rhythm, the retina and light]. *Klin Monbl Augenheilkd* 186:175–179
- Reme CE, Young RW (1977) The effects of hibernation on cone visual cells in the ground squirrel. *Invest Ophthalmol Vis Sci* 16:815–840
- Rosenbaum DM, Degterev A, David J et al (2010) Necroptosis, a novel form of caspase-independent cell death, contributes to neuronal damage in a retinal ischemia-reperfusion injury model. *J Neurosci Res* 88:1569–1576
- Ryhanen T, Hyttinen JM, Kopitz J et al (2009) Crosstalk between Hsp70 molecular chaperone, lysosomes and proteasomes in autophagy-mediated proteolysis in human retinal pigment epithelial cells. *J Cell Mol Med* 13:3616–3631
- Seibenhener ML, Geetha T, Wooten MW (2007) Sequestosome 1/p62--more than just a scaffold. *FEBS Lett* 581:175–179
- Settembre C, Fraldi A, Jahreiss L et al (2008) A block of autophagy in lysosomal storage disorders. *Hum Mol Genet* 17:119–129
- Viiri J, Hyttinen JM, Ryhanen T et al (2010) p62/sequestosome 1 as a regulator of proteasome inhibitor-induced autophagy in human retinal pigment epithelial cells. *Mol Vis* 16:1399–1414
- Wang AL, Lukas TJ, Yuan M et al (2009a) Autophagy and exosomes in the aged retinal pigment epithelium: possible relevance to drusen formation and age-related macular degeneration. *PLoS One* 4:e4160
- Wang AL, Boulton ME, Dunn WA, Jr. et al (2009b) Using LC3 to monitor autophagy flux in the retinal pigment epithelium. *Autophagy* 5:1190–1193
- Wang T, Lao U, Edgar BA (2009c) TOR-mediated autophagy regulates cell death in Drosophila neurodegenerative disease. *J Cell Biol* 186:703–711
- Wu BX, Darden AG, Laser M et al (2006) The rat Apg3p/Aut1p homolog is upregulated by ischemic preconditioning in the retina. *Mol Vis* 12:1292–1302
- Yorimitsu T, Klionsky DJ (2005) Autophagy: molecular machinery for self-eating. *Cell Death Differ* 12 Suppl 2:1542–1552

Part II
Neuroprotection, Drugs and Novel
Protective Therapies

Chapter 13

Regeneration of Cone Outer Segments Induced by CNTF

Rong Wen, Weng Tao, Lingyu Luo, Deqiang Huang, Konrad Kauper,
Paul Stabila, Matthew M. LaVail, Alan M. Laties, and Yiwen Li

Keywords CNTF • Cone • Retinal degeneration • Cone outer segments
• Neuroprotection • Regeneration • S334ter rat • PNA • Cone ERG

13.1 Introduction

Hereditary retinal degenerations are a major cause of blindness and effective treatments are still being sought (Hartong et al. 2006). Among these conditions, the worldwide prevalence of retinitis pigmentosa, a group of inherited retinal degenerations, is about 1 in 4,000 for a total of more than 1 million affected individuals with well over 100 genes implicated. Although most mutations responsible for RP only affect rod photoreceptors directly, cones undergo a secondary degeneration (Delyfer et al. 2004; Hartong et al. 2006). Since cones are responsible for our central and color vision, rescue of the cones has become a major research challenge for therapeutic discovery and development.

R. Wen (✉) • L. Luo • D. Huang • Y. Li
Bascom Palmer Eye Institute, Miller School of Medicine,
University of Miami, Miami, FL 33136, USA
e-mail: rwen@med.miami.edu

W. Tao • K. Kauper • P. Stabila
Neurotech USA, Lincoln, RI 02865, USA

M.M. LaVail
Beckman Vision Center, University of California, San Francisco, CA 94143, USA

A.M. Laties
Departments of Ophthalmology, School of Medicine,
University of Pennsylvania, Philadelphia, PA, USA

We investigated the secondary cone degeneration in a retinal degeneration model, the S334ter-3 rats. In these rats, rod degeneration starts at postnatal day (PD) 8, peaks at PD 12–13, and most rods are degenerated by PD 20 (Liu et al. 1999). Cone degeneration starts with an early sign of COS loss, which in these animals occurs in many round or irregular areas across the retina (Li et al. 2010). When treated with CNTF, degenerating cones regenerate COS (Li et al. 2010). These results provide evidence that in early stages, CNTF reverses secondary cone degeneration. Sustained delivery of CNTF helps cones to maintain COS and their functions.

13.2 Materials and Methods

Homozygous S334ter rats and Sprague-Dawley rats were used. Intravitreal injections were carried out with 33-gauge needles. The left eyes were injected with recombinant human CNTF protein (10 $\mu\text{g}/5 \mu\text{L}$), and the right ones with phosphate-buffered saline (PBS) (5 μL) and served as control. CNTF was injected intravitreally at a given time point and retinas were collected 10 days later. CNTF-secreting microdevices were implanted in the vitreous at postnatal day (PD) 20 and eyes were collected 140 days later. Flat-mounted retinas were stained with fluorescent-conjugated peanut agglutinin (PNA) or antibodies against cone arrestin (CAR) and examined by confocal microscopy. Photopic ERG responses were elicited by 1 ms white flashes of 2.5 log cd s/m² in the Ganzfeld sphere with white background illumination of 30 cd s/m².

13.3 Results

13.3.1 Loss of COS in Early Stages of Cone Degeneration

At PD 10, PNA staining is evenly distributed across the retina (Fig. 13.1a). Loss of PNA staining is detected at PD12 when rod degeneration is at its peak (not shown). By PD 20, loss of COS appears in many small round or irregularly shaped PNA-negative areas (Fig. 13.1a). PNA staining outside those areas is similar to that of PD 10. Loss of COS progresses with age (Fig. 13.1a–f).

Since PNA only stains COS, antibodies against CAR were used as a marker to identify cone cells (Zhu et al. 2002). At PD 20, cells inside PNA-negative areas are positive of CAR, indicating they are cones (Fig. 13.2a). By PD 90, however, only a few CAR-positive cells remained in the PNA-negative areas (Fig. 13.2b). Thus, by PD 90, most of the cones in the PNA-negative areas were degenerated.

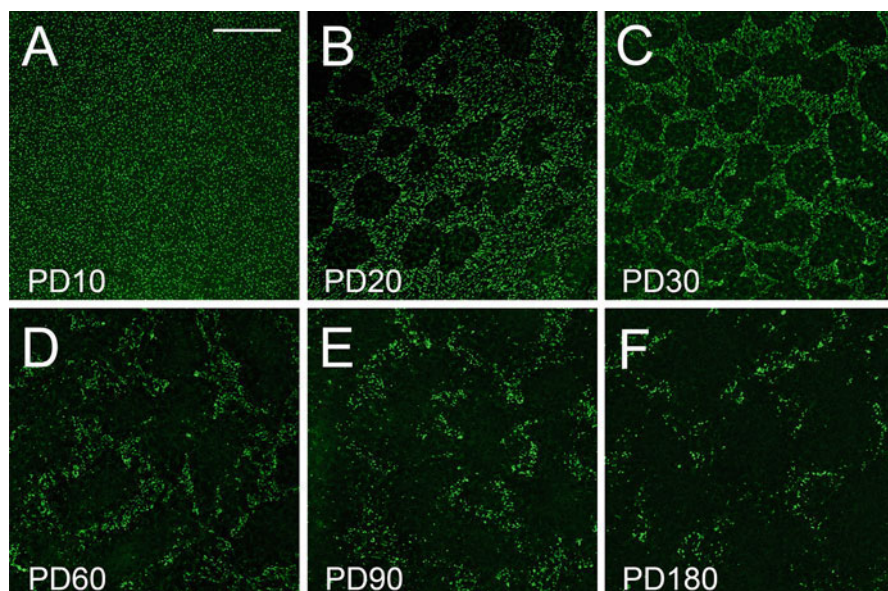


Fig. 13.1 Loss of COS. Flat-mounted retinas of different ages were stained with PNA. Loss of PNA staining is concentrated in small round or irregularly shaped areas and progressive with age. Scale bar: 200 μm (Modified from Li et al. 2010)

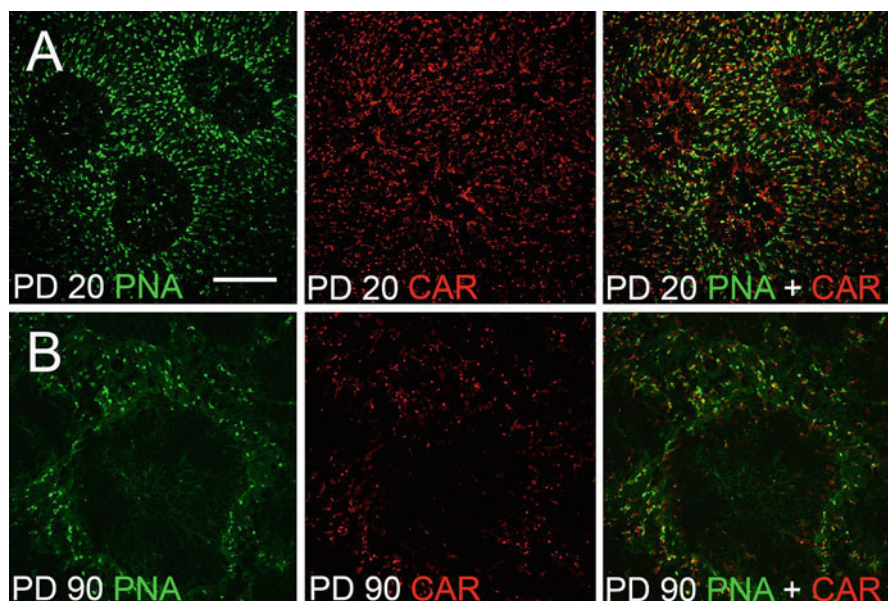


Fig. 13.2 Loss of cones. Flat-mounted retinas of S334ter-3 rats were double-stained with PNA and antibodies against cone arrestin (CAR). Many CAR-positive cells were found in the PNA-negative areas at PD 20 (a), but only a few remained in the PNA-negative areas at PD 90 (b). Scale bars: 100 μm (Modified from Li et al. 2010)

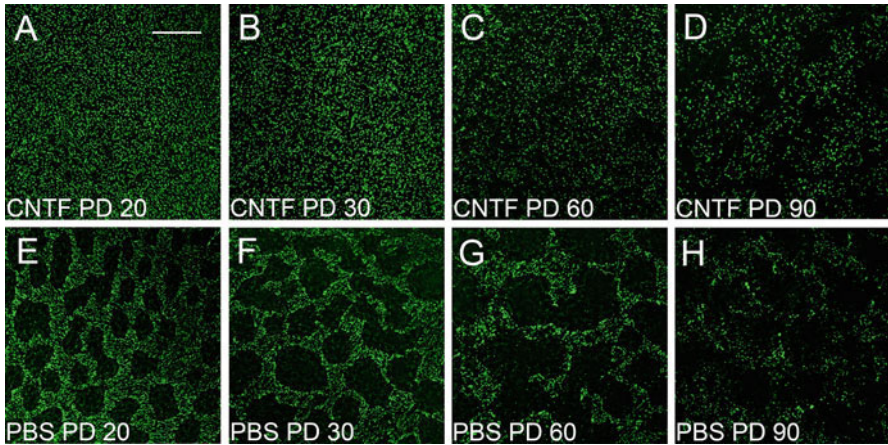


Fig. 13.3 Effect of CNTF on PNA-positive cells. Flat-mounted retinas of different ages were stained with PNA. After CNTF treatment, no PNA-negative areas were seen at PD 20 (a), whereas many PNA-negative areas appeared in PBS-treated retinas (e). The PNA-negative areas completely disappeared in PD 30 and 60 CNTF-treated retinas (b, c), as compared to the PBS-treated fellow eyes (f, g). This effect became less dramatic in PD 60 retinas (d), compared to PBS-treated retinas (h). Scale bar: 200 μm (Modified from Li et al. 2010)

13.3.2 *CNTF Promotes COS Regeneration*

Retinas treated with CNTF at PD 10 (endpoint PD 20) had no obvious PNA-negative areas (Fig. 13.3a), unlike PBS-treated ones in which many PNA-negative areas appeared (Fig. 13.3e). In most cases, PNA-negative areas completely disappeared in CNTF-treated retinas between PD 20 and 50 (endpoints PD 30–60) (Fig. 13.3b, c). In contrast, PBS-treated fellow retinas had many PNA-negative areas (Fig. 13.3f, g). This effect became less dramatic at PD 80 (endpoint PD 90, Fig. 13.3d) and almost disappeared in retinas of PD 170 (endpoint PD 180, not shown).

CNTF-induced reappearance of PNA-positive cells (Fig. 13.3a, b) suggests COS regeneration. To confirm this observation, eyes were treated with CNTF at PD 35 and retinas were examined at PD 45. Indeed, the density of PNA-positive cells in CNTF-treated retinas of PD 45 was significantly more than in the PD 35 controls before the treatment started (Fig. 13.4a).

Long-term effect of CNTF was achieved by using CNTF-secreting microdevices (Tao 2006; Tao et al. 2006; Tao and Wen 2007), which were implanted in the left eyes and control devices in the right eyes at PD 20, and retinas were collected at PD160. The densities of PNA-positive cells in CNTF-treated retinas are significantly more than in the control retinas (Fig. 13.4b). In another experiment, CNTF-secreting devices were implanted in the left eyes and control devices in the right eyes at PD 30. Cone ERGs were recorded at PD 135. The cone b-wave amplitude in CNTF-treated eyes is significantly higher than in control eyes (Fig. 13.4c, d).

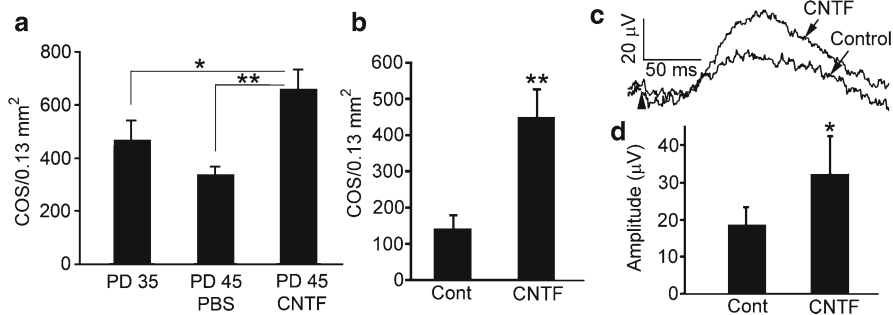


Fig. 13.4 Regeneration of COS and long-term effects. To demonstrate regeneration of COS, retinas were treated with either PBS or CNTF at PD 35 and collected by PD45 (a). PNA-positive cell counts in CNTF-treated retinas are 657 ± 76 ($n=4$), significantly more than in PBS treated (334 ± 33 , $n=3$), or untreated at PD 35 before the treatment (467 ± 73 , $n=3$) (a, ANOVA and Bonferroni test). To see the long-term effects of CNTF, CNTF-secreting microdevices were implanted at PD 20 and retinas were collected by PD 160 (b). PNA-positive cells are significantly more in CNTF-treated retinas (446 ± 80) than the controls (141 ± 40) (b, mean \pm SD, $n=3$, Student's t test). Cone ERGs were recorded at PD 135 from eyes implanted at PD 30. Representative cone b-waves are shown in panel C (arrowhead indicates the onset of flash, c). The amplitude of cone b-wave in CNTF-treated eyes (32.46 ± 10.02 μ V, mean \pm SD, $n=3$) is significantly higher than the control (17.70 ± 4.78 μ V, $n=3$) (d, Student's t test). * $P < 0.05$; ** $P < 0.01$ (Modified from Li et al. 2010)

13.4 Discussion

Loss of COS constitutes a prelude to cone degeneration, followed by cone cell death with a delay. In the S334ter-3 rats, the delay of cone death is about 2 months. PNA-negative patches are readily observable at PD20, but the cones in the PNA-negative areas are visibly alive. In contrast, cones are scarce to nonexistent in the PNA-negative areas in retinas by PD 90. This is also reflected in the CNTF-induced COS regeneration. Although partially responsive up to PD 60, regenerative potential has dramatically decreased in retinas by PD 80. A 2-month window is rather large considering the rapid rate of rod degeneration (10 days) in these animals. Although the time frame shifts, a strong parallel exists in patients with RP. In most clinical cases, rod degeneration in RP patients is much slower, and cone death should occur much later.

It is rather surprising that degenerating cones remain capable of regenerating COS, indicating that to a certain degree cone degeneration is reversible. COS are functional organelles that initiate the conversion of photons into neuronal signals. Regeneration COS should restore the light-sensing function of cones. This is very significant since it is possible that, in RP patients, degenerating cones may also be capable of regenerating COS. In that case, it is possible to stimulate those cones to regenerate COS and to restore vision to some extent.

Reports from CNTF clinical trials in patients with RP are consistent with our preclinical observations. In a Phase I clinical trial, three patients with late-stage RP

had significant improvement of vision after implantation of a device that delivers CNTF to the retina (Sieving et al. 2006). Recently, adaptive optics scanning laser ophthalmoscopy was used to observe three patients with retinal degeneration over a two-year interval (Talcott et al. 2010). While cone density significantly decreased in the sham-treated eyes, no decrease in cone density occurred in the CNTF-treated eye (Talcott et al. 2010). Together, these findings challenge us to rethink our goals in treating retinal degenerations. As a useful first step, we may want to emphasize early cone protection while continuing efforts to find ways to restore vision in late-stage RP patients.

CNTF has been shown to protect rod photoreceptors in different animal models (LaVail et al. 1992, 1998; Cayouette and Gravel 1997; Cayouette et al. 1998; Chong et al. 1999; Caffè et al. 2001; Liang et al. 2001; Bok et al. 2002; Tao et al. 2002). Our data support long-term sustained delivery CNTF as a therapy to benefit RP patients by preserving cone function and useful vision.

Acknowledgments We thank Dr. Cheryl Craft for anti cone-arrestin antibodies; Dr. Ying Song, Dr. Lian Zhao, and Yun Liu for technical assistance. Supported by Grants from NIH: R01EY015289 (RW), R01EY018586 (RW), R01EY001919 (MML), R01EY006842 (MML), Hope for Vision (RW), the James and Esther King Biomedical Research Program of the State of Florida (YL), the Department of Defense (W81XWH-09-1-0674, RW), and NIH Core Grants P30EY14801, P30EY002162, the Foundation Fighting Blindness (MML), and unrestricted grants from Research to Prevent Blindness, Inc., New York, NY to Bascom Palmer Eye Institute, Beckman Vision Center, and Scheie Eye Institute.

References

- Bok D, Yasumura D, Matthes MT et al (2002) Effects of adeno-associated virus-vectored ciliary neurotrophic factor on retinal structure and function in mice with a P216L rds/peripherin mutation. *Exp Eye Res* 74:719–735
- Caffè AR, Soderpalm AK, Holmqvist I et al (2001) A combination of CNTF and BDNF rescues rod photoreceptors but changes rod differentiation in the presence of RPE in retinal explants. *Invest Ophthalmol Vis Sci* 42:275–282
- Cayouette M, Gravel C (1997) Adenovirus-mediated gene transfer of ciliary neurotrophic factor can prevent photoreceptor degeneration in the retinal degeneration (rd) mouse. *Hum Gene Ther* 8:423–430
- Cayouette M, Behn D, Sendtner M et al (1998) Intraocular gene transfer of ciliary neurotrophic factor prevents death and increases responsiveness of rod photoreceptors in the retinal degeneration slow mouse. *J Neurosci* 18:9282–9293
- Chong NH, Alexander RA, Waters L et al (1999) Repeated injections of a ciliary neurotrophic factor analogue leading to long-term photoreceptor survival in hereditary retinal degeneration. *Invest Ophthalmol Vis Sci* 40:1298–1305
- Delyfer MN, Leveillard T, Mohand-Said S et al (2004) Inherited retinal degenerations: therapeutic prospects. *Biol Cell* 96:261–269
- Hartong DT, Berson EL, Dryja TP (2006) Retinitis pigmentosa. *Lancet* 368:1795–1809
- LaVail MM, Unoki K, Yasumura D et al (1992) Multiple growth factors, cytokines, and neurotrophins rescue photoreceptors from the damaging effects of constant light. *Proc Natl Acad Sci U S A* 89:11249–11253

- LaVail MM, Yasumura D, Matthes MT et al (1998) Protection of mouse photoreceptors by survival factors in retinal degenerations. *Invest Ophthalmol Vis Sci* 39:592–602
- Li Y, Tao W, Luo L et al (2010) CNTF induces regeneration of cone outer segments in a rat model of retinal degeneration. *PLoS One* 5:e9495
- Liang FQ, Aleman TS, Dejneka NS et al (2001) Long-term protection of retinal structure but not function using RAAV.CNTF in animal models of retinitis pigmentosa. *Mol Ther* 4:461–472
- Liu C, Li Y, Peng M et al (1999) Activation of caspase-3 in the retina of transgenic rats with the rhodopsin mutation s334ter during photoreceptor degeneration. *J Neurosci* 19:4778–4785
- Sieving PA, Caruso RC, Tao W et al (2006) Ciliary neurotrophic factor (CNTF) for human retinal degeneration: phase I trial of CNTF delivered by encapsulated cell intraocular implants. *Proc Natl Acad Sci U S A* 103:3896–3901
- Talcott K, E., Ratnam K, Sundquist SM et al (2010) Longitudinal study of cone photoreceptors during retinal degeneration and in response to ciliary neurotrophic factor treatment. *Invest Ophthalmol Vis Sci* (in press)
- Tao W (2006) Application of encapsulated cell technology for retinal degenerative diseases. *Expert Opin Biol Ther* 6:717–726
- Tao W, Wen R (2007) Application of encapsulated cell technology for retinal degenerative diseases. In: Tombran-Tink J, Barnstable CJ (eds) *Retinal Degenerations*. Humana Press
- Tao W, Wen R, Laties AM (2006) Cell-based delivery systems: Development of encapsulated cell technology for ophthalmic applications. In: Jaffe JJ, Ashton P, Pearson PA (eds) *Intraocular drug delivery*. Humana Press, New York, NY
- Tao W, Wen R, Goddard MB et al (2002) Encapsulated cell-based delivery of CNTF reduces photoreceptor degeneration in animal models of retinitis pigmentosa. *Invest Ophthalmol Vis Sci* 43:3292–3298
- Zhu X, Li A, Brown B et al (2002) Mouse cone arrestin expression pattern: light induced translocation in cone photoreceptors. *Mol Vis* 8:462–471

Chapter 14

Glucocorticoid-Dependent Mechanisms in Photoreceptor Survival

Marisa A. Cubilla, Mauricio M. Castañeda, Tomás P. Bachor,
and Angela M. Suburo

Keywords Glucocorticoids • Glucocorticoid receptor • Mifepristone • Dexamethasone • Light-induced retinal degeneration • Rhodopsin • Caspase-3 • Cleaved caspase-3 • Apoptosis

14.1 Introduction

Glucocorticoids (GCs) act directly on photoreceptors (PRs), as shown by immediate ERG changes in normal rats receiving intravenous GCs (Abraham et al. 1998). These changes are blocked by mifepristone (MFP), an antagonist of the GC receptor (GR). Endogenous GCs or exogenous dexamethasone (DEX) prevent light-induced degeneration (Wenzel et al. 2001), whereas intravitreal flucinolone acetate preserves PRs in RCS rats (Glybina et al. 2009).

A single GR gene can be translated into several different proteins. GR α is a ligand-dependent transcription factor regulating most GC effects, whereas GR β does not bind GCs but suppresses GR α activity (Cidlowski 2009). The GR α can positively or negatively regulate gene expression and interacts directly with other transcription factors (Jacques et al. 2010).

Continuous light triggers PR cell death by excessive activation of the transduction cascade (Fain 2006). Death results from activation of several signaling pathways, including caspase-3 cleavage (Organisciak and Vaughan 2010). GR ligands are increasingly used in different retinal diseases (Edelman 2010), and antagonists have been advocated for treatment of serous chorioretinopathy (Gemenetzi et al. 2010), therefore we need a deeper understanding of GC pathways involved in PR

M.A. Cubilla • M.M. Castañeda • T.P. Bachor • A.M. Suburo (✉)
Facultad de Ciencias Biomédicas, Universidad Austral,
Pilar 1629AHJ, Buenos Aires, Argentina
e-mail: amsuburo@cas.austral.edu.ar

survival. We report here the effects of DEX and MFP on rhodopsin (RHO) levels and caspase-3 activation in a model of low-level and continuous light.

14.2 Materials and Methods

Balb-c male mice (35–45 days of age) were bred and cared in accordance with the ARVO Statement for the Use of Animals in Ophthalmic and Vision Research. Standard illumination was 12-h light:12-h dark, ≤ 60 lx. Animals were left in complete darkness during 24 h. The next day, at noon, mice were randomly separated. The control group returned to standard illumination and experimental groups were housed for 2 or 4 days under 1,500 lx. The latter received DEX (10 mg/kg/day, sc, Sidus, Buenos Aires), MFP (30 mg/kg/2 days, sc, Sigma-Aldrich, St Louis, MO), and MFP and DEX in consecutive but separate injections (M+D), or similar volumes of propylene glycol, the vehicle (VHC). Mice were given 1 mL of 5% dextrose ip as required. They were euthanatized at noon, after 1 h of complete darkness to allow full separation of the retinal pigment epithelium (RPE).

Immunohistochemistry, immunofluorescence, and Western blots were done as described (Torbidoni et al. 2005, 2006; Iribarne et al. 2008), using the following primary antibodies: GR α (N499, a gift from M. Garabedian, New York University School of Medicine, NY), Glyceraldehyde 3-phosphate dehydrogenase (GAPDH, Santa Cruz Biotechnology), RHO (antibody B6-30, a gift from J. Nathans, Johns Hopkins University School of Medicine, MD), and cleaved caspase-3 (CC-3, 9661, Cell Signaling Technology Inc, MA). Three samples were studied for each marker and each experimental condition.

14.3 Results

14.3.1 GRs in Control and Light-Exposed Retinas

In control retinas, GR α immunoreactivity appeared in all nuclear retinal layers, but staining was lowest in the outer nuclear layer (ONL) and RPE (Fig. 14.1a). Cells of the ganglion cell layer (GCL) always showed high immunoreactivity. After exposure to 1,500 lx during 2 days, structural damage was limited to the dorsolateral quadrant, which showed shorter PR outer segments (OS) and a slight reduction in ONL rows. However, all PR nuclei now displayed strong GR α immunoreactivity. After 4 days of light exposure, OS damage appeared in every region of the retina, but was more severe in the dorsotemporal quadrant, where only a few ONL rows remained. Every retinal nuclear layer showed intense GR α immunostaining, higher than in 2-day-exposed retinas. No increase was detected in the RPE (Fig. 14.1b, c).

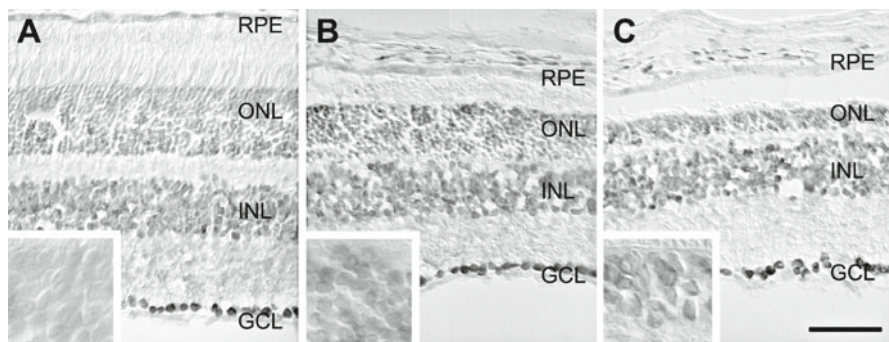


Fig. 14.1 GR immunostaining in retinal cryosections through the dorsolateral quadrant. (a) Under standard illumination conditions, GR immunoreactivity appeared in every nuclear layer, being stronger in the GCL than in the INL and ONL. The RPE displayed nuclear and cytoplasmic staining. (b) In a mouse exposed during 2 days, the retina showed a reduced ONL with short outer segments. PR nuclei immunoreactivity was stronger than in the unexposed retinas. (c) After a 4-day exposure, OS were absent and the ONL only retained a few nuclear rows. Remaining PR nuclei showed strong GR immunostaining. Bar, 50 μm . *Insets*. PR nuclei are enlarged to show immunoreactivity changes in exposed retinas. The same bar equals to 15 μm

14.3.2 Rhodopsin

In VHC mice exposed during 2 days, RHO decreased to about 70% of nonexposed and nontreated control levels. MFP mice showed a greater decrease, to 40% of controls. DEX treatment blocked the effects of light, even in mice receiving MFP (Fig. 14.2a).

After a 4-day exposure, RHO in VHC mice dropped to less than 20% of controls. In MFP mice, RHO could not be detected even after developing blots beyond the saturation point for other groups. RHO was only slightly decreased in M+D mice (Fig. 14.2b). VHC mice exposed during 4 days and returned to standard illumination for another 6 days showed partial recovery of control RHO levels, but this protein remained barely detectable in mice receiving MFP during exposure (not shown).

14.3.3 Activation of Caspase-3

CC-3 is not detected in control retinas (Torbidoni et al. 2006). After a 2-day exposure, a few CC-3⁺ cells appeared in the ONL of the dorsotemporal quadrant (<1 per 40 \times field). More CC-3⁺ cells (2–5 per 40 \times field) appeared in every ONL region of MFP mice exposed during the same period (Fig. 14.3a, b). A similar pattern was observed after 4 days of 1,500 lx. CC-3⁺ cells were always restricted to the ONL.

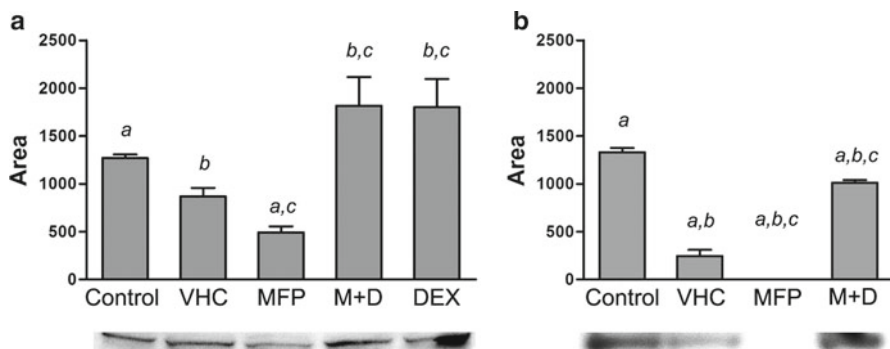


Fig. 14.2 Levels of RHO protein in control and light-exposed mice. Bars represent mean \pm SE of three different experiments. Means with the same letter are significantly different from each other (ANOVA and Tukey's test). (a) Two-day exposure; *a* and *b*, $P < 0.05$; *c*, $P < 0.01$. (b) Four-day exposure; *a-c*, $P < 0.01$

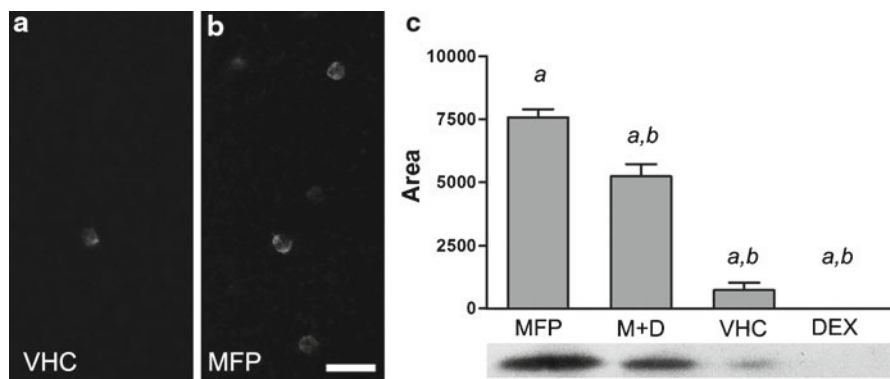


Fig. 14.3 (a, b) Wholemouts showing immunofluorescent CC-3⁺ nuclei in the ONL of retinas exposed during 2 days after VHC or MFP injection. Bar, 20 μ m. (c) Levels of CC-3 protein in mice exposed during 4 days. Means with the same letter are significantly different from each other (ANOVA and Tukey's test); *a* and *b*, $P < 0.01$

Western blots also showed higher levels of CC-3 in MFP than in VHC mice. Large amounts of the activated caspase could still be detected after 4 days of light exposure in MFP and M+D mice. By contrast, no CC-3 could be detected in exposed mice treated with DEX (Fig. 14.3c).

14.4 Discussion

We explored the distribution of GR α immunoreactivity during the early phases of a 1,500 lx-induced retinal degeneration model (Torbidoni et al. 2005). Changes of GR α in retinas subjected to 1,500 lx indicated that glucocorticoid nuclear signaling

contributed to the PR damage response. Nuclear translocation of GR has also been described in another model of light damage (Wenzel et al. 2001). Strong nuclear immunoreactivity suggested a build-up of endogenous ligands in light-exposed retinas, since hormone activation leads to the translocation of GR α from the cytoplasm to the nucleus (Nishi 2010). GR transcription and translation might also be upregulated. Further studies should clarify involvement of the different GR splicing variants (Hinds et al. 2010).

Light-induced PR degeneration is initiated by OS damage (Organisciak and Vaughan 2010). Consistent with that phenomenon, a 30% of RHO protein was lost after 2 days of light exposure. Mice receiving MFP showed even lower RHO levels. However, in mice receiving DEX, or both MFP and DEX, light exposure during 2 days did not affect RHO levels. MFP effects on RHO levels were completely reversed by DEX, indicating that they were mediated by GR α . Little RHO recovery was found in MFP mice returned to standard illumination, suggesting that PR death would be increased. This was confirmed by amounts of CC-3 in the different experimental groups. CC-3 enzymatic activity, protein, and immunoreactivity gradually increase after 2 and 4 days of light exposure (Torbidoni et al. 2006). VHC mice displayed a similar pattern, whereas higher numbers of CC-3 immunoreactive ONL nuclei and larger amounts of CC-3 protein appeared in MFP mice. DEX administration lessened the MFP-dependent CC-3 increase, but M+D mice still showed higher CC-3 levels than VHC mice. The different effects of DEX on MFP-induced changes of RHO and CC-3 would imply that cell death mechanisms were still active in spite of RHO preservation. DEX could block caspase-3 cleavage and preserve RHO by different mechanisms. Larger amounts of DEX might be required to prevent cell death than to preserve RHO. For example, downregulation of AP-1 activity after 52 mg/kg DEX is associated to survival of light-damaged PRs (Wenzel et al. 2001), whereas downregulation of AP-1 after 1.8 mg/kg DEX did not protect PRs in a RHO mutant dog model (Gu et al. 2009). Other mechanisms are possible. Activation of calpain, a protease involved in light-induced retinal degeneration (Imai et al. 2010), is prevented by DEX and probably exacerbated by MFP (Shuto et al. 2009). In addition, we have shown that the antiapoptotic molecule Bcl-X_L disappears during light exposure, but remains at normal levels when DEX is given (Cubilla et al. 2010). Other steroid hormones and receptors might be involved in PR survival, since endogenous GCs but not DEX can bind to the mineralocorticoid receptor (Nishi 2010). This receptor is expressed by PRs and seems to be actively involved in retinal maintenance (Wilkinson-Berka et al. 2009). MFP can also block the progesterone receptor, but this seems an unlikely protection mechanism, since progesterone has been found ineffective in a rat light-induced retinal degeneration model (Kaldi and Berta 2004).

Acknowledgments MAC and MMC are research fellows from the Consejo Nacional de Investigaciones Científicas y Técnicas (CONICET), Argentina. MAC was also a fellow of ANPCyT, MINCYT, during the initial phase of this project. AMS is Principal Researcher from CONICET. Studies reported here were funded by grants from Universidad Austral and ANPCyT (PICT 21399/2004 and PICTO 2008 0090). We are very grateful to Guillermo Gastón and Soledad Arregui for their skilful technical assistance.

References

- Abraham I, Palhalmi J, Szilagyi N et al (1998) Glucocorticoids alter recovery processes in the rat retina. *Neuroreport* 9:1465–1468
- Cidlowski JA (2009) Glucocorticoids and their actions in cells. *Retina* 29:S21–23
- Cubilla MA, Castañeda MM, Luzzani GA et al (2010) Glucocorticoid receptors in light-induced retinal degeneration. In: Association for Research in Vision and Ophthalmology, Inc. (ARVO) Annual Meeting Fort Lauderdale Florida
- Edelman JL (2010) Differentiating intraocular glucocorticoids. *Ophthalmologica* 224 Suppl 1:25–30
- Fain GL (2006) Why photoreceptors die (and why they don't). *Bioessays* 28:344–354
- Gemenetzi M, De Salvo G, Lotery AJ (2010) Central serous chorioretinopathy: an update on pathogenesis and treatment. *Eye (Lond)*
- Glybina IV, Kennedy A, Ashton P et al (2009) Photoreceptor neuroprotection in RCS rats via low-dose intravitreal sustained-delivery of fluocinolone acetonide. *Invest Ophthalmol Vis Sci* 50:4847–4857
- Gu D, Beltran WA, Pearce-Kelling S et al (2009) Steroids do not prevent photoreceptor degeneration in the light-exposed T4R rhodopsin mutant dog retina irrespective of AP-1 inhibition. *Invest Ophthalmol Vis Sci* 50:3482–3494
- Hinds TD, Jr., Ramakrishnan S, Cash HA et al (2010) Discovery of Glucocorticoid Receptor- β in Mice with a Role in Metabolism. *Mol Endocrinol* 24:1715–1727
- Imai S, Shimazawa M, Nakanishi T et al (2010) Calpain inhibitor protects cells against light-induced retinal degeneration. *J Pharmacol Exp Ther* 335:645–652
- Iribarne M, Ogawa L, Torbidoni V et al (2008) Blockade of endothelinergic receptors prevents development of proliferative vitreoretinopathy in mice. *Am J Pathol* 172:1030–1042
- Jacques E, Semlali A, Boulet LP et al (2010) AP-1 overexpression impairs corticosteroid inhibition of collagen production by fibroblasts isolated from asthmatic subjects. *Am J Physiol Lung Cell Mol Physiol* 299:L281–287
- Kaldi I, Berta A (2004) Progesterone administration fails to protect albino male rats against photostress-induced retinal degeneration. *Eur J Ophthalmol* 14:306–314
- Nishi M (2010) Imaging of transcription factor trafficking in living cells: lessons from corticosteroid receptor dynamics. *Methods Mol Biol* 647:199–212
- Organisciak DT, Vaughan DK (2010) Retinal light damage: mechanisms and protection. *Prog Retin Eye Res* 29:113–134
- Shuto M, Higuchi K, Sugiyama C et al (2009) Endogenous and exogenous glucocorticoids prevent trimethyltin from causing neuronal degeneration of the mouse brain in vivo: involvement of oxidative stress pathways. *J Pharmacol Sci* 110:424–436
- Torbidoni V, Iribarne M, Suburo AM (2006) Endothelin receptors in light-induced retinal degeneration. *Exp Biol Med (Maywood)* 231:1095–1100
- Torbidoni V, Iribarne M, Ogawa L et al (2005) Endothelin-1 and endothelin receptors in light-induced retinal degeneration. *Exp Eye Res* 81:265–275
- Wenzel A, Grimm C, Seeliger MW et al (2001) Prevention of photoreceptor apoptosis by activation of the glucocorticoid receptor. *Invest Ophthalmol Vis Sci* 42:1653–1659
- Wilkinson-Berka JL, Tan G, Jaworski K et al (2009) Identification of a retinal aldosterone system and the protective effects of mineralocorticoid receptor antagonism on retinal vascular pathology. *Circ Res* 104:124–133

Chapter 15

HDAC Inhibition Prevents *Rd1* Mouse Photoreceptor Degeneration

Javier Sancho-Pelluz and François Paquet-Durand

Keywords Retinitis pigmentosa • HDAC • Photoreceptor degeneration • *rd1* mouse • Retinal explant culture • Trichostain A • Neuroprotection • PARP

15.1 Introduction

Retinitis pigmentosa (RP) is a heterogeneous group of inherited retinal diseases. In the most typical progression, mutation-induced rod photoreceptor death precedes mutation-independent cone cell death. The progressive loss of photoreceptors leads to typical clinical symptoms, such as night blindness, tunnel vision, and accumulation of pigment deposits.

The *rd1* mouse is a well-known animal model for studies on RP (Sancho-Pelluz et al. 2008). It carries a mutation in the gene encoding for the β -subunit of rod photoreceptor cGMP phosphodiesterase-6 (Bowes et al. 1990), causing cGMP accumulation and leading to different alterations, such as overactivation of PARP (Paquet-Durand et al. 2007), and eventually to photoreceptor cell death.

Histone modifications, such as acetylation, may influence chromatin structure, DNA packaging, and ultimately transcription (Wade 2001). The enzymes directly regulating acetylation balance are histone acetyltransferases (HATs), which add acetyl groups to lysine residues, and histone deacetylases (HDACs), which remove

J. Sancho-Pelluz (✉)

Department of Ophthalmology, Columbia University, New York, NY 10032, USA

e-mail: fjs2115@columbia.edu

F. Paquet-Durand

Division of Experimental Ophthalmology, Institute for Ophthalmic Research,
University of Tübingen, Tübingen, Germany

acetyl groups. Generally, an increase of histone acetylation levels is accompanied by increased transcription, while low levels are associated with silencing of gene transcription (Kruszewski and Szumiel 2005).

We analyzed the expression of HDACs in retinas of wild-type and *rd1* animals and studied their enzymatic activity *in vivo* and *in vitro*. Photoreceptor cell death was preceded by activation of HDACs and, importantly, HDAC inhibition was strongly neuroprotective, proposing a pivotal position for HDACs within the metabolic pathways leading to cell death.

15.2 Materials and Methods

15.2.1 Animals

Animals were housed under standard white cyclic lighting and had *ad libitum* access to food and water. C3H *rd1/rd1* (*rd1*) and control C3H wild-type (*wt*) mice were used. All procedures were performed in accordance with the ARVO statement for the use of animals in ophthalmic and visual research. Because of the critical changes at postnatal day (P) 11 (Sancho-Pelluz et al. 2008), most comparisons between *rd1* and *wt* were carried out at this age.

15.2.2 *In Vitro* Retinal Explant Cultures

Retinas from P5 *rd1* and *wt* animals were used to generate retinal explants as described before (Paquet-Durand et al. 2009). The first 2 days, the retina was left in R16 culture medium (Invitrogen Ltd, Paisley, UK) without treatment. At P7, cultures were exposed to Trichostatin A (TSA, 1 μ M), an HDAC inhibitor (HDACi), or kept as untreated control. Explants were cultured until P11 for short-term cultures (P5+2+4), or until P28, for long-term cultures (P5+2+21).

15.2.3 HDAC Assay

Fluor de Lys Fluorescent Assay System Assay (Biomol, Hamburg, Germany) was originally intended to measure HDAC activity in tissue homogenates. It was adapted for use on 4% PFA fixed retinal cryosections and performed as described in (Sancho-Pelluz et al. 2010).

15.2.4 TUNEL and Immunostaining

The terminal deoxynucleotidyl transferase dUTP nick end labeling (TUNEL) assay (Roche Diagnostics, Mannheim, Germany) and immunostaining were performed on retinal cryosections from *wt*, TSA-treated and -untreated *rd1* retinas. Primary antibodies were from Cell Signaling (Danvers, MA, USA; acetylated lysine, Sirt2; HDAC2, HDAC5, Rhodopsin) and Alexis Biochemicals (Lörrach, Germany; PAR). Corresponding secondary antibodies, Alexa 488, were from Molecular Probes (Eugene, OR, USA). Sections were mounted in Vectashield with DAPI (Vector Labs, Burlingame, CA, USA).

15.3 Results

15.3.1 Study of Expression and Activity of HDACs in *wt* and *rd1* Retina

Immunohistology revealed no changes in expression of the two major HDAC classes at P11. Class I HDAC2 (Fig. 15.1a, b) and class II HDAC5 (Fig. 15.1b, c) were expressed in nuclei of the outer nuclear layer (ONL), inner nuclear layer (INL), and ganglion cell layer (GCL).

While the ONL of *wt* P11 animals seems to be devoid of visible HDAC activity (Fig. 15.1e), *rd1* presented some ONL cell bodies with elevated HDAC activity (*arrowheads* in Fig. 15.1f). In *wt* mouse ONL, an antibody detecting acetylation of lysine residues showed uniform staining of the photoreceptor population (Fig. 15.1g). In contrast to this, the *rd1* ONL presented conspicuous “gaps” in the staining (*arrowheads* in Fig. 15.1h), which indicated nonacetylated nuclei. These colocalized with positive TUNEL staining (*arrow* in Fig. 15.1i, j), suggesting that hypoacetylation was related to the degenerative process. HDAC activity positive cells did not colocalize with TUNEL staining (Fig. 15.1l), implying that HDAC overactivation preceded the final stages of cell death.

15.3.2 HDAC I/II Inhibitors Protect *rd1* Photoreceptors Regulating PARP Activity

After short-term culture (P5+2+4) with/without TSA, HDAC activity assay was used to ascertain successful HDAC inhibition. Nontreated retinal cultures still presented HDAC activity (*arrowheads* in Fig. 15.1m), whereas TSA-treated retinas did

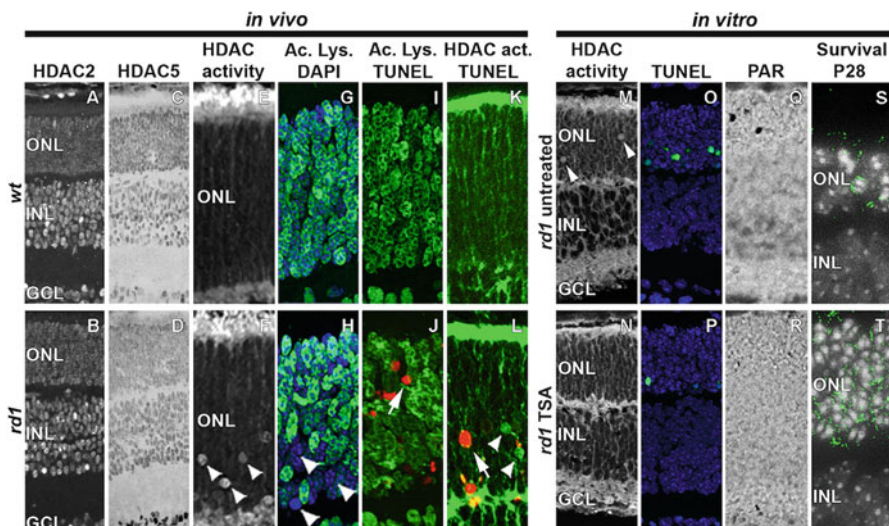


Fig. 15.1 HDACs in *rd1* and *wt* retinas. Antibodies labeling different HDAC classes were used in retinal sections showing no difference in expression between *wt* and *rd1* mice (a–d). HDACs are overactivated in *rd1* when compared to *wt* (e, f). Level of acetylation is lower in the ONL of *rd1* animals (arrowheads in h) compared to the *wt* (g). Those hypoacetylated cells matched with TUNEL assay (arrow in j). HDAC overactivated cells (arrowheads in i) do not correlate with TUNEL-positive cells (arrow in i). TSA treated *rd1* retinal explants do not present HDAC-activity-positive cells (n) compared to the untreated situation (arrowheads in m). TSA seemed to reduce the number of TUNEL-positive cells in short-term cultures (o, p). PAR expression was also reduced in ONL of treated animals, therefore PARP activity decreased (q, r). The rescue of cells was obvious when the treatment was prolonged until 28 days (s, t). Most remaining cells seemed to be rods according to the rhodopsin expression (green in t)

not show positive cells in the ONL (Fig. 15.1n). Photoreceptor viability was evaluated using the TUNEL assay. In *rd1* retina, 1 μ M of TSA significantly decreased the rate of cell death compared to untreated retina (Fig. 15.1o, p).

We had previously found strong activation of PARP to be causally related to photoreceptor cell death in *rd1* retina (Paquet-Durand et al. 2007). Immunostaining for poly-ADP-ribosylated proteins (PAR), the product of PARP, was performed to identify a possible relation between HDACs and PARP. In *rd1* explants, the number of PAR positive cells was reduced by TSA treatment (Fig. 15.1q, r), implying that activation of PARP in *rd1* photoreceptors took place downstream of HDAC activity.

Since short-term TSA treatment (until P11) had reduced photoreceptor cell death as evidenced by the TUNEL assay, we used long-term cultures (until P28) to test for pro-survival effects of TSA. Here, TSA treatment almost doubled the number of

surviving *rdl* photoreceptor rows (Fig. 15.1s, t) with the majority of surviving *rdl* photoreceptors showing rhodopsin expression (green). In *rdl*-cultured retina, since outer segments do not develop properly, rhodopsin aggregates predominantly in the cytoplasm of photoreceptors (Bowes et al. 1988).

15.4 Discussion

HDAC activity has been linked to diverse cellular processes, such as gene expression, cytoskeletal modifications, cell division, and differentiation (Haberland et al. 2009). HDAC inhibition can have opposite effects in different paradigms, promoting cell death in carcinogenic tissue while supporting rescue in some neurological disorders (Morrison et al. 2007). Any modification of HDAC activity, and thereby of histone acetylation and transcription, may have critical effects on the viability of the cell.

When the HDAC class I/II inhibitor TSA was applied in short-term retinal explants from *rdl* animals, a reduction in dying cells was noted. This decrease transformed into a significant prosurvival effect in the long-term treatment, with an ONL thickness that was roughly doubled. At that age (P28), in untreated *rdl* mouse, rods are almost completely gone. The remaining ONL contains one or two rows of photoreceptors, mainly cones. Furthermore, rhodopsin was expressed in most of the surviving *rdl* photoreceptors in treated retinas (Bowes et al. 1988), whereas in the nontreated most of the ONL cells were rhodopsin negative, indicating that in this case the surviving cells were mostly cones. The rescue promoted by the inhibition of HDAC suggests that HDAC overactivation was a cause and not a consequence of photoreceptor cell death.

In degenerating *rdl* retina, PARP is overactivated and promoting cell death (Paquet-Durand et al. 2007; Sahaboglu et al. 2010). Since PARP activity may be regulated by acetylation on specific lysine residues (Haenni et al. 2008), HDACs might directly control PARP activity. Our results showing reduced accumulation of PAR after HDAC I/II inhibition also suggest a link, direct or indirect, between high HDAC activity and overactivation of PARP. Furthermore, PARP activity colocalizes to a large extent with TUNEL-positive cells (Paquet-Durand et al. 2007), while HDAC activity correlation with TUNEL is only minor. Therefore, HDAC activity appears to temporally precede PARP in *rdl* photoreceptor cell death mechanisms (Fig. 15.2).

Taken together, increased HDAC activity in degenerating *rdl* photoreceptors was found to be causally involved in cell death and possibly connected to downstream activation of PARP. This highlights HDACs as novel targets for the pharmacological treatment of RP and related neurodegenerative diseases.

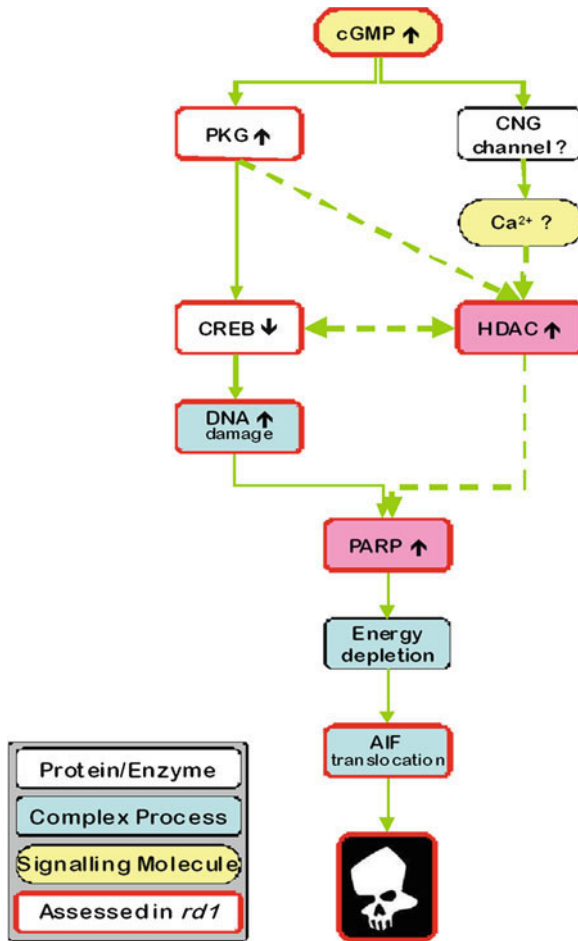


Fig. 15.2 Role of HDACs in the molecular cell death pathways during *rd1* photoreceptor degeneration. A mutation in PDE6 induces deregulation of cGMP, which causes PKG activation and possibly Ca²⁺-ion influx via CNG ion channels. CREB expression and activity is lower in the *rd1* mouse retina. Overactivation of HDACs might be involved in CREB downregulation. Since CREB regulates a number of genes protecting against oxidative stress, its downregulation may cause DNA damage and therefore activation of PARP. Excessive activity of HDAC might further contribute to PARP overactivation. This may lead to energy depletion and translocation of apoptosis-inducing factor (AIF) from mitochondria to the nucleus. Eventually, AIF activates endonucleases which cause DNA fragmentation and precipitate cell death. *Arrows*: activating interaction. *Dotted lines*: unclear interaction. (Diagram modified after Sancho-Pelluz et al. 2008)

Acknowledgments We thank Beckman, Bernard and Shirlee Brown Glaucoma Lab, Foundation Fighting Blindness, Schneeweiss Stem Cell Fund, Jonas Family Fund, Bernard Becker-Association of University Professors in Ophthalmology-Research to Prevent Blindness (RPB), and EY018213. The Kerstan Foundation and the German research Institute (PA175 1/1-1).

References

- Bowes C, Li T, Danciger M et al (1990) Retinal degeneration in the *rd* mouse is caused by a defect in the beta subunit of rod cGMP-phosphodiesterase. *Nature* 347:677–680
- Bowes C, van Veen T, Farber DB (1988) Opsin, G-protein and 48-kDa protein in normal and *rd* mouse retinas: developmental expression of mRNAs and proteins and light/dark cycling of mRNAs. *Exp Eye Res* 47:369–390
- Haberland M, Montgomery RL, Olson EN (2009) The many roles of histone deacetylases in development and physiology: implications for disease and therapy. *Nat Rev Genet* 10:32–42
- Haenni SS, Hassa PO, Altmeyer M et al (2008) Identification of lysines 36 and 37 of PARP-2 as targets for acetylation and auto-ADP-ribosylation. *Int J Biochem Cell Biol* 40:2274–2283
- Kruszewski M, Szumiel I (2005) Sirtuins (histone deacetylases III) in the cellular response to DNA damage – facts and hypotheses. *DNA Repair* 4:1306–1313
- Morrison BE, Majdzadeh N, D’Mello SR (2007) Histone deacetylases: focus on the nervous system. *Cell Mol Life Sci* 64:2258–2269
- Paquet-Durand F, Hauck SM, van Veen T et al (2009) PKG activity causes photoreceptor cell death in two retinitis pigmentosa models. *J Neurochem* 108:796–810
- Paquet-Durand F, Silva J, Talukdar T et al (2007) Excessive activation of poly(ADP-ribose) polymerase contributes to inherited photoreceptor degeneration in the retinal degeneration mouse 1. *J Neurosci* 27:10311–10319
- Sahaboglu A, Tanimoto N, Kaur J et al (2010) PARP1 gene knock-out increases resistance to retinal degeneration without affecting retinal function. *PLoS One*, accepted, in press
- Sancho-Pelluz J, Alavi MV, Sahaboglu A et al (2010) Excessive HDAC activation is critical for neurodegeneration in the *rdl* mouse. *Cell Death Dis* 1:e24
- Sancho-Pelluz J, Arango-Gonzalez B, Kustermann S et al (2008) Photoreceptor cell death mechanisms in inherited retinal degeneration. *Mol Neurobiol* 38:253–269
- Wade PA (2001) Transcriptional control at regulatory checkpoints by histone deacetylases: molecular connections between cancer and chromatin. *Hum Mol Genet* 10:693–698

Chapter 16

Neuroprotective Dose Response in RCS Rats Implanted with Microphotodiode Arrays

Machelle T. Pardue, Moon K. Kim, Tiffany A. Walker,
Amanda E. Faulkner, Alan Y. Chow, and Vincent T. Ciavatta

Keywords Retinal degeneration • Retinitis pigmentosa • RCS rats • Electroretinogram • Retinal function • Light • Subretinal • Microphotodiode array

16.1 Introduction

Implantation of a subretinal MPA has been shown to preserve retinal function and structure in RCS rats (Pardue et al. 2005a, b). In these studies, RCS rats were implanted at 21 days of age and then followed for 8 or 17 weeks. All animals were housed in a normal 12:12 light cycle (~100 lx) and then exposed to ERG flash stimuli such that the 8-week group received weekly testing with a long protocol (17 steps) and the 17-week group received biweekly testing with a short protocol (nine steps). The implanted RCS rats with 8 weeks of weekly ERG testing showed significantly greater ERG b-wave amplitudes and greater photoreceptor counts, whereas the implanted RCS rats from the 17 weeks group did not show any functional or morphological benefits. Since microphotodiodes produce electrical currents in proportion to

M.T. Pardue (✉) • V.T. Ciavatta
Rehabilitation Research and Development Center of Excellence,
Atlanta VA Medical Center, Decatur, GA 30033, USA

Department of Ophthalmology, Emory University, Atlanta, GA, USA
e-mail: mpardue@emory.edu

M.K. Kim • T.A. Walker • A.E. Faulkner
Rehabilitation Research and Development Center of Excellence,
Atlanta VA Medical Center, Decatur, GA 30033, USA

A.Y. Chow
Optobionics Corp., Naperville, IL, USA

the intensity of incident light, we hypothesize that this difference in neuroprotection is due to the increased current output from the MPA device in the 8-week group undergoing weekly ERG with a long protocol. Furthermore, exposing the eye to greater light levels and therefore increased electrical current may produce greater neuroprotective effects. Here, we examined the dose response of subretinal electrical stimulation by exposing RCS rats implanted with electrically active MPAs to variable durations and combinations of two different light regimens: pulsing incandescent bulbs and flashes from xenon bulbs of an ERG Ganzfeld.

16.2 Materials and Methods

16.2.1 Implantation of RCS Rats with MPAs

Dystrophic RCS rats, originally obtained from Matthew LaVail of the University of California, San Francisco were used in this study. RCS rats ($n=28$) were implanted monocularly at 21 days of age with an MPA device, as previously described (Ball et al. 2001). Briefly, the rats were anesthetized with ketamine (60 mg/kg)/xylazine (7.5 mg/kg) and the pupils dilated with 1% tropicamide. After preparing a sterile field, the eye was rotated inferiorly and a 1.5 mm incision made through all layers of the orbit, approximately 2 mm from the superior limbus. Saline was placed on the eye and a localized retinal detachment formed over the course of 5 min. The implant was then gently inserted into the subretinal space and confirmation of the implant location made by fundus examination.

The MPA device was a 1.0 mm diameter, 25- μm thick silicon disc that contained a series of photodiodes with iridium oxide surface electrodes ($9\times 9\ \mu\text{m}$), as previously described (Chow et al. 2001, 2002). The spectral responsivity of the MPA device ranged from 300 to 1,400 nm, peaking at ~ 840 nm (Chow et al. 2001; DeMarco et al. 2007). For the stimuli used here, the current output varied depending on the light stimuli from environmental to incandescent to xenon flash stimuli (see Table 16.1).

16.2.2 Light Dosing

Implanted RCS rats ($n=24$) were divided into three different groups to received incandescent light exposure ($350\ \text{cd}/\text{m}^2$ at 0.25 Hz) on a customized rack. Rats were exposed to chronic (12 h/day, 7 days/week; $n=5$), daily (1 h/day, 7 days/week; $n=8$), or weekly (1 h/week; $n=11$) treatments. The “light rack” consisted of 4 in. elongated incandescent bulbs hung 6 in. apart around the circumference of the normal rodent shoebox caging. The bulbs were placed to optimize exposure to the rats inside the cage. All animals were exposed to the incandescent lighting at the same time of the day using an automatic timer. Rats were provided with food and water and could roam freely in the cages. For animals with hourly light exposure, their behavior was monitored and recorded by an observer every 10–15 min.

Table 16.1 Current output from the MPA device in response to different light stimuli

	Environmental light	Incandescent light	Xenon flash
Wavelength (nm)	500–650	400–1,000	400–1,400
Light intensity (cd/m ² or *cd s/m ²)	4.5–86	350	3.9 × 10 ⁻⁴ –137 “**”
Stimulus current (μA/cm ²)	3.0 × 10 ⁻³ –0.3	5.5	0.01–1,680

16.2.3 Retinal Function Testing

ERGs were recorded from each rat to measure retinal function. All incandescent light exposure groups had biweekly ERGs. However, six rats that were exposed to 1 h/week incandescent lighting had ERG testing weekly. ERG recordings were performed as previously described (Pardue et al. 2005b). Briefly, rats were dark-adapted overnight, anesthetized with ketamine (60 mg/kg)/xylazine (7.5 mg/kg), and pupils dilated (1% tropicamide, 1% cyclopentolate). Dark and light-adapted ERGs were recorded using a nine step intensity series (biweekly ERGs) or a 17 step intensity series (weekly ERGs). Scotopic stimuli ranged from 3.9×10^{-4} to 137 cd s/m², while photopic stimuli ranged from 0.15 to 75 cd s/m².

16.2.4 Morphological Assessment of Photoreceptor Numbers

After 8 weeks of follow-up, all RCS rats were euthanized (anesthetic overdose) and both eyes were enucleated and fixed in 2% paraformaldehyde/2.5% glutaraldehyde. Following dehydration in a graded alcohol series and embedding in plastic resin (Embed 812/DER 736; Electron Microscopy, Fort Washington, PA), vertical sections were cut at 0.5 μm and stained with toluidine blue. Sections through the center of the implant were photographed such that eight locations across the retina were imaged (Pardue et al. 2005b). Photoreceptor nuclei counts were made in each location based on five separate measurements.

16.3 Results

16.3.1 Effects of Light Exposure on Retinal Function in Implanted RCS Rats

ERG responses in rats exposed to variable incandescent lighting regimens were not significantly different. Figure 16.1a shows representative ERG waveforms from rats at 2 and 8-weeks post-op. As seen previously, retinal function in the RCS rats decreased rapidly from 2 to 8 weeks postimplantation and was nearly unrecordable at 8 weeks postimplantation (11 weeks of age) (Pardue et al. 2005b). At 2 weeks

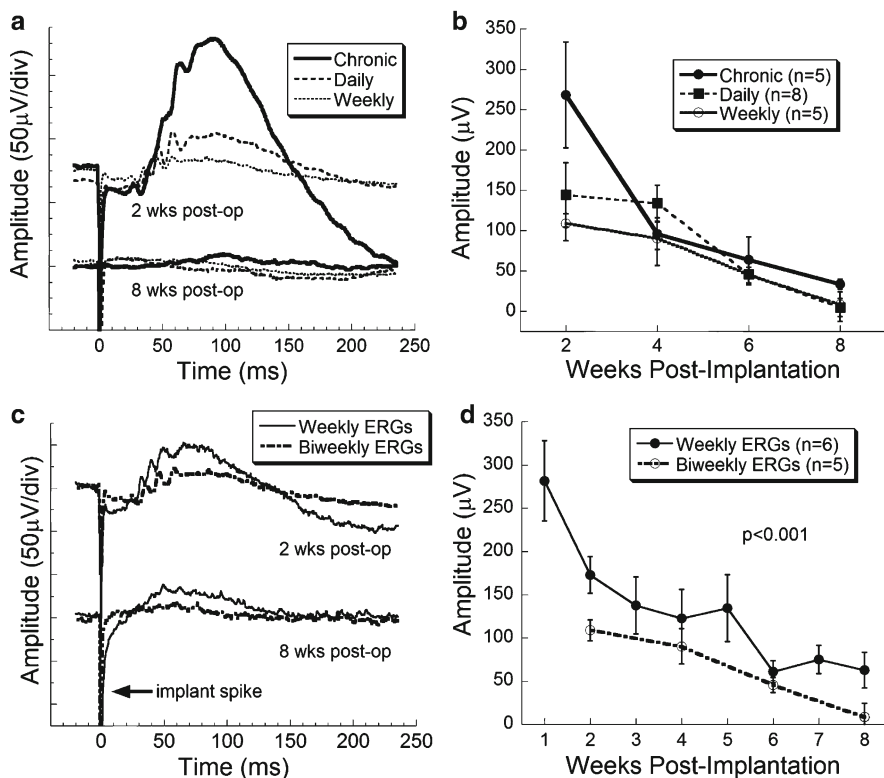


Fig. 16.1 ERGs recorded from implanted RCS rats while exposed to different lighting conditions. (a) Representative waveforms to bright flashes (137 cd s/m²) from implanted RCS rats exposed to chronic, daily or weekly incandescent light exposure. (b) Average max dark-adapted b-wave across time to a bright flash from implanted RCS rats exposed to incandescent lights. No significant differences were seen between groups. (c) Representative waveforms to bright flashes (137 cd s/m²) from implanted RCS rats that received ERG testing every 2 weeks or weekly. (d) Average max dark-adapted b-wave amplitude across weeks of implantation in implanted RCS rats exposed to different frequencies of xenon flashes. RCS rats receiving weekly ERGs had significantly larger b-wave amplitudes across the testing period ($p=0.024$)

after implantation, the chronic exposure group had significantly larger ERGs; however, this difference was diminished by 8 weeks post-op. Figure 16.1b shows the maximum b-wave amplitude in response to the brightest flash for each time-point. No statistical differences were found.

In contrast, frequency of exposure to the xenon flash affected retinal function. Figure 16.1c shows that implanted RCS rats undergoing weekly ERG testing had larger ERG waveforms at 2 and 8 weeks post-op. Examination of the max b-wave response (Fig. 16.1d) shows that the weekly ERG response were greater throughout the testing period (main effect of two-way repeated ANOVA, $F(1, 43)=7.33$, $p=0.024$).

16.3.2 Effect of Light Exposure on Photoreceptor Survival in Implanted RCS Rats

Exposure of the implanted RCS rats to different light regimens did not affect the number of photoreceptors present at 8 weeks after implantation. The average number of photoreceptors present in rats exposed to chronic incandescent lighting was 91.66 ± 74.64 (average \pm SD) vs. daily with 117.33 ± 33.67 and weekly with 86.08 ± 28.92 . Implanted RCS rats that received weekly ERGs also did not have significant more photoreceptors 156.14 ± 60.82 compared to biweekly ERGs 86.08 ± 28.92 , although there was a trend for greater numbers of photoreceptors.

16.4 Discussion

The current output estimated from the MPA device in response to different lighting conditions increased from sub-microamp with environmental lighting to 1,800 \times larger with incandescent lights to as much as 560,000 \times greater with xenon flashes. While current output changes greatly over these lighting conditions, our findings show that increasing the incandescent lighting exposure did not result in greater preservation of retinal function. However, increasing exposure to xenon flashes from biweekly to weekly significantly increased retinal preservation in the implanted RCS rats.

While we have calculated the current output from the MPA device based on in vitro recordings in a chamber (see Table 16.1), these measurements do not necessarily accurately predict the current output in the cage environment. The light intensity varies within the cage depending on how far the animal is from the light source. Additionally, since there is a gradient current output from the MPA in response to light and animals were free to roam around the cage during the light exposure, it is unknown if the MPA received full light exposure during periods of light dosing. During the light exposure period, particularly with chronic incandescent light exposure, rats slept greater than 50% of the time. The dose of incident light reaching the subretinal implant during the exposure time is likely to be less than the actual output of the light source.

Xenon flashes presented with the ERG testing ranged from 3.9×10^{-4} to 137 cd s/m² and potentially increased current to the implant from 0.01 to 1,680 μ A/cm². The increased preservation of retinal function with weekly ERGs may be due to the pulses of very high current (3–5 per intensity) or may be due to the increasing current output in a stepwise fashion that was produced from the MPA device as increasing intensities were presented. It should also be noted that the weekly ERG recording provided a higher “dose” of current earlier (1-week postimplantation) in the course of degeneration. It is possible that this exposure to high levels of current at 1-week postimplantation upregulated growth factors, such as fibroblast growth factor 2 (Ciavatta et al. 2009) that could increase the survival of photoreceptors. It does appear that the

preservation of retinal function in the weekly ERG group is due to current output from the subretinal device since prior studies have shown that naïve rats or rats with inactive devices receiving weekly ERGs did not have preserved photoreceptor function (Pardue et al. 2005a, b).

While prior studies have shown that subretinal electrical stimulation preserves photoreceptor at 8 weeks after implantation with an MPA device (Pardue et al. 2005b), our experiments did not show any increased survival of photoreceptors with weekly vs. biweekly xenon flash exposure. This may indicate that neurotrophic factors upregulated by the subretinal current may enhance function in to surviving cells, but not stop apoptotic pathways.

One complication of this study is that white light was used to increase current output from the MPA device. White light can have detrimental effects on photoreceptor survival. While the light levels used here were below those used to induce light damage models of retinal degenerations, it may have confounded our results by increasing photoreceptor death in the degenerating retina (Reme 2005). Future studies will use infrared light to stimulate MPA devices since the MPA is sensitive at these wavelengths and infrared has not been reported to be damaging to the retina.

Acknowledgments This study was supported by the Department of Veterans Affairs, Research to Prevent Blindness, and National Eye Institute Grant P30EY0636.

References

- Ball SL, Pardue MT, Chow AY et al (2001) Subretinal implantation of photodiodes in rodent models of photoreceptor degeneration. In: Hollyfield JG, Anderson RE, LaVail MM (eds) IX International Symposium on Retinal Degeneration. Kluwer/Plenum Press, NY
- Chow AY, Pardue MT, Chow VY et al (2001) Implantation of silicon chip microphotodiode arrays into the cat subretinal space. *IEEE Trans Neural Syst Rehabil Eng* 9:86–95
- Chow AY, Pardue MT, Perlman JI et al (2002) Subretinal implantation of semiconductor-based photodiodes: durability of novel implant designs. *J Rehabil Res Dev* 39:313–321
- Ciavatta VT, Kim M, Wong P et al (2009) Retinal expression of Fgf2 in RCS rats with subretinal microphotodiode array. *Invest Ophthalmol Vis Sci* 50:4523–4530
- DeMarco PJ, Jr., Yarbrough GL, Yee CW et al (2007) Stimulation via a subretinally placed prosthetic elicits central activity and induces a trophic effect on visual responses. *Invest Ophthalmol Vis Sci* 48:916–926
- Pardue MT, Phillips MJ, Yin H et al (2005a) Possible sources of neuroprotection following subretinal silicon chip implantation in RCS rats. *J Neural Eng* 2:S39–47
- Pardue MT, Phillips MJ, Yin H et al (2005b) Neuroprotective effect of subretinal implants in the RCS rat. *Invest Ophthalmol Vis Sci* 46:674–682
- Reme CE (2005) The dark side of light: rhodopsin and the silent death of vision the proctor lecture. *Invest Ophthalmol Vis Sci* 46:2671–2682

Chapter 17

Treatment with 670-nm Light Protects the Cone Photoreceptors from White Light-Induced Degeneration

Rizalyn S. Albarracin and Krisztina Valter

Keywords Retinal degeneration • 670-nm light treatment • Light damage • Photoreceptor cell death • Near-infrared treatment • Photobiomodulation • Cones

17.1 Introduction

Photoreceptor cell death and the loss of functional vision are common pathological features of retinal degenerative diseases such as age macular degeneration (AMD) and retinitis pigmentosa (RP) (Remé et al. 1998). Exposure to excessive light has been shown to lead to tissue damage, similar to those observable in AMD (Rutar et al. 2010). Thus, the light damage model may be a suitable tool in exploring therapeutic strategies to slow the progression of retinal dystrophies. In this model, photoreceptors are the most susceptible to severe damage, especially, in an area 2-mm supero-temporal to the optic disk known as the “hotspot”. In this area, extensive cell death, erosion of the blood retina barrier and an obliteration of the choroidal vessels are evident, while in the surrounding zone, the retina shows signs of long-term instability. Moreover, the structural changes of the retina are paralleled with global loss of retinal function.

Irradiation with 670-nm light is a new emerging therapy that has been shown to be beneficial in treating a variety of disease conditions both in the laboratory and the clinic. This is also synonymous to near-infrared (NIR) treatment, low level light therapy (LLLT) and photobiomodulation (PBM). We recently demonstrated that

R.S. Albarracin (✉) • K. Valter
Research School of Biology, The Australian National University, Canberra, ACT 0200, Australia
ARC Centre of Excellence for Vision Sciences, The Australian
National University, Canberra, ACT 0200, Australia
e-mail: rizalyn.albarracin@anu.edu.au

pre-treatment with 670-nm light in retinas damaged by white light has downregulated the expression of cytokine *ccl2* and muted the stress response of the retina, as seen by the expression levels of *gfap* and *fgf* genes (Natoli et al. 2010). In the current study, we investigated the effects of treatment with 670-nm light on cone photoreceptor function and structure in light-induced damage in SD albino rats, using three treatment paradigms, prior to, during or post-BL exposure.

17.2 Materials and Methods

All experimental procedures were conducted in accordance with the ARVO Statement for the Use of Animals in Ophthalmic and Vision Research and the protocols approved by The Australian National University Animal Ethics Committee. Sprague-Dawley (SD) rats were born and reared in dim (<5 lx) cyclic light (12 h/12 h on/off) conditions prior to experimentation, food pellets and water were provided ad libitum. Animals were used when aged P80–100. Animals were divided into six groups ($n=8$ /groups). In the first group, animals were not exposed to either 670-nm light or damaging white light (control). Animals in the second group were exposed to damaging white light only (LD) and in the third group they were exposed to 670-nm light only for 5 consecutive days (670-nm control). In the remaining groups, animals were exposed to damaging bright white light (BL) as well as treated with 670-nm light following one of three paradigms. Light damage was induced by exposure to 1,000 lx white light for 24 h, as described earlier (Rutar et al. 2010). Light treatment was performed using 670-nm LED array (Quantum Devices, WI, USA) held at 1 in. (2.5 cm) distance from the animals' eyes, for 3 min. The energy fluence achieved was 9 J/cm² at eye level. In one group, treatment was given 1× daily on 5 consecutive days prior to BL (pre-conditioned). In the second group, animals were treated 1 day prior to BL, then 2× daily during and immediately after BL (mid-conditioned). The third group received treatment immediately after the cessation of BL once a day for 5 days (post-conditioned). From here onwards, the three treatment paradigms will be referred to as Precon, Midcon and Postcon, respectively.

Cone photoreceptor function was assessed by full-field electroretinogram (ERG), using a double-flash paradigm (Chrysostomou et al. 2009). Apoptotic cell death was assessed by TdT-mediated dUTP nick end labelling (TUNEL). Immunolabeling using antibodies against rabbit polyclonal rhodopsin and mouse monoclonal L/M opsins was used to assess protein expression and localisation. Real-time quantitative PCR (RT-qPCR) was performed to examine changes in *opn1mw* gene expression using StepOne Plus qPCR machine and software. Data were analysed using a two-tailed Student's *t* test with $P<0.05$ considered to represent a statistically significant difference. All values are mean \pm 1 SEM.

17.3 Results

17.3.1 *Effects of 670-nm Light on Bright Light-Induced Photoreceptor Cell Death*

Compared to normal control, the sustained exposure of the retina to BL induced a significant amount of TUNEL+ profiles (Fig. 17.1a, b). The average TUNEL+ profiles in LD group ranged from 300 to 400 cells/mm in the ONL, mostly localised in the hotspot area. In 670 nm-treated retinas, TUNEL+ profiles were significantly reduced compared to LD control. The amount of TUNEL+ cell count for the Precon group was 16 cells/mm (Fig. 17.1a), while Midcon animals produced 75 cells/mm (Fig. 17.1b). The rate of cell death in both treated groups decreased significantly compared to controls ($P < 0.05$). Animals from Postcon group were excluded from the TUNEL analysis because, in this treatment group, retinas were analysed 1 week after BL, when the presence of TUNEL+ profiles is decreased considerably owing to the transitory nature of DNA fragmentation during apoptosis. In this model, apoptosis has been shown to peak after 24 h of exposure to damaging light and prevails for up to 3 days of recovery followed by a rapid drop in numbers.

17.3.2 *670-nm Light Mitigates Loss of Outer Segments Following Photic Injury*

Immunohistochemistry, using antibodies against rhodopsin and L/M opsins, was performed to identify the outer segments (OS) of the rod and cone photoreceptors. Figure 17.2 depicts a segment of the superior retina, where the hotspot is usually present. In control animals, high density of rhodopsin and L/M opsins are evenly distributed across the outer retina (Fig. 17.2a). By contrast, exposure to damaging light caused a focal loss of OS, most significantly in this area (Fig. 17.2b), and to a lesser extent in the surrounding penumbra (not shown). Following 670-nm light treatment, the damaging effects of BL on the OS were less severe in comparison to the non-treated retinas as indicated in Fig. 17.2d–f. Only a shortening of OSs was observed in retinas from Precon and Midcon groups (Fig. 17.2d, e). Postcon retinas revealed more prominent shortening and disorganisation of OSs, but these changes did not reach the severity found in LD controls (Fig. 17.2b, f). Treatment with 670 nm-treated only did not cause any significant changes in immunoreactivity (Fig. 17.2c).

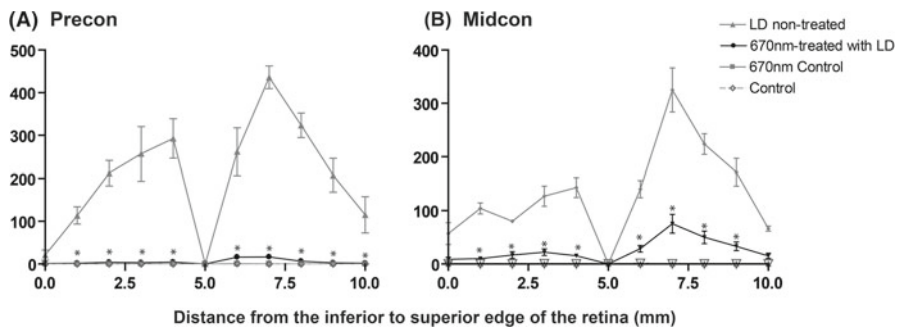


Fig. 17.1 Distribution and frequency of TUNEL+ profiles in retinal sections from Precon and Midcon groups (a, b). *Statistically significant differences ($P < 0.05$)

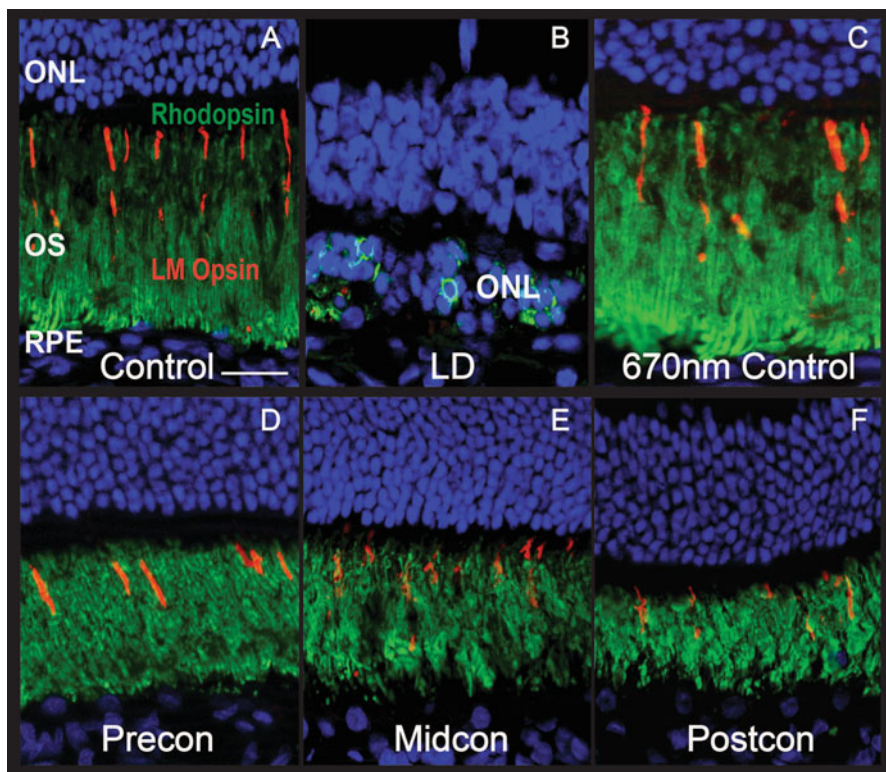


Fig. 17.2 Immunohistochemical labelling of photoreceptor outer segments with antibodies against rhodopsin (green) and L/M opsins (red). Scale bar represents 25 μ M

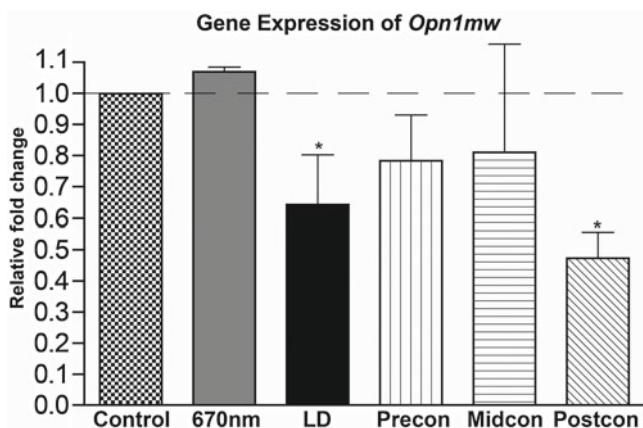


Fig. 17.3 Quantitative real-time PCR analysis of *opn1mw* gene in BL-exposed SD retinas treated with 670 nm light. The *dashed line* indicates fold ratio of 1. *Statistically significant differences ($P < 0.05$)

17.3.3 Regulation of Cone Opsin Gene by 670-nm Light

To validate the expression of outer segment proteins described in the previous section, the regulatory effect of 670 nm in *opn1mw* gene was examined 1-week post-BL exposure using RT-qPCR. The *opn1mw* gene encodes the medium-wavelength cone opsin. Changes in gene expression were compared to control levels that were normalised to 1. As shown in Fig. 17.3, exposure to BL caused a 60% decrease in the expression of *opn1mw* compared to normal control that was statistically significant ($P < 0.05$). Treatment with 670-nm light alone did not cause significant change in *opn1mw* gene expression. In Precon and Midcon-treated groups, *opn1mw* expression was slightly downregulated only by 10–20%, though in the latter group, greater variability of the data was found. These changes are not statistically significant compared to the control ($P < 0.05$). By contrast, *opn1mw* expression in Postcon group was down to 70%, which was similar to the LD retina.

17.3.4 670-nm Light Maintains Retinal Function Following Photoc Injury

The effects of damaging light on the physiological status of treated and non-treated retinas were examined using double-flash full-field ERG paradigm. Figure 17.4 illustrates the average cone b-wave amplitudes analysed from eight animals in each group. Changes in functional response were expressed as ratio of amplitudes analysed 1 week after exposure to BL or treatment and amplitudes measured on the same

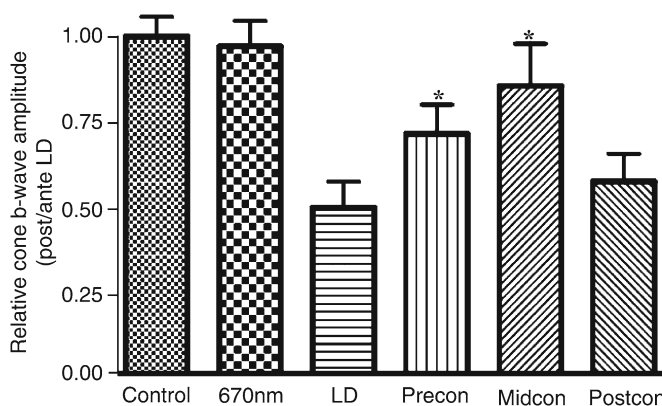


Fig. 17.4 Analysis of the relative cone b-wave ERG responses in treated and non-treated retinas 7 days after BL exposure. *Statistically significant differences ($P < 0.05$)

animal prior to experimentation. The value of 1 indicates no change. A significant, approximately 50% decrease in cone b-wave amplitude was observed in the non-treated BL-exposed retinas compared to controls ($P < 0.05$). Treatment with 670 nm light, in the Precon and Midcon groups, produced a 30 and a 25% loss, respectively, which represent a significant protection of function in these treatment groups compared to control. No significant difference was observed in Postcon retinas when compared to the non-treated BL-exposed animals. Treatment with 670-nm light alone did not cause change in cone b-wave amplitudes.

17.4 Discussion

In our present study, we evaluated the potential protective benefits of 670-nm light using the established light-induced damage model in rodent retina. Firstly, our results are consistent with previous findings that exposure to damaging levels of light induces major structural damage and histopathological changes predominantly in the photoreceptor and retinal pigment epithelial cells (Noell et al. 1966).

Treatment with 670-nm light is an emerging therapeutic modality; it has been shown to rescue cell death, promotes wound healing and provides anti-inflammatory relief in various diseases in humans and animal models (Whelan et al. 2001; Liang et al. 2006; Natoli et al. 2010). In the current study, we observed that 670-nm light produced a remarkable level of protection to photoreceptors damaged by bright light. Preconditioning the retina proved to be sufficient in ameliorating retinal damage from light exposure. Similarly, treating the retina during the BL exposure promotes protection of photoreceptors. As a result, the observed prevention of cell death leads

to maintenance of retinal integrity and recovery of functional vision. Our findings seem to suggest that 670-nm light possibly acts on broad cell signalling pathways common to tissues. Recently, our group has demonstrated that pre-treatment with 670 nm in light-exposed retina caused significant reduction in the expression of pro-inflammatory cytokine *ccl2*, and stress factors *GFAP* and *fgf-2* (Natoli et al. 2010). This implicates the possible involvement of pathways modulating cellular stress, apoptosis and inflammation.

The level of functional preservation observed between the three paradigms varies. The results from Precon and Midcon groups showed better preservation cones responses and structures compared to Postcon retinas. Quantitative assessment in Postcon animals revealed no significant functional recovery at all which is further supported with a significant downregulation of *opn1mw* gene expression and the more extensive structural damage in this group. Considering, however, that there was a morphological preservation of photoreceptors and OS density present in Postcon retinas when compared to controls, its functional outcome came as a surprise. We believe that the functional loss is only temporary as the retina attempts to repair the damage. One important aspect in resolving tissue injuries and stress is the production growth factors within the damaged tissues. The involvement of 670-nm light in enhancing production of growth factors in wounded tissues was previously presented by Whelan and colleagues in 2001. In our current model, 670-nm light may have stimulated the production of the neuroprotective CNTF and growth factor *fgf-2*. These factors have been associated to the reduction of retinal function that may explain the reduction of photoreceptor ERG response observed in this series (Valter et al. 2005).

The outer segments of the photoreceptors have been suggested to display regenerative properties in various animal models as supported by a recent study that cone outer segments have the capacity to regrow in retinas treated with CNTF (Li et al. 2010). The ability of the outer segments to regenerate proves to be an attractive therapeutic target for rescue strategies in animal models for retinal degeneration. In the current study, the severe damage or loss of photoreceptors was stalled by the treatment of 670-nm light. In Precon and Midcon groups, the damage was limited mainly to the shortening of OS, while in the Postcon group a more severe, but still potentially reversible damage occurred. Early investigation from our group revealed a gradient of CNTF upregulation in all treated groups where Postcon showed the most immunoreactivity. Taken together, 670-nm light has the potential to slow the process of retinal degeneration. Considering its direct effects on apoptosis, this treatment may be extended to clinical studies on therapeutic interventions for human degenerative diseases such as AMD and RP. Although the functional responses did not recover to the level of the normal retina, given ample time to recover, 670-nm light may have the capacity to promote better functional outcome as the outer segments regenerate. Thus, 670-nm light represents a novel therapeutic modality to stabilise the retina against photoreceptor degeneration.

Acknowledgments This work was supported by the Australian Research Council through the ARC Centre of Excellence in Vision Science (CE0561903).

References

- Chrysostomou V, Stone J, Valter K (2009) Life history of cones in the rhodopsin-mutant P23H-3 rat: evidence of long-term survival. *Invest Ophthalmol Vis Sci* 50:2407–2416
- Li Y, Tao W, Luo L et al (2010) CNTF Induces Regeneration of Cone Outer Segments in a Rat Model of Retinal Degeneration. *PLoS ONE* 5:e9495
- Liang HL, Whelan HT, Eells JT et al (2006) Photobiomodulation partially rescues visual cortical neurons from cyanide-induced apoptosis. *Neuroscience* 139:639–649
- Natoli R, Zhu Y, Valter K et al (2010) Gene and noncoding RNA regulation underlying photoreceptor protection: microarray study of dietary antioxidant saffron and photobiomodulation in rat retina. *Mol Vis* 16:1801–1822
- Noell WK, Walker VS, Kang BS et al (1966) Retinal damage by light in rats. *Invest Ophthalmol* 5:450–473
- Remé CE, Grimm C, Hafezi F et al (1998) Apoptotic cell death in retinal degenerations. *Prog Ret Eye Res* 17:443–464
- Rutar M, Provis J, Valter K (2010) Brief exposure to damaging light causes focal recruitment of macrophages, and long-term destabilization of photoreceptors in the albino rat retina. *Curr Eye Res* 35:631–643
- Valter, K, Bisti S, Gargini C et al (2005) Time course of neurotrophic factor upregulation and retinal protection against light-induced damage after optic nerve section. *Invest Ophthalmol Vis Sci* 46:1748–1754
- Whelan HT, Smits RL, Buchman EV et al (2001) Effect of NASA Light-Emitting Diode Irradiation on Wound Healing. *J Clin Laser Med & Surg* 19:305–314

Chapter 18

Dark-Rearing the *rd10* Mouse: Implications for Therapy

Therese Cronin, Arkady Lyubarsky, and Jean Bennett

Keywords Dark-rearing • Phosphodiesterase 6b • *rd10* Mouse model • Rod ON-bipolar cells • Electroretinogram

18.1 Introduction

Gene-based, pharmacological, and prosthetic therapies have been investigated for the prevention or reversal of photoreceptor cell death in retinal degeneration (RD). Retinitis pigmentosa (RP) and allied forms of RD can be triggered by a wide range of deleterious mutations, over 170 identified thus far: in the retina it seems “anything that can go wrong will go wrong.” This calls for several therapeutic approaches, which in the absence of alternatives have to be tested in mouse models. The efficiency of the test depends on the model; it should neither degenerate too fast nor too slow. In the extensively studied *rd1* mouse (Bowes et al. 1990; Punzo and Cepko 2007), the effects of the phosphodiesterase 6b (*PDE6β*) mutation are so severe, arising between PN5 and PN14, that several layers of photoreceptor cells are lost before the retinal circuitry has reached full maturation. By contrast, the relatively recently characterized *rd10* mouse shows the first signs of degeneration at PN18 (Chang et al. 2002). For this reason, the *rd10* model is of great value for early-stage therapeutic testing, balancing a significant retinal pathology with a slower rate of progression and thus the opportunity to achieve rescue. Such a rescue strategy should depend on the nature of the mutation, whether it precipitates a null, leaky, gain-of-function, or dominant-negative phenotype. In the case of the *rd10* mouse, the *PDE6β* point mutation changes codon 560 of exon 13 from an arginine to a cysteine.

T. Cronin (✉) • A. Lyubarsky • J. Bennett
F.M. Kirby Center for Molecular Ophthalmology,
University of Pennsylvania, Philadelphia, PA 19104, USA
e-mail: therese@mail.med.upenn.edu

Although the pathophysiological mechanism of this *rd10* mutation has yet to be elucidated, the gradual degeneration of the *rd10* phenotype is characteristic of a leaky, haplo-insufficient state, as further implied by complementarity mating with wild-type (WT) and *rd1* mice (Chang et al. 2007). This suggests that a *PDE6 β* gene replacement approach should achieve rescue. The therapeutic window available may be extended by dark-rearing the mouse from birth, a unique feature of the *rd10* retina that was originally reported by Chang and colleagues (2007) (Pang et al. 2008). This protective effect of dark-rearing has yet to be explained and may result from at least three possible mechanisms, (1) a gain-of-function in the *rd10 PDE6 β* molecule may cause light-evoked activity to be toxic to the cell, (2) altered synaptic development, as may occur by dark-rearing (Vistamehr and Tian 2004), may mask the retinal phenotype, (3) secondary cues for cell death may be accelerated by light and delayed by dark-rearing. In this preliminary study, the ERG, histology, and transcript levels of crucial retinal genes are compared between cyclic-light-reared and dark-reared mice, termed LR-*rd10* and DR-*rd10*, respectively. The data show that the ONL of the DR-*rd10* mouse is protected from cell death with some ONL function preserved until at least PNM2.5. Furthermore, the downstream circuitry of the rod ON-bipolar cells (RBCs) is maintained in the DR-*rd10* mice. The protective effect of light restriction in the *rd10* mouse may provide insight into disease management and treatment strategies for patients with retinal degeneration caused by recessive photoreceptor mutations.

18.2 Methods

18.2.1 Mice

All procedures were approved by the Institutional Animal Care and Use Committee of the University of Pennsylvania and complied with the ARVO Statement for the Use of Animals in Ophthalmic and Vision Research. C57Bl/6J and *PDE6 β ^{rd10}/J* mice were obtained from Jackson laboratories (ME).

18.2.2 Electroretinography

ERG recordings followed procedures described previously (Lyubarsky et al. 2002). Wild-type C57Bl/6J mice were dark-adapted overnight; *rd10* mice have been raised in dark from birth. Animals were anesthetized with a cocktail containing (in mg/g body weight): 25 ketamine, 10 xylazine, and 1000 urethane. The pupil was dilated with 1% tropicamide saline solution (Mydracil; Alconox, New York, NY), and the mouse was placed on a custom-made thermo-stabilized stage maintained at 37°C. Two miniature cups with embedded platinum wires made of UV-transparent plastic serving as recording electrodes were placed in electrical contact with the corneas.

A platinum wire loop placed in the mouth served as a reference and a ground electrode. Full-field ERG were recorded with Espion Electrophysiology System (Diagnosys LLC, Lowell, MA) modified by the manufacturer for experiments with mice by substituting LEDs with emission maximum at 365 nm for standard blue cones. Intensities of green and white stimuli were defined in scotopic units according to the manufacturer's instruction, and they were converted into the units of photon flux and number of photoisomerizations/photoreceptor as described by Lyubarsky et al. (2004).

18.2.3 Immunolabeling and Imaging

Immunolabeling of retinal cryosections was carried out according to previously described protocols (Sherry et al. 2006; Phillips et al. 2010). Antibodies used were rabbit PKC α (1/1000, Sigma, St. Louis, MO), rabbit VAMP-2 (1/500, ab3347 Abcam, MA), rabbit synapsin-1 (1/500, ab8), all raised in rabbit and detected using alexafluor-labeled secondary anti-rabbit antibodies (1/500, Molecular Probes, OR). Specificity of labeling methods was confirmed by omitting primary antibody. Confocal microscopy was performed using a Leica confocal microscope. Images were captured using a 40 \times oil immersion objective and stacked images processed using Image J.

18.2.4 Quantitative Real-Time PCR

RNA samples were harvested from whole eyes using RNeasy kit (Qiagen) and used for single-strand cDNA synthesis from oligoDT primers. Primers amplifying a 150–200 bp amplicon of genes in enriched sets were designed using the Whitehead Institute Primer3 program. Thermal cycler conditions for the RTPCR system (Applied Biosystems 7500) were 50°C for 2 min, 95°C for 10 min, 40 cycles of 15 s at 95°C followed by 1 min at 60°C. PCRs were performed in triplicate for each sample and relative quantitation was calculated using the Pfaffl formula with 18S rRNA as reference.

18.3 Results

18.3.1 Preservation of Function Until PNM3 in the DR-*rd10* Mouse

The retinal function of DR-*rd10* was compared to that of LR-*rd10* mice using flash ERG at a range of ages from postnatal day (P) 21 to postnatal month (PNM) 3. The saturating a-wave response from dark-adapted mice is reduced compared to WTs for

both DR-*rd10*s and LR-*rd10*s, from P21; however, the DR response amplitude is twice that of the LR response and is maintained until at least 7 weeks long after the a-wave of LR-*rd10*s is lost. Even more striking is a dark-adapted b-wave response close to that of the WT, suggesting that not only is downstream synaptic signaling intact, but may even be undergoing a compensatory effect, with a b/a ratio increased compared to WT.

18.3.2 Immunohistochemical Analysis of the Effect of DR on *rd10* Retinal Remodeling

There is considerable evidence for anatomical reshaping of inner retinal neurons during retinal degeneration. Early disorganization and alteration in size of rod bipolar cell (RBC) terminals has been reported in *rd10* mice at PN30 (Puthussery et al. 2009). In both DR-*rd10* as well as LR-*rd10* mice, we observe remodeling of the RBC dendrites. At this advanced stage, cone outer segments are evident only in DR-*rd10* mice (Fig. 18.2a). It was of interest to examine the extent to which synaptic connections of the inner retina may be influencing the rate of degeneration in the DR-*rd10* mouse. Antibody against VAMP-2, the principal SNARE protein of retinal synapses, stains both ribbon and conventional synapses in the outer and inner plexiform layers (OPL and IPL), (Phillips et al. 2010). While VAMP-2 staining is completely diminished in the OPL of the *rd10* mouse reared under cyclic light, staining is maintained in the dark-reared *rd10* (Fig. 18.2b). Antibody against synapsin-1 labels the conventional synapses of amacrine cells in the IPL, previously synapsin-1 labeling had been observed ectopically in puncta of the INL and GCL of *rd10* retinas (Phillips et al. 2010). Spread of this synaptic marker into the OPL is observed in LR-*rd10* mice. By contrast, a more intense and confined labeling of conventional synapses is evident in DR-*rd10* compared to LR-*rd10* (Fig. 18.2c).

18.3.3 *QrtPCR* Analysis of Candidate Retinal Genes

While rhodopsin expression is lost by PNM2.5 in LR-*rd10* mice, the expression in DR-*rd10* is maintained at 79% of WT levels. DR-*rd10* *PDE6 β* expression levels are also close to WT. GS expression in Müller glia, possibly indicative of a continued retinal response to glutamate, is found to be maintained in both LR-*rd10* and DR-*rd10* mice.

18.4 Discussion

Light restriction has been shown to slow degenerations in 15 of 20 rodent strains surveyed (reviewed by Paskowitz et al. 2006; Valter et al. 2009). Particularly robust findings have been documented in the RCS rat (Dowling and Sidman 1962; Kaiz

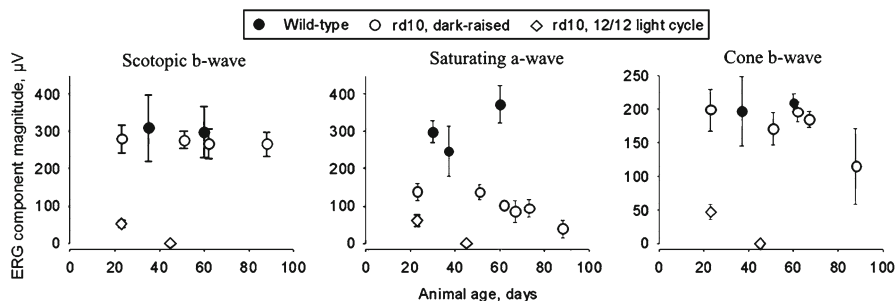


Fig. 18.1 Time course of changes in the ERG in *rd10* mice: no decline at least in the first 2 months

and Auerbach 1979), the P23H-3 transgenic mouse (Naash et al. 1996) and rat (Bicknell et al. 2002), and in the rhodopsin-mutant dog (Cideciyan et al. 2005). However, it is in the *rd10* mouse that the protective effect of dark-rearing is most evident (Chang et al. 2007). An effort is made in this preliminary study to characterize this effect and improve our understanding of the nature of the *rd10* mutation. A therapeutic strategy that takes advantage of this protective effect may be translated to human patients with photoreceptor-based RD mutations. Recently, it has been demonstrated that bipolar cells of the *rd10* retina undergo histochemical and morphological changes during the course of degeneration with loss of nearly a quarter of RBCs and a differential loss of responsiveness to glutamate (Gargini et al. 2007; Puthussery et al. 2009). A survival strategy for those RBCs that remain may be observed in the extension of processes to the remaining cones of the ONL (Puthussery et al. 2009). Our results imply that the protective effects of dark-rearing are a consequence of altered synaptic contacts in the OPL that preserved function of both the ONL and INL. Significant preservation of rod photoreceptor and RBC function is found in DR-*rd10* mice compared to LR-*rd10* mice until PNM3 (Fig. 18.1) and OPL synaptic contacts are more prevalent in the DR *rd10* than in the age-matched LR-*rd10* (Fig. 18.2). The normal scotopic b-wave in ERG suggests that these RBC-photoreceptor synapses are functional.

In the *rd/rd* retina, it has been hypothesized that the RBCs do not receive sufficient input from healthy photoreceptors to enable normal development of glutamate signaling pathways (Chua et al. 2009). In the case of the *rd10* model, it may be the *maintenance* of glutamate signaling pathway that is compromised, as the inner retina somehow succumbs to secondary effects of the *PDE6β* mutation. As the DR-*rd10* is never challenged with light, the undisrupted glutamate flow may help maintain downstream signaling pathways. This initial investigation offers evidence of the extent of this protective effect. It suggests that appropriately timed light restriction at the time of accelerated degeneration may help support retinal circuitry prior to therapy and maximize the chance of a positive outcome. Alternatively, it may be possible to address the primary cause of retinal degeneration in this model – such as

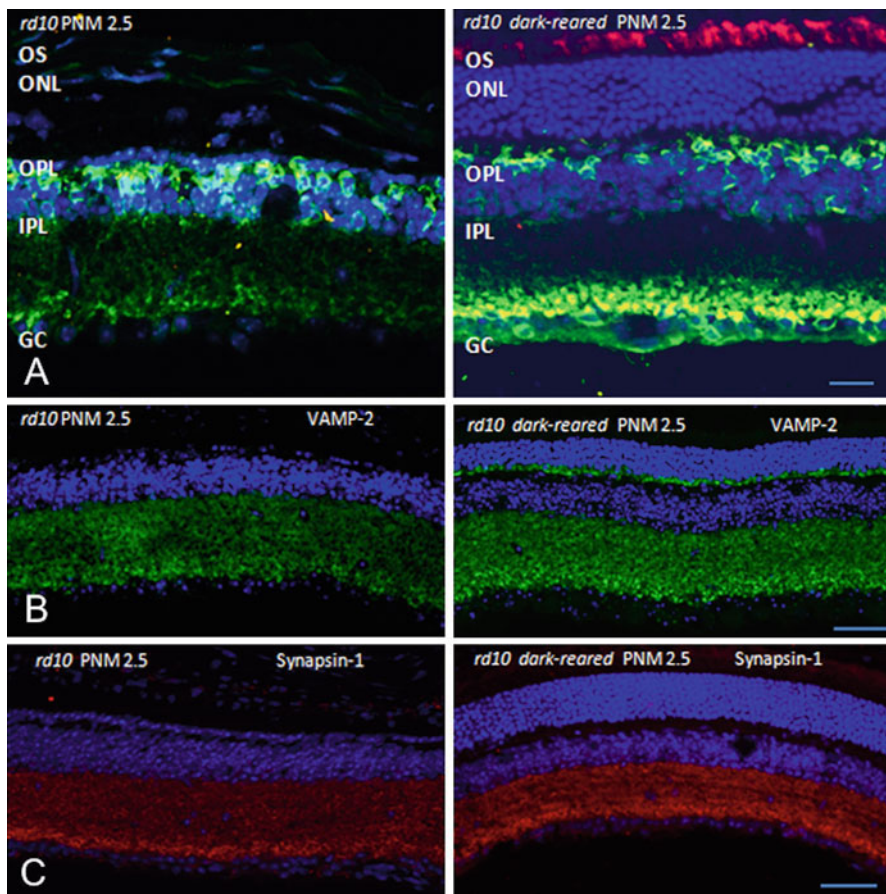


Fig. 18.2 Immunolabelling of LR-*rd10* vs. DR-*rd10* mice at PNM2.5. (a) PNA (red) and PKC α (green) expression. (b) VAMP-2 and (c) Synapsin-1 Scale bar, 50 μ M

alterations in glutamate release/replacement. Evidently, further investigation is needed before the exact nature of the dark-rearing protective effect can be understood in the *rd10* mice.

Up to 21 mutations have been found within the PDE6 β catalytic domain in patients with recessive RP (<http://www.hgmd.cf.ac.uk/>). This preliminary study into long-term maintenance of rod function in the dark-reared *rd10* mouse suggests that approaches to maintain rod function may be extrapolated to human patients.

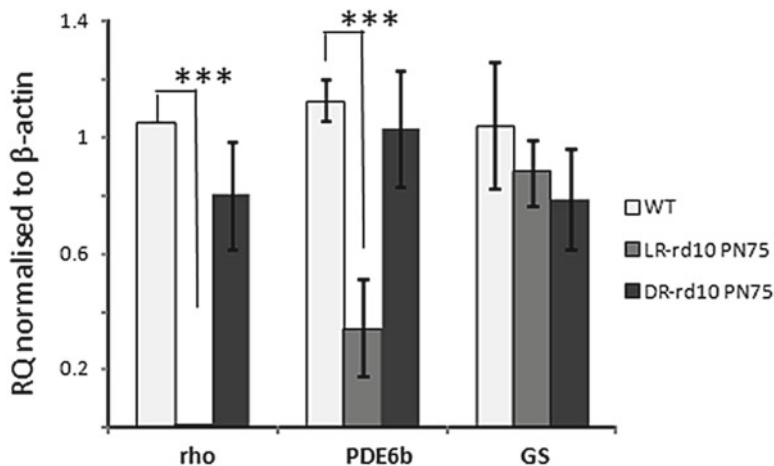


Fig. 18.3 Retinal gene expression in light-reared (LR) vs. dark-reared (DR) *rd10* mice at PNM2.5

Acknowledgments We thank Wei Zhang for technical assistance. This study was supported by FFB Center Grant #C-GT-0607-0390-UPA02 and Hope for Vision.

References

- Bicknell IR, Darrow R, Barsalou L et al (2002) Alterations in retinal rod outer segment fatty acids and light-damage susceptibility in P23H rats. *Mol Vis*, 8:333–340
- Bowes C, Li T, Danciger M et al (1990) Retinal degeneration in the rd mouse is caused by a defect in the beta subunit of rod cGMP-phosphodiesterase. *Nature* 347:677–680
- Chang B, Hawes NL, Hurd RE et al (2002) Retinal degeneration mutants in the mouse. *Vision Res* 42:517–525
- Chang B, Hawes NL, Pardue MT et al (2007) Two mouse retinal degenerations caused by missense mutations in the beta-subunit of rod cGMP phosphodiesterase gene. *Vision Res* 47:624–633
- Chua J, Fletcher EL, Kalloniatis M (2009) Functional remodeling of glutamate receptors by inner retinal neurons occurs from an early stage of retinal degeneration. *J Comp Neurol* 514:473–491
- Cideciyan AV, Jacobson SG, Aleman TS et al (2005) In vivo dynamics of retinal injury and repair in the rhodopsin mutant dog model of human retinitis pigmentosa. *Proc Natl Acad Sci U S A* 102:5233–5238
- Dowling JE, Sidman RL (1962) Inherited retinal dystrophy in the rat. *J Cell Biol* 14:73–109
- Gargini C, Terzibasi E, Mazzoni F et al (2007) Retinal organization in the retinal degeneration 10 (*rd10*) mutant mouse: a morphological and ERG study. *J Comp Neurol* 500:222–238
- Kaizt M, Auerbach E (1979) Retinal degeneration in RCS rats raised under ambient light levels. *Vision Res* 19:79–81

- Lyubarsky AL, Lem J, Chen J et al (2002) Functionally rodless mice: transgenic models for the investigation of cone function in retinal disease and therapy. *Vision Res* 42:401–415
- Lyubarsky AL, Daniele LL, Pugh EN (2004) From candelas to photoisomerizations in the mouse eye by rhodopsin bleaching in situ and the light-rearing dependence of the major components of the mouse ERG. *Vision Res* 44:3235–3251
- Naash ML, Peachey NS, Li ZY et al (1996) Light-induced acceleration of photoreceptor degeneration in transgenic mice expressing mutant rhodopsin. *Invest Ophthalmol Vis Sci* 37:775–782
- Pang J, Boye SL, Kumar A et al (2008) AAV-mediated gene therapy for retinal degeneration in the rd10 mouse containing a recessive PDEbeta mutation. *Invest Ophthalmol Vis Sci* 49:4278–4283
- Paskowitz DM, LaVail MM, Duncan JL (2006) Light and inherited retinal degeneration. *The Brit J Ophthalmol* 90:1060–1066
- Phillips MJ, Otteson DC, Sherry DM (2010) Progression of neuronal and synaptic remodeling in the rd10 mouse model of retinitis pigmentosa. *J Comp Neurol* 518: 2071–2089
- Punzo C, Cepko C (2007) Cellular responses to photoreceptor death in the rd1 mouse model of retinal degeneration. *Invest Ophthalmol Vis Sci* 48:849–857
- Puthussery T, Gayet-Primo J, Pandey S et al (2009) Differential loss and preservation of glutamate receptor function in bipolar cells in the rd10 mouse model of retinitis pigmentosa. *The Euro J Neurosci* 29:1533–1542
- Sherry DM, Mitchell R, Standifer KM et al (2006) Distribution of plasma membrane-associated syntaxins 1 through 4 indicates distinct trafficking functions in the synaptic layers of the mouse retina. *BMC Neurosci* 7:54
- Valter K, Kirk DK, Stone J (2009) Optimising the structure and function of the adult P23H-3 retina by light management in the juvenile and adult. *Exp Eye Res* 89:1003–1011
- Vistamehr S, Tian N (2004) Light deprivation suppresses the light response of inner retina in both young and adult mouse. *Vis Neurosci* 21:23–37

Chapter 19

Intravitreal Injection of Erythropoietin Glycosylation Analogs Does Not Protect Rod Photoreceptor Cells from Light-Induced Damage

Masaki Tanito, Feng Li, and Robert E. Anderson

Keywords Retinal light damage • Erythropoietin • Outer nuclear layer thickness • Electroretinogram

19.1 Introduction

Previous experimental studies using bright light exposure to rodent eyes have shown that light stress causes photoreceptor cell damage (Noell et al. 1966) and that the apoptotic pathway, the common fate of photoreceptors in retinitis pigmentosa and

M. Tanito (✉)

Department of Ophthalmology, University of Oklahoma Health Sciences Center, Oklahoma City, OK, USA

Dean A. McGee Eye Institute, Oklahoma City, OK, USA

Department of Ophthalmology, Shimane University Faculty of Medicine, Izumo, Shimane, Japan
e-mail: mtanito@med.shimane-u.ac.jp

F. Li

Department of Ophthalmology, University of Oklahoma Health Sciences Center, Oklahoma City, OK, USA

Dean A. McGee Eye Institute, Oklahoma City, OK, USA

R.E. Anderson

Department of Ophthalmology, University of Oklahoma Health Sciences Center, Oklahoma City, OK, USA

Dean A. McGee Eye Institute, Oklahoma City, OK, USA

Department of Cell Biology, University of Oklahoma Health Sciences Center, Oklahoma City, OK, USA

age-related macular degeneration, is the main cause of light-induced cell death (Wenzel et al. 2005). Thus, light-induced damage in the albino rat is a suitable model system to study stress-induced retinal degenerations. The cytokine erythropoietin (Epo), a glycoprotein produced by the kidney in adults and by liver in the fetus, is responsible for erythropoiesis and is best known for treatment of anemia. Recent evidence suggested that Epo has nonhematopoietic biological effects on angiogenesis, brain development, wound healing, and neuroprotection (Arcasoy 2008). Systemic administration of Epo has been shown to be protective against light-induced retinal degenerations (Rex et al. 2004). Aranesp (darbepoetin alfa; Amgen, Thousand Oaks, CA) and AMG114 (Amgen), hyperglycosylated forms of Epo, are recently developed glycosylation analogs of Epo with an extended circulating half-life in vivo. In the current study, the efficacy of two Epo compounds (Aranesp and AMG114) was tested in a rat model of light-induced retinal degeneration. The drugs were administered by intravitreal injection.

19.2 Materials and Methods

19.2.1 Light Exposure

All procedures were carried out according to the ARVO Statement for the Use of Animals in Ophthalmic and Vision Research and the University of Oklahoma Health Sciences Center (OUHSC) Guidelines for Animals in Research. All protocols were reviewed and approved by the Institutional Animal Care and Use Committees of the OUHSC and the Dean A. McGee Eye Institute. Sprague-Dawley (Harlan Sera-Lab; Indianapolis, IN) rats were born and raised in our vivarium and kept under dim cyclic light (5 lx, 12 h on/off, 7 a.m.–7 p.m.) prior to experimentation.

Unanesthetized rats (6–7 weeks of age) were exposed to 2,700 lx diffuse, cool, white fluorescent light for 6 h (9 a.m.–3 p.m.) as described previously (Tanito et al. 2007, 2008). After exposure, the rats were returned to the dim cyclic light environment for 7 days, after which their electroretinograms (ERG) were recorded; they were then euthanized and their eyes enucleated. One-hundred and thirty rats were divided into ten groups of 10 or 20 rats each (Table 19.1). Groups 1–6 were given intravitreal injections in one eye of either Aranesp or AMG114 at three different doses, each calculated to be at the levels of 0.2, 2, 20 ng in the eye, 48 h before the damaging light exposure. Doses of Epo-analogs injected were decided based on the previous study by Rex et al. (2004). The contralateral eye was injected with carrier. These six groups were exposed to damaging light. Groups 7–8 were injected in one eye with 20 ng Aranesp or AMG114 and in the other eye with carrier. These two groups were not exposed to light and served as controls for drug toxicity to the retina. Groups 9–10 were not injected with drug. Group 9 was exposed to light and Group 10 served as an unexposed control. The identity and dose levels of the drugs

Table 19.1 Animal groups

Group	Number of rats	Treatment		
		Left eye	Right eye	Light exposure
1	20	Vehicle	Aranesp (20 mU)	Yes
2	20	Aranesp (200 mU)	Vehicle	Yes
3	10	Vehicle	Aranesp (2,000 mU)	Yes
4	20	AMG114 (20 mU)	Vehicle	Yes
5	10	Vehicle	AMG114 (200 mU)	Yes
6	10	AMG114 (2,000 mU)	Vehicle	Yes
7	10	Vehicle	Aranesp (2,000 mU)	No
8	10	AMG114 (2,000 mU)	Vehicle	No
9	10	Uninjected	Uninjected	Yes
10	10	Uninjected	Uninjected	No

used in this study were masked to the examiners until the experimental results had been recorded and the data analyzed.

19.2.2 Intravitreal Injection

Intravitreal injections were done between 12 p.m. and 1 p.m. 2 days before light exposure. This allowed enough time for the animals to recover from anesthesia and to determine if there were any untoward effects of the injection, such as injury cataract or infection. In addition, the endogenous neuroprotective cytokine response that protects against light damage (Faktorovich et al. 1992; Wen et al. 1995) was reduced after two days. After anesthesia with Ketamine (120 mg/kg) and xylazine (6 mg/kg), the rat eyes were dilated with 1% tropicamide and topically anesthetized with 0.5% Proparacaine·HCl. The animals were placed on a sterile pad over a regulated heating pad and the eyes magnified under an operating microscope. Both eyes and surrounding skin and hair were bathed with a 5% solution of betadine followed by sterile saline. Two microliters of drug or vehicle were taken up by a microsyringe with a 33-gauge needle and injected into the vitreal space through a small incision created by penetration with a 30-gauge beveled needle at the limbus on the superior side of the eye. Subsequent to the injection, an erythromycin ophthalmic ointment (E. Fougere & CO, Melville, NY) was applied to the corneal surface to reduce the risk of infection and to prevent corneal opacifications. Injected animals were kept in the operation room for several hours for recovery. We supplied Tylenol in the drinking water (1–2 mg/mL drinking water; 15–30 of 32 mg/mL pediatric elixir/500 mL bottle), starting 24 h before the surgery and continuing for 4 days thereafter. Injected rats were monitored carefully for signs of ocular inflammation and cataract formation.

19.2.3 ERG Recording and Outer Nuclear Layer Thickness Measurement

Seven days after the light exposure, ERGs were recorded to estimate retinal function and outer nuclear layer (ONL) thickness was measured on retinal sections to estimate retinal structure in the animals from groups 1–10 (ERG results are not available for Group 8, a nonexposed control group). The methods for ERG recordings and ONL thickness measurements were described previously (Tanito et al. 2007, 2008). Throughout the experiments, all animals were checked for signs of infection and cataract formation. No animals developed infection and three were eliminated from the study (one in Group 5 and two in Group 8) because of cataract or anesthetic overdose.

19.3 Results

The ERG a- and b-wave amplitudes (Fig. 19.1) and ONL thickness (Fig. 19.2) were not significantly different between light and left eyes in Groups 9 and 10, indicating good reproducibility, and in Groups 7 and 8 (no ERGs), indicating that neither drug was toxic to the retina. There were no significant left eye/right eye differences in any rats in Groups 1–6, indicating no retinal protection by Epo functionally or structurally.

19.4 Discussion

Previous studies have shown that up-regulation of Epo in the retina by systemic hypoxic preconditioning, Epo-expressing transgenic mice, or intraperitoneal injection of Epo provides retinal protection from light damage (Grimm et al. 2002, 2004; Ranchon Cole et al. 2007). Rex et al. (2004) reported that overexpression of Epo delivered by adeno-associated vectors is protective against retinal light damage when administered systemically, but not intraocularly. Thus, assuming all of these studies are correct, there is a basic difference between Epo delivered to the retina from the systemic circulation and Epo delivered intraocularly. Ranchon-Cole et al. (2007) reported that mechanisms such as free radical scavenging or antioxidant facilitating activity are independent of retinal protection mediated by systemic Epo, perhaps through an indirect effect of Epo such as increase in hematocrit level (Rex et al. 2004) or postadministrative modifications of Epo by nonretinal tissues.

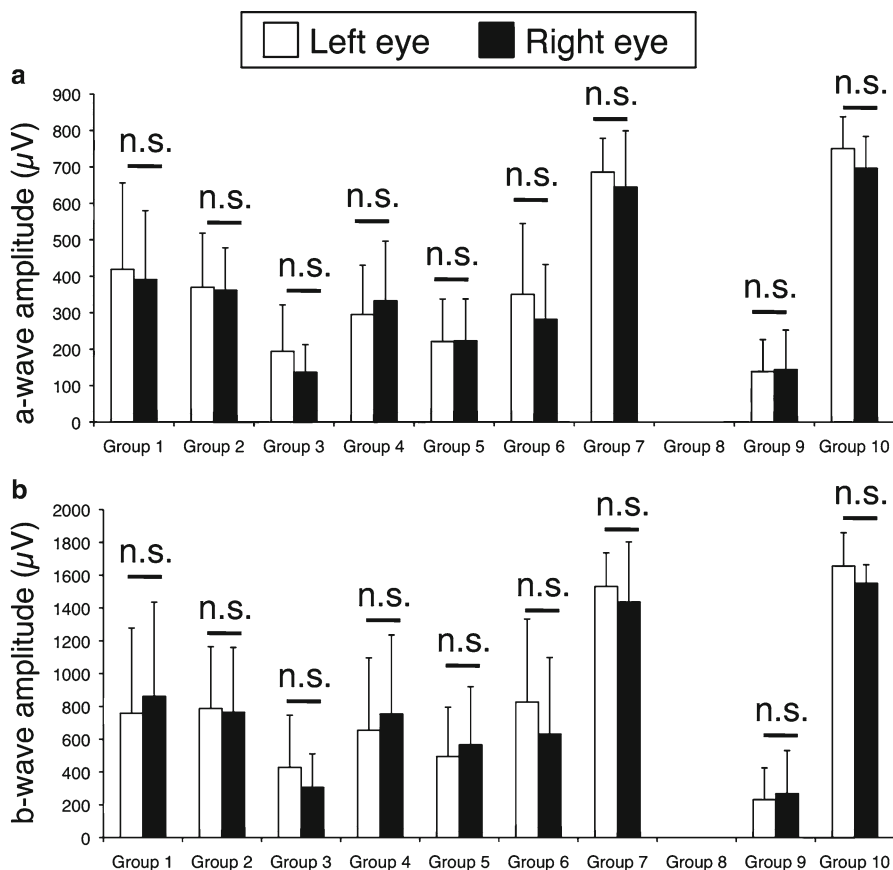


Fig. 19.1 ERG Amplitudes. The means (\pm SD) of ERG a-wave amplitudes are shown in (a). (b) b-Wave amplitudes. ERG values for Group 8 are not available; n.s. indicates not significant by paired *t* test between right and left eyes

These are possibilities that should be tested. More recently, absence or very low levels of Epo receptor expression was reported in nonhematopoietic cells such as endothelial, cardiac, neuronal, renal, and tumor cells (Sinclair et al. 2010; Swift et al. 2010) and may explain the discrepancy.

In conclusion, Epo glycosylation analogs such as Aranesp and AMG114 injected intravitreally do not protect rod photoreceptor cells from light-induced cell death.

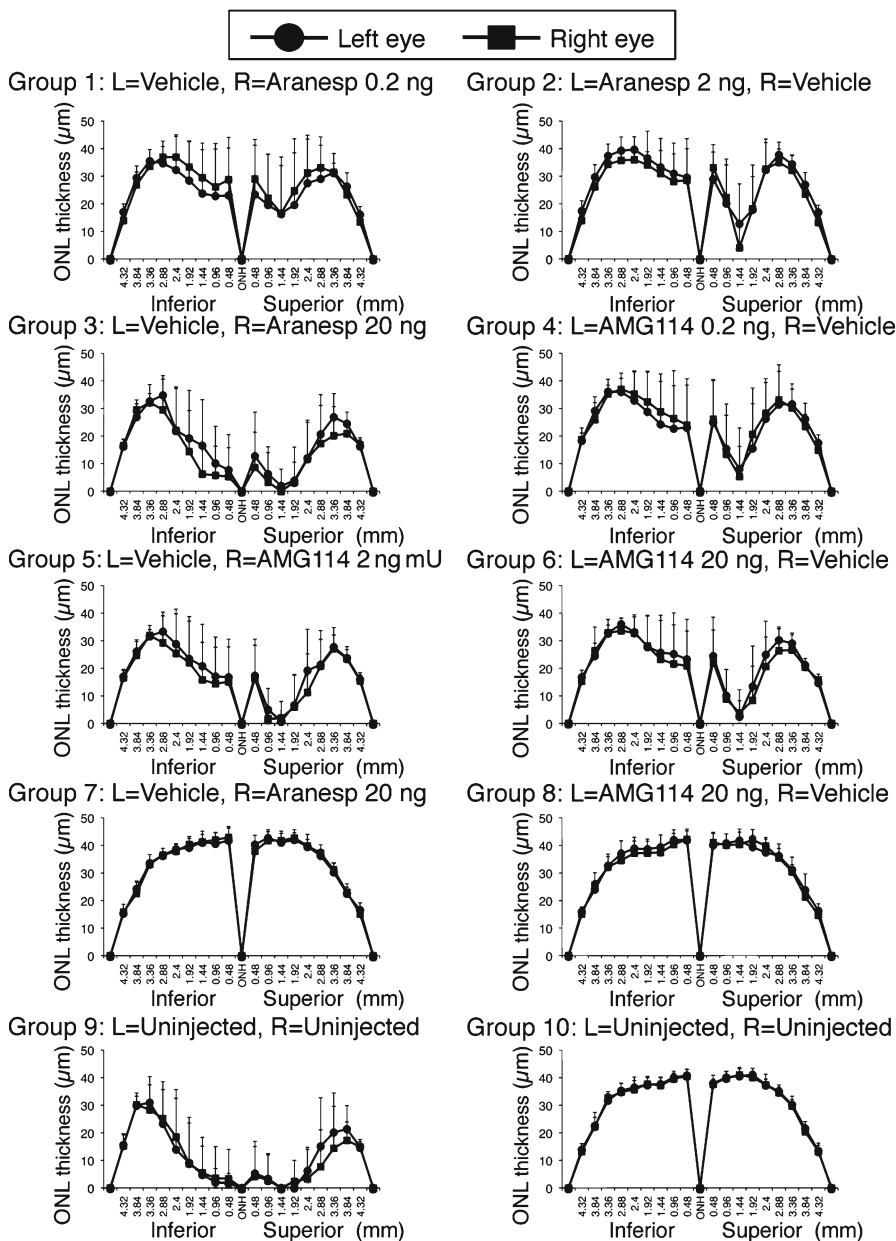


Fig. 19.2 ONL thickness measurements. The means (\pm SD) of ONL thickness (μm) are shown on the y axis. The units on the x axis are the distances (mm) from the optic nerve head (ONH) along the vertical meridian to the inferior and superior ora serrata

Acknowledgments The authors are grateful to Mark Dittmar (Dean A. McGee Eye Institute) for maintaining the animals used in this study and to Louisa J. Williams and Linda S. Boone (Dean A. McGee Eye Institute) for their excellent retinal section preparation. This study was supported by a contract from Amgen, Inc. (Thousand Oaks, CA) and grants from the National Eye Institute (EY04149, EY00871, and EY12190); National Center for Research Resources (RR17703); Research to Prevent Blindness, Inc.; and the Foundation Fighting Blindness.

References

- Arcasoy MO (2008) The non-haematopoietic biological effects of erythropoietin. *Br J Haematol* 141:14–31
- Faktorovich EG, Steinberg RH, Yasumura D et al (1992) Basic fibroblast growth factor and local injury protect photoreceptors from light damage in the rat. *J Neurosci* 12:3554–3567
- Grimm C, Wenzel A, Groszer M et al (2002) HIF-1-induced erythropoietin in the hypoxic retina protects against light-induced retinal degeneration. *Nat Med* 8:718–724
- Grimm C, Wenzel A, Stanescu D et al (2004) Constitutive overexpression of human erythropoietin protects the mouse retina against induced but not inherited retinal degeneration. *J Neurosci* 24:5651–5658
- Noell WK, Walker VS, Kang BS et al (1966) Retinal damage by light in rats. *Invest Ophthalmol* 5:450–473
- Ranchon Cole I, Bonhomme B, Doly M (2007) Pre-treatment of adult rats with high doses of erythropoietin induces caspase-9 but prevents light-induced retinal injury. *Exp Eye Res* 85:782–789
- Rex TS, Allocca M, Domenici L et al (2004) Systemic but not intraocular Epo gene transfer protects the retina from light- and genetic-induced degeneration. *Mol Ther* 10:855–861
- Sinclair AM, Coxon A, McCaffery I et al (2010) Functional erythropoietin receptor is undetectable in endothelial, cardiac, neuronal, and renal cells. *Blood* 115:4264–4272
- Swift S, Ellison AR, Kassner P et al (2010) Absence of functional EpoR expression in human tumor cell lines. *Blood* 115:4254–4263
- Tanito M, Kaidzu S, Ohira A et al (2008) Topography of retinal damage in light-exposed albino rats. *Exp Eye Res* 87:292–295
- Tanito M, Li F, Elliott MH et al (2007) Protective effect of TEMPOL derivatives against light-induced retinal damage in rats. *Invest Ophthalmol Vis Sci* 48:1900–1905
- Wen R, Song Y, Cheng T et al (1995) Injury-induced upregulation of bFGF and CNTF mRNAs in the rat retina. *J Neurosci* 15:7377–7385
- Wenzel A, Grimm C, Samardzija M et al (2005) Molecular mechanisms of light-induced photoreceptor apoptosis and neuroprotection for retinal degeneration. *Prog Retin Eye Res* 24:275–306

Chapter 20

Relieving Bottlenecks in RNA Drug Discovery for Retinal Diseases

**Jack M. Sullivan, Edwin H. Yau, R. Thomas Taggart,
Mark C. Butler, and Tiffany A. Kolniak**

Keywords Retinal degenerations • Macular degenerations • Gene therapy
• Posttranscriptional gene silencing • Ribozyme • Hammerhead ribozyme • shRNA
• siRNA • High throughput screening • Breakthrough technology development

J.M. Sullivan (✉)

Department of Ophthalmology, University at Buffalo, State University of New York (SUNY),
SUNY Eye Institute, Buffalo, NY 14209, USA

Department of Pharmacology and Toxicology, University at Buffalo,
State University of New York (SUNY), SUNY Eye Institute, Buffalo, NY 14209, USA

Department of Physiology and Biophysics, University at Buffalo,
State University of New York (SUNY), SUNY Eye Institute, Buffalo, NY 14209, USA

Department of Neuroscience Program, University at Buffalo,
State University of New York (SUNY), SUNY Eye Institute, Buffalo, NY 14209, USA

VA Western New York Healthcare System, Buffalo, NY 14215, USA

The Ross Eye Institute of University at Buffalo, Buffalo, NY 14209, USA

e-mail: jackmsullivanm PhD@yahoo.com

E.H. Yau

Department of Ophthalmology, University at Buffalo,
State University of New York (SUNY), SUNY Eye Institute, Buffalo, NY 14209, USA

Department of Pharmacology and Toxicology, University at Buffalo,
State University of New York (SUNY), SUNY Eye Institute, Buffalo, NY 14209, USA

R.T. Taggart • M.C. Butler

Department of Ophthalmology, University at Buffalo, State University of New York (SUNY),
SUNY Eye Institute, Buffalo, NY 14209, USA

T.A. Kolniak

Department of Ophthalmology, University at Buffalo, State University of New York (SUNY),
SUNY Eye Institute, Buffalo, NY 14209, USA

Department of Neuroscience Program, University at Buffalo, State University of New York
(SUNY), SUNY Eye Institute, Buffalo, NY 14209, USA

20.1 Introduction

Currently, only one nucleic acid drug is approved for human disease by the Food and Drug Administration (Vitravene™, fomiversen, ISIS 2922). This singular success is testament to the difficulties that exist in development of PTGS agents over the last three decades. We encountered the biocomplexity intrinsic to development of PTGS agents in RDD for retina-directed therapeutics. The steps in the process of RDD are similar to the development of small molecule drugs except that in RDD, the drug is a delivered or expressed macromolecular RNA molecule (Fig. 20.1). We critically detailed the bottlenecks at each step in RDD that limit the efficiency and success of PTGS agent development (Sullivan and Taggart 2007). Here, we present an overview of established and emerging technologies to address these bottlenecks, some of which were established in this lab.

20.2 Materials and Methods

To demonstrate the complexity of mRNA structure, we folded human peripherin mRNA (*RDS*, *PRPH2*) into secondary structures with Mfold, which first finds the minimal free energy structure (Zuker 2003). *RDS* is a disease target mRNA in autosomal

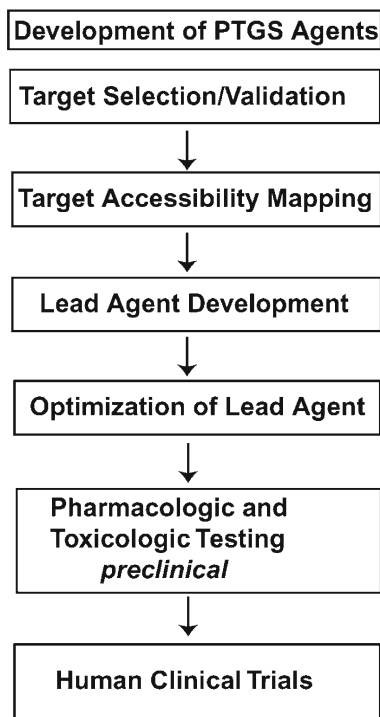


Fig. 20.1 Process of RNA drug discovery. Steps in PTGS development

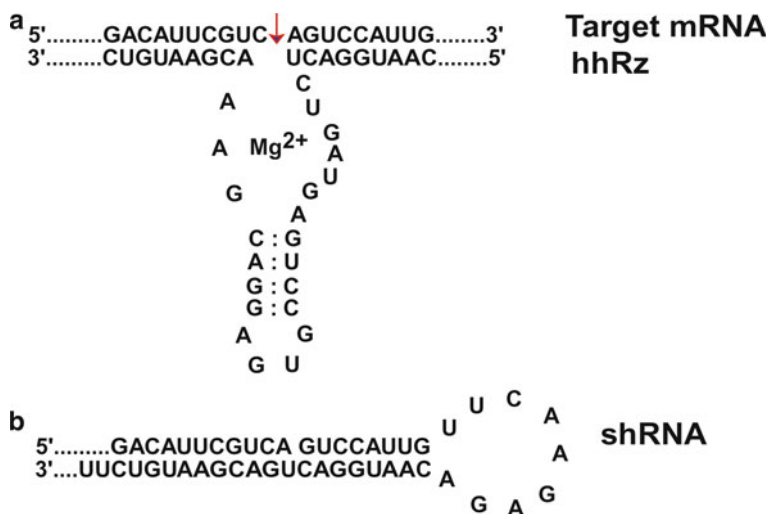


Fig. 20.2 Ribozyme and shRNA Agents. (a) Hammerhead ribozyme structure. (b) shRNA structure

dominant retinitis pigmentosa and macular dystrophies and is expressed in rod and cone photoreceptors (Boon et al. 2008).

20.3 Variables in RDD

20.3.1 Agents of PTGS

PTGS agents interact with target mRNAs on the basis of complementary Watson–Crick base pairing. We focus on ribozymes and shRNA agents that could constitute gene-based therapeutics. PTGS agents contain an engineered region that is antisense to an accessible region in the target mRNA (Fig. 20.2). The hammerhead ribozyme (hhRz) has its catalytic core situated between two antisense flanks that anneal to the target mRNA and position the enzyme to cleave after an NUH↓ triplet (N=G, A, U, C; U=U, H=C, A, U). The hhRz catalyzes a transesterification reaction based on RNA chemistry. After cleavage, the release of the target fragments is critical to allow enzymatic turnover and avoid product inhibition. The total antisense span of the hhRz should be at least 12 nt which is sufficient for good specificity with respect to the human transcriptome. The hhRz can be expressed within the context of a structured (chimeric) RNA that provides stability, appropriate cellular trafficking (to colocalize with target mRNA), and cellular stability (resistance to nucleases). The short hairpin RNA (shRNA) is a double-stranded stem loop element that contains a guide or antisense strand (complementary to the target mRNA region) and its complement separated by a short engineered loop. The cytoplasmic RNase

Dicer cleaves off the loop to generate a short interfering RNA (siRNA). Cellular proteins interact with the siRNA, then select and orient the guide strand to form the RNA-induced silencing complex (RISC). RISC binds to the target mRNA, and the protein components cleave the target RNA. RISC uses a seed sequence of 7–8 nt to interact with the target mRNA and within this seed the process is mismatch-tolerant. It is not surprising that there are typically many off-target effects with shRNA as compared to the hhRz which, relatively, is expected to have higher specificity for cleaving the target mRNA and potentially lower toxicity.

20.3.2 Validating Appropriate Disease Target mRNAs

The target mRNA expresses a protein, which is expected to contribute to the disease process. In an autosomal dominant hereditary retinal degeneration, the mutant mRNA encodes a protein that could have gain-of-function toxic properties or dominant negative properties that promote cellular compromise and ultimate cell death and vision loss. Also, the loss of the wild type (WT) mRNA and protein may create a state of haploinsufficiency that may contribute to cellular demise. To solve the simultaneous problem of gain-of-function toxicity of mutant gene products and WT haploinsufficiency, it may be necessary to express both a PTGS agent to knockdown the mutant (and WT) proteins and a variant WT allele to reconstitute WT protein expression with an mRNA that cannot be cleaved by the PTGS agent. Albeit complex, a knockdown-reconstitute strategy could allow use of a single therapeutic PTGS agent for all or most mutant alleles of a dominant disease gene.

PTGS agents have therapeutic potential for retinal degenerations, where the targets are human WT mRNAs and proteins. For example, age-related macular degeneration is a multifactorial disease process with pathophysiological contributions originating from oxidative stress, accumulation of toxic retinoids (e.g., A2E), and local inflammation. Investigation of cellular disease pathways can validate WT mRNA targets and proteins that, if reduced by PTGS agents, could ameliorate disease states.

20.3.3 Target mRNA Structure and Determinations of Accessibility

Annealing of a PTGS agent to a target mRNA is the rate limiting step in PTGS reaction kinetics. Annealing cannot occur if the targeted region is in a preexisting state of stable secondary or tertiary structure, or is protein coated. The PTGS agent must colocalize to the cellular compartment with the target mRNA to allow collision-mediated annealing, and the PTGS agent must be in sufficient local concentration to drive the second-order annealing reaction forward. The capacity of the PTGS to anneal will depend upon the local accessibility of the target mRNA. mRNA and

Fig. 20.3 Target mRNA structure and accessibility. The most stable *PRPH2* mRNA structure predicted by Mfold (-993 kCal/mol)



viral RNA targets have profoundly limiting secondary structures that constrain the number of large and kinetically-stable single stranded platforms able to support PTGS annealing. Accessibility is rare in any target mRNA. An example of extensive secondary structures present in a disease target (human *RDS*) mRNA is shown (Fig. 20.3). There are few, if any, large single stranded regions. The primary and critical challenge in RDD is to identify those rare regions in the target mRNA which are accessible to rapid PTGS ligand annealing. Any perturbing intrinsic RNA structures or extrinsic structures (e.g., protein coating) that occlude the annealing platform will prevent or delay annealing events at physiological temperatures. The conformational folding space of the target mRNA can be sampled by combinatorial HTS procedures. Computational HTS approaches are used to assess RNA target secondary structures. There are number of algorithms available such as MFold (Zuker 2003), SFold (Ding et al. 2004), and OligoWalk (Mathews et al. 1999). We combine the outputs of these algorithms to analyze target mRNA structure in a bioinformatics approach that we call multiparameter prediction of RNA accessibility (Abdelmaksoud et al. 2009).

It is also critical to experimentally probe the accessibility of a target mRNA to which PTGS agents will be designed. Randomized short oligodeoxynucleotides (ODN) can be presented to the folded target mRNA and then RNaseH added to promote cleavage within rare regions of annealing. RNA primer extension analysis can then be used to identify the region of the probe binding and cleavage (Ho et al. 1998). Similar approaches that use reverse transcriptase to initiate cDNA synthesis from regions of ODN binding can also be used to identify accessible platforms (Allawi et al. 2001). We recently developed a novel approach based on reverse transcription and ODN probes to rapidly identify stable single stranded accessible regions that contain hhRz cleavage sites in target mRNAs in their native folding state(s) (Sullivan and Taggart 2007).

20.3.4 Screening Large Numbers of PTGS Agents to Identify a Lead Candidate

In any accessible platform(s) there are typically multiple potential hhRz or shRNA cleavage sites. Once rare regions of accessibility are identified, it may be necessary to construct a substantial set of PTGS agents to test efficacy and identify a lead candidate that exerts the greatest knockdown of target mRNA/protein. The design of a PTGS expression plasmid should be such that the small RNA is expressed to abundance in cultured cells (e.g., an RNA polymerase III promoter). The PTGS agent may be inserted within an RNA chimera to provide support, cellular stability, and cell compartment colocalization with target mRNA. The vector should be modified such that ligation of adaptors containing the PTGS cDNA is efficient. The cell line chosen should have high transfection efficiency with commercially available reagents (e.g., HEK293S cells, Lipofectamine). Conventional molecular biological tools such as RT/PCR and western analysis are slow, low throughput approaches with substantial variability; and do not permit rapid, efficient, and reliable identification of the lead PTGS candidate. A more efficient approach is to identify a means of directly or indirectly coupling the expression of the target gene to the expression of a convenient reporter molecule that can be rapidly and efficiently analyzed under HTS assays (Yau and Sullivan 2007; Yau and Sullivan submitted). Examples of such reporter genes could be secreted alkaline phosphatase or rapid decay forms of EGFP. The critical factor is that reporter expression represents the steady-state accumulation of the target mRNA. The PTGS agent and the target-reporter plasmid can be cotransfected into naïve cultured cells or the PTGS expression plasmid can be delivered into a stable cell line engineered to express the target-reporter construct. Output reads from the HTS reporter screen (e.g., SEAP enzyme assay, EGFP fluorescence) are then rank-ordered to identify the lead candidate PTGS plasmid that promotes the greatest target knockdown.

20.3.5 Optimizing the Lead Candidate

If the PTGS agent is an hhRz, the lead candidate may be subject to several rational modifications to obtain a more effective knockdown agent. The antisense flanks of the hhRz govern both target mRNA molecular recognition and specificity as well as the product leaving rates and enzymatic turnover efficiency (Stage-Zimmermann and Uhlenbeck 1998). The enzymatic core of the ribozyme is evolutionarily optimized and changes are typically deleterious, but stem II-loop elements that support the core can be altered with potential to enhance knockdown. Addition of upstream (5') tertiary accessory elements can potentially enhance efficacy by driving the enzyme structure into a catalytically active state (Khvorova et al. 2003). The expression of the

PTGS agent in a protective RNA chimera (e.g., a tRNA, adenoviral VAI RNA) with defined structure and cellular trafficking streams can facilitate colocalization with target mRNA and increase the half-life of the PTGS agent in the cell (Lieber and Strauss 1995; Koseki et al. 1999).

20.3.6 The Vector, PTGS Expression Construct, and Animal Testing

For a gene-based therapy, there must be a vector to deliver the PTGS expression construct to appropriate cells. A variety of engineered viruses (e.g., rAAV) (Flannery et al. 1997) and nanoparticles, which have properties of synthetic viruses (Farjo et al. 2006), offer potential for high transduction efficiency to promote PTGS expression in as many diseased cells as possible. An optimized surgical approach is needed to maximize therapeutic vector delivery and target cell transduction. Visualization of surgical delivery of vector insures correct compartmental access in the eye (e.g., subretinal space) and allows quantitation of the areal extent of delivery (e.g., fraction of retina coverage by delivered volume). Quantitative measurement of target cell transduction (e.g., expression of a nontoxic fluorescent protein) should be used to normalize measured rescue (e.g., ERG). In many mouse-based preclinical studies, such measures are limited by the imaging technology. The small mouse eye has a constrained pupillary aperture (~1 mm dilated) that limits both the input of light and the collection of the output specular image. As a facilitating technology, we developed a stereo bright-field and fluorescence microscope that allows real time visualization within the neonatal mouse eye during and after subretinal or intraocular injections (Butler and Sullivan 2010).

20.3.7 Appropriate Targets (Human)

Many animal models exist for retinal degenerations. In the context of PTGS agents under development for potential clinical translation, it is critical to understand that an animal mRNA is unlikely to represent the same conformational landscape as a PTGS receptor as would a human cognate mRNA target. This results due to sequence divergence at the 5 and 3'UT regions, codon differences, and third position bias. RNA folding into secondary structures is a local process, and even when the primary sequences of an animal and human target are identical over the region of PTGS annealing, the secondary structures can indeed be different and this can impact efficacy. Our view for PTGS studies intended toward human clinical translation is that the mRNA targets expressed in preclinical animal models be true full length human mRNAs.

20.4 Conclusions

PTGS agents have great therapeutic potential for retinal degenerations. The overview presented here will hopefully provide both direction and incentive for other motivated groups to share the challenges of RDD. Viral and nanoparticle vector technology for retinal or ocular gene therapy is advanced. Gene therapy clinical trial for Leber congenital amaurosis due to autosomal recessive (*null*) mutations in the *RPE65* gene is demonstrating early safety and efficacy profiles when the delivered genetic construct expresses a WT protein (den Hollander et al. 2010). If fully successful, this initial therapeutic trial could establish the eye as an organ for vector based gene therapy for other recessive conditions, and ultimately for expressed PTGS agents that act to knockdown expression of specific validated disease targets as a path to cell preservation and sustenance of vision.

Acknowledgments We thank the National Eye Institute (R01 EY13433, PI: Sullivan) (R24 EY016662, PI: M Slaughter), the Veterans Administration (Merit Grant 1I01BX000669-01), an Unrestricted grant from Research to Prevent Blindness, and a grant from the Oishei Foundation (Buffalo, NY).

References

- Abdelmaksoud H, Yau EH, Zuker M et al (2009) Development of lead hammerhead ribozyme candidates against human rod opsin for retinal degeneration therapy. *Exp. Eye Res* 88:859–879
- Allawi HT, Dong F, Ip HS et al (2001) Mapping of RNA accessible sites by extension of random oligonucleotide libraries with reverse transcriptase. *RNA* 7:314–327
- Boon CJF, den Hallander AI, Hoyng CB et al (2008) The spectrum of retinal dystrophies caused by mutations in the *peripherin/RDS* gene. *Prog Ret Eye Res* 27:213–225
- Butler MC, Sullivan JM (2010) A novel real-time *in vivo* mouse retinal imaging system. *Invest Ophthalmol Vis Sci* 51:3103
- Den Hollander AI, Black A, Bennet J et al (2010). Lighting a candle in the dark: advances in genetics and gene therapy of recessive retinal dystrophies. *J Clin Invest* 120: 3042–3053
- Ding Y, Chan CY, Lawrence CE (2004) Sfold web server for statistical folding and rational design of nucleic acids. *Nucleic Acids Res* 32 (supp):W135–W141
- Farjo R, Skaggs J, Quiambao AB et al (2006) Efficient non-viral ocular gene transfer with compacted DNA nanoparticles. *PLoS One* 1:e38
- Flannery JG, Zolotukhin S, Vaquero MI et al (1997) Efficient photoreceptor-targeted gene expression *in vivo* by recombinant adeno-associated virus. *Proc Natl Acad Sci U S A* 94:6916–6921
- Ho SP, Bao Y, Leshner T, Malhotra R et al (1998) Mapping of RNA accessible sites for antisense experiments with oligonucleotide libraries. *Nat Biotechnol* 16:56–63
- Khvorova A, Lescoute A, Westhof E et al (2003) Sequence elements outside the hammerhead ribozyme catalytic core enable intracellular activity. *Nature Struct Biol* 10: 708–712
- Koseki S, Tanabe T, Tani K et al (1999) Factors governing the activity *in vivo* of ribozymes transcribed by RNA polymerase III. *J Virol* 73:1868–1877
- Lieber A, Strauss M (1995) Selection of efficient cleavage sites in target mRNAs by using a ribozyme expression library. *MolCell. Biol* 15:540–551

- Mathews DH, Burkard ME, Freier SM et al (1999) Predicting oligonucleotide affinity to nucleic acid targets. *RNA* 5:1458–1469
- Stage-Zimmermann TK, Uhlenbeck OC (1998) Hammerhead ribozyme kinetics. *RNA* 4:875–889
- Sullivan JM, Taggart RT (2007) Novel and enhanced approaches to determined local mRNA accessibility. *Invest Ophthalmol Vis Sci* 48:4605
- Yau EH, Sullivan JM (2007) High throughput cellular screening for ribozyme development against arbitrary mRNA targets. *Invest Ophthalmol Vis Sci* 48:1681
- Zuker M (2003) Mfold web server for nucleic acid folding and hybridization prediction. *Nucleic Acids Res* 31:3406–3415

Chapter 21

On Further Development of Barrier Modulation as a Technique for Systemic Ocular Drug Delivery

Finnian Hanrahan, Matthew Campbell, Anh T. Nguyen, Mayu Suzuki, Anna-Sophia Kiang, Lawrence C. Tam, Oliviero L. Gobbo, Sorcha Ní Dhubhghaill, Marian M. Humphries, Paul F. Kenna, and Pete Humphries

Keywords Blood-retinal barrier • Drug delivery • Tight junction • Claudin-5 • Barrier modulation • Retinal pigmented epithelium • IMPDH1

21.1 Introduction

The use of the monoclonal antibody Lucentis® to treat neovascularization in wet AMD has been a huge milestone in the treatment of retinal degeneration. However, the blood-retinal barrier (BRB) remains the largest obstacle to the treatment of retinal conditions, with up to 98% of low-molecular-weight drugs not crossing the BRB (Pardridge 2007). The majority of therapeutics used to treat the retina currently, such as Lucentis®, are delivered via intraocular injection. This requires repeated visits to clinics, great discomfort for patients, as well as the risk of endophthalmitis, cataract, retinal detachment and toxic vitreitis (Ness et al. 2010).

The BRB is made up of two distinct parts – the inner and outer BRB. The iBRB is formed by cells of the retinal vascular endothelium, while the oBRB is formed by the cells of the retinal pigmented epithelium (RPE). In both cases, the crucial part of the barrier is the tight junction, a protein complex that spans the plasma membrane at the apical end of contacting endothelial or epithelial cells. These tight junction complexes limit paracellular transport between the cells of the iBRB and oBRB.

F. Hanrahan (✉) • M. Campbell • A.T. Nguyen • M. Suzuki • A.-S. Kiang • L.C. Tam
• S.N. Dhubhghaill • M.M. Humphries • P.F. Kenna • P. Humphries
Ocular Genetics Unit, Smurfit Institute of Genetics, Trinity College Dublin, Dublin 2, Ireland
e-mail: hanrahfe@tcd.ie

O.L. Gobbo
School of Pharmacy and Pharmaceutical Sciences,
Trinity College Dublin, Dublin 2, Ireland

Tight junctions are made up of at least three different types of membrane-spanning proteins – occludin, members of the junctional adhesion molecule family of proteins and claudin proteins (Ben-Yosef et al. 2003), as well as many structural and transport proteins inside the cell, such as zona occludens proteins (Anderson and Van Itallie 2008).

21.2 Therapeutic Delivery Across the iBRB

This lab has recently reported that using systemically injected small interfering RNA (siRNA) targeting claudin-5, a tight junction component of the iBRB and not of the oBRB, the iBRB was modulated to allow for the selective passive diffusion of low-molecular-weight compounds from the blood to the retina, 24 and 48 h post injection of siRNA (Campbell et al. 2009). This technique was used to treat a number of animal models of retinopathies.

One model was a mouse knockout of the IMPDH1 gene, in which animals demonstrate a gradual and age-dependent degeneration of their retinal outer segments due to a lack of guanosine triphosphate (GTP), of which IMPDH1 is the rate-limiting enzyme in its de novo synthesis (Gu et al. 2003). In these animals, GTP was delivered systemically following suppression of claudin-5. Electroretinography (ERG) readouts were observed to improve in animals that had received claudin-5 siRNA, while no improvement was observed in animals administered nontargeting (NT) siRNA (Fig. 21.1). Claudin-5 siRNA without GTP, meanwhile, resulted in no improvement in the ERG, indicating that modulation of the iBRB alone had not caused this improvement in the ERG. These results demonstrate that suppression of claudin-5 at the iBRB was sufficient to allow GTP – a 523-Da molecule which is normally unable to cross the BRB – to diffuse across the iBRB into the retina where it had an effect (Campbell et al. 2009).

This technique was demonstrated to be size-selective as well as transient, with microperoxidase – molecular weight 1,881 Da – being maintained within retinal microvessels even while claudin-5 was suppressed, and levels of claudin-5 expression and full barrier strength were shown to return to normal 72 h post-siRNA injection. Concomitantly, no cell death was observed, and neuronal transcription profiles remained largely unchanged as a result of barrier modulation (Campbell et al. 2009).

Claudin-5 is expressed in the endothelial cells of the iBRB and not in RPE cells of the oBRB (Bai et al. 2008; Tachikawa et al. 2008), and as such, the delivery of therapeutics following claudin-5 suppression results in the delivery of the therapeutic across the iBRB alone. What remains to be investigated is whether there would be any advantage in the delivery of low-molecular-weight therapeutics across the oBRB alone, or both the iBRB and oBRB.

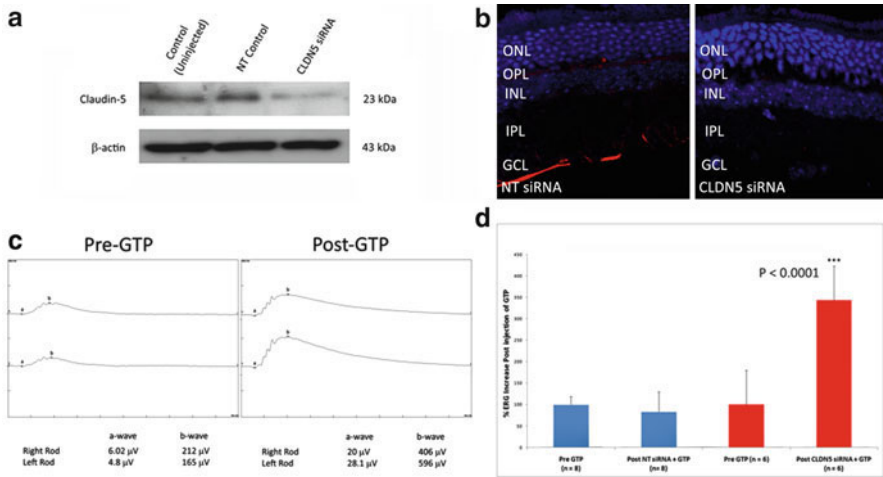


Fig. 21.1 Improvement in ERG results following systemic GTP delivery across the modulated iBRB. **(a)** Western blot illustrating decreased levels of claudin-5 in the retinas of IMPDH1^{-/-} mice 48 h after systemic injection of claudin-5 siRNA. **(b)** Immunohistochemical analysis of claudin-5 levels (*red*) counterstained with DAPI (*blue*), at 40 \times objective. A decrease in claudin-5 levels is apparent after claudin-5 siRNA delivery. **(c)** ERG tracings in IMPDH1^{-/-} mice before and after injection with GTP 48 h after claudin-5 siRNA delivery. Well-formed **(a, b)** were observed following treatment. **(d)** Graph of electrical readout of rod photoreceptors expressed as percentage changes. A significant increase (***, $P < 0.0001$) in rod-isolated ERG was observed in mice receiving claudin-5 siRNA and GTP compared with mice receiving NT siRNA and GTP (modified from Campbell et al. 2009)

21.3 The oBRB and Its Potential in Barrier Modulation

The RPE that constitutes the oBRB is located at the interface between the photoreceptor outer segments on its apical side and Bruch membrane on its basolateral side, with the choriocapillaris beyond (Simo et al. 2010). One of the main functions of the RPE is the maintenance of the oBRB – important for the homeostatic microenvironment of the retina – as well as the transport of nutrients, ions, and water. However, unlike the retinal endothelial vasculature, the RPE also protects against photo-oxidation, phagocytoses shed photoreceptor outer segments, re-isomerises all-*trans*-retinal into 11-*cis*-retinal – a molecule necessary for photo-transduction, and secretes factors essential to the integrity of the retina, including immunosuppressive factors and growth factors (Simo et al. 2010). Indeed, transplanted RPE cells have been observed to slow the progression of retinal degeneration in animal models without forming a functional BRB (Litchfield et al. 1997).

Despite these differences in characteristics and anatomy, the oBRB has been investigated to a far lesser extent. The barrier selectivity of the RPE appears to be

very similar to its endothelial counterpart (Steuer et al. 2005), despite an apparent difference in transepithelial resistance (Rizzolo 2007), and changes in RPE tight junction size selectivity appear to follow alterations in the levels of tight junction proteins such as claudins and occludin (Abe et al. 2003). One example where delivery across the oBRB could potentially be beneficial would be for the delivery of anti-angiogenic substances, such as sunitinib (molecular weight 400 Da), to conditions such as wet AMD where choroidal neovascularization is the central pathology. This is because it is the RPE which secretes VEGF across both its apical and basolateral membranes (Peng et al. 2010), and so hypothetically delivery of anti-angiogenic therapies here could maximise their effect.

Another potential benefit of oBRB modulation is improvement of the therapeutic window of a drug. 9-cis-retinyl acetate, for instance, has been demonstrated to partially rescue cone photoreceptor loss in an animal model of Leber's congenital amaurosis, even when delivered by oral gavage or intraperitoneally (Maeda et al. 2009). To generate this effect, however, a very high dose of the artificial chromophore was required, and side effects of this treatment could be quite negative (Palczewski 2010). In this case, and in the case of many other drugs which do manage to cross the oBRB, the therapeutic window of these therapeutics, as well as their efficacy, could be greatly improved by their delivery across a modulated oBRB. In the case of 11-cis-retinal replacements such as 9-cis-retinyl acetate, delivery across the oBRB might be preferable due to 11-cis-retinal's production being in the RPE, therefore delivery across the oBRB would be more akin to its natural delivery pattern, as well as improving the therapeutic window. Delivery across the oBRB as well as the iBRB would maximise this improvement, and this could hypothetically be done by suppressing the tight junction protein occludin, which is expressed in both the iBRB (Leal et al. 2010) and the oBRB (Miura et al. 2010).

One final strategy behind targeting the oBRB rather than the iBRB for delivery of therapeutics is that, by modulating the iBRB by systemic siRNA delivery, the blood-brain barrier is also modulated due to the apparent equivalence in tight junction protein composition (Campbell et al. 2008). For some therapeutics, this would be undesirable if they have psychoactive properties or are neuronally damaging. One way to circumvent this problem would be to subretinally inject an AAV carrying a claudin-5 shRNA under the control of an inducible promoter. Another option, however, would be to target the oBRB and not the iBRB, for instance by suppression of claudin-1 which does not appear to be prominently expressed in the endothelial barrier (Xu et al. 2005).

21.4 Closing Remarks

As has been previously demonstrated (Campbell et al. 2009), modulation of the iBRB by the suppression of tight junction proteins holds much promise for the delivery of therapeutics that could aid in combatting many conditions of the retina. Modulation of the oBRB, in conjunction with or in the absence of iBRB modulation,

could aid in the efficient and safe delivery of therapeutics to the retina, as well as potentially opening up new therapeutic opportunities unique to delivery across the oBRB.

References

- Abe T, Sugano E, Saigo Y et al (2003) Interleukin-1beta and barrier function of retinal pigment epithelial cells (ARPE-19): aberrant expression of junctional complex molecules. *Invest Ophthalmol Vis Sci* 44:4097–4104
- Anderson JM, Van Itallie CM (2008) Tight junctions. *Curr Biol* 18:R941–943
- Bai L, Zhang Z, Zhang H et al (2008) HIV-1 Tat protein alter the tight junction integrity and function of retinal pigment epithelium: an in vitro study. *BMC Infect Dis* 8:77
- Ben-Yosef T, Belyantseva IA, Saunders TL et al (2003) Claudin 14 knockout mice, a model for autosomal recessive deafness DFNB29, are deaf due to cochlear hair cell degeneration. *Hum Mol Genet* 12:2049–2061
- Campbell M, Kiang AS, Kenna PF et al (2008) RNAi-mediated reversible opening of the blood-brain barrier. *J Gene Med* 10:930–947
- Campbell M, Nguyen AT, Kiang AS et al (2009) An experimental platform for systemic drug delivery to the retina. *Proc Natl Acad Sci U S A* 106:17817–17822
- Gu JJ, Tolin AK, Jain J et al (2003) Targeted disruption of the inosine 5'-monophosphate dehydrogenase type I gene in mice. *Mol Cell Biol* 23(18):6702–12
- Leal EC, Martins J, Voabil P et al (2010) Calcium dobesilate inhibits the alterations in tight junction proteins and leukocyte adhesion to retinal endothelial cells induced by diabetes. *Diabetes* 59:2637–2645
- Litchfield TM, Whiteley SJ, Lund RD (1997) Transplantation of retinal pigment epithelial, photoreceptor and other cells as treatment for retinal degeneration. *Exp Eye Res* 64:655–666
- Maeda T, Cideciyan AV, Maeda A et al (2009) Loss of cone photoreceptors caused by chromophore depletion is partially prevented by the artificial chromophore pro-drug, 9-cis-retinyl acetate. *Hum Mol Genet* 18:2277–2287
- Miura Y, Klettner A, Noelle B et al (2010) Change of morphological and functional characteristics of retinal pigment epithelium cells during cultivation of retinal pigment epithelium-choroid perfusion tissue culture. *Ophthalmic Res* 43:122–133
- Ness T, Feltgen N, Agostini H et al (2010) Toxic vitritis outbreak after intravitreal injection. *Retina* 30:332–338
- Palczewski K (2010) Retinoids for treatment of retinal diseases. *Trends Pharmacol Sci* 31:284–295
- Pardridge WM (2007) Blood-brain barrier delivery. *Drug Discov Today* 12:54–61
- Peng S, Adelman RA, Rizzolo LJ (2010) Minimal effects of VEGF and anti-VEGF drugs on the permeability or selectivity of RPE tight junctions. *Invest Ophthalmol Vis Sci* 51:3216–3225
- Rizzolo LJ (2007) Development and role of tight junctions in the retinal pigment epithelium. *Int Rev Cytol* 258:195–234
- Simo R, Villarroel M, Corraliza L et al (2010) The retinal pigment epithelium: something more than a constituent of the blood-retinal barrier – implications for the pathogenesis of diabetic retinopathy. *J Biomed Biotechnol* 2010:190724
- Steuer H, Jaworski A, Elger B et al (2005) Functional characterization and comparison of the outer blood-retina barrier and the blood-brain barrier. *Invest Ophthalmol Vis Sci* 46:1047–1053
- Tachikawa M, Toki H, Tomi M et al (2008) Gene expression profiles of ATP-binding cassette transporter A and C subfamilies in mouse retinal vascular endothelial cells. *Microvasc Res* 75:68–72
- Xu H, Dawson R, Crane IJ et al (2005) Leukocyte diapedesis in vivo induces transient loss of tight junction protein at the blood-retina barrier. *Invest Ophthalmol Vis Sci* 46:2487–2494

Chapter 22

An Application for Mammalian Optic Nerve Repair by Fish Regeneration-Associated Genes

Yoshiki Koriyama, Kayo Sugitani, Toru Matsukawa, and Satoru Kato

Keywords Optic nerve • Regeneration • Survival • Retinal ganglion cell • Repair • Apoptosis

22.1 Introduction

In the adult mammalian CNS, axonal injury leads to retrograde neuronal degeneration and death in cell soma. Aguayo et al. reported that optic nerve transection induced cell death over 90% of total retinal ganglion cells (RGCs) within 2 weeks in adult rat (Villegas-Pérez et al. 1993). However, fish optic nerve injury never leads to widely spreading cell death of RGCs (Koriyama et al. 2007). Goldfish can regrow their axons toward the visual center and finally restore their visual function after optic nerve injury (Stuermer et al. 1992). It takes about a half-year from start of axonal regrowth to complete restoration of vision. We classified this fish optic nerve regeneration process as three stages, early (0–5 days): preparation period, middle (1–6 weeks): axon outgrowth and synapse connection period, and late (2–6 months): synapse refinement period (Kato et al. 1999, 2007). We were interested in the key molecules involved in the early stage of regeneration process. Especially, we focused on the differences of cell death and survival signaling between rat and fish. Thus, we found two molecules, insulin-like growth factor (IGF-I, Koriyama et al. 2007) and neural nitric oxide synthase (nNOS, Koriyama et al. 2009). In addition, we

Y. Koriyama • T. Matsukawa • S. Kato (✉)

Department of Molecular Neurobiology, Kanazawa University, Kanazawa 920-8640, Japan
e-mail: satoru@med.kanazawa-u.ac.jp

K. Sugitani

Division of Health Sciences, Kanazawa University, Kanazawa 920-8640, Japan

Table 22.1 Regeneration molecules derived from goldfish after ON injury

Molecules	Days of upregulation after ONI	Localization of protein		
		ONL	INL	GCL
From cell signaling study				
IGF-I	2 days	±	+	+++
nNOS	5 days	+	++	+++
From differential hybridization study				
Transglutaminase	5 days	±	+	+++
Purpurin	2 days	+	++	+++

ONI optic nerve injury; *ONL* outer nuclear layer; *INL* inner nuclear layer; *GCL* ganglion cell layer

constructed a cDNA library from axotomized goldfish retina. In our study, differential screening of the cDNA library was performed to identify the gene of which expression is upregulated in fish retina 5 days, after optic nerve injury. Following this extension, we cloned the CNS regeneration-candidate molecules such as transglutaminase (TG, Sugitani et al. 2006) and purpurin (Matsukawa et al. 2004). In Table 22.1, we summarize the neurite outgrowth-promoting factors which we cloned from fish retina by two strategies of cell signaling study and differential hybridization study. Further, we attempted to regenerate rat RGCs by using these molecules derived from regenerating goldfish retina.

22.2 IGF-I

Many trophic factors, such as nerve growth factor (Turner et al. 1980) and brain-derived neurotrophic factor (Mey and Thanos 1993), have been reported to be useful for RGCs survival and regenerating their optic nerve. To characterize the RGC survival signaling after nerve injury, we evaluated, the survival signal, Akt phosphorylation levels in the goldfish retina. Amounts of phospho-Akt (p-Akt) in the goldfish retina rapidly increased 4–5 fold at the protein level by 3–5 days after nerve injury. Furthermore, level of IGF-I, which activates the Akt, increased 2 days earlier than that of p-Akt in the goldfish retina. The addition of IGF-I to the goldfish retinal explants dramatically induces axon outgrowth. On the contrary, the levels of rat IGF-I were rapidly decreased from RGCs 1–2 days just prior to the inactivation of p-Akt by optic nerve injury. The supplementation with IGF-I into the rat retina induced upregulation of p-Akt expression and cell survival of RGCs both in vitro and in vivo. Furthermore, IGF-I drastically enhanced neurite outgrowth even in rat retinal explant cultures. These data suggest that IGF-I is required for axonal regeneration in both goldfish and rat RGCs.

22.3 nNOS

Nitric oxide (NO) signaling results in both neurotoxic and neuroprotective effects in CNS neurons after nerve lesioning. We investigated the role of NO signaling on optic nerve regeneration in the goldfish. Levels of nNOS mRNA and protein increased in the RGCs 5 days and peaked at 20 days after injury (Koriyama et al. 2009). The period corresponds to the axonal elongation stage in the goldfish optic nerve regeneration process. NO stimulates soluble guanylate cyclase and produces cGMP. In retinal explant culture study, cGMP analog and NO donor promoted neurite outgrowth, whereas specific nNOS inhibitor and siRNA suppressed it from adult fish RGCs. Intraocular injection of cGMP analog also promoted the axonal regeneration from injured RGCs in vivo (Koriyama et al. 2009). The data all together indicate that NO-cGMP system is activated and thereby promotes optic nerve regeneration in the goldfish retina after injury.

22.4 TG

TGs are a family of enzymes that catalyze protein cross-linking reactions as described before (Sugitani et al. 2006). The retinal TG mRNA increases from 5 days and peaked at 20 days after injury in goldfish. Localization of increased mRNA is limited to the ganglion cell layer (GCL). TG inhibitor and siRNA dramatically suppressed the axon outgrowth from goldfish retinal explants. In contrast, the levels of TG protein decreased in rat RGCs within 1–3 days after injury. Furthermore, the addition of recombinant TG to retinal explant cultures induced striking axon outgrowth from adult rat RGCs. We expect that TG also acts as a neuroregenerative molecule against rat RGCs.

22.5 Purpurin

A secretory retinol-binding protein, purpurin, was originally discovered as an adhesion-mediating protein from chick retina (Schubert and LaCorbiere 1985). We cloned purpurin from the retinal cDNA library with differential hybridization of normal and axotomized goldfish retinas. The levels of purpurin mRNA peaked at 2–5 days after injury (Matsukawa et al. 2004). The purpurin proteins were diffusely localized in all retinal layers, especially in the GCL after injury (Fig. 22.1b) compared to intact retina (Fig. 22.1a). In retinal explant culture study in Fig. 22.2, retinol itself did not affect any changes on the control neurite length (Fig. 22.2d); however, recombinant purpurin significantly induced neurite outgrowth (Fig. 22.2b). Furthermore, the combination of purpurin and retinol (ret) promoted the axon

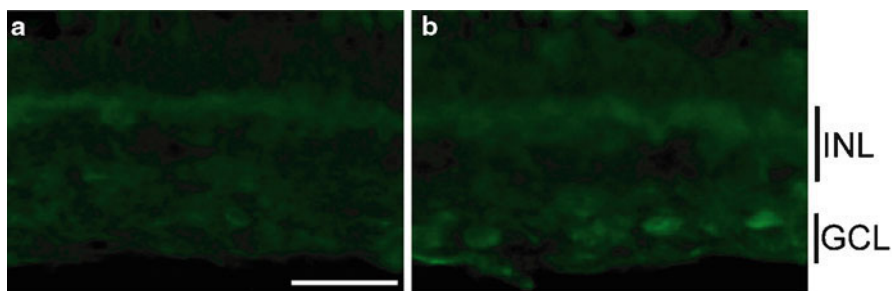


Fig. 22.1 Immunohistochemical study of purpurin in the goldfish retina. Retinal sections from goldfish were incubated with antipurpurin antibody. (a) Intact retina (b) 5 days after optic nerve injury. *INL* inner nuclear layer; *GCL* ganglion cell layer. Scale bar=100 μ m

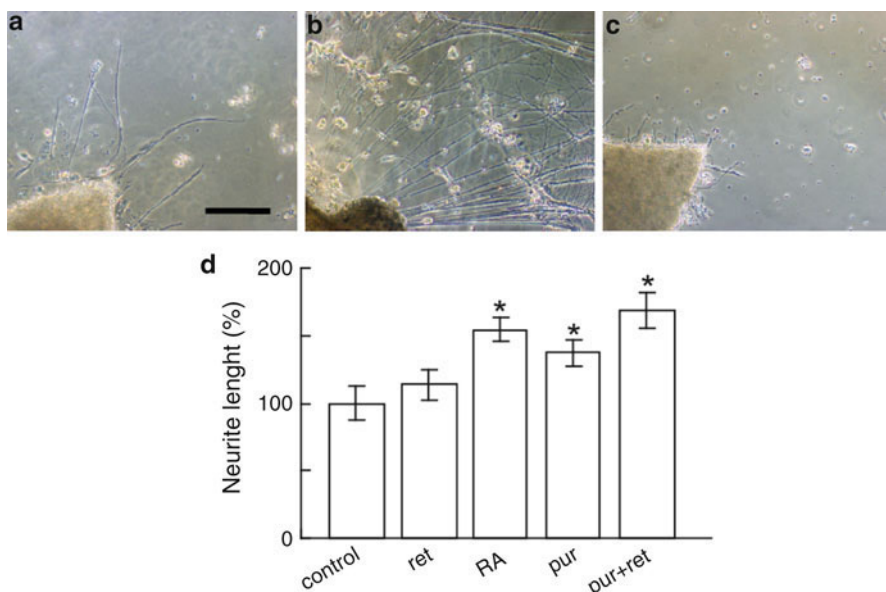


Fig. 22.2 Neurite outgrowth in adult goldfish retinas in culture. Retinal explants were cultured for 5 days. (a) Scrambled siRNA of purpurin. (b) Purpurin (1 μ g/mL). (c) siRNA of purpurin. Scale bar=100 μ m. (d) Neurite length with the addition of purpurin and retinoids to the 5-day-optic nerve-injured retina. Note a drastic enhancement of neurite length with the addition of purpurin (Pur). Purpurin plus retinol (ret) and retinoic acid (RA). * $P < 0.01$ vs. control, + $P < 0.01$ vs. purpurin alone

elongation compared to purpurin alone (Fig. 22.2d). Scrambled siRNA of purpurin did not affect any change in neurite outgrowth (Fig. 22.2a). However, siRNA of pupurin significantly inhibited the axon outgrowth of purpurin (Fig. 22.2c).

22.6 Future Study for Overcoming Mammalian CNS Injury

The supplementation of IGF-I or TG certainly induced axon outgrowth in rat retinal explant culture. Recently, there is a paper that TG suppresses the upregulation of the hypoxia-induced, proapoptotic genes and protects against ischemic-induced neuronal death (Filiano et al. 2008). TG might potentially act as retinal neuroprotectants and neurite outgrowing molecules. As an application study of rat optic nerve regeneration by NO, we recently demonstrated that NO-producing chemical (1R)-isoPropyloxygenipin (IPRG001) exerts RGC neuroprotective action both in vitro and in vivo, through the Nrf2/antioxidant response element pathway by S-nitrosylation against oxidative stress (Koriyama et al. 2010). Moreover, IPRG001 also induced axon outgrowth mediated by NO production from rat RGC lines (Y. Koriyama, unpublished data). These data strongly suggest that NO must be the key molecule which induces optic nerve regeneration. Purpurin significantly increases the neurite length compared to the control. These results suggest that purpurin itself induces neurite outgrowth mediated by its cell signaling such as adhesion molecules-associated signaling and by increase of intracellular levels of retinoic acid because purpurin also acts as a retinol-binding protein. In preliminary data, recombinant purpurin protein induced neurite outgrowth from rat RGC lines (Koriyama unpublished data). These findings strongly indicate that purpurin is one of the high-potential tools for rescuing RGC apoptosis caused by a variety of glaucomatous conditions. Recently, Harvey's group reviewed gene therapy studies for improving the RGCs survival and regeneration. (Harvey et al. 2009). Gene transfer techniques seem to be useful for our application study of mammalian optic nerve repair by fish-derived genes such as purpurin. Taken together, the goldfish regeneration-associated genes become a useful therapeutic tool to rescue degenerative neuronal diseases.

References

- Filiano AJ, Bailey CD, Tucholski J et al (2008) Transglutaminase 2 protects against ischemic insult, interacts with HIF1beta, and attenuates HIF1 signaling. *FASEB J* 22:2662–2675
- Harvey AR, Hellström M, Rodger J (2009) Gene therapy and transplantation in the retinofugal pathway. *Prog Brain Res* 175:151–161
- Kato S, Devadas M, Okada K et al (1999) Fast and slow recovery phases of goldfish behavior after transection of the optic nerve revealed by a computer image processing system. *Neuroscience* 93:907–914
- Kato S, Koriyama Y, Matsukawa T et al (2007) Optic nerve regeneration in goldfish. In: Becker CG, Becker T (eds) *Model Organisms in Spinal Cord Regeneration*, Wiley-VCH, Weinheim
- Koriyama Y, Homma K, Sugitani K et al (2007) Upregulation of IGF-I in the goldfish retinal ganglion cells during the early stage of optic nerve regeneration. *Neurochem Int* 50:749–756
- Koriyama Y, Yasuda R, Homma K et al (2009) nNOS, Nitric oxide-cGMP signaling regulates axonal elongation during optic nerve regeneration in the goldfish in vitro and in vivo. *J Neurochem* 110:890–901

- Koriyama Y, Chiba K, Yamazaki M et al (2010) Long-acting genipin derivative protects retinal ganglion cells from oxidative stress models in vitro and in vivo through the Nrf2/antioxidant response element signaling pathway. *J Neurochem* 115:79–91
- Matsukawa T, Sugitani K, Mawatari K et al (2004) Role of purpurin as a retinol-binding protein in goldfish retina during the early stage of optic nerve regeneration: its priming action on neurite outgrowth. *J Neurosci* 24:8346–8353
- Mey J, Thanos S (1993) Intravitreal injections of neurotrophic factors support the survival of axotomized retinal ganglion cells in adult rats in vivo. *Brain Res* 602:304–317
- Schubert D, LaCorbiere M (1985) Isolation of an adhesion-mediating protein from chick neural retina adherens. *J Cell Biol* 101:1071–1077
- Stuermer CA, Bastmeyer M, Bähr M et al (1992) Trying to understand axonal regeneration in the CNS of fish. *J Neurobiol* 23:537–550
- Sugitani K, Matsukawa T, Koriyama Y et al (2006) Upregulation of retinal transglutaminase during the axonal elongation stage of goldfish optic nerve regeneration. *Neuroscience* 142: 1081–1092
- Turner JE, Delaney RK, Johnson JE (1980) Retinal ganglion cell response to nerve growth factor in the regenerating and intact visual system of the goldfish (*Carassius auratus*). *Brain Res* 197:319–330
- Villegas-Pérez MP, Vidal-Sanz M, Rasminsky M (1993) Rapid and protracted phases of retinal ganglion cell loss follow axotomy in the optic nerve of adult rats. *J Neurobiol* 24: 23–36

Chapter 23

The Mechanism of Fenretinide (4-HPR) Inhibition of β -carotene Monooxygenase 1. New Suspect for the Visual Side Effects of Fenretinide

Eugenia Poliakov, Alexander Gubin, James Laird, Susan Gentleman,
Robert G. Salomon, and T. Michael Redmond

Keywords β -carotene monooxygenase 1 • BCMO1 • β -carotene • Fenretinide
• 4-HPR • Noncompetitive inhibition • Retinoid

23.1 Introduction

4-hydroxy(phenyl)retinamide (4-HPR) or fenretinide is a synthetic retinoid derivative. Fenretinide is the most extensively studied retinoid for the chemoprevention and treatment of a cancer because it is far less toxic than other retinoids (Veronesi et al. 2006). The very common adverse events are diminished dark adaptation (Camerini et al. 2001). Symptoms occurring during fenretinide treatment tend to abate with termination of treatment. Recently, the beneficial effects of fenretinide administration also were demonstrated in a mouse model of Stargardt disease (ABCA4^{-/-}) (Radu et al. 2005) and in treatment of Stargardt patients. It has been extensively demonstrated that fenretinide forms a tight complex with plasma retinol-binding protein (RBP4) and thus interferes with the retinol transport (Berni et al. 1993; Zanotti and Berni 2004). The effects of fenretinide on vision and bisretinoid accumulation in the eye were attributed to its ability to reduce plasma levels of RBP4 and retinol. However, recently the role of RBP4 in mediating visual fenretinide effects was questioned because fenretinide treatment of both wt and RBP4^{-/-} animals showed comparable levels of 11-cis retinal regeneration (Golczak et al. 2008). Additionally, fenretinide prevention of high fat-induced obesity, insulin resistance, and hepatic stenosis was not observed in RBP4^{-/-} animals, and thus the anti-adiposity

E. Poliakov • A. Gubin • S. Gentleman • T.M. Redmond (✉)
LRCMB, National Eye Institute, NIH, Bldg 6, Room, 6 Center Dr. MSC0608,
Bethesda, MD 20892, USA
e-mail: Redmond@helix.nih.gov

J. Laird • R.G. Salomon
Department of Chemistry, Case Western Reserve University, Cleveland, OH, USA

effects of fenretinide are independent of the RBP4-lowering effect (Motani et al. 2009; Preitner et al. 2009).

On the other hand, all-trans retinal, the aldehyde form of vitamin A, can be synthesized locally in the tissues by the cleavage of β -carotene and thus β -carotene monooxygenase 1 (BCMO1) might supply all-trans retinal as an accessory source of vitamin A for the visual cycle (Chichili et al. 2005). In this report, we describe the mechanism of fenretinide inhibition of mouse BCMO1 which may be responsible for the visual effects of fenretinide.

23.2 Materials and Methods

23.2.1 Constructs

Recombinant Δ 336-345BCMO1 was produced by inserting at the 341 aa codon position of BCMO1 the modified transposon cassette Tn5/Kan (Epicentre Biotechnologies) with terminal BSG1 sites and then removing this cassette along with an additional 15 nucleotides on each side with BSG1 enzyme.

23.2.2 Protein Expression and Enzyme Assays

Recombinant His-tag mouse BCMO1 and BCMO1 Δ 336-345 was produced in *E.coli* and purified using Talon CellThru resin as described previously (Poliakov et al. 2005). β -carotene was delivered in 1% Octylthioglucoside. Activity was measured in the presence of fenretinide in DMSO or DMSO alone (not more than 5% of total volume). All other inhibitors were delivered in aqueous or ethanol solutions.

23.2.3 HPLC Analysis of Retinoids and Carotenoids

Retinoids were extracted with acetonitrile and separated by RP-HPLC in acetonitrile: 125 mM ammonium acetate (76:24).

23.2.4 Synthesis of Fenretinine, 15-[(4-Hydroxyphenyl)Amino] Retinal (1)

Synthesis of fenretinine was done by Alane reduction of amide based on previously described synthesis of dopamine-uptake inhibitors (He et al. 1993). To a flame-dried 15 mL round bottom flask was added fenretinide (6 mg, 15.3 μ mol) and freshly

distilled, dry tetrahydrofuran (2 mL). While stirring at room temperature, a solution of aluminum hydride in tetrahydrofuran (200 μ L of an approximately 0.7 M AlH_3 solution, 0.14 mmol, prepared as described in Yoon and Brown 1968) was added dropwise via syringe. Some bubbling occurred, along with the change of the bright yellow solution to an orange-red. Stirring was continued for 2 h and monitored by TLC (R_f of starting material=0.15, R_f of product=0.28 in 25% ethyl acetate/hexanes). The reaction mixture was poured into 5 mL of cold (0°C) 15% aqueous sodium hydroxide solution and extracted 3 times with chloroform. The organic extract was dried over anhydrous sodium sulfate, filtered, and concentrated to give crude fenretinine, which was purified by flash chromatography using ethyl acetate/hexanes to give product 1 as clear slightly yellow oil (2.8 mg, 93% based on recovered starting material).

^1H NMR (400 MHz, CDCl_3) δ 6.70 (d, $J=8.8$ Hz, 2H), 6.62–6.51 (3H), 6.27 (d, $J=15.2$ Hz, 1H), 6.18–6.03 (3H), 5.61 (t, $J=6.7$ Hz, 1H), 3.82 (d, $J=6.5$ Hz, 2H), 2.00 (t, $J=7.6$ Hz, 2H), 1.94 (s, 3H), 1.88 (s, 3H), 1.70 (d, $J=5.2$ Hz, 3H), 1.64–1.54 (m, 2H), 1.49–1.42 (m, 2H), 1.24 (s, 3H), 1.01 (d, $J=4.8$ Hz, 3H). ^{13}C NMR (100 MHz, CDCl_3) δ . HRMS (FT-ICR): m/z calculated for $\text{C}_{26}\text{H}_{35}\text{NO}^+$ (M^+) 377.27186, found.

23.2.5 Tertiary Structure Modeling and Molecular Docking

A model based on the crystal structure of apocarotenoid oxygenase was constructed for both wild-type BCMO1 and the truncated form of BCMO1 using the Swiss Model repository (Arnold et al. 2006; Kiefer et al. 2009) as previously described (Poliakov et al. 2005, 2009). Docking of fenretinide was modeled using the Autodock Vina program (Trott and Olson 2010)

23.3 Results

23.3.1 Fenretinide is a Potent Inhibitor of BCMO1

We tested fenretinide for its inhibitory potential in our in vitro assay system. β -carotene cleavage activity was monitored by measurement of all-trans retinal concentration after 1 h. We performed experiments with increasing concentrations of fenretinide (range 0–50 M) without preincubation with the inhibitor. We found that fenretinide substantially inhibited BCMO1 activity with no activity detected at 50 μM of fenretinide. In contrast, other retinoids, retinyl acetate and retinyl palmitate, did not inhibit BCMO1 catalytic activity at 50 μM . We also tested various biologically active aromatic compounds (resveratrol, capsaicin) and demonstrated that they also do not affect BCMO1 catalytic activity at 50 μM (Table 23.1).

Table 23.1 Cleavage activity of BCMO1 in the presence of candidate inhibitors

Inhibitor	Activity in the presence of 50 μM inhibitor (% of wt)
Retinyl palmitate	98.6 \pm 13.4
Retinyl acetate	98.7 \pm 3.9
Capsaicin	94.0 \pm 19.9
Resveratrol	100.6 \pm 10.6

23.3.2 *Fenretinide Demonstrates Noncompetitive Inhibition Behavior*

In the presence of the inhibitor, K_m is not significantly changed; however, V_{\max} changed substantially in the presence of varying inhibitor concentrations. K_i was calculated from the formula:

$$K_i = V_{\max, \text{app}}[I] / V_{\max}$$

We determined that the average K_i is 1.5 μM (Fig. 23.1).

Noncompetitive inhibition occurs when both inhibitor and substrate bind simultaneously to the enzyme, and binding of one does not influence the affinity of either species to complex with the enzyme (IC_{50} for the noncompetitive inhibitor is not changed at various substrate concentrations and $K_i = 1.2 \mu\text{M}$ from Cornish-Bowden plot) (Fig. 23.2).

23.3.3 *Fenretinide Does Not Inhibit Catalytic Activity of BCMO1 Δ 337-346 Mutant*

To study the mechanism of inhibition, we created a mutant BCMO1 with portion of the metazoan loop deleted, BCMO1 Δ 336-345. This mutant had significantly impaired activity and exhibited a sigmoidal kinetics which could be explained by sigmoidal cooperative substrate binding to a slowly fluctuating monomeric enzyme (Qian 2008) (data not shown). This mutant was not significantly inhibited by fenretinide (90% of activity at 50 μM fenretinide). We modeled BCMO1 on the ACO crystal structure template in the presence of substrate in the binding cleft (PDB ID: 2BIW) as the best choice for carotenoid cleavage activity (Kloer et al. 2005). However, ACO does not contain a metazoan loop to serve as template for this portion of the enzyme. Modeling attempts with the RPE65 crystal structure as a template for the loop were unsuccessful due to the collapsed substrate binding cleft of the crystallized protein in the absence of substrate (Kiser et al. 2009). Docking of fenretinide was performed using AutodockVina with full-length and truncated protein modeled on ACO template (Fig. 23.3a, b). Accordingly, we propose that the metazoan loop is allowing this retinoid to bind to BCMO1.

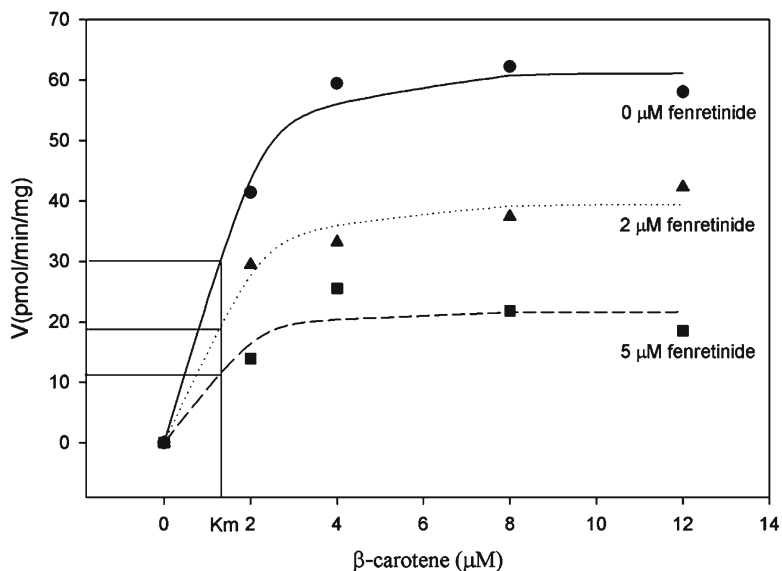


Fig. 23.1 Michaelis-Menten plot of BCMO1 activity at three concentrations of fenretinide. Circles, 0 μM fenretinide; triangles, 2 μM fenretinide; squares, 5 μM fenretinide

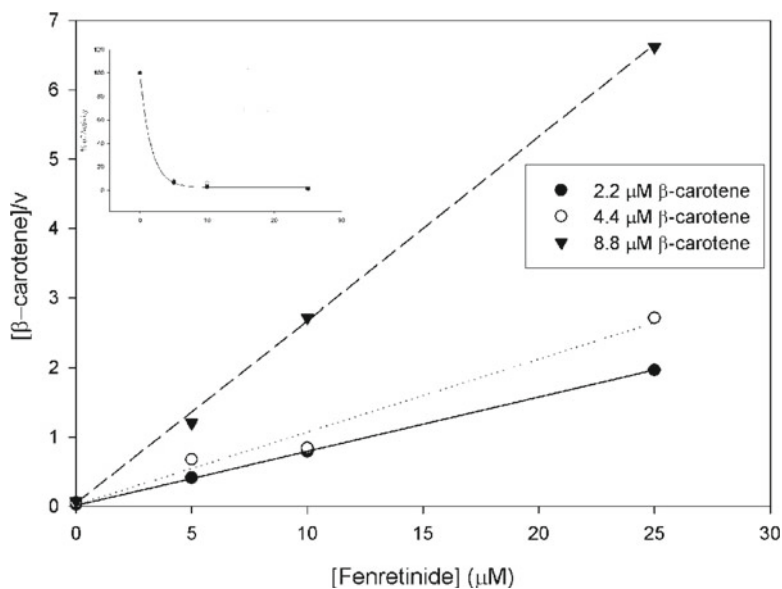


Fig. 23.2 Cornish-Bowden plot of inhibition of BCMO1 by fenretinide at three concentrations of β -carotene

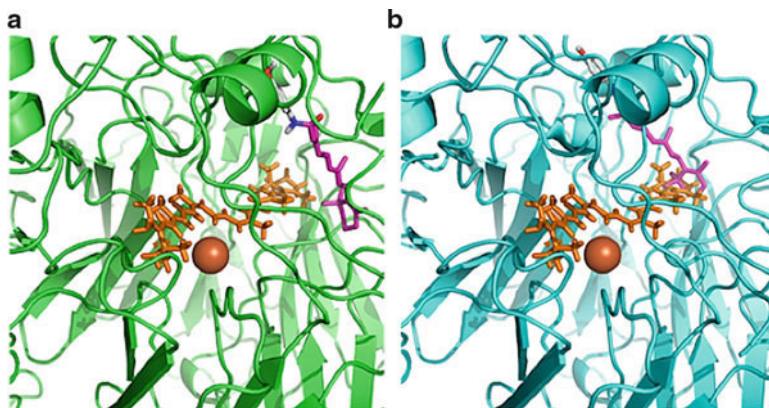


Fig. 23.3 Docking of fenretinide in models of BCMO1 and BCMO1 Δ 336-345. (a), wt BCMO1; (b), mutant BCMO1 Δ 336-345. The β -carotene is shown in orange. Fenretinide is shown in magenta

23.3.4 Amine Analog of Fenretinide (Fenretinine) Is Not an Inhibitor of BCMO1

To determine the structural components of fenretinide-specific binding, we synthesized amine analog of fenretinide by selective reductive amination. The compound was dissolved in DMSO and used for in vitro assay. Fenretinine at 50 μ M concentration did not show any significant inhibition of BCMO1 (data not shown).

23.4 Discussion

In this report, we describe and analyze a strong specific inhibitory effect of fenretinide on BCMO1 with $K_i \sim 1.2 \mu\text{M}$. In contrast, other retinoids (retinyl esters) or bioactive aromatic compounds with similarities to carotenoids are not effective inhibitors of BCMO1. Moreover, even the structural amino analog of fenretinide (fenretinine) is not an inhibitor of BCMO1. Thus, the inhibitory effect is unique for fenretinide. We found that fenretinide is a noncompetitive inhibitor of BCMO1, which means that it and substrate bind simultaneously to the enzyme and that binding of one does not influence the affinity of the other. Therefore, fenretinide does not bind in the substrate tunnel, as we would intuitively predict for a retinoid. To investigate the mechanism of fenretinide binding, we constructed BCMO1 Δ 337-346 truncated protein and found that this mutant protein is not inhibited by fenretinide. The most favorable docking position of fenretinide on the full-length BCMO1 structural model suggests that fenretinide is not bound in the substrate tunnel. Moreover, docking fenretinide on the truncated protein model shows that it could not

accommodate fenretinide without clash with β -carotene. BCMO1 is considered to be a local backup source of vitamin A. While the effect of fenretinide on RBP4 and retinol transport is well described (Formelli et al. 1989; Lewis et al. 1996), the simultaneous inhibition of BCMO1 by fenretinide could provide an additional explanation for the visual side effects of this drug.

Acknowledgments We would like to thank Dr. K. Palczewski for the enthusiastic support of this project. We would like to acknowledge Dr. W. Samuel for kindly providing fenretinide.

References

- Arnold K, Bordoli L, Kopp J et al (2006) The SWISS-MODEL workspace: a web-based environment for protein structure homology modelling. *Bioinformatics* 22:195–201
- Berni R, Clerici M, Malpeli G et al (1993) Retinoids: in vitro interaction with retinol-binding protein and influence on plasma retinol. *Faseb J* 7:1179–1184
- Camerini T, Mariani L, De Palo G et al (2001) Safety of the synthetic retinoid fenretinide: long-term results from a controlled clinical trial for the prevention of contralateral breast cancer. *J Clin Oncol* 19:1664–1670
- Chichili GR, Nohr D, Schaffer M et al (2005) beta-Carotene conversion into vitamin A in human retinal pigment epithelial cells. *Invest Ophthalmol Vis Sci* 46:3562–3569
- Formelli F, Carsana R, Costa A et al (1989) Plasma retinol level reduction by the synthetic retinoid fenretinide: a one year follow-up study of breast cancer patients. *Cancer Res* 49:6149–6152
- Golczak M, Maeda A, Bereta G et al (2008) Metabolic basis of visual cycle inhibition by retinoid and nonretinoid compounds in the vertebrate retina. *J Biol Chem* 283:9543–9554
- He X, Raymon LP, Mattson MV et al (1993) Further studies of the structure-activity relationships of 1-[1-(2-benzo[b]thienyl)cyclohexyl]piperidine. Synthesis and evaluation of 1-(2-benzo[b]thienyl)-N,N-dialkylcyclohexylamines at dopamine uptake and phencyclidine binding sites. *J Med Chem* 36:4075–4081
- Kiefer F, Arnold K, Kunzli M et al (2009) The SWISS-MODEL Repository and associated resources. *Nucleic Acids Res* 37:D387–392
- Kiser PD, Golczak M, Lodowski DT et al (2009) Crystal structure of native RPE65, the retinoid isomerase of the visual cycle. *Proc Natl Acad Sci U S A* 106:17325–17330
- Kloer DP, Ruch S, Al-Babili S et al (2005) The structure of a retinal-forming carotenoid oxygenase. *Science* 308:267–269
- Lewis KC, Zech LA, Phang JM (1996) Effects of chronic administration of N-(4-hydroxyphenyl) retinamide (4-HPR) in rats on vitamin A metabolism in the eye. *Eur J Cancer* 32A:1803–1808
- Motani A, Wang Z, Conn M et al (2009) Identification and characterization of a non-retinoid ligand for retinol-binding protein 4 which lowers serum retinol-binding protein 4 levels in vivo. *J Biol Chem* 284:7673–7680
- Poliakov E, Gentleman S, Cunningham FX, Jr. et al (2005) Key role of conserved histidines in recombinant mouse beta-carotene 15,15'-monooxygenase-1 activity. *J Biol Chem* 280:29217–29223
- Poliakov E, Gentleman S, Chander P et al (2009) Biochemical evidence for the tyrosine involvement in cationic intermediate stabilization in mouse beta-carotene 15, 15'-monooxygenase. *BMC Biochem* 10:31
- Preitner F, Mody N, Graham TE et al (2009) Long-term Fenretinide treatment prevents high-fat diet-induced obesity, insulin resistance, and hepatic steatosis. *Am J Physiol Endocrinol Metab* 297:E1420–1429
- Qian H (2008) Cooperativity and specificity in enzyme kinetics: a single-molecule time-based perspective. *Biophys J* 95:10–17

- Radu RA, Han Y, Bui TV et al (2005) Reductions in serum vitamin A arrest accumulation of toxic retinal fluorophores: a potential therapy for treatment of lipofuscin-based retinal diseases. *Invest Ophthalmol Vis Sci* 46:4393–4401
- Trott O, Olson AJ (2010) AutoDock Vina: Improving the speed and accuracy of docking with a new scoring function, efficient optimization, and multithreading. *J Comput Chem* 31:455–461
- Veronesi U, Mariani L, Decensi A et al (2006) Fifteen-year results of a randomized phase III trial of fenretinide to prevent second breast cancer. *Ann Oncol* 17:1065–1071
- Yoon NM, Brown HC (1968) Selective Reductions .12. Explorations in Some Representative Applications of Aluminum Hydride for Selective Reductions. *J Am Chem Soc* 90:2927
- Zanotti G, Berni R (2004) Plasma retinol-binding protein: structure and interactions with retinol, retinoids, and transthyretin. *Vitam Horm* 69:271–295

Part III
Gene Therapy

Chapter 24

Gene Augmentation Trials Using the Rpe65-Deficient Dog: Contributions Towards Development and Refinement of Human Clinical Trials

Simon M. Petersen-Jones, Matthew J. Annear, Joshua T. Bartoe, Freya M. Mowat, Susie E. Barker, Alexander J. Smith, James W. Bainbridge, and Robin R. Ali

Keywords Leber congenital amaurosis • RPE65 • Canine model • Briard • Gene therapy • Gene augmentation • AAV2 • Immune response • Repeated injection • Subretinal injection

24.1 Introduction

Spontaneous mutations in *RPE65* result in an early-onset retinal dystrophy in humans, dogs, and mice. In humans, the resultant condition is classified as Leber congenital amaurosis (LCA) type II. LCA affects about 1 in 80,000 people (Stone 2007) and LCAII (due to *RPE65* mutations) has been estimated to account for between 6 and 11% of all LCA cases (Thompson et al. 2000; den Hollander et al. 2008).

Mice with a spontaneously occurring nonsense mutation in *Rpe65* have been identified (the *Rd12* mouse) (Pang et al. 2005) and an engineered *Rpe65* knockout mouse has also been utilized extensively (Redmond et al. 1998).

In the 1980s, some dogs of the Briard breed in Sweden were recognized as having an early-onset loss of dim-light vision with variable loss of daytime vision. This was initially described as a congenital stationary night blindness (Narfström et al. 1989). Subsequent molecular studies showed the condition resulted from a four base-pair deletion in the *Rpe65* gene resulting in a frame shift and premature stop codon (Veske et al. 1999). The same gene mutation was identified in Briard dogs in

S.M. Petersen-Jones (✉) • M.J. Annear • J.T. Bartoe • F.M. Mowat
Department of Small Animal Clinical Sciences, Michigan State University,
East Lansing, MI, 48824, USA
e-mail: peter315@cvm.msu.edu

S.E. Barker • A.J. Smith • J.W. Bainbridge • R.R. Ali
Department of Genetics, UCL Institute of Ophthalmology, London, EC1V 9EL, UK

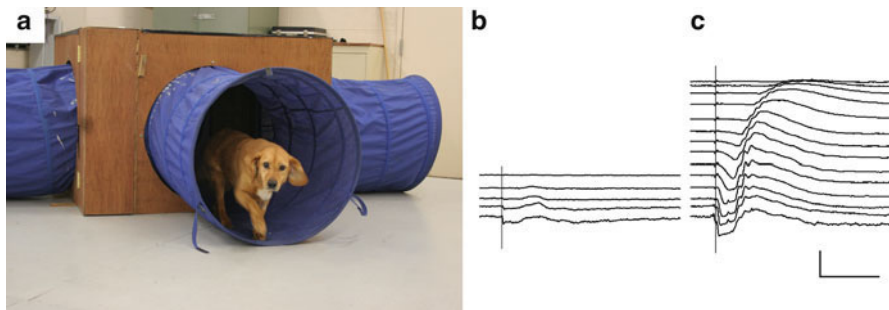


Fig. 24.1 (a) Rpe65-deficient dog successfully exiting a four-choice vision testing device (Gearhart et al. 2008) following gene augmentation therapy. (b) Dark-adapted ERG intensity: response series from a Rpe65-deficient dog prior to gene therapy and (c) 4 months following sub-retinal injection with an AAV2/2 *hRPE65p:hRPE65* construct (Annear et al. 2011). Note the dramatic improvement in ERG waveforms following therapy. Response threshold is markedly improved and waveforms are of a typical shape for a canine. Flash intensities for (b, c) from *bottom* (brightest) to *top* were 2.38, 1.9, 1.36, 0.85, 0.39, 0.0, -0.39, -0.79, -1.19, -1.6, -2.0, -2.41, -2.79, -3.18 log cdS/m². Size bars: vertical = 100 μ V; horizontal = 50 ms

the USA (Aguirre et al. 1998). The affected dogs have a lack of detectable Rpe65 protein, disruption of the retinoid cycle, and a lack of 11-*cis*-retinal supply to the photoreceptors from the retinal pigment epithelium (Acland et al. 2005). 11-*cis*-retinal is required for the formation of the normal visual pigments. Similarly to young LCAII patients, Rpe65-deficient dogs have residual vision and are able to negotiate their way out of a simple four-choice vision testing device under normal room lighting conditions (Fig. 24.1a); however, as lighting is dimmed, their choice of exit tunnel becomes random (Gearhart et al. 2008). The loss of dim-light vision is reflected in the markedly raised threshold of rod-mediated ERG responses (Fig. 24.1b).

Unlike many other retinal dystrophies, severe visual deficits of Rpe65-deficient animals and LCAII patients in the early stages of the condition are the result of severely reduced photoreceptor function rather than due to photoreceptor cell loss. Photoreceptors do eventually degenerate with cones apparently being lost more rapidly than rods, although the rate of loss does differ between species. In mice, cones are lost rapidly (Znoiko et al. 2005) and their function can only be rescued by early gene therapy intervention using fast-acting viral vectors (Pang et al. 2010), whereas in humans although there is a loss of photoreceptors over the first decade of life, some residual responses from severely desensitized rods and cones are detectable in older patients (Jacobson et al. 2005, 2009). Unlike mice, Rpe65-deficient dogs maintain cones relatively late into the disease process (Wrigstad et al. 1994). In addition to the slow degeneration of photoreceptors, the disruption in the retinoid cycle results in the accumulation of lipid droplets in the retinal pigment epithelium (Wrigstad et al. 1994).

Therapeutic intervention to introduce a normal copy of *RPE65* (gene augmentation) requires the survival of photoreceptors capable of function and of retinal pigment epithelium capable of supporting the retinoid cycle. The relatively slow loss of photoreceptors provides a “window of opportunity” for gene augmentation therapy early in the disease process.

24.2 Gene Therapy Proof-of-Principle Trials in Rpe65-Deficient Dogs

Ground-breaking gene therapy studies using subretinally administered adeno-associated viral (AAV) vectors to introduce a normal copy of the *Rpe65* gene in the Rpe65-deficient dog model resulted in remarkable improvement in retinal function as assessed by ERG (Acland et al. 2001). Subsequently additional studies by the same and other groups of investigators showed the safety and efficacy of this approach in the dog. Efficacy was shown by assessment of improvement in several measure of visual function including ability to negotiate an obstacle course; improvement in ERG thresholds, waveform, and amplitudes; improvement in the transient pupillary light reflex; a reduction in nystagmus (a feature of the condition in dogs and humans); and increased visual cortical activity in response to visual stimuli as assessed by functional MRI (Narfström et al. 2003a, 2003b, 2005; Ford et al. 2003; Acland et al. 2005; Le Meur et al. 2007; Aguirre et al. 2007; Bennicelli et al. 2008).

24.3 Phase I/II Clinical Trials in LCAII Patients

Following the success of the proof-of-principle studies in the dog, three groups enrolled LCAII patients for phase I/II gene therapy clinical trials. All three trials utilized subretinally injected AAV vectors to deliver the human *RPE65* cDNA, although features of the construct and the dose and volume injected varied between the groups. Testing of outcomes was performed by a number of different measures as summarized in a recent comprehensive review (Cideciyan 2010). Importantly, all three trials showed the safety of the approach, with no serious adverse effects and also evidence of efficacy (Bainbridge et al. 2008; Maguire et al. 2008; Hauswirth et al. 2008). LCAII patients have regional variations in photoreceptor degeneration across the retina suggesting that identification of surviving photoreceptors and targeting therapy to the regions containing those photoreceptors may be an important part of the therapeutic regime (Jacobson et al. 2005, 2009).

Gene augmentation therapy is still in its infancy and further studies are required for optimization. The canine Rpe65-deficient dog which was critical in the development of the human gene therapy trials is certain to be utilized for assessment of

modification of the treatment regimes. Most recently, the dog has been used to investigate whether immunological response to treatment in one eye precludes successful treatment in the second eye.

24.4 Safety and Efficacy of Treatment of the Second Eye of Rpe65-Deficient Dogs

Immune responses to viral vector capsid following gene therapy have been shown in some studies to interfere with expression of the transgene on repeat administration (Halbert et al. 1997, 1998, 2000; Wang et al. 2007). Studies in mice showed that previous intravitreal AAV administration interfered with transgene expression in the second eye when the second injection was intravitreal (Li et al. 2008), but not when it was subretinal (Li et al. 2009). However, Barker et al. showed that previous subretinal AAV delivery in one eye did not interfere with the efficacy of vector administration in the second eye at lower doses, but higher doses reduced the efficacy of transgene expression (Barker et al. 2009).

In a study using Rpe65-deficient dogs, we injected subretinally one eye of nine dogs with an AAV2/2-*hRpe65p.hRPE65* construct and 85–180 days later applied the same treatment to the second eye. Rescue of retinal function was assessed by vision testing (Fig. 24.1a) and ERG (Fig. 24.1c). Despite the induction of a neutralizing antibody response to the AAV2/2 capsid, there was no significant difference in outcomes in the second treated eyes compared to the first eyes. Functional rescue was maintained in all successfully treated eyes for the duration of the study (up to 2 years). The impact of several variables (including total vector dose and the neutralizing antibody response) on the mean rod and cone ERG rescue was investigated. Neither vector dose nor neutralizing antibody response correlated with the ERG measures of outcome (Annear et al. 2011).

In a separate study, Amado et al. reported improvement in pupillary light reflexes and abilities to negotiate obstacles following treatment of Rpe65-deficient dogs in both eyes treated about 2 weeks apart (Amado et al. 2010). However, data illustrating the results of the testing were not provided and assessment of rescue by more sensitive measures such as ERG was not performed. Both studies showed that in the Rpe65-deficient dog immune response to the viral capsid occurs and at the doses used did not interfere with functional rescue when the second eye was treated. These findings support the future gene augmentation treatment of the second eye of human LCAII patients.

Acknowledgments This work was supported by the British Retinitis Pigmentosa Society, The Midwest Eye Banks and Transplantation Center Research Program and Michigan State University College of Veterinary Medicine Purebred Dog Endowment Fund. JWB is a Wellcome Trust Advanced Fellow. RRA and JWB are investigators at The NIHR Centre for Ophthalmology at UCL and Moorfields Eye Hospital.

References

- Acland GM, Aguirre GD, Bennett J et al (2005) Long-term restoration of rod and cone vision by single dose rAAV-mediated gene transfer to the retina in a canine model of childhood blindness. *Mol Ther* 12:1072–1082
- Acland GM, Aguirre GD, Ray J et al (2001) Gene therapy restores vision in a canine model of childhood blindness. *Nat Genet* 28:92–95
- Aguirre GD, Baldwin V, Pearce-Kelling S et al (1998) Congenital stationary night blindness in the dog: common mutation in the RPE65 gene indicates founder effect. *Mol Vis* 4:23
- Aguirre GK, Komaromy AM, Cideciyan AV et al (2007) Canine and human visual cortex intact and responsive despite early retinal blindness from RPE65 mutation. *PLoS Med* 4:e230
- Amado D, Mingozzi F, Hui D et al (2010) Safety and efficacy of subretinal readministration of a viral vector in large animals to treat congenital blindness. *Sci Transl Med* 2:21ra16
- Annear MJ, Bartoe JT, Barker SE et al (2011) Gene therapy in the second eye of RPE65-deficient dogs improves retinal function. *Gene Ther* 18(1):53–61
- Bainbridge JW, Smith AJ, Barker SS et al (2008) Effect of gene therapy on visual function in Leber's congenital amaurosis. *N Engl J Med* 358:2231–2239
- Barker SE, Broderick CA, Robbie SJ et al (2009) Subretinal delivery of adeno-associated virus serotype 2 results in minimal immune responses that allow repeat vector administration in immunocompetent mice. *J Gene Med* 11:486–497
- Bennicelli J, Wright JF, Komaromy A et al (2008) Reversal of blindness in animal models of leber congenital amaurosis using optimized AAV2-mediated gene transfer. *Mol Ther* 16:458–465
- Cideciyan AV (2010) Leber congenital amaurosis due to RPE65 mutations and its treatment with gene therapy. *Prog Retin Eye Res* 29:398–427
- den Hollander AI, Roepman R, Koenekoop RK et al (2008) Leber congenital amaurosis: genes, proteins and disease mechanisms. *Prog Retin Eye Res* 27:391–419
- Ford M, Bragadottir R, Rakoczy PE et al (2003) Gene transfer in the RPE65 null mutation dog: relationship between construct volume, visual behavior and electroretinographic (ERG) results. *Doc Ophthalmol* 107:79–86
- Gearhart PM, Gearhart CC, Petersen-Jones SM (2008) A novel method for objective vision testing in canine models of inherited retinal disease. *Invest Ophthalmol Vis Sci* 49:3568–3576
- Halbert CL, Rutledge EA, Allen JM et al (2000) Repeat transduction in the mouse lung by using adeno-associated virus vectors with different serotypes. *J Virol* 74:1524–1532
- Halbert CL, Standaert TA, Aitken ML et al (1997) Transduction by adeno-associated virus vectors in the rabbit airway: efficiency, persistence, and readministration. *J Virol* 71:5932–5941
- Halbert CL, Standaert TA, Wilson CB et al (1998) Successful readministration of adeno-associated virus vectors to the mouse lung requires transient immunosuppression during the initial exposure. *J Virol* 72:9795–9805
- Hauswirth WW, Aleman TS, Kaushal S et al (2008) Treatment of leber congenital amaurosis due to RPE65 mutations by ocular subretinal injection of adeno-associated virus gene vector: short-term results of a phase I trial. *Hum Gene Ther* 19:979–990
- Jacobson SG, Aleman TS, Cideciyan AV et al (2009) Defining the residual vision in leber congenital amaurosis caused by RPE65 mutations. *Invest Ophthalmol Vis Sci* 50:2368–2375
- Jacobson SG, Aleman TS, Cideciyan AV et al (2005) Identifying photoreceptors in blind eyes caused by RPE65 mutations: Prerequisite for human gene therapy success. *Proc Natl Acad Sci U S A* 102:6177–6182
- Le Meur G, Stieger K, Smith AJ et al (2007) Restoration of vision in RPE65-deficient Briard dogs using an AAV serotype 4 vector that specifically targets the retinal pigmented epithelium. *Gene Ther* 14:292–303
- Li Q, Miller R, Han PY et al (2008) Intraocular route of AAV2 vector administration defines humoral immune response and therapeutic potential. *Mol Vis* 14:1760–1769

- Li W, Kong F, Li X et al (2009) Gene therapy following subretinal AAV5 vector delivery is not affected by a previous intravitreal AAV5 vector administration in the partner eye. *Mol Vis* 15:267–275
- Maguire AM, Simonelli F, Pierce EA et al (2008) Safety and efficacy of gene transfer for Leber's congenital amaurosis. *N Engl J Med* 358:2240–2248
- Narfström K, Bragadottir R, Redmond TM et al (2003a) Functional and structural evaluation after AAV.RPE65 gene transfer in the canine model of Leber's congenital amaurosis. *Adv Exp Med Biol* 533:423–430
- Narfström K, Katz ML, Bragadottir R et al (2003b) Functional and structural recovery of the retina after gene therapy in the RPE65 null mutation dog. *Invest Ophthalmol Vis Sci* 44:1663–1672
- Narfström K, Vaegan, Katz M et al (2005) Assessment of structure and function over a 3-year period after gene transfer in RPE65^{-/-} dogs. *Doc Ophthalmol* 111:39–48
- Narfström K, Wrigstad A, Nilsson SE (1989) The Briard dog: a new animal model of congenital stationary night blindness. *Br J Ophthalmol* 73:750–756
- Pang J, Boye SE, Lei B et al (2010) Self-complementary AAV-mediated gene therapy restores cone function and prevents cone degeneration in two models of Rpe65 deficiency. *Gene Ther* 17:815–826
- Pang JJ, Chang B, Hawes NL et al (2005) Retinal degeneration 12 (rd12): a new, spontaneously arising mouse model for human Leber congenital amaurosis (LCA). *Mol Vis* 11:152–162
- Redmond TM, Yu S, Lee E et al (1998) Rpe65 is necessary for production of 11-cis-vitamin A in the retinal visual cycle. *Nat Genet* 20:344–351
- Stone EM (2007) Leber congenital amaurosis - a model for efficient genetic testing of heterogeneous disorders: LXIV Edward Jackson Memorial Lecture. *Am J Ophthalmol* 144:791–811
- Thompson DA, Gyurus P, Fleischer LL et al (2000) Genetics and phenotypes of RPE65 mutations in inherited retinal degeneration. *Invest Ophthalmol Vis Sci* 41:4293–4299
- Veske A, Nilsson SE, Narfström K et al (1999) Retinal dystrophy of swedish Briard/Briard-beagle dogs is due to a 4-bp deletion in RPE65. *Genomics* 57:57–61
- Wang Z, Allen JM, Riddell SR et al (2007) Immunity to adeno-associated virus-mediated gene transfer in a random-bred canine model of Duchenne muscular dystrophy. *Hum Gene Ther* 18:18–26
- Wrigstad A, Narfström K, Nilsson SE (1994) Slowly progressive changes of the retina and retinal pigment epithelium in Briard dogs with hereditary retinal dystrophy. A morphological study. *Doc Ophthalmol* 87:337–354
- Znoiko SL, Rohrer B, Lu K et al (2005) Downregulation of cone-specific gene expression and degeneration of cone photoreceptors in the Rpe65^{-/-} mouse at early ages. *Invest Ophthalmol Vis Sci* 46:1473–1479

Chapter 25

Gene Therapy Restores Missing Cone-Mediated Vision in the CNGA3^{-/-} Mouse Model of Achromatopsia

Stylianos Michalakis, Regine Mühlfriedel, Naoyuki Tanimoto, Vidhyasankar Krishnamoorthy, Susanne Koch, M. Dominik Fischer, Elvir Becirovic, Lin Bai, Gesine Huber, Susanne C. Beck, Edda Fahl, Hildegard Büning, Jennifer Schmidt, Xiangang Zong, Tim Gollisch, Martin Biel, and Mathias W. Seeliger

Keywords CNGA3 • Cyclic nucleotide-gated channel • Achromatopsia • ACHM2 • Gene therapy • rAAV • Adeno-associated virus • Gene replacement • Rod monochromacy • Cone photoreceptor

25.1 Introduction

Mutations in the genes CNGA3 and CNGB3 that encode either of the two types of cone cyclic nucleotide-gated (CNG) subunits account together for approximately 75% of all cases of complete achromatopsia (Kohl et al. 2005), a hereditary, autosomal recessive disorder characterized by lack of cone photoreceptor function. The complete unresponsiveness of cones in achromatopsia has grave consequences for vision, particularly with respect to the densely cone-packed human fovea. In addition to the lack of color discrimination, achromats suffer from very poor visual acuity, pendular nystagmus, and photophobia (Kohl et al. 1998).

S. Michalakis • S. Koch • E. Becirovic • L. Bai • J. Schmidt • X. Zong • M. Biel
Department of Pharmacy, Center for Integrated Protein Science Munich (CIPSM),
Center for Drug Research, Ludwig-Maximilians-Universität München, Munich, Germany

R. Mühlfriedel • N. Tanimoto • M.D. Fischer • G. Huber • S.C. Beck • E. Fahl
• M.W. Seeliger (✉)
Division of Ocular Neurodegeneration, Centre for Ophthalmology, Institute for Ophthalmic
Research, Eberhard Karls-Universität, Tübingen, Germany
e-mail: see@uni-tuebingen.de

V. Krishnamoorthy • T. Gollisch
Visual Coding Group, Max Planck Institute of Neurobiology, Martinsried, Germany

H. Büning
Department I of Internal Medicine and Center for Molecular Medicine Cologne,
University of Cologne, Cologne, Germany

We have previously shown that genetic inactivation of *CNGA3* in mice – in close agreement with the human phenotype – leads to selective loss of cone-mediated light responses (Biel et al. 1999) accompanied by morphological, structural, and molecular changes, and finally results in cone cell death (Michalakis et al. 2005).

Here, we set out to design a curative gene replacement strategy using recombinant adeno-associated viral vectors (rAAV) to restore cone function in the *CNGA3*^{-/-} mouse model.

25.2 Materials and Methods

25.2.1 rAAV Production Vectors and Subretinal rAAV Injections

293T cells were cotransfected with a viral vector (pAAV2.1-mBP-CNGA3) that expresses mouse *CNGA3* under control of a 0.5-kb mouse SWS opsin promoter (Akimoto et al. 2004), pAdDeltaF6 (Auricchio et al. 2001) and pAAV2/5Y719F (Petr-Silva et al. 2009) plasmids followed by iodixanol-gradient (Grieger et al. 2006) purification, ion exchange chromatography (HiTrap Q ÄKTA Basic FPLC system, GE Healthcare, Germany), and by further concentration using Amicon Ultra-4 Centrifugal Filter Units (Millipore, Germany). Physical titers were determined by qPCR (LightCycler 480, Roche Applied Science, Germany). 1–1.5 μ L rAAV particles were injected into the subretinal space using the NanoFil subretinal injection Kit (WPI, Germany) with a 34-gauge beveled needle. The procedure was monitored immediately following the injections using scanning laser ophthalmoscopy (Seeliger et al. 2005) and optical coherence tomography (Fischer et al. 2009). All procedures concerning animals were approved by local authorities (Regierungspräsidium Tübingen and Regierung von Oberbayern).

25.2.2 Electrophysiological Analysis

ERG analysis was performed 6, 10, and 11 weeks after injection according to procedures described elsewhere (Seeliger et al. 2001; Tanimoto et al. 2009). Spike trains of retinal ganglion cells were recorded extracellularly with commercial planar multielectrode arrays (Multi Channel Systems, Reutlingen, Germany). During recordings, the retina was continuously superfused with Ames medium, buffered with 22 mM NaHCO₃ and 5% CO₂/95% O₂ (pH 7.4), and maintained at 35°C. To visually stimulate the retina, the screen of a CRT monitor was focused with standard optics onto the photoreceptor layer, covering the recorded piece of retina. Periodic flashes were produced by switching the monitor display every 1 s between black and white, with a contrast (white–black)/(white + black)=0.97. Overall, light level was controlled with neutral density filters in the light path.

25.2.3 *Immunohistochemistry*

The immunohistochemical procedure and antibody dilutions were described previously (Michalakis et al. 2005). Laser scanning confocal micrographs were collected using a LSM 510 meta microscope (Carl Zeiss, Germany).

25.2.4 *Behavior*

The experiment was performed at 111.0 ± 2.2 lux. The day after habituation to the water ($21 \pm 1^\circ\text{C}$, made opaque by the addition of nontoxic white dye) mice were trained for 6 trials to associate a red rectangle with a stable visible platform that was placed in a swimming pool (120 cm in diameter, 70 cm high, white plastic) filled with water up to a depth of 30 cm. The position of the platform was changed from trial to trial in a pseudorandom order to avoid association of the platform with distal spatial cues. On the following day, the animals had to discriminate between two visible platforms. One platform was stable (marked with the red rectangle; correct choice) and the other platform sank when a mouse climbed onto it (marked with a green rectangle; incorrect choice). Trials were terminated if the mouse climbed on one of the two platforms.

25.3 Results

We produced viral vector particles that drive expression of the mouse CNGA3 cDNA under control of a 0.5-kb-fragment of the mouse blue opsin (*S*-opsin) promoter (Akimoto et al. 2004) with a Y719F-modified AAV5 capsid (AAV5-mBP-CNGA3) that results in higher resistance to proteasomal degradation (Petr-Silva et al. 2009). We delivered $6\text{--}9 \times 10^9$ rAAV genomic particles into the subretinal space within the central to ventral part of the retina of 12–14-day-old CNGA3^{-/-} mice and monitored the procedure immediately following the injections using scanning laser ophthalmoscopy (Seeliger et al. 2005) and optical coherence tomography (Fischer et al. 2009).

At 10 weeks posttreatment, clear signs of a functional restoration of cone photoreceptor function were found in Ganzfeld electroretinograms (ERGs) (Fig. 25.1). No differences between the treated eyes (TE), untreated eyes (UE), or wild-type (wt) eyes were detectable at dim-light levels (Fig. 25.1a, top row), demonstrating regular rod function. A prominent rescue effect on cones was found in the light adapted (photopic) part of the protocol (Fig. 25.1a, bottom), in which rods are non-responsive due to desensitization.

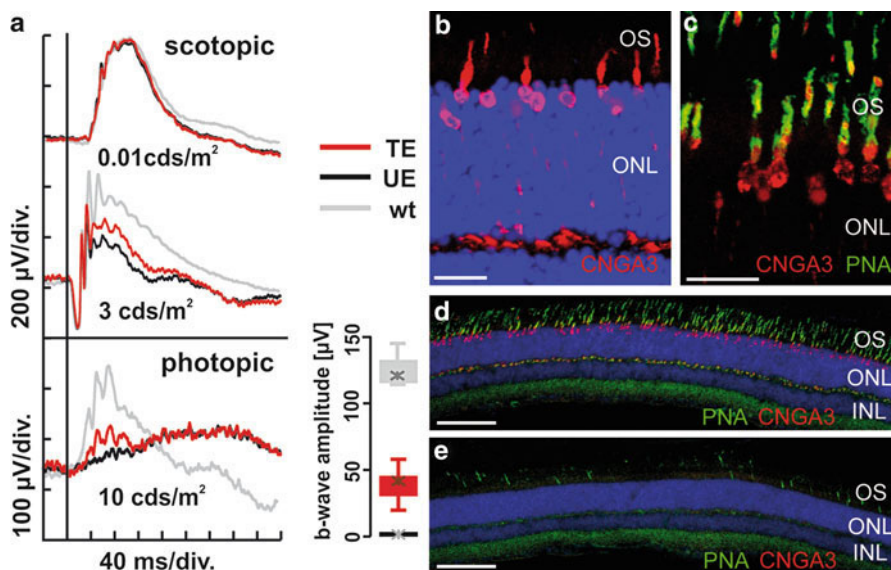


Fig. 25.1 Restoration of cone-mediated ERG, establishment of cone CNG channel, and delay of cone degeneration in treated CNGA3^{-/-} cones. **(a)** Single flash ERG. Scotopic rod system response (*top*): no difference between the treated eye (TE), untreated eye (UE), and the wt eye. Mixed rod/cone system response (*center*): amplitude increase in the TE relative to the UE indicative for cone system function improvement. Photopic conditions (traces *bottom left*, corresponding box plot *bottom right*): substantial restoration of cone system function. **(b–c)** Cone-specific expression of CNGA3 (*red*) in a treated area of a CNGA3^{-/-} retina. **(c)** Colabeling with the cone marker peanut agglutinin (PNA) indicates presence of rescued CNGA3 in cone outer segments (COS, PNA, *green*; CNGA3, *red*). **(d–e)** The treatment preserves a high number of cones. Retinal slices of age-matched treated and untreated CNGA3^{-/-} mice were stained with the cone marker PNA (*green*) and anti-CNGA3 (*red*). Scale bars mark 20 μm in **(a–b)** and 100 μm in **(c–d)**. In **(a, c–d)**, nuclei are stained with Hoechst dye (*blue*). INL inner nuclear layer; ONL outer nuclear layer; OS (photoreceptor) outer segments

Following ERG measurements, eyes were removed, fixed, cryo-sectioned, and processed for immunohistochemistry. We found expression of CNGA3 in cone photoreceptors within the injected, but not the untreated part of the retina (Fig. 25.1b, c). The CNGA3 protein was specifically expressed in cones and localized throughout the cone photoreceptor (Fig. 25.1b). The CNGA3 protein that was produced as a result of our therapy was able to restore COS expression and localization of CNGB3 (not shown) and to reduce the degenerative process in the retina. In line with this, high numbers of cones were still present in the ventral retina of treated but not untreated (age-matched) CNGA3^{-/-} mice (Fig. 25.1d, e).

Having shown by electroretinography that treated cones acquired the ability to generate regular light-evoked signals and to activate respective bipolar cells, we examined next whether these signals are capable of exciting ganglion cells in a regular fashion. To this end, we performed multielectrode array recordings to

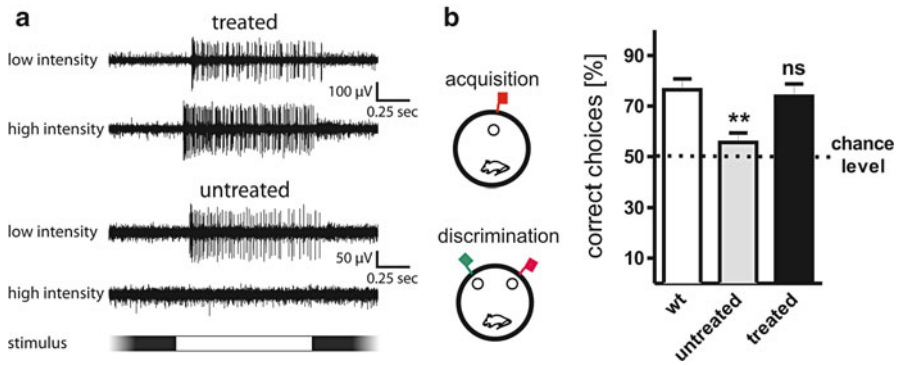


Fig. 25.2 Gene replacement therapy restores responsiveness of ganglion cells to photopic stimuli and enables cone-mediated central vision in *CNGA3*^{-/-} mice. **(a)** Spike trains of different types of ON ganglion cells from treated (*top*) and untreated *CNGA3*^{-/-} mice (*bottom*) in response to periodic flashes of light at two different intensity levels. Stimulus phase is indicated at the *bottom*. The spike trains obtained from the treated mice show reliable response patterns for both applied light intensities. By contrast, ganglion cells from untreated retinas do not respond to light flashes at the highest light level, which corresponds to photopic conditions. **(b)** Behavioral test for cone-mediated vision. Mice were trained to associate a red-colored cue with a stable visible platform (acquisition). Subsequently, the mice had to discriminate between two visible platforms (discrimination), a stable platform (positioned next to a red cue = correct choice) and a platform that sank when a mouse climbed onto it (positioned next to a green cue = incorrect choice). The graph shows the mean percentage of correct choices for 6 trials during the discrimination test. Statistical significance (*t*-test) of differences from comparisons with wild type is shown on top of bars (***p* < 0.01; *ns* non significant)

measure the spiking activity of ganglion cells from isolated retinas of treated and untreated eyes of *CNGA3*^{-/-} mice (Fig. 25.2a). As expected for a retina limited to rod function only, ganglion cells from untreated *CNGA3*^{-/-} mice responded well at low light levels, but did not show any light-evoked activity under photopic conditions (Fig. 25.2a). Much in contrast, many neurons in treated regions displayed strong light-evoked activity for both low and high light levels (Fig. 25.2a). This indicates that transmission of cone signals to the inner retina was reestablished in the treated retinas.

Finally, we aimed at assessing whether the restoration of retinal cone-mediated signaling enabled treated *CNGA3*^{-/-} mice to develop cone vision-guided behavior. We therefore designed a simple test for vision-guided behavior in mice that highly depends on cone-mediated vision under photopic light conditions. The mice were trained in a cued water maze to associate a red cue with a stable visible platform (day one). On day two, the mice had to discriminate between two randomly arranged visible platforms, a stable platform marked with a red cue (correct choice), and a platform that sank when a mouse climbed onto it marked with a green cue (incorrect choice). Wild-type mice were able to differentiate between the two platforms based on the visual cues and performed significantly above chance level (Fig. 25.2b). This indicates that wild-type mice were able to differentiate between the two cues.

Note that the mice may have used differences in the spectral identity, luminous intensity, or some combination of the two to discriminate between the two visual cues. The fact that cone-mediated vision is essential for stimulus discrimination, however, was confirmed by the fact that *CNGA3*^{-/-} mice were not able to solve this task; their performance was not significantly different from the 50% chance level (Fig. 25.2b). Treated *CNGA3*^{-/-} mice, on the other hand, performed significantly better than untreated *CNGA3*^{-/-} mice (Fig. 25.2a). Moreover, treated *CNGA3*^{-/-} mice showed no significant difference to the wild-type control mice in this test. This confirms that our gene replacement therapy is sufficient to restore cone-mediated visual behavior.

25.4 Discussion

Cone vision is the most important visual quality in daytime environment. Inherited diseases such as achromatopsia lead to dysfunction and later degeneration of cone photoreceptors and are currently untreatable. We here show that the principal subunit of the cone CNG channel (*CNGA3*) could successfully be produced in congenitally nonfunctional cone photoreceptors of *CNGA3*^{-/-} mice. The electrophysiological recordings in combination with the behavioral data provide clear evidence that retinas with cones that are completely nonfunctional from birth can become capable of generating signals that higher visual centers can process in a way that permits the animal to successfully discriminate objects based on cone-mediated signals and take respective action. This proof-of-concept in mice is very promising and relevant for future human use of this kind of therapeutic strategy.

Although it will take some time until the results of long-term follow-up experiments are available, the preserved number of cones suggests that the treatment also ameliorates the progressive cone degeneration.

Acknowledgments We thank Peter Humphries (Trinity College Dublin) for providing *Rho*^{-/-} mice, James M. Wilson (Univ Pennsylvania) and Alberto Auricchio (TIGEM) for the gift of AAV plasmids. This work was supported by the Deutsche Forschungsgemeinschaft (Se837/6-1, Se837/7-1, and Bi484/4-1), the German Ministry of Education and Research (BMBF 0314106), the European Union (EU HEALTH-F2-2008-200234), and the Max Planck Society.

References

- Akimoto M, Filippova E, Gage PJ et al (2004) Transgenic mice expressing Cre-recombinase specifically in M- or S-cone photoreceptors. *Invest Ophthalmol Vis Sci* 45:42–47
- Auricchio A, Hildinger M, O'Connor E et al (2001) Isolation of highly infectious and pure adeno-associated virus type 2 vectors with a single-step gravity-flow column. *Hum Gene Ther* 12:71–76

- Biel M, Seeliger M, Pfeifer A et al (1999) Selective loss of cone function in mice lacking the cyclic nucleotide-gated channel CNG3. *Proc Natl Acad Sci U S A* 96:7553–7557
- Fischer MD, Huber G, Beck SC et al (2009) Noninvasive, in vivo assessment of mouse retinal structure using optical coherence tomography. *PLoS One* 4:e7507
- Grieger JC, Choi VW, Samulski RJ (2006) Production and characterization of adeno-associated viral vectors. *Nat Protoc* 1:1412–1428
- Kohl S, Marx T, Giddings I et al (1998) Total colourblindness is caused by mutations in the gene encoding the alpha-subunit of the cone photoreceptor cGMP-gated cation channel. *Nat Genet* 19:257–259
- Kohl S, Varsanyi B, Antunes GA et al (2005) CNGB3 mutations account for 50% of all cases with autosomal recessive achromatopsia. *Eur J Hum Genet* 13:302–308
- Michalakakis S, Geiger H, Haverkamp S et al (2005) Impaired opsin targeting and cone photoreceptor migration in the retina of mice lacking the cyclic nucleotide-gated channel CNGA3. *Invest Ophthalmol Vis Sci* 46:1516–1524
- Petrs-Silva H, Dinculescu A, Li Q et al (2009) High-efficiency transduction of the mouse retina by tyrosine-mutant AAV serotype vectors. *Mol Ther* 17:463–471
- Seeliger MW, Grimm C, Stahlberg F et al (2001) New views on RPE65 deficiency: the rod system is the source of vision in a mouse model of Leber congenital amaurosis. *Nat Genet* 29:70–74
- Seeliger MW, Beck SC, Pereyra-Munoz N et al (2005) In vivo confocal imaging of the retina in animal models using scanning laser ophthalmoscopy. *Vis Res* 45:3512–3519
- Tanimoto N, Muehlfriedel RL, Fischer MD et al (2009) Vision tests in the mouse: Functional phenotyping with electroretinography. *Front Biosci* 14:2730–2737

Chapter 26

Functional Rescue of P23H Rhodopsin Photoreceptors by Gene Delivery

Marina S. Gorbatyuk, Oleg S. Gorbatyuk, Matthew M. LaVail,
Jonathan H. Lin, William W. Hauswirth, and Alfred S. Lewin

Keywords Gene delivery • Gene therapy • ER stress • P23H rhodopsin • ERG
• siRNA • BiP/Grp78 • Transgenic rats • Folding

26.1 Introduction

Autosomal dominant Retinitis Pigmentosa (ADRP) is an inherited retinal disorder, which leads to progressive death of photoreceptor (PR) and significant visual impairment. The rhodopsin-linked form of RP affects approximately 1 in 30,000 people and is associated with over 100 different genetic modifications within the misfolded rhodopsin (*RHO*) gene (<http://www.sph.uth.tmc.edu/RetNet>). Progress in developing gene therapies for dominant RP has been slower compared to recessive forms of this retinopathy, but some advances in this field have been made lately. As any dominant disease, the treatment of ADRP correcting the primary genetic defect most likely requires a removal of the defective gene product in PR cells.

M.S. Gorbatyuk (✉)
Department of Cell Biology and Anatomy, University of North Texas Health Science Center,
Fort Worth, TX 76107, USA
e-mail: Marina.Gorbatyuk@unthsc.edu

O.S. Gorbatyuk • A.S. Lewin
Department of Molecular Genetics and Microbiology, University of Florida,
Gainesville, FL 32610, USA

M.M. LaVail
Beckman Vision Center, University of California, San Francisco, CA 94143, USA

J.H. Lin
Department of Pathology, University of California at San Diego, La Jolla, CA 92093, USA

W.W. Hauswirth
Department of Ophthalmology, University of Florida, Gainesville, FL 32610, USA

However, alternative therapeutic approaches exist, such as modulation of cellular signaling caused by the accumulation of misfolded RHO. In the current study, we set out to determine what effects overexpressing wild-type (WT) RHO, the ER resident chaperone *BiP/GRP78*, and transcriptional activator of heat shock proteins (HSPs), *HSF1*, would have on retinal function in P23H transgenic rats, as assessed by electroretinography (ERG).

The idea of testing the WT RHO in P23H RHO PR was originated from studies on transgenic mice, carrying mutated rhodopsin (*RHO*) transgene on different genetic backgrounds, suggesting that the increased amount of WT RHO in ADRP PRs might be beneficial for vision of these animals (Frederick et al. 2001). Justification of overexpression of BiP protein was based on its chaperoning (Hoshino et al. 2007) and anti-apoptotic activities *in vivo* and *in vitro* (Miyake et al. 2000). The master regulator of chaperone gene transcription, *HSF1*, has also been shown to suppress polyglutamine aggregates *in vivo* and cause a therapeutic effect (Fujikake et al. 2008). Therefore, we employed a gene delivery approach with a help of adeno-associated viruses (AAV) to validate these therapeutic genes as candidates for ADRP gene therapy in P23H RHO transgenic rats.

26.2 Materials and Methods

26.2.1 Animals

Homozygous transgenic P23H line 3 *RHO* rats were used in this experiment. All animal procedures were performed according to the guidelines of the ARVO statement for the “Use of Animals in Ophthalmic and Vision Research.” Subretinal injection of P23H RHO-3 rats with 2 μ L of AAV-expressing mouse *Rho*-resistant gene 301 (referred to WT), human *GRP78* (*BiP*), and *HSF-1* cDNA with titer of 10^{11} – 10^{12} /per genome was performed on postnatal day (P) 15 in P23H RHO pups, as described before (Gorbatyuk et al. 2010). Control eyes were injected with AAV-GFP.

26.2.2 Transient Transfection of HeLa Cells and Immunohistochemistry

We used Lipofectamine 2000 and pcDNA3.1 plasmids-expressing mouse P23H *RHO*, WT *RHO*, and human *GRP78* under control of the CMV promoter to perform transfection in HeLa cells. At 48 h, cells were fixed with Pen-Fix, and immunohistochemistry was performed by using the 1D4 antibody against rhodopsin and anti-Flag antibody. Cy-2- and Cy-3-conjugated secondary antibodies were applied to detect RHO and the Flag epitope tag, respectively.

26.2.3 ERG

The procedure was performed as described before (Gorbatyuk et al. 2010). Scotopic ERG responses were measured with 10 μ s flashes of white light at 2.68 cd-s/m² intensity. Differences in a- and b-wave amplitudes between simultaneously recorded test and control eyes were the primary measure of outcome.

26.2.4 Histology

Rats were intracardially perfused with 2% paraformaldehyde and 2.5% glutaraldehyde, and eyes were removed from euthanized animals, postfixed and embedded in epoxy resin (Gorbatyuk et al. 2010). Mean outer nuclear layer (ONL) thickness of the entire retina or specific region of the eye was compared between the AAV-*BiP* and control-injected eyes.

26.3 Results

26.3.1 Functional Preservation of P23H RHO Photoreceptors as a Result of Overexpression of Mouse RHO 301

We used the *Rho* 301 gene in a “cut-and-replace” experiment as a resistant target for siRNA301. *Rho* 301 encodes the WT mouse rod opsin protein. In rats, we tested this gene independently to validate the therapeutic effect of WT RHO. We injected pups at P15 to analyze them by scotopic ERG at 1 and 3 months postinjection. Results of this analysis demonstrated that both a- and b-waves responses were elevated in Rho301-treated eyes (Fig. 26.1) at 1 month posttreatment. A-wave amplitude was

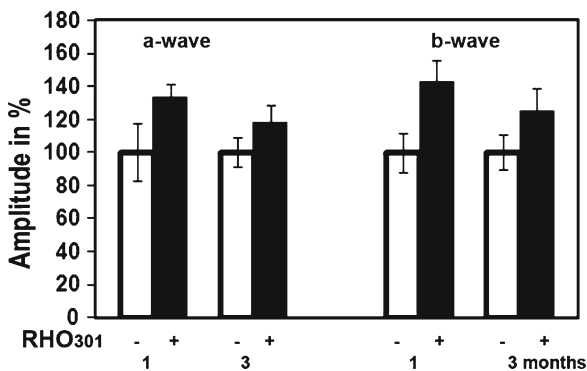


Fig. 26.1 Overexpression of mouse RHO301 leads to functional preservation of P23H RHO-3 photoreceptors

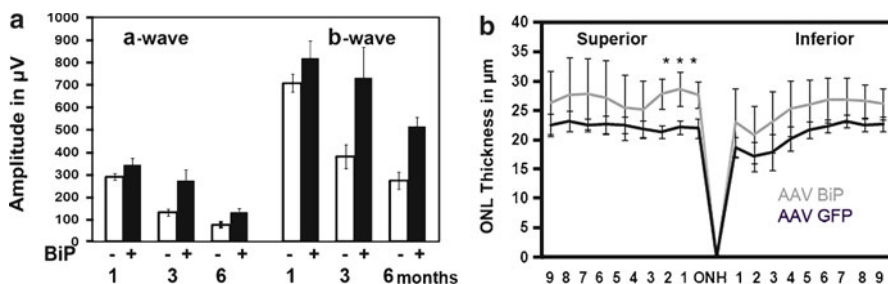


Fig. 26.2 Overexpression of human BiP/GRP78 protein leads to steady therapeutic effect over 6 months measured (a) by scotopic ERG and (b) by histological analysis

increased by 33% and b-wave amplitude by 42%. However, at 3 months following injection, the therapeutic effect was only 18 and 34% ($p < 0.05$), respectively, for a- and b-wave amplitudes compared to the GFP-treated eye.

26.3.2 *Functional Preservation of P23H RHO Photoreceptors as a Result of Increased Expression of Human BiP/Grp78*

Following injection, we analyzed animals over 6 months by ERG and then euthanized them for histological analysis. The results of this experiment are shown in Fig. 26.2a. AAV5-BiP treatment led to the rescue of retinal activity in P23H RHO rats. In BiP-treated eyes, a- and b-wave response amplitudes were higher than in control (GFP-injected) eyes, and this protection was consistent over 6 months. A-wave amplitudes were increased from 18 to 78% and b-wave amplitudes were amplified by 15–89%. The peak of therapeutic activity occurs at 3 months postinjection; the a-wave was increased by 110% and b-wave was increased by 92%, $p < 0.05$, relative to the control-injected eyes.

26.3.3 *Preservation of Retinal Integrity in P23H RHO Rats as a Result of Overexpression of Human BiP/GRP78*

To determine if this therapeutic effect corresponded to preservation of retinal integrity, we enucleated euthanized rats and processed the retinas for histological analysis in order to measure the thickness of the ONL. Morphometric analysis of individual retinas showed small but significant changes in individual sectors of central inferior hemisphere in BiP-treated retina (Fig. 26.2b). The differences in the lengths of ONL in three individual sectors in the superior hemisphere were from 25 to 30%, $p < 0.05$.

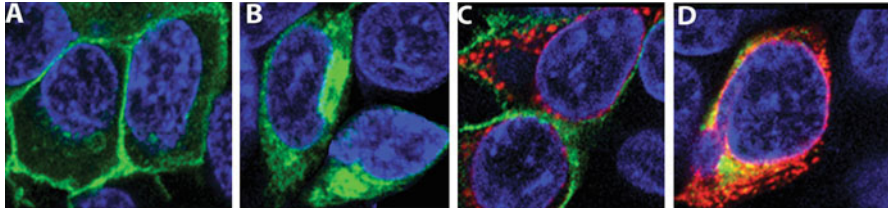


Fig. 26.3 Immunostaining of HeLa cells cotransfected with wild-type RHO, P23H RHO, and BiP-Flag. (a) Immunostaining analysis demonstrated the localization of wild-type RHO to the cell membrane and (b) P23H RHO retained within the ER (green). (c) Overexpression of BiP-Flag (red) did not affect the trafficking of WT RHO and (d) did not promote the distribution of P23H RHO to the cytoplasm

26.3.4 Elevation of BiP Protein Level Does Not support the Trafficking of P23H RHO to the Cell Membrane

To determine if the increase in the level of BiP would promote opsin folding and localization to the cell membrane, we performed cotransfection of HeLa cells with plasmids-expressing P23H opsin and BiP-Flag protein. The Flag epitope sequence was placed in front of KDEL fragment and served as a tag for detection of exogenous BiP protein. Results of the experiment are presented in Fig. 26.3 and suggest that the WT RHO, which served as a control, localized to the plasma membrane and the BiP-Flag overexpression did not interfere with this distribution. However, the coexpression of P23H RHO and BiP-Flag proteins in cells had no effect on the mislocalization of P23H RHO in the cytoplasm. This experiment indicated that extra BiP protein in the ER did not permit exit of P23H RHO from the ER and delivery to the cell membrane.

26.3.5 Functional Preservation of P23H RHO Photoreceptors as a Result of Overexpression of HSF1

To determine if the HSF1 overexpression had a therapeutic effect in P23H RHO retina, we injected pups with AAV-*HSF1* and then monitored them by ERG recording for 3 months (Fig. 26.4). We observed an increase of over 35% for both a- and b-wave amplitudes ($p < 0.05$) in HSF1-treated eyes relative to the AAV-GFP-treated eyes.

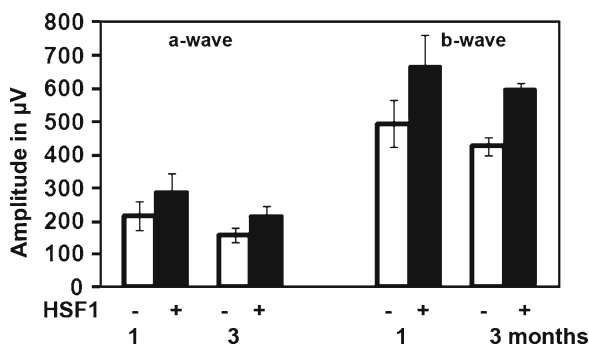


Fig. 26.4 Overexpression of HSF1 in P23H RHO-3 photoreceptors leads to sustained preservation of a- and b-wave amplitudes of the scotopic ERG

26.4 Discussion

The P23H mutation of rhodopsin belongs to a class (Class II) that is retained in the ER and is later translocated to the cytoplasm for degradation. It causes PR cell death by a dominant negative mechanism. The dominant negative effect of misfolded RHO is associated with its ability to recruit the WT RHO to form aggresomes, therefore keeping the WT RHO from trafficking to the disk membrane. Therefore, we tested the hypothesis that increased expression of WT RHO would lead to enhancement of PR function in P23H transgenic rats, assuming that newly synthesized RHO escapes from the ER and translocates to the outer segments of PRs. Analysis of ERG results demonstrated that the highest therapeutic effect was observed at 1 month postinjection and was slightly diminished after that. It suggests that the deleterious effect of mutated RHO overcomes the boost normal RHO in RPs, first and second, that expression of exogenous RHO has to be optimized by manipulations with expression cassette, viral dose, and time of injection. We note, however, that in P23H transgenic mice, we have seen a beneficial effect of overexpression of RHO for up to 6 months (Mao et al. submitted for publication.)

Gene therapy for PRs expressing P23H RHO can be addressed either by directly targeting the mutant protein or by reprogramming different pathways in the cellular response to misfolded protein. For example, it has been shown that pharmacological chaperones such as geldanamycin, radicicol, and 17-AAG cause the induction of HSPs and are able to lessen the deleterious impact of P23H RHO (Mendes and Cheetham 2008). Moreover, the impact of misfolded protein can be overcome by reducing protein aggregation and promoting degradation of the aggregation-prone species. Consequently, we decided to validate new therapeutic targets and to manipulate the level of molecular chaperones in P23H RHO ADRP.

Overexpression of ER-resident BiP/Grp78 protein led to sustained elevation of ERG a- and b-wave amplitudes by almost twofold compared to control eyes and

abolished the retinal degeneration in P23H RHO PR. This therapeutic effect was not necessarily linked to promoting the trafficking of RHO to the cell membrane, but likely was associated with modulation of cellular signaling (Gorbatyuk et al. 2010). Currently, we are testing this chaperone in other models of neurodegenerative diseases.

Another inducer of molecular chaperones, HSF1, has been reported to be involved in a prevention of ADRP in RP10 mouse model via inhibition of Hsp90 and an induction of Hsp70 (Tam et al. 2010). Therefore, it was not surprising that the gene delivery of HSF1 preserved the ERG response in P23H RHO transgenic rats. We hypothesize that due to overexpression of HSF1, the levels of HSP70, HSP 40, and other chaperones were elevated and that this elevation activates prosurvival cellular pathways in P23H RHO RP cells.

Thus, our data suggest that it may not be necessary to improve RHO folding to improve PR viability. Manipulation of cell death and prosurvival pathways and shifting the balance in PR cells toward cell survival could be a reliable therapeutic approach for preserving vision in people with ADRP caused by RHO mutations.

Acknowledgments This study was supported by FFB: TA-GT-4090-0479-UFL, TA-GT-0507-0384, by C-NP-0706-0353-UCSF, by NIH: EY020905, EY11123, EY08571, EY02162, EY01919, EY06842, EY018313, and EY020846.

References

- Frederick JM, Krasnoperova NV, Hoffmann K et al (2001) Mutant rhodopsin transgene expression on a null background. *Invest Ophthalmol Vis Sci* 42:826–833
- Fujikake N, Nagai Y, Popiel HA et al (2008) Heat shock transcription factor 1-activating compounds suppress polyglutamine-induced neurodegeneration through induction of multiple molecular chaperones. *J Biol Chem* 283:26188–26197
- Gorbatyuk MS, Knox T, LaVail MM et al (2010) Restoration of visual function in P23H rhodopsin transgenic rats by gene delivery of BiP/Grp78. *Proc Natl Acad Sci U S A* 107:5961–5966
- Hoshino T, Nakaya T, Araki W et al (2007) Endoplasmic reticulum chaperones inhibit the production of amyloid-beta peptides. *Biochem J* 402:581–589
- Mendes HF, Cheetham ME (2008) Pharmacological manipulation of gain-of-function and dominant-negative mechanisms in rhodopsin retinitis pigmentosa. *Hum Mol Genet* 17:3043–3054
- Miyake H, Hara I, Arakawa S et al (2000) Stress protein GRP78 prevents apoptosis induced by calcium ionophore, ionomycin, but not by glycosylation inhibitor, tunicamycin, in human prostate cancer cells. *J Cell Biochem* 77:396–408
- Tam LC, Kiang AS, Campbell M et al (2010) Prevention of autosomal dominant retinitis pigmentosa by systemic drug therapy targeting heat shock protein 90 (Hsp90). *Hum Mol Genet* 19(22): 4421–36

Chapter 27

Gene Delivery of Wild-Type Rhodopsin Rescues Retinal Function in an Autosomal Dominant Retinitis Pigmentosa Mouse Model

Haoyu Mao, Marina S. Gorbatyuk, William W. Hauswirth,
and Alfred S. Lewin

Keywords Gene delivery • Rhodopsin • Autosomal dominant retinitis pigmentosa

27.1 Introduction

Retinitis pigmentosa (RP) is a neurodegenerative disease with the prevalence of 1/4,000 and almost 1.5 million patients globally (Hartong et al. 2006; Daiger et al. 2007), with autosomal dominant retinitis pigmentosa (ADRP) accounting for 40% of clinical cases. The primary symptoms of ADRP are gradual loss of night vision followed by loss of peripheral vision, but central vision is diminished late in the disease (van Soest et al. 1999; Farrar et al. 2002). Currently, there is no cure for the disease. Mutations in rhodopsin (*RHO*) are associated with over 25% of ADRP cases (Daiger et al. 2007). The first identified *RHO* mutation, P23H (proline 23 substituted by histidine), is associated with 12% ADRP patients in the U.S. (Dryja et al. 1990; van Soest et al. 1999; Daiger et al. 2007). Several P23H transgenic animal models, including mouse, rat, fly, and frog models, have been developed and used to test gene and pharmacological therapies (Olsson et al. 1992; Roof et al. 1994; Bush et al. 2000; Organisciak et al. 2003; Ranchon et al. 2003; Galy et al. 2005;

H. Mao (✉) • A.S. Lewin
Department of Molecular Genetics and Microbiology, University of Florida,
Gainesville, FL, USA
e-mail: maohaoyu@ufl.edu

M.S. Gorbatyuk
Department of Cell Biology and Anatomy, University of North Texas Health Science
Center at Fort Worth, Fort Worth, TX, USA

W.W. Hauswirth
Department of Molecular Genetics and Microbiology, University of Florida,
Gainesville, FL, USA
Department of Ophthalmology, University of Florida, Gainesville, FL, USA

Gorbatyuk et al. 2005a, 2007a, 2008; Tam and Moritz 2006). Despite the genetic heterogeneity of ADRP, our group and others have explored a “resect and replace” gene therapy employing RNA interference (RNAi) or catalytic RNA enzymes (ribozymes) (Georgiadis et al. 2010; Lewin et al. 1998; Sullivan et al. 2002; Gorbatyuk et al. 2005b, 2007b, 2008; Kiang et al. 2005). For this allele-independent method, expression of both the mutant and wild-type gene is suppressed and a resistant allele is introduced (Sullivan et al. 2002; Cashman et al. 2005; Kiang et al. 2005; Tessitore et al. 2006; Gorbatyuk et al. 2007a, b, 2008). This approach should be applicable to ADRP genes, like *RHO* which are affected by many different mutations. In present studies, however, we introduced a single gene, *RHO301*, to express normal rhodopsin protein. The increased production of normal rhodopsin rescued photoreceptor function in P23H mice, suggesting that gene therapy with normal gene is possible for treatment of this class of ADRP mutation.

27.2 Materials and Methods

27.2.1 *RHO301 Gene Cloning*

The mouse *RHO* (Genbank, BC013125) cDNA we employed contained 109 bp 5' UTR and 159 bp 3' UTR. It also contained five silent mutations to eliminate siRNA301 recognition site. Expression was driven by a mouse opsin proximal promoter, and the insert was packaged in adeno-associated virus (AAV) serotype 5 capsids at a titer of 2×10^{12} vg/mL.

27.2.2 *Experiment with Animal Models*

All animal procedures were approved by the University of Florida Institutional Animal Care and Use Committee in accordance with the ARVO statement for the “Use Animals in Ophthalmic and Vision Research.” P23H mice (line 37) containing a human P23H *RHO* transgene (Dryja et al. 1990) were bred with C57BL/6J wild-type mice (Jackson Laboratories) to obtain the transgenic P23H *RHO*, mouse *RHO* +/+ mice. Subretinal AAV injections with 1 μ L AAV5 *RHO301* (2×10^9 viral particles) were performed as described by Timmers et al. (Dryja et al. 1990; Olsson et al. 1992; Timmers et al. 2001). Only right eyes were injected with virus.

27.2.3 *Electroretinography (ERG)*

After subretinal injection, retinal function was measured at 1, 2, 3, and 6 months time points postinjection. AAV5-*RHO301*-injected P23H mice were analyzed by simultaneous full-field ERG of a UTAS-E 2000 Visual Electrodiagnostic System

(LKC). The a-wave amplitudes were measured from baseline to the peak in the cornea-negative direction, and b-wave amplitudes were measured from cornea-negative peak to major cornea-positive peak. The results from each group of mice were averaged and the means were compared statistically by using Student's *t*-test for paired data and ANOVA for multiple groups.

27.2.4 Histological Analysis for the Outer Nuclear Layer

At 6 months postinjection, the mice were euthanized, and the retinas were fixed and prepared for plastic sectioning after perfusion. Dissected tissues were postfixed in 1% osmium tetroxide and maintained in 0.1 M cacodylate buffer overnight. Tissues were embedded in an epoxy resin and stained with toluidine blue. The thickness of the outer nuclear layer (ONL) was measured at ten equally spaced superior and inferior loci using the MBF Stereoinvestigator on a Zeiss microscope. Mean readings were averaged from ten measurements. Differences between the ONL thickness of left control eyes and that of right treated eyes were analyzed by using Student's *t*-test for paired samples.

27.3 Results

27.3.1 Expression of AAV-Delivered *RHO301*

The *RHO301* was constructed by introducing five silent mismatches into a normal mouse *RHO* cDNA to eliminate the binding site of siRNA301 (Gorbatyuk et al. 2007b, 2008). At postnatal day 15, *RHO301* was delivered by subretinal injection. We analyzed mRNA and protein levels of *RHO301* 1 month postsubretinal injection. Compared to *RHO* mRNA levels in untreated left eyes, we obtained an almost twofold increase of total *RHO* mRNA in treated right eyes indicating successful *RHO301* delivery (data not shown). Opsin protein was increased by 50% in right injected eyes as detected by immunoblot using mouse antirhodopsin monoclonal antibodies (1D4, data not shown).

27.3.2 Retinal Structure Integrity in AAV Gene-Delivered P23H Mice

To analyze the structural integrity of retina, the ONL thickness was measured to determine the photoreceptors survival. In eyes expressing *RHO301*, ONL thickness was remarkably elevated compared to untreated eyes (Fig. 27.1a, b). Six months

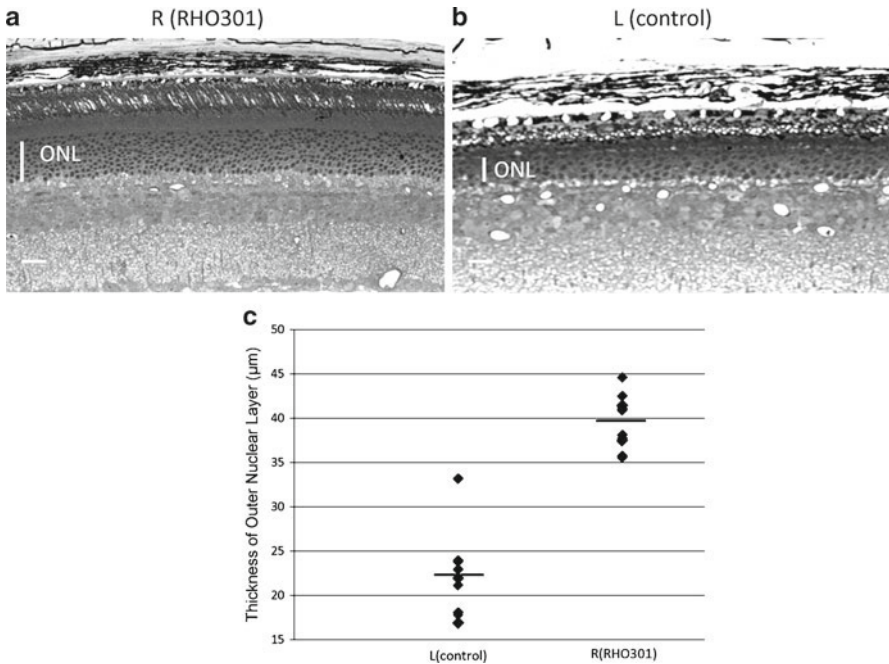


Fig. 27.1 The structural integrity of P23H retinas via *RHO301* gene transfer. Six months after injection, the thickness of ONL was measured in (a) AAV-*RHO301*-injected P23H right retinas and compared with (b) untreated left retinas. The white caliper bar is 10 µm. (c) Significant increase of the ONL thickness was detected in the *RHO301*-injected (right) eyes of P23H mice (labeled as R *RHO301*) compared with the ONL of untreated (left) eyes (labeled as L control) in the whole retina ($p < 0.05$)

survival of photoreceptors was approximately double in treated eyes when averaged over the entire retina (Fig. 27.1c).

27.3.3 Rescued Retinal Function Observed in AAV-*RHO301*-Injected P23H Eyes

But were surviving rod cells functional? The full-field electroretinogram (ERG) was measured to assess retinal function in P23H transgenic mice. *RHO301* gene transfer consistently improved both the a-wave and b-wave responses of P23H mice compared to untreated control eyes in a 6-month time-course with different intensities readings (Fig. 27.2a, b). At 6 months postinjection, there was an almost three-fold increase of a-wave amplitude in treated eyes compared with untreated eyes at

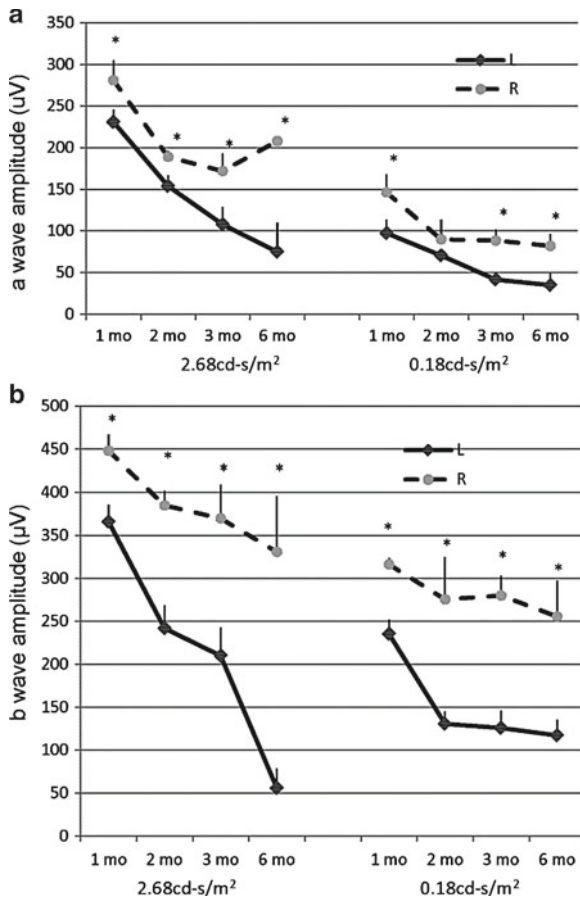


Fig. 27.2 *RHO301* gene delivery protects retinas of P23H mice. The scotopic ERG a- and b-wave amplitudes measured at 0.18 and 2.68 cd-s/m² luminance, from 1 to 6 months following injection of *RHO301* (gray circles) in right eyes. Untreated left eyes of transgenic mice (black diamonds) showed retinal degeneration with decreased amplitudes. (a) In ERG a-wave response, the amplitudes of right treated eyes were significantly increased compared with that of left untreated eyes at different time points (**p* < 0.05, shown as statistical significance). (b) At both 0.18 and 2.68 cd-s/m² luminance, the b-wave amplitudes of right injected eyes significantly higher than those of left untreated eyes at all four different time points (**p* < 0.05, shown as statistical significance at 1, 2, 3, and 6 months time points)

the highest light intensity with 2.68 cd-s/m² luminance (Fig. 27.2a). At same time point, 80% of the b-wave amplitude was maintained in AAV-*RHO301*-treated P23H eyes (Fig. 27.2b). Therefore, the retinal degeneration in P23H mice was dramatically slowed by delivery of functional *RHO*. These results are consistent with the preserved retinal structure in AAV-*RHO301*-injected P23H eyes.

27.4 Discussion

In this study, we used viral mediated gene transfer in P23H *RHO* transgenic mice model to test the hypothesis that supplementation of degenerating retina with functional *RHO* would reduce the rate of retinal degeneration in photoreceptors affected by a dominant rhodopsin mutation. Since we have already tested its cognate siRNA301 in vitro and in vivo, these experiments also validated the resistant cDNA, necessary for the replacement step of the “resect and replace” strategy. Our results not only confirmed those of Fredrick et al. that transgenic overexpression of *RHO* could benefit mice carrying the P23H *RHO* gene (Frederick et al. 2001), but also demonstrated that viral delivery of normal *RHO* can be beneficial to reduce the rate of retinal degeneration in ADRP photoreceptors.

Human clinical trials of gene therapy for a recessive retinal degeneration have shown promise in restoring vision (Bainbridge et al. 2008; Cideciyan et al. 2009; Simonelli et al. 2010) and suggest that gene transfer to the retina is safe. It is possible that gene transfer of *RHO* may be applicable to other Class II rhodopsin mutations that lead to RP by mechanisms similar to the P23H mutation (Mendes et al. 2005). Therefore, the increase of rhodopsin expression by wild-type gene delivery using AAV is a potential treatment for a large number of people with ADRP.

References

- Bainbridge JWB, Smith AJ, Barker SS et al (2008) Effect of gene therapy on visual function in Leber's congenital amaurosis. *N Engl J Med* 358:2231–2239
- Bush RA, Kononen L, Machida S et al (2000) The effect of calcium channel blocker diltiazem on photoreceptor degeneration in the rhodopsin Pro23His rat. *Invest Ophthalmol Vis Sci* 41:2697–2701
- Cashman SM, Binkley EA, Kumar-Singh R (2005) Towards mutation-independent silencing of genes involved in retinal degeneration by RNA interference. *Gene Ther* 12:1223–1228
- Cideciyan AV, Hauswirth WW, Aleman TS et al (2009) Human RPE65 gene therapy for Leber congenital amaurosis: persistence of early visual improvements and safety at 1 year. *Hum Gene Ther* 20:999–1004
- Daiger SP, Bowne SJ, Sullivan LS (2007) Perspective on genes and mutations causing retinitis pigmentosa. *Arch Ophthalmol* 125:151–158
- Dryja TP, McGee TL, Reichel E et al (1990) A point mutation of the rhodopsin gene in one form of retinitis pigmentosa. *Nature* 343:364–366
- Farrar GJ, Kenna PF, Humphries P (2002) On the genetics of retinitis pigmentosa and on mutation-independent approaches to therapeutic intervention. *EMBO J* 21:857–864
- Frederick JM, Krasnoperova NV, Hoffmann K et al (2001) Mutant rhodopsin transgene expression on a null background. *Invest Ophthalmol Vis Sci* 42:826–833
- Galy A, Roux MJ, Sahel JA et al (2005) Rhodopsin maturation defects induce photoreceptor death by apoptosis: a fly model for RhodopsinPro23His human retinitis pigmentosa. *Hum Mol Genet* 14:2547–2557
- Georgiadis A, Tschernutter M, Bainbridge JW et al (2010) AAV-mediated knockdown of peripherin-2 in vivo using miRNA-based hairpins. *Gene Ther* 17:486–493
- Gorbatyuk M, Justilien V, Liu J et al (2007a) Preservation of photoreceptor morphology P23H rats using an allele independent and function in ribozyme. *Exp Eye Res* 84:44–52

- Gorbatyuk M, Justilien V, Liu J et al (2007b) Suppression of mouse rhodopsin expression in vivo by AAV mediated siRNA delivery. *Vis Res* 47:1202–1208
- Gorbatyuk MS, Hauswirth WW, Lewin AS (2008) Gene therapy for mouse models of ADRP. *Adv Exp Med Biol* 613:107–112
- Gorbatyuk MS, Timmers AMM, Pang JJ et al (2005a) Rescue of vision in P23H rats with an rAAV delivered ribozyme targeting mouse opsin. *Invest Ophthalmol Vis Sci* 46
- Gorbatyuk MS, Pang JJ, Thomas J et al (2005b) Knockdown of wild-type mouse rhodopsin using an AAV vectored ribozyme as part of an RNA replacement approach. *Mol Vis* 11:648–656
- Hartong DT, Berson EL, Dryja TP (2006) Retinitis pigmentosa. *Lancet* 368:1795–1809
- Kiang AS, Palfi A, Ader M et al (2005) Toward a gene therapy for dominant disease: validation of an RNA interference-based mutation-independent approach. *Mol Ther* 12:555–561
- Lewin AS, Drenser KA, Hauswirth WW et al (1998) Ribozyme rescue of photoreceptor cells in a transgenic rat model of autosomal dominant retinitis pigmentosa. *Nat Med* 4:967–971
- Mendes HF, van der Spuy J, Chapple JP et al (2005) Mechanisms of cell death in rhodopsin retinitis pigmentosa: implications for therapy. *Trends Mol Med* 11:177–185
- Olsson JE, Gordon JW, Pawlyk BS et al (1992) Transgenic mice with a rhodopsin mutation (Pro23His): a mouse model of autosomal dominant retinitis pigmentosa. *Neuron* 9:815–830
- Organisciak DT, Darrow RM, Barsalou L et al (2003) Susceptibility to retinal light damage in transgenic rats with rhodopsin mutations. *Invest Ophthalmol Vis Sci* 44:486–492
- Ranchon I, LaVail MM, Kotake Y et al (2003) Free radical trap phenyl-N-tert-butyl nitron protects against light damage but does not rescue P23H and S334ter rhodopsin transgenic rats from inherited retinal degeneration. *J Neurosci* 23:6050–6057
- Roof DJ, Adamian M, Hayes A (1994) Rhodopsin accumulation at abnormal sites in retinas of mice with a human P23H rhodopsin transgene. *Invest Ophthalmol Vis Sci* 35:4049–4062
- Simonelli F, Maguire AM, Testa F et al (2010) Gene Therapy for Leber's Congenital Amaurosis is Safe and Effective Through 1.5 Years After Vector Administration. *Mol Ther* 18:643–650
- Sullivan JM, Pietras KM, Shin BJ et al (2002) Hammerhead ribozymes designed to cleave all human rod opsin mRNAs which cause autosomal dominant retinitis pigmentosa. *Mol Vis* 8: 102–113
- Tam BM, Moritz OL (2006) Characterization of rhodopsin P23H-induced retinal degeneration in a *Xenopus laevis* model of retinitis pigmentosa. *Invest Ophthalmol Vis Sci* 47:3234–3241
- Tessitore A, Parisi F, Denti MA et al (2006) Preferential silencing of a common dominant rhodopsin mutation does not inhibit retinal degeneration in a transgenic model. *Mol Ther* 14:692–699
- Timmers A, Zhang H, Squitieri A et al (2001) Subretinal injections in rodent eyes: effects on electrophysiology and histology of rat retina. *Mol Vis* 7:131–137
- van Soest S, Westerveld A, de Jong PT et al (1999) Retinitis pigmentosa: defined from a molecular point of view. *Surv Ophthalmol* 43:321–334

Chapter 28

Retinal Degeneration and Cellular Suicide

Wai Gin Fong and Catherine Tsilfidis

Keywords Apoptosis • Autophagy • Retinitis pigmentosa • XIAP • Retinal degeneration • Programmed cell death • Retina

28.1 Programmed Cell Death Pathways

Apoptosis, the most well-documented form of programmed cell death (PCD), is characterized by chromatin condensation, cytoplasmic blebbing, and DNA fragmentation. The central mediators of apoptosis are a family of cysteine aspartases (Caspases), whose cleavage and activation directly lead to the morphology and DNA breakup seen in apoptotic cells (Liston et al. 2003). Apoptosis pathways can be subdivided into extrinsic, receiving signals from cell surface receptors, or intrinsic, receiving internal signals through the mitochondria. In the extrinsic signaling pathway, ligand-bound cell surface receptors such as TNF or Fas recruit procaspase 8 to form the death-inducing signaling complex (DISC) (see Fig. 28.1). Aggregation of the DISC induces the cleavage and release of active caspase 8, which in turn catalyses the cleavage and activation of the effector caspases 3 and 7. Effector caspases directly execute the apoptotic program through the destruction of vital proteins and the activation of DNases. The intrinsic pathway is initiated by internal signals to the mitochondria, which causes leakage of cytochrome c into the cytoplasm. Cytochrome

W.G. Fong

Ottawa Hospital Research Institute, Ottawa General Hospital, Ottawa, ON, Canada K1H 8L6

C. Tsilfidis (✉)

Ottawa Hospital Research Institute, Ottawa General Hospital, Ottawa, ON, Canada K1H 8L6

Department of Cellular and Molecular Medicine, University of Ottawa, 501 Smyth Road, Ottawa, ON, Canada K1H 8L6

e-mail: ctsilfidis@ohri.ca

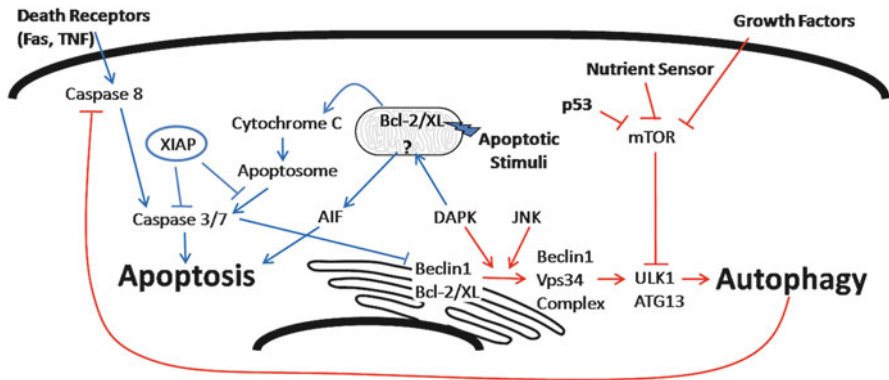


Fig. 28.1 Interaction between apoptosis and autophagy pathways. *Blue lines* represent the apoptosis pathway. *Red lines* represent the autophagy pathway

c recruits Apaf-1 and procaspase 9 to form the apoptosome, a complex which can directly activate effector caspases (Liston et al. 2003) (see Fig. 28.1).

Autophagy is a self-degradative process by which the cell compartmentalizes and recycles internal components through lysosomal degradation. Although considered a type II form of PCD, autophagy can be self-protective through the removal of damaged organelles and protein aggregates, and nutrient recycling (Eisenberg-Lerner et al. 2009). Three distinct forms of autophagy, macroautophagy, microautophagy, and chaperone-mediated autophagy, have been defined based on how the target protein or structure enters the lysosome (Massey et al. 2004; Klionsky 2005). Macroautophagy is a very well-characterized system in yeast and the most well-studied system in retinal disease models. This process begins with the formation of a phagophore, a double membrane vesicle which recognizes and engulfs target proteins and organelles to form an autophagosome. The autophagosome then fuses with lysosomes to form an autolysosome, which breaks down and recycles the target (Glick et al. 2010). In yeast, a family of autophagy-related genes (Atg) regulate the induction (Atg 1, 13, 17) and formation (Atg 6, 14 and Vps 34) of the phagophore, target recognition (Atg 11, 19) and completion of the autophagosome (Atg 8, 12). This system is well conserved in higher organisms with the majority of yeast Atg proteins having mammalian homologs, including Ulk1/2 (Atg1), Beclin1 (Atg 6), and LC3 (Atg 8) (Mizushima 2007; Glick et al. 2010) (see Fig. 28.1).

Though normally active at a low basal level, autophagy is ramped up during periods of low nutrient conditions, loss of growth factor support, and oxidative stress. The target of rapamycin (TOR) kinase, normally activated by the amino acid-dependent or the insulin/PI3K signaling pathways (Hietakangas and Cohen 2009), acts as a central regulator by blocking phagophore formation through the phosphorylation of Atg13 (Diaz-Troya et al. 2008). Upon loss of proper signaling events or repression from internal sensors, TOR activity is abrogated and autophagy allowed to proceed (see Fig. 28.1). Alternatively, mammalian autophagy is also controlled by Bcl2, which binds Beclin1 and prevents phagophore formation (Liang et al. 2006).

The phosphorylation of Bcl2 through Jnk1 prevents Beclin1 binding and allows activation of the autophagic program (Wei et al. 2008) (see Fig. 28.1).

The complex interaction between apoptosis and autophagy are just beginning to be elucidated. Depending on the system, both forms of PCD can work in concert or in parallel to augment cell death, or autophagy can antagonize apoptosis through the removal of cell death-inducing agents such as protein aggregates or damaged organelles. Significant signaling crosstalk exists between these two systems, as seen in the inhibition of TOR by the pro-apoptotic p53 (Feng et al. 2005), the aforementioned interaction between the anti-apoptotic Bcl2 and the pro-autophagic Beclin1, and the dual activating role of DAPk in both forms of PCD (Gozuacik et al. 2008) (see Fig. 28.1). It is likely that the PCD observed in complex systems will always be the combined result of multiple cell death pathways.

28.2 Cell Death in Inherited Retinal Dystrophies

The progressive loss of vision via photoreceptor cell death is a shared trait of all inherited retinal diseases, including Retinitis Pigmentosa (RP) and Leber Congenital Amaurosis (LCA). Numerous diverse gene mutations have been linked to this class of retinal dystrophies, indicating the sensitivity of the retina to changes in a variety of different pathways. The types of cell death within the affected retina are also variable, with different or multiple forms of cell death discovered in different models of the same disease. The challenge for researchers is to tease out the initial cause of cell death in these diseases from the resulting downstream cell death due to loss of trophic support or oxidative stress.

In the case of RP, the challenge for researchers is readily apparent, with as many as 47 genes linked to the various forms of RP (<http://www.sph.uth.tmc.edu/retnet>). In addition, several syndromes, including Usher's and Bardet-Biedl, have a RP component in addition to other nonocular deficits, indicating other mutations that can cause uncontrolled photoreceptor death in the retina (Hartong et al. 2006). Nyctalopia or night blindness is usually the early stage of this disease, caused by the initial wave of cell death specifically targeting rod photoreceptors. This is followed by the loss of peripheral vision and, eventually, the loss of central vision produced by progressive cone photoreceptor death. Outer nuclear layer thinning due to photoreceptor loss, and pigment deposits in the retina are hallmarks of the late stages of RP (Doonan and Cotter 2004).

The morphological characteristics of apoptosis, including chromatin condensation and DNA fragmentation, have been observed in all human samples and animal models of RP (Li and Milam 1995). However, the correlation of caspase activation and photoreceptor cell death is less clear. In the *rd/rd* mouse model, which contains a functional deletion of peripherin 2, activation of caspase 3 has been correlated with peak photoreceptor death (Hughes et al. 2004). This is also true for the S334ter mutant of rhodopsin in rats, where both photoreceptor death and caspase 3 activity peaks at postnatal day 11–12 and the intraocular injection of the caspase 3 inhibitor

z-DEVD-fmk afforded partial protection from cell death (Liu et al. 1999). On the other hand, there is contradictory evidence in the *rd1* mouse model, which has a mutation in the *Pde6b* gene encoding the β -subunit of cGMP-PDE (Farber 1995). Jomary et al. (2001) found caspase 8 and 3 activation, as well as cytochrome c release, in *rd1* mice, whereas others found neither caspase cleavage nor cytochrome c release in the same mouse model (Doonan et al. 2003). Caspase 3 inhibitor or caspase 3 deletion delayed the onset of disease, but was unable to block photoreceptor cell death entirely (Yoshizawa et al. 2002; Zeiss et al. 2004).

Some have suggested alternatives to classic apoptosis in the *rd1* mouse model. ER stress and elevated calcium can induce the activation of calpain, a calcium-activated cysteine protease, and trigger a caspase-independent pathway of apoptosis through the release of apoptosis-inducing factor (AIF) from the mitochondria (Sanges and Marigo 2006). AIF released into the cytosol migrates to the nucleus where it can induce the nuclear condensation and DNA fragmentation seen in apoptosis. This phenomenon is also seen in Royal College of Surgeons (RCS) rats, a model for childhood onset rod-cone dystrophy, which indicates that this form of caspase-independent apoptosis may not be *rd1* specific (Mizukoshi et al. 2010).

Lohr et al. (2006) analyzed several different markers of cell death, including apoptosis, autophagy, oxidative stress, and neuroinflammation, and attempted to correlate their activation with TUNEL positive cells in *rd1*, *rds*, and light damage murine models. The study indicated that in *rd* and light-damaged mice, all markers correlated strongly with TUNEL positive cells, indicating multiple cell death pathways ran in parallel (Lohr et al. 2006). In *rds* mice, autophagy markers lagged after cell death, suggesting a cleanup role for autophagy in these mice. Autophagy is also activated during cone cell death in several RP mouse models and the addition of insulin, which blocks autophagy through TOR kinase, prolongs the life of these cone photoreceptors (Punzo et al. 2009). It appears that multiple methods of cell death can run in parallel and share responsibility for both rod and photoreceptor cell death in RP models.

28.3 Cell Death in Retinal Damage Models

The retina is a highly sensitive organ to direct physical or chemical damage, as well as to the oxidative stress and the loss of trophic support that follows. Waves of photoreceptor death occur in damaged retinas days after the initial insult, culminating in loss of vision. Several animal models have been developed that mimic human disease, including retinal detachments and retinal ischemia.

Retinal detachment is a physical separation that occurs between the neural retina and the underlying RPE. Photoreceptor cell death through apoptosis is seen within 24 h and peaks 2–3 days postdetachment. Activation of caspase 3, 7, and 9 precedes maximum TUNEL positive cells, implicating the intrinsic pathway of apoptosis (Zacks et al. 2003). However, Fas is upregulated before caspase 9 activation, and the inhibition of Fas postdetachment decreases levels of activated caspase 9 and

TUNEL positive cells, suggesting a role for Fas in the triggering of apoptosis (Zacks et al. 2004).

In retinal ischemia, blood vessel occlusion and subsequent reperfusion induce numerous death signals including hypoxia, glutamate toxicity, and oxidative stress. In addition to necrosis, apoptosis is triggered quickly in the retina beginning 2 h postischemia in the ganglion cell layer and 9 h postischemia in the inner nuclear layer (INL), with peak apoptosis occurring after 24 h (Katai and Yoshimura 1999). Apoptosis correlates with caspase 3 upregulation in photoreceptors in the inner and outer nuclear layer and amacrine neurons (Singh et al. 2001).

28.4 Retina Rescue by Blocking PCD

The prevalence and importance of PCD in retinal degenerations makes it an ideal target to combat these diseases. By directly blocking PCD pathways, retinal structure and function can be preserved regardless of the cell death trigger underlying the disease. To this end, synthetic peptide caspase inhibitors have been designed to specifically block effector caspase-3 and 7 (z-DEVD-fmk). In RP animal models, z-DEVD-fmk partially protected the retina of the rhodopsin S334ter mutant rat (Liu et al. 1999) and the tubby mouse, a model of Usher's Syndrome (Bode and Wolfrum 2003). Though effective, peptide inhibitors have limited cell penetration and half-life (Lamkanfi et al. 2003) and recent studies question the specificity of peptide caspase inhibitors, especially at high concentrations (Berger et al. 2006; Pereira and Song 2008).

Alternatively, targeted gene therapy to block specific PCD pathways in retinal cells is also an interesting option. In autophagy, a gene target that specifically inhibits the cell death pathway without blocking basal/prosurvival autophagy has yet to be elucidated. However, several protein families are known to play important roles in the control of apoptosis. The Bcl-2 family controls mitochondrial potential and permeability, including cytochrome c release into the cytoplasm, which plays a pivotal role in the activation of the intrinsic apoptotic pathway. In one study, RP model *rdls* mice crossed with Bcl-2 transgenic mice driven by the rhodopsin promoter had a twofold preservation of photoreceptors compared to littermates, as measured by ONL thickness and photoreceptor cell counts (Nir et al. 2000). Although Bcl-2 has potential as a treatment in RP, the oncogenic potential of this protein likely excludes it as a gene therapy candidate in humans.

The X-linked inhibitor of apoptosis (XIAP) protein is the most potent member of the IAP family of caspase inhibitors. Structurally, XIAP consists of three baculoviral IAP repeat (BIR) domains which are necessary for caspase binding, a ubiquitin binding domain (UBA) and a RING zinc finger (Galban and Duckett 2010). XIAP inhibits both the pro- and active forms of several different caspases, including the effector caspases 3 and 7 and the intrinsic pathway apoptosome member caspase 9 (see Fig. 28.1). The E3 ubiquitin ligase activity associated with the carboxy-terminal RING domain can target bound caspases for degradation (Suzuki et al. 2001).

The ability of XIAP to inhibit vital effector caspases allows it to effectively block both the intrinsic and extrinsic apoptosis pathways and protect cells from a wide variety of insults.

The overexpression of XIAP through an adeno-associated viral vector (AAV-XIAP) is able to preserve photoreceptors in several models of retinal disease. In rat models of RP with rhodopsin mutations P23H and S334ter, we found that a single subretinal injection of AAV XIAP at day 14–17 preserved retinal thickness specifically in the injected region at week 28. In P23H rats, retinal function, as measured by electroretinograms (ERGs), was partially maintained in the XIAP-treated eye vs. the untreated contralateral eye or GFP-treated animals. Interestingly, no functional protection was seen in S334ter rats despite the preservation of retinal structure (Leonard et al. 2007). Similarly, pretreatment with subretinal AAV-XIAP provided long-term protection in murine models of retinal ischemia (Renwick et al. 2006), retinal detachment (Zadro-Lamoureux et al. 2009), and chemical damage by *N*-methyl-*N*-nitrosourea (MNU) (Petrin et al. 2003a, b).

The success of AAV-XIAP in these *in vivo* models highlights the usefulness of direct caspase inhibition for the treatment of diverse retinal degenerative diseases. Although AAV-XIAP did not infect all cells, it was able to preserve the structure and function of the infected region of the retina. The results would be greatly improved with a wider spread of virus to maximize the treated area. In addition, alternative methods of XIAP delivery, such as protein transduction, need to be explored for the treatment of acute disease where pretreatment with AAV-XIAP is not possible.

28.5 Looking into the Future

The simple phenotype of retinal degeneration belies the complexity underlying these diseases. The vast array of mutations and complicated interplay between signaling events makes a single gene therapy target difficult to find. The prevalence of PCD in these dystrophies offers common ground in the effort to preserve vision. Inhibition of PCD, particularly apoptosis, not only protects individual cells, but also helps maintain the interconnected and inter-reliant web of the retina. Improvements in delivery and spread will only enhance the prospects of PCD inhibition as a viable treatment for human disease.

References

- Berger AB, Sexton KB, Bogoy M (2006) Commonly used caspase inhibitors designed based on substrate specificity profiles lack selectivity. *Cell Res* 16:961–963
- Bode C, Wolfrum U (2003) Caspase-3 inhibitor reduces apoptotic photoreceptor cell death during inherited retinal degeneration in tubby mice. *Mol Vis* 9:144–150

- Diaz-Troya S, Perez-Perez ME, Florencio FJ et al (2008) The role of TOR in autophagy regulation from yeast to plants and mammals. *Autophagy* 4:851–865
- Doonan F, Cotter TG (2004) Apoptosis: a potential therapeutic target for retinal degenerations. *Curr Neurovasc Res* 1:41–53
- Doonan F, Donovan M, Cotter TG (2003) Caspase-independent photoreceptor apoptosis in mouse models of retinal degeneration. *J Neurosci* 23:5723–5731
- Eisenberg-Lerner A, Bialik S, Simon HU et al (2009) Life and death partners: apoptosis, autophagy and the cross-talk between them. *Cell Death Differ* 16:966–975
- Farber DB (1995) From mice to men: the cyclic GMP phosphodiesterase gene in vision and disease. The Proctor Lecture. *Invest Ophthalmol Vis Sci* 36:263–275
- Feng Z, Zhang H, Levine AJ et al (2005) The coordinate regulation of the p53 and mTOR pathways in cells. *Proc Natl Acad Sci U S A* 102:8204–8209
- Galban S, Duckett CS (2010) XIAP as a ubiquitin ligase in cellular signaling. *Cell Death Differ* 17:54–60
- Glick D, Barth S, Macleod KF (2010) Autophagy: cellular and molecular mechanisms. *J Pathol* 221:3–12
- Gozuacik D, Bialik S, Raveh T et al (2008) DAP-kinase is a mediator of endoplasmic reticulum stress-induced caspase activation and autophagic cell death. *Cell Death Differ* 15:1875–1886
- Hartong DT, Berson EL, Dryja TP (2006) Retinitis pigmentosa. *Lancet* 368:1795–1809
- Hietakangas V, Cohen SM (2009) Regulation of tissue growth through nutrient sensing. *Annu Rev Genet* 43:389–410
- Hughes EH, Schlichtenbrede FC, Murphy CC et al (2004) Minocycline delays photoreceptor death in the rds mouse through a microglia-independent mechanism. *Exp Eye Res* 78:1077–1084
- Jomary C, Neal MJ, Jones SE (2001) Characterization of cell death pathways in murine retinal neurodegeneration implicates cytochrome c release, caspase activation, and bid cleavage. *Mol Cell Neurosci* 18:335–346
- Katai N, Yoshimura N (1999) Apoptotic retinal neuronal death by ischemia-reperfusion is executed by two distinct caspase family proteases. *Invest Ophthalmol Vis Sci* 40:2697–2705
- Klionsky DJ (2005) The molecular machinery of autophagy: unanswered questions. *J Cell Sci* 118:7–18
- Lamkanfi M, Declercq W, Depuydt B et al (2003) The Caspase Family. In: Los M, Walczak H (eds) *Caspases: Their Role in Cell Death and Cell Survival*. Landes Bioscience and Kluwer Academic, New York
- Leonard KC, Petrin D, Coupland SG et al (2007) XIAP protection of photoreceptors in animal models of retinitis pigmentosa. *PLoS One* 2:e314
- Li ZY, Milam AH (1995) Apoptosis in retinitis pigmentosa. In: Anderson R, LaVail M, Hollyfield J (eds) *Degenerative Diseases of the Retina*. Plenum Press, New York
- Liang C, Feng P, Ku B et al (2006) Autophagic and tumour suppressor activity of a novel Beclin1-binding protein UVRAG. *Nat Cell Biol* 8:688–699
- Liston P, Fong WG, Korneluk RG (2003) The inhibitors of apoptosis: there is more to life than Bcl2. *Oncogene* 22:8568–8580
- Liu C, Li Y, Peng M et al (1999) Activation of caspase-3 in the retina of transgenic rats with the rhodopsin mutation s334ter during photoreceptor degeneration. *J Neurosci* 19:4778–4785
- Lohr HR, Kuntchithapatham K, Sharma AK et al (2006) Multiple, parallel cellular suicide mechanisms participate in photoreceptor cell death. *Exp Eye Res* 83:380–389
- Massey A, Kiffin R, Cuervo AM (2004) Pathophysiology of chaperone-mediated autophagy. *Int J Biochem Cell Biol* 36:2420–2434
- Mizukoshi S, Nakazawa M, Sato K et al (2010) Activation of mitochondrial calpain and release of apoptosis-inducing factor from mitochondria in RCS rat retinal degeneration. *Exp Eye Res* 91:353–361
- Mizushima N (2007) Autophagy: process and function. *Genes Dev* 21:2861–2873
- Nir I, Kedzierski W, Chen J et al (2000) Expression of Bcl-2 protects against photoreceptor degeneration in retinal degeneration slow (rds) mice. *J Neurosci* 20:2150–2154

- Pereira NA, Song Z (2008) Some commonly used caspase substrates and inhibitors lack the specificity required to monitor individual caspase activity. *Biochem Biophys Res Commun* 377:873–877
- Petrin D, Baker A, Brousseau J et al (2003a) XIAP protects photoreceptors from n-methyl-n-nitrosourea-induced retinal degeneration. *Adv Exp Med Biol* 533:385–393
- Petrin D, Baker A, Coupland SG et al (2003b) Structural and functional protection of photoreceptors from MNU-induced retinal degeneration by the X-linked inhibitor of apoptosis. *Invest Ophthalmol Vis Sci* 44:2757–2763
- Punzo C, Kornacker K, Cepko CL (2009) Stimulation of the insulin/mTOR pathway delays cone death in a mouse model of retinitis pigmentosa. *Nat Neurosci* 12:44–52
- Renwick J, Narang MA, Coupland SG et al (2006) XIAP-mediated neuroprotection in retinal ischemia. *Gene Ther* 13:339–347
- Sanges D, Marigo V (2006) Cross-talk between two apoptotic pathways activated by endoplasmic reticulum stress: differential contribution of caspase-12 and AIF. *Apoptosis* 11:1629–1641
- Singh M, Savitz SI, Hoque R et al (2001) Cell-specific caspase expression by different neuronal phenotypes in transient retinal ischemia. *J Neurochem* 77:466–475
- Suzuki Y, Nakabayashi Y, Takahashi R (2001) Ubiquitin-protein ligase activity of X-linked inhibitor of apoptosis protein promotes proteasomal degradation of caspase-3 and enhances its anti-apoptotic effect in Fas-induced cell death. *Proc Natl Acad Sci U S A* 98:8662–8667
- Wei Y, Pattingre S, Sinha S et al (2008) JNK1-mediated phosphorylation of Bcl-2 regulates starvation-induced autophagy. *Mol Cell* 30:678–688
- Yoshizawa K, Kiuchi K, Nambu H et al (2002) Caspase-3 inhibitor transiently delays inherited retinal degeneration in C3H mice carrying the rd gene. *Graefes Arch Clin Exp Ophthalmol* 240:214–219
- Zacks DN, Zheng QD, Han Y et al (2004) FAS-mediated apoptosis and its relation to intrinsic pathway activation in an experimental model of retinal detachment. *Invest Ophthalmol Vis Sci* 45:4563–4569
- Zacks DN, Hanninen V, Pantcheva M et al (2003) Caspase activation in an experimental model of retinal detachment. *Invest Ophthalmol Vis Sci* 44:1262–1267
- Zadro-Lamoureux LA, Zacks DN, Baker AN et al (2009) XIAP effects on retinal detachment-induced photoreceptor apoptosis [corrected]. *Invest Ophthalmol Vis Sci* 50:1448–1453
- Zeiss CJ, Neal J, Johnson EA (2004) Caspase-3 in postnatal retinal development and degeneration. *Invest Ophthalmol Vis Sci* 45:964–970

Chapter 29

Suppression of *rds* Expression by siRNA and Gene Replacement Strategies for Gene Therapy Using rAAV Vector

Hilda Petrs-Silva, Douglas Yasumura, Michael T. Matthes,
Matthew M. LaVail, Alfred S. Lewin, and William W. Hauswirth

Keywords *rds*/peripherin • Retinitis pigmentosa • Photoreceptor degeneration
• Gene therapy • Adeno-associated viral vector • siRNA • Gene replacement

29.1 Introduction

Autosomal dominant retinitis pigmentosa (ADRP) is a genetically heterogeneous disease and the most prevalent hereditary cause of blindness, with more than one million individuals affected worldwide (Hartong et al. 2006). Mutations in *rds* (retinal degeneration slow/peripherin) are one of the most common causes associated with ADRP, accounting for approximately 10% of the cases (Fingert et al. 2008). RDS is a transmembrane glycoprotein localized to the rim region of outer segment (OS) disks in rods and cones (Wrigley et al. 2000). Mice carrying a naturally occurring null mutant fail to form photoreceptor OSs. Heterozygotes have a partial phenotype of short, disorganized OSs (Ma et al. 1995) suggesting a haploinsufficiency. Thus far, over 90 human mutations in *rds* have been identified and result in a wide spectrum of retinal dystrophies, in which the common feature is the visual loss

H. Petrs-Silva (✉) • W.W. Hauswirth
Departments of Ophthalmology, Institute of Biophysics, CCS, UFRJ,
Rio de Janeiro 21941-902, Brazil
e-mail: hilda.ufl@gmail.com

D. Yasumura • M.T. Matthes • M.M. LaVail
Beckman Vision Center, University of California San Francisco, San Francisco, CA, USA

A.S. Lewin
Departments of Ophthalmology, Institute of Biophysics, CCS, UFRJ,
Rio de Janeiro 21941-902, Brazil
Departments of Molecular Genetics and Microbiology,
University of Florida, Gainesville, FL, USA

associated with the gradual death of photoreceptor cells. To date, attempts to achieve structural and functional rescue in animal models of *rds*-induced retinal degeneration have not been successful. Disease may be caused by reduction in the level of wild-type protein (haploinsufficiency), by a gain of a deleterious function or by a combination of both.

Gene therapy may be a promising approach for treating RDS/peripherin disease. Upon subretinal injection of recombinant adeno-associated virus (rAAV) vector containing *rds*, null mice responded with increases in rhodopsin synthesis, correction of rod OS formation and restoration of visual function over the first 14 weeks following treatment (Ali et al. 2000; Schlichtenbrede et al. 2003). However, treatment did not result in long-term preservation of photoreceptors (Sarra et al. 2001). Because of the dominant nature of this class of disease, simple gene replacement therapy is usually insufficient to overcome the expression of the mutant allele. Rather, the therapeutic approach for dominant negative mutations must be to either eliminate the mutated gene or repair its mutation together with gene replacement. The critical importance of RDS in photoreceptor OS integrity suggests that a suppression and replacement strategies may be useful. Because there are at least 90 different disease-causing dominant mutations in *rds*, targeted gene elimination or repair for each separate mutation becomes problematic. Therefore, gene therapy aimed at dominant genes, like *rds*, requires either mutation-independent suppression of mutated allele expression or an increase in the expression of the wild-type allele, or both. One approach to suppress expression is with small interfering RNA (siRNA). The silencing mechanism is based on ubiquitous cellular processes, in which the interference RNA degrades mRNA in a sequence-specific manner, upon introduction of double-stranded RNA (Hammond et al. 2000).

The objective of this work is to develop an effective therapy for genetic retinal disease associated with mutations in *rds*. For this, we propose the development of an siRNA to eliminate the endogenous *rds* mutant and wild-type mRNA, followed by a replacement therapy where an siRNA-resistant version of *rds* is supplied simultaneously. The siRNA and the resistant *rds* will be delivered to photoreceptor cells of diseased mice retinas through rAAV.

29.2 Materials and Methods

29.2.1 Cell Transfection

HEK-293 cells were grown in 24-well plates at 30–50% confluence for overnight and then cotransfected with 10 pmol of synthetic siRNA (Applied Biosystems) and 200 ng of plasmid using Lipofectamine 2000 (Invitrogen). A scrambled siRNA was used as negative control. After 72 h mRNA was collected.

29.2.2 RNA Isolation and Semiquantitative Real-Time PCR

Total RNA was extracted using RNeasy Kit as per manufacturer's instructions (Qiagen). Total RNA (2 µg) was reverse transcribed (RT) using First Strand Kit (GE), with the same amount of RNA for each reaction. RT RNA was mixed with SYBER Green and applied to 96-well plates for real-time PCR using commercially available primer pairs from SA.Biosciences (Qiagen). A two-step cycling program was employed (1 cycle 10 min at 95°C followed by 40 cycles of 15 s at 95°C and 1 min at 60°C). Data analysis was done following SA.Biosciences protocol.

29.2.3 AAV Production

AAV vectors were produced by plasmid cotransfection of HEK-293 cells as described by Zolotukhin et al. (2002). Vector titer was determined as DNase-resistant vector genomes by real-time PCR relative to a standard.

29.2.4 Subretinal Injection

All procedures in animals were handled according to the ARVO Statement for the Use of Animals in Ophthalmic and Vision Research and the guidelines of the Institutional Animal Care and Use Committee at the University of Florida. Eyes were injected as described by Timmers et al. (2001).

29.2.5 Electroretinogram

Mice were dark adapted overnight, and all procedures were carried out under dim red light. Mice were anesthetized and eyes were dilated. Hydroxypropyl methylcellulose 2.5% was applied to each eye to prevent corneal dehydration and to allow for optimal electrical conductivity. Mice were placed onto a platform with their entire head inside the Ganzfeld stimulus dome. Electroretinograms (ERGs) were recorded using gold loop cornea electrodes. Aluminum hub needles placed subcutaneously between the eyes and in a hind leg were used for the reference and ground electrodes, respectively. ERGs were recorded using a PC-based control and recording unit (Toennies Multiliner Vision). Scotopic rod ERG luminance response functions were elicited through a series of five white flashes of high intensity (0.7 log cd s/m²).

29.2.6 Statistical Analysis

Differences between groups were evaluated using one-way ANOVA for analysis of variance followed by Dunnett's posttest for group comparison. Differences were considered significant at P value of less than 0.01.

29.3 Results

29.3.1 Synthetic siRNAs Targeted to *rds* Reduces Transduction In Vitro in HEK-293 Cells

Initially two synthetic siRNAs were tested for its specificity and efficacy to decrease *rds* expression in HEK-293 cells cotransfected with siRNAs and a plasmid expressing *rds* from the CMV promoter, through semiquantitative real-time PCR. Both siRNAs were able to reduce more than 50% of *rds* expression in vitro, when compared with a scrambled siRNA used as a control (Fig. 29.1).

29.3.2 Effect of siRNA Directed to *rds* In Vivo in Photoreceptors by rAAV-5 Vector

To determine the effect of these siRNAs targeted to *rds* in vivo, both siRNAs were cloned in rAAV vector under the control of the H1 RNA polymerase III promoter. As a reporter, we used the green fluorescent protein (GFP) gene under the control of chicken beta-actin (CBA) promoter in the same AAV5 vector. Six-week old C57Bl/6

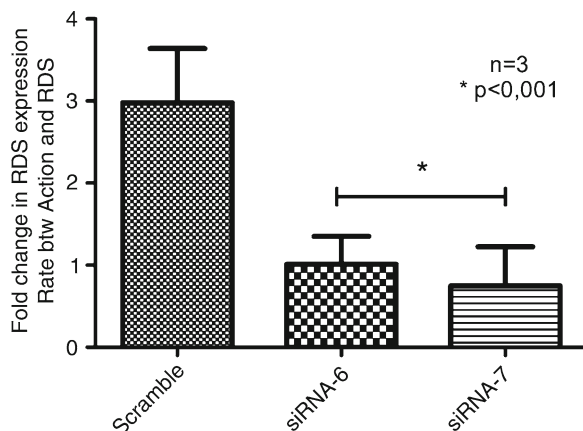


Fig. 29.1 HEK-293 cells cotransfected with plasmid containing *rds* and synthetic siRNA for 72 h followed by RNA extraction and real-time PCR to analyze *rds* expression

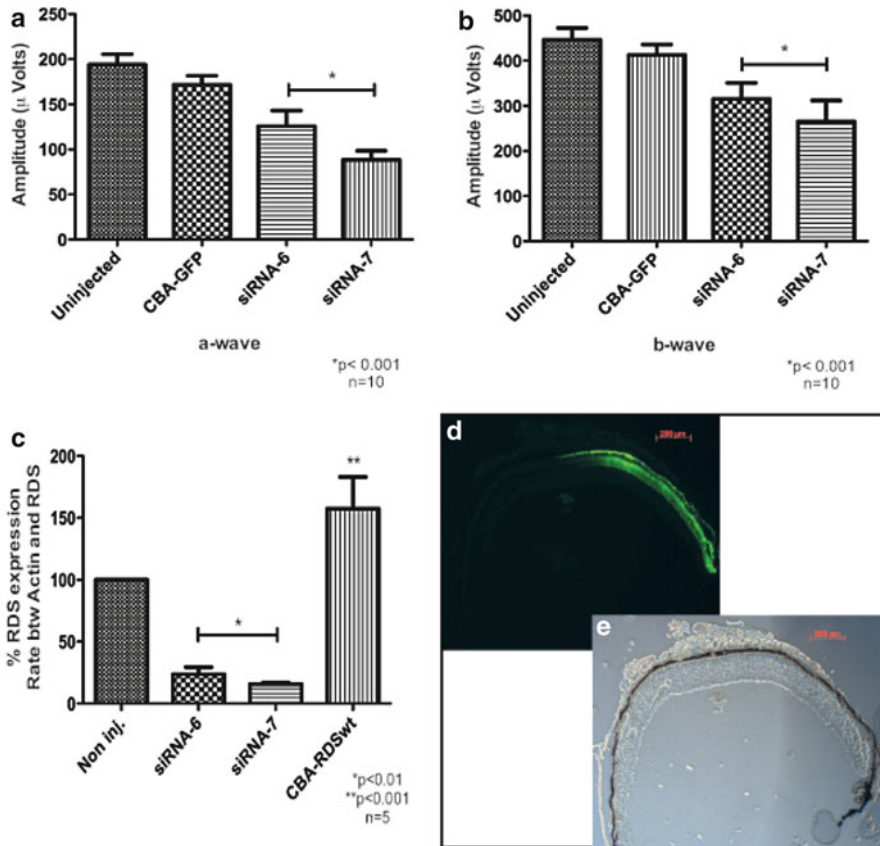


Fig. 29.2 Reduction of *rd5* in mice by siRNA delivered by rAAV to photoreceptors. Functional analysis by ERG: graphics show maximal amplitude of a-wave (**a**) and b-wave (**b**). Analysis of *rd5* expression in the presence of siRNA6 or 7 (**c**): total RNA was extracted and analyzed using real-time PCR. Transverse section of the retina showing its intact structure through bright field (**d**) and a fluorescent picture of the same field (**e**) showing GFP expression in approximately 1/2 of the retina, corresponding to rAAV transduced area

mice were injected subretinally with 1 μ L of the vectors (10^9 vg). Right eyes received rAAV with siRNA and left eyes were uninjected or received rAAV with only GFP. One month after infection, full-field scotopic ERGs were recorded. Both a- and b-wave amplitudes were reduced around 30–50% with both siRNAs directed to *rd5* (Fig. 29.2a, b). Control injected or uninjected eyes showed no change in ERG response. Reduction in ERG responses was paralleled by a reduction in RDS mRNA content in the retinas measured by real-time PCR at the same time point (Fig. 29.2c). In contrast, injection with rAAV containing the *rd5* gene led to an increase in *rd5* mRNA levels. The distribution of AAV infection was determined by detection of GFP expression through fluorescence microscopy (Fig. 29.2d). Since we do not transduce the entire retina, RNA knockdown by siRNA must have been very efficient on a per cell basis.

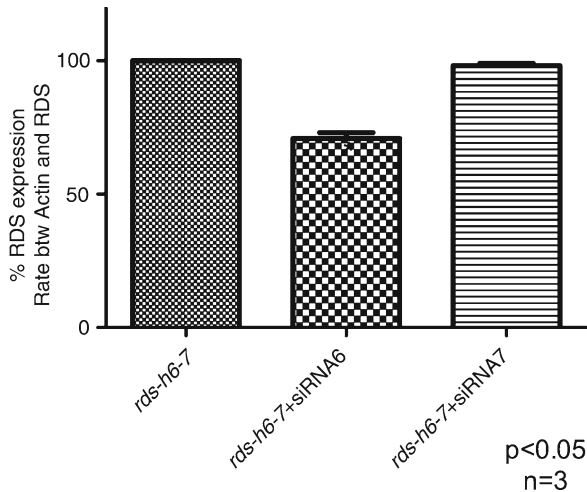


Fig. 29.3 HEK-293 cells cotransfected with plasmid containing resistant *rds-h6-7* and siRNA6 or 7 for 72 h followed by RNA extraction and real-time PCR to analyze *rds-h6-7* expression

29.3.3 Construction of *rds* Resistant to siRNA

In order to construct an *rds* gene resistant to the action of siRNAs6 and 7, we changed all possible nucleotides in each siRNA recognition site without changing the amino acid coding and called the modified cDNA, *rds h6-7*. The resistance of the *rds-h6-7* to siRNAs6 and 7 was initially analyzed in HEK-293 cells. Cells were cotransfected with the *rds-h6-7* under CBA promoter plus each synthetic siRNA. At 72 h postinfection, total RNA was collected and the amount of *rds* expression was analyzed through real-time PCR. *Rds-h6-7* was completely resistant to siRNA7 but was only partially resistant to siRNA6 in vitro (Fig. 29.3).

29.3.4 Proof of Principal for Combination Therapy for *rds* Using AAV Vector in Photoreceptors In Vivo

To test the feasibility of a combination therapy for *rds*-related diseases, an rAAV vector containing *rds-h6-7* was constructed. Combination injection was done with rAAV2/5 expressing siRNA6 or 7 and the *rds-h6-7* in the subretinal space of C57Bl/6 mice. A total of 1 μ L of the vectors was injected, both at 10^9 vg/ μ L. One month after injection, simultaneous full-field scotopic ERGs were recorded. There was a slight decrease in a-wave amplitude in the presence of siRNA6, confirming that *rds-h6-7* is not completely resistant to the action of siRNA6 (Fig. 29.4a). However, there was no significant change in amplitude in the combination *rds-h6-7* and siRNA7

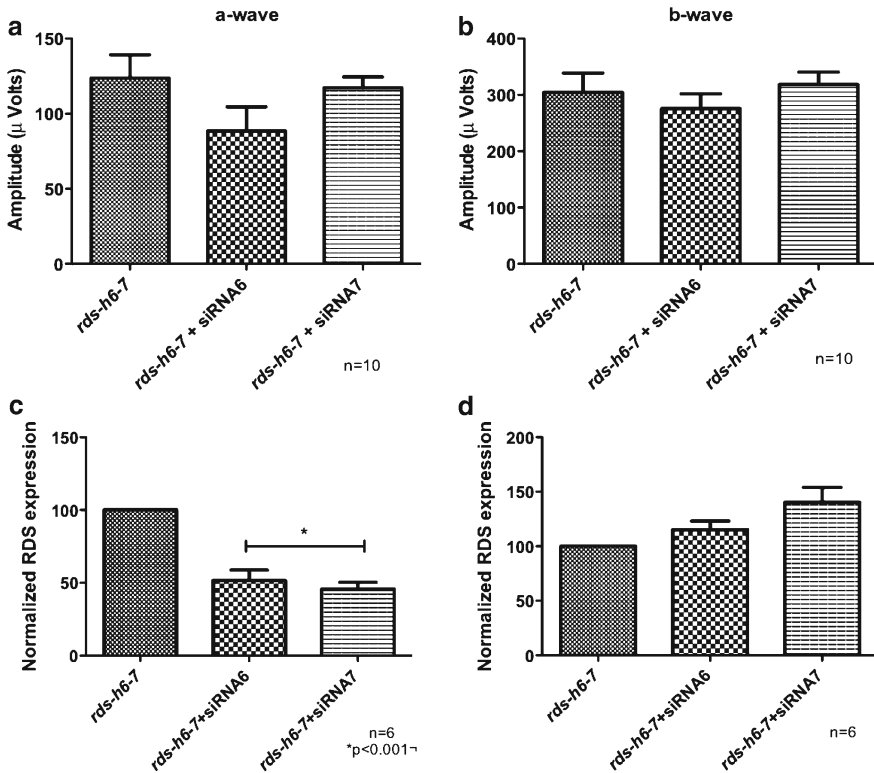


Fig. 29.4 Coinfection of photoreceptors in vivo with siRNA6 or 7 plus resistant *rds* delivered by rAAV – reposition of *rds* expression by its resistant version. Functional analysis by ERG: graphics show maximal amplitude of a-wave (a) and b-wave (b). Analysis by real-time PCR of total *rds* expression (c) and only of resistant *rds* with a distinct primer (d). PCR values for *rds* were normalized to the levels of β -actin in the same samples

(Fig. 29.4a). There was no significant difference in b-wave amplitudes between the eyes injected with *rds-h6-7* alone and *rds-h6-7* plus either siRNA. It is important to note that siRNA7 was the most effective reducing ERG (Fig. 29.2). These results suggest that even in the presence of siRNA7 directed to downregulate the expression of the wild-type *rds* in mouse photoreceptors, the coexpression of an *rds* allele resistant to this siRNA is capable of maintaining the function of these cells in vivo.

To examine RNA replacement, we analyzed *rds* expression by real-time PCR. First, we analyzed the total amount of *rds* expression, including endogenous and resistant genes, using a pair of primers that recognize both transcripts. We measured a reduction of 50% of the total *rds* with both siRNAs, indicating that some *rds* was degraded. We also designed a pair of primers specific for the resistant version of the *rds* delivered by AAV. There was no reduction of the exogenous *rds* with either

siRNA6 or siRNA7. These results confirm that the resistant version of *rd5* is resistant to the action of the siRNA7 and partially resistant to siRNA6, that downregulate only the endogenous transcript.

29.4 Discussion

The results showed that siRNA-based small hairpin RNA can efficiently and specifically silence RDS in vivo 1 month after AAV2/5-mediated delivery to the photoreceptors, leading to a nearly 50% reduction in *rd5* expression in the retina, and also leading to a reduction in the electrophysiological function of the photoreceptors detected by decrease of the electroretinogram a- and b-wave amplitudes. The reduction of 50% in *rd5* expression might be related with the area of the retina covered by the injection that was also around 50%. In this study, we also designed a version of *rd5* resistant to the action of the siRNA, and we showed that the presence of this resistant version together with siRNA prevented the decrease in the ERG response, while endogenous *rd5* expression was reduced by the siRNA. This result suggests that the exogenous-resistant version of *rd5* was able to provide the amount of *rd5* expression necessary to preserve the physiological function of the photoreceptors.

These results represent the proof of principle for the effectiveness of a combination therapy using siRNA to suppress *rd5* expression and gene replacement by adding a copy of *rd5* resistant to the action of the siRNA. This strategy can be applied by gene therapy using rAAV vector to deliver both the siRNA and the resistant gene into photoreceptor cells in order to treat retinal diseases caused by mutations in *rd5/peripherin*. The strategy of knocking down gene expression with siRNA delivered by rAAV vectors could also be adapted to other autosomal dominant eye diseases.

The heterogeneity in many dominant disease-causing genes represents a significant challenge with respect to development of viable gene therapy. As an example, *rd5*-related retina diseases are caused by over 90 different mutations within the gene, each of which could require a unique gene therapy. However, our approach overcomes this problem with an siRNA directed to a region in which no mutations have been described. This siRNA would be effective for the downregulation of all the mutants described so far in *rd5* gene and also the normal allele. In order to maintain *rd5* expression, the resistant version of *rd5* would complement this RNA knockdown. This approach should be applicable for most exon mutations in the *rd5/peripherin* gene leading to autosomal dominant disease. For loss-of-function mutations, however, using AAV to deliver the wild-type gene might be sufficient.

References

- Ali RR, Sarra GM, Stephens C et al (2000) Restoration of photoreceptor ultrastructure and function in retinal degeneration slow mice by gene therapy. *Nat Genet* 25:306–310
- Fingert JH, Oh K, Chung M et al (2008) Association of a novel mutation in the retinol dehydrogenase 12 (RDH12) gene with autosomal dominant retinitis pigmentosa. *Arch Ophthalmol* 126: 1301–1307

- Hammond SM, Bernstein E, Beach D, Hannon GJ (2000) An RNA-directed nuclease mediates post-transcriptional gene silencing in *Drosophila* cells. *Nature* 404:293–296
- Hartong DT, Berson EL, Dryja TP (2006) Retinitis pigmentosa. *Lancet* 368:1795–809
- Ma J, Norton JC, Allen AC et al (1995) Retinal degeneration slow (*rds*) in mouse results from simple insertion of a t haplotype-specific element into protein-coding exon II. *Genomics* 28:212–219
- Sarra GM, Stephens C, de Alwis M et al (2001) Gene replacement therapy in the retinal degeneration slow (*rds*) mouse: the effect on retinal degeneration following partial transduction of the retina. *Hum Mol Genet* 10:2353–2361
- Schlichtenbrede FC, da Cruz L, Stephens C et al (2003) Long-term evaluation of retinal function in Prph2Rd2/Rd2 mice following AAV-mediated gene replacement therapy. *J Gene Med* 5: 757–764
- Timmers AM, Zhang H, Squitieri A et al (2001) Subretinal injections in rodent eyes: effects on electrophysiology and histology of rat retina. *Mol Vis* 7:131–137
- Wrigley JD, Ahmed T, Nevett CL et al (2000) Peripherin/*rds* influences membrane vesicle morphology. Implications for retinopathies. *J Biol Chem* 275:13191–13194
- Zolotukhin S, Potter M, Zolotukhin I et al (2002) Production and purification of serotype 1, 2, and 5 recombinant adeno-associated viral vectors. *Methods* 28:158–167

Chapter 30

Silencing the Expression of *CTRP5/C1QTNF5* and *ELOVL4* Genes by Small Interfering RNA

Venkata Ramana Murthy Chavali*, Vidyullatha Vasireddy*, and Radha Ayyagari

Keywords CTRP5 • C1QTNF5 • ELOVL4 • siRNA • Small interfering RNA • Late-onset retinal degeneration • STGD3 • L-ORD • Stargardt-like macular degeneration

30.1 Introduction

Inherited retinal degenerations are a group of heterogeneous diseases characterized by the progressive loss of photoreceptors and the retinal pigment epithelium (RPE). Several genetic mutations which are responsible for the pathology of these retinal diseases in both human and animal models have been described. A significant proportion of retinal degenerations are inherited in a dominant manner (RetNet). The dominant mutations cause retinal phenotypes either by dominant-negative or haploinsufficiency mechanisms. Dominant-negative mechanism has been implicated in the pathology of two macular degenerations, Stargardt-like macular degeneration (STGD3) and late-onset retinal degenerations (L-ORD) (Zhang et al. 2001; Hayward et al. 2003; Ayyagari et al. 2004). STGD3 is an inherited form of early onset autosomal dominant macular degeneration caused due to a 5-bp deletion mutation in the elongation of very long chain fatty acid-4 (*ELOVL4*) gene, whereas an S163R encoding missense mutation in the C1q tumor necrosis factor-5 (*C1QTNF5/CTRP5*) gene causes L-ORD (Hayward et al. 2003; Maugeri et al. 2004; Vasireddy et al. 2010). Using in vitro and in vivo models considerable progress has been made in establishing the disease mechanism underlying STGD3 and L-ORD (Vasireddy et al. 2005; Shu et al. 2006a). The mutant proteins of *ELOVL4* and *CTRP5* are

*Equal contribution authors

V.R.M. Chavali • V. Vasireddy • R. Ayyagari (✉)
Department of Ophthalmology, Shiley Eye Center, University of California San Diego,
La Jolla, CA 92037, USA
e-mail: rayyagari@ucsd.edu

found to interact with their respective wild-type protein and alter the trafficking of the wild-type protein, making them unavailable for their normal function (Vasireddy et al. 2005; Shu et al. 2006a).

Potential therapies to treat dominant retinal degeneration and neurodegeneration are being actively pursued. Silencing the mutant allele and selective removal of the mutant protein are two promising strategies to treat dominant diseases due to mutations that exert dominant-negative effect. Ribozyme and RNA interference (RNAi) mediated technologies have been proven to be efficient in either controlling the expression of mutant allele or complete knockdown of gene expression in several degenerative diseases (Campbell et al. 2009). Here, we describe the efficacy of siRNA probes designed to specifically silence the wild-type and mutant *ELOVL4* (human) transcript and both wild type and mutant transcripts of mouse and human *CTRP5/CIQTNF5* genes. Our studies using transfected cells indicated selective and successful knockdown of *ELOVL4* and *CTRP5* genes by the siRNA probes we tested.

30.2 Materials and Methods

30.2.1 siRNA Designing

The siRNA targeting human *ELOVL4* (mutant) and both the human *CTRP5* and mouse *Ctrp5* (wild type and mutant) are custom designed in our lab and synthesized by Applied biosystems-Lifetechnologies, Carlsbad, CA. Predesigned siRNA of *ELOVL4*, that can target the wild-type allele were obtained from Applied Biosystems. The following siRNAs (represented 5'-3') were used in our study: UGUAGAAGAAAGAGAAAUatg- *ELOVL4* #1 antisense; GUUUUUGACA AGAUCAAActg- *Ctrp5* #2 siRNA antisense; AGAAAUCCAGAGAAGGUACtg- *Ctrp5* #3 siRNA antisense; AUUCUUCACCAGAUCAAActg- *CTRP5* #4 siRNA antisense; GGCAAUGGAUUCGCCAUUCtt- *CTRP5* #5 siRNA antisense. The Cy3-labeled Silencer GFP (eGFP) siRNA (Cat#4626, Life-technologies, Carlsbad, CA) was used as a positive control for both transfection and as a measure of knockdown efficiency, and the Silencer negative control siRNA (Cat# 4611, Lifetechnologies, Carlsbad, CA) was used as a negative control in our experiments.

30.2.2 Cell Culture and Transfection of siRNA

Cos-7 cells were cultured in DMEM with 10% fetal bovine serum and antibiotics. For immunocytochemistry, cells were seeded on dual chamber slides (Lab-Tek, Nalge Nunc, Naperville, IL). For quantitative real-time PCR (qRT-PCR), cells were seeded in 10-cm culture dish and grown to a confluence of 70–80%. After 24 h of seeding, cells were transfected with GFP tagged wild type *ELOVL4* or mutant *ELOVL4*;

co-transfected with both GFP tagged wild type and mutant *ELOVL4* protein expressing constructs and the siRNA targeting wild type or mutant *ELOVL4* allele.

Another set of Cos-7 cells were cotransfected with a wild-type human *CTRP5*-GFP or wild-type mouse *Ctrp5*-GFP fusion protein expression constructs (pEG-FPC1-h*CTRP5*-GFP or pEFGPC1-m*Ctrp5*-GFP) and corresponding siRNA that targets the human or mouse *CTRP5/Ctrp5* RNA transcripts. For all the transfection experiments involving qRT-PCR, GAPDH siRNA was used as internal control. Transfection efficiency of siRNA was tested by using the Cy3-labeled siRNA. The transfection experiments were performed using Lipofectamine 2000 reagent (Life technologies, Carlsbad, CA) (Chavali et al. 2010).

30.2.3 Quantitative Real-Time PCR

In vitro qRT-PCR analysis was performed using Cos-7 cells transfected with *ELOVL4/CTRP5* constructs and siRNA. After 48 h posttransfection, RNA was isolated from the cell pellets, and cDNA was prepared as reported earlier (Mandal et al. 2006). Comparative Ct method was used to calculate the expression levels of *CTRP5* and *ELOVL4* (Mandal et al. 2006; Raz-Prag et al. 2006).

30.2.4 Immunofluorescence Analysis of Transfected Cos-7 Cells

After 48 h of transfection cells expressing the GFP fusion tag constructs were fixed and mounted with mounting medium containing DAPI as reported earlier (Chavali et al. 2010). Images were captured using a confocal microscope (LSM 510, Carl Zeiss Meditec, Inc., CA).

30.3 Results

The efficiency of siRNA in controlling the expression of the *ELOVL4* and *CTRP5* genes was studied using Cos-7 cells expressing these genes.

30.3.1 siRNA-Mediated Suppression of *ELOVL4* mRNA

To test the efficacy of siRNA that targets the wild-type *ELOVL4*, Cos-7 cells were transfected with a vector containing GFP-tagged wild-type *ELOVL4* and siRNA (50 and 100 nM) that targets the wild-type *ELOVL4*. Expression of *ELOVL4* in the

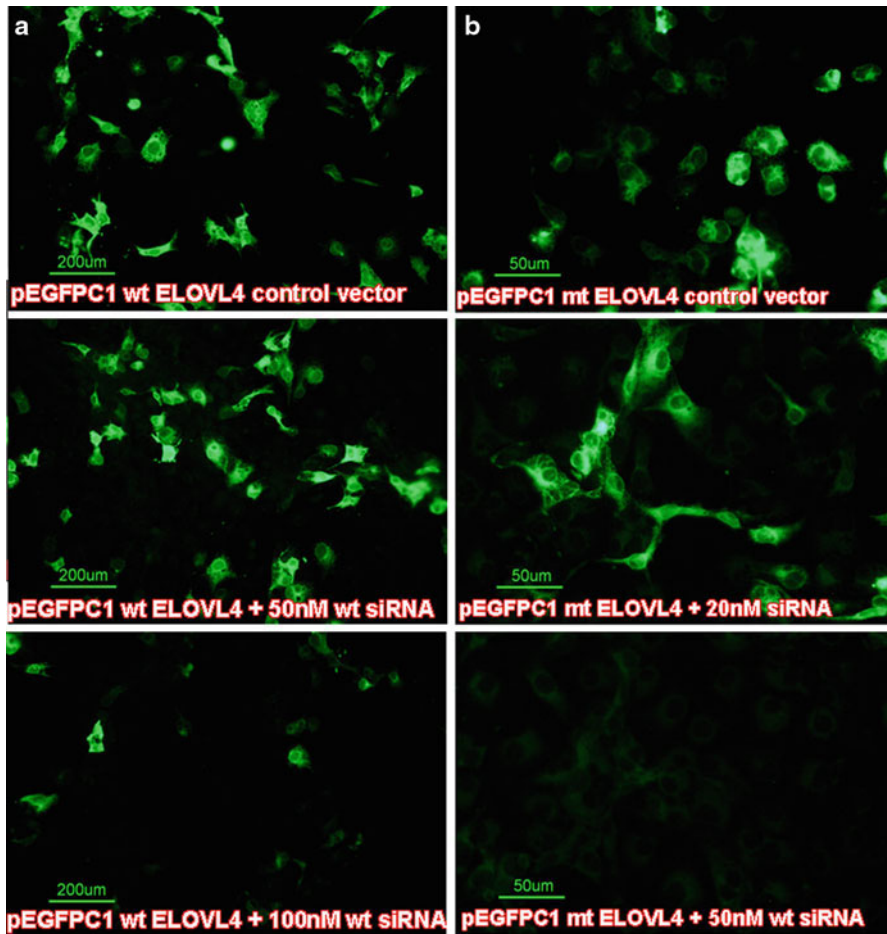


Fig. 30.1 Knockdown of human ELOVL4 protein expression. Expression of human ELOVL4 protein after cotransfection of Cos-7 cells with (a) vector expressing the wild-type *ELOVL4*-GFP fusion tag protein and an siRNA that targets the wild-type protein, (b) vector expressing mutant *ELOVL4*-GFP fusion tag along with siRNA that targets the mutant protein was done using immunocytochemistry analysis. The GFP fluorescence from GFP fusion protein expression is shown in green. The nuclei are stained using DAPI

presence of siRNA was evaluated by immunocytochemistry (Fig. 30.1). The ELOVL4 protein observed by the GFP fluorescence indicated a decrease in its expression in the presence of siRNA in a dose-dependent manner. Maximum silencing of wild-type ELOVL4 protein was achieved at a concentration of 100 nM (Fig. 30.1a).

Affect of the siRNA that targets the mutant ELOVL4 was also studied at 25 and 50 nM concentrations in cells expressing mutant ELOVL4-GFP fusion protein. Substantial decrease in the number of cells showing GFP fluorescence was observed

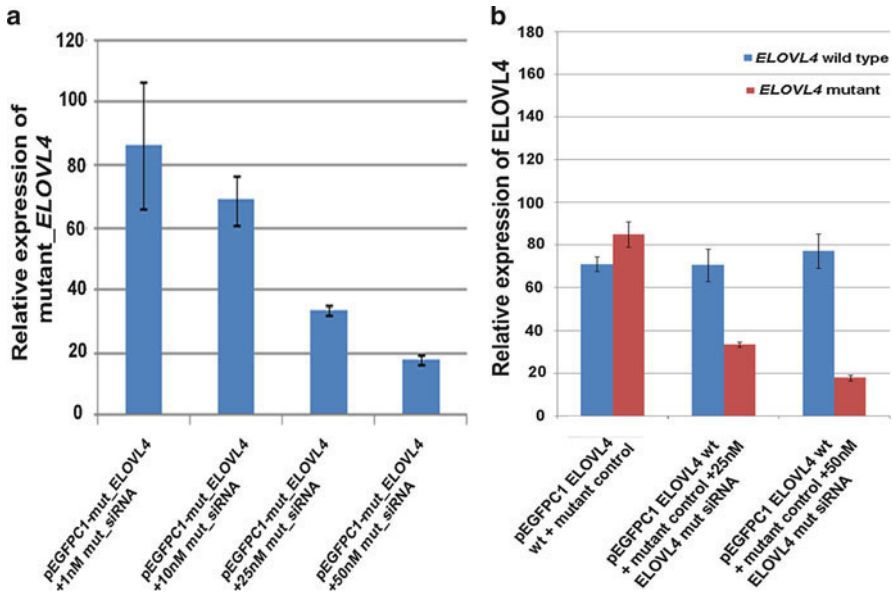


Fig. 30.2 Expression analysis of human *ELOVL4* transcripts in the presence of siRNA. (a) Quantitative RT-PCR analysis of human mutant *ELOVL4* transcript levels in Cos-7 cells, 48 h after cotransfection with vector expressing the human mutant *ELOVL4*-GFP fusion tag protein and different concentrations of siRNA that targets the mutant protein. (b) Quantitative expression levels of the wild type and mutant *ELOVL4* transcript when measured in cells transfected with vectors expressing wild-type *ELOVL4*-GFP tag and mutant *ELOVL4*-GFP tag protein and siRNA that targets the mutant *ELOVL4* at different concentrations

in the presence of siRNA (#1) at 25 nM concentration, where as very few cells with GFP expression were noted when siRNA was present at 50 nM concentration (Fig. 30.1b). Measurement of mutant *ELOVL4* transcript levels in these cells by qRT-PCR showed 70–80% reduction in its expression compared to that of control cells. These results indicate the specificity of the siRNA designed to target the mutant *ELOVL4* allele (Fig. 30.2a).

As STGD3 is a dominant disease, both the wild type and mutant alleles are coexpressed in these patients. Therefore, physiologically it is important to evaluate the affect of siRNA targeted to the mutant *ELOVL4* in cells coexpressing the wild type and mutant alleles. Cos-7 cells were cotransfected with separate constructs containing wild type or mutant *ELOVL4* and siRNA targeting the mutant allele. Evaluation of the expression of wild type and mutant *ELOVL4* mRNA in these cells by qRT-PCR showed dose-dependent decrease in the levels of mutant transcript while the levels of wild-type *ELOVL4* transcript remained unaltered. This demonstrates that the mutant *ELOVL4* siRNA specifically targets the mutant allele while sparing the wild-type *ELOVL4* allele (Fig. 30.2b).

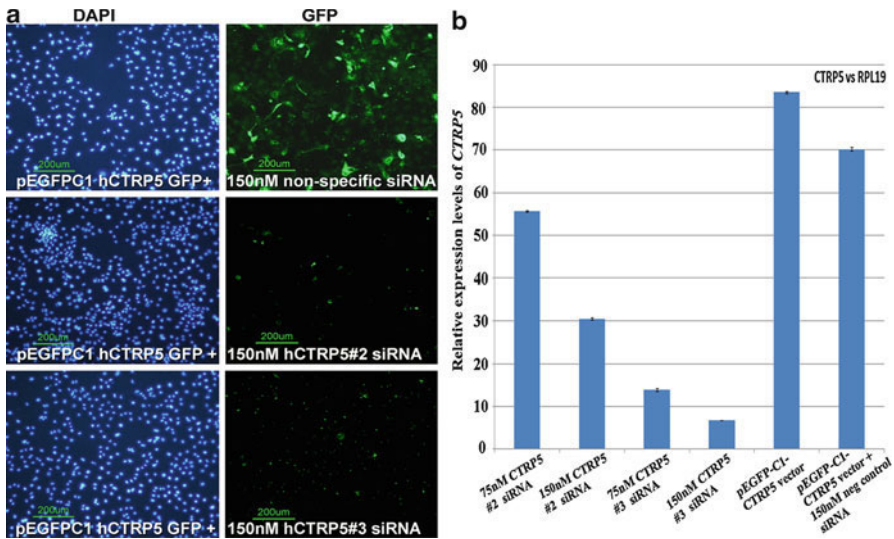


Fig. 30.3 Knockdown of human *CTRP5* mRNA and protein expression by small interfering RNA (*CTRP5*#4, *CTRP5*#5). (a) Expression of human *CTRP5* protein after cotransfection of both siRNA and *CTRP5*-GFP fusion tag constructs using immunocytochemistry analysis. The GFP fluorescence resulting from *CTRP5* expression is shown in green. The nuclei are stained using DAPI. (b) Quantitative RT-PCR analysis of human *CTRP5* mRNA levels in Cos-7 cells, 48 h after cotransfection of human *CTRP5*-GFP fusion tag expressing constructs with 75 and 150 nM concentrations of both the siRNA or a silence negative control siRNA (Ambion) (error bars, $n = 3$)

30.3.2 siRNA Mediated Knockdown of *CTRP5/Ctrp5*

Independent siRNA probes that target human or mouse *CTRP5* were designed and their affect was tested at 75 and 150 nM concentrations in Cos-7 cells expressing the *CTRP5* protein. Transfection efficiency of siRNA probes was monitored by using Cy3-tagged siRNA probes. Expression of *CTRP5* were studied by qRT-PCR and immunocytochemistry.

Immunofluorescence analysis of Cos-7 cells transfected with *CTRP5*-GFP fusion protein expressing construct and two siRNA probes (#4 and #5 in Fig. 30.3.1) showed dramatic decrease in the number of cells expressing *CTRP5* protein in presence of both the siRNA tested (Fig. 30.3a). The two siRNA probes that target the human wild-type *CTRP5* showed effective silencing (25–85%) of the wild-type transcript when measured by qRT-PCR (Fig. 30.3b). The nonspecific negative control siRNA did not affect the expression of *CTRP5* even at the highest concentration tested (150 nM (Fig. 30.3b)).

Another set of two siRNA probes (#2 and #3 in Fig. 30.4.1) designed to target the mouse wild-type *Ctrp5* showed near complete knockdown of the expression of *Ctrp5*-GFP fusion protein in Cos-7 cells at a concentration of 150 nM (Fig. 30.4a). Consistent with these observations, expression levels of *Ctrp5* transcript were found

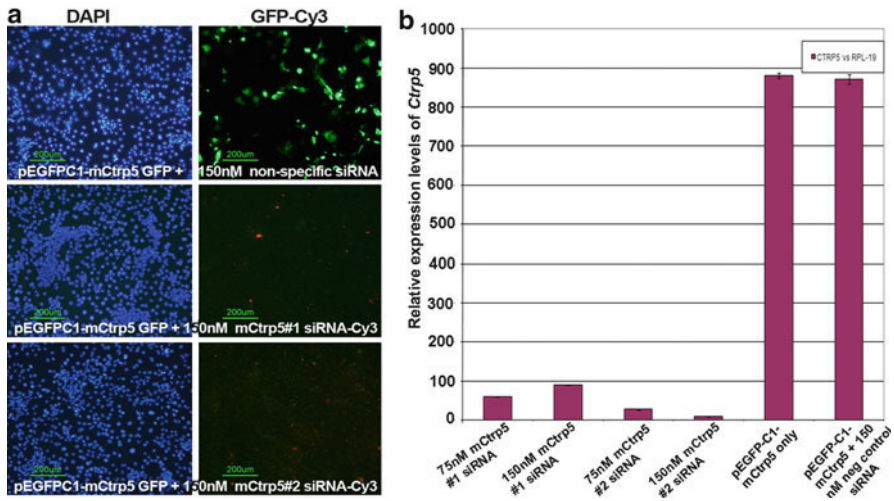


Fig. 30.4 Knockdown of mouse *Ctrp5* mRNA and protein expression by siRNA (*Ctrp5*#2, *Ctrp5*#3) in Cos-7 cells. (a) Expression analysis of mouse *Ctrp5* protein, 48 h after cotransfection of both siRNA (150 nM concentration) and *Ctrp5*-GFP fusion tag constructs using immunocytochemistry analysis. The GFP fluorescence resulting from *Ctrp5* expression is shown in green and Cy3 tag showing the localization of the siRNA in cells is shown in red. The nuclei are stained using DAPI. (b) Quantitative RT-PCR analysis of mouse *Ctrp5* mRNA levels in Cos-7 cells cotransfected with mouse *Ctrp5*-GFP fusion tag expressing constructs and siRNA with 75 and 150 nM concentrations of both the siRNA or a 150-nM concentration of silence negative control siRNA (Ambion) (error bars, $n=3$)

to be significantly low (~5%) compared to that in control cells (n). The negative control siRNA did not have any effect on the expression of the *Ctrp5* in the Cos7 cells. The siRNA probes designed to selectively knockdown the mutant *CTRP5/Ctrp5* alleles with S163R mutation were found to be ineffective (data not shown).

30.4 Discussion

Over the past decade, the development of genomic technologies enabled to effectively knockdown the expression of specific genes to understand their function. RNAi has been found to be a valuable tool for achieving gene silencing (Devi 2006). In this study, the siRNA probes that can effectively silence the expression of wild type and mutant *ELOVL4* and the wild-type *CTRP5/Ctrp5* genes, which are involved in causing two different forms of dominant macular degenerations (STGD3 and L-ORD) in humans, have been studied (Zhang et al. 2001; Hayward et al. 2003; Ayyagari et al. 2004).

Studies on *CTRP5* and *ELOVL4* genes demonstrated that the underlying mechanism of STGD3 and L-ORD due to mutations in these genes is likely to be due to

the dominant-negative effect exerted by the mutant proteins (Hayward et al. 2003; Vasireddy et al. 2005; Shu et al. 2006a, 2006b). The S163R mutant CTRP5 protein is reported to be secretion deficient, misfolded, retained within the endoplasmic reticulum (ER) causing ER stress (Mandal et al. 2006; Shu et al. 2006a). Impaired secretion of the mutant CTRP5 protein may underlie the pathophysiology of L-ORD (Mandal et al. 2006). Characterization of siRNA probes that selectively knockdown the expression of the *CTRP5* and *ELOVL4* genes have potential implications in developing new therapeutic strategies to treat L-ORD and STGD3.

To evaluate the therapeutic potential of the designed siRNA, it is important to experimentally test the efficacy of the siRNA in silencing the mutant transcript using in vivo models. A few mouse models showing STGD3 phenotype are known (Karan et al. 2005; Vasireddy et al. 2006, 2007). A knockin mouse model for STGD3 mouse with the 5 bp-deletion mutation in the heterozygous state developed late-onset retinal degeneration similar to the phenotype observed in STGD3 patients whereas the homozygous mice with 5 bp-mutation die within hours after their birth (Vasireddy et al. 2007). The *ELOVL4* has been shown to catalyze the steps involved in the elongation of long chain fatty acids (Agbaga et al. 2008). Mutations in this gene are predicted to affect its function in fatty acid chain elongation. The siRNA that targets the mutant *ELOVL4* may rescue the retinal phenotype by selective silencing of the expression of the mutant protein. Similarly, the siRNA that target the wild-type CTRP5 protein can thus be used to evaluate the function of CTRP5/ Ctrp5.

Both STGD3 and L-ORD are late-onset progressive degenerations that cause irreversible loss of vision. Genetic testing enables the presymptomatic diagnosis of individuals at risk to develop these diseases for administering therapies to delay or prevent the onset of disease. Ability to selectively silence the mutant transcript may facilitate development of effective therapies for these conditions. Our current studies demonstrating the efficacy of siRNA probes in silencing the expression of the *ELOVL4* and *CTRP5* genes are the first and important steps to establish such therapies. Additional evaluation of these probes and achieving stable silencing of these mutant proteins in vivo may offer promise in treating these conditions.

References

- Agbaga MP, Brush RS, Mandal MN et al (2008) Role of Stargardt-3 macular dystrophy protein (*ELOVL4*) in the biosynthesis of very long chain fatty acids. *Proc Natl Acad Sci USA* 105:12843–12848
- Ayyagari R, Mandal MA, Karoukis AJ et al (2004) Early-onset long anterior lens zonules and late-onset macular degeneration phenotype is caused by a CTRP5 gene mutation. *Invest Ophthalmol Vis Sci* 46:3363–3371
- Campbell M, Nguyen AT, Kiang AS et al (2009) An experimental platform for systemic drug delivery to the retina. *Proc Natl Acad Sci U S A* 106:17817–17822
- Chavali VR, Sommer JR, Petters RM et al (2010) Identification of a promoter for the human C1Q-tumor necrosis factor-related protein-5 gene associated with late-onset retinal degeneration. *Invest Ophthalmol Vis Sci* 51:5499–5507
- Devi GR (2006) siRNA-based approaches in cancer therapy. *Cancer Gene Ther* 13:819–829

- Hayward C, Shu X, Cideciyan AV et al (2003) Mutation in a short-chain collagen gene, *CTRP5*, results in extracellular deposit formation in late-onset retinal degeneration: a genetic model for age-related macular degeneration. *Hum Mol Genet* 12:2657–2667
- Karan G, Lillo C, Yang Z et al (2005) Lipofuscin accumulation, abnormal electrophysiology, and photoreceptor degeneration in mutant *ELOVL4* transgenic mice: a model for macular degeneration. *Proc Natl Acad Sci U S A* 102:4164–4169
- Mandal MN, Vasireddy V, Reddy GB et al (2006) *CTRP5* is a membrane-associated and secretory protein in the RPE and ciliary body and the S163R mutation of *CTRP5* impairs its secretion. *Invest Ophthalmol Vis Sci* 47:5505–5513
- Maugeri A, Meire F, Hoyng CB et al (2004) A novel mutation in the *ELOVL4* gene causes autosomal dominant Stargardt-like macular dystrophy. *Invest Ophthalmol Vis Sci* 45:4263–4267
- Raz-Prag D, Ayyagari R, Fariss RN et al (2006) Haploinsufficiency is not the key mechanism of pathogenesis in a heterozygous *Elovl4* knockout mouse model of STGD3 disease. *Invest Ophthalmol Vis Sci* 47:3603–3611
- RetNet In: <http://www.sph.uth.tmc.edu/Retnet/>
- Shu X, Tulloch B, Lennon A et al (2006a) Disease mechanisms in late-onset retinal macular degeneration associated with mutation in *C1QTNF5*. *Hum Mol Genet* 15:1680–1689
- Shu X, Tulloch B, Lennon A et al (2006b) Biochemical characterisation of the *C1QTNF5* gene associated with late-onset retinal degeneration. A genetic model of age-related macular degeneration. *Adv Exp Med Biol* 572:41–48
- Vasireddy V, Wong P, Ayyagari R (2010) Genetics and molecular pathology of Stargardt-like macular degeneration. *Prog Retin Eye Res* 29(3):191–207
- Vasireddy V, Vijayarathy C, Huang J et al (2005) Stargardt-like macular dystrophy protein *ELOVL4* exerts a dominant negative effect by recruiting wild-type protein into aggregates. *Mol Vis* 11:665–676
- Vasireddy V, Jablonski MM, Mandal MN et al (2006) *Elovl4* 5-bp-deletion knock-in mice develop progressive photoreceptor degeneration. *Invest Ophthalmol Vis Sci* 47:4558–4568
- Vasireddy V, Uchida Y, Salem N, Jr. et al (2007) Loss of functional *ELOVL4* depletes very long-chain fatty acids (> or = C28) and the unique omega-O-acylceramides in skin leading to neonatal death. *Hum Mol Genet* 16:471–482
- Zhang K, Kniazeva M, Han M et al (2001) A 5-bp deletion in *ELOVL4* is associated with two related forms of autosomal dominant macular dystrophy. *Nat Genet* 27:89–93

Chapter 31

Gene Therapy Strategies for Usher Syndrome Type 1B

David S. Williams and Vanda S. Lopes

Keywords Adeno-associated virus • Gene therapy • Lentivirus • Melanosome • *MYO7A* • Photoreceptor • Opsin • Retinal pigment epithelium • Usher syndrome

31.1 Introduction

Usher syndrome type 1 is characterized by profound congenital deafness, followed by progressive retinal degeneration. Usher syndrome type 1B (Usher 1B) accounts for about half of all cases of Usher 1 (Astuto et al. 2000; Bharadwaj et al. 2000; Ouyang et al. 2005), and is caused by mutations in the *MYO7A* gene, which encodes an unconventional myosin (Weil et al. 1995).

Use of cochlear implants to treat the deafness of Usher 1 patients is now quite common. Infants who receive these implants become well integrated into the speaking community and most are able to attend mainstream schools (Blanchet et al. 2007; Liu et al. 2008). There is currently no treatment for their ensuing retinal degeneration; however, Usher 1B appears to be quite suitable for gene therapy, involving the addition of a wild-type gene. First, inheritance of Usher 1B is recessive, suggesting that it results from loss of *MYO7A* function. Studies on *Myo7a*-mutant mice support this conclusion. Second, because of their congenital deafness, Usher 1 patients are often identified genetically early in life, before the onset of any retinal degeneration. In addition to the loss of photoreceptor cells, many cases of retinal degenerations involve remodeling of the inner retina, which may be irreversible (Jones and Marc 2005), so early application of gene therapy is important. In this short review, we discuss gene therapy strategies that use different viruses for delivering *MYO7A* to the retina in order to prevent blindness.

D.S. Williams (✉) • V.S. Lopes
Departments of Ophthalmology and Neurobiology, UCLA School of Medicine,
Los Angeles, CA 90095, USA
e-mail: dswilliams@ucla.edu

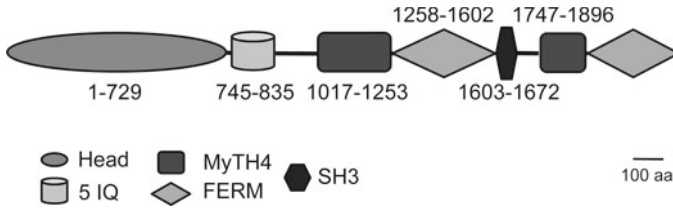


Fig. 31.1 Schematic representation of the domain structure MYO7A. *IQ* isoleucine-glutamine motif; *MyTH4* myosin tail homology 4; *FERM* band4.1, ezrin, radixin, and moesin; *SH3* Scr homology 3 domain

31.2 MYO7A Gene

The *MYO7A* gene is over 100 kb, with a coding region of just under 7 kb (Chen et al. 1996; Weil et al. 1996; Kelley et al. 1997; Levy et al. 1997). It encodes a protein that contains a myosin motor head, a lever arm, a putative coiled coil, and a tail (Fig. 31.1). The lever arm binds light chains, including calmodulin (Udovichenko et al. 2002), and the tail domain contains a repeat of MyTH4 and FERM domains (Chen et al. 1996; Weil et al. 1996). Mutations causing Usher 1 have been identified all along the *MYO7A* sequence. They include missense mutations in the motor domain (Weston et al. 1996), the first MyTH4 domain (Cuevas et al. 1999; Bharadwaj et al. 2000), the first FERM domain (Janecke et al. 1999), the second MyTH4 domain (Bharadwaj et al. 2000), and the second FERM domain (Bharadwaj et al. 2000; Jacobson et al. 2009), suggesting that the entire cDNA (and not a “minigene” version) is required for successful therapy.

Most of retinal *MYO7A* is present in the retinal pigment epithelium (RPE), as first shown by immunofluorescence studies of rat retina (Hasson et al. 1995). El-Amraoui reported the protein to be present also in the photoreceptor cells of amphibians, birds, and primates, although they failed to detect it in rodent retinas (El-Amraoui et al. 1996). Subsequent immunoelectron microscopy (Liu et al. 1997) and phenotype studies of *Myo7a*-mutant mice (see below) (Liu et al. 1999) indicated that *MYO7A* is located and functions in the region of the photoreceptor connecting cilium (Williams 2008).

Two main isoforms of *MYO7A* were detected in a human retinal cDNA library. They differed by the presence or absence of a 114-bp segment corresponding to the 5' end of exon 34 (Weil et al. 1996). However, quantitative analysis of the expression of these two isoforms has determined that a significant level of only the shorter isoform is expressed in both the photoreceptor and RPE cells (unpublished results), indicating that delivery of a cDNA encoding just the shorter isoform should be sufficient for gene therapy.

31.3 *Myo7a*-Mutant Mice

Mice possessing mutations in *Myo7a*, the orthologue of the Usher 1B gene, have been described (Gibson et al. 1995). There are a variety of alleles, at least one of which, the shaker1^{4626SB}, is a null allele (Hasson et al. 1997; Liu et al. 1999). *Myo7a*-mutant mice are deaf and have vestibular dysfunction (Holme and Steel 2002), like Usher 1B patients, but none of the alleles appears to undergo retinal degeneration (Lillo et al. 2003). Nevertheless, mutant phenotypes have been identified in both the RPE and photoreceptor cells (Fig. 31.2). In the RPE, melanosomes are mislocalized and possess aberrant motility (Liu et al. 1998; Gibbs et al. 2004; Lopes et al. 2007). Phagosomes are also mislocalized and digested more slowly (Gibbs et al. 2003). In the photoreceptor cells, the concentration of opsin is increased in the connecting cilium, suggesting defective transport to the base of the outer segment and/or a breakdown in a distal ciliary diffusion barrier (Liu et al. 1999). These mutant phenotypes represent amenable assays to test for the presence of functional protein, and so can be used in experiments testing the efficacy of gene therapy with *Myo7a*-mutant mice.

The localization of MYO7A in the RPE and photoreceptor cells, together with the presence of phenotypes in the RPE and photoreceptor cells of *Myo7a*-mutant mice, suggests that both the RPE and photoreceptor cells would need to be transduced with wild-type *MYO7A* for successful retinal gene therapy. This suggestion is supported by a study of mice that contained mosaics of MYO7A-positive and MYO7A-null cells in their tissues. In these mice, the photoreceptor phenotype was demonstrated to be cell autonomous and not secondary to lack of MYO7A in the adjacent RPE (Jacobson et al. 2008).

31.4 Lentivirus-Mediated Gene Therapy

The first experiments to test for efficacious *MYO7A* gene therapy used an HIV-1-derived lentivirus to carry *MYO7A* cDNA following injection into the subretinal space of *Myo7a*-null mice (Hashimoto et al. 2007). The smaller of the two main isoforms (lacking the 114-bp segment) was used. *MYO7A*, driven by a chimeric promoter, containing an element each from the *CMV* and native *MYO7A* promoters, was thus found to be expressed in the RPE cells. No significant levels of MYO7A were detected in the photoreceptor cells; however, a small and sufficient amount was deemed to be present, for corrected phenotypes were evident in both the RPE and photoreceptor cells in the region of the injection. As might be expected for a virus that can integrate into the chromosomes at different sites (Bushman 2003; Mitchell et al. 2004), the resulting levels of MYO7A varied among different RPE cells, and cells that had a mean level that was 65% lower than wildtype still possessed mislocalized melanosomes (Hashimoto et al. 2007). More recently, this study has been repeated using a lentivirus derived from equine infectious anemia virus

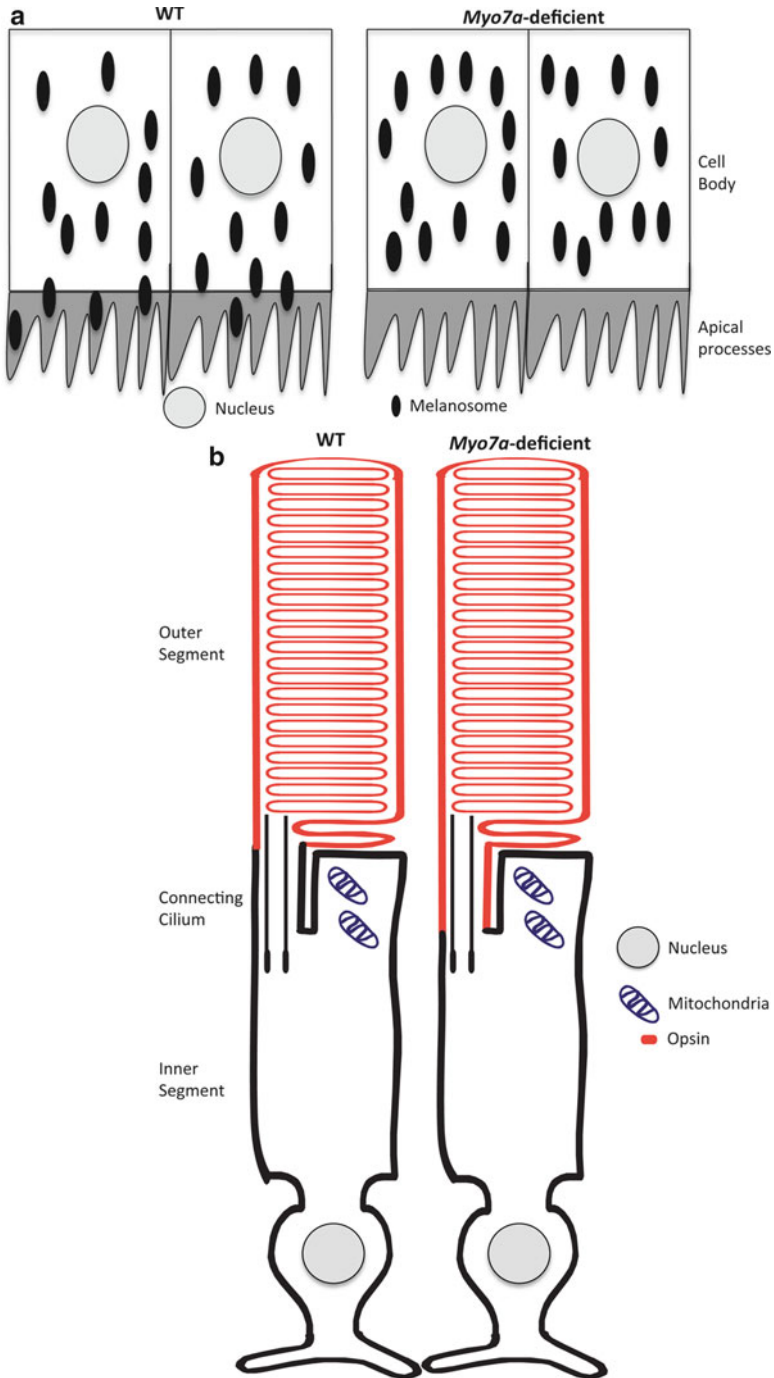


Fig. 31.2 Schematic representation of two mutant phenotypes present in the retinas of *Myo7a*-deficient mice. **(a)** Melanosomes are absent from the apical region of the RPE (Liu et al. 1998). **(b)** The concentration of opsin is increased in the connecting cilium (Liu et al. 1999)

(EIAV) and the same *CMV-MYO7A* promoter. In this case, higher titers of virus have been obtained, and, following injection, *MYO7A* has been detected at wild-type levels in the photoreceptor connecting cilium, as well as in the RPE cells (unpublished results).

To obviate variable expression among transduced cells, as well as the possibility of undesirable insertional mutagenesis, an approach is to use an integration-deficient lentivirus (Yanez-Munoz et al. 2006). Mature RPE and photoreceptor cells do not divide, so that integration is not required to maintain the introduced gene. Preliminary results suggest that comparable titers of integration-proficient and integration-deficient HIV-1-based lentivirus, carrying *MYO7A*, as above, correct mutant phenotypes the RPE and photoreceptor cells with similar efficacy.

31.5 AAV-Mediated Gene Therapy

In one of the most successful clinical applications of gene therapy so far, an adeno-associated virus (AAV) has been used to deliver *RPE65* cDNA to the RPE, and thus improve the vision of patients with Leber's congenital amaurosis (LCA), caused by *RPE65* mutations (Bainbridge et al. 2008; Cideciyan et al. 2008; Hauswirth et al. 2008; Maguire et al. 2008). However, AAV was considered to be inappropriate for delivering *MYO7A* cDNA, as it is 1–2 kb larger than the reported carrying capacity of AAV (Grieger and Samulski 2005). Nevertheless, we tested whether an AAV5 vector, containing *MYO7A* cDNA under a *CMV* promoter, could effect *MYO7A* expression in primary cultures of RPE cells from *Myo7a*-null mice. Transduction and *MYO7A* expression was indicated by the detection of *MYO7A* protein on western blots (Fig. 3 in Allocca et al. 2008).

Recent studies (Dong et al. 2010; Lai et al. 2010; Wu et al. 2010) have found that genomes larger than 5 kb are only partially packaged by AAV, resulting in fragments of the larger genomes, none of which is larger than 5 kb, consistent with earlier studies on AAV packaging limits (Grieger and Samulski 2005). However, these recent studies also demonstrate that, following infection, the fragments can be reassembled into transgenes that are larger than the capsid packaging limit, thus explaining the ability of an AAV vector to deliver *MYO7A* cDNA.

The ability of AAV2 and AAV5 vectors to deliver *MYO7A* to the RPE and photoreceptors of *Myo7a*-mutant mice has now been tested. A ubiquitous promoter, CBA (chicken beta-actin), was used. *MYO7A* was detected in the RPE and photoreceptor connecting cilium at levels that were comparable in proportion to that found in wild-type retinas. The levels were related to the amount of virus that was injected, with the highest concentration of virus resulting in levels that were ~2-fold higher than wild-type levels. Correction of the RPE and photoreceptor cell phenotypes, without any pathological effects, was observed over a range of virus concentrations and consequential *MYO7A* levels (unpublished results).

31.6 Conclusion: The Best Strategy for Usher 1B Gene Therapy?

MYO7A gene therapy can be achieved using either lentiviral or AAV vectors. Transduction of photoreceptor cells by lentiviruses has been reported to be rather inefficient (Kostic et al. 2003; Gruter et al. 2005). However, in the case of retinal *MYO7A*, of which only 2–3% is in the photoreceptors and the remainder in the RPE, relatively poor transduction of photoreceptor cells seems to be acceptable, and may in fact be desirable when using ubiquitous promoters. Expression level was also not a problem with AAV2 or AAV5 delivery of *MYO7A*. Episomal *MYO7A* has an advantage over integrating DNA, so that an integration-deficient lentivirus or AAV would be a preferred vector on that basis. A perceived disadvantage of the AAV vectors may be that the partial packaging results in DNA fragments whose precise nature is unknown. Even though the fragments have been found to reassemble into functional *MYO7A*, it may be preferable to design a strategy whereby the fragments are preconstructed.

Acknowledgments We are grateful to Drs. Samuel Jacobson, Bill Hauswirth, Katie Binley, Xian-Jie Yang, and their respective laboratories for discussions and collaborative research. We are supported by grants from the NIH and NNRI. DSW is a Jules and Doris Stein RPB Professor.

References

- Allocca M, Doria M, Petrillo M et al (2008) Serotype-dependent packaging of large genes in adeno-associated viral vectors results in effective gene delivery in mice. *J Clin Invest* 118: 1955–64
- Astuto LM, Weston MD, Carney CA et al (2000) Genetic heterogeneity of Usher syndrome: analysis of 151 families with Usher type I. *Am J Hum Genet* 67: 1569–74
- Bainbridge JW, Smith AJ, Barker SS et al (2008) Effect of gene therapy on visual function in Leber's congenital amaurosis. *N Engl J Med* 358: 2231–9
- Bharadwaj AK, Kaszlejna JP, Huq S et al (2000) Evaluation of the myosin VIIA gene and visual function in patients with Usher syndrome type I. *Exp Eye Res* 71: 173–81
- Blanchet C, Roux AF, Hamel C et al (2007) [Usher type I syndrome in children: genotype/phenotype correlation and cochlear implant benefits]. *Rev Laryngol Otol Rhinol (Bord)* 128: 137–43
- Bushman F D (2003) Targeting survival: integration site selection by retroviruses and LTR-retrotransposons. *Cell* 115: 135–8
- Chen ZY, Hasson T, Kelley PM et al (1996) Molecular cloning and domain structure of human myosin-VIIa, the gene product defective in Usher syndrome 1B. *Genomics* 36: 440–448
- Cideciyan AV, Aleman TS, Boye SL et al (2008) Human gene therapy for RPE65 isomerase deficiency activates the retinoid cycle of vision but with slow rod kinetics. *Proc Natl Acad Sci U S A* 105: 15112–7
- Cuevas JM, Espin SC, Millan JM et al (1999) Identification of three novel mutations in the *MYO7A* gene. *Hum Mutat* 14: 181
- Dong B, Nakai H, Xiao W (2010) Characterization of genome integrity for oversized recombinant AAV vector. *Mol Ther* 18: 87–92
- El-Amraoui A, Sahly I, Picaud S et al (1996) Human Usher 1B/mouse shaker-1: the retinal phenotype discrepancy explained by the presence/absence of myosin VIIA in the photoreceptor cells. *Hum Mol Genet* 5: 1171–8

- Gibbs D, Azarian SM, Lillo C et al (2004) Role of myosin VIIa and Rab27a in the motility and localization of RPE melanosomes. *J Cell Sci* 117: 6473–83
- Gibbs D, Kitamoto J, Williams DS (2003) Abnormal phagocytosis by retinal pigmented epithelium that lacks myosin VIIa, the Usher syndrome 1B protein. *Proc Natl Acad Sci U S A* 100: 6481–86
- Gibson F, Walsh J, Mburu P et al (1995) A type VII myosin encoded by mouse deafness gene shaker-1. *Nature* 374: 62–64
- Grieger JC, Samulski RJ (2005) Packaging capacity of adeno-associated virus serotypes: impact of larger genomes on infectivity and postentry steps. *J Virol* 79: 9933–44
- Gruter O, Kostic C, Crippa SV et al (2005) Lentiviral vector-mediated gene transfer in adult mouse photoreceptors is impaired by the presence of a physical barrier. *Gene Ther* 12: 942–7
- Hashimoto T, Gibbs D, Lillo C et al (2007) Lentiviral gene replacement therapy of retinas in a mouse model for Usher syndrome type 1B. *Gene Ther* 14: 584–94
- Hasson T, Heintzelman MB, Santos-Sacchi J et al (1995) Expression in cochlea and retina of myosin VIIa, the gene product defective in Usher syndrome type 1B. *Proc. Natl. Acad. Sci. USA* 92: 9815–19
- Hasson T, Walsh J, Cable J et al (1997) Effects of shaker-1 mutations on myosin-VIIa protein and mRNA expression. *Cell Motility and the Cytoskeleton* 37: 127–38
- Hauswirth WW, Aleman TS, Kaushal S et al (2008) Treatment of leber congenital amaurosis due to RPE65 mutations by ocular subretinal injection of adeno-associated virus gene vector: short-term results of a phase I trial. *Hum Gene Ther* 19: 979–90
- Holme RH and Steel KP (2002) Stereocilia defects in waltzer (Cdh23), shaker1 (Myo7a) and double waltzer/shaker1 mutant mice. *Hear Res* 169: 13–23
- Jacobson SG, Aleman TS, Sumaroka A et al (2009) Disease boundaries in the retina of patients with Usher syndrome caused by MYO7A gene mutations. *Invest Ophthalmol Vis Sci* 50: 1886–94
- Jacobson SG, Cideciyan AV, Aleman TS et al (2008) Usher syndromes due to MYO7A, PCDH15, USH2A or GPR98 mutations share retinal disease mechanism. *Hum Mol Genet* 17: 2405–15
- Janecke AR, Meins M, Sadeghi M et al (1999) Twelve novel myosin VIIA mutations in 34 patients with Usher syndrome type I: confirmation of genetic heterogeneity. *Hum Mutat* 13: 133–40
- Jones, BW and Marc RE (2005) Retinal remodeling during retinal degeneration. *Exp Eye Res* 81: 123–37
- Kelley PM, Weston MD, Chen ZY et al (1997) The genomic structure of the gene defective in Usher syndrome type 1b (MYO7A). *Genomics* 40: 73–9
- Kostic C, Chiodini F, Salmon P et al (2003) Activity analysis of housekeeping promoters using self-inactivating lentiviral vector delivery into the mouse retina. *Gene Ther* 10: 818–21
- Lai Y, Yue Y, Duan D (2010) Evidence for the failure of adeno-associated virus serotype 5 to package a viral genome ≥ 8.2 kb. *Mol Ther* 18: 75–9
- Levy G, Levi-Acobas F, Blanchard S et al (1997) Myosin VIIA gene: heterogeneity of the mutations responsible for Usher syndrome type 1B. *Hum Mol Genet* 6: 111–6
- Lillo C, Kitamoto J, Liu X et al (2003) Mouse models for Usher syndrome 1B. *Adv Exp Med Biol* 533: 143–150
- Liu X, Ondek B, Williams DS (1998) Mutant myosin VIIa causes defective melanosome distribution in the RPE of shaker-1 mice. *Nat. Genet.* 19: 117–118
- Liu X, Udovichenko IP, Brown SDM et al (1999) Myosin VIIa participates in opsin transport through the photoreceptor cilium. *J. Neurosci.* 19: 6267–6274
- Liu X, Vansant G, Udovichenko IP et al (1997) Myosin VIIa, the product of the Usher 1B syndrome gene, is concentrated in the connecting cilia of photoreceptor cells. *Cell Motil. Cytoskel.* 37: 240–252
- Liu XZ, Angeli SI, Rajput K et al (2008) Cochlear implantation in individuals with Usher type 1 syndrome. *Int J Pediatr Otorhinolaryngol* 72: 841–7
- Lopes VS, Ramalho JS, Owen DM et al (2007) The ternary Rab27a-Myrip-Myosin VIIa complex regulates melanosome motility in the retinal pigment epithelium. *Traffic* 8: 486–99
- Maguire AM, Simonelli F, Pierce EA et al (2008) Safety and efficacy of gene transfer for Leber's congenital amaurosis. *N Engl J Med* 358: 2240–8

- Mitchell RS, Beitzel BF, Schroder AR et al (2004) Retroviral DNA integration: ASLV, HIV, and MLV show distinct target site preferences. *PLoS Biol* 2: E234
- Ouyang XM, Yan D, Du LL et al (2005) Characterization of Usher syndrome type I gene mutations in an Usher syndrome patient population. *Hum Genet* 116: 292–9
- Udovichenko IP, Gibbs D, Williams DS (2002) Actin-based motor properties of native myosin VIIa. *J Cell Sci* 115: 445–450
- Weil D, Blanchard S, Kaplan J et al (1995) Defective myosin VIIA gene responsible for Usher syndrome type 1B. *Nature* 374: 60–61
- Weil D, Levy G, Sahly I et al (1996) Human myosin VIIA responsible for the Usher 1B syndrome: a predicted membrane-associated motor protein expressed in developing sensory epithelia. *Proc Natl Acad Sci U S A* 93: 3232–3237.
- Weston MD, Kelley PM, Overbeck LD et al (1996) Myosin VIIA mutation screening in 189 Usher syndrome type 1 patients. *Am J Hum Genet* 59: 1074–83
- Williams DS (2008) Usher syndrome: Animal models, retinal function of Usher proteins, and prospects for gene therapy. *Vision Res* 48: 433–41
- Wu Z, Yang H, Colosi P (2010) Effect of genome size on AAV vector packaging. *Mol Ther* 18: 80–6
- Yanez-Munoz RJ, Balaggan KS, MacNeil A et al (2006) Effective gene therapy with nonintegrating lentiviral vectors. *Nat Med* 12: 348–53

Part IV
Blood Vessels, Angiogenesis, and
Neovascularization

Chapter 32

Neovascularization: Ocular Diseases, Animal Models and Therapies

Xue Cai, Steven A. Sezate, and James F. McGinnis

Keywords Neovascularization • Nanoceria • Ocular diseases • Animal models • Nanoparticles • Reactive oxygen species • Diabetic retinopathy • Age-related macular degeneration • Retinopathy of prematurity • VEGF • PEDF • CNV • RNV • *Vldlr*

32.1 Introduction

Exudative (“wet” form) age-related macular degeneration (AMD), retinopathy of prematurity (ROP), and diabetic retinopathy (DR) are severe diseases and the leading causes of blindness affecting all age groups. The common characteristics of these neovascular diseases include abnormal new blood vessels in the eye, which form choroidal neovascularizations (CNV) or retinal neovascularizations (RNV). Documented data demonstrated that angiogenic and angiostatic factors such as vascular endothelial growth factor (VEGF) and pigment epithelium derived factor (PEDF) respectively, play pivotal roles in the pathogenesis of ocular neovascularization (Bird 2010; Sapiaha et al. 2010).

X. Cai • S.A. Sezate

Department of Ophthalmology, Dean McGee Eye Institute, University of Oklahoma Health Sciences Center, Oklahoma City, OK 73104, USA

J.F. McGinnis (✉)

Department of Ophthalmology, Dean McGee Eye Institute, University of Oklahoma Health Sciences Center, Oklahoma City, OK 73104, USA

Department of Cell Biology, University of Oklahoma Health Sciences Center, Oklahoma City, OK 73104, USA

Oklahoma Center for Neuroscience, University of Oklahoma Health Sciences Center, Oklahoma City, OK 73104, USA
e-mail: james-mcginnis@ouhsc.edu

32.2 Neovascular Ocular Diseases

32.2.1 Age-Related Macular Degeneration

AMD is the leading cause of blindness among adults in developed countries. It is characterized by subretinal deposits (drusen) with or without evidence of damage to underlying RPE (retinal pigment epithelium). AMD which involves CNV is categorized as “wet” or neovascular AMD in contrast to “dry” AMD. The actual cause of this disease is unknown but is multifactorial in nature with variable phenotypes, rates of progression, and involvement of environmental factors (Edwards and Malek 2007).

32.2.2 Retinopathy of Prematurity

ROP, or oxygen induced retinopathy (OIR), is the most prevalent ocular disease seen in the neonate, and is the dominant cause of severe visual disorders in childhood in the Western world. It is characterized by retardation of the development of the normal retinal vascular system due to microvascular degeneration. Subsequently, ischemia and retinal hypoxia result in excessive neovascularization and development as compensatory blood vessels which eventually lead to fibrous scars and retinal detachment (Gibson et al. 1989).

32.2.3 Diabetic Retinopathy

DR, another leading cause of blindness in industrialized countries, is characterized by formation of defective retinal microvessels which subsequently lead to leakage of blood through the blood-retinal barrier into the eye and loss of vision. Accumulating evidence suggests that a primary cause of DR is chronic inflammation although many other factors such as erythropoietin (EPO), renin-angiotensin, oxidative stress, insulin receptor signaling, etc., are associated with DR (Cheung et al. 2010).

32.3 Animal Models

The animal models for neovascular diseases are either naturally occurring, generated by expression of transgenes, or are laser/chemical-induced (Grossniklaus et al. 2010). Because of the multiple characteristics of these diseases, there is no perfect model which includes all of the complications.

32.3.1 *Choroidal Neovascularization*

The CNV animal models for wet AMD are induced by laser photocoagulation, which disrupts Bruch's membrane (BM) resulting in the development of CNV within 2–3 weeks. This model is currently popular and used in many laboratories but the variable rate of CNV and transient CNV leakage are major disadvantages of this animal model (Tobe et al. 1998).

32.3.2 *Vldlr*

Mutation in the very low density lipoprotein receptor (*Vldlr*) gene causes a distinct form of AMD called RAP (retinal angiomatous proliferation). In the mouse model, new blood vessels originate from the outer plexiform layer at postnatal day (P) 13–14, pass through the outer nuclear layer, invade the subretinal space and choroid, and cause RPE disruption, BM exposure and photoreceptor degeneration with significant fibrosis (Dorrell et al. 2009, Hu et al. 2008). Decreased mRNA levels of rhodopsin and cone-opsin were detected around 2 months of age, but retinal degeneration and ERG reduction occur at 6 months of age (Dorrell et al. 2009).

32.3.3 *Vascular Endothelial Growth Factor*

The transgenic CNV model mimicking DR and AMD was generated by introducing human VEGF₁₆₅ (AAV-hVEGF₁₆₅) into the mice. CNV leakage was detected in these mice at 2 months of age and persisted for more than 20 months (Lai et al. 2005a). Using the reverse tetracycline transactivator (rtTA) inducible promoter system to control the time of VEGF expression in the transgenic mice resulted in prominent VEGF expression, rapid neovascularization within 3–4 days, and severe retinal damage (Ohno-Matsui et al. 2002).

32.3.4 *Ins2^{Akita}*

The spontaneously occurring Akita (*Ins2^{Akita+/-}*) mouse represents the early stage of DR (type I diabetes). A point mutation in the *Insulin 2* gene causes the rapid onset of hyperglycemia and hypoinsulinemia, detectable at 4 weeks (Yoshioka et al. 1997). After the onset of hyperglycemia, increases occur in retinal vascular permeability by 8 weeks, more acellular capillaries and leukocytes are seen about 31–36 weeks and thinning of the inner nuclear layer, inner plexiform layer and ganglion cell loss are noticeable after 22 weeks (Barber et al. 2005). These changes and their effects are similar to those found in toxin-induced animal models for DR.

32.3.5 *Ins2^{Akita}VEGF*

The Akimba (*Ins2^{Akita}VEGF^{+/-}*) mouse was generated by crossing the Akita mouse (Yoshioka et al. 1997) with Kimba (*VEGF^{+/+}*) mouse (Lai et al. 2005a). The Akimba mice retain the key characteristics of the parents; RNV and hyperglycemia by 8 weeks of age and enhanced photoreceptor cell loss, thinning of the retina, neovascularization, fibroses and edema by 25 weeks of age (Rokoczy et al. 2010).

32.3.6 *Oxygen Induced Retinopathy*

The ROP rodent model is induced by exposing the newborn rodent to 75–80% oxygen for the first 5–10 days followed by recovery in room air for 5–15 days. The high oxygen inhibits angiogenesis and promotes retinal avascularity which, when exposed to normoxia, actually produces hypoxia, disregulated angiogenesis and delicate, porous vessels which grow through the retina into the vitreous. These neovessels then can leak blood and/or produce retinal detachment and loss of vision (Ricci 1990).

32.4 Therapeutic Treatment of Ocular Neovascular Diseases

Imbalance of growth factors (e.g., VEGF which stimulates growth and PEDF which suppresses growth) has been implicated in the growth of excessive blood vessels (Bird 2010). It is critical when treating ocular neovascular diseases that only the newly formed pathological blood vessels be targeted without affecting the existing vessels. One strategy is to suppress ocular NV by inhibiting VEGF levels without causing pathogenesis (Bird 2010; Sapienza et al. 2010). Anti-VEGF therapy has promising clinical benefits, but the effect is temporary and requires frequent intravitreal injections (Bird 2010) because multiple redundant signaling pathways exist (Friedlander 2009). Also, efficacy and safety over long time periods have not been demonstrated.

32.4.1 *Targeting Pathology and Angiogenic Pathways*

Antiangiogenic drugs such as Lodamin, and carboxyamidotriazole, or nerve growth factor receptor inhibitor K252a significantly regressed or inhibited the ocular NV in laser-induced CNV (Benny et al. 2010; Afzal et al. 2010) and OIR in mice (Liu et al. 2010). TM601, by targeting annexin 2, regressed ocular NV and reduced ocular leakage (Lima e Silva et al. 2010). Blockage of CCR3 (eosinophil/mass cell

chemokine receptor) which is specifically expressed in CNV endothelial cells of AMD patients or its ligand, eotaxin, inhibited CNV in injury-induced CNV mice. This strategy has proven more effective than VEGF-A neutralization (Takeda et al. 2009). Sphingosine-1-phosphate is a bioactive lipid molecule which stimulates angiogenesis. A monoclonal antibody against it, Sonopcizumab, significantly suppressed RNV in OIR mice and reduced the leakage in laser-induced CNV mice (Xie et al. 2009). siRNA targeting of EPO significantly reduced its expression and RNV in OIR mice (Xiong et al. 2009).

32.4.2 Targeting VEGF-Dependent Pathway

The helper-dependent adenovirus (HD-Ad) vector, expressing a soluble form of the VEGF receptor (sFlt-1) in a constitutive (HD-Ad/CMV-sFlt-1) or doxycycline (dox)-inducible (HD-Ad/S-M2/CMV-sFlt-1) manner, inhibited RNV by more than 60% in OIR rats (Lamartina et al. 2007). AAV-mediated gene delivery (AAV-sFlt) to laser-induced CNV in mice and monkeys leads to sustained sFlt expression and regression of CNV for 7 months (mice) and 18 months (monkeys). The photoreceptor population and retinal function were retained (Lai et al. 2005b). Similarly, AAV2-sFLT01 inhibition of angiogenesis in OIR mice up to 12 month was reported (Pechan et al. 2009). A siRNA-expressing vector targeting either human HIF-1 α (hypoxia inducible factor-1 alpha) or human VEGF₁₆₅ or targeting both resulted in downregulating target gene expression in OIR mice and thereby decreased RNV (Jiang et al. 2009). The Wnt pathway inhibitor DKK1 was shown to attenuate RNV and blood vessel leakage in streptozotocin (STZ)-induced diabetic and OIR rats (Chen et al. 2009). Recently, a combination of angiostatic therapies targeting multiple angiogenic pathways was experimentally proven to achieve a more profound inhibition of neovascularization than blocking of a single pathway in OIR (Friedlander 2009).

32.4.3 Nanomedicine

Nanomedicine has primarily involved the application of nanotechnology to deliver drugs, therapeutic genes, and peptides to inhibit neovascularization and prevent retinal cell apoptosis (Ellis-Behnke and Jonas 2011). Cerium oxide nanoparticles (nanoceria), by mimicking the activity of the neuroprotective enzymes super oxide dismutase and catalase (Singh et al. 2010), catalytically destroy reactive oxygen species (ROS). We showed that less than one half nanogram of nanoceria was capable of providing almost complete protection in vivo to rat photoreceptors against light damage (Chen et al. 2006). Metal nanoparticles have also been reported to have antioxidants, antiapoptosis and antiaging effects (Ellis-Behnke and Jonas 2011). In our lab we recently employed nanoceria to therapeutically treat inherited

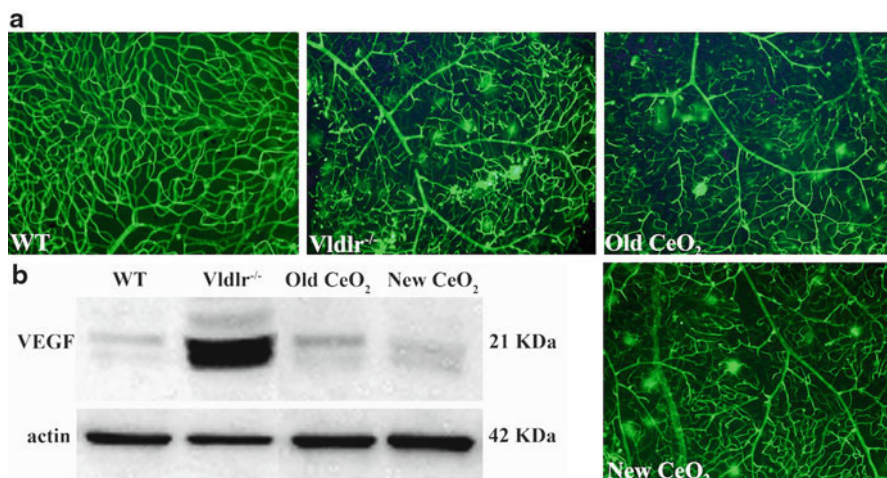


Fig. 32.1 Nanoceria (CeO_2) greatly inhibit the development of abnormal retinal blood vessels and reduce VEGF expression in *Vldlr*^{-/-} mice. Nanoceria were injected at P7 and retina flatmounts, at P21, show fluorescent staining of blood vessels with isolectin conjugated to Alexa Fluor 488 (**a**). Wild type (WT) retina has no abnormal blood vessels while *Vldlr*^{-/-} retina exhibits many enlarged vessels and blebs. Treatment with old (6 years) or new (1 month) nanoceria greatly reduces the vascular enlargements and blebs in the *Vldlr*^{-/-} retina. Western blot data (**b**) show that VEGF levels are greatly reduced by nanoceria treatment compared to uninjected age-matched *Vldlr*^{-/-} retinas

illicit angiogenesis in *Vldlr*^{-/-} mice. As a proof-of-principle and to test the shelf life of nanoceria, we intravitreally injected the *Vldlr*^{-/-} neonates at P7 with 1 μL of nanoceria, which had been stored at room temperature for 6 years or 1 month. The eyes were harvested at P21 and analyzed for either intraretinal vascular lesions or the expression of VEGF. As shown in Fig. 32.1, the retinal vascular lesions were equally inhibited by nanoceria regardless of storage time (Fig. 32.1a). Similarly, the overexpression of VEGF in the *Vldlr*^{-/-} retina was inhibited to the same extent by old and new nanoceria (Fig. 32.1b). The stability of the ROS scavenging activity of the nanoceria supports their potential for therapeutic use over extended periods of time.

32.4.4 Regenerative Medicine

An alternative approach using stem cell-based therapy, has suggested a new strategy for treating vascular eye diseases (Marchetti et al. 2010). Adult bone-marrow (BM)-derived endothelial progenitor cells (EPCs) were reported to be capable of being incorporated into existing blood vessels and forming vascular mosaics with endogenous retinal vascular endothelial cells (Otani et al. 2002) after injection into the

vitreous of new born mice. Ritter et al. reported that adult BM-derived myeloid progenitor cells can differentiate into microglia and promote vascular repair in an OIR mouse model (Ritter et al. 2006).

32.5 Conclusion

For each of the three major blinding diseases (DR, AMD, and ROP), there have been significant advancements in therapeutic treatments which have improved the quality of life for patients with these diseases. However, none of the therapies have yet been shown to relieve all of the symptoms and/or be beneficial over long periods of time. The single protein/gene targeted therapies such as anti-VEGF have had very positive effects, especially on AMD, but the potency appears to decrease over time. Laser treatment has been most effective for treatment of ROP although less so for DR. The ideal therapy would target an upstream node (e.g., ROS), common to many diseases, and would retain its effectiveness for extended periods of time. One such strategy is the use of regenerative nanoceria which, by acting on ROS would be expected to have a broad spectrum effect on all the downstream targets including illicit neovascularization, inflammation, vascular leakage, and retinal degeneration.

References

- Afzal A, Caballero S, Pali SS et al (2010) Targeting retinal and choroid neovascularization using the small molecule inhibitor carboxyamidotriazole. *Brain Res Bull* 81:320–326
- Barber AJ, Antonetti DA, Kern TS et al (2005) The Ins2Akita mouse as a model of early retinal complications in diabetes. *Invest Ophthalmol Vis Sci* 46:2210–2218
- Benny O, Nakai K, Yoshimura T et al (2010) Broad spectrum antiangiogenic treatment for ocular neovascular diseases. *PLoS One* 5 pII:e12515
- Bird AC (2010) Therapeutic targets in age-related macular disease. *J Clin Invest* 120:3033–3041
- Chen J, Patil S, Seal S et al (2006) Rare earth nanoparticles prevent retinal degeneration induced by intracellular peroxides. *Nat Nanotechnol* 1:142–150
- Chen Y, Hu Y, Zhou T et al (2009) Activation of the Wnt pathway plays a pathogenic role in diabetic retinopathy in humans and animal models. *Am J Pathol* 175:2676–2685
- Cheung N, Mitchell P, Wong TY (2010) Diabetic retinopathy. *Lancet* 376:124–136
- Dorrell MI, Aguilar E, Jacobson R et al (2009) Antioxidant or neurotrophic factor treatment preserves function in a mouse model of neovascularization-associated oxidative stress. *J Clin Invest* 119:611–623
- Edwards AO, Malek G (2007) Molecular genetics of AMD and current animal models. *Angiogenesis* 10:119–132
- Ellis-Behnke R, Jonas JB (2011) Redefining tissue engineering for nanomedicine in ophthalmology. *Acta Ophthalmol* e108–e114
- Friedlander M (2009) Combination angiostatic therapies: targeting multiple angiogenic pathways. *Retina* 29:S27–29
- Gibson DL, Sheps SB, Schechter MT et al (1989) Retinopathy of prematurity: a new epidemic? *Pediatrics* 83:486–492
- Grossniklaus HE, Kang SJ, Berglin L (2010) Animal models of choroidal and retinal neovascularization. *Prog Retin Eye Res* 29:500–519

- Hu W, Jiang A, Liang J et al (2008) Expression of VLDLR in the retina and evolution of subretinal neovascularization in the knockout mouse model's retinal angiomatous proliferation. *Invest Ophthalmol Vis Sci* 49:407–415
- Jiang J, Xia XB, Xu HZ et al (2009) Inhibition of retinal neovascularization by gene transfer of small interfering RNA targeting HIF-1 α and VEGF. *J Cell Physiol* 218:66–74
- Lai CM, Dunlop SA, May LA et al (2005a) Generation of transgenic mice with mild and severe retinal neovascularisation. *Br J Ophthalmol* 89:911–916
- Lai CM, Shen WY, Brankov M et al (2005b) Long-term evaluation of AAV-mediated sFlt-1 gene therapy for ocular neovascularization in mice and monkeys. *Mol Ther* 12:659–668
- Lamartina S, Cimino M, Roscilli G et al (2007) Helper-dependent adenovirus for the gene therapy of proliferative retinopathies: stable gene transfer, regulated gene expression and therapeutic efficacy. *J Gene Med* 9:862–874
- Limae Silva R, Shen J, Gong YY et al (2010) Agents that bind annexin A2 suppress ocular neovascularization. *J Cell Physiol* 225:855–864
- Liu X, Wang D, Liu Y et al (2010) Neuronal-driven angiogenesis: role of NGF in retinal neovascularization in an oxygen-induced retinopathy model. *Invest Ophthalmol Vis Sci* 51:3749–3757
- Marchetti V, Krohne TU, Friedlander DF et al (2010) Stemming vision loss with stem cells. *J Clin Invest* 120:3012–3021
- Ohno-Matsui K, Hirose A, Yamamoto S et al (2002) Inducible expression of vascular endothelial growth factor in adult mice causes severe proliferative retinopathy and retinal detachment. *Am J Pathol* 160:711–719
- Otani A, Kinder K, Ewalt K et al (2002) Bone marrow-derived stem cells target retinal astrocytes and can promote or inhibit retinal angiogenesis. *Nat Med* 8:1004–1010
- Pechan P, Rubin H, Lukason M et al (2009) Novel anti-VEGF chimeric molecules delivered by AAV vectors for inhibition of retinal neovascularization. *Gene Ther* 16:10–16
- Ricci B (1990) Oxygen-induced retinopathy in the rat model. *Doc Ophthalmol* 74:171–177
- Ritter MR, Banin E, Moreno SK et al (2006) Myeloid progenitors differentiate into microglia and promote vascular repair in a model of ischemic retinopathy. *J Clin Invest* 116:3266–3276
- Rokoczy E, Rashman I, Binz N et al (2010) Characterization of a mouse model of hyperglycemia and retinal neovascularization. *Am J Pathol* 177
- Sapieha P, Joyal JS, Rivera JC et al (2010) Retinopathy of prematurity: understanding ischemic retinal vasculopathies at an extreme of life. *J Clin Invest* 120:3022–3032
- Singh S, Kumar A, Karakoti A, et al. (2010) Unveiling the mechanism of uptake and sub-cellular distribution of cerium oxide nanoparticles. *Mol Biosyst* 6:1813–1820
- Takeda A, Baffi JZ, Kleinman ME et al (2009) CCR3 is a target for age-related macular degeneration diagnosis and therapy. *Nature* 460:225–230
- Tobe T, Ortega S, Luna JD et al (1998) Targeted disruption of the FGF2 gene does not prevent choroidal neovascularization in a murine model. *Am J Pathol* 153:1641–1646
- Xie B, Shen J, Dong A et al (2009) Blockade of sphingosine-1-phosphate reduces macrophage influx and retinal and choroidal neovascularization. *J Cell Physiol* 218:192–198
- Xiong SQ, Xia XB, Xu HZ et al (2009) Suppression of retinal neovascularization by small-interference RNA targeting erythropoietin. *Ophthalmologica* 223:306–312
- Yoshioka M, Kayo T, Ikeda T et al (1997) A novel locus, Mody4, distal to D7Mit189 on chromosome 7 determines early-onset NIDDM in nonobese C57BL/6 (Akita) mutant mice. *Diabetes* 46:887–894

Chapter 33

Retinal Neovascular Disorders: Mouse Models for Drug Development Studies

Rosanne M. Yetemian and Cheryl M. Craft

Keywords Retinal neovascularization • Neovascular disorders • Age-related macular degeneration • Diabetic retinopathy • Retinopathy of prematurity • Mouse models • Drug development

33.1 Introduction

Neovascularization is a hallmark of several eye diseases leading to visual impairment, and its epidemiological impact is substantial (Lee et al. 1998). In retinal degenerative disease models, neovascularization is the process by which the choroid and/or retina become infiltrated with new blood vessels. In retinal neovascularization (RNV), sprouting retinal vessels penetrate the inner limiting membrane (ILM) and grow into the vitreous, and in some cases, grow through the avascular outer retina into the subretinal space (Campochiaro 2000). Numerous clinical and

R.M. Yetemian

Mary D. Allen Laboratory for Vision Research, Doheny Eye Institute, Keck School of Medicine, University of Southern California, Los Angeles, CA 90033-9224, USA

Department of Ophthalmology, Keck School of Medicine of the University of Southern California, Los Angeles, CA 90033-9224, USA

Regulatory Affairs, Abbott Medical Optics, Inc., Santa Ana, CA 92705, USA

C.M. Craft (✉)

Mary D. Allen Laboratory for Vision Research, Doheny Eye Institute, Keck School of Medicine, University of Southern California, Los Angeles, CA 90033-9224, USA

Department of Ophthalmology, Keck School of Medicine of the University of Southern California, Los Angeles, CA 90033-9224, USA

Department of Cell & Neurobiology, Keck School of Medicine of the University of Southern California, Los Angeles, CA 90033-9224, USA

e-mail: ccraft@usc.edu

experimental observations indicate that ischemia (or hypoxia) is the driving force behind RNV (Michaelson and Steedman 1949). Occlusion of retinal vessels leading to ischemia is a feature of diseases with RNV, including diabetic retinopathy (DR) and retinopathy of prematurity (ROP) (Campochiaro 2000).

Choroidal neovascularization (CNV) is characterized by new blood vessels emanating from the choroid into the subretinal pigment epithelium, subretinal space, or both (Qazi et al. 2009). This leads to the formation of neovascular membranes, which include vascular endothelial cells, retinal pigment epithelial (RPE) cells, and macrophages (Das and McGuire 2003). Vascular endothelial growth factor (VEGF) and platelet-derived growth factor (PDGF) are essential mediators in the development of CNV, which is the primary form of neovascularization in age-related macular degeneration (AMD) patients. Although multiple factors have been implicated in the development of neovascularization, future studies are warranted in the identification of novel treatment strategies. To better understand the current mouse models available to study RNV and CNV, a brief review of the retinal diseases characterized by neovascularization is examined below.

33.2 Proliferative Diabetic Retinopathy

The most common cause of blindness among Americans between the ages of 20–74 is DR. This disorder can be classified as either nonproliferative or proliferative. Whereas nonproliferative DR is characterized by venous dilation, retinal hemorrhage, and microaneurysms, proliferative DR is characterized by abnormal new vessel and fibrous tissue proliferation on the surface of the retina (Lee et al. 1998). Ischemia of the inner retinal layers causes the release of VEGF, stimulating new blood vessel formation locally and in other regions of the eye (Besirli and Johnson 2009). For diabetics, RNV is the major contributor to blindness, and treatment of neovascularization can reduce severe visual loss from 50% to approximately 5% per year (Lee et al. 1998).

33.3 Retinopathy of Prematurity

ROP is characterized by RNV that eventually affects the vitreous, causes retinal detachment, and inevitable blindness in premature infants (Lee et al. 1998). ROP, like DR, is primarily characterized by RNV and less by CNV. The disease can progress in two phases: (1) delayed retinal vascular growth after birth and partial regression of existing vessels followed by (2) hypoxia-induced pathological vessel growth (Chen and Smith 2007). ROP develops through conditions of excessive hyperoxia and hypoxia leading to deregulation of VEGF expression. Serum insulin-like growth factor 1 (IGF-1) has also shown to directly correlate with the severity of ROP in the clinic. Taken together, the pathophysiology of ROP is similar to that of other retinal disease with RNV.

33.4 Age-Related Macular Degeneration

A multifactorial cause of photoreceptor degeneration, AMD accounts for more than half of all blindness and visual impairment in developed countries primarily affecting individuals over 60 (Ting et al. 2009). Patients with AMD are categorized as having nonexudative (dry) or exudative (wet) stage forms of the disease. Dry AMD patients exhibit large, poorly demarcated drusen and RPE abnormalities. Wet AMD is characterized by local regions of RPE atrophy and growth of new blood vessels from the choroid that penetrate Bruch's membrane and enter the retina where they can leak and cause damage. Genetic association studies on AMD patients identified Complement Factor H (CFH) and Age-related Maculopathy Susceptibility 2 (ARMS) genes as contributors to AMD (Wright et al. 2010), with the effect sizes of these two susceptibility alleles unusually large by the standard of most complex traits. Current successful therapeutic strategies for treating AMD and improving visual quality include the use of anti-VEGF medicines.

33.5 Genetic Mouse Models for Neovascularization

The distinction between RNV and CNV in mouse models is important in that they are used to determine the type of disease for which they are most appropriate. For example, DR and ROP are both primarily characterized by RNV, and AMD, which may also be associated with RNV, exhibits CNV as the primary mechanism for neovascularization in the eye.

Transgenic mouse models for RNV provide an adequate resource for the characterization of this phenomenon. One example is the *rho/VEGF* transgenic mouse, which develops retinal and subretinal neovascularization (SRN) as a consequence of VEGF expression driven by the rhodopsin promoter. This model is a close representation to patients with retinal angiomatous proliferation (RAP) (Miller 1997). The development of VEGF₁₆₅ overexpressing transgenic mice driven by the truncated rhodopsin promoter developed phenotypes ranging from mild to severe RNV and are also used in RNV studies (Miller 1997).

The reverse tetracycline transactivator (rtTA) inducible promoter system coupled with the rhodopsin (*rho/rtTa-TRE/VEGF*) or interphotoreceptor retinoid-binding protein (IRBP) promoter (*IRBP/rtTA-TRE/VEGF*) has been used to control the onset of VEGF expression in the retina (Grossniklaus et al. 2010). The addition of doxycycline in these mice activates the expression levels of VEGF, and subsequently causes extensive RNV. In comparison to *rho/VEGF* mice, these transgenic models are associated with total retinal detachment and higher ocular levels of VEGF mRNA and protein (Ohno-Matsui et al. 2002).

A recently identified knockout mouse that also exhibits RNV is the *Nrl^{-/-}Grk1^{-/-}* mouse. The neural retina leucine zipper knockout (*Nrl^{-/-}*), which lacks the transcription factor responsible for normal rod photoreceptor development, leads to a retinal

phenotype with all cone photoreceptors that include an enhanced number of S-cones and a normal number of M-cones. The double knockout that lacks the G-protein-coupled receptor kinase 1 gene (*Nrl^{-/-}Grk1^{-/-}*) involved in phototransduction recovery exhibits a light independent age-related degeneration (Zhu et al. 2003, 2006). These mice exhibit an RNV phenotype similar to RAP and retinal vascularization that is first observed at 1 month and is mediated by the inflammatory response (Yetemian et al. 2010; Yetemian 2010).

Relevant models of CNV can be found in transgenic knockout mice where CNV is a phenotypic distinction. One such model is the monocyte chemoattractant protein-1 (*Ccl2*) or its receptor CC-chemokine receptor-2 (*Ccr2*) deficient mouse, which are both current models for AMD (Ambati et al. 2003). These transgenic mice lacking either *Ccl2* or *Ccr2* fail to recruit macrophages to the RPE or Bruch's membrane, thereby allowing the accumulation of complement factor C5a and IgG, both of which induce VEGF production (Ambati et al. 2003).

Other transgenic knockout mice that exhibit a CNV phenotype include mice that overexpress Apolipoprotein E (*ApoE*) that were fed a high fat diet and developed AMD like lesions (Malek et al. 2005). Disruption of ceruloplasmin and hephaestin in mice causes iron overload and subsequent AMD-like changes. These mice develop RPE abnormalities and photoreceptor degeneration (Hahn et al. 2004). Knockout mice for the very low density lipoprotein receptor gene (*Vldlr^{TM1Her}*) develop new blood vessels in the outer plexiform layer (OPL) of the retina as well as choroidal anastomoses by 3 months (Heckenlively et al. 2003). The transgenic mouse line (*mcd/mcd*) exhibits features associated with geographic atrophy and AMD. The *mcd/mcd* mice express a mutated form of cathepsin D that is enzymatically inactive, thereby impairing photoreceptor outer segment phagocytosis by RPE cells (Rakoczy et al. 2002). Also, the Cu, Zn superoxide dismutase-deficient mouse (*Sod^{-/-}*) has been shown to exhibit fundus and histological evidence of CNV in approximately 10% of *Sod^{-/-}* mice.

Another model for neovascularization similar to AMD is the spontaneous autosomal semidominant mouse mutation Belly spot and tail (*Bst*), which arose in the C57/Bl6J inbred strain at the Jackson Laboratory (Smith et al. 1999). The mutation was mapped to chromosome 16, 1.9 ± 1.1 cM from *D16Mit168*, and these mice have late closure of the optic fissure, delayed retinal differentiation, decreased number of retinal ganglion cells, and coloboma of the optic nerve and retina (Smith et al. 1999). A highly variable phenotype, aging *Bst*+ mice were found to have SRN. SRN begins in the choroid with vascular invasion through Bruch's membrane into the subretinal space, and can lead to CNV in the form of subretinal hemorrhage that may undergo fibrosis and cause more retinal damage (Smith et al. 1999).

33.6 Nongenetic Models for Neovascularization

Animal models for the study of RNV include hypoxia-induced, vascular occlusion, and intraocular injection of pro-angiogenic molecules. Hypoxia-induced models have been developed in several species and is performed by exposing mice to hyperoxia, then placing them in normoxic conditions, causing an ischemic situation that

initiates rapid abnormal neovascularization. This model has proven to delineate the molecular changes in neovascular eye disease and directly correlates to ROP (Ashton 1966; Chen and Smith 2007). Occlusion of retinal veins by laser photocoagulation or photodynamic therapy has also been used in RNV studies (Ham et al. 1997).

Animal models for nongenetically induced CNV include laser and surgically induced models. Experimental laser-induced mice were created using spot treatments from a krypton laser to create photocoagulation injuries to Bruch's membrane (Ryan 1979; Tobe et al. 1998). The laser-induced model is currently well established and is also used in preclinical trials for the study of anti-angiogenic drugs. Although the physical insult to Bruch's membrane differs from the long-term chronic conditions that occur in human AMD, the models closely mimic natural cellular responses that occur in human CNV. Surgically induced forms of CNV are also currently in practice and are done primarily by the injection of synthetic peptides, viral vectors containing VEGF, and inert synthetic materials (Grossniklaus et al. 2010).

33.7 Use of Mouse Models for Neovascularization in Preclinical Drug Testing

The discovery that VEGF plays a significant role in neovascularization spurred the development of several anti-VEGF pharmacological treatments such as Bevacizumab (Avastin), Ranizumab (Lucentis), (Genentech, Inc.), and Pegaptanib (Macugen) (Eyetechnology, Inc.). Bevacizumab (BVZ) is a full-length humanized monoclonal antibody that binds all isoforms of VEGF-A, Ranizumab (RBZ) is the 48 kDa form of BVZ, and Pegaptanib is a 28-base ribonucleic acid aptamer that binds to VEGF₁₆₅. All are FDA approved, and the extensive preclinical studies for each involved the use of some of the mouse models discussed above. A study by Katsuki et al. compared the effects of intraocular RBZ and BVZ injections using *rho/VEGF* and doxycycline-treated *Tet/opsin/VEGF* mice to demonstrate not only safety but also efficacy in suppression of SRN (Katsuki et al. 2009). A study funded by Eyetechnology, Inc. used a murine model of ROP in their preclinical testing for Pegaptanib, among several other animal models for RNV (Eyetechnology Study Group 2002). It is apparent from the preclinical testing conducted on these three currently marketed treatments for AMD that the mouse models utilized were influential in the development of these drugs and will continue to be utilized during the development of future treatments for neovascularization.

33.8 Conclusion

Despite their similarities in structure and function, the retinas of humans and mice are quite unique and do present challenges when compared. Mice, for example, have only two opsin expressing cones when compared to humans and lack a defined

macula. Nevertheless, they have similar morphology and neuronal structures that are extremely comparable to the human retina and are extensively used in many disease studies. DR, ROP, and AMD are the leading forms of retinal dystrophy in the aging human population, and mouse models are becoming increasingly useful in identifying causative mechanisms and therapeutic targets to protect against these diseases.

As we learn more about neovascularization, we will continue to develop and explore new animal models for the treatment and prevention of disease. This short review is not a comprehensive study on all the available mouse models for preclinical testing, but it summarizes significant trends and variability in RNV research and the high impact mouse models have in human disease studies. Mouse models are crucial to understanding the molecular and cellular mechanism behind retinal degeneration and will continue to provide avenues for potential therapeutic advancement.

Acknowledgments We thank members of the Mary D. Allen Laboratory for scientific discussions. CMC is the Mary D. Allen Chair in Vision Research, DEI, and a Research to Prevent Blindness (RPB) Senior Scientific Investigator. This work was supported, in part, by NIH Grant EY015851 (CMC), EY03040 (DEI), RPB (DEI & CMC), Dorie Miller, William Hansen Sandberg Memorial Scholarship (RMY), Tony Gray Foundation, Mary D. Allen Foundation (Dr. Richard Newton Lolley Memorial Scholarship [RMY]), and an RD2010 Travel Award (RMY).

References

- Ambati J, Anand A, Fernandez S et al. (2003) An animal model of age-related macular degeneration in senescent Ccl-2- or Ccr-2-deficient mice. *Nat Med* 9:1390–1397
- Ashton N (1966) Oxygen and the growth and development of retinal vessels. In vivo and in vitro studies. The 33 Francis I. Proctor Lecture. *Am J Ophthalmol* 62:412–435
- Besirli CG, Johnson MW (2009) Proliferative diabetic retinopathy. *Mayo Clin Proc* 84:1054
- Campochiaro PA (2000) Retinal and choroidal neovascularization. *J Cell Physiol* 184:301–310
- Chen J, Smith LE (2007) Retinopathy of prematurity. *Angiogenesis* 10:133–140
- Eyetech Study Group (2002) Preclinical and phase 1A clinical evaluation of an anti-VEGF pegylated aptamer (EYE001) for the treatment of exudative age-related macular degeneration. *Retina* 22:43–52
- Das A, McGuire PG (2003) Retinal and choroidal angiogenesis: pathophysiology and strategies for inhibition. *Prog Retin Eye Res* 22:721–748
- Grossniklaus HE, Kang SJ, Berglin L (2010) Animal models of choroidal and retinal neovascularization. *Prog Retin Eye Res* 29:500–519
- Hahn P, Qian Y, Dentchev T et al. (2004) Disruption of ceruloplasmin and hephaestin in mice causes retinal iron overload and retinal degeneration with features of age-related macular degeneration. *Proc Natl Acad Sci USA* 101:13850–13855
- Ham DI, Chang K, Chung H (1997) Preretinal neovascularization induced by experimental retinal vein occlusion in albino rats. *Korean J Ophthalmol* 11:60–64
- Heckenlively JR, Hawes NL, Friedlander M et al. (2003) Mouse model of subretinal neovascularization with choroidal anastomosis. *Retina* 23:518–522
- Katsuki M, Akiko M, Matsuoka M et al. (2009) Effects of intraocular ranibizumab and bevacizumab in transgenic mice expressing human vascular endothelial growth factor. *Ophthalmology* 116:1748–1754
- Lee P, Wang CC, Adamis AP (1998) Ocular neovascularization: an epidemiologic review. *Survey of Ophthalmology* 43:245–269

- Lolley, RN, Schmidt, SY, Farber DB (1974) Alterations in cyclic AMP metabolism associated with photoreceptor degeneration in C3H mouse. *J Neurochem* 22:701–707
- Malek G, Johnson LV, Mace BE et al. (2005) Apolipoprotein E allele-dependent pathogenesis: a model for age-related retinal degeneration. *Proc Natl Acad Sci USA* 102:11900–11905
- Michaelson IC, Steedman HF (1949) Injection of the retinal vascular system in enucleated eyes. *Br J Ophthalmol* 33:376–379
- Miller JW (1997) Vascular endothelial growth factor and ocular neovascularization. *Am J Pathol* 151:13–23
- Ohno-Matsui K, Hirose A, Yamamoto S, et al. (2002) Inducible expression of vascular endothelial growth factor in adult mice causes severe proliferative retinopathy and retinal detachment. *Am J Pathol.* 160:711–719
- Qazi Y, Maddula S, Ambati BK (2009) Mediators of ocular angiogenesis. *J Genet* 88:495–515
- Rakoczy PE, Zhang D, Robertson T, et al. (2002) Progressive age-related changes similar to age-related macular degeneration in a transgenic mouse model. *Am J Pathol* 161:1515–1524
- Ryan SJ (1979) The development of an experimental model of subretinal neovascularization in disciform macular degeneration. *Trans Am Ophthalmol Soc* 77:707–745
- Smith RS, Simon JW, Zabeleta A et al. (1999) The *bst* locus on mouse chromosome 16 is associated with age-related subretinal neovascularization. *PNAS* 97:2191–2195
- Ting AY, Lee TK, MacDonald IM (2009) Genetics of age-related macular degeneration. *Curr Opin Ophthalmol* 20:369–376
- Tobe T, Ortega S, Luna JD et al. (1998) Targeted disruption of the *FGF2* gene does not prevent choroidal neovascularization in a murine model. *Am J Pathol* 153:1641–1646
- Wright AF, Chakarova CF, Abd El-Aziz MM et al. (2010) Photoreceptor degeneration: genetic and mechanistic dissection of a complex trait. *Nat Rev Genet* 11:273–284
- Yetemian RY, Brown BM, Craft CM (2010) Neovascularization, enhanced inflammatory response, and age-related cone dystrophy in the *Nrl*^{-/-}*Grk1*^{-/-} mouse retina. *Invest Ophthalmol Vis Sci* 51:6196–6206
- Yetemian RY (2010) Elements of photoreceptor homeostasis: investigating phenotypic manifestations and susceptibility to photoreceptor degeneration in genetic knockout models for retinal disease. Dissertation. University of Southern California. ProQuest, LLC. Ann Arbor, MI
- Zhu X, Brown BM, Li A, et al. (2003) GRK1-dependent phosphorylation of S and M opsins and their binding to cone arrestin during cone phototransduction in the mouse retina. *Journal of Neurosci* 23:6152–6160
- Zhu X, Brown BM, Rife L, Craft CM (2006) Slowed photoresponse recovery and age related degeneration in cones lacking G protein-coupled receptor kinase 1. In *Advances in Experimental Medicine and Biology, Retinal Degenerative Diseases* 572:133–139. Hollyfield JG, Anderson RE, LaVail MM, eds. Springer

Chapter 34

A Review and Update on the Molecular Basis of Pathogenesis of Sorsby Fundus Dystrophy

Heidi Stöhr and Bela Anand-Apte

Keywords Sorsby fundus dystrophy • Choroidal neovascularization • Bruch's membrane • TIMP3 • Extracellular matrix • Angiogenesis • VEGF • AMD

34.1 Introduction

SFD is a rare autosomal dominant macular degeneration that was first described in four pedigrees by Sorsby in 1949 (Sorsby et al. 1949). Forty-five years later, a positional candidate gene approach identified the *TIMP3* gene on chromosome 22q12.3 as the causative gene associated with SFD (Weber et al. 1994). A susceptibility locus for AMD has recently been identified near the *TIMP3* locus (Chen et al. 2010). There is a considerable degree of clinical overlap between SFD and the more prevalent AMD. Thus, the elucidation of SFD pathophysiology is believed to contribute to the identification of potential common pathways underlying different forms of macular dystrophies and to the development of therapeutic interventions.

H. Stöhr (✉)

Institute of Human Genetics, University Regensburg,
Franz-Josef-Strauss-Allee 11, 93053 Regensburg, Germany
e-mail: heidi.stoehr@klinik.uni-regensburg.de

B. Anand-Apte

Department of Ophthalmic Research, Cole Eye Institute, 9500 Euclid Avenue,
Cleveland, OH 44195, USA

34.2 Clinical Manifestations of SFD and Therapeutic Intervention

SFD is characterized by a sudden decrease in central vision during the fourth or fifth decade of life as a consequence of CNV and subretinal hemorrhage. Some patients may be aware of difficulties in dark adaptation and color vision for a decade or more before losing central vision. Within a few years, patients develop disciform atrophic macular scars surrounded by massive pigmentation that often extend into the retinal mid-periphery and is then accompanied by a loss of ambulatory vision. Preneovascular fundus examination shows diffuse or focal subretinal yellow-white deposits at the level of BM that affect the entire posterior pole (Polkinghorne et al. 1989). Clinical heterogeneity concerning age of onset, disease progression, fundus appearance, and nyctalopia is common within and between SFD families (Felbor et al. 1997; Sivaprasad et al. 2008).

Histopathological analyses of donor eyes from SFD patients revealed thickening of BM and atrophy of the retinal pigment epithelium (RPE) and choroid (Capon et al. 1989; Fariss et al. 1998). The lipid-containing deposits were located between the RPE and the elastic layer of BM. In addition, the elastic layer of BM was morphologically altered in the diseased eye (Chong et al. 2000). Immunohistochemistry showed that the accumulations contained an increased amount of TIMP3 (Fariss et al. 1998). On the basis of these findings, it has been proposed that the subretinal deposits create a diffusion barrier for nutrients from the choroid vessels to the RPE and photoreceptor cells. In support of this hypothesis, high doses of oral vitamin A supplementation reversed night blindness in early stages of SFD (Jacobson et al. 1995). Other treatment strategies for the management of SFD include anti-VEGF and angiostatic steroid therapies (Sivaprasad et al. 2008).

34.3 Mutation Spectrum of TIMP3 in SFD

The identification of *TIMP3* as the disease-causing gene defined SFD as a distinct nosological entity with full penetrance but variable expressivity. Up to now, nine missense mutations in exon 5 of the *TIMP3* gene have been found to introduce amino acid substitutions E139K (Saihan et al. 2009), S156C (Felbor et al. 1995), H158R (Lin et al. 2006), G166C (Felbor et al. 1997), G167C (Jacobson et al. 1995), Y168C (Weber et al. 1994), S170C (Barbazetto et al. 2005), Y172C (Jacobson et al. 2002), and S181C (Weber et al. 1994) in the C-terminal domain of the TIMP3. Furthermore, a nonsense mutation (E139X) (Clarke et al. 2001) and a splice mutation (Tabata et al. 1998) were identified in SFD, which are predicted to generate a truncated TIMP3 molecule lacking most of the C-terminal region. Although large phenotypic variability impedes genotype–phenotype correlation, the S156C mutation goes along with early manifestation and rapid progression of the disease (Felbor et al. 1995), whereas patients with the H158R and the splice site mutations exhibit late onset and mild SFD (Lin et al. 2006; Tabata et al. 1998).

34.4 Advances in the Elucidation of the Pathogenesis of SFD

Unlike the other soluble members of the TIMP family, TIMP3 is tightly sequestered to the ECM. It is an endogenous inhibitor of matrix metalloproteases (MMPs) and certain ADAM and ADAMTS proteins, enzymes that degrade matrix components and catalyze the shedding of ectodomains from cell surface proteins (Brew and Nagase 2010). Furthermore, TIMP3 has various additional functions including proapoptotic and antiangiogenic activities. On the basis of the dominant pattern of inheritance, either haploinsufficiency of TIMP3 or gain of function of mutant TIMP3, both causing deleterious effects on ECM remodeling, appears likely to be involved in SFD pathology.

34.4.1 Molecular Characteristics of Mutant TIMP3

Most of the 11 SFD-related *TIMP3* mutations cause an odd number of cysteines in the respective molecules. It has been shown that mutant TIMP3 proteins with an additional cysteine have a higher tendency to dimerize and multimerize when electrophoretically separated under nonreducing conditions (Langton et al. 2000; Yeow et al. 2002; Weber et al. 2002; Arris et al. 2003). This was demonstrated to be true also for proteins harboring the E139K mutation (Saihan et al. 2009), implying that SFD mutations in general favor the formation of intermolecular disulfide bridges. From the observation that ECM-bound mutant TIMP3 proteins have greater stability than wild-type TIMP3 *in vitro* (Langton et al. 2005), it has been assumed that turnover-resistant TIMP3 aggregates disturb ECM homeostasis leading to BM thickening. While this may be an appealing hypothesis, experimental evidence for an increased resistance of endogenous mutant TIMP3 to degradation has been lacking (Soboleva et al. 2003). Furthermore, TIMP3 is internalized by LRP-mediated endocytosis in cartilage (Troeborg et al. 2008) indicating additional mechanisms that regulate extracellular levels of TIMP3. Protease inhibitory activities and ECM binding appears to be retained in TIMP3 proteins carrying different SFD-related mutations (Langton et al. 2000; Yeow et al. 2002; Soboleva et al. 2003; Fogarasi et al. 2008). Overexpression of S156C-TIMP3 mutation in endothelial cells, however, resulted in reduced binding to the ECM, increased glycosylation, and decreased MMP inhibitory activity (Qi et al. 2009), and confirmed an earlier study demonstrating that S156C-TIMP3 expressed in RPE cells does not dimerize and show altered MMP inhibition (Qi et al. 2002). Thus, the capacity of mutant TIMP3 to multimerize, to interact with the ECM and to exert inhibitory functions seems to be dependent on the experimental conditions used by different laboratories including the type of mutants and cell culture systems. Given the unique composition of the choroid-BM-RPE complex, a tissue-specific impact of mutant TIMP3 molecules is conceivable to cause SFD.

34.4.2 *Clues from Animal Models*

Gene-targeted mouse lines with TIMP3 deficiency and knock-in mice carrying the S156C-TIMP3 mutation were generated to further study SFD pathogenesis. TIMP3-deficient mice develop abnormal vessels with dilated capillaries throughout the choroid (Janssen et al. 2008) due to a local disruption of both ECM and angiogenic homeostasis. In addition, unbalanced matrix degradation by MMPs and uncontrolled cleavage of the cytokine TNF- α by TACE in the absence of TIMP3 has been found to cause pulmonary alveolar enlargement (Leco et al. 2001), enhanced susceptibility to cardiomyopathy (Fedak et al. 2004), chronic hepatic inflammation and impaired liver regeneration after partial hepatectomy (Mohammed et al. 2004), and antigen-induced arthritis (Mahmoodi et al. 2005). An increased abundance of TIMP3 was detected in BM and in the ECM of primary cell cultures established from mice carrying the *Timp3*^{S156C} allele (Weber et al. 2002; Soboleva et al. 2003). *Timp3*^{S156C} knock-in mice, however, display only slight abnormalities in the inner aspect of BM and RPE basal microvilli (Weber et al. 2002). The reason for an absence of typical SFD-related symptoms like BM thickening and CNV in either TIMP3 knock-out nor *Timp3*^{S156C} mice may lie in the short life span of the mouse. TIMP3 interacts with EFEMP1, the protein associated with autosomal dominant Drayton honeycomb retinal dystrophy (DHRD) (Klenotic et al. 2004). Interestingly, knock-in mice carrying the DHRD-associated R345W mutation in the *Efemp1* gene develop large deposits of abnormal material between BM and the RPE that contains EFEMP1 and TIMP3 (Fu et al. 2007). It remains to be determined whether manifestation of SFD-like phenotypes in the TIMP3 mouse models can be induced by certain genetic backgrounds or physiological challenges.

34.4.3 *Molecular Mechanisms of Angiogenesis in SFD*

Over the past few years, significant progress has been made toward understanding the role of TIMP3 in VEGF-mediated angiogenesis and the possible pathophysiological mechanisms that are responsible for the CNV phenotype in SFD. TIMP3 is a potent inhibitor of VEGF-mediated angiogenesis with a novel function of blocking VEGF binding to VEGFR2 independent of its MMP inhibitory function (Qi et al. 2003). Concomitant with an abnormal choroid vasculature (Janssen et al. 2008), TIMP3-deficient mice show increased laser-induced CNV (Ebrahim et al. 2011). Interestingly, S156C-TIMP3 expression in endothelial cells resulted in an increase in the levels of the mature form of VEGFR2 protein on the surface of the cells, which was sufficient to increase VEGF binding and subsequent VEGFR2 autophosphorylation and MAP kinase phosphorylation with downstream consequences of enhanced VEGF-dependent migration and tube formation (Qi et al. 2009). Since both recombinant TIMP3 proteins (WT and S156C-TIMP3) can block the binding of VEGF to VEGFR2 in vitro (Fogarasi et al. 2008), the loss of angioinhibitory

activity seen with mutant TIMP3 in endothelial cells is most likely due to the upregulation of the VEGFR2, suggesting a gain of function. The mechanisms by which mutant TIMP3 regulates the posttranscriptional processing of VEGFR2 is unknown and remains to be examined.

34.5 TIMP3 and AMD

It has long been suggested that TIMP3 also plays a role in the pathogenesis of AMD due to the strong similarity between the clinical phenotypes of AMD and SFD, the large accumulation of TIMP3 in drusen in AMD (Kamei and Hollyfield 1999) as well as in the subretinal deposits in SFD patients (Fariss et al. 1998). While genetic studies have failed to identify mutations in the coding region of *TIMP3* in patients with AMD, the recent discovery of a single-nucleotide polymorphism located within a large intron of the synapsin III (*SYN3*) gene and approximately 100 kb upstream of the first exon of *TIMP3* that confers susceptibility to AMD (Chen et al. 2010), has led to a resurgence of interest in this protein. Future efforts are now directed toward the identification and mechanism of action of the functional allele at the *SYN3/TIMP3* locus.

References

- Arris CE, Bevitt DJ, Mohamed J et al (2003) Expression of mutant and wild-type TIMP3 in primary gingival fibroblasts from Sorsby's fundus dystrophy patients. *Biochim Biophys Acta* 1638:20–28
- Barbazetto IA, Hayashi M, Klais CM et al (2005) A novel TIMP3 mutation associated with Sorsby fundus dystrophy. *Arch Ophthalmol* 123:542–543
- Brew K, Nagase H (2010) The tissue inhibitors of metalloproteinases (TIMPs): an ancient family with structural and functional diversity. *Biochim Biophys Acta* 1803:55–71
- Capon MRC, Marshall J, Krafft JI et al (1989) Sorsby's fundus dystrophy: a light and electron microscopic study. *Ophthalmology* 96:1769–1777
- Chen W, Stambolian D, Edwards AO et al (2010) Genetic variants near TIMP3 and high-density lipoprotein-associated loci influence susceptibility to age-related macular degeneration. *Proc Natl Acad Sci USA* 107:7401–7406
- Chong NH, Alexander RA, Gin T et al (2000) TIMP-3, collagen, and elastin immunohistochemistry and histopathology of Sorsby's fundus dystrophy. *Invest Ophthalmol Vis Sci* 41:898–902
- Clarke M, Mitchell KW, Goodship J et al (2001) Clinical features of a novel TIMP-3 mutation causing Sorsby's fundus dystrophy: implications for disease mechanism. *Br J Ophthalmol* 85:1429–1431
- Ebrahem Q, Qi J, Sugimoto M et al. (2011) Increased neovascularization in mice lacking tissue inhibitor of metalloproteinases-3. *Invest Ophthalmol Vis Sci* 52:6117–6123
- Fariss RN, Apte SS, Luthert PJ et al (1998) Accumulation of tissue inhibitor of metalloproteinases-3 in human eyes with Sorsby's fundus dystrophy or retinitis pigmentosa. *Br J Ophthalmol* 82:1329–1334
- Fedak PW, Smookler DS, Kassiri Z et al (2004) TIMP-3 deficiency leads to dilated cardiomyopathy. *Circulation* 110:2401–2409

- Felbor U, Stöhr H, Amann T et al (1995) A novel Ser156Cys mutation in the tissue inhibitor of metalloproteinases-3 (TIMP3) in Sorsby's fundus dystrophy with unusual clinical features. *Hum Mol Genet* 4:2415–2416
- Felbor U, Benkowitz C, Litt M et al (1997) A founder mutation in TIMP3, Ser181Cys, presents with variable expressivity of Sorsby fundus dystrophy. *Arch Ophthalmol* 115:1569–1571
- Fogarasi M, Janssen A, Weber BH et al (2008) Molecular dissection of TIMP3 mutation S156C associated with Sorsby fundus dystrophy. *Matrix Biol* 27:381–292
- Fu L, Garland D, Yang Z et al (2007) The R345W mutation in EFEMP1 is pathogenic and causes AMD-like deposits in mice. *Hum Mol Genet* 16:2411–2422
- Jacobson SG, Cideciyan AV, Regunath G et al (1995) Night blindness in Sorsby's fundus dystrophy reversed by vitamin A. *Nat Genet* 11:27–32
- Jacobson SG, Cideciyan AV, Bennett J et al (2002) Novel mutation in the TIMP3 gene causes Sorsby fundus dystrophy. *Arch Ophthalmol* 120:376–379
- Janssen A, Hoellenriegel J, Fogarasi M et al (2008) Abnormal vessel formation in the choroid of mice lacking tissue inhibitor of metalloproteinase-3. *Invest Ophthalmol Vis Sci* 49:2812–2822
- Kamei M, Hollyfield JG (1999). *Invest Ophthalmol Vis Sci* 40:2367–2375
- Klenotic PA, Munier FL, Marmorstein LY et al (2004) Tissue inhibitor of metalloproteinases-3 (TIMP-3) is a binding partner of epithelial growth factor-containing fibulin-like extracellular matrix protein 1 (EFEMP1). Implications for macular degenerations. *J Biol Chem* 279:30469–30473
- Langton KP, McKie N, Curtis A et al (2000) A novel tissue inhibitor of metalloproteinases-3 mutation reveals a common molecular phenotype in Sorsby's fundus dystrophy. *J Biol Chem* 275:27027–27031
- Langton KP, McKie N, Smith BM et al (2005) Sorsby's fundus dystrophy mutations impair turnover of TIMP-3 by retinal pigment epithelial cells. *Hum Mol Genet* 14:3579–3586
- Leco KJ, Waterhouse P, Sanchez OH et al (2001) Spontaneous air space enlargement in the lungs of mice lacking tissue inhibitor of metalloproteinases-3 (TIMP-3). *J Clin Invest* 108:817–829
- Lin RJ, Blumenkranz MS, Binkley J et al (2006) A novel His158Arg mutation in TIMP3 causes a late-onset form of Sorsby fundus dystrophy. *Am J Ophthalmol* 142:839–848
- Mahmoodi M, Sahebjam S, Smookler D et al (2005) Links Lack of tissue inhibitor of metalloproteinases-3 results in an enhanced inflammatory response in antigen-induced arthritis. *Am J Pathol* 166:1733–1740
- Mohammed FF, Smookler DS, Taylor SE et al (2004) Abnormal TNF activity in *Timp3*^{-/-} mice leads to chronic hepatic inflammation and failure of liver regeneration. *Nat Genet* 36:969–977
- Polkinghorne PJ, Capon MRC, Berninger T et al (1989) Sorsby's fundus dystrophy: a clinical study. *Ophthalmology* 96: 1763–1768
- Qi JH, Dai G, Luthert P et al (2009) S156C mutation in tissue inhibitor of metalloproteinases-3 induces increased angiogenesis. *J Biol Chem* 284:19927–19936
- Qi JH, Ebrahem Q, Moore N et al (2003) A novel function for tissue inhibitor of metalloproteinases-3 (TIMP3): inhibition of angiogenesis by blockage of VEGF binding to VEGF receptor-2. *Nat Med* 9:407–415
- Qi JH, Ebrahem Q, Yeow K et al (2002) Expression of Sorsby's fundus dystrophy mutations in human retinal pigment epithelial cells reduces matrix metalloproteinase inhibition and may promote angiogenesis. *J Biol Chem* 277:13394–13400
- Saihan Z, Li Z, Rice J et al (2009) Clinical and biochemical effects of the E139K missense mutation in the TIMP3 gene, associated with Sorsby fundus dystrophy. *Mol Vis* 15:1218–1230
- Sivaprasad S, Webster AR, Egan CA et al (2008) Clinical Course and Treatment Outcomes of Sorsby Fundus Dystrophy. *Am J Ophthalmol* 146:228–234
- Soboleva G, Geis B, Schrewe H et al (2003) Sorsby fundus dystrophy mutation *Timp3*(S156C) affects the morphological and biochemical phenotype but not metalloproteinase homeostasis. *J Cell Physiol* 197:149–156
- Sorsby A, Mason MEJ, Gardner N (1949) A fundus dystrophy with unusual features (late onset and dominant inheritance of a central retinal lesion showing oedema, haemorrhage and exudates developing into generalised choroidal atrophy with massive pigment proliferation). *Br J Ophthalmol* 33: 67–97

- Tabata Y, Isashiki Y, Kamimura K et al (1998) A novel splice site mutation in the tissue inhibitor of the metalloproteinases-3 gene in Sorsby's fundus dystrophy with unusual clinical features. *Hum Genet* 103:179–182
- Troeberg L, Fushimi K, Khokha R et al (2008) Calcium pentosan polysulfate is a multifaceted exosite inhibitor of aggrecanases. *FASEB J* 22:3515–3524
- Weber B, Vogt G, Pruett RC et al (1994) Mutations in the tissue inhibitor of metalloproteinases-3 (TIMP3) in patients with Sorsby's fundus dystrophy. *Nat Genet* 8:352–356
- Weber BH, Lin B, White K et al (2002) A mouse model for Sorsby fundus dystrophy. *Invest Ophthalmol Vis Sci* 43:2732–2740
- Yeow KM, Kishnani NS, Hutton M et al (2002) Sorsby's fundus dystrophy tissue inhibitor of metalloproteinases-3 (TIMP-3) mutants have unimpaired matrix metalloproteinase inhibitory activities, but affect cell adhesion to the extracellular matrix. *Matrix Biol* 21:75–88

Chapter 35

The Importance of Hypoxia-Regulated, RPE-Targeted Gene Therapy for Choroidal Neovascularization

George W. Smith, C. Kathleen Dorey, Howard Prentice, and Janet Blanks

Keywords HIF-1 • Hypoxia • Gene therapy • Retinal pigment epithelium • Choroidal neovascularization • Age-related macular degeneration • Endostatin

35.1 Introduction

Age-related macular degeneration (AMD) is the leading cause of irreversible blindness among adults over the age of 60 in the western world (Ambati et al. 2003; Klein et al. 2004; Zarbin 2004). Currently, in the United States alone, almost two million people suffer from AMD and over seven million more are at risk (Friedman et al. 2004). Acute loss of central vision associated with the “wet” (neovascular) form of AMD is the result of unstable, new blood vessels that grow into the subretinal space from the choroid, the vascular bed behind Bruch’s membrane that supplies

G.W. Smith (✉)

Department of Ophthalmology, John A. Moran Eye Center,
University of Utah, Salt Lake City, UT, USA
e-mail: tyler.smith@hsc.utah.edu

C.K. Dorey

Department of Medicine, Virginia Tech Carilion School of Medicine, Roanoke, VA, USA

H. Prentice

Charles E. Schmidt College of Biomedical Science,
Florida Atlantic University, Boca Raton, FL, USA

Center for Complex Systems and Brain Science, Florida Atlantic University,
Boca Raton, FL, USA

J. Blanks

Department of Biomedical Science, Florida Atlantic University, Boca Raton, FL, USA

Center for Complex Systems and Brain Science,
Florida Atlantic University, Boca Raton, FL, USA

the posterior retina. These abnormal vessels leak fluid and disrupt the sensitive environment of the RPE and photoreceptors, which can cause sudden loss of vision (Green 1999). Although affecting only 20% of AMD-afflicted individuals, the most severe vision loss is associated with the neovascular form (Fine et al. 2000). While the specific pathological events that culminate in subretinal neovascularization are not completely clear, it is thought that age-related changes in the retina, including overwhelming oxidative stress and diminished RPE cell function (Robison et al. 1980; Young 1988; Dorey et al. 1989; Holz et al. 1999; Wassell et al. 1999), initiate local chronic inflammation (Johnson et al. 2000; Anderson et al. 2002), hypoxia (Mousa et al. 1999), and retinal ischemia (Ozaki et al. 1999). Prevention of this pathological angiogenic process, commonly called choroidal neovascularization, or CNV, is a major target for AMD treatment strategies (D'Amato and Adamis 1995; Do 2009). Conventional therapies include repeated intraocular injections of expensive anti-VEGF agents, such as pegaptanib, bevacizumab, and ranibizumab, have short-term effects and are typically administered after vision loss has already occurred. Gene therapy, on the other hand, has the potential to deliver effective doses of anti-angiogenic proteins with a single injection. Though the advantages over conventional methods may seem obvious, potentially damaging complications of constituent transgene expression are concerns that need to be addressed before moving gene therapy for AMD into the clinical arena.

The need for a long-term, regulated, and relatively inexpensive therapeutic option that can be made widely available has yet to be fulfilled. With that goal in mind, a gene therapy platform that exploits the pathological conditions within the retina to drive local production of an angiostatic gene product could be an advantageous new option for treatment of neovascular AMD.

35.2 Constitutive vs. Regulated Expression

An ideal therapeutic approach for the treatment of wet AMD would be to inhibit or reverse overwhelming oxidative stress, substantial inflammatory cytokine production, and neovascularization in the posterior retina. One of the concerns in engineering a gene therapy vector to inhibit neovascularization is how much or how often should the transgene product be produced. The clear choices available are constitutive or regulated production of a gene therapy effector protein. Constitutive production of anti-apoptotic agents has been widely reported in the brain (Mandel et al. 1997; Dong et al. 2005), cardiovascular system (Yin et al. 2004; Zhuo et al. 2009), retina (Bennett et al. 1998; Green et al. 2001; Schuettauf et al. 2004), and other tissues (Murakami et al. 1998; Eaton et al. 2002). In the eye, Takahashi has shown that constitutive expression of endostatin attenuates VEGF-induced vascular leakage, neovascularization, and retinal detachment (Takahashi et al. 2003). Balaggan reported that constitutive expression of endostatin, following subretinal administration, led to a 40% and 60% decrease in CNV area compared to uninjected and null virus, respectively (Balaggan et al. 2006).

While constitutive expression may seem promising, the potential for drawbacks in retinas of patients continuously exposed to high levels of transgene product cannot be ignored. For example, in nondiseased regions of the eye, elevated endostatin could have a range of effects that may alter endogenous cell-to-cell communication and interactions. The possibility of deleterious effects of constitutive endostatin expression in the retina should be analyzed in the future.

Regulation of gene therapy can be achieved by exogenous agents (tetracycline, rapamycin, etc., which allow a switch through an external intervention), or alternatively with an intrinsic stimulus derived from the physiological or pathological status of the tissue (hypoxia, oxidative stress, inflammation, etc.) Gene therapy, regulated by exogenous agents, which involve systemic administration of an activator drug, such as an antibiotic, typically results in low efficiency of regulation with leaky activity in the uninduced state (Agha-Mohammadi et al. 2004). Also, in many diseases where therapeutic intervention would be most effective at the onset of pathology, timing the exogenous trigger may be difficult, especially when the initial pathological events are hard to detect. On the other hand, intrinsically regulated therapies can be auto-initiated by endogenous sensors that are triggered by disease onset, thereby eliminating the decision of when to initiate treatment.

35.3 RPE-Specific Promoters

While the natural anatomical barriers help contain viral vectors within portions of the eye, there is still some concern about the effects of ubiquitous and constitutively expressed transgenes. Tissue-specific promoters offer an additional level of regulation that reduce transgene expression in nontarget cells, and thereby help to minimize any damaging effects of vector-based expression in surrounding healthy tissue. In the eye, different tissue-specific promoters have been used to target photoreceptors (Bennett et al. 1998; Ali et al. 2000; Hauswirth et al. 2000) or RPE cells for retinal degenerations (Kachi et al. 2006). RPE-specific gene expression has been accomplished by using upstream portions of the RPE65 promoter or the vitelliform macular dystrophy (VMD2) promoter (Boulanger et al. 2000; Fraefel et al. 2005; Balaggan et al. 2006). Specifically, RPE-specific gene therapy utilized the RPE65 promoter to deliver RPE65 and rescue vision in RPE65^{-/-} retinal dystrophic dogs (Le Meur et al. 2007).

Both the RPE65 and VMD2 promoters have been used to deliver anti-angiogenic agents with RPE cell-specific expression pattern. Balaggan et al. used a portion of the VMD2 promoter for RPE cell-specific delivery of endostatin and angiostatin by lentiviral vectors and obtained significant reduction of both neovascularization and vascular hyperpermeability in experimental CNV (Balaggan et al. 2006). Similarly, Kachi et al. found significant suppression of experimental CNV in mice treated with equine infectious anemia viral vectors expressing both endostatin and angiostatin (or endostatin alone) driven by the VMD2 promoter (Kachi et al. 2009). Fraefel and colleagues demonstrated efficient, yet transient transfection of rat RPE with GFP by

using the upstream region of the RPE65 promoter in a herpes simplex vector (Kachi et al. 2006). RPE-specific promoters give the advantage of targeting the local environment of CNV development, but regulating their activity can be difficult.

35.4 Hypoxia-Regulated Expression

Another method for controlling transgene expression is to take advantage of endogenous transcription regulatory mechanisms that cells use to adapt to specific microenvironments, like hypoxia or oxidative stress. In certain stressful and potentially pathological conditions, cells have developed abilities to sense and respond to such challenging situations by upregulating genes that are involved in overcoming the stress, such as metabolic enzymes and antioxidants, and downregulating genes that are not necessary for preserving cellular integrity. This is achieved by cis-acting regulatory elements incorporated in and around promoters of genes, which can then be turned off or on by specific transcription factors, or trans-acting elements. This cis/trans regulation can be harnessed as a way to regulate transgene expression in certain pathological situations.

In the retina, increased oxidative stress, hypoxia, and inflammation are known to be the initiating factors leading to enhanced VEGF expression and subsequent development of neovascular AMD. Elevated levels of VEGF have been found in neovascular lesions in both AMD eyes (Sheridan et al. 2009), and laser-induced CNV (Yang et al. 2009). While VEGF is the key angiogenic stimulus, its expression is intrinsically regulated by HIF-1 in response to hypoxia, inflammation, and oxidative stress (Ozaki et al. 1999; Caniggia et al. 2000; Sandau et al. 2001; Stiehl et al. 2002; Jung et al. 2003; Yang et al. 2009). Increased levels of HIF-1 have also been found in CNV lesions from both AMD patients and laser-induced CNV (Vinores et al. 2006; Zhang et al. 2007; Sheridan et al. 2009). Zhang et al. have shown that inhibition of HIF-1 by shRNA can effectively reduce VEGF-induced neovascularization in the laser model (Zhang et al. 2010). Also, Vinores et al. described that removal of the HRE (the binding site for HIF-1) from the VEGF promoter resulted in a tenfold reduction in the size of laser-induced CNV lesions in mice (Vinores et al. 2006). These lines of evidence strongly support selection of the HRE as the basis for a regulated gene therapy approach to the treatment of CNV.

Hypoxia-regulated gene therapy has been proposed as an improved expression strategy for a range of diseases, including cancer, cardiovascular disease, retinal diseases, and ischemic disorders. The regulatory elements conferring hypoxia regulation are primarily HIF-1 binding sites, which were identified and characterized by Semenza et al. (Semenza et al. 1991). The hypoxia-response elements (HREs) were first combined with tissue-specific promoters to target gene expression to ischemic myocardium by Prentice et al. (1997). Importantly, they observed that gene expression declined rapidly when the tissue returned to normoxia. Since then, hypoxia regulation has been used to significantly induce activity of tissue-specific promoters

in cell culture (Binley et al. 1999), as well as animal models of myocardial ischemia (Tang et al. 2005) and cancer (Ruan et al. 2001). Furthermore, Bainbridge has demonstrated that incorporation of multiple copies of the HRE into a promoter resulted in significantly enhanced GFP expression in areas of laser-induced hypoxia in the mouse model (Bainbridge et al. 2003). One concern with their results is that considerable GFP expression was detected in the normoxic controls, indicating substantial normoxic activity from their HRE-enhanced promoter. This may seem a surprising result, but may be explained by the possibility of either leaky basal expression or additional normoxic regulators of the HIF-1 pathway.

Ideally, a hypoxia-regulated gene therapy vector not only should drive enhanced expression in hypoxic conditions, but should also be minimally active in normoxia. Webster et al. developed an elegant solution to silencing hypoxia-regulated gene expression by creating a cassette that includes multiple copies of the HRE and a neuronal silencer element (NRSE) that inactivates transgene expression in tissues other than neurons (Schoenherr and Anderson 1995; Webster 2003). In this valuable construct, it is likely that the binding of HIF-1 to the HRE displaces the trans-acting silencing factor (regulator of the silencer). Promoters containing this element provided robust hypoxia induction of gene expression in ischemic cardiac tissue both in vivo and in vitro (Webster 2003). In exploiting the NRSE in hypoxia responsive promoters, Webster and colleagues subsequently combined three copies of both the HRE and neuron-restrictive silencer in alternating order to construct a hybrid, hypoxia-regulated silencer element, the HRSE (Hernandez et al. 2000). In an analysis of applications for retinal disease, we previously reported that hypoxia-induced, RPE cell-specific expression of a reporter gene was further enhanced by the addition of six hypoxia responsive elements to the promoter (Dougherty et al. 2008). Combining both the HRSE and six additional copies of the HRE regulatory element as upstream regulators of the RPE65 cell-specific promoter resulted in hypoxia-induced transcriptional activation in ARPE-19 cells that was more than 50-fold greater than the activity of the native RPE65 promoter (Dougherty et al. 2008). Additionally, incorporation of multiple neuron-restrictive silencer elements within the HRSE provides nearly 80% reduction in normoxic activity relative to unregulated RPE65 promoter (Dougherty et al. 2008).

35.5 Effectiveness of Endostatin

Selecting an appropriate therapeutic transgene to effectively treat a multifactorial disease such as AMD can be daunting, especially when the complex pathological mechanisms are not fully understood. Fortunately, the angiogenic response in wet AMD is better understood, and many different therapeutic agents have been shown to effectively inhibit pathological neovascularization. The two prevailing approaches are directly blocking VEGF (using antibodies or soluble receptors, etc.) or indirectly inhibiting the angiogenic response to VEGF with endogenous molecules like PEDF,

endostatin, and angiostatin. The latter approach may be more advantageous since directly blocking VEGF may also attenuate its neurotrophic effects on photoreceptors and cell survival effects on the RPE and choriocapillaris. While PEDF, endostatin, and angiostatin are all powerful endogenous angiogenesis inhibitors, endostatin is of particular interest due to its broad range effects on migrating endothelial cells and its relatively small cDNA size, which allow it to easily fit into the small “payload” of some vectors, like adeno-associated virus (AAV). Additionally, unregulated lentiviral delivery of endostatin in a mouse model of laser-induced CNV successfully reduced lesion area by 60% compared to null virus and 40% compared to untreated eyes, and had no harmful effects on established retinal vasculature at 1 year postinjection (Balaggan et al. 2006). The study also reported that unregulated angiostatin had a similar effect on CNV lesion area (50 and 30% reduction in lesion area vs. null virus and uninjected eyes, respectively), though not as much as the endostatin vector. While both vectors similarly reduced neovascular leakage, only the endostatin vector significantly increased apoptosis of neovascular cells within the lesion compared to the null virus (Balaggan et al. 2006). These results suggest that although endostatin and angiostatin have similar mechanisms of action on migrating endothelial cells, endostatin may be a more effective instigator of vessel regression.

35.6 Conclusions

Preliminary experiments employing both HRES and HRE regulatory elements, in combination with the RPE65 promoter, to drive hypoxia-regulated endostatin expression in a mouse model of laser-induced CNV have resulted in significant reduction in mean CNV lesion area (almost 80% compared to PBS-injected controls; unpublished data). Six-month prophylactic treatment with the same vector also showed similar reduction in CNV area; however, more research is needed to establish how successful this highly regulated gene therapy vector can be.

An additional important benefit of our pathology-initiated, site-specific therapeutic platform is the potential for prophylactic application. A major problem with treating AMD is that available therapies are administered after significant damage to the retina has already occurred. Current diagnostic tools, together with genetic predisposition, can only predict the likelihood of disease onset, and if initial signs of AMD are evident, then retinal pathology has, most likely, already begun. Our preliminary data indicates that the hypoxia-regulated, RPE-specific vector can be administered at least 6 months prior to pathology onset, and still be pathology-initiated and fully therapeutically viable. Such a treatment option would overcome the clinical question of when to administer therapy to people with high risk of developing AMD, and would reduce the need for frequent clinical checkups in patients at high risk for CNV.

References

- Agha-Mohammadi S, O'Malley M, Etemad A et al (2004) Second-generation tetracycline-regulatable promoter: repositioned tet operator elements optimize transactivator synergy while shorter minimal promoter offers tight basal leakiness. *J Gene Med* 6:817–828
- Ali RR, Sarra GM, Stephens C et al (2000) Restoration of photoreceptor ultrastructure and function in retinal degeneration slow mice by gene therapy. *Nat Genet* 25:306–310
- Ambati J, Ambati BK, Yoo SH et al (2003) Age-related macular degeneration: etiology, pathogenesis, and therapeutic strategies. *Surv Ophthalmol* 48:257–293
- Anderson DH, Mullins RF, Hageman GS et al (2002) A role for local inflammation in the formation of drusen in the aging eye. *Am J Ophthalmol* 134:411–431
- Bainbridge JW, Mistry A, Binley K et al (2003) Hypoxia-regulated transgene expression in experimental retinal and choroidal neovascularization. *Gene Ther* 10:1049–1054
- Balagagan KS, Binley K, Esapa M et al (2006) EIAV vector-mediated delivery of endostatin or angiostatin inhibits angiogenesis and vascular hyperpermeability in experimental CNV. *Gene Ther* 13:1153–1165
- Bennett J, Zeng Y, Bajwa R et al (1998) Adenovirus-mediated delivery of rhodopsin-promoted bcl-2 results in a delay in photoreceptor cell death in the rd/rd mouse. *Gene Ther* 5:1156–1164
- Binley K, Iqbal S, Kingsman A et al (1999) An adenoviral vector regulated by hypoxia for the treatment of ischaemic disease and cancer. *Gene Ther* 6:1721–1727
- Boulanger A, Liu S, Henningsgaard AA et al (2000) The upstream region of the Rpe65 gene confers retinal pigment epithelium-specific expression in vivo and in vitro and contains critical octamer and E-box binding sites. *J Biol Chem* 275:31274–31282
- Caniggia I, Mostachfi H, Winter J et al (2000) Hypoxia-inducible factor-1 mediates the biological effects of oxygen on human trophoblast differentiation through TGFbeta(3). *J Clin Invest* 105:577–587
- D'Amato RJ, Adamis AP (1995) Angiogenesis inhibition in age-related macular degeneration. *Ophthalmology* 102:1261–1262
- Do DV (2009) Antiangiogenic approaches to age-related macular degeneration in the future. *Ophthalmology* 116:S24–26
- Dong Z, Zhou L, Del Villar K et al (2005) JIP1 regulates neuronal apoptosis in response to stress. *Brain Res Mol Brain Res* 134:282–293
- Dorey CK, Wu G, Ebenstein D et al (1989) Cell loss in the aging retina. Relationship to lipofuscin accumulation and macular degeneration. *Invest Ophthalmol Vis Sci* 30:1691–1699
- Dougherty CJ, Smith GW, Dorey CK et al (2008) Robust hypoxia-selective regulation of a retinal pigment epithelium-specific adeno-associated virus vector. *Mol Vis* 14:471–480
- Eaton D, Gilham DE, O'Neill A et al (2002) Retroviral transduction of human peripheral blood lymphocytes with Bcl-X(L) promotes in vitro lymphocyte survival in pro-apoptotic conditions. *Gene Ther* 9:527–535
- Fine SL, Berger JW, Maguire MG et al (2000) Age-related macular degeneration. *N Engl J Med* 342:483–492
- Fraefel C, Mendes-Madeira A, Mabon O et al (2005) In vivo gene transfer to the rat retina using herpes simplex virus type 1 (HSV-1)-based amplicon vectors. *Gene Ther* 12:1283–1288
- Friedman DS, O'Colmain BJ, Munoz B et al (2004) Prevalence of age-related macular degeneration in the United States. *Arch Ophthalmol* 122:564–572
- Green ES, Rendahl KG, Zhou S et al (2001) Two animal models of retinal degeneration are rescued by recombinant adeno-associated virus-mediated production of FGF-5 and FGF-18. *Mol Ther* 3:507–515
- Green WR (1999) Histopathology of age-related macular degeneration. *Mol Vis* 5:27
- Hauswirth WW, LaVail MM, Flannery JG et al (2000) Ribozyme gene therapy for autosomal dominant retinal disease. *Clin Chem Lab Med* 38:147–153

- Hernandez OM, Discher DJ, Bishopric NH et al (2000) Rapid activation of neutral sphingomyelinase by hypoxia-reoxygenation of cardiac myocytes. *Circ Res* 86:198–204
- Holz FG, Schutt F, Kowitz J et al (1999) Inhibition of lysosomal degradative functions in RPE cells by a retinoid component of lipofuscin. *Invest Ophthalmol Vis Sci* 40:737–743
- Johnson LV, Ozaki S, Staples MK et al (2000) A potential role for immune complex pathogenesis in drusen formation. *Exp Eye Res* 70:441–449
- Jung YJ, Isaacs JS, Lee S et al (2003) IL-1beta-mediated up-regulation of HIF-1alpha via an NFkappaB/COX-2 pathway identifies HIF-1 as a critical link between inflammation and oncogenesis. *FASEB J* 17:2115–2117
- Kachi S, Esumi N, Zack DJ et al (2006) Sustained expression after nonviral ocular gene transfer using mammalian promoters. *Gene Ther* 13:798–804
- Kachi S, Binley K, Yokoi K et al (2009) Equine infectious anemia viral vector-mediated codelivery of endostatin and angiostatin driven by retinal pigmented epithelium-specific VMD2 promoter inhibits choroidal neovascularization. *Hum Gene Ther* 20:31–39
- Klein R, Peto T, Bird A et al (2004) The epidemiology of age-related macular degeneration. *Am J Ophthalmol* 137:486–495
- Le Meur G, Stieger K, Smith AJ et al (2007) Restoration of vision in RPE65-deficient Briard dogs using an AAV serotype 4 vector that specifically targets the retinal pigmented epithelium. *Gene Ther* 14:292–303
- Mandel RJ, Spratt SK, Snyder RO et al (1997) Midbrain injection of recombinant adeno-associated virus encoding rat glial cell line-derived neurotrophic factor protects nigral neurons in a progressive 6-hydroxydopamine-induced degeneration model of Parkinson's disease in rats. *Proc Natl Acad Sci U S A* 94:14083–14088
- Mousa SA, Lorelli W, Campochiaro PA (1999) Role of hypoxia and extracellular matrix-integrin binding in the modulation of angiogenic growth factors secretion by retinal pigmented epithelial cells. *J Cell Biochem* 74:135–143
- Murakami H, Yayama K, Chao L et al (1998) Human kallikrein gene delivery protects against gentamycin-induced nephrotoxicity in rats. *Kidney Int* 53:1305–1313
- Ozaki H, Yu AY, Della N et al (1999) Hypoxia inducible factor-1alpha is increased in ischemic retina: temporal and spatial correlation with VEGF expression. *Invest Ophthalmol Vis Sci* 40:182–189
- Prentice H, Bishopric NH, Hicks MN et al (1997) Regulated expression of a foreign gene targeted to the ischaemic myocardium. *Cardiovasc Res* 35:567–574
- Robison WG, Jr., Kuwabara T, Bieri JG (1980) Deficiencies of vitamins E and A in the rat. Retinal damage and lipofuscin accumulation. *Invest Ophthalmol Vis Sci* 19:1030–1037
- Ruan H, Su H, Hu L et al (2001) A hypoxia-regulated adeno-associated virus vector for cancer-specific gene therapy. *Neoplasia* 3:255–263
- Sandau KB, Zhou J, Kietzmann T et al (2001) Regulation of the hypoxia-inducible factor 1alpha by the inflammatory mediators nitric oxide and tumor necrosis factor-alpha in contrast to desferrioxamine and phenylarsine oxide. *J Biol Chem* 276:39805–39811
- Schoenherr CJ, Anderson DJ (1995) The neuron-restrictive silencer factor (NRSF): a coordinate repressor of multiple neuron-specific genes. *Science* 267:1360–1363
- Schuettauf F, Vorwerk C, Naskar R et al (2004) Adeno-associated viruses containing bFGF or BDNF are neuroprotective against excitotoxicity. *Curr Eye Res* 29:379–386
- Semenza GL, Neufeldt MK, Chi SM et al (1991) Hypoxia-inducible nuclear factors bind to an enhancer element located 3' to the human erythropoietin gene. *Proc Natl Acad Sci U S A* 88:5680–5684
- Sheridan CM, Pate S, Hiscott P et al (2009) Expression of hypoxia-inducible factor-1alpha and -2alpha in human choroidal neovascular membranes. *Graefes Arch Clin Exp Ophthalmol* 247:1361–1367
- Stiehl DP, Jelkmann W, Wenger RH et al (2002) Normoxic induction of the hypoxia-inducible factor 1alpha by insulin and interleukin-1beta involves the phosphatidylinositol 3-kinase pathway. *FEBS Lett* 512:157–162

- Takahashi K, Saishin Y, Silva RL et al (2003) Intraocular expression of endostatin reduces VEGF-induced retinal vascular permeability, neovascularization, and retinal detachment. *FASEB J* 17:896–898
- Tang YL, Tang Y, Zhang YC et al (2005) A hypoxia-inducible vigilant vector system for activating therapeutic genes in ischemia. *Gene Ther* 12:1163–1170
- Vinorez SA, Xiao WH, Aslam S et al (2006) Implication of the hypoxia response element of the Vegf promoter in mouse models of retinal and choroidal neovascularization, but not retinal vascular development. *J Cell Physiol* 206:749–758
- Wassell J, Davies S, Bardsley W et al (1999) The photoreactivity of the retinal age pigment lipofuscin. *J Biol Chem* 274:23828–23832
- Webster KA (2003) Therapeutic angiogenesis: a complex problem requiring a sophisticated approach. *Cardiovasc Toxicol* 3:283–298
- Yang XM, Wang YS, Zhang J et al (2009) Role of PI3K/Akt and MEK/ERK in mediating hypoxia-induced expression of HIF-1 α and VEGF in laser-induced rat choroidal neovascularization. *Invest Ophthalmol Vis Sci* 50:1873–1879
- Yin H, Chao L, Chao J (2004) Adrenomedullin protects against myocardial apoptosis after ischemia/reperfusion through activation of Akt-GSK signaling. *Hypertension* 43:109–116
- Young RW (1988) Solar radiation and age-related macular degeneration. *Surv Ophthalmol* 32:252–269
- Zarbin MA (2004) Current concepts in the pathogenesis of age-related macular degeneration. *Arch Ophthalmol* 122:598–614
- Zhang C, Wang YS, Wu H et al (2010) Inhibitory efficacy of hypoxia-inducible factor 1 α short hairpin RNA plasmid DNA-loaded poly (D, L-lactide-co-glycolide) nanoparticles on choroidal neovascularization in a laser-induced rat model. *Gene Ther* 17:338–351
- Zhang P, Wang Y, Hui Y et al (2007) Inhibition of VEGF expression by targeting HIF-1 α with small interference RNA in human RPE cells. *Ophthalmologica* 221:411–417
- Zhuo Y, Chen PF, Zhang AZ et al (2009) Cardioprotective effect of hydrogen sulfide in ischemic reperfusion experimental rats and its influence on expression of survivin gene. *Biol Pharm Bull* 32:1406–1410

Chapter 36

What Is the Role of CCR3 in Choroidal Neovascularization?

Yiwen Li, Deqiang Huang, Xin Xia, Zhengying Wang,
Lingyu Luo, and Rong Wen

Keywords CNV • Matrigel • CCR3 • SB328437 • AMD • Angiogenesis • VEGF-A • Rapamycin

36.1 Introduction

Age-related macular degeneration (AMD) is the leading cause of blindness in the elderly in the developed world (Klein et al. 1992). AMD presents in two distinct forms: the geographic atrophy and the exudative or “wet” AMD. The wet AMD is characterized by choroidal neovascularization (CNV) in which new blood vessels from the choroid invade the macula area, resulting in retinal edema, hemorrhage, retinal detachment, and disciform scar formation, which eventually destroy the structure of the retina and lead to irreversible loss of central vision. Compiling evidence indicates that vascular endothelial growth factor A (VEGF), the major regulator of vasculogenesis and angiogenesis (Ferrara and Davis-Smyth 1997), is critical in CNV development (Das and McGuire 2003; Grisanti and Tatar 2008; Penn et al. 2008). Clinically, neutralization of VEGF has become standard care in the treatment of wet AMD (Rosenfeld et al. 2005; Brown et al. 2006; Rosenfeld et al. 2006; Emerson and Lauer 2007; Lin and Rosenfeld 2007; Chappelow and Kaiser 2008).

Recently, CCR3 has been reported to play a critical role of in CNV development and CCR3 targeting is believed to be superior to VEGF neutralization in CNV suppression (Takeda et al. 2009). In our attempts to investigate the role of CCR3 in CNV development, no CNV inhibition was observed when CCR3 was blocked

Y. Li (✉) • D. Huang • X. Xia • Z. Wang • L. Luo • R. Wen
Bascom Palmer Eye Institute, University of Miami, Miller School of Medicine,
Miami, FL 33136, USA
e-mail: yli2@med.miami.edu

by either a small molecule CCR3 antagonist SB 328437 or CCR3-neutralizing antibodies in the Matrigel CNV model in mouse and rat, whereas VEGF neutralization by VEGF-neutralizing antibodies effectively suppressed CNV. Rapamycin, an inhibitor of the mammalian target of rapamycin (mTOR), also inhibited CNV efficaciously. These results lead us to conclude that CCR3 plays no role in CNV development and that CCR3 targeting is unlikely to be a promising therapy for CNV.

36.2 Materials and Methods

36.2.1 *Animals and Subretinal Injection of Matrigel*

CNV was induced in adult Sprague Dawley rats and BALB/c mice by subretinal injection of Matrigel transsclerally, as described (Zhao et al. 2007; Cao et al. 2010). Matrigel (growth factor reduced) was diluted with phosphate buffered saline (PBS) or PBS containing substances to be tested at a 3:1 ratio (75% gel). The injection volume was 1.2 μL for rats, 0.8 μL for mice. CCR3-specific antagonist SB 328437, CCR3-neutralizing antibodies (CCR3 ab) (clone 83103, R & D Systems), VEGF-neutralizing antibodies (VEGF ab) (R & D Systems), or rapamycin was dissolved in PBS or dimethyl sulfoxide then PBS. Final concentration is 1 $\mu\text{g}/\mu\text{L}$ of CCR3 ab or VEGF ab, 10 $\mu\text{g}/\mu\text{L}$ of SB 328437 or rapamycin.

36.2.2 *Visualization of Blood Vessels and Measurement of CNV*

Blood vessels were labeled with a solution containing DiI, as described (Li et al. 2008). Animals were killed and perfused with DiI. Eyecups were embedded in 5% agarose and cut to obtain serial vibratome sections (100 μm thick) to cover the entire Matrigel area. Sections were examined by confocal microscopy. CNV area was calculated as described (Cao et al. 2010) and analyzed statistically by Kruskal-Wallis and Dunn's test. Data are expressed as mean \pm SD. Double asterisks: $P < 0.01$; Triple asterisks: $P < 0.001$.

36.3 Results

36.3.1 *Development of CNV in the Matrigel Model*

Angiogenic sprouts are detected as early as in 4 days after Matrigel injection. The CNV network is well developed in 10 days after injection and increases progressively in size (Cao et al. 2010). Figure 36.1 shows a typical CNV network in the Matrigel-injected area. The 3D reconstruction of the CNV network in the entire

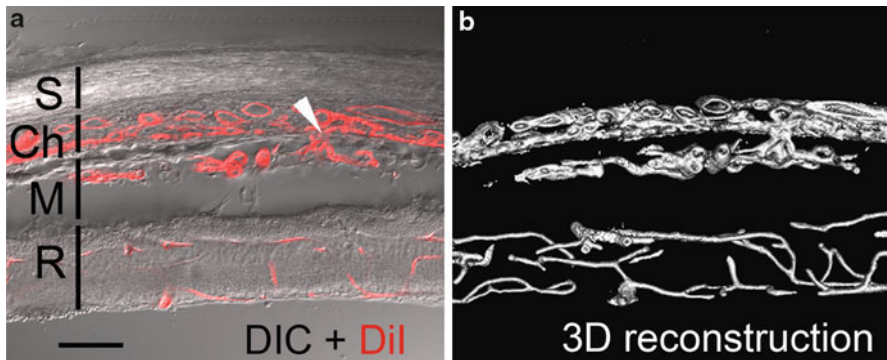


Fig. 36.1 CNV induced by subretinal Matrigel. CNV network was well developed in a rat eye 10 days after Matrigel injection. (a) Shows a DIC image of a retinal section (*gray*) superimposed to a confocal fluorescent image (*red*). The site of CNV entering the Matrigel area is indicated by an *arrowhead* (a). A 3D-reconstruction of vasculature in the entire thickness of the section is shown in (b). Layers of the eye are: *S* sclera; *Ch* choroid; *M* Matrigel; *R* retina. Scale bar: 100 μ m

thickness of the section clearly shows the origin of the new blood vessels and the interconnection (Fig. 36.1b).

36.3.2 CCR3 Targeting and CNV Development in Rats and Mice

CCR3 was blocked by a specific antagonist SB328437 and CCR3-neutralizing antibodies at the optimal concentrations reported to inhibit CNV (Takeda et al. 2009). Figure 36.2 shows representative images of CNV in rat eyes. Neither SB328437 nor CCR3 ab inhibited CNV. In many eyes treated with SB328437 (Fig. 36.2b) or CCR3 ab (Fig. 36.2c), the extent of CNV seemed to be larger than that typically seen in untreated controls (Fig. 36.2a). In contrast, minimal CNV was found in eyes treated with VEGF ab (Fig. 36.2d) or rapamycin (Fig. 36.2e). In fact, CNV was completely absent in 10 out of 14 eyes treated with VEGF-A antibodies, and 13 out of 16 in rapamycin-treated eyes in rat. In the 10 mouse eyes treated with rapamycin, only one had minimal CNV, whereas the other 9 had none.

Quantitative data show in rat the CNV area in control eyes is 3.63 ± 1.64 ($n=13$), 6.83 ± 5.31 ($n=15$) in SB328437, and 7.55 ± 3.91 ($n=16$) in CCR3 ab treated eyes (Fig. 36.3a). No statistically significant difference was found between control eyes and eyes treated with SB328437 or CCR3 ab (Fig. 36.3a). In contrast, the CNV areas are 0.19 ± 0.32 ($n=14$) in the eyes treated with VEGF ab, and 0.05 ± 0.12 ($n=16$) in rapamycin-treated eyes (Fig. 36.3a). CNV inhibition by both VEGF ab and rapamycin is highly significant when compared with the control eyes ($P < 0.01$), or eyes treated with SB328437 or CCR3 ab ($P < 0.001$) (Fig. 36.3a).

In mouse, the results are very similar. CNV area is 1.29 ± 0.92 ($n=14$) in control eyes, 2.03 ± 2.1 ($n=15$) in eyes treated with SB328437, and 2.2 ± 1.89 ($n=22$) in

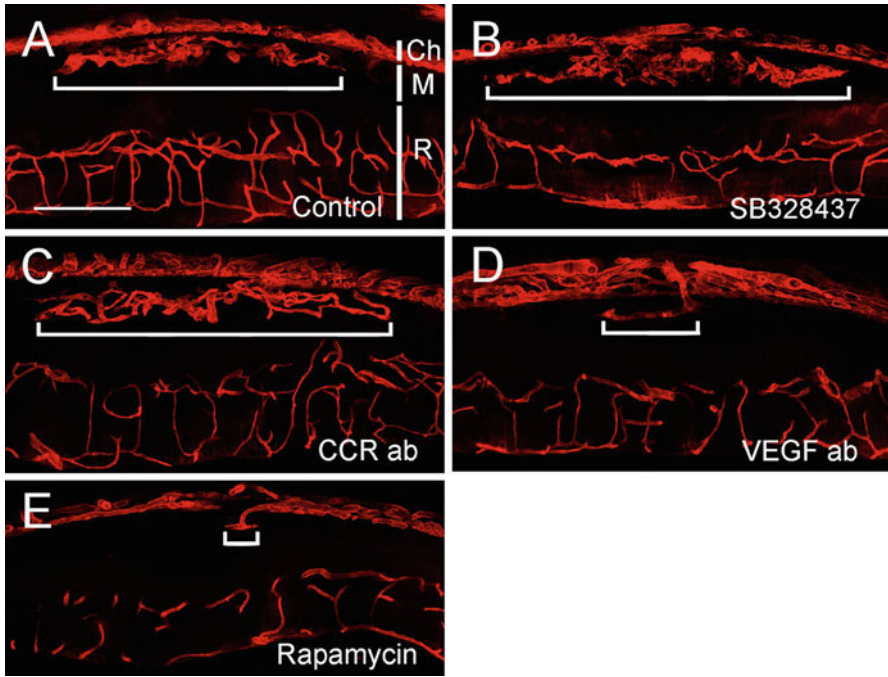


Fig. 36.2 Effects of SB328437, CCR3 ab, VEGF ab, or rapamycin on CNV in rats. Eyes were injected with Matrigel alone or mixed with SB328437, CCR3 ab, VEGF ab, or rapamycin and collected 12 days later. Extensive CNV was seen in the control eyes (a) as well as the eyes treated with SB328437 (b), CCR3 ab (c). Minimal CNV was found in eyes treated with VEGF ab (d) or rapamycin (e). The width of CNV is indicated by a horizontal bar in each section. The layers of the eye are indicated by vertical white bars in (a): Ch choroids; M Matrigel; R retina. Scale bar: 200 μm

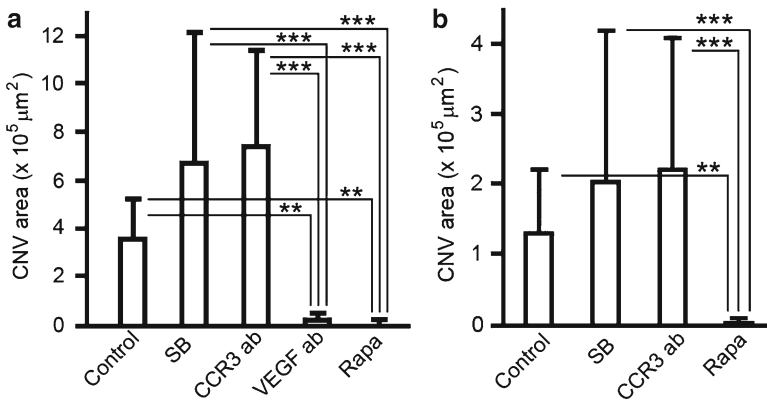


Fig. 36.3 Quantification of CNV area. The CNV area of each eye was calculated as described (Cao et al. 2010). No statistically significant difference was found between the control eyes and eyes treated with SB328437 or CCR3 ab in rat (a) or in mouse (b). The CNV area in eyes treated with VEGF ab in rat (a) or in rapamycin treated eyes in both rat (a) and mouse (b) are significantly smaller than the control eyes (a, b) (** $P < 0.01$) or eyes treated with SB328437 (a, b) or CCR3 ab (a) (***) ($P < 0.001$)

eyes treated with CCR3 ab (Fig. 36.3b). Again, no statistically significant difference was found between control eyes and eyes treated with SB328437 or CCR3 ab in mouse (Fig. 36.3b). The CNV area in rapamycin-treated eyes is 0.008 ± 0.024 ($n=10$) (Fig. 36.3b), significantly smaller than in the control eyes ($P < 0.01$) or eyes treated with SB328437 or CCR3 ab ($P < 0.001$) (Fig. 36.3b).

36.4 Discussion

We have demonstrated the failure of CNV inhibition by CCR3 targeting with either CCR3 ab or CCR3 antagonist SB328437 in the subretinal Matrigel models of CNV. On the other hand, VEGF neutralization and mTOR targeting with rapamycin significantly suppressed CNV.

The Matrigel CNV model was first reported in rat (Wen et al. 2002). Subsequently, it was found in rabbit that subretinal Matrigel induces highly permeable neovascularization (Qiu et al. 2006). The Matrigel-induced CNV has been characterized recently in details in rat (Cao et al. 2010). The Matrigel induced CNV increases in size progressively, which is accompanied by infiltration of leukocytes and myofibroblasts as well as deposition of collagen (Cao et al. 2010). These features resemble the inflammatory reaction and fibrosis in wet AMD in patients, showing that the Matrigel model closely mimics the CNV in patients with wet AMD. VEGF neutralization and rapamycin treatment effectively suppressed CNV in the Matrigel model (Cao et al. 2010) (present work), consistent with findings from the laser-induced CNV model (Kwak et al. 2000; Saishin et al. 2003; Dejneka et al. 2004) and demonstrating the similarity between the two models. It is therefore unlikely that the discrepancy between our findings and the report showing the CCR3 targeting was more effective than VEGF neutralization (Takeda et al. 2009) is due to the difference in the CNV models used. The concentrations of CCR3 inhibitors used in our experiments were reportedly the optimal concentrations for CNV inhibition in the laser-induced CNV model (Takeda et al. 2009), which should have been sufficient for CCR3 inhibition, especially considering that the inhibitors were delivered in situ (in gel).

Our data confirm the efficacy of VEGF neutralization on CNV suppression, consistent with the critical role of VEGF in CNV development and maintenance reported by many previous studies. In addition, nearly complete inhibition of CNV by rapamycin in our study is in agreement with a previous report showing that systemically administered rapamycin significantly suppressed laser-induced CNV in mouse (Dejneka et al. 2004).

In summary, our attempts to investigate the role of CCR3 in CNV in the Matrigel CNV model yield consistent negative results in two species, leading to the conclusion that CCR3 is not critically in CNV development and maintenance. CCR3 targeting therefore is unlikely to be a viable therapeutic approach for CNV. On the other hand, our results support the therapeutic strategies to suppress CNV with anti-VEGF agents and rapamycine.

Acknowledgments This work was supported by grants from the James and Esther King Biomedical Research Program of the State of Florida (YL), National Institutes of Health (R01EY015289 to RW, R01EY018586 to RW), Hope for Vision (RW), and the Department of Defense (W81XWH-09-1-0674 to RW). It was also supported by NIH core grant P30EY14801 and an unrestricted grant from Research to Prevent Blindness Inc. to Bascom Palmer Eye Institute.

References

- Brown DM, Kaiser PK, Michels M et al (2006) Ranibizumab versus verteporfin for neovascular age-related macular degeneration. *N Engl J Med* 355:1432–1444
- Cao J, Zhao L, Li Y et al (2010) A subretinal matrigel rat choroidal neovascularization (CNV) model and inhibition of CNV and associated inflammation and fibrosis by VEGF Trap. *Invest Ophthalmol Vis Sci* 51:6009–6017
- Chappelov AV, Kaiser PK (2008) Neovascular age-related macular degeneration: potential therapies. *Drugs* 68:1029–1036
- Das A, McGuire PG (2003) Retinal and choroidal angiogenesis: pathophysiology and strategies for inhibition. *Prog Retin Eye Res* 22:721–748
- Dejneka NS, Kuroki AM, Fosnot J et al (2004) Systemic rapamycin inhibits retinal and choroidal neovascularization in mice. *Mol Vis* 10:964–972
- Emerson MV, Lauer AK (2007) Emerging therapies for the treatment of neovascular age-related macular degeneration and diabetic macular edema. *BioDrugs* 21:245–257
- Ferrara N, Davis-Smyth T (1997) The biology of vascular endothelial growth factor. *Endocr Rev* 18:4–25
- Grisanti S, Tatar O (2008) The role of vascular endothelial growth factor and other endogenous interplayers in age-related macular degeneration. *Prog Retin Eye Res* 27:372–390
- Klein R, Klein BE, Linton KL (1992) Prevalence of age-related maculopathy. The Beaver Dam Eye Study. *Ophthalmology* 99:933–943
- Kwak N, Okamoto N, Wood JM et al (2000) VEGF is major stimulator in model of choroidal neovascularization. *Invest Ophthalmol Vis Sci* 41:3158–3164
- Li Y, Song Y, Zhao L et al (2008) Direct labeling and visualization of blood vessels with lipophilic carbocyanine dye DiI. *Nat Protoc* 3:1703–1708
- Lin RC, Rosenfeld PJ (2007) Antiangiogenic therapy in neovascular age-related macular degeneration. *Int Ophthalmol Clin* 47:117–137
- Penn JS, Madan A, Caldwell RB et al (2008) Vascular endothelial growth factor in eye disease. *Prog Retin Eye Res* 27:331–371
- Qiu G, Stewart JM, Sadda S et al (2006) A new model of experimental subretinal neovascularization in the rabbit. *Exp Eye Res* 83:141–152
- Rosenfeld PJ, Brown DM, Heier JS et al (2006) Ranibizumab for neovascular age-related macular degeneration. *N Engl J Med* 355:1419–1431
- Rosenfeld PJ, Schwartz SD, Blumenkranz MS et al (2005) Maximum tolerated dose of a humanized anti-vascular endothelial growth factor antibody fragment for treating neovascular age-related macular degeneration. *Ophthalmology* 112:1048–1053
- Saishin Y, Takahashi K, Lima Silva R et al (2003) VEGF-TRAP(R1R2) suppresses choroidal neovascularization and VEGF-induced breakdown of the blood-retinal barrier. *J Cell Physiol* 195:241–248
- Takeda A, Baffi JZ, Kleinman ME et al (2009) CCR3 is a target for age-related macular degeneration diagnosis and therapy. *Nature* 460:225–230
- Wen et al (2002) IOVS 2002; 43:ARVO E-abstract 1297
- Zhao L, Wang Z, Liu Y et al (2007) Translocation of the retinal pigment epithelium and formation of sub-retinal pigment epithelium deposit induced by subretinal deposit. *Mol Vis* 13:873–880

Chapter 37

Intermittent But Not Constant High Glucose Induces ER Stress and Inflammation in Human Retinal Pericytes

Yimin Zhong, Joshua J. Wang, and Sarah X. Zhang

Keywords Endoplasmic reticulum stress • Inflammation • Retinal pericyte • MCP-1 • CHOP • Diabetic retinopathy

37.1 Introduction

Increased inflammatory cytokines in the retina are closely associated with retinal pathologies in diabetic retinopathy (Li et al. 2009b). Pericytes, along with endothelial cells, are the major cell components of retinal capillaries. Pericytes activated by oxidized lipids secrete high levels of inflammatory cytokines, such as macrophage chemoattractant protein 1 (MCP-1) (Zhang et al. 2008). In addition, pericyte injury and cell death are considered as a hallmark pathological change in diabetic retinopathy. Although the mechanisms underlying diabetes-induced pericyte injury are not fully understood, studies suggest that fluctuating glucose, when compared to constantly increased glucose concentration, is more detrimental to vascular cells, including pericytes (Quagliaro et al. 2003; Beltramo et al. 2009). In addition, fluctuating glucose stimulates a greater increase in inflammatory cytokine production from endothelial cells than stable high glucose (Piconi et al. 2004). However, it is unclear whether glucose fluctuation influences inflammatory mediators in pericytes.

Y. Zhong

Department of Medicine, Endocrinology and Diabetes, Harold Hamm Oklahoma Diabetes Center, University of Oklahoma Health Sciences Center, Oklahoma City, OK 73104, USA

State Key Laboratory of Ophthalmology, Zhongshan Ophthalmic Center, Sun Yat-sen University, Guangzhou 510060, China

J.J. Wang • S.X. Zhang (✉)

Department of Medicine, Endocrinology and Diabetes, Harold Hamm Oklahoma Diabetes Center, University of Oklahoma Health Sciences Center, Oklahoma City, OK 73104, USA
e-mail: xin-zhang@ouhsc.edu

Moreover, we recently demonstrated that endoplasmic reticulum (ER) stress is implicated in retinal inflammation during diabetes (Li et al. 2009a). In the present study, we evaluated the effects of intermittent and constant high glucose and the role of ER stress in inflammatory factor production in retinal pericytes.

37.2 Materials and Methods

37.2.1 Materials

Sodium 4-phenyl butyrate and tauroursodeoxycholic acid were purchased from Calbiochem (San Diego, CA). Anti-VEGF, anti-ATF4, and anti-CHOP antibodies were obtained from Santa Cruz Biotechnology (Santa Cruz, CA). Anti-nucleoporin p62 antibody was from BD Biosciences Pharmingen (San Diego, CA). Anti-KDEL (for detection of GRP78) and anti- β -actin antibodies were obtained from Abcam (Cambridge, MA). Horse-radish peroxidase-conjugated secondary antibodies were obtained from Vector Laboratories (Burlingame, CA).

37.2.2 Cell Culture

Primary human retinal pericytes (HRP) were purchased from Clonetics, Inc. (Walkersville, MD). Cells were maintained in Dulbecco's modified Eagle's medium (DMEM) containing 10% fetal bovine serum (FBS) and 1% antibiotic/antimycotic. After reaching 50% of confluence, cells were exposed to the following experimental conditions for 8 days with medium replaced every 2 days: (1) normal glucose (5 mM); (2) constant high glucose (HG, 25 mM); (3) normal and high glucose alternating every 48 h. On day 8, cells were quiescent in DMEM with 1% FBS for 24 h. Medium were collected and cells harvested for analysis.

37.2.3 Western Blot Analysis

Western blot analysis was performed as described previously (Li et al. 2009a). Briefly, cells were lysed in radioimmunoprecipitation assay lysis buffer. Nuclear and cytoplasmic extracts were prepared using a Nuclear Extract Kit (Active Motif, Carlsbad, CA) following manufacturer's instructions. Twenty-five micrograms of protein were dissolved by SDS-PAGE. Primary antibodies used for blotting include: anti-KDEL (1:5,000), anti-ATF4 (1:500), anti-GADD153 (1:500), anti-VEGF (1:500), anti- β -actin (1:5,000), and anti-nucleoporin p62 (1:2,000) antibodies.

37.2.4 Quantification of MCP-1 Secretion in Pericytes

MCP-1 secreted into the medium was measured using the DuoSet ELISA kit for human MCP-1 (R&D Systems, Minneapolis, MN) according to manufacturer's instructions as described previously (Zhang et al. 2008).

37.2.5 Statistical Analysis

Data were expressed as mean \pm SD. Statistical analysis was performed using Student *t*-test when comparing two groups, or ANOVA with Bonferroni's post hoc test when comparing three or more groups. Statistical significance was accepted as $P < 0.05$.

37.3 Results

37.3.1 High Glucose Suppresses GRP78 Expression in HRP

Glucose regulated protein (GRP78), also known as heat shock 70 kDa protein 5 (hsp70-5 or hspA5) or immunoglobulin heavy chain-binding protein (BiP), is a prominent ER chaperone that promotes appropriate protein folding. Pharmaceutical induction of GRP78 expression or overexpression of GRP78 gene in the retina protect retinal ganglion cells and photoreceptors from ER stress-induced apoptosis and cell death, suggesting that GRP78 is a cyto-protective factor in retinal cells (Gorbatyuk et al. 2010; Inokuchi et al. 2008). In the present study, we examined expression of GRP78 in HRP after exposure to constant or intermittent high glucose for 8 days. We found that GRP78 level was decreased in both constant and intermittent high glucose-treated cells when compared to cells exposed to normal glucose. Intermittent glucose induced a more remarkable decrease in GRP78 expression when compared to constant high glucose (Fig. 37.1a, b), indicative of an inhibitory effect of high glucose on GRP78 expression.

37.3.2 Intermittent But Not Constant High Glucose Activates ATF4/CHOP and Increases MCP-1 Secretion in HRP

Activating transcription factor 4 (ATF4) and its target gene C/EBP homologous protein (CHOP) are important ER stress response genes that trigger inflammatory and apoptotic cascades (Endo et al. 2006). We next determined the effect of high glucose on ATF4 and CHOP expression. As both ATF4 and CHOP are transcription factors, which translocate into the nucleus when activated, we thus measured the

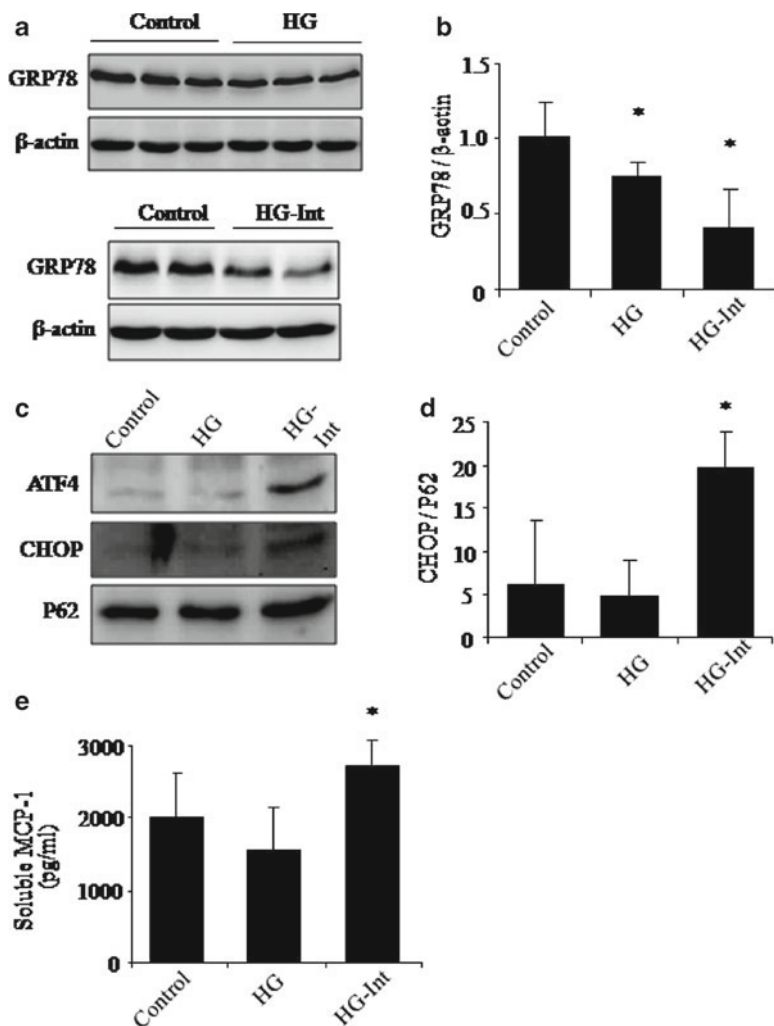


Fig. 37.1 Effects of intermittent and constant high glucose on ER stress and MCP-1 secretion in HRP. HRP were exposed to constant high glucose (HG), intermittent high glucose (HG-Int), or normal glucose (Control) for 8 days. (a) GRP78 expression in cells exposed to constant high glucose (upper panel) or intermittent high glucose (lower panel). Representative blots from three independent experiments. (b) Quantification of GRP78 expression by densitometry (mean \pm SD, $n=3$). (c, d) Nuclear levels of ATF4 and CHOP evaluated by Western blot analysis and semiquantified by densitometry (mean \pm SD, $n=3$). (e) Soluble MCP-1 secreted into the medium measured by ELISA (mean \pm SD, $n=3$). * $P<0.05$ vs. control

level of ATF4 and CHOP protein in nuclear extract from HRP. We found that ATF4 and CHOP are expressed at very low level in cells cultured in normal glucose. Exposure to constant high glucose did not alter ATF4 or CHOP expression. In contrast, intermittent high glucose induced a significant increase in nuclear levels of ATF4 and CHOP, suggesting an activation of ER stress in HRP (Fig. 37.1c, d).

To determine if induction of ER stress by glucose fluctuation is associated with increased inflammation, we measured MCP-1 secretion from HRP after treatment with constant or intermittent high glucose for 8 days. We found that intermittent high glucose induced a significant increase in MCP-1 secretion when compared to normal glucose and constant high glucose, while constant high glucose had no effect on MCP-1 secretion (Fig. 37.1e). These results corroborate the changes in ATF4 and CHOP expression, suggesting that only intermittent, but not constant, high glucose induces ER stress and inflammatory mediators in HRP.

37.3.3 Inhibition of ER Stress by Chemical Chaperones Alleviates Inflammatory Cytokine Expression in HRP Exposed to Intermittent High Glucose

Sodium 4-phenyl butyrate (PBA) and tauroursodeoxycholic acid (TUDCA) are small molecule chaperones that suppress the induction of ER stress (Li et al. 2009a). To investigate if ER stress plays a role in glucose fluctuation-induced inflammation in pericytes, HRP were pretreated with TUDCA or PBA for 8 h, followed by incubation with intermittent high glucose for 8 days. MCP-1 secreted into the medium was measured by ELISA. We found that TUDCA and PBA dose dependently decreased intermittent high glucose-induced MCP-1 secretion from HRP. Vascular endothelial growth factor (VEGF) is a key proinflammatory cytokine in the pathogenesis of vascular leakage and retina neovascularization in diabetic retinopathy (Li et al. 2009a). We also measured VEGF expression in HRP by Western blot analysis. The results show that VEGF expression was markedly increased by intermittent high glucose, and the increase was largely abolished by ER stress inhibitor TUDCA and PBA. As CHOP is a key mediator of ER stress-induced inflammatory response and apoptosis, we further examined CHOP expression in HRP treated with TUDCA or PBA. We found that TUDCA and PBA effectively suppressed the induction of CHOP expression by intermittent high glucose. These results collectively suggest that ER stress plays a critical role in glucose fluctuation-induced inflammation in HRP (Fig. 37.2).

37.4 Discussion

The endoplasmic reticulum (ER) has long been recognized as a cellular factory for protein processing. Intriguingly, emerging evidence suggests that the ER also acts as a principal stress sensor that initiates numerous intracellular signaling pathways implicated in pathological conditions, such as inflammation and apoptosis. C/EBP homologous protein (CHOP), a target gene of ATF4, is a key mediator of ER stress-associated inflammatory and apoptotic processes. Inhibition of CHOP expression attenuates inflammation and prevents caspase activation and apoptotic cascade in

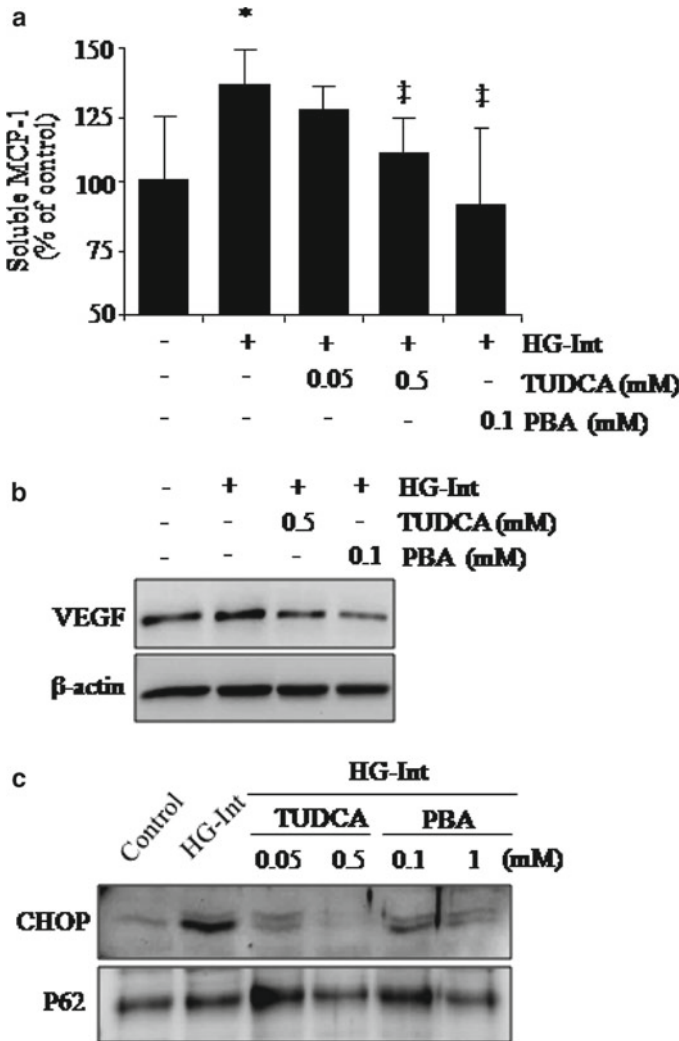


Fig. 37.2 Chemical chaperones ameliorate intermittent high glucose-induced inflammatory cytokine production and CHOP expression. HRP were exposed to intermittent high glucose (HG-Int) with or without the chemical chaperones TUDCA and PBA for 8 days. (a) Secretion of MCP-1 into the medium was measured by ELISA (mean±SD, n=4). *P<0.05 vs. control. ‡P<0.05 vs. HG-Int. (b) Expression of VEGF was determined by Western blot analysis. (c) Nuclear level of CHOP was determined by Western blot analysis in nuclear extract. Representative blots from three independent experiments

cells exposed to LPS or diabetic stressors(Song et al. 2008). Our recent study shows that CHOP and ATF4 expression is significantly elevated, accompanied by increased retinal inflammation and vascular leakage, in the retina in diabetic animals (Li et al. 2009a). Induction of ER stress is sufficient to induce inflammatory cytokine

expression in the retina. Conversely, suppression of ER stress using small molecule ER chaperones significantly alleviates diabetes- and ischemia-induced retinal inflammation, suggesting ER stress is a potential mediator of inflammatory damage of retinal cells in diabetic retinopathy. In the present study, we further addressed the role of ER stress in high glucose-induced inflammation in pericytes. We found that exposure of HRP to intermittent high glucose induces ATF4 and CHOP activation and inflammatory cytokine expression. Moreover, inhibition of ATF4 and CHOP by chemical chaperones largely reversed fluctuating high glucose-induced VEGF and MCP-1 expression. These results suggest that ATF4 and CHOP activation secondary to ER stress contributes to pericyte inflammation in diabetes.

Although we have shown that glucose fluctuation induces ER stress in pericytes, the mechanisms underlying the activation of ATF4/CHOP pathway remain poorly understood. GRP78 is recognized as a protective factor against ER stress-induced inflammation and cell damage. We found that persistent high glucose for 8 days suppressed GRP78 expression, but did not induce ATF4 and CHOP activation. In contrast, intermittent exposure to high glucose caused a more marked decrease in GRP78 expression, accompanied by increased ATF4 and CHOP expression. The association between decreased GRP78 expression and activation of ATF4 and CHOP remains to be elucidated. In addition, Ikesugi and associates reported glucose deprivation, but not high glucose, elicits ER stress in rat retinal pericytes (Ikesugi et al. 2006). It is possible that the repetitive shift from high glucose to normal glucose during glucose fluctuation induces ER stress, while GRP78 suppression compromises the protein folding capacity of the ER, resulting in exaggerated ATF4/CHOP activation and inflammation in retinal pericytes. In addition, increased ATF4/CHOP activation may also contribute to pericyte apoptosis induced by glucose fluctuation. Future studies are warranted to investigate how ER stress-associated apoptotic pathway is implicated in retinal cell death in diabetic retinopathy.

Acknowledgments This work was supported by National Institutes of Health grant EY019949; Research Award 5-2009-475 from Juvenile Diabetes Research Foundation; Research Grants HR07-167 and HR10-060 from Oklahoma Center for the Advancement of Science and Technology; Research Grant M2010088 from American Health Assistance Foundation; and Dr. William Talley Research Award from Harold Hamm Oklahoma Diabetes Center.

References

- Beltramo E, Berrone E, Tarallo S et al (2009) Different apoptotic responses of human and bovine pericytes to fluctuating glucose levels and protective role of thiamine. *Diabetes Metab Res Rev* 25:566–576
- Endo M, Mori M, Akira S et al (2006) C/EBP Homologous Protein (CHOP) Is Crucial for the Induction of Caspase-11 and the Pathogenesis of Lipopolysaccharide-Induced Inflammation. *J Immunol* 176:6245–6253
- Gorbatyuk MS, Knox T, LaVail MM et al. (2010) Restoration of visual function in P23H rhodopsin transgenic rats by gene delivery of BiP/Grp78. *Proc Natl Acad Sci U S A* 107:5961–5966
- Ikesugi K, Mulhern ML, Madson CJ et al (2006) Induction of endoplasmic reticulum stress in retinal pericytes by glucose deprivation. *Curr Eye Res* 31:947–953

- Inokuchi Y, Nakajima Y, Shimazawa M et al (2008) Effects of an Inducer of BiP, a Molecular Chaperon, on Endoplasmic Reticulum (ER) Stress-Induced, Limits Retinal Cell Death. *Invest Ophthalmol Vis Sci* 50:334–344
- Li J, Wang JJ, Yu Q et al (2009a) Endoplasmic Reticulum Stress is implicated in Retinal Inflammation and Diabetic Retinopathy. *FEBS Lett* 183:1521–1527
- Li J, Wang JJ, Chen D et al (2009b) Systemic administration of HMG-CoA reductase inhibitor protects the blood-retinal barrier and ameliorates retinal inflammation in type 2 diabetes. *Exp Eye Res* 89:71–78
- Piconi L, Quagliari L, Da Ros R et al (2004) Intermittent high glucose enhances ICAM-1, VCAM-1, E-selectin and interleukin-6 expression in human umbilical endothelial cells in culture: the role of poly(ADP-ribose) polymerase. *J Thromb Haemost* 2:1453–1459
- Quagliari L, Piconi L, Assaloni R et al (2003) Intermittent High Glucose Enhances Apoptosis Related to Oxidative Stress in Human Umbilical Vein Endothelial Cells. *Diabetes* 52: 2795–2804
- Song B, Scheuner D, Ron D et al (2008) Chop deletion reduces oxidative stress, improves beta cell function, and promotes cell survival in multiple mouse models of diabetes. *J Clin Invest* 118:3378–3389
- Zhang SX, Wang JJ, Dashti A et al (2008) Pigment epithelium-derived factor (PEDF) mitigates inflammation and oxidative stress in retinal pericytes exposed to oxidized-LDL. *J Mol Endocrinol* 41:135–143

Chapter 38

Regulation of Retinal Vascular Permeability by Betacellulin

Masahiko Sugimoto, Alecia Cutler, Gregory Grossman, and Bela Anand-Apte

Keywords Diabetic retinopathy • Retinal vascular permeability • Diabetic macular edema • Betacellulin • Epidermal growth factor receptor

38.1 Introduction

Diabetes mellitus (DM) and its retinal complications: DM is a chronic disease that has developed into a worldwide epidemic with the number of cases expected to reach 300 million by the year 2025. Diabetic retinopathy is a common sequelae of both type I (insulin dependent) and type II (insulin independent) diabetes and is the most common cause of blindness in working age adults in the United States of America (Klein and Klein 2010). Severity of hyperglycemia and duration of the disease in addition to hypertension are strong risk factors for the development of diabetic retinopathy. Intervention studies have determined that while intensive treatment of diabetes reduced the development of diabetic retinopathy (Group 1993a, 1995; Group et al. 2008), it was associated with a two to threefold increased risk of severe hypoglycemia (Group 1993a) as well as an increased risk of mortality from cardiovascular disease (Ismail-Beigi et al. 2010). However, the fundamental pathophysiological mechanisms that lead to diabetic retinopathy as a consequence of hyperglycemia have not been established. Identifying the downstream effectors specific for the development of retinopathy will allow the therapeutic targeting of these pathologies.

M. Sugimoto • A. Cutler • G. Grossman • B. Anand-Apte (✉)
Department of Ophthalmology, Cole Eye Institute, Cleveland Clinic Lerner College of Medicine
at Case Western Reserve University, Cleveland, OH, USA
e-mail: anandab@ccf.org

38.2 Betacellulin: Structure and Expression

Betacellulin (BTC), a member of the epidermal growth factor (EGF) family, was originally isolated from the conditioned medium of a mouse pancreatic b-tumor cell line (Shing et al. 1993). Mature secreted BTC is a 32-kDa glycoprotein composed of 80 amino acid residues (Asp1-Tyr80) generated by cleavage of a 178 amino acid membrane-anchored precursor protein (pro-BTC). The carboxyterminal 50-residue region of BTC (Arg31-Tyr80) contains the conserved consensus sequence of the EGF family of proteins (Miura et al. 2002). Many of EGF family members are proteolytically processed and the active forms of the proteins released from cells. Cleavage of the membrane-anchored forms of BTC to release a secreted form occurs principally by ADAM-10 (a disintegrin and metalloprotease-10) (Sahin et al. 2004; Blobel 2005; Sanderson et al. 2005; Sahin and Blobel 2007) as well as endothelin-1 (Sanderson et al. 2006).

Strong BTC mRNA expression has been detected in a number of tissues including pancreas, liver, kidney, and small intestine in addition to somewhat lower expression in heart, lung, liver, skeletal muscle, kidney, prostate, testis, ovary, and colon (Sasada et al. 1993; Seno et al. 1996). In the eye, BTC protein is synthesized by retinal pigment epithelial, endothelial, and Muller cell lines (Anand-Apte et al. 2010). In the pancreas, BTC expression has been localized to islet cell populations closely associated with insulin-producing b-cells (Miyagawa et al. 1999).

38.3 Biological Function of BTC

BTC is unique among members of the EGF family in its ability to regulate pancreatic islet physiology. BTC can induce the proliferation of fetal pancreatic cells (Sundaresan et al. 1998; Demeterco et al. 2000) and stimulate the conversion of non- β -cells into β -like insulin-producing cells (Mashima et al. 1996; Watada et al. 1996; Yoshida et al. 2002; Li et al. 2005). BTC has the potential to induce the differentiation of β -cells within the islets of embryonic pancreatic explant cultures (Huotari et al. 2002) and enhance insulin secretion by islet cells (Dahlhoff et al. 2009). These properties have led to experiments examining the specific β -cell proliferative properties of BTC in diabetic models. Injection of recombinant BTC significantly reduced blood glucose levels (Ogata et al. 2004) and promoted b-cell regeneration (Yamamoto et al. 2000; Li et al. 2003) and glucose tolerance in streptozotocin-induced diabetic as well as pancreatectomized rats (Li et al. 2001). More recently, it has been demonstrated that adenoviral-mediated expression of BTC could result in a significant remission of metabolic diabetes following a single treatment (Shin et al. 2008).

38.4 Betacellulin Induces Angiogenesis

BTC is a growth factor that signals predominantly via the ErbB1 and ErbB4 receptors, but is also capable of binding and activating ErbB1/ErbB2, ErbB1/ErbB3, ErbB1/ErbB4, ErbB2/ErbB3, and ErbB2/ErbB4 (Alimandi et al. 1997). BTC induces angiogenesis via activation of EGF receptors, mitogen-activated protein kinase, and phosphatidylinositol 3'-kinase/Akt in endothelial cells. In addition, BTC stimulates the growth and migration of vascular smooth muscle cells (Mifune et al. 2004) as well as wound healing and associated angiogenesis (Schneider et al. 2008) which indicates a potential role for this protein in vascular remodeling. Earlier studies have reported that overexpression of BTC by hepatocellular carcinoma cells along with EGF receptor expression in tumor endothelial cells is correlated with a significantly higher microvascular density which suggests that BTC can enhance vascularity via a paracrine pathway (Moon et al. 2006).

38.5 Role of Betacellulin in the Retina in Diabetes

While the general role of BTC in vascular endothelial functions has been studied, its specific role in the retina is currently unclear. Initial reports of the proliferative effect of BTC on RPE cells (Shing et al. 1993; Shing and Folkman 1996) and its pro-angiogenic functions suggested that it might play a role in proliferative diabetic retinopathy (PDR). We have recently reported that RPE cells, retinal endothelial cells, and Muller cells secrete BTC (Anand-Apte et al. 2010). While diabetic mice do not demonstrate PDR, they do show increased retinal vascular permeability (Poulaki et al. 2002). In addition, we have determined that in a mouse model of diabetes, soluble cleaved BTC is increased in the retina and contributes to increased retinal vascular permeability (Anand-Apte et al. 2010). ADAMs and ADAM-10 in particular have been recently reported to be novel regulators of vascular permeability (Shing et al. 1993; Ponnuchamy and Khalil 2008; Schulz et al. 2008). The cleavage of membrane-anchored forms of BTC to release a secreted form occurs principally by ADAM-10 (a disintegrin and metalloprotease-10) (Sahin et al. 2004; Blobel 2005; Sanderson et al. 2005; Sahin and Blobel 2007). Our recent studies show that ADAM-10 is increased concomitantly with cleaved soluble BTC in the retinas of diabetic mice as well as humans (Anand-Apte et al. 2010). Intravitreal injection of soluble BTC resulted in a dramatic increase of retinal vascular permeability and retinal hemorrhage in mice with a potency similar to that obtained with vascular endothelial growth factor (VEGF). Thus, BTC is a potent permeability factor that could play a critical role in the development of increased retinal vascular permeability in diabetic retinopathy and be a potential therapeutic target in this disease.

38.6 Future Vision

The pancreatic β -cell inducing properties of BTC make it a viable candidate for gene therapy in diabetes to increase insulin secretion in patients with diabetes (Chen et al. 2007; Shin et al. 2008; Kodera et al. 2009; Yechoor et al. 2009). However, our studies indicate that BTC also has properties of increasing retinal vascular leakage that could contribute to the development of diabetic retinopathy. It is possible that there may be unique signaling pathways utilized by BTC in the pancreas and retina that could be targeted to inhibit the deleterious effects of BTC in the retina. The ability to treat retinal diseases locally vs. systemically may be another approach to address this issue. In the meanwhile, it will be prudent to proceed with caution with regard to the use of BTC as a therapy for the metabolic symptoms of diabetes and ensure careful long-term monitoring of the retinal health status of any patients participating in trial studies.

References

- Alimandi M, Wang LM, Bottaro D et al (1997) Epidermal growth factor and betacellulin mediate signal transduction through co-expressed ErbB2 and ErbB3 receptors. *Embo J* 16:5608–5617
- Anand-Apte B, Ebrahem Q, Cutler A et al (2010) Betacellulin induces increased retinal vascular permeability in mice. *PLoS ONE* 5:e13444
- Blobel CP (2005) ADAMs: key components in EGFR signalling and development. *Nat Rev Mol Cell Biol* 6:32–43
- Chen S, Ding J, Yu C et al (2007) Reversal of streptozotocin-induced diabetes in rats by gene therapy with betacellulin and pancreatic duodenal homeobox-1. *Gene Ther* 14:1102–1110
- Dahlhoff M, Dames PM, Lechner A et al (2009) Betacellulin overexpression in transgenic mice improves glucose tolerance and enhances insulin secretion by isolated islets in vitro. *Mol Cell Endocrinol* 299:188–193
- Demeterco C, Beattie GM, Dib SA et al (2000) A role for activin A and betacellulin in human fetal pancreatic cell differentiation and growth. *J Clin Endocrinol Metab* 85:3892–3897
- Group AC, Patel A, MacMahon S et al (2008) Intensive blood glucose control and vascular outcomes in patients with type 2 diabetes. *N Engl J Med* 358:2560–2572
- Group DR (1995) The effect of intensive diabetes treatment on the progression of diabetic retinopathy in insulin-dependent diabetes mellitus. The Diabetes Control and Complications Trial. *Arch Ophthalmol* 113:36–51
- Group TDCaCTR (1993a) The effect of intensive treatment of diabetes on the development and progression of long-term complications in insulin-dependent diabetes mellitus. The Diabetes Control and Complications Trial Research Group. *N Engl J Med* 329:977–986
- Huotari MA, Miettinen PJ, Palgi J et al (2002) ErbB signaling regulates lineage determination of developing pancreatic islet cells in embryonic organ culture. *Endocrinology* 143:4437–4446
- Ismail-Beigi F, Craven T, Banerji MA et al (2010) Effect of intensive treatment of hyperglycaemia on microvascular outcomes in type 2 diabetes: an analysis of the ACCORD randomised trial. *Lancet* 376:419–430
- Klein R, Klein BE (2010) Are individuals with diabetes seeing better?: a long-term epidemiological perspective. *Diabetes* 59:1853–1860
- Kodera T, Yamada S, Yamamoto Y et al (2009) Administration of conophylline and betacellulin-delta4 increases the beta-cell mass in neonatal streptozotocin-treated rats. *Endocr J* 56:799–806

- Li L, Seno M, Yamada H et al (2001) Promotion of beta-cell regeneration by betacellulin in ninety percent-pancreatectomized rats. *Endocrinology* 142:5379–5385
- Li L, Seno M, Yamada H et al (2003) Betacellulin improves glucose metabolism by promoting conversion of intraislet precursor cells to beta-cells in streptozotocin-treated mice. *Am J Physiol Endocrinol Metab* 285:E577–583
- Li WC, Horb ME, Tosh D et al (2005) In vitro transdifferentiation of hepatoma cells into functional pancreatic cells. *Mech Dev* 122:835–847
- Mashima H, Ohnishi H, Wakabayashi K et al (1996) Betacellulin and activin A coordinately convert amylase-secreting pancreatic AR42J cells into insulin-secreting cells. *J Clin Invest* 97:1647–1654
- Mifune M, Ohtsu H, Suzuki H et al (2004) Signal transduction of betacellulin in growth and migration of vascular smooth muscle cells. *Am J Physiol Cell Physiol* 287:C807–813
- Miura K, Doura H, Aizawa T et al (2002) Solution structure of betacellulin, a new member of EGF-family ligands. *Biochem Biophys Res Commun* 294:1040–1046
- Miyagawa J, Hanafusa O, Sasada R et al (1999) Immunohistochemical localization of betacellulin, a new member of the EGF family, in normal human pancreas and islet tumor cells. *Endocr J* 46:755–764
- Moon WS, Park HS, Yu KH et al (2006) Expression of betacellulin and epidermal growth factor receptor in hepatocellular carcinoma: implications for angiogenesis. *Hum Pathol* 37:1324–1332
- Ogata T, Park KY, Seno M et al (2004) Reversal of streptozotocin-induced hyperglycemia by transplantation of pseudoislets consisting of beta cells derived from ductal cells. *Endocr J* 51:381–386
- Ponnuchamy B, Khalil RA (2008) Role of ADAMs in endothelial cell permeability: cadherin shedding and leukocyte rolling. *Circ Res* 102:1139–1142
- Poulaki V, Qin W, Jousen AM et al (2002) Acute intensive insulin therapy exacerbates diabetic blood-retinal barrier breakdown via hypoxia-inducible factor-1alpha and VEGF. *J Clin Invest* 109:805–815
- Sahin U, Blobel CP (2007) Ectodomain shedding of the EGF-receptor ligand epigen is mediated by ADAM17. *FEBS Lett* 581:41–44
- Sahin U, Weskamp G, Kelly K et al (2004) Distinct roles for ADAM10 and ADAM17 in ectodomain shedding of six EGFR ligands. *J Cell Biol* 164:769–779
- Sanderson MP, Abbott CA, Tada H et al (2006) Hydrogen peroxide and endothelin-1 are novel activators of betacellulin ectodomain shedding. *J Cell Biochem* 99:609–623
- Sanderson MP, Erickson SN, Gough PJ et al (2005) ADAM10 mediates ectodomain shedding of the betacellulin precursor activated by p-aminophenylmercuric acetate and extracellular calcium influx. *J Biol Chem* 280:1826–1837
- Sasada R, Ono Y, Taniyama Y et al (1993) Cloning and expression of cDNA encoding human betacellulin, a new member of the EGF family. *Biochem Biophys Res Commun* 190:1173–1179
- Schneider MR, Antsiferova M, Feldmeyer L et al (2008) Betacellulin regulates hair follicle development and hair cycle induction and enhances angiogenesis in wounded skin. *J Invest Dermatol* 128:1256–1265
- Schulz B, Pruessmeyer J, Maretzky T et al (2008) ADAM10 regulates endothelial permeability and T-Cell transmigration by proteolysis of vascular endothelial cadherin. *Circ Res* 102:1192–1201
- Seno M, Tada H, Kosaka M et al (1996) Human betacellulin, a member of the EGF family dominantly expressed in pancreas and small intestine, is fully active in a monomeric form. *Growth Factors* 13:181–191
- Shin S, Li N, Kobayashi N et al (2008) Remission of diabetes by beta-cell regeneration in diabetic mice treated with a recombinant adenovirus expressing betacellulin. *Mol Ther* 16:854–861
- Shing Y, Folkman J (1996) *Betacellulin*: Blackwell Scientific Publications

- Shing Y, Christofori G, Hanahan D et al (1993) Betacellulin: a mitogen from pancreatic beta cell tumors. *Science* 259:1604–1607
- Sundaresan S, Roberts PE, King KL et al (1998) Biological response to ErbB ligands in nontransformed cell lines correlates with a specific pattern of receptor expression. *Endocrinology* 139:4756–4764
- Watada H, Kajimoto Y, Miyagawa J et al (1996) PDX-1 induces insulin and glucokinase gene expressions in alphaTC1 clone 6 cells in the presence of betacellulin. *Diabetes* 45:1826–1831
- Yamamoto K, Miyagawa J, Waguri M et al (2000) Recombinant human betacellulin promotes the neogenesis of beta-cells and ameliorates glucose intolerance in mice with diabetes induced by selective alloxan perfusion. *Diabetes* 49:2021–2027
- Yeboor V, Liu V, Paul A et al (2009) Gene therapy with neurogenin 3 and betacellulin reverses major metabolic problems in insulin-deficient diabetic mice. *Endocrinology* 150:4863–4873
- Yoshida S, Kajimoto Y, Yasuda T et al (2002) PDX-1 induces differentiation of intestinal epithelial IEC-6 into insulin-producing cells. *Diabetes* 51:2505–2513

Chapter 39

Presence of RPE-Produced VEGF in a Timely Manner Is Critical to Choroidal Vascular Development

Meili Zhu, Yanyan Bai, Lixin Zheng, and Yun-Zheng Le

Keywords Development • Choroidal vasculature • VEGF • RPE • Inducible
• Knockout

39.1 Introduction

Choroidal blood circulation is responsible for approximately 80% of blood supplies to the eye. Abnormality in choroidal vascular system and its interaction with the RPE is associated with many ocular diseases, such as age-related macular degeneration (AMD), the number one cause of blindness in people over 65 years of age in the

M. Zhu • Y. Bai

Department of Medicine Endocrinology, University of Oklahoma Health Sciences Center,
Oklahoma City, OK 73104, USA

Harold Hamm Oklahoma Diabetes Center, University of Oklahoma Health Sciences Center,
Oklahoma City, OK 73104, USA

L. Zheng

Department of Ophthalmology, University of Oklahoma Health Sciences Center, Oklahoma City,
OK 73104, USA

Dean A. McGee Eye Institute, Oklahoma City, OK 73104, USA

Y.-Z. Le (✉)

Department of Medicine Endocrinology, University of Oklahoma Health Sciences Center,
Oklahoma City, OK 73104, USA

Harold Hamm Oklahoma Diabetes Center, University of Oklahoma Health Sciences Center,
Oklahoma City, OK 73104, USA

Dean A. McGee Eye Institute, Oklahoma City, OK 73104, USA

Departments of Cell Biology, University of Oklahoma Health Sciences Center,
Oklahoma City, OK 73104, USA

e-mail: Yun-Le@ouhsc.edu

United States. Information regarding choroidal vascular development may yield mechanistic insights about ocular diseases with defects in choroidal vasculatures. Unfortunately, at present little is known about the regulatory mechanisms of choroidal vascular development. Previous studies suggest that RPE-produced vascular endothelial growth factor (VEGF) may be involved in the development of choroidal vessels (Gogat et al. 2004; Marneros et al. 2005; Yi et al. 1998; Zhao and Overbeek 2001). We therefore took advantage of our inducible RPE-specific VEGF knockout (KO) mice and determined the temporal requirement of the RPE-produced VEGF in choroidal vascular development. In this chapter, we discuss the results and conclusion of this study. In addition, we report an improved procedure to evaluate choroidal vascular density in mice, which is more advantageous than our methodology published previously (Le 2010).

39.2 Methods

39.2.1 *Animal Experiments*

All experiments that utilized animals were performed according to the ARVO Statement for the Use of Animals in Ophthalmic and Vision Research and were approved by Institutional Animal Care and Use Committee at the University of Oklahoma Health Sciences Center. Electroretinography (ERG) and doxycycline (dox) induction for RPE-specific VEGF KO were performed as described previously (Le et al. 2010).

39.2.2 *Quantification of Choroidal Vascular Density*

Choroidal vascular density was estimated with images generated either by immunostaining with anti-CD31 antibody or by perfusion with fluorescein isothiocyanate (FITC)-conjugated concanavalin A. Immunostaining of choroidal vessels with anti-CD31 antibody was performed as described previously (Le 2010). For perfusion with FITC-concanavalin A, we adopted a procedure commonly used in the analysis of leukostasis in diabetic mice (Wang et al. 2010). Briefly, after deep anesthetization, the animals were perfused with 10 mL of phosphate saline buffer (PBS) containing heparin (0.1 mg/mL) through the left ventricle. The animals were then perfused with FITC-concanavalin A (20 $\mu\text{g/mL}$ in PBS; pH 7.4; 5 mg/kg body weight) to label choroidal endothelial cells. Excessive unbound lectin was then removed by perfusion with another 10 mL of PBS. The eyeballs were removed and fixed in 4% paraformaldehyde for 1 h. Choroids were then dissected and flat-mounted. For pigmented animals, the dissected choroids were treated with 0.25% trypsin/EDTA at 37°C for 1 h. Pigments were brushed off by a human hair loop before

mounting. Images of choroidal vessels were obtained by fluorescent microscopy. Choroidal vascular densities were quantified with Adobe Photoshop Software as described previously (Le 2010). In this process, images were converted to black–white ones that were used to calculate the density of choroidal vessels in two dimensions.

39.3 Results

39.3.1 Choroidal Vascular Density

A previous study demonstrated that the loss of the RPE-produced VEGF at embryonic day 10 (E10) caused dramatic defects, including absence of choriocapillaris, occurrence of microphthalmia, and complete loss of visual function (Marneros et al. 2005). To determine the temporal requirement of the RPE-produced VEGF in choroidal vascular development, we generated tetracycline-inducible RPE-specific VEGF KO mice. Using a semiquantitative procedure, we examined the choroidal vascular density in conditional VEGF KO mice after dox induction at various time points during embryonic development. Inducing VEGF disruption in the RPE with dox at E10–12 resulted in 31 and 21% reduction in the density of choroidal capillaries and large vessels, respectively (Le et al. 2010). Dox induction at E13–15 in conditional VEGF KO mice caused 20 and 9% reduction in the density of choroidal capillaries and large vessels, respectively (Le et al. 2010). Dox induction at E16–18 or anytime afterward did not have any apparent effect on choroidal vascular density in conditional VEGF KO mice (Le et al. 2010). These results suggest that the RPE-produced VEGF is required for choroidal vascular development during early organogenesis.

39.3.2 Retinal Integrity

As a result of defects in the development of choroidal vasculature, the conditional VEGF KO mice with dox induction at E10–12 demonstrated a reduction in photoreceptor function and outer nuclear layer (ONL) thickness. Dox induction at E10–12 caused 39 and 41% of reduction in scotopic ERG a-wave and b-wave amplitudes, respectively (Le et al. 2010). As expected, there was a 25% reduction in photoreceptor ONL thickness in these conditional VEGF KO mice. Dox induction at E13–15 caused 34 and 17% of reduction in scotopic ERG a-wave and b-wave amplitudes in conditional VEGF KO mice, with a marginal reduction (7%) in photoreceptor ONL thickness (Le et al. 2010). No significant change in photoreceptor function and ONL thickness was observed in conditional VEGF KO mice if dox induction occurred after E15 (Le et al. 2010). However, we did not detect any development defects in the RPE and retinal vasculature of the conditional VEGF KO mice with dox induction at any time during organogenesis (Le et al. 2010).

39.4 Discussion

Previous studies suggest that fibroblast growth factors (FGFs) and VEGF are major factors involved in the development of choroidal vasculature (Gogat et al. 2004; Rousseau et al. 2003; Yi et al. 1998; Zhao and Overbeek 2001). Upregulation of VEGF and its receptors in the RPE and the underlying mesenchyme in mammals has been observed during development (Gogat et al. 2004; Yi et al. 1998; Zhao and Overbeek 2001). A high level of VEGF expression in the RPE from E10.5 until at least P7 in mice (Saint-Geniez et al. 2006; Zhao and Overbeek 2001) has led to the assumption that the RPE-produced VEGF is required for choroidal development and maturation in this entire period. To our surprise, RPE-produced VEGF is not required for the development or maturation of choroidal vasculature after early organogenesis. This result, along with that from a previous study (Marneros et al. 2005), suggests that the RPE-produced VEGF is required for the formation of choroidal vasculature from the beginning of ocular vascular development to embryonic day 15. This time frame is inline with a previous finding suggesting that FGF-2 may be required for choroidal vascular development after E12.5 (Rousseau et al. 2003). However, disruption of both FGF-1 and FGF-2 did not result in any apparent defect in choroidal vasculature (Miller et al. 2000). These observations support the notion that FGF-1 and FGF-2 may exert their functions synergistically with VEGF. In this case VEGF may play a more prominent role in early choroidal vascular development. The identity of other growth factor(s) responsible for the maturation of choroidal vessels after E15 is not clear.

As the development of rod photoreceptor cells occurs after early organogenesis in mice (Cepko et al. 1996), the reduced scotopic ERG amplitudes and photoreceptor ONL thickness in E10-15 induced conditional VEGF KO mice are likely secondary defects to choroidal vascular abnormality. By controlling the inducible disruption of VEGF after organogenesis, we can generate a mouse model of VEGF-null in the RPE with no apparent developmental defects in the eye. Therefore, this animal model may be useful for addressing the postdevelopmental function of the RPE-produced VEGF and for investigating the relationship between the RPE and choroidal vasculature, which is important to the understanding of pathogenic mechanisms of AMD.

A major challenge in choroidal vascular biology is the difficulties in imaging/analyzing the density of mouse choroidal vessels. We previously developed a method for quantifying choroidal vascular density with immunostained choroid flat-mounts (Le 2010). We have since modified our methodology. In our hands, the method described in this chapter is more advantageous. In the new procedure, we labeled the choroidal vessels through the perfusion of fluorescently labeled concanavalin A in mice, which gave a more uniform staining pattern for choroidal vessels. As a result, we were able to demonstrate a much clearer image for choroidal vessels from pigmented mice (Fig. 39.1). Moreover, this procedure is more reproducible and can be completed in a shorter time.

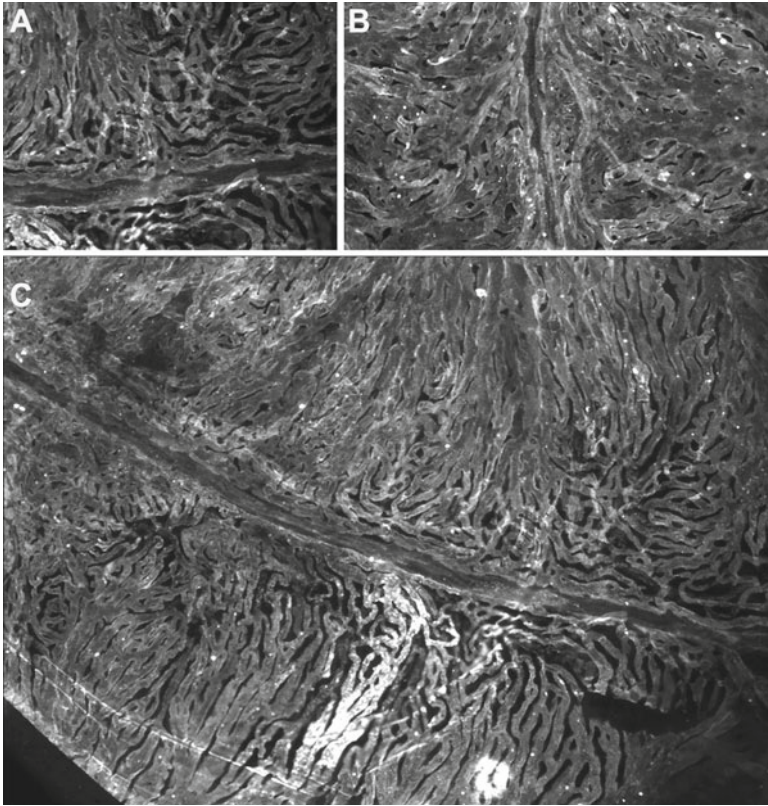


Fig. 39.1 Fluorescent microscopic images of choroid flat-mounts from 1-month-old pigmented mice perfused with FITC-concanavalin A. **(a)** Enlarged image of choriocapillaris. **(b)** Enlarged image of large choroidal vessels. **(c)** Image of the four petals of a choroid flat-mount. Choroidal vessels from pigmented mice can be clearly visualized

Acknowledgments This study was supported partially by American Health Assistance Foundation grant M2008-059, Foundation Fighting Blindness grant BR-CMM-0808-0453-UOK, Beckman Initiative for Macular Research Grant 1003, NIH grants R01EY20900, P20RR17703, P20RR024215, and P30EY12190. American Diabetes Association grant 1-10-BS-94, Oklahoma Center for Advancement of Science and Technology Contract HR09-058, and Unrestricted Research Awards from Hope for Vision and Research to Prevent Blindness.

References

- Cepko CL, Austin CP, Yang X et al (1996) Cell fate determination in the vertebrate retina. *Proc Natl Acad Sci USA* 93:589–95
- Gogat K, Le Gat L, Van Den Berghe L et al (2004) VEGF and KDR gene expression during human embryonic and fetal eye development. *Invest Ophthalmol Vis Sci* 45:7–14

- Le YZ (2010) Computer-assisted semi-quantitative analysis of choroidal density. *Adv Exp Med Biol* 664:211–216
- Le, YZ, Bai Y, Zhu M et al (2010) Temporal requirement of RPE-derived VEGF in the development of choroidal vasculature. *J Neurochem* 112:1584–1592
- Marneros AG, Fan J, Yokoyama Y, et al (2005) Vascular endothelial growth factor expression in the retinal pigment epithelium is essential for choriocapillaris development and visual function. *Am J Pathol* 167:1451–9
- Miller DL, Ortega S, Bashayan O et al (2000) Compensation by fibroblast growth factor 1 (FGF1) does not account for the mild phenotypic defects observed in FGF2 null mice. *Mol Cell Biol* 20:2260–8
- Rousseau B, Larrieu-Lahargue F, Bikfalvi A et al (2003) Involvement of fibroblast growth factors in choroidal angiogenesis and retinal vascularization. *Exp Eye Res* 77:147–56
- Saint-Geniez M, Maldonado AE, D'Amore PA (2006) VEGF expression and receptor activation in the choroid during development and in the adult. *Invest Ophthalmol Vis Sci* 47:3135–42
- Wang J, Xu X, Elliott M et al (2010) Müller cell-derived VEGF is essential for diabetes-induced retinal inflammation and vascular leakage. *Diabetes* 59:2297–3005
- Yi X, Mai LC, Uyama M et al (1998) Time-course expression of vascular endothelial growth factor as related to the development of the retinochoroidal vasculature in rats. *Exp Brain Res* 118:55–60
- Zhao S, Overbeek PA (2001) Regulation of choroid development by the retinal pigment epithelium. *Mol Vis* 7:277–82

Chapter 40

Vasohibin-1 and Retinal Pigment Epithelium

Yumi Ishikawa, Nobuhiro Nagai, Hideyuki Onami, Norihiro Kumasaka, Ryosuke Wakusawa, Hikaru Sonoda, Yasufumi Sato, and Toshiaki Abe

Keywords Vasohibin • VEGF • Retinal pigment epithelium • Hypoxia • Cell dynamics • Cobalt chloride

40.1 Introduction

Choroidal neovascularization (CNV) leads to subretinal hemorrhages, exudative lesions, serous retinal detachment, and disciform scars in patients with age-related macular degeneration (AMD) (Bressler et al. 1998). Vascular endothelial growth factor (VEGF), a pro-angiogenic factor, plays a major role in the development of CNV (Spilisbury et al. 2000). Recently, anti-VEGF treatment for patients with AMD has developed and reported good results (Krzystolik et al. 2002; Rosenfeld et al. 2006). However, there are many problems, such as repeated intravitreal injections, side effects (Pilli et al. 2008), suppression of the important physiological VEGF function (Alon et al. 1995), and further not all patients respond well to this therapy (Lux et al. 2007). Vasohibin-1 is a VEGF-inducible gene in human cultured endothelial cells (ECs) with antiangiogenic properties (Watanabe et al. 2004; Sonoda et al. 2006). Vasohibin-1 is induced by several pro-angiogenic factors such as VEGF and

Y. Ishikawa • N. Nagai • H. Onami • N. Kumasaka • R. Wakusawa • T. Abe (✉)
Division of Clinical Cell Therapy, United Center for Advanced Research and Translational
Medicine (ART), Tohoku University Graduate School of Medicine, 1-1 Seiryomachi Aobaku
Sendai, Miyagi, Japan
e-mail: toshi@oph.med.tohoku.ac.jp

H. Sonoda
Discovery Research Laboratories, Shionogi and Co. Ltd, Osaka, Japan

Y. Sato
Department of Vascular Biology, Institute of Development, Aging, and Cancer,
Tohoku University Graduate School of Medicine, Miyagi, Japan

basic fibroblast growth factor (bFGF) (Watanabe et al. 2004). We showed that the vasohibin-1/VEGF ratio might play a role for clinical significance of CNV in patients with AMD using surgically excised CNV membranes (Wakusawa et al. 2008). The membranes included not only ECs but also retinal pigment epithelium (RPE). In this report, we examined the effects of vasohibin-1 on RPE.

40.2 Methods

40.2.1 RPE Preparation

We used commercially available rat RPE cell line, RPE-J. RPE-J was cultured in DMEM/F-12 medium with 4% fetal bovine serum (FBS; Sigma, St. Louis MO) with 5% CO₂ supply at 33°C. Human vasohibin-1 cDNA with antineomycin gene vector was transduced into RPE-J as we previously reported (Abe et al. 2008). Cells that were stably introduced the vector were selected by antibiotics. We selected 18 clones on both vasohibin-1 cDNA and only vector-transduced RPE-Js. Cobalt chloride (100–300 μM) and low glucose (0–100 μM) and oxygen supply (2%) were used for hypoxic stress. Vasohibin-1 was supplied from Shionogi and Co. Ltd, Osaka, Japan and VEGF and other chemicals were purchased from Wako (Tokyo Japan).

40.2.2 Real-Time RPE Impedance Analysis and MTS Assay

Dynamic cellular biology of the cultured RPE was monitored using Real-Time Cell Analyzer (RTCA), xCELLigence System (Roche Applied Science, Mannheim, Germany). The system evaluates cellular events in real time measuring electrical impedance at an electrode/solution interface at the bottom of cell culture plates. The system provides cell number, viability, morphology, and adhesion described as Cell Index (CI). RPE proliferation was also evaluated by 3-(4, 5-dimethylthiazol-2-yl)-5-(3-carboxymethoxyphenyl)-2-(4-sulfophenyl)-2H-tetrazolium, inner salt (MTS) assay, and counting cell number for each condition.

40.2.3 Extraction of mRNA, cDNA Generation, Reverse-Transcriptase, and Real-Time Polymerase Chain Reaction (RT-PCR)

mRNA was extracted and cDNAs were generated from the cells according to the manufacturer's instructions (Pharmacia Biotech Inc., Uppsala, Sweden). Semiquantitative real-time PCR was carried out by the primer sets described below (LightCycleST300:Roche, Basel, Swiss). The sequences were 5'-TCT GCT CTC

TTG GGT GCA AT-3' and 5'-TTC CGG TGA GAG GTC CGG TT-3' for VEGF, 5'-GAT TCC CAT ACC AAG TGT GCC-3' and 5'-ATG TGG CGG AAG TAG TTC CC-3' for vasohibin-1, and 5'-CATCACCATCTTCCAGGAGC-3' and 5'-CATGAGTCCTTCCACGATACC-3' for GAPDH. All data were normalized to the GAPDH expression level, thus giving the relative expression level.

40.2.4 Western Blot Analysis for Vasohibin-1 and VEGF

Cells were collected and used for western blotting analysis after sonication, as we reported previously (Abe et al. 2008). Cells were washed in ice-cold Dalbecco's phosphate buffered saline (DPBS) 3 times, and then immediately sonicated in lysis buffer. After blotting on Immune-Blot PVDF Membrane (BIO-RAD Laboratories, CA), it was incubated overnight in mouse antivasohibin-1 or anti-VEGF antibody (Santa Cruz) at 4°C and visualized using an enhanced chemiluminescence system (ECL Plus, GE Healthcare) according to the manufacturer's instructions.

40.3 Results

40.3.1 Vasohibin-1 Expression

Vasohibin-1 expression in the RPE was confirmed by real-time PCR and western blot analysis. When we cultured the cells with cobalt chloride, a pseudo-hypoxic condition, or low oxygen (2%), 1% serum, and no glucose, gradual upregulation of VEGF gene was observed with 100- μ M cobalt chloride (Fig. 40.1a). Conversely, statistically significant low vasohibin-1 expression was observed with 100- μ M cobalt chloride at more than 12-h culture when compared to those of standard culture or less than 6-h culture (Fig. 40.1b). Western blot analysis showed that vasohibin-1 expression seemed to be downregulated at more than 36-h culture with 100- μ M cobalt chloride (Fig. 40.1c).

40.3.2 RPE Dynamics and Proliferation by Vasohibin-1

An RTCA was used to monitor dynamic changes in the properties of RPE cells during the culture. The parameter of CI shows cell viability, number, morphology, and adhesion to the bottom of the plates. When we cultured the cells under standard condition as described above, we found no difference of CI even though we added VEGF (Fig. 40.2a) and/or vasohibin-1 (Fig. 40.2b). When we added VEGF (0.2–10 nM) in the culture medium at 2% oxygen, 1% serum, and no glucose, we found that VEGF enhanced CI (Fig. 40.2c). Statistically significant difference was observed when we cultured the cells more than 15 h after treatments with 1 and 2-nM VEGF.

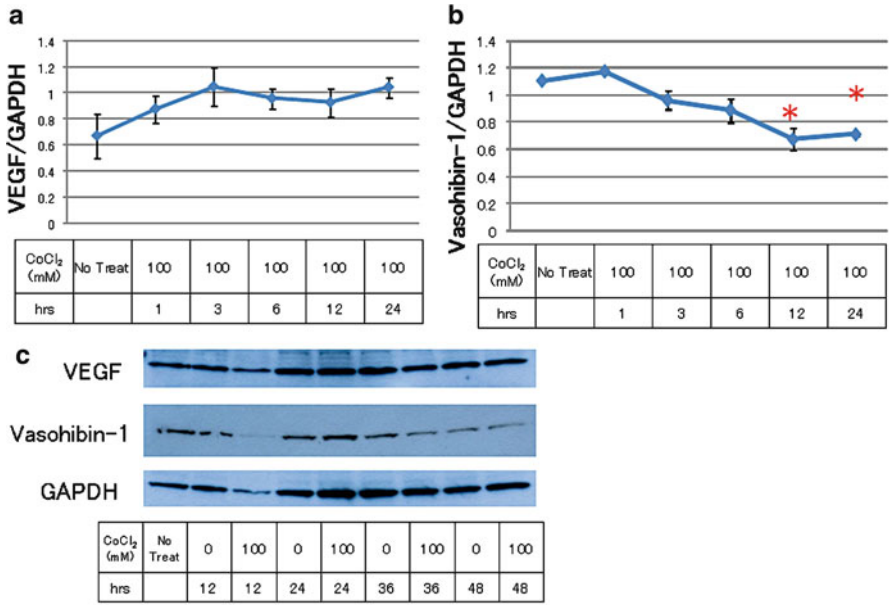


Fig. 40.1 Real-time PCR of VEGF (a) and vasohibin-1 (b) genes is shown. VEGF gene was upregulated in RPE-J with cobalt chloride during successive culture whereas vasohibin-1 gene was suppressed. Western blot analysis (c) shows decreased vasohibin-1 expression at the condition

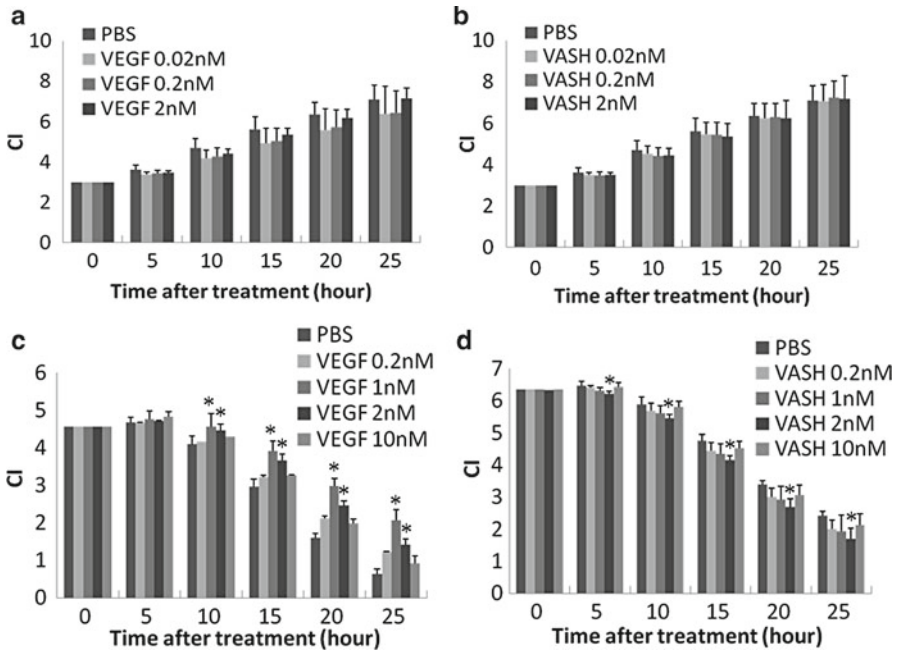


Fig. 40.2 Cell Index of RTCA shows that VEGF enhanced CI at hypoxic condition (a), conversely vasohibin-1 reduced CI only at hypoxic condition (b). The results were not observed at normal condition

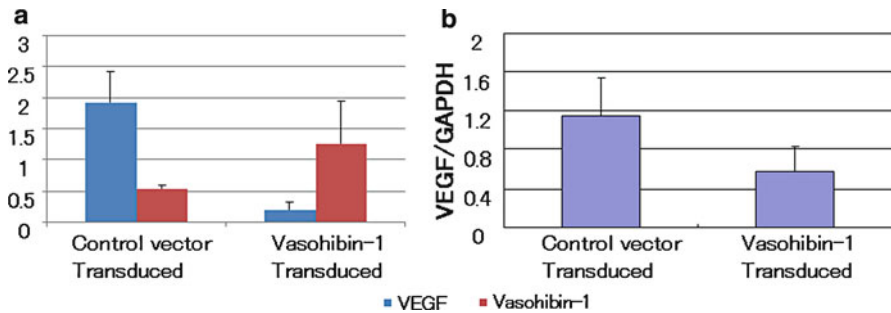


Fig. 40.3 Human vasohibin-1 gene was transduced into RPE-J. We selected 18 clones on both vasohibin-1 gene transduced and only vector-transduced RPE-J. Statistically significant less VEGF gene expression was observed in vasohibin-1 gene-transduced cDNA when compared to that of vector-transduced cDNA (a). Western blot analysis also showed comparable results (b)

Conversely, when we applied vasohibin-1 (0.2–10 nM) in the culture medium at 2% oxygen, 1% serum, and no glucose, we found that vasohibin-1 showed lower CI (Fig. 40.2d). Statistically significant difference was observed at 2-nM vasohibin-1. Vasohibin-1 application also showed statistically significant small cell number either 300- μ M cobalt chloride or 2% oxygen, 1% serum, and no glucose. When we performed MTS assay, statistically significant less cell proliferation was also observed at these indicated conditions. When we examined the apoptotic cells, there was no significant difference. Human vasohibin-1 gene-transduced RPE-J showed statistically significant less VEGF expression when compared to those of vector-transduced cell by real-time PCR and western blot analysis (Fig. 40.3a, b).

40.4 Discussion

Vasohibin-1 is an endogenous antiangiogenic agent that is induced by variable pro-angiogenic factors such as VEGF and bFGF. Vasohibin-1 was reported to inhibit the sprouting of new vessels and to support vascular maturation processes (Kimura et al. 2009). These antiangiogenic properties were detected after recombinant vasohibin-1 was used for corneal and retinal neovascularization (Watanabe et al. 2004). We have found that vasohibin-1 is expressed on ECs of choroidal and retinal vessels, human CNV membranes (Wakusawa et al. 2008), and proliferative membranes of diabetic retinopathy (Sato et al. 2009). In addition, we suggested that the vasohibin-1/VEGF ratio was related to the activity of the CNV (Wakusawa et al. 2008). RPE is known for secreting VEGF from its basal side to choriocapillaris direction and performs important function for the survival of the vascular ECs and nonvascular cells developmentally and also in adults (Alon et al. 1995). This mechanism also maintains low VEGF concentration at subretinal space (Peng et al. 2010). Because of this specific function, we examined the correlation of vasohibin-1 and VEGF on RPE. From the results of present study, vasohibin-1 was expressed in RPE and the

expression was suppressed under hypoxic condition in RPE-J. Vasohibin-1 was also suspected to inhibit VEGF function of rat RPE. Interestingly, these results were observed only at hypoxic conditions and not in standard culture condition. Together with the previous reports, these results may show that vasohibin-1 may not suppress physiological VEGF function. External vasohibin-1 may participate as one of the molecules that suppress the pathological CNV.

In summary, we examined vasohibin-1 expression in rat RPE and the effects under normal or hypoxic condition. Vasohibin-1 expression was suppressed under hypoxic conditions. External vasohibin-1 plays an important role on RPE, especially in hypoxic condition, and suppresses VEGF function on rat RPE.

Acknowledgments This study was supported in part by grants from Grants-in-Aid for Scientific Research 20592030, 21592214 from the Japan Society for the Promotion of Science, Chiyoda-ku, Tokyo, Japan and Suzuken Memorial Foundation.

References

- Abe T, Wakusawa R, Seto H et al (2008) Topical doxycycline can induce expression of BDNF in transduced retinal pigment epithelial cells transplanted into the subretinal space. *Invest Ophthalmol Vis Sci* 49: 3631–3639
- Alon T, Hemo I, Itin A et al (1995) Vascular endothelial growth factor acts as a survival factor for newly formed retinal vessels and has implications for retinopathy of prematurity. *Nat Med* 1: 1024–1028
- Bressler NM, Bressler SB, Fine SL (1998) Age-related macular degeneration. *Surv Ophthalmol* 32: 375–413
- Kimura H, Miyashita H, Suzuki Y et al (2009) Distinctive localization and opposed roles of vasohibin-1 and vasohibin-2 in the regulation of angiogenesis. *Blood* 113: 4810–4818
- Krzystolik MG, Afshari MA, Adamis AP et al (2002) Prevention of experimental choroidal neovascularization with intravitreal anti-vascular endothelial growth factor antibody fragment. *Arch Ophthalmol* 120: 338–346
- Lux A, Llacer H, Heussen FMA et al (2007) Non-responders to bevacizumab (Avastin) therapy of choroidal neovascular lesions. *Am J Ophthalmol* 91: 1318–1322
- Peng S, Adelman RA, Rizzolo LJ (2010) Minimal effects of VEGF and anti-VEGF drugs on the permeability or selectivity of RPE tight junctions. *Invest Ophthalmol Vis Sci* 51: 3216–3225
- Pilli S, Kotsolis A, Spaide RF et al (2008) Endophthalmitis associated with intravitreal anti-vascular endothelial growth factor therapy injections in an office setting. *Am J Ophthalmol* 145: 879–882
- Rosenfeld PJ, Brown DM, Heier JS et al (2006) MARINA Study Group. Ranibizumab for neovascular age-related macular degeneration. *N Engl J Med* 355: 1419–1431
- Sato H, Abe T, Wakusawa R et al (2009) Vitreous levels of vasohibin-1 and vascular endothelial growth factor in patients with proliferative diabetic retinopathy. *Diabetologia* 52: 359–361
- Sonoda H, Ohta H, Watanabe K et al (2006) Multiple processing forms and their biological activities of a novel angiogenesis inhibitor vasohibin. *Biochem Biophys Res Commun* 342: 640–646
- Spilisbury K, Garrett KL, Shen WY et al (2000) Overexpression of vascular endothelial growth factor (VEGF) in the retinal pigment epithelium leads to the development of choroidal neovascularization. *Am J Pathol* 157: 135–144
- Wakusawa R, Abe T, Sato H et al (2008) Expression of vasohibin, an antiangiogenic factor, in human choroidal neovascular membranes. *Am J Ophthalmol* 146: 235–243
- Watanabe K, Hasegawa Y, Yamashita H et al (2004) Vasohibin as an endothelium-derived negative feedback regulator of angiogenesis. *J Clin Invest* 114: 898–907

Part V
Genotype/Phenotype

Chapter 41

Polymorphic Variation of RPGRIP1L and IQCB1 as Modifiers of X-Linked Retinitis Pigmentosa Caused by Mutations in RPGR

Abigail T. Fahim, Sara J. Bowne, Lori S. Sullivan, Kaylie D. Webb, Jessica T. Williams, Dianna K. Wheaton, David G. Birch, and Stephen P. Daiger

Keywords Retinitis pigmentosa • Retinal degeneration • RPGR • Genetic modifier • Ciliopathy

41.1 Introduction

The inherited retinal dystrophies, including retinitis pigmentosa, Leber congenital amaurosis, cone-rod dystrophy, and others, are a remarkably heterogeneous group of blinding disorders displaying both genetic and phenotypic diversity. They encompass a spectrum of diseases all resulting in photoreceptor loss and eventual blindness, but differ in age of onset, severity, cone- or rod-predominance, and associated findings. Some forms of disease are syndromic while other forms are retina-specific. Over 150 different genes have been implicated to date in all inherited retinal dystrophies, and retinitis pigmentosa alone is caused by over 40 genes, many displaying allelic heterogeneity, and some demonstrating both dominant and recessive modes of inheritance (RetNet; <http://www.sph.uth.tmc.edu/retnet/>).

Certain genetic causes of retinal degeneration appear particularly prone to variable expressivity. For example, many instances of extreme phenotypic variability

A.T. Fahim • S.J. Bowne • L.S. Sullivan • J.T. Williams • S.P. Daiger (✉)
Human Genetics Center, School of Public Health,
University of Texas Health Science Center at Houston, Houston, TX 77030, USA
e-mail: stephen.p.daiger@uth.tmc.edu

K.D. Webb
Retina Foundation of the Southwest, Dallas, TX 75231, USA

D.K. Wheaton • D.G. Birch
Retina Foundation of the Southwest, Dallas, TX 75231, USA

Department of Ophthalmology, University of Texas Southwestern Medical Center,
Dallas, TX 75231, USA

have been reported for mutations in RPGR (retinitis pigmentosa GTPase regulator), which causes over 70% of X-linked RP in addition to cone and cone-rod dystrophy and atrophic macular dystrophy (Ayyagari et al. 2002; Demirci et al. 2002; Yang et al. 2002). RPGR localizes to the connecting cilium in photoreceptors and is thought to play a role in protein transport (Roepman et al. 2000; Hong et al. 2003; Khanna et al. 2005). Until recently, the “GTPase regulator” function of RPGR was largely speculative, but recent evidence shows that RPGR interacts with the GTPase RAB8A and that disease-causing mutations in RPGR disrupt this interaction (Murga-Zamalloa et al. 2010). X-linked RP demonstrates marked variable expressivity among both affected males, who demonstrate a wide range of severity, and female carriers, who may or may not have clinical symptoms (Souied et al. 1997; Grover et al. 2000). In addition, there have been multiple reports of diagnoses of both X-linked retinitis pigmentosa and cone-rod dystrophy within the same family (Keith et al. 1991; Walia et al. 2008).

Some of the observed phenotypic diversity is undoubtedly due to considerable allelic heterogeneity: over 100 different RPGR mutations have been found to date in families with X-linked retinitis pigmentosa (XIRP) (Human Gene Mutation Database; <http://www.hgmd.cf.ac.uk/>). However, the same mutation often results in varying degrees of clinical severity, and sometimes different diagnoses, both across families and within families. This variable expressivity suggests the presence of either genetic or environmental modifiers, or both, playing a substantial role in disease expression.

This study aimed to categorize the clinical diversity in a cohort of 98 affected males from 56 families with RPGR mutations, and to test candidate modifier genes for association with disease severity. Ninety-eight affected males with 44 different RPGR mutations were included. Candidate modifier genes were chosen according to the following criteria: (1) the protein is known to interact with RPGR, (2) the protein has polymorphic amino acid substitutions, and (3) the gene contains known retinal disease-causing mutations. Based on these criteria, coding SNPs in RPGR-interacting protein 1 (RPGRIP1) (Boylan and Wright 2000; Dryja et al. 2001), RPGRIP1-like (RPGRIP1L) (Arts et al. 2007; Delous et al. 2007; Khanna et al. 2009), centrosomal protein 290 kDa (CEP290) (den Hollander et al. 2006; Sayer et al. 2006; Baala et al. 2007), and IQ motif containing B1 (IQCB1 aka nephrocystin-5) (Otto et al. 2005) were chosen for analysis. This study describes and categorizes phenotypic severity in a cohort of 98 males with RPGR mutations and reports two SNPs in candidate modifier genes associated with disease severity.

41.2 Materials and Methods

41.2.1 Patients and Clinical Assessment

This study was performed in accordance with the Declaration of Helsinki and informed consent was obtained from all participants. The research was approved by the Committees for Protection of Human Subjects at the University of Texas Health

Table 41.1 Males with XIRP were divided into grades 1, 2, and 3 according to the clinical criteria shown in the table

Severity	ERG	Visual field
Grade 1	$\geq 10 \mu\text{V}$ 30 Hz flicker in teens (1–5 μV in 30s)	Good central 30° field sensitivity
Grade 2	1–5 μV 30 Hz flicker in teens	Marked central field constriction; some sensitivity beyond 20°
Grade 3	$< 1 \mu\text{V}$ 30 Hz flicker in teens/20s	Marked central field constriction

Science Center at Houston and the University of Texas Southwestern Medical Center. Ninety-eight affected males from 56 families were enrolled. Clinical assessment included manifest refraction and best-corrected visual acuity, Humphrey visual fields, frequency domain optical coherence tomography, dark-adapted threshold, full-field electroretinogram, and multifocal electroretinogram.

Fifty-four of the 98 affected males had 3 or more visits at least 1 year apart. For these individuals, log cone 31 Hz flicker ERG amplitude was plotted as a function of patient age and linear regression analysis was used to determine the predicted amplitude at age 18 (Berson et al. 1985; Birch et al. 1999; Berson 2007). The 54 patients with multiple visits were characterized as grade 1 (mild), grade 2 (moderate), or grade 3 (severe) based on the derived cone 31 Hz flicker ERG amplitude at age 18, supplemented by Humphrey visual fields. Supplementary measures, along with cone ERG amplitude, were also used to characterize the 44 patients with a single visit. Criteria used to categorize patients as grade 1, 2, or 3 are summarized in Table 41.1.

41.2.2 Genotyping Candidate Modifier Loci

Blood samples were collected in EDTA-coated tubes, and DNA was extracted using the Genra Puregene blood kit (Qiagen, Valencia, CA). DNA sequences containing SNPs of interest were amplified from 37.5 ng genomic DNA per reaction with either AmpliTaq Gold 360 (Applied Biosystems) or PyroMark PCR Kit (Qiagen). The PyroMark PCR reactions included two specific primers, one of which contained an M13 tail, and a universal biotinylated M13 primer, as described by Guo and Milewicz (2003). PCR conditions for PyroMark reactions were as follows: 95°C for 15 min, 45 cycles of 94°C for 30 s, 52°C for 30 s, and 72°C for 30 s, followed by extension at 72°C for 10 min. Reactions were run on a PSQ HS 96A Instrument (Qiagen).

41.2.3 Data Analysis

Family-based association testing was performed using the DFAM procedure in PLINK (<http://pngu.mgh.harvard.edu/purcell/plink/>) (Purcell et al. 2007). As this

analysis requires a dichotomous phenotype, patients with grade 1 or 3 RP were compared, while patients with grade 2 RP were excluded.

41.3 Results

41.3.1 Phenotypic Heterogeneity Between and Within Families

Ninety-eight affected males from 56 families with mutations in RPGR were ascertained and categorized as grade 1 (mild), 2 (moderate), or 3 (severe) according to the clinical criteria in Table 41.1. The cohort included 21 grade 1, 34 grade 2, and 43 grade 3 affected males. RPGR mutations have historically been fully penetrant in the hemizygous state, consistent with the absence of known nonpenetrance in our cohort. Representative fundus photos, ERGs, and visual fields from each category are shown in Fig. 41.1. Most pedigrees were too small to assess intrafamilial phenotypic variability. However, Fig. 41.2 shows one of the largest pedigrees in the study, which demonstrated marked phenotypic heterogeneity.

41.3.2 Modifier SNPs

Coding SNPs with $MAF \geq 2\%$ in RPGRIP1, RPGRIP1L, CEP290, and IQCB1 (a.k.a. NPHP5) were sequenced in the cohort of 98 affected males and in 99 available family members. Family-based association testing was performed using the

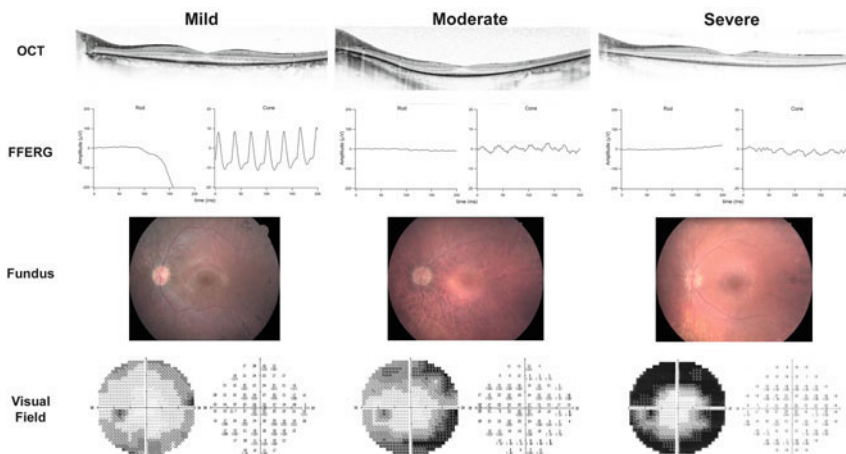


Fig. 41.1 Shown are OCT scans, fFERGs, fundus photos, and visual fields from representative mild (grade 1), moderate (grade 2), and severe (grade 3) males from families enrolled in this study

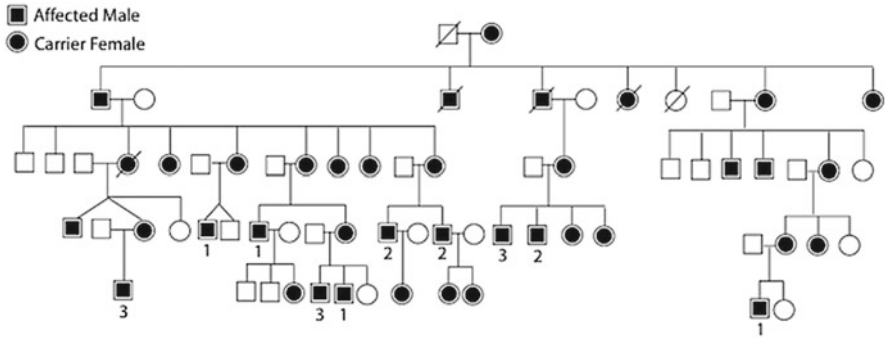


Fig. 41.2 A large pedigree with XIRP is shown with phenotypic variability. 1 = grade 1, 2 = grade 2, 3 = grade 3

Table 41.2 The results of the family-based association testing are shown

Gene	SNP	<i>p</i> value
RPGRIP1	P96Q	0.622
	K192E	0.367
	A547S	0.684
	E1033Q	0.294
RPGRIP1L	A229T	0.564
	R744Q	0.049
	G1025S	0.523
	D1264N	0.920
CEP290	K838E	0.698
	L906W	NA
IQCB1	I393N	0.044
	C434Y	0.977

Coding SNPs that were sequenced in the 98 affected males are shown with their respective *p* values calculated using the DFAM procedure in PLINK. *p* values <0.05 are shown in bold

DFAM test in PLINK (Purcell et al. 2007) comparing individuals with grade 1 (mild) and grade 3 (severe) RP. Two coding SNPs showed significant association: rs1141528 (I393N) in IQCB1 and rs2302677 (R744Q) in RPGRIP1L (Table 41.2). In IQCB1, the minor allele (asparagine) at position 393 was associated with more severe disease ($p=0.044$). In RPGRIP1L, the common allele (arginine) at position 744 was associated with more severe disease ($p=0.049$).

41.4 Discussion

This study described and categorized the clinical diversity in a cohort of 98 affected males from 56 families with RPGR mutations, and demonstrated association in the cohort between severe disease and coding SNPs in two proteins known to interact

with RPGR. In IQCB1, residue 393 lies in one of two calmodulin-binding domains, and interaction between IQCB1 and calmodulin has been previously demonstrated (Otto et al. 2005). Studies have shown that calmodulin is an important modulator of the cGMP-gated cation channel in rods (Chen et al. 1994). IQCB1 I393N is a predicted benign variant by PolyPhen-2 (Adzhubei et al. 2010). In RPGRIP1L, residue 744 lies in the linker region between two C2 domains and is predicted to be probably damaging by PolyPhen-2 (Delous et al. 2007; Adzhubei et al. 2010).

There have been three prior reports of coding SNPs in cilia proteins acting as genetic modifiers in ciliopathies. In a group of 602 patients with various syndromic ciliopathies caused by mutations in different genes, the threonine allele at the A229T coding SNP in RPGRIP1L was associated with increased frequency of retinopathy as part of the syndromic phenotype (Khanna et al. 2009). Furthermore, the authors demonstrated that the associated protein variant disrupted binding of RPGRIP1L to RPGR. Of note, the A229T SNP was sequenced in our cohort, but no association with disease severity was found. A similar modifying effect was found in nephronophthisis, a hereditary fibrocystic renal disease with variable retinopathy most commonly caused by mutations in NPHP1. In a group of 306 patients with nephronophthisis, the minor allele at a coding SNP in AHI1, a cilia protein that interacts with NPHP1, was associated with increased frequency of retinopathy (Louie et al. 2010). The same variant in AHI1 was also found to be associated with neurologic symptoms in nephronophthisis (Tory et al. 2007). As there are no reports of direct interaction between AHI1 and RPGR, SNPs in AHI1 were not included in our study.

Genetic modifiers achieve a remarkable genetic phenomenon: the generation of a complex genetic trait superimposed on an underlying Mendelian trait. Discovery of modifier genes leads to new investigations in the biology of disease and in potential therapeutics. In addition, genotyping modifier loci in patients may have prognostic utility. This study and future studies of retinitis pigmentosa modifier genes help to define the total genetic contribution to disease and to understand the complexity of phenotypic variation in this otherwise Mendelian disease.

Acknowledgments We thank James Hixson for the monosomic cell line DNA, Hemaxi Patel for assistance in visual function testing, and Martin Klein for assistance in creating Fig. 41.1. This work was funded by the Foundation Fighting Blindness and NEI/NIH grant EY007142 to SPD.

References

- Adzhubei IA, Schmidt S, Peshkin L et al (2010) A method and server for predicting damaging missense mutations. *Nat Methods* 7:248–249
- Arts HH, Doherty D, van Beersum SE et al (2007) Mutations in the gene encoding the basal body protein RPGRIP1L, a nephrocystin-4 interactor, cause Joubert syndrome. *Nat Genet* 39:882–888
- Ayyagari R, Demirci FY, Liu J et al (2002) X-linked recessive atrophic macular degeneration from RPGR mutation. *Genomics* 80:166–171

- Baala L, Audollent S, Martinovic J et al (2007) Pleiotropic effects of CEP290 (NPHP6) mutations extend to Meckel syndrome. *Am J Hum Genet* 81:170–179
- Berson EL (2007) Long-term visual prognoses in patients with retinitis pigmentosa: the Ludwig von Sallmann lecture. *Exp Eye Res* 85:7–14
- Berson EL, Sandberg MA, Rosner B et al (1985) Natural course of retinitis pigmentosa over a three-year interval. *Am J Ophthalmol* 99:240–251
- Birch DG, Anderson JL, Fish GE (1999) Yearly rates of rod and cone functional loss in retinitis pigmentosa and cone-rod dystrophy. *Ophthalmology* 106:258–268
- Boylan JP, Wright AF (2000) Identification of a novel protein interacting with RPGR. *Hum Mol Genet* 9:2085–2093
- Chen TY, Illing M, Molday LL et al (1994) Subunit 2 (or beta) of retinal rod cGMP-gated cation channel is a component of the 240-kDa channel-associated protein and mediates Ca(2+)-calmodulin modulation. *Proc Natl Acad Sci USA* 91:11757–11761
- Delous M, Baala L, Salomon R et al (2007) The ciliary gene RPGRIP1L is mutated in cerebello-oculo-renal syndrome (Joubert syndrome type B) and Meckel syndrome. *Nat Genet* 39:875–881
- Demirci FY, Rigatti BW, Wen G et al (2002) X-linked cone-rod dystrophy (locus COD1): identification of mutations in RPGR exon ORF15. *Am J Hum Genet* 70:1049–1053
- den Hollander AI, Koenekoop RK, Yzer S et al (2006) Mutations in the CEP290 (NPHP6) gene are a frequent cause of Leber congenital amaurosis. *Am J Hum Genet* 79:556–561
- Dryja TP, Adams SM, Grimsby JL et al (2001) Null RPGRIP1 alleles in patients with Leber congenital amaurosis. *Am J Hum Genet* 68:1295–1298
- Grover S, Fishman GA, Anderson RJ et al (2000) A longitudinal study of visual function in carriers of X-linked recessive retinitis pigmentosa. *Ophthalmology* 107:386–396
- Guo DC, Milewicz DM (2003) Methodology for using a universal primer to label amplified DNA segments for molecular analysis. *Biotechnol Lett* 25:2079–2083
- Hong DH, Pawlyk B, Sokolov M et al (2003) RPGR isoforms in photoreceptor connecting cilia and the transitional zone of motile cilia. *Invest Ophthalmol Vis Sci* 44:2413–2421
- Keith CG, Denton MJ, Chen JD (1991) Clinical variability in a family with X-linked retinal dystrophy and the locus at the RP3 site. *Ophthalmic Paediatr Genet* 12:91–98
- Khanna H, Hurd TW, Lillo C et al (2005) RPGR-ORF15, which is mutated in retinitis pigmentosa, associates with SMC1, SMC3, and microtubule transport proteins. *J Biol Chem* 280:33580–33587
- Khanna H, Davis EE, Murga-Zamalloa CA et al (2009) A common allele in RPGRIP1L is a modifier of retinal degeneration in ciliopathies. *Nat Genet* 41:739–745
- Louie CM, Caridi G, Lopes VS et al (2010) AHI1 is required for photoreceptor outer segment development and is a modifier for retinal degeneration in nephronophthisis. *Nat Genet* 42:175–180
- Murga-Zamalloa CA, Atkins SJ, Peranen J et al (2010) Interaction of retinitis pigmentosa GTPase regulator (RPGR) with RAB8A GTPase: implications for cilia dysfunction and photoreceptor degeneration. *Hum Mol Genet* 19:3591–3598
- Otto EA, Loeys B, Khanna H et al (2005) Nephrocystin-5, a ciliary IQ domain protein, is mutated in Senior-Loken syndrome and interacts with RPGR and calmodulin. *Nat Genet* 37:282–288
- Purcell S, Neale B, Todd-Brown K et al (2007) PLINK: a tool set for whole-genome association and population-based linkage analyses. *Am J Hum Genet* 81:559–575
- Roepman R, Bernoud-Hubac N, Schick DE et al (2000) The retinitis pigmentosa GTPase regulator (RPGR) interacts with novel transport-like proteins in the outer segments of rod photoreceptors. *Hum Mol Genet* 9:2095–2105
- Sayer JA, Otto EA, O'Toole JF et al (2006) The centrosomal protein nephrocystin-6 is mutated in Joubert syndrome and activates transcription factor ATF4. *Nat Genet* 38:674–681
- Souied E, Segues B, Ghazi I et al (1997) Severe manifestations in carrier females in X linked retinitis pigmentosa. *J Med Genet* 34:793–797

- Tory K, Lacoste T, Burglen L et al (2007) High NPHP1 and NPHP6 mutation rate in patients with Joubert syndrome and nephronophthisis: potential epistatic effect of NPHP6 and AHI1 mutations in patients with NPHP1 mutations. *J Am Soc Nephrol* 18:1566–1575
- Walia S, Fishman GA, Swaroop A et al (2008) Discordant phenotypes in fraternal twins having an identical mutation in exon ORF15 of the RPGR gene. *Arch Ophthalmol* 126:379–384
- Yang Z, Peachey NS, Moshfeghi DM et al (2002) Mutations in the RPGR gene cause X-linked cone dystrophy. *Hum Mol Genet* 11:605–611

Chapter 42

RPGRIP1 and Cone–Rod Dystrophy in Dogs

Tatyana Kuznetsova, Barbara Zangerl, and Gustavo D. Aguirre

Keywords *RPGRIP1* • Polymorphism • Cone–rod dystrophy • Protein network
• Photoreceptor cilia

42.1 Introduction

Cone–rod dystrophies (*crd*) affect the cone and rod photoreceptors resulting in reduced visual acuity followed by severe loss of central and color vision that often progresses to complete blindness. The onset of clinical disease in man ranges from early to late adulthood, and inherited as X-linked, autosomal dominant or, most commonly, autosomal recessive. Mutations in over 20 genes have been identified to cause *crd* (RetNet db). Canine models have been developed for several human retinal degenerations (Aguirre and Acland 2006); in terms of *crd*, the standard wire-haired dachshund (SWHD), miniature long-haired dachshund (MLHD), pit bull and Glen of Imaal terriers are the only dog breeds thus far affected with *crd*, and the involved genes have been identified in all except pit bull terriers (Goldstein et al. 2010; Kijas et al. 2004; Mellersh et al. 2006; Ropstad et al. 2007).

A canine autosomal recessive, early-onset *crd* (*crd1*) was described in MLHDs (Mellersh et al. 2006). The *crd1* locus was mapped to a region of CFA15 syntenic to HSA14 and containing *RPGRIP1* (the retinitis pigmentosa GTPase interacting protein 1). This gene encodes a ciliary protein that plays an important role in maintenance and function of the cilium. In man, mutations in *RPGRIP1* are associated with Leber congenital amaurosis (Dryja et al. 2001), and cone–rod dystrophy (Hameed et al. 2003). Sequence analysis of canine *RPGRIP1* revealed a 44-nucleotide insertion in exon 2 that was proposed to be responsible for the disease in MLHD as

T. Kuznetsova (✉) • B. Zangerl • G.D. Aguirre
Department of Clinical Studies, Section of Ophthalmology, School of Veterinary Medicine,
University of Pennsylvania, Philadelphia, PA 19104, USA
e-mail: tatyanak@vet.upenn.edu

it altered the reading frame by introducing a premature stop codon (Mellersh et al. 2006). Subsequent studies, however, indicate that only ~80% of homozygous mutant MLHDs had the disease (Miyadera et al. 2009). The genotype–phenotype discordance suggests that another mutation in the same or different gene may contribute to the disease. In this review, we examine the RPGRIP1 protein interactome with the view of selecting possible interacting genes that could be associated with the *crd1* phenotype.

42.2 Focus on the *RPGRIP1*: What Makes It Special?

Human *RPGRIP1* encompasses 25 (24 coding) exons (Dryja et al. 2001), and is expressed in amacrine neurons, photoreceptors and, at reduced levels, in many other eye tissues (Roepman et al. 2000). Knockout studies indicated that RPGRIP1 is required for morphogenesis of the outer segment (OS) discs (Zhao et al. 2003), and plays an important role in OS formation, particularly in rods (Won et al. 2009). Moreover, *RPGRIP1* is subject to multiple splicing leading to numerous isoforms with species-specific subcellular localization patterns, e.g., connecting cilium, photoreceptor inner segment and OS (Castagnet et al. 2003; Mavlyutov et al. 2002), and the basal body of cells with primary cilia (Shu et al. 2005), suggesting that different isoforms may perform cell-specific functions.

RPGRIP1 is a component of the cilia protein network, but details about its molecular function and interacting proteins are incomplete. In retina, RPGRIP1 was identified as a part of different protein complexes including RPGR (Roepman et al. 2000), NPHP4 (Roepman et al. 2005), and/or RanB (Castagnet et al. 2003). It directly interacts with RPGR via its C-terminal domain (RID; Roepman et al. 2000). The C2 domain specifically binds with NPHP4 (Roepman et al. 2005), which is part of a multifunctional complex localized in actin- and microtubule-based structures. Mutations in the NPHP4 gene are linked to nephronophthisis type 4, Senior–Løken syndrome in man (Mollet et al. 2002), and *crd* in dogs (SWHD) (Wiik et al. 2008). To better understand the potential role and functioning of RPGRIP1 in the cilium, and identify potential candidate proteins that influence the *crd1* phenotype, a putative molecular network was generated based on results of integrated information of protein–protein interactions or colocalization of ciliary proteins.

42.3 Characterization of the RPGRIP1-Associated Protein Network

In spite of the fact that the exact function of the RPGRIP1 is still unclear, interaction with RPGR and NPHP4 establishes connection to several cellular processes (Fig. 42.1). Mutations in many of these genes have been shown to have a retinal phenotype.

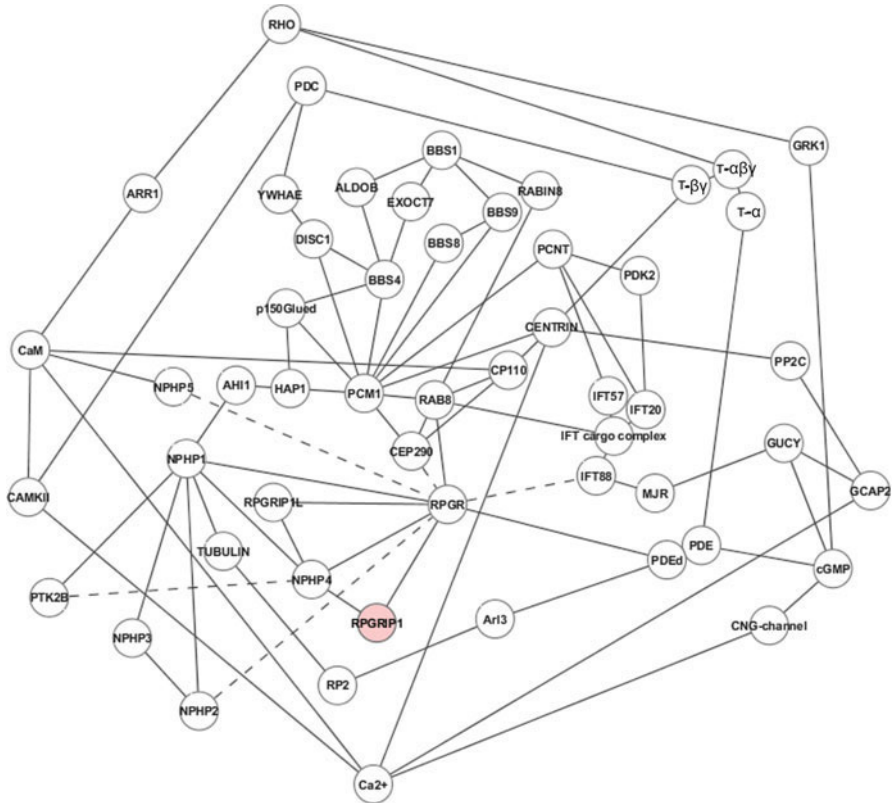


Fig. 42.1 Putative *RPGRIP1*-associated protein network. The connections are based on reported protein–protein interactions (for description and references, please see text). Direct interactions are shown by *solid lines*; interactions that are shown by *dotted lines* represent indirect interactions (e.g., for those that were identified by immunoprecipitation analysis)

42.3.1 *RPGRIP1* Is a Component of the Transport Network for Cilia Assembly

RPGRIP1 interacts with *RPGR* anchoring it to the connecting cilium. *RPGR* isoforms were found associated with intraflagellar transport polypeptide *IFT88* and the *p150Glued* subunit of the dynactin transport machinery (Khanna et al. 2005) suggesting involvement of *RPGR* in regulation of transport in primary cilia. *IFT88* interacts directly with the molecular chaperone *MRJ* which acts as a cargo receptor for photoreceptor-specific guanylate cyclase (*GUCY*) and plays a critical role in formation or stabilization of the IFT-cargo complexes (Roepman and Wolfrum 2007) (Fig. 42.1).

Another *RPGR*-interacting partner is *PDEδ* (Linari et al. 1999). *PDEδ* binds and specifically stabilizes the GTP-bound form of *Arl3*, which belongs to the ARF small

GTPase family, by strongly decreasing the dissociation rate of GTP (Zhang et al. 2004). The retinitis pigmentosa RP2 protein, which links pericentriolar vesicle transport between the Golgi and the primary cilium, is a GTPase-activating protein for Arl3. Depletion of RP2 and dysregulation of Arl3 resulted in dispersal of vesicles cycling cargo from the Golgi complex to the cilium.

42.3.2 RPGRIP1 Involvement in Regulating Cytoskeleton Dynamics and Ciliogenesis

There is a group of proteins in the RPGRIP1-associated interactome with different functions that are part of a complex cellular machine regulating cytoskeletal function and integrity (Fig. 42.1). RPGRIP1-interacting partner RPGR was found in a protein complex with CEP290 (NPHP6), a microtubule motor protein (Khanna et al. 2005), suggesting involvement of RPGR in microtubule organization. Although a centrosomal protein, CEP290 also was localized in the basal bodies of the ciliary apparatus in different cell types, including the photoreceptor cilium. CEP290 interacts with a component of centriolar satellites PCM1 which is implicated in some BBS proteins function (Kim et al. 2008), and localizes to centriolar satellites in a PCM1- and microtubule-dependent manner. PCM1 plays a role in the recruitment of some centrosomal proteins including centrin and pericentrin (PCNT), and is required for the organization of the cytoplasmic microtubule network. CEP290 interaction with PCM1 is important for the ciliary targeting of RAB8, a small GTPase involved with BBS protein complex to promote ciliogenesis (Kim et al. 2008). Direct or indirect interactions with other proteins, e.g., RABIN8, CP110, BSS1, and others, also are important for ciliogenesis (Nachury et al. 2007; Tsang et al. 2008).

RPGR has been proposed as a regulator of some NPHP protein complexes in the mammalian retina (Murga-Zamalloa et al. 2010). The RCC1-like domain of RPGR interacts with the N-terminal part of NPHP4, an RPGRIP1-interacting partner. In the retina, RPGR also interacts directly with RPGRIP1L (NPHP8) and NPHP1, a protein that interacts with NPHP4, NPHP2, and tubulin (Mollet et al. 2002; Murga-Zamalloa et al. 2010). RPGR, NPHP5, and CaM were detected in a common multi-protein complex in the retina, and NPHP5 was shown to directly interact with CaM (Otto et al. 2005).

One form of NPHP1-interacting protein is AHI1, a cilium-localized protein that was shown to cause a form of Joubert syndrome (Eley et al. 2008). AHI1 is required for photoreceptor OS development, and null mice fail to form OS and have abnormal distribution of opsin throughout their photoreceptors. AHI1 binds huntingtin-associated protein 1 (HAP1), which interacts with PCM1 and with the p150Glued subunit of dynactin transport machinery. It was found that BBS4 acts as an adaptor that connects p150Glued with PCM1, and thus assists the centrosomal recruitment of PCM1 and is associated with some centrosomal proteins.

42.3.3 *Components of Molecular Networks Regulating Cellular Transport and Cytoskeleton Dynamics Show Connection with Visual Pathway*

Figure 42.1 also includes a group of molecules from the visual signaling cascade, including RHO, GRK1, transducin ($T\alpha\beta\gamma$), GUCY, PDE, ARR1, and others that “border” the *RPGRIP1*-associated network. Interaction of CP110 with different proteins, e.g., CaM and centrin, is an example of intersection of signaling pathways (Tsang et al. 2006). Ca^{2+} ions are required for the activation of centrin isoforms and for centrin/transducin ($T\beta\gamma$) complex formation. Centrin functions are regulated not only by Ca^{2+} -binding but also by site-specific phosphorylation/dephosphorylation. A changeover of assembly and disassembly of centrin/transducin complexes may regulate the diffusion of transducin through the connecting cilium (Trojan et al. 2008).

The network represented on the Fig. 42.1 carries limited information and does not show any pathways in detail but is presented as an overview of the *RPGRIP1* interactome, and to provide clues as to what other proteins may interact with *RPGRIP1* and determine the phenotype/disease outcome in the mutant dogs.

42.4 *Dogs with Retinal Degeneration Show Significant Phenotypic Variation with RPGRIP1 Mutation Ins44*

The *crdl* “causative” *RPGRIP1* Ins44 mutation was initially completely associated with disease status in an inbred research colony (Mellersh et al. 2006). A recent study of a general MLDH population identified substantial genotype–phenotype discordance: 16% of normal controls were homozygous for the insertion, while 20% of dogs with retinal degeneration did not carry the insertion on both chromosomes (Miyadera et al. 2009). Additionally, four other breeds were identified to carry Ins44 including English Springer Spaniels (ESSs; in dogs affected with PRA, ~30% were homozygous for Ins44), Beagles (allelic frequency 27.8%), French Bulldogs (12.5%), and Labrador Retriever (3%), with some variation in the length of the polyA insertion (Miyadera et al. 2009). That result in ESSs is in good agreement with our own data. Depending on the survey conducted (unpublished), the clinical incidence of retinal degeneration in ESSs is ~3%, yet the number of dogs that are homozygous for the mutation ranges from ~20 to 40%. These observations resulted in the suggestion that the *RPGRIP1* Ins44 mutation represents a predisposing factor for disease rather than the causative mutation. This possibility could be explained by several different hypotheses.

First, *RPGRIP1* undergoes multiple splicing, and some its isoforms can delete exon 2 which is the site of the putative mutation (Kuznetsova et al. 2011). Moreover, a subset of *RPGRIP1* isoforms can be driven from internal alternative promoter(s) located at 3' of the mutation. In both cases those isoforms could provide protein

function independent of the exon 2 Ins44 genotype. This hypothesis could be tested by investigating RPGRIP1 protein expression in dogs with Ins44.

Second, it has been demonstrated that Ins44 contains a prolonged polyA tract. In many cases, including a recent report (Miyadera et al. 2009), such polynucleotide tracts are polymorphic. This suggests that DNA polymerase fidelity defects with the replication of long polynucleotide repeats, some chromosomes carrying the insertion may not consist of a 44, but 43, 45, or 47 nucleotide repeat. In those cases the mutation would not necessarily result in a premature stop codon, but at a modified RPGRIP1 N-terminus and could partially explain variation in disease phenotype in dogs with Ins44.

Lastly, Ins44 alone may not be sufficient to cause disease, but be dependent on a second mutation in *RPGRIP1* or a different gene. Based on outcross/intercross/backcross studies carried out in our lab, the potential modifier gene is most likely located inside the mapped 1.74 Mb region of canine chromosome 15 containing *RPGRIP1* (Miyadera et al. 2009). In this case cosegregation of a haplotype with *crdl* would explain better the cases of the disease and be in agreement that Ins44 alone highly associated with *crdl* in the inbred population.

In summary, RPGRIP1 is an important signaling component inside the cilia. *RPGRIP1* primary mRNA undergoes an extensive splicing resulting in the formation of multiple isoforms. To date, the exact role of RPGRIP1 protein isoforms in cilia function is unknown, but published data about RPGRIP1 interacting molecules support the role of this protein in the cytoskeleton dynamic and transport of ciliary proteins. Reconstruction and analysis of the putative RPGRIP1-associated molecular network offers opportunities to further investigate the molecular mechanisms of cone-rod dystrophy in dogs.

Acknowledgments This study was supported by Morris Animal Foundation, EY-06855, 17549, Foundation Fighting Blindness Center Grant, and Van Sloun Fund

References

- Aguirre GD, Acland GM (2006) Models, Mutants and Man: Searching for Unique Phenotypes and Genes in the Dog Model of Inherited Retinal Degeneration. The Dog and Its Genome. In: Ostrander EA, Giger U, Lindblad-Toh K (eds). Cold Spring Harbor, NY, Cold Spring Harbor Laboratory Press: 291–325
- Castagnet P, Mavlyutov T, Cai Y et al (2003) RPGRIP1s with distinct neuronal localization and biochemical properties associate selectively with RanBP2 in amacrine neurons. *Hum Mol Genet* 12:1847–1863
- Dryja TP, Adams SM, Grimsby JL et al (2001) Null RPGRIP1 alleles in patients with Leber congenital amaurosis. *Am J Hum Genet* 68:1295–1298
- Eley L, Gabrielides C, Adams M et al (2008) Joubertin localizes to collecting ducts and interacts with nephrocystin-1. *Kidney Int* 74:1139–1149
- Goldstein O, Mezey JG, Boyko AR et al (2010) ADAM9 mutation in Canine Cone-Rod Dystrophy 3 (*crdl3*) establishes homology with human CORD9. *Mol Vis* 16:1549–1569

- Hameed A, Abid A, Aziz A et al (2003) Evidence of RPGRIP1 gene mutations associated with recessive cone-rod dystrophy. *J Med Genet* 40:616–619
- Khanna H, Hurd TW, Lillo C et al (2005) RPGR-ORF15, which is mutated in retinitis pigmentosa, associates with SMC1, SMC3, and microtubule transport proteins. *J Biol Chem* 280:33580–33587
- Kijas JW, Zangerl B, Miller B et al (2004) Cloning of the canine ABCA4 gene and evaluation in canine cone-rod dystrophies and progressive retinal atrophies. *Mol Vis* 10:223–232
- Kim J, Krishnaswami SR, Gleeson JG (2008) CEP290 interacts with the centriolar satellite component PCM-1 and is required for Rab8 localization to the primary cilium. *Hum Mol Genet* 17:3796–3805
- Kuznetsova T, Zangerl B, Goldstein O et al (2011) Structural organization and expression pattern of the canine RPGRIP1 isoforms in retinal tissue. *Invest Ophthalmol Vis Sci* 52:2989–2998
- Linari M, Ueffing M, Manson F et al (1999) The retinitis pigmentosa GTPase regulator, RPGR, interacts with the delta subunit of rod cyclic GMP phosphodiesterase. *Proc Natl Acad Sci USA* 96:1315–1320
- Mavlyutov TA, Zhao H, Ferreira PA (2002) Species-specific subcellular localization of RPGR and RPGRIP isoforms: Implications for the phenotypic variability of congenital retinopathies among species. *Hum Mol Genet* 11:1899–1907
- Mellersh CS, Bournsnel ME, Pettitt L et al (2006) Canine RPGRIP1 mutation establishes cone-rod dystrophy in miniature longhaired dachshunds as a homologue of human Leber congenital amaurosis. *Genomics* 88:293–301
- Miyadera K, Kato K, Aguirre-Hernandez J et al (2009) Phenotypic variation and genotype-phenotype discordance in canine cone-rod dystrophy with an RPGRIP1 mutation. *Mol Vis* 15:2287–2305
- Mollet G, Salomon R, Gribouval O et al (2002) The gene mutated in juvenile nephronophthisis type 4 encodes a novel protein that interacts with nephrocystin. *Nat Genet* 32:300–305
- Murga-Zamalloa CA, Desai NJ, Hildebrandt F et al (2010) Interaction of ciliary disease protein retinitis pigmentosa GTPase regulator with nephronophthisis-associated proteins in mammalian retinas. *Mol Vis* 16:1373–1381
- Nachury MV, Loktev AV, Zhang Q et al (2007) A core complex of BBS proteins cooperates with the GTPase Rab8 to promote ciliary membrane biogenesis. *Cell* 129:1201–1213
- Otto EA, Loeyes B, Khanna H et al (2005) Nephrocystin-5, a ciliary IQ domain protein, is mutated in senior-loken syndrome and interacts with RPGR and calmodulin. *Nat Genet* 37:282–288
- Roepman R, Wolfrum U (2007) Protein networks and complexes in photoreceptor cilia. *Subcell Biochem* 43:209–235
- Roepman R, Letteboer SJ, Arts HH et al (2005) Interaction of nephrocystin-4 and RPGRIP1 is disrupted by nephronophthisis or Leber congenital amaurosis-associated mutations. *Proc Natl Acad Sci USA* 102:18520–18525
- Roepman R, Bernoud-Hubac N, Schick DE et al (2000) The retinitis pigmentosa GTPase regulator (RPGR) interacts with novel transport-like proteins in the outer segments of rod photoreceptors. *Hum Mol Genet* 9:2095–2105
- Ropstad EO, Bjerkas E, Narfstrom K (2007) Clinical findings in early onset cone-rod dystrophy in the standard wire-haired dachshund. *Vet Ophthalmol* 10:69–75
- Shu X, Fry AM, Tulloch B et al (2005) RPGR ORF15 isoform co-localizes with RPGRIP1 at centrioles and basal bodies and interacts with nucleophosmin. *Hum Mol Genet* 14:1183–1197
- Trojan P, Krauss N, Choe HW et al (2008) Centrioles in retinal photoreceptor cells: Regulators in the connecting cilium. *Prog Retin Eye Res* 27:237–259
- Tsang WY, Bossard C, Khanna H et al (2008) CP110 suppresses primary cilia formation through its interaction with CEP290, a protein deficient in human ciliary disease. *Dev Cell* 15:187–197
- Tsang WY, Spektor A, Luciano DJ et al (2006) CP110 cooperates with two calcium-binding proteins to regulate cytokinesis and genome stability. *Mol Biol Cell* 17:3423–3434
- Wiik AC, Wade C, Biagi T et al (2008) A deletion in nephronophthisis 4 (NPHP4) is associated with recessive cone-rod dystrophy in standard wire-haired dachshund. *Genome Res* 18:1415–1421

- Won J, Gifford E, Smith RS et al (2009) RPGRIP1 is essential for normal rod photoreceptor outer segment elaboration and morphogenesis. *Hum Mol Genet* 18:4329–4339
- Zhang H, Liu XH, Zhang K et al (2004) Photoreceptor cGMP phosphodiesterase delta subunit (PDEdelta) functions as a prenyl-binding protein. *J Biol Chem* 279:407–413
- Zhao Y, Hong DH, Pawlyk B et al (2003) The retinitis pigmentosa GTPase regulator (RPGR)-interacting protein: Subservicing RPGR function and participating in disk morphogenesis. *Proc Natl Acad Sci USA* 100:3965–3970

Chapter 43

High-Throughput Approaches for the Genetic Diagnosis of Retinal Dystrophies

Esther Pomares, Gemma Marfany, and Roser Gonzàlez-Duarte

Keywords Retinal dystrophies • Genetic testing • Mutational screening • SNP-cosegregation chip • DNA microarrays • Next-generation sequencing

43.1 Introduction

Currently, there is no laboratory or research center that offers a comprehensive clinical and genetic diagnosis of retinal dystrophies. From the clinical side, some reports attest to the fact that most patients visit on average seven ophthalmologists before an accurate diagnosis of their visual disorder is attained (Koenekoop et al. 2007). From the genetics side, the conventional mutational screening of all the reported candidates for retinal disorders – with neither major genes nor prevalent mutations – would involve the analysis of more than 1,400 exons and/or sequence at least 300 kb (Booij et al. 2011), clearly too burdensome in time and budget for most laboratories. An added nontrivial difficulty is the fact that a significant proportion of the causative genes remains unknown, even though in the last years the number of candidates has been steadily increasing and nearly 150 genes have been reported to date (<http://www.sph.uth.tmc.edu/Retnet/>). The rapid development of high-throughput technologies based on DNA chips and SNP-genotyping has completely revolutionized molecular testing and novel gene search. An accurate comparison of the existing technologies based on direct and indirect (cosegregation) screenings shows that only a combination of approaches provides nowadays the most effective diagnosis.

E. Pomares • G. Marfany • R. Gonzàlez-Duarte (✉)
Departament de Genètica, Universitat de Barcelona, Barcelona 08028, Spain
Institut de Biomedicina, Universitat de Barcelona, Barcelona 08028, Spain
CIBERER, Instituto de Salud Carlos III, Barcelona, Spain
e-mail: rgonzalez@ub.edu

The future holds promise in this burgeoning field as new potent and affordable methodologies – together with deeper knowledge of genes and mutations involved in retinal pathologies – pave the path for new effective therapies.

43.2 Direct Molecular Diagnosis of Retinal Dystrophies

A brief account of the late techniques used to unveil known – or new – mutations in retinal dystrophy genes by direct analysis of the patients' DNA, pointing their major strengths and pitfalls, is presented below (summarized in Table 43.1).

43.2.1 Mutation Screening Chips

The commercially available microarrays, developed by Asper Ophthalmics (<http://www.asperbio.com/asper-ophthalmics>) and based on the APEX methodology, allow the direct screening of nearly all reported mutations for particular retinal disorders (such as Retinitis Pigmentosa, Leber Congenital Amaurosis, and Stargardt's disease) using a cost-effective approach (Klevering et al. 2004; Zernant et al. 2005). Their high versatility (new mutations are periodically included in the chips) and celerity of diagnosis (less than 24 h after the sample is received) make them some of the most preferred tools for genetic testing. However, given that only known single nucleotide mutations among the wide panoply of pathogenic variants – many of them private – are screened, the proportion of the cases successfully diagnosed is moderate (Table 43.1) (Henderson et al. 2007; Koenekoop et al. 2007). Besides, there is a small percentage of misdiagnosis (false negatives as well as false positives) due to the inherent technical error associated to hybridization on high-throughput microarrays (Henderson et al. 2007). Verification by conventional sequencing of all the detected mutations is strictly required.

43.2.2 Resequencing Chips

To overcome some of the shortfalls of mutation-based chips as well as to identify new mutations, resequencing microarrays (Affymetrix, Palo Alto, CA) for autosomal recessive RP diagnosis have been designed (Mandal et al. 2005; RetChipv1.0, <http://www.hgm2010.org/viewabsdetail-word.php?id=255&pn=P029-T>). Although the resequencing methodology is robust, deletions and insertions (except for very small indels) usually remain undetected. Other features calling for improvement in these first microarrays were: (1) the restricted number of included candidates; (2) the exclusion of exons from duplicated genes or highly similar sequences; (3) the low flexibility to add new genes once the chips had been designed and produced;

Table 43.1 Comparative assessment of the currently available methodologies for molecular diagnosis of retinal dystrophies

	Overall efficiency ¹	Main strengths/limitations	Diagnostic/research tool	Cost (in €) per sample
Direct				
Mutation microarray ²	35–45%	Celerity and low cost/only reported mutations	Yes/no	250
Resequencing chips	60–70%	Robustness and new mutations/only known genes	Yes/no	1,500–3,000 ³
Next-generation sequencing	99%	Screening all genes/high number of unfiltered unique variants	No/yes	2,000–3,000
Indirect				
Homozygosity mapping	40% (all cases) / (consanguinity) 99%	Wide genome search/common ancestry required	No/yes	500 ³
Cosegregation chips	60–70%	Reliability and informativeness/familial cases and only known genes	Yes/yes	80 ³

¹The efficiency on allele detection is calculated as the average of molecular diagnosis success for all retinal dystrophy cases (dominant, recessive, sporadic)

²Commercially available

³Cost after optimization (several samples are analyzed in parallel)

and (4) the high overall costs. Recently, improved resequencing chips have been launched aiming to increase the gene testing capacity: e.g., all mutation-containing exons (100) of 19 RP genes are included in a 30-kb-capacity Affymetrix custom genechip (Clark et al. 2010) or, a more comprehensive chip of 300 kb, which covers all the coding exons of 90 retinal disease genes and allows the analysis of many patients at once through a DNA-pooling strategy, in a fast and cost-effective manner (Booij et al. 2011). Again, the results support the robustness of the methodology, but the chips are not suitable to deal with the increasing number of candidates, and the limitations of the technique hinder the analysis of highly similar sequences.

43.2.3 Next-Generation Sequencing of Target Genes

Massive parallel next-generation sequencing has revolutionized the speed and budget to produce large amounts of sequence data, becoming a promising alternative for genotyping (Biesecker 2010). Indeed, the first report on this powerful technique targeted to the exons of a selected list of 46 retinal disease genes, and applied to familial and sporadic cases has demonstrated that DNA-pooling strategies coupled to ultrasequencing is a very effective approach (Bowne et al. 2011). Nonetheless, the massive amount of data generated by this strategy requires wide bioinformatics support for processing and filtering, as hundreds of potentially pathogenic variants have to be sorted out. Assets on the positive side are: the deep sequence coverage associated to this approach, the reliability of the gathered data, the possibility of DNA pooling, and the unrestricted flexibility on the number and type of sequences to study. Together, these features will push deep sequencing-based strategies to the forefront of high-throughput genetic testing as the costs plummet down.

43.3 Indirect Molecular Diagnosis of Retinal Dystrophies

Indirect high-throughput strategies rely on the use of single nucleotide polymorphisms (SNPs) to detect mendelian inheritance and cosegregation with the genomic region where the disease causing gene is presumably located.

43.3.1 Homozygosity Mapping

In recessively inherited retinal disorders, around 60% of the families are consanguineous (Pomares et al. 2007), and the affected family members are homozygous by descent, that is, they share two copies of the same pathogenic allele. Indeed, homozygosity mapping is a very valuable approach under consanguinity, but it is also useful in the diagnosis of sporadic patients, assuming that homozygosity due to unknown common ancestry is the most frequent case in rare diseases (Thiadens et al. 2009;

Bandah-Rozenfeld et al. 2010; Littink et al. 2010). Genome-wide analysis (GWA) with Affymetrix SNP microarrays allows the screening of all reported causative genes that are homozygous in the patient (Littink et al. 2010). When all candidates are excluded this approach pinpoints the remaining homozygous regions where a search for a new candidate should be undertaken. A bioinformatic analysis plus a careful assessment of the genetic data is required to determine the minimum length of homozygous consecutive SNPs to be considered, as well as detect low polymorphic regions to be excluded from further analysis. However, dominant or compound heterozygous cases are not suitable for homozygosity mapping.

43.3.2 Cosegregation SNP-Chips

Bearing diagnosis in mind as a first aim, we designed a cost-effective, robust, and fast strategy of high-throughput genotyping based on a comprehensive cosegregation study of familial cases. So far, three versatile SNP-based chips for the molecular diagnosis of dominant and recessive inherited retinal dystrophies have been devised (Pomares et al. 2007; Pomares et al. 2010; Pomares et al. in prep). Focusing on the reported retinal disease genes, all the SNPs were specifically selected based on both, their close physical position to each candidate (covering from the 5' to the 3' end) and high informativeness. The main asset of these chips is the rapid and reliable inclusion/exclusion of many candidates in a single genotyping step, highlighting those to be further analyzed in order to identify the causal mutation. Remarkably, considering that exclusion of all known candidates is a prerequisite for novel gene search, these chips stand out as valuable tools to single out suitable families for genome-wide linkage analysis. Overall, this strategy is highly efficient on recessive familial cases (85% on average), particularly in consanguineous families, where even a single patient can be diagnosed. Of note, haplotype SNP conservation in unrelated patients strongly hints at a shared mutation due to a founder effect. Although the efficiency of the diagnosis depends on the structure of the pedigree and consanguinity degree, this strategy applies to all types of inheritance, even to sporadic cases analyzed under the assumption of unknown common ancestry (Table 43.1) (Pomares et al. in prep).

43.4 Optimized Multitiered Strategy for Efficient Molecular Diagnosis

After careful consideration and based on daily practice, we have developed an optimized cost-effective multitiered strategy based on the following steps:

1. After accurate clinical diagnosis, a direct mutational screening chip for the disease, if available, will be prioritized. If only one pathogenic allele is detected, full mutational screening of the candidate will be performed.
2. Assuming that no pathogenic variant is identified, the cosegregation SNP chip will be our second choice. In familial cases, whether dominant, recessive, or X-linked, all available samples will be genotyped for haplotype cosegregation

analysis. If consanguineous cases are studied, homozygosity will add a further constraint to cosegregation, making the diagnosis of even a single patient viable. Sporadic cases are also amenable for testing under the homozygosity criterion.

3. If the number of nonexcluded candidates is below three genes (medium-sized genes), direct mutational screening will be undertaken. Otherwise, either a custom-designed resequencing chip, or exon amplification of retinal disease genes coupled to next-generation DNA sequencing are advised.
4. Finally, this tiered-strategy underscores those families suitable for novel gene search, after all candidates have been excluded. Depending on the genetic informativeness, the next choice will rely on either genome wide SNP-linkage analysis or next-generation sequencing after exome capture.

43.5 Future Venues and Concluding Remarks

The advent of next-generation DNA sequencing following the enrichment of individual whole exomes is opening new scenarios for the genetic diagnosis of highly heterogeneous diseases, as novel unreported genes may be identified not only in large families, but also in single patients (Ng et al. 2009; Choi et al. 2009). Although the costs are currently not affordable for routine diagnosis, a substantial decrease is foreseeable in the near future. Nonetheless, given that each individual human genome bears around 20,000 rare SNP variants, half of them potentially pathogenic, the identification of the causative mutation demands the confluence of bioinformatics, evolutionary biology, molecular genetics, and functional assays. These novel genes will increase the molecular repertoire and widen the basic knowledge of this group of heterogeneous disorders.

Once most of the retinal dystrophies causative genes are identified, the direct mutational screening and cosegregation SNP-chips will become the tools of choice for routine genetic testing. As the efficiency of the molecular diagnosis increases, it will have a major impact on the welfare of the patients and their families, who have endured the uncertainties of partial diagnoses and unpredictable prognoses. In this promising new era where gene and cell therapies for hitherto untreatable and highly incapacitating diseases – such as retinal dystrophies – are emerging (Stone 2009), accurate, rapid, and cost-effective genetic diagnosis is urgent, and the benefits derived undeniable.

Acknowledgments We would like to acknowledge the generous support from the patients, their families, and patient's associations, particularly to Andrés Mayor (Fundaluce, Hospital Central de Asturias). E. P. is under contract by CIBERER. This study was supported by grants SAF2009-08079 (Ministerio de Ciencia e Innovación, Gobierno de España) and SGR2009-1427 (Generalitat de Catalunya), CIBERER (U718), Fundaluce and ONCE to R.G.-D. We apologize to all the colleagues whose contributions to the genetic testing of retinal dystrophies could not be quoted due to space limitations.

References

- Bandah-Rozenfeld D, Mizrahi-Meissonnier L, Farhy C et al (2010) Homozygosity mapping reveals null mutations in FAM161A as a cause of autosomal-recessive retinitis pigmentosa. *Am J Hum Genet* 87:382–391
- Biesecker LG (2010) Exome sequencing makes medical genomics a reality. *Nat Genet* 42:13–14
- Booij JC, Bakker A, Kulumbetova J et al (2011) Simultaneous mutation detection in 90 retinal disease genes in multiple patients using a custom-designed 300-kb resequencing chip. *Ophthalmology* 118:160–167
- Bowne SJ, Sullivan LS, Koboldt DC et al (2011) Identification of disease-causing mutations in autosomal dominant retinitis pigmentosa (adRP) using next-generation DNA sequencing. *Invest Ophthalmol Vis Sci* 52:494–503
- Choi M, Scholl UI, Weizhen J et al (2009) Genetic diagnosis by whole exome capture and massively parallel DNA sequencing. *Proc Natl Acad Sci USA* 106:19096–19101
- Clark GM, Crowe P, Muszynska D et al (2010) Development of a diagnostic genetic test for simplex and autosomal recessive retinitis pigmentosa. *Ophthalmology* 117:2169–77.e3
- Henderson RH, Waseem N, Searle R et al (2007) An assessment of the apex microarray technology in genotyping patients with Leber congenital amaurosis and early-onset severe retinal dystrophy. *Invest Ophthalmol Vis Sci* 48:5684–5689
- Klevering BJ, Yzer S, Rohrschneider K et al (2004) Microarray-based mutation analysis of the ABCA4 (ABCR) gene in autosomal recessive cone-rod dystrophy and retinitis pigmentosa. *Eur J Hum Genet* 12:1024–1032
- Koenekoop RK, Lopez I, den Hollander AI et al (2007) Genetic testing for retinal dystrophies and dysfunctions: benefits, dilemmas and solutions. *Clin Experiment Ophthalmol* 35:473–485
- Littink KW, Koenekoop RK, van den Born LI et al (2010) Homozygosity mapping in patients with cone-rod dystrophy: novel mutations and clinical characterizations. *Invest Ophthalmol Vis Sci* 51(11):5943–5951
- Mandal MN, Heckenlively JR, Burch T et al (2005) Sequencing arrays for screening multiple genes associated with early-onset human retinal degenerations on a high-throughput platform. *Invest Ophthalmol Vis Sci* 46:3355–3362
- Ng SB, Turner EH, Robertson PD et al (2009) Targeted capture and massive parallel sequencing of 12 human exomes. *Nature* 461:272–278
- Pomares E, Marfany G, Brion MJ et al (2007) Novel high-throughput SNP genotyping cosegregation analysis for genetic diagnosis of autosomal recessive retinitis pigmentosa and Leber congenital amaurosis. *Hum Mutat* 28:511–516
- Pomares E, Riera M, Permanyer J et al (2010) Comprehensive SNP-chip for Retinitis Pigmentosa-Leber Congenital Amaurosis diagnosis: new mutations and detection of mutational founder effects. *Eur J Hum Genet* 18:118–124
- Stone EM (2009) Progress towards effective treatments for human photoreceptor degenerations. *Curr Opin Genet Dev* 19:283–289
- Thiadens AA, den Hollander AI, Roosing S et al (2009) Homozygosity mapping reveals PDE6C mutations in patients with early-onset cone photoreceptor disorders. *Am J Hum Genet* 85:240–247
- Zernant J, Kulm M, Dharmaraj S et al (2005) Genotyping microarray (disease chip) for Leber Congenital Amaurosis: detection of modifier alleles. *Invest Ophthalmol Vis Sci* 46:3052–3059

Chapter 44

Genes and Mutations in Autosomal Dominant Cone and Cone-Rod Dystrophy

Susanne Kohl, Veronique Kitiratschky, Monika Papke, Simone Schaich, Alexandra Sauer, and Bernd Wissinger

Keywords Cone dystrophy • Cone-rod dystrophy • Retinal degeneration • PRPH2 • CRX • GUCA1A • GUCY2D • AIPL1 • UNC119 • PROM1 • PITPNM3

44.1 Introduction

Cone- (CD) and cone-rod dystrophies (CRD) are characterized by decreased visual acuity, color vision defects, and photoaversion in case of a clinical diagnosis of CD. In many instances, CD progress to a more generalized CRD by concomitant loss of both cones and rods, with additional progressive loss in peripheral vision and night blindness. The clinical course of CRD is generally more severe, eventually leading to legal blindness. CDs/CRDs belong to the rare hereditary retinal dystrophies with an estimated prevalence of 1: 40,000 (Hamel 2007), and are genetically heterogeneous with all modes of inheritance documented. To date, ten genes (*AIPL1*, *CRX*, *GUCA1A*, *GUCY2D*, *PITPNM3*, *PROM1*, *PRPH2*, *RIMS1*, *SEMA4A*, *UNC119*) for the autosomal dominant forms of CD/CRD are listed in RetNet (RetNet: <http://www.sph.uth.tmc.edu/Retnet/home.htm>). We have tried to assess the mutation spectrum and prevalence of eight of these genes within our cohort of 52 patients and families with autosomal dominant CD/CRD.

S. Kohl (✉) • V. Kitiratschky • M. Papke • S. Schaich • A. Sauer • B. Wissinger
Department for Ophthalmology, Molecular Genetics Laboratory,
Institute for Ophthalmic Research, University Tuebingen,
Roentgenweg 11, S Tuebingen 72076, Germany
e-mail: susanne.kohl@uni-tuebingen.de

44.2 Materials and Methods

44.2.1 Patients and Clinical Examinations

Patients with a clinical diagnosis of cone dystrophy (CD) or cone-rod dystrophy (CRD), and a family history consistent with an autosomal dominant mode of inheritance were included in the study and recruited at the Centre for Ophthalmology, Tübingen, Germany and ophthalmic specialist centers throughout Europe and the United States of America. The diagnosis of adCD or adCRD was based on standard ophthalmologic assessment (fundus examination, color vision, visual field and visual acuity testing) and electroretinography (ERG). Venous blood was taken from patients and family members after informed consent. Total genomic DNA was extracted according to standard procedures. The study followed the tenets of the Declaration of Helsinki and was approved by the local ethical committee.

44.2.2 Genetic Analyses

Mutation screening of all coding exons and flanking intronic sequences of the *PRPH2*, *CRX*, *GUCAIA*, *AIPL1* and *UNC119* gene was performed by DNA sequencing of PCR amplified genomic DNA according to standard procedures. Mutation analysis of the *GUCY2D* gene was performed for all coding exons and flanking intronic sequences for 19 subjects, the remaining 33 patients were only analyzed for alterations at codon 838 in exon 13 by PCR/RFLP analysis with the restriction enzyme HhaI, followed by sequencing for confirmation (Kitiratschky et al. 2008b). Mutation scanning for the common mutation c.1117C>T p.Arg373Cys in *PROM1* was performed by sequencing of exon 11. Mutation scanning in *PITPNM1* was performed in a collaboration project by dHPLC and sequencing (Köhn et al. 2010). Novel sequence variants were excluded in 100 healthy controls and segregation analysis was performed in all cases for which samples from additional family members were available by either PCR/RFLP analysis or sequencing.

44.3 Results

44.3.1 Mutation Spectrum

Our patient collection comprised 52 independent families with a primary clinical diagnosis of cone (CD; $n=36$) or cone-rod dystrophy (CRD; $n=16$) and a family history consistent with an autosomal dominant mode of inheritance. Sixteen different heterozygous mutations in five of the eight analyzed genes were detected in 25 independent patients (Table 44.1). One patient was shown to have a mutation in

Table 44.1 Mutations in patients with autosomal dominant cone (adCD) and cone-rod dystrophy (adCRD)

Gene	Mutation at nucleotide position	Mutation at polypeptide level	Reference	Number of families (segregation in family)	Clinical diagnosis
<i>PRPH2</i>	c.510C>T	p.Arg172Trp	Wells et al. (1993)	1 (1)	adCD
<i>PRPH2</i>	c.556G>A	p.Asp186Asn	Novel	1 (1)	adCD
<i>PRPH2</i>	c.595A>G	p.Asn199Asp	Novel	1	adCD
<i>PRPH2</i>	c.866C>T	p.Ser289Leu	Kohl et al. (1997)	1	adCD
<i>PRPH2</i>	c.583C>G	p.Arg195Gly	Novel	1 (1)	adCD
<i>PRPH2</i>	c.920deIT	p.Leu307ArgfsX*17	Grüning et al. (1994)	1 (1)	adCRD
<i>CRX</i>	c.636deIC	p.Ser213ProfsX*6	Kitiratschky et al. (2008a)	1 (1)	adCD/adCRD
<i>CRX</i>	c.495deIAinsTTT	p.Ala166LeufsX*22	Novel	1 (1)	adCD
<i>GUCA1A</i>	c.265G>A	p.Glu89Lys	Kitiratschky et al. (2009)	1	adCD
<i>GUCA1A</i>	c.300T>A	Asp100Gln	Kitiratschky et al. (2009)	1 (1)	adCD
<i>GUCA1A</i>	c.451C>T	p.Leu151Phe	Sokal et al. (2005)	1 (1)	adCD
<i>GUCA1A</i>	c.476G>T	p.Gly159Val	Kitiratschky et al. (2009)	1 (1)	adCD
<i>GUCY2D</i>	c.2512C>T	p.Arg838Cys	Kelsell et al. (1998)	7 (6)/1 (1)	adCD/adCRD
<i>GUCY2D</i>	c.2512C>G	p.Arg838Gly	Kitiratschky et al. (2008b)	1	adCRD
<i>GUCY2D</i>	c.2513G>A	p.Arg838His	Payne et al. (2001)	3 (2)	adCD
<i>PROM1</i>	c.1117C>T	p.Arg373Cys	Michaelides et al. (2010)	1	adCRD

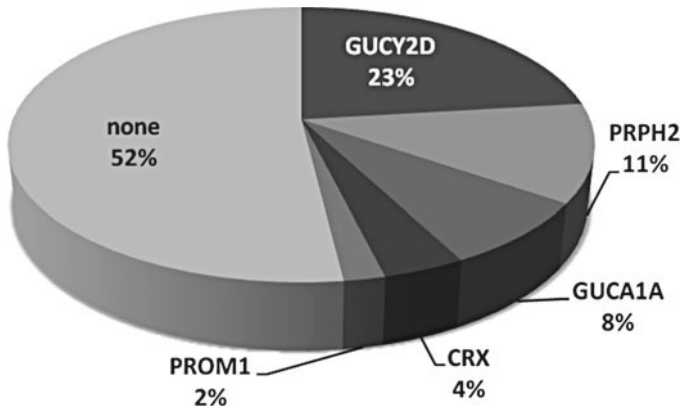


Fig. 44.1 Prevalence of mutations in the investigated genes in our collection of 52 patients with autosomal dominant cone and cone-rod dystrophies

PROM1 (2%), 2 independent families carried a mutation in *CRX* (4%), 4 were observed in *GUCA1A* (8%), 6 in *PRPH2* (12%) and 12 patients had mutations in *GUCY2D* (24%) (Fig. 44.1). Except for the mutations in *CRX*, and a 1 bp-deletion in *PRPH2*, all other mutations were missense mutations. No pathogenic variants were identified in *AIPL1*, *PITPNM3*, and *UNC119*. Segregation analysis could be performed in 18 of the 25 families and showed concordant segregation of the mutation with the disease phenotype in the respective family.

44.4 Discussion

GUCY2D and *GUCA1A* encode the retina specific guanylate cyclase (RetGC1) and its activating protein (GCAP1), respectively, which are expressed in rod and cone photoreceptors. Excitation of the photoreceptors decreases the intracellular concentration of cGMP and Ca^{2+} . GCAP1 works as a Ca^{2+} -sensor that detects changes in Ca^{2+} concentration and stimulates the membrane bound RetGC1 in a Ca^{2+} -dependent manner, thereby replenishing the cGMP pool of the photoreceptor. Thus, RetGC1 and GCAP1 mediate the recovery of rod and cone responses and are important to regain the dark-adapted state after excitation of the photoreceptor (Lamb and Pugh 2006).

GUCY2D gene mutations were identified in 12 (23%) of 52 patients. Interestingly, all mutations affect codon 838 of the gene. Arg838 was substituted by a cysteine codon in eight patients (c.2512C>T p.Arg838Cys), by a histidine codon in three (c.2513G>A p.Arg838His) and by a glycine codon in one patient (c.2512C>G p.Arg838Gly) (Kitiratschky et al. 2008b). Haplotype analysis showed that among six independent p.Arg838Cys mutation carriers, only two shared a common haplotype and that none of the p.Arg838His mutation carriers did, indicating that Arg838 is a true mutation hotspot related to adCD/CRD. According to our study *GUCY2D* is the

major gene responsible for adCD/CRD, with CD being the predominant phenotype as reported recently (Hunt et al. 2010).

GUCAIA mutations were identified in four unrelated patients (7.6%). All mutations affect amino acid residues that are evolutionary highly conserved and locate in functionally important domains of the protein: p.Glu89Lys and p.Gly159Val are located in the flanking helices of the Ca²⁺-binding EF-hand 3 and 4, while p.Asp100Glu and p.Leu151Phe are situated in the Ca²⁺-binding loops (Kitiratschky et al. 2009). Most patients presented with adCD and one patient had adCRD.

The transcription factor CRX is important for transactivation of many retina-specific expressed genes. It is expressed in rod and cone photoreceptors and cells of the inner nuclear layer early in development and expression is maintained throughout life. The transactivation domain of CRX has been localized to the C-terminus of the protein (Swaroop et al. 2010). We have identified two frame-shift mutations in the *CRX* gene in two independent families. In the first case, we identified a disease causing 1 bp-deletion, c.636delC, in a family with adCRD and marked intrafamilial variability (Kitiratschky et al. 2008a). The mutation results in a frame-shift after amino acid residue Ser213, and introduces a premature termination codon in the ultimate exon of *CRX* (p.Ser213ProfsX*6), resulting in a severely truncated protein that is expected to have reduced transactivation activity. Phenotypically, all affected family members showed signs of CD with reduced cone ERG, but only patients from one family branch also showed a reduced rod ERG, with some even displaying a negative combined rod-cone response. The second family was shown to carry a novel indel-mutation, c.495delAinsTTT, resulting in a frame-shift after amino acid residue Arg166, and also in a severely truncated CRX polypeptide (p.Ala166LeufsX*22). The patients in this family presented with slowly progressive CRD starting at their 20 to 30s. Severity in this family varied substantially within different individuals, some presenting with a marked negative ERG.

PRPH2, formerly known as *RDS*, encodes peripherin – a surface glycoprotein in the outer segment of rod and cone photoreceptor – which functions as an adhesion molecule involved in morphogenesis and stabilization of the outer segment discs. Retinal dystrophies associated with heterozygous *PRPH2* gene mutations show high phenotypic variability ranging from central to peripheral retinal dystrophies, namely adult vitelliform macular dystrophy, pattern dystrophy, fundus flavimaculatus-like dystrophy, central areolar choroidal dystrophy, macular dystrophy, CD/CRD, and retinitis pigmentosa (Boon et al. 2008). In many instances, intrafamilial phenotypic heterogeneity is observed. We have identified mutations in *PRPH2* in six individuals of our cohort. Except for c.920delT, all other mutations were missense substitutions. The mutations p.Arg172Trp, p.Asp186Asn, p.Arg195Gly, and p.Asn199Asp affect highly conserved amino acid residues that are located within the second intradiscal D2 loop, which is involved in dimerization as well as heteromeric interactions with ROM1 (Ding et al. 2005). The mutation p.Ser289Leu is located at the C-terminus extending into the cytoplasmic space. This C-terminus is truncated in case of the c.920delT mutation that results in a frame-shift and premature translation termination after 17 altered amino acid residues (p.Leu307ArgfsX*17). The patient was diagnosed with CRD, yet the mutation was originally described in

a patient with autosomal dominant retinitis pigmentosa (Grüning et al. 1994), and we have observed the mutation before in a patient with macular dystrophy (unpublished data), again highlighting the fact that the same mutation in *PRPH2* can result in very different phenotypes, probably due to additional modifying factors or the genetic background. All other patients with *PRPH2* mutations presented within this study were diagnosed with CD, although the mutation p.Arg172Trp is commonly associated with an autosomal dominant Stargardt-like macular dystrophy.

Mutations in *PROM1* have been identified in autosomal recessive retinitis pigmentosa (Maw et al. 2000), and later certain mutations have been associated with autosomal dominant CRD and bull's-eye macular dystrophy (Michaelides et al. 2010). This prompted us to screen our patient sample for the mutation c.1117C>T p.Arg373Cys, which led to the identification of one adCRD patient with this mutation. *PROM1* encodes the five transmembrane domain protein Prominin which contains two large, highly glycosylated extracellular loops and a cytoplasmic tail (Corbeil et al. 2001). It is specifically associated with plasma membrane protrusions (Corbeil et al. 2000), but its function and specific molecular interactions remain largely unknown. In the retina, *PROM1* is found at the base of the photoreceptor outer segments, where the new disk membranes are formed.

We have not found any putatively pathogenic mutations in *AIPL1*, *PITPNM3*, and *UNC119*. Only single reports relate these genes to autosomal dominant CD / CRD (Sohocki et al. 2000; Köhn et al. 2007, 2010; Kobayashi et al. 2000). *AIPL1* encodes a protein with TPR motifs, which are found in proteins that mediate a variety of functions, including nuclear transport and protein chaperone activity. Mutations in *AIPL1* are common in autosomal recessive Lebers congenital amaurosis. Few missense mutations in *PITPNM3* have been observed and discussed with respect to adCD and macular dystrophy. *PITPNM3* is the human homolog of the *Drosophila* rdgB protein, which is highly expressed in the retina and has been proposed to be required for membrane turnover of photoreceptor cells. *UNC119* is a photoreceptor synaptic protein homologous to *C. elegans* neuroprotein unc119, and the protein localizes to rod and cone ribbon synapses. Yet in this patient sample, none of the patients carried a mutation in these genes. Therefore our study does not support a role of these genes in adCD/adCRD.

Acknowledgments We thank all patients participating and all clinicians contributing patients to this study, and Britta Baumann for excellent technical assistance. This study was supported by the German Research Council DFG (KFO134:Ko2176/2-1).

References

- Boon CJ, den Hollander AI, Hoyng CB et al (2008) The spectrum of retinal dystrophies caused by mutations in the peripherin/RDS gene. *Prog Retin Eye Res* 27:213–35
- Corbeil D, Röper K, Fargeas CA et al (2001) Prominin: a story of cholesterol, plasma membrane protrusions and human pathology. *Traffic* 2:82–91

- Corbeil D, Röper K, Hellwig A et al (2000) The human AC133 hematopoietic stem cell antigen is also expressed in epithelial cells and targeted to plasma membrane protrusions. *J Biol Chem* 275:5512–20
- Ding XQ, Stricker HM, Naash MI (2005) Role of the second intradiscal loop of peripherin/rds in homo and hetero associations. *Biochemistry* 44:4897–904
- Grüning G, Millan JM, Meins M et al (1994) Mutations in the human peripherin/RDS gene associated with autosomal dominant retinitis pigmentosa. *Hum Mutat* 3:321–3
- Hamel CP (2007) Cone rod dystrophies. *Orphanet J Rare Dis.* 2:1–7
- Hunt DM, Buch P, Michaelides M (2010) Guanylate cyclases and associated activator proteins in retinal disease. *Mol Cell Biochem* 334:157–68
- Kelsell RE, Gregory-Evans K, Payne AM et al (1998) Mutations in the retinal guanylate cyclase (RETGC-1) gene in dominant cone-rod dystrophy. *Hum Mol Genet* 7:1179–84
- Kitiratschky VB, Behnen P, Kellner U et al (2009) Mutations in the GUCA1A gene involved in hereditary cone dystrophies impair calcium-mediated regulation of guanylate cyclase. *Hum Mutat* 30:E782–96
- Kitiratschky VB, Nagy D, Zabel T et al (2008a) Cone and cone-rod dystrophy segregating in the same pedigree due to the same novel CRX gene mutation. *Br J Ophthalmol* 92:1086–91
- Kitiratschky VB, Wilke R, Renner AB et al (2008b) Mutation analysis identifies GUCY2D as the major gene responsible for autosomal dominant progressive cone degeneration. *Invest Ophthalmol Vis Sci* 49:5015–23
- Kobayashi A, Higashide T, Hamasaki D et al (2000) HRG4 (UNC119) mutation found in cone-rod dystrophy causes retinal degeneration in a transgenic model. *Invest Ophthalmol Vis Sci* 41:3268–77
- Kohl S, Christ-Adler M, Apfelstedt-Sylla E et al (1997) RDS/peripherin gene mutations are frequent causes of central retinal dystrophies. *J Med Genet* 34:620–6
- Köhn L, Kadzhaev K, Burstedt MS et al (2007) Mutation in the PYK2-binding domain of PITPNM3 causes autosomal dominant cone dystrophy (CORD5) in two Swedish families. *Eur J Hum Genet* 15:664–71
- Köhn L, Kohl S, Bowne SJ et al (2010) PITPNM3 is an uncommon cause of cone and cone-rod dystrophies. *Ophthalmic Genet* 31:139–40
- Lamb TD, Pugh EN Jr (2006) Phototransduction, dark adaptation, and rhodopsin regeneration the proctor lecture. *Invest Ophthalmol Vis Sci* 47:5137–52
- Maw MA, Corbeil D, Koch J et al (2000) A frameshift mutation in prominin (mouse)-like 1 causes human retinal degeneration. *Hum Mol Genet* 9:27–34
- Michaelides M, Gaillard MC, Escher P et al (2010) The PROM1 mutation p.R373C causes an autosomal dominant bull's eye maculopathy associated with rod, rod-cone, and macular dystrophy. *Invest Ophthalmol Vis Sci* 51:4771–80
- Payne AM, Morris AG, Downes SM et al (2001) Clustering and frequency of mutations in the retinal guanylate cyclase (GUCY2D) gene in patients with dominant cone-rod dystrophies. *J Med Genet* 38:611–4
- Sohocki MM, Perrault I, Leroy BP et al (2000) Prevalence of AIPL1 mutations in inherited retinal degenerative disease. *Mol Genet Metab* 70:142–50
- Sokal I, Dupps WJ, Grassi MA et al (2005) A novel GCAP1 missense mutation (L151F) in a large family with autosomal dominant cone-rod dystrophy (adCORD). *Invest Ophthalmol Vis Sci* 46:1124–32
- Swaroop A, Kim D, Forrest D (2010) Transcriptional regulation of photoreceptor development and homeostasis in the mammalian retina. *Nat Rev Neurosci* 11:563–76
- Wells J, Wroblewski J, Keen J et al (1993) Mutations in the human retinal degeneration slow (RDS) gene can cause either retinitis pigmentosa or macular dystrophy. *Nat Genet* 3:213–8

Chapter 45

The Power of Homozygosity Mapping: Discovery of New Genetic Defects in Patients with Retinal Dystrophy

**Karin W. Littink, Anneke I. den Hollander, Frans P.M. Cremers,
and Rob W.J. Collin**

Keywords Homozygosity mapping • Retinal dystrophy • Retinitis pigmentosa
• Cone-rod dystrophy • Mutation • Gene identification • Nonconsanguineous
• Identity-by-descent

45.1 Introduction

Monogenic retinal dystrophies (RD) affect approximately 1:2,000 individuals, which corresponds to more than two million people worldwide (Berger et al. 2010), and account for ~5% of blindness worldwide. For two types of retinal dystrophy that will be discussed in this chapter (autosomal recessive cone-rod dystrophy (arCRD) and retinitis pigmentosa (arRP)), approximately half of the genetic causes

K.W. Littink

The Rotterdam Eye Hospital, PO Box 70030, 3000 LM Rotterdam, The Netherlands

Department of Human Genetics, Radboud University Nijmegen Medical Centre,
route 855, PO Box 9101, 6500 HB Nijmegen, The Netherlands

A.I. den Hollander • R.W.J. Collin (✉)

Department of Human Genetics, Radboud University Nijmegen Medical Centre,
route 855, PO Box 9101, 6500 HB Nijmegen, The Netherlands

Department of Ophthalmology, Radboud University Nijmegen Medical Centre,
route 400, PO Box 9101, 6500 HB Nijmegen, The Netherlands

Nijmegen Centre for Molecular Life Sciences, Radboud University Nijmegen Medical Centre,
PO Box 9101, 6500 HB Nijmegen, The Netherlands

e-mail: r.collin@antrg.umcn.nl

F.P.M. Cremers

Department of Human Genetics, Radboud University Nijmegen Medical Centre,
route 855, PO Box 9101, 6500 HB Nijmegen, The Netherlands

Department of Human Genetics, Nijmegen Centre for Molecular Life Sciences, Radboud
University Nijmegen Medical Centre, PO Box 9101, 6500 HB Nijmegen, The Netherlands

remain unsolved. Until now, the majority of new genes and gene mutations have mainly been discovered through the candidate gene approach, screening of genes involved in animal models, and the positional cloning approach. A derivative of the positional cloning approach is homozygosity mapping, a method that has mainly been used in consanguineous families. As summarized in this mini-review, homozygosity mapping can also be a powerful tool to identify genetic defects underlying retinal disease in nonconsanguineous families.

45.1.1 *Homozygosity Mapping*

In autosomal recessive diseases, affected individuals carry mutations in both copies of the same gene. In case an affected individual carries a homozygous mutation, the same mutation is inherited from both parents. Assuming that the mutation in both parents originates from the same ancestral allele, not only the mutation but also the surrounding chromosomal region will be identical on both chromosomes in the patient. Such region is called “homozygous” or “identical by descent (IBD)”. Although the size of the chromosome and the local recombination rate influence this formula, as a rule of thumb, the resulting size (S) of the homozygous region depends on the number of generations (n) between the ancestor carrying the recessive DNA variant and the patient carrying the homozygous region: $S = 100 \text{ Mb}/n$ (Woods et al. 2006). Thus, the average size of a homozygous region carrying the causal defect in a single patient of a first-cousin marriage will be 33 Mb (Fig. 45.1a), whereas this region will measure ~ 7 Mb in a patient from a nonconsanguineous family in which the common ancestor lived 14 generations ago (Fig. 45.1b).

Homozygous regions present in an individual’s DNA can be detected by using arrays on which thousands of single nucleotide polymorphisms (SNPs) equally distributed over the genome can be genotyped. When an SNP call on one allele is identical to that on the other allele, the SNP is called homozygous. Significant stretches of consecutive homozygous SNPs together compose a homozygous region. These regions can be homozygous by chance, for example in genomic regions that have limited haplotype diversity. However, as shown in Fig. 45.1, stretches of homozygous SNPs can also indicate that a genomic region originates from a common ancestor.

45.2 The Efficacy of Homozygosity Mapping in Different Types of Families and Populations

45.2.1 *Consanguineous vs. Nonconsanguineous Families*

Due to the structure of the pedigree (Fig. 45.1a), individuals from consanguineous families that are affected by a recessive disease almost exclusively carry their mutation in a homozygous state. As a consequence, homozygosity mapping has been

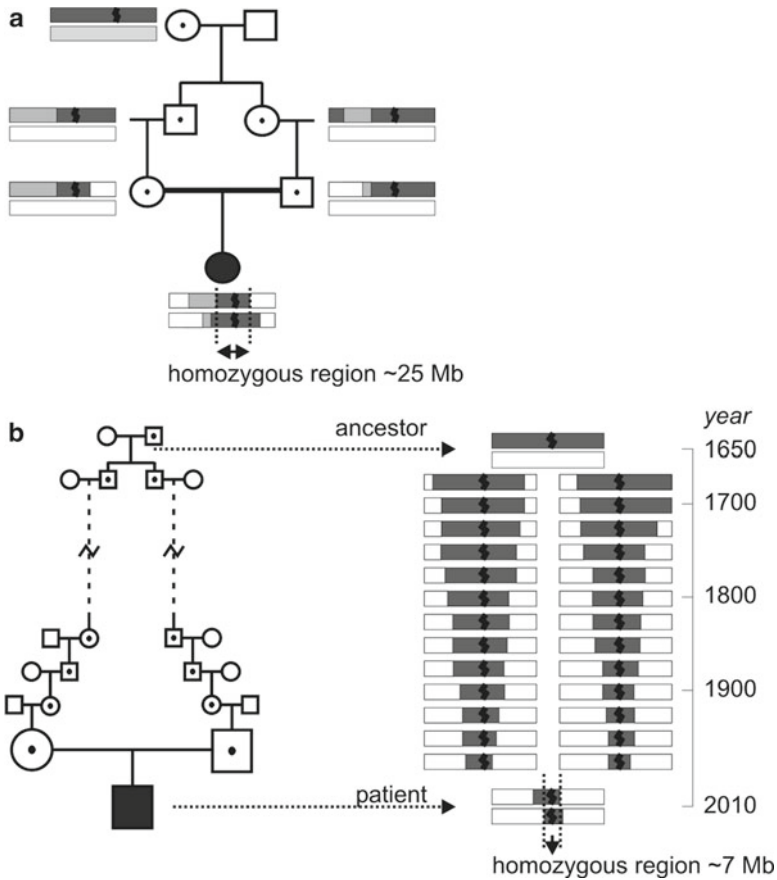


Fig. 45.1 Schematic presentation of the transfer of a mutation and the surrounding chromosomal region through different generations. Every generation, the original ancestral chromosome becomes “smaller” due to recombination between homologous chromosomes. **(a)** In consanguineous families, the mutation is likely inherited from a recent common ancestor. When the ancestral mutation is passed on via father and mother to their child, part of the original haplotype is still present, and in the child will be present as an identical-by-descent (i.e., homozygous) region. **(b)** Patients from nonconsanguineous families may also have a common ancestor via the paternal and maternal line, and thus carry a homozygous mutation. When an ancestor who carried the mutation lived several generations ago, more recombinations took place, and as a result, the homozygous region containing the mutation in a patient will be smaller

successfully used for many years to identify the genetic defect underlying recessive disorders in these families. In addition, consanguineous families often have large sibships, which allow a direct comparison of homozygous regions between affected and unaffected siblings, and facilitate the mapping of a genomic region that presumably harbors the genetic defect. However, also in the Dutch population, where consanguineous marriages are uncommon, ~35% of patients with a recessive

retinal dystrophy carry their mutation homozygously (FPMC, unpublished data). We hypothesize that most of these patients will carry their mutation homozygously because their parents are distantly related (Fig. 45.1b). This is especially likely in areas where little migration occurred over the past centuries (McQuillan et al. 2008). Homozygosity mapping could thus also lead to the identification of the genetic defect in patients of nonconsanguineous families.

To test this hypothesis, we performed genome-wide homozygosity mapping in two large cohorts of patients with arCRD or arRP, respectively (Littink et al. 2010; Collin et al. 2011). Homozygosity mapping can be used to find mutations in known genes residing in homozygous regions, and to scrutinize conspicuous homozygous regions for novel disease genes.

Approximately 40% of arCRD patients carry mutations in *ABCA4*, often a combination of a null mutation and a moderately severe *ABCA4* mutation (Maugeri et al. 1999). After excluding arCRD patients who carried one or two known mutations in *ABCA4*, we performed homozygosity mapping in 95 remaining arCRD families that originated from the Netherlands, Germany, or eastern Canada. Six sporadic patients and one family with two affected siblings were reported to be consanguineous (~7%). All known arCRD genes that resided in homozygous regions were screened for mutations. In the consanguineous patients, three genes were screened in three families, which led to the identification of the causative mutation in one family. Nine genes were screened in DNA of nonconsanguineous patients, and in four a mutation was detected. In conclusion, we identified the genetic defect in 2 out of 7 consanguineous patients (28%), and in 6 out of 88 nonconsanguineous families (7%). This percentage seems to show a much higher efficiency in identifying the genetic defect in consanguineous patients. However, if we take into account the number of genes screened per group of patients, one mutation was detected out of three genes screened in consanguineous patients, while nine screened genes led to four causative mutations in nonconsanguineous patients, showing a similar “success rate” for the different groups.

The arRP cohort consisted of 186 families that almost exclusively live in the Netherlands. Twenty-one families appeared to be consanguineous, and in the majority of cases originated from countries in which consanguineous marriages are more common, like Turkey and Morocco. In 13 of these 21 patients, one or more of their homozygous regions contained one of the known arRP genes, and sequence analysis of the corresponding genes revealed homozygous mutations in seven patients. However, since several patients had multiple homozygous regions encompassing different arRP genes, the total “sequence effort” was 21. Therefore, the “success rate” of screening consanguineous patients was calculated to be 0.33.

In the remaining group of 165 nonconsanguineous families, the number of homozygous regions was small, and varied in size between ~1.0 and 38.5 Mb. Compared to the consanguineous patients, a much smaller percentage of patients carried homozygous regions that overlapped with known arRP genes. However, in

the 29 patients from whom their homozygous regions contained one of the known arRP genes, homozygous mutations were found in 16 cases. Only in three nonconsanguineous patients, their homozygous regions encompassed two different arRP genes, resulting in a total of 32 “sequence efforts” and thereby yielding a success rate of 0.5 for this group. Thus, although the chances that a nonconsanguineous patient carries his or her genetic defect in a homozygous state is smaller compared to consanguineous patients, our data indicate that once a significant homozygous region overlaps with a known gene, the sequencing effort will be more efficient in nonconsanguineous patients compared to consanguineous patients.

Besides identifying homozygous mutations in known retinal dystrophy genes, our homozygosity mapping approach has also led to the identification of novel arCRD/arRP genes. In both our arCRD and arRP cohorts, multiple patients had a homozygous region overlapping with a known arRP locus on chromosome 6, the RP25 locus (Ruiz et al. 1998). Due to the relatively small size of some of the homozygous regions in our nonconsanguineous patients, the region overlapping with the RP25 locus was relatively small, and contained only five genes, which resulted in the identification of *EYS* (Collin et al. 2008). In addition, homozygosity mapping in two nonconsanguineous Dutch families recently aided the discovery of two other novel arRP genes, *C2ORF71* and *IMPG2* (Collin et al. 2010; Bandah-Rozenfeld et al. 2010). It should be noted though that these two families had four and three affected siblings, respectively, and as a result there was only a single shared homozygous region in both families, whereas isolated patients on average carry five of such regions.

45.2.2 *Successfulness Based on Population Composition*

As exemplified above, as well as in other studies, homozygosity mapping has been shown to be a powerful tool to identify the genetic defect in nonconsanguineous patients with several autosomal recessive diseases living in the Netherlands, Germany, eastern Canada (den Hollander et al. 2007; Littink et al. 2010; Collin et al. 2011), Lebanon (Megarbane et al. 2009), United Kingdom (Connell et al. 2010), and Japan (Hamanoue et al. 2009). However, when looking more carefully to the patient’s origin, many patients have migrated from a country with a higher percentage of consanguineous marriages as observed in for instance the Netherlands or Germany. The proportion of the genome that is homozygous (the inbreeding coefficient) is usually higher in populations that have a history of consanguinity (McQuillan et al. 2008). Patients from these populations thus have a higher chance to carry a homozygous mutation. However, also in populations with a high migration rate, as in northern America, certain immigrant groups may cluster together and form a relatively isolated population as well, as seen in the French-Canadian population in eastern Canada.

45.3 Conclusions

45.3.1 *Strengths, Limitations, and Future Perspectives of Homozygosity Mapping*

Homozygosity mapping can be a powerful, but not necessarily an efficient method to detect new genes and new mutations in consanguineous as well as nonconsanguineous patients. The main strength of homozygosity mapping is that it is a cost-effective way to perform a genome-wide analysis of regions that might harbor individual genetic defects, especially in genetically heterogeneous recessive disorder, like arCRD and arRP. The main limitation of homozygosity mapping however is that, it will never detect compound heterozygous mutations. In consanguineous families, patients almost exclusively carry their mutation homozygously, although the disadvantage is that their genome carries many homozygous stretches and as such many candidate genes reside within these regions. In contrast, in nonconsanguineous patients only small parts of their genome are homozygous, but there is a significant chance that these patients carry the causative mutations in a compound heterozygous state. In theory, homozygosity mapping will probably be most effective in nonconsanguineous families from whom there is evidence that the patients' parents share a common ancestor, which is most likely in populations with limited migration. Therefore, it is important to document the origin of the parents and grandparents of patients with autosomal recessive diseases.

Finally, with the introduction of new sequencing technologies, collectively called “next generation sequencing” (NGS), an analysis of all known retinal dystrophy genes will become feasible. In a research setting, NGS already led to the identification of new disease genes (Nikopoulos et al. 2010), and it is likely to be instrumental to identify many new retinal dystrophy genes in the near future.

Currently, NGS is deployed to sequence all exons of the whole genome (“exome sequencing”). Using this method, it will still be a challenge to detect the causative variant among thousands of variants. At this stage, conspicuously large homozygous regions may decrease the number of variants that need to be verified (Krawitz et al. 2010).

Thus, although genetic screening technologies are booming, homozygosity mapping has proven to be powerful and cost-effective to identify the genetic defect in consanguineous as well as in a subset of nonconsanguineous patients, and will remain useful as long as both the costs and the data analysis of NGS will remain challenging.

References

- Bandah-Rozenfeld D, Collin RWJ, Banin E et al (2010) Mutations in IMPG2, encoding interphotoreceptor matrix proteoglycan 2, cause autosomal-recessive retinitis pigmentosa. *Am J Hum Genet* 87:199–208
- Berger W, Kloekener-Gruissem B, Neidhardt J (2010) The molecular basis of human retinal and vitreoretinal diseases. *Prog Retin Eye Res* 29:335–375

- Collin RWJ, Littink KW, Klevering BJ et al (2008) Identification of a 2 Mb human ortholog of *Drosophila* eyes shut/spacemaker that is mutated in patients with retinitis pigmentosa. *Am J Hum Genet* 83:594–603
- Collin RWJ, Safieh C, Littink KW et al (2010) Mutations in C2ORF71 cause autosomal-recessive retinitis pigmentosa. *Am J Hum Genet* 86:783–788
- Collin RWJ, van den Born LI, Klevering BJ et al (2011) High-resolution homozygosity mapping is a powerful tool to detect novel mutations causative for autosomal recessive RP in the Dutch population. *Invest Ophthalmol Vis Sci* 52:2227–2239
- Connell F, Kalidas K, Ostergaard P et al (2010) Linkage and sequence analysis indicate that CCBE1 is mutated in recessively inherited generalised lymphatic dysplasia. *Hum Genet* 127:231–241
- den Hollander AI, Lopez I, Yzer S et al (2007) Identification of novel mutations in patients with Leber congenital amaurosis and juvenile RP by genome-wide homozygosity mapping with SNP microarrays. *Invest Ophthalmol Vis Sci* 48:5690–5698
- Hamanoue H, Megarbane A, Tohma T et al (2009) A locus for ophthalmo-acromelic syndrome mapped to 10p11.23. *Am J Med Genet A* 149A:336–342
- Krawitz PM, Schweiger MR, Rodelsperger C et al (2010) Identity-by-descent filtering of exome sequence data identifies PIGV mutations in hyperphosphatasia mental retardation syndrome. *Nat Genet* 42:827–829
- Littink KW, Koenekoop RK, van den Born LI et al (2010) Homozygosity mapping in patients with cone-rod dystrophy: novel mutations and clinical characterizations. *Invest Ophthalmol Vis Sci* 51:5943–5951
- Maugeri A, van Driel MA, van de Pol DJ et al (1999) The 2588G->C mutation in the ABCR gene is a mild frequent founder mutation in the Western European population and allows the classification of ABCR mutations in patients with Stargardt disease. *Am J Hum Genet* 64:1024–1035
- McQuillan R, Leutenegger AL, Abdel-Rahman R et al (2008) Runs of homozygosity in European populations. *Am J Hum Genet* 83:359–372
- Megarbane A, Slim R, Nurnberg G et al (2009) A novel VPS13B mutation in two brothers with Cohen syndrome, cutis verticis gyrata and sensorineural deafness. *Eur J Hum Genet* 17:1076–1079
- Nikopoulos K, Gilissen C, Hoischen A et al (2010) Next-generation sequencing of a 40 Mb linkage interval reveals TSPAN12 mutations in patients with familial exudative vitreoretinopathy. *Am J Hum Genet* 86:240–247
- Ruiz A, Borrego S, Marcos I, Antinolo G (1998) A major locus for autosomal recessive retinitis pigmentosa on 6q, determined by homozygosity mapping of chromosomal regions that contain gamma-aminobutyric acid-receptor clusters. *Am J Hum Genet* 62:1452–1459
- Woods CG, Cox J, Springell K et al (2006) Quantification of homozygosity in consanguineous individuals with autosomal recessive disease. *Am J Hum Genet* 78:889–896

Chapter 46

Development and Validation of a Canine-Specific Profiling Array to Examine Expression of Pro-apoptotic and Pro-survival Genes in Retinal Degenerative Diseases

Sem Genini, William A. Beltran, and Gustavo D. Aguirre

Keywords Dog model • Retinal degenerative diseases • RNA expression profiling array • Real-time quantitative reverse transcription-PCR • Pro-apoptosis genes • Pro-survival genes • Cell death • Cell survival • Madin–Darby canine kidney cells • Staurosporin

46.1 Introduction

Photoreceptors, like other specialized cells, have the innate ability to die through varied molecular mechanisms, and in response to multiple insults, whether genetic or acquired (Melino et al. 2005). Since the description of apoptosis as one of the final pathways in photoreceptor cell death (Chang et al. 1993; Portera-Cailliau et al. 1994), many studies have examined different molecules and mechanisms involved in the process.

Multiple pathways have been reported to be relevant for both retinal cell death (Cottet and Schorderet 2009; Doonan et al. 2005; Kunchithapautham and Rohrer 2007; Lohr et al. 2006; Rohrer et al. 2004; Sancho-Pelluz et al. 2008; Werdehausen et al. 2007) and survival (Barnstable and Tombran-Tink 2006; Bazan 2006; Jomary et al. 2006; Ueki et al. 2009; Wenzel et al. 2005). These are dependent on the underlying mutation, the model, whether naturally occurring or induced, the speed of the degenerative process, the cell class involved, and other factors. Despite the abundance of such studies, the signaling pathways and molecular mechanisms that link the mutations to the observed phenotypes are still unknown for many of the photoreceptor degenerative diseases.

S. Genini • W.A. Beltran (✉) • G.D. Aguirre
Department of Clinical Studies, University of Pennsylvania, Section of Ophthalmology,
School of Veterinary Medicine, 3900 Delancey Street, Philadelphia, PA 19104, USA
e-mail: wbeltran@vet.upenn.edu

One of these diseases is canine X-linked progressive retinal atrophy 2 (XLPR2), caused by a 2-bp deletion in exon ORF15 of the *RPGR* gene (Zhang et al. 2002). In two recent studies from our group, we characterized by TUNEL labeling the time course of cell death in affected dogs (Beltran et al. 2006), and identified by microarray analysis a number of nonclassical apoptosis and mitochondria-related genes that seemed to be involved in the degenerative process (Genini et al. 2010). However, limitations of the latter study included the use of a custom canine cDNA array with a limited number of genes, and without relevant pro- and antiapoptotic genes. Although for humans and rodent models a comprehensive suite of commercially available products can be used to analyze RNA and protein expressions of a large panel of genes associated with biological pathways or specific disease states, these tools do not work or are currently not available for the dog.

The aim of this study was to fill this gap by developing and validating a canine-specific real-time quantitative reverse transcription-PCR (qRT-PCR) profiling array containing key genes that are directly or indirectly involved in pro-apoptotic and pro-survival processes, autophagy, and/or are related to microglia/macrophages, cells that have been recently associated with retinal disease processes (Langmann 2007; Sasahara et al. 2008).

46.2 Materials and Methods

46.2.1 Development of the Canine-Specific qRT-PCR Array

The canine-specific custom-designed qRT-PCR profiling array (Table 46.1) was developed in conjunction with Applied Biosystems (ABI, Foster City, CA). Canine-specific sequences of selected genes, identified from studies in other species, were submitted to ABI to develop gene-specific TaqMan assays (http://www3.applied-biosystems.com/AB_Home/index.htm). These contained unlabeled forward and reverse primers and FAM dye-labeled TaqMan MGB probes. The Ingenuity Pathway Analysis (IPA, Ingenuity System Inc., Redwood City, CA) database was interrogated with the 96 genes on the array to better characterize biological functions and pathways involved.

46.2.2 Validation of the qRT-PCR Array Using Madin–Darby Canine Kidney (MDCK) Cells

46.2.2.1 Cell Culture

MDCK cells were grown to 80% confluency in 60-mm Petri dishes in Dulbecco's modified Eagle's medium (DMEM, with low glucose and L-glutamine, without sodium bicarbonate) supplemented with 10% fetal bovine serum (FBS), 1% penicillin

Table 46.1 List of the 96 genes included in the profiling array

Gene symbol (alternative symbol)	Gene description	Gene category	TaqMan [®] assay	Location on array
<i>I8S</i>	Eukaryotic 18S rRNA	7	Hs99999901_s1	A1
<i>AIFM1 (AIF)</i>	Apoptosis-inducing factor; mitochondrion-associated 1	1	Cf02636601_m1	A2
<i>SLC25A4 (ANTF-1)</i>	Solute carrier family 25, member 4	1	Cf02730291_g1	A3
<i>APAF1</i>	Apoptotic peptidase-activating factor 1	1	Cf02695305_m1	A4
<i>ATG3</i>	Autophagy-related 3 homolog	3	Cf00684119_m1	A5
<i>ATG5</i>	Autophagy-related 5 homolog	3	Cf02637561_m1	A6
<i>ATG7</i>	Autophagy-related 7 homolog	3	Cf02656560_m1	A7
<i>ATG12</i>	Autophagy-related 12 homolog	3	Cf02641158_m1	A8
<i>BAD (BBC2/BCL2L8)</i>	BCL2-antagonist of cell death	1	Cf02627333_m1	A9
<i>BAK1</i>	BCL2-antagonist/killer 1	1	Cf02627218_m1	A10
<i>BAX</i>	BCL2-associated X protein	1	Cf02622186_g1	A11
<i>BBC3 (PUMA)</i>	BCL2-binding component 3	1	Cf02708330_m1	A12
<i>BCL2</i>	B-cell CLL/lymphoma 2	4	Cf02622425_m1	B1
<i>BCL2L1 (BAM/BIM)</i>	BCL2-like 1	1	Cf00708025_s1	B2
<i>PABPN1 (BCL2L2)</i>	Poly(A)-binding protein, nuclear 1	4	Cf02664611_m1	B3
<i>BCL2L1 (BCL-XL)</i>	BCL2-like 1	4	Cf02622161_m1	B4
<i>BDNF</i>	Brain-derived neurotrophic factor	4, 5	Cf02622349_g1	B5
<i>BECN1 (ATG6)</i>	Beclin 1	3	Cf02643377_m1	B6
<i>BID</i>	BH3-interacting domain death agonist	1	Cf03460096_m1	B7
<i>GRP78 (BIP)</i>	78 kDa glucose-regulated protein	4	Cf02631877_m1	B8
<i>BNIP3 (NIP3)</i>	BCL2/adenovirus E1B 19 kDa-interacting protein 3	1	Cf02654885_m1	B9
<i>BNIP3L (NIX)</i>	BCL2/adenovirus E1B 19 kDa-interacting protein 3-like	1	Cf03460134_m1	B10
<i>CASP10</i>	Caspase 10	1	Cf03460108_m1	B11
<i>CASP14</i>	Caspase 14	2	Cf03460139_m1	B12
<i>CASP2</i>	Caspase 2	1	Cf02624522_m1	C1
<i>CASP3</i>	Caspase 3	1	Cf02622232_m1	C2
<i>CASP4</i>	Caspase 4	1	Cf02623472_m1	C3

(continued)

Table 46.1 (continued)

Gene symbol (alternative symbol)	Gene description	Gene category	TaqMan [®] assay	Location on array
<i>CASP6</i>	Caspase 6	1	Cf02652513_m1	C4
<i>CASP7</i>	Caspase 7	1	Cf03460102_m1	C5
<i>CASP8</i>	Caspase 8	1	Cf02627553_m1	C6
<i>CASP9 (APAF3)</i>	Caspase 9	1	Cf02627331_m1	C7
<i>SFRS2IP (CASP11)</i>	Splicing factor, arginine/serine-rich 2, interacting protein	2	Cf02703447_m1	C8
<i>CAPN1</i>	Calpain 1, (mu/I) large subunit	1	Cf02704115_m1	C9
<i>CAPN2</i>	Calpain 2, (mu/II) large subunit	1	Cf02645870_m1	C10
<i>CAST</i>	Calpastatin	2	Cf02664849_m1	C11
<i>CTSD</i>	Cathepsin D	3	Cf02625552_m1	C12
<i>CTSS</i>	Cathepsin S	3	Cf02625930_m1	D1
<i>CCL2</i>	Chemokine (C-C motif) ligand 2	4, 5	Cf02671955_g1	D2
<i>CD40 (TNFRSF5)</i>	TNF receptor superfamily member 5	2, 4, 5	Cf02626290_m1	D3
<i>CD40LG (CD154/TNFSF5)</i>	CD40 ligand	2, 4, 5	Cf02623314_m1	D4
<i>PTPRC (CD45)</i>	Protein tyrosine phosphatase, receptor type C	1, 5	Cf02653185_m1	D5
<i>CNTF</i>	Ciliary neurotrophic factor	4, 5	Cf03460095_sH	D6
<i>CREB1</i>	cAMP responsive element-binding protein 1	4	Cf02667607_m1	D7
<i>CYCS</i>	Cytochrome c, somatic	1	Cf02640410_g1	D8
<i>TYROBP (DAP12/KARAP)</i>	TYRO protein tyrosine kinase-binding protein	5	Cf02642009_m1	D9
<i>DIABLO (SMAC/SMAC3)</i>	Diablo homolog	1	Cf02665346_m1	D10
<i>ENDOG</i>	Endonuclease G	1	Cf02703061_u1	D11
<i>FADD (GIG3/MORT1)</i>	FAS-associated death domain-containing protein	1	Cf03460155_m1	D12
<i>FAS (TNFRSF6/APO-1/CD95)</i>	TNF receptor superfamily, member 6	1	Cf02651136_m1	E1
<i>FASLG (TNFSF6/CD95L/CD178)</i>	FAS ligand	1	Cf02625215_s1	E2
<i>BFGF (FGF2)</i>	Basic fibroblast growth factor	4, 5	Cf03460065_g1	E3
<i>DDIT3 (GADD153/CHOP10)</i>	DNA-damage-inducible transcript 3	2	Cf02654858_m1	E4
<i>GAPDH</i>	Glyceraldehyde-3-phosphate dehydrogenase	7	Hs02786624_g1	E5
<i>GDNF</i>	Glial cell-derived neurotrophic factor	4, 5	Cf02691052_s1	E6

<i>HIF1A</i>	Hypoxia-inducible factor 1, alpha subunit	4	Cf02741632_m1	E7
<i>HRK (DP5/IHARAKIRI)</i>	BCL2-interacting protein	1	Cf02702255_g1	E8
<i>HSPB1 (HSP27)</i>	Heat shock 27 kDa protein 1	4	Cf02628297_m1	E9
<i>HSPD1 (HSP60)</i>	Heat shock 60 kDa protein 1 (chaperonin)	1, 4	Cf026668830_gH	E10
<i>HSP70 (HSPA1)</i>	Heat shock protein 70	4	Cf02622418_g1	E11
<i>HSP86 (HSP90AA1)</i>	Heat shock protein HSP90-alpha	4	Cf03460183_sl	E12
<i>IGF1R (CD221)</i>	Insulin-like growth factor 1 receptor	4	Cf02625178_m1	F1
<i>IL6 (IFNB2)</i>	Interleukin 6	2, 5	Cf02624282_m1	F2
<i>IL10</i>	Interleukin 10	4, 5	Cf02624265_m1	F3
<i>MAP1LC3A (LC3)</i>	Microtubule-associated protein 1 light chain 3 alpha	3	Cf02630406_m1	F4
<i>LYZ</i>	Lysozyme	3	Cf02642933_m1	F5
<i>PRKCZ (PKC2)</i>	Protein kinase C, zeta	4	Cf02674616_m1	F6
<i>PRDX3</i>	Peroxiredoxin 3	4	Cf03460191_sH	F7
<i>NGF</i>	Nerve growth factor	4, 5	Cf02625041_sl	F8
<i>NTF3</i>	Neurotrophin 3	4, 5	Cf02700489_sl	F9
<i>NTF4</i>	Neurotrophin 4	4	Cf02705704_sl	F10
<i>SOD1</i>	Superoxide dismutase 1, soluble	1, 4	Cf02624276_m1	F11
<i>STAT1</i>	Signal transducer and activator of transcription 1	1	Cf02662970_m1	F12
<i>STAT3</i>	Signal transducer and activator of transcription 3	4, 5	Cf02666647_m1	G1
<i>BIRC5 (IAP4)</i>	Baculoviral IAP repeat-containing 5 (survivin)	4	Cf02628995_m1	G2
<i>TNFA</i>	Tumor necrosis factor alpha	1, 2, 5	Cf02628236_m1	G3
<i>TNFRSF1A</i>	Tumor necrosis factor receptor superfamily, member 1A	1, 2	Cf02622751_m1	G4
<i>TNFRSF21 (DR6)</i>	Tumor necrosis factor receptor superfamily, member 21	2	Cf03460083_sl	G5
<i>TNFRSF25 (APO-3/DDR3)</i>	Tumor necrosis factor receptor superfamily, member 25	1, 2	Cf02653814_g1	G6
<i>TNFSF10 (APO-2L/TRAIL)</i>	Tumor necrosis factor (ligand) superfamily, member 10	1, 2	Cf03460069_m1	G7
<i>TNFRSF9 (4-1BB/CD137)</i>	Tumor necrosis factor receptor superfamily, member 9	2	Cf03460132_m1	G8
<i>TNFRSF8 (CD153/CD30L)</i>	Tumor necrosis factor (ligand) superfamily, member 8	2	Cf03460158_m1	G9

(continued)

Table 46.1 (continued)

Gene symbol (alternative symbol)	Gene description	Gene category	TaqMan® assay	Location on array
<i>TP53</i>	Tumor protein p53	1	Cf02623148_m1	G10
<i>TP73</i>	Tumor protein p73	1, 4	Cf02680478_mH	G11
<i>TRADD</i>	TNFRSF1A-associated via death domain	1, 2	Cf02661903_m1	G12
<i>TRAF2 (TRAP)</i>	TNF receptor-associated factor 2	2	Cf02662893_m1	H1
<i>TRAF3</i>	TNF receptor-associated factor 3	2	Cf02659700_m1	H2
<i>XIAP (API3/BIRC4)</i>	X-linked inhibitor of apoptosis	4	Cf02625207_m1	H3
<i>ACTB</i>	Actin, beta	7	Hs03023880_g1	H4
<i>RHO</i>	Rhodopsin	6	Cf02625669_m1	H5
<i>OPN1SW</i>	Opsin 1 (cone pigments), short-wave-sensitive, blue opsin	6	Cf03460200_m1	H6
<i>OPN1LW</i>	Opsin 1 (cone pigments), long-wave-sensitive, red/green opsin	6	Cf02622926_m1	H7
<i>ARR3 (CAR/ARRX)</i>	Retinal cone arrestin 3	6	Cf03460116_m1	H8
<i>VIM</i>	Vimentin	6	Cf02668853_g1	H9
<i>GFAP</i>	Glial fibrillary acidic protein	6	Cf02655695_m1	H10
<i>PKCA (PRKCA)</i>	Protein kinase C, alpha	6	Cf02655322_m1	H11
<i>BEST1 (VMD2)</i>	Bestrophin 1	6	Cf02697409_gH	H12

Genes are reported with their symbols (in parenthesis the alternative symbols), descriptions, categories, TaqMan assay numbers (ABI), and location on the array. Main categories were (1) pro-death, mitochondria-dependent; (2) pro-death, mitochondria-independent; (3) autophagy; (4) pro-survival; (5) microglia/macrophage related; (6) positive control expressed in retina; (7) housekeeping

and streptomycin, 1% sodium pyruvate, and 1% MEM nonessential amino acids (Sigma-Aldrich, St. Louis, MO). At 5 and 10 h prior to cell collection, control cells received fresh supplemented DMEM, while treated cells received fresh supplemented DMEM containing 10 μ M staurosporin (Sigma-Aldrich). For each time point (5 or 10 h) and cell type (control or staurosporin-treated), the experiment was done in duplicate, one Petri dish was used to assess cellular viability and the other for qRT-PCR analysis.

46.2.2.2 Assessment of Cellular Viability

Cellular viability of the cultured control and staurosporin-treated MDCK cells was assessed with a LIVE/DEAD[®] Viability/Cytotoxicity Assay Kit (Invitrogen-Life Technologies, Carlsbad, CA) following the manufacturer's recommendation. Petri dishes containing the cells were examined by epifluorescence microscopy (Axioplan, Carl Zeiss Mediatech, Oberkochen, Germany). Images were digitally captured (Spot 4.0 camera), and displayed with a graphics program (Photoshop, Adobe, Mountain View, CA).

46.2.2.3 qRT-PCR Analysis

MDCK cells used for qRT-PCR analysis were harvested by adding PBS and removing the cells from the Petri dishes with a plastic 16-cm cell scraper. Total RNA from cell pellets was extracted, DNase treated, and reverse-transcribed as previously described (Genini et al. 2010). qRT-PCR reactions containing 30 ng of mixed cDNA at a ratio of 2:1 (5:10 h) also were performed as recently described (Genini et al. 2010).

46.3 Results

We developed a profiling array containing 96 canine-specific TaqMan probes to test the expression of genes related to pro-apoptotic and antiapoptotic processes. The selected genes belong to seven main categories that inform on signaling pathways and disease mechanisms, e.g., (1) pro-death, mitochondria-dependent; (2) pro-death, mitochondria-independent; (3) autophagy; (4) pro-survival; (5) microglia/macrophage related; (6) expressed in retina [rods or cones (*ARR3*, *OPN1SW*, *OPN1MW*, and *RHO*), Müller cells and astrocytes (*GFAP* and *VIM*), bipolar cells (*PKCA*), and in the retinal pigment epithelium (*BEST1*)]; (7) housekeeping genes (*18S*, *ACTB*, and *GAPDH*). Table 46.1 provides a summary of the 96 genes included in the array with their symbols, descriptions, categories, TaqMan assay numbers (ABI), and location on the array.

Table 46.2 Five most significant IPA biological functions (“molecular and cellular functions” or “disease and disorders”) and canonical pathways identified with the 96 genes included in the profiling array

IPA biological functions

Molecular and cellular functions

- Cell death
- Cell-mediated immune response
- Cellular development
- Cellular function and maintenance
- DNA replication, recombination, and repair

Diseases and disorders

- Inflammatory disease
- Immunological disease
- Cancer
- Neurological disease
- Skeletal and muscular disorders

IPA canonical pathways

- Death receptor signaling
 - Apoptosis signaling
 - Induction of apoptosis by HIV 1
 - TNFR1 signaling
 - Tumoricidal function of hepatic natural killer cells
-

To evaluate in detail and to confirm the nature of the 96 selected genes, we analyzed them with the IPA program. As expected, the five most relevant IPA molecular and cellular functions identified were cell death, cell-mediated immune response, cellular development, function, and maintenance, as well as DNA replication, recombination, and repair (Table 46.2). Inflammatory disease, immunological disease, neurological disease, cancer, and skeletal and muscular disorders were the five IPA biological functions related to “diseases and disorders” with the highest number of genes (Table 46.2). Furthermore, relevant IPA pathways included death receptor signaling, apoptosis signaling, TNFR1 signaling, induction of apoptosis by HIV1, and tumoricidal function of hepatic natural killer cells (Table 46.2).

The profiling array was validated, and the functionality of the TaqMan assays was tested, with RNA extracted from control and staurosporin-treated MDCK cells. To examine the highest number of genes possible, we mixed with a ratio of 2:1 the cDNAs of the staurosporin-treated cells at 5 h (to detect early apoptotic genes) and 10 h (to detect late apoptotic genes). The cDNAs from age-matched untreated cells at 5 and 10 h post addition of fresh DMEM were processed similarly. While the untreated cells were mostly all alive at 5 h (Fig. 46.1a) and 10 h (Fig. 46.1c), several staurosporin-treated cells were dead at 5 h (Fig. 46.1b) and almost all at 10 h (Fig. 46.1d) of treatment.

The qRT-PCR results showed that retina-specific control genes did not amplify (*BEST1*, *OPN1LW*, and *OPN1SW*), or had very high CT values between 35 and 38

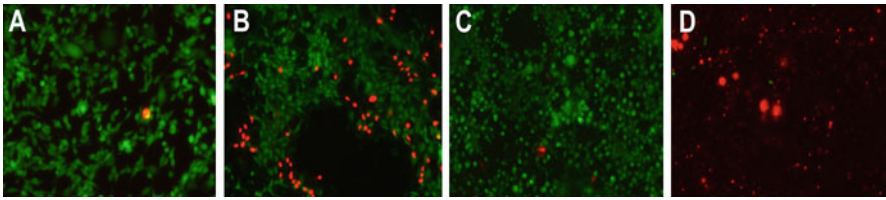


Fig. 46.1 LIVE/DEAD viability/cytotoxicity assay showing live (*green*) or dead (*red*) cells in control ((a) 5 h; (c) 10 h) or staurosporin-treated ((b) 5 h; (d) 10 h) MDCK cultures. Note the marked reduction in number of live cells after 10 h exposure to staurosporin

(*ARR3*, *GFAP*, and *RHO*) in both untreated and treated cells. Furthermore, the additional genes *BNIP3L*, *BID*, *CASP14*, *CD40*, *CD40LG*, *FADD*, *IL10*, *TNFA*, *TNFRSF9*, *TNFSF8*, *TNFRSF21*, and *TYROBP* did not amplify in MDCK cells. For the remaining genes, CT values ranged from 10 (*18S*) to 34 (*FASLG*, *NTF3*, *NTF4*, *PRDX3*, *PTPRC*, and *TP73*). The calculated mean CT values of *GAPDH* and *ACTB* were used for normalization because they did not change between treated and control samples, while *18S* was excluded as it was unstable and highly variable.

A total of eight genes (*BCL2L1*, *BCL2L11*, *CASP10*, *CCL2*, *DDIT3*, *HSP70*, *NGF*, and *TRAF2*) showed fold change (FC) differences >3 in control vs. staurosporin-treated cells, while four (the retinal genes *ARR3*, *GFAP*, and *RHO*, as well as *IL6*) showed opposite regulation. The expressions of *BNIP3*, *TNFA*, and *GFAP* were also assessed with single assays done separately. The same experimental conditions used for qRT-PCR on the profiling array were applied, with the exception that the quantity of cDNA was augmented to 100 ng per gene and that other primers for *BNIP3* (Genini et al. 2010) were used. The results demonstrated no changes in expression of *BNIP3*, upregulation of *GFAP* (raw CT values of 34 and 36, respectively), and *TNFA* (raw CT values of 35 and 37, respectively) in staurosporin-treated vs. control cells.

46.4 Discussion and Conclusions

In the present study, we developed a qRT-PCR profiling array containing key genes that are directly or indirectly involved in pro-apoptotic and pro-survival processes, autophagy, and/or are related to microglia/macrophages. For all the selected genes, canine-specific TaqMan assays are now inventoried and available for the research community. The array was validated in canine origin MDCK cell cultures treated with staurosporin, and we identified a number of genes that are important in pro-apoptotic and pro-survival processes, defined as part of signaling pathways that activate apoptosis, attempt to block apoptosis, or attempt to down- or upregulate protective cell functions. A precise and final classification of one gene to one category was a very complex task, because several genes fit into different categories depending on several factors (e.g., cell type, disease, age, interacting molecules) and because this classification is a dynamic process that alters as more information becomes available.

Specific characterization of the selected genes with IPA confirmed their expected biological functions and pathways, including cell death and cell-mediated immune response, and provided additional information to better evaluate and dissect the general pattern of the genes on the profiling array.

A few genes, in particular those that are retinal-specific, could not be successfully amplified in MDCK cells with 30 ng of cDNA. This might be due to absence or very low levels of gene expression in MDCK cells, as shown with the single assay for *TNFA* that worked when we used 100 ng of cDNA. Alternatively, this may have been caused by primers not annealing to the sequence of interest. MDCK cells were used for this initial validation step in order to save precious and limited canine retina samples; however, additional validation with RNA from retina will clarify the reasons for the failed amplification of certain genes.

This profiling array will be useful in future studies to identify genes, molecular mechanisms, and signaling pathways associated with photoreceptor degeneration in XLPRA2 and also additional canine models, e.g., *rcd1*, *rcd2*, XLPRA1, that carry mutations in other genes known to cause retinal degeneration in humans. Inclusion of three housekeeping genes used for normalization in the profiling array represents an advantage as it will enable selection of the optimal combination for each different experiment that will be performed.

It is expected that such quantitative analyses of gene expression will be valuable in identifying common, as well as disease-specific pro-death/pro-survival pathways that may represent future novel therapeutic targets.

Acknowledgments This study was supported by the Foundation Fighting Blindness (FFB), NIH Grants EY06855, 13132, and 17549, Fight for Sight Nowak Family Grant, the Van Sloun Fund for Canine Genetic Research, and Hope for Vision. The authors thank Rupa Gosh for technical assistance with qRT-PCR experiments.

References

- Barnstable CJ, Tombran-Tink J (2006) Molecular mechanisms of neuroprotection in the eye. *Adv Exp Med Biol* 572:291–295
- Bazan NG (2006) Cell survival matters: docosahexaenoic acid signaling, neuroprotection and photoreceptors. *Trends Neurosci* 29:263–271
- Beltran WA, Hammond P, Acland GM et al (2006) A frameshift mutation in RPGR exon ORF15 causes photoreceptor degeneration and inner retina remodeling in a model of X-linked retinitis pigmentosa. *Invest Ophthalmol Vis Sci* 47:1669–1681
- Chang GQ, Hao Y, Wong F (1993) Apoptosis: final common pathway of photoreceptor death in *rd*, *rds*, and rhodopsin mutant mice. *Neuron* 11:595–605
- Cotter S, Schorderet DF (2009) Mechanisms of apoptosis in retinitis pigmentosa. *Curr Mol Med* 9:375–383
- Doonan F, Donovan M, Cotter TG (2005) Activation of multiple pathways during photoreceptor apoptosis in the *rd* mouse. *Invest Ophthalmol Vis Sci* 46:3530–3538
- Genini S, Zangerl B, Slavik J et al (2010) Transcriptional Profile Analysis of RPGRORF15 Frameshift Mutation Identifies Novel Genes Associated with Retinal Degeneration. *Invest Ophthalmol Vis Sci* 51:6038–6050

- Jomary C, Cullen J, Jones SE (2006) Inactivation of the Akt survival pathway during photoreceptor apoptosis in the retinal degeneration mouse. *Invest Ophthalmol Vis Sci* 47:1620–1629
- Kunchithapautham K, Rohrer B (2007) Apoptosis and autophagy in photoreceptors exposed to oxidative stress. *Autophagy* 3:433–441
- Langmann T (2007) Microglia activation in retinal degeneration. *J Leukoc Biol* 81:1345–1351
- Lohr HR, Kuntchithapautham K, Sharma AK et al (2006) Multiple, parallel cellular suicide mechanisms participate in photoreceptor cell death. *Exp Eye Res* 83:380–389
- Melino G, Knight RA, Nicotera P (2005) How many ways to die? How many different models of cell death? *Cell Death Differ* 12(Suppl 2):1457–1462
- Portera-Cailliau C, Sung CH, Nathans J et al (1994) Apoptotic photoreceptor cell death in mouse models of retinitis pigmentosa. *Proc Natl Acad Sci USA* 91:974–978
- Rohrer B, Pinto FR, Hulse KE et al (2004) Multidestructive pathways triggered in photoreceptor cell death of the rd mouse as determined through gene expression profiling. *J Biol Chem* 279:41903–41910
- Sancho-Pelluz J, Arango-Gonzalez B, Kustermann S et al (2008) Photoreceptor cell death mechanisms in inherited retinal degeneration. *Mol Neurobiol* 38:253–269
- Sasahara M, Otani A, Oishi A et al (2008) Activation of bone marrow-derived microglia promotes photoreceptor survival in inherited retinal degeneration. *Am J Pathol* 172:1693–1703
- Ueki Y, Le YZ, Chollangi S et al (2009) Preconditioning-induced protection of photoreceptors requires activation of the signal-transducing receptor gp130 in photoreceptors. *Proc Natl Acad Sci USA* 106:21389–21394
- Wenzel A, Grimm C, Samardzija M et al (2005) Molecular mechanisms of light-induced photoreceptor apoptosis and neuroprotection for retinal degeneration. *Prog Retin Eye Res* 24:275–306
- Werdehausen R, Braun S, Essmann F et al (2007) Lidocaine induces apoptosis via the mitochondrial pathway independently of death receptor signaling. *Anesthesiology* 107:136–143
- Zhang Q, Acland GM, Wu WX et al (2002) Different RPGR exon ORF15 mutations in Canids provide insights into photoreceptor cell degeneration. *Hum Mol Genet* 11:993–1003

Chapter 47

The Chromosome 10q26 Susceptibility Locus in Age-Related Macular Degeneration

Chloe M. Stanton, Kevin J. Chalmers, and Alan F. Wright

Keywords Age-related macular degeneration • HTRA1 • ARMS2 • Chromosome 10 • Protease • Extracellular matrix • TGF-beta

47.1 Introduction

Age-related macular degeneration (AMD) is the leading cause of blindness in developed countries, affecting at least 20 million people aged over 65 years of age worldwide (Friedman et al. 2004). It is a genetically complex disease, arising through the interaction of genetic and environmental factors (Klein et al. 2004). Linkage analysis and genome-wide association studies (GWAS) have identified two genomic regions containing major AMD susceptibility loci. A risk allele in either locus accounts for an estimated 71% population-attributable risk of AMD; individuals carrying risk alleles at both loci have an estimated 40-fold increase in risk of developing AMD (Yang et al. 2006; Cameron et al. 2007).

The first AMD susceptibility locus on chromosome 1 (1q25-31) contains the complement factor H (*CFH*) and other complement-related genes. This has highlighted the role of the alternative complement pathway and inflammatory processes in AMD pathogenesis (Iyengar et al. 2004; Majewski et al. 2003; Klein et al. 2006; Haines et al. 2005; Edwards et al. 2005; Hageman et al. 2005). Subsequently, risk variants in other genes involved in the alternative complement pathway have been reported, including factor B and complement component *C3* (Gold et al. 2006; Yates et al. 2007).

The pathological role of the second major susceptibility locus, in chromosomal region 10q26 – which has an equivalent impact on AMD risk as *CFH* – is much less

C.M. Stanton (✉) • K.J. Chalmers • A.F. Wright
MRC Human Genetics Unit, Institute of Genetics and Molecular Medicine,
Western General Hospital, Crewe Road, Edinburgh EH4 2XU, UK
e-mail: chloe.stanton@hgu.mrc.ac.uk

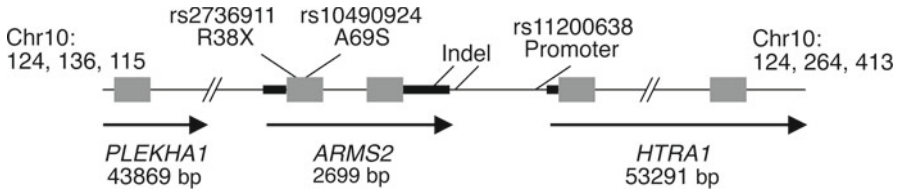


Fig. 47.1 The chromosome 10q26 locus. Location of variants on chromosome 10 reported to be associated with AMD susceptibility (not drawn to scale). Grey shaded regions represent coding sequences of candidate genes; untranslated regions are shown in *black*. Nucleotide positions and distances along chromosome 10 are derived from the NCBI Entrez gene database. Figure adapted from Allikmets and Dean (2008)

clear (Majewski et al. 2003; Seddon et al. 2003; Weeks et al. 2004; Fisher et al. 2005). Association studies refined the region likely to contain causative alleles (Jakobsdottir et al. 2005; Rivera et al. 2005) but three genes *PLEKHA1*, *LOC387715* (*ARMS2*) and *HTRA1* lie in a 200-kb region of strong linkage disequilibrium (LD), shown in Fig. 47.1. Thus, identification of the gene or the variant(s) influencing susceptibility to AMD has proved remarkably difficult.

47.2 Unravelling the Genetic Association Locus in Chromosomal Region 10q26

Rivera et al. (2005) studied chromosome 10q26 in two independent AMD case-control cohorts and found that the strongest association with AMD ($p = 10^{-34}$) arose from SNP rs10490924, encoding an amino acid substitution of alanine to serine at position 69 (A69S) in the hypothetical locus *LOC387715*, subsequently called *ARMS2* (Fig. 47.1). A Chinese study then identified the risk allele of SNP rs11200638, which was in complete LD with the *ARMS2* A69S polymorphism, as potentially causal (Dewan et al. 2006). Individuals homozygous for the minor (A) allele had a tenfold increased risk of wet AMD (Rivera et al. 2005; Dewan et al. 2006). The same SNP was also associated with AMD in Caucasians (Yang et al. 2006) and in particular with the risk of developing dry AMD (Cameron et al. 2007).

The rs11200638 SNP was proposed to affect putative binding sites for transcription factor AP2 α and serum response factor (SRF) in the promoter region of *HTRA1* (Fig. 47.1). Transcription of *HTRA1* was shown to be up-regulated by the AA genotype compared with the GG genotype (Dewan et al. 2006). Increased levels of *HTRA1* mRNA and protein were detected in RPE from four AMD-affected individuals carrying the AA risk allele (Yang et al. 2006). Thus, it was proposed that increased *HTRA1* activity may increase susceptibility to AMD. However, subsequent studies failed to consistently replicate these findings. Several studies found no significant difference in *HTRA1* mRNA or protein in retina and placental samples of known genotype, and no increased promoter activity by luciferase assays (Kanda et al. 2007, 2010; Chowers et al. 2008). Furthermore, the region surrounding

rs11200638 does not bind the transcription factor AP2 α (Kanda et al. 2007). However, others utilised the same techniques to show that there is a difference in promoter activity, mRNA and protein levels for *HTRA1* in carriers of the risk allele (An et al. 2010; Yang et al. 2010).

47.3 The Contribution of *ARMS2* to the AMD Association in Chromosomal Region 10q26

ARMS2 is conserved only in chimpanzees and encodes a 12-kDa protein of unknown function (Kanda et al. 2007). The contradictory evidence for *HTRA1* expression differences led to investigation of variants in *ARMS2* as the true risk alleles for AMD in 10q26. Kanda and colleagues evaluated the contribution of SNPs in a 220-kb region spanning *PLEKHA1*, *ARMS2* and *HTRA1* to the association with AMD and proposed that the A69S variant in *ARMS2* was causal but the majority of association studies were unable to separate the impact of *ARMS2* from *HTRA1* SNPs (Wang et al. 2010).

A 372 base pair deletion and a 54 base pair insertion in the 3' untranslated region (UTR) of *ARMS2* (indel in Fig. 47.1) was found to be significantly associated with AMD ($p=10^{-29}$) in 760 AMD cases and 549 controls (Fritsche et al. 2008). The indel was strongly associated ($r^2>0.88$) with rs10490924 and several other SNPs, forming a risk haplotype with an eightfold increased risk of AMD for homozygous individuals. The deletion removed a polyadenylation signal, whilst insertion of an AU-rich element reportedly led to rapid mRNA decay in individuals with the indel polymorphism. As a consequence, expression of *ARMS2* was not detected in homozygous carriers of the indel variant (Fritsche et al. 2008).

Interestingly, a second coding change in *ARMS2* – R38X – also results in reduced *ARMS2* mRNA and protein (Yang et al. 2010). This mutation is not present on the risk haplotype but is weakly protective, suggesting that loss of *ARMS2* protein function may be necessary but not sufficient to cause AMD.

Subsequent work showed that the indel is more complex, consisting of two adjacent indels, 17 base pairs apart (Wang et al. 2010). Again, the indel was strongly associated with AMD ($p=10^{-13}$), and was in strong LD with rs10490924 ($D' 0.99$) but it did not appear to affect stability of the *ARMS2* transcript, nor was it associated with lower levels of *ARMS2* mRNA in retina or white blood cells. The authors speculated that A69S is the biologically relevant variant at the chromosome 10q26 locus, although the functional consequences were unknown.

Previous reports had identified *ARMS2* expression in only the placenta and the retina (Jakobsdottir et al. 2005; Fritsche et al. 2008). However, Wang et al. (2010) showed that *ARMS2* is ubiquitously expressed after screening 18 tissues by RT-PCR. Kanda et al. (2007) and Fritsche et al. (2008) used immunostaining to show intense *ARMS2* staining in the retinal photoreceptor layer, localised to mitochondria and proposed a role for *ARMS2* in mitochondrial homeostasis. In contrast, Kortvely

et al. (2010) identified ARMS2 as a secreted protein, present at high levels in the choroid. This highlights the controversy and uncertainty regarding the roles of ARMS2 and HTRA1 in AMD susceptibility.

47.4 The Potential Role of HTRA1 in AMD

HTRA1 is a member of the mammalian HtrA (high temperature requirement A) serine protease family, first identified in *Escherichia coli* as a heat shock protein (Clausen et al. 2002). Four members of this highly conserved family have been described in humans; each having a characteristic trypsin-like catalytic domain paired with one or more C-terminal PDZ domains (Hu et al. 1998; Gray et al. 2000; Clausen et al. 2002; Nie et al. 2003). HTRA1 also has an N-terminal secretory signal sequence, an insulin-like growth factor (IGF) domain and a Kazal-type serine protease inhibitor domain (Zumbrunn and Trueb 1996). The serine peptidase activity of HTRA1 is regulated by ligand binding to the PDZ domain (Murwantoko et al. 2004). Auto-activation may occur via N-terminal cleavage of the Kazal inhibitory domain (Hu et al. 1998).

HTRA1 is secreted in a variety of tissues, with strongest expression in placenta (Zumbrunn and Trueb 1996). Its expression is up-regulated in osteoarthritis and in Duchenne muscular dystrophy, conditions in which degradation of the extracellular matrix (ECM) may be important (Hu et al. 1998; Bakay et al. 2002; Grau et al. 2006).

Oka et al. (2004) reported that HTRA1 inhibits BMP and TGF β signalling, and regulates availability of IGFs by cleaving IGF-binding proteins. Loss-of-function mutations in HTRA1 cause uncontrolled TGF β signalling, leading to cerebral autosomal recessive arteriopathy with subcortical infarcts and leukoencephalopathy (CARASIL; Hara et al. 2009). TGF β is a known regulator of ECM deposition and angiogenesis, both of which are important in AMD.

HTRA1 is expressed in human RPE, and is detected in drusen in AMD eyes (Dewan et al. 2006; Yang et al. 2006). A proposed role for HTRA1 in AMD pathogenesis is degradation of ECM proteoglycans (Grau et al. 2006). Collagens have been identified as binding partners of HTRA1 using a combination of approaches (Murwantoko et al. 2004; De Luca et al. 2004). HTRA1 degrades matrix proteins, including Gla and decorin in vitro, and regulates physiological and pathological matrix mineralisation (Canfield et al. 2007). Proteomic approaches identified many HTRA1-interacting proteins and suggested an intriguing link to regulation of the complement pathway through cleavage of clusterin, vitronectin and fibromodulin (Chamberland et al. 2009; An et al. 2010).

In summary, HTRA1 is able to bind and degrade components of the ECM, consistent with a role in AMD pathogenesis. HTRA1 may be involved in neovascularisation, wound healing following chronic inflammation, complement regulation and thickening of Bruch's membrane with age. However, much work remains to be done to clarify the relative roles of HTRA1 and/or ARMS2 in AMD susceptibility.

References

- Allikmets R, Dean M (2008) Bringing age-related macular degeneration into focus. *Nat Genet* 40: 820–821
- An E, Sen S, Park SK et al (2010) Identification of novel substrates for the serine protease HTRA1 in the human RPE secretome. *Invest Ophthalmol Vis Sci* 51:3379–3386
- Bakay M, Zhao P, Chen J et al (2002) A web-accessible complete transcriptome of normal human and DMD muscle. *Neuromuscul Disord* 12:S125–S141
- Cameron DJ, Yang Z, Gibbs D et al (2007) HTRA1 Variant Confers Similar Risks to Geographic Atrophy and Neovascular Age-Related Macular Degeneration. *Cell Cycle* 6:1122–1125
- Canfield AE, Hadfield KD, Rock CF et al (2007) HtrA1: a novel regulator of physiological and pathological matrix mineralization? *Biochem Soc Trans* 35:669–671
- Chamberland A, Wang E, Jones AR et al (2009) Identification of a novel HtrA1-susceptible cleavage site in human aggrecan: evidence for the involvement of HtrA1 in aggrecan proteolysis in vivo. *J Biol Chem* 284:27352–27359
- Chowers I, Meir T, Lederman M et al (2008) Sequence variants in *HTRA1* and *LOC387715/ARMS2* and phenotype and response to photodynamic therapy in neovascular age-related macular degeneration in populations from Israel. *Mol Vis* 14:2263–2271
- Clausen T, Southan C, Ehrmann M (2002) The HtrA Family of Proteases Implications for Protein Composition and Cell Fate. *Mol Cell* 10:443–455
- De Luca A, De Falco M, Fedele V et al (2004) The serine protease HtrA1 is upregulated in the human placenta during pregnancy. *J Histochem Cytochem* 52:885–892
- Dewan A, Liu M, Hartman S et al (2006) HTRA1 promoter polymorphism in wet age-related macular degeneration. *Science* 314:989–992
- Edwards AO, Ritter R, Abel KJ et al (2005) Complement factor H polymorphism and age-related macular degeneration. *Science* 308:421–424
- Fisher Sa, Abecasis GR, Yashar BM et al (2005) Meta-analysis of genome scans of age-related macular degeneration. *Hum Mol Genet* 14:2257–2264
- Friedman DS, O’Colmain BJ, Muñoz B et al (2004) Prevalence of age-related macular degeneration in the United States. *Arch Ophthalmol* 122:564–572
- Fritsche LG, Loenhardt T, Janssen A et al (2008) Age-related macular degeneration is associated with an unstable *ARMS2 (LOC387715)* mRNA. *Nat Genet* 40:892–896
- Gold B, Merriam JE, Zernant J et al (2006) Variation in factor B (BF) and complement component 2 (C2) genes is associated with age-related macular degeneration. *Nat Genet* 38:458–462
- Grau S, Richards PJ, Kerr B et al (2006) The role of human HtrA1 in arthritic disease. *J Biol Chem* 281:6124–6129
- Gray CW, Ward RV, Karran E et al (2000) Characterization of human HtrA2, a novel serine protease involved in the mammalian cellular stress response. *FEBS J* 267:5699–5710
- Hageman GS, Anderson DH, Johnson LV et al (2005) A common haplotype in the complement regulatory gene factor H (HF1/CFH) predisposes individuals to age-related macular degeneration. *Proc Natl Acad Sci USA* 102:7227–7232
- Haines JL, Hauser Ma, Schmidt S et al (2005) Complement factor H variant increases the risk of age-related macular degeneration. *Science* 308:419–421
- Hara K, Shiga A, Fukutake T et al (2009) Association of HTRA1 mutations and familial ischemic cerebral small-vessel disease. *N Engl J Med* 360:1729–1739
- Hu SI, Carozza M, Klein M et al (1998) Human HtrA, an evolutionarily conserved serine protease identified as a differentially expressed gene product in osteoarthritic cartilage. *J Biol Chem* 273:34406–34412
- Iyengar SK, Song D, Klein BEK et al (2004) Dissection of genomewide-scan data in extended families reveals a major locus and oligogenic susceptibility for age-related macular degeneration. *Am J Hum Genet* 74:20–39

- Jakobsdottir J, Conley YP, Weeks DE et al (2005) Susceptibility genes for age-related maculopathy on chromosome 10q26. *Am J Hum Genet* 77:389–407
- Kanda A, Chen W, Othman M et al (2007) A variant of mitochondrial protein LOC387715/ARMS2, not HTRA1, is strongly associated with age-related macular degeneration. *Proc Natl Acad Sci U S A* 104:16227–16232
- Kanda A, Stambolian D, Chen W et al (2010) Age-related macular degeneration-associated variants at chromosome 10q26 do not significantly alter ARMS2 and HTRA1 transcript levels in the human retina. *Mol Vis* 16:1317–1323
- Klein R, Peto T, Bird A et al (2004) The epidemiology of age-related macular degeneration. *Am J Ophthalmol* 137:486–495
- Klein RJ, Zeiss C, Chew EY et al (2006) Complement Factor H Polymorphism in Age-Related Macular Degeneration. *Science* 308:385–389
- Kortvely E, Hauck SM, Duetsch G et al (2010) ARMS2 is a constituent of the extracellular matrix providing a link between familial and sporadic age-related macular degenerations. *Invest Ophthalmol Vis Sci* 51:79–88
- Majewski J, Schultz DW, Weleber RG et al (2003) Age-related macular degeneration--a genome scan in extended families. *Am J Hum Genet* 73:540–550
- Murwantoko, Yano M, Ueta Y et al (2004) Binding of proteins to the PDZ domain regulates proteolytic activity of HtrA1 serine protease. *Biochem J* 381:895–904
- Nie G-y, Hampton A, Li Y et al (2003) Identification and cloning of two isoforms of human high-temperature requirement factor A3 (HtrA3), comparison of its tissue distribution with HtrA1 and HtrA2. *Biochem J* 371:39–48
- Oka C, Tsujimoto R, Kajikawa M et al (2004) HtrA1 serine protease inhibits signaling mediated by Tgfbeta family proteins. *Development* 131:1041–1053
- Rivera A, Fisher SA, Fritsche LG et al. (2005) Hypothetical LOC387715 is a second major susceptibility gene for age-related macular degeneration, contributing independently of complement factor H to disease risk. *Hum Mol Genet.* 14(21):3227–3236
- Seddon JM, Santangelo SL, Book K et al (2003) A genomewide scan for age-related macular degeneration provides evidence for linkage to several chromosomal regions. *Am J Hum Genet* 73:780–790
- Wang G, Spencer KL, Scott WK et al (2010) Analysis of the indel at the ARMS2 3'UTR in age-related macular degeneration. *Hum Genet* 127:595–602
- Weeks DE, Conley YP, Tsai H-J et al (2004) Age-related maculopathy: a genomewide scan with continued evidence of susceptibility loci within the 1q31, 10q26, and 17q25 regions. *Am J Hum Genet* 75:174–189
- Yang Z, Camp NJ, Sun H et al (2006) A variant of the HTRA1 gene increases susceptibility to age-related macular degeneration. *Science* 314:992–993
- Yang Z, Tong Z, Chen Y et al (2010) Genetic and functional dissection of HTRA1 and LOC387715 in age-related macular degeneration. *PLoS Genet* 6:e1000836
- Yates JRW, Sepp T, Matharu BK et al (2007) Complement C3 variant and the risk of age-related macular degeneration. *N Engl J Med* 357:553–561
- Zumbrunn J, Trueb B (1996) Primary structure of a putative serine protease specific for IGF-binding proteins. *FEBS Lett* 398:187–192

Chapter 48

Congenital Stationary Night Blindness: Mutation Update and Clinical Variability

Nidhi Lodha, Catrina M. Loucks, Chandree Beaulieu,
Jillian S. Parboosingh, and N. Torben Bech-Hansen

Keywords CSNB • CSNB1A • CSNB2A • *CANAI1F* • *NYX* • *GRM6* • *TRMP1*

48.1 Introduction

Congenital stationary night blindness (CSNB) represents a group of low vision disorders in which patients exhibit a negative ERG, reduced visual acuity, impaired night vision, myopia, nystagmus, and strabismus (Miyake et al. 1986; Héon and Musarella 1994; Miyake 2006; Lodha et al. 2009) with abnormal retinal neurotransmission (Tremblay et al. 1995) and different modes of genetic inheritance (Bech-Hansen et al. 1998a, b; Strom et al. 1998; Bech-Hansen et al. 2000; Zeitz et al. 2005a, b; Zeitz 2007; Bellone et al. 2008; Audo et al. 2009; Li et al. 2009; Nakamura et al. 2010). Analysis of individuals with CSNB diagnosed based on a negative ERG has revealed *CANAI1F* mutations in the patients with incomplete X-linked CSNB (CSNB2A), *NYX* mutations in patients with complete X-linked CSNB (CSNB1A), and *GRM6* and *TRMP1* mutations in patients with complete autosomal recessive CSNB (CSNB1B and CSNB1C). Several reports have revealed phenotypic variability among genetically defined CSNB1 and CSNB2 patients (Boycott et al. 2000; Jacobi et al. 2002; Allen et al. 2003), though limited information is available on the genotype–phenotype correlation in patients with CSNB.

N. Lodha (✉) • C.M. Loucks • C. Beaulieu • J.S. Parboosingh • N.T. Bech-Hansen
Department of Medical Genetics, University of Calgary, Heritage Medical Research Building,
Room No 258, Calgary, AB, Canada

Alberta Children's Hospital Research Institute, University of Calgary, Calgary, AB, Canada
e-mail: nlodha@ucalgary.ca

In this report we describe the type and distribution of mutations in *CACNA1F*, *NYX*, *GRM6*, *TRMP1*, and *CAPB4* genes in a cohort of 199 patients with CSNB together with the worldwide experience. In addition, we have analyzed the degree of clinical variability of 182 genetically defined patients with X-linked CSNB in an effort to refine the phenotype of patients with CSNB.

48.2 Methods

48.2.1 Subjects

A total of 199 patients were contributed by the CSNB Study Group for genetic analysis from Canada (Alberta, British Columbia, Nova Scotia, Ontario, Quebec), Denmark, Finland, Netherlands, United Kingdom, and USA (California, Georgia, Illinois, Missouri, New York, Oregon, Pennsylvania, Texas, Wisconsin) (manuscript in preparation). Furthermore, a retrospective chart review of 182 patients (males, except for 1 female; from 52 different families) with genetically defined X-linked CSNB (CSNB1A and CSNB2A) was undertaken. Clinical data collected included visual acuity (VA), refractive error (ref), color vision (CV), where available electrophysiological (ERG), dark adaptation (DA), nystagmus, strabismus, and complaint of impaired night vision.

48.2.2 Analyses

48.2.2.1 Genetic Analysis

Genomic DNA was PCR-amplified using a series of primers designed to amplify the coding and flanking intronic regions of the *CACNA1F*, *NYX*, *GRM6*, *TRMP1*, and *CAPB4* genes (see Boycott et al. 2001). PCR fragments were then sequenced and sequence variants were evaluated for their consequence on the encoded protein (e.g., nonsense, frameshift, or missense that involved a change in a highly conserved residue; analysis by PolyPhen).

48.2.2.2 Statistical Analysis

Within-group variability for individual clinical measures was calculated and variability between groups was compared using the variability ratio test. Binary variables (nystagmus, strabismus, impaired night vision) were compared using χ -square analysis (O'Brien 1981).

48.3 Results

48.3.1 Genetic Analysis

In a total of 199 patients diagnosed clinically with CSNB, 112 for X-linked iCSNB, 73 for X-linked cCSNB, and 14 with ar-cCSNB, we have identified a total of 116 unique mutations (65 unpublished; manuscript in preparation) in 159 (80%) of these families. Of the mutations, 69 were in *CACNA1F* (Table 48.1, Fig. 48.1), 32 in *NYX* (Table 48.2), seven in *GRM6* (Table 48.3), and eight in *TRMP1* (Table 48.4). No mutations were identified in *CAPB4*. *CACNA1F* mutations were distributed across the coding region from exon 2 to 47 (Fig. 48.1), while *NYX* mutations predominated in conserved or immediately adjacent residues across the leucine-rich repeats of *NYX*. The *CACNA1F* mutations were identified among patients originally diagnosed

Table 48.1 Unique *CACNA1F* mutations in patients with CSNB2A

Mutation type	Calgary experience (%)	World experience (%)
Missense point mutation	25 (36)	34 (37)
Nonsense point mutation	14 (20)	19 (21)
Splicing	9 (13)	15 (16)
Frameshift deletion	11 (16)	13 (14)
In-frame deletion	4 (6)	4 (4)
In-frame deletion/insertion	2 (3)	2 (2)
Frameshift duplication	3 (4)	3 (3)
Frameshift insertion	1 (1)	2 (2)
Total	69 (100)	92 (100)

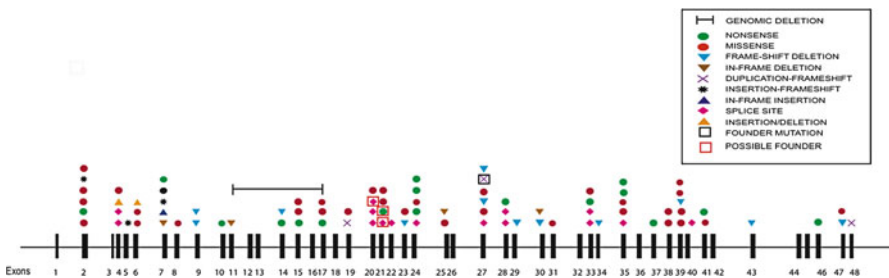




Fig. 48.1 Distribution of *CACNA1F* mutations in patients with CSNB2A. Genomic organization of *CACNA1F* on the X-chromosome between nucleotides 48,087,757 and 48,116,066 showing the distribution of 92 unique mutations (65 from our studies plus published mutations from other labs). The *CACNA1F* gene codes for the α_1 -subunit of the voltage-gated calcium channel $Ca_v1.4$. □: founder mutation in *CACNA1F* c.3166dupC (exon 27, frameshift mutation in patients with Dutch-German Mennonite ancestry). The following *CACNA1F* mutations show multiple occurrences:  c.2576+1G>A (Exon 20 splice mutation) in 8 families from Canada and United States.  c.2683C>T (Exon 21 nonsense mutation) in 7 European families

Table 48.2 Unique *NYX* mutations in patients with CSNB1A

Mutation type	Calgary experience (%)	World experience (%)
Missense point mutation	17 (53)	22 (46)
Nonsense point mutation	4 (13)	6 (13)
Splicing	2 (6)	3 (6)
Frameshift deletion	3 (9)	6 (13)
In-frame deletion	1 (3)	5 (10)
In-frame deletion/insertion	1 (3)	2 (4)
In-frame duplication	4 (13)	4 (8)
Total	32 (100)	48 (100)

Table 48.3 Unique *GRM6* mutations in patients with CSNB1B

Mutation type	Calgary experience	World experience
Missense point mutation	4	10
Nonsense point mutation	0	4
Splicing	1	1
Frameshift deletion	2	2
Frameshift duplication	0	2
Total	7	19

Table 48.4 Unique *TRMP1* mutations in patients with CSNB1C

Mutation type	Calgary experience	World experience (%)
Missense point mutation	3	20 (44)
Nonsense point mutation	2	8 (18)
Splicing	2	10 (22)
Frameshift deletion	1	5 (11)
Regulatory	0	1 (2)
Silent	0	1 (2)
Total	8	45 (100)

with incomplete X-linked CSNB (iCSNB or CSNB2A), Åland Island eye disease (AIED and AIED-like), and Åland eye disease (AED) (Strom et al. 1998; Boycott et al. 2001; Jalkanen et al. 2007) suggesting that these conditions are the same genetic condition (Rosenberg, Lodha, Bech-Hansen, manuscripts in preparation). We consistently observed the *CACNA1F* founder mutation (c.3166dupC, exon 27) among individuals from Canada with a Dutch-German Mennonite ancestry (Orton et al. 2008). A 24-bp deletion mutation in *NYX*, which results in the loss of the RACPAACA amino acids in the N-terminal Cys-rich region of nyctalopin, was detected in 12 North American CSNB families. Of 164 CSNB mutations known worldwide (Bech-Hansen, manuscript in preparation), we note that 18 of 48 unique *NYX* mutations, 24 of 93 unique *CACNA1F* mutations, 7 of 17 unique *GRM6* mutations, and 3 of 45 unique *TRMP1* mutations have been detected in more than one family. No mutations were identified in 40 of 199 CSNB patients (20%); the clinical picture and the family histories of these patients were not inconsistent with CSNB and autosomal inheritance.

Table 48.5 Clinical features of X-linked CSNB

Measures	CSNB1A (<i>NYX</i>) <i>n</i> =43	CSNB2A (<i>CACNA1F</i>) <i>n</i> =139
Visual acuity ^a	$m=0.35\pm0.25$, $r=0.05-1$	$m=0.50\pm0.34$, $r=0.00-1.78$
Refraction ^b	$m=-9.19\pm4.61$, $r=-26$ to -0.25	$m=-3.78\pm5.76$, $r=-21$ to 12.25
Impaired night vision	97.2% (<i>n</i> =36)	39% (<i>n</i> =128)
Nystagmus	40% (<i>n</i> =10)	52.5% (<i>n</i> =137)
Strabismus	29.4% (<i>n</i> =17)	24% (<i>n</i> =131)
Dark adaptation	NA	95% (<i>n</i> =40)
-ve ERG (b/a ratio)	100% (<i>n</i> =64 eyes)	75% (<i>n</i> =52 eyes)

-ve ERG negative electroretinogram; NA not applicable; *m* mean; *r* range

^aVision measured in log MAR

^bRefraction measured in diopters

Table 48.6 Clinical variability observed in patients with X-linked CSNB

Clinical features	Variability ^a CSNB1A	Variability ^a CSNB2A	<i>F</i> value	<i>p</i> value
Visual acuity	0.06 (<i>n</i> =43)	0.12 (<i>n</i> =149)	1.85	<0.05
Refractive error	21.25 (<i>n</i> =43)	33.18 (<i>n</i> =149)	1.57	<0.05
b/a ratio	0.02 (<i>n</i> =64 eyes)	0.11 (<i>n</i> =52 eyes)	8.15	<0.001
Impaired night vision	<i>n</i> =36	<i>n</i> =128		0.41
Nystagmus	<i>n</i> =10	<i>n</i> =137		0.57
Strabismus	<i>n</i> =17	<i>n</i> =131		1

^aVariability: a measure of data distribution reflects how far the data points are from the mean (O'Brien, 1981)

48.3.2 Clinical Variability

Clinical and ERG data were collected from 182 genetically defined patients with CSNB (43 CSNB1A from 14 families and 139 CSNB2A from 38 families). Summary ERG reports were available on all patients, though detailed reports have so far only been available on 79 patients.

Almost all patients (181 out of 182) with X-linked CSNB, CSNB1A and CSNB2A, had abnormal visual acuity (Table 48.5). Patients with CSNB1A had more severely impaired night vision compared to patients with CSNB2A (Table 48.5), and both groups of patients had abnormal ERGs (summary ERG of scotopic and photopic ERG information). All patients with CSNB1A had an abnormal rod-isolated response; negative bright-flash ERGs, normal to square cone a-waves, normal cone b-waves, and normal 30 Hz flicker responses, while patients with CSNB2A had reduced to normal isolated rod responses, abnormal cone ERGs and 30-Hz flicker. However, only 75% of the CSNB2A patients had negative bright-flash ERGs. Nystagmus and strabismus were present in some but not all patients (CSNB1A: 40%, 29.4%; CSNB2A: 52.5%, 24%, respectively) suggesting that these are secondary diagnostic feature of both CSNB1A and CSNB2A. Our statistical analysis of the variability of the clinical and ERG presentations revealed that patients with CSNB2A had more variable phenotype with respect to the visual acuity, refractive error, and the b/a wave ratio than those with CSNB1A (Table 48.6).

The analysis of clinical data in our cohort shows that all of the patients with CSNB1A exhibit the diagnostic characteristics of negative ERG, abnormal visual acuity, impaired night vision, and myopia (Table 48.5). Most of the patients with CSNB2A (99%) have abnormal vision, though only 75% of these patients had the characteristic negative ERG and only 39% of these patients had impaired night vision. The statistical analysis of visual acuity, refractive error, and b/a ratio of ERG waves confirms that the clinical phenotype of CSNB1A is less variable than the clinical phenotype of CSNB2A (Table 48.6).

48.4 Discussion

Mutation analyses in clinically recognized CSNB patients have provided useful diagnostic information and revealed the spectrum and distribution of sequence changes in *CACNA1F*, *NYX*, *GRM6*, *TRMP1*, and *CAPB4* genes (Tables 48.1–48.4). Definitive DNA diagnosis of CSNB was established in 80% of cases in a cohort of 199 unrelated patients analyzed in our laboratory. Combining our mutation information with that of published reports, a total of 209 mutations are known in *CACNA1F*, *NYX*, *GRM6*, *TRMP1*, and *CAPB4*. Within this cumulative data set, we note that the majority of mutations were identified in a single family with only 27% of mutations being detected in more than one family. This finding varied between genes with *TRMP1* having the fewest mutations (6%) detected in more than one family and *GRM6* having the highest rate (41%) with *NYX* and *CACNA1F* having recurrence rates of 37 and 25%. Moreover, mutations in *NYX* and *CACNA1F* represent the most common causes of cCSNB and iCSNB, respectively, which support the notion that X-linked CSNB is the more common form of CSNB. *GRM6* and *TRMP1* mutations were equally common (10% combined) in cCSNB patients. These results have implications for diagnostic labs. The absence of *CAPB4* mutation in the Calgary CSNB cohort might be due to a low incidence together with a bias of ascertainment of ar-iCSNB. From published reports, four of five patients in whom *CAPB4* mutations were identified did not complain of impaired night vision and had ERGs with severely reduced cone function and only negligibly reduced rod function together with abnormal vision, color vision, and photophobia, characteristics similar to cone–rod dystrophy (Zeitig et al. 2006; Zeitig 2007; Littink et al. 2009). For CSNB patients in whom the genetic causes are still to be discovered, mutations are likely to be found among genes for other proteins that function in photoreceptor pre- and postsynaptic processes that affect retinal neurotransmission.

The analysis of clinical data from our cohort shows that all of the patients with CSNB1A exhibit the diagnostic characteristics of negative ERG, abnormal visual acuity, impaired night vision, and myopia (Table 48.5). Almost all (99%) the patients with CSNB2A have abnormal vision, though only 75% of these patients had the characteristic negative ERG and a minority of these patients had impaired night

vision (Table 48.5). Nystagmus and strabismus are present only in 50% or less of patients with CSNB1A and CSNB2A (Table 48.5), suggesting that both of these diagnostic features are not primary, as originally suggested (Miyake et al. 1986).

The clinical phenotype (reduced visual acuity and refractive error) and ERG features were found to be more variable among patients with CSNB2A than among patients with CSNB1A (Table 48.6). Such variability may be explained by various factors, including the presence of other genetic factors modifying the phenotype (Boycott et al. 2000; Allen et al. 2003; Zeitz et al. 2007) and environmental factors acting before or after birth.

The “negative bright”-flash ERG has been considered diagnostic for CSNB and a requisite feature of a defect in the retinal neurotransmission. However, our findings revealed that the negative ERG is *not* invariably present in patients with mutations in the *CACNA1F* gene, as 13 of 52 patients with CSNB2A in whom detailed ERG analysis was available did not have a *negative* bright-flash ERG. Patients with a presynaptic defect due to *CACNA1F* mutations show that both the cone and rod pathways are affected in patients with CSNB2A (Miyake et al. 1986; Tremblay et al. 1995). These findings show that CSNB2A is a cone–rod disorder rather than strictly a night blindness disorder with a predominant rod defect. The cases that present with nonnegative bright-flash ERGs could possibly be explained by a milder retinal neurotransmission deficit. This observation would suggest that the presence of a negative ERG, though normally present, should not be taken as pathognomonic of this subtype of CSNB, as patients with an abnormal, but nonnegative bright-flash ERG could be misdiagnosed, and potentially lead to unnecessary investigations and patient mismanagement.

A comprehensive clinical assessment, detailed family history, and robust ERG data will aid in the diagnosis of CSNB. The constant clinical findings in patients with X-linked CSNB are abnormal vision and abnormal ERGs. However, the absence of a negative bright-flash scotopic ERG or complaint of impaired night vision does not exclude a diagnosis of CSNB.

48.5 Conclusions

Mutations in the *CACNA1F*, *NYX*, *GRM6*, and *TRPM1* genes established the genetic cause of CSNB in 80% of patients in a cohort of 199. Some patients with mutations in *CACNA1F* (CSNB2A) presented with an abnormal but nonnegative ERG. Furthermore, X-linked CSNB patients with CSNB2A showed greater variability in the key phenotypic features (reduced visual acuity, refractive error, and b/a wave ratio) than those patients with CSNB1A. Furthermore, CSNB1A patients invariably complained of night blindness, while those with CSNB2A infrequently did consistent with the notion that the later is more correctly a cone–rod disorder.

References

- Allen L E Zito I Bradshaw K et al (2003) Genotype-phenotype correlation in British families with X linked congenital stationary night blindness. *Br J Ophthalmol* 87:1413–1420
- Audo I Kohl S Leroy B P et al (2009) TRPM1 is mutated in patients with autosomal-recessive complete congenital stationary night blindness. *American Journal of Human Genetics* 85:720–729
- Bech-Hansen N T Boycott K M Gratton K J et al (1998a) Localization of a gene for incomplete X-linked congenital stationary night blindness to the interval between DXS6849 and DXS8023 in Xp11.23. *Hum Genet* 103:124–130
- Bech-Hansen N T Naylor M J Maybaum T A et al (1998b) Loss-of-function mutations in a calcium-channel alpha1-subunit gene in Xp11.23 cause incomplete X-linked congenital stationary night blindness. *Nat Genet* 19:264–267
- Bech-Hansen N T Naylor M J Maybaum T A et al (2000) Mutations in NYX, encoding the leucine-rich proteoglycan nyctalopin, cause X-linked complete congenital stationary night blindness. *Nat Genet* 26:319–323
- Bellone R R Brooks S A Sandmeyer L et al (2008) Differential gene expression of TRPM1, the potential cause of congenital stationary night blindness and coat spotting patterns (LP) in the Appaloosa horse (*Equus caballus*). *Genetics* 179:1861–1870
- Boycott K M Maybaum T A Naylor M J et al (2001) A summary of 20 CACNA1F mutations identified in 36 families with incomplete X-linked congenital stationary night blindness, and characterization of splice variants. *Hum Genet* 108:91–97
- Boycott K M Pearce W G and Bech-Hansen N T (2000) Clinical variability among patients with incomplete X-linked congenital stationary night blindness and a founder mutation in CACNA1F. *Can J Ophthalmol* 35:204–213
- Héon E and Musarella M A (1994) Congenital stationary night blindness: a critical review for molecular approaches. Chur, Switzerland, Harwood Academic
- Jacobi F K Andreasson S Langrova H et al (2002) Phenotypic expression of the complete type of X-linked congenital stationary night blindness in patients with different mutations in the NYX gene. *Graefes Arch Clin Exp Ophthalmol* 240:822–828
- Jalkanen R Bech-Hansen N T Tobias R et al (2007) A Novel CACNA1F Gene Mutation Causes Aland Island Eye Disease. *Invest Ophthalmol Vis Sci* 48:2498–2502
- Li Z Sergouniotis P I Michaelides M et al (2009) Recessive mutations of the gene TRPM1 abrogate ON bipolar cell function and cause complete congenital stationary night blindness in humans. *Am J Hum Genet* 85:711–719
- Littink K W van Genderen M M Collin R W et al (2009) A novel homozygous nonsense mutation in CABP4 causes congenital cone-rod synaptic disorder. *Invest Ophthalmol Vis Sci* 50:2344–2350
- Lodha N Tobias R Brennan R et al (2009) Phenotypic variability in genetically defined X-linked Congenital Stationary Night Blindness. *Arvo Abstract Book, Inv. Ophthalmol. & Vis. Sci, Program 3721*
- Miyake Y (2006) *Congenital Stationary Night Blindness*. London, England, The Mit Press
- Miyake Y Yagasaki K Horiguchi M et al (1986) Congenital stationary night blindness with negative electroretinogram. A new classification. *Arch Ophthalmol* 104:1013–1020
- Nakamura M Sanuki R Yasuma T R et al (2010) TRPM1 mutations are associated with the complete form of congenital stationary night blindness. *Molecular Vision* 16:425–437
- O'Brien R G (1981) A simple test for variance effects in experimental designs. *Psychological Bulletin* 83:570–574
- Orton N C Innes A M Chudley A E et al (2008) Unique disease heritage of the Dutch-German Mennonite population. *Am J Med Genet A* 146A:1072–1087
- Strom T M Nyakatura G Apfelstedt-Sylla E et al (1998) An L-type calcium-channel gene mutated in incomplete X-linked congenital stationary night blindness. *Nat Genet* 19:260–263
- Tremblay F Laroche R G and De Becker I (1995) The electroretinographic diagnosis of the incomplete form of congenital stationary night blindness. *Vision Res* 35:2383–2393

- Zeit C (2007) Molecular genetics and protein function involved in nocturnal vision Christina Zeit. *Expert Review of Ophthalmology* 2:467–485
- Zeit C Forster U Neidhardt J et al (2007) Night blindness-associated mutations in the ligand-binding, cysteine-rich, and intracellular domains of the metabotropic glutamate receptor 6 abolish protein trafficking. *Hum Mutat* 28:771–780
- Zeit C Kloeckener-Gruissem B Forster U et al (2006) Mutations in CABP4, the gene encoding the Ca²⁺-binding protein 4, cause autosomal recessive night blindness. *Am J Hum Genet* 79: 657–667
- Zeit C Minotti R Feil S et al (2005a) Novel mutations in CACNA1F and NYX in Dutch families with X-linked congenital stationary night blindness. *Mol Vis* 11:179–183
- Zeit C van Genderen M Neidhardt J et al (2005b) Mutations in GRM6 cause autosomal recessive congenital stationary night blindness with a distinctive scotopic 15-Hz flicker electroretinogram. *Invest Ophthalmol Vis Sci* 46:4328–4335

Chapter 49

Serum Biomarkers and Trafficking Defects in Peripheral Tissues Reflect the Severity of Retinopathy in Three Brothers Affected by Choroideremia

Natalia Strunnikova, Wadih M. Zein, Chris Silvin, and Ian M. MacDonald

Keywords CSNB • CSNB1A • CSNB2A • *CANA1F* • *NYX* • *GRM6* • *TRMP1*

49.1 Introduction

Choroideremia (CHM) is an X-linked disorder of trafficking whose primary manifestations in humans are those of a progressive chorioretinopathy. Clinical and basic research has carefully defined the ocular manifestations of the disorder and progressive stages of the retinopathy (Jacobson et al. 2006). Additional important information on the pathogenesis of this disorder has come from the study of animal models, by creating tissue-specific knockouts of the *chm* gene in photoreceptors and the retinal pigment epithelium (RPE), which demonstrated cell–autonomous degeneration in these layers (Tolmachova et al. 2006).

Typical of a sex-linked disorder, males are predominantly affected, whereas females are carriers. Nonrandom inactivation of the normal X-chromosome, has been traditionally used to explain findings in affected females; however, an alternate hypothesis may be that insufficiency of total REP activity explains the manifestations of CHM (Rak et al. 2004). Our recent studies have demonstrated that REP1 depletion has effects on phagocytosis and intracellular trafficking in nonocular tissues like skin fibroblasts and monocytes with a large degree of variability in the manifestations in patients carrying different *CHM* mutations (Strunnikova et al. 2009).

N. Strunnikova • W.M. Zein

Ophthalmic Genetics and Visual Function Branch, National Eye Inst/NIH, Bethesda, MD 20892, USA

C. Silvin

Genetics and Molecular Biology Branch, National Human Genome Research Institute NIH, Bethesda, MD 20892, USA

I.M. MacDonald (✉)

Department of Ophthalmology, University of Alberta, 10240 Kingsway Ave, Edmonton, AB 10240, Canada

e-mail: Ian.M.Macdonald@albertahealthservices.ca

The potential contribution of the genetic background of the individual in disease development has not been evaluated in CHM patients. Here, we used monocytes from three brothers carrying the same mutation in CHM gene to evaluate differences in vesicle transport, lysosomal acidification, and rates of proteolytic degradation. We demonstrated previously the variability of the clinical phenotypes of the brothers was reflected in functional differences of intracellular vesicle transport in their peripheral tissues. In addition, CHM fibroblasts secreted significantly lower levels of some cytokine/growth factors including macrophage MCP1, PEDF, TNF- α , FGF, and IL-8 (Strunnikova et al. 2009). Here we observed that serum levels of PEDF, VEGF, and MCP1 factors vary significantly between the brothers carrying the same mutation in the *CHM* gene. Altered acidification in lysosomes, reduced rates of proteolytic degradation, and altered secretion of growth factors may correlate with cellular effects in the retina of CHM patients and help predict changes in disease progression.

49.2 Methods

49.2.1 *Characterization of the Patient Population*

The study was approved by the CNS Institutional Review Board of the NIH (08-E1-#017). Three brothers (age 13–18) of Caucasian origin with the clinical diagnosis of CHM were accrued to the National Eye Institute of the NIH, Bethesda, MD. Six Caucasian healthy males (age 21–34) with normal vision and no ocular pathology acted as age-matched controls. Subjects underwent fundus imaging (OIS, Sacramento, California, USA) and optical coherence tomography (OCT) using Stratus 3 OCT (Carl Zeiss Meditec Inc, Dublin, CA). Peripheral blood samples (36 mL) were collected (Vacutainer CPT, Becton Dickinson, NJ) and mononuclear cells were sorted using AutoMax into CD14+ and CD14– populations. Levels of IL8, MCP1, TNF α , EGF, VEGF, and PEDF were determined in blood serum by commercial technology (SearchLight/Aushon BioSystems, Inc, Woburn, MA). Genomic DNA was isolated from peripheral blood monocytes, PCR amplified, and sequenced (MacDonald et al. 2004). Molecular genetic testing of the *CHM* gene was undertaken through the National Ophthalmic Genotyping Network, eyeGENE™.

49.2.2 *Confocal Microscopy and FACS Analysis on Phagocytosing CD14+ Monocyte Population from CHM Patients and Controls*

Monocytes for live cell imaging were plated on eight-well chamber slides 24 h before feeding (Lab-Tek; Nalge Nunc International, Naperville, IL). Phagocytosis in monocytes was tracked by pHrodo™ BioParticles® conjugate (pH-dependent dye conjugated with *E. coli*, Invitrogen, Carlsbad, CA) using fluorescence-activated cell

sorting (FACS) and live cell imaging analysis. Confocal microscopy was performed on a laser scanning confocal microscope (Leica Microsystems, Exton, PA) using 63× objective. pHrodo™ BioParticles® conjugates were visualized by exciting with a 568-nm laser beam and collecting emissions between 580 and 650 nm. Differences in rate of proteolytic degradation between the CHM patients and controls were determined using self-quenched conjugate of DQ™-ovalbumin with BODIPY FL dye (Molecular Probes, Eugene, OR). The increase in fluorescence corresponding to the rate of degradation of engulfed DQ-ovalbumin was measured using FACS analysis at different time points following feeding. Samples were analyzed on a FACStar plus flowcytometer (Becton-Dickinson, Mountain View, CA) with 488 nm excitation and 530 nm band pass filter for FITC. For all analyses, at least 10,000 cells were assessed in each sample.

49.3 Results

49.3.1 *Clinical Variation between the Members of the CHM Affected Family*

Clinical data from patients carrying the same *CHM* mutation are shown in Figs. 49.1a and 49.2b. From the fundus images (Fig. 49.1a), phenotypic variability in these three brothers carrying the same mutation (Fig. 49.1b) is clearly apparent compared to a normal control. The oldest brother (CHM3, age 18) shows areas of significant retinal pigment epithelial depigmentation and loss, along with atrophy of the choroidal vasculature. The youngest brother (CHM2, age 13) has more retinal pigment epithelial atrophy than his older brother (CHM1, age 16). While each brother maintains normal central acuity, the oldest brother has lost considerable visual field, consistent with the fundus image (CHM3). Whereas one would have expected a clear progression in the fundus images and field loss in all brothers, their phenotypes do not reflect that and illustrate the phenotypic variability inherent in this disorder. The OCT images of the CHM-affected brothers can be compared to a normal patient (Fig. 49.2b). The least affected sibling (CHM1, age 16) has what would appear a normal RPE and retinal architecture with little apparent remodeling in the retina. The OCT retinal image of his older sibling (CHM3, age 18) shows marked loss of the outer segments, outer nuclear layer, and RPE in the area beyond the central retina (consistent with the fundus photograph, Fig. 49.1a).

49.3.2 *Clinical and Functional Variability Between the Individuals Carrying the Same CHM Mutation*

Trafficking defects in peripheral cells from normal controls and the three CHM patients carrying the same mutation, but with variation in severity of the disease (Fig. 49.1a), were evaluated using *E. coli* particles conjugated with a pH-dependent

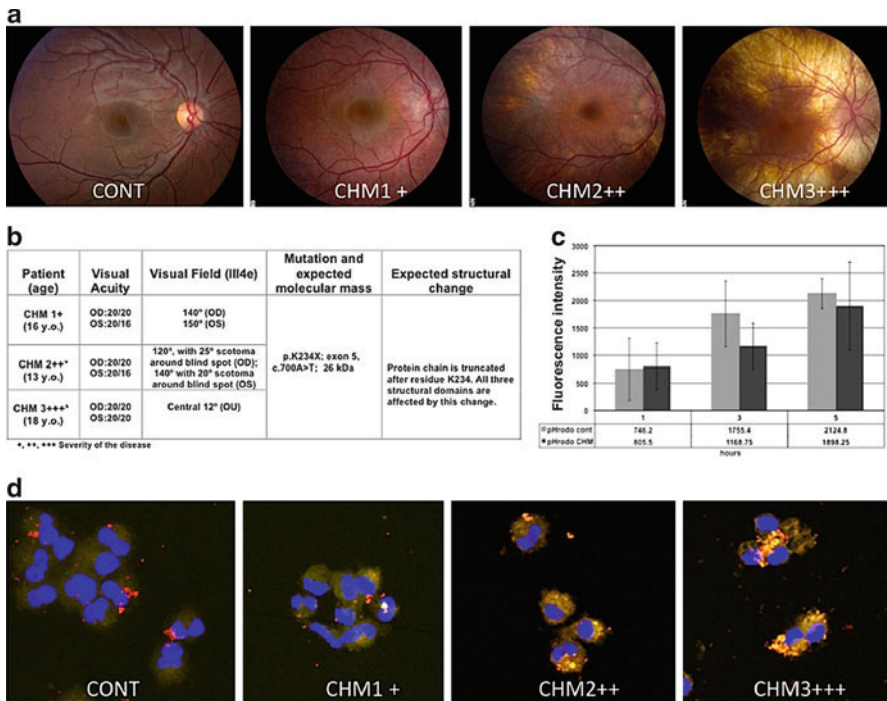


Fig. 49.1 Clinical and phenotypic variation in patients carrying the same mutation in the *CHM* gene. (a) Fundus photography of control (CONT) and three brothers carrying the same *CHM* mutations with different severity of the disease (from less to more severe: CHM1+, CHM2++, CHM3+++). (b) Clinical characteristics of CHM patients and effect of the *CHM* mutation. (c) Differences in lysosomal acidification in monocytes from CHM and control patients determined by FACS in older patient population using *E. coli* BioParticles® (Strunnikova et al. 2009). (d) Differences in the uptake and fluorescence levels of monocytes fed with BioParticles® from CHM affected brothers and control patients (confocal images, control, patients CHM1+, CHM2++ and CHM3+++)

fluorescent dye (pHrodo™ BioParticles®). FACS analysis of monocytes derived from older patients carrying different mutations (Strunnikova et al. 2009) exhibited lower levels of fluorescence intensity following the feeding compared to control (Fig 49.1c). Here we used peripheral cells from young CHM-affected brothers (age 13, 16, and 18) carrying the same *CHM* mutation to determine if differences in the disease manifestations could be correlated with trafficking and phagocytic. Confocal microscopy of the monocytes following feeding with BioParticles® demonstrated a large degree of variation in the fluorescent intensities of the cells derived from the brothers which could be the result of pH change within the phagolysosomes or increased uptake of the particles by the monocytes of patients CHM2 and CHM3 with more advanced disease. The efficiency of lysosome-mediated degradation by monocytes was further evaluated with DQ™-ovalbumin particles with BODYPY

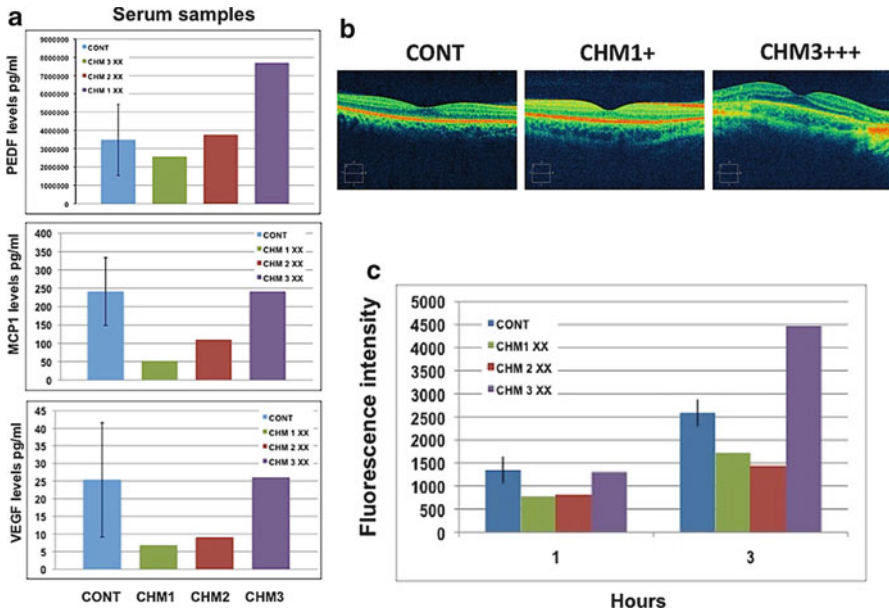


Fig. 49.2 Variation in rates of proteolytic degradation in monocytes and levels of serum cytokine in CHM patients carrying the same mutation. **(a)** Levels of PDGF, VEGF and MCP1 in the serum of brothers carrying the same *CHM* mutation (CHM1, CHM2, CHM3). **(b)** OCT of control subject, a brother with the least severe disease (CHM1) and the most severe disease (CHM3). **(c)** The efficiency of lysosome-mediated proteolytic degradation by monocytes from affected brothers (CHM1, CHM 2, CHM3) and control assessed with DQTM-ovalbumin particles. Increase in fluorescence intensity, was measured by FACS. Data was expressed as a mean fluorescence intensity of the cells \pm SED (when applicable) at 1 and 3 h following the feeding

FL dye. Using this system, we evaluated proteolytic abilities of the monocytes of the CHM patients. FACS analysis of the monocytes from age-matched controls and the CHM-affected brothers, following feeding with DQTM-ovalbumin particles, confirmed a large degree of variability in the rates of DQTM-ovalbumin degradation by the cells between the brothers carrying the same mutation, which reflected difference in their clinical status (Fig. 49.2c). A possible explanation could be that in younger patients with more severe disease and active degeneration of the retina, more inflammatory cytokines are released into the blood stream causing an alteration of the function of peripheral cells. To evaluate this hypothesis, we measured serum levels of PDGF, VEGF, and MCP1 factors and determined that they vary significantly between the brothers with highest levels observed in the serum of patient CHM3 with the most severe disease and lowest levels in the serum of the least affected patient, CHM1 (Fig. 49.2a). Phenotypic variability in peripheral cells of the younger patients and levels of cytokines in serum (CHM 1–3) could therefore be potentially associated with the differences in their disease development and could reflect variability in disease progression.

49.4 Discussion

Citations on variability in the phenotype of CHM patients are few and a unifying hypothesis to explain the variability of disease has been lacking to date. Variable electrophysiologic responses from the retina in CHM-affected males within the same family and unrelated families have been reported (Sieving et al. 1986). Our observations on trafficking defects in peripheral tissues of CHM patients may begin to explain some phenomena that we observe as phenotypic variability in CHM. The disorder of trafficking in specific tissues, such as the eye may be related to the total REP activity in that tissue (Rak et al. 2004). An example of the phenotypic variability between the female carriers of the same mutation in the CHM gene was described earlier (Rudolph et al. 2003). The potential contribution of the individual's genetic background to the phenotypic variability was not previously evaluated in patients carrying the same *CHM* mutation. Analysis of the serum and peripheral cells from patients could be a useful approach to evaluate differences in disease stage. Some degenerative retinal conditions including AMD have demonstrated systemic alterations in circulating levels of different biomarkers; for example, an increase in complement components C5a, Bb, and C-reactive protein levels independently associated with advanced AMD (Reynolds et al. 2009). In a similar fashion, we observed that levels of PEDF, VEGF, and MCP1 in serum from CHM patients were altered more in patients with more severe disease compared to controls and the mildly symptomatic brother. Potentially, active degeneration of the retina in symptomatic patients could stimulate a release of the inflammatory cytokines to the blood stream affecting the function of monocytes. We demonstrated that variability in trafficking defects and lysosomal function in peripheral cells of the CHM patients could depend on the mutation they carry and possibly be correlated with the extent of their RPE dysfunction. The trafficking defects that we observed in peripheral cells of CHM patients could also be demonstrated in *CHM* knockdown experiments on human fetal RPE cells in culture (Gordiyenko et al. 2009; Strunnikova et al. 2009). REP-1 depletion had a measurable effect, reducing the level of acidification of phagolysosomes in the RPE cells. Gene replacement is currently being planned as a potential therapy for CHM. In addition, a number of nonsense mutations in the *CHM* gene have been reported, similarly to speculations about therapy for the *CFTR* gene in CF (Becq 2010), there may be the opportunity to allow read through of nonsense mutations in the *CHM* gene (Moosajee et al. 2008) and thereby increase total REP function. Younger CHM patients may differ with older patients exhibiting more defects and higher levels of cytokines than older patients, at the end stage of their disease. The measures of trafficking in peripheral tissues and cytokine serum levels of CHM patients may provide useful correlations that reflect active changes in the retinal phenotype, development of the disease, and may provide an opportunity to test pharmacologic compounds that normalize these parameters.

References

- Becq F (2010) Cystic fibrosis transmembrane conductance regulator modulators for personalized drug treatment of cystic fibrosis: progress to date. *Drugs* 70:241–259
- Gordiyenko NV, Fariss RN, Zhi C et al (2009) Silencing of the CHM gene alters phagocytic and secretory pathways in the retinal pigment epithelium. *Invest Ophthalmol Vis Sci* 51:1143–1150
- Jacobson SG, Cideciyan AV, Sumaroka A et al (2006) Remodeling of the human retina in choroideremia: rab escort protein 1 (REP-1) mutations. *Invest Ophthalmol Vis Sci* 47:4113–4120
- MacDonald IM, Sereda C, McTaggart K et al (2004) Choroideremia gene testing. *Expert Rev Mol Diagn* 4:478–484
- Moosajee M, Gregory-Evans K, Ellis CD et al (2008) Translational bypass of nonsense mutations in zebrafish *rep1*, *pax2.1* and *lamb1* highlights a viable therapeutic option for untreatable genetic eye disease. *Hum Mol Genet* 17:3987–4000
- Rak A, Pylypenko O, Niculae A et al (2004) Structure of the Rab7:REP-1 complex: insights into the mechanism of Rab prenylation and choroideremia disease. *Cell* 117:749–760
- Reynolds R, Hartnett ME, Atkinson JP et al (2009) Plasma complement components and activation fragments: associations with age-related macular degeneration genotypes and phenotypes. *Invest Ophthalmol Vis Sci* 50:5818–5827
- Rudolph G, Preising M, Kalpadakis P et al (2003) Phenotypic variability in three carriers from a family with choroideremia and a frameshift mutation 1388delCCinsG in the REP-1 gene. *Ophthalmic Genet* 24:203–214
- Sieving PA, Niffenegger JH, Berson EL (1986) Electroretinographic findings in selected pedigrees with choroideremia. *Am J Ophthalmol* 101:361–367
- Strunnikova NV, Barb J, Sergeev YV et al (2009) Loss-of-function mutations in Rab escort protein 1 (REP-1) affect intracellular transport in fibroblasts and monocytes of choroideremia patients. *PLoS One* 4:e8402
- Tolmachova T, Anders R, Abrink M et al (2006) Independent degeneration of photoreceptors and retinal pigment epithelium in conditional knockout mouse models of choroideremia. *J Clin Invest* 116:386–394

Part VI
New Animal Models of Retinal
Degeneration

Chapter 50

Translational Vision Research Models Program

Jungyeon Won, Lan Ying Shi, Wanda Hicks, Jieping Wang,
Juergen K. Naggert, and Patsy M. Nishina

Keywords Retinal degeneration • Mouse • ENU mutagenesis • Translational vision research models • *Pde6a* • *Tulp1* • *Rhodopsin*

50.1 Introduction

A number of chemical mutagenesis screens for eye phenotypes have been carried out in zebrafish and mice (Baird et al. 2002; Thaung et al. 2002; Jablonski et al. 2005; Favor and Neuhäuser-Klaus 2000; Malick et al. 2002). The most commonly used mutagen, *N*-ethyl-*N*-nitrosourea (ENU) (Hitotsumachi et al. 1985) induces point mutations resulting in a range of consequences including total or partial loss-of-function, dominant-negative or gain-of-function alleles (Justice et al. 1997; Brown and Nolan 1998; Hrabe de Angelis and Balling 1998).

Screening for chemically induced mutants provides an important source of models to study the effects of single gene mutations found in human patients. Additionally, new mutations within the same gene provide allelic series in which splice variants or domain-specific effects can be queried. Mutations in novel genes that lead to retinal disorders can be discovered using a forward genetic approach. Finally, the mouse models can be used as a resource to test therapies.

J. Won • L.Y. Shi • W. Hicks • J. Wang • J.K. Naggert • P.M. Nishina (✉)
The Jackson Laboratory, 600 Main Street, Bar Harbor, ME 04609, USA
e-mail: patsy.nishina@jax.org

50.2 Materials and Methods

50.2.1 *Origins of Mice and Husbandry*

C57BL/6J (B6) mutagenized offspring were generated (Won et al. 2011). In some cases, mice were exposed to 12,000 lx for 1 h in a mirrored box to screen for susceptibility to light-induced damage (Budzynski et al. 2010).

Once heritability of the observed ocular phenotype was established (Won et al. 2011), mutants were bred and maintained in the JAX Research Animal Facility. Mice were provided with NIH 6% fat chow diet and acidified water, with 12:12-h dark:light cycle in pressurized individual ventilation caging. Procedures utilizing mice were approved by the Institutional Animal Care and Use Committee.

50.2.2 *Clinical Evaluation and Electrorretinography*

Mice, dark-adapted for a minimum of 1 h, were treated with atropine and examined by indirect ophthalmoscopy with a 60 or 78 diopter aspheric lens. The equipment and protocol for ERG were those previously described (Hawes et al. 2000).

50.2.3 *Genetic Mapping and Mutational Analysis*

For mapping purposes, phenotypically affected mice were mated with DBA/2J mice to generate F1 offspring that were intercrossed. Resulting F2 progeny were phenotyped by indirect ophthalmoscopy. Tail tip DNA from a minimum of ten affected and ten unaffected mice were pooled and subjected to a genome wide scan using 48–80 simple sequence length polymorphic (SSLP) markers distributed throughout the genome. Samples used in the DNA pools were tested individually to confirm the map location (Taylor et al. 1994). Additional F2 progeny were generated and tested with either SSLP or single nucleotide polymorphic markers to narrow the region around the disease loci.

Total RNA was isolated from whole eyes and brains (Life Technologies) of affected mutants and B6 control mice. RNA quantity was determined using a NanoDrop spectrophotometer (Thermo Scientific) and RNA quality was evaluated with an Agilent Technologies 2100 Bioanalyzer. cDNA was generated using a Retroscript kit (Ambion). Primers to sequence the coding region of the candidate genes were designed from exon sequences obtained from the Ensembl Database. RT-PCR DNA fragments sequenced on an Applied Biosystems 3730XL system were compared (Won et al. 2011).

50.2.4 Histological Analysis

Enucleated eyes, fixed overnight in cold methanol/acetic acid solution (3:1, v/v), were paraffin embedded and cut into 6 μm sections, stained with hematoxylin and eosin (H & E) and examined by light microscopy.

50.3 Results and Discussion

50.3.1 A New Mutation in Phosphodiesterase 6A, cGMP-Specific, Rod, Alpha (*Pde6a*)

Tvrm58 mutants, identified by indirect ophthalmoscopy, segregated in a recessive manner and presented with a mottled, grainy fundus appearance, typical of retinal degeneration models (data not shown). The mutation was mapped to chromosome 18 between markers, *D18Mit123* and *D18Mit207*. Due to the map location and phenotypic similarity to two alleles of *Pde6a*, *Pde6a^{nmf282}* and *Pde6a^{nmf363}* (Sakamoto et al. 2009), a complementation test was carried out in which homozygous *tvrm58* mice were outcrossed with homozygous *Pde6a^{nmf363}* mice. Compound heterozygous animals (*tvrm58/+*, *Pde6a^{nmf282/+}*) exhibited severe retinal degeneration (data not shown), indicating that *tvrm58* was a new allele of *Pde6a*. Using direct sequencing, we determined that nucleotide 2019 (nm_14086), normally a thymidine, was mutated to cytosine in *tvrm58* mutants. The mutation is predicted to cause a substitution of amino acid 638Leu (CTC) to Pro (CCC) (L638P; Fig. 50.1a). The 638Leu residue is located within the conserved metal dependent phosphohydrolase HD domain (NCBI conserved domain ID: smart00471) and in the PDEase-I domain (amino acid 558–801, NCBI conserved domain ID: pfam00233), and is highly conserved from humans to zebrafish. Interestingly, the two previous mutations identified in *Pde6a^{nmf282}* and *Pde6a^{nmf363}* mice V685M and D670G, respectively, occurred within the same domains.

By light microscopy, the retinas of *Pde6a^{tvrm58}* mutants appeared to develop normally and were similar to controls at 2 weeks of age. Therefore, the disease progression of *Pde6a^{tvrm58}* mutants is slower than that observed for *Pde6a^{nmf282}* and *Pde6a^{nmf363}*, which show ~70% and ~20% photoreceptor loss, respectively (Sakamoto et al. 2009), at the same age. By 3 weeks, the outer nuclear layer (ONL) was reduced to 2–3 nuclei thickness (Fig. 50.1b).

50.3.2 A New Mutation in Tubby-Like Protein 1

Tvrm124 was mapped to chromosome 17, between markers *D17Mit113* and *D17Mit62*. The (tubby-like protein 1, Tulp1) *Tulp1* gene was located within the critical region and a complementation test showed that compound heterozygous

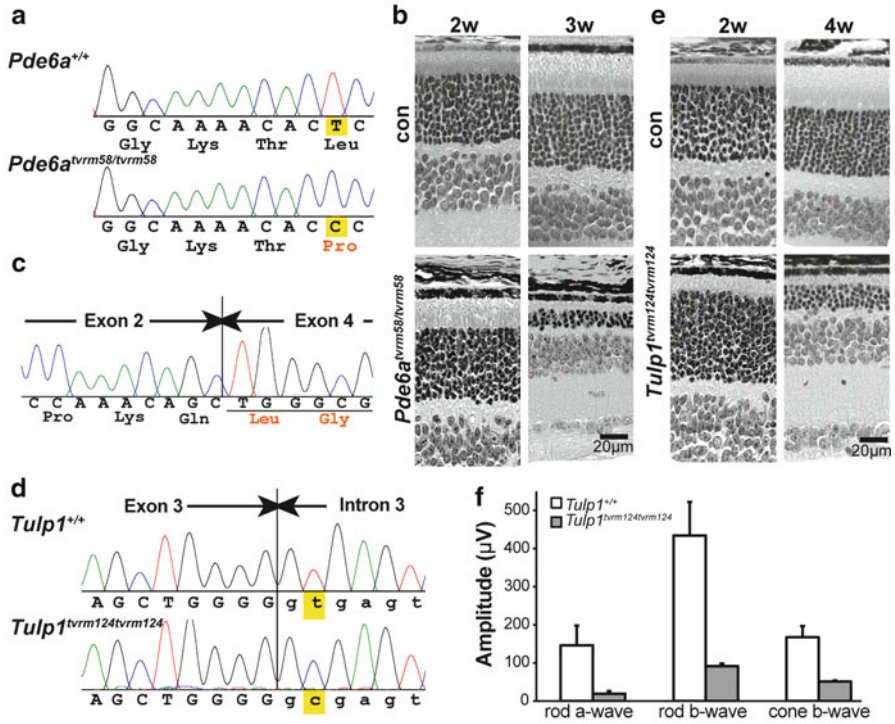


Fig. 50.1 (A-B) *Pde6a*^{tvrm58} (a) A T–C transition in *Pde6a*^{tvrm58} results in an amino acid substitution 638Leu to Pro. (b) Retinal histology of control and *Pde6a*^{tvrm58} mutants at 2 and 3 weeks of age. At 2 weeks, photoreceptor loss was not observed in *Pde6a*^{tvrm58} mutants but by 3 weeks their number was greatly reduced (~25% of control). (c–e) *Tulp1*^{tvrm124} (c) Exon 3 is skipped in *tvrm124* cDNA, causing a frame shift (red characters) that is predicted to produce a truncated protein. (d) Sequencing of control and *Tulp1*^{tvrm124} genomic DNA revealed a single base T to A substitution (highlighted), at the conserved splice donor site in intron 3 of *Tulp1*. Upper case letters indicate exon sequences, lower case letters, intronic sequences. (e) Retinal histology of control and *Tulp1*^{tvrm124} mutant at 2 and 4 weeks of age. (f) ERGs from 4-week-old control and *Tulp1*^{tvrm124} mutant animals. In *Tulp1*^{tvrm124} mice, both dark and light-adapted responses were significantly reduced

B6-*tvrm124*/+, B6.129-*Tulp1*^{tmlPjn+/-} mice were affected, confirming that *tvrm124* was a new *Tulp1* allele. Direct sequencing of *Tulp1*^{tvrm124} retinal cDNA showed that exon 3 was skipped, causing a frame shift (Fig 50.1c). If translated, the protein is predicted to terminate prematurely, 26 amino acids after the frame shift. Sequencing of genomic DNA showed that the splice donor site in intron 3 of *Tulp1*^{tvrm124} mice was altered with the second nucleotide changed from a thymidine to a cytosine (Fig. 50.1d).

Histological analysis of *Tulp1*^{tvrm124} mutants showed preservation of the ONL at 2 weeks of age. However, photoreceptor outer segments at the same age were barely detectable (Fig. 50.1e). By 4 weeks, only 4–6 layers of photoreceptor cell bodies in

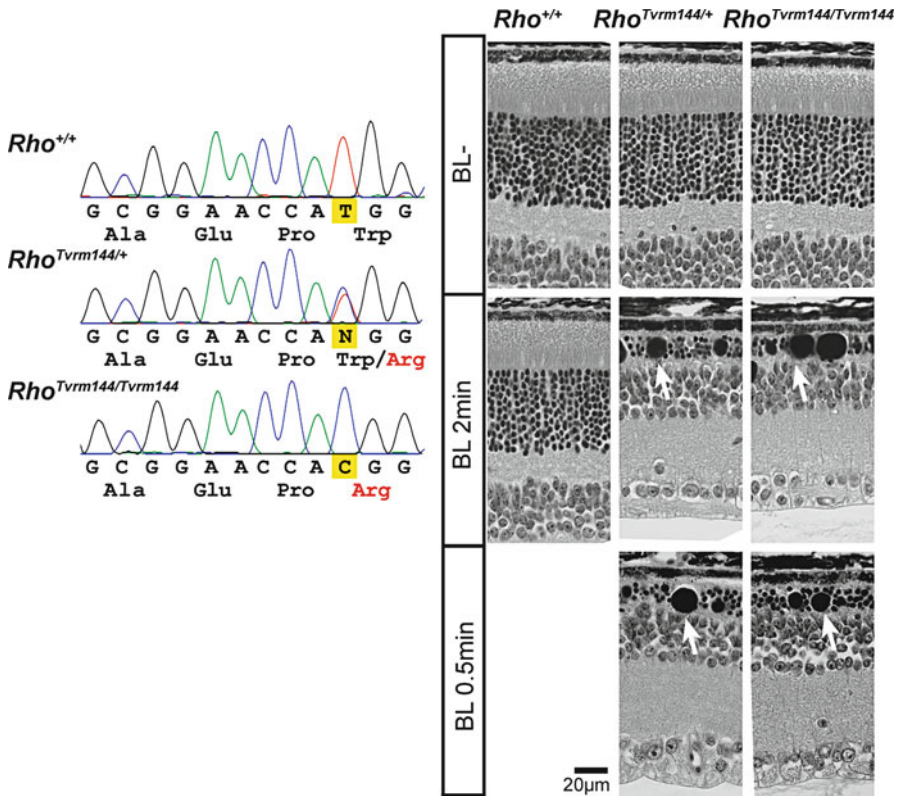


Fig. 50.2 *Rho*^{*Tvrml144*}. (a) A T–C transition in the *Rho* gene results in an amino acid change from 35Trp to Arg. (b) Retinal histology of control, heterozygous *Rho*^{*Tvrml144*/+}, and homozygous *Rho*^{*Tvrml144*/*Tvrml144*} at 1 month of age. Retinas were normal in all animals with no light stimulation (BL–). After bright light exposure (BL; 12,000 lx), control animals were not affected. However, both *Rho*^{*Tvrml144*/+} and *Rho*^{*Tvrml144*/*Tvrml144*} mutants showed severe photoreceptor loss with chromatin aggregation (arrows) after 0.5 and 2 min BL exposure

the ONL remained, resembling the *Tulp1* null allele (Ikeda et al. 2000). Similarly, cone and rod photoreceptor function, assessed by ERG, was severely impaired at 4 weeks (Fig. 50.1f) (Ikeda et al. 2000).

50.3.3 A New Mutation in Rhodopsin

The light sensitive *Tvrml144* mutants were identified by routine exposure of G3 mice to high intensity light prior to screening by indirect ophthalmoscopy. Because the fundi of heterozygous *Tvrml144* mice bleached following light exposure, we hypothesized that the effect was caused by a mutation in rhodopsin. By direct sequencing of retinal cDNA from *Rho*^{*Tvrml144*} mice, a base pair substitution was observed.

A thymidine at nucleotide 181 (nm_145383) was substituted with a cytosine, which is predicted to cause a nonsynonymous change of residue 35 from tryptophan to arginine (Fig. 50.2a). Tryptophan35, an evolutionarily conserved residue from human to zebrafish is located in the amino terminal domain of rhodopsin.

Retinas of *Rho*^{Tvrm144} mice raised in standard vivarium conditions were normal at all ages examined as were retinas of homozygous *Rho*^{Tvrm144} mice examined at one and 2 months of age (Fig. 50.2b, data not shown). However, 30 s of bright light exposure (12,000 lx) was sufficient to cause photoreceptor degeneration in both *Rho*^{Tvrm144/+} and *Rho*^{Tvrm144/Tvrm144} retinas when sampled 1 week after exposure. Photoreceptor nuclei were reduced to 2–3 layers, and photoreceptor outer and inner segments and outer plexiform layers were severely thinned compared to controls (Fig. 50.2b). Chromatin aggregation was observed centrally. No consistent difference in severity of light-induced degeneration was observed between mice of either genotype.

Previously *Rho* alleles showed spontaneous and panretinal degeneration, even when mice were reared from birth in darkness (Naash et al. 1996). Photoreceptors in homozygous rhodopsin null mutants raised in ambient light showed slow degeneration in previous knock-out and knock-in studies (Chan et al. 2004; Humphries et al. 1997). Photoreceptor nuclei were preserved in heterozygous mutants of these knock-out/knock-in models at all ages observed, but outer segments were thinned or disorganized. Outer segments were severely thinned or absent in homozygous null animals as early as P15. On the other hand, previous reports of mouse models bearing rhodopsin missense mutations show diverse phenotypes. For example, *Rho*^{R3}, C185R mutants show rapid photoreceptor degeneration (Liu et al. 2010), while photoreceptor cells were retained in other missense mutants (Wang et al. 2005). Like *Rho*^{Tvrm144} mice, heterozygous *Rho*^{Tvrm1} and *Rho*^{Tvrm4} mice raised in standard vivarium lighting did not exhibit morphological changes until exposed to bright light (Budzynski et al. 2010).

50.4 Summary

ENU mutagenesis is an efficient method to identify new animal models of ocular disease. The new alleles described herein will be a useful resource to further examine the role of the affected molecules and the effects of their disruption within the retina.

References

- Baird PN, Guymer RH, Chiu D et al (2002) Generating mouse models of retinal disease using ENU mutagenesis. *Vision Res* 42:479–485
- Brown SD, Nolan PM (1998) Mouse mutagenesis-systematic studies of mammalian gene function. *Hum Mol Genet* 7:1627–633
- Budzynski E, Gross AK, McAlear SD et al (2010) Mutations of the opsin gene (Y102H and I307N) lead to light-induced degeneration of photoreceptors and constitutive activation of phototransduction in mice. *J Biol Chem* 285:14521–14533

- Chan F, Bradley A, Wensel TG et al (2004) Knock-in human rhodopsin-GFP fusions as mouse models for human disease and targets for gene therapy. *Proc Natl Acad Sci USA* 101: 9109–9114
- Favor J, Neuhäuser-Klaus A (2000) Saturation mutagenesis for dominant eye morphological defects in the mouse *Mus musculus*. *Mamm Genom* 11:520–525
- Hawes NL, Chang B, Hageman GS et al (2000) Retinal degeneration 6 (*rd6*): a new mouse model for human retinitis punctata albescens. *Invest Ophthalmol Vis Sci* 41:3149–3157
- Hitotsumachi S, Carpenter DA, Russell WL (1985) Dose-repetition increases the mutagenic effectiveness of N-ethyl-N-nitrosourea in mouse spermatogonia. *Proc Natl Acad Sci USA* 82: 6619–6621
- Hrabe de Angelis M, Balling R (1998) Large scale ENU screens in the mouse: genetics meets genomics. *Mutat Res* 400:25–32
- Humphries MM, Rancourt D, Farrar GJ et al (1997) Retinopathy induced in mice by targeted disruption of the rhodopsin gene. *Nat Genet* 15:216–219
- Ikeda S, Shiva N, Ikeda A et al (2000) Retinal degeneration but not obesity is observed in null mutants of the tubby-like protein 1 gene. *Hum Mol Genet* 9:155–163
- Jablonski MM, Wang X, Lu L et al (2005) The Tennessee Mouse Genome Consortium: identification of ocular mutants. *Vis Neurosci* 22:595–604
- Justice MJ, Zheng B, Woychik RP et al (1997) Using targeted large deletions and high-efficiency N-ethyl-N-nitrosourea mutagenesis for functional analyses of the mammalian genome. *Methods* 13:423–436
- Liu H, Wang M, Xia CH et al (2010) Severe retinal degeneration caused by a novel rhodopsin mutation. *Invest Ophthalmol Vis Sci* 51:1059–1065
- Malicki JJ, Pujic Z, Thisse C et al (2002) Forward and reverse genetic approaches to the analysis of eye development in zebrafish. *Vision Res* 42:527–533
- Naash MI, Ripps H, Li S et al (1996) Polygenic disease and retinitis pigmentosa: albinism exacerbates photoreceptor degeneration induced by the expression of a mutant opsin in transgenic mice. *J Neurosci* 16:7853–7858
- Sakamoto K, McCluskey M, Wensel TG et al (2009) New mouse models for recessive retinitis pigmentosa caused by mutations in the *Pde6a* gene. *Hum Mol Genet* 18:178–192
- Taylor BA, Navin A, Phillips SA (1994) PCR-amplification of simple sequence repeat variants from pooled DNA samples for rapidly mapping new mutations of the mouse. *Genomics* 21:626–632
- Thaug C, Arnold K, Jackson IJ et al (2002) Presence of visual head tracking differentiates normal sighted from retinal degenerate mice. *Neurosci Lett* 325:21–24
- Wang Z, Wen XH, Ablonczy Z et al (2005) Enhanced shutoff of phototransduction in transgenic mice expressing palmitoylation-deficient rhodopsin. *J Biol Chem* 280:24293–24300
- Won J, Shi LY, Hicks W et al. (2011) Mouse model resources for vision research. *J Ophthalmol* 39:1384

Chapter 51

Zebrafish: A Model System for the Investigation of Novel Treatments for Retinal Disease

Cheryl Y. Gregory-Evans

Keywords Zebrafish • Retinal disease • Treatment • Chemical mutagenesis • Morpholino • Transgenic • Embryogenesis • Eye development • Small molecule screen

51.1 Introduction

In a relatively short space of time, the zebrafish has moved from a popular hobbyist species to an experimental model of major significance. From its simple origins in the Ganges River in India, this freshwater tropical fish has become a rising star of the genetic model organisms for biomedical research. George Streisinger at the University of Oregon pioneered its use for studying embryogenesis (Streisinger et al. 1986; Grunwald and Streisinger 1992; Kimmel et al. 1995), and it was brought to the forefront of vision research by John Dowling at Harvard University (Schmitt and Dowling 1994; Fadool et al. 1997). In this chapter, morphological and genetic attributes to the zebrafish system are discussed alongside recent work highlighting the versatility for studying retinal degeneration.

51.2 Morphological and Embryological Features

Adult zebrafish are small (~4 cm) and mate year round, with females being able to spawn on a weekly basis and are reproductively capable for about 1.5 years. They lay clutches of embryos of around 100–200 per mating which develop synchronously.

C.Y. Gregory-Evans (✉)
Department of Ophthalmology, University of British Columbia, Vancouver, BC, Canada
e-mail: cge30@eyecarecentre.org

The extra-uterine development and optical transparency during early development make the zebrafish system superior to the mouse for studying real-time effects in loss- and gain-of-function mutants. The eyes begin to develop at the 6 somite stage (Kimmel et al. 1995) with the optic lobes evaginating from the diencephalon (Schmitt and Dowling 1994). After lens induction at 14–15 somites, the retina becomes distinct from the RPE at about 18 somites. At about 32 h post-fertilization (hpf) the ganglion cells differentiate (Schmitt and Dowling 1999) and by 72 hpf the zebrafish larvae show their first visual response (Easter and Nicola 1996). The zebrafish has an elaborate tetrachromatic color vision system, mediated by long-wave, middlewave, shortwave, and UV-sensitive cones (Robinson et al. 1993).

51.3 Zebrafish Genetic Resources

Ten years ago the complete mitochondrial DNA sequence for *D. rerio* was published (Broughton et al. 2001). The 16,596 base pairs code for 13 protein coding genes, an origin of replication, 2 rRNAs and 22 tRNA genes, identical to the common mitochondrial vertebrate form. At around the same time the Sanger Institute initiated the zebrafish genome sequencing project and since then has released several genome assemblies, the latest being Zv9 in September 2010 (http://www.sanger.ac.uk/Projects/D_rerio/). This is the finished version, meaning that the error rate is about 1 in 50,000 bases and all nonrepetitive DNA has been sequenced. The gene structures can be viewed at several genome browsers (ENSEMBL (www.ensembl.org), UCSC (www.genome.ucsc.edu), and the Zebrafish Genome Resource at NCBI (<http://www.ncbi.nlm.nih.gov/genome/guide/zebrafish/>)). There is also a dedicated online database of genetic, genomic, developmental information, publications, and molecular tools for zebrafish, the Zebrafish Information Network (www.zfin.org; Sprague et al. 2006). An NIH initiative known as The Zebrafish Gene Collection (ZGC, <http://zgc.nci.nih.gov/>) supports the production of cDNA libraries, clones and sequences of expressed genes for zebrafish. All resources generated by the ZGC are publicly accessible to the biomedical research community.

51.3.1 Genetic Screens

One of the most significant features of the zebrafish model system is the ability to carry out large-scale forward genetic screens to investigate specific developmental processes without any prior knowledge of the genes involved. The chemical mutagen *N*-ethyl-*N*-nitrosourea (ENU) has been used to generate loss-of-function mutants (Haffter et al. 1996). Several large scale ENU mutagenesis screens have identified genes important to development (Driever et al. 1996; Haffter et al. 1996). Fish from these screens have been reanalyzed using behavioral screens to find visually

impaired mutants (Neuhauss et al. 1999; Brockerhoff et al. 1995; Maurer et al. 2011). Independent ENU screens have also been specifically designed to identify visual mutants (Brockerhoff et al. 1998; Muto et al. 2005). This has resulted in a large number of recessive mutants, many with retinal defects that are models for human retinal degenerations (Malicki et al. 1996).

While chemically based screens have been instrumental in generating mutant phenotypes, positional cloning of these mutations is laborious. Retrovirus-mediated insertional mutagenesis provides an attractive alternative since the affected gene can be easily identified. The mutants generated from this type of screen (Amsterdam et al. 2004) have been reanalyzed for visual defects (Gross et al. 2005). While highly informative, forward genetic screens do not identify mutations in genes with redundant function or dominant-negative effect. The gain-of-function approach increases the efficiency of phenotype-based screens since the analysis can be performed in the F1 generation, in contrast to the F3 generation used for loss-of-function screens. Such an approach has identified new genes expressed in the retina (Maddison et al. 2009).

51.3.2 *Mutant Strain Repositories*

The mutant zebrafish lines obtained through mutagenesis screens are available through a number of zebrafish repositories or from the original investigators. The Zebrafish International Resource Center (ZIRC, www.zebrafish.org/zirc) is housed on the University of Oregon. It maintains and provides wildtype and mutant strains either as embryos or as frozen sperm and distributes these to the research community. The Zebrafish Genome Project funded by the Wellcome Trust Sanger Institute, UK facilitates the positional cloning of genes uncovered from genetic screens in the zebrafish (http://www.sanger.ac.uk/Projects/D_erio/mutres/faqs.shtml). If your gene of interest does not have a corresponding mutant you can request that a mutant be developed.

51.4 **Functional Assessment in Zebrafish**

Direct assignment of gene function in zebrafish is facilitated by the use of targeted “knockdown” technology (Nasevicius and Ekker 2000) using selective antisense morpholino oligonucleotides (MOs) available from GeneTools (<http://www.genetools.com/>). The results of this approach can be seen in real-time during the first few days of development (Fig. 51.1a). However, gene knockdown in zebrafish is complicated by the fact that a large number of genes are duplicated, which may compensate for the loss of function of the targeted homolog. Some duplicate genes have been lost, whereas other duplicated genes are retained with subfunctionalization of

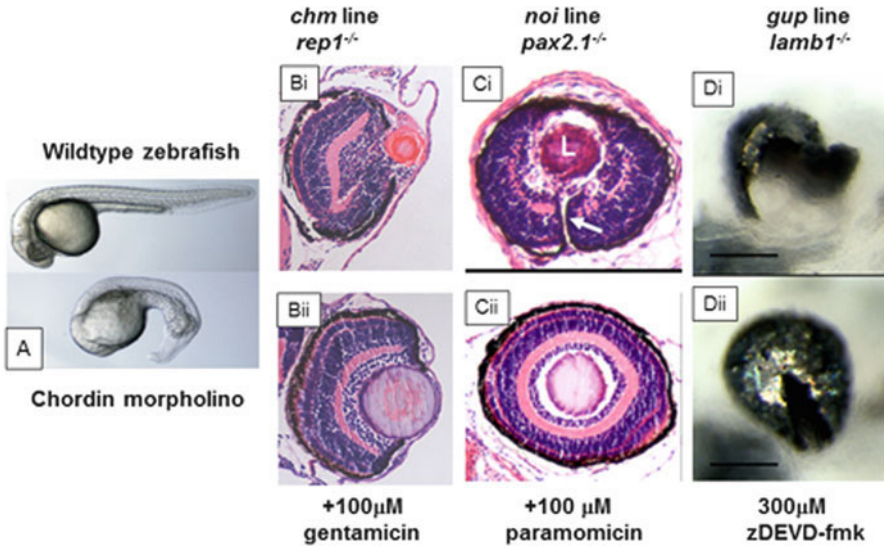


Fig. 51.1 Chemical treatments to zebrafish mutants. (a) Chordin morpholino knockdown in wild-type fish. (b) Zebrafish eye histology in 6-day-old *chm* mutant before (Bi) and after treatment (Bii) with gentamicin, restoring appearance of retinal lamination. (c) Zebrafish eye histology in 6-day-old *noi* mutant before (Ci) and after treatment (Cii) with paramomycin, causing closure of the optic fissure (arrow). (d) Zebrafish eye anatomy in 6-day-old *gup* mutant before (Di) and after treatment (Dii) with caspase inhibitor zDEVD-fmk, reducing the size of the coloboma

the two copies or a new function assigned to one of the copies (Wagner 1998). Knockdown experiments should be carefully controlled by testing at least one mismatch and one scrambled control oligomer. Whenever possible, the levels of both the target protein and one or more control proteins should be evaluated in samples treated with experimental and control morpholinos. ZFIN maintains and curates a morpholino database that has entries for 277 zebrafish genes which have been successfully targeted.

The ability to regulate gene expression both temporally and spatially has been a recent advance in the zebrafish tool box (Davison et al. 2007; Asakawa et al. 2008). The binary Gal4/UAS system relies on the ability of the transcription factor Gal4 to drive gene expression of other genes under the regulation of Gal4-responsive upstream activator sequences (UAS). For example, in a GAL4 activator fish line (Tg-*hsp70:GAL4*), the activator protein GAL4 is present but has no target gene to activate. In a UAS fish line, UAS is fused to the target gene which is silent in the absence of the GAL4 activator. When the GAL4 and UAS lines are crossed, the target genes can be turned on in the double-transgenic progeny when embryos are exposed to heat shock, at a time when the gene expression is required.

51.5 Drug Discovery

Validating new drug targets remains a bottleneck in drug discovery, as most small molecule discovery efforts rely on high-throughput screening using simplified *in vitro* reactions or cell-based assays. Chemical suppression screens in zebrafish were pioneered in 2004 by Randall Peterson's group at Harvard, who were working on the *gridlock* mutant, which displayed abnormal bifurcation of the lateral dorsal aorta with blockage of the circulation to the trunk. From a 5,000 small-molecule screen, two overcame the blood circulation problem (Peterson et al. 2004). More recently, a zebrafish line expressing GFP under the control of the endothelial-specific *flil* gene was screened with 2,000 small molecules to identify compounds that could modulate the retinal vascular network. Four chemicals were found that either altered blood vessel morphology or resulted in loss of retinal vessels (Kitambi et al. 2009).

We have used this approach (Moosajee et al. 2008) to test the ability of aminoglycosides and cell death inhibitors to delay retinal degeneration in the *chm* (*rep1^{-/-}*) model of choroideremia and in two ocular coloboma mutants, *noi* (*pax2^{-/-}*) and *gup* (*lamb1^{-/-}*). The zebrafish were assayed simultaneously in a 96-well plate format so that drugs could be added to the aquatic environment allowing absorption into the fish. We found that either aminoglycosides (Fig. 51.1b, c) or caspase inhibitors (Fig. 51.1d) were able to ameliorate the phenotypic defects in these mutant zebrafish, validating this zebrafish system for identifying modifiers of eye defects.

Although chemical suppression screens have discovered new compounds to ameliorate disease, there are a few caveats to note: (1) it can be difficult to predict the influence of pharmacokinetic and bioavailability in whole-organism screens; (2) it can be difficult to assess the specificity of a drug's effect without some knowledge of its specific target; (3) genetic mutations in fish need to faithfully recapitulate the human disease in question; and (4) there are limitations in zebrafish physiology (e.g., the zebrafish heart has two chambers whereas the human heart has four). These latter two caveats are less problematic for retinal degeneration mutants due to the similar physiology. Thus, the effect of chemical compounds can be directly assayed *in vivo* by using retinal behavioral screen readouts.

51.6 Conclusion

The combination of genetic, developmental, and physiological attributes places the zebrafish as a forefront model for identifying novel treatments for retinal degeneration. Small-molecule screening is a powerful approach to drug discovery, and the use of zebrafish allows for inexpensive high-throughput testing of chemicals in the context of the whole organism. Our experience suggests that chemical screens will be an important addition to the existing genetic, cell biological, and biochemical technologies. Emerging investigation into complex behavioral and physiologic phenotypes will lead to an unprecedented insight into whole organism phenotypic screening in the near future.

References

- Amsterdam A, Nissen RM, Sun Z et al (2004) Identification of 315 genes essential for early zebrafish development. *Proc Natl Acad Sci USA* 101:12792–12797
- Asakawa K, Suster ML, Mizusawa K et al (2008) Genetic dissection of neural circuits by Tol2 transposon-mediated Gal4 gene and enhancer trapping in zebrafish. *Proc Natl Acad Sci USA* 105:1255–1260
- Brockerhoff SE, Hurley JB, Janssen-Bienhold U et al (1995) A behavioral screen for isolating zebrafish mutants with visual system defects. *Proc Natl Acad Sci USA* 92:10545–10549
- Brockerhoff SE, Dowling JE, Hurley JB (1998) Zebrafish retinal mutants. *Vision Res* 38:1335–1339
- Broughton RE, Milam JE, Roe BA (2001) The complete sequence of the zebrafish (*Danio rerio*) mitochondrial genome and evolutionary patterns in vertebrate mitochondrial DNA. *Genome Res* 11:1958–1967
- Davison JM, Akitake CM, Goll MG et al (2007) Transactivation from Gal4-VP16 transgenic insertions for tissue-specific cell labeling and ablation in zebrafish. *Dev Biol* 304:811–824
- Driever W, Solnica-Krezel L, Schier AF et al (1996) A genetic screen for mutations affecting embryogenesis in zebrafish. *Development* 123:37–46
- Easter SS, Nicola GN (1996) The development of vision in the zebrafish (*Danio rerio*). *Dev Biol* 180:646–663
- Fadool JM, Brockerhoff SE, Hyatt GA et al (1997) Mutations affecting eye morphology in the developing zebrafish (*Danio rerio*). *Dev Genet* 20:288–295
- Gross JM, Perkins BD, Amsterdam A et al (2005) Identification of zebrafish insertional mutants with defects in visual system development and function. *Genetics* 170:245–261
- Grunwald DJ, Streisinger G (1992) Induction of recessive lethal and specific locus mutations in the zebrafish with ethyl nitrosourea. *Genet Res* 59:103–116
- Haffter P, Granato M, Brand M et al (1996) The identification of genes with unique and essential functions in the development of the zebrafish, *Danio rerio*. *Development* 123:1–36
- Kimmel CB, Ballard WW, Kimmel SR et al (1995) Stages of embryonic development of the zebrafish. *Dev Dyn* 203:253–310
- Kitambi SS, McCulloch KJ, Peterson RT et al (2009) Small molecule screen for compounds that affect vascular development in the zebrafish retina. *Mech Dev* 126:464–477
- Maddison LA, Lu J, Victoroff T et al (2009) A gain-of-function screen in zebrafish identifies a guanylate cyclase with a role in neuronal degeneration. *Mol Genet Genomics* 281:551–563
- Malicki J, Neuhauss SC, Schier AF et al (1996) Mutations affecting development of the zebrafish retina. *Development* 123:263–273
- Maurer CM, Schönthaler HB, Mueller KP et al (2010) Distinct Retinal Deficits in a Zebrafish Pyruvate Dehydrogenase-Deficient Mutant. *J Neurosci* 30:11962–11972
- Moosajee M, Gregory-Evans K, Ellis CD et al (2008) Translational bypass of nonsense mutations in zebrafish *rep1*, *pax2.1* and *lamb1* highlights a viable therapeutic option for untreatable genetic eye disease. *Hum Mol Genet* 17:3987–4000
- Muto A, Orger MB, Wehman AM et al (2005) Forward genetic analysis of visual behavior in zebrafish. *PLoS Genet* 1:e66
- Nasevicius A, Ekker SC (2000) Effective targeted gene ‘knockdown’ in zebrafish. *Nat Genet* 26:216–220
- Neuhauss SC, Biehmaier O, Seeliger MW et al (1999) Genetic disorders of vision revealed by a behavioral screen of 400 essential loci in zebrafish. *J Neurosci* 19:8603–8615
- Peterson RT, Shaw SY, Peterson TA, et al (2004) Chemical suppression of a genetic mutation in a zebrafish model of aortic coarctation. *Nat Biotechnol* 22:595–599
- Robinson J, Schmitt EA, Hárosi FI et al (1993) Zebrafish ultraviolet visual pigment: absorption spectrum, sequence, and localization. *Proc Natl Acad Sci USA* 90:6009–6012
- Schmitt EA, Dowling JE (1994) Early eye morphogenesis in the zebrafish, *Brachydanio rerio*. *J Comp Neurol* 344:532–542

- Schmitt EA, Dowling JE (1999) Early retinal development in the zebrafish, *Danio rerio*: light and electron microscopic analyses. *J Comp Neurol* 404:515–536
- Sprague J, Bayraktaroglu L, Clements D et al (2006) The Zebrafish Information Network: the zebrafish model organism database. *Nucl Acids Res* 34: Database issue D581–D585
- Streisinger G, Singer F, Walker C et al (1986) Segregation analyses and gene-centromere distances in zebrafish. *Genetics* 112:311–319
- Wagner A (1998) The fate of duplicated genes: loss or new function? *Bioessays* 20:785–788

Chapter 52

Retinal Degeneration in the Fly

Nansi Jo Colley*

Keywords *Drosophila melanogaster* • Compound eye • Rhodopsin • Invertebrate phototransduction • Retinitis pigmentosa • Age-related macular degeneration • Photoreceptor • Protein trafficking • Secretory pathway

52.1 Introduction

The first mutations in *Drosophila* known to cause retinal degeneration were identified in the 1960s by the pioneering studies of Bill Pak and co-workers (Pak 1995). At that time, the clinical significance of the findings was not fully appreciated. The revolutionary finding that put flies into the spotlight was the one showing that genes controlling development in flies could also do so in humans. In the 1980s, homeodomain-containing transcription factors were found to be essential during development in *Drosophila*. Almost identical homeodomain-containing genes were found in the genomes of a wide range of organisms, including humans and mice (Lawrence 1992). This knowledge led to the conclusion that organisms as different as flies and humans contain nearly identical genes with similar functions.

At the turn of the twentieth century in the hands of Thomas Hunt Morgan, the founding father of *Drosophila* research, *Drosophila* emerged as a powerful genetic workhorse (Rubin and Lewis 2000). In 1910, Morgan identified the first mutation in *Drosophila*, which was a spontaneous mutation that caused a normally red-eyed fly to be white eyed (Fig. 52.1a). This first allele transformed our understanding of

*Reprinted from Colley (2010), with permission from Elsevier. Copyright Elsevier 2010.

N.J. Colley (✉)

Department of Ophthalmology and Visual Sciences and Department of Genetics, and
UW-Eye Research Institute, University of Wisconsin, Madison, WI, 53792, USA
e-mail: njcolley@wisc.edu

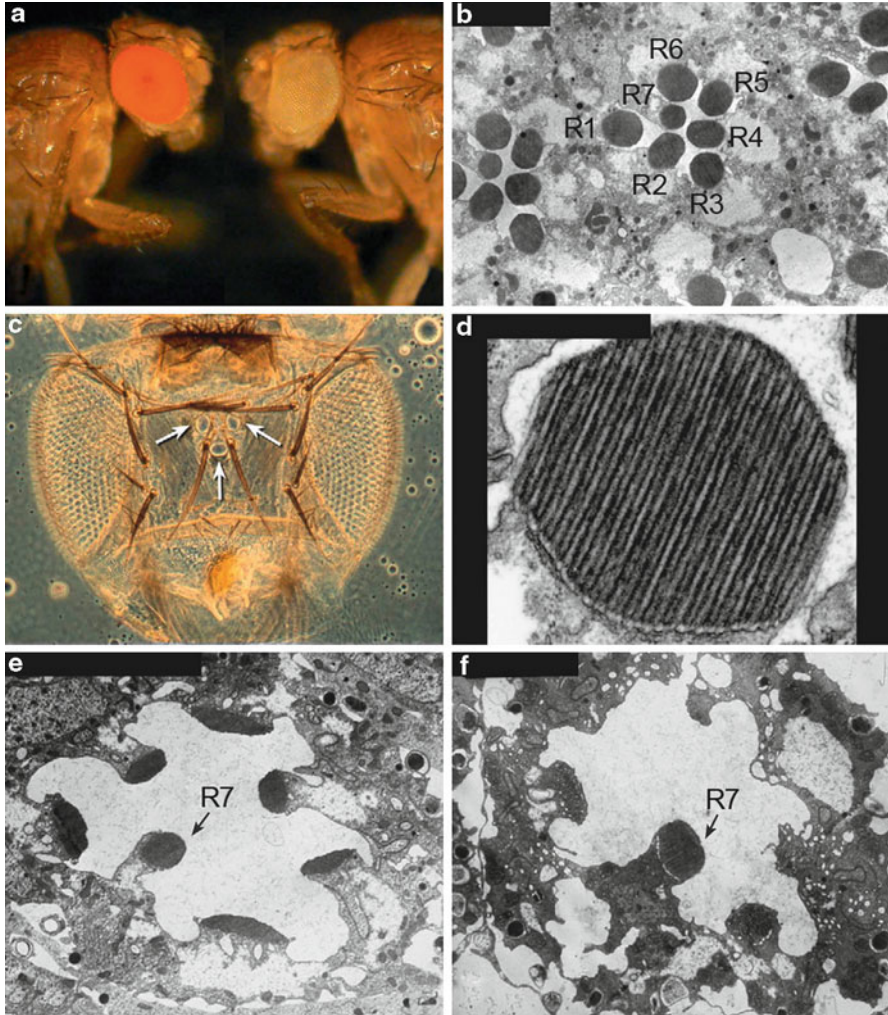


Fig. 52.1 (a) Wild-type red-eyed fly, Canton S compared to a white-eyed mutant fly, w^{1118} . (b) Cross section through the compound eye showing the R1-7 photoreceptor cells and their photosensitive rhabdomeres (R). The R8 photoreceptor cell is located below the plane of the section. (c) The adult *Drosophila* visual system showing the two compound eyes and the three simple eyes (ocelli) located on the top of the head (arrows). (d) A higher magnification of a rhabdomere showing the microvilli. The rhabdomeres are made up of about 60,000 microvilli and are 50 nm in diameter and 1–2 μ m in length. (e) A newly eclosed $ninaE^{117}$ mutant fly, showing the reduced size of the rhabdomeres. $ninaE^{117}$ is a null allele, so the flies completely lack Rh1 rhodopsin expressed in the R1-6 photoreceptor cells. (f) Six-day-old $ninaE^{117}$ fly, showing that the rhabdomeres of the R1-6 photoreceptor cells are almost completely gone, but the R7 cell rhabdomere remains

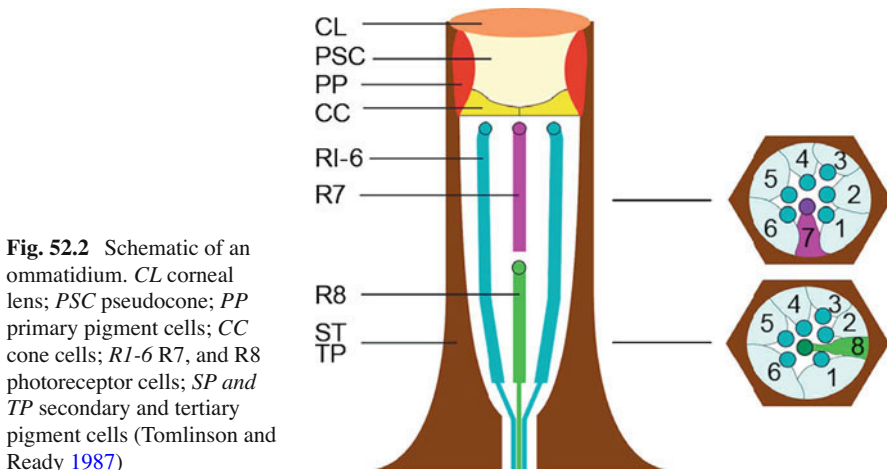
genetics and heredity. The white gene encodes a membrane-associated, adenosine triphosphate (ATP)-binding cassette, (ABC)-type multidrug transporter required for the transport of pigment precursors involved in eye pigment biosynthesis. In humans, mutations in the *ABCA4* gene (also *ABCR*) account for approximately 3% of

autosomal recessive retinitis pigmentosa (RP) and are linked to both recessive cone-rod dystrophy and recessive Stargardt macular dystrophy. The *ABCA4* transporter serves as a flippase in the retinoid cycle. When the *ABCA4* gene is mutated, toxic detergent-like by-products accumulate in the retinal pigment epithelium (RPE) leading to severe pathology (Bok 2007). Therefore, the white gene, discovered at the turn of the century, was subsequently found to encode an ABC-type transporter required for eye pigment biosynthesis in *Drosophila*, and is related to another ABC-type transporter in the human eye that is involved in the retinoid cycle and several types of retinal diseases.

52.2 The Compound Eye and Phototransduction

The *Drosophila* compound eye is composed of approximately 800 individual eye units called ommatidia (Figs. 52.1c and 52.2). The major rhodopsin in the eye, Rh1, is encoded by the *ninaE* gene, and displays 22% amino acid identity with human rhodopsin and 37% identity with human melanopsin. Each *Drosophila* photoreceptor cell contains a photoreceptive rhabdomere, which is comprised of approximately 60,000 tightly packed microvilli, containing the rhodopsin photopigments and other components of the phototransduction cascade (Fig. 52.1b, d). The rhabdomeres are functionally equivalent to the vertebrate photoreceptor outer segments (Fig. 52.3).

Phototransduction in *Drosophila* utilizes a signaling cascade in which light stimulation of Rh1 leads to the activation of the G protein (Gq) and the stimulation of phospholipase C beta (PLC-beta), leading to the opening of the cation-selective transient receptor potential (TRP) and TRP-like (TRPL) channels. The photoreceptors depolarize as intracellular calcium dramatically rises. The *Drosophila* phototransduction cascade shares some similarities with the phototransduction cascade in



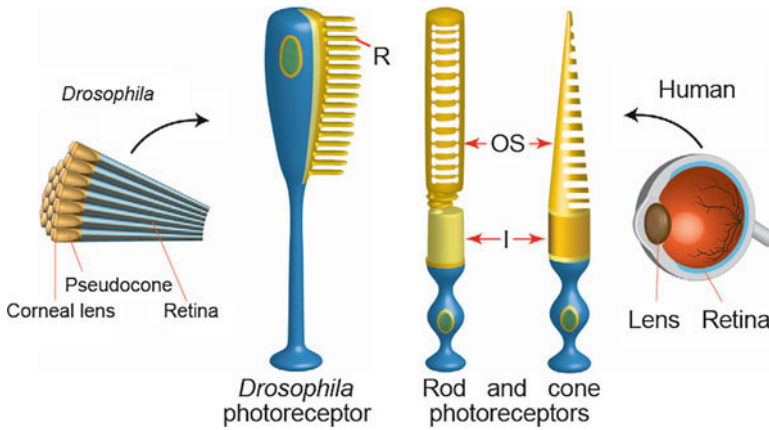


Fig. 52.3 The *Drosophila* photoreceptor cell compared with human rod and cone photoreceptor cells. In *Drosophila*, the pseudocone cone (also called the crystalline cone) and the corneal lens are the lens elements, and they are secreted by the underlying cone cells. The *Drosophila* lens is comprised of droscrySTALLIN, which is similar to insect cuticular proteins. *R* rhabdomere; *OS* outer segments; *I* inner segments; *N* nucleus (Chang and Ready 2000)

mammalian rod and cone photoreceptor cells. Both cascades are initiated by light-activation of rhodopsin that in turn leads to the stimulation of G proteins. Phototransduction in *Drosophila* as well as in humans is terminated when arrestin binds to light-stimulated rhodopsin and prevents the binding of rhodopsin to the G-protein. However, notable differences are that rod and cone channels are gated by cyclic nucleotides and they close in response to light, leading to a hyperpolarizing response (Minke and Parnas 2006; Hardie and Postma 2008).

Although certain features of phototransduction in *Drosophila* differ from rod and cone phototransduction, *Drosophila* phototransduction shares many common features with signaling in intrinsically photosensitive retinal ganglion cells (ipRGCs) (Panda et al. 2005). These cells function in circadian rhythm entrainment and pupil constriction. The light response in ipRGCs is initiated with absorption of light by melanopsin, which is more similar to *Drosophila* Rh1 than to the photopigments in rods and cones (Provencio et al. 1998). Light-stimulated melanopsin is thought to activate a phosphoinositide-cascade leading to the opening of DAG-sensitive TRPC6/7 channels (Panda et al. 2005; Sekaran et al., 2007; Graham et al. 2008). Therefore, *Drosophila* photoreceptor cells and ipRGCs share similar phototransduction cascades. Further, TRPM1 channels have been identified in ON-bipolar cells (Koike et al. 2010) and mutations in TRPM1 are implicated in autosomal-recessive congenital stationary night blindness (Audo et al. 2009). With the discovery of TRPC6/7 in ipRGCs and TRPM1 channels in ON-bipolar cells, findings in the fly may be relevant for understanding the mechanisms in the ipRGC and the ON-bipolar cells in the vertebrate retina.

52.3 Genetic Screens Identify Retinal Degeneration Loci

Several forward genetic screens in *Drosophila* led to an explosion in the identification of many genes involved in retinal degeneration and understanding their counterparts in human disease. The electroretinogram (ERG) genetic screening approach was pioneered by Bill Pak and co-workers in the 1960s and led to the isolation of over 200 ERG-defective mutants (Pak 1995). In the 1980s, the development of gene-cloning techniques for *Drosophila* made it possible to isolate the corresponding genes. For example, the major rhodopsin in *Drosophila*, Rh1, was cloned and determined to be encoded by the *neither inactivation nor after potential E* (*ninaE*) locus. The *ninaE* mutants isolated in the original ERG screen were found to harbor mutations in the structural gene for the major rhodopsin in *Drosophila*, Rh1. In addition, the first evidence that mutations in a rhodopsin gene led to retinal degeneration came from these elegant studies in the 1980s in *Drosophila* (Stephenson et al. 1983; O'Tousa et al. 1985, 1989; Zuker et al. 1985). The use of the ERG in *Drosophila* continues to be an effective strategy to identify mutants in phototransduction and also in loci in retinal degeneration.

The DPP is a sensitive phenotype in the eye that can be easily assessed in live flies. It is based on the precise packing of the photoreceptor cells. Any mutation leading to, even subtle, structural alterations in photoreceptor cells will cause attenuation in the DPP. For example, a reduction in rhodopsin levels in the R1-6 photoreceptor cells in *ninaE* mutants, leads to structural alterations in the photoreceptor cells (Fig. 52.1e, f) and attenuation in the DPP. A variety of mutants were isolated by this method, including dominant alleles of *ninaE* (rhodopsin), and alleles of two chaperones, *ninaA* (cyclophilin) and *calnexin* (Ondek et al. 1992; Colley et al. 1995; Rosenbaum et al. 2006). Both the ERG and the DPP screens accelerated the pace of identifying mutations that cause retinal degeneration in *Drosophila*.

52.4 Retinal Degenerations in Flies and Humans

Since the initial findings, that mutations in *Drosophila* rhodopsin lead to retinal degeneration, over 100 mutations in human rhodopsin have been found to cause autosomal dominant RP (adRP). The first mutation identified in adRP patients, published by Dryja et al. (1990), was a mutation that caused a proline residue located near the N-terminus of rhodopsin to be replaced by a histidine residue (Pro23His). A great majority of these mutants, including Pro23His, produce misfolded rhodopsin that is improperly transported through the secretory pathway (Roof et al. 1994). However, the mechanism by which the mutant rhodopsins cause dominant retinal degeneration was determined in *Drosophila*. It was found that rhodopsin mutations act dominantly to cause retinal degeneration by the mutant protein interfering with the maturation of normal rhodopsin (Colley et al. 1995; Kurada and O'Tousa 1995).

These studies in *Drosophila* provided a mechanistic explanation for the cause of certain forms of adRP

It is now widely appreciated that retinal defects and retinal degeneration can be triggered by mutations in almost every component of the photoreceptor cells. One class of retinal degenerations involves defects in rhodopsin maturation. In *Drosophila*, as in humans, rhodopsin is synthesized and glycosylated in the ER, binds its vitamin-A-derived chromophore at a lysine residue in the seventh transmembrane domain, is transported through the various compartments of the Golgi, and is delivered to its final destination for phototransduction. The mechanisms that regulate rhodopsin maturation, such as its folding, glycosylation, chaperone interaction, chromophore attachment, and transport are key to photoreceptor survival in flies and humans.

In flies, the transport of Rh1 from the ER to the rhabdomere requires the cyclophilin, *NinaA*. Cyclophilins are known to display peptidyl-prolyl *cis-trans* isomerase and are thought to play a role in protein folding during biosynthesis. Consistent with a role in protein folding, *NinaA* resides in the ER. In addition, *NinaA* is detected in secretory transport vesicles together with Rh1, and forms a specific and stable complex with Rh1, consistent with a role as a chaperone in the secretory pathway (Colley et al. 1991; Baker et al. 1994). Similarly, in mammals a cyclophilin-like protein (RanBP2/Nup358) was found to act as a chaperone for red/cone opsin biogenesis (Ferreira et al. 1996). Another chaperone required for Rh1 biosynthesis in *Drosophila* is calnexin (Rosenbaum et al. 2006). Mutations in *ninaA*, *ninaE*, and *calnexin* all lead to severe retinal pathology in flies. In mammalian photoreceptors, calnexin is also expressed in the ER. Although calnexin is not required for the expression of rod rhodopsin, cone M-opsin, or melanopsin in the mouse, we have shown that it is required for proper retinal morphology (Kraus et al. 2010). Mechanisms that regulate rhodopsin maturation, such as its folding, chaperone interaction, and transport are essential for photoreceptor health in flies and humans (Colley 2010).

52.5 Summary

Many genes are functionally equivalent between flies and humans. In addition, the same, or similar, mutations cause disease in both species. In fact, nearly three-fourths of all human disease genes have related sequences in *Drosophila*. The fly has a relatively small genome, made up of about 13,600 genes in four pairs of chromosomes. However, despite the dramatic differences in size and apparent complexity between humans and flies – we have less than twice as many genes as a fly – our genome is estimated to be made up of only 20,000–25,000 genes contained in 23 pairs of chromosomes. Therefore, despite the fly's perceived simplicity, or our perceived complexity, our genetic makeup may not be all that different. Its versatility for genetic manipulation and convenience for unraveling fundamental biological processes continue to guarantee the fly a place in the spotlight for unraveling the basis of and therapeutic treatments for human eye diseases.

Acknowledgments Our research, on retinal degeneration in *Drosophila*, is supported by funding from the National Eye Institute (R01 EY08768), the Retina Research Foundation, and the Retina Research Foundation/Walter H. Helmerich Research Chair. I gratefully acknowledge C. Vang, E. Rosenbaum, and B. Larson for assistance with preparing the manuscript and figures.

References

- Audo I, Kohl S, Leroy BP et al (2009) TRPM1 is mutated in patients with autosomal-recessive complete congenital stationary night blindness. *Am J Hum Genet* 85:720–729
- Baker EK, Colley NJ, Zuker CS (1994) The cyclophilin homolog NinaA functions as a chaperone, forming a stable complex in vivo with its protein target rhodopsin. *EMBO Journal* 13:4886–4895
- Bok D (2007) Contributions of genetics to our understanding of inherited monogenic retinal diseases and age-related macular degeneration. *Arch Ophthalmol* 125:160–164
- Chang HY, Ready DF (2000) Rescue of photoreceptor degeneration in rhodopsin-null *Drosophila* mutants by activated Rac1. *Science* 290:1978–1980
- Colley NJ (2010) Retinal Degeneration through the Eye of the Fly. *Encyclopedia of the Eye* 4:54–61
- Colley NJ, Baker EK, Stammes MA et al (1991) The cyclophilin homolog ninaA is required in the secretory pathway. *Cell* 67:255–263
- Colley NJ, Cassill JA, Baker EK et al (1995) Defective intracellular transport is the molecular basis of rhodopsin-dependent dominant retinal degeneration. *Proc Natl Acad Sci USA* 92:3070–3074
- Dryja TP, McGee TL, Reichel E et al (1990) A point mutation of the rhodopsin gene in one form of retinitis pigmentosa. *Nature* 343:364–366
- Ferreira PA, Nakayama TA, Pak WL et al (1996) Cyclophilin-related protein RanBP2 acts as chaperone for red/green opsin. *Nature* 383:637–640
- Graham DM, Wong KY, Shapiro P et al (2008) Melanopsin ganglion cells use a membrane-associated rhabdomic phototransduction cascade. *J Neurophysiol* 99:2522–2532
- Hardie RC, Postma M (2008) Phototransduction in Microvillar Photoreceptors of *Drosophila* and Other Invertebrates. San Diego, CA: Academic Press
- Koike C, Numata T, Ueda H et al (2010) TRPM1: A vertebrate TRP channel responsible for retinal ON bipolar function. *Cell Calcium* 48:95–101
- Kraus A, Groenendyk J, Bedard K et al (2010) Calnexin deficiency leads to dysmyelination. *J Biol Chem* 285:18928–18938
- Kurada P, O'Tousa JE (1995) Retinal degeneration caused by dominant rhodopsin mutations in *Drosophila*. *Neuron* 14:571–579
- Lawrence PA (1992) *The Making of a Fly The Genetics of Animal Design*. Cambridge: Blackwell Scientific Publications
- Minke B, Parnas M (2006) Insights on TRP channels from in vivo studies in *Drosophila*. *Annu Rev Physiol* 68:649–684
- O'Tousa JE, Leonard DS, Pak WL (1989) Morphological defects in ora photoreceptors caused by mutation in R1-6 opsin gene of *Drosophila*. *J Neurogenetics* 6:41–52
- O'Tousa JE, Baehr W, Martin RL et al (1985) The *Drosophila* ninaE gene encodes an opsin. *Cell* 40:839–850
- Ondek B, Hardy RW, Baker EK et al (1992) Genetic dissection of cyclophilin function: saturation mutagenesis of the *Drosophila* cyclophilin homolog ninaA. *Journal of Biological Chemistry* 267:16460–16466
- Pak WL (1995) *Drosophila* in vision research. The Friedenwald Lecture. *Invest Ophthalmol Vis Sci* 36:2340–2357
- Panda S, Nayak SK, Campo B et al (2005) Illumination of the Melanopsin Signaling Pathway. *Science* 307:600–604
- Provencio I, Jiang G, De Grip WJ et al (1998) Melanopsin: An opsin in melanophores, brain, and eye. *Proc Natl Acad Sci USA* 95:340–345

- Roof DJ, Adamian M, Hayes A (1994) Rhodopsin accumulation at abnormal sites in retinas of mice with a human P23H rhodopsin transgene. *Investigative Ophthalmology & Visual Science* 35:4049–4062
- Rosenbaum EE, Hardie RC, Colley NJ (2006) Calnexin is essential for rhodopsin maturation, Ca²⁺ regulation, and photoreceptor cell survival. *Neuron* 49:229–241
- Rubin GM, Lewis EB (2000) A Brief History of *Drosophila's* Contributions to Genome Research. *Science* 287:2216–2218
- Sekaran, S., Lall, G.S., Ralphs, K.L., Wolstenholme, A.J., Lucas, R.J., Foster, R.G., and Hankins, M.W. (2007). 2-Aminoethoxydiphenylborane is an acute inhibitor of directly photosensitive retinal ganglion cell activity in vitro and in vivo. *J Neurosci* 27, 3981–3986
- Stephenson RS, O'Tousa J, Scavarda NJ et al (1983) *Drosophila* mutants with reduced rhodopsin content. *Symposia of the Society for Experimental Biology* 36:477–501
- Tomlinson A, Ready DF (1987) Cell fate in the *Drosophila* ommatidium. *Developmental Biology* 123:264–275
- Zuker CS, Cowman AF, Rubin GM (1985) Isolation and structure of a rhodopsin gene from *D. melanogaster*. *Cell* 40:851–858

Chapter 53

Looking into Eyes: Rhodopsin Pathologies in *Drosophila*

Ana Griciuc, Liviu Aron, and Marius Ueffing

Keywords Retinitis pigmentosa • Retinal degeneration • Rhodopsin • *Drosophila* • Photoreceptor • Retina • Phototransduction • Autophagy • ER stress

53.1 Introduction

The capacity to see the world around us is a unique experience and one of the best understood processes in biology. The small insect *Drosophila melanogaster* has played a central role in our understanding of vision. *Drosophila* was the first organism in which the process of phototransduction (PT) was subjected to genetic analysis. This revealed that many anatomical and physiological aspects of vision are conserved from insects to mammals (Wang and Montell 2007; Sanes and Zipursky 2010). In addition, the detailed analysis of RD caused by altered PT has uncovered many pathological mechanisms of retinal disease, most of which were subsequently found to operate in mammals.

RP represents a heterogeneous group of retinal dystrophies in which death of photoreceptor neurons (PNs) leads to progressive blindness. RP is caused by mutations in at least 181 genes, and is arguably the most complex genetic disorder in man (Daiger 2004; Daiger et al. 2007). Most cases of RP are autosomal dominant

A. Griciuc • M. Ueffing (✉)

Department of Protein Science, Helmholtz Zentrum Muenchen-German Research Center for Environmental Health, 85764, Neuherberg, Germany

Institute for Ophthalmic Research, Center for Ophthalmology,

University of Tuebingen, 72076, Tuebingen, Germany

e-mail: marius.ueffing@uni-tuebingen.de

L. Aron (✉)

Department of Pathology, Harvard Medical School, Boston, MA 02115, USA

e-mail: liviu@hms.harvard.edu

(i.e., ADRP), while a minority of cases exhibit a recessive pattern of inheritance (Daiger et al. 2007). Alterations in rhodopsin (Rho) structure and/or dynamics have emerged as central pathogenic events in RP. Thus, *Rho* mutations account for at least 25% of all RP cases; and defects in PT that involve alterations in Rho dynamics are associated with other RP mutations (Hamel 2006; Daiger et al. 2007). Here, we highlight pathogenic mechanisms linking altered Rho states to RP, with a focus on *Drosophila* studies. Excellent reviews cover the study of RP mechanisms and emerging therapies, and the utility of other systems in understanding RP (Kennan et al. 2005; Mendes et al. 2005; Hartong et al. 2006; Sancho-Pelluz et al. 2008; Rivas and Vecino 2009; Shintani et al. 2009).

53.2 The Dark Side of Rhodopsin

The *Drosophila* compound eye is composed of approx. 800 “eyes” or ommatidia. Each ommatidium contains eight PNs (R1-8) and additional nonneuronal cells that support vision. PNs are divided into six outer photoreceptors (R1-R6), sensitive to light contrast and mediating motion detection, and two inner PNs (R7-8) responsible for color detection (Cook and Desplan 2001). R1-6 PNs express a single Rho ortholog, called *Rh1*, which is encoded by the *ninaE* locus (O’Tousa et al. 1985; Zuker et al. 1985); R7-8 PNs express a combination of *Rh3-6* genes (Cook and Desplan 2001).

Rh1 is a seven-transmembrane G protein-coupled receptor that localizes to rhabdomeres – the light-sensing organelles of PNs – where it interacts with light particles. Activated Rh1 binds the G_q protein, which becomes activated and recruits the phospholipase C (NorpA). NorpA hydrolytic activity leads to the opening of TRP or TRPL Ca²⁺ channels (Fig. 53.1). Rh1 is inactivated by GPRK1-mediated phosphorylation and binding to Arrestin 2 (Arr2; Dolph et al. 1993) and via a novel dCAMTA/dFbx14 pathway, which is poorly defined (Han et al. 2006). Arr2 is phosphorylated by Ca²⁺/calmodulin-dependent kinase II (CaMKII) and detaches from phosphorylated Rh1, which becomes substrate of the Ca²⁺/CaM-dependent protein phosphatase RDGC. In contrast to vertebrate PT (involving cyclic GMP), fly PT is mediated by phosphoinositol (PI) signaling. The pool of PI 4,5-biphosphate (PIP₂) necessary for PT is continuously regenerated from diacylglycerol (DAG); the DAG kinase (RDGA) and the PI transfer protein RDGB are important for this reconversion (Wang and Montell 2007).

Abnormalities in PT are a major cause of RD in *Drosophila* and humans, and virtually all mutations that affect PT components result in severe RD in the fly (Wang and Montell 2007). A second collection of mutants are those carrying mutations in the *Rh1* gene. *Rh1* mutations were first associated with RD in the fly. Inactivation of the *Rh1* gene causes RD (O’Tousa et al. 1989; Leonard et al. 1992), and several *Rh1* gain-of-function (GOF) mutations were isolated, which induce a slow and progressive RD (Colley et al. 1995; Kurada and O’Tousa 1995; Kurada et al. 1998). Subsequently, loss-of-function (LOF) and GOF Rho mutations were

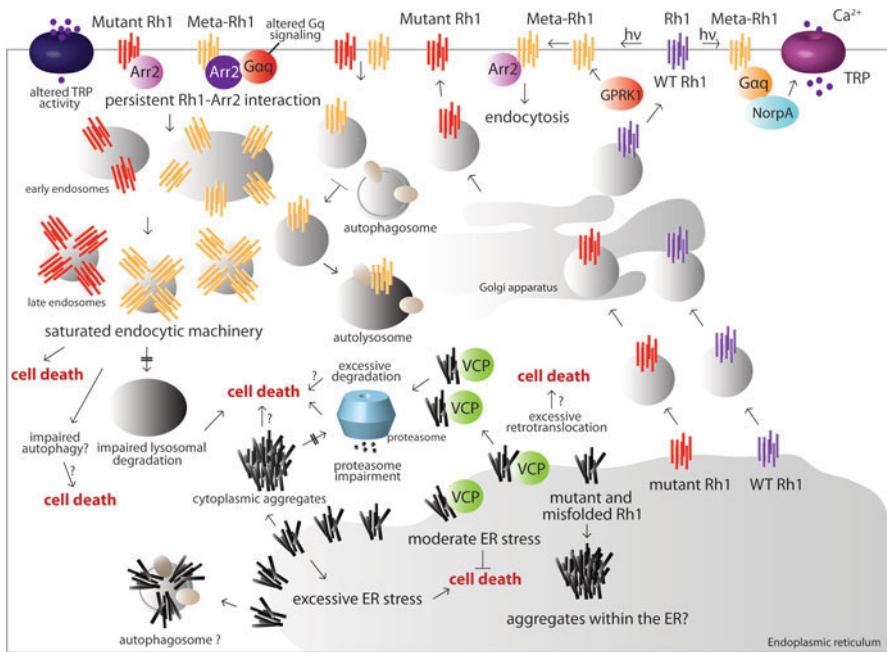


Fig. 53.1 Pathways leading to retinal degeneration in *Drosophila*. Work in *Drosophila* uncovered several pathways linking altered Rh1 states to retinal degeneration. Altered phototransduction emerged as a major contributor to cell death. Mutations in several PT cascade components (including Rh1) stabilize the interaction between Rh1 and Arr2, which in turn causes massive Rh1 endocytosis. Internalized Rh1 fails to reach the lysosomal compartment and accumulates in late endosomes, causing cell death via yet unidentified mechanisms. One potential mechanism might be autophagy impairment. Mutations that cause Rh1 misfolding lead to Rh1 retention in the ER, and to ER stress. Excessive ER stress is pro-apoptotic, while moderate ER stress appears to be protective. Interestingly, excessive Rh1 retrotranslocation and/or proteasomal degradation (mediated by VCP) appears to cause RD. It is unclear (i) whether insoluble cytosolic Rh1 aggregates are pathogenic or whether soluble Rh1 oligomers are more toxic than insoluble aggregates; (ii) how Rh1 degradation (via both ERAD and autophagy) is implemented under conditions of ER stress and how it causes RD, and (iii) whether different Rh1 folding mutants exhibit differential activation of ER stress, ERAD and autophagic machineries

discovered in patients with recessive RP and ADRP, respectively (Daiger et al. 2007). The first and most common Rho mutation to be associated with ADRP is a proline-to-histidine substitution in codon 23 (P23H; Dryja et al. 1990); remarkably, more than 120 Rho mutations have been linked to ADRP (Daiger et al. 2007). Rho mutations have been divided into at least six classes, based on their biochemical and cellular properties (Mendes et al. 2005). In *Drosophila*, dominant *Rh1* mutations causing RD affect (i) the C-terminus of the protein and do not cause Rh1 misfolding, but alter its targeting to the outer segment or (ii) the intradiscal/transmembrane domains causing Rh1 misfolding and retention within the ER.

53.3 Pathogenic Mechanisms Underlying RD in *Drosophila*

Detailed investigation of mutant flies that exhibit RD allowed the identification of several pathogenic mechanisms (Fig. 53.1). Below, we highlight some of these mechanisms, with a focus on Rh1-mediated pathologies.

53.3.1 Abnormalities in the PT Cascade

The tight regulation of Rh1 levels and activation status is critical for PN viability. Failure to uncouple activated Rh1 from the G protein leads to constitutive activation of the PT and to RD. Several mutants, such as *norpA*, *arr2*, *rdgB*, *rdgC*, or *trp* display abnormally stable Rh1-Arr2 complexes, which cause constitutive activation of PT (Alloway and Dolph 1999; Alloway et al. 2000; Kiselev et al. 2000); RD in these mutants is suppressed by vitamin A deprivation, which reduces Rh1 levels (Knust 2007). One prominent consequence of altered PT is an imbalance of Ca²⁺ levels. Thus, in *rdgA* mutants, failure to metabolize DAG leads to excessive Ca²⁺ influx through TRP channels, and *TRP LOF* mutations suppress RD (Raghu et al. 2000). Abnormally low TRP activity also causes RD, by reducing Ca²⁺ influx into PNs, which appears to stabilize the Rh1-Arr2 interaction (Wang et al. 2005). Interestingly, a constitutively active *TRP* mutant – *trp^{P365}* – that leads to excessive Ca²⁺ influx into PNs also exhibits RD (Yoon et al. 2000). Another defect found in PT mutants is altered G protein signaling. A novel *Rh1* mutant, *Rh1^{pp100}*, causes degeneration by increasing the binding of mutant Rh1 to Arr2 and by elevating the cytosolic levels of G_qα; interestingly, these two processes appear to be independent (Iakhine et al. 2004). The protein TADR associates with Rh1 and loss of TADR function causes Rh1-dependent (but Arr2- and NorpA-independent) degeneration, by inhibiting the membrane detachment of G_q during light stimulation (Ni et al. 2008).

53.3.2 Altered Rh1 Endocytosis and Autophagy

A consequence of the prolonged interaction between Rh1 and Arr2 is the rapid internalization of Rh1-Arr2 complexes by receptor-mediated endocytosis. Increased Rh1 endocytosis leads to PN desensitization via a novel Gq-mediated, Arr2-independent and tetraspanin-dependent mechanism (Han et al. 2007). Excessive Rh1 endocytosis leads to RD in several mutants, including *rdgB*, *rdgC*, *arr1/2*, and *norpA*, (Knust 2007; Wang and Montell 2007). A remarkable finding is the noncell autonomous regulation of Rh1-Arr2 interaction by the secreted enzyme ceramidase (CDase; which is involved in sphingolipid metabolism; Acharya et al. 2008). The Rh1-Arr2 complex is further regulated by the endocytic adaptor AP-2, which interacts with Arr2 and promotes Rh1-Arr2 internalization; inhibition of AP-2 function

suppressed cell death caused by excessive endocytosis in *norpA* mutants (Orem et al. 2006). A primary cause of PN degeneration in *norpA* and other mutants exhibiting Rh1 pathogenic endocytosis was suggested to be the failure of lysosomal degradation of Rh1, which instead accumulates in late endosomes (Chinchore et al. 2009). Accumulation of Rh1 in late endosomes might also result from impaired lysosome-mediated autophagy. Thus, autophagy inhibition caused Rh1 accumulation in late endosomes and RD in wild-type (WT) PNs, and Rab7 overexpression (which promotes Rh1 trafficking from late endosomes to lysosomes) rescued this effect (Midorikawa et al. 2010). Remarkably, autophagy induction (by overexpressing the mediators TSC1/2 or Atg1) suppressed RD in *norpA* flies, by stimulating the clearance of Rh1-Arr2 complexes; however, autophagy stimulation did not suppress RD in *ninaE^{RH27}* flies (Wang et al. 2009). Therefore, autophagy stimulation might represent a new therapeutic strategy for a subset of *Rho*-linked RP (see also Mendes and Cheetham 2008).

53.3.3 Impaired Rh1 Maturation, Trafficking, and Proteasomal Clearance

Impairment of Rho biogenesis and transport causes RD in both flies and humans. In *Drosophila*, Rh1 requires the chaperones NinaA (Colley et al. 1991; Stamnes et al. 1991) and Calnexin (Rosenbaum et al. 2006) but also 3-hydroxyretinal (Ahmad et al. 2006) to mature. The GTP-binding protein Rab1 mediates Rh1 transport between ER and the Golgi complex (Satoh et al. 1997); Rab6 mediates Rh1 trafficking within the Golgi and post-Golgi compartments (Shetty et al. 1998); and Rab11 facilitates Rh1 transport from the post-Golgi compartment to rhabdomeres (Satoh et al. 2005). The helix 8 in the C-terminal region of Rh1 is critical for its rhabdomeric localization (Kock et al. 2009).

How do defects in Rh1 maturation and transport cause RD? One possible mechanism is the absence of WT Rh1 from rhabdomeres, as seen in *Rh1* LOF mutants. Thus, besides its critical role in PT, Rh1 is essential for rhabdomere morphogenesis. Rh1 activates the Rho GTPase Drac1 to control cytoskeleton organization in rhabdomeres (Chang and Ready 2000).

A second mechanism linking Rh1 maturation defects to RD is the accumulation of high levels of Rh1 in the ER, which causes toxicity. Several dominant Rh1 alleles were isolated in *Drosophila* and found to cause light-dependent RD (Colley et al. 1995; Kurada and O'Tousa 1995). In flies carrying these alleles, mutant Rh1 localizes to the endoplasmic reticulum (ER) and impairs the maturation of the endogenous WT Rh1; intriguingly, the presence of both mutant and WT Rh1 is required for toxicity (Colley et al. 1995; Kurada and O'Tousa 1995; Kurada et al. 1998). This suggests that both conformers interact to cause toxicity in PNs (see also Griuciu et al. 2010b). More recently, Giangrande and colleagues generated transgenic flies in which the most common RP-linked *Rho* mutation, *Rho^{P23H}* (its equivalent in flies is *Rh1^{P37H}*), was expressed in R1-6 PNs, under the control of a promoter identical to

the endogenous Rh1 promoter; these flies underwent light- and age-dependent RD (Galy et al. 2005). The use of a small hsv tag allowed the differential analysis of mutant and WT Rh1 conformers, and revealed that Rh1^{P37H} exhibited a dual localization – being present both in rhabdomeres and the ER – while it did not interfere with the maturation of its endogenous WT counterpart. This suggests that RD in *Rh1*^{P37H} flies is due to a toxic (GOF) effect caused by Rh1^{P37H} accumulation in the ER, rather than absence of WT Rh1 from rhabdomeres (dominant negative [DN] effect). The presence of misfolded Rh1 in the ER causes ER stress, both in *Drosophila* (Ryoo et al. 2007) and mammals (Lin et al. 2007). Interestingly, moderate ER stress protects against RD in the fly (Mendes et al. 2009). To understand how ER-based Rh1^{P37H} leads to RD, we inactivated the ER-associated degradation (ERAD) effector VCP/ter94, an ATP-dependent chaperone that mediates Rho^{P23H} extraction from the ER and proteasomal degradation in mammalian cell cultures (Griciuc et al. 2010a). VCP inactivation increased the levels of misfolded Rh1^{P37H}, indicating that VCP is required for Rh1^{P37H} degradation in vivo. VCP ablation also activated the Ire1/Xbp1 ER stress pathway but, remarkably, strongly suppressed Rh1^{P37H}-induced RD; moreover, treatment of *Rh1*^{P37H} flies with VCP/ERAD or proteasome inhibitors potently suppressed RD (Griciuc et al. 2010b). These results suggest that (i) excessive retrotranslocation and/or degradation of Rh1^{P37H} represents a new pathway to cell death in the *Rh1*^{P37H} retina and (ii) partial inhibition of ERAD might be neuroprotective. Working with another Rh1 mutant (*ninaE*^{G69D}), Kang and Ryoo (2009) found that enhancement of ERAD function (by overexpression of ERAD components Hrd1 or EDEM2) rescued the loss of mature Rh1 and RD; interestingly, ERAD inhibition (by Hrd1 or EDEM2 RNAi) also rescued the loss of Rh1, but the effects on RD have not been investigated (Kang and Ryoo 2009). Collectively, these results suggest that early induction of ERAD might protect against RD by clearing the mutant Rh1 from the ER, while chronic ERAD is pro-apoptotic. It remains to be determined whether different Rh1 mutations lead to different levels of ER stress and ERAD activity and whether they cause RD via a GOF or DN mechanism, or both. It is therefore possible that, similar to autophagy, the effects of ERAD manipulation on RD might depend on the Rh1 mutation being investigated.

53.3.4 Pathways to Cell Death in RD

A major pathway to RD has been found to be the programmed cell death (PCD or apoptosis), which is promoted by the activation of *reaper*, *hid*, or *grim* genes and inhibited by *Diap1* or the caspase inhibitor *P35* (Steller 2008). This pathway appears to mediate RD in several mutants, including *rdgC*, *ninaE*^{RH27} (Davidson and Steller 1998), and *Rh1*^{P37H} (Galy et al. 2005). However, RD in the *norpA* mutant (Hsu et al. 2004) appears to be PCD-independent. Further studies in RD mutants will reveal the similarities and differences in the initiation and implementation of cell death programs as well as their underlying biochemical interactions.

53.4 Conclusions

The use of *Drosophila* to study Rho pathologies has greatly advanced our understanding of RD and its underlying mechanisms. It is remarkable to see how often the mechanisms of disease in *Drosophila* resemble those in mammals, despite differences in anatomy and physiology between these species. These pathological processes are likely to be central events in retinal disease, given their evolutionary conservation. Further genetic and proteomic investigations are required to dissect the intricate network of biochemical interactions that link alterations in Rh1 function to PN cell death. It is important to determine whether the various Rh1 altered states (e.g., caused by different Rh1 mutations) lead to distinct molecular pathologies or whether distinct sets of pathological pathways are shared between these altered cellular environments. Many secrets of visual physiology and pathology still remain hidden in the tiny eyes of *Drosophila*. These secrets will undoubtedly passionate the existing and future scholars of retinal dystrophies and could bring valuable clues about how to fight retinal disease in humans.

Acknowledgments Work in the Ueffing laboratory is supported by the EU Grant NEUROTRAIN (MEST-CT-2005-020235), RETNET (MRTN-CT-2003-504003) and EVI-GENORET (LSHG-CT-2005-512036 to MU).

References

- Acharya JK, Dasgupta U, Rawat SS et al (2008) Cell-nonautonomous function of ceramidase in photoreceptor homeostasis. *Neuron* 57:69–79
- Ahmad ST, Joyce MV, Boggess B et al (2006) The role of *Drosophila* ninaG oxidoreductase in visual pigment chromophore biogenesis. *J Biol Chem* 281:9205–9209
- Alloway PG, Dolph PJ (1999) A role for the light-dependent phosphorylation of visual arrestin. *Proc Natl Acad Sci USA* 96:6072–6077
- Alloway PG, Howard L, Dolph PJ (2000) The formation of stable rhodopsin-arrestin complexes induces apoptosis and photoreceptor cell degeneration. *Neuron* 28:129–138
- Chang HY, Ready DF (2000) Rescue of photoreceptor degeneration in rhodopsin-null *Drosophila* mutants by activated Rac1. *Science* 290:1978–1980
- Chinchore Y, Mitra A, Dolph PJ (2009) Accumulation of rhodopsin in late endosomes triggers photoreceptor cell degeneration. *PLoS Genet* 5:e1000377
- Colley NJ, Baker EK, Stammes MA et al (1991) The cyclophilin homolog ninaA is required in the secretory pathway. *Cell* 67:255–263
- Colley NJ, Cassill JA, Baker EK et al (1995) Defective intracellular transport is the molecular basis of rhodopsin-dependent dominant retinal degeneration. *Proc Natl Acad Sci USA* 92:3070–3074
- Cook T, Desplan C (2001) Photoreceptor subtype specification: from flies to humans. *Semin Cell Dev Biol* 12:509–518
- Daiger SP (2004) Identifying retinal disease genes: how far have we come, how far do we have to go? *Novartis Found Symp* 255:17–27; discussion 27–36, 177–178
- Daiger SP, Bowne SJ, Sullivan LS (2007) Perspective on genes and mutations causing retinitis pigmentosa. *Arch Ophthalmol* 125:151–158

- Davidson FF, Steller H (1998) Blocking apoptosis prevents blindness in *Drosophila* retinal degeneration mutants. *Nature* 391:587–591
- Dolph PJ, Ranganathan R, Colley NJ et al (1993) Arrestin function in inactivation of G protein-coupled receptor rhodopsin in vivo. *Science* 260:1910–1916
- Dryja TP, McGee TL, Reichel E et al (1990) A point mutation of the rhodopsin gene in one form of retinitis pigmentosa. *Nature* 343:364–366
- Galy A, Roux MJ, Sahel JA et al (2005) Rhodopsin maturation defects induce photoreceptor death by apoptosis: a fly model for RhodopsinPro23His human retinitis pigmentosa. *Hum Mol Genet* 14:2547–2557
- Griciuc A, Aron L, Piccoli G et al (2010a) Clearance of Rhodopsin(P23H) aggregates requires the ERAD effector VCP. *Biochim Biophys Acta* 1803:424–434
- Griciuc A, Aron L, Roux MJ et al (2010b) Inactivation of VCP/ter94 suppresses retinal pathology caused by misfolded rhodopsin in *Drosophila*. *PLoS Genet* 6
- Hamel C (2006) Retinitis pigmentosa. *Orphanet J Rare Dis* 1:40
- Han J, Reddig K, Li HS (2007) Prolonged G(q) activity triggers fly rhodopsin endocytosis and degradation, and reduces photoreceptor sensitivity. *EMBO J* 26:4966–4973
- Han J, Gong P, Reddig K et al (2006) The fly CAMTA transcription factor potentiates deactivation of rhodopsin, a G protein-coupled light receptor. *Cell* 127:847–858
- Hartong DT, Berson EL, Dryja TP (2006) Retinitis pigmentosa. *Lancet* 368:1795–1809
- Hsu CD, Whaley MA, Frazer K et al (2004) Limited role of developmental programmed cell death pathways in *Drosophila* norpA retinal degeneration. *J Neurosci* 24:500–507
- Iakhine R, Chorna-Ornan I, Zars T et al (2004) Novel dominant rhodopsin mutation triggers two mechanisms of retinal degeneration and photoreceptor desensitization. *J Neurosci* 24:2516–2526
- Kang MJ, Ryoo HD (2009) Suppression of retinal degeneration in *Drosophila* by stimulation of ER-associated degradation. *Proc Natl Acad Sci USA* 106:17043–17048
- Kennan A, Aherne A, Humphries P (2005) Light in retinitis pigmentosa. *Trends Genet* 21:103–110
- Kiselev A, Socolich M, Vinos J et al (2000) A molecular pathway for light-dependent photoreceptor apoptosis in *Drosophila*. *Neuron* 28:139–152
- Knust E (2007) Photoreceptor morphogenesis and retinal degeneration: lessons from *Drosophila*. *Curr Opin Neurobiol* 17:541–547
- Kock I, Bulgakova NA, Knust E et al (2009) Targeting of *Drosophila* rhodopsin requires helix 8 but not the distal C-terminus. *PLoS One* 4:e6101
- Kurada P, O'Tousa JE (1995) Retinal degeneration caused by dominant rhodopsin mutations in *Drosophila*. *Neuron* 14:571–579
- Kurada P, Tonini TD, Serikaku MA et al (1998) Rhodopsin maturation antagonized by dominant rhodopsin mutants. *Vis Neurosci* 15:693–700
- Leonard DS, Bowman VD, Ready DF et al (1992) Degeneration of photoreceptors in rhodopsin mutants of *Drosophila*. *J Neurobiol* 23:605–626
- Lin JH, Li H, Yasumura D et al (2007) IRE1 signaling affects cell fate during the unfolded protein response. *Science* 318:944–949
- Mendes CS, Levet C, Chatelain G et al (2009) ER stress protects from retinal degeneration. *EMBO J* 28:1296–1307
- Mendes HF, Cheetham ME (2008) Pharmacological manipulation of gain-of-function and dominant-negative mechanisms in rhodopsin retinitis pigmentosa. *Hum Mol Genet* 17:3043–3054
- Mendes HF, van der Spuy J, Chapple JP et al (2005) Mechanisms of cell death in rhodopsin retinitis pigmentosa: implications for therapy. *Trends Mol Med* 11:177–185
- Midorikawa R, Yamamoto-Hino M, Awano W et al (2010) Autophagy-dependent rhodopsin degradation prevents retinal degeneration in *Drosophila*. *J Neurosci* 30:10703–10719
- Ni L, Guo P, Reddig K et al (2008) Mutation of a TADR protein leads to rhodopsin and Gq-dependent retinal degeneration in *Drosophila*. *J Neurosci* 28:13478–13487
- O'Tousa JE, Leonard DS, Pak WL (1989) Morphological defects in oraJK84 photoreceptors caused by mutation in R1-6 opsin gene of *Drosophila*. *J Neurogenet* 6:41–52
- O'Tousa JE, Baehr W, Martin RL et al (1985) The *Drosophila* ninaE gene encodes an opsin. *Cell* 40:839–850

- Orem NR, Xia L, Dolph PJ (2006) An essential role for endocytosis of rhodopsin through interaction of visual arrestin with the AP-2 adaptor. *J Cell Sci* 119:3141–3148
- Raghu P, Usher K, Jonas S et al (2000) Constitutive activity of the light-sensitive channels TRP and TRPL in the *Drosophila* diacylglycerol kinase mutant, rdgA. *Neuron* 26:169–179
- Rivas MA, Vecino E (2009) Animal models and different therapies for treatment of retinitis pigmentosa. *Histol Histopathol* 24:1295–1322
- Rosenbaum EE, Hardie RC, Colley NJ (2006) Calnexin is essential for rhodopsin maturation, Ca²⁺ regulation, and photoreceptor cell survival. *Neuron* 49:229–241
- Ryoo HD, Domingos PM, Kang MJ et al (2007) Unfolded protein response in a *Drosophila* model for retinal degeneration. *EMBO J* 26:242–252
- Sancho-Pelluz J, Arango-Gonzalez B, Kustermann S et al (2008) Photoreceptor cell death mechanisms in inherited retinal degeneration. *Mol Neurobiol* 38:253–269
- Sanes JR, Zipursky SL (2010) Design principles of insect and vertebrate visual systems. *Neuron* 66:15–36
- Satoh A, Tokunaga F, Kawamura S et al (1997) In situ inhibition of vesicle transport and protein processing in the dominant negative Rab1 mutant of *Drosophila*. *J Cell Sci* 110 (Pt 23):2943–2953
- Satoh AK, O'Tousa JE, Ozaki K et al (2005) Rab11 mediates post-Golgi trafficking of rhodopsin to the photosensitive apical membrane of *Drosophila* photoreceptors. *Development* 132:1487–1497
- Shetty KM, Kurada P, O'Tousa JE (1998) Rab6 regulation of rhodopsin transport in *Drosophila*. *J Biol Chem* 273:20425–20430
- Shintani K, Shechtman DL, Gurwood AS (2009) Review and update: current treatment trends for patients with retinitis pigmentosa. *Optometry* 80:384–401
- Stamnes MA, Shieh BH, Chuman L et al (1991) The cyclophilin homolog ninaA is a tissue-specific integral membrane protein required for the proper synthesis of a subset of *Drosophila* rhodopsins. *Cell* 65:219–227
- Steller H (2008) Regulation of apoptosis in *Drosophila*. *Cell Death Differ* 15:1132–1138
- Wang T, Montell C (2007) Phototransduction and retinal degeneration in *Drosophila*. *Pflugers Arch* 454:821–847
- Wang T, Jiao Y, Montell C (2005) Dissecting independent channel and scaffolding roles of the *Drosophila* transient receptor potential channel. *J Cell Biol* 171:685–694
- Wang T, Lao U, Edgar BA (2009) TOR-mediated autophagy regulates cell death in *Drosophila* neurodegenerative disease. *J Cell Biol* 186:703–711
- Yoon J, Ben-Ami HC, Hong YS et al (2000) Novel mechanism of massive photoreceptor degeneration caused by mutations in the trp gene of *Drosophila*. *J Neurosci* 20:649–659
- Zuker CS, Cowman AF, Rubin GM (1985) Isolation and structure of a rhodopsin gene from *D. melanogaster*. *Cell* 40:851–858

Chapter 54

Müller Glia as a Source of Neuronal Progenitor Cells to Regenerate the Damaged Zebrafish Retina

Craig M. Nelson and David R. Hyde

Keywords Retinal regeneration • Zebrafish • Stat3 • Asc11a • Pax6 • Müller glia • Phagocytosis • TNF α

54.1 Models of Retinal Damage in Zebrafish

The zebrafish retina exhibits robust neuronal regeneration. Different damage paradigms have been used to characterize the cellular and molecular basis of the retinal cell regeneration response. Retinal damage can be induced by either constant intense light (Vihtelic and Hyde 2000; Bernardos et al. 2007), focused heat (Raymond et al. 2006), neurotoxins (Fimbel et al. 2007; Sherpa et al. 2008), full-thickness needle puncture, or surgical lesions (Hitchcock et al. 1992; Cameron and Carney 2000; Faillace et al. 2002; Fausett and Goldman 2006), or the expression of the *E. coli nitroreductase* transgene in the presence of metronidazole (Montgomery et al. 2010). In all of these damage models, the Müller glia reentered the cell cycle and produced a transient-amplifying population of multipotent neuronal progenitors that migrated to the damaged area and differentiated into the neuronal classes that were lost (Cameron and Carney 2000; Fausett and Goldman 2006; Raymond et al. 2006; Kassen et al. 2007). The regeneration response in all of these models is highly specific, such that the only neuronal cell types that are regenerated correspond to the neuronal types that were lost.

C.M. Nelson • D.R. Hyde (✉)

Department of Biological Sciences and the Center for Zebrafish Research,
University of Notre Dame, 027 Galvin Life Science Building, Notre Dame, IN 46556, USA
e-mail: dhyde@nd.edu

54.2 Regeneration of the Light-Damaged Zebrafish Retina

While most of the damage models result in the loss of several different neuronal cell classes, the light-lesion model causes only photoreceptor cell loss. After 36 h of constant light, the ONL has lost a significant number of nuclei; and the Müller glia in the INL start expressing PCNA (Fig. 54.1b, arrows). After 51 h, the Müller glial cells initiate the production of a transiently amplifying population of neuronal progenitor cells (Fig. 54.1c). The Müller glia and INL neuronal progenitors can also be detected by BrdU-incorporation subsequent to a wide variety of insults (Vihtelic and Hyde 2000; Yurco and Cameron 2005; Fausett and Goldman 2006; Raymond et al. 2006; Bernardos et al. 2007). By 68 h, the number of PCNA-labeled neuronal progenitor cells increases as they become fusiform-shaped and cluster around the Müller glial processes. Additionally, the neuronal progenitors begin migrating along the Müller glial cell processes from the INL to the ONL (Fig. 54.1d). After 96 h in constant light, the neuronal progenitor cells continue proliferating and migrate to the ONL (Fig. 54.1e), where they start to differentiate into either rod or cone photoreceptors.

The regeneration specificity observed in all of these models, whereby only the neuronal cell types that are damaged or lost are regenerated, suggests that the signals that are required to induce and direct regeneration may involve both general (required for the regeneration of all neuronal cell types) and specific for individual cell types. Furthermore, identification of these regeneration signals and the underlying pathways may reveal the molecular keys necessary to stimulate a similar regeneration response in the damaged or diseased human retina, which currently cannot regenerate.

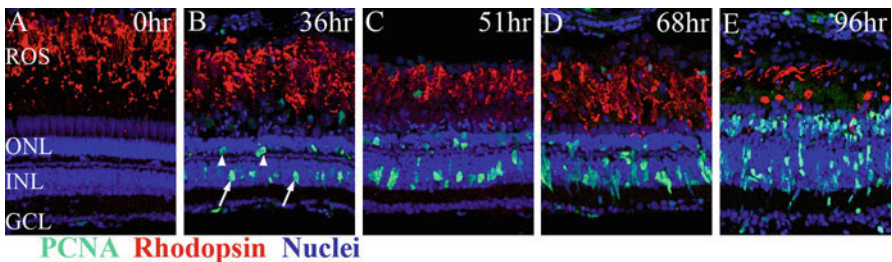


Fig. 54.1 Timecourse of light-induced photoreceptor cell death and regeneration. Dark-adapted adult *albino* zebrafish were kept in constant light for either 0 (a), 36 (b), 51 (c), 68 (d), or 96 h (e). Frozen retinal sections were labeled with anti-rhodopsin polyclonal antiserum (red), anti-PCNA monoclonal antibody (green), and the nuclear stain To-Pro-3 (blue). At 0 h, there is minimal cell proliferation in the undamaged retina (a). By 36 h of constant light, both ONL residing rod precursor cells and a subset of Müller glia in the INL are proliferating (b, arrowheads and arrows, respectively). The dividing Müller glia yield columns of proliferating neuronal progenitor cells (c, d), which then migrate to the ONL (e). ROS rod outer segments; ONL outer nuclear layer; INL inner nuclear layer; GCL ganglion cell layer

To identify such signals, gene microarray analyses have been performed on zebrafish retinas that were light-damaged (Kassen et al. 2007; Craig et al. 2010), Müller glia that were isolated from light-damaged and undamaged retinas (Qin et al. 2009), retinas that were mechanically excised to remove a small retinal patch (Cameron et al. 2005), or retinas that had undergone an optic nerve crush (McCurley and Callard 2010). However, the loss of only rods and cones in the light-damaged retina should simplify the identification of transcriptional and protein expression changes required for neuronal regeneration relative to the other damage models that result in the loss of a greater number of neuronal cell types.

54.3 Induction of Müller Glial Proliferation in the Light-Damaged Zebrafish Retina

After 24 h of constant intense light, which corresponds to the time when maximal cell death occurs in the light-damaged retina, a subset of Müller glia possessed a weak cytoplasmic TUNEL signal (Bailey et al. 2010). Additionally, light damage of a rod-specific transgenic reporter line, *Tg(XIRho:EGFP)^{rl}*, caused some Müller glia to contain both TUNEL signal and EGFP, suggesting that these Müller glia engulfed apoptotic photoreceptor cell bodies (Bailey et al. 2010). Intravitreal injection of *O*-phospho-L-serine (L-SOP), which mimics the phosphatidylserine head group and partially blocks phagocytosis of apoptotic cells, immediately prior to starting the constant light treatment did not alter light-induced photoreceptor cell death (Bailey et al. 2010). However, intravitreal injection of L-SOP significantly reduced the number of PCNA-positive Müller glia and the number of regenerated cone photoreceptors (Bailey et al. 2010). This suppression was not through the group III metabotropic glutamate receptors (mGluRs). This suggested that Müller glial engulfment of apoptotic photoreceptors is at least one mechanism to activate the proliferative response.

Using a proteomics approach, we found that tumor necrosis factor α (TNF α) protein expression by photoreceptors increased after 16 h of constant light relative undamaged controls and colocalized with Müller glia after 36 h of light (Nelson and Hyde, unpublished data). Furthermore, the TNF α receptor superfamily member a, colocalized with PCNA-positive Müller glia in the INL after 36 h of light damage (Nelson and Hyde, unpublished data). TNF α signaling through this receptor has been shown to induce both apoptotic and proliferative pathways (MacEwan 2002). Knockdown of TNF α protein expression immediately prior to light damage resulted in a significantly reduced number of proliferating Müller glia, but did not affect levels of photoreceptor death, relative to controls (Nelson and Hyde, unpublished results). Thus, TNF α signaling represents another process that is required to initiate Müller glia proliferation during photoreceptor regeneration.

54.4 Transcription Factors Required for Maximal Müller Glial Cell Proliferation

Recent work has also shed light on some of the transcription factors utilized by zebrafish Müller glia during dedifferentiation and the initial cell division (Fausett et al. 2008; Kassen et al. 2007). Microarray studies revealed that both the Achaete-scute complex-like 1a (*Ascl1a*) and Signal transducer and activator of transcription 3 (*Stat3*) proteins increased in expression shortly after retinal damage. The role of these proteins in the regenerative response was tested by the intravitreal injection and then electroporation of specific morpholinos, which are modified oligonucleotides that are designed to be complementary to the 5' region of specific mRNAs and block the translation of the mRNA (Thummel et al. 2008). Knockdown of either *Ascl1a* or *Stat3* protein expression by intravitreal injection and electroporation of morpholinos immediately prior to retinal injury resulted in a significantly reduced number of proliferating Müller glia (Fausett et al. 2008; Kassen and Hyde, unpublished data). Importantly, reduced expression of either *Ascl1a* or *Stat3* had no effect on the expression of the other, and knocking down both simultaneously did not further inhibit Müller glia proliferation (Kassen and Hyde, unpublished data). This suggests that these two mechanisms for the initiation of Müller glial-dependent regeneration act in separate but parallel and functionally redundant pathways relative to one another.

Stat3 signaling can act downstream of many different transmembrane *Jak/Stat* receptors that will bind to a wide variety of extracellular secreted growth factors and cytokines including *Fgf*, *Egf*, interleukins, interferons, *TNF α* , and ciliary neurotrophic factor (*CNTF*; Aaronson and Horvath 2002; Miscia et al. 2002). Intravitreal injection of *CNTF* into undamaged zebrafish eyes resulted in increased *Stat3* expression and the proliferation of a subset of Müller glia (Kassen et al. 2009). Knockdown of *Stat3* in these *CNTF*-injected eyes inhibited proliferation (Kassen et al. 2009), which suggested that *CNTF* can stimulate Müller glia proliferation in a *Stat3*-dependent manner. However, the requirement of *CNTF* to induce Müller glia proliferation in the light-damaged retina remains unknown, as are the upstream signaling molecules that are ultimately responsible for the increased expression of *Stat3* and *Ascl1a*.

54.5 Proteins That Are Required for Neuronal Progenitor Cell Proliferation

Zebrafish possess two *Pax6* proteins, one encoded by the *pax6a* gene and the other encoded by the *pax6b* gene. The *Pax6a* protein was expressed in ganglion and amacrine cells and the neuronal progenitor cells in the light-damaged retina, while *Pax6b* was only expressed in the neuronal progenitor cells. Morpholino-mediated knockdown of the *Pax6b* protein did not affect Müller glial cell division, but blocked the subsequent first cell division of the neuronal progenitors (Thummel et al. 2010).

Knockdown of the paralogous Pax6a protein blocked later neuronal progenitor cell divisions, which is required to generate the maximal number of neuronal progenitors (Thummel et al. 2010). This work defined distinct roles for the Pax6a and Pax6b proteins in regulating neuronal progenitor cell proliferation in the adult zebrafish retina.

54.6 Future Directions

Studying the proteins and processes that are required for the Müller glial-dependent regeneration of the light-damaged zebrafish retina will identify what is required to induce Müller glia proliferation, amplification of the resulting neuronal progenitor cells, the migration of the neuronal progenitors to the proper nuclear layer and their differentiation into the specific neuronal cell classes that were lost. Comparison of the regenerative response in the light-damaged retina relative to the other damage models should reveal general features of regeneration and specific details that differentiate the regeneration of one type of neuronal class from another. This information will provide us with models for why the damaged mammalian retina is unable to regenerate and allow us to develop mechanisms to induce a regenerative response in the human retina.

References

- Aaronson DS, Horvath CM (2002) A road map for those who don't know JAK-STAT. *Science* 296:1653–1655
- Bailey TJ, Fossum SL, Fimbel SM et al (2010) The inhibitor of phagocytosis, O-phospho-L-serine, suppresses Müller glia proliferation and cone cell regeneration in the light-damaged zebrafish retina. *Exp Eye Res* 91:601–612
- Bernardos RL, Barthel LK, Meyers JR et al (2007) Late-stage neuronal progenitors in the retina are radial Müller glia that function as retinal stem cells. *J Neurosci* 27:7028–7040
- Cameron DA, Carney LH (2000) Cell mosaic patterns in the native and regenerated inner retina of zebrafish: implications for retinal assembly. *J Comp Neurol* 416:356–367
- Cameron DA, Gentile KL, Middleton FA et al (2005) Gene expression profiles of intact and regenerating zebrafish retina. *Mol Vis* 11:775–791
- Craig SEL, Thummel R, Ahmed H et al (2010) The zebrafish galectin Drgal1-L2 is expressed by proliferating Müller glia and photoreceptor progenitors and regulates the regeneration of rod photoreceptors. *Invest Ophthalmol Vis Sci* 51:3244–3252
- Faillace MP, Julian D, Korenbrot JI (2002) Mitotic activation of proliferative cells in the inner nuclear layer of the mature fish retina: regulatory signals and molecular markers. *J Comp Neurol* 451:127–141
- Fausett BV, Goldman D (2006) A role for alpha1 tubulin-expressing Müller glia in regeneration of the injured zebrafish retina. *J Neurosci* 26:6303–6313
- Fausett BV, Gumerson JD, Goldman D (2008) The proneural basic helix-loop-helix gene *ascl1a* is required for retina regeneration. *J Neurosci* 28:1109–1117
- Fimbel SM, Montgomery JE, Burket CT et al (2007) Regeneration of inner retinal neurons after intravitreal injection of ouabain in zebrafish. *J Neurosci* 27:1712–1724

- Hitchcock PF, Lindsey Myhr KJ, Easter SS Jr et al (1992) Local regeneration in the retina of the goldfish. *J Neurobiol* 23:187–203
- Kassen SC, Ramanan V, Montgomery JE et al (2007) Time course analysis of gene expression during light-induced photoreceptor cell death and regeneration in *albino* zebrafish. *Dev Neurobiol* 67:1009–1031
- Kassen SC, Thummel R, Campochiaro LA et al (2009) CNTF induces photoreceptor neuroprotection and Müller glial cell proliferation through two different signaling pathways in the adult zebrafish retina. *Exp Eye Res* 88:1051–1064
- MacEwan, D (2002) TNF receptor subtype signalling: differences and cellular consequences. *Cell Signal* 14:477–492
- McCurley AT, Callard GV (2010) time course analysis of gene expression patterns in zebrafish eye during optic nerve regeneration. *J Exp Neurosci* 13:17–33
- Miscia S, Marchisio M, Grilli A et al (2002) Tumor necrosis factor alpha (TNF-alpha) activates Jak1/Stat3-Stat5B signaling through TNFR-1 in human B cells. *Cell Growth Differ* 13:13–8
- Montgomery JE, Parsons MJ, Hyde DR (2010) A novel model of retinal ablation demonstrates that the origin of regenerated rod photoreceptors is dependent on the extent of damage. *J Comp Neurol* 518:800–814
- Qin Z, Barthel LK, Raymond PA (2009) Genetic evidence for shared mechanisms of epimorphic regeneration in zebrafish. *Proc Natl Acad Sci USA* 106:9310–9315
- Raymond PA, Barthel LK, Bernardos RL et al (2006) Molecular characterization of retinal stem cells and their niches in adult zebrafish. *BMC Dev Biol* 6:36
- Sherpa T, Fimbel SM, Mallory DE et al (2008) Ganglion cell regeneration following whole-retina destruction in zebrafish. *Dev Neurobiol* 68:166–181
- Thummel R, Enright JM, Kassen SC et al (2010) Pax6a and Pax6b control novel regulatory points during neuronal progenitor cell proliferation in the regenerating zebrafish retina. *Exp Eye Res* 90:572–582
- Thummel R, Kassen SC, Montgomery JE et al (2008) Inhibition of Müller glial cell division blocks regeneration of the light-damaged zebrafish retina. *Dev Neurobiol* 68:392–408
- Vihtelic TS, Hyde DR (2000) Light-induced rod and cone cell death and regeneration in the adult *albino* zebrafish (*Danio rerio*) retina. *J Neurobiol* 44:289–307
- Yurco P, Cameron DA (2005) Responses of Müller glia to retinal injury in adult zebrafish. *Vis Res* 45:991–1002

Chapter 55

The Genetics of Outer Segment Morphogenesis in Zebrafish

Alison L. Reynolds, Oliver E. Blacque, and Breandán N. Kennedy

Keywords Zebrafish • Photoreceptor • Outer segment • Mutants • Blindness • Intraflagellar transport • Phototransduction

55.1 Introduction

55.1.1 *Photoreceptor Outer Segments*

Photoreceptors are vision-enabling sensory cells positioned in the outer retina. These cells detect light, and contain morphological and molecular specialisations that convert photons into nerve impulses during phototransduction. Morphologically, vertebrate photoreceptors contain outer segments (OS), inner segments (IS), nuclear regions and synaptic terminals (Fig. 55.1). The OS is a modified sensory cilium joined to the IS by a connecting cilium. OS contain stacked membranous discs in which phototransduction initiates.

55.1.2 *Significance of Photoreceptor Outer Segments*

Understanding OS morphogenesis is significant biologically and biomedically. Inherited human blindness can result from mutations that cause defective or absent OS, compromising phototransduction and visual function. As the photoreceptor OS

A.L. Reynolds (✉) • O.E. Blacque • B.N. Kennedy (✉)
UCD School of Biomedical and Biomolecular Sciences, UCD Conway Institute,
University College Dublin, Belfield, Dublin 4, Ireland
e-mail: alison.reynolds@ucd.ie; brendan.kennedy@ucd.ie

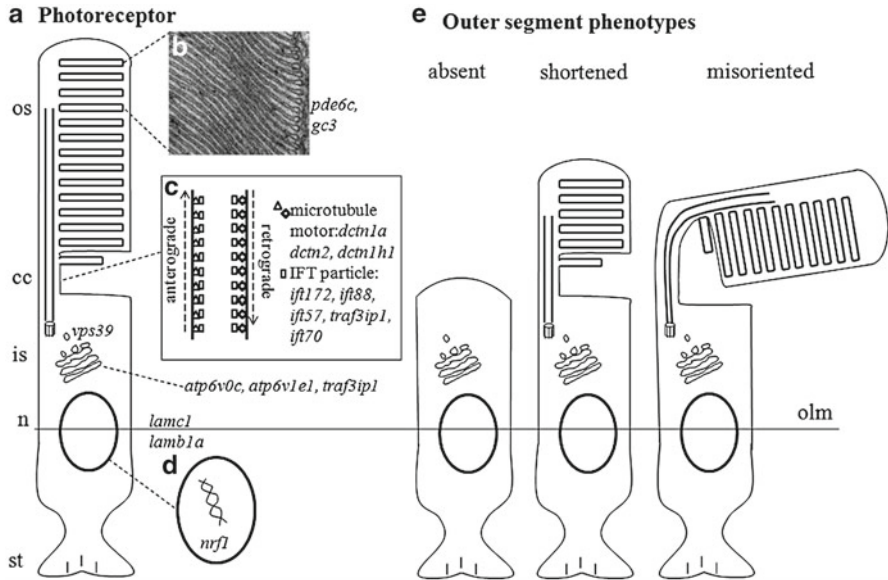


Fig. 55.1 Schematic of a normal photoreceptor (a) showing cellular compartments: outer segment (os), connecting cilium (cc), inner segment (is), nucleus (n), synaptic terminal (st) and the cellular location of genes mutated in zebrafish OS mutants. (b) Transmission electron micrograph of zebrafish OS at 6 days post fertilisation. (c) Microtubule-dependent transport along the cc (*triangle* and *diamond shapes* microtubule-dependent motors, *rectangle shape* intraflagellar trafficking particle). (d) Nucleus. (e) Schematic of main OS phenotypes identified in zebrafish mutants: OS absent, OS shortened and OS misoriented (see Table 55.1). *OLM* outer limiting membrane

is a highly compartmentalised modified cilium, it serves as an excellent model to understand intraflagellar transport (IFT), which is central to cilium formation and maintenance. Primary cilia possess key signalling and transport functions in many vertebrate organs, and defects are associated with blindness, cystic kidneys and bone abnormalities.

55.1.3 Study of Photoreceptor Outer Segment Morphogenesis in Zebrafish

Zebrafish exhibit cone-mediated visual function by 3 days post fertilisation (dpf). This facilitates studies of cone function/dysfunction and complements studies in rod-dominant rodents. Zebrafish development proceeds rapidly, patterning the retina with cells equivalent to mammalian retina (Schmitt and Dowling 1999; Tsujikawa and Malicki 2004a). The ex utero development of zebrafish larvae is associated with maternal stores of wildtype genes/proteins in the yolk. This maternal expression often enables mutants to develop to larval stages, revealing retinal phenotypes

obscured in equivalent mammalian mutants due to embryonic lethality. Here, we review zebrafish mutants with OS defects and refer to some “morphant” studies that characterise OS genes using morpholino knockdown.

55.2 Zebrafish Mutant Screens

Randomly mutating the zebrafish genome has generated many mutants with phenotypic defects in OS morphogenesis and the unbiased identification of genes required for this process. Zebrafish mutants can be generated using either the chemical mutagen *N*-ethyl-*N*-nitrosourea to induce point mutations, or retroviruses to generate insertional mutants (Solnica-Krezel et al. 1994; Neuhauss et al. 1999; Mohideen et al. 2003; Amsterdam et al. 2004; Gross et al. 2005; Muto et al. 2005; Wehman et al. 2005). Mutants with OS defects are identified indirectly via screens for larvae with morphological defects in eye size or visual function. Visual mutants are often analysed by light/electron microscopy revealing a subset of mutants with defects in OS morphogenesis. The majority of mutants display recessive inheritance of the phenotype. In chemical mutants, the causative mutation can often be identified by mapping the mutation to a chromosome and evaluating candidate genes (Johnson et al. 1995). For insertional mutants, the mutated gene can be identified more readily using inverse PCR (Amsterdam and Hopkins 2004).

55.3 Zebrafish Outer Segment Mutants

Mutants with defects in OS morphogenesis fall into three categories: no OS, shortened OS or abnormal OS – often described as misoriented relative to the RPE (Fig. 55.1). In many cases, failure of OS formation leads to photoreceptor degeneration. There follows a brief description of OS mutants, divided broadly by gene function (Table 55.1).

55.3.1 Mutations in Genes Encoding Phototransduction Proteins

To date, only two mutants have been identified in which phototransduction genes cause OS defects: *pde6c* and *gc3*. Both genes are central to cone phototransduction relating to the timing of phenotypic screens in larvae, when vision is predominantly cone-mediated (Bilotta et al. 2001). The gene encoding a subunit of cone-specific cGMP phosphodiesterase is mutated in *pde6c* and *els* mutants (Stearns et al. 2007; Nishiwaki et al. 2008). These mutants show pan-retinal cone degeneration, beginning at 4 dpf in *pde6c* and 6 dpf in *els*. Both mutants exhibit OS defects. *pde6c* mutants

Table 55.1 Thirty-three zebrafish mutants with outer segment defects divided by gene function

Locus	Gene/Chr	Outer segment defect	Other affected systems
Genes encoding phototransduction proteins			
<i>el1/pde6c</i>	<i>pde6c/12</i>	Shortened	–
<i>zat</i>	<i>gc3/5</i>	Thinner	–
Genes encoding intracellular trafficking proteins			
<i>curly</i>	<i>ift57/2</i>	Shorter	Kidney, heart, body axis
<i>ovl</i>	<i>ift88/13, 9</i>	Absent	
<i>moe</i>	<i>ift172/20</i>	Absent	
<i>eli</i>	<i>traq3ip1/9</i>	Absent	
<i>mok</i>	<i>dcm1a/7</i>	Infrequent, disorganised	Heart, kidney, liver, CNS, olfaction
<i>ako</i>	<i>dcm2/6</i>	Mostly absent*	
<i>cnb</i>	<i>dync1h1/17</i>	Absent	Hair cells
<i>flr</i>	<i>ift70/3</i>	Absent	
<i>lbk</i>	<i>vps39/17</i>	Shorter	Kidney, body axis, hydrocephalus
<i>atp6v0c</i>	<i>atp6v0c/3</i>	Undeveloped/absent	Liver, pigment, intestine
<i>atp6v1e1</i>	<i>atp6v1e1/4</i>	Undeveloped/absent	Pigment, brain, liver, gut, CNS
Genes encoding structural proteins			
<i>gup</i>	<i>lamb1a/25</i>	Shorter	Pigment, brain, liver, gut, CNS, skeleton
<i>sly</i>	<i>lamc1/2</i>	Shorter	RPE, RGC, ST, lens, notochord, ISV, brain, muscle
Transcription factors			
<i>nrf</i>	<i>nrf1/4</i>	Fewer, deformed	RGC, Lens, ST, notochord, ISV, brain, muscle
Gene function other and unknown			
<i>odc1</i>	<i>odc1/14, 17</i>	Shorter/absent	Brain
<i>wrb</i>	<i>pwil15</i>	Shorter/absent	–
<i>fad</i>	<i>unk/2</i>	Shorter/absent	Heart, ear
<i>nbd</i>	<i>unk/?</i>	Rod OS shorter (adult)	Pigment
<i>nbe</i>	<i>unk/?</i>	Rod OS shorter (adult)	–

<i>nbj</i>	<i>unk</i> /?	Rod OS shorter (adult)	–
<i>nbg</i>	<i>unk</i> /?	Rod OS shorter (adult)	–
<i>rys</i>	<i>rys</i> /9	Shorter/absent	RPE
<i>tli</i>	<i>tli</i> /23	Absent	Pigment
<i>umm_s332</i>	<i>umm_s332</i> /?	Less PRs shorter	RPE
<i>umm_s507</i>	<i>umm_s507</i> /?	Less PRs shorter	–
<i>she</i>	<i>umm_s545</i> /?	Less PRs shorter	RPE
<i>vos</i>	<i>vos</i> /23	Less PRs shorter*	–
<i>wud</i>	<i>wud</i> /8	COS shorter (adult)	–
<i>yoi</i>	<i>yoi</i> /25	COS shorter (adult)	–
<i>bru</i>	<i>bru</i> /3	OS and IS absent	Pigment
<i>nie</i>	<i>nie</i> /?	Less PRs, malformed*	–

OS outer segment; PRs photoreceptors; RPE retinal pigmented epithelium; IS inner segment; RGC retinal ganglion cell; ON optic nerve; ST synaptic terminal (of photoreceptors); CNS central nervous system; ISV intersegmental vessel; * residual OS misoriented; *unk* unknown. References describing the OS defect are given in the text.

show extensive degeneration of cones and stubby OS at 5 dpf (Stearns et al. 2007). Although *els* mutants have stubby OS and mislocalisation of both rod and cone opsin, the OS ultrastructure appears normal at 6 dpf (Nishiwaki et al. 2008). *zatoichi* (*zat*) mutants are homozygous for a null mutation in the gene encoding cone-specific guanylyl cyclase 3, the ortholog of human *GUCY2D* (Muto et al. 2005). Although *pde6c*, *els* and *zat* mutants have defective visual function, the defect in OS morphology is less severe in *zat* mutants. *zat* OS are elongated but thinner than in wildtype (unpublished).

Both *pde6c* and *gc3* regulate cGMP levels. Aberrant cGMP levels may explain the photoreceptor degeneration observed in *zat*, *pde6c* and *els* mutants. However, OS defects may be explained by transport functions recently ascribed to retinal guanylate cyclases and cGMP-phosphodiesterases. Knockout of the mouse *Pde6d* subunit results in shorter rod OS, which correlate with impaired transport of *Pde6c* to the OS (Zhang et al. 2007; Karan et al. 2008). Furthermore, knockout of mouse guanylate cyclase 1 (*Gucy2e*) disrupts transport of *Pde6c* to OS (Karan et al. 2008; Karan et al. 2010). In the latter, guanylate cyclase-bearing membranes are proposed to transport peripheral membrane proteins required for OS morphogenesis from the endoplasmic reticulum.

55.3.2 Mutations in Intracellular Trafficking Genes

The largest class of mutants with OS morphogenesis defects involves intracellular trafficking-associated genes – related specifically to IFT, molecular motors and membrane transport.

55.3.2.1 Intraflagellar Transport Particle B proteins

IFT is a bidirectional motility of protein complexes along cilia, driven anterograde by kinesin-2 and retrograde by cytoplasmic dynein 2, and requiring the IFT particle, which consists of >20 proteins grouped into IFT-A and IFT-B subcomplexes. IFT is essential for cilium formation because it is thought to be a primary mechanism for transporting and distributing protein cargos (docked to IFT particles/motors) within the organelle (Blacque et al. 2008). As no proteins (and lipid) are synthesised in the OS, OS proteins must be transported from the IS via the relatively narrow connecting cilium to ensure normal visual function. Since many OS proteins are rapidly turned over (e.g. rhodopsin) and some OS structures are continually remodelled (e.g. membranous discs), high levels of active transport into the OS are required. Hence it is not surprising that IFT genes are highly represented in zebrafish mutants with OS defects.

OS defects have been found in four IFT-B subunit mutants – *ovl* (*ift88*), *curly* (*ift57*), *moe* (*ift172*) and *ftr* (*ift70*). In all cases, IS appear grossly normal; however, in *ovl*, *ftr* and *moe* mutants, OS are almost never formed (Doerre and Malicki 2002;

Tsujikawa and Malicki 2004b; Krock and Perkins 2008; Sukumaran and Perkins 2009). In contrast, OS form but fail to extend in *curly* mutants (Krock and Perkins 2008), which indicates that not all zebrafish IFT-B proteins contribute equally to OS formation and IFT-directed protein transport. Consistent with OS formation defects, all four mutants display opsin accumulation within IS, particularly at the apical membrane. Also, disorganised membrane material is observed near the connecting cilium of *curly* mutants (Krock and Perkins 2008), indicating that the final steps of IS transport also requires IFT-B proteins. Since most mouse IFT-B gene mutants are embryonic lethal prior to retinal differentiation, zebrafish is a leading vertebrate model for investigating the role of IFT particle genes in OS formation and in the wider question of protein transport into and out of a vertebrate cilium.

55.3.2.2 Microtubule-Dependent Molecular Motors

OS defects are found in mutant alleles of three subunits of cytoplasmic dynein motor complexes, namely *mok/dctn1a* (p150 glued subunit of dynactin), *akol/dctn2* (p50 dynamitin subunit of dynactin) and *cnbdync1h1* (cytoplasmic dynein heavy chain 1) (Doerre and Malicki 2001; Jing and Malicki 2009; Insinna et al. 2010). In *mok* fish, OS number is reduced, and those which do develop are smaller, severely disorganised and lost during the first 12 h of development, with opsin mislocalised to the IS (Doerre and Malicki 2001). OS are missing in most *ako* mutant retinas, with those remaining orientated sideways or basally (Jing and Malicki 2009). In *cnb* mutants, very few OS are observed and rhodopsin is mislocalised in IS (Insinna et al. 2010). In *mok*, *ako* and *cnb* mutants, abnormal OS formation is followed by a pan-retinal degeneration of the photoreceptor cell layer. Phenotypic differences between dynein 1 and dynactin subunit mutants may indicate differential requirements for OS formation. In support, morpholino knockdown of both dynactin subunits mostly caused IS polarity defects, without affecting the OS (Insinna et al. 2010). This has led to the suggestion that zebrafish dynein 1 functions independently of the dynactin adaptor in OS formation, but together with this adaptor in facilitating transport events (e.g. post-Golgi vesicle trafficking) required for proper establishment of IS polarity. It is not known whether dynein 1 operates in OS as a retrograde IFT motor, similar to that described for dynein 2 in many organisms, including zebrafish (Krock et al. 2009).

Mutant alleles of zebrafish kinesin-2 motor subunits have yet to be isolated. However, morpholinos targeting *kif17* (which forms a homodimeric kinesin-2 motor) exhibit a near total failure of OS formation in the central retina, together with mislocalisation of opsin to perinuclear regions (Insinna et al. 2008). Similarly, overexpression of a dominant negative variant of KIF17 causes immediate OS maintenance defects (Insinna et al. 2009). In contrast, overexpression of a dominant negative variant of KIF3B (a subunit of the canonical heterotrimeric kinesin-2 motor, kinesin II) results in early defects in IS membrane systems indicating that zebrafish kinesin II serves broader roles to KIF17 in photoreceptor cells, both within the IS and OS (Insinna et al. 2009).

55.3.2.3 Membrane Transport

At least four mutants associated with membrane transport possess OS defects. The *lbk* allele (disrupted *vps39* subunit of the HOPS complex involved in endolysosomal protein sorting), exhibits reduced OS length due to aberrant trafficking of endosomal vesicles (Schonthaler et al. 2008). Mutants of subunits of the V-ATPase complex, *atp6v0c* and *atp6v1e1* possess underdeveloped and absent OS (Nuckels et al. 2009), in addition to defects in cell proliferation and enhanced apoptosis. Since V-ATPases play roles in proton, protein and intracellular transport, as well as synaptic vesicle exocytosis and hedgehog signalling (Nuckels et al. 2009), membrane transport defects may underpin the OS defects in *atp6v0c* and *atp6v1e1* mutants. Finally, the *eli* mutant (disruption of *traf3ip1* gene) fails to form OS (Doerre and Malicki 2002). Membrane transport defects are associated with this phenotype because *eli* physically interacts with Rabaptin 5, an effector of the endosomal RAB5 GTPase, and can dislodge IFT20 from Golgi membranes when over-expressed (Omori et al. 2008; Follit et al. 2009). Since *eli* also interacts with IFT20 and binds to mouse IFT-B complexes as IFT54, *eli* may act as a bridging mechanism between the IFT particle and protein involved in ciliary membrane transport (Omori et al. 2008; Follit et al. 2009).

55.3.3 Mutations in Genes Encoding Structural Proteins

Mutants in genes encoding laminin subunits (*lamc1* and *lamb1a*) show defects in OS elongation (Biehler et al. 2007). Both *sly* and *gup* mutants exhibit severely shortened OS prior to photoreceptor degeneration. Laminins, heterotrimeric extracellular matrix proteins expressed in the outer limiting membrane and interphotoreceptor matrix maintain photoreceptor structure (Libby et al. 2000). Mutations in genes encoding laminin subunits may result in loss of structural support to OS, and failure to elongate.

55.3.4 Mutations in Genes Encoding Transcription Factors

The *nrf* mutant encodes a transcription factor, similar to human nuclear respiratory factor 1 (Becker et al. 1998). Photoreceptors are mostly absent in *nrf* mutants at 5 dpf, however those that form have correctly polarised but deformed OS. Loss of the *nrf1* gene causes extensive apoptosis at onset of visual function, possibly due to *nrf1* failing to correctly target the anti-apoptotic gene *bcl-2* (Becker et al. 1998). In mammals, the transcription factors *Crx* and *Nrl* are required for OS morphogenesis as they regulate expression of key OS structural and phototransduction proteins (Furukawa et al. 1999; Mears et al. 2001).

55.3.5 Other Outer Segment Mutants

Mutations in *wrb* and *odc1* genes lead to *pwi* and *odc1* mutants, both of which show little or no OS (Gross et al. 2005). *Odc1* encodes ornithine decarboxylase 1, an enzyme catalysing the biosynthesis of putrescine, a precursor for γ -aminobutyric acid. *wrb* encodes tryptophan-rich basic protein. The role of either gene in the retina is poorly understood, however inhibiting *odc* in developing rabbit retina disrupts cone morphology (Withrow et al. 2002).

Many OS mutants in novel genes or the causative genes remain unidentified. The *fad* mutant, a model for the pigment and blood-clotting disorder Hermansky–Pudlak syndrome (Bahadori et al. 2006), has shorter, misaligned OS. Four mutants with adult-onset night blindness have been identified, namely *nbd*, *nbe*, *nbf* and *nbg*, showing a variety of rod OS defects: OS thinning (*nbd*), severe degeneration and OS shortening (*nbe*), shortening of OS and degeneration (*nbf*) and a moderate rod OS degeneration (*nbg*) (Maaswinkel et al. 2003; Maaswinkel et al. 2005). It is possible that these late-onset mutants may be caused by a primary defect in known rod genes.

Five mutants were identified in screens for retinal stem cell mutants: *rys*, *she*, *unm_s322*, *unm_s507* and *unm_s545* (Wehman et al. 2005). *rys* mutants have shortened OS centrally and are missing OS peripherally. *she*, *unm_s322* and *unm_s507* mutants have a reduced number of photoreceptors with shortened OS. *wud* and *yoi* mutants both exhibit shortened or misaligned cone OS in adults (Muto et al. 2005). *tli* mutants fail to form OS (Nishiwaki et al. 2008). *vos* mutants have fewer photoreceptors and degenerated OS, and the few OS which form are misaligned and lie parallel (not perpendicular) to the RPE (Mohideen et al. 2003). *nie* mutants are similar, having fewer photoreceptors and those OS which form are misoriented and have an abnormal shape. *Bru* mutants fail to form either inner or outer segments (Doerre and Malicki 2002).

55.4 Conclusion

Forward genetic screens in zebrafish are an alternative and unbiased approach to uncovering genes necessary for normal visual function. The abundance of maternally-expressed genes in zebrafish allows some mutants to develop to larval stages, contrasting with the embryonic lethality of equivalent mutants in mammals. This has enabled phenotypic characterisation of novel genes associated with OS defects, such as those observed in transport and structure (Biehlmaier et al. 2007; Sukumaran and Perkins 2009).

Abnormal OS morphogenesis is associated with many human retinal disorders: (*retinitis pigmentosa*, cone rod dystrophy, Leber congenital amaurosis) and ciliopathies (Adams et al. 2007; den Hollander et al. 2008). Several overlapping classes of genes are mutated in zebrafish and human retinal dystrophies e.g. transport proteins, phototransduction proteins, transcription factors and structural proteins

(RETNET <http://www.sph.uth.tmc.edu/retnet/>). Of the 208 loci identified in human retinal disease, mutations have been found in 167 genes (~80%), with the causative mutation unknown in the remaining 20%. It is possible that some of the classes of genes responsible for OS morphogenesis defects in zebrafish may cause human retinal disorders.

References

- Adams N, Awadein A, Toma H (2007) The retinal ciliopathies. *Ophthalmic Genet* 28:113–25
- Amsterdam A, Hopkins N (2004) Retroviral-mediated insertional mutagenesis in zebrafish. *Methods Cell Biol* 77:3–20
- Amsterdam A, Nissen R, Sun Z et al (2004) Identification of 315 genes essential for early zebrafish development. *Proc Natl Acad Sci USA* 101:12792–12797
- Bahadori R, Rinner O, Schonhaler HB et al (2006) The Zebrafish fade out Mutant: A Novel Genetic Model for Hermansky-Pudlak Syndrome. *Invest Ophthalmol Vis Sci* 47:4523–4531
- Becker TS, Burgess SM, Amsterdam AH et al (1998) Not really finished is crucial for development of the zebrafish outer retina and encodes a transcription factor highly homologous to human Nuclear Respiratory Factor-1 and avian Initiation Binding Repressor. *Development* 125:4369–4378
- Biehmaier O, Makhankov Y, Neuhaus SCF (2007) Impaired retinal differentiation and maintenance in zebrafish laminin mutants. *Invest Ophthalmol Vis Sci* 48:2887–2894
- Bilotta J, Saszik S, Sutherland SE (2001) Rod contributions to the electroretinogram of the dark-adapted developing zebrafish. *Dev Dyn* 222:564–570
- Blacque O, Cevik S, Kaplan O (2008) Intraflagellar transport: from molecular characterisation to mechanism. *Front Biosci* 13:2633–52
- den Hollander AI, Roepman R, Koenekoop RK et al (2008) Leber congenital amaurosis: Genes, proteins and disease mechanisms. *Prog Retin Eye Res* 27:391–419
- Doerre G, Malicki J (2001) A mutation of early photoreceptor development, mikre oko, reveals cell-cell interactions involved in the survival and differentiation of zebrafish photoreceptors. *J Neurosci* 21:6745–6757
- Doerre G, Malicki J (2002) Genetic analysis of photoreceptor cell development in the zebrafish retina. *Mech Dev* 110:125–138
- Follit JA, Xu F, Keady BT et al (2009) Characterization of mouse IFT complex B. *Cell Motil Cytoskeleton* 66: 457–468
- Furukawa T, Morrow EM, Li T et al (1999) Retinopathy and attenuated circadian entrainment in Crx-deficient mice. *Nat Genet* 23:466–470
- Gross JM, Perkins BD, Amsterdam A et al (2005) Identification of zebrafish insertional mutants with defects in visual system development and function. *Genetics* 170:245–261
- Insinna C, Baye L, Amsterdam A et al (2010) Analysis of a zebrafish *dync1h1* mutant reveals multiple functions for cytoplasmic dynein 1 during retinal photoreceptor development. *Neural Dev* 5:12
- Insinna C, Humby M, Sedmak T et al (2009) Different roles for KIF17 and kinesin II in photoreceptor development and maintenance. *Dev Dyn* 238:2211–2222
- Insinna C, Pathak N, Perkins B et al (2008) The homodimeric kinesin, Kif17, is essential for vertebrate photoreceptor sensory outer segment development. *Dev Biol* 316:160–170
- Jing X, Malicki J (2009) Zebrafish ale oko, an essential determinant of sensory neuron survival and the polarity of retinal radial glia, encodes the p50 subunit of dynactin. *Development* 136:2955–2964
- Johnson SL, Africa D, Horne S et al (1995) Half-Tetrad Analysis in Zebrafish: Mapping the *ros* mutation and the centromere of linkage group I. *Genetics* 139:1727–1735
- Karan S, Frederick J, Baehr W (2010) Novel functions of photoreceptor guanylate cyclases revealed by targeted deletion. *Mol Cell Biochem* 334:141–55

- Karan S, Zhang H, Li S et al. (2008) A model for transport of membrane-associated phototransduction polypeptides in rod and cone photoreceptor inner segments. *Vision Res* 48:442–452
- Krock B, Mills-Henry I, Perkins B (2009) Retrograde intraflagellar transport by cytoplasmic dynein-2 is required for outer segment extension in vertebrate photoreceptors but not arrestin translocation. *Invest Ophthalmol Vis Sci* 50:5463–5471
- Krock BL, Perkins BD (2008) The intraflagellar transport protein IFT57 is required for cilia maintenance and regulates IFT-particle-kinesin-II dissociation in vertebrate photoreceptors. *J Cell Sci* 121:1907–1915
- Libby RT, Champlaud M-F, Claudepierre T et al (2000) Laminin expression in adult and developing retinae: evidence of two novel CNS laminins. *J Neurosci* 20:6517–6528
- Maaswinkel H, Mason B, Li L (2003) ENU-induced late-onset night blindness associated with rod photoreceptor cell degeneration in zebrafish. *Mech Ageing Dev* 124:1065–1071
- Maaswinkel H, Riesbeck LE, Riley ME et al (2005) Behavioral screening for nightblindness mutants in zebrafish reveals three new loci that cause dominant photoreceptor cell degeneration. *Mech Ageing Dev* 126:1079–1089
- Mears AJ, Kondo M, Swain PK et al (2001) Nrl is required for rod photoreceptor development. *Nat Genet* 29:447–452
- Mohideen MAP, Beckwith LG, Tsao-Wu GS et al (2003) Histology-based screen for zebrafish mutants with abnormal cell differentiation. *Dev Dyn* 228:414–423
- Muto A, Orger MB, Wehman AM et al (2005) Forward genetic analysis of visual behavior in zebrafish. *PLoS Genet* 1:e66
- Neuhauß SCF, Biehmaier O, Seeliger MW et al (1999) Genetic disorders of vision revealed by a behavioral screen of 400 essential loci in zebrafish. *J Neurosci* 19:8603–8615
- Nishiwaki Y, Komori A, Sagara H et al (2008) Mutation of cGMP phosphodiesterase 6[alpha]-subunit gene causes progressive degeneration of cone photoreceptors in zebrafish. *Mech Dev* 125:932–946
- Nuckels RJ, Ng A, Darland T et al (2009) The vacuolar-ATPase complex regulates retinoblast proliferation and survival, photoreceptor morphogenesis, and pigmentation in the zebrafish eye. *Invest Ophthalmol Vis Sci* 50:893–905
- Omori Y, Zhao C, Saras A et al (2008) elipsa is an early determinant of ciliogenesis that links the IFT particle to membrane-associated small GTPase Rab8. *Nat Cell Biol* 10:437–444
- Schmitt E, Dowling J (1999) Early retinal development in the zebrafish, *Danio rerio*: light and electron microscopic analyses. *J Comp Neurol* 404:515–536
- Schonhaler HB, Fleisch VC, Biehmaier O et al (2008) The zebrafish mutant *lbk/vam6* resembles human multisystemic disorders caused by aberrant trafficking of endosomal vesicles. *Development* 135:387–399
- Solnica-Krezel L, Schier A, Driever W (1994) Efficient recovery of ENU-induced mutations from the zebrafish germline. *Genetics* 136:1–20
- Stearns G, Evangelista M, Fadool JM et al (2007) A mutation in the cone-specific PDE6 gene causes rapid cone photoreceptor degeneration in zebrafish. *J Neurosci* 27:13866–13874
- Sukumaran S, Perkins BD (2009) Early defects in photoreceptor outer segment morphogenesis in zebrafish *ift57*, *ift88* and *ift172* intraflagellar transport mutants. *Vision Res* 49:479–489
- Tsujikawa M, Malicki J (2004a) Genetics of photoreceptor development and function in zebrafish. *Int J Dev Biol* 48:925–34
- Tsujikawa M, Malicki J (2004b) Intraflagellar transport genes are essential for differentiation and survival of vertebrate sensory neurons. *Neuron* 42:703–716
- Wehman AM, Staub W, Meyers JR et al (2005) Genetic dissection of the zebrafish retinal stem-cell compartment. *Dev Biol* 281:53–65
- Withrow C, Ashraf S, O'Leary T et al (2002) Effect of polyamine depletion on cone photoreceptors of the developing rabbit retina. *Invest Ophthalmol Vis Sci* 43:3081–3090
- Zhang H, Li S, Doan T et al (2007) Deletion of PrBP/delta impedes transport of GRK1 and PDE6 catalytic subunits to photoreceptor outer segments. *Proc Natl Acad Sci USA* 104:8857–62

Chapter 56

Factor XIII_A Induction in the Retina and Optic Nerve After Optic Nerve Lesion in Goldfish

Kayo Sugitani, Kazuhiro Oogai, Hiroshi Nakashima, and Satoru Kato

Keywords Factor XIII_A • Optic nerve regeneration • Retinal ganglion cells • Wound healing • Transglutaminase • Neurite outgrowth

56.1 Introduction

Coagulation factor XIII is a plasma transglutaminase (TG) that consists of two catalytic A subunits and two noncatalytic B subunits as a heterotetramer (A₂B₂) (Schwartz et al. 1973). In blood, factor XIII promotes clot stability by catalyzing the formation of covalent cross-linking reactions in polymerized fibrin. Additionally, in the cellular form, factor XIII_A exists as a homodimer of A subunits (A₂) in the platelet, monocytes, macrophages, megakaryocytes, and various tissues including lung, kidney, stomach, skin, esophagus, liver, testis, bone, spleen etc. (Derrick et al. 1993). The variety of tissue distributions of factor XIII_A suggests that it has an important role in multiple biological functions. Moreover, the involvement of factor XIII_A in wound healing has been suggested from the reports of factor XIII_A-deficient patients (Ariëns et al. 2002; Hsieh and Nugent 2008). Optic nerve injury in fish induced the regeneration-associated genes, such as transcription factors, neurotrophic factors, and anti-apoptotic factors in adult fish (Koriyama et al. 2007; Becker and Becker 2008; Nagashima et al. 2009). In our previous study, retinal TG (TG_R), belongs to TG family, was identified as an upregulated gene 20–40 days after

K. Sugitani (✉) • K. Oogai • H. Nakashima
Division of Health Sciences, Graduate School of Medicine,
Kanazawa University, 5-11-80 Kodatsuno, Kanazawa 920-0942, Japan
e-mail: sugitani@kenroku.kanazawa-u.ac.jp

S. Kato
Department of Molecular Neurobiology, Graduate School of Medicine, Kanazawa University,
13-1 Takara-machi, Kanazawa, Ishikawa 920-8640, Japan

optic nerve lesion (Sugitani et al. 2006). The present study showed that cellular factor XIII_A was induced more rapidly than TG_R in damaged retina and optic nerve after nerve injury. We discussed the physiological role of FXIII_A in optic nerve regeneration.

56.2 Materials and Methods

56.2.1 Experiment with Animals

Adult common goldfish (*Carassius auratus*; body length about 7–8 cm) were used throughout this study. Goldfish were anesthetized with ice-cold water. The optic nerve was sectioned 1 mm away from the posterior of the eyeball with scissors. After surgery, goldfish were kept in water tanks at 22 ± 1°C for 1–40 days. All animal cares were performed according to the guidelines for animal experiments of Kanazawa University. We paid specific attention to minimize the number of experimental animals and their suffering.

56.2.2 Cloning of Goldfish Neural Factor XIII_A

To identify the genes whose expression was specifically upregulated during the early stage of optic nerve regeneration, a cDNA library was prepared from the goldfish retina 24 h after optic nerve transection. Positive clones were selected by screening the cDNA library using the 600 bp cDNA probes for factor XIII_A generated as referring to zebrafish and blowfish factor XIII_A cDNA. Sequencing analysis was performed using the ABI Prism 310 Genetic Analyzer (Applied Biosystems, Foster City, CA, USA) and a BigDyeTerminator V.1.1 Cycle Sequencing Kit (Applied Biosystems).

56.2.3 In Situ Hybridization

Tissue fixation and cryosectioning were carried out as described previously (Barthel and Raymond 1993). Briefly, eyes were enucleated, bisected, and fixed in 4% paraformaldehyde solution containing 0.1 M phosphate buffer (pH 7.4) and 5% sucrose for 2 h at 4°C. After infiltration with increasing concentrations of sucrose (5–20%), followed by overnight incubation in 20% sucrose at 4°C, the eyes were embedded in OCT compound, and sectioned at a thickness of 12 μm. In situ hybridization was performed on goldfish retinas and optic nerve using digoxigenin-labeled RNA probes which were generated from factor XIII_A cDNA amplified by PCR in the pGEM-T vector (Promega, Madison, WI, USA).

56.2.4 Retinal Explant Culture

Goldfish retinal explant culture was performed using naïve (intact) retina. Briefly, the retina was isolated under sterile conditions, and cut into 0.5 mm squares using scissors. Retinal explants were cultured on polyornithine-coated 35 mm culture dishes in 0.5 mL L-15 medium (Invitrogen) in 20 mM Hepes buffer (pH 7.4) containing 10% FCS, 100 U penicillin, and 100 µg/mL streptomycin at 28°C. Effects of recombinant factor XIIIa (1–100 ng/mL) were tested by adding to the culture medium. Neurite outgrowth from the retinal explants was assayed by measuring the length and density of neurites in each explant (total 40–50 explants) in 35 mm dish. Finally, the percentage of explants showing positive neurite outgrowth was compared under various culture conditions.

56.3 Results

56.3.1 Changes in Factor XIIIa Gene Expression in the Retina and Optic Nerve After Optic Nerve Injury

To obtain a full-length cDNA for factor XIIIa, we screened a cDNA library prepared from goldfish retinas at 1 day after optic nerve transection. One positive clone was isolated as a 2,580 bp fragment from 300,000 plaques screened, and the cDNA was identified as full-length of coagulation factor XIII A subunit (factor XIIIa) encoded 744 amino acid residues with a predicted molecular mass of 83.8 kDa.

The expression of factor XIIIa mRNA in the goldfish retina and optic nerve was investigated after optic nerve transection using in situ hybridization. Very weak signals for the factor XIIIa could be seen in the inner nuclear layer and the ganglion cell layer of control retina (Fig. 56.1a). The signals of factor XIII mRNA in the retina started to increase at 1 day and peaked at 3–10 days (Fig. 56.1b) and then

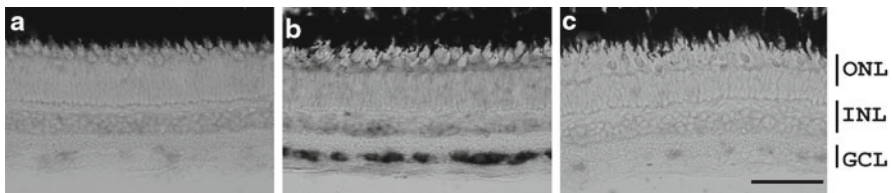


Fig. 56.1 In situ hybridization of factor XIIIa mRNA in goldfish retina after optic nerve injury. (a) Faint signals of factor XIIIa mRNA are observed in the inner nuclear layers (INL) and the ganglion cell layers (GCL) of control retina. (b) Seven days after axotomy, levels of factor XIII mRNA increased only in the GCL. (c) Expression of factor XIIIa mRNA in the GCL gradually decreased to control levels by 20 days after axotomy. Scale bar = 50 µm

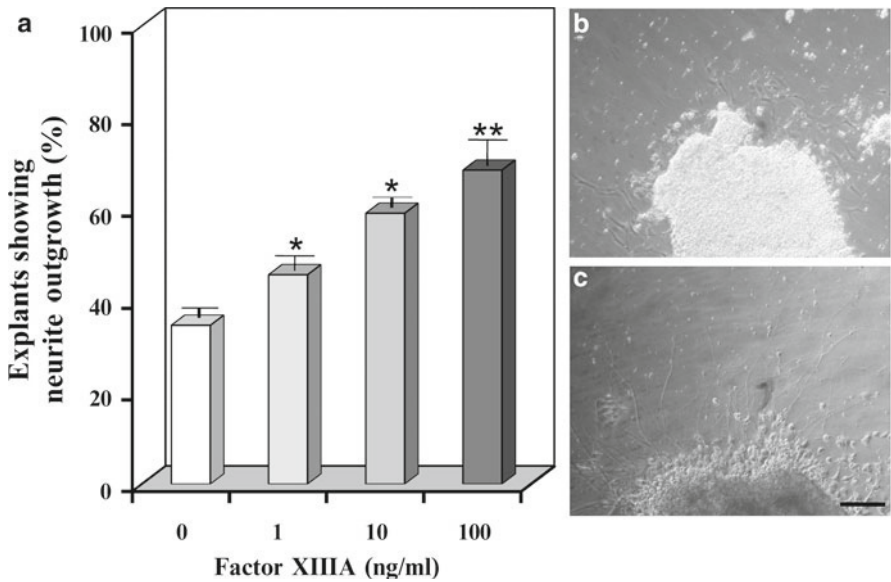


Fig. 56.2 Explant culture of adult goldfish naïve retinas treated with recombinant factor XIIIa protein. (a) Graphical representation of the neurite outgrowth for 2 days of culture. The x axis indicates concentrations of the factor XIIIa, the y axis on the left indicates percentage of explants which have more than five neurites. (b) No addition. (c) Recombinant factor XIIIa protein (100 ng/mL). Recombinant factor XIIIa increased number of explant with long neurites compared with the controls (* $P < 0.05$, ** $P < 0.01$ increased relative to control). Values represent mean \pm SD from five independent experiments. Scale bar = 200 μ m

decreased by 20 days after axotomy (Fig. 56.1c). Changes in factor XIIIa gene expression were localized only in the ganglion cell layer (Fig. 56.1b). In addition, factor XIIIa mRNA was also upregulated in the optic nerve lesion site (nonneuronal cells?) within a few days after optic nerve injury (data not shown).

56.3.2 Recombinant Factor XIIIa Protein Clearly Induced Neurite Outgrowth

Figure 56.2a shows a histogram of neurite outgrowth after treatment of recombinant factor XIIIa protein in the goldfish naïve retinal explant culture. Recombinant factor XIIIa protein enhanced neurite outgrowth in naïve retina (Fig. 56.2c) compared with the control culture (Fig. 56.2b) and this effect was dose dependent (Fig. 56.2a). Interestingly, these effects were observed only in the naïve retina.

56.4 Discussion

In this study, we used goldfish retinas for characterization of the cellular factor XIIIa. Eitan et al. demonstrated that a crude neural TG (factor XIIIa) enzyme prepared from injured goldfish optic nerves could partially regenerate injured rat optic nerves *in vivo* (Eitan et al. 1994). To investigate the functional role of factor XIIIa in CNS regeneration at a genetic level, we identified a full-length factor XIIIa cDNA clone using a retinal cDNA library from axotomized goldfish retinas (Matsukawa et al. 2004a). The cDNA clone for factor XIIIa encoded 744 amino acid residues with a molecular mass of 84 kDa. Three hours after goldfish optic nerve transection, a pretty number of factor XIIIa positive cells accumulate on the surrounding area of the optic nerve injured site (data not shown). Levels of factor XIIIa mRNA started to increase in the retina 1–3 days and peaked at 5–10 days after axotomy. Furthermore, we clearly showed that the increase in factor XIIIa mRNA was localized only in the retinal ganglion cells (RGCs).

TG family catalyzes posttranslational, covalent protein cross-linking reactions in diverse processes in nervous systems (Lesort et al. 2000). During goldfish optic nerve regeneration, we showed that expression of two types of TG gene, factor XIIIa and TG_R, was observed in the RGCs. However, these different types of TG are upregulated in different stage of optic nerve regeneration. TG_R is upregulated in the second stage (1–6 weeks after axotomy), which corresponds to the period of axonal elongation to the target and start of synaptic connection in the tectum (Sugitani et al. 2006). On the other hand, factor XIIIa is upregulated in the first stage, which corresponds to the period of preparation for axonal regrowth (Matsukawa et al. 2004b). In our culture study, we clearly demonstrated that recombinant factor XIIIa protein induced neurite outgrowth from naïve retina, but not from primed retina. By contrast, recombinant TG_R protein induced a drastic extension of long and thick neurites only from primed retina in which optic nerve had sectioned 5–7 days previously. These results correspond with the peak period of upregulation for these two types of TGs. Previous reports showed that fibronectin and collagen are putative substrates for factor XIIIa in wound healing (Ariëns et al. 2002). However, it remains unsolved what are the target substrates for cellular factor XIIIa in the optic nerve regeneration.

References

- Ariëns RA, Lai TS, Weisel JW et al (2002) Role of factor XIII in fibrin clot formation and effects of genetic polymorphisms. *Blood* 100:743–754
- Becker CG, Becker T (2008) Adult zebrafish as a model for successful central nervous system regeneration. *Restor Neurol Neurosci* 26:71–80
- Barthel LK, Raymond PA (1993) Subcellular localization of alpha-tubulin and opsin mRNA in the goldfish retina using digoxigenin-labeled cRNA probes detected by alkaline phosphatase and HRP histochemistry. *J Neurosci Methods* 50:145–152

- Derrick EK, Barker JN, Khan A et al (1993) The tissue distribution of factor XIIIa positive cells. *Histopathology* 22:157–162
- Eitan S, Solomon A, Lavie V et al (1994) Recovery of visual response of injured adult rat optic nerves treated with transglutaminase. *Science* 264:1764–1768
- Hsieh L, Nugent D (2008) Factor XIII deficiency. *Haemophilia* 14:1190–1200
- Koriyama Y, Homma K, Sugitani K et al (2007) Upregulation of IGF-I in the goldfish retinal ganglion cells during the early stage of optic nerve regeneration. *Neurochem Int* 50:749–756
- Lesort M, Tucholski J, Miller ML et al (2000) Tissue transglutaminase: a possible role in neurodegenerative diseases. *Prog Neurobiol* 61:439–463
- Matsukawa T, Arai K, Koriyama Y et al (2004b) Axonal regeneration of fish optic nerve after injury. *Biol Pharm Bull* 27:445–451
- Matsukawa T, Sugitani K, Mawatari K et al (2004a) Role of purpurin as a retinol-binding protein in goldfish retina during the early stage of optic nerve regeneration: its priming action on neurite outgrowth. *J Neurosci* 24:8346–8353
- Nagashima M, Sakurai H, Mawatari K et al (2009) Involvement of retinoic acid signaling in goldfish optic nerve regeneration. *Neurochem Int* 54:229–236
- Schwartz ML, Pizzo SV, Hill RL et al (1973) Human Factor XIII from plasma and platelets. Molecular weights, subunit structures, proteolytic activation, and cross-linking of fibrinogen and fibrin. *J Biol Chem* 248:1395–1407
- Sugitani K, Matsukawa T, Koriyama Y et al (2006) Upregulation of retinal transglutaminase during the axonal elongation stage of goldfish optic nerve regeneration. *Neuroscience* 142:1081–1092

Part VII
Analysis of Retinal Degeneration by
Imaging and Functional Testing

Chapter 57

Imaging the Photoreceptor Mosaic with Adaptive Optics: Beyond Counting Cones

Pooja Godara, Melissa Wagner-Schuman, Jungtae Rha,
Thomas B. Connor Jr., Kimberly E. Stepien, and Joseph Carroll*

Keywords Adaptive optics • Cone degeneration • Photoreceptor • RPE • Retinal imaging

57.1 Introduction

The use of AO imaging systems to image the living human retina is becoming increasingly widespread. A number of groups are utilizing AO technology to examine photoreceptors in the normal (Roorda and Williams 2002; Putnam et al. 2005; Jonnal et al. 2010) and diseased (Choi et al. 2006; Wolfing et al. 2006; Duncan et al. 2007; Carroll et al. 2008; Chen et al. 2010) retina. Owing to their high contrast, identifying cones in AO images has proved relatively easy – semi-automated techniques to identify cone photoreceptors are now widely used (Li and Roorda 2007; Rossi and Roorda 2010). Thus, a major focus in the analysis and interpretation of AO images

*Pooja Godara and Melissa Wagner-Schuman contributed equally to this work

P. Godara • J. Rha • T.B. Connor Jr. • K.E. Stepien
Department of Ophthalmology, Medical College of Wisconsin, Milwaukee, WI 53226, USA

M. Wagner-Schuman
Department of Ophthalmology, Medical College of Wisconsin, Milwaukee, WI 53226, USA

Departments of Ophthalmology and Biophysics, Medical College of Wisconsin,
Milwaukee, WI 53226, USA

J. Carroll (✉)
Department of Ophthalmology, Medical College of Wisconsin, Milwaukee, WI 53226, USA

Departments of Ophthalmology and Biophysics, Medical College of Wisconsin,
Milwaukee, WI 53226, USA

Departments of Ophthalmology and Biophysics, and Cell Biology, Neurobiology, and Anatomy,
Medical College of Wisconsin, Milwaukee, WI 53226, USA
e-mail: jcarroll@mcw.edu

has been density, spacing, or regularity of the cone mosaic. However, we believe that there may exist other important features in these images that may not get captured by these metrics. It is important to establish what other features should be captured from these images and begin to discuss what they might mean, specifically with regard to photoreceptor health.

Here, we describe three cases with unusual AO retinal images. This descriptive case series demonstrates that while AO imaging has shed enormous light on the cellular basis of visual abnormalities in retinal degenerations, several questions remain. While the underlying disease etiology is uncertain in these examples, the presence or absence of the cones is secondary to potentially more meaningful features involving the photoreceptor mosaic. A similar logic applies to optical coherence tomography images – there is more data to be gained from these images than just retinal or sublayer thickness (i.e., inner segment/outer segment (IS/OS) reflectivity). Continued development of new image analysis metrics should increase the clinical utility of both imaging modalities.

57.2 Materials and Methods

Three patients who presented with different retinal conditions were evaluated. All patients underwent a comprehensive clinical examination, fundus photography, and slit lamp biomicroscopy. SD-OCT line scans were obtained with the Biotigen SD-OCT (Biotigen, Inc., Durham, NC, USA) as previously described (Tanna et al. 2010). Images of the cone photoreceptor mosaic were obtained and processed using a flood-illuminated AO ophthalmoscope as previously described (Rha et al. 2009). Participants provided written informed consent, and research was approved by the local Institutional Review Board.

57.3 Results

57.3.1 Case 1

Patient 1 was a 15-year-old boy referred for evaluation of macular drusen. He was asymptomatic and reported no particular visual complaints at that time. Visual acuity was 20/20 OU. Clinical examination was significant for bilateral scattered, well-defined, fine, hard drusen in the central macula and extending radially into the temporal midperiphery (Fig. 57.1). Family history was noteworthy for the patient's father was diagnosed with similar findings at age 30, macular degenerative changes in the paternal grandfather, and an aunt and uncle having severe macular degeneration findings. A diagnosis of dominant drusen also known as Doyme's honeycomb dystrophy was made. The high-resolution SD-OCT images from the patient's right eye revealed retinal pigment epithelium (RPE) excrescences with underlying moderately reflective material consistent with drusen, though not all druse could be seen

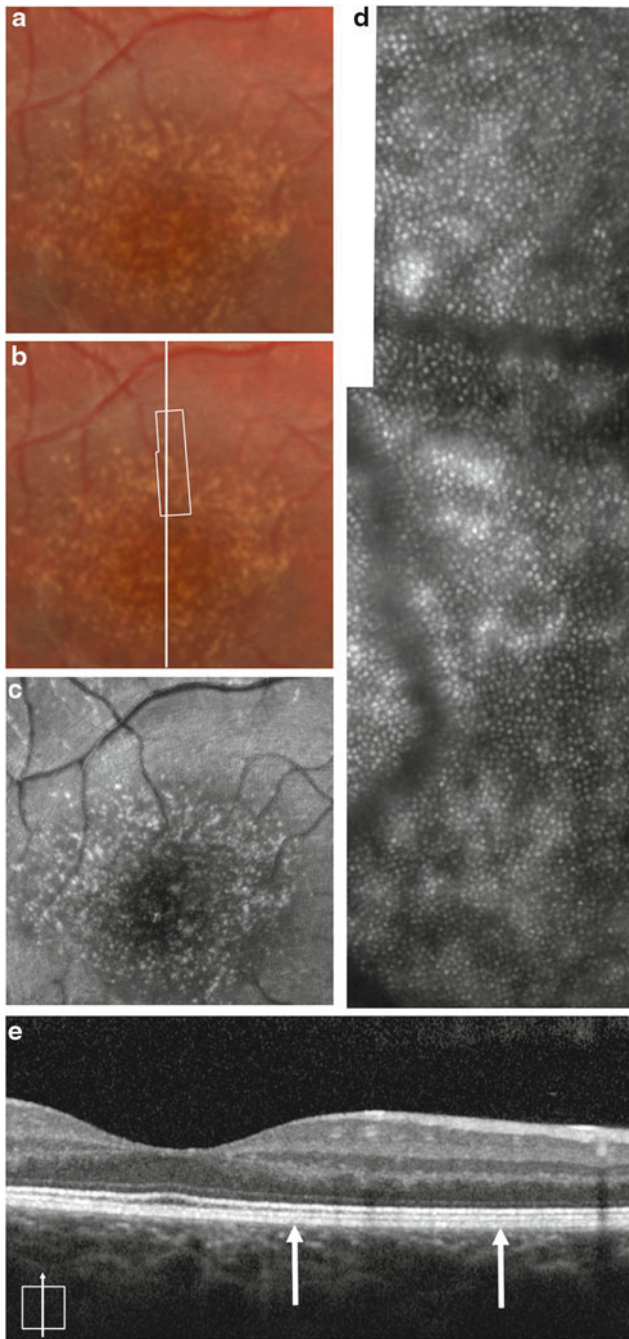


Fig. 57.1 Multimodal imaging of a patient with dominant drusen. Color fundus photograph (**a**, **b**) and autofluorescence (**c**) images showing numerous scattered drusen in central fundus. The *white box* in (**b**) represents the area of the AO image (**d**). (**e**) High-resolution SD-OCT image taken at the location of the horizontal line (**b**). *Thin vertical arrows* represent the boundary of the retinal area imaged with AO

on the SD-OCT images (Fig. 57.1). AO imaging revealed a regular photoreceptor mosaic with areas of hyper-reflectivity coinciding with the location of the drusen. Though the photoreceptor mosaic is regular and undisrupted, the areas of hyper-reflectivity are different from what is seen in normal retina. In normal retinas, the RPE absorbs light that is not captured by cones resulting in the high contrast between reflective cones and the nonreflective RPE. In the data from patients with albinism published by our group (McAllister et al. 2010), we observed similar heterogeneous patterns of reflectivity due to melanin clumping (where the absence of melanin caused an increase in reflectivity and a reduction in the local cone contrast). Thus in the current patient, we believe that the increased reflectivity associated with the drusen can be attributed to increased scatter from the RPE (not likely due to decreased melanin, but rather accumulation of some other material). It may be that local cone contrast could be used in conjunction with OCT-based measures of drusen anatomy (Khanifar et al. 2008; Jain et al. 2010) to monitor drusen progression – even though the density and regularity of the overlying cone photoreceptors may remain unchanged. AO flood-illuminated systems may differ with AOSLO systems in capturing this altered reflectivity.

57.3.2 Case 2

Patient 2 was a 17-year-old girl who presented for evaluation of decreased vision with a family history significant for retinal dystrophy. Visual acuity without correction was 20/40 +2 OD 20/30 –1 OS, and color vision was decreased. Fundus exam showed subtle bull’s eye pigmentation in the macular region, left eye greater than right. The high-resolution SD-OCT images from the patient’s right eye revealed preserved retinal layers in the central fovea with loss of the IS/OS layer and the external limiting membrane (ELM) in the perifoveal region in a ring like fashion corresponding to the bull’s eye lesion. Figure 57.2 shows images from the area where the IS/OS was absent, yet significant structure remains. The low frequency hypo-reflective structures are probably RPE cells, as the average spacing of these structures (13.1 μm) is similar to previous reports (Roorda et al. 2007). However, the smaller hyper-reflective structures may or may not represent cone structure; the SD-OCT image would suggest an absence of cones. As such, algorithms which simply detect bright spots (Xue et al. 2007) will lead to misinterpretation of the images. That said, it is difficult to reconcile what (if not cones) these structures could be. Correlating microperimetry with high-resolution images certainly appears to be the way forward in interpreting difficult images like these (Yoon et al. 2009).

57.3.3 Case 3

Patient 3 was a 35-year-old woman referred for abnormal pigmentary changes in her retina and complaints of difficulty with night vision. Past ocular history was significant for being told she had a “weird” appearance of her retina 11 years prior

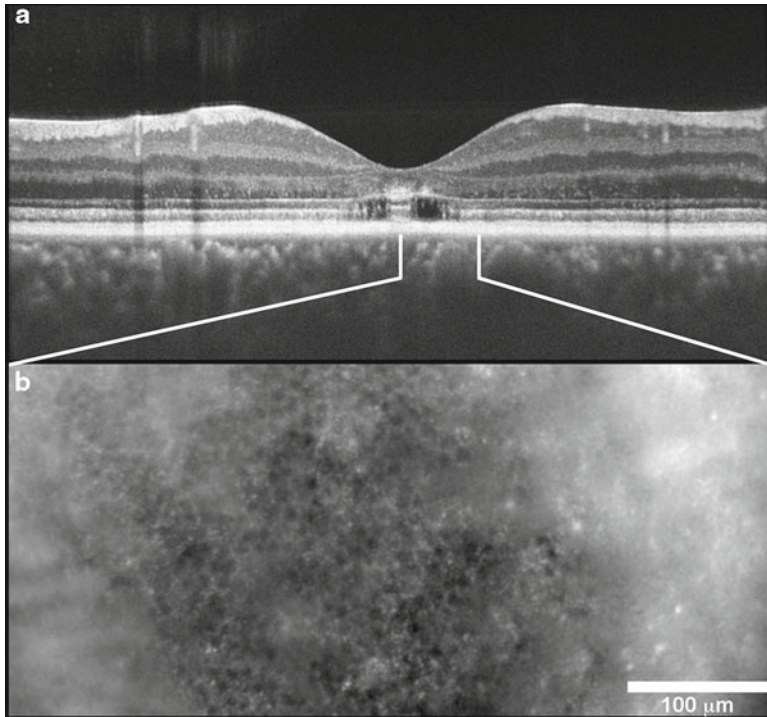


Fig. 57.2 Image from a patient with a bull's eye maculopathy. **(a)** SD-OCT scan shows that retinal layers are preserved in a small island in the central macula with loss of the IS/OS layer and the ELM in the perifoveal region. The *white lines* indicate the area imaged with AO in **(b)**

to this examination. Family history was significant for her father having macular dystrophy with degenerative changes at 45 years of age. Her visual acuity without correction was 20/25 –1 OD and 20/25 OS. Fundus exam revealed a mottled appearance of the retina bilaterally. In the posterior pole of the right eye there are focal areas of atrophy seen both superior and inferior to the fovea. AO images of the retina had a varied appearance (Fig. 57.3). Near the foveal center, some cones appeared with inverted contrast, yet they remained regularly integrated with the surrounding normally reflective cones. The cone spacing here is near normal values (3.99 vs. 4.49 μm). However at 2.0° from the fovea, cone spacing is increased in the patient (7.42 vs. 5.58 μm), indicating lower cone density. In addition, the cones take on a “bubble-wrap” type appearance, which has been described before (Duncan et al. 2007; Godara et al. 2010). The raised appearance results from a nonuniform reflectance across the cone aperture. Measures of cone density or cone spacing do not capture the abnormal appearance of these cells, which may be a transient indicator of cone health and should be investigated further.

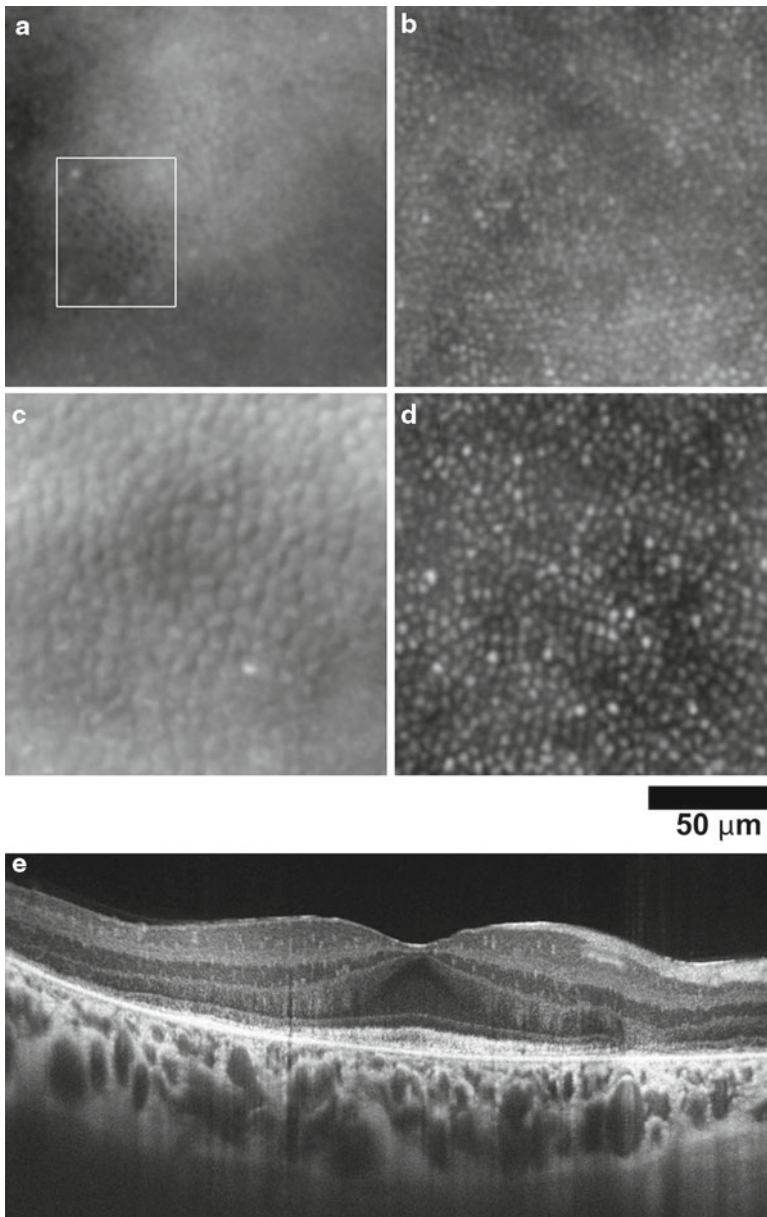


Fig. 57.3 Images from a patient with focal areas of retinal atrophy and visual loss (**a, c**) and a normal control (**b, d**). At 0.5° eccentricity (**a, b**), a small patch of cones in the patient (**a, white box**) appears with inverted contrast compared to normal. At 2.0° eccentricity (**c, d**), the cones in the patient (**c**) appear raised, owing to nonuniform reflectivity across the cone aperture. (**e**) SD-OCT image through the fovea, showing diffuse disruption of the IS/OS layer at the locations imaged with AO

57.4 Discussion

AO retinal imaging has rapidly advanced as a clinical imaging tool in the last decade. Now, we have the ability not only to image photoreceptors consistently at the same location but also to follow up the changes longitudinally over time. The above clinical examples highlight the need to have a better understanding of the information present in these AO images (beyond cone density or regularity), as this information is likely to increase the clinical utility of AO imaging.

Acknowledgments The authors thank B. Schroeder and P.M. Summerfelt for technical assistance. J. Carroll is the recipient of a Career Development Award from Research to Prevent Blindness. This study was supported by NIH grants P30EY001931 and R01EY017607, The Thomas M. Aaberg, Sr. Retina Research Fund, and an unrestricted grant from Research to Prevent Blindness. This investigation was conducted in a facility constructed with support from Research Facilities Improvement Program Grant Number C06 RR-RR016511 from the National Center for Research Resources, NIH. Additional support comes from the Clinical and Translational Science Institute and the Biotechnology Innovation Center, NIH CTSA Grant UL1 RR 031973.

References

- Carroll J, Choi SS, Williams DR (2008) In vivo imaging of the photoreceptor mosaic of a rod monochromat. *Vis Res* 48:2564–2568
- Chen YF, Roorda A, Duncan JL (2010) Advances in imaging of Stargardt disease. *Adv Exp Med Biol* 664:333–340
- Choi SS, Doble N, Hardy JL et al (2006) In vivo imaging of the photoreceptor mosaic in retinal dystrophies and correlations with visual function. *Invest Ophthalmol Vis Sci* 47:2080–2092
- Duncan JL, Zhang Y, Gandhi J et al (2007) High-resolution imaging with adaptive optics in patients with inherited retinal degeneration. *Invest Ophthalmol Vis Sci* 48:3283–3291
- Godara P, Rha J, Tait DM et al (2010) Unusual adaptive optics findings in a patient with bilateral maculopathy. *Arch Ophthalmol* 128:253–254
- Jain N, Farsiu S, Khanifar AA et al (2010) Quantitative comparison of drusen segmented on SD-OCT versus drusen delineated on color fundus photographs. *Invest Ophthalmol Vis Sci* 51:4875–4883
- Jonnal RS, Besecker JR, Derby JC et al (2010) Imaging outer segment renewal in living human cone photoreceptors. *Opt Express* 18:5257–5270
- Khanifar AA, Koreishi AF, Izatt JA et al (2008) Drusen ultrastructure imaging with spectral domain optical coherence tomography in age-related macular degeneration. *Ophthalmology* 115:1883–1890
- Li KY, Roorda A (2007) Automated identification of cone photoreceptors in adaptive optics retinal images. *J Opt Soc Am A* 24:1358–1363
- McAllister JT, Dubis AM, Tait DM et al (2010) Arrested development: High-resolution imaging of foveal morphology in albinism. *Vis Res* 50:810–817
- Putnam NM, Hofer HJ, Doble N et al (2005) The locus of fixation and the foveal cone mosaic. *J Vis* 5:632–639
- Rha J, Schroeder B, Godara P et al (2009) Variable optical activation of human cone photoreceptors visualized using short coherence light source. *Opt Lett* 34:3782–3784
- Roorda A, Williams DR (2002) Optical fiber properties of individual human cones. *J Vis* 2: 404–412

- Roorda A, Zhang Y, Duncan JL (2007) High-resolution in vivo imaging of the RPE mosaic in eyes with retinal disease. *Invest Ophthalmol Vis Sci* 48:2297–2303
- Rossi EA, Roorda A (2010) The relationship between visual resolution and cone spacing in the human fovea. *Nat Neurosci* 13:156–157
- Tanna H, Dubis AM, Ayub N et al (2010) Retinal imaging using commercial broadband optical coherence tomography. *Br J Ophthalmol* 94:372–376
- Wolfing JI, Chung M, Carroll J et al (2006) High-resolution retinal imaging of cone-rod dystrophy. *Ophthalmology* 113:1014–1019
- Xue B, Choi SS, Doble N et al (2007) Photoreceptor counting and montaging of en-face retinal images from an adaptive optics fundus camera. *J Opt Soc Am A* 24:1364–1372
- Yoon MK, Roorda A, Zhang Y et al (2009) Adaptive optics scanning laser ophthalmoscopy images in a family with the mitochondrial DNA T8993C mutation. *Invest Ophthalmol Vis Sci* 50:1838–1847

Chapter 58

Baseline Imaging Reveals Preexisting Retinal Abnormalities in Mice

Brent A. Bell, Charles Kaul, Mary E. Rayborn, and Joe G. Hollyfield

Keywords Fundus • Baseline • Imaging • Mice • Retina • Lesion • Abnormalities • Scanning laser • Ophthalmoscope • Optical coherence tomography

58.1 Introduction

Noninvasive intraocular imaging in small animals is becoming increasingly popular among vision researchers. Imaging instruments originally designed for clinical use in humans have found utility in the research laboratory (Hawes et al. 1999; Huber et al. 2009; Luhmann et al. 2009). Several instruments are now commercially available that can be used to obtain images of the rodent eye. Thanks to the extensive development required for clinical use, these devices are now very robust, user-friendly and relatively easy to operate. In the last few years, some instruments have undergone technical improvements to further enhance the quality of images obtained in rodents, especially mice. These changes improve light coupling efficiency and collection, provide for a larger field of view (FOV) with wide-field objectives, permit automatic real-time signal averaging and auto-tracking software, and enhance spatial and axial resolution when coupled with better scanning systems. Many have already reported the benefit these enhanced systems offer for characterization of small animal retinal morphology. Morphological changes, such as mutant phenotypes (Hawes et al. 1999), retinal lesions and degeneration (Fischer et al. 2009; Huber et al. 2009; Ruggeri et al. 2009), and age-related structural changes (Luhmann et al. 2009), are just a few examples. In addition, hybrid instruments combining more than one imaging modality (e.g., both scanning laser ophthalmoscopy (SLO)

B.A. Bell • C. Kaul • M.E. Rayborn • J.G. Hollyfield (✉)
Department of Ophthalmology, Cole Eye Institute (i31),
Cleveland Clinic Lerner College of Medicine, Cleveland, OH 44195, USA
e-mail: hollyfj@ccf.org

and spectral-domain optical coherence tomography (OCT)) are now available. The benefits of a multiple modality instrument have been previously reported for mice (Kocaoglu et al. 2007).

These imaging devices enable rapid, noninvasive nondestructive observations of retinal morphology *in vivo*. The collected images provide information that is similar to histological analysis and for routine structural analysis, may ultimately replace this tedious time and resource-consuming technology (Huber et al. 2009).

Imaging becomes even more powerful and clearly distances itself from histology when data collection occurs sequentially over multiple time points. This form of repeated imaging, including one set of baseline images collected prior to commencement of any planned experiments, can be an invaluable asset to any experimental study. First, baseline imaging is extremely important because it will reveal potentially problematic animals that may have preexisting pathology. Undetected, these animals may complicate and confound the analyses that are planned many days or months following the initiation of an experimental manipulation. Second, it could save substantial resources lost when experiments utilize undetected, compromised animals. Third, serial imaging over the course of a study allows an assessment of sequential changes. And finally, this technology permits each animal to serve as its own control if imaging is performed prior to initiation of experiments (Eter et al. 2008).

After identifying profound retinal abnormalities in presumably “normal,” untreated animals, we implemented routine baseline imaging with SLO and OCT to identify mice with atypical retinas. Our objective was to evaluate the utility and importance of using one or more retinal imaging techniques to establish baseline structure levels prior to commencement of extensive research studies with those animals. We have determined prevalence levels for retinal changes in several mouse strains, including wild-type and transgenic knockout lines.

58.2 Materials and Methods

58.2.1 *Animal Models*

Imaging data were collected from mice ranging in age from 2 to 14 months post partum. Mice studied included C57BL/6J and BALB/c, complement knockouts C3, C4, factor B, factor H, and SOD1 (see Table 58.1 for mouse numbers). C57BL/6J and BALB/c were obtained from reputable vendors (The Jackson Laboratory, Bar Harbour, ME and Taconic Farms, Inc., Hudson, NY). All knockouts were bred and maintained in-house in the Biological Resources Unit (BRU) at The Cleveland Clinic (CC). Animals were housed with cyclic fluorescent lighting (12/12-h light/dark) and provided food and water *ad libitum*. The CC Institutional Animal Care and Use Committee (IACUC) approved all experiments.

Table 58.1 Summary of results for mice imaged at 2–4 (i.e., baseline) or 6–14 months

Age (months)	Details	C57BL/6J	BALB/ cAnNTac	BALB/cJ	SOD1 ^{+/+} , SOD1 ^{-/-}	C3 ^{-/-}	C4 ^{-/-}	fH ^{-/-}	fB ^{-/-}
2-4	Mice imaged (#)	66	30	15	7	21	41	124	42
	Mice with retinal abnormalities (#)	1	1	15	1	1	7	7	1
	Prevalence of abnormalities (%)	1.5	3.3	100	14.3	4.8	17.1	5.6	2.4
6-14	Mice imaged (#)	17	-	-	13	43	22	8	12
	Mice with retinal abnormalities (#)	1	-	-	1	2	3	0	1
	Prevalence of abnormalities (%)	5.9	-	-	7.7	4.7	13.6	0	8.3

58.2.2 *Imaging Procedures*

Mice were anesthetized with 90 mg/kg of sodium pentobarbital. Cycloplegia was induced by administration of 2 μ L of 0.5% Mydrin[®]-P Tropicamide/Phenylephrine combination drops (Santen Pharmaceutical Co., Ltd, Japan). Drops were gently massaged into the eye using the lids followed by rinsing with balanced saline solution (BSS) (Alcon Laboratories, Inc., Ft. Worth, TX). Mice were then placed into an oxygenated chamber for 5 min and then removed for imaging with an HRA2 SLO (Heidelberg Engineering, Vista, CA), OCT (Bioptigen, Inc. Research Triangle Park, NC), and occasionally, color fundus photography (Paques et al. 2007; Luhmann et al. 2009; Gabriele et al. 2010). SLO imaging included collection of dark-field reflectance and autofluorescent (AF) images with both blue (488 nm) and IR (795 and 830 nm). Using a 55° wide-field lens, SLO images of the retina were obtained with the optic nerve centrally positioned in the FOV. Additional views of the peripheral regions were obtained to further investigate the nasal, temporal, superior, and inferior quadrants. Eyes were occasionally rehydrated with BSS and mechanically massaged to simulate blinking as needed during imaging. After SLO imaging, the mouse was transferred to the OCT system where a volumetric scan (300 A-scans/B-scan \times 300 B-scans/volume) with a 50° lens and axial resolution of \sim 7 μ m was collected with the optic nerve again centrally located. After imaging, both eyes received Bacitracin Zinc and Polymyxin B Sulfate ophthalmic ointment (Bausch & Lomb, Inc., Tampa, FL) to prevent corneal dehydration during recovery. Mice were placed in a warmed, oxygenated chamber and then returned to normal vivarium following recovery.

58.2.3 *Histology*

Histological processing has been previously described (Hollyfield et al. 2008).

58.3 Results

Over 450 mice were evaluated using visible-light fundus, SLO, and OCT imaging. Imaging procedures and animal recovery were successful in that only six mice expired as result of being anesthetized and imaged. Using primarily SLO and OCT, two independent observers identified retinal abnormalities (Fig. 58.1) that were obvious and readily apparent.

Figure 58.1 is an example of a retinal abnormality found in a SOD1^{+/+} mouse by SLO and visible-light fundus imaging that was later confirmed by histology. The lesion found was quite expansive (0.3 \times 0.5 mm) but thin and was later identified as a doubling of the retinal pigment epithelium (RPE) by histology. Despite the thin

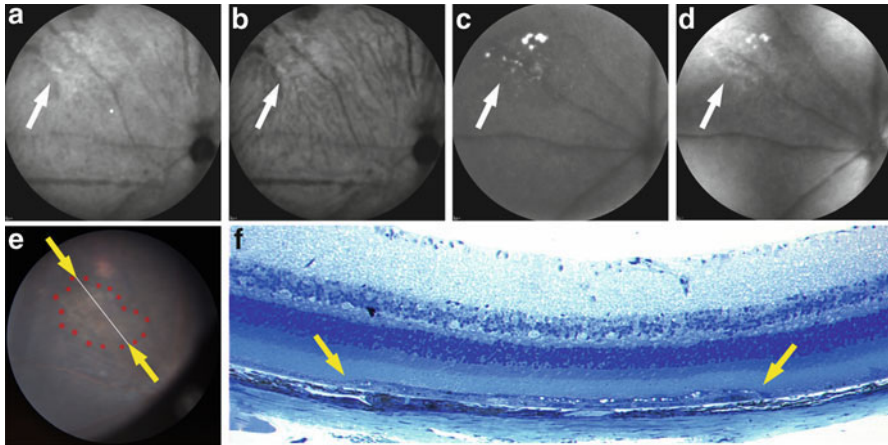


Fig. 58.1 A prominent abnormality found superior-temporal in a naïve, 4-month-old, *SOD1^{+/+}* mouse. IR reflectance (**a**), IR dark-field (**b**), autofluorescence (**c**), and red free dark-field (**d**) images of the lesion collected using an HRA2 SLO. *White arrows (a–d)* point to the lesion detected by all four HRA2 imaging mode settings. Notice that each mode reveals different characteristics about the lesion. IR images (**a**, **b**) reveal suspicious irregularities that are faintly visible against the background mosaic that originates from the choriocapillaris. The AF image (**c**) shows hyperfluorescent AFF of varying size and intensity within the region of irregularity seen by IR. The red free image (**d**) shows the outline of a well-demarcated lesion that encompasses the foci observed by AF. A visible fundus image (**e**) of the lesion shows a discolored region (encircled by *red dots*) relative to dark background. The spot superior to the lesion with *pinkish-hue* is a vortex vein. Lesion histology (**f**) reveals RPE layer duplication, large vacuoles, and outer nuclear layer thinning. The location of the histology section (**f**) is denoted by the *dashed white line* in the visible fundus photo (**e**). *Yellow arrows* identify transitions between normal and abnormal tissue (**e**, **f**)

nature of this lesion, adequate contrast was still obtained with all four SLO image collection modes and visible-light fundus photography. The discovery of an abnormality in this animal prompted the implementation of baseline imaging for all mice enrolled into future experimental studies.

In addition to retinal abnormalities, suspected developmental abnormalities were also observed in many mice. These included retinal arteriole-venous malformations, hyaloid vessel remnants or “floaters”, and cataracts. These observations were not considered within the scope of this study, as our primary focus was lesions involving or originating from the outer retina.

First, we rapidly screened both eyes of each mouse to obtain SLO images. Second, suspected abnormalities in the SLO images were carefully screened by OCT to determine if the finding was substantiated in both imaging modalities. In many cases, abnormalities found by SLO could not be resolved or detected by OCT (i.e., false positives), and in far fewer instances, vice versa. Figure 58.2 is an example of abnormalities easily visualized by SLO but difficult to delineate by OCT. The images are from a 2-month old BALB/cJ mouse that had extensive findings at baseline detected primarily by SLO IR reflectance and AF imaging. This mouse strain

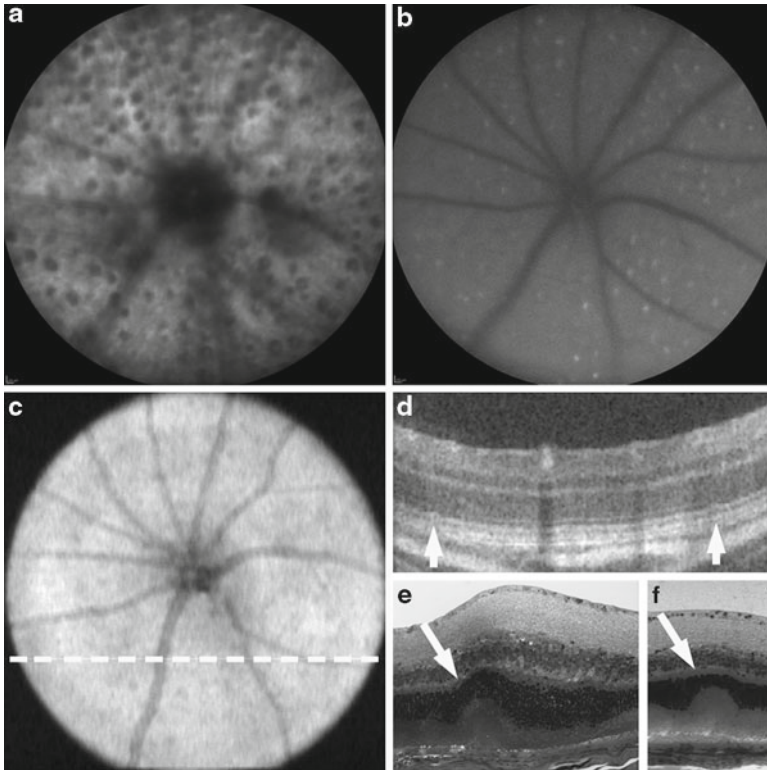


Fig. 58.2 Baseline SLO and OCT images collected from a 2-month-old BALB/cJ mouse. IR reflectance (a) and AF (b) SLO images collected show widely distributed, circular, punctate lesions and smaller AFF, respectively. The AFF seen by AF are in close proximity and overlap with the circular lesions observed by IR and thus the two observations appear to be related. OCT en-face image (c) denotes orientation of the B-scan image (d). The B-scan image shows subtle deviations (arrows) in the transition zone between inner and outer photoreceptor matrix but otherwise is an unremarkable, normal-looking image of a mouse retina. By contrast, histology of this animal (e, f) revealed that the lesions are pronounced retinal infoldings

from this particular vendor exhibited widely distributed circular abnormalities. These abnormalities were found bilaterally in all eyes (30/30) surveyed from 15 total mice. However, the number of abnormalities observed per eye was variable and ranged from approximately one to several dozen as shown in Fig. 58.2a. Autofluorescent foci (AFF) in Fig. 58.2b are superimposed over many of the circular patterns seen by SLO IR in Fig. 58.2a, which implies that they are interrelated. Some of these observations have been previously documented in BALB/c mice from a different vendor (Huber et al. 2009). The AFF have also been documented by multiple groups and are reported as being activated microglia and macrophages (Xu et al. 2008; Luhmann et al. 2009). Our histological analysis of the eyes from these mice revealed that the observed abnormalities are retinal infoldings (see Fig. 58.2e, f).

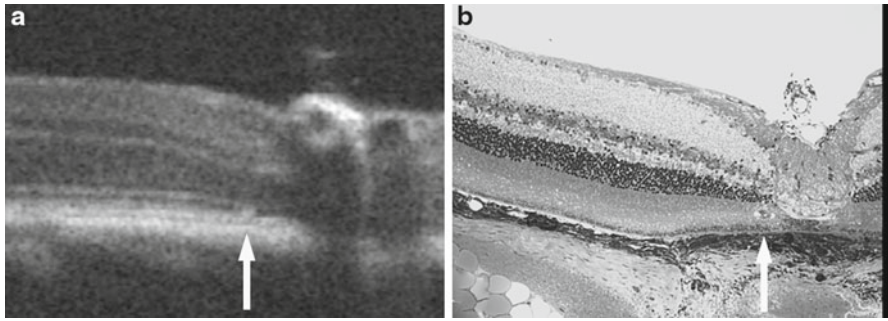


Fig. 58.3 OCT and histology from a 2-month-old $C4^{-/-}$ mouse. (a) B-scan showing that OCT is capable of resolving remarkably small abnormalities within the photoreceptor layer. (b) Histology of the retina verified that OCT detected a single RPE cell abnormality that impacts approximately half the thickness of the photoreceptor layer

For SLO, a suspected abnormality met one or more of the following criteria: (1) an irregular pattern relative to background mosaic architecture seen with IR reflectance and dark-field imaging (see Figs. 58.1a, b and 58.2a), (2) punctate or clustered, AFF in AF images (Figs. 58.1c and 58.2b), and (3) faint hypofluorescent areas in AF images (no example shown). A majority of abnormalities found with SLO were found to have a combination of both conditions “1” and “2” simultaneously. By contrast, condition “3” was quite rare in our study and seen only in a few mice.

A suspected OCT abnormality was defined as remarkable if it was seen as being morphologically different relative to adjacent, like tissues or layers of the retina (see Fig. 58.3). Figure 58.3 is an OCT image of a minute abnormality observed near the optic nerve in a $C4^{-/-}$ mouse. This particular lesion presents a challenge to imaging systems as it is juxtaposed to the optic nerve, under thick nerve tissue and retinal vasculature. This lesion was not detected by SLO and represents the smallest lesion that would have been recorded as an abnormality by OCT. In addition, the suspected abnormality also impacted, at a minimum, a significant portion of the photoreceptor outer segments or more of the retinal tissue with regard to length and/or thickness (Fig. 58.4e). Figure 58.4 shows images from a $C4^{-/-}$ mouse that had unremarkable SLO images but clearly showed an abnormal length of RPE and outer segments within the photoreceptor matrix.

The results from this evaluation are summarized in Table 58.1. The table is categorically divided into two age groups for the various mouse types investigated. For each age group and mouse type, the three subcategories include the total number of animals imaged, the number observed with abnormalities, and the percentage found with abnormalities (i.e., prevalence frequency). The frequency of fundus abnormalities in young mice, ranked from lowest to highest, is as follows: C57BL/6J (1.5%), factor $B^{-/-}$ (2.4%), BALB/cAnNTac (3.3%), $C3^{-/-}$ (4.8%), factor $H^{-/-}$ (5.6%), $SOD1^{+/, -/}$ (14.3%), $C4^{-/-}$ (17.1%), and BALB/cJ (100%). The frequency in middle-aged animals, ranked from lowest to highest, is as follows: factor $H^{-/-}$ (0%), $C3^{-/-}$ (4.7%), C57BL/6J (5.9%), $SOD1^{+/, -/}$ (7.7%), factor $B^{-/-}$ (8.3%), and $C4^{-/-}$

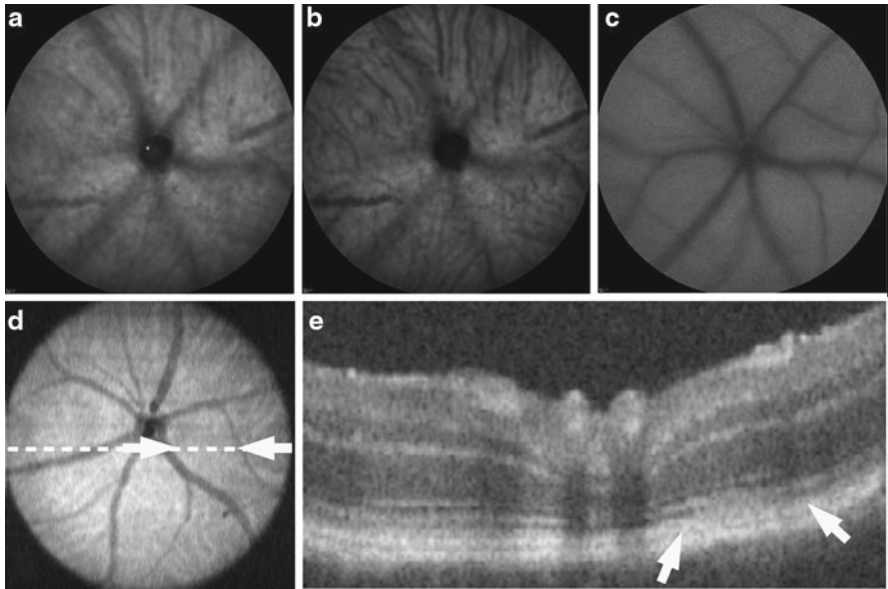


Fig. 58.4 Baseline SLO and OCT images collected from a 2-month-old $C4^{-/-}$ mouse. Images shown are IR reflectance (a), IR dark-field (b), and AF (c) collected by SLO that appear unremarkable with no indication of abnormalities. OCT en-face image (d) denotes orientation of the B-scan image (e), which clearly reveals a lesion in the outer photoreceptor matrix. The lesion appears as a “fuzzy” region between the RPE and transition zone that delineates the inner and outer photoreceptor matrix segments

(13.6%). Fewer mice in the 6–14 month age range were available for evaluation than the young, 2–4-month-old mice and thus, the frequency of retinal abnormalities (i.e., Factor H group for example) in the 6–14-month age group must be interpreted cautiously since fewer animals have been evaluated. No BALB/c mice were available for imaging at 6–14 months of age.

Overall, if all animals imaged at baseline (i.e., mice 2–4 months of age, $n=346$) are pooled, then the average prevalence of retinal abnormalities is 9.5% (33 abnormalities observed in 346 total mice). If the BALB/cJ mice ($n=15$), which exhibited a 100% incidence of abnormalities, are excluded then the frequency drops to 5.7% (19/331). Thus, one may expect to find an abnormality in approximately 1 out of every 20 mice. Important to note, however, is that the frequency of retinal abnormalities is subject to the type of mouse used and can vary depending on the vendor.

58.4 Discussion

Our screening process involves two separate imaging instruments to identify preexisting abnormalities in mouse retinas. In our opinion, from a qualitative perspective, the combined approach increases the sensitivity and specificity for detection of retinal

abnormalities. We have also found it prudent to utilize more than one imaging mode (i.e., IR and AF combined with SLO for example) to enhance the ability to contrast abnormalities within the normal retinal background. Originally, our baseline imaging used primarily SLO imaging and to a limited extent, visible fundus photography. We began to incorporate OCT imaging after many suspected abnormalities found by SLO could not be located by histology despite comprehensive serial sectioning of those tissues. In order to address this problem, we incorporated *in vivo* OCT imaging immediately following SLO imaging, to determine if a suspected SLO finding was a true or false positive. Only after the addition of OCT did we observe a reduction in SLO false positives. Thus, a tiered approach utilizing both imaging modalities is important as SLO is limited to a two-dimensional view of the retina whereas OCT provides the missing dimension (in-depth morphology) that SLO does not reveal.

There are challenges with *in vivo* retinal imaging in the small mouse eye (i.e., adequate plane of anesthesia, time limitations due to lens cataract formation, motion artifact due to respiration, etc.). Features such as auto-tracking help minimize these problems. However, not all instruments have this capability and, as a result, only a portion of the collected information is useful at times. For example, the respiration artifact of an animal causes partial image blurring if an instrument does not have auto-tracking. However, imaging with a second instrument does not require much additional time, and the overlap obtained by integrating the results of the two systems serves to minimize the weaknesses and deficiencies encountered with a single instrument. Simply stated, imaging with more than one instrument provides an opportunity to obtain a “second opinion” while the animal is already prepared.

The use of noninvasive ocular imaging is an undisputed, useful tool for rapidly obtaining information about retinal morphology in mice. By evaluating a sizeable cohort of animals, we determined the prevalence of retinal abnormalities in some specific knockout lines and in wild-type strains. Although others have reported sequential imaging studies in mice (Luhmann et al. 2009), to the best of our knowledge, this is the first study to document the number and percentage of retinal abnormalities found in a substantial cohort of animals at baseline. Surprisingly, numerous abnormalities occur in presumably normal mice at early ages, both in wild-type and knockout animals. This observation is not only limited to mice as we have also observed retinal abnormalities in two rat strains as well (unpublished data). At this time, the cause for these abnormalities is unknown but we hypothesize that inbreeding could be a factor as many animal models, even wild types like the C57BL/6J, have been inbred for many years to maintain strain characteristics. Many of the animals used were obtained from vendors where environmental conditions (e.g., light intensity/duration) are unknown and could have caused these changes. In addition, mutations can occur spontaneously (Hawes et al. 1999). These findings reported here underscore the importance of performing baseline and serial imaging to properly characterize animals before going forward with extensive experiments. At first glance a frequency of 5–10% does not seem like a problematic number; nevertheless, without baseline testing one cannot be assured that a frequency ranging from 10 to 100% will not occur. This study has indeed demonstrated that a sizeable number

of animals have retinal abnormalities and that the range can be extensive and varies among strains.

Unfortunately, noninvasive imaging is not without limitations. Approximately, 50% of the retina cannot be surveyed due to instrument limitations and optics of the mouse eye. Thus, the prevalence findings we have shown here could be even higher if one were to perform comprehensive serial histological sections of these retinas.

In addition, proper animal preparation with regard to anesthesia and pupil dilation is crucial for obtaining the best images for detecting abnormalities. If not performed carefully, the development of lens and/or corneal opacities (i.e., cataracts) limits image quality and detection sensitivity. Yet another limitation of imaging is instrumentation cost as these systems are quite expensive to procure. In our case, this expense was immediately offset when a group of mice ordered from a reputable vendor for an extensive and costly long-term study revealed numerous retinal abnormalities that could have potentially caused confusing and confounding results upon completion of the study.

Abnormal pathology is undoubtedly a dynamic process undergoing continual change. Lesions are not going to be presented with the same characteristics across various strains and models and even with respect to individual animals within a strain. Genetic mutations are always possible and baseline imaging will improve our chances of catching these spontaneous and spurious events. The intra- and inter-variability shown among these models suggests that a comprehensive baseline imaging session prior to the commencement of experiments would be a beneficial addition to any proposed research study.

Acknowledgments The authors would like to thank the Foundation Fighting Blindness, Research to Prevent Blindness, Wolf Foundation, and NIH R01EY014240 for providing financial support. The authors also thank Dr. Nancy B. Bell for constructive input and assistance in the preparation of this chapter.

References

- Eter N, Engel DR, Meyer L et al (2008) In vivo visualization of dendritic cells, macrophages, and microglial cells responding to laser-induced damage in the fundus of the eye. *Invest Ophthalmol Vis Sci* 49:3649–3658
- Fischer MD, Huber G, Beck SC et al (2009) Noninvasive, in vivo assessment of mouse retinal structure using optical coherence tomography. *PLoS One* 4:e7507
- Gabriele ML, Ishikawa H, Schuman JS et al (2010) Reproducibility of Spectral-Domain Optical Coherence Tomography Total Retinal Thickness Measurements in Mice. *Invest Ophthalmol Vis Sci*
- Hawes NL, Smith RS, Chang B et al (1999) Mouse fundus photography and angiography: a catalogue of normal and mutant phenotypes. *Mol Vis* 5:22
- Hollyfield JG, Bonilha VL, Rayborn ME et al (2008) Oxidative damage-induced inflammation initiates age-related macular degeneration. *Nat Med* 14:194–198
- Huber G, Beck SC, Grimm C et al (2009) Spectral domain optical coherence tomography in mouse models of retinal degeneration. *Invest Ophthalmol Vis Sci* 50:5888–5895

- Kocaoglu OP, Uhlhorn SR, Hernandez E et al (2007) Simultaneous fundus imaging and optical coherence tomography of the mouse retina. *Invest Ophthalmol Vis Sci* 48:1283–1289
- Luhmann UF, Robbie S, Munro PM et al (2009) The drusenlike phenotype in aging Ccl2-knockout mice is caused by an accelerated accumulation of swollen autofluorescent subretinal macrophages. *Invest Ophthalmol Vis Sci* 50:5934–5943
- Paques M, Guyomard JL, Simonutti M et al (2007) Panretinal, high-resolution color photography of the mouse fundus. *Invest Ophthalmol Vis Sci* 48:2769–2774
- Ruggeri M, Tsechpenakis G, Jiao S et al (2009) Retinal tumor imaging and volume quantification in mouse model using spectral-domain optical coherence tomography. *Opt Express* 17:4074–4083
- Xu H, Chen M, Manivannan A et al (2008) Age-dependent accumulation of lipofuscin in perivascular and subretinal microglia in experimental mice. *Aging Cell* 7:58–68

Chapter 59

Correlation Between Spectral Domain OCT Retinal Nerve Fibre Layer Thickness and Multifocal Pattern Electroretinogram in Advanced Retinitis Pigmentosa

Ieva Sliesoraityte, Eric Troeger, Antje Bernd, Anne Kurtenbach,
and Eberhart Zrenner

Keywords Retinitis pigmentosa • Multifocal pattern electroretinography • Retinal nerve fibre layer • Ganglion cell • Retinal cell survival

59.1 Introduction

Retinitis pigmentosa (RP) is a group of heterogeneous diseases and the most common cause of inherited blindness worldwide (Zrenner et al. 1999). The primary occurrence of RP is marked by photoreceptor dysfunction which is followed by rods and secondary cone loss, eventually leading to retinal atrophy.

Previous *in vivo* works reported that even in the late stages of retinal degeneration approximately one third of ganglion cells are preserved morphologically (Humayun et al. 1999; Villegas-Pérez et al. 1998). However, as well as the significant change in retinal ganglion cells (RGC) morphology in a classical animal model of RP, a remarkable change in electrophysiological properties of RGC has been reported (Chen et al. 2005). Moreover, a negative remodelling was observed, causing radical changes in retinal structure in mature transgenic and knockout retinal degeneration models (Jones et al. 2005). To date the morphological and functional mechanisms involved in RP degeneration, particularly in advanced stages, are not fully understood. By combining recent advances in electrophysiology and retinal imaging modalities, our research was focused on morphological alterations and functional assessments of RGC situated at the temporal region. To the best of our knowledge, our project group for the first time reports the correlation between spectral-domain OCT retinal nerve fibre layer thickness and multifocal pattern electroretinograms in retinitis pigmentosa patients.

I. Sliesoraityte (✉) • E. Troeger • A. Bernd • A. Kurtenbach • E. Zrenner
Centre for Ophthalmology, Institute for Ophthalmic Research, University of Tuebingen,
72076, Tuebingen, Germany
e-mail: sliesoraityte@yahoo.com

59.2 Materials and Methods

59.2.1 Study Population

This analysis is based on baseline data from 12 patients (24 eyes) with established RP diagnosis and a spectrum of disease severity and 12 healthy controls (24 eyes) enrolled in a prospective observational case–control study. Participants included in this report were recruited from the Institute for Ophthalmic Research at the Tuebingen University Eye hospital. All patients had full explanations of the procedures and informed written consent was obtained. The study was approved by the Ethical Committee of the Medical Faculty, University of Tuebingen and was conducted according to the tenets of the Declaration of Helsinki.

Inclusion criteria were defined as age 18 years or older at the time of enrolment, with a diagnosis of retinitis pigmentosa (based on the history of night blindness, impairment of peripheral visual fields, reduction of electroretinogram rod and cone amplitudes, and the presence of characteristic fundus pigmentary changes) and a visual field of less or equal to 10°. Participants were excluded if the best corrected visual acuity (BCVA) was less than 0.01, refraction error more than ± 8 dioptres or with any other pathology, which could lead to inability to maintain a steady fixation, with a previous history of glaucoma, IOP >22 mmHg and/or <10 mmHg, any origin of macular edema (e.g. diabetic macular edema, vitreous traction, etc.), any systemic (e.g. epilepsy) or eye diseases and/or topical medication usage that might influence mfPERG readings, and media opacity that may have precluded quality macular scans.

59.2.2 Electrophysiological Recordings

Electrophysiological recordings were carried out using the VERIS 4.9.1 system (Electro-Diagnostic Imaging, Inc., Redwood City, CA). DTL fibre electrodes were used for mfPERG response measurements. Reference and ground skin electrodes were attached to the ipsilateral temple and forehead, respectively. Recordings were performed with best optical correction with undilated pupils, and pupil size ranged between 3 and 4 mm in both groups.

Multifocal PERG recordings were assessed using a pattern of 19 hexagonal elements, each consisting of 25 triangles, alternating between black and white (Stiefelmeyer et al. 2003; Langrová et al. 2007). The stimulus was generated on an Iiyama monitor and viewed at a distance of 38 cm, which stimulated the central 38° of the visual field. Each of 19 hexagonal elements of the mfPERG stimulus was alternated between 102 and 1 cd/m², i.e. ~98% contrast. The frame rate was 75 Hz. The m-sequence length was 215–1 elements corresponding to a total recording time of 7 min 17 s for each condition. The continuous mfPERG recordings were amplified by 100 K, filtered with a frequency bandpass of 3–100 Hz, and sampled at 502 Hz. Additionally, software created by one of the authors was applied for accurate topographical correspondence of waveforms to corresponding measures of retinal

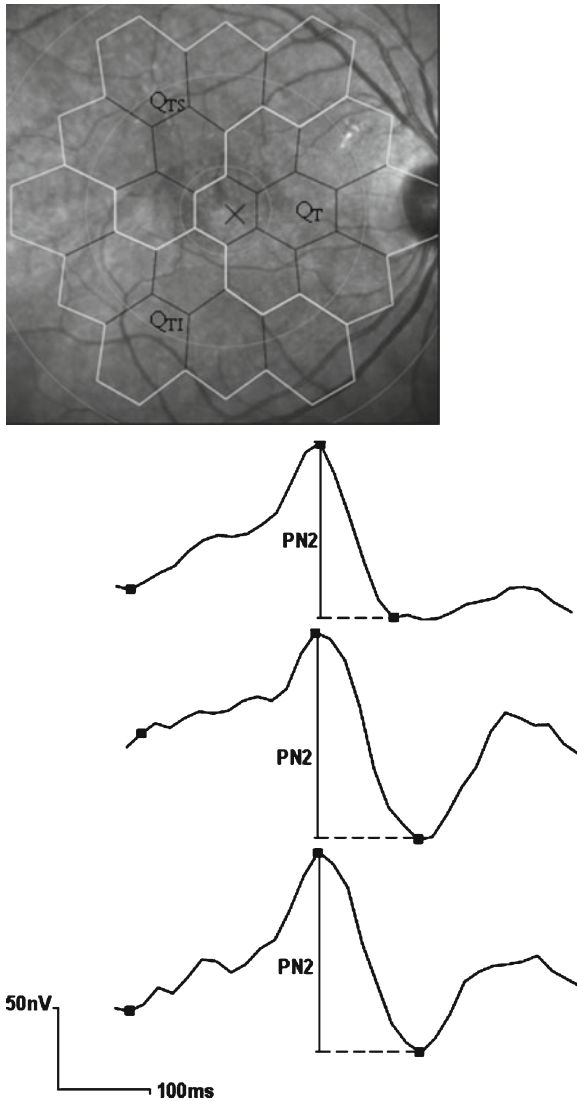


Fig. 59.1 Inner retinal recordings using multifocal pattern electroretinogram (mfPERG). (a) Grouping into three regions, i.e. temporal superior (Q_{TS}), temporal (Q_T) and temporal inferior (Q_{TI}) quadrants, while each of them comprising six elements; (b) amplitude of the positive-to-negative (PN2) component measured as a vertical distance from the highest point through the second negative peak

nerve fibre layer thickness within the peripapillary region, i.e. temporal superior (Q_{TS}), temporal (Q_T) and temporal inferior (Q_{TI}) regions, each of them comprising six elements. (Fig. 59.1a). The amplitudes of the positive-to-negative (PN2) component were measured as the vertical distance from the first peak to the second negative deflection was evaluated (Fig. 59.1b).

59.2.3 Retinal Nerve Fibre Layer Imaging

Spectral domain-optical coherence tomography (Heidelberg Engineering, Dossenheim, Germany) was used to detect retinal nerve fibre layer thickness in retinitis pigmentosa subjects. Circular $15 \times 15^\circ$ scan angle (4.4×4.4 mm) images were centred on the optic disc, each being composed of 768 A-scans \times 73 B-scans, with 61 μm distance between each B-scan and with each B-scan resampled nine times. A circle grid, composed of three circles of 1, 2.22 and 3.45 mm diameter, was centred on the optic disc by an experienced operator. Internal fixation was used on all patients to obtain Spectral domain-OCT scans. The operator was appointed to monitor and ensure that the scan quality, indicated by a horizontal bar turning red in the presence of poor signal strength, was under acceptable limits throughout the scan acquisition. The circle grid allowed calculation of the retinal thickness at each diameter for the nasal.

59.3 Results

59.3.1 Basic Characteristics of Study Cohort

The study group consisted of 12 RP patients (7 men and 5 women) and 12 healthy subjects (7 men and 5 women), who served as an age-matched control group. Duration of RP ranged from 1 to 27 years (average 13 ± 8 years) and the area of the kinetic visual field for III (4)e target size ranged from 60.5 to 722.8 deg^2 (mean 343.9 ± 213.29 deg^2). Basic characteristics of the participants are shown in Table 59.1. There were no statistically significant differences in demographical

Table 59.1 Basic characteristics of the study cohort

Variables	Retinitis pigmentosa	Healthy controls	<i>p</i> value
Age (years)	44 ± 14	39 ± 6	$p = 0.211$
BCVA	0.5 ± 0.23	1.2 ± 0.16	$p < 0.001^*$
IOP (mmHg)	16.8 ± 1.8	14.6 ± 2.27	$p = 0.022^*$
R1-PN2 implicit time (ms)	44.3 ± 9.57	44.8 ± 5.79	$p = 0.878$
R1-PN2 amplitude (nV)	90.7 ± 57.5	245.2 ± 80.32	$p < 0.001^*$
R2-PN2 implicit time (ms)	46.2 ± 8.43	39.6 ± 3.39	$p = 0.019^*$
R2-PN2 amplitude (nV)	28.0 ± 9.25	188.6 ± 52.24	$p < 0.001^*$
R3-PN2 implicit time (ms)	47.1 ± 11.38	38.0 ± 2.45	$p = 0.013^*$
R3-PN2 amplitude (nV)	31.3 ± 14.88	166.5 ± 37.87	$p < 0.001^*$
CMT (μm)	264.0 ± 92.32	288.3 ± 25.88	$p = 0.390$

* $p < 0.05$

RP retinitis pigmentosa; BCVA best corrected visual acuity; IOP intraocular pressure; R1, R2, R3 concentric ring 1, 2 and 3; PN2 positive-to-negative component in multifocal pattern electroretinogram; RNFLT retinal nerve fibre layer thickness

Table 59.2 Retinal fibre layer thickness measurements, mfPERG P-N2 component amplitude and implicit time within each peripapillary region

	Variables	Retinitis pigmentosa	Healthy controls	<i>p</i> value*
Temporal superior	RNFLT (μm)	139.1 \pm 45.93	130.7 \pm 14.95	<i>p</i> =0.556
	Amplitude PN2 (nV)	41.9 \pm 14.56	173.7 \pm 52.06	<i>p</i> <0.001*
	Implicit time PN2 (ms)	52.75 \pm 9.71	36.5 \pm 4.06	<i>p</i> <0.001*
Temporal	RNFLT (μm)	109.4 \pm 33.92	78.9 \pm 15.56	<i>p</i> =0.01*
	Amplitude PN2 (nV)	52.8 \pm 25.54	171.4 \pm 46.10	<i>p</i> <0.001*
	Implicit time PN2 (ms)	47.0 \pm 9.18	37.6 \pm 2.61	<i>p</i> =0.002*
Temporal inferior	RNFLT (μm)	152.7 \pm 30.95	143.6 \pm 14.98	<i>p</i> =0.370
	Amplitude PN2 (nV)	42.2 \pm 16.81	200.3 \pm 49.63	<i>p</i> <0.001*
	Implicit time PN2 (ms)	49.0 \pm 8.07	42.2 \pm 16.81	<i>p</i> =0.003*

**p*<0.05

RNFLT retinal nerve fibre layer thickness; PN2 positive-to-negative component in mfPERG (multifocal pattern electroretinogram)

characteristics between groups. Significantly decreased amplitude and prolonged implicit time of the mfPERG component P1N2 within three concentric rings were observed in RP patients.

59.3.2 Inner Retina Structure–Function Relation

Significant decrease of mfPERG of P1N2 component amplitude and implicit time was observed in temporal superior, temporal and temporal inferior region comparing RP subjects with healthy controls. Table 59.2 shows retinal fibre layer thickness and mfPERG of P1N2 component amplitude, and implicit time in particular peripapillary region. Regardless of reduced mfPERG amplitudes and prolonged implicit time of P1N2 component in RP patients, RNFL thickness is comparable to that of healthy controls.

A scatter plot together with the corresponding regression profile between mfPERG of P1N2 component amplitude and RNFL thickness within temporal superior and temporal regions in RP subjects and healthy controls is shown in Fig. 59.2. The linear regression profile of mfPERG of P1N2 component amplitude and RNFL thickness is of the same character in RP and healthy controls, i.e. increasing in temporal superior, and slightly decreasing in temporal region. However, the association was statistically significant neither in RP nor in healthy controls. Moreover, there was no statistically significant difference in the above-mentioned association comparing RP and healthy controls. Multiple linear regression models were then used to examine the correlation of the P1N2 component of mfPERG adjusted for age, RP duration and visual acuity with retinal nerve fibre layer thickness measures. No significant difference between adjusted (age, RP duration and visual acuity) and nonadjusted (crude) models were determined analysing RNFLT and P1N2 amplitude in particular segments.

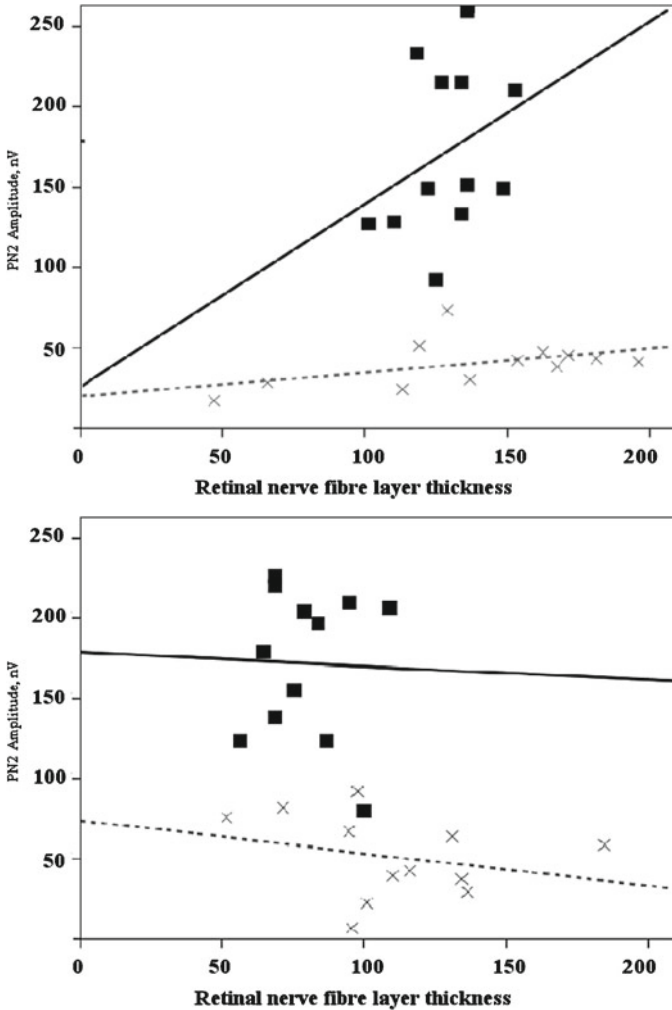


Fig. 59.2 Inner retina structure and function relation in peripapillary regions. Regression analysis between PIN2 component amplitude and retinal nerve fibre layer thickness in RP subjects (*crosses* and *dashed line*) and healthy controls (*squares* and *solid line*) within Q_{TS} (temporal superior (a)), Q_T (temporal (b)) peripapillary regions

59.4 Discussion

In this study we examined the relationship between retinal nerve fibre layer thickness and ganglion cell functions as assessed by electrophysiological means in retinitis pigmentosa patients with concentric visual fields smaller than 10° of visual angle. After controlling for age, RP duration and visual acuity, we found reduced amplitudes and prolonged implicit times in patients, without significant changes in retinal

nerve fibre layer thickness within temporal superior, temporal and temporal inferior peripapillary regions compared to healthy subjects.

Retinitis pigmentosa involves the progressive death of photoreceptors, and several studies have shown that inner retinal cells undergo various degree of remodelling in mutant inherited models (Strettoi et al. 2003; Cuenca et al. 2004). Therefore, it was anticipated that the consequence of progressive retinitis pigmentosa will be the loss of ganglion cells. However, our findings suggest that diminution of photoreceptors sensory input observed in retinitis pigmentosa patients might attenuate certain ganglion cells function, but do not induce diffuse transneuronal alterations in the neighbouring cell layers, which would be accompanied with detectable loss of RGC and/or diminished retinal nerve fibre layer thickness. These results are consistent with studies examining RGC survival in the mouse model of inherited photoreceptor degeneration, where remarkable preservation of RGC structure, survival and projections to higher visual centres was observed well beyond the death of photoreceptors (Mazzoni et al. 2008). Recently, it was proved in human RP studies (Walia and Fishman 2008; Rangaswamy et al. 2010).

Common pathophysiological processes may underlie the preserved capabilities of RGC to transmit information of action potentials despite the loss of photoreceptors, even in advanced RP cases. It is well known that RGC are still active in the absence of light and fire even if deprived from their photoreceptor input. This also explains the blind patients' ability to report grey instead of black in complete darkness. Moreover, 2–3% of melanopsin-containing RGC are important in circadian light responses (Ruggiero et al. 2009). They may provide light-modulated input to the inner retina with feedback to amacrine and bipolar cells under very bright light, although not be able to provide spatial resolution (Güler et al. 2008).

In conclusion, this chapter shows reduced retinal ganglion cell function without significant disruption of retinal nerve fibre layer thickness in advanced retinitis pigmentosa subjects. These findings provide support for the notion of ongoing intraretinal signal processing within the inner retina after diffuse rod and cone loss in late stages of inherited photoreceptor degenerative diseases. However, long-term studies with larger samples are warranted to gain information about ganglion cells morphology and function in patients with retinitis pigmentosa after many years of blindness.

Acknowledgments We thank Pro-Retina (Aachen, Germany) for providing financial support to IS.

References

- Chen ZS, Yin ZQ, Chen S et al (2005) Electrophysiological changes of retinal ganglion cells in Royal College of Surgeons rats during retinal degeneration. *Neuroreport* 16:971–975
- Cuenca N, Pinilla I, Sauv e Y et al (2004) Regressive and reactive changes in the connectivity patterns of rod and cone pathways of P23H transgenic rat retina. *Neuroscience* 127:301–317
- G ler AD, Ecker JL, Lall GS et al (2008) Melanopsin cells are the principal conduits for rod-cone input to non-image-forming vision. *Nature* 453:102–105

- Humayun MS, Prince M, de Juan Jr. E et al (1999) Morphometric analysis of the extramacular retina from postmortem eyes with retinitis pigmentosa. *Invest Ophthalmol Vis Sci* 40:143–148
- Jones BW, Watt CB, Marc RE (2005) Retinal remodelling. *Clin Exp Optom* 88:282–291
- Langrová H, Jägle H, Zrenner E et al (2007) The multifocal pattern electroretinogram (mfPERG) and cone-isolating stimuli. *Vis Neurosci* 24:805–816
- Mazzoni F, Novelli E, Strettoi E (2008) Retinal ganglion cells survive and maintain normal dendritic morphology in a mouse model of inherited photoreceptor degeneration. *J Neurosci* 28:14282–14292
- Rangaswamy NV, Patel HM, Locke KG et al (2010) A comparison of visual field sensitivity to photoreceptor thickness in retinitis pigmentosa. *Invest Ophthalmol Vis Sci* 51:4213–4219
- Ruggiero L, Allen CN, Lane Brown R et al (2009) The development of melanopsin-containing retinal ganglion cells in mice with early retinal degeneration. *Eur J Neurosci* 29:359–367
- Stiefelmeyer S, Neubauer AS, Berninger T (2003) The multifocal pattern electroretinogram in glaucoma. *Vis Res* 44:103–112
- Strettoi E, Pignatelli V, Rossi C et al (2003) Remodeling of second-order neurons in the retina of rd/rd mutant mice. *Vis Res* 43:867–877
- Villegas-Pérez MP, Lawrence JM, Vidal-Sanz M et al (1998) Ganglion cell loss in RCS rat retina: a result of compression of axons by contracting intraretinal vessels linked to the pigment epithelium. *J Comp Neurol* 392:58–77
- Walia S, Fishman GA (2008) Retinal nerve fiber layer analysis in RP patients using Fourier-domain OCT. *Invest Ophthalmol Vis Sci* 49:3525–3528
- Zrenner E, Stett A, Weiss S et al (1999) Can subretinal microphotodiodes successfully replace degenerated photoreceptors? *Vis Res* 39: 2555–2567

Chapter 60

Imaging Human Postmortem Eyes with SLO and OCT

Nika Bagheri, Brent A. Bell, Vera L. Bonilha, and Joe G. Hollyfield

Keywords Scanning laser ophthalmoscope • Optical coherence tomography • Macular hole • Retinal pigment epithelium detachment • Age-related macular degeneration • Retinitis pigmentosa

60.1 Introduction

The confocal scanning laser ophthalmoscope (SLO) and the spectral-domain optical coherence tomography (OCT) are two imaging systems that have rapidly revolutionized clinical ophthalmology. SLO is a noncontact, high-resolution imaging system that is now a worldwide standard in macular diagnostics. It has multiple imaging modes that provide contrast for imaging a variety of retinal conditions (Sharp and Manivannan 1997). Currently, SLO is used to evaluate a wide spectrum of retinal and choroidal diseases (Hassenstein and Meyer 2009). OCT provides in-depth structural detail of retinal morphology with an axial resolution of several microns. Today, this “noninvasive optical-biopsy” is used extensively for early diagnosis and precise monitoring of glaucoma and retinal diseases (Geitzenauer et al. 2010). These two instruments continue to make substantial advances in clinical ophthalmology (Da Pozzo et al. 2009; Wolf-Schnurrbusch et al. 2008; Imamura et al. 2009).

Here, we describe the use of SLO and OCT as the initial assessment to (1) screen “normal” postmortem eyes for retinal lesions, and (2) better characterize retinal lesions in eyes with suspected pathology prior to histological analysis. Just as the combination of SLO and OCT provides a comprehensive diagnostic assessment in the clinic, the combination of these two modalities ensures comprehensive characterization of retinal lesions prior to histopathology.

N. Bagheri • B.A. Bell • V.L. Bonilha • J.G. Hollyfield (✉)
Department of Ophthalmology, Cole Eye Institute (i31),
Cleveland Clinic Lerner College of Medicine, Cleveland, OH 44195, USA
e-mail: hollyfj@ccf.org

60.2 Materials and Methods

60.2.1 Tissue Preparation

Postmortem human eyes were obtained through the donor eye program of the Foundation Fighting Blindness (donations #777, #779, #784, #846, #908). Five donors (6 eyes) are described (Table 60.1). The first three donors' eyes had no grossly visible pathology. #846 had a fibrovascular scar consistent with end-stage age-related macular degeneration (AMD). #908 had extensive degeneration from retinitis pigmentosa (RP). Globes were initially fixed in 4% paraformaldehyde and 0.5% glutaraldehyde in 0.1 M phosphate buffer and later stored in 2% paraformaldehyde in the same buffer. Globes were bisected near the equator, dividing the globe into an anterior and posterior pole; the latter was used in this analysis.

60.2.2 Bright-Field Macroscopic Imaging

Prior to imaging, each eye was placed in a custom holder to stabilize the posterior pole; this allows it to be immersed in phosphate buffered saline, minimizing surface reflectance artifact. The first set of images collected used conventional bright-field macrophotography with a Zeiss AxioCam MRC5 camera equipped with a Zoom 7000 Navitar macro video lens. Illumination was accomplished using a flexible, bifurcated fiber-optic coupled to a tungsten-halogen light source. Images were taken using Zeiss AxioVision AC Rel 4.5 software.

60.2.3 Scanning Laser Ophthalmoscope

The next set of images was collected using SLO Heidelberg Retina Angiograph 2 (HRA2, Heidelberg Engineering, Inc.) equipped with a 55° wide field objective. The SLO housing was positioned so that the lens was directed down onto the aqueous surface for optimal imaging of the fundus. A $1,000 \pm 2.5 \mu\text{m}$ ruby sphere was placed on the optic nerve head to provide a reference scale. Autofluorescence (AF) and infrared (IR) images were obtained. Lesion areas were estimated based on the mean of five separate hand drawn outlines using ImageJ software.

Table 60.1 Human donor eye information

Donation #	779	777	784	846	908
Eye(s)	OD	OD	OU	OD	OD
Age (years)	74	74	95	71	79
Gender	Female	Female	Female	Male	Male
Postmortem interval	10.5 h	6.5 h	4 h	7 h	11 h

60.2.4 Optical Coherence Tomography

The final set of images was collected using Spectral-domain OCT (Biotigen, Inc.) operating at a peak wavelength of 840 and a 55 nm bandwidth with a 50° field of view (300 A-scans/B-scan by 300 B-scans/volume). The eye was positioned directly below the OCT objective.

60.3 Results

60.3.1 Normal Retina

Fundus images of #779 show an opaque appearance around the fovea consistent with edema (Fig. 60.1a). SLO AF images collect lipofuscin autofluorescence signal from the RPE. IR images penetrate farther into tissue, showing choroidal vasculature.

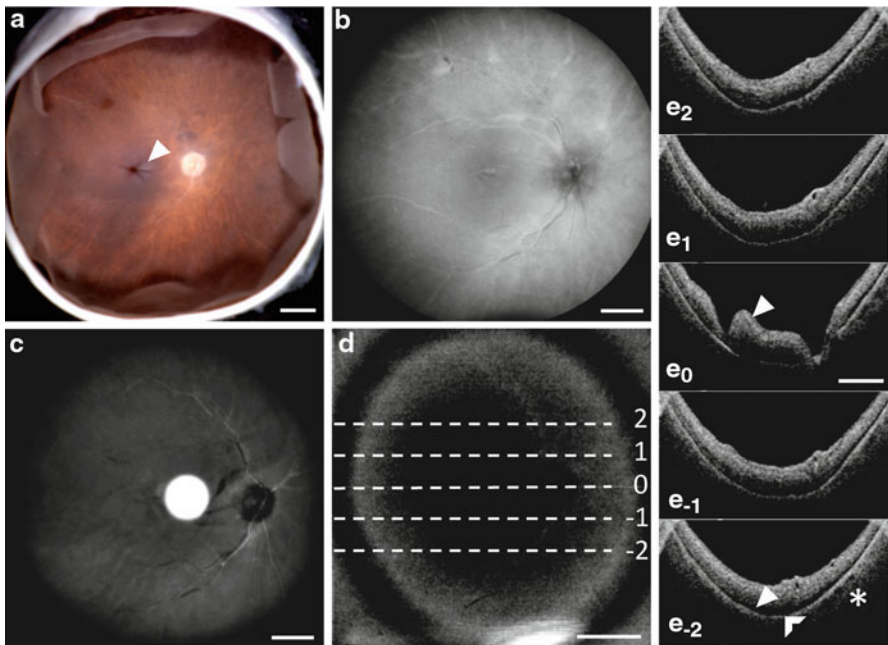


Fig. 60.1 Imaging characterizes a normal donor eye. (a) Macroscopic fundus image shows an opaque appearance around the fovea consistent with edema (*closed arrow*). (b, c) SLO AF and IR images show no pathology. (d) *Dashed lines* on OCT fundus image indicate B-scan image planes. (E_2 – E_{-2}) OCT is unremarkable at levels shown in (d) except for mild macular edema at 0 (*closed arrow*). The inner retina becomes opaque postmortem making retinal lamina difficult to differentiate; however, the photoreceptor layer (*closed arrow*), RPE (*open arrow*), and choroid (*asterisk*) remain visible. Scale = 2 mm

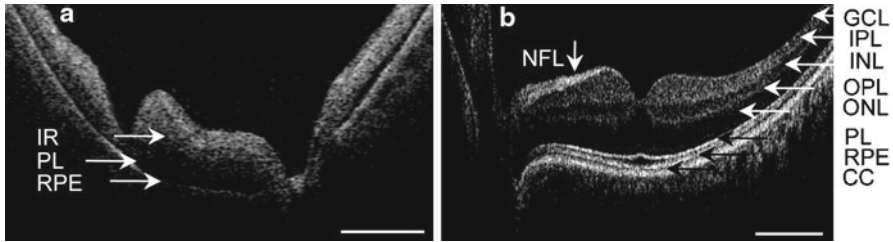


Fig. 60.2 Postmortem (a) and in vivo (b) OCT B-scans of normal human retinas. *IR* inner retina; *NFL* nerve fiber layer; *GCL* ganglion cell layer; *IPL* inner plexiform layer; *INL* inner nuclear layer; *OPL* outer plexiform layer; *ONL* outer nuclear layer; *ELM* external limiting membrane; *PL* photoreceptor inner and outer segments; *RPE* retinal pigment epithelium; *CC* choriocapillaris. Scale=2 mm

SLO imaging is unremarkable (Fig. 60.1b, c). OCT shows minor macular edema (Fig. 60.1d, 60.1E₂-E₂). However, comparison of OCT from in vivo eyes with OCT from postmortem eyes shows that postmortem changes are accompanied by the loss of distinct retinal lamella (compare Fig. 60.2a, b).

60.3.2 Macular Hole

Fundus images of #777 show an opaque appearance around the fovea consistent with edema. In addition, exudate is seen around the optic nerve (Fig. 60.3a). SLO AF images show decreased autofluorescence around the optic nerve and macula (Fig. 60.3b). SLO IR images show increased reflectance around the optic nerve and within an oval-shaped area at the center of the macula (Fig. 60.3c). OCT imaging reveals a macular hole (Fig. 60.3d). At the center of the macular hole, an isolated retinal fragment corresponds to the small area of decreased autofluorescence in Fig. 60.3b. The hole corresponds to the oval-shaped area of increased reflectance in Fig. 60.3c. The perimacular area of decreased reflectance in Fig. 60.3c is due to increased scattering of light from retinal elevation surrounding the macular hole, which attenuates signal from the choroid.

60.3.3 RPE Detachment

Fundus images of #784 OD and OS show prominent choroidal vessels and exudate around the optic nerve (Fig. 60.4a). SLO AF images of both eyes have a subtle, halo-shaped area of increased autofluorescence at the fovea (Fig. 60.4b). OCT imaging reveals bilateral, focal RPE detachment centered on the fovea (Fig. 60.4c, d). The halo-shaped area of increased autofluorescence corresponds to changes in the elevation of the RPE in the region of detachment. The AF laser penetrates the epithelial

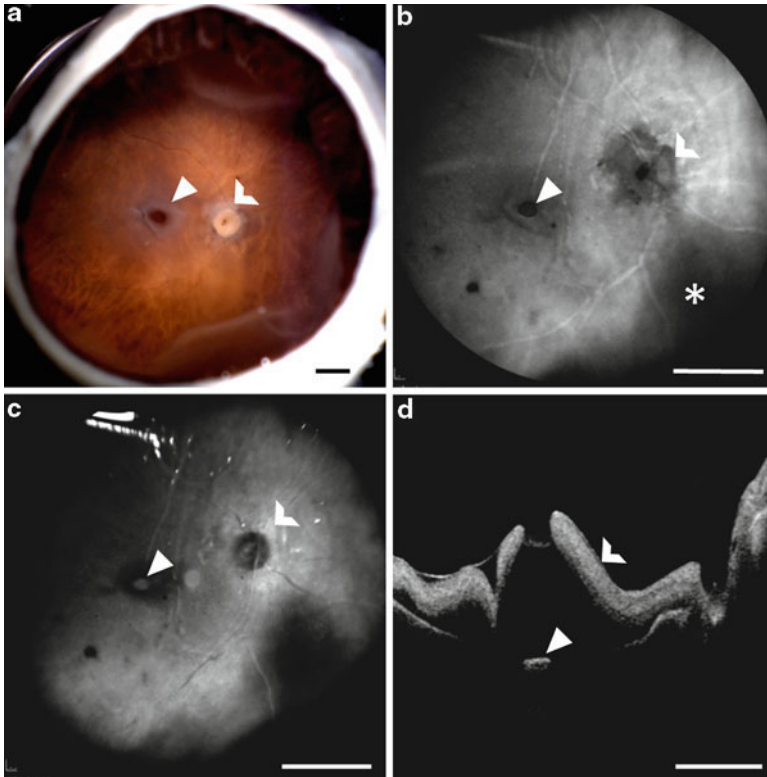


Fig. 60.3 Imaging of normal donor eye reveals macular hole. (a) Macroscopic fundus image shows an opaque appearance around the fovea consistent with edema (*closed arrow*) and exudate around the optic nerve (*open arrow*). (b) SLO AF image shows a small area of decreased autofluorescence at the macula (*closed arrow*) and a well-demarcated area of decreased autofluorescence around the optic nerve (*open arrow*). Dark areas in periphery are due to retinal detachment (*asterisk*). (c) SLO IR image shows increased reflectance around the optic nerve corresponding to the region in (b) and consistent with RPE degeneration (*open arrow*). An oval-shaped area of increased reflectance at the center of the macula (*closed arrow*) is surrounded by a larger area of decreased reflectance. (d) OCT B-scan of the optic nerve and fovea reveals a macular hole with a piece of detached retina (*closed arrow*) and retinal elevation surrounding the hole (*open arrow*). Scale=2 mm

surface at a tangential angle rather than a right angle, appearing as if the retinal thickness is increased adjacent to the detachment.

60.3.4 AMD Retina

Fundus images of #846 show a fibrovascular scar consistent with end-stage AMD (Fig. 60.5a). SLO AF imaging shows absence of autofluorescence in a large, central area similar to the fibrovascular scar (Fig. 60.5b). However, macroscopic image

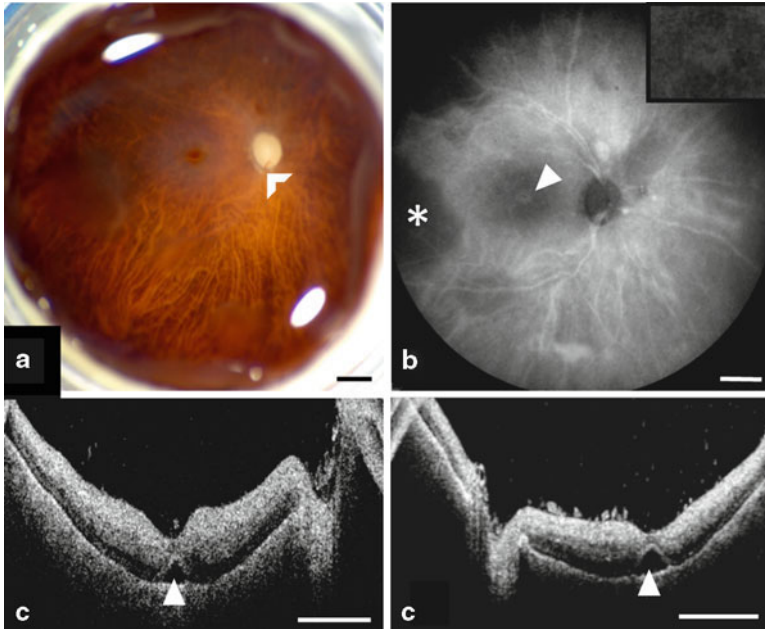


Fig. 60.4 Imaging a pair of eyes from a normal donor reveals bilateral RPE detachment. (a) Macroscopic fundus images show RPE atrophy allowing for visualization of choroidal vessels and exudate around the optic nerve (*open arrow*) (OS not shown). (b) SLO AF images of both eyes have a subtle, halo-shaped area of increased autofluorescence at the fovea (*closed arrow, inset*) (OS not shown). Dark areas in periphery are due to retinal detachment (*asterisk*). (c, d) OCT B-scan of the optic nerve and fovea shows bilateral, focal RPE detachment centered on the fovea (*closed arrows*). Scale = 2 mm

estimates the lesion area to be $66.0 \pm 1.22 \text{ mm}^2$ whereas AF image estimates the lesion area to be $75.9 \pm 0.60 \text{ mm}^2$. SLO shows a 13% larger lesion than conventional bright-field macrophotography. A *t* test of the macroscopic lesion estimate versus the AF lesion estimate shows a significant difference ($p < 0.0001$) likely due to improved contrast with SLO. OCT also reveals areas with subretinal fibrosis (Fig. 60.5C₂-C₋₂).

60.3.5 RP Retina

Fundus images of #908 show prominent choroidal vessels indicating atrophy of the overlying RPE and numerous bone spicule pigment deposits in the periphery encroaching on the macula (Fig. 60.6a). SLO AF imaging shows loss of autofluorescence consistent with RPE atrophy (Fig. 60.6b). OCT reveals thinning, degenerate retina toward the periphery and RPE detachment (Fig. 60.6C₂-C₋₂). Bone spicule pigment deposits are not evident with OCT.

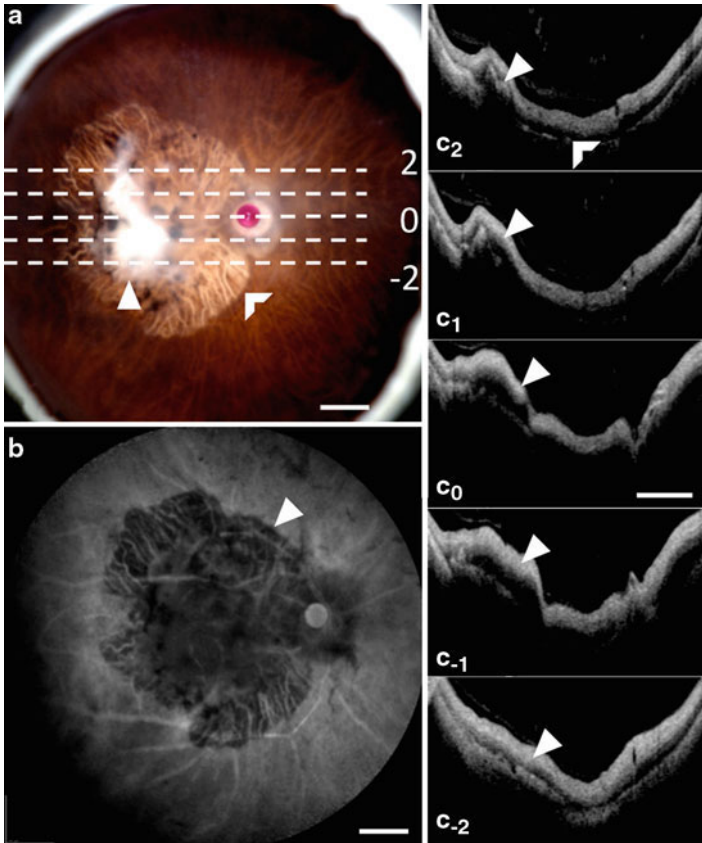


Fig. 60.5 Imaging characterizes an end-stage AMD eye. **(a)** Macroscopic fundus image shows a fibrovascular scar (*closed arrow*) and a central area of RPE atrophy allowing visualization of choroidal vessels (*open arrow*). The ruby sphere is placed on the optic nerve head for magnification reference. *Dashed lines* indicate OCT image planes. **(b)** SLO AF image shows a large, well-defined area of decreased autofluorescence encompassing the optic nerve and macula (*closed arrow*) which corresponds to the central lesion in **(a)**. Areas with autofluorescence correspond to the remaining area with RPE. C_2 - C_{-2} : OCT B-scans indicated in **(a)** reveal bright collections directly above the RPE which raise the inner retinal layer and are consistent with fibrovascular scar (*closed arrows*). Small, *dome-shaped* irregularities below the RPE layer may be drusen (*open arrow*). Scale=2 mm

60.4 Discussion

Although human donor eyes are invaluable to research, the vast majority are received with minimal clinical history and usually without fundus images. Here, we have attempted to address this perpetual challenge by applying the same technology used in the clinic to postmortem eyes.

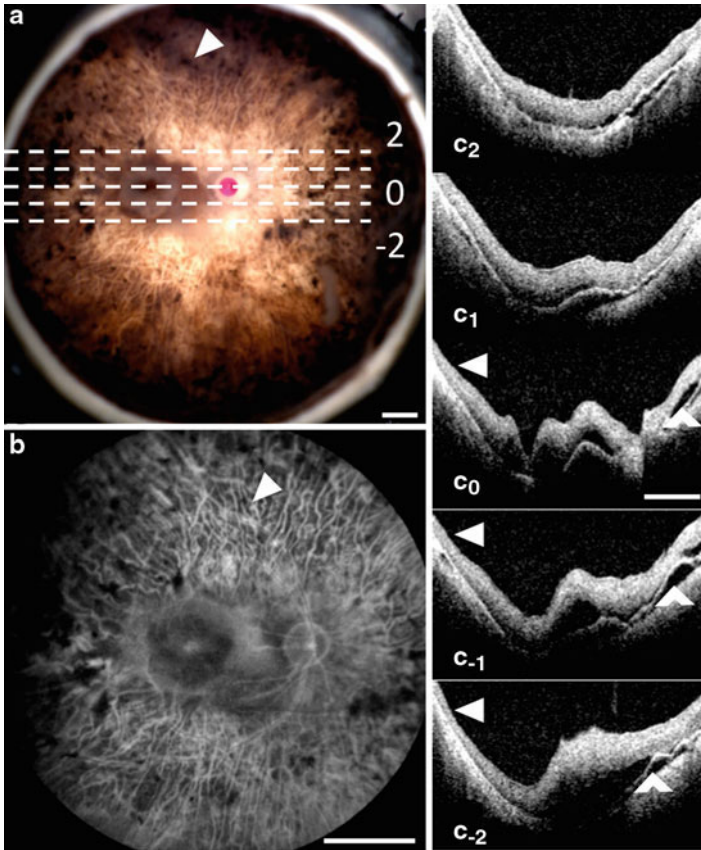


Fig. 60.6 Imaging characterizes an RP eye. (a) Macroscopic fundus image shows prominent choroidal vessels indicative of RPE atrophy and bone spicule pigment deposits (*closed arrow*) in the periphery. The ruby sphere is placed on the optic nerve head for magnification reference. *Dashed lines* indicate OCT image planes. (b) SLO AF image shows loss of autofluorescence indicating RPE atrophy (*closed arrow*), particularly in the periphery and mid-periphery. C_2 – C_{-2} : OCT B-scans indicated in (a) reveal thin, degenerate retina at the margins (*closed arrows*). RPE detachment is also seen (*open arrows*). Scale=2 mm

In vivo imaging with SLO allows for angiography and provides detailed retinal and choroidal vasculature (Jorzik et al. 2005). Postmortem imaging with the AF and IR modes of SLO identifies areas with absent or atrophied RPE. SLO imaging with AF and IR of postmortem eyes reveals features of RPE and choroid similar to those of in vivo eyes. Potential retinal detachment, however, substantially reduces the quality of images of postmortem eyes as compared to in vivo eyes. Tissue fixatives may further exacerbate the degree of retinal detachment from the RPE-choroid complex. In addition, the retina becomes less transparent in postmortem eyes. Both conditions compromise signal collection from structures underlying the retina and contribute to reduced image quality in postmortem eyes.

In vivo imaging with OCT shows detailed retinal architecture, including distinct retinal lamina (Yaqoob et al. 2005). It also resolves localized changes in retinal thickness between the macula and periphery. Postmortem changes mask the lamellar features of the inner retina, and allow resolution only of the photoreceptor layer, RPE, and choroid. Figure 60.2 clearly shows a difference in resolution of retinal lamina in in vivo and postmortem images. Despite the stark contrast in image quality, OCT imaging of postmortem eyes shows the thickness of the inner retina and RPE, and visualizes changes at sections throughout tissue with an in-depth resolution of several microns.

In vivo imaging is optimal; however, postmortem imaging with SLO and OCT provides more detail than the standard photographic image of the posterior pole. Information obtained from imaging regarding the location and size of retinal lesions also allows for targeted histopathology. To the best of our knowledge, the use of SLO for retinal imaging in human postmortem eyes has been reported only by two other groups (Bindewald et al. 2004; Olsen 2008). These earlier studies, however, removed the neural retina prior to imaging to improve visualization of the RPE-choroid complex. The removal of the neural retina for imaging limits the usefulness of the procedure when subsequent histology of the specimens is required. OCT has been used on human postmortem eyes primarily for corneal studies (Wolf et al. 2004; Johnson et al. 2007). OCT also has been used for retinal imaging of human postmortem eyes (Chauhan and Marshall 1999; Ugarte et al. 2006). However, this is the first time OCT has been routinely applied in conjunction with SLO and macroscopic imaging to screen and characterize a range of retinal pathology in postmortem donor eyes.

In summary, the use of both SLO and OCT in the initial assessment of postmortem eyes prior to histological analysis provides useful information about locations and types of different retinal lesions. As described above, #777 and #784 appeared normal in macroscopic fundus images, but in fact were found to have a macular hole and bilateral RPE detachment, respectively. Without knowing the clinical history of #777, it is impossible to determine if the isolated retinal fragment at the base of the macular hole was present at the time of death or if it was an artifact of fixation. Similarly, it is unknown if the bilateral RPE detachments were present at the time of death or were fixation artifacts. Aside from finding lesions that were not detected by macroscopic imaging, SLO and OCT further characterized known retinal lesions. The combination of SLO and OCT shows the full extent of retinal pathology and clarifies the locations of specific inclusions. Despite the valuable information imaging provides, it is important to be wary of using a single imaging instrument which may provide an incomplete picture of retinal pathology. The combination of SLO and OCT is critical to accurately interpreting pathology, and provides a more thorough means to identify retinal lesions in donor eyes.

Acknowledgments This work was supported by the Foundation Fighting Blindness, Columbia, MD and Research to Prevent Blindness, New York, NY. Figure 60.2b was reprinted with permission from Bioptigen, Inc. The authors thank Charlie Kaul and Dr. Lisa Kuttner-Kondo for their constructive comments and enthusiastic support.

References

- Bindewald A, Jorzik JJ, Loesch A et al (2004) Visualization of retinal pigment epithelial cells in vivo using digital high-resolution confocal scanning laser ophthalmoscopy. *Am J Ophthalmol* 137:556–558
- Chauhan DS, Marshall J (1999) The interpretation of optical coherence tomography images of the retina. *Invest Ophthalmol Vis Sci* 40:2332–2342
- Da Pozzo S, Marchesan R, Ravalico G (2009) Scanning laser polarimetry - a review. *Clin Experiment Ophthalmol* 37:68–80
- Geitzenauer W, Hitzenberger CK, Schmidt-Erfurth UM (2010) Retinal optical coherence tomography: past, present and future perspectives. *Br J Ophthalmol*
- Hassenstein A, Meyer CH (2009) Clinical use and research applications of Heidelberg retinal angiography and spectral-domain optical coherence tomography - a review. *Clin Experiment Ophthalmol* 37:130–143
- Imamura Y, Fujiwara T, Margolis R et al (2009) Enhanced depth imaging optical coherence tomography of the choroid in central serous chorioretinopathy. *Retina* 29:1469–1473
- Johnson CS, Mian SI, Moroi S et al (2007) Role of corneal elasticity in damping of intraocular pressure. *Invest Ophthalmol Vis Sci* 48:2540–2544
- Jorzik JJ, Bindewald A, Dithmar S et al (2005) Digital simultaneous fluorescein and indocyanine green angiography, autofluorescence, and red-free imaging with a solid-state laser-based confocal scanning laser ophthalmoscope. *Retina* 25:405–416
- Olsen TW (2008) The Minnesota Grading System using fundus autofluorescence of eye bank eyes: a correlation to age-related macular degeneration (an AOS thesis). *Trans Am Ophthalmol Soc* 106:383–401
- Sharp PF, Manivannan A (1997) The scanning laser ophthalmoscope. *Phys Med Biol* 42:951–966
- Ugarte M, Hussain AA, Marshall J (2006) An experimental study of the elastic properties of the human Bruch's membrane-choroid complex: relevance to ageing. *Br J Ophthalmol* 90:621–626
- Wolf AH, Neubauer AS, Priglinger SG et al (2004) Detection of laser in situ keratomileusis in a postmortem eye using optical coherence tomography. *J Cataract Refract Surg* 30:491–495
- Wolf-Schnurrbusch UE, Enzmann V, Brinkmann CK et al (2008) Morphologic changes in patients with geographic atrophy assessed with a novel spectral OCT-SLO combination. *Invest Ophthalmol Vis Sci* 49:3095–3099
- Yaqoob Z, Wu J, Yang C (2005) Spectral domain optical coherence tomography: a better OCT imaging strategy. *Biotechniques* 39:S6–13

Chapter 61

In Vivo Assessment of Rodent Retinal Structure Using Spectral Domain Optical Coherence Tomography

M. Dominik Fischer, Gesine Huber, Francois Paquet-Durand, Peter Humphries, T. Michael Redmond, Christian Grimm, and Mathias W. Seeliger

Keywords Optical coherence tomography • Imaging • Mouse models • Retinal degeneration • Light damage • Rhodopsin • RPE65 • Rd1

61.1 Introduction

Optical coherence tomography (OCT) is an established diagnostic tool in clinical ophthalmology and continues to play a significant role in vision science (Drexler and Fujimoto 2008). Only recently, commercially available OCT instruments with Spectral Domain technology (SD-OCT) were adapted with custom software and hardware to allow widespread application of this powerful tool in animal research (Knott et al. 2011; Fischer et al. 2009; Huber et al. 2009). As SD-OCT imaging is noninvasive, it is ideally suited to study changes of retinal structure in a longitudinal study design. This bears a major advantage over cross-sectional study designs, which are necessary for morphometric analysis by histology, as interindividual differences

M.D. Fischer (✉) • G. Huber • M.W. Seeliger
Division of Ocular Neurodegeneration, Institute for Ophthalmic Research,
Centre for Ophthalmology, Schleichstrasse 12-16, Tuebingen 72076, Germany
e-mail: Dominik.Fischer@med.uni-tuebingen.de

F. Paquet-Durand
Division for Experimental Ophthalmology, Institute for Ophthalmic Research,
Centre for Ophthalmology, Tuebingen 72076, Germany

P. Humphries
Department of Genetics, The Ocular Genetics Unit, Trinity College Dublin, Dublin 2, Ireland

T.M. Redmond
Laboratory of Retinal Cell and Molecular Biology, National Eye Institute, National Institutes of Health, Bethesda, MD, USA

C. Grimm
Department of Ophthalmology, Laboratory of Retinal Cell Biology, University of Zurich,
Sternwartstrasse 14 8091, Zurich, Switzerland

can be excluded as confounding effect. This is even more important in preclinical testing of experimental therapeutic strategies, where, e.g., surgical procedures (gene therapy, stem cell implantation) can be hard to standardize leading to some degree of variability within the treated cohort. Histology is a time consuming and costly procedure that provides (ultra-)high structural resolution and the option for subsequent analysis such as immunohistochemistry. However, preparatory protocols for histology impact on tissue dimensions (Hanstede and Gerrits 1983; Buttery et al. 1991) and functionally important changes in retinal integrity, such as edema formation or focal detachments, may be misinterpreted as handling artifacts *ex vivo*. SD-OCT can be used to overcome some of these obstacles, while reducing the number of animals needed in each study, which has ethical as well as economic implications. Here, we present data obtained by SD-OCT imaging of mouse models with induced (light damage) and inherited retinal degenerations.

61.2 Materials and Methods

61.2.1 Animals

Animals were housed under standard white cyclic lighting (12 h/12 h; 60 lux), had free access to food and water, and were used irrespective of gender. *Rho*^{-/-} (Humphries et al. 1997), *RPE65*^{-/-} (Redmond et al. 1998), C57/BL6/J (Charles River Laboratories), C3H *rd1/rd1* (*rd1*), and control C3H wild-type (wt) mice (Frasson et al. 1999) were used. Light damage was performed as previously described (Joly et al. 2009). All procedures were performed in accordance with the local ethics committee, German laws governing the use of experimental animals, and the ARVO statement for the use of animals in ophthalmic and visual research.

61.2.2 Retinal Imaging

A detailed protocol for anesthesia and imaging is described elsewhere (Seeliger et al. 2005; Fischer et al. 2009). Briefly, mice were anesthetized by subcutaneous injection of ketamine (66.7 mg/kg) and xylazine (11.7 mg/kg); their pupils dilated with tropicamide eye drops (Mydriaticum Stulln, Pharma Stulln, Germany) before image acquisition. A custom-made contact lens was used to avoid corneal dehydration and edema. Imaging and analysis was performed using the proprietary software package Eye Explorer version 3.2.1.0 from Heidelberg Engineering as previously described (Huber et al. 2009).

61.2.3 Histology

Animals were sacrificed and enucleated for histological analysis. After orientation was marked, the eyes were fixed overnight in 2.5% glutaraldehyde prepared in

0.1 M cacodylate buffer and processed as prescribed previously (Samardzija et al. 2006). For the timeline analysis of *rd1* mice, eyes were directly embedded, frozen, and sectioned as previously prescribed (Huber et al. 2009).

61.3 Results

Cross-sectional SD-OCT imaging in C57BL/6 animals (P28) provided in vivo data on normal murine retinal layer composition (Fig. 61.1a, b). Laminal organization correlated well with ex vivo light microscopy studies.

Focal light damage produced a selective loss of the outer retina in the exposed region, which borders a site of edema formation. The edema as functional significant alteration of retinal integrity is only visible in vivo and does not endure the tissue processing required for histology (Fig. 61.1c–g).

Rhodopsin was shown to serve not only as visual pigment but also as a structural protein of the discs in the rod outer segments (ROS). Indeed, ROS are never formed in rhodopsin (*rho*) deficient mice (Humphries et al. 1997). SD-OCT imaging in *rho*^{-/-} (P28) animals demonstrates a complete lack of ROS in vivo while the outer nuclear layer (ONL) appeared only marginally thinner compared to wt retina (data not shown). The entire retina showed absence of ROS, while the outer limiting membrane seems not to be disturbed and can be distinguished from the RPE signal by a distance roughly equivalent to inner segment remnants.

The protein *RPE65* regenerates the visual pigment rhodopsin in the retinal pigment epithelial cells (Redmond et al. 1998). In *RPE65*^{-/-} mice, the defective regenerating cycle causes accumulation of retinyl esters as lipid droplets in RPE cells. Image resolution of SD-OCT in *RPE65*^{-/-} mice at 11 months of age could not detect intracellular lipid accumulations in vivo. However, cross-sectional images revealed a reduction of ONL thickness reflecting the slow photoreceptor degeneration (data not shown).

The rapid degenerative process in the *rd1* mouse retina is caused by a loss of function mutation in the gene encoding the β subunit of the rod cGMP phosphodiesterase 6 (PDE6 β) (Bowes et al. 1990). Already at about P10 first signs of photoreceptors cell loss become evident while the vast majority of rod photoreceptor nuclei have disappeared by P21 (Paquet-Durand et al. 2007; Sancho-Pelluz et al. 2008). Iterative SD-OCT imaging of *rd1* mice at P11 and P28 reflected the severe retinal degeneration within only 17 days. At P28, the outer retina lacked plexiform/nuclear layers and photoreceptor segments and the inner nuclear layer (INL) seemed to border the RPE almost directly (data not shown).

61.4 Discussion

OCT is established as valuable tool to analyze and monitor structural changes in the retina. Virtual cross sections of the retina obtained with latest generation SD-OCT devices begin to approach the level of low power micrographs gained from light microscopy. Because this is achieved in a noninvasive manner, this technique does

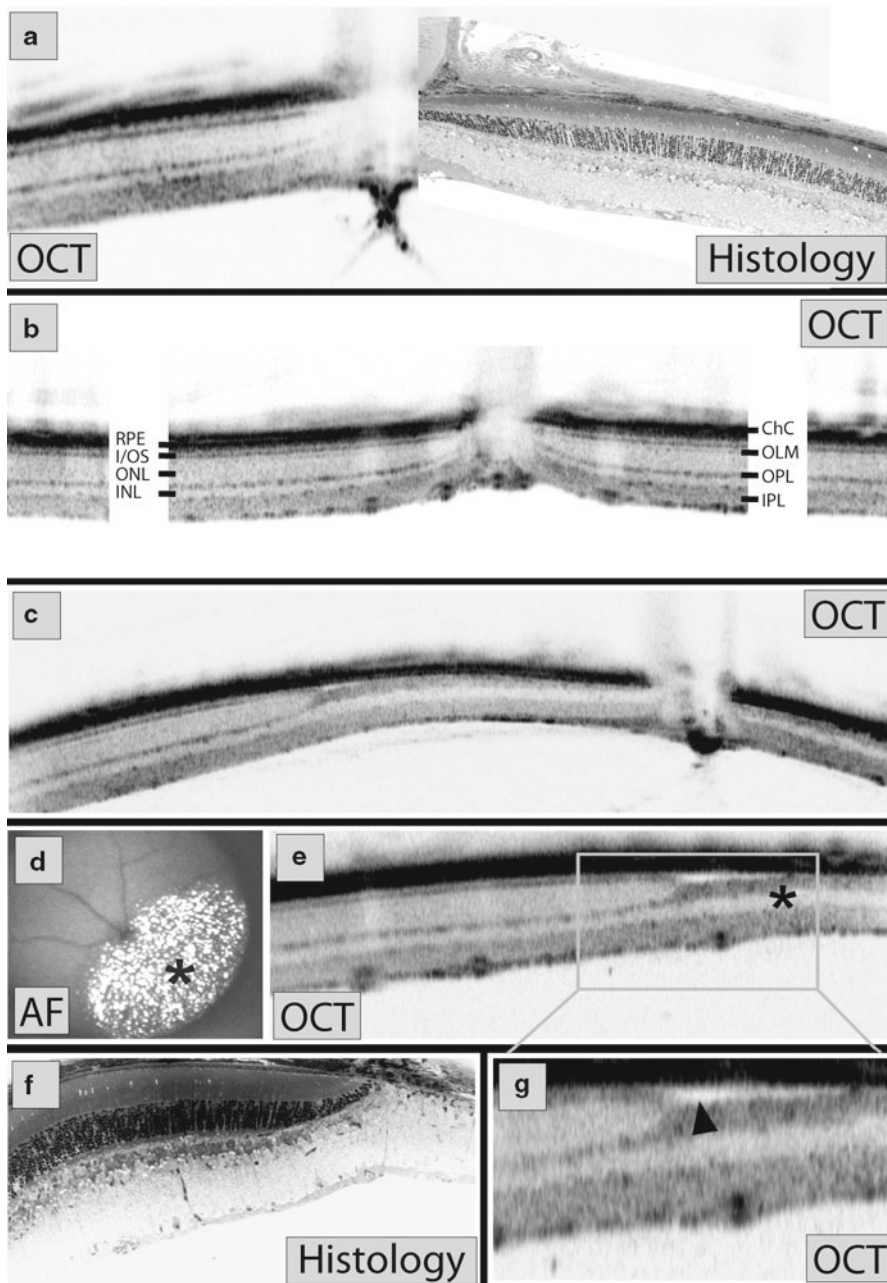


Fig. 61.1 Retinal cross sections in C57BL/6 mice with (a, b) naïve retinal structure and (c–g) after focal light damage. (a) Virtual B-scan and histologic section through the optic nerve head displaying a Bergmeister’s papilla. (b) Identification of individual retinal layers. (c) Optical coherence tomography (OCT) section across the central retina, containing adjacent damaged and nondamaged areas. (d) Demarcation of the damaged area in vivo by scanning laser ophthalmoscopy autofluorescence (AF) imaging based on fluorescent photoreceptor debris (marked by an *asterisk*). (e) Transition zone between damaged (marked by an *asterisk*) and nondamaged retina. (f, g) Comparison of light-induced retinal damage in histology and OCT. The *arrowhead* in the OCT image points toward focal edema formation

not only redefine genotype/phenotype correlation in the clinical setting, but also heralds a new era of noninvasive longitudinal studies with animal models that mimic respective disease characteristics. Here, we present data from commonly used wild-type mice and models of light-induced and inherited retinal degeneration using the Spectralis™ HRA+OCT platform.

The data from C57BL/6 wild-type mice established the comparability of virtual SD-OCT cross sections and histologic data in normal murine retina (Fig. 61.1a, b). While the origin of the distinct components within the reflectivity profile in virtual cross sections has continuously been subject to debate, it is generally thought (Drexler and Fujimoto 2008; Fischer et al. 2008; Srinivasan et al. 2008) that – from vitreous to sclera – the first thin hyperreflective line resembles the nerve fiber layer (NFL) followed by the less reflective ganglion cell layer (GCL). The consecutive thick band of higher reflective properties, the inner plexiform layer (IPL), is approximated by a band of low reflectance, the INL. The outer plexiform layer (OPL) appears as a thin stripe with a signal intensity comparable to that of the IPL. The outer retina is composed of a thick band, the ONL with similar signal intensity as in the INL. Apparently, both nuclear layers share the low signal intensity because they scatter and/or reflect light to a much lesser extent than both plexiform layers. Located just distal to the ONL is the external limiting membrane (ELM), which is formed by adherence junctions between distal photoreceptor cell bodies and apical villi of Müller glia cells. Photoreceptor inner and outer segments appear with the same signal intensity as the cell bodies, whereas the inner/outer segment (IOS) border generates a strong reflectance signal possibly due to the high mitochondrial content in the ellipsoid region (Fischer et al. 2008).

Photoreceptor apoptosis is a common final path of many forms of induced and inherited retinal degenerations. Typically, degenerating photoreceptor cell bodies and their inner and outer segments in the outer retina are subsequently removed without major alterations of the inner retinal layers. Whereas most genetic defects leading to photoreceptor degeneration affect the retina gradually both in terms of topographical distribution and pace, focal light exposure produces sharply delineated lesions adjacent to practically normal retina within hours, allowing a direct comparison between damaged and nondamaged areas (Fig. 61.1c–g). Upon photoreceptor degeneration, lipid-rich debris accumulates as it overwhelms the uptake capacity of the retinal pigment epithelium and glial cells. Due to its autofluorescent quality, it nicely demarcates the area of damage. In mouse models of inherited retinal degeneration, characteristic changes could be demonstrated with noninvasive SD-OCT imaging. While resolution is weaker when compared to conventional histology, the advantage of having an undistorted morphology together with topological information could be particularly useful when assessing retinal degeneration types that do not show a uniform progression in the entire retina. Here, we present the efficacy of a commercially available SD-OCT in small animal retinal imaging and provide in vivo structural data on mouse models of retinal degeneration. This method will be valuable in studies on dynamic changes of retinal structure through the natural course of disease and help to monitor effects of experimental therapeutic strategies.

Acknowledgments We thank Dr. C. Burchard for critical discussions and insightful comments. This work was supported by the Deutsche Forschungsgemeinschaft (DFG, grants Se837/5-2, Se837/6-1, Se837/7-1, and PA1751/1–1), the German Ministry of Education and Research (BMBF grant 0314106), the European Union grants LSHG-CT-512036, EU HEALTH-F2-2008-200234, and EU MEST-CT-2005–020235, and a contribution of the Tistou and Charlotte Kerstan Foundation to the OCT equipment.

References

- Bowes C, Li T, Danciger M et al (1990) Retinal degeneration in the rd mouse is caused by a defect in the beta subunit of rod cGMP-phosphodiesterase. *Nature* 347:677–680
- Buttery RG, Hinrichsen CF, Weller WL et al (1991) How thick should a retina be? A comparative study of mammalian species with and without intraretinal vasculature. *Vision Res* 31:169–187
- Drexler W, Fujimoto JG (2008) State-of-the-art retinal optical coherence tomography. *Prog Retin Eye Res* 27:45–88
- Fischer MD, Fleischhauer JC, Gillies MC et al (2008) A new method to monitor visual field defects caused by photoreceptor degeneration by quantitative optical coherence tomography. *Invest Ophthalmol Vis Sci* 49:3617–3621
- Fischer MD, Huber G, Beck SC et al (2009) Noninvasive, in vivo assessment of mouse retinal structure using optical coherence tomography. *PLoS One* 4:e7507
- Frasson M, Picaud S, Leveillard T et al (1999) Glial cell line-derived neurotrophic factor induces histologic and functional protection of rod photoreceptors in the rd/rd mouse. *Invest Ophthalmol Vis Sci* 40:2724–2734
- Hanstede JG, Gerrits PO (1983) The effects of embedding in water-soluble plastics on the final dimensions of liver sections. *J Microsc* 131:79–86
- Huber G, Beck SC, Grimm C et al (2009) Spectral domain optical coherence tomography in mouse models of retinal degeneration. *Invest Ophthalmol Vis Sci* 50:5888–5895
- Humphries MM, Rancourt D, Farrar GJ et al (1997) Retinopathy induced in mice by targeted disruption of the rhodopsin gene. *Nat Genet* 15:216–219
- Joly S, Franke M, Ulbricht E et al (2009) Cooperative Phagocytes. *Am J Pathol* 174:2310–2323
- Knott EJ, Sheets KG, Zhou Y et al (2011) Spatial correlation of mouse photoreceptor-RPE thickness between SD-OCT and histology. *Exp Eye Res* 92:155–160
- Paquet-Durand F, Silva J, Talukdar T et al (2007) Excessive activation of poly(ADP-ribose) polymerase contributes to inherited photoreceptor degeneration in the retinal degeneration 1 mouse. *J Neurosci* 27:10311–10319
- Redmond TM, Yu S, Lee E et al (1998) Rpe65 is necessary for production of 11-cis-vitamin A in the retinal visual cycle. *Nat Genet* 20:344–351
- Samardzija M, Wenzel A, Auenberg S et al (2006) Differential role of Jak-STAT signaling in retinal degenerations. *Faseb J* 20:2411–2413
- Sancho-Pelluz J, Arango-Gonzalez B, Kustermann S et al (2008) Photoreceptor cell death mechanisms in inherited retinal degeneration. *Mol Neurobiol* 38:253–269
- Seeliger MW, Beck SC, Pereyra-Munoz N et al (2005) In vivo confocal imaging of the retina in animal models using scanning laser ophthalmoscopy. *Vision Res* 45:3512–3519
- Srinivasan VJ, Monson BK, Wojtkowski M et al (2008) Characterization of outer retinal morphology with high-speed, ultrahigh-resolution optical coherence tomography. *Invest Ophthalmol Vis Sci* 49:1571–1579

Chapter 62

Rod Photoreceptor Temporal Properties in Retinal Degenerative Diseases

Yuquan Wen, Kirsten G. Locke, Donald C. Hood, and David G. Birch

Keywords Retinitis pigmentosa • Cone–rod dystrophy • Stargardt disease • Retinal degeneration • Electroretinography • Phototransduction • Rhodopsin • Peripherin/rds • ABCA4

62.1 Introduction

Among the many genetic causes of retinal degenerative disease (RDD), some predominantly affect the rods, while others predominantly affect the cones (*RetNet*, <http://www.sph.uth.tmc.edu/RetNet/disease.htm>). Because rhodopsin, for example, is unique to the rods (Liebman et al. 1974), rhodopsin mutations cause the characteristic early night blindness typical of retinitis pigmentosa (RP). Initial loss of rods is followed by secondary cone degeneration as the disease progresses (Petters et al. 1997; Koenekoop 2009; Punzo et al. 2009).

In contrast to RP, patients with cone–rod dystrophy (CRD) initially exhibit dysfunction of the cone photoreceptors and rod-mediated losses are minimal in the early stages. However, in later stage of CRD, rods also degenerate, causing elevated dark-adapted thresholds and reduction in the amplitude of dark-adapted rod

Y. Wen (✉) • K.G. Locke

Rose–Silverthorne Retinal Degenerations Laboratory, Retina Foundation of the Southwest,
9900 N Central Expressway, Suite 400, Dallas, TX 75231, USA
e-mail: ywen@retinafoundation.org

D.C. Hood

Department of Psychology and Ophthalmology, Columbia University, New York, NY, USA

D.G. Birch

Rose–Silverthorne Retinal Degenerations Laboratory, Retina Foundation of the Southwest,
9900 N Central Expressway, Suite 400, Dallas, TX 75231, USA

Department of Ophthalmology, University of Texas Southwestern Medical Center,
Dallas, TX 75390, USA

electroretinogram (ERG) (Fishman 1976). Stargardt disease represents a variant of CRD, with dystrophy limited primarily to the posterior pole. It is predominantly an autosomal recessive macular dystrophy caused by ABCA4 (ATP-binding cassette, subfamily A, member 4) mutations (Allikmets et al. 1997a, b; Fishman 2010).

It is unknown whether rod photoresponse kinetics are altered in these human RDDs, although studies in laboratory models of RP showed earlier-than-normal rod photoresponse recovery (Niculescu 2004; Kraft et al. 2005; Wen et al. 2006; Wen 2008; Wen and Kraft 2008). Here, we use paired-flash full-field ERG to characterize the rod photoresponse recovery kinetics in patients with primary rod degeneration (RP), patients with secondary rod degeneration (CRD), and patients with degeneration limited to the posterior pole (Stargardt disease).

62.2 Materials and Methods

62.2.1 Subjects

Patients were recruited from the database of the Southwest Eye Registry at the Retina Foundation of the Southwest. They included 18 patients with autosomal dominant retinitis pigmentosa (adRP) reported previously (Wen et al. 2011), 5 patients with CRD, and 4 patients with Stargardt disease. The 18 adRP patients included 10 patients harboring rhodopsin mutations and 8 patients harboring peripherin/rds mutations. Included within the 5 patients diagnosed with CRD were two autosomal recessive/isolate CRD patients heterozygous for an ABCA4 mutation (ABCA4: Asn-965-Ser or Ala-192-Thr) and one autosomal dominant patient carrying a peripherin/rds mutation (Arg-172-Trp). Individuals with normal eye exams ($n=13$) provided normative values.

In order to ensure reliable analysis of pair-flash ERG results, patients were recruited only if they retained a dark-adapted rod response amplitude of greater than 10 μ V to a ISCEV (International Society for Clinical Electrophysiology of Vision) standard rod stimulus. The tenets of the Declaration of Helsinki were followed and all subjects gave written informed consent after a full explanation of the procedures was given. All procedures were approved by the institutional review board of University of Texas Southwestern Medical Center, Dallas, TX.

62.2.2 Evaluation of the Rod Inactivation Kinetics Using Paired-Flash ERG

Prior to paired-flash ERG, the pupil of the left eye was dilated (1% tropicamide and 2.5% phenylephrine hydrochloride), and the patient was dark adapted for 45 min. Paired-flash ERG was recorded in a ganzfeld dome. A bipolar contact lens

(Burian-Allen electrode, Hansen Laboratories, Coralville, IA) was used to record the signals. Details of pair-flash ERG recording were previously described (Birch et al. 1995; Pepperberg et al. 1997). Briefly, a test flash (achromatic, 2.4 log scot td-s) was delivered prior to the probe flash ($\lambda_{\text{cut-off}}=470$ nm, 4.2 log scot td-s) with variable inter-stimulus-interval (ISI). The cone response at short (i.e., 200 ms) ISIs was subtracted from the response to the probe flash to provide a rod-only response at each ISI.

62.3 Results

62.3.1 Rod Photoresponse Recovery Kinetics in RDDs

To determine whether rod photoresponse recovery kinetics in patients with RDDs is different from normal, we derived T_{sat} from these patients using the paired-flash paradigm. Figure 62.1a–d shows the rod-only response to probe flash at indicated ISI after a fixed test flash in a normal subject (Fig. 62.1a), a patient with CRD (Fig. 62.1b), a patient with Stargardt disease (Fig. 62.1c), and a patient with RP (Fig. 62.1d), respectively. Figure 62.2 shows the relative recovery of the rod response to the test flash from saturation (A/A_{max}), where A is the derived rod response amplitude of the test flash at a particular time point ($t=$ ISI) after the test flash ($A(t)=A_{\text{max}}-A_{\text{probe}}(t)$) (Pepperberg et al. 1997). The relative recovery of rod photoresponse was fitted with an exponential recovery function ($A/A_{\text{max}}=\exp[-(t-T_{\text{sat}})/\tau]$), where T_{sat} indicates the initiation of rod recovery from saturation from the test flash. Technically, T_{sat} is the horizontal intercept of the exponential fit. In Fig. 62.2, the T_{sat} derived from the patient with RP is 254 ms, which is shorter than that derived from the normal subject ($T_{\text{sat}}=555$ ms), the patient with CRD ($T_{\text{sat}}=523$ ms) and the patient with Stargardt disease ($T_{\text{sat}}=580$ ms).

Figure 62.3 and Table 62.1 show T_{sat} values for 13 normal subjects, 5 patients with CRD, 4 patients with Stargardt disease, and 18 patients with adRP. T_{sat} derived from 5 patients with CRD was 473 ± 113 (SD) ms, which is not different from the normal 544 ± 92 (SD) ms ($P=0.26$) (Fig. 62.3; Table 62.1). T_{sat} derived from 4 patients with Stargardt disease was 491 ± 98 (SD) ms, which is not different from the normal 544 ± 92 (SD) ms ($P=0.38$) (Fig. 62.3; Table 62.1). However, T_{sat} derived from 18 patients with adRP was 331 ± 99 (SD) ms, which is 39% shorter from the normal average ($P<0.001$) (Fig. 62.3; Table 62.1). Two patients with adRP showed T_{sat} values (489 and 520 ms) within the 99% confidence interval (CI) of normal (Fig. 62.3). These two highest T_{sat} values were derived from two patients who carried peripherin/rds mutation but retained normal ERG amplitudes at the time of pair-flash ERG recording.

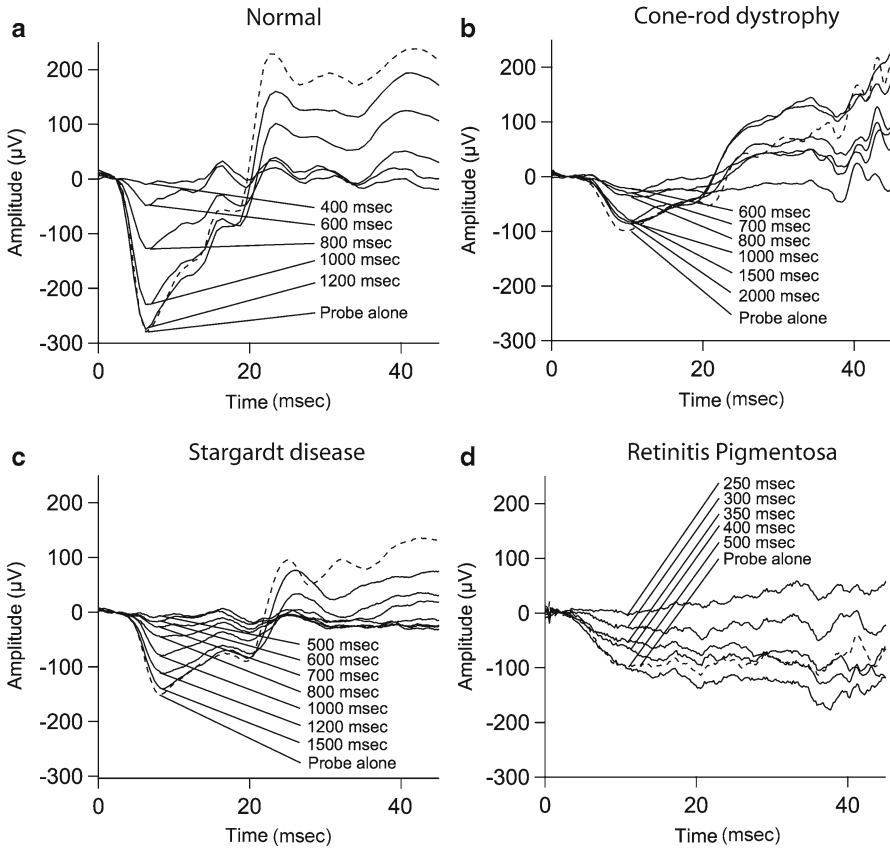


Fig. 62.1 Representative photoreponse recovery mediated by rod photoreceptors in normal subject and retinal degenerative diseases (RDDs). Representative rod-only waveforms generated by a probe flash at various inter-stimulus-interval (ISI) after a fixed test flash recorded from a normal subject (**a**), a patient with cone-rod dystrophy (CRD) (**b**), a patient with Stargardt disease (**c**), and a patient with RP (**d**). The rod-mediated photoreponse shows little recovery at ISIs of 500–600 ms in normal, CRD, and Stargardt disease (**a–c**). However, by an ISI of 500 ms, the rod-mediated photoreponse is fully recovered in the patient with RP

62.3.2 T_{sat} Is Correlated with Dark-Adapted Rod Amplitude in adRP

The ISCEV standard dark-adapted ERG rod response has been recognized as a surrogate marker for rod activity (Marmor et al. 2009). Figure 62.4 shows the relationship between T_{sat} and the ISCEV standard rod response amplitude in the 18 patients with adRP. A significant correlation exists between these two indices of rod

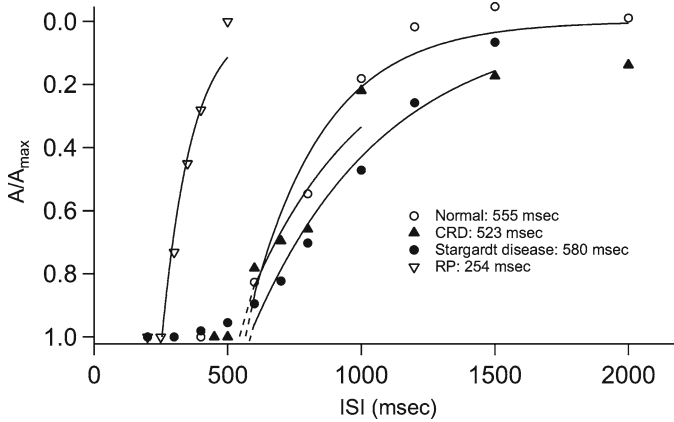


Fig. 62.2 Deriving T_{sat} from patients with RP, CRD, and Stargardt disease. T_{sat} was derived from the rod-mediated photoresponse recovery shown in Fig. 62.1 using an exponential fit model ($A/A_{max} = \exp[-(t - T_{sat})/\tau]$) (Birch et al. 1995; Pepperberg et al. 1997). T_{sat} derived from the patient with RP ($T_{sat} = 254$ ms) is shorter than normal ($T_{sat} = 555$ ms). However, T_{sat} derived from patients with CRD ($T_{sat} = 523$ ms) and Stargardt disease ($T_{sat} = 580$ ms) is comparable to normal ($T_{sat} = 555$ ms)

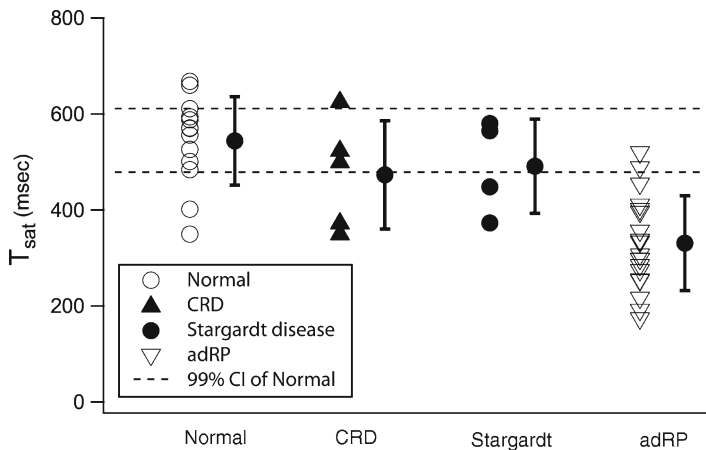


Fig. 62.3 T_{sat} derived from normal subject and RDDs. T_{sat} derived from 13 normal subjects, 5 patients with CRD, 4 patients with Stargardt disease, and 18 patients with autosomal dominant retinitis pigmentosa (adRP). Average value and standard deviation of each group is shown next to the scatter plot. Broken line: 99% confidence interval of normal T_{sat} distribution

dysfunction in patients with adRP (Pearson’s Correlation Coefficient=0.54, $P=0.01$) (Fig. 62.4). Thus, as ISCEV rod response diminishes, T_{sat} generally becomes shorter in patients with adRP. All patients with adRP with reduced rod amplitude also showed faster than normal recovery times.

Table 62.1 Characterization of rod recovery kinetics with T_{sat} in patients with RDDs and normal subjects

	Count	T_{sat} (ms)	Reduction	Significance (P)
Normal	13	544 ± 92 (SD)		
CRD	5	473 ± 113		0.26
Stargardt	4	491 ± 98		0.38
adRP	18	331 ± 99	39%	<0.001

This table presents the statistical results of T_{sat} in patients with CRD, Stargardt disease, or adRP. Statistical significance was calculated using two-tailed unpaired student t -test between sampled normal subjects and patients with RDDs

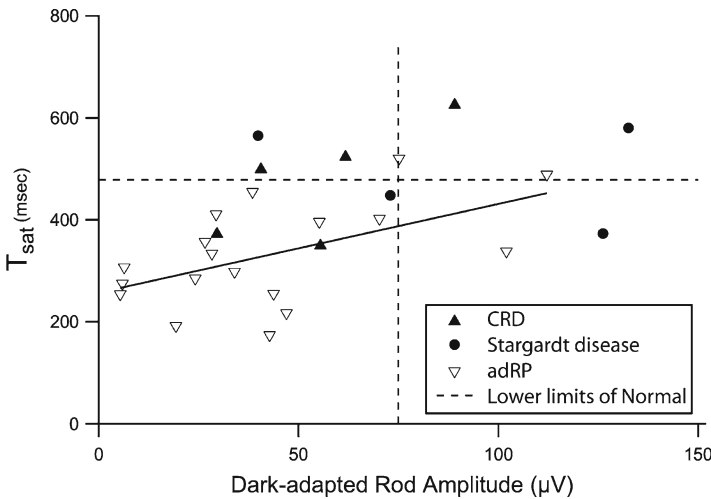


Fig. 62.4 Relationship between T_{sat} and the ISCEV standard rod response amplitude in patients with CRD, Stargardt disease, and adRP. A significant correlation (*solid line*) exists between these two indices of rod dysfunction in 18 adRP (Pearson’s Correlation Coefficient=0.54, $P=0.01$). These indices do not appear to be related in patients with CRD or Stargardt disease. *Broken line*: lower limit of normal T_{sat} and ISCEV rod amplitude (75 μ V)

The results from the patients with CRD (solid triangles) and Stargardt disease (solid circles) suggest that the correlation does not hold in these diseases (Fig. 62.4). Note that three of these patients exhibited normal T_{sat} values despite rod amplitudes less than 75 μ V, the lower limit of normal adult subjects (Birch and Anderson 1992).

62.4 Discussion

Previously, we reported that rods in retinitis pigmentosa, regardless of the inheritance pattern, recover earlier than normal (Wen et al. 2011). In this study, we found that patients with CRD and Stargardt disease show normal rod photoresponse recovery kinetics. This reinforces the suggestion that shortened rod photoresponse

recovery is a result of primary rod degeneration in RP. This finding is consistent with previous invasive studies in laboratory animals. Kraft et al. (2005) showed that transgenic rods with pro-347-leu and pro-347-ser rhodopsin, both of which associated with human adRP, have earlier-than-normal time-to-peak, diminished sensitivity to light, and reduced integration time. In addition, it has been reported that rods with the *Mertk* mutation, which is associated with autosomal recessive RP in human (Gal et al. 2000), showed earlier-than-normal recovery (Niculescu 2004; Wen et al. 2006). Furthermore, rods that survived transient light damage in albino rat exhibited earlier-than-normal recovery (Wen 2008; Wen and Kraft 2008). Contrary to shortened rod recovery in RP, prolonged rod photoresponse recovery was observed in a type of cone dystrophy associated with *GCAP1* mutations (Jiang et al. 2008). In this study, we found that CRD caused by *ABCA4* mutations ($T_{\text{sat}} = 523$ and 499 ms) is not associated with either shortened or elongated rod photoresponse recovery.

Rod photoresponse recovery kinetics can be manipulated by genetic engineering in laboratory animals (He et al. 1998; Chen et al. 2000; Kraft et al. 2006; Krispel et al. 2006; Tsang et al. 2007). Moreover, it has been shown that rods are able to recover to normal recovery kinetics in a transient light damage model (Wen 2008; Wen and Kraft 2008). Because normal T_{sat} is specific to healthy rods, rod recovery kinetics could serve as biomarker for treatment efficacy in clinical studies and trials.

Acknowledgments We thank Dr. Dianna Hughbanks-Wheaton and Kaylie Clark at the Southwest Eye Registry and the Daiger lab at UT Houston for coordinating and performing genetic testing. This investigation was supported by US National Institutes of Health grant (NEI R01 09076) to D.G.B and D.C.H. and the Foundation Fighting Blindness.

References

- Allikmets R, Shroyer NF, Singh N et al (1997a) Mutation of the Stargardt disease gene (*ABCR*) in age-related macular degeneration. *Science* 277:1805–1807
- Allikmets R, Singh N, Sun H et al (1997b) A photoreceptor cell-specific ATP-binding transporter gene (*ABCR*) is mutated in recessive Stargardt macular dystrophy. *Nat Genet* 15:236–246
- Birch DG, Anderson JL (1992) Standardized full-field electroretinography. Normal values and their variation with age. *Arch Ophthalmol* 110:1571–1576
- Birch DG, Hood DC, Nusinowitz S et al (1995) Abnormal activation and inactivation mechanisms of rod transduction in patients with autosomal dominant retinitis pigmentosa and the pro-23-his mutation. *Invest Ophthalmol Vis Sci* 36:1603–1614
- Chen CK, Burns ME, He W et al (2000) Slowed recovery of rod photoresponse in mice lacking the GTPase accelerating protein *RGS9-1*. *Nature* 403:557–560
- Fishman GA (1976) Progressive human cone-rod dysfunction (dystrophy). *Trans Sect Ophthalmol Am Acad Ophthalmol Otolaryngol* 81:OP716–724
- Fishman GA (2010) Historical evolution in the understanding of Stargardt macular dystrophy. *Ophthalmic Genet* 31:183–189
- Gal A, Li Y, Thompson DA et al (2000) Mutations in *MERTK*, the human orthologue of the RCS rat retinal dystrophy gene, cause retinitis pigmentosa. *Nat Genet* 26:270–271
- He W, Cowan CW, Wensel TG (1998) *RGS9*, a GTPase accelerator for phototransduction. *Neuron* 20:95–102

- Jiang L, Wheaton D, Bereta G et al (2008) A novel GCAP1(N104K) mutation in EF-hand 3 (EF3) linked to autosomal dominant cone dystrophy. *Vision Res* 48:2425–2432
- Koenekoop RK (2009) Why do cone photoreceptors die in rod-specific forms of retinal degenerations? *Ophthalmic Genet* 30:152–154
- Kraft TW, Allen D, Petters RM et al (2005) Altered light responses of single rod photoreceptors in transgenic pigs expressing P347L or P347S rhodopsin. *Mol Vis* 11:1246–1256
- Kraft TW, Sandoval IM, Boye SL et al (2006) Dramatically altered rod responses in rat retina overexpressing R9AP and RGS9-1. In: Society for Neuroscience Atlanta, GA
- Krispel CM, Chen D, Melling N et al (2006) RGS expression rate-limits recovery of rod photoreponses. *Neuron* 51:409–416
- Liebman PA, Jagger WS, Kaplan MW et al (1974) Membrane structure changes in rod outer segments associated with rhodopsin bleaching. *Nature* 251:31–36
- Marmor MF, Fulton AB, Holder GE et al (2009) ISCEV Standard for full-field clinical electroretinography (2008 update). *Doc Ophthalmol* 118:69–77
- Niculescu DM (2004) Physiological Characterization of the Light Response of Rod Photoreceptors in the Dystrophic Royal College of Surgeons Rat. In: *Physiological Optics Birmingham, AL: University of Alabama at Birmingham*
- Pepperberg DR, Birch DG, Hood DC (1997) Photoresponses of human rods in vivo derived from paired-flash electroretinograms. *Vis Neurosci* 14:73–82
- Petters RM, Alexander CA, Wells KD et al (1997) Genetically engineered large animal model for studying cone photoreceptor survival and degeneration in retinitis pigmentosa. *Nat Biotechnol* 15:965–970
- Punzo C, Kornacker K, Cepko CL (2009) Stimulation of the insulin/mTOR pathway delays cone death in a mouse model of retinitis pigmentosa. *Nat Neurosci* 12:44–52
- Tsang SH, Woodruff ML, Janisch KM et al (2007) Removal of phosphorylation sites of gamma subunit of phosphodiesterase 6 alters rod light response. *J Physiol* 579:303–312
- Wen Y (2008) Physiological Characterization of the Light Response of Rod Photoreceptors in the Light Damaged Rat. In: *Neurobiology Birmingham, Alabama: University of Alabama at Birmingham*
- Wen Y, Kraft TW (2008) Altered Light Response of Rod Photoreceptors Surviving Light Damage. In: *ARVO 2008 Annual Meeting Fort Lauderdale, Florida, USA*
- Wen Y, Niculescu DM, Kraft TW (2006) Desensitization of retinal photoreceptors during disease: not a story of equivalent light. In: Society for Neuroscience Atlanta, GA
- Wen Y, Locke KL, Hood DC, Birch DG (2011) Rod photoreceptor temporal properties in retinitis pigmentosa. *Exp Eye Res* 92(3):202–208

Chapter 63

ERG Critical Flicker Frequency Assessment in Humans

Kristen E. Bowles and Timothy W. Kraft

Keywords Critical flicker frequency • Aging • Electroretinogram • Flicker • Scotopic • Photopic

63.1 Introduction

Knowledge of how retinal signaling changes with age in healthy eyes may provide insights to susceptibility in age-related diseases such as age-related macular degeneration. As a person ages, there is a continuous decline of rod and ganglion cell density. The rate of cell loss is higher from the second to fourth decade of life compared to the fourth through ninth decade (Gao and Hollyfield 1992). As rod cell density decreases, the diameter of the remaining photoreceptor increases. Yet remaining photoreceptors appeared disorganized; older photoreceptors contain refractile bodies within the outer segment layer and nuclei can be dislocated to the inner segment (Curcio et al. 1993). By contrast, cone density loss did not correlate with the aging process; however, a high degree of cone density variation was seen within the age groups (Gao and Hollyfield 1992; Curcio et al. 1993).

Neither the results of psychophysical testing nor the standard electrophysiology testing shows a decrease in retinal function matching these anatomical findings. Functional loss is not statistically significant until the sixth decade of life when compared to young adults. Specifically, critical flicker frequency (CFF), or the highest frequency at which a periodic waveform is perceived as flickering, showed a slow continuous loss of CFF with increasing age. Depending on the retinal adaptation state and size of the stimuli, CFF was not statistically lower until approximately

K.E. Bowles • T.W. Kraft (✉)

Department of Vision Sciences, University of Alabama at Birmingham,
924 18th Street South, Birmingham, AL 35223, USA
e-mail: twkraft@uab.edu

the seventh decade compared to the second decade of life (Misiak 1947; Coppinger 1955; Loranger 1959). The retinal responses to the ISCEV standard tests also slowly decrease with age similar to psychophysical results. B-wave amplitude of the scotopic maximum response, which measures primary bipolar cell response, decreases only modestly until the sixth decade of life. Beyond the sixth decade of life, b-wave amplitude decreases at a faster rate and is statistically lower than amplitudes during the second decade (Birch and Anderson 1992).

To look for a more sensitive test of functional loss, one that might correlate with anatomical findings, the current study measures the retinal response to flickering stimuli in subjects 20–29 and 50–58 years of age. The present study includes ISCEV standard electroretinograms (ERG) tests and CFF measures under scotopic and photopic lighting conditions.

63.2 Materials and Methods

63.2.1 *Subject Selection and Preparation*

Subjects were volunteers; inclusion criteria were healthy male subjects between the ages 20 and 29 years or between the ages 50 and 58 years with refractive error less than -6.0 diopters, no systemic disease with known ocular manifestations such as diabetes, or existing ocular disease including ocular hypertension. All research adhered to the tenets of the Declaration of Helsinki and UAB IRB regulations. Subjects were dark adapted for 20 min and received 1% proparacaine and tropicamide in the tested eye. ERGs were recorded using the Espion system with the Colorburst mini-ganzfeld stimulator and DTL electrodes (Diagnosys, Lowell, MA).

63.2.2 *ERG Protocol*

To maximize retinal sensitivity for the dim flickering stimuli, a variation of the ISCEV standard protocol was created. The testing order was as follows: rod threshold, combined response, two scotopic CFF protocols, light adaptation, photopic flicker CFF protocols, and finally cone flash and 30 Hz flicker. Other than the additional CFF protocols, the ISCEV standard parameters were used (Marmor et al. 2004). CFF protocols began with the lowest frequency and progressively increased.

A full field flicker ERG protocol was used to find scotopic and photopic CFF. Flicker frequencies for scotopic testing ranged from 4 to 16 Hz at mean luminosities of 0.0035 and 0.009 cd/m^2 . Scotopic luminosities were obtained by adding 0.4 and 0.6 Log unit Wratten neutral density filters and a 0.9 ND Kodak filter to the Colorburst stimulator. Flicker frequencies for photopic testing ranged from 25 to 72 Hz

at mean luminosities of 10 and 40 cd/m². Data were collected with a sampling frequency of 5,000 Hz and a band pass filtered between 0 and 1,000 Hz. Stimulus wavelength was 530 nm. The subject fixated on a small red LED with the “non-tested” eye. Scotopic flicker frequency up to 32 Hz was tested in a few subjects to assess for a flicker null phenomenon; however, flicker was not detected at either scotopic or photopic luminosity.

Flicker data was analyzed using fast Fourier transforms (FFTs) (IGOR PRO v. 5.03, Wavemetrics Inc., Lake Oswego, OR). Noise was calculated after subtracting drift and then averaging data from 2 to 20 Hz for scotopic data and 20 to 160 Hz for photopic data, excluding the FFT points corresponding to the driving frequency ± 1.5 Hz. For example, for a 4 Hz stimulus, data from 2.5 to 5.5 Hz were omitted when determining the rms noise. The magnitude of the FFT peak corresponding stimulus frequency was measured, and the baseline noise was subtracted. Responses were considered significant if the magnitude of the fundamental response was two standard deviations above the averaged noise. A semi-log plot of magnitude vs. frequency was fitted with a linear regression extrapolated to threshold (set as one standard deviation above the noise, 3.8 μ V). A two tailed *t*-test was performed on the averaged data for both groups; significance was set at $p=0.05$.

63.3 Results

All individual ISCEV standard ERG results were within normal limits. However, as a group the older subjects had a significantly slower implicit time for the b-wave (107 vs. 94 ms) and smaller amplitude in the 30 Hz flicker test (75 vs. 107 μ V, $p=0.03$).

At all luminosities tested, 0.0032, 0.009, 10, and 40 cd/m², all subjects showed a decrease in flicker amplitude with increasing stimulus frequency.

63.3.1 Scotopic CFF

Figure 63.1a presents results that determined CFF at the dimmest background luminance tested, 0.0035 cd/m². The averaged flicker response curve for both groups showed a linear decline in magnitude with increasing flicker frequency up to 10 Hz, after which the slope was shallower. Individual CFFs were found by fitting a linear regression to the highest four frequency measurements for each individual subject (Table 63.1). Only one subject from each group produced a measurable response at 16 Hz. The younger subjects had higher variability in CFF compared to the older subject group at this intensity. The two groups had comparable slopes. No statistical significance was seen between the older and younger CFF values (14.0 ± 1.2 vs. 17.3 ± 1.6 Hz, mean \pm s.e.m.; $p=0.13$).

Results at the brighter scotopic luminance tested, 0.009 cd/m², also produced a linear decline with increasing frequency (Fig. 63.1b). The older group's CFF was 14.3 ± 0.1 Hz while that of the younger group was 16.3 ± 1.2 Hz (Table 63.1),

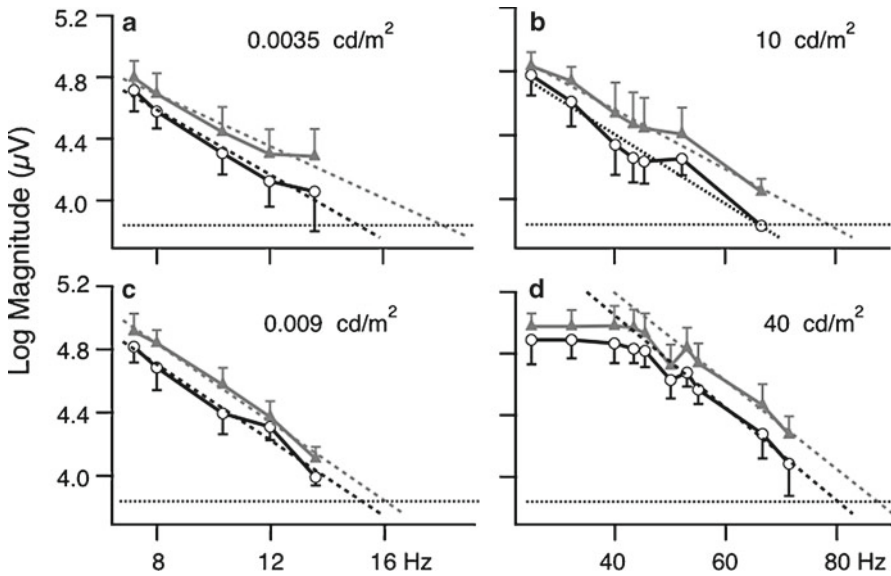


Fig. 63.1 Group averages for younger (*filled triangles*, +st. dev.) and older subjects (*open circles*, -st. dev.) at the four intensities tested. (a) Results at 0.0035 cd/m²; (b) group averages at 0.009 cd/m²; (c) group averages at 10 cd/m²; (d) group averages at 40 cd/m². *Horizontal dashed line* represents threshold. Note that the linear regressions, shown by the *thick dashed lines*, are fitted to mean results, whereas the results in the table were derived from individual fits

and these are not significantly different ($p=0.12$). The linear regression fit the mean curves produced parallel slopes (slope = -0.12). There was one outlier in the younger group at this luminosity, with a rather shallow slope (-0.07) and higher CFF (23 Hz).

63.3.2 Photopic CFF

At 10 cd/m², the CFF of the older group was statistically lower than that of the younger group ($p < 0.05$). The decrease in amplitude was not monotonic, but showed a plateau between 46 and 53 Hz in both age groups (Fig. 63.1c). The older subjects CFF ranged from 53.3 to 68.1 Hz, with an average of 61.9 ± 2.6 Hz. The younger group's CFF ranged from 53.0 to 87.4 Hz, with an average of 72.4 ± 4.2 Hz. Another indicator of greater flicker sensitivity in the younger subjects was that four out of seven older subjects had responses to the 66 Hz stimulus while six of eight younger subjects registered a measurable response.

At the brightest mean luminance, 40 cd/m², the averaged results for both groups generated curves with a plateau at the lower frequencies tested, 25–46 Hz, which then dropped off in a roughly linear fashion as seen in Fig. 63.1d. CFF was determined by fitting a line to the highest four frequencies and extrapolating to threshold.

Table 63.1 Critical flicker frequency (CFF)

Older subject	Age	0.0035 cd/m ²	0.009 cd/m ²	10 cd/m ²	40 cd/m ²	Younger subject	Age	0.0035 cd/m ²	0.009 cd/m ²	10 cd/m ²	40 cd/m ²
G1P2	51	14.5	15.0	54.6	88.0	G2P8	27	17.0	15.8	53.0	84.2
G1P3	51	13.2	14.1	66.6	80.4	G2P9	25	22.4	15.8	87.4	97.3
G1P6	58	18.8	14.0	68.1	80.4	G2P10 ^a	24			60.6	84.7
G1P7	58	11.4	14.6	53.3	69.1	G2P11	27	13.0	13.6	71.4	86.5
G1P9	51	17.7	14.3	67.8	93.2	G2P12	20	23.0	15.0	78.1	83.2
G1P11	54	11.1	13.9	56.3	75.1	G2P13	28	18.0	16.3	79.2	82.2
G1P12	53	11.5	14.2	66.4	87.1	G2P14	28	15.1	14.4	71.1	89.5
						G2P15	25	12.4	23.0	78.2	93.9

Individual ages and CFF results for two groups of subjects tested at four different mean luminositities

^aOne subject did not complete scotopic testing

The averaged CFF for the older group was 81.9 ± 3.1 Hz and for the younger group averaged CFF was 87.7 ± 2.1 Hz. Slopes of the linear regression fit to the mean older and younger groups were almost identical, -0.038 and -0.036 , respectively. The older group did not have a significantly lower CFF as compared to the younger group ($p=0.13$).

63.4 Discussion

This study assessed normal variation in CFF in two age groups of adult males. Subjects were considered “normal” after an unremarkable routine eye exam. This assessment was confirmed when ISCEV standard ERG results showed a-wave and b-wave amplitude and implicit timing within normal limits. Previous studies have shown that the standard combined b-wave amplitude slowly decreases with age, up to 55 years, whereas beyond 55 years a steep decline in b-wave amplitude was observed (Birch and Anderson 1992). We found no change in b-wave amplitude between younger males, mean 25.5 years old, and older males, 53.7 years old, but we did observe a slower b-wave in the group 3 decades older.

Because significant anatomical changes are seen by the fourth decade of life, it is possible other types of electrophysiological testing might show changes earlier in the aging process than the fifth decade.

The standard ISCEV flicker test at 30 Hz on a rod saturating background showed significantly lower amplitude in our older group. In addition, the older groups' CFF was statistically lower than the younger group at a mean background of 10 cd/m^2 but not at 40 cd/m^2 . It is possible that in the lower photopic range the aging effect is more pronounced; however, larger sample sizes might verify the general photopic decline of flicker sensitivity in older subjects.

There are very few studies of scotopic ERG CFF. Instead, previous work has been measured by psychophysical methods (Aguilar and Stiles 1954; Conner and MacLeod 1977; Hecht and Smith 1936; Odom et al. 1992). Our scotopic electrophysiologic CFF results agreed with previous psychophysical data and did not show a change in CFF at scotopic levels. Scotopic testing with a 32 Hz stimulus was conducted to test for the null flicker effect, and none was found. Therefore, the results suggest that the post-photoreceptor rod pathway remains robust in its flicker detection despite the statically decreased rod density seen between these two age groups in anatomic studies.

References

- Aguilar M, Stiles WS (1954) Saturation of the rod mechanism of the retina at high levels of stimulation. *Optica Acta* 1:59–65
- Birch DG, Anderson JL (1992) Standardized full-field electroretinogram. Normal values and their variation with age. *Arch Ophthalmol* 110:1571–1576

- Conner JD, MacLeod DI (1977) Rod photoreceptors detect rapid flicker. *Science* 195:698–699
- Coppinger NW (1955) The relationship between critical flicker frequency and chronological age for varying levels of stimulus brightness. *J Geront* 10:48–52
- Curcio CA, Millican CL, Allen KA et al (1993) Aging of the human photoreceptor mosaic: Evidence for selective vulnerability of rods in central retina. *Invest Ophthalmol Vis Sci* 34:3278–3296
- Gao H, Hollyfield JG (1992) Aging of the human retina. Differential loss of neurons and retinal pigment epithelium cells. *Invest Ophthalmol Vis Sci* 33:1–17
- Hecht S, Smith EL (1936) Intermittent stimulation by light. VI. Area and the relation between critical frequency and intensity. *J Gen Physiol* 19: 979–991
- Loranger AW (1959) Critical flicker frequency and some intellectual functions in old age. *J Geront* 14:323–327
- Marmor MF, Holder GE, Seeliger MW et al (2004) Standard for clinical electroretinography (2004 update) *Doc Ophthalmol* 108:107–114
- Misiak H (1947) Age and sex differences in critical flicker frequency. *J Exp Physiol* 37:318–322
- Odom JV, Reits D, Burger N, et al (1992) Flicker electroretinograms: A systems analytic approach. *Optom Vis Sci* 69:106–116

Part VIII
Mechanisms of Retinal Degeneration

Chapter 64

Biology of Retinoschisin

Camasamudram Vijayasathy, Lucia Ziccardi, and Paul A. Sieving

Keywords X-linked retinoschisis • Retinoschisin • Discoidin domain • Mutations • Retina • Photoreceptors • Bipolar cells • Synapse • Gene therapy

64.1 Introduction

The vertebrate retina is a light sensitive neural tissue lining the inner surface of the eye. The basic functional unit of the retina is comprised of photoreceptors, bipolar, horizontal, amacrine, and ganglion cells, which, in each point in the visual field, operate to capture light, process and integrate visual information before delivering it to the brain. The sequential positioning of the cellular components through the retinal depth, and the parallel arrangements of many such basic units across the entire retina contribute to the creation of a mosaic pattern. Many studies reveal an important role of adhesion molecules and their binding partners in controlling retinal patterning (Galli-Resta et al. 2008). Retinoschisin (RS1) is one of the proteins implicated in maintenance of retinal architecture. In young males, loss of RS1 function due to mutations in the X-linked retinoschisis gene (*RS1*; MIM: 312700) leads to splitting within the retinal layers, which impairs visual-signal processing

C. Vijayasathy
Section for Translation Research in Retinal and Macular Degeneration,
National Institute on Deafness and Other Communication Disorders,
National Institutes of Health, Bethesda, MD 20892, USA

L. Ziccardi
Neurophthalmology Unit, Fondazione “G.B. Bietti” IRCCS, Via Livenza,
300198 Rome, Italy

P.A. Sieving (✉)
National Eye Institute, National Institutes of Health, Bethesda, MD 20892, USA
e-mail: paulsieving@nei.nih.gov

and leads to progressive vision loss in the condition known as X-linked juvenile retinoschisis (XLRS) (Sauer et al. 1997).

64.2 *RS1* Gene and Protein

The human *RS1* gene on the X-chromosome spans 32.43 kb of DNA, consisting of six exons that encode a 12-kb mRNA (NM_000330.3*) which is translated into a 224 amino acid retina-specific secretory protein, RS1 (NP_000321.1). RS1 is prominently expressed by the rod and cone inner segments, including the foveal and macular cone photoreceptors, and bipolar cells (Molday et al. 2001; Reid et al. 2003). RS1 expression occurs early in postnatal development of the mouse retina and by P7 is apparent in the newly formed outer plexiform layer (OPL) (Takada et al. 2004). Pinealocytes, which are evolutionarily related to the photoreceptors, also express RS1, but the role in the pineal gland is not known (Takada et al. 2006). The 24-kDa RS1 protein encodes two functional sites of conserved sequence motifs, the N-terminus signal sequence (aa 1–21/23) that directs protein translocation to the exterior of the cell, and a long and highly conserved sequence motif termed the discoidin domain (exons 4–6; aa 64–219) (Wu et al. 2005; Vijayasarathy et al. 2006). The discoidin domain apparently contributes to the adhesive function of RS1 to preserve the retinal cell architecture and to establish proper synaptic connectivity (Takada et al. 2008). RS1 is a peripheral membrane protein bound by ionic forces to the outer leaflet of the photoreceptor inner segment plasma membrane (Vijayasarathy et al. 2007). The functional conformation of RS1 is an octamer with eight subunits joined together by Cys(59)–Cys(223) intermolecular disulfide bonds (Wu et al. 2005). Subunits within the octamer are further organized into dimers mediated by Cys(40)–Cys(40) bonds.

64.3 *RS1* Interactions

RS1 binds specifically to the anionic phospholipids for example, phosphatidylserine (PS) in the presence of Ca^{2+} (Vijayasarathy et al. 2007). Several other possible RS1 interacting ligands were identified: Na^+/K^+ ATPase and the sterile alpha and TIR motif-containing protein, SARM1 (Molday et al. 2007), alphaB crystallin and beta2 laminin (Steiner-Champlaud et al. 2006), and L-type voltage-gated calcium channel (LVGCC) (Shi et al. 2009). However, the structural basis for these interactions has not been defined. Imaging with atomic force microscopy provided biophysical evidence that RS1 causes major reorganization of PS-containing supported bilayers in the presence of calcium cations (Kotova et al. 2010). Membrane proteins often preferentially reside and function optimally within lipid domains enriched in certain types of lipids, and it is likely that a lipid-binding protein, such as RS1, may act to stabilize membrane microdomains into which membrane proteins assemble, such as Na^+/K^+ ATPase, SARM, and LVGCC. RS1 bound by phospholipids on the membrane surface can form a multimolecular stabilizing scaffold that participates in cell–matrix, cell–cell interactions, and cytoskeleton organization.

64.4 X-Linked Retinoschisis Mutations

XLRS patients harbor a wide spectrum of *RS1* mutations, with the majority occurring in the discoidin domain. Mutations are known to occur across the entire gene, including both the introns and the exons, and include missense, nonsense, frame-shift (deletions/insertions), and splice-site mutations (The Retinoschisis Consortium: <http://www.dmd.nl/rs/consortium.html>). The molecular consequences have been shown to affect RS1 biosynthesis in multiple ways, including the processing of pre-RNA transcript, translation initiation, ability to mature in the secretory pathway, and the ability to achieve a biologically active octamer conformation due to misfolding (Wu and Molday 2003; Wang et al. 2006; Vijayasarathy et al. 2009, 2010). Two major biochemical signatures emerge from these point mutations: an RS1-null phenotype results from an absolute lack of RS1 protein, whereas others give a signature of functionally incompetent misfolded mutant RS1 molecules. While some misfolded proteins (Leu12His and Leu13Pro) are disposed by the large ATP-dependent proteolytic machine involving the 26S proteasome (endoplasmic reticulum-associated degradation), other misfolded mutants (Glu72Lys, Arg102Trp, Arg213Trp, Asn179Asp, and Pro192S) are stabilized in the cell and form high molecular mass aggregates (Vijayasarathy et al. 2010).

64.5 Clinical Pathology

XLRS is transmitted in an X-linked recessive pattern that causes male-only disease, while the female carriers have no symptoms. In rare cases, skewed X-chromosome inactivation leads to XLRS phenotype heterozygous females (Rodriguez et al. 2005). Historically, XLRS lesions were thought to be related to a defect in Müller cells, which span the thickness of the retina (Mooy et al. 2002). The principle clinical pathology in XLRS includes vitreo-retinal dystrophy characterized by splitting of inner retinal layers and alterations of the vitreous body, peripheral retinal schisis with vitreous veils, inner retinal holes and tractions in half of the affected males, and a selective b-wave reduction on electroretinogram (ERG) recordings (George et al. 1996; Tantri et al. 2004; Sikkink et al. 2007; Lesch et al. 2008; Vijayasarathy et al. 2009). Abnormalities in the ERG a-wave have been observed at least in some patients (Bradshaw et al. 1999) but in many ERG a-wave remains normal (Khan et al. 2001). The stellate spoke-like maculopathy with microcysts seen at young ages may progress to macular atrophy during the third to fifth decades of life (Vijayasarathy et al. 2009). Patients experience an early onset central vision reduction. Schisis cavities may lead to ruptured vessels and vitreous bleeds, or retinal detachments may occur. XLRS patients display a particularly high clinical variability with a remarkably broad spectrum of phenotypes (Hiriyantha et al. 2001). A strict correspondence between genetic mutations and clinical severity has been sought but not found, although males harboring RS1 missense mutations seem to present a less

severe phenotype than those carrying null mutations (Bradshaw et al. 1999; Pimenides et al. 2005; Vijayasarathy et al. 2009, 2010; Sergeev et al. 2010). Genetic factors such as tyrosinase gene (*Tyr*) that modulate severity and disease penetrance have been mapped in mouse models of XLRs (Johnson et al. 2010) but have not been identified for human XLRs.

64.6 Molecular Pathology

Knockout mouse models have been helpful in deducing the molecular mechanisms of the retinal degeneration and in evaluating the strategies for gene therapy. The *RS1* knockout mice share several important clinical features with human XLRs disease (Weber et al. 2002; Zeng et al. 2004; Jablonski et al. 2005; Kjellstrom et al. 2007). Consistent with a role for *RS1* in maintaining photoreceptor stability, electron microscopy showed profound pathological alterations in the morphology of rod inner segments in the absence of *RS1* protein (Johnson et al. 2006; Takada et al. 2008). The pre- and postsynaptic processes, along with synaptic terminal proteins (*PSD 95* and *mGluR6*), were displaced from the OPL into the outer nuclear layer, and rod nuclei can be shifted into the inner segment region. Reduced areal density of synaptic vesicles at the photoreceptor presynapse was also found. Bipolar and photoreceptor cells both express *RS1*. Despite the deficiency of *RS1* in *RS1*-KO bipolar cells, the inner plexiform layer appeared morphologically intact, suggesting that bipolar axons are targeted correctly in the proximal retina. These findings imply that (a) *RS1* acts locally to maintain the photoreceptor inner segment stability and architecture; (b) the loss of integrity of OPL, inner nuclear layer, and photoreceptor cells is a major pathologic feature of the retina of the *RS1*-KO mice; (c) *RS1* appears to be needed for preservation of synaptic structures but not for synaptogenesis; (d) early effects on synaptic structure contribute to the functional deficit reflected in the b-wave reduction; and (e) axonal degeneration or axonal retraction stemming from a defect in photoreceptor homeostasis may contribute to synaptic loss in XLRs disease.

64.7 Prospects for Gene Therapy

Lack of a dominant-negative effect of XLRs mutations in carrier females provides evidence that gene transfer may be successful for XLRs patients. The *RS1* gene was introduced into the mouse models of XLRs both by a subretinal injection approach (AAV5-*RS1* vector using opsin promoter) and through intravitreal delivery of AAV8-*RS1* vector using a *RS1* promoter (Janssen et al. 2008; Park et al. 2009) at different stages of disease: early at P15, P30, P60 or late at 7 months. The vitreal route for *RS1* gene administration would be safer than subretinal injection which requires retinal surgical manipulation and vitrectomy. Overall, the gene therapy treatments in XLRs mice lead to improvement in both retinal ERG function and

morphology, and the rate and extent of degeneration were less pronounced in the treated eye than in the untreated eye of the same animal (Park et al. 2009). Gene transfer at advanced stages of the disease (7 months of age) showed poor response (Janssen et al. 2008). Treatment with AAV8-hRS p4-RS1 vector by vitreal administration resulted in robust tissue-specific RS1 expression in photoreceptor inner segments lying deep in the retina (Park et al. 2009). Most importantly, cellular expression of RS1 was correctly targeted with this vector and was not seen in ocular tissues that do not normally express RS1 (optic nerve, retinal fiber layer, peripheral cornea, or ciliary body). The results hold promise for future clinical trials in human patients and as a new therapeutic strategy for XLR5 treatment.

References

- Bradshaw K, George N, Moore A et al (1999) Mutations of the XLR5 gene cause abnormalities of photoreceptor as well as inner retinal responses of the ERG. *Doc Ophthalmol* 98:153–173
- Galli-Resta L, Leone P, Bottari D et al (2008) The genesis of retinal architecture: an emerging role for mechanical interactions? *Prog Retin Eye Res* 27:260–283
- George ND, Yates JR, Moore AT (1996) Clinical features in affected males with X-linked retinoschisis. *Arch Ophthalmol* 114:274–280
- Hirianna KT, Singh-Parikshak R, Bingham EL et al (2001) Searching for genotype-phenotype correlations in X-linked juvenile retinoschisis. In: *New Insights Into Retinal Degenerative Diseases*. (Anderson RE LVM, Hollyfield JG, ed), pp 45–53. New York: : Plenum Publishers
- Jablonski MM, Dalke C, Wang X et al (2005) An ENU-induced mutation in Rs1h causes disruption of retinal structure and function. *Mol Vis* 11:569–581
- Janssen A, Min SH, Molday LL et al (2008) Effect of late-stage therapy on disease progression in AAV-mediated rescue of photoreceptor cells in the retinoschisin-deficient mouse. *Mol Ther* 16:1010–1017
- Johnson BA, Ikeda S, Pinto LH, Ikeda A (2006) Reduced synaptic vesicle density and aberrant synaptic localization caused by a splice site mutation in the Rs1h gene. *Vis Neurosci* 23:887–898
- Johnson BA, Cole BS, Geisert EE, et al. (2010) Tyrosinase is the modifier of retinoschisis in mice. *Genetics* 186:1337–1344
- Khan NW, Jamison JA, Kemp JA et al (2001) Analysis of photoreceptor function and inner retinal activity in juvenile X-linked retinoschisis. *Vision Res* 41:3931–3942
- Kjellstrom S, Bush RA, Zeng Y et al (2007) Retinoschisin gene therapy and natural history in the Rs1h-KO mouse: long-term rescue from retinal degeneration. *Invest Ophthalmol Vis Sci* 48:3837–3845
- Kotova S, Vijayarath C, Dimitriadis EK et al (2010) Retinoschisin (RS1) interacts with negatively charged lipid bilayers in the presence of Ca²⁺: an atomic force microscopy study. *Biochemistry* 49:7023–7032
- Lesch B, Szabo V, Kanya M et al (2008) Clinical and genetic findings in Hungarian patients with X-linked juvenile retinoschisis. *Mol Vis* 14:2321–2332
- Molday LL, Wu WW, Molday RS (2007) Retinoschisin (RS1), the protein encoded by the X-linked retinoschisis gene, is anchored to the surface of retinal photoreceptor and bipolar cells through its interactions with a Na/K ATPase-SARM1 complex. *J Biol Chem* 282:32792–32801
- Molday LL, Hicks D, Sauer CG et al (2001) Expression of X-linked retinoschisin protein RS1 in photoreceptor and bipolar cells. *Invest Ophthalmol Vis Sci* 42:816–825
- Mooy CM, Van Den Born LI, Baarsma S et al (2002) Hereditary X-linked juvenile retinoschisis: a review of the role of Muller cells. *Arch Ophthalmol* 120:979–984

- Park TK, Wu Z, Kjellstrom S et al (2009) Intravitreal delivery of AAV8 retinoschisin results in cell type-specific gene expression and retinal rescue in the Rs1-KO mouse. *Gene Ther* 16:916–926
- Pimenides D, George ND, Yates JR et al (2005) X-linked retinoschisis: clinical phenotype and RS1 genotype in 86 UK patients. *J Med Genet* 42:e35
- Reid SN, Yamashita C, Farber DB (2003) Retinoschisin, a photoreceptor-secreted protein, and its interaction with bipolar and muller cells. *J Neurosci* 23:6030–6040
- Rodriguez FJ, Rodriguez A, Mendoza-Londono R et al (2005) X-linked retinoschisis in three females from the same family: a phenotype-genotype correlation. *Retina* 25:69–74
- Sauer CG, Gehrig A, Warneke-Wittstock R et al (1997) Positional cloning of the gene associated with X-linked juvenile retinoschisis. *Nat Genet* 17:164–170
- Sergeev YV, Caruso RC, Meltzer MR et al (2010) Molecular modeling of retinoschisin with functional analysis of pathogenic mutations from human X-linked retinoschisis. *Hum Mol Genet* 27:27
- Shi L, Jian K, Ko ML et al (2009) Retinoschisin, a new binding partner for L-type voltage-gated calcium channels in the retina. *J Biol Chem* 284:3966–3975
- Sikkink SK, Biswas S, Parry NR et al (2007) X-linked retinoschisis: an update. *J Med Genet* 44:225–232
- Steiner-Champlaud MF, Sahel J, Hicks D (2006) Retinoschisin forms a multi-molecular complex with extracellular matrix and cytoplasmic proteins: interactions with beta2 laminin and alphaB-crystallin. *Mol Vis* 12:892–901
- Takada Y, Vijayasarathy C, Zeng Y et al (2008) Synaptic pathology in retinoschisis knockout (Rs1-/-) mouse retina and modification by rAAV-Rs1 gene delivery. *Invest Ophthalmol Vis Sci* 49:3677–3686
- Takada Y, Fariss RN, Muller M, Bush RA, Rushing EJ, Sieving PA (2006) Retinoschisin expression and localization in rodent and human pineal and consequences of mouse RS1 gene knockout. *Mol Vis* 12:1108–1116
- Takada Y, Fariss RN, Tanikawa A et al (2004) A retinal neuronal developmental wave of retinoschisin expression begins in ganglion cells during layer formation. *Invest Ophthalmol Vis Sci* 45:3302–3312
- Tantri A, Vrabec TR, Cu-Unjieng A et al (2004) X-linked retinoschisis: a clinical and molecular genetic review. *Surv Ophthalmol* 49:214–230
- Vijayasarathy C, Takada Y, Zeng Y et al (2007) Retinoschisin is a peripheral membrane protein with affinity for anionic phospholipids and affected by divalent cations. *Invest Ophthalmol Vis Sci* 48:991–1000
- Vijayasarathy C, Gawinowicz MA, Zeng Y et al (2006) Identification and characterization of two mature isoforms of retinoschisin in murine retina. *Biochem Biophys Res Commun* 349:99–105
- Vijayasarathy C, Ziccardi L, Zeng Y et al (2009) Null retinoschisin-protein expression from an RS1 c354del1-ins18 mutation causing progressive and severe XLRS in a cross-sectional family study. *Invest Ophthalmol Vis Sci* 50:5375–5383
- Vijayasarathy C, Sui R, Zeng Y, et al (2010) Molecular mechanisms leading to null-protein product from retinoschisin (RS1) signal-sequence mutants in X-linked retinoschisis (XLRS) disease. *Hum Mutat* 31:1251–1260
- Wang T, Zhou A, Waters CT, O'Connor E et al (2006) Molecular pathology of X linked retinoschisis: mutations interfere with retinoschisin secretion and oligomerisation. *Br J Ophthalmol* 90:81–86
- Weber BH, Schrewe H, Molday LL et al (2002) Inactivation of the murine X-linked juvenile retinoschisis gene, Rs1h, suggests a role of retinoschisin in retinal cell layer organization and synaptic structure. *Proc Natl Acad Sci USA* 99:6222–6227
- Wu WW, Molday RS (2003) Defective discoidin domain structure, subunit assembly, and endoplasmic reticulum processing of retinoschisin are primary mechanisms responsible for X-linked retinoschisis. *J Biol Chem* 278:28139–28146
- Wu WW, Wong JP, Kast J, Molday RS (2005) RS1, a discoidin domain-containing retinal cell adhesion protein associated with X-linked retinoschisis, exists as a novel disulfide-linked octamer. *J Biol Chem* 280:10721–10730
- Zeng Y, Takada Y, Kjellstrom S et al (2004) RS-1 Gene Delivery to an Adult Rs1h Knockout Mouse Model Restores ERG b-Wave with Reversal of the Electronegative Waveform of X-Linked Retinoschisis. *Invest Ophthalmol Vis Sci* 45:3279–3285

Chapter 65

Transcriptome Analyses to Investigate the Pathogenesis of RNA Splicing Factor Retinitis Pigmentosa

Michael H. Farkas, Greg R. Grant, and Eric A. Pierce

Keywords RNA-seq • Next-generation sequencing • Retinitis pigmentosa • RNA splicing factors • *Prpf* • Transcriptome

65.1 Introduction

Retinitis pigmentosa (RP) is a progressive rod–cone dystrophy that is characterized by night blindness, loss of peripheral vision, which can eventually lead to complete loss of vision (Hartong et al. 2006). RP primarily affects the rod photoreceptors and retinal pigment epithelium (RPE), and is the most common inherited retinal dystrophy, affecting as many as 1:1,000–1:3,500 people worldwide (Bunker et al. 1984; Grondahl 1987; Haim et al. 1992; Xu et al. 2006).

Displaying all modes of Mendelian inheritance, RP is genetically heterogeneous. To date 46 loci have been identified for nonsyndromic RP, leading to the identification of 36 causative genes (RetNet 2009). Genes implicated in RP encode components of the phototransduction cascade, retinal transcription factors, photoreceptor structural proteins, cilia proteins, and ubiquitously expressed components of the spliceosome. Currently, genes encoding five spliceosomal components have been identified in autosomal dominant RP (adRP). These include the pre-mRNA processing factors 3, 8, and 31 (*PRPF3*, 8, and *31*), RP9, and SNRNP200 (Maita et al. 2005; McKie et al. 2001; Vithana et al. 2001; Zhao et al. 2009).

M.H. Farkas • E.A. Pierce (✉)

Ocular Genomics Institute, Berman Gund Laboratory, Department of Ophthalmology, Massachusetts Eye and Ear Infirmary, 243 Charles St., Boston, MA 02114, USA
e-mail: eric_pierce@meei.harvard.edu

G.R. Grant

Penn Center for Bioinformatics, University of Pennsylvania, Philadelphia, PA 19104, USA

Mutations in splicing factors are of particular interest because these proteins are ubiquitously expressed and required for proper splicing of pre-mRNA in all cell types, yet mutations in *PRPF3*, *8*, and *31*, RP9, and SNRNP200 are only known to cause retinal disease. The spliceosome is a dynamic complex consisting of five small nucleolar ribonucleoproteins (snRNPs); U1, U2, U4/U6, and U5 (Grainger and Beggs 2005). The U1 and U2 snRNPs are the first to bind a pre-mRNA by recognizing the 5' splice site and branch site, respectively. This interaction along with the binding of auxiliary splicing proteins defines the intron/exon boundaries and recruits the U4/U6-U5 tri-snRNP. Following a series of protein and RNA rearrangements, the U4/U6-U5 tri-snRNP becomes the catalytic component that drives splicing (Beggs et al. 1995; Farkas et al. 2010). The five splicing factors implicated in adRP are all components of the U4/U6-U5 tri-snRNP.

65.2 The Retinal Pigment Epithelium Is the Primary Tissue Affected by Mutations in the Pre-mRNA Processing Factors 3, 8, and 31

An intriguing aspect of question about RP caused by mutations in spliceosomal components is how the identified mutations result in a tissue-specific disease. Prior to the generation of animal models with single codon mutations in the *Prpf3* and *8* genes, mimicking the most common mutations found in patients with this disease and *Prpf31*-knockout animals that mimic the null alleles found in most *PRPF31* patients, it was unclear which retinal cell type was adversely affected (Graziotto et al. 2011). Ultrastructural analyses of the retinas of the gene-targeted mice indicated above showed that the RPE degenerated prior to the photoreceptors. The RPE of wild-type animals appears normal with long apical microvilli interdigitating the photoreceptor outer segments and visible basal infoldings. The RPE of mutant animals, however, shows a loss of basal infoldings, extensive vacuolization, and amorphous deposits between the RPE and Bruch's membrane (Fig. 65.1).

Interestingly, the mutations that lead to the RNA splicing factor forms of RP are not unlike disease-causing mutations in other spliceosomal components with regard to the tissue specificity of pathogenesis. A better studied spliceosome-associated disease is spinal muscular atrophy (SMA), which is an autosomal recessive neurodegenerative disorder characterized by degeneration of α -motor neurons in the spinal cord leading to muscular atrophy, and ultimately paralysis (Zhang et al. 2008). The SMA disease gene produces a ubiquitously expressed SMN1 (survival of motor neurons) protein that is necessary for the biogenesis and assembly of pre-mRNA processing factors, and other ribonucleoprotein complexes, involved in splicing. Mutations in the *SMN1* gene lead to this disease resulting in an altered snRNP stoichiometry affecting only motor neurons. It is hypothesized that the altered snRNP composition in turn results in generation of aberrant mRNA transcripts which are responsible for disease (Zhang et al. 2008).

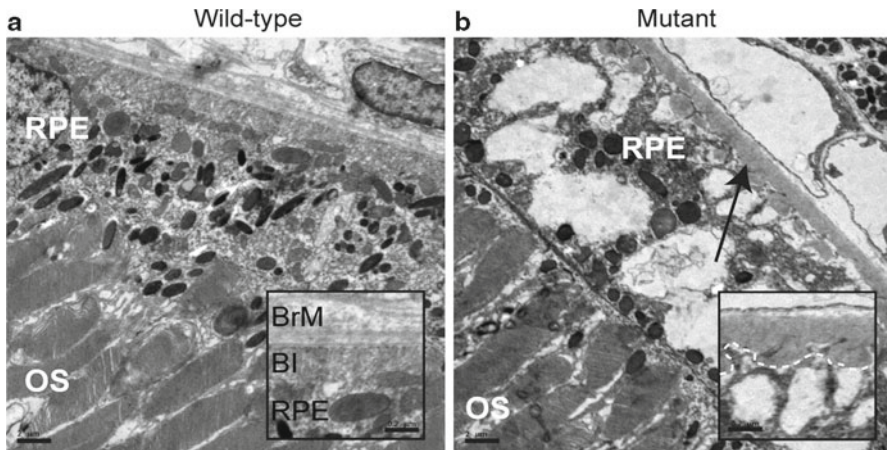


Fig. 65.1 Electron microscopy of representative retina and RPE from 2-year-old homozygous *Prpf3*-T494M, *Prpf8*-H2309P, and heterozygous 1-year-old *Prpf31* knockout mice. (a) Representative wild-type control image for all three mouse models. (b) Representative image for all three mouse models showing vacuoles in the RPE. In the *Prpf3*-T494M and *Prpf8*-H2309P mice, loss of basal infoldings and accumulation of amorphous material between Bruch's membrane and the RPE is evident (arrow). These changes are not evident in the control samples. Scale bars: (a, b) 2 μ m; inset scale bars 0.2 μ m. OS outer segments; RPE retinal pigment epithelium

65.3 Identifying Aberrantly Spliced Transcripts Using Next-Generation Sequencing

Similar to mutations in the *SMN1* gene, mutations in the pre-mRNA processing factors are believed to cause RP via production of aberrantly spliced transcripts. Identification of these transcripts is a challenging task given the number of expressed genes and the complexity of the transcriptome with thousands of genes in the mouse, many of which can be alternatively spliced (Bult et al. 2008). Until recently it has been difficult to study splicing-associated diseases in great enough detail to be effective. Exon microarrays have been useful, but have many disadvantages such as limited probe sets that only cover annotated splice junction boundaries, high levels of background, and low sensitivity (Teng and Xiao 2009). The development of next-generation sequencing (NGS) technologies provided the ability to fully interrogate the transcriptome and has overcome many of the limitations of microarrays (Shendure 2008).

65.3.1 Next-Generation Sequencing Platforms

Multiple platforms exist for NGS-based transcriptome analyses (reviewed in more detail in Simon et al. 2009; Ansorge 2009). Similar to microarrays, NGS analyses provide quantitative expression data. However, NGS analyses also provide data for

novel splicing events with greater sensitivity and less background (Shendure 2008). In many cases, the best platform to study splicing is a trade-off between the number of sequencing reads generated and the length of the sequence. Our lab has demonstrated that at least 100 million 108 bp paired-end reads are necessary for full coverage of the mouse neural retina transcriptome (Farkas et al. 2010). This is consistent with data from transcriptome analyses of other tissues and organisms (Blencowe et al. 2009).

65.3.2 An Overview of RNA-Seq

Although the protocols for the generation of cDNA libraries from total RNA are rapidly evolving, the principles underlying the process stay the same. High quality mRNA is isolated and fragmented to a user-defined length (currently 250–350 bp). The fragmented mRNA is then converted to double-stranded cDNA and common adapters are ligated to the ends of the cDNA (Wang et al. 2009). Following sequencing, the data is aligned to the genome or transcriptome and can be analyzed for gene expression, expression of individual exons, alternative/aberrant splicing, insertion/deletions, and polymorphisms.

65.3.3 Bioinformatic Analysis of RNA-Seq Data

The generation of NGS technology applications for RNA sequencing (RNA-seq) applications quickly outpaced the available algorithms for aligning and analyzing the resulting sequence data. Unlike genomic resequencing, RNA-seq requires the ability to align reads that can span multiple exons that can be tens of thousands of bases apart. One option to overcome this obstacle is to align reads to a transcriptome database. While this is a good method for quickly aligning millions of reads that cross annotated splice junctions, it is incapable of identifying reads that cross novel junctions. Identifying novel junctions in normal tissues is an important step toward identifying aberrant transcripts in disease tissues since the two types must be compared to differentiate normal from abnormal.

Algorithms designed to tackle the issues presented by RNA-seq data are continually being developed and adapted (Li and Homer 2010). Most are geared toward aligning data quickly and less compute-intensive. However, this often sacrifices sensitivity and leads to a loss of data. With the advent of Cloud Computing (McPherson 2009; Langmead et al. 2010), there is no longer a need for ultra-efficient algorithms that sacrifice data quality, but rather the ability to develop algorithms that maximize the number reads aligned in a manner that is more sensitive and accurate. We have developed the RNA-seq Ultimate Mapper (RUM) that is based on the alignment algorithms Bowtie to align ungapped reads to the genome and transcriptome followed by a gapped alignment using BLAT (Blast-like

Alignment Tool) (Langmead et al. 2009; Kent 2002; Farkas et al. 2010). Using Bowtie, millions of reads that map to both the genome and the annotated transcriptome can quickly be aligned. BLAT is a gapped aligner that is more computationally intensive and slower than Bowtie, but allows for the alignment of reads that span novel junctions. The combination of these two algorithms provides speed, accuracy, and the ability to identify previously unannotated transcripts.

65.4 RNA-Seq Analyses of RNA Splicing Factor Mutant Mice

Preliminary analyses of the neural retinas and RPE of wild-type and splicing factor mutant mice using RUM have revealed that there are thousands of novel/aberrant transcripts being produced in the mutant animals. Since all of the splicing factors are part of the U4/U6-U5 tri-snRNP and they all interact within this complex, we hypothesized that a common splicing mechanism is deficient. Thus, it is logical to compare all data sets for a common set of aberrant transcripts. When this is performed on the preliminary RNA-seq data produced for the *Prpf3*, *8*, and *31* mouse models, as few as 52 transcripts are in common among all three mutant mice. These results suggest that pathogenic splicing errors are not widespread in RP. Two likely outcomes from the generation of aberrant transcripts are production of truncated proteins or the absence of protein production due to nonsense-mediated decay of the aberrant transcript. Given these outcomes, we will test candidate aberrant transcripts for pathogenic effects in the RPE and neural retina using both cell culture and mouse models.

65.5 Future Experimental Approaches

Obvious limitations exist to studying human RNA splicing factor RP disease in gene-targeted mouse models. For example, species-based differences in gene expression and alternative splicing may complicate identification of the cause for RNA splicing factor RP. However, it is not usually possible to obtain high quality ocular tissues from patients affected with RP. A potential solution to this problem is the use of retinal cells differentiated from patient-specific induced pluripotent stem (iPS) cells (Yu et al. 2007, 2009). The generation of iPS-derived RPE and retinal cells has recently been reported (Buchholz et al. 2009; Carr et al. 2009). It is possible that iPS-derived retinal cells from patients with RNA splicing factor RP could provide a source of human cells for transcriptome analyses, although the suitability of these cells for such studies remains to be/will need to be evaluated (Buchholz et al. 2009; Carr et al. 2009; Ozsolak et al. 2010).

RNA-seq is a continuously evolving method for studying molecularly complex diseases such as the RNA splicing factor forms of RP. As the methodology and bioinformatic approaches continue to develop and expand, many questions regarding

aberrant splicing and the affect on various tissues may be answered. Furthermore, the characterization of the transcriptomes in normal cells and tissues such as the retina and RPE will help answer other basic biological questions as well. For example, a more thorough annotation of these transcriptomes will aid research into other retinal diseases, as well as provide insight into splice site preference at a single tissue level.

Acknowledgments This work has been supported by the Ruth-Kirschstein National Research Service Award, Foundation Fighting Blindness, Penn Genome Frontiers Institute, Rosanne Silbermann Foundation, F.M. Kirby Foundation, and Research to Prevent Blindness.

References

- Ansorge WJ (2009) Next-generation DNA sequencing techniques. *New Biotechnol* 25:195–203
- Beggs JD, Teigelkamp S, Newman AJ (1995) The role of PRP8 protein in nuclear pre-mRNA splicing in yeast. *J Cell Sci Suppl* 19:101–105
- Blencowe BJ, Ahmad S, Lee LJ (2009) Current-generation high-throughput sequencing: deepening insights into mammalian transcriptomes. *Genes Dev* 23:1379–1386
- Buchholz DE, Hikita ST, Rowland TJ et al (2009) Derivation of functional retinal pigmented epithelium from induced pluripotent stem cells. *Stem Cells* 27:2427–2434
- Bult CJ, Eppig JT, Kadin JA et al (2008) The Mouse Genome Database (MGD): Mouse biology and model systems. *Nuc Acid Res* 36:D724–D728
- Bunker CH, Berson EL, Bromley WC et al (1984) Prevalence of retinitis pigmentosa in Maine. *Am J Ophthalmol* 97:357–365
- Carr AJ, Vugler AA, Hikita ST et al (2009) Protective effects of human iPS-derived retinal pigment epithelium cell transplantation in the retinal dystrophic rat. *PLoS ONE* 4:e8152
- Farkas MH, Bujakowska K, Krishan, A et al (2010) Characterization of aberrant splicing by next generation high-throughput RNA-seq in mice with targeted mutations in *Prpf3*, *Prpf8*, and *Prpf31*. *Invest Ophthalmol Vis Sci* 51:ARVO E-Abstract 3667
- Grainger RJ, Beggs JD (2005) Prp8 protein: At the heart of the spliceosome. *RNA* 11:533–557
- Graziotto JJ, Farkas MH, Bujakowska KM et al (2011) Three gene targeted mouse models of RNA splicing factor RP show late onset RPE and retinal degeneration. *Invest Ophthalmol Vis Sci* 52(1):190–198
- Grondahl J (1987) Estimation of prognosis and prevalence of retinitis pigmentosa and Usher syndrome in Norway. *Clin Genet* 31:255–264
- Haim M, Holm NV, Rosenberg T (1992) Prevalence of retinitis pigmentosa and allied disorders in Denmark. I Main results. *Acta Ophthalmol (Copenh)* 70:178–186
- Hartong DT, Berson EL, Dryja TP (2006) Retinitis pigmentosa. *Lancet* 368:1795–1809
- Kent WJ (2002) BLAT – the BLAST-like alignment tool. *Genome Res* 12:656–664
- Langmead B, Hansen K, Leek J (2010) Cloud-scale RNA-sequencing differential expression analysis with Myrna. *Genome Biol* 11:R83
- Langmead B, Trapnell C, Pop M et al (2009) Ultrafast and memory-efficient alignment of short DNA sequences to the human genome. *Genome Biol* 10:R25
- Li H, Homer N (2010) A survey of sequence alignment algorithms for next-generation sequencing. *Brief Bioinform* 11:473–483
- Maita H, Kitaura H, Ariga H, Iguchi-Arigo SM (2005) Association of PAP-1 and Prp3p, the products of causative genes of dominant retinitis pigmentosa, in the tri-snRNP complex. *Exp Cell Res* 302:61–68
- McKie AB, McHale JC, Keen TJ et al (2001) Mutations in the pre-mRNA splicing factor gene *PRPC8* in autosomal dominant retinitis pigmentosa (RP13). *Hum Mol Genet* 10:1555–1562

- McPherson JD (2009) Next-generation gap. *Nat Meth* 6:S2–S5
- Ozsolak F, Goren A, Gymrek M et al (2010) Digital transcriptome profiling from attomole-level RNA samples. *Genome Res* 20:519–525
- RetNet (2009) RetNet Web site address. <http://www.sph.uth.tmc.edu/Retnet/>
- Shendure J (2008) The beginning of the end for microarrays? *Nat Meth* 5:585–587
- Simon SA, Zhai J, Nandety RS et al (2009) Short-read sequencing technologies for transcriptional analyses. *Annu Rev Plant Biol* 60:305–333
- Teng X, Xiao H (2009) Perspectives of DNA microarray and next-generation DNA sequencing technologies. *Sci C Life Sci* 52:7–16
- Vithana EN, Abu-Safieh L, Allen MJ et al (2001) A human homolog of yeast pre-mRNA splicing gene, PRP31, underlies autosomal dominant retinitis pigmentosa on chromosome 19q13.4 (RP11). *Mol Cell* 8:375–381
- Wang Z, Gerstein M, Snyder M (2009) RNA-Seq: a revolutionary tool for transcriptomics. *Nat Rev Genet* 10:57–63
- Xu L, Hu L, Ma K, et al (2006) Prevalence of retinitis pigmentosa in urban and rural adult Chinese: The Beijing Eye Study. *Eur J Ophthalmol* 16:865–866
- Yu J, Hu K, Smuga-Otto K et al (2009) Human induced pluripotent stem cells free of vector and transgene sequences. *Science* 324:797–801
- Yu J, Vodyanik MA, Smuga-Otto K et al (2007) Induced pluripotent stem cell lines derived from human somatic cells. *Science* 318:1917–1920
- Zhang Z, Lotti F, Dittmar K et al (2008) SMN deficiency causes tissue-specific perturbations in the repertoire of snRNAs and widespread defects in splicing. *Cell* 133:585–600
- Zhao C, Bellur DL, Lu S et al (2009) Autosomal-dominant retinitis pigmentosa caused by a mutation in SNRNP200, a gene required for unwinding of U4/U6 snRNAs. *Am J Hum Genet* 85:617–627

Chapter 66

The Role of the X-linked Retinitis Pigmentosa Protein RP2 in Vesicle Traffic and Cilia Function

Nele Schwarz, Alison J. Hardcastle, and Michael E. Cheetham

Keywords Retinal degeneration • RP2 • Arl3 • UNC119 • Membrane • Photoreceptor outer segment • Cilia • Vesicle traffic • NSF • PC2

66.1 Introduction

RP is a genetically heterogeneous group of diseases characterised by night blindness and loss of peripheral vision, as the rod photoreceptor cells dysfunction and die followed by cone photoreceptor cell death. X-linked RP (XLRP) is the most severe form of RP with mutations in the *RP2* gene accounting for approximately 15% of all XLRP cases (Schwahn et al. 1998; Hardcastle et al. 1999). The 350 amino acid RP2 protein is ubiquitously expressed and does not appear to be enriched in retina (Chapple et al. 2000), but patients with *RP2* mutations appear to have only a retinal pathology without other organ involvement.

66.2 RP2 Structure

RP2 contains a homology domain with tubulin cofactor C (TBCC) (Schwahn et al. 1998), which acts with other cofactor chaperones (TBCA, TBCB, TBCD, and TBCE) in the tubulin folding pathway (Tian et al. 1996). Determination of the RP2 crystal structure revealed that the TBCC-like domain forms a right-handed parallel beta-helix containing seven coils, similar to cyclase-associated protein (Kuhnel et al. 2006). The C-terminus of RP2 shows structural similarity with nucleoside

N. Schwarz • A.J. Hardcastle • M.E. Cheetham (✉)
UCL Institute of Ophthalmology, 11-43 Bath Street, London, EC1V 9EL, UK
e-mail: michael.cheetham@ucl.ac.uk

diphosphate kinase 1 (NDK1, Evans et al. 2006; Kuhnel et al. 2006), but lacks the catalytic residues that mediate the transfer of phosphate to generate nucleoside triphosphates (Yoon et al. 2006). Most of the reported RP2 missense mutations lie within residues conserved with TBCC, or another related protein TBCCD1 (Stephan et al. 2007), suggesting a potential overlap in function for this family of proteins. This hypothesis was supported by *in vitro* studies that showed RP2, in conjunction with TBCD, could partly substitute for TBCC function as a tubulin GTPase-activating protein (GAP) (Bartolini et al. 2002); however, RP2 was not able to replace TBCC in the tubulin heterodimerisation reaction (Bartolini et al. 2002), and TBCC does not compensate for RP2 in rods of XLRP patients (Grayson et al. 2002).

The small GTPase, ADP ribosylation factor (Arf)-like protein, Arl3, was the first identified RP2 interacting partner (Bartolini et al. 2002). Arl3 is a ubiquitous microtubule associated protein, which localises to the connecting cilium in photoreceptors (Grayson et al. 2002). Arl3 knock-out mice develop retinal degeneration and polycystic kidneys, suggesting cilia dysfunction (Schrick et al. 2006). The structure of the RP2:Arl3 complex and subsequent detailed biochemical analyses revealed that RP2 is a GAP for Arl3 and therefore a negative regulator for Arl3, not an effector as previously thought (Veltel et al. 2008). Pathogenic mutations, e.g., R118H, disrupt the Arl3 GAP activity. Furthermore, RP2 could replace the yeast homologue of the TBCC family, CIN2, to act as a GTPase for the yeast Arl protein CIN4 suggesting that this GAP activity is a conserved function of the TBCC family (Veltel et al. 2008).

A common function of TBCC domain proteins may be linked to centrioles. For example, a *Chlamydomonas* protein of the TBCCD1 clade (ASQ2) is required for mother–daughter centriole linkage and mitotic spindle orientation (Feldman and Marshall 2009). Disruption of mammalian TBCCD1 caused the dissociation of the centrosome from the nucleus and disorganisation of the Golgi apparatus (Gonçalves et al. 2010). In another study, a *Trypanosoma* protein with the RP2 class of TBCC domain (TbRP2), but no other similarity to human RP2, was linked to flagella function (Stephan et al. 2007). TbRP2 localised to the mature basal body of the flagellum. Loss of TbRP2 caused shortened flagella and defects in axonemal microtubule formation, but had no effect on other microtubule structures (Stephan et al. 2007).

Collectively, these findings suggested that mutations and/or loss of RP2 may cause XLRP by disrupting Arl3-related small GTPase signalling and affecting the centriole-associated function. Recent data confirm a role for RP2 and Arl3 in cilia function and suggest a role in protein and vesicle traffic.

66.3 RP2 Cilia Localisation and Function

Posttranslational modification by myristoylation (at G2) and palmitoylation (at C3) at the N-terminal dual acylation motif (MGCXFSK) target RP2 to the plasma membrane and detergent-resistant membranes (Chapple et al. 2000, 2003). Mutations affecting this motif (e.g., deletion of S6 or disruption of G2) prevent membrane

association (Chapple et al. 2000, 2002; Schwahn et al. 2001), illustrating that these modifications are vital for correct localisation and function of RP2. Studies in fixed human retina detected RP2 on the cytoplasmic face of the plasma membrane in all the cell types in the retina (Grayson et al. 2002). More recently, detailed investigation in unfixed mouse retina detected RP2 in the ciliary apparatus at the cilium-associated centriole and the basal body of photoreceptor cells, in addition to the plasma membrane (Evans et al. 2010). Myristoylation was essential for RP2 localisation at the basal body of human retinal epithelial (RPE) cells (Evans et al. 2010) and renal epithelium cell cilia (Hurd et al. 2010).

In addition to the enrichment of RP2 at the photoreceptor cilia base, RP2 localises to the periciliary ridge and the Golgi complex in mouse retina (Evans et al. 2010). The periciliary ridge, Golgi complex and basal body function in close association with each other to regulate inner to outer segment export of proteins in photoreceptor cells. Therefore, RP2 is ideally localised to couple the movement of proteins destined for cilia from the endomembrane system to the base of the cilium and via intraflagellar transport (IFT) into the cilium itself. Depletion of RP2 by siRNA or overexpression of a constitutively active GTP form of Arl3 (Arl3-Q71L), which mimics loss of RP2's GAP activity, led to fragmentation of the Golgi network in RPE cells and dispersal of components of the IFT machinery, such as IFT20, from the peribasal body pool (Evans et al. 2010).

A model has been proposed in which RP2 and Arl3, together with the Arl3 interactor human retinal gene (HRG) 4 (or Unc119), could function in the transport of prenylated proteins to intracellular transport vesicles in the connecting cilium (Veltel and Wittinghofer 2009). In this model, HRG4 would only bind to prenylated proteins after dissociation from Arl3-GTP. This dissociation is induced by RP2 binding to Arl3-GTP, which stimulates GTP hydrolysis and releases HRG4 from the transient ternary complex, thereby allowing it to deliver, or remove, prenylated proteins from a membrane. RP2 recruits Arl3-Q71L to the plasma membrane and both proteins decorate intracellular vesicles, particularly in the Golgi (Evans et al. 2010). Therefore, expression of constitutively active Arl3 with its GAP, RP2, sequesters and concentrates both proteins at a normally transient interaction site on internal vesicles. This suggests both Arl3 and RP2 can bind vesicles and may regulate vesicle traffic. Furthermore, HRG4 may act in concert with Arl3-GTP to deliver, or remove, proteins from a range of intracellular membranes. After delivery of vesicles to the base of the cilium, RP2 may also function as a docking signal for IFT vesicles, allowing specific unloading of the cargo at the ciliary base (Fig. 66.1).

66.4 New RP2 Interaction Partners

Recently, two new RP2 interaction partners were identified, N-ethylmaleimide sensitive factor (NSF, Holopainen et al. 2010) and polycystin 2 (PC2, Hurd et al. 2010). NSF is a ubiquitous ATPase involved in vesicle-membrane fusion by associating with the soluble NSF attachment factor receptor (SNARE) complex (Söllner et al. 1993;

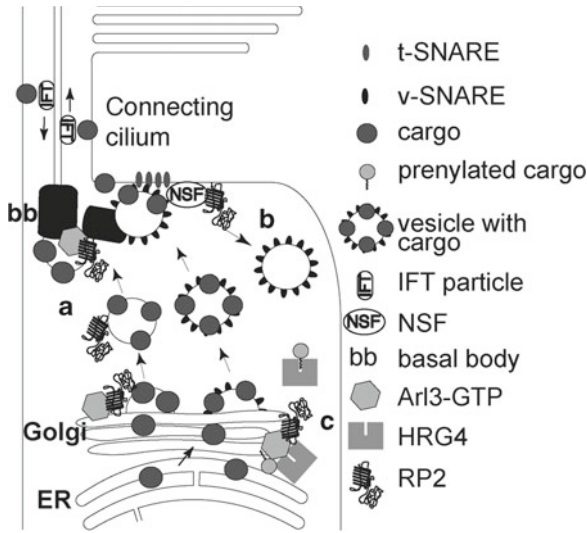


Fig. 66.1 RP2 localization and function in photoreceptor cells. (a) RP2 links pericentriolar vesicle transport between the Golgi and the primary cilium. Following fusion of vesicles with the pericentriolar membrane surrounding the basal body (bb) cargo is transported into the cilium by intraflagellar transport (IFT). (b) RP2 co-localises with NSF, which is important for disassembly of used NSF receptor attachment complexes (SNAREs). Vesicular SNAREs (vSNARE) attach post-Golgi to the vesicle coat and bind to plasma membrane SNAREs (tSNARE). (c) RP2, Arl3-GTP and HRG4 form a transient ternary complex. RP2 stimulated GTP hydrolysis by Arl3 facilitates the insertion and removal of prenylated proteins into membranes by HRG4

Mayer et al. 1996). RP2 and NSF co-localise at the base of the outer segment in mouse retina (Holopainen et al. 2010), suggesting a role for RP2 in regulation of SNARE-mediated protein delivery to the ciliary base or periciliary ridge (Fig. 66.1).

Additionally, RP2 co-localised with PC2 in cilia of renal epithelial cells and was involved in trafficking and secretion of PC2. RNAi mediated knock-down of RP2 caused cilia swelling and accumulation of PC2 at the distal tip (Hurd et al. 2010), a morphology similar to that seen in motile cilia of the respiratory tract in Bardet-Biedl syndrome knock-out mice (Shah et al. 2008). Therefore, RP2 could play a role in retrograde trafficking or possibly secretion of proteins from the cilia tip. This is of special interest as photoreceptors regularly shed the distal portion of the outer segment for phagocytosis by the RPE and disruption of this process is associated with retinal degeneration. PC2 dysfunction leads to polycystic kidney disease (Harris and Torres 2009), while patients with mutations in RP2 only display a retinal disease phenotype. It is therefore unclear whether the proposed trafficking or secretion defect of PC2 in RP2 patients has a clinical manifestation.

66.5 Conclusions

The localisation of RP2 to basal bodies and cilia in photoreceptors and kidney cells has linked RP2 dysfunction with ciliopathies. To increase our understanding of RP2 function, it is important to identify the mechanisms by which RP2 regulates vesicle trafficking to the primary cilium and thereby contributes to cilia maintenance and function. This is especially important as RP2 and its interaction partners are ubiquitously expressed proteins, yet patients with RP2 mutations appear to have only a retinal pathology. The identification of retina-specific interaction partners or future detailed analyses of RP2 in the retina may clarify why the loss of RP2 leads specifically to RP.

Acknowledgements This work is supported by the British Retinitis Pigmentosa Society.

References

- Bartolini F, Bhamidipati A, Thomas S et al (2002) Functional overlap between Retinitis Pigmentosa 2 protein and the tubulin-specific chaperone cofactor C. *J Biol Chem* 277:14629–14634
- Chapple JP, Hardcastle AJ, Grayson C et al (2000) Mutations in the N-terminus of the X-linked retinitis pigmentosa protein RP2 interfere with the normal targeting of the protein to the plasma membrane. *Hum Mol Genet* 9:1919–1926
- Chapple JP, Hardcastle AJ, Grayson C et al (2002) Delineation of the plasma membrane targeting domain of the X-linked retinitis pigmentosa protein RP2. *Invest Ophthalmol Vis Sci* 43:2015–2020
- Chapple JP, Grayson C, Hardcastle AJ et al (2003) Organization on the plasma membrane of the retinitis pigmentosa protein RP2: investigation of association with detergent-resistant membranes and polarized sorting. *Biochem J* 372:427–433
- Gonçalves J, Nolasco S, Nascimento R et al (2010) TBCCD1, a new centrosomal protein, is required for centrosome and Golgi apparatus positioning. *EMBO* 11:194–200
- Evans RJ, Hardcastle AJ, Cheetham ME (2006) Focus on molecules: X-linked Retinitis Pigmentosa 2 protein, RP2. *Exp Eye Res* 82:543–544
- Evans RJ, Schwarz N, Nagel-Wolfrum K et al (2010) The retinitis pigmentosa protein RP2 links pericentriolar vesicle transport between the Golgi and the primary cilium. *Hum Mol Genet* 19:1358–1367
- Feldman JL, Marshall WF (2009) ASQ2 encodes a TBCC-like protein required for mother-daughter centriole linkage and mitotic spindle orientation. *Curr Biol* 19:1238–1243
- Grayson C, Bartolini F, Chapple JP et al (2002) Localization in the human retina of the X-linked retinitis pigmentosa protein RP2, its homologue cofactor C and the RP2 interacting protein Arl3. *Hum Mol Genet* 11:3065–3074
- Hardcastle AJ, Thiselton DJ, van Maldergem L et al (1999) Mutations in the RP2 gene cause disease in 10% of families with familial X-linked retinitis pigmentosa assessed in this study. *Am J Hum Genet* 64:1210–1215
- Harris PC, Torres VE (2009) Polycystic Kidney Disease. *Ann Rev Med* 60:321–337
- Holopainen JM, Cheng CL, Molday LL et al (2010) Interaction and localization of the retinitis pigmentosa protein RP2 and NSF in retinal photoreceptor cells. *Biochem* 49:7439–7447
- Hurd T, Zhou W, Jenkins P et al (2010) The retinitis pigmentosa protein RP2 interacts with polycystin 2 and regulates cilia-mediated vertebrate development. *Hum Mol Genet* 19:4330–4344

- Kuhnel K, Veltel S, Schlichting I et al (2006) Crystal structure of the human retinitis pigmentosa 2 protein and its interaction with Arl3. *Structure* 14:367–378
- Mayer A, Wickner W, Haas A (1996) Sec18p (NSF)-driven release of Sec17p (alpha-SNAP) can precede docking and fusion of yeast vacuoles. *Cell* 85:83–94
- Schrick JJ, Vogel P, Abuin A et al (2006) ADP-ribosylation factor-like 3 is involved in kidney and photoreceptor development. *Am J Pathol* 168:1288–1298
- Schwahn U, Lenzer S, Dong J et al (1998) Positional cloning of the gene for X-linked retinitis pigmentosa 2. *Nat Genet* 19:327–332
- Schwahn U, Paland N, Techritz S et al (2001) Mutations in the X-linked RP2 gene cause intracellular misrouting and loss of the protein. *Hum Mol Genet* 10:1177–1183
- Shah AS, Farmen SL, Moninger TO et al (2008) Loss of Bardet-Biedl syndrome proteins alters the morphology and function of motile cilia in airway epithelia. *Proc Natl Acad Sci* 105:3380–3385
- Söllner T, Bennet MK, Whiteheart SW et al (1993) A protein assembly-disassembly pathway in vitro that may correspond to sequential steps of synaptic vesicle docking, activation, and fusion. *Cell* 75:409–418
- Stephan A, Vaughan S, Shaw MK et al (2007) An essential quality control mechanism at the eukaryotic basal body prior to intraflagellar transport. *Traffic* 8:1323–1330
- Tian G, Huang Y, Rommelaere H et al (1996) Pathway leading to correctly folded β -tubulin. *Cell* 86:287–296
- Veltel S, Gasper R, Eisenacher E et al (2008) The retinitis pigmentosa 2 gene product is a GTPase-activating protein for Arf-like 3. *Nat Struct Mol Biol* 15:373–380
- Veltel S, Wittinghofer A (2009) RPGR and RP2: targets for the treatment of X-linked retinitis pigmentosa? *Expert Opin Ther Targets* 13:1239–1251
- Yoon JH, Qiu J, Cai S et al (2006) The retinitis pigmentosa-mutated RP2 protein exhibits exonuclease activity and translocates to the nucleus in response to DNA damage. *Exp Cell Res* 312:1323–1334

Chapter 67

***Caenorhabditis elegans* as a Model Organism for Ciliopathies and Related Forms of Photoreceptor Degeneration**

Calvin A. Mok and Elise Héon

Keywords Bardet–Biedl syndrome • *C. elegans* • Photoreceptor degeneration • Primary cilia • Ciliopathy • Model organism

67.1 Introduction

Bardet–Biedl syndrome (BBS) is an autosomal recessive, pleiotropic disorder with an incidence of approximately 1 in 150,000 individuals in North American and European populations (Beales et al. 1997). This congenital disorder’s primary features include a combination of obesity, cystic renal and digit anomalies and always photoreceptor degeneration leading to vision loss by the second decade of life. Secondary features can include anosmia, diabetes, subclinical hearing loss and liver dysfunction among others (Baker and Beales 2009). To date, 16 genes have been identified as associated with the manifestation of BBS in most human patients (OMIM #209900). This genetic heterogeneity is associated with a high number of private and novel mutations the validation of which can be challenging with no

C.A. Mok

The Program in Genetics and Genome Biology, The Hospital for Sick Children,
555 University Avenue, Toronto, ON, Canada, M5G 1X8

Samuel Lunenfeld Research Institute, Mount Sinai Hospital, Toronto, ON, Canada, M5G 1X5

E. Héon (✉)

The Program in Genetics and Genome Biology, The Hospital for Sick Children,
555 University Avenue, Toronto, ON, Canada, M5G 1X8

Department of Ophthalmology and Vision Sciences, The Hospital for Sick Children,
555 University Avenue, Toronto, ON, Canada, M5G 1X8

e-mail: elise.heon@sickkids.ca

straightforward biological assay. A number of BBS proteins (*BBS1/2/4/5/7/8/9*) have been shown to form a complex; the BBSome, which promotes ciliogenesis (Loktev et al. 2008). The pleiotropic nature of this disease has been linked to the role of these proteins in the possible function and maintenance of an evolutionarily conserved organelle known as the primary cilium (for review, see Zaghoul and Katsanis 2009).

The primary cilium is normally a non-motile, 9+0 microtubule doublet structure protruding from the surface cell membranes. This organelle can participate in a number of chemo-, thermo-, and mechanosensory roles (Evans et al. 2006). Furthermore, the primary cilium is involved in a number of important signalling pathways that include Wnt, Sonic Hedgehog (Shh) and planar cell polarity (PCP) (Huangfu et al. 2003; Lin et al. 2003; Corbit et al. 2005; 2008; Ross et al. 2005; Rohatgi et al. 2007; Jones et al. 2008). Each of these pathways can play important roles in developmental morphology as well as later roles in cell proliferation and cell signalling.

In mammalian systems, cilia are thought to be present nearly ubiquitously, even if only transiently in some cell types (Marshall and Nonaka 2006). The photoreceptor outer segment complexes are the largest mammalian sensory cilia as they are bridged by a modified primary cilium. Dysfunction of this “bridge” has been implicated in BBS as well as a number of growing ciliopathies including Nephronophthisis, Leber’s congenital amaurosis, Senior–Løken syndrome and Joubert syndrome (Zaghoul and Katsanis 2009).

Both vertebrate and invertebrate systems have been key to elucidating the cellular functions of BBS proteins (Tobin and Beales 2009; Zaghoul and Katsanis 2009). Murine models have recapitulated a large number of human BBS features (excepting digit anomalies) although the exact aetiology of many of these features remains unclear. The pathology of vision loss clearly indicates that photoreceptors are initially normal, implying relatively normal development. The progression of the vision loss implies a complex pathogenesis related in some form to photoreceptor survival itself.

67.2 *C. elegans* BBS Proteins Play a Role in IFT Transport

The nematode *Caenorhabditis elegans* was instrumental in initially identifying the possible molecular functions of BBS proteins (Ou et al. 2005; Pan et al. 2006). Specifically, a number of BBS genes share orthologs with *C. elegans* (Inglis et al. 2006). These genes are expressed by 60 sensory neurons and their protein products localise at the ciliated endings of dendrites to undergo intraflagellar transport (IFT) (Blacque et al. 2004). The absence of these proteins results in disrupted IFT, loss of ciliary function as noted by defects in the uptake of the lipophilic dye DiI and morphological defects to cilia structure (Blacque et al. 2004).

Ou et al. used the *C. elegans* IFT motor movement phenotype to identify an important role for BBS proteins in maintaining motor kinetics. Two motors, heterotrimeric kinesin-II and homodimeric OSM-3 act co-ordinately to transport

IFT-B and IFT-A raft proteins, respectively, along the middle segment of *C. elegans* cilia (Ou et al. 2005). At the distal segment, OSM-3 acts alone to transport both IFT-A and IFT-B rafts. The absence of BBS-1, -7, or -8 proteins, however, caused a dissociation of kinesin-II and OSM-3 such that these motors move separately at 1.3 and 0.5 $\mu\text{m/s}$, respectively (Ou et al. 2005; Pan et al. 2006). This dissociation leads to the accumulation of IFT-B proteins at the distal end of the primary cilium. It was thus concluded that BBS proteins serve to associate IFT-A and IFT-B rafts in order to facilitate turnover of machinery for eventual retrograde transport.

Lechtreck et al. chose to examine the molecular functions of the BBS proteins in the flagellated organism *Chlamydomonas reinhardtii* (Lechtreck et al. 2009). Here they identified a number of known non-phototactic mutants as having genetic lesions to *bbs* genes. *C. reinhardtii* BBS proteins regulate the accumulation of signalling proteins.

It was confirmed that flagellar assembly was normal in *bbs4* mutants although they did not exhibit an axonemal response to Ca^{2+} ions, thereby indicating functional defects to this structure. Lechtreck et al. further confirmed the presence of a BBSome-like complex in *C. reinhardtii* consisting of at least BBS1, -5, -7, and -8 although it was present in sub-stoichiometric amounts in comparison to other ciliary components when examined by immunofluorescence microscopy.

The absence of BBS4 protein led to an accumulation of signalling proteins in the flagellar axoneme that were not present in wild-type fractions. The authors attributed these changes in protein complement as defects to either the exclusion or removal of these proteins from the flagellum. Interestingly, newly forming flagella in *bbs4* mutants displayed normal phototactic behaviours that were later lost in these animals, supporting their theory of accumulation-related defects.

67.3 BBS Proteins Function in RPE Cells

Jin et al. have shown that BBS proteins may play a role outside of IFT using retinal pigment epithelium (RPE) cultures (Jin et al. 2010). Jin et al. first identified the presence of BBSome components in RPE extracts. Using bioinformatic techniques, they further identified that BBSome components have canonical coat-like structural elements. These elements are similar to those found on COPI and COPII which participate in the transport of proteins between the Golgi and endoplasmic reticulum (McMahon and Mills 2004; Staggs et al. 2007).

These findings prompted Jin et al. to identify that BBSome components are indeed recruited to membrane structures such as liposomes via the action of the Arf-like GTPase, ARL6, which is not a component of the BBSome but is also known as BBS3. Lastly, Jin et al. surmised that certain classes of membrane proteins may be targeted by the BBSome/ARL6 complex and confirmed that the ciliary targeting signal of the GPCR SSTR3 and similar variants can associate non-ciliary proteins to the BBSome, causing their localization at the ciliary membrane. Thus BBSome proteins may have dual functions in both IFT function and in the accumulation or targeting of specific membrane proteins to the ciliary membrane.

67.4 *C. elegans* Have Phototransduction Components

Of the approximately 20,000 protein-coding genes in *C. elegans*, 35% are estimated to have human homologs (Lai et al. 2000). Regardless, *C. elegans* has a large theoretical ciliome which resembles that of other ciliomes from varying species (for review, see Inglis et al. 2006) likely due to the high level of conservation in the function of this organelle. Despite the relative complexity of its ciliome, *C. elegans* is not capable of “visual” perception. However, these nematodes are capable of photosensation through a number of ciliated neurons (Ward et al. 2008; Liu et al. 2010). More recently, Liu et al. investigated whether or not the putative photoreceptor neurons of *C. elegans* had similar functional dynamics to human photoreceptors by exploring the role of G-protein coupled receptors (GPCRs), guanylate cyclases (GCs) and phosphodiesterases (PDEs) in this *C. elegans* signal transduction pathway (Liu et al. 2010).

Liu et al. confirmed that the dissociation of GPCRs by the membrane permeable peptide mSIRK disrupted the light-mediated response in *C. elegans*. Unlike the vertebrate receptor, however, PDEs did not appear to play a role in this signal cascade, likely due to low GC activity in dark conditions. They next identified a seven transmembrane domain receptor mutant (*lite-1*) in a forward genetics screen for phototaxis defects. Liu et al. concluded that despite the presence of similar components in light transduction, the roles of GCs and PDEs are different from that of vertebrate photoreceptors. Furthermore, the overall signal transduction cascade appears to begin with a complex involving the taste receptor-like protein LITE-1 as opposed to homologs of opsins.

67.5 Is *C. elegans* a Good Animal Model to Study Photoreceptor Degeneration?

Although putative photoreceptor neurons in *C. elegans* do not follow conventional vertebrate pathways (Liu et al. 2010), many biological pathways are highly conserved in this model to offer a strong genetic organism in dissecting the basis of photoreceptor degeneration. Namely, the high conservation of the ciliome with an emphasis on the biogenesis, maintenance and function of the cilium, makes *C. elegans* an ideal model for studying ciliopathic forms of photoreceptor degeneration. Furthermore, a number of phototransduction genes associated with vision loss (beyond those of BBS proteins) are conserved in *C. elegans*. For example, homologs of cyclic nucleotide-gated ion channels, cGMP-dependent protein kinases, PDEs and guanylate cyclases, despite differing roles to vertebrates in phototransduction, still play a role in the aetiology of retinal degeneration.

We hypothesized that a number of signalling pathways will remain functionally conserved across multiple genomes, including that of the nematode. By accurately analysing the phenotypic characteristics of *C. elegans* *bbs* mutants, we can use the

power of this genetic model to identify the aetiology of *bbs* phenotypes. In doing so, we can begin to model the role of cilia in *C. elegans* and have the potential to identify new signalling pathways that can then be explored in human syndromes such as BBS. *C. elegans* provides a relatively inexpensive and rapid approach to deciphering basic biological questions related to vision loss.

References

- Baker K, Beales PL (2009) Making sense of cilia in disease: the human ciliopathies. *Am J Med Genet C Semin Med Genet* 151C:281–295
- Beales PL, Warner AM, Hitman GA et al (1997) Bardet-Biedl syndrome: a molecular and phenotypic study of 18 families. *J Med Genet* 34:92–98
- Blacque OE, Reardon MJ, Li C et al (2004) Loss of *C. elegans* BBS-7 and BBS-8 protein function results in cilia defects and compromised intraflagellar transport. *Genes Dev* 18:1630–1642
- Corbit KC, Aanstad P, Singla V et al (2005) Vertebrate Smoothed functions at the primary cilium. *Nature* 437:1018–1021
- Corbit KC, Shyer AE, Dowdle WE et al (2008) Kif3a constrains beta-catenin-dependent Wnt signalling through dual ciliary and non-ciliary mechanisms. *Nat Cell Biol* 10:70–76
- Evans JE, Snow JJ, Gunnarson AL et al (2006) Functional modulation of IFT kinesins extends the sensory repertoire of ciliated neurons in *Caenorhabditis elegans*. *J Cell Biol* 172:663–669
- Huangfu D, Liu A, Rakeman AS et al (2003) Hedgehog signalling in the mouse requires intraflagellar transport proteins. *Nature* 426:83–87
- Inglis PN, Borojevich KA, Leroux MR (2006) Piecing together a ciliome. *Trends Genet* 22:491–500
- Jin H, White SR, Shida T et al (2010) The conserved Bardet-Biedl syndrome proteins assemble a coat that traffics membrane proteins to cilia. *Cell* 141:1208–1219
- Jones C, Roper VC, Foucher I et al (2008) Ciliary proteins link basal body polarization to planar cell polarity regulation. *Nat Genet* 40:69–77
- Lai CH, Chou CY, Ch'ang LY et al (2000) Identification of novel human genes evolutionarily conserved in *Caenorhabditis elegans* by comparative proteomics. *Genome Res* 10:703–713
- Lechtreck KF, Johnson EC, Sakai T et al (2009) The *Chlamydomonas reinhardtii* BBSome is an IFT cargo required for export of specific signaling proteins from flagella. *J Cell Biol* 187:1117–1132
- Lin F, Hiesberger T, Cordes K et al (2003) Kidney-specific inactivation of the KIF3A subunit of kinesin-II inhibits renal ciliogenesis and produces polycystic kidney disease. *Proc Natl Acad Sci USA* 100:5286–5291
- Liu J, Ward A, Gao J et al (2010) *C. elegans* phototransduction requires a G protein-dependent cGMP pathway and a taste receptor homolog. *Nat Neurosci* 13:715–722
- Loktev AV, Zhang Q, Beck JS et al (2008) A BBSome subunit links ciliogenesis, microtubule stability, and acetylation. *Dev Cell* 15:854–865
- Marshall WF, Nonaka S (2006) Cilia: tuning in to the cell's antenna. *Curr Biol* 16:R604–614
- McMahon HT, Mills IG (2004) COP and clathrin-coated vesicle budding: different pathways, common approaches. *Curr Opin Cell Biol* 16:379–391
- Ou G, Blacque OE, Snow JJ et al (2005) Functional coordination of intraflagellar transport motors. *Nature* 436:583–587
- Pan X, Ou G, Civelekoglu-Scholey G et al (2006) Mechanism of transport of IFT particles in *C. elegans* cilia by the concerted action of kinesin-II and OSM-3 motors. *J Cell Biol* 174:1035–1045
- Rohatgi R, Milenkovic L, Scott MP (2007) Patched1 regulates hedgehog signaling at the primary cilium. *Science* 317:372–376

- Ross AJ, May-Simera H, Eichers ER et al (2005) Disruption of Bardet-Biedl syndrome ciliary proteins perturbs planar cell polarity in vertebrates. *Nat Genet* 37:1135–1140
- Stagg SM, LaPointe P, Balch WE (2007) Structural design of cage and coat scaffolds that direct membrane traffic. *Curr Opin Struct Biol* 17:221–228
- Tobin JL, Beales PL (2009) The nonmotile ciliopathies. *Genet Med* 11:386–402
- Ward A, Liu J, Feng Z et al (2008) Light-sensitive neurons and channels mediate phototaxis in *C. elegans*. *Nat Neurosci* 11:916–922
- Zaghloul NA, Katsanis N (2009) Mechanistic insights into Bardet-Biedl syndrome, a model ciliopathy. *J Clin Invest* 119:428–437

Chapter 68

Towards a Pathological Mechanism for IMPDH1-Linked Retinitis Pigmentosa

Dharia A. McGrew and Lizbeth Hedstrom

Keywords IMP dehydrogenase • Retinitis pigmentosa • Rhodopsin • Leber congenital amaurosis • Purine metabolism • Translation regulation

68.1 Introduction

Up to 1 in 3,500 individuals is affected by retinitis pigmentosa (RP), a common form of inherited blindness (Hartong et al. 2006). The onset, severity, and progression of disease varies widely even within families (Hamel 2006). RP is characterized by degeneration of the rod photoreceptors via apoptosis, which is followed by the secondary death of cone photoreceptors. Patients experience impaired night and peripheral vision followed by the progressive narrowing of the visual field. The molecular mechanisms that trigger the apoptotic pathway are poorly understood (Berger et al. 2010).

Over 40 genes have been linked to various forms of RP (RetNet <http://www.sph.uth.tmc.edu/retnet/>). Novel RP genes are identified on a regular basis, and yet a significant number of alleles remain unmapped. Most RP genes are involved in phototransduction. Rhodopsin mutations alone account for ~25% of cases. However, several RP-linked genes are ubiquitously expressed. One of the most curious of such genes is the RP10 allele, which is linked to the gene for inosine 5'-monophosphate dehydrogenase (*IMPDH1*) (Bowne et al. 2002; Kennan et al. 2003). *IMPDH1*-linked RP accounts for approximately 2% of autosomal dominant RP. *IMPDH1* is

D.A. McGrew
Department of Biology, Brandeis University, Waltham, MA 02453, USA

L. Hedstrom (✉)
Department of Biology, Brandeis University, Waltham, MA 02453, USA

Department of Chemistry, Brandeis University, Waltham, MA 02453, USA
e-mail: hedstrom@brandeis.edu

also linked to a more severe retinal degeneration, Leber congenital amaurosis (LCA) (Bowne et al. 2006a, b).

Cellular replication, transcription, signaling, and other processes all require the biosynthesis of nucleotides. IMPDH catalyzes the oxidation of IMP to XMP, the rate limiting step in de novo guanine nucleotide production. Because of its pivotal role in cell proliferation, inhibitors of IMPDH are useful for immunosuppressive, antiviral, and cancer chemotherapy. The enzymatic properties of IMPDH are well characterized (Hedstrom 2009). However, *IMPDH1* knockout mice develop normal retina and do not get RP, suggesting that disease is not simply the result of the depletion of guanine nucleotides (Aherne et al. 2004).

68.2 IMPDH and the Retina

Humans have two genes for IMPDH referred to as type I and type II (Hedstrom 2009). These proteins share 84% sequence identity and have very similar enzymatic properties. In general, type I is constitutively expressed while type II is upregulated in rapidly proliferating cells. Both isoforms are expressed in most cell types, although some cells have one or the other as the predominant form (Gu et al. 2003). Type II is expressed in the developing eye. Only type I appears to be expressed in the adult eye where it is restricted to the photoreceptors and bipolar cells (Aherne et al. 2004). This isoform switch coordinates with the laminar organization of retinal layers that occurs around the time of eye opening (Gunter et al. 2008). IMPDH type I is found in the inner segment, outer nuclear layer and synaptic terminals in photoreceptors, and the cytoplasm and nucleus of other cells (Bowne et al. 2006a; Gunter et al. 2008; Tam et al. 2008).

68.3 IMPDH Structure and Function

The functional unit of IMPDH is a tetramer. Each monomer has a catalytic α/β barrel core. An additional subdomain is situated on the opposite end from the active site and contains two cystathionine β -synthase (CBS) repeats (Fig. 68.1; Sintchak et al. 1996). Removal of the subdomain has no effect on IMPDH activity (Hedstrom 2009). The adRP-linked mutations cluster at the interface of the subdomain and catalytic core, away from the active site of the enzyme (Fig. 68.1a). At least three mutations are clearly pathogenic (R224P, D226N, and R231P) and at least four others are likely pathogenic (T116M, R238E, V268I, and H372P). Two mutations (R105W and N198K) are linked to LCA (Bowne et al. 2006b). As expected from their location, pathogenic mutations do not have an effect on the enzymatic activity or oligomerization. Instead, the RP mutations must perturb the function of the subdomain (Mortimer and Hedstrom 2005). CBS repeats are found in a variety of proteins, where they often bind adenine nucleotides (Kemp 2004), although this role may not be applicable in IMPDH (Mortimer and Hedstrom 2005). Work with bacterial

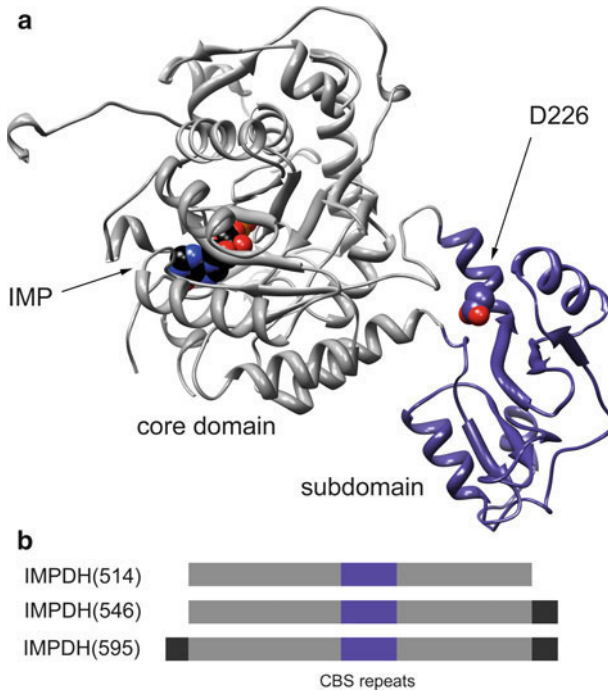


Fig. 68.1 (a) Crystal structure of an IMPDH monomer (*Streptococcus pyogenes*, PDB: 1ZFJ; this is the only crystal structure where the subdomain is completely visible). Each monomer is made up of an α/β barrel core domain (gray) and a subdomain of unknown function (purple). The active site is shown with IMP substrate (black spacefill). The position of the most common pathogenic mutation D226N (spacefill) can be seen at the interface of the two domains. (b) Scheme showing the differences between the canonical IMPDH1(514), IMPDH1(546), and IMPDH1(595)

IMPDH has suggested that the subdomain regulates intracellular levels of adenine nucleotides, although the mechanism of this process has not yet been elucidated (Pimkin and Markham 2008; Pimkin et al. 2009). Our work suggests that IMPDH bind single stranded nucleic acids, and that this activity is mediated by the subdomain (McLean et al. 2004).

68.4 Retinal Splice Variants

The “canonical form” of IMPDH1 expressed in most cells has 514 amino acids but there are two variants expressed in the retina generated by alternative splicing of mRNA (Gunter et al. 2008; Spellacy et al. 2007). These forms are referred to as IMPDH1(546) and IMPDH1(595), respectively. Both contain a C-terminal extension of 32 amino acids while IMPDH1(595) has an additional N-terminal extension (Fig. 68.1b). The retinal isoforms have identical enzymatic activity to IMPDH1(514) in our hands (Xu et al. 2008), but others observed increased enzymatic activity in

the IMPDH1(595) (Gunter et al. 2008). Similar retinal IMPDH1 isoforms are found in many organisms, suggesting that they have a conserved function unique to photoreceptors (Spellicy et al. 2007).

68.5 IMPDH and Translation

IMPDH binds single-stranded nucleic acids with high affinity (McLean et al. 2004), although the physiological role of this activity remains unclear. Curiously, IMPDH has been found associated with chromatin and telomeres in yeast (Cornuel et al. 2002; Park and Ahn 2010). Our work finds the enzyme associated with polyribosomes, suggesting that IMPDH (described in more detail below). These observations suggest that IMPDH may play a part in replication, transcription, and/or translation distinct from its role in guanine nucleotide biosynthesis. Importantly, the pathogenic adRP mutations reduce the affinity of the interaction with nucleic acids (Mortimer and Hedstrom 2005; Bowne et al. 2006b), suggesting that perturbation of this activity may cause disease (note: we reported that IMPDH1(546) and IMPDH1(595) do not bind nucleic acids) (Xu et al. 2008), but it now appears that these initial protein preparations contained contaminating RNA. Subsequent changes to the purification method yielded preparations of the retinal variants that bind nucleic acid with picomolar affinity (A. Butterworth, D. McGrew and L. Hedstrom, unpublished observations).

Canonical IMPDH and both retinal splice variants co-sediment with polyribosomes in lysates prepared from tissue culture cells and retina (Mortimer et al. 2008). Treatment with puromycin or RNase disrupts polyribosomes and also shifts IMPDH to the lower molecular weight fractions, demonstrating that IMPDH is part of the polyribosome complex. This observation suggests that IMPDH plays a role in translation regulation. Deletion of the subdomain reduces, but does not abolish, the association of IMPDH with polyribosomes (Mortimer et al. 2008). The most common adRP mutation, D226N, also decreases the association of IMPDH1 with polyribosomes. These observations suggest that the pathogenic mutations perturb the translation of a protein critical to rod photoreceptor function, leading to RP (Fig. 68.2).

IMPDH-associated transcripts were isolated from bovine retina by IMP affinity chromatography and cloned. This experiment identified rhodopsin mRNA as a retinal IMPDH1-associated transcript. This interaction was confirmed in a nascent chain immunoprecipitation experiment. Rhodopsin-translating polyribosomes were isolated with a monoclonal antibody that recognizes the N-terminal sequence of rhodopsin (Mortimer et al. 2008). IMPDH co-precipitated with the rhodopsin-translating polyribosomes. This interaction can be recapitulated in tissue culture cells expressing human *RHO* and IMPDH(546). Taken together, these observations suggest that the “moonlighting” function of retinal IMPDH1 may involve the regulation of rhodopsin mRNA.

Rhodopsin makes up ~95% of the protein in the rod disks (Sung and Chuang 2010). Mutations in rhodopsin account for the majority of RP cases, so the association

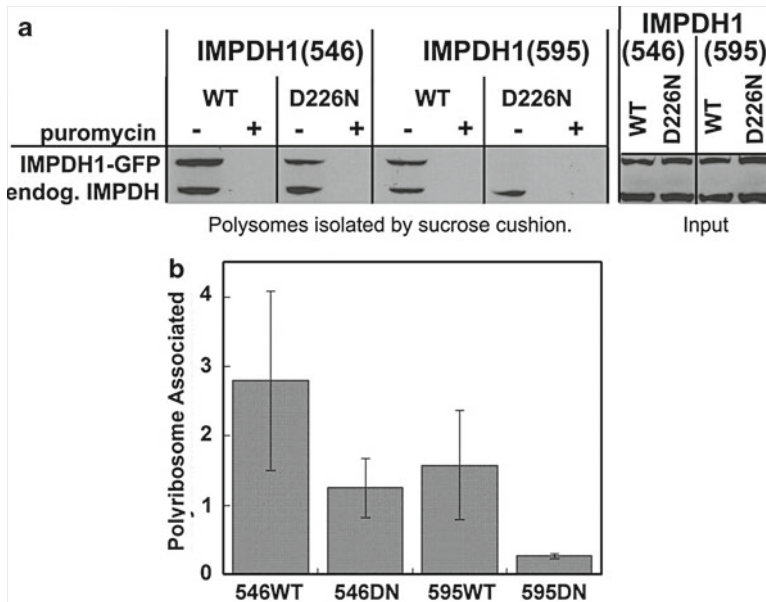


Fig. 68.2 The D226N mutation decreases the association of IMPDH1(595) with polyribosomes. (a) Lysates were prepared from HEK cells expressing GFP-tagged retinal IMPDH1 isoforms, and total polyribosomes were collected by sedimentation through a sucrose cushion. Failure of IMPDH1 to sediment after puromycin treatment demonstrates polyribosome association. Samples were analyzed by immunoblotting with monoclonal antibody recognizing IMPDH. (b) Composite data from three experiments as in (a). The endogenous IMPDH band was used to normalize the amount of GFP-tagged IMPDH1 in the polyribosomes. The units are arbitrary. This figure was originally published in *The Journal of Biological Chemistry* (Mortimer et al. (2008)). © The American Society for Biochemistry and Molecular Biology)

of IMPDH with the biosynthesis of rhodopsin suggests an appealing mechanism of disease. Although little is known about the posttranscriptional control of rhodopsin mRNA, every other step in the biosynthesis of rhodopsin is tightly controlled by the cell, and virtually any perturbation of rhodopsin expression RP (Kanda et al. 2007; Mendes et al. 2005).

68.6 Summary

IMPDH has a function in the retina, apparently independent of its enzymatic activity, mediated by retina-specific variants. This moonlighting activity may involve the posttranscriptional regulation of rhodopsin mRNA. The adRP mutation D226N has reduced binding to nucleic acids and reduced association with polyribosomes. If this mutation perturbs the biosynthesis of rhodopsin in some way, this would explain a link between IMPDH and the mechanism of retinal degeneration.

References

- Aherne A, Kennan A, Kenna PF et al (2004) On the molecular pathology of neurodegeneration in IMPDH1-based retinitis pigmentosa. *Hum Mol Genet* 13:641–650
- Berger W, Kloeckener-Gruissem B, Neidhardt J et al (2010) The molecular basis of human retinal and vitreoretinal diseases. *Prog Retin Eye Res* 29(5):335–375
- Bowne SJ, Sullivan LS, Blanton SH et al (2002) Mutations in the inosine monophosphate dehydrogenase 1 gene (IMPDH1) cause the RP10 form of autosomal dominant retinitis pigmentosa. *Hum Mol Genet* 11(5):559–568
- Bowne SJ, Liu Q, Sullivan LS et al (2006a) Why do mutations in the ubiquitously expressed housekeeping gene IMPDH1 cause retinaspecific photoreceptor degeneration? *Invest Ophthalmol Vis Sci* 47:3754–3765
- Bowne SJ, Sullivan LS, Mortimer SE et al (2006b) Spectrum and frequency of mutations in IMPDH1 associated with autosomal dominant retinitis pigmentosa and leber congenital amaurosis. *Invest Ophthalmol Vis Sci* 47:34–42
- Cornuel JF, Moraillon A, Gueron M (2002) Participation of yeast inosine 5'-monophosphate dehydrogenase in an in vitro complex with a fragment of the C-rich telomeric strand. *Biochimie* 84:279–289
- Gu JJ, Tolin AK, Jain J et al (2003) Targeted disruption of the inosine 5'-monophosphate dehydrogenase type I gene in mice. *Mol Cell Biol* 23:6702–6712
- Gunter JH, Thomas EC, Lengefeld N et al (2008) Characterisation of inosine monophosphate dehydrogenase expression during retinal development: Differences between variants and isoforms. *Int J Biochem Cell Biol* 40:1716–1728
- Hamel C (2006) Retinitis pigmentosa. *Orphanet J Rare Dis* 1:40
- Hartong DT, Berson EL, Dryja TP (2006) Retinitis pigmentosa. *Lancet* 368:1795–1809
- Hedstrom L (2009) IMP dehydrogenase: Structure, mechanism, and inhibition. *Chem Rev* 109:2903–2928
- Kanda A, Friedman JS, Nishiguchi KM et al (2007) Retinopathy mutations in the bZIP protein NRL alter phosphorylation and transcriptional activity. *Hum Mutat* 28:589–598
- Kemp BE (2004) Bateman domains and adenosine derivatives form a binding contract. *J Clin Invest* 113:182–184
- Kennan A, Aherne A, Bowne SJ et al (2003) On the role of IMPDH1 in retinal degeneration. *Adv Exp Med Biol* 533:13–18
- McLean JE, Hamaguchi N, Belenky P et al (2004) Inosine 5'-monophosphate dehydrogenase binds nucleic acids in vitro and in vivo. *Biochem J* 379:243–251
- Mendes HF, van der Spuy J, Chapple JP et al (2005) Mechanisms of cell death in rhodopsin retinitis pigmentosa: Implications for therapy. *Trends Mol Med* 11:177–185
- Mortimer SE, Hedstrom L (2005) Autosomal dominant retinitis pigmentosa mutations in inosine 5'-monophosphate dehydrogenase type I disrupt nucleic acid binding. *Biochem J* 390:41–47
- Mortimer SE, Xu D, McGrew D et al (2008) IMP dehydrogenase type 1 associates with polyribosomes translating rhodopsin mRNA. *J Biol Chem* 283:36354–36360
- Park JH, Ahn SH (2010) IMP dehydrogenase is recruited to the transcription complex through serine 2 phosphorylation of RNA polymerase II. *Biochem Biophys Res Commun* 392:588–592
- Pimkin M, Markham GD (2008) The CBS subdomain of inosine 5'-monophosphate dehydrogenase regulates purine nucleotide turnover. *Mol Microbiol* 68:342–359
- Pimkin M, Pimkina J, Markham GD (2009) A regulatory role of the bateman domain of IMP dehydrogenase in adenylate nucleotide biosynthesis. *J Biol Chem* 284:7960–7969
- Sintchak MD, Fleming MA, Futer O et al (1996) Structure and mechanism of inosine monophosphate dehydrogenase in complex with the immunosuppressant mycophenolic acid. *Cell* 85:921–930
- Spellacy CJ, Daiger SP, Sullivan LS et al (2007) Characterization of retinal inosine monophosphate dehydrogenase 1 in several mammalian species. *Mol Vis* 13:1866–1872

- Sung CH, Chuang JZ (2010) The cell biology of vision. *J Cell Biol* 190:953–963
- Tam LC, Kiang A, Kennan A et al (2008) Therapeutic benefit derived from RNAi-mediated ablation of IMPDH1 transcripts in a murine model of autosomal dominant retinitis pigmentosa (RP10). *Hum Mol Genet* 17:2084–2100
- Xu D, Cobb G, Spellicy CJ et al (2008) Retinal isoforms of inosine 5'-monophosphate dehydrogenase type 1 are poor nucleic acid binding proteins. *Arch Biochem Biophys* 472:100–104

Chapter 69

Calpain and Photoreceptor Apoptosis

Anh T.H. Nguyen, Matthew Campbell, Paul F. Kenna, Anna-Sophia Kiang, Lawrence Tam, Marian M. Humphries, and Peter Humphries

Keywords Calpain • Photoreceptor apoptosis • Light-induced retinal damage • Blood retina barrier • Barrier modulation • Claudin-5 • Retinitis pigmentosa • Age-related macular degeneration

69.1 Introduction

Apoptosis has been thought to be the mode of cell death in various neurodegenerative conditions such as Huntington's disease, Alzheimer's diseases, age-related macular degeneration, glaucoma and retinitis pigmentosa. However, the actual mechanism of this process is not fully understood. In the classical sense, apoptosis involves activation of various caspases which in turn cleave different intracellular proteins leading to cytoskeletal destruction, DNA fragmentation and autophagocytosis. There are two major apoptotic pathways. The extrinsic pathway occurs upon ligands binding to cell-surface receptors resulting in activation of pro-caspase 8 which then cleaves downstream caspases. On the other hand, cellular stress such as oxidative stress triggers release of cytochrome c from the mitochondria into the cytosol in the intrinsic pathway. Cytochrome c then forms a complex with Apaf-1 that turns pro-caspase 9 into its active form initiating a caspase cascade. However, the two apoptosis pathways are not mutually exclusive. Caspase 8 can interact with Bid, a pro-apoptotic protein of the Bcl-2 family which then leads to release of mitochondrial cytochrome c into the cytoplasm. Recently, the mechanism of apoptosis has been questioned since studies in which caspases were inhibited by pharmacologic inhibition or genetic manipulation did not necessarily increase cellular survival. Furthermore,

A.T.H. Nguyen (✉) • M. Campbell • P.F. Kenna • A.-S. Kiang • L. Tam • M.M. Humphries
• P. Humphries

The Ocular Genetics Unit, Smurfit Institute of Genetics, Trinity College Dublin, Dublin, Ireland
e-mail: nguyentat@tcd.ie

accumulating evidence showing calpain activation during apoptosis (Nath et al. 1996) suggests that apoptosis could occur in a caspase-independent fashion.

69.2 Calpain Activation

Calpain activation has been highly implicated in various neuronal pathological conditions such as Alzheimer's disease, Parkinson's disease and Huntington's disease (Nixon 2003; Bizat et al. 2005). In addition, calpain-mediated proteolysis has been observed in retinal degeneration in several animal models of RP and glaucoma (Donovan and Cotter 2002; Doonan et al. 2003; Huang et al. 2010). Calpain is ubiquitously expressed in the central nervous system (Kawashima et al. 1988). In the retina, calpain is present in most layers, including photoreceptor outer segments, plexiform layers (Azarian et al. 1993), ganglion cell and nerve fibre layers (Persson et al. 1993; Azuma and Shearer 2008). The calpain family consists of 14 members of calcium-dependent cysteine proteases. There are two types of calpain present in the brain including calpain 1 (μ -calpain) and calpain 2 (m-calpain) based on their requirements of Ca^{2+} concentrations for activation (Li et al. 2004; Suzuki et al. 2004). Both types have the same regulatory subunit (25–30 kDa) but distinct catalytic subunits (72–80 kDa) (Suzuki et al. 1987). Calpain is normally present in the cytoplasm as inactive form and then transferred to the membrane upon stimulation (Suzuki et al. 2004). However, Mizukoshi et al. (2010) suggested that inactive calpain is transferred to and activated in mitochondria in RCS rat retinal degeneration. Calpain has been shown to cleave many intracellular proteins involved in apoptosis, cell adhesion and cell migration. For example, calpain cleaves proteins involved in apoptosis such as pro-caspase-12, pro-caspase-3, PARP, Bax, p53 and p35 (Wood et al. 1998; McGinnis et al. 1999; Lee et al. 2000; Tan et al. 2006). In addition, calpain also cleaves alpha fodrin, a 280 kDa neuroskeletal protein, the cleavage of which is an important early event in apoptosis, into fragments of 145 and 150 kDa (Sakamoto et al. 2000). Also, calpain inhibition in endothelial cells and lymphocytes reduces cell migration but stabilizes focal adhesions in CHO cells and fibroblasts (Potter et al. 1998; Kulkarni et al. 1999; Glading et al. 2000; Rock et al. 2000).

Most retinal and neuronal degenerations seem to share a common end point at which apoptosis leads to cell death. Calpain activation has been implicated in various pathological conditions, thus inhibition of calpain has been investigated in the development of treatments for these diseases. A highly specific endogenous calpain inhibitor is calpastatin which binds to calpain in its inactive form in the ER. Interestingly, the calpain–calpastatin association has been shown to be both dependent (Goll et al. 2003) and independent (Melloni et al. 2006) on Ca^{2+} concentrations. Intravitreal injection of calpastatin into the rd1 mouse model for RP-reduced photoreceptor cell death (Paquet-Durand et al. 2010). However, treatment of rd mouse retinal explants with the calpain inhibitor ALLN effectively reduced cleavage of alpha fodrin but did not protect photoreceptor survival (Doonan et al. 2005). Moreover, many other calpain inhibitors cross inhibit other cysteine proteases such as caspases and cathepsins. On the other hand, the same is true for so-called

caspase-specific inhibitors such as zVAD-fmk and z-DEVD-fmk which also potently inhibit calpains (Paquet-Durand et al. 2007). In addition, SNJ-1945, a novel oral calpain inhibitor, significantly reduces cell loss in the ganglion cell layer and thinning of the inner plexiform layer induced by NMDA (Shimazawa et al. 2010).

69.3 Light Ablation Model

In addition to transgenic mouse models, light-induced retinal degeneration has been used in various studies for investigating photoreceptor cell death. This model has certain advantages over transgenics such as faster rate of photoreceptor cell death, more or less the same stage of apoptosis in affected photoreceptors and the severity of retinal damage can be altered by light intensity and duration of light exposure. Several light damage protocols have been developed using fluorescent white light, broadband green light or narrow band blue light on mice or rats and variation of these protocols has helped to identify different pathways of photoreceptor apoptosis induced by light (Wenzel et al. 2005). For example, Donovan and Cotter (2002) show that photoreceptor cell death in light-induced retinal degeneration Balb/c mice does not involve activation of various caspases such as caspase 3 (an important apoptosis executioner), caspase 8, 9, 7 and 1. The authors also suggested that zVAD-fmk, a pan-caspase inhibitor did not protect photoreceptor from apoptosis indicating light-induced retinal degeneration is caspase independent. On the other hand, they showed Ca²⁺ channel blocker diltiazem-inhibited calpain activity and photoreceptor apoptosis in this light-induced damage model. In contrast, caspase 3 was shown to be upregulated in the retina after exposure of Sprague–Dawley rats to blue light (Wu et al. 2002) while calpain was observed to be highly upregulated but played no vital role in photoreceptor apoptosis in retinas from light-ablated Wistar rats (Perche et al. 2009). Thus, these studies indicate that apoptosis is a complicated process involving not only caspases but also other proteins including calpains.

69.4 Systemic Delivery of Calpain Inhibitors

Intraocular injection of therapeutic agents is widely used experimentally in rodent models of retinal degeneration; however, regular intravitreal injection in humans poses a high risk of severe endophthalmitis and is a far from optimal treatment of retinopathies. Using an RNAi approach, we have shown that hydrodynamic injection in mice of siRNA targeting the tight junction protein claudin-5 results in a transient opening of the inner blood–retina barrier to molecules of up to 800 Da in a reversible manner (Campbell et al. 2008). In this regard, we have undertaken a series of experiments using light-induced retinal degeneration in BalB/c mice (Campbell et al. 2009). As calpain activity has been highly implicated in light-induced photoreceptor cell apoptosis, we selected the calpain inhibitor ALLM (401 Da) as a potential protective agent of this form of cell death. Indeed, many calpain inhibitors have been used to protect against photoreceptor cell death in this

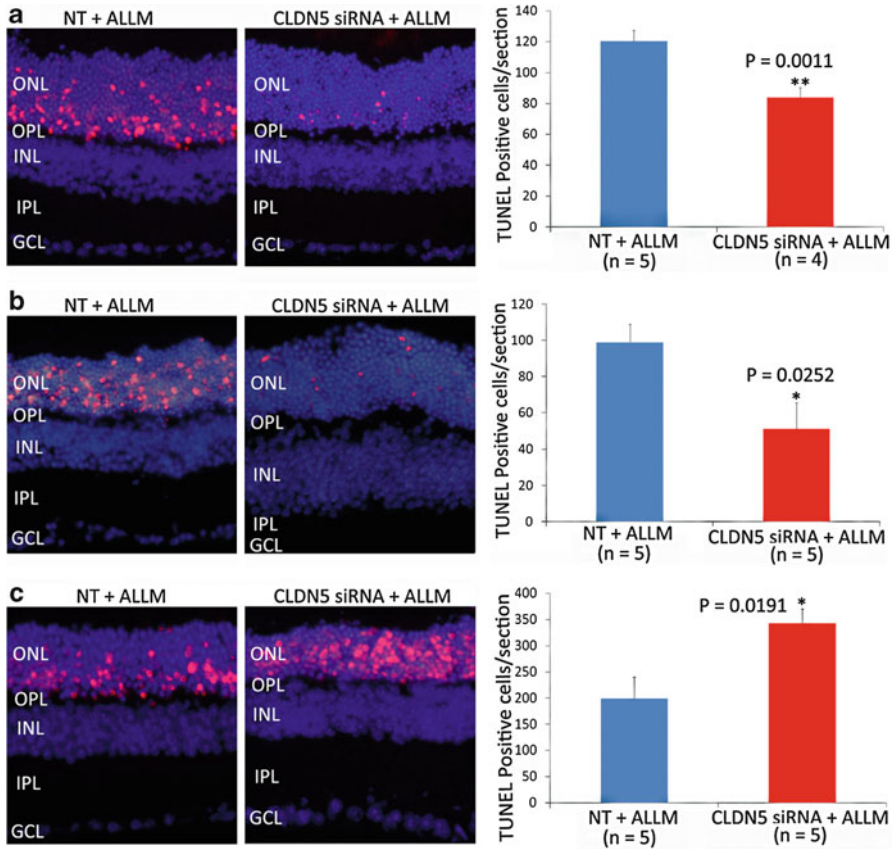


Fig. 69.1 Effects of either a Claudin-5 or NT siRNA together with a potent calpain inhibitor, ALLM, on light-induced retinal degeneration Balb/c mice. Claudin-5 or NT siRNA was administered to Balb/c mice 48 h prior injection of 20 mg/kg ALLM. Mice were dark adapted for 24 h prior to exposure to white light of 7,900 lux for 2 h (**a**, **b**). At 12 and 24 h after light ablation, TUNEL positive nuclei present in the ONL of retinal sections of mice injected with Claudin-5 siRNA were significantly less than those injected with NT siRNA (** $P=0.0011$) and ($P=0.0252$). (**c**) However, there were significantly more TUNEL positive nuclei in Claudin-5 sections compared to NT sections at 48 h post light exposure ($P=0.0191$)

model but by direct intraocular injection rather than systemic administration. Following suppression of claudin-5 at the inner blood retina barrier (iBRB), we administered an intraperitoneal injection of the calpain inhibitor prior to light induction of photoreceptor apoptosis. ALLM has a very low rate of diffusion across the iBRB and offers little or no protection when administered systemically prior to light ablation. We have shown that following RNAi-mediated opening of the iBRB prior to injection of a calpain inhibitor (ALLM) in BalB/c mice, the extent of photoreceptor apoptosis compared to mice injected with a non-targeting siRNA is significantly reduced. Experimentally, the retinal microvasculature can in principle be transiently modulated to allow the delivery of a wide range of low molecular weight pharmacological agents with proven efficacies in neuroprotection (Fig. 69.1).

69.5 Conclusion

Calpain inhibition may be a potential target for future drug development. Currently, most calpain inhibitors are injected directly into the retina due to their low rate of diffusion across the iBRB. However, of patients treated with Lucentis for AMD, this method has been implicated as a cause of endophthalmitis in 2% (Montezuma et al. 2007). Thus, the proof of principle showing systemic delivery of ALLM following neuronal barrier modulation in the retina could prove a new effective delivery method for many other low molecular weight drugs to treat a variety of retinopathies and neuropathies.

Acknowledgements We thank Caroline Woods, David Flynn and Rebecca Robertson for animal husbandry. The Ocular Genetics Unit at TCD is supported by Science Foundation Ireland, The Wellcome Trust, European Vision Institute, EVI-Genoret Grant LSHG-CT-2005-512036, Fighting Blindness Ireland and Enterprise Ireland.

References

- Azarian SM, Schlamp CL, Williams DS (1993) Characterization of calpain II in the retina and photoreceptor outer segments. *J Cell Sci* 105 (Pt 3):787–798
- Azuma M, Shearer TR (2008) The role of calcium-activated protease calpain in experimental retinal pathology. *Surv Ophthalmol* 53:150–163
- Bizat N, Galas MC, Jacquard C et al (2005) Neuroprotective effect of zVAD against the neurotoxin 3-nitropropionic acid involves inhibition of calpain. *Neuropharmacology* 49:695–702
- Campbell M, Kiang AS, Kenna PF et al (2008) RNAi-mediated reversible opening of the blood-brain barrier. *J Gene Med* 10:930–947
- Campbell M, Nguyen AT, Kiang AS et al (2009) An experimental platform for systemic drug delivery to the retina. *Proc Natl Acad Sci USA* 106:17817–17822
- Donovan M, Cotter TG (2002) Caspase-independent photoreceptor apoptosis in vivo and differential expression of apoptotic protease activating factor-1 and caspase-3 during retinal development. *Cell Death Differ* 9:1220–1231
- Doonan F, Donovan M, Cotter TG (2003) Caspase-independent photoreceptor apoptosis in mouse models of retinal degeneration. *J Neurosci* 23:5723–5731
- Doonan F, Donovan M, Cotter TG (2005) Activation of multiple pathways during photoreceptor apoptosis in the rd mouse. *Invest Ophthalmol Vis Sci* 46:3530–3538
- Glading A, Chang P, Lauffenburger DA et al (2000) Epidermal growth factor receptor activation of calpain is required for fibroblast motility and occurs via an ERK/MAP kinase signaling pathway. *J Biol Chem* 275:2390–2398
- Goll DE, Thompson VF, Li H et al (2003) The calpain system. *Physiol Rev* 83:731–801
- Huang W, Fileta J, Rawe I et al (2010) Calpain activation in experimental glaucoma. *Invest Ophthalmol Vis Sci* 51:3049–3054
- Kawashima S, Hayashi M, Saito Y et al (1988) Tissue distribution of calcium-activated neutral proteinases in rat. *Biochim Biophys Acta* 965:130–135
- Kulkarni S, Saido TC, Suzuki K et al (1999) Calpain mediates integrin-induced signaling at a point upstream of Rho family members. *J Biol Chem* 274:21265–21275
- Lee MS, Kwon YT, Li M et al (2000) Neurotoxicity induces cleavage of p35 to p25 by calpain. *Nature* 405:360–364

- Li H, Thompson VF, Goll DE (2004) Effects of autolysis on properties of μ - and m -calpain. *Biochim Biophys Acta* 1691:91–103
- McGinnis KM, Gnegy ME, Park YH et al (1999) Procaspase-3 and poly(ADP)ribose polymerase (PARP) are calpain substrates. *Biochem Biophys Res Commun* 263:94–99
- Melloni E, Averna M, Stifanese R et al (2006) Association of calpastatin with inactive calpain: a novel mechanism to control the activation of the protease? *J Biol Chem* 281:24945–24954
- Mizukoshi S, Nakazawa M, Sato K et al (2010) Activation of mitochondrial calpain and release of apoptosis-inducing factor from mitochondria in RCS rat retinal degeneration. *Exp Eye Res* 91:353–361
- Montezuma SR, Sobrin L, Seddon JM (2007) Review of genetics in age related macular degeneration. *Semin Ophthalmol* 22:229–240
- Nath R, Raser KJ, Stafford D et al (1996) Non-erythroid alpha-spectrin breakdown by calpain and interleukin 1 beta-converting-enzyme-like protease(s) in apoptotic cells: contributory roles of both protease families in neuronal apoptosis. *Biochem J* 319(Pt 3):683–690
- Nixon RA (2003) The calpains in aging and aging-related diseases. *Ageing Res Rev* 2:407–418
- Paquet-Durand F, Johnson L, Ekstrom P (2007) Calpain activity in retinal degeneration. *J Neurosci Res* 85:693–702
- Paquet-Durand F, Sanges D, McCall J et al (2010) Photoreceptor rescue and toxicity induced by different calpain inhibitors. *J Neurochem* 115:930–940
- Perche O, Doly M, Ranchon-Cole I (2009) Calpains are activated by light but their inhibition has no neuroprotective effect against light-damage. *Exp Eye Res* 89:989–994
- Persson H, Kawashima S, Karlsson JO (1993) Immunohistochemical localization of calpains and calpastatin in the rabbit eye. *Brain Res* 611:272–278
- Potter DA, Tirnauer JS, Janssen R et al (1998) Calpain regulates actin remodeling during cell spreading. *J Cell Biol* 141:647–662
- Rock MT, Dix AR, Brooks WH et al (2000) Beta1 integrin-mediated T cell adhesion and cell spreading are regulated by calpain. *Exp Cell Res* 261:260–270
- Sakamoto YR, Nakajima TR, Fukiage CR et al (2000) Involvement of calpain isoforms in ischemia-reperfusion injury in rat retina. *Curr Eye Res* 21:571–580
- Shimazawa M, Suemori S, Inokuchi Y et al (2010) A novel calpain inhibitor, ((1S)-1-(((1S)-1-Benzyl-3-cyclopropylamino-2,3-di-oxopropyl)amino)carbonyl)-3-methylbutyl)carbamic acid 5-methoxy-3-oxapentyl ester (SNJ-1945), reduces murine retinal cell death in vitro and in vivo. *J Pharmacol Exp Ther* 332:380–387
- Suzuki K, Hata S, Kawabata Y et al (2004) Structure, activation, and biology of calpain. *Diabetes Suppl* 1:S12–18
- Suzuki K, Imajoh S, Emori Y et al (1987) Calcium-activated neutral protease and its endogenous inhibitor. Activation at the cell membrane and biological function. *FEBS Lett* 220:271–277
- Tan Y, Dourdin N, Wu C et al (2006) Ubiquitous calpains promote caspase-12 and JNK activation during endoplasmic reticulum stress-induced apoptosis. *J Biol Chem* 281:16016–16024
- Wenzel A, Grimm C, Samardzija M et al (2005) Molecular mechanisms of light-induced photoreceptor apoptosis and neuroprotection for retinal degeneration. *Prog Retin Eye Res* 24:275–306
- Wood DE, Thomas A, Devi LA et al (1998) Bax cleavage is mediated by calpain during drug-induced apoptosis. *Oncogene* 17:1069–1078
- Wu J, Gorman A, Zhou X et al (2002) Involvement of caspase-3 in photoreceptor cell apoptosis induced by in vivo blue light exposure. *Invest Ophthalmol Vis Sci* 43:3349–3354

Chapter 70

Ceramide Signaling in Retinal Degeneration

Hui Chen, Julie-Thu A. Tran, Richard S. Brush, Anisse Saadi,
Abul K. Rahman, Man Yu, Douglas Yasumura, Michael T. Matthes,
Kelly Ahern, Haidong Yang, Matthew M. LaVail,
and Md Nawajes A. Mandal

Keywords Ceramide • Retinal degeneration • Apoptosis • Photoreceptor • RPE

70.1 Introduction

Ceramide (Cer) is the key metabolite of cellular sphingolipids, which are a family of membrane lipids with important structural roles in the regulation of the fluidity and subdomain structure of the lipid bilayer, especially lipid rafts (Tsui-Pierchala et al. 2002; Martin et al. 2005); it also has crucial functional roles in receptor function, in membrane conductance, in cell–cell interactions, and in the internalization of pathogens (Huwiler et al. 2000; Hannun and Obeid 2008). But their role in signaling, since the discovery of Cer as a mediator of apoptotic cell death, received wider attention in the last two decades (Obeid et al. 1993; Hannun and Obeid 2008). It is now an established fact that bioactive sphingolipids, such as Cer, ceramide-1-phosphate (C1P), sphingosine (Sph), and sphingosine-1-phosphate (S1P), maintain cellular

H. Chen

Department of Ophthalmology, OUHSC, Oklahoma City, OK 73104, USA

Dean A. McGee Eye Institute, 608 S. L. Young Boulevard, DMEI 414,
Oklahoma City, OK 73104, USA

Ophthalmology Department of Sichuan Academy of Medical Sciences & Sichuan
Provincial People's Hospital, Chengdu City, Sichuan Province 610072, China

J.-T.A. Tran • R.S. Brush • A. Saadi • A.K. Rahman • M. Yu • M.N.A. Mandal (✉)
Department of Ophthalmology, OUHSC, Oklahoma City, OK 73104, USA

Dean A. McGee Eye Institute, 608 S. L. Young Boulevard, DMEI 414,
Oklahoma City, OK 73104, USA
e-mail: mmandal@ouhsc.edu

D. Yasumura • M.T. Matthes • K. Ahern • H. Yang • M.M. LaVail
Beckman Vision Center, University of California, San Francisco, CA 94143, USA

homeostasis by regulating cell growth, apoptosis, inflammation, angiogenesis, and neovascularization (Olivera and Spiegel 1993; Spiegel and Milstien 2003; Futerman and Hannun 2004; Hannun and Obeid 2008). The processes of apoptotic cell death are integral to major retinal diseases including Retinitis Pigmentosa (RP), Stargardt's disease, Leber's congenital amaurosis (LCA), and age-related macular degeneration (AMD) (Glazer and Dryja 2002; Allikmets 2004; Haddad et al. 2006; Hartong et al. 2006). Recent evidence suggests a strong correlation between Cer signaling and survival and homeostasis of photoreceptor and retinal pigment epithelial (RPE) cells, which is the focus of this review.

70.2 An Overview of Ceramide Metabolism in the Cell

There are two major pathways that exist for Cer production in the cell. The first is the *de novo* biosynthesis of ceramide, which takes place in the endoplasmic reticulum (ER) through condensation of L-serine and palmitoyl-CoA by the enzyme serine-palmitoyl transferase (SPT) followed by sequential generation of 3-ketodihydrosphingosine (3-keto-DHS), dihydrosphingosine (DHS), and dihydroceramide, before finally being converted into Cer. The second pathway for cellular Cer generation is from the hydrolysis of higher-order sphingolipids, mainly sphingomyelin (SM), in the plasma membrane by the action of sphingomyelinase (SMase, or sphingomyelin phosphodiesterase, SMPD) enzymes. The catabolic pathway of ceramide degradation is catalyzed by a group of enzymes called ceramidases (or ASAH, acyl-sphingosine-amido-hydrolase), which deacetylate Cer to yield Sph and a fatty acid. Both Cer and Sph can be phosphorylated by specific kinases to form C1P and S1P, respectively.

70.3 Ceramide in Photoreceptor Apoptosis

Photoreceptor death by apoptosis is the hallmark of most retinal degenerative disorders (Chang et al. 1993; Portera-Cailliau et al. 1994; Carella 2003). Recently, from *in vitro* studies, Cer has been established as an essential second messenger in the activation of apoptosis in photoreceptors. In rat retina neuronal cultures, Nora Rotstein's group showed that addition of cell-permeable short-chain C₂-Cer triggers photoreceptor apoptosis, whereas inhibition of synthesis of endogenous Cer protects photoreceptors from oxidative stress-induced (paraquat) apoptosis (German et al. 2006). In a mouse retina-derived 661W cell line, treatment with sodium nitropruside showed an increase in Cer levels, while inhibition of this increased Cer by desipramine, an inhibitor of SMase enzymes, protected these cells from oxidative stress-induced apoptosis, suggesting a role of Cer in oxidative stress-induced photoreceptor cell death (Sanvicens and Cotter 2006). In our lab, we tested cell-permeable C₈-Cer and BSA-conjugated C₁₆-Cer (physiological Cer) in 661W cells and found

both these ceramides caused cell death in a dose-dependent manner; we also observed an increase in Cer H_2O_2 -treated 661W cells (Mandal et al. unpublished data), providing additional support of Cer's role as a death mediator in retinal cells. In another recent publication, Rotstein's group showed that enhanced formation of Cer and its subsequent breakdown to Sph, which was induced by oxidative stress, triggered photoreceptor apoptosis in cultured rat retina neurons (Abraham et al. 2010). In summary, these evidences point toward a key role for Cer as a common mediator of photoreceptor cell apoptosis in culture, especially due to oxidative stress.

Evidence is gradually accumulating on the role of Cer in photoreceptor cell death *in vivo*, too. The first evidence came from *Drosophila* studies, in which Acharya et al. detected increased Cer in arrestin2 (*arr2*) and phospholipase C (*plc*) mutant photoreceptors. Further, transgenic overexpression of neutral Ceramidase (nCDase or ASAH2), an enzyme that reduces Cer level by breaking Cer into Sph and free fatty acid, showed prevention of photoreceptors from Cer-induced cell death (Acharya et al. 2003, 2004). They also showed that preventing *de novo* biosynthesis of Cer suppresses retinal degeneration in *Drosophila* phototransduction mutants. Noteworthy, overexpression of ceramidase in tissues distant from photoreceptors suppresses photoreceptor degeneration in an arrestin mutant and facilitates membrane turnover in a rhodopsin null mutant (Acharya et al. 2008). Mutation in ceramide kinase gene in *Drosophila* leads to photoreceptor degeneration, also by accumulation of excess Cer, and provides additional evidence of Cer involvement in photoreceptor cell death (Dasgupta et al. 2009). In mutants, the accumulated Cer subsequently leads to loss of phospholipase C activity and inhibits phototransduction, which is then accompanied by severe degeneration of photoreceptors. Overexpression of ceramidase in these cells decreased Cer levels and rescued PLC activity and cell death (Dasgupta et al. 2009).

Further, in a mammalian model (rabbit), involvement of Cer has been associated with a gradual loss of photoreceptor cells in an experimental model of retinal detachment (Ranty et al. 2009). Using light-damaged albino rat models and with genetic models of retinal dystrophies (RCS and P23H1 rats), we found an integral association of increased Cer level with photoreceptor cell death (Mandal et al. unpublished data). A recent publication shows that ceramide levels increase with progression of photoreceptor degeneration in *Rd10* mice and that inhibiting *de novo* ceramide biosynthesis by myriocin (a powerful inhibitor of SPT enzyme) can preserve photoreceptor structure and function in this mouse model of RP (Strettoi et al. 2010).

In human, mutations in *Ceramide kinase like (CERKL)* gene are found to be associated with inherited RP (RP26) (Tuson et al. 2004; Auslender et al. 2007). The function of CERKL is not yet known, but is potentially involved in the Cer metabolic pathway, suggesting a direct link between human retinal degeneration and Cer-mediated apoptosis. Additionally, in several inherited sphingolipid metabolism defect diseases commonly known as "lipid storage disease," such as Krabbe's disease (Brownstein et al. 1978), Niemann-Pick disease (Robb and Kuwabara 1973), Sandhoff disease (Sango et al. 2008), and Gaucher disease (Seidova et al. 2009), retinal impairment and vision loss due to retinal neuronal cell death are often present and accompanied by Cer accumulation. Increased level of Cer was found

in retinas of patients with Farber disease, caused by a mutation in *Ceramidase* gene (also known as ceramidase deficiency) (Zarbin et al. 1985, 1988). Furthermore, increased Cer was found in the brain of patients with the juvenile form of Batten disease (Puranam et al. 1997), in which neuronal apoptosis is thought to be the cause of RP in these patients. Cer is also shown to alter the chloride channel activity of Bestrophin protein, and Cer accumulation is suggested to enhance inflammation in the retina in Best vitelliform macular dystrophy (VMD) patients (Xiao et al. 2009). In summary, the changes in Cer level in human and mouse-inherited retinal diseases, proof of Cer involvement in *Drosophila* photoreceptor degeneration, involvement of Cer in cell death in vitro, and the association between Cer changes and retinal neuronal death in the sphingolipid metabolic diseases underscore the significance of Cer and its metabolites in the death of retina photoreceptors and retina degeneration diseases.

70.4 Ceramide Signaling in RPE Cell Death

RPE atrophy (cell death) followed by or concomitant with photoreceptor cell death is the final outcome of all forms of RP. In dry AMD, the atrophy to the RPE cell in the macular region is considered to be the primary pathology and is also common in the early stage of wet AMD. Recent evidences have shown that Cer participates in activating RPE cell death. In cultured human RPE (hRPE) cells, treatment with the chemical oxidants tBH and H₂O₂ led to Cer generation, which signaled for RPE apoptosis (Barak et al. 2001). In another study, laser exposure induced hRPE apoptosis with concomitant Cer production (Barak et al. 2005). Further studies on the overexpression of Sphingomyelin phosphodiesterase-3 (SMPD3), a key enzyme responsible for Cer production from SM, showed enhanced RPE cell death and arrested cell proliferation, with the percentage of apoptotic cells increasing proportionally with the amount of transfected *SMPD3* DNA (Zhu et al. 2010). Interestingly, the short-chain C₂-Cer selectively induced apoptosis in the nonpolarized RPE cultures, but not in fully differentiated and polarized RPE cells. This has a relevance with AMD since nonpolarized RPE cells are found in late AMD lesions, and Cer may play a critical role in their apoptosis (Zhu et al. 2010). The studies on the mechanisms of Cer-induced RPE apoptosis indicated the role of increasing ROS production, mitochondrial membrane permeability transition (MPT), and caspase-3 activation (Kannan et al. 2004).

70.5 Conclusion

Cer is known as a deadly second messenger in the cell and is now known to play a role in various forms of photoreceptor cell death. This discovery has a significant impact from a therapeutic point of view; Cer synthesis can be targeted for retinal

degenerative diseases and evidence has already started accumulating from *Drosophila* and mammalian studies (Acharya et al. 2003; Strettoi et al. 2010). Cer metabolism is complex and other bioactive Cer metabolites, such as C1P and S1P, also play important roles in cell growth, differentiation, inflammation, and neovascularization, which are relevant in many forms of retinal degenerative diseases, recently reviewed in Rotstein et al. (2010) and which is beyond the scope of this review.

Acknowledgments Our study is supported by NIH grants RR17703 and EY12190, Knight's Templar Eye Foundation, and Research to Prevent Blindness.

References

- Abraham CE, Miranda GE, Agnolazza DL et al (2010) Synthesis of sphingosine is essential for oxidative stress-induced apoptosis of photoreceptors. *Invest Ophthalmol Vis Sci* 51:1171–1180
- Acharya JK, Dasgupta U, Rawat SS et al (2008) Cell-nonautonomous function of ceramidase in photoreceptor homeostasis. *Neuron* 57:69–79
- Acharya U, Mowen MB, Nagashima K et al (2004) Ceramidase expression facilitates membrane turnover and endocytosis of rhodopsin in photoreceptors. *Proc Natl Acad Sci USA* 101:1922–1926
- Acharya U, Patel S, Koundakjian E et al (2003) Modulating sphingolipid biosynthetic pathway rescues photoreceptor degeneration. *Science* 299:1740–1743
- Allikmets R (2004) Leber congenital amaurosis: a genetic paradigm. *Ophthalmic Genet* 25:67–79
- Auslender N, Sharon D, Abbasi AH et al (2007) A common founder mutation of CERKL underlies autosomal recessive retinal degeneration with early macular involvement among Yemenite Jews. *Invest Ophthalmol Vis Sci* 48:5431–5438
- Barak A, Morse LS, Goldkorn T (2001) Ceramide: a potential mediator of apoptosis in human retinal pigment epithelial cells. *Invest Ophthalmol Vis Sci* 42:247–254
- Barak A, Goldkorn T, Morse LS (2005) Laser induces apoptosis and ceramide production in human retinal pigment epithelial cells. *Invest Ophthalmol Vis Sci* 46:2587–2591
- Brownstein S, Meagher-Villemure K, Polomeno RC et al (1978) Optic nerve in globoid leukodystrophy (Krabbe's disease). Ultrastructural changes. *Arch Ophthalmol* 96:864–870
- Carella G (2003) Introduction to apoptosis in ophthalmology. *Eur J Ophthalmol* 13 Suppl 3:S5–10
- Chang GQ, Hao Y, Wong F (1993) Apoptosis: final common pathway of photoreceptor death in rd, rds, and rhodopsin mutant mice. *Neuron* 11:595–605
- Dasgupta U, Bamba T, Chiantia S et al (2009) Ceramide kinase regulates phospholipase C and phosphatidylinositol 4, 5, bisphosphate in phototransduction. *Proc Natl Acad Sci USA* 106:20063–20068
- Futerman AH, Hannun YA (2004) The complex life of simple sphingolipids. *EMBO Rep* 5:777–782
- German OL, Miranda GE, Abraham CE et al (2006) Ceramide is a mediator of apoptosis in retina photoreceptors. *Invest Ophthalmol Vis Sci* 47:1658–1668
- Glazer LC, Dryja TP (2002) Understanding the etiology of Stargardt's disease. *Ophthalmol Clin North Am* 15:93–100, viii
- Haddad S, Chen CA, Santangelo SL et al (2006) The genetics of age-related macular degeneration: a review of progress to date. *Surv Ophthalmol* 51:316–363
- Hannun YA, Obeid LM (2008) Principles of bioactive lipid signalling: lessons from sphingolipids. *Nat Rev Mol Cell Biol* 9:139–150
- Hartong DT, Berson EL, Dryja TP (2006) Retinitis pigmentosa. *Lancet* 368:1795–1809

- Huwiler A, Kolter T, Pfeilschifter J et al (2000) Physiology and pathophysiology of sphingolipid metabolism and signaling. *Biochim Biophys Acta* 1485:63–99
- Kannan R, Jin M, Gamulescu MA et al (2004) Ceramide-induced apoptosis: role of catalase and hepatocyte growth factor. *Free Radic Biol Med* 37:166–175
- Martin RE, Elliott MH, Brush RS et al (2005) Detailed characterization of the lipid composition of detergent-resistant membranes from photoreceptor rod outer segment membranes. *Invest Ophthalmol Vis Sci* 46:1147–1154
- Obeid LM, Linardic CM, Karolak LA et al (1993) Programmed cell death induced by ceramide. *Science* 259:1769–1771
- Olivera A, Spiegel S (1993) Sphingosine-1-phosphate as second messenger in cell proliferation induced by PDGF and FCS mitogens. *Nature* 365:557–560
- Portera-Cailliau C, Sung CH, Nathans J et al (1994) Apoptotic photoreceptor cell death in mouse models of retinitis pigmentosa. *Proc Natl Acad Sci USA* 91:974–978
- Puranam K, Qian WH, Nikbakht K et al (1997) Upregulation of Bcl-2 and elevation of ceramide in Batten disease. *Neuropediatrics* 28:37–41
- Ranty ML, Carpentier S, Cournot M et al (2009) Ceramide production associated with retinal apoptosis after retinal detachment. *Graefes Arch Clin Exp Ophthalmol* 247:215–224
- Robb RM, Kuwabara T (1973) The ocular pathology of type A Niemann-Pick disease. A light and electron microscopic study. *Invest Ophthalmol* 12:366–377
- Rotstein NP, Miranda GE, Abraham CE et al (2010) Regulating survival and development in the retina: key roles for simple sphingolipids. *J Lipid Res* 51:1247–1262
- Sango K, Yamanaka S, Ajiki K et al (2008) Involvement of retinal neurons and pigment epithelial cells in a murine model of sandhoff disease. *Ophthalmic Res* 40:241–248
- Sanvicens N, Cotter TG (2006) Ceramide is the key mediator of oxidative stress-induced apoptosis in retinal photoreceptor cells. *J Neurochem* 98:1432–1444
- Seidova SF, Kotliar K, Foerger F et al (2009) Functional retinal changes in Gaucher disease. *Doc Ophthalmol* 118:151–154
- Spiegel S, Milstien S (2003) Sphingosine-1-phosphate: an enigmatic signalling lipid. *Nat Rev Mol Cell Biol* 4:397–407
- Strettoi E, Gargini C, Novelli E et al (2010) Inhibition of ceramide biosynthesis preserves photoreceptor structure and function in a mouse model of retinitis pigmentosa. *Proc Natl Acad Sci USA* 107:18706–18711
- Tsui-Pierchala BA, Encinas M, Milbrandt J et al (2002) Lipid rafts in neuronal signaling and function. *Trends Neurosci* 25:412–417
- Tuson M, Marfany G, Gonzalez-Duarte R (2004) Mutation of CERKL, a novel human ceramide kinase gene, causes autosomal recessive retinitis pigmentosa (RP26). *Am J Hum Genet* 74:128–138
- Xiao Q, Yu K, Cui YY et al (2009) Dysregulation of human bestrophin-1 by ceramide-induced dephosphorylation. *J Physiol* 587:4379–4391
- Zarbin MA, Green WR, Moser HW et al (1985) Farber's disease. Light and electron microscopic study of the eye. *Arch Ophthalmol* 103:73–80
- Zarbin MA, Green WR, Moser AB et al (1988) Increased levels of ceramide in the retina of a patient with Farber's disease. *Arch Ophthalmol* 106:1163
- Zhu D, Sreekumar PG, Hinton DR et al (2010) Expression and regulation of enzymes in the ceramide metabolic pathway in human retinal pigment epithelial cells and their relevance to retinal degeneration. *Vision Res* 50:643–651

Chapter 71

Endoplasmic Reticulum-Associated Degradation (ERAD) of Misfolded Glycoproteins and Mutant P23H Rhodopsin in Photoreceptor Cells

Heike Kroeger, Wei-Chieh Chiang, and Jonathan H. Lin

Keywords Misfolded proteins • ERAD • ER • Quality control • P23H rhodopsin • Photoreceptor cells

71.1 The Endoplasmic Reticulum: Protein Folding and Quality Control

ER-resident chaperones are among the first proteins that interact with a nascent polypeptide chain. For instance, BiP/Grp78, an Hsp70 orthologue, detects and binds unfolded hydrophobic regions of a nascent polypeptide chain in an ATP-dependent process (Hendershot et al. 1995). ER-resident J-domain co-chaperones, ERdj1 and ERdj2, regulate the interaction between BiP/Grp78 and the nascent peptide (Blond-Elguindi et al. 1993).

The initial step of ER glycoprotein modification involves attachment of a Glc3Man9GlcNAc2-core glycan onto a nascent polypeptide chain that is further processed by activities of Glucosidase I and II (Aebi et al. 2009). On removal of glucose residues, the monoglycosylated N-glycan becomes a substrate for ER-resident lectins, calreticulin (CRT) and calnexin (CNX). CRT and CNX both require Ca²⁺ for their activities; CNX is ER membrane-bound, while CRT is soluble in the ER lumen (Wada et al. 1991; Peterson et al. 1995). Both lectins promote protein folding by stabilizing folding sequences, preventing aggregation of unfolded proteins, and facilitating disulfide-bond formation through association with ER oxidoreductase, ERp57, a protein disulfide isomerase (PDI) homologue (Oliver et al. 1999; Ellgaard 2004).

H. Kroeger • W.-C. Chiang • J.H. Lin (✉)

Department of Pathology, University of California, San Diego, La Jolla, CA 92093-0612, USA
e-mail: jlin@ucsd.edu

Glycoproteins that fail to fold correctly are subject to a quality control process (Trombetta and Parodi 2003). A key quality control sensor of the ER is UGGT1, which recognizes structural formation of misfolded proteins and alters their glycosylation stage to regenerate monoglycosylated glycans, which subsequently renews binding to CNX and CRT and reentrance into the ER protein-folding cycle (Trombetta and Helenius 2000). This cycle continues until the native conformation of the protein is achieved, or failing this, until the protein is targeted for disposal by endoplasmic reticulum-associated degradation (ERAD) (Lippincott-Schwartz et al. 1988). Some ER-retained proteins can also be modified by mannosidases, which may act as a timer for glycoprotein degradation and thus prevent glycoproteins from becoming permanently trapped in the reglucosylation/folding cycle (Fagioli and Sitia 2001).

71.2 Recognition Misfolded Proteins in the ER

The complete mechanism for recognizing misfolded ER proteins is poorly understood. One step in directing glycoprotein substrates to the ERAD machinery is the formation of the Man₇N-glycan with a 1,6-linked mannose (Hosokawa et al. 2010a). Various ER-resident enzymes are able to trim mannose residues, such as ER mannosidase I, a member of the glycosyl hydrolase 47 family, which also includes the ER degradation enhancing α -mannosidase-like proteins 1–3 (EDEM1–3) and Golgi mannosidases (Aebi et al. 2009). EDEM1 enhances ERAD through its ability to extract misfolded glycoproteins from the CNX/CRT cycle (Molinari et al. 2003; Oda et al. 2003). EDEM1 and EDEM3 also trim mannose residues from N-glycan (Hirao et al. 2006; Hosokawa et al. 2010b). By contrast, EDEM2 has no enzymatic activity, but still increases turnover of misfolded proteins in the ER and likely plays nonenzymatic roles in ERAD (Mast et al. 2005). The mammalian PDI orthologue, ERdj5, is a cochaperone of EDEM1 and BiP/Grp78. ERdj5 recognizes misfolded proteins and reduces disulfide bonds via its reductase activity, which is important for protein dislocation (Ushioda et al. 2008).

71.3 From Quality Control to Dislocation for ERAD

How are misfolded proteins targeted for dislocation from the ER to the cytosol? OS-9 and XTP3-B are ER lectin-like proteins that contain mannose 6-phosphate receptor homology domains and N-linked glycosylation sites. OS-9 and XTP3-B may recognize and transfer misfolded proteins to an ER membrane-bound dislocation complex (Christianson et al. 2008; Hosokawa et al. 2008; Bernasconi et al. 2010). OS-9 interacts further with the ER-luminal Hsp90 homologue, 94 kDa glucose-regulated protein (Grp94), to deliver ERAD substrates to the dislocation complex. The complex contains the E3 ubiquitin ligase (HRD), the membrane adaptor

protein (Sel1L), and a membrane-embedded pore that forms the dislocation channel (Christianson et al. 2008; Hosokawa et al. 2008; Mueller et al. 2008). Sel1L is a type I transmembrane glycoprotein, which interacts with the ERAD components HRD1, Derlin1, and Derlin2 as well as with the cytoplasmic protein p97/VCP (valosin-containing protein) (Lilley and Ploegh 2005). OS-9 and XTP3-B associate with the HRD1-Sel1L ubiquitin ligase complex and XTP3-B is able to recognize both glycosylated and nonglycosylated ERAD substrates and facilitate their degradation (Hosokawa et al. 2008). Additional proteins and regulatory steps are likely to be involved in determining how misfolded proteins are selected for ERAD and delivered to the ER dislocation channel.

71.4 Cytosolic Events of ERAD

The dislocation and translocation of an ERAD substrate from the ER to cytosol requires activity of AAA-ATPases such as p97/VCP (Ye et al. 2001; Jarosch et al. 2002). p97/VCP forms homohexamers, which associate with the cofactors Ufd1 (ubiquitin fusion degradation 1) and Npl4 (nuclear protein localization 4) to extract substrates from the ER membrane (Bays et al. 2001; Ye et al. 2001; Braun et al. 2002) using energy provided by ATP hydrolysis (Zhang et al. 2000).

ERAD substrates are further ubiquitinated once in the cytosol through a process that requires three cytosolic enzymes. E1 activates ubiquitin in an ATP-dependent manner; E2 then conjugates activated ubiquitin through a thiol-ester bond to its essential cysteine residue, and the E3 ligase transfers ubiquitin onto one or more lysine residues or the N-terminus of the target proteins (Weissman 2001). The E4 ubiquitin-chain-extension enzyme is also shown to be involved in the ERAD degradation pathway (Richly et al. 2005).

The ubiquitinated substrate is ultimately degraded by the proteasome. The 26S proteasome is a large cytosolic protease complex, consisting of a 20S core particle that is capped by the 19S regulatory particle (Finley 2009). Four heptameric rings, two outer α subunits, and two inner β subunits form a barrel-shaped structure with proteolytic activity in the central cavity (Groll et al. 1997). The core particle entrance is very narrow and requires partial unfolding of the substrate for entrance (Finley 2009). The regulatory particle contains ATPase subunits and plays an important role in substrate recognition, unfolding, and translocation of target proteins into the core particle (Finley 2009). Proteins that target polyubiquitinated substrates to the proteasome include: Rad23 (radiation sensitive 23); Dsk2 (dominant suppressor of Kar1); Rpn10 (regulatory particle non-ATPase10); and Rpn13 (Finley 2009). Before proteolysis, proteasome-associated deubiquitin (DUBs) enzymes cleave and shorten the ubiquitin chain of target proteins resulting in the insertion of the substrate into the proteasome. Human proteasomes have three distinct DUB's, RPN11, UCH37 and USP14, which are associated with the regulatory particle (Finley 2009). Deubiquitin hydrolases remove the polyubiquitin chain, and ubiquitin proteins are recycled. Additionally, cytosolic N-glycanase removes oligosaccharides from

ERAD substrates to allow translocation into the proteasome (Blom et al. 2004; Misaghi et al. 2004). N-glycanase interacts with other ERAD components and Rad23 (Suzuki et al. 2001). The regulatory particle then unfolds the substrate and translocates it to the core particle for degradation.

71.5 ERAD in Retinitis Pigmentosa

In retinitis pigmentosa arising from the P23H rhodopsin (Rho) mutation, P23H Rho proteins are misfolded in the ER/Golgi and associate with CNX, BiP/Grp78 and Grp94 (Fig. 71.1a) (Anukanth and Khorana 1994; Noorwez et al. 2009). Recent studies implicate ERAD in the removal of misfolded P23H Rho. EDEM1 recognizes mutant Rho in the ER lumen and targets it for ERAD (Fig. 71.1b) (Kang and Ryoo 2009; Kosmaoglou et al. 2009). The complete mechanism of how mutant

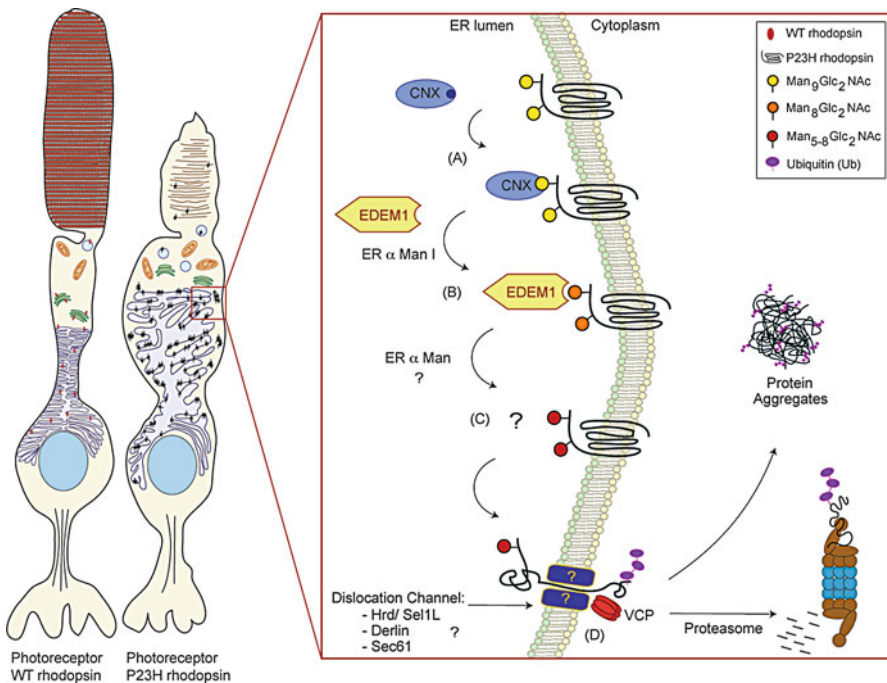


Fig. 71.1 Model of P23H rhodopsin clearance in photoreceptors by ERAD (a). Misfolded P23H rhodopsin (Rho) is a glycoprotein that interacts with calnexin (CNX) during folding. (b) Misfolded P23H Rho is trapped in the quality control/folding cycle and becomes a target for ER α -mannosidase I. After removal of mannose residues, mutant Rho is recognized by EDEM1. (c) Once associated to EDEM1, P23H Rho may be further demannosylated and modified by other ER-resident chaperones, which also promote the delivery of P23H Rho to the membrane-bound dislocation channel. (d) p97/VCP extracts P23H Rho through the channel into the cytosol, where it will be degraded by the proteasome or form aggregates

Rho is dislocated from the ER membrane to the cytosol is unknown, but the AAA-ATPase p97/VCP is one factor in the dislocation and delivery of P23H Rho to the proteasome (Fig. 71.1d) (Griciuc et al. 2010a, b). In vitro studies have shown that misfolded P23H Rho is ubiquitinated and targeted for proteasomal degradation (Sung et al. 1991; Illing et al. 2002; Saliba et al. 2002). Many other ERAD components are likely to be involved in the identification and delivery of P23H Rho to ERAD (Fig. 71.1c).

Acknowledgments We thank M. LaVail for helpful suggestions on this manuscript and grant support from the Hope for Vision Foundation, the Karl Kirchgessner Foundation, and the NIH (EY018313, EY020846). W.C. Chiang received postdoctoral support from the Fight-for-Sight Foundation.

References

- Aebi M, Bernasconi R, Clerc S et al (2009) N-glycan structures: recognition and processing in the ER. *Trends Biochem Sci* 35:74–82
- Anukanth A, Khorana HG (1994) Structure and function in rhodopsin. Requirements of a specific structure for the intradiscal domain. *J Biol Chem* 269:19738–19744
- Bays NW, Wilhovskiy SK, Goradia A et al (2001) HRD4/NPL4 is required for the proteasomal processing of ubiquitinated ER proteins. *Mol Biol Cell* 12:4114–4128
- Bernasconi R, Galli C, Calanca V et al (2010) Stringent requirement for HRD1, SEL1L, and OS-9/XTP3-B for disposal of ERAD-LS substrates. *J Cell Biol* 188:223–235
- Blom D, Hirsch C, Stern P et al (2004) A glycosylated type I membrane protein becomes cytosolic when peptide: N-glycanase is compromised. *EMBO J* 23:650–658
- Blond-Elguindi S, Cwirla SE, Dower WJ et al (1993) Affinity panning of a library of peptides displayed on bacteriophages reveals the binding specificity of BiP. *Cell* 75:717–728
- Braun S, Matuschewski K, Rape M et al (2002) Role of the ubiquitin-selective CDC48(UFD1/NPL4) chaperone (segregase) in ERAD of OLE1 and other substrates. *EMBO J* 21:615–621
- Christianson JC, Shaler TA, Tyler RE et al (2008) OS-9 and GRP94 deliver mutant alpha1-antitrypsin to the Hrd1-SEL1L ubiquitin ligase complex for ERAD. *Nat Cell Biol* 10:272–282
- Ellgaard L (2004) Catalysis of disulphide bond formation in the endoplasmic reticulum. *Biochem Soc Trans* 32:663–667
- Fagioli C, Sitia R (2001) Glycoprotein quality control in the endoplasmic reticulum. Mannose trimming by endoplasmic reticulum mannosidase I times the proteasomal degradation of unassembled immunoglobulin subunits. *J Biol Chem* 276:12885–12892
- Finley D (2009) Recognition and processing of ubiquitin-protein conjugates by the proteasome. *Annu Rev Biochem* 78:477–513
- Griciuc A, Aron L, Piccoli G et al (2010a) Clearance of Rhodopsin (P23H) aggregates requires the ERAD effector VCP. *Biochim Biophys Acta* 1803:424–434
- Griciuc A, Aron L, Roux MJ et al (2010b) Inactivation of VCP/ter94 suppresses retinal pathology caused by misfolded rhodopsin in *Drosophila*. *PLoS Genet* 6
- Groll M, Ditzel L, Lowe J et al (1997) Structure of 20S proteasome from yeast at 2.4 Å resolution. *Nature* 386:463–471
- Hendershot LM, Wei JY, Gaut JR et al (1995) In vivo expression of mammalian BiP ATPase mutants causes disruption of the endoplasmic reticulum. *Mol Biol Cell* 6:283–296
- Hirao K, Natsuka Y, Tamura T et al (2006) EDEM3, a soluble EDEM homolog, enhances glycoprotein endoplasmic reticulum-associated degradation and mannose trimming. *J Biol Chem* 281:9650–9658

- Hosokawa N, Kamiya Y, Kato K (2010a) The role of MRH domain-containing lectins in ERAD. *Glycobiology* 20:651–660
- Hosokawa N, Wada I, Nagasawa K et al (2008) Human XTP3-B forms an endoplasmic reticulum quality control scaffold with the HRD1-SEL1L ubiquitin ligase complex and BiP. *J Biol Chem* 283:20914–20924
- Hosokawa N, Tremblay LO, Sleno B et al (2010b) EDEM1 accelerates the trimming of alpha1,2-linked mannose on the C branch of N-glycans. *Glycobiology* 20:567–575
- Illing ME, Rajan RS, Bence NF et al (2002) A rhodopsin mutant linked to autosomal dominant retinitis pigmentosa is prone to aggregate and interacts with the ubiquitin proteasome system. *J Biol Chem* 277:34150–34160
- Jarosch E, Taxis C, Volkwein C et al (2002) Protein dislocation from the ER requires polyubiquitination and the AAA-ATPase Cdc48. *Nat Cell Biol* 4:134–139
- Kang MJ, Ryoo HD (2009) Suppression of retinal degeneration in *Drosophila* by stimulation of ER-associated degradation. *Proc Natl Acad Sci USA* 106:17043–17048
- Kosmaoglou M, Kanuga N, Aguila M et al (2009) A dual role for EDEM1 in the processing of rhodopsin. *J Cell Sci* 122:4465–4472
- Lilley BN, Ploegh HL (2005) Multiprotein complexes that link dislocation, ubiquitination, and extraction of misfolded proteins from the endoplasmic reticulum membrane. *Proc Natl Acad Sci USA* 102:14296–14301
- Lippincott-Schwartz J, Bonifacino JS, Yuan LC et al (1988) Degradation from the endoplasmic reticulum: disposing of newly synthesized proteins. *Cell* 54:209–220
- Mast SW, Diekmann K, Karavog K et al (2005) Human EDEM2, a novel homolog of family 47 glycosidases, is involved in ER-associated degradation of glycoproteins. *Glycobiology* 15:421–436
- Misaghi S, Pacold ME, Blom D et al (2004) Using a small molecule inhibitor of peptide: N-glycanase to probe its role in glycoprotein turnover. *Chem Biol* 11:1677–1687
- Molinari M, Calanca V, Galli C et al (2003) Role of EDEM in the release of misfolded glycoproteins from the calnexin cycle. *Science* 299:1397–1400
- Mueller B, Klemm EJ, Spooner E et al (2008) SEL1L nucleates a protein complex required for dislocation of misfolded glycoproteins. *Proc Natl Acad Sci USA* 105:12325–12330
- Noorwez SM, Sama RR, Kaushal S (2009) Calnexin improves the folding efficiency of mutant rhodopsin in the presence of pharmacological chaperone 11-cis-retinal. *J Biol Chem* 284:33333–33342
- Oda Y, Hosokawa N, Wada I et al (2003) EDEM as an acceptor of terminally misfolded glycoproteins released from calnexin. *Science* 299:1394–1397
- Oliver JD, Roderick HL, Llewellyn DH et al (1999) ERp57 functions as a subunit of specific complexes formed with the ER lectins calreticulin and calnexin. *Mol Biol Cell* 10:2573–2582
- Peterson JR, Ora A, Van PN et al (1995) Transient, lectin-like association of calreticulin with folding intermediates of cellular and viral glycoproteins. *Mol Biol Cell* 6:1173–1184
- Richly H, Rape M, Braun S et al (2005) A series of ubiquitin binding factors connects CDC48/p97 to substrate multiubiquitylation and proteasomal targeting. *Cell* 120:73–84
- Saliba RS, Munro PM, Luthert PJ et al (2002) The cellular fate of mutant rhodopsin: quality control, degradation and aggresome formation. *J Cell Sci* 115:2907–2918
- Sung CH, Schneider BG, Agarwal N et al (1991) Functional heterogeneity of mutant rhodopsins responsible for autosomal dominant retinitis pigmentosa. *Proc Natl Acad Sci USA* 88:8840–8844
- Suzuki T, Park H, Kwofie MA et al (2001) Rad23 provides a link between the Png1 deglycosylating enzyme and the 26S proteasome in yeast. *J Biol Chem* 276:21601–21607
- Trombetta ES, Helenius A (2000) Conformational requirements for glycoprotein reglucosylation in the endoplasmic reticulum. *J Cell Biol* 148:1123–1129
- Trombetta ES, Parodi AJ (2003) Quality control and protein folding in the secretory pathway. *Annu Rev Cell Dev Biol* 19:649–676
- Ushioda R, Hoseki J, Araki K et al (2008) ERdj5 is required as a disulfide reductase for degradation of misfolded proteins in the ER. *Science* 321:569–572

- Wada I, Rindress D, Cameron PH et al (1991) SSR alpha and associated calnexin are major calcium binding proteins of the endoplasmic reticulum membrane. *J Biol Chem* 266: 19599–19610
- Weissman AM (2001) Themes and variations on ubiquitylation. *Nat Rev Mol Cell Biol* 2:169–178
- Ye Y, Meyer HH, Rapoport TA (2001) The AAA ATPase Cdc48/p97 and its partners transport proteins from the ER into the cytosol. *Nature* 414:652–656
- Zhang X, Shaw A, Bates PA et al (2000) Structure of the AAA ATPase p97. *Mol Cell* 6: 1473–1484

Chapter 72

Protein Misfolding and Potential Therapeutic Treatments in Inherited Retinopathies

Lawrence C.S. Tam, Anna-Sophia Kiang, Matthew Campbell, James Keaney, G. Jane Farrar, Marian M. Humphries, Paul F. Kenna, and Pete Humphries

Keywords Retinitis pigmentosa • Protein misfolding • Heat shock protein • Rhodopsin • IMPDH1 • RDS-peripherin • Chaperones • Gene therapy

72.1 Introduction

The folding of a protein begins at the ribosome whereby newly synthesized polypeptides undergo dynamic conformational changes before they reach their most stable and functional native state. However, folding intermediates may be affected by debilitating conditions such as mutations, translational errors, or environmental stress that prevent them from adopting their native states, creating an accumulation of nonproductive intermediates known as misfolded conformers. Both prokaryotic and eukaryotic cells have evolved and established an extensive protein quality control system that acts to facilitate either refolding of misfolded protein species by molecular chaperones or their removal by proteolytic degradation (Hartl and Hayer-Hartl 2009; Rubinsztein 2006). The main chaperone classes that prevent the accumulation of misfolded proteins are heat shock proteins (Hsp) (Bukau et al. 2006). Heat shock protein 90 (Hsp90; 90 kDa) is one of the most abundant molecular chaperones in eukaryotic cells, and it functions in essential housekeeping functions such as cellular trafficking, cell growth, signal transduction, and differentiation (Pratt and Toft 2003). The protein quality control system can adapt to various levels of stress imposed by misfolded proteins through the induction of stress responses and modulation of cellular molecular chaperone levels (Goldberg 2003; Guisbert et al. 2008). However, when the population of misfolded proteins exceeds the refolding

L.C.S. Tam (✉) • A.-S. Kiang • M. Campbell • J. Keaney • G.J. Farrar • M.M. Humphries
• P.F. Kenna • P. Humphries
Department of Genetics, The Ocular Genetics Unit, Trinity College Dublin, Dublin 2, Ireland
e-mail: lawrencet@tcd.ie

and removal capacity of a cell, aberrant protein aggregates can manifest in two different ways. First, the misfolded protein can acquire new, toxic gain-of-function associated with its aggregation (e.g., mutations in *RHO* causing autosomal dominant RP [adRP]) (Illing et al. 2002; Rajan and Kopito 2005). Secondly, the function of a protein is lost as a result of the protein's inability to attain a functional conformation, and thus results in clearance via proteasome degradation with a consequent "loss-of-function" phenotype (e.g., *BBS6* causing Bardet-Biedl syndrome) (Hiroiyama et al. 2007).

72.2 Protein Misfolding in Photoreceptor Cells

Autosomal dominant forms of RP represent up to 30% of all cases, and within this category, approximately 40% of cases are caused by mutations within the *RHO*, *IMPDH1*, and *RDS-peripherin* genes (Dryja et al. 1990; Farrar et al. 1991; Kennan et al. 2002; Bowne et al. 2002). To date, over 140 point mutations identified in the rhodopsin gene are known to cause adRP, and almost one-sixth of those may be implicated in disease pathology through protein misfolding (Illing et al. 2002). In particular, extensive studies into the pathological mechanism of mutant P23H opsin have increased our understanding of the role that protein misfolding plays in photoreceptor cell death. In brief, the P23H mutation renders rhodopsin extremely aggregation prone, leading to the recruitment of endoplasmic reticulum (ER)-resident chaperones (e.g., BiP and GRP94) and initiation of the unfolded protein response (UPR) to disengage protein synthesis and favor protein degradation. Accumulation of misfolded opsin within the ER imposes serious cellular stress and ER-localized chaperones retro-translocate mutant opsins from the ER to the ubiquitin-proteasome system (UPS) for degradation in the cytosol (Illing et al. 2002; Saliba et al. 2002; Mendes et al. 2005). When the UPS becomes overloaded with mutant opsins, the buildup of toxicity may initiate a detrimental cascade leading to photoreceptor cell death through apoptosis (Illing et al. 2002; Mendes et al. 2005). To date, more than 100 different mutations in the *RDS* gene have been identified to cause a wide array of diseases ranging from adRP to various forms of cone-dominant macular dystrophies (<http://www.retina-international.org.sci-news/rdsmut.htm>). A recent study was carried out on the *RDS* gene carrying a missense mutation (N244K) which can cause both rod-dominant and cone-dominant dystrophies (Conley et al. 2010). Biochemical analysis revealed that this particular mutation may be associated with a loss-of-function haploinsufficiency phenotype by causing *RDS* to misfold, and thus negatively affecting its normal trafficking and assembly with *ROM1*. In our laboratory, we reported that one of the missense mutations (Arg224Pro) in the *IMPDH1* gene responsible for the RP10 form of adRP, causes significant protein tertiary structural perturbation pushing the folding equilibrium toward intermediates that have a propensity to misfold and aggregate, resulting in the formation of insoluble protein aggregates in cell cytosol (Kennan et al. 2002; Aherne et al. 2004). Furthermore, we also showed that adeno-associated virus (AAV)-mediated expression

of mutant human IMPDH1 in the RP10 mouse model impairs visual function and induces rapid photoreceptor cell death (Tam et al. 2008). Although the exact mechanism of toxicity acquired by mutant IMPDH1 still remains to be elucidated, the pathological hallmarks displayed in the RP10 mouse model suggest that it is likely to be a dominant negative effect similar to that observed in the P23H mutant rhodopsin mouse model (Olsson et al. 1992).

72.3 Therapeutic Strategies for Inhibiting Protein Aggregation and Related Toxicity

To date, protein misfolding has been implicated in an increasing number of human disorders including both neurodegenerative and retinal conditions (Ross and Poirier 2004; Surguchev and Surguchov 2009). In principle, all the key steps involved in the formation of pathological protein aggregates may be considered as feasible targets for inhibiting or attenuating disease onset and progression (Bartolini and Andrisano 2010). However, there is not a single target in which, once inhibited, will ultimately inhibit the progression of protein aggregation. The difficulties in effectively overcoming protein aggregation might be due to the fact that our knowledge of the molecular mechanisms for protein aggregation is still limited, and that more than one single event is involved in the initial and subsequent steps of aggregation. In general, current therapeutic strategies employed to halt protein aggregation are focused on targeting specific steps of the aggregation process or related toxic events and can be categorized as follows.

72.3.1 *Inhibition of Conformational Shift*

A beta-sheet breaker consists of a modified core sequence of the target protein that shows affinity for the native monomer and is unable to assume an ordered beta-sheet structure (Wisniewski and Sadowski 2008). Beta-sheet breakers have been designed against amyloid-beta fibrillation for Alzheimer's disease (AD) treatment and against prion PrP^c conversion (Rocha et al. 2009; Soto et al. 2000). However, peptide based structures have short half-lives and poor bioavailability due to enzymatic degradation in the bloodstream (Adessi and Soto 2002).

72.3.2 *Enhancing Chaperone Activities*

Manipulation of the cellular chaperone machinery has been evaluated in many model systems to counteract protein misfolding (Sittler et al. 2001; Warrick et al. 1999). The augmentation of heat shock proteins has demonstrated beneficial effects in many overexpression studies of different disease models. For example, Gorbatyuk

et al. (2010) showed that AAV-mediated overexpression of an ER homologue of Hsp70 (BiP/Grp78) significantly reduced photoreceptor cell death and maintained visual function in the transgenic P23H rhodopsin rat model. Currently, many low-molecular-weight agents have demonstrated the ability to increase cellular expression of Hsp70 through the inhibition of Hsp90 (Sloan et al. 2009). In our laboratory, we demonstrated that both intravitreal and systemic administration of a Hsp90 inhibitor, 17-allylamino-17-demethoxygeldanamycin (17-AAG), in the RP10 mouse model significantly inhibited the accumulation of protein aggregates in the retina and protected the photoreceptor cells from degeneration (Tam et al. 2010).

72.3.3 *Inhibition of Factors Mediating Cell Toxicity*

Cell apoptosis, mitochondria dysfunction, and oxidative stress have all been linked to neuronal cell death, and are considered as potential targets for the treatment of aggregation. For example, oxidative stress has been linked to neuronal cell death and evidence of oxidative damage has been identified in AD, Parkinson's disease (PD) and amyotrophic lateral sclerosis (ALS) patients (Andersen 2004). Oxidative alterations of aggregation-prone proteins such as alpha-synuclein, amyloid-beta and SOD1 are known to cause protein misfolding and impaired clearance of aggregates (Hashimoto et al. 1999a, b; Raichur et al. 2006). Therefore, antioxidants have been widely investigated as potential therapeutic agents, and have been shown to effectively inhibit the formation of amyloid-beta and alpha-synuclein fibrils (Ono and Yamada 2006).

72.3.4 *Gene Therapy*

Gene therapy can be used effectively to alleviate the burden derived from the accumulation of misfolded proteins by suppression of aggregation-prone proteins prior to translation using RNA interference. For example, our laboratory demonstrated that AAV-mediated delivery of short hairpin RNA (shRNA) significantly ablated human mutant IMPDH1 at both the RNA and protein levels and protected the outer nuclear layer (ONL) from degeneration in a mouse model of RP10 (Tam et al. 2008). O'Reilly et al. also showed that subretinal delivery of AAV expressing a codon-modified rhodopsin replacement gene in the presence of rhodopsin-targeting shRNAs significantly protected the ONL of the retina in P23H mice on a *RHO*^{-/-} background (O'Reilly et al. 2007).

72.4 **Conclusions**

In this review, we provide a brief overview of how protein misfolding contributes to specific forms of retinal disorder, and also of current therapeutic strategies for the treatment of harmful consequences caused by misfolded proteins. However, there

are still many gaps in our understanding of the basic biological mechanisms involved in protein misfolding. In many conformational disorders, a specific gain or loss of function leading to toxicity still remains difficult to elucidate. In particular, protein misfolding in retinal disorders such as RP can elicit both narrow and broad pathological effects in cells. For example, different mutations in the rhodopsin gene can show different cellular defects ranging from accumulation of aggregates in the endoplasmic reticulum (ER) to improper trafficking to the outer segment and dysregulated activation of the phototransduction pathway. Finally, owing to the heterogeneity of the steps involved in protein misfolding disorders, it may be possible to employ a combination of protein-specific and disease-specific therapeutic agents as well as protein homeostasis enhancers to increase the efficacy of treatment.

Acknowledgments The Ocular Genetics Unit at TCD is supported by grants from Science Foundation Ireland (07-IN.1.B1778); The MRC/HRB (FB06HUM); The Wellcome Trust (083866/2/07/2); Enterprise Ireland (PC/2008/0006); Fighting Blindness Ireland (FB09HUM); IRCSET (G30364/G30409).

References

- Adessi C, Soto C (2002) Converting a peptide into a drug: strategies to improve stability and bioavailability. *Curr Med Chem* 9:963–978
- Aherne A, Kennan A, Kenna PF et al (2004) On the molecular pathology of neurodegeneration in IMPDH1-based retinitis pigmentosa. *Hum Mol Genet* 13:641–650
- Andersen JK (2004) Oxidative stress in neurodegeneration: cause or consequence? *Nat Rev Neurosci* 5:S18–S25
- Bartolini M, Andrisano V (2010) Strategies for the inhibition of protein aggregation in human diseases. *ChemBioChem* 11:1018–1035
- Bowne SJ, Sullivan LS, Blanton SH et al (2002) Mutations in the inosine monophosphate dehydrogenase 1 gene (IMPDH1) cause the RP10 form of autosomal dominant retinitis pigmentosa. *Hum Mol Genet* 11:559–568
- Bukau B, Weissman J, Horwich A (2006) Molecular chaperones and protein quality control. *Cell* 125:443–451
- Conley SM, Stricker HM, Naash MI (2010) Biochemical analysis of phenotypic diversity associated with mutations in codon 244 of the retinal degeneration slow gene. *Biochemistry* 49:905–911
- Dryja TP, McGee TL, Reichel E et al (1990) A point mutation of the rhodopsin gene in one form of retinitis pigmentosa. *Nature* 343:364–366
- Farrar GJ, Kenna P, Jordan SA et al (1991) A three-base-pair deletion in the peripherin-RDS gene in one form of retinitis pigmentosa. *Nature* 354: 478–480
- Goldberg AL (2003) Protein degradation and protection against misfolded or damaged proteins. *Nature* 426:895–899
- Gorbatyuk MS, Knox T, LaVail MM et al (2010) Restoration of visual function in P23H rhodopsin transgenic rats by gene delivery of BiP/Grp78. *Proc Natl Acad Sci USA* 107:5961–5966
- Guisbert E, Yura T, Rhodius VA (2008) Convergence of molecular, modelling, and systems approaches for an understanding of the Escherichia coli heat shock response. *Microbiol Mol Biol Rev* 72:545–554
- Hartl FU, Hayer-Hartl M (2009) Converging concepts of protein folding in vitro and in vivo. *Nature Struct Mol Biol* 16:574–581
- Hashimoto M, Hsu LJ, Xia Y (1999a) Oxidative stress induces amyloid-like aggregate formation of NACP/alpha-synuclein in vitro. *Neuroreport* 10:717–721

- Hashimoto M, Takeda A, Hsu LJ (1999b) Role of cytochrome c as a stimulator of alpha-synuclein aggregation in Lewy body disease. *J Biol Chem* 274:28849–28852
- Hiroshima S, Yamazaki Y, Kitamura A (2007) MKKS is a centrosome-shuttling protein degraded by disease-causing mutations via CHIP-mediated ubiquitination. *Mol Biol Cell* 19:899–911
- Illing ME, Rajan RS, Bence NF (2002) A rhodopsin mutant linked to autosomal dominant retinitis pigmentosa is prone to aggregate and interacts with the ubiquitin proteasome system. *J Biol Chem* 277:34150–34160
- Kennan A, Aherne A, Palfi A et al (2002) Identification of an IMPDH1 mutation in autosomal dominant retinitis pigmentosa (RP10) revealed following comparative microarray analysis of transcripts derived from retinas of wild-type and Rho(2/2) mice. *Hum Mol Genet* 11, 547–557
- Mendes HF, van der Spuy J, Chapple JP et al (2005) Mechanisms of cell death in rhodopsin retinitis pigmentosa: implications for therapy. *Trends Mol Med* 11:177–185
- O'Reilly M, Palfi A, Chadderton N et al (2007) RNA interference-mediated suppression and replacement of human rhodopsin in vivo. *Am J Hum Genet* 81:127–135
- Olsson JE, Gordon JW, Pawlyk BS et al (1992) Transgenic mice with a rhodopsin mutation (Pro23His): a mouse model of autosomal dominant retinitis pigmentosa. *Neuron* 9:815–830
- Ono K, Yamada J (2006) Antioxidant compounds have potent anti-fibrillogenic and fibril-destabilizing effects for alpha-synuclein fibrils in vitro. *J Neurochem* 97:115–115
- Pratt WB, Toft DO (2003) Regulation of signalling protein function and trafficking by the hsp90/hsp70-based chaperone machinery. *Exp Biol Med* 228:111–133
- Raichur A, Vali S, Gorin F (2006) Dynamic modelling of alpha-synuclein aggregation for the sporadic and genetic forms of Parkinson's disease. *Neuroscience* 142:859–870
- Rajan RS, Kopito RR (2005) Suppression of wild-type rhodopsin maturation by mutants linked to autosomal dominant retinitis pigmentosa. *J Biol Chem* 280:1284–1291
- Rocha S, Cardoso I, Borner H (2009) Design and biological activity of beta-sheet breaker peptide conjugates. *Biochem Biophys Res Commun* 380:397–401
- Ross CA, Poirier MA (2004) Protein aggregation and neurodegenerative disease. *Nat Med* 10: S10–S17.49
- Rubinsztein DC (2006) The roles of intracellular protein degradation pathways in neurodegeneration. *Nature* 443:780–786
- Saliba RS, Munro PMG, Luthert PJ (2002) The cellular fate of mutant rhodopsin: quality control, degradation and aggregate formation. *J Cell Sci* 115:2907–2918
- Sittler A, Lurz R, Lueder G et al (2001) Geldanamycin activates a heat shock response and inhibits huntingtin aggregation in a cell culture model of Huntington's disease. *Hum Mol Genet* 10:1307–1315
- Sloan LA, Fillmore MC, Churcher I (2009) Small-molecule modulation of cellular chaperones to treat protein misfolding disorders. *Curr Opin Drug Discov Dev* 12:666–681
- Soto C, Kacsak RJ, Saborio GP (2000) Reversion of prion protein conformational changes by synthetic beta-sheet breaker peptides. *Lancet* 355:192–197
- Surguchev A, Surguchov A (2009) Conformational diseases: Looking into the eyes. *Brain Res Bull* 81:12–24
- Tam LC, Kiang AS, Campbell M et al (2010) Prevention of autosomal dominant retinitis pigmentosa by systemic drug therapy targeting heat shock protein 90 (Hsp90). *Hum Mol Genet* 19: 4421–4436
- Tam LC, Kiang AS, Kennan A et al (2008) Therapeutic benefit derived from RNAi-mediated ablation of IMPDH1 transcripts in a murine model of autosomal dominant retinitis pigmentosa (RP10). *Hum Mol Genet* 17:2084–2100
- Warrick JM, Chan HY, Gray-Board GL et al (1999) Suppression of polyglutamine-mediated neurodegeneration in *Drosophila* by the molecular chaperone HSP70. *Nat Genet* 23:425–428
- Wisniewski T, Sadowski M (2008) Preventing beta-amyloid fibrillization and deposition: beta-sheet breakers and pathological chaperone inhibitors. *BMC Neurosci* 9:S5

Chapter 73

Development of a Cellular Model of Rod Opsin Retinitis Pigmentosa

Matthew Adamowicz, Antonius Song, Samuel Wadsworth,
Abraham Scaria, and Catherine O’Riordan

Keywords Rod opsin • Autosomal dominant retinitis pigmentosa • P23H opsin • Cellular model • Unfolded protein response • Autophagy

73.1 Introduction

Retinitis pigmentosa (RP) is the most common cause of inherited retinal degeneration which is clinically characterized by night blindness and the loss of peripheral vision. Mutations in the rod visual pigment, rhodopsin, are recognized as the most common cause of autosomal dominant RP (ADRP) with a single base substitution in codon 23 (P23H) of the rhodopsin gene accounting for ~7% of all cases of dominant retinitis pigmentosa in the US, (Dryja et al. 1990). Much data supports the view that rhodopsin RP is a protein-misfolding disease in which the misfolding or misassembly of a mutant protein alters its cellular fate and induces cell death (Gregensen et al. 2006). In culture, the P23H mutant protein, unlike wild-type (WT) protein, causes retention in the ER, induction of the unfolded protein response (UPR), inhibition of the proteasome, and aggregation into oligomeric high molecular weight species that form intracellular inclusions (Saliba et al. 2002). Similarly P23H rhodopsin mislocalizes and/or aggregates in the rod cells of animal RP models (Olsson et al. 1992), suggesting that cellular models may be predictive of in vivo models of this disease. Here, we report on the development of a rhodopsin RP cellular model to allow a better understanding of the precise mechanisms by which rhodopsin misfolding leads to photoreceptor death. Understanding the molecular and cellular consequences of rod opsin mutations and the underlying disease mechanisms in ADRP are essential to develop future therapies for this class of retinal dystrophy.

M. Adamowicz • A. Song • S. Wadsworth • A. Scaria • C. O’Riordan (✉)
Genzyme Corporation, 49 New York Avenue, Framingham, MA 01701, USA
e-mail: catherine.oriordan@genzyme.com

73.2 Materials and Methods

73.2.1 *Generation of Expression Vectors*

The 1,047 bp ORF sequences of human wild-type and P23H-mutant rhodopsin were synthesized with 5' EcoRI and 3' HindIII ends by DNA 2.0 (Menlo Park, CA, USA). Each rhodopsin ORF was subcloned into the EcoRI and HindIII sites of pcDNA3.1 (-) (Invitrogen). Expression was driven by the CMV promoter.

73.2.2 *Western Blotting*

Proteins were resolved using SDS-PAGE on a NuPage 4–12% gradient (Invitrogen) in MOPS buffer. Proteins were transferred to a nitrocellulose membrane using the I-Blot system (Invitrogen). The membrane was blocked briefly in PBS-T (PBS containing 0.05% Tween-20 and 0.1% I-Block) (Applied Biosystems). Rhodopsin was detected using PBS-T containing 1 µg/mL of the anti-Rhodopsin mouse antibody 1D4 (Abcam).

73.2.3 *TUNEL Assay Detection of Apoptosis*

Apoptosis was determined using the APO-BrdU TUNEL Assay (Invitrogen) per the manufacturer's instructions.

73.2.4 *Immunofluorescence*

RPE cells were fixed in 4% paraformaldehyde and permeabilized in 0.5% Triton X-100. The cells were blocked in 5% normal goat serum (NGS), 0.2% BSA, 50 mM NH₄Cl, 25 mM glycine, and 25 mM lysine and then incubated in PBS with 0.2% BSA, 0.1% Triton X-100, 5% NGS (antibody solution), 10 µg/mL antibody to Rhodopsin (R9153; Sigma), and 1 µg/mL mouse anti α -tubulin (Fitzgerald). Subsequently the cells were incubated in a secondary antibody solution containing 2 µg/mL anti-rabbit Alexafluor 488 (Invitrogen), 2 µg/mL anti-mouse Alexafluor555 (Invitrogen), and 1 µg/mL DAPI.

73.2.5 *Gene Expression Analysis*

RNA was purified using the RNEasy kit (Qiagen) according to the manufacturer's instructions. The cDNA was synthesized using Promega's Reverse Transcription System and analyzed in a Taqman gene expression assay for BIP, CHOP,

beta-glucuronidase, or Rhodopsin (Applied Biosystems). The relative expression of each gene was compared to the beta-glucuronidase gene using the Delta-Delta C_t method of calculating gene expression. Autophagy related genes were quantified using the human autophagy array (SA Biosciences). Fold upregulation was determined using the RT² Profiler PCR Array Data Analysis tool available from SA Biosciences.

73.3 Results

73.3.1 *P23H Opsin Protein Has Altered Intracellular Trafficking*

We compared the fate of WT and P23H opsin following transient transfection of human retinal pigmented epithelial cells (RPE). The localization of the opsins was investigated by confocal immunofluorescence using anti-rhodopsin antibody. In the case of the wild-type protein the majority of the protein was processed to the plasma membrane, (Fig. 73.1a), indicating normal biogenesis. By contrast, the mutant P23H showed a perinuclear/reticular distribution characteristic of ER retention with almost no localization to the cell surface (Fig. 73.1a). Aggregation of wild-type rhodopsin and the RP-linked mutant P23H was assessed by SDS-PAGE immunoblot analysis of detergent soluble extracts from RPE cells transiently expressing either protein (Fig. 73.1b). Wild-type rhodopsin migrated predominantly as a diffuse band at a molecular mass of ~40 kDa. This species corresponds to monomeric, mature rhodopsin containing N-linked glycans. P23H rhodopsin differed markedly from wild-type rhodopsin in terms of mobility. The majority of P23H migrated as dimers and oligomers (Fig. 73.1b) and was sensitive to endo H, indicating that it remains core glycosylated (Fig. 73.1c). Endo glycosidase H is specific for high mannose N-linked oligosaccharide structures typical of proteins that have not matured beyond the ER. Together, these data confirm that in RPE cells wild-type rhodopsin is able to fold and mature beyond the ER, whereas the P23H mutant unable to fold productively, is retained within the ER and is more prone to forming nonnative oligomers.

73.3.2 *Activation of UPR and Autophagy*

We assessed P23H rhodopsin's ability to induce ER stress in transfected RPE cells by measuring the levels of two markers of the UPR, BiP (binding immunoglobulin protein), and CHOP (C/EBP homologous protein). Increased BiP mRNA levels were detected in cells transiently expressing both WT and P23H rhodopsin (Fig. 73.2a) suggesting that increasing the folding load of the ER per se induced the UPR. However, BiP mRNA expression was significantly higher in cells expressing

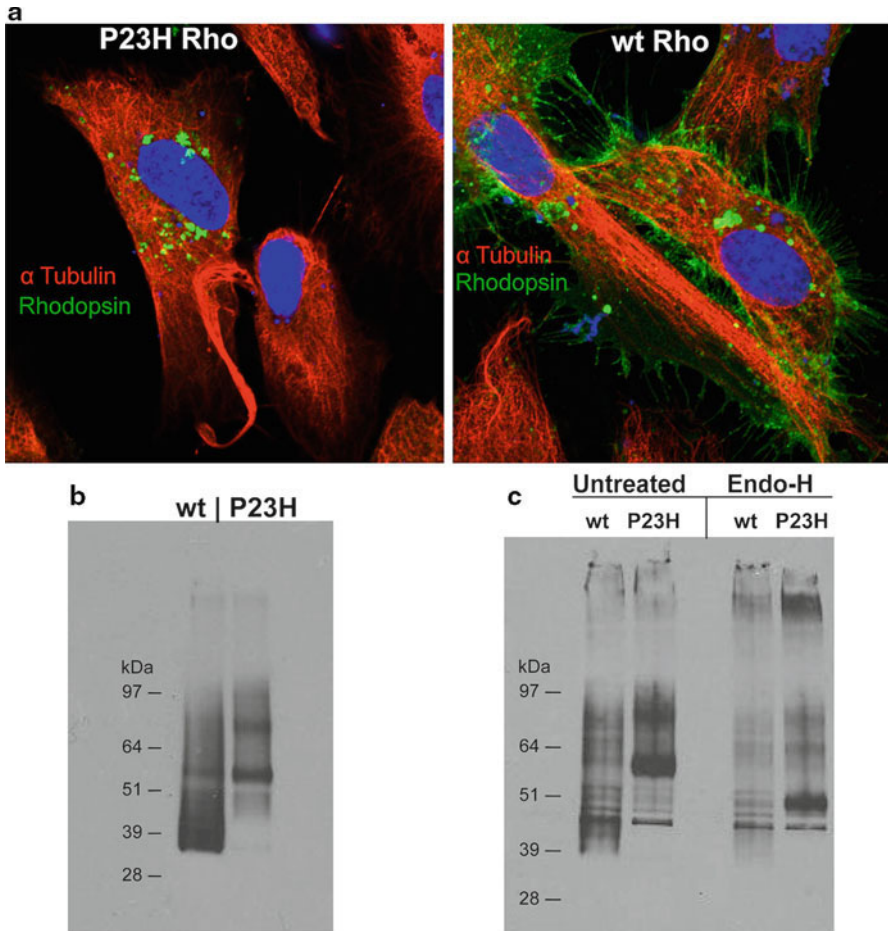


Fig. 73.1 (a) Confocal microscopy images of RPE cells transfected with either WT or P23H rhodopsin. Cells were stained for α -tubulin (red) and rhodopsin (green), DNA was visualized using DAPI (blue). (b) Western blot of RPE cells transfected with either WT or P23H rhodopsin and probed with the monoclonal 1D4 rhodopsin antibody. (c) Western blot of RPE cells transfected with P23H rhodopsin. Cell lysates were either left untreated, or incubated overnight in 0.05 mU of endoglycosidase H

P23H rhodopsin (43-fold over untransfected cells) as compared with cells expressing WT rhodopsin (14-fold increase over untransfected cells), (Fig. 73.2a). The rhodopsin mRNA levels were identical in cells expressing WT and mutant forms of the protein (Fig. 73.2a). Thus, P23H rhodopsin is a more potent inducer of BiP than WT rhodopsin, presumably because of its folding defect. We next examined CHOP expression and found cells expressing the WT opsin protein showed a 15-fold induction of CHOP compared to untransfected cells, while cells expressing P23H mutant showed a 23-fold induction (Fig. 73.2a). As CHOP is a UPR-induced transcription

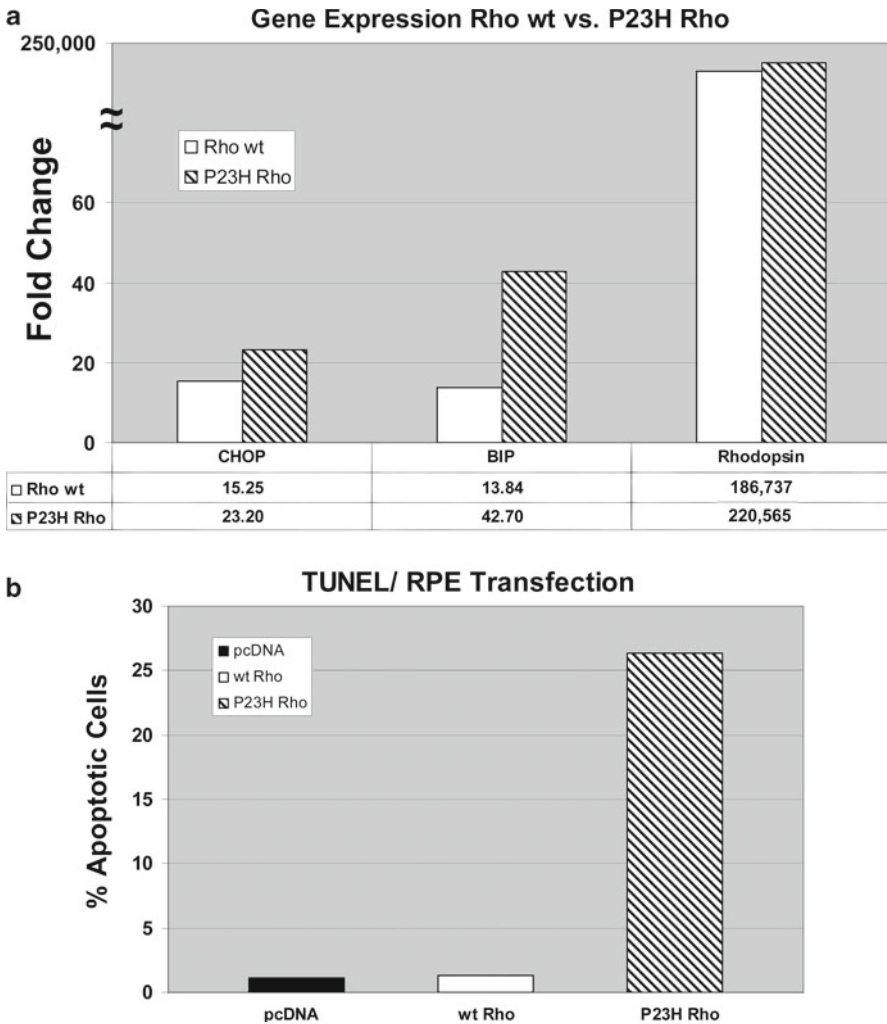


Fig. 73.2 (a) Taqman gene expression analysis of BIP (GRP78), CHOP, and rhodopsin in RPE cells transiently transfected with either WT Rho or P23H Rho. Fold upregulation was determined using the Delta-Delta C_t method relative to beta-glucuronidase. (b) Terminal deoxynucleotidyl transferase dUTP nick end labeling (*TUNEL*) measurement of apoptosis using flow cytometry in RPE cells transfected with WT Rho, P23 Rho, or control pcDNA vector

factor that mediates apoptosis (Lin et al. 2007), we measured the relative levels of apoptosis between WT and P23H mutant expressing cells. In agreement with the mRNA levels of CHOP, *TUNEL* assay results confirm that RPE cells transiently expressing the P23H mutant are more apoptotic than those expressing the wild-type opsin (Fig. 73.2b). One consequence of the UPR is activation of another major cellular pathway, autophagy (Kroemer et al. 2010). Gene expression analysis of RPE

cells expressing either WT or mutant opsin revealed that many markers of the canonical autophagy pathway were preferentially induced in cells expressing the P23H mutant. For example, autophagy related protein 16L2 (ATG16L2), ATG10 and ATG9B were upregulated twofold, while LC3 (MAP1LC3B) was upregulated 2.7-fold.

73.4 Discussion

This study reports on the development of a cellular model of rod opsin RP, that can be exploited to identify the mechanisms of cell death associated with opsin protein-misfolding and to evaluate therapeutic approaches for potential treatments. This study confirms earlier reports (Saliba et al. 2002; Illing et al. 2002), and shows that a mutation linked to ADRP, P23H, results in the production of a misfolded and aggregation prone form of rhodopsin that is retained within the ER. Thus, experimental conditions used in our cellular model induced a protein misfolding that resembles pathological processes associated with an inherited mutation. The UPR has been postulated to play a role in the pathogenesis of protein misfolding diseases (Schroder and Kaufman 2005). Individual UPR target genes can be assigned cytoprotective or proapoptotic functions. For example, expression of the ER chaperone BiP protects cells from ER stress, whereas CHOP, a transcription factor induced by the PERK branch of the UPR, promotes cell death (Lin et al. 2007). This study shows that cells expressing both WT and P23H opsin induced BiP concomitant with the need to fold large amounts of rhodopsin. However cells expressing the mutant opsin protein showed a greater induction consistent with additional ER stress due to the folding defect. Similarly cells expressing the P23H mutant opsin were more apoptotic, due in part to increased levels of the proapoptotic protein CHOP. The predominant outcome of ER stress is the induction of autophagy, a tightly regulated pathway involving the lysosomal degradation of cytoplasmic organelles through the formation of autophagosomes (Kroemer et al. 2010). Cells expressing the P23H opsin had increased markers of the canonical autophagic pathway, including ATG16, ATG9b, ATG10, and LC3. ATG16 interacts with clathrin and connects the endocytic pathway to autophagy (Ravikumar et al. 2010) while ATG9b and ATG10 are involved in autophagosome formation along with LC3 (MAP1LC3B). As autophagy plays a major role in protein degradation, the upregulation of this pathway in P23H expressing cells is significant. Autophagy induction maybe an attempt to degrade mutant rhodopsin and restore cellular homeostasis analogous to the role autophagy plays in removing aggregated mutant Huntingtin protein (Ravikumar et al. 2004). Unmitigated autophagy may eventually result in cellular apoptosis, and whether autophagy is contributing to the apoptotic cell death observed in P23H expressing cells (Fig. 73.2b) has yet to be determined.

The precise mechanism by which rhodopsin misfolding leads to photoreceptor death still remains to be clarified. The autosomal dominant cellular model described here, reveals that many cellular pathways including ER stress, autophagy, and apoptosis

are induced in response to P23H opsin expression. Understanding these pathways will allow the development of effective therapies for this currently untreatable form of retinal dystrophy.

References

- Dryja TP, McGee T, Reichel E et al (1990) A point mutation of the rhodopsin gene in one form of retinitis pigmentosa. *Nature* 343:364–366
- Gregensen N, Bross P, Vang S et al (2006) Protein misfolding and human disease. *Annu Rev Genomics Hum Genet* 7:103–124
- Illing M, Rajan S, Bence N et al (2002) The rhodopsin mutant linked to autosomal dominant retinitis pigmentosa is prone to aggregate and interacts with the ubiquitin proteasome system. *J Biol Chem* 277:34150–34160
- Kroemer G, Marino G and Levine B (2010) Autophagy and the Integrated Stress response. *Mol Cell* 40:280–293
- Lin J, Li H, Yasumura D et al (2007) IRE1 Signaling affects cell fate during the unfolded protein response. *Science* 318:944–949
- Olsson J, Gordon J, Pawlyk B et al (1992) Transgenic mice with a rhodopsin mutation (Pro23His): a mouse model of autosomal dominant retinitis pigmentosa. *Neuron* 9:815–830
- Ravikumar B, Vacher C, Berger Z et al (2004) Inhibition of mTOR induces autophagy and reduces toxicity of polyglutamine. *Nature Genet* 36:585–595
- Ravikumar B, Moreau K, Jahreiss L et al (2010) Plasma membrane contributes to the formation of pre-autophagosomal structures. *Nat Cell Biol* 12:747–757
- Saliba R, Munro P, Luther P et al (2002) The cellular fate of mutant rhodopsin: quality control degradation and aggresome formation. *J Cell Sci* 115:2907–2918
- Schroder M and Kaufman RJ (2005) The mammalian unfolded protein response. *Annu Rev Biochem* 74:739–789

Chapter 74

A Brief Account of Rho GTPases in Retinal Physiology and Pathophysiology

Severin Reinhard Heynen, Omolara O. Ogunshola, and Christian Grimm

Keywords Rho GTPases • Rac1 • Cdc42 • Retina • Photoreceptor • Development
• Cytoskeleton • Degeneration

74.1 Introduction

Rho GTPases, proteins of the Ras superfamily of GTPases, have multifaceted roles in the cell including regulation of the cytoskeleton, cell growth, development, and apoptosis (Hall and Nobes 2000; Aznar and Lacal 2001; Govek et al. 2005). RAC1, CDC42, and gene family member A (RHOA) are the classical and most studied members of the 25 Rho GTPases identified to date (Wennerberg and Der 2004). They are best known for their role in the generation of filopodia, lamellipodia, and stress fibers in the cell (Hall and Nobes 2000).

This family of GTPases can be activated or inactivated depending on their binding to GTP or GDP, respectively. Proteins such as guanine nucleotide exchange factors (GEF), GTPase-activating proteins (GAP), and guanine-nucleotide dissociation inhibitors (GDI) regulate and facilitate the exchange of GDP to GTP and catalyze triphosphate hydrolysis (Paduch et al. 2001). Active Rho GTPases initiate downstream

S.R. Heynen (✉) • C. Grimm

Laboratory of Retinal Cell Biology, Department of Ophthalmology, University of Zurich,
Wagistrasse 14, 8952, Schlieren, Switzerland

Zurich Center for Integrative Human Physiology, Zurich, Switzerland
e-mail: severin.heynen@usz.ch

O.O. Ogunshola

Zurich Center for Integrative Human Physiology, Zurich, Switzerland

Institute of Veterinary Physiology, University of Zurich,
Winterthurerstrasse 260, 8057, Zurich, Switzerland

signaling cascades through interactions with effector proteins such as p21-activated kinases (PAK), mixed lineage kinases (MLK), and Rho-associated kinases (ROCK) (Teramoto et al. 1996; Jaffer and Chernoff 2002; Zhao and Manser 2005; Yoshimura et al. 2006; Wells and Jones 2010).

Many Rho GTPases have overlapping functions but also have distinct niches. For example, RAC1 and RHOA are both implicated in the formation of lamellipodia during gastrulation in *Xenopus* (Tahinci and Symes 2003). However, RAC1 and RHOA have antagonistic roles in cellular movement. RAC1 is required to extend lamellipodia toward the direction of movement thereby generating the force for forward motion. On the other hand, RHOA is involved in microfilament disassembly at the lagging end, allowing the cell to contract and move in one direction (Raftopoulou and Hall 2004).

This review focuses on various functions of Rho GTPases in the retina. A brief overview of their roles during retinal development, in the organization of the photoreceptor cytoskeleton, and during photoreceptor degeneration will be presented.

74.2 Rho GTPases in Retinal Development

During retinal development, Rho GTPases are involved in several pre- and postnatal processes. The formation of the optic cup through the invagination of the optic vesicle (Chow and Lang 2001; Rembold et al. 2006) has been proposed to be partially dependent on lens-retinal tethering. Loss of CDC42, or pharmacological disruption of actin–myosin interactions, lead to reduced lens pit invagination and suggests a role for CDC42 in optic cup formation (Chauhan et al. 2009).

Processes of retinal development such as axonogenesis have been shown to involve Rho GTPases (Ruchhoeft et al. 1999; Yuan et al. 2003). Studies in *Drosophila* have shown that the RAC1 GEF, VAV, is involved in photoreceptor axon guidance to ganglion cells during retinal development. Mutant VAV generated disorganized photoreceptor to ganglion cell connections in the eye. Expression of nonfunctional RAC1 or RAC2 rescued these flies from this phenotype suggesting a role for this GTPase in photoreceptor axon guidance (Malartre et al. 2010). The localization of RAC1, CDC42, and RHOA in the neuroretinal and plexiform layers during retinal development in mice (Mitchell et al. 2007) may suggest that Rho GTPases have similar roles in axon guidance in the mammalian retina as was shown in the fly.

The developmental functions of Rho GTPases also extend to postnatal processes involved in the morphogenesis of photoreceptors. For example, Mushroom bodies tiny (MBT), a CDC42 effector protein in *Drosophila*, localizes to rhabdomeric adherens junctions and is essential for photoreceptor morphogenesis (Schneeberger and Raabe 2003). A null allele of *Mbt* causes changes in twinstar/cofilin activation that affects actin organization at adherens junctions resulting in a disorganized rhabdomeric morphology (Menzel et al. 2007). MBT localization and activity requires CDC42 and a loss of function studies of CDC42 showed a similar photoreceptor morphology as MBT-null flies (Schneeberger and Raabe 2003). Rho GTPases are

localized in most cells, including photoreceptors, during postnatal development in the mouse retina (Mitchell et al. 2007) suggesting that these proteins may be of similar importance as CDC42 is in *Drosophila*.

It is clear that Rho GTPases have important roles in photoreceptor morphogenesis; however, most of the research has been done in *Drosophila*. Studies in mammalian systems will help to increase our understanding of the developmental role of Rho GTPases in the retina.

74.3 Rho GTPases and the Photoreceptor Cytoskeleton

Investigations into the structural role of Rho GTPases in photoreceptors have been performed in the non-inverted retina of cephalopodes like the octopus. These retinas possess rhabdomeres which contain the light sensitive photopigments. Actin microvilli span the rhabdoms and change their length depending on the light conditions which affects rhabdomere extension and light absorption capacity (Robles et al. 1995; Torres et al. 1997). In dark conditions, when the cross sections of the rhabdoms increase, Rho GTPase activities were found primarily in membranous rhabdomeric fractions. In contrast, in light conditions GTPases were inactive and found primarily in soluble fractions (Gray et al. 2008). Gray and colleagues hypothesized that the correlation between GTPase activity and the change in actin microvilli length at different light intensities indicates an active role of Rho GTPases in the regulation of rhabdomere light sensitivity. Supporting this hypothesis, rhabdomeres maintained in darkness ceased to increase their size normally when Rho GTPases were inhibited (Miller et al. 2005).

The role of Rho GTPases in the mammalian retina is unclear. Some studies suggest that these proteins have a role in the regulation of phototransduction. It was shown that RHOA is able to bind photoexcited rhodopsin (Wieland et al. 1990; Balasubramanian and Slepak 2003) and that RAC1 can be activated by light in lipid rafts of bovine photoreceptor outer segments (Wieland et al. 1990; Balasubramanian and Slepak 2003). Additionally, Rho GTPases may be involved in the regulation of physiological processes in photoreceptors including disc formation, rod outer segment length regulation, and disc shedding. All these processes rely on actin cytoskeleton dynamics (Steinberg et al. 1980; Williams 1988; Chaitin 1989; Chaitin and Burnside 1989; Hale et al. 1996) and may be modulated by the action of Rho GTPases. However, it is clear that neither RAC1 nor CDC42 is essential to maintain photoreceptor integrity and outer segment structure in the mature mouse retina. Conditional knockdowns of either protein in adult photoreceptor cells did not lead to acute alterations in photoreceptor or retinal physiology (Haruta et al. 2009; Heynen et al. in press). Deciphering the regulation pathways of cytoskeleton dynamics in mammalian photoreceptor cells also requires detailed investigations into emerging nonclassical Rho GTPases (Wennerberg and Der 2004). WRCH-1 (Wnt-1 responsive *Cdc42* homolog), a recently emerged nonclassical Rho GTPases similar to CDC42, is involved in actin-dependent filopodia projections

(Aspenstrom et al. 2004). These projections differ structurally from CDC42-induced filopodia suggesting that WRCH-1 may activate a different set of effector proteins leading to the observed morphological differences. Therefore, nonclassical Rho GTPases, having similar functions to the classical three, may be of interest in the study of the photoreceptor cytoskeleton.

74.4 Rho GTPases in Photoreceptor Degeneration and Survival

Retinitis pigmentosa (RP) is a heterogeneous class of retinal dystrophies that ultimately lead to blindness through the degeneration of photoreceptor cells (Portera-Cailliau et al. 1994; Curcio et al. 1996). It has become increasingly evident that mutations in cytoskeletal components lead to photoreceptor degeneration and RP. The RP1 protein is important in disc formation, disc stacking, and protein transport (Liu et al. 2002, 2003, 2004). Mutations in mouse RP1 result in disorganized disc stacking and mislocalization of rhodopsin, indicating the involvement of cytoskeletal components. Retinas expressing a mutant RP1 protein show a progressive loss of photoreceptors (Gao et al. 2002). Since Rho GTPases are regulators of the cellular cytoskeleton, they may play a role in photoreceptor degenerative processes. Supporting this hypothesis, photoreceptor degeneration in rhodopsin knockout *Drosophila* flies can be rescued by a constitutively expressed active form of *Drosophila Rac1 (Drac1)* (Chang and Ready 2000). Therefore, rhodopsin may be involved in organizing the actin cytoskeleton via *Drac1*. However, recent work in mice suggests a different role for RAC1 during photoreceptor degeneration. RAC1 localized to the perikaryal region in photoreceptor cells during retinal degeneration induced by exposure to high levels of visible light (Belmonte et al. 2006). Inactivation of RAC1 using a conditional knockdown strategy rendered photoreceptors resistant to light-induced degeneration (Haruta et al. 2009). Thus, RAC1 can rescue photoreceptors in *Drosophila* whereas in mice it might be involved in a pro-apoptotic process. The reason for this discrepancy is unclear. However, species and especially structural differences of photoreceptors in *Drosophila* and mouse could play a role.

In a study similar to Haruta and colleagues, we investigated the function of CDC42 during photoreceptor death in four mouse models of retinal degeneration. CDC42 localized to the perinuclear region of some photoreceptors after toxic light exposure and in *Rd1*, *Rd10*, and VPP mice suggesting a role for this protein in retinal degeneration. However, rod photoreceptor-specific ablation of CDC42 did not affect retinal degeneration after light exposure and in the VPP mouse model (Heynen et al. *in press*). Together these results suggest that although CDC42 responds to photoreceptor degeneration by changing its cellular localization, it does not influence the progression of degeneration.

Even though it is clear that some Rho GTPases participate in retinal degeneration, their signaling mechanisms are not completely understood. Shedding light on Rho GTPase pathways in the retina may provide ways of protecting photoreceptors against death.

74.5 Conclusion

A body of work over the past few decades has shown that Rho GTPases play important functions in photoreceptor development, physiology, and pathophysiology. It is clear that Rho GTPases play a defined role in rhabdomic changes in length and size dependent on different lighting conditions. Yet their role in mammalian photoreceptors still remains unknown. Recent experiments have implicated an Rho GTPase, RAC1, in photoreceptor degeneration and neuroprotection. These observations make Rho GTPases an interesting and important protein target in the investigation of blinding diseases.

Acknowledgments I would like to thank members of the lab, especially Marijana Samardzija as well as Christian Grimm, for the continued help and support. This work was supported by a cooperative project grant from the Center of Integrative Human Physiology (ZIHP) of the University of Zurich and by the Swiss National Science Foundation (SNF #3100A0-117760).

References

- Aspenstrom P, Fransson A, Saras J (2004) Rho GTPases have diverse effects on the organization of the actin filament system. *Biochem J* 377:327–337
- Aznar S, Lacal JC (2001) Rho signals to cell growth and apoptosis. *Cancer Lett* 165:1–10
- Balasubramanian N, Slepak VZ (2003) Light-mediated activation of Rac-1 in photoreceptor outer segments. *Curr Biol* 13:1306–1310
- Belmonte MA, Santos MF, Kihara AH et al (2006) Light-Induced photoreceptor degeneration in the mouse involves activation of the small GTPase Rac1. *Invest Ophthalmol Vis Sci* 47:1193–1200
- Chaitin MH (1989) Immunogold localization of actin and opsin in rds mouse photoreceptors. *Prog Clin Biol Res* 314:265–274
- Chaitin MH, Burnside B (1989) Actin filament polarity at the site of rod outer segment disk morphogenesis. *Invest Ophthalmol Vis Sci* 30:2461–2469
- Chang HY, Ready DF (2000) Rescue of photoreceptor degeneration in rhodopsin-null *Drosophila* mutants by activated Rac1. *Science* 290:1978–1980
- Chauhan BK, Disanza A, Choi SY et al (2009) Cdc42- and IRSp53-dependent contractile filopodia tether presumptive lens and retina to coordinate epithelial invagination. *Development* 136:3657–3667
- Chow RL, Lang RA (2001) Early eye development in vertebrates. *Annu Rev Cell Dev Biol* 17:255–296
- Curcio CA, Medeiros NE, Millican CL (1996) Photoreceptor loss in age-related macular degeneration. *Invest Ophthalmol Vis Sci* 37:1236–1249
- Gao J, Cheon K, Nusinowitz S et al (2002) Progressive photoreceptor degeneration, outer segment dysplasia, and rhodopsin mislocalization in mice with targeted disruption of the retinitis pigmentosa-1 (Rp1) gene. *Proc Natl Acad Sci USA* 99:5698–5703
- Govek EE, Newey SE, Van Aelst L (2005) The role of the Rho GTPases in neuronal development. *Genes Dev* 19:1–49
- Gray SM, Kelly S, Robles LJ (2008) Rho signaling mediates cytoskeletal re-arrangements in octopus photoreceptors. *Am Malacol Bull* 26:19–26
- Hale IL, Fisher SK, Matsumoto B (1996) The actin network in the ciliary stalk of photoreceptors functions in the generation of new outer segment discs. *J Comp Neurol* 376:128–142

- Hall A, Nobes CD (2000) Rho GTPases: molecular switches that control the organization and dynamics of the actin cytoskeleton. *Philos Trans R Soc Lond B Biol Sci* 355:965–970
- Haruta M, Bush RA, Kjellstrom S et al (2009) Depleting Rac1 in mouse rod photoreceptors protects them from photo-oxidative stress without affecting their structure or function. *Proc Natl Acad Sci USA* 106:9397–9402
- Heynen SR, Tanimoto N, Joly S, Seeliger MW, Samardzija M, Grimm C. Retinal degeneration modulates intracellular localization of CDC42 in photoreceptors. *Molecular Vision* in press
- Jaffer ZM, Chernoff J (2002) p21-activated kinases: three more join the Pak. *Int J Biochem Cell Biol* 34:713–717
- Liu Q, Zuo J, Pierce EA (2004) The retinitis pigmentosa 1 protein is a photoreceptor microtubule-associated protein. *J Neurosci* 24:6427–6436
- Liu Q, Lyubarsky A, Skalet JH et al (2003) RP1 is required for the correct stacking of outer segment discs. *Invest Ophthalmol Vis Sci* 44:4171–4183
- Liu Q, Zhou J, Daiger SP et al (2002) Identification and subcellular localization of the RP1 protein in human and mouse photoreceptors. *Invest Ophthalmol Vis Sci* 43:22–32
- Malartre M, Ayaz D, Amador FF et al (2010) The guanine exchange factor vav controls axon growth and guidance during Drosophila development. *J Neurosci* 30:2257–2267
- Menzel N, Schneeberger D, Raabe T (2007) The Drosophila p21 activated kinase Mbt regulates the actin cytoskeleton and adherens junctions to control photoreceptor cell morphogenesis. *Mech Dev* 124:78–90
- Miller AM, Ramirez T, Zuniga FI et al (2005) Rho GTPases regulate rhabdom morphology in octopus photoreceptors. *Vis Neurosci* 22:295–304
- Mitchell DC, Bryan BA, Liu JP et al (2007) Developmental expression of three small GTPases in the mouse eye. *Mol Vis* 13:1144–1153
- Paduch M, Jelen F, Otlewski J (2001) Structure of small G proteins and their regulators. *Acta Biochim Pol* 48:829–850
- Portera-Cailliau C, Sung CH, Nathans J et al (1994) Apoptotic photoreceptor cell death in mouse models of retinitis pigmentosa. *Proc Natl Acad Sci USA* 91:974–978
- Raftopoulou M, Hall A (2004) Cell migration: Rho GTPases lead the way. *Dev Biol* 265:23–32
- Rembold M, Loosli F, Adams RJ et al (2006) Individual cell migration serves as the driving force for optic vesicle evagination. *Science* 313:1130–1134
- Robles LJ, Camacho JL, Torres SC et al (1995) Retinoid cycling proteins redistribute in light-/dark-adapted octopus retinas. *J Comp Neurol* 358:605–614
- Ruchhoeft ML, Ohnuma S, McNeill L et al (1999) The neuronal architecture of Xenopus retinal ganglion cells is sculpted by rho-family GTPases in vivo. *J Neurosci* 19:8454–8463
- Schneeberger D, Raabe T (2003) Mbt, a Drosophila PAK protein, combines with Cdc42 to regulate photoreceptor cell morphogenesis. *Development* 130:427–437
- Steinberg RH, Fisher SK, Anderson DH (1980) Disc morphogenesis in vertebrate photoreceptors. *J Comp Neurol* 190:501–508
- Tahinci E, Symes K (2003) Distinct functions of Rho and Rac are required for convergent extension during Xenopus gastrulation. *Dev Biol* 259:318–335
- Teramoto H, Coso OA, Miyata H et al (1996) Signaling from the small GTP-binding proteins Rac1 and Cdc42 to the c-Jun N-terminal kinase/stress-activated protein kinase pathway. A role for mixed lineage kinase 3/protein-tyrosine kinase 1, a novel member of the mixed lineage kinase family. *J Biol Chem* 271:27225–27228
- Torres SC, Camacho JL, Matsumoto B et al (1997) Light-/dark-induced changes in rhabdom structure in the retina of Octopus bimaculoides. *Cell Tissue Res* 290:167–174
- Wells CM, Jones GE (2010) The emerging importance of group II PAKs. *Biochem J* 425:465–473
- Wennerberg K, Der CJ (2004) Rho-family GTPases: it's not only Rac and Rho (and I like it). *J Cell Sci* 117:1301–1312
- Wieland T, Ulibarri I, Gierschik P et al (1990) Interaction of recombinant rho A GTP-binding proteins with photoexcited rhodopsin. *FEBS Lett* 274:111–114

- Williams DR (1988) Topography of the foveal cone mosaic in the living human eye. *Vision Res* 28:433–454
- Yoshimura T, Arimura N, Kaibuchi K (2006) Molecular mechanisms of axon specification and neuronal disorders. *Ann N Y Acad Sci* 1086:116–125
- Yuan XB, Jin M, Xu X et al (2003) Signalling and crosstalk of Rho GTPases in mediating axon guidance. *Nat Cell Biol* 5:38–45
- Zhao ZS, Manser E (2005) PAK and other Rho-associated kinases--effectors with surprisingly diverse mechanisms of regulation. *Biochem J* 386:201–214

Chapter 75

Molecular Clues to Bothnia-Type Retinal Dystrophy

Xiaoqin He, Joel Lobsiger, and Achim Stocker

Keywords Cellular retinaldehyde-binding protein • 11-*cis*-retinal • Bothnia-type retinal dystrophy • X-ray crystallography structure • R234W

75.1 Introduction

In retinal pigment epithelium (RPE), cellular retinaldehyde-binding protein (CRALBP) is the major acceptor of 11-*cis*-retinol in the isomerization step of the rod visual cycle. It serves as a substrate carrier for 11-*cis*-retinol dehydrogenase (RDH 5), facilitating the oxidation of 11-*cis*-retinol to 11-*cis*-retinal. CRALBP also protects bound ligands from photoisomerization (Saari et al. 2001). The arginine-to-tryptophan missense mutation in position 234 (R234W) in the *RLBP1* gene is associated with the autosomal recessive disease Bothnia-type retinal dystrophy, and impairs regeneration of visual pigment (Burstedt et al. 1999). The rod–cone dystrophy occurs predominantly in northern Sweden with patients losing peripheral and central vision gradually. In this study, we report the X-ray crystallographic structures of CRALBP and its disease causing mutant R234W and provide a molecular explanation of the disease mechanism.

X. He • A. Stocker (✉)

Department of Chemistry and Biochemistry, University of Bern,
Freiestrasse 3, Bern, Switzerland
e-mail: achim.stocker@ibc.unibe.ch

J. Lobsiger

Institute for Molecular Biology and Biophysics, ETH Zürich, Zürich, Switzerland

75.2 Materials and Methods

75.2.1 Protein Expression, Purification, and Crystallization

The proteins CRALBP WT and R234W were cloned, expressed, purified, and crystallized as described previously (He et al. 2009). Hexagonal crystals of CRALBP WT in complex with 11-*cis*-retinal were formed in 1.0M K/Na tartrate, 0.1M Tris-HCl (pH 7.0), 0.2M Li₂SO₄ after 3 days. The space group was P6₅22 with $a = 71.92 \text{ \AA}$, $b = 71.92 \text{ \AA}$, $c = 303.20 \text{ \AA}$, $\alpha = 90^\circ$, $\beta = 90^\circ$, $\gamma = 120^\circ$. Monoclinic crystals of R234W in complex with 11-*cis*-retinal were formed in 20% (wt./vol.) PEG 3000, 0.1M Hepes (pH 7.5), 0.2M NaCl. The crystals have a C2 space group with $a = 87.93 \text{ \AA}$, $b = 57.88 \text{ \AA}$, $c = 75.15 \text{ \AA}$, $\alpha = 90^\circ$, $\beta = 122.846^\circ$, $\gamma = 90^\circ$. The structure of R234W was solved by SAD using selenomethionine-labeled protein; the structure of CRALBP WT was subsequently solved by molecular replacement using the atomic model of R234W and the program Phaser (Qian et al. 2007).

75.2.2 Illumination of 11-*cis*-Retinal

Illumination of 11-*cis*-retinal and its complexes with CRALBP WT and R234W was performed according to the methods of Saari and Bredberg (1987). The time-dependent photoisomerization of 11-*cis*-retinal in ethanol, CRALBP WT, or R234W was plotted respectively, by recording the remaining amount of 11-*cis*-retinal after being exposed to light every 5 s. The first-order rate constants (k) from the slopes of the plots of $\log a/a_0$ vs. time were calculated. The following values were used to calculate quantum yield Φ_{R234W} : $\Phi_{CRALBP} = 0.07$; $\epsilon_{CRALBP} = \epsilon_{R234W} = 15,400 \text{ (M}^{-1} \text{ cm}^{-1}\text{)}$.

75.3 Results

75.3.1 The Structure Determination of CRALBP WT and R234W

The crystallographic structure model of CRALBP WT comprises residues 23–306 of 317 residues; the residues 1–22 are missing due to the different crystal contacts. The N-terminal domain comprises five α helices. The C-terminal $\alpha\beta\alpha$ sandwich comprises a 5- β -strand sheet forming hydrophobic floor for retinal binding, two α helices packed on one side, and four α helices on the other side forming the ligand pocket with the β -sheet. The electron density map of the C11–C15 terminal tail is poorly defined, suggesting that this part of the ligand is slightly disordered in the less tightly packed ligand-binding pocket (Fig. 75.1).



Fig. 75.1 Closer look at the environment of the ligand 11-*cis*-retinal both CRALBP WT (*gray*) and R234W (*pink*). Retinal is buried deeper into the ligand-binding cavity by a dramatic structural change in the loop region. In CRALBP WT, R234 is part of a cluster of three pairs of positively charged residues (R103–K104, K236–R234, and K261–265) at the protein surface. The mutation to tryptophan in R234W changed the potential distribution at the surface patch, which might mediate interactions with specific acidic lipids

The structure model of the R234W mutant comprises residues 57–306 of 317 and the 11-*cis*-retinal ligand tail is well visible. The one-amino-acid mutation caused structural changes of 1 Å root mean square deviation over all C α atoms. A rather big conformational transition occurred in the loop where the apolar indole ring of W234 is buried between the N-terminal α helices and the C-terminal $\alpha\beta\alpha$ sandwich. Extensive van der Waals interactions are formed between tryptophan and nearby residues, and K104 and K261 are pushed over 5.4 and 3.4 Å respectively. Residues 227–238 are moved by an average 2.3 Å deviation comparing to wild type. Side chains of F198, F235, and I238 in the ligand-binding pocket are flipped in a domino-like manner; consequently, the pocket size is reduced (He et al. 2009) (Fig. 75.2).

Fig. 75.2 Comparison of the ligand-binding cavity of CRALBP WT (*gray*) and R234W (*pink*). The pocket volumes were calculated using the program VOIDOO and a rolling probe with a radius of 1.0 Å. The R234W volume is $5.989 \times 10^2 \text{ \AA}^3$, CRALBP WT volume is $6.454 \times 10^2 \text{ \AA}^3$. Pictures are drawn using PyMol (Delano 2002)

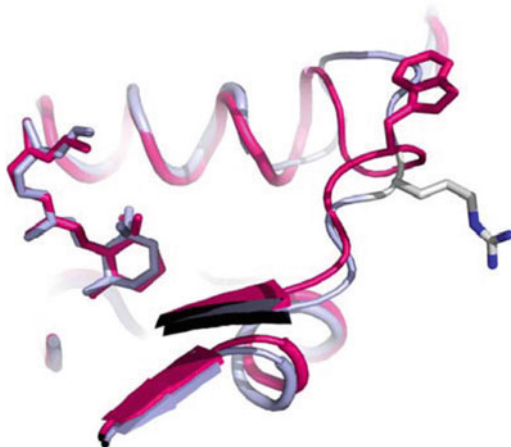


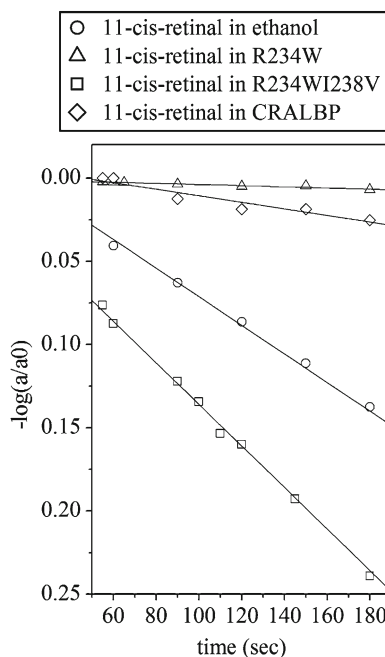
Fig. 75.3 Time courses of the photoisomerization of 11-*cis*-retinal in the presence of ethanol, wild-type CRALBP, or R234W.

The amount present at $t=0$ is a_0 ; the amount present after illumination is a . For a first-order decay process, $a = a_0 e^{-kt}$. The first-order rate constants calculated from this experiment are

$$k_{\text{ethanol}} = 0.859 \times 10^{-3} \text{ s}^{-1};$$

$$k_{\text{CRALBP}} = 0.197 \times 10^{-3} \text{ s}^{-1};$$

$$k_{\text{R234W}} = 0.035 \times 10^{-3} \text{ s}^{-1}$$



75.3.2 Photoisomerization of 11-*cis*-Retinal

We determined first-order rate constants for the photoisomerization of 11-*cis*-retinal in ethanol, CRALBP WT, or R234W using the method described by Saari and Bredberg (Fig. 75.3). The measurements revealed a fivefold reduction of R234W photosensitivity ($191.5 \text{ M}^{-1} \text{ cm}^{-1}$) relative to CRALBP WT. The reduction must be

Table 75.1 Crystallographic statistics

	Wild-type CRALBP	R234W Se-Met
Crystal parameters	P6 ₃ 22 $a=71.9 \text{ \AA}$, $b=71.9 \text{ \AA}$, $c=303.2 \text{ \AA}$ $\alpha=90^\circ$, $\beta=90^\circ$, $\gamma=120^\circ$	C121 $a=87.9 \text{ \AA}$, $b=57.9 \text{ \AA}$, $c=75.6 \text{ \AA}$ $\alpha=90^\circ$, $\beta=122.85^\circ$, $\gamma=90^\circ$
Molecules/asymmetric unit	1	1
Data collection		
Wavelength (Å)	0.9762	0.9793
No. crystals	1	1
Resolution (Å) (outer shell)	50.0–3.0 (3.2–3.0)	50–1.7 (1.8–1.7)
No. observations	10,3496 (14,433)	38,0336 (46,406)
No. unique reflections	9,692 (1,499)	67,824 (9,663)
Mean redundancy	10.7 (9.6)	5.6 (4.8)
Completeness (%)	99.5 (99.6)	97.4 (86.1)
R_{sym} (%)	0.059 (0.53)	0.048 (0.58)
$I/\sigma(I)$	22.8 (4.1)	19.8 (2.7)
Phasing		
Se sites		5
FOM (SAD phases)		0.49
Refinement		
Resolution range (Å)	48.1–3.0	45.6–1.7
No. reflections working set	9,690	67,814
No. reflections test set	970	6,775
$R_{\text{work}}/R_{\text{free}}$ (%)	23.9/27.2	16.7/18.4
RMS bonds (Å)	0.004	0.005
RMS angles (°)	0.74	1.18
Residues included	23–306	57–306
Ramachandran statistics		
Generously allowed (%)	99.65	100.00
Not allowed (%)	0.35	n.a.

attributed to the local increase in packing density through the I238 C δ methyl group, because the extinction coefficient of CRALBP and R234W decreased equally from 25,000 to 15,400 M⁻¹ cm⁻¹ after binding 11-*cis*-retinal. The result is consistent with crystallographic data (Table 75.1).

75.4 Discussion

The molecular basis of retinoid transportation by CRALBP was not well understood due to the lack of structural data. The crystal structure of CRALBP here provides insight into stereospecific binding and into chemical protection of 11-*cis*-retinal in the human eye. The clinical phenotype of Bothnia-type Retinal Dystrophy is caused by the R234W mutation in CRALBP, and leads to a defective retinal metabolism. The crystal structure of the pathologic R234W mutation of CRALBP reveals impaired 11-*cis*-retinal release through stabilization of the ligand complex and

disruption of a conserved basic surface patch with putative loss of lipid stimulation of retinoid transfer. The results of our study suggest that impaired 11-*cis*-retinal release may be a major cause of night blindness and retinal pathology in patients carrying the R234W missense mutation in the *RLBP1* gene. This study may help elucidate CRALBP's role in visual cycle regulation, and provide further information in search of Bothnia-type retinal dystrophy treatment.

Acknowledgments We thank National Eye Institute, National Institutes of Health, for the generous gift of 11-*cis*-retinal. Data collection was performed at the Swiss Light Source, Beam-line X06DA (PXIII), Villigen, Switzerland, and at the European Synchrotron Radiation Facility, Beamline ID29, Grenoble, France. This study was supported by the Berne University Research Foundation.

References

- He X, Lobsiger J, Stocker A (2009) Bothnia dystrophy is caused by domino-like rearrangements in cellular retinaldehyde-binding protein mutant R234W. *Proc Natl Acad Sci* 106:18545–18550
- Saari JC, Nawrot M, Kennedy BN et al (2001) Visual cycle impairment in cellular retinaldehyde binding protein (CRALBP) knockout mice results in delayed dark adaptation. *Neuron* 29:739–748
- Burstedt MS, Sandgren O, Holmgren G et al (1999) Bothnia dystrophy caused by mutations in the cellular retinaldehyde-binding protein gene (RLBP1) on chromosome 15q26. *Invest Ophthalmol Vis Sci* 40:995–1000
- Qian B, Raman S, Das R et al (2007) High-resolution structure prediction and the crystallographic phase problem. *Nature* 450:259–264
- Saari JC, Bredberg DL (1987) Photochemistry and stereoselectivity of cellular retinaldehyde-binding protein from bovine retina. *J Biol Chem* 262:7618–7622
- Delano ML (2002) The PyMOL Molecular Graphics System (Delano ML, Palo Alto, CA)

Chapter 76

A Novel Missense Mutation in Both *OPNILW* and *OPNIMW* Cone Opsin Genes Causes X-Linked Cone Dystrophy (XLCOD5)

Jessica C. Gardner, Tom R. Webb, Naheed Kanuga, Anthony G. Robson, Graham E. Holder, Andrew Stockman, Caterina Ripamonti, Neil D. Ebenezer, Olufunmilola Ogun, Sophie Devery, Genevieve A. Wright, Eamonn R. Maher, Michael E. Cheetham, Anthony T. Moore, Michel Michaelides, and Alison J. Hardcastle*

Keywords Cone opsin • Cone dystrophy • X-linked • XLCOD5 • Opsin array

76.1 Introduction

XLCOD and XLCORD are heterogeneous disorders in which progressive visual loss results from cone cell degeneration, with a variable degree of rod loss. Onset of disease occurs within the first or second decade and is characterised by loss of cone function leading to colour vision disturbance, photophobia and loss of central vision. Maculopathy is often observed (Michaelides et al. 2006). The most common cause of XLCOD/XLCORD is mutation of exon *ORF15* in the *RPGR* gene (Demirci et al. 2002; Yang et al. 2002; Ebenezer et al. 2005).

Genetic mapping in a British family defined a new locus for XLCOD on Xq26.1-pter (XLCOD5). Subsequent candidate gene screening identified the causative

*The authors Jessica C. Gardner and Tom R. Webb contributed equally.

J.C. Gardner • T.R. Webb • N. Kanuga • A. Stockman • C. Ripamonti • N.D. Ebenezer
• O. Ogun • M.E. Cheetham • A.J. Hardcastle (✉)
UCL Institute of Ophthalmology, 11-43 Bath Street, London EC1V 9EL, UK
e-mail: a.hardcastle@ucl.ac.uk

A.G. Robson • G.E. Holder • A.T. Moore • M. Michaelides (✉)
UCL Institute of Ophthalmology, 11-43 Bath Street, London EC1V 9EL, UK

Moorfields Eye Hospital, City Road, London EC1V 2PD, UK
e-mail: michel.michaelides@ucl.ac.uk

S. Devery • G.A. Wright
Moorfields Eye Hospital, City Road, London EC1V 2PD, UK

E.R. Maher
West Midlands Regional Genetics Service, Birmingham Women's Hospital,
Birmingham B15, UK

mutation as a novel missense substitution (c.529T>C; p.W177R) in both *OPNILW* and *OPNIMW* cone opsin genes. We also investigated the functional consequences of this mutation.

76.2 Materials and Methods

76.2.1 Ophthalmic Assessment

A three generation family with a clinical diagnosis of XLCOD was ascertained at Moorfields Eye Hospital, UK. The study adhered to tenets of the Declaration of Helsinki and informed consent was obtained. Four affected males and two obligate carriers were fully assessed. Ophthalmic examination included colour fundus photography, autofluorescence imaging, colour vision testing, full-field ERG, and pattern ERG (PERG). Psychophysical measurements and dark-adaptation tests were performed in selected cases (see Gardner et al. 2010).

76.2.2 Molecular Genetic Analysis

DNA was isolated from peripheral blood and used for two point linkage analysis (Gardner et al. 2010). The cone opsin gene array on Xq28 was initially screened for mutations in an affected male. The locus control region, LCR, and six exons with the flanking intronic regions of the *OPNILW* and *OPNIMW* opsin genes were amplified and sequenced as described previously (Gardner et al. 2009). Following the preliminary screen of the array, *OPNILW* and *OPNIMW* exons 2, 3 and 4 were amplified independently using gene-specific primers in order to confirm the presence or absence of an exon in the array and to identify *OPNILW*- and *OPNIMW*-specific haplotypes. Further analysis involved the pairing of gene-specific primers with co-amplifying primers in a strategy designed to establish the relationship of each *OPNILW* and *OPNIMW* exon to its neighbour. Sequence changes were tested for segregation. PCR products of Exon 3 (co-amplification of *OPNILW* and *OPNIMW* genes) in over 200 control chromosomes were analysed using an MspI restriction digest assay that was diagnostic for the mutation.

76.2.3 Immunoblotting and Immunocytochemistry

To create cone opsin constructs with a 1D4 epitope for transient transfection, we subcloned 1D4-tagged green (*OPNIMW*) opsin with a C203R mutation from pGrnC203R (Kazmi et al. 1997) into pBK-CMV. Using site-directed mutagenesis, we made a wild-type green opsin construct and a construct with the W177R mutation.

Primary antibodies used were 1D4 and anti-calnexin (Sigma). Secondary antibodies used were HRP-conjugated goat anti-mouse (Pierce) and Alexa Fluor 488 anti-mouse or Alexa Fluor 594 anti-rabbit (Invitrogen). 9-*cis*-retinal was from Sigma. SK-N-SH cells were maintained, transfected, and rescue experiments (9-*cis*-retinal) conducted, essentially as previously described (Mendes and Cheetham 2008; Kosmaoglou et al. 2009). For immunocytochemistry, cells were seeded on chamber slides and transfected with 1D4 epitope-tagged cone opsin constructs, fixed 24 h posttransfection with 4% paraformaldehyde and permeabilised in 0.1% Triton X-100. Cells transfected with cone opsins were incubated with 1D4 (0.5 µg/mL) and anti-calnexin (1:600), followed by secondary antibodies (1:2,000). Images were taken with a Zeiss LSM 700 laser scanning confocal microscope.

76.3 Results

76.3.1 Phenotype of the *XLCOD5* Family

Affected subjects were between 14 and 82 years of age. All had experienced gradual deterioration of colour vision and visual acuity. Four affected males were studied in detail. All had bilateral macular atrophy and severe generalised cone system dysfunction on ERG, but rod function was preserved. PERGs indicated severe macular dysfunction. Short-wavelength flash ERGs were subnormal in one affected male. The obligate carriers showed mild generalised cone system dysfunction with moderate macular involvement. Colour vision tests revealed good tritan discrimination. Psychophysical tests in two affected males showed dramatic loss of L- and M-cone sensitivity and reduced sensitivity in obligate carriers. S-cone sensitivity was markedly reduced in the eldest affected male, but was normal in the younger males (phenotype data are described in detail in Gardner et al. 2010).

76.3.2 Molecular Genetic Analysis

A prior study of this family did not identify a mutation in *RPGR* (Ebenezer et al. 2005). Haplotype analysis excluded *RPGR* and two other candidate genes, *RP2* and *CACNA1F*, on Xp. A reconstructed, linked haplotype on Xq confirmed segregation of XLCOD with markers DXS0984, DXS1227, DXS8045 and DXS1073 between Xq26.1-qter (see Gardner et al. 2010). Linkage analysis revealed a significant LOD score ($Z_{\max} = 2.41$) for marker DXS8045 on Xq27.3. The linked region included the cone opsin gene array on Xq28, which was considered a candidate for XLCOD. An initial mutation screen of the array revealed an intact LCR and a full complement of exons for *OPNIMW*; however, no *OPNILW*-specific exon 3 was identified. Further analysis revealed that the *OPNIMW* exon 3 sequence

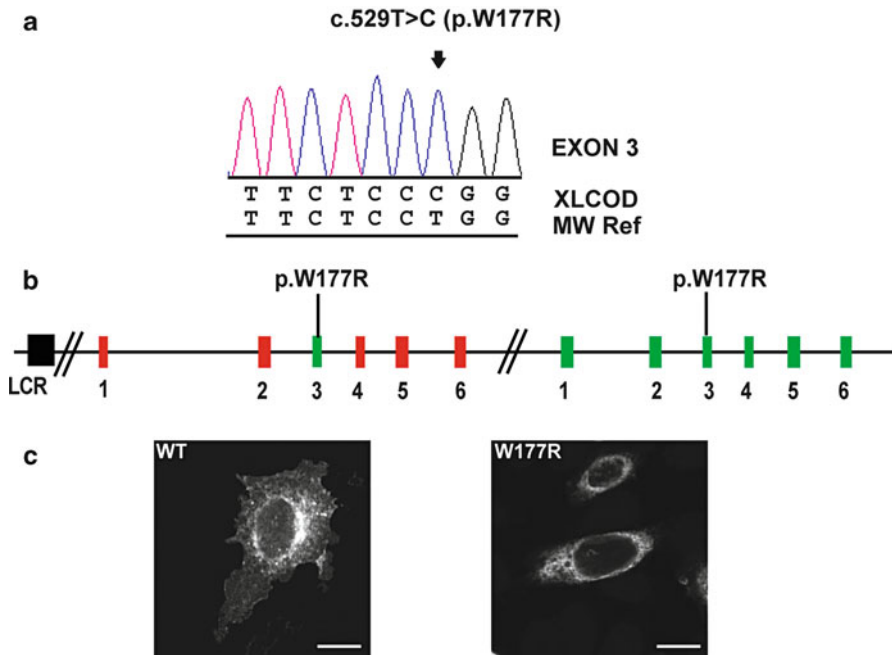


Fig. 76.1 Analysis of the cone opsin array in XLCOD5. **(a)** Exon 3 sequence with a novel missense mutation, c.529T>C (p.W177R), highlighted with an arrow. *OPNIMW* reference sequence also shown. **(b)** Schematic of the cone opsin gene array in the XLCOD5 family. Both *OPNILW* and *OPNIMW* genes contain identical copies of mutant *OPNIMW* exon 3 with the c.529T>C missense mutation (p.W177R). **(c)** Comparison of the cellular localisation of WT and W177R mutant MW opsin. The majority of WT MW opsin is correctly targeted to the plasma membrane, whereas no MW W177R mutant opsin was correctly trafficked, all is retained in the ER. Scale bar 10 μ M

contained a novel missense mutation, c.529T>C, that changed a highly conserved Trp residue to Arg at p.177 (W177R) (Fig. 76.1a). The genomic organisation of the array in the XLCOD5 family was established, and affected members were found to have an *OPNILW* gene harbouring a W177R mutant *OPNIMW* exon 3, followed by a *OPNIMW* gene containing an identical W177R mutant *OPNIMW* exon 3 (Fig. 76.1b). The W177R mutation was not detected in over 200 chromosomes, equivalent to over 400 *OPNILW* and *OPNIMW* genes. Analysis of the intervening sequence flanking the mutant *OPNIMW* exon 3 of both *OPNILW* and *OPNIMW* genes revealed that the two genes shared a minimum identical region of *OPNIMW*-derived sequence of 492 bp, from IVS2-170 to IVS3+25. This suggests that W177R was transferred in a block of exon 3 sequence from the *OPNIMW* gene into the *OPNILW* gene by gene conversion.

Cone opsins contain a hepta-helical transmembrane domain and W177 is a highly conserved residue located in helix IV (Gardner et al. 2010). We investigated the effects of W177R in cone opsin (referred to herein as MW W177R) and the rod

opsin equivalent (W161R) in transiently transfected cells. We also compared MW W177R with MW C203R, a misfolding mutation that causes blue cone monochromacy (BCM) (Kazmi et al. 1997), and with rod opsin mutant P23H, a misfolding mutation which is a common cause of retinitis pigmentosa (RP) (Saliba et al. 2002; Illing et al. 2002). Our results show that wild-type (WT) MW cone opsin is processed in the ER and correctly targeted to the plasma membrane, but the W177R mutant resulted in misfolding and retention in the ER (Fig. 76.1c). In addition, in contrast to WT rod opsin which localises to the plasma membrane, P23H and W161R localised exclusively to the ER, demonstrating that W161R causes misfolding of rod opsin (Gardner et al. 2010).

In previous studies, treatment of mutant P23H rod opsin with 11-*cis*-retinal or 9-*cis*-retinal has been shown to improve the folding and trafficking of the mutant protein (Saliba et al. 2002; Noorwez et al. 2004). We investigated the effect of 9-*cis*-retinal on MW W177R, MW C203R and W161R in rod opsin. Our results showed that 9-*cis*-retinal did not alleviate the misfolding or ER retention of MW W177R and had no effect on localisation of W161R rod opsin. In contrast, 9-*cis*-retinal treatment of P23H partially restored traffic of P23H to the plasma membrane (Gardner et al. 2010).

76.4 Discussion

We describe a new locus for cone dystrophy (XLCOD5) and the identification of a novel missense mutation in the cone opsin gene array on Xq28. This mutation was present in both *OPNILW* and *OPNIMW* cone opsin genes as a result of a gene conversion event transferring exon 3 of the *OPNIMW* gene into the *OPNILW* gene. Previously, only three point mutations in the cone opsin gene array (C203R, P307L, and R247X) have been described, associated with stationary red/green colour vision disorders or with a BCM phenotype (Nathans et al. 1986, 1989, 1993; Reyniers et al. 1995; Ueyama et al. 2002; Michaelides et al. 2005). We have identified a novel misfolding missense mutation of the *OPNILW* and *OPNIMW* cone opsins that causes early-onset progressive cone dystrophy. XLCOD5 was differentiated from BCM by the phenotype, including the absence of nystagmus and evidence of progression and psychophysical evidence of cone cell death, including loss of SW cones (Michaelides et al. 2004).

Conservation of the mutated tryptophan residue across opsins and species and comparative modelling of the structure of the cone opsins with the crystal structure of rhodopsin (Palczewski et al. 2000; Stenkamp et al. 2002) predicted that the W177R mutation would result in a major conformational change. We surmised that a build up of misfolded W177R cone opsins, in both red and green cone photoreceptors, could cause cone dystrophy in a similar manner to class II rod opsin misfolding mutants, such as P23H, causing retinitis pigmentosa (Mendes et al. 2005). Our investigation shows that the MW W177R mutant and its rod opsin equivalent, W161R, were retained in the ER and formed inclusions targeted for degradation by

the proteasome (Gardner et al. 2010). These results indicate that cone degeneration in this family is probably the result of an accumulation of structurally abnormal W177R opsin in the ER. Although treatment with the pharmacological chaperone 9-*cis*-retinal partially alleviated the trafficking defect of the P23H rod mutant, it had no effect on the processing of MW W177R, MW C203R and W161R rod opsin mutants.

In addition to our study, recent research on other families with a variety of phenotypes has identified rare mutations and combinations of polymorphisms in the *OPNILW* and *OPNIMW* genes, which strengthens the hypothesis that a wider spectrum of retinal dystrophies is attributable to the cone opsin array than has previously been recognised (Carroll et al. 2009; Mizrahi-Meissonier et al. 2010). Phenotypes can range from stationary congenital disorders of cone function, to BCM with progression in later life, to early-onset retinal degeneration (XLCOD5). Correlations between genotype and phenotype are beginning to emerge and will be greatly aided with the advent of high-resolution adaptive optics imaging of the retinal mosaic and functional analyses, which may help to advance our understanding of the phenotypic effects of a variety of mutations in the cone opsin array (Wagner Schuman et al. 2010).

Acknowledgements This research was supported by funding from Fight for Sight UK, The British Retinitis Pigmentosa Society, Wellcome Trust, Moorfields Special Trustees and the National Institute for Health Research UK to the Biomedical Research Centre for Ophthalmology Michel Michaelides is supported by an FFB Career Development Award.

References

- Carroll J, Baraas RC, Wagner-Schuman M et al (2009) Cone photoreceptor mosaic disruption associated with Cys203Arg mutation in the M-cone opsin. *Proc Natl Acad Sci USA* 106(48):20948–20953
- Demirci FY, Rigatti BW, Wen G et al (2002) X-linked cone-rod dystrophy (locus COD1): identification of mutations in RPGR exon ORF15. *Am J Hum Genet* 70:1049–1053
- Ebenezer ND, Michaelides M, Jenkins SA et al (2005) Identification of novel RPGR ORF15 mutations in X-linked progressive cone-rod dystrophy (XLCORD) families. *Invest Ophthalmol Vis Sci* 46:1891–1898
- Gardner JC, Michaelides M, Holder GE et al (2009) Blue cone monochromacy: causative mutations and associated phenotypes. *Mol Vis* 15:876–884
- Gardner JC, Webb TR, Kanuga N et al (2010) X-linked cone dystrophy caused by mutation of the red and green cone opsins. *Am J Hum Genet* 87:26–39
- Illing ME, Rajan RS, Bence NF et al (2002) A rhodopsin mutant linked to autosomal dominant retinitis pigmentosa is prone to aggregate and interacts with the ubiquitin proteasome system. *J Biol Chem* 277:34150–34160
- Kazmi MA, Sakmar TP, Ostrer H (1997) Mutation of a conserved cysteine in the X-linked cone opsins causes color vision deficiencies by disrupting protein folding and stability. *Invest Ophthalmol Vis Sci* 38:1074–1081
- Kosmaoglou M, Kanuga N, Aguilà M et al (2009) A dual role for EDEM1 in the processing of rod opsin. *J Cell Sci* 122:4465–4472
- Mendes HF, van der Spuy J, Chapple JP et al (2005) Mechanisms of cell death in rhodopsin retinitis pigmentosa: implications for therapy. *Trends Mol Med* 11:177–185

- Mendes HF and Cheetham ME (2008) Pharmacological manipulation of gain-of-function and dominant-negative mechanisms in rhodopsin retinitis pigmentosa. *Hum Mol Genet* 17:3043–3054
- Michaelides M, Hardcastle AJ, Hunt DM et al (2006) Progressive cone and cone-rod dystrophies: phenotypes and underlying molecular genetic basis. *Surv Ophthalmol* 51:232–258
- Michaelides M, Hunt DM and Moore AT (2004) The cone dysfunction syndromes. *Br J Ophthalmol* 88:291–297
- Michaelides M, Johnson S, Simunovic MP et al (2005) Blue cone monochromatism: a phenotype and genotype assessment with evidence of progressive loss of cone function in older individuals. *Eye* 19:2–10
- Mizrahi-Meissonnier L, Merin S, Banin E et al (2010) Variable retinal phenotypes caused by mutations in the X-linked photopigment gene array. *Invest Ophthalmol Vis Sci* 51(8):3884–3892
- Nathans J, Maumenee IH, Zrenner E et al (1993) Genetic heterogeneity among blue-cone monochromats. *Am J Hum Genet* 53:987–1000
- Nathans J, Piantanida TP, Eddy RL et al (1986) Molecular genetics of inherited variation in human color vision. *Science* 232:203–210
- Nathans J, Davenport CM, Maumenee IH et al (1989) Molecular genetics of human blue cone monochromacy. *Science* 245:831–838
- Noorwez SM, Malhora R, McDowell JH et al (2004) Retinoids assist the cellular folding of the autosomal dominant retinitis pigmentosa mutant P23H. *J Biol Chem* 279:16278–16284
- Palczewski K, Kumasaka T, Hori T et al (2000) Crystal Structure of Rhodopsin: A G Protein-Coupled Receptor. *Science* 289:739–745
- Reyniers E, Van Thienen MN, Meire F et al (1995) Gene conversion between red and defective green opsin gene in blue cone monochromacy. *Genomics* 29:323–328
- Saliba RS, Munro PG, Luthert PJ et al (2002) The cellular fate of mutant rhodopsin: quality control, degradation and aggresome formation. *J Cell Sci* 115:2907–2918
- Stenkamp RE, Filipek S, Driessen CG et al (2002) Crystal structure of rhodopsin: a template for cone visual pigments and other G protein-coupled receptors. *Biochem Biophys Acta* 1565:168–182
- Ueyama H, Kuwayama S, Imai H et al (2002) Novel missense mutations in red/green opsin genes in congenital color-vision deficiencies. *Biochem Biophys Res Commun* 294:205–209
- Wagner-Schuman M, Neitz J, Rha J et al (2010) Color-deficient cone mosaics associated with Xq28 opsin mutations: a stop codon versus deletions. *Vision Res* 50(23):2396–2402
- Yang Z, Peachey NS, Moshfeghi DM et al (2002) Mutations in the RPGR gene cause X-linked cone dystrophy. *Hum Mol Genet* 11(5):605–611

Chapter 77

A Potential Cytosolic Function of Bestrophin-1

Olaf Strauß, Rudgar Neussert, Claudia Müller, and Vladimir M. Milenkovic

Keywords VMD2 • BEST1 • Ca²⁺-signaling • Ca²⁺ stores • Endoplasmic reticulum • Vitelliform macular dystrophy • Best disease • Endogenously expressed bestrophin-1

77.1 Introduction

Mutations in the VMD2 or BEST1 gene (MIM 607854) can lead to various types of retinal degenerations (Boon et al. 2009; Hartzell et al. 2008). Over 100 distinct mutations have been identified and associated with the respective disorder (http://www-huge.uni-regensburg.de/BEST1_database/). The gene product of BEST1, bestrophin-1, was found to function as Ca²⁺-dependent anion channel and modulator of activity of voltage-dependent L-type Ca²⁺ channels (Hartzell et al. 2008; Rosenthal et al. 2006; Yu et al. 2008). Mutations were found to lead to a loss of function. However, these observations could not explain how mutations lead to retinal degeneration or were in contradiction to findings in bestrophin-1 mouse models.

O. Strauß (✉) • C. Müller • V.M. Milenkovic
Experimental Ophthalmology, Eye Hospital, University Health Center Regensburg,
Regensburg, Germany
e-mail: strauss@eye-regensburg.de

R. Neussert
Experimental Ophthalmology, Eye Hospital,
University Hospital Hamburg-Eppendorf, Hamburg, Germany

77.2 Best's Vitelliforme Macular Dystrophy

The most common BEST1-associated disease is Best's vitelliforme macular dystrophy which also led to the name of the BEST gene product bestrophin-1 (Boon et al. 2009; Marquardt et al. 1998; Petrukhin et al. 1998). The disease is an autosomal-dominant inherited form of macular dystrophy with juvenile onset (Boon et al. 2009). It is characterized by a fast accumulation of lipofuscin in the retina and the development of a central bull's eye or egg-yolk like lesion. A hallmark of the diagnosis of the disease is the reduction of the light-peak in the patient's electro-oculogram, a signal which is generated by activation of Cl channels in the basolateral membrane of the retinal pigment epithelium (RPE) (Arden and Constable 2006). In the eye, bestrophin-1 was found to be expressed only in the RPE (Marmorstein et al. 2000). Thus, it is likely that mutation-dependent change of bestrophin-1 function leads to retinal degeneration by alteration of RPE function, a close interaction partner of the photoreceptors (Strauss 2005). However, so far it is not known which function of the RPE is changed in Best's disease.

77.3 The Function of Bestrophin-1

Bestrophin-1 is a membrane protein (Milenkovic et al. 2009) which appeared in over-expression studies to function as a Ca^{2+} -dependent anion channel in the cell membrane (Hartzell et al. 2008) and modulator of voltage-dependent L-type channels (Burgess et al. 2008; Reichhart et al. 2010; Rosenthal et al. 2006; Yu et al. 2008).

In nearly all cases, mutations lead to a loss of anion channel conductance. (Hartzell et al. 2008; Sun et al. 2002; Tsunenari et al. 2003; Yu et al. 2006). The loss of anion conductance could possibly explain the decreased light-peak in the patient's electro-oculogram: if bestrophin-1 is the basolateral Cl channel of the RPE, then a loss of function would lead to reduction of the light-peak. This conclusion is challenged by observations made in bestrophin-1 knock-out or knock-in mouse models. Here, a signal of the DC-electroretinogram corresponding with the light-peak in the electro-oculogram (Peachey et al. 2002) did not correlate with either absence of bestrophin-1 or the presence of a mutant bestrophin-1 with loss of anion channel activity (Marmorstein et al. 2006; Zhang et al. 2010).

77.4 The Localization of Bestrophin-1

Histological analysis of Best's patient eyes revealed that bestrophin-1 has lost its basolateral localization (Mullins et al. 2005). Thus, the localization of bestrophin-1 seems to be of importance for its function and mislocalization is probably associated with the patho-physiology underlying the retinal degeneration in Best's disease. However, the subcellular localization of the bestrophin-1 was so far not thoroughly investigated.

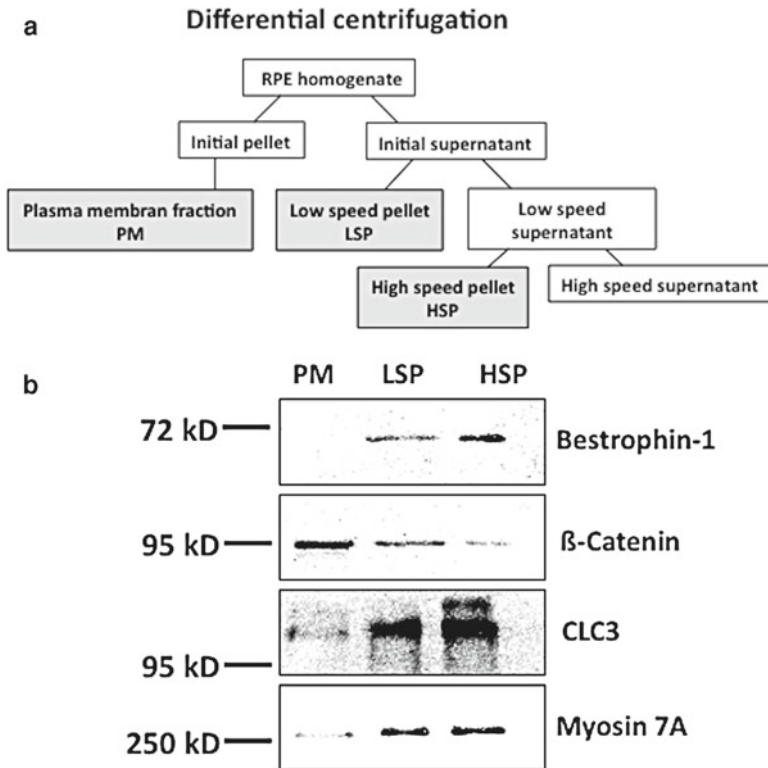


Fig. 77.1 Analysis of subcellular bestrophin-1 localization by biochemical methods. **(a)** Scheme of differential centrifugation which was used to separate fractions of membrane proteins from either plasma membrane or cytosolic membrane structures. A homogenate was established from freshly isolated porcine RPE cells. Initial pellet (PM): $19,000g \times 20'$; supernatant: $41,000g \times 20'$ resulting in low speed pellet (LSP); supernatant: $160,000g \times 75'$ resulted in the high speed pellet (HSP). **(b)** Western-blot analysis of the pellets obtained by differential centrifugation. Equal amounts of protein were loaded to the blot. The blot was stained for bestrophin-1, β -catenin, CLC-3, and myosin-7A. Bestrophin-1 was mainly found in the fraction which showed the highest enrichment of cytosolic membrane proteins (The antibodies against CLC-3 were a kind gift from Thomas Jentsch; figure from Neussert et al. 2010.)

We analyzed the subcellular localization of endogenously expressed bestrophin-1 (Neussert et al. 2010). After differential centrifugation of membrane proteins from freshly isolated porcine RPE cells, we found largest proportion of bestrophin-1 or intracellular Cl channel CLC-3 in the fraction of cytosolic membrane proteins (Fig. 77.1). Thus, a large proportion of endogenously expressed bestrophin-1 is in the cytoplasmic structures of RPE cells. Furthermore, we analyzed the subcellular localization of bestrophin-1 in fresh sections of the porcine retina (Fig. 77.2). In stainings for the membrane protein cadherin and for bestrophin-1, we found both proteins at the basolateral side of the RPE but with separate localization. Thus, bestrophin-1 seems to be localized in vesicular structures close to the membrane. This is supported by a study investigating endogenously expressed bestrophin-1

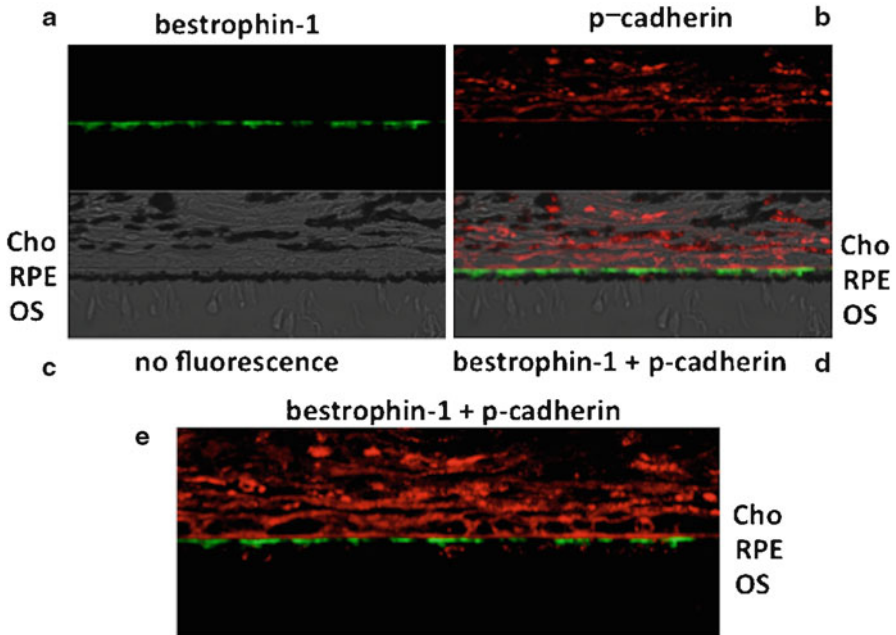


Fig. 77.2 Subcellular localization of bestrophin-1 in cryo-sections of the porcine retina detected by costaining for pan-cadherin. **(a)** Staining for bestrophin-1 in the RPE showing the basolateral localization. **(b)** Staining of the same section against pan-cadherin showing localization in the cell of the choroid and in the basolateral membrane of the RPE. **(c)** Light-microscopic picture of the section shown in **(a, b)**. **(d)** Overlay picture of **(a–c)** showing that the larger proportion of bestrophin-1 is not in the cell membrane together with cadherin. Bestrophin-1 is close to the basolateral membrane (*green*) below the pan-cadherin (*red*). Absence of *yellow pixels* reveals that there is no overlap of bestrophin-1 and pan-cadherin staining. **(e)** Overlay picture at higher magnification showing only weak colocalization of bestrophin-1 and cadherin (*Cho* choroid; *RPE* retinal pigment epithelium; *OS* photoreceptor outer segments; *ONL* outer nuclear layer; from Neussert et al. 2010)

in epithelial airway cells (Barro-Soria et al. 2010). In these cells, bestrophin-1 is colocalized with proteins of the endoplasmic reticulum calreticulin, calnexin, and stim1 (stromal interacting molecule 1). Also, a study using overexpressed bestrophin-1 reported that a large proportion of bestrophin-1 was found in the cytoplasm (Milenkovic et al. 2009).

With the conclusion that bestrophin-1 is an intracellular Cl channel, the family of bestrophins resembles somewhat the family of ClC Cl channels (Jentsch et al. 2002). Some members function as Cl channels in the cell membrane, while others function as Cl channels in cytosolic membranes such as vesicles. The function of the cytoplasmic Cl channels would be to transport counter-ions to cations which are accumulated in these vesicles by active transport. The hypothesis that endogenously expressed bestrophin-1 is a cytoplasmic Cl channel could also explain why the membrane conductance for Cl⁻ in RPE cells from bestrophin-1 knock-out mice is not different to that of RPE cells from wild-type mice (Marmorstein et al. 2006).

77.5 Cytoplasmic Function of Bestrophin-1

So if bestrophin-1 is a cytoplasmic Cl channel what might be its function? As described above, bestrophin-1 was found to be colocalized with calreticulin, calnexin, and stim1 (Barro-Soria et al. 2010). In addition, bestrophin-1 possibly physically interacts with stim1. Stim1 is involved in intracellular Ca^{2+} signaling by activating store-operated Ca^{2+} channels in the cell membrane after Ca^{2+} depletion from these stores (Putney 2005) and it regulates the Ca^{2+} reuptake into these Ca^{2+} stores (Brandman et al. 2007). Thus, bestrophin-1 is probably in membranes of endoplasmic reticulum Ca^{2+} stores. Indeed activation of Ca^{2+} -dependent Cl channels in the plasma membrane in response to increases in intracellular-free Ca^{2+} after depletion of Ca^{2+} stores was modulated by the presence of bestrophin-1 (Barro-Soria et al. 2010). The group concluded that bestrophin-1 provides a pathway to transport Cl^- as a counter-ion when Ca^{2+} is accumulated into the Ca^{2+} stores by active ion transport. We could support this conclusion by studying the endogenously expressed bestrophin-1 in the mouse RPE (Neussert et al. 2010). RPE cells from bestrophin-1 knock-out mice showed increased levels of basal intracellular Ca^{2+} compared to that of wild-type mice (Fig. 77.3a). This seems to result from a less efficient accumulation of Ca^{2+} into endoplasmic reticulum Ca^{2+} stores (Fig. 77.3b). Furthermore, when analyzing ATP-stimulated Ca^{2+} transients in mouse RPE cells, we found that ATP-receptor activation recruited Ca^{2+} by 90% from Ca^{2+} stores of the endoplasmic reticulum which was not the case in cells from bestrophin-1 knock-out mice (Fig. 77.4). Thus, bestrophin-1 modulates intracellular Ca^{2+} signaling.

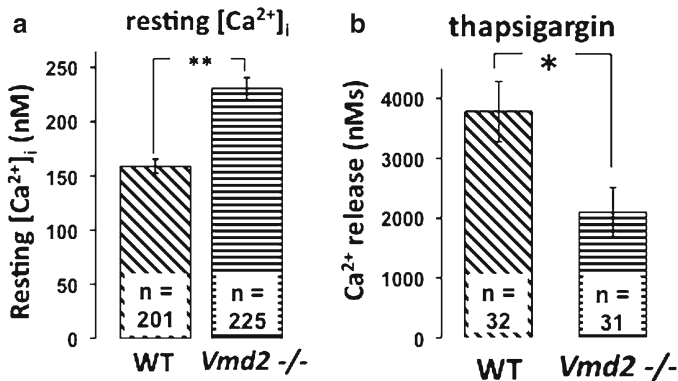


Fig. 77.3 Ca^{2+} homeostasis in mouse RPE cells. (a) Comparison of resting Ca^{2+} levels. Cells from *Vmd2*^{-/-} mice showed significantly increased Ca^{2+} levels (** $p < 0.01$). The number “*n*” depicts the number of investigated cells from at least ten mice. (b) Comparison of Ca^{2+} release from cytosolic stores by thapsigargin application: the Ca^{2+} release was quantified by integration of the area below the Ca^{2+} -increases during thapsigargin application. “*n*” depicts the number of cells of at least four cell cultures. * $p < 0.05$ (from Neussert et al. 2010)

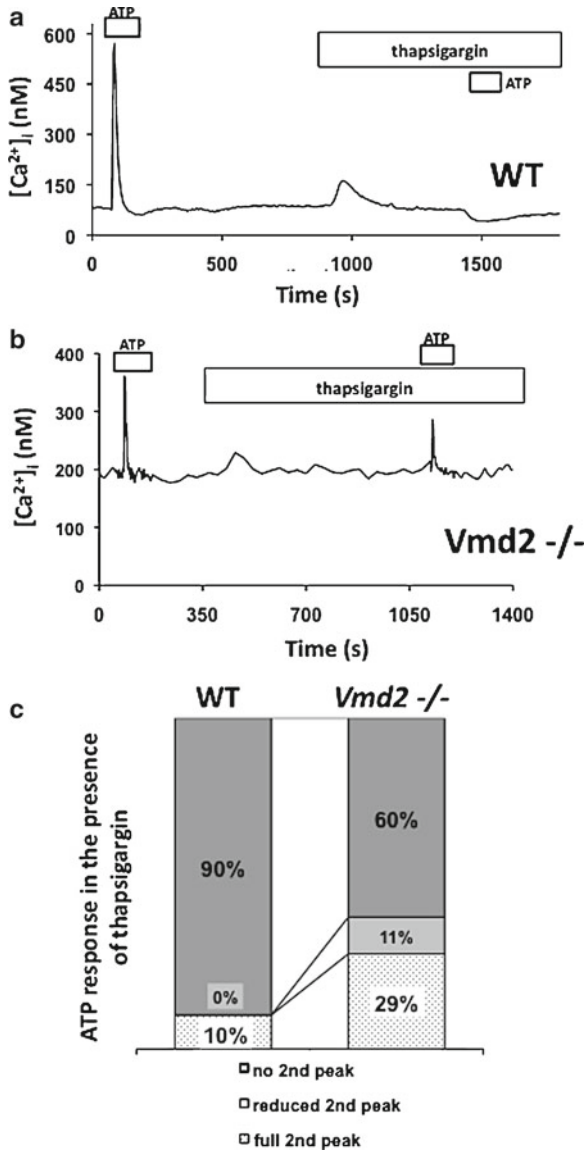


Fig. 77.4 Contribution of endoplasmic reticulum Ca^{2+} stores to ATP-dependent Ca^{2+} signaling in RPE cells. **(a)** Comparison of resting Ca^{2+} levels. Cells from *Vmd2*^{-/-} mice showed significantly increased Ca^{2+} levels (** $p < 0.01$). The number “ n ” depicts the number of investigated cells from at least ten mice. **(b)** Comparison of Ca^{2+} release from cytosolic stores by thapsigargin application: the Ca^{2+} release was quantified by integration of the area below the Ca^{2+} increases during thapsigargin application. “ n ” depicts the number of cells of at least four cell cultures. * $p < 0.05$ (from Neussert et al. 2010). **(c)** Effect of thapsigargin on ATP-induced Ca^{2+} transients in wild-type mouse cells: The figure shows the mean values of eight simultaneous recordings. A first ATP application shows the normal ability to react to ATP application. After recovery, thapsigargin (1 μM) was applied leading to a transient increase in $[\text{Ca}^{2+}]_i$. In the presence of thapsigargin, the ATP-induced

This function could explain observations from several studies showing that bestrophin-1 modulates Cl^- transport or membrane conductance for Cl^- more indirectly (Barro-Soria et al. 2009, 2010). In addition, Ca^{2+} -signals in the RPE of bestrophin-1 knock-out or W93C knock-in mice were different compared to that of wild-type mice (Marmorstein et al. 2006; Neussert et al. 2010; Zhang et al. 2010).

In summary, the aspect of intracellular bestrophin-1 function opens new routes to understand the role of bestrophin-1 for cell function of the RPE: regulation of cell function by modulation of intracellular Ca^{2+} signaling. This conclusion helps to understand differing observations from mouse models and overexpression studies and is therefore complementary to the published observations on bestrophin-1 function.

References

- Arden GB and Constable PA (2006) The electro-oculogram. *Prog Retin Eye Res* 25: 207–248
- Barro-Soria R, Aldeni F, Almaca J et al (2010) ER-localized bestrophin 1 activates Ca^{2+} -dependent ion channels TMEM16A and SK4 possibly by acting as a counterion channel. *Pflugers Arch* 459: 485–497
- Barro-Soria R, Spitzner M, Schreiber R et al (2009) Bestrophin-1 enables Ca^{2+} -activated Cl^- conductance in epithelia. *J Biol Chem* 284: 29405–29412
- Boon CJ, Klevering BJ, Leroy BP et al (2009) The spectrum of ocular phenotypes caused by mutations in the BEST1 gene. *Prog Retin Eye Res* 28: 187–205
- Brandman O, Liou M, Park WS et al (2007) STIM2 is a feedback regulator that stabilizes basal cytosolic and endoplasmic reticulum Ca^{2+} levels. *Cell* 131: 1327–1339
- Burgess R, Millar ID, Leroy BP et al (2008) Biallelic mutation of BEST1 causes a distinct retinopathy in humans. *Am J Hum Genet* 82: 19–31
- Hartzell HC, Qu Z, Yu K et al (2008) Molecular physiology of bestrophins: multifunctional membrane proteins linked to best disease and other retinopathies. *Physiol Rev* 88: 639–672
- Jentsch TJ, Stein V, Weinreich F et al (2002) Molecular structure and physiological function of chloride channels. *Physiol Rev* 82: 503–568
- Marmorstein AD, Marmorstein LY, Rayborn M et al (2000) Bestrophin, the product of the Best vitelliform macular dystrophy gene (VMD2), localizes to the basolateral plasma membrane of the retinal pigment epithelium. *Proc Natl Acad Sci USA* 97: 12758–12763
- Marmorstein LY, Wu J, McLaughlin P et al (2006) The light peak of the electroretinogram is dependent on voltage-gated calcium channels and antagonized by bestrophin (best-1). *J Gen Physiol* 127: 577–589

←

Fig. 77.4 (continued) rise in $[\text{Ca}^{2+}]_i$ was abolished. Note: the trace shows a mean value of eight recordings which includes all types of reactions to thapsigargin application. **(b)** Example for an effect of thapsigargin on ATP-induced Ca^{2+} transients in *Vmd2*^{-/-} mouse cells: The figure shows the mean values of eight simultaneous recordings. A first ATP application shows the normal ability to react to ATP application. After recovery, thapsigargin (1 μM) was applied having no effects on $[\text{Ca}^{2+}]_i$. Note: the trace shows a mean value of eight recordings which includes all types of reactions to thapsigargin application: such as full second peak, reduced second peak, or no second peak. **(c)** Frequency distribution of thapsigargin effects on ATP responses in cells from either wild-type or *Vmd2*^{-/-} mice (from Neussert et al. 2010)

- Marquardt A, Stohr H, Passmore LA et al (1998) Mutations in a novel gene, VMD2, encoding a protein of unknown properties cause juvenile-onset vitelliform macular dystrophy (Best's disease). *Hum Mol Genet* 7: 1517–1525
- Milenkovic VM, Soria RB, Aldehni F et al (2009) Functional assembly and purinergic activation of bestrophins. *Pflugers Arch* 458: 431–441
- Mullins RF, Oh KT, Heffron E et al (2005) Late development of vitelliform lesions and flecks in a patient with best disease: clinicopathologic correlation. *Arch Ophthalmol* 123: 1588–1594
- Neussert R, Muller C, Milenkovic VM et al (2010) The presence of bestrophin-1 modulates the Ca^{2+} recruitment from Ca^{2+} stores in the ER. *Pflugers Arch* 460: 163–175
- Peachey NS, Stanton JB, Marmorstein (2002) Noninvasive recording and response characteristics of the rat DC-electroretinogram. *Vis Neurosci* 19: 693–701
- Petrukhin K, Koisti MJ, Bakall B et al (1998) Identification of the gene responsible for Best macular dystrophy. *Nat Genet* 19: 241–247
- Putney JW Jr (2005) Capacitative calcium entry: sensing the calcium stores. *J Cell Biol* 169: 381–382
- Reichhart N, Milenkovic VM, Halsband CA et al (2010) Effect of bestrophin-1 on L-type Ca^{2+} channel activity depends on the Ca^{2+} channel beta-subunit. *Exp Eye Res* 91: 630–639
- Rosenthal R, Bakall B, Kinnick T et al (2006) Expression of bestrophin-1, the product of the VMD2 gene, modulates voltage-dependent Ca^{2+} channels in retinal pigment epithelial cells. *Faseb J* 20: 178–180
- Strauss O (2005) The retinal pigment epithelium in visual function. *Physiol Rev* 85: 845–881
- Sun H, Tsunenari T, Yau KW et al (2002) The vitelliform macular dystrophy protein defines a new family of chloride channels. *Proc Natl Acad Sci USA* 99: 4008–4013
- Tsunenari T, Sun H, Williams J et al (2003) Structure-function analysis of the bestrophin family of anion channels. *J Biol Chem* 278: 41114–41125
- Yu K, Cui Y, Hartzell HC (2006) The bestrophin mutation A243V, linked to adult-onset vitelliform macular dystrophy, impairs its chloride channel function. *Invest Ophthalmol Vis Sci* 47: 4956–4961
- Yu K, Xiao Q, Cui G et al (2008) The best disease-linked Cl⁻ channel hBest1 regulates Ca^v1 (L-type) Ca^{2+} channels via src-homology-binding domains. *J Neurosci* 28: 5660–5670
- Zhang Y, Stanton JB, Wu J et al (2010) Suppression of Ca^{2+} signaling in a mouse model of Best disease. *Hum Mol Genet* 19: 1108–1118

Chapter 78

Modeling the Structural Consequences of *BEST1* Missense Mutations

Karina E. Guziewicz, Gustavo D. Aguirre, and Barbara Zangerl

Keywords *BEST1* • Bestrophin-1 • Canine multifocal retinopathy • Best vitelliform macular dystrophy • Comparative protein modeling • Missense mutations

78.1 Introduction

Bestrophinopathies are a group of inherited retinal disorders primarily caused by point mutations scattered throughout the entire *BEST1* gene. In humans, most of these sequence alterations lead to Best vitelliform macular dystrophy (BVMD), and in dogs cause *cmr*, a retinal phenotype modeling BVMD (Guziewicz et al. 2007, 2011; Zangerl et al. 2010).

The *BEST1* gene product, bestrophin-1 (Best1), is embedded in the basolateral plasma membrane of the RPE, where it functions as a Ca²⁺ dependent anion channel (Marmorstein et al. 2000; Hartzell et al. 2008). Two different topological models of human bestrophin-1 (hBest1) have been proposed. Based on the hydropathy profile analysis, Tsunenari et al. predicted six hydrophobic domains with five transmembrane-spanning segments for the native hBest1 (Tsunenari et al. 2003). Milenkovic et al. proposed a plausible alternative model with four membrane-spanning regions that places residues 95–229 within the cytoplasmic matrix, forming an extensive intracellular loop (Milenkovic et al. 2007). Both models locate the N and C termini on the cytosolic side, and both predict transmembrane domains within the highly evolutionarily conserved N-terminal part of the protein.

Although remarkable progress has been made toward understanding the bestrophin-1 physiology (Sun et al. 2002; Yu et al. 2007; Milenkovic et al. 2007;

K.E. Guziewicz • G.D. Aguirre • B. Zangerl (✉)

Section of Ophthalmology, Department of Clinical Studies, School of Veterinary Medicine, University of Pennsylvania, Ryan Veterinary Hospital, 3900 Delancey Street, Room 2020, Philadelphia, PA 19104, USA
e-mail: bzangerl@vet.upenn.edu

Qu et al. 2009), our understanding of its complex function and pathological mechanism is still at an early stage. Hitherto, the molecular consequences of altered residues defining three mutational hotspots of the bestrophin-1 molecule (6–30aa, 80–105aa, and 293–312aa) have been the most extensively studied (for review see Hartzell et al. 2008; Boon et al. 2009). These studies established a primary link between *BEST1* mutations and the anion channel malfunction, and provided multiple clues how a particular amino acid substitution may interfere with the protein functionality. In most cases, diminished or absent Cl⁻ current, altered anion permeability or defective membrane integration in association with bestrophinopathies have been reported (Hartzell et al. 2008; Boon et al. 2009; Xiao et al. 2010). Despite the indisputable advancements made in elucidation of bestrophin-1 pathogenic effects, expression and molecular kinetics of mutant transcripts, potential structural consequences, and its impact on the intracellular processing, were either not examined at all or just outlined in few cases (Hartzell et al. 2008; Boon et al. 2009).

We previously described three spontaneous canine bestrophin-1 (cBest1) mutations responsible for *cmr*, an autosomal recessive retinal disorder recognized in numerous dog breeds (Guziewicz et al. 2007; Zangerl et al. 2010). The distinct sequence alterations in *cBEST1* include a nonsense transition (C₇₃T/R₂₅X) located in the first coding exon (*cmr1*), a missense substitution (G₄₈₂A/G₁₆₁D) affecting a conserved glycine residue (*cmr2*), and a frameshift mutation (C₁₃₈₈del/P₄₆₃FS) resulting in a truncated protein shortened by 92 C-terminal aa (*cmr3*) (Guziewicz et al. 2007; Zangerl et al. 2010). Detailed studies on molecular consequences of *cmr1* mutation verified the *BEST1* null phenotype, where C₇₃T/R₂₅X premature stop encodes for a truncated protein not detectable in the homozygous mutant animals or in an in vitro model system (Guziewicz et al. 2011).

In the *cmr2* model, the small (75 Da), neutral, and non-hydrophilic glycine residue at position 161 is replaced by a much larger (133 Da) highly hydrophilic and negatively charged aspartic acid. We speculated that this drastic amino acid change may cause defective intracellular trafficking due to the incorrect folding of the mutant protein that cannot pass the endoplasmic reticulum (ER) quality control system. Indeed, the in-depth characterization of pathogenic effects of G₄₈₂A/G₁₆₁D revealed mislocalization of the *cmr2*-bestrophin to the perinuclear space of the cells. Moreover, confocal immunofluorescence microscopy analysis indicated co-localization of *cmr2* mutant protein with an ER marker, calnexin (Guziewicz et al. 2011). To further support our hypothesis on *cmr2* protein misfolding and retention in the ER, we used computational approaches to predict the potential structural consequences of the G₁₆₁D alteration.

78.2 Materials and Methods

78.2.1 Topology Prediction

Topological model of canine bestrophin-1 (NP_001091014) was predicted in silico using Classification and Secondary Structure Prediction of Membrane Proteins SOSUI Server v1.11 (<http://bp.nuap.nagoya-u.ac.jp/sosui/>; Hirokawa et al. 1998).

The model was verified by TopPred II algorithm (Transmembrane Topology Prediction of Membrane Proteins: <http://mobylye.pasteur.fr/cgi-bin/portal.py>; Claros and von Heijne 1994). Transmembrane segment hydrophobicity scores were calculated according to the GES scale with a cutoff of (–c) 1.8 and (–p) 0.7 (Engelman et al. 1986).

78.2.2 Prediction of Protein Structure

Protein Homology/analogy Recognition Engine (PHYRE Server version 0.2) (<http://www.sbg.bio.ic.ac.uk/phyre/>; Bennett-Lovsey et al. 2008) was used to perform the secondary fold recognition analysis and tertiary structure prediction for cBest1 (1–296aa) and hBest1 (25–301aa) protein segments. For the putative cBest1 wild-type (WT) structure the estimated precision value (EPV) reached 85% with an e-value of 0.46; for the *cmr2* mutant protein EPV of 75% and e-value of 0.7 was considered. The putative model structures for hBest1 WT (EPV of 80%, e-value of 0.5) and hBest1 I₂₀₁T mutant (EPV of 85%, e-value of 0.43) were compared to the canine specific predictions. All structures were evaluated on 3D molecule viewer module of the Vector NTI™ 10 software package (Invitrogen).

78.3 Results

78.3.1 Canine Bestrophin-1 Topology

In silico analysis predicted four transmembrane-spanning regions for the native cBest1, orienting the N and C termini to the cytoplasm (Fig. 78.1). According to the SOSUI algorithm, the four most probable transmembrane segments are located at amino acids 32–54, 73–94, 231–253, and 265–287. This model further predicts large, relatively hydrophobic intracellular loop (95–230aa), harboring the G161 residue mutated in *cmr2* (Fig. 78.1). To test whether the location of the transmembrane domains is affected by the *cmr2* mutation, the G₁₆₁D change was introduced into the protein sequence, and analyzed with the SOSUI algorithm. No effect on the cBest1 topological model was noted with the G₁₆₁D substitution. The putative cBest1 topology model was verified by TopPred II algorithm (data not shown).

78.3.2 Comparative Protein Modeling

The highly evolutionarily conserved N-terminal part (1–296aa fragment) was used for secondary and tertiary structure prediction of the native cBest1 or the G₁₆₁D mutant variant (Fig. 78.2). Figure 78.2c–d₁ illustrates the detailed structural

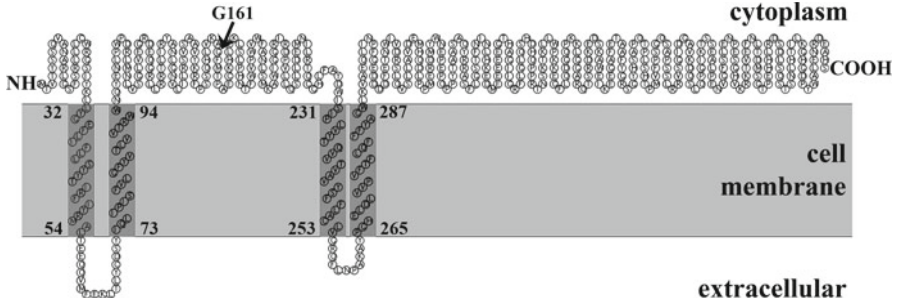


Fig. 78.1 A representative model of canine bestrophin-1 topology. Two independent computational algorithms (SOSUI, TopPred II) were used to estimate the number of transmembrane domains of the cBest1. Both, the hydropathy index of Kyte and Doolittle and the Goldman, Engelman, and Steitz (GES) hydrophobicity scale, predict four cBest1 transmembrane segments

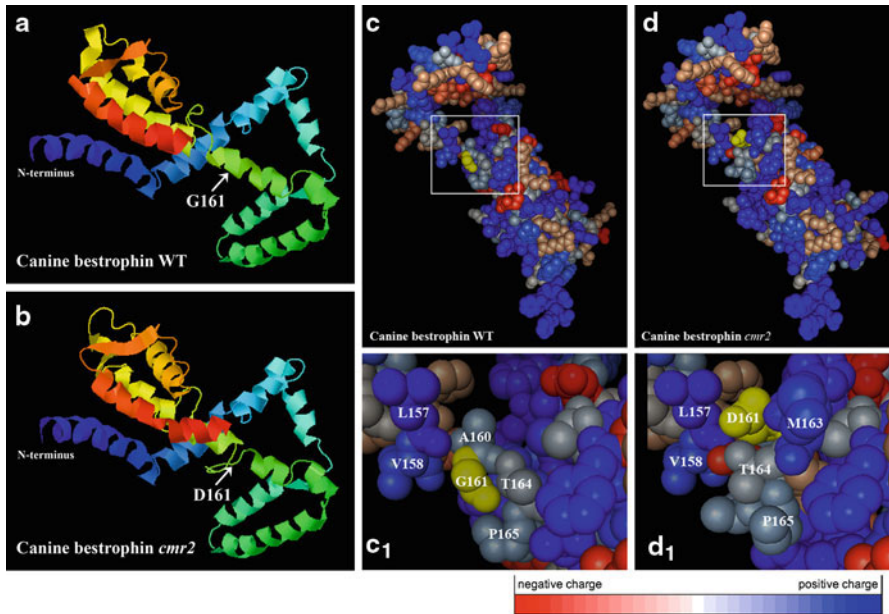


Fig. 78.2 3D representation of the native and *cmr2* mutant 295aa long N-terminal cBest1 fragment. **(a, b)** Overview of the tertiary structure predictions; structural changes caused by G₁₆₁D substitution are indicated by *arrows*. **(c, d)** Detailed structural environment of the wild-type residues in the native cBest1 **(c)** in comparison to the *cmr2* mutant **(d)**. Amino acids G161 (WT) and D161 (*cmr2*) are highlighted in *yellow*. **(c₁, d₁)** Higher resolution views of the regions denoted by the *white square* in **(c)** and **(d)**; Note the significant changes in the amino acid constellations induced by G₁₆₁D replacement. Color code bar: negatively charged aa are labeled in *red*, whereas positively charged are marked in *blue*

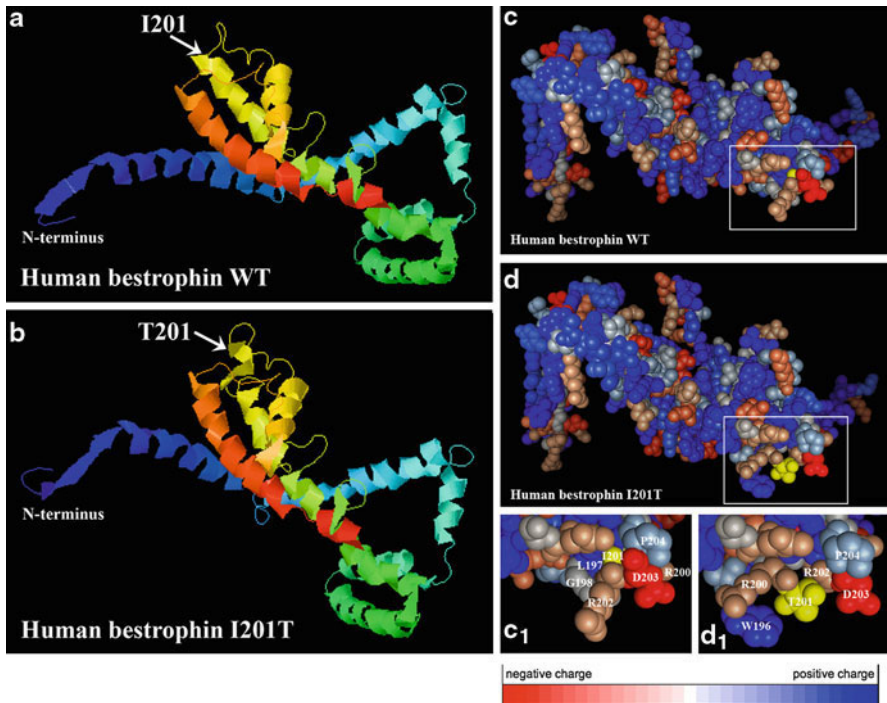


Fig. 78.3 Computational prediction of 3D models for the native hBest1 and $I_{201}T$ mutant variant (amino acids 25–301). *Arrows* indicate position of I_{201} WT residue (**a**) and T_{201} mutant (**b**). Panels (**c**, **d**) illustrate details of the putative tertiary structure calculated for the native hBest1 (**c**) vs. $I_{201}T$ mutant (**d**); (**c**₁) and (**d**₁) show magnifications of the portion denoted by the *white square* in the images (**c**) and (**d**). Wild-type residue I_{201} and mutant T_{201} are highlighted in *yellow*. Note the striking rearrangement of molecular interactions surrounding the T_{201} residue (**d**₁). Color code bar: negatively charged aa are labeled in *red*, whereas positively charged are marked in *blue*

environment of the wild-type residues in the native cBest1 in comparison to the *cmr2* mutant model. Replacement of Gly by Asp at position 161 dramatically affects protein structure leading to disrupted intramolecular interactions of neighboring residues (Fig. 78.2b, d–d₁). To assess the relevance of the canine specific findings to human bestrophinopathies, a putative 3D structure for hBest1 (25–301aa fragment) WT or comparable $T_{602}C/I_{201}T$ mutant variant associated with Best disease (Lotery et al. 2000) was predicted by the same algorithm (Fig. 78.3). Significant changes in the $I_{201}T$ mutant protein inducing conformational rearrangements and altered inter-residue interactions are demonstrated in Fig. 78.3d–d₁. Note that only three-dimensional models of $EPV \geq 75\%$ were considered.

78.4 Discussion

Membrane proteins play a crucial role in biological systems as ion channels, pores, and receptors. Understanding their structure and dynamics is essential to expand our knowledge on fundamental aspects of cellular homeostasis. However, only a small fraction of these important proteins has been isolated so far, and the function of most still remains ambiguous. Reasons for this lag include difficulties in expressing such proteins in significant quantities, in isolating and purifying them considering their amphipathic character, and in crystallizing them (<http://www.che.udel.edu/cobre/>). The recent rapid advances in computer sciences have accelerated their applications to understand complex biological systems, which helped to tackle some of the experimental difficulties. As a consequence, theoretical simulations and computational design methods are now an integral part of biomedical research, becoming an exceptionally useful and powerful means for studying membrane proteins architecture and properties (Casadio et al. 2003). We used two independent computational topology algorithms to assess the putative topology model for cBest1 (Fig. 78.1). Our in silico prediction strongly supports the experimental hBest1 topology model of Milenkovic et al. (2007), which further suggests similar topology for all vertebrate bestrophins. Both models consist of four transmembrane domains in the N-terminus of the protein, separated by a larger intracellular loop, and orienting the C-terminus toward the cytosol (Fig. 78.1; Milenkovic et al. 2007).

The majority of the disease-causing missense mutations identified in humans affect folding or trafficking, rather than specifically affecting protein function (Sanders and Myers 2004). To date, all examined missense changes in the hBest1 were associated with functional consequences, implicating an impaired channel activity. This study demonstrates the potential structural consequences of G₁₆₁D (*cmr2*) and comparable hBest1 point mutation, I₂₀₁T, predicted by comparative modeling of the N-terminal part of bestrophin-1. Both analyzed mutations are substitutions replacing a highly evolutionary conserved amino acid with a much bulkier residue (*cmr2*) of different biochemical properties (*cmr2*, I₂₀₁T). Such dramatic changes often affect structure of the encoded protein in the immediate vicinity of the residue, creating electrostatic disturbances and altering the intramolecular interactions (Figs. 78.2c₁, d₁ and 78.3c₁, d₁).

The predicted structural rearrangements caused by G₁₆₁D are in good agreement with previous experiments. Wild type cBest1 is processed in the ER and targeted to the plasma membrane, reflecting normal biogenesis and trafficking of bestrophin-1, but the *cmr2* mutant is retained in the ER (Guziewicz et al. 2011). These data indicate that at least a subset of *BEST1* missense mutations may lead to the protein misassembly, and its build-up in the ER. Since the BVMD and *cmr* are disorders where subretinal deposits accumulate, this mechanism may have an influence on the nature of lesions observed as well as on the disease progression. To support this hypothesis detailed studies are required to further analyze the molecular changes in the early events of the structurally defective bestrophin-1 folding.

Bestrophins are recognized as one of the most mysterious proteins of all known ion channels. To date, Best1 function and kinetics are still not fully understood. Our studies provided new insights into molecular pathology of point mutations associated with *cmr* and Best disease, which is central to the pathogenesis of bestrophinopathies. Additional studies will be required to explore the biochemical and cellular consequences of *BEST1* mutations, and clarify their impact on protein structure with relation to disease onset and progression.

Acknowledgments This study was supported by The Foundation Fighting Blindness, NEI/NIH grant EY06855, EY17549, The Van Sloun Fund for Canine Genetic Research, Hope for Vision, and P30EY-001583.

References

- Bennett-Lovsey RM, Herbert AD, Sternberg MJ et al (2008) Exploring the extremes of sequence/structure space with ensemble fold recognition in the program Phyre. *Proteins* 70:611–625
- Boon CJ, Klevering BJ, Leroy BP et al (2009) The spectrum of ocular phenotypes caused by mutations in the *BEST1* gene. *Prog Retin Eye Res* 28:187–205
- Casadio R, Fariselli P, Martelli PL (2003) In silico prediction of the structure of membrane proteins: is it feasible? *Brief Bioinform* 4:341–348
- Claros MG, von Heijne G (1994) TopPred II: An Improved Software For Membrane Protein Structure Predictions. *Comput Appl Biosci* 10:685–686
- Engelman DM, Steitz TA, Goldman A (1986) Identifying nonpolar transbilayer helices in amino acid sequences of membrane proteins. *Annu Rev Biophys Biophys Chem* 15:321–353
- Guziewicz KE, Zangerl B, Lindauer SJ et al (2007) Bestrophin gene mutations cause canine multifocal retinopathy: a novel animal model for best disease. *Invest Ophthalmol Vis Sci* 48:1959–1967
- Guziewicz KE, Slavik J, Lindauer SJP et al (2011) Molecular consequences of *BEST1* gene mutations in canine multifocal retinopathy predict functional implications for human bestrophinopathies. *Invest Ophthalmol Vis Sci* 52:4497–4505
- Hartzell HC, Qu Z, Yu K et al (2008) Molecular physiology of bestrophins: multifunctional membrane proteins linked to best disease and other retinopathies. *Physiol Rev* 88:639–672
- Hirokawa T, Boon-Chieng S, and Mitaku S (1998) SOSUI: classification and secondary structure prediction system for membrane proteins. *Bioinformatics* 14:378–379
- Lotery AJ, Munier FL, Fishman GA et al (2000) Allelic variation in the *VMD2* gene in best disease and age-related macular degeneration. *Invest Ophthalmol Vis Sci* 41:1291–1296
- Marmorstein AD, Marmorstein LY, Rayborn M et al (2000) Bestrophin, the product of the Best vitelliform macular dystrophy gene (*VMD2*), localizes to the basolateral plasma membrane of the retinal pigment epithelium. *Proc Natl Acad Sci USA* 97:12758–12763
- Milenkovic VM, Rivera A, Horling F et al (2007) Insertion and topology of normal and mutant bestrophin-1 in the endoplasmic reticulum membrane. *J Biol Chem* 282:1313–1321
- Qu Z, Cheng W, Cui Y et al (2009) Human disease-causing mutations disrupt an N-C-terminal interaction and channel function of bestrophin 1. *J Biol Chem* 284:16473–16481
- Sanders CR, Myers JK (2004) Disease-related misassembly of membrane proteins. *Annu Rev Biophys Biomol Struct* 33:25–51
- Sun H, Tsunenari T, Yau KW et al (2002) The vitelliform macular dystrophy protein defines a new family of chloride channels. *Proc Natl Acad Sci USA* 99:4008–4013
- Tsunenari T, Sun H, Williams J et al (2003) Structure-function analysis of the bestrophin family of anion channels. *J Biol Chem* 278:41114–41125

- Xiao Q, Hartzell HC, Yu K (2010) Bestrophins and retinopathies. *Pflugers Arch* 460: 559–569
- Yu K, Qu Z, Cui Y et al (2007) Chloride channel activity of bestrophin mutants associated with mild or late-onset macular degeneration. *Invest Ophthalmol Vis Sci* 48:4694–4705
- Zangerl B, Wickström K, Slavik J et al (2010) Assessment of canine *BEST1* variations identifies new mutations and established an independent bestrophinopathy model (*cmr3*) in Lapponian Herders. *Mol Vis* 16:2791–2804

Chapter 79

Microglial Activation and Transcriptomic Changes in the Blue Light-Exposed Mouse Retina

Stefanie Ebert, Yana Walczak, Charlotte Remé, and Thomas Langmann

Keywords Mouse retina • Blue light damage • Retinal degeneration • Microglia • MacGreen mice • Transcriptomics • Regeneration • AMD

79.1 Introduction

Apoptosis is a general hallmark of photoreceptor degeneration in retinal dystrophies (Wenzel et al. 2005). Light damage is a useful model to analyze different features of photoreceptor apoptosis (Reme et al. 1998). Exposure to visible light activates the transcription factor AP-1 (Suter et al. 2000; Wenzel et al. 2000) and its inhibition by corticosteroids is protective (Wenzel et al. 2001).

Light-induced photoreceptor degeneration causes activation of microglia (Noell 1980; Ng and Streilein 2001). White light-evoked photoreceptor death is accompanied by microglial migration from the plexiform layers to the outer nuclear layer (Zhang et al. 2005). Accumulation of microglia occurs simultaneously with photoreceptor degeneration, suggesting that they play a role in retinal degeneration (Santos et al. 2010). Following blue light exposure, resident microglia and invading cells rapidly migrated to the lesion site and phagocytosed dying photoreceptors (Joly et al. 2009).

Despite these indications that microglia are activated and connected to apoptosis in light-damaged retinas, the underlying mechanisms are not well understood. Here, we present histological and molecular analyses in microglia-specific reporter mice following blue light damage of the retinas.

S. Ebert • Y. Walczak • T. Langmann (✉)
Institute of Human Genetics, University of Regensburg,
Franz Josef Strauss Allee 11, 93055 Regensburg, Germany
e-mail: thomas.langmann@klinik.uni-regensburg.de

C. Remé
University of Zurich, Lab for Retinal Cell Biology, Restelbergstrasse 53, 8044 Zurich,
Switzerland

79.2 Materials and Methods

79.2.1 Blue Light Exposure of MacGreen Mice

MacGreen mice, which express eGFP under the control of the *Csf1r* promoter (Sasmono et al. 2003), were used for blue light exposure experiments as described previously (Grimm et al. 2001; Joly et al. 2009). Briefly, eyes were exposed to blue light (410 ± 10 nm) for 2 min before mice were returned to their regular 12 h light dark rhythm. Control animals were dark adapted and exposed mice were sacrificed after 12, 24, and 72 h. All procedures were performed in accordance with the ARVO statement for the use of animals in ophthalmic and vision research.

79.2.2 Retinal Cross Sections and Whole Mounts

Immunohistochemical analyses were carried out using retinal sections and retinal whole mounts as described previously (Ebert et al. 2009).

79.2.3 RNA Isolation and Reverse Transcription

Total RNA was extracted from retinas using the Qiagen RNeasy Mini Kit. First-strand cDNA synthesis was performed with the Fermentas RevertAid™ H Minus First Strand cDNA Synthesis Kit.

79.2.4 DNA Microarrays

RNAs from blue light-exposed and dark-adapted MacGreen retinas were analyzed with duplicate Affymetrix 430 2.0 arrays according to the Affymetrix standard protocol. MIAME criteria were met (Brazma et al. 2001). The Gene Expression Dynamics Inspector was used to create self-organizing maps (Eichler et al. 2003). Each tile of the mosaic represents an individual cluster and is color-coded to represent high or low expression. Differentially regulated transcripts were identified with the Genomatix ChipInspector program.

79.2.5 Quantitative Real-Time PCR

Amplifications of 50 ng cDNA were performed with an ABI7900HT machine using TaqMan Universal PCR Master Mix, 200 nM primers, and 0.25 μ L dual-labeled LNA probes. Results were analyzed using the $\Delta\Delta$ Ct method for relative quantification. Primer sequences and Roche Library Probes are listed in Table 79.1.

Table 79.1 Primer pairs and Roche library probes used for qRT-PCR validation

Gene	F-primer (5'-3')	R-primer (5'-3')	Roche library probe
Agt211	CAGCTGGGCATGGAAATA	AGCACAGCCAAGCCAACCT	47
ATPase	GGCACAATGCAGGAAAGG	TCAGCAGGCACATAGATAGCC	77
Ch25h	AAGACCTGGGCTGTCCAG	GCCTCCCTTGCTTATGGT	68
Chi3l1	AGCAGTATTTCACCCTGTAT	CGCTGAGCAGGAGTTTCTCT	20
Crispld2	GAGTGTCCATCCAGCTACGG	TTTATGCTTGTGAGGGCTTTTCTC	27
Fut11	TTTGGGAAAGTCGAAAGAGATTC	CCTTGCCAATAATCTGTAGCC	11
Gpr37	CCCTGGTCACTTCCATGAG	CACCCAGAGAAAGCCACCTC	2
Irgm1	AAGCCACTAACATCGAATCA	TGCCTTATCTCACTTAATACTCCTCA	82
Il-33	ACCCACGAAAAGATATTCACTAAAA	CAAGCAAAGGATCTTCTCTAGAAAT	13
Len2	CCATCTATGAGCTACAAGAGAACAAAT	TCGTATCCAGTAGCCGACAGC	58
Parp10	TGCGGGCCCTTTTATAGCA	TGCAGCAAATGGGTGTGAC	56
Pgf	CTGGGTGGCTGTGCATT	GGCACCACTTCCACTTCTGT	3
Rfx2	CTCATCAATGCCATGAGTGG	TGCGAAGGCACCTTACAACAC	62
Rlbp1	CCCCTCGGATCTCAAGAAG	TTTGAACCTGGCTGGGAAT	1
Serpina3n	ACATCGGGAGTCAAGTATCAC	CCATCTTCTGTGTCTGCGAGTC	20
Sprr1a	CCTGAAGACCTGATCACCGA	AGGCAATGGGACTATAAGC	66
Steap4	TGGTCAAAGCATTTAACACCCAT	GTCAATTTCCACAGACAAACACC	64
Timpl	GCAAAGAGCTTTCTCAAAGACC	AGGGATAGATAAACAGGGAACACT	76
Tim4sf1	CTGTGTCAATTTGGCATCACT	GCACITTGACCACATAGAGGA	29
Timbim1	GCTGTCTTCCCTTGTACCTTACC	AAAGATGGTGTGAGCAAGATGATGT	74

79.3 Results

79.3.1 *Microglia Accumulate in Blue Light-Induced Retinal Lesions*

To visualize microglia in blue light-induced retinal lesions, whole mounts of MacGreen retinas were analyzed. Dark-adapted MacGreen mice showed a normal retinal morphology (Fig. 79.1a). In contrast, a defined lesion was present in the retinas of MacGreen mice 72 h after blue light exposure (Fig. 79.1b, circled area).

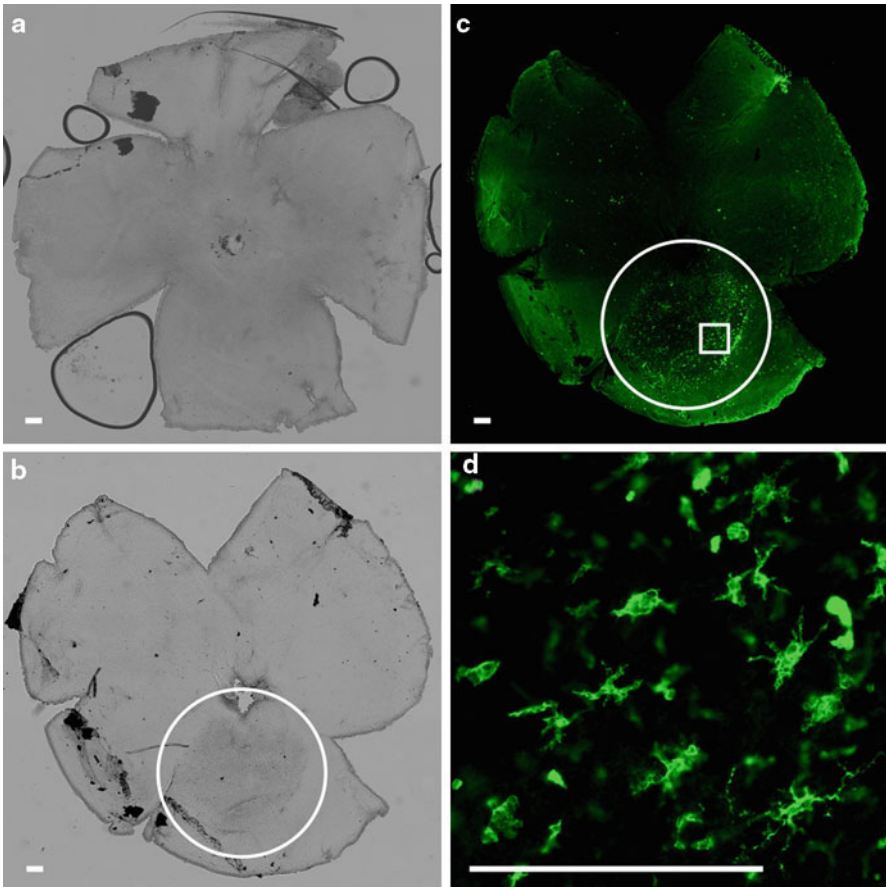


Fig. 79.1 Whole mount analysis of blue light-exposed MacGreen retinas. (a–d) Brightfield and immunofluorescence microscopy images of dark-adapted and 72 h blue light-exposed MacGreen retinas. (b, c) The *white circle* indicates the lesion site. (c, d) eGFP⁺ amoeboid microglia at the lesion center. Scale bar, 200 μ m

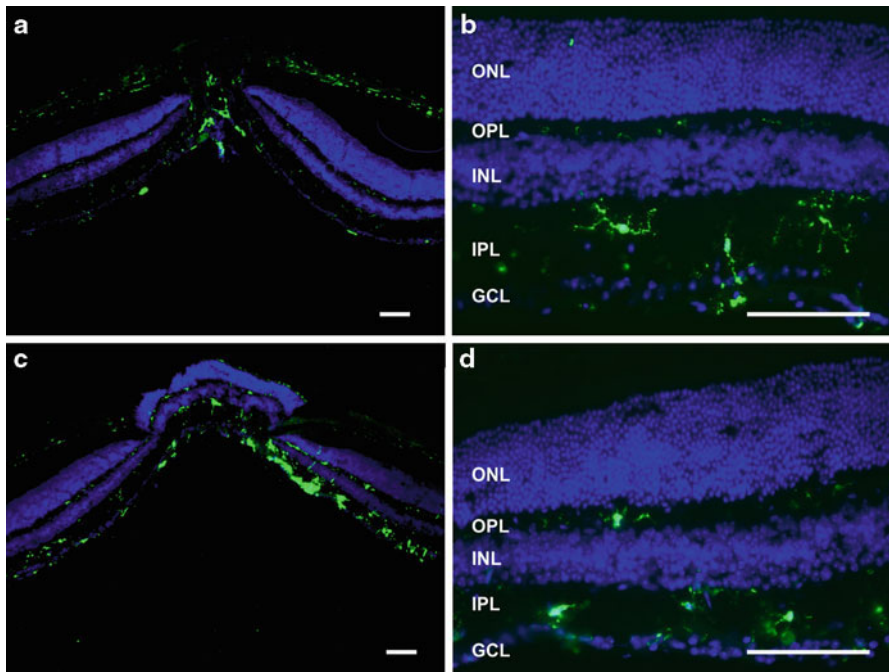


Fig. 79.2 Cryosections of blue light-exposed MacGreen retinas. eGFP⁺ microglia in dark-adapted (**a, b**) and blue light-exposed retinas (**c, d**). Counter staining of nuclei with DAPI. *ONL* outer nuclear layer; *OPL* outer plexiform layer; *INL* inner nuclear layer; *IPL* inner plexiform layer; *GCL* ganglion cell layer. Scale bar, 100 μ m

Closer examination of this region revealed local proliferation and migration of eGFP⁺ microglia toward the lesion center (Fig. 79.1c) and identified many eGFP⁺ microglia with amoeboid morphology (Fig. 79.1d).

We then characterized the distribution of microglia within the retinal layers. Nonexposed retinas showed exclusively ramified eGFP⁺ microglia in the ganglion cell layer and both plexiform layers (Fig. 79.2a, b). Seventy-two hours after light damage, many eGFP⁺ microglia were detected close to the central lesion (Fig. 79.2c). These cells had bloated cell bodies and short pseudopodia typical for alerted microglia (Fig. 79.2d).

79.3.2 Transcriptomic Changes in the Blue Light-Exposed Retina

Next, transcriptomic analyses were performed to define the molecular events in the blue light-exposed retina. DNA microarrays were carried out with RNAs from dark-adapted MacGreen retinas and MacGreen retinas 12, 24, and 72 h after blue light damage.

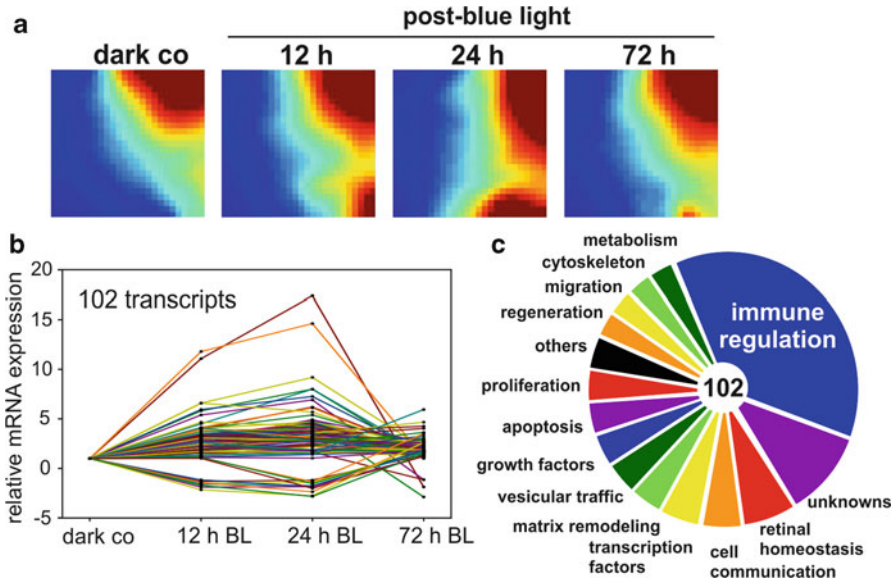


Fig. 79.3 DNA-microarray analysis of blue light-induced retinal tissue. (a) Gene expression dynamics inspector analysis. (b) Significance analysis of microarrays. (c) Pie chart of functional categories and pathways

We first used self-organizing maps to identify transcriptome activity via “gestalt” recognition (Eichler et al. 2003). These maps facilitate the identification of global patterns and each mosaic tile represents a gene cluster, with blue color indicating low and red high expression. The four maps showed major changes in retinal gene expression following blue light exposure (Fig. 79.3a). Especially, the expression levels of the bottom right gene clusters increased at 12 h, reached a peak at 24 h, and then declined at 72 h after light damage (Fig. 79.3a).

Next, we applied the Significance Analysis of Microarrays algorithm to identify transcripts with differential expression. Thereby, we detected 102 significantly regulated transcripts after blue light exposure compared to controls (Fig. 79.3b and Table 79.2). The majority of these transcripts showed increased expression after 12 h and peaked at 24 h, indicating a rapid response in the retinal transcriptome (Fig. 79.3b).

We then grouped these transcripts into functional categories (Fig. 79.3c). The largest group with 38 genes was immune regulation, followed by 11 uncharacterized transcripts and 7 genes related to retinal homeostasis. Thus, immune responses dominate the retinal transcriptome in this model of retinal degeneration. The remaining transcripts scattered into several other groups, indicating pleiotropic effects of blue light damage.

The differential expression of selected transcripts was then validated by qRT-PCR (Table 79.3). We could verify the expression profiles of all 19 transcripts, albeit with differences in the magnitude of regulation. As shown with the DNA microarrays, the strongest expression changes were noted 24 h after blue light exposure (Table 79.3). Several upregulated transcripts correspond to microglial activation

Table 79.2 Expression changes of all 102 differentially expressed transcripts in the retina of blue light-damaged retinas

Nr.	Gene ID	Gene symbol	Gene name	FC 12 h BL	FC 24 h BL	FC 72 h BL
1	20716	Serpina3n	Serine (or cysteine) peptidase inhibitor, clade A, member 3N	11.8	14.6	1.2
2	16819	Lcn2	Lipocalin 2	11.1	17.4	-1.9
3	17750	Mt2	Metallothionein 1	6.6	5.7	1.7
4	21857	Timp1	Tissue inhibitor of metalloproteinase 1	6.6	9.2	2.0
5	546546	Serpina3h	Serpin peptidase inhibitor, clade E (nexin, plasminogen activator inhibitor type 1), member 3	5.9	7.3	1.6
6	117167	Steap4	Six-transmembrane epithelial antigen of the prostate 4	5.8	8.0	1.2
7	17873	Gadd45b	Growth arrest and DNA-damage-inducible 45 beta	5.4	6.9	-1.1
8	17748	Mt1	Transmembrane 4 superfamily member 1	4.7	4.3	1.0
9	12654	Chi3l1	Chitinase 3-like 1	4.5	8.0	1.5
10	68713	Ifitm1	Interferon-induced transmembrane protein 1	4.1	6.1	1.7
11	20753	Spr1a	Small proline-rich protein 1A	4.1	2.8	1.5
12	17112	Tm4sf1	Transmembrane 4 superfamily member 1	4.0	3.1	2.7
13	20296	Ccl2	Chemokine (C-C motif) ligand 2	4.0	4.7	2.3
14	12609	Cebpd	CCAAT/enhancer-binding protein (C/EBP), delta	4.0	5.4	2.1
15	13615	Edn2	Endothelin 2	4.0	6.2	1.8
16	11504	Adamts1	A disintegrin-like and metalloproteinase (reprolysin type) with thrombospondin type 1 motif, 1	3.9	3.9	1.6
17	18414	Osmr	Oncostatin M receptor	3.7	3.8	1.2
18	27279	Tnfrsf12a	Tumor necrosis factor receptor superfamily, member 12A	3.5	3.7	2.0
19	21816	Tgm1	Transglutaminase 1, K polypeptide	3.4	4.5	1.5
20	78892	Crispld2	Cysteine-rich secretory protein LCCL domain containing 2	3.4	3.0	2.5
21	17869	Myc	Myelocytomatosis oncogene	3.3	4.3	1.7
22	77125	Il33	Interleukin 33	3.3	4.1	1.7
23	17105	Lyz2	Lysozyme 2	3.2	3.6	1.2
24	215474	Sec22c	SEC22 vesicle trafficking protein homolog C	3.2	4.7	1.7
25	56297	Arl6	ADP-ribosylation factor-like 6	3.2	4.1	2.3
26	19659	Rbp1	Retinol-binding protein 1, cellular	3.1	4.3	1.6

(continued)

Table 79.2 (continued)

Nr.	Gene ID	Gene symbol	Gene name	FC 12 h BL	FC 24 h BL	FC 72 h BL
27	20848	Stat3	Signal transducer and activator of transcription 3	3.1	3.8	2.3
28	69660	Tmbim1	Transmembrane BAX inhibitor motif containing 1	3.1	3.5	2.3
29	16007	Cyr61	Cysteine-rich protein 61	3.1	2.8	2.5
30	108052	Slc14a1	Solute carrier family 14 (urea transporter), member 1 (kidd blood group)	3.1	3.7	1.3
31	100048827	LOC100048827		3.0	4.6	1.0
32	12642	Ch25h	Cholesterol 25-hydroxylase	2.9	3.1	2.2
33	14173	Fgf2	Fibroblast growth factor 2	2.9	4.4	1.6
34	100045296	LOC100045296		2.9	3.6	1.3
35	12702	Soxs3	Suppressor of cytokine signaling 3	2.9	4.2	1.7
36	16878	Lif	Leukemia inhibitory factor	2.9	3.5	1.4
37	12661	Ch11	Cell adhesion molecule with homology to L1CAM	2.9	4.7	-2.9
38	15368	Hmox1	Heme oxygenase (decycling) 1	2.9	3.8	2.2
39	12266	C3	Complement component 3	2.8	4.9	1.1
40	100048759	LOC100048759		2.8	4.9	2.7
41	15944	Irgm1	Immunity-related GTPase family, M	2.8	4.8	1.2
42	14283	Fosl1	FOS-like antigen 1	2.7	2.7	2.6
43	19725	Rfx2	Regulatory factor x, 2 (influences HLA class II expression)	2.7	3.3	4.0
44	19128	Prosl1	Protein S (alpha)	2.7	2.8	2.6
45	74249	Lrrc2	Leucine-rich repeat containing 2	2.7	3.8	1.8
46	634286	LOC634286		2.7	3.8	1.7
47	14726	Pdpm	Podoplanin	2.6	4.0	1.8
48	68794	Finc	Filamin C, gamma (actin-binding protein 280)	2.6	1.9	1.5
49	11910	Atf3	Activating transcription factor 3	2.6	3.8	2.2
50	100047489	LOC100047489		2.6	3.9	2.5
51	13618	Ednrb	Endothelin receptor type B	2.5	4.9	1.5
52	21346	Tagln2	Transgelin 2	2.4	3.2	1.0

53	66929	Asf1b	ASF1 anti-silencing function 1 homolog B (<i>Saccharomyces cerevisiae</i>)	2.4	3.6	4.7
54	80285	Parp9	Phosphoinositide-3-kinase adaptor protein 1	2.4	3.8	4.3
55	20302	Ccl3	Chemokine (C-C motif) ligand 3	2.3	3.8	1.7
56	14190	Fgl2	Fibrinogen-like protein 2	2.3	1.9	1.7
57	19039	Lgals3bp	Lectin, galactoside-binding, soluble, 3 binding protein	2.3	2.3	1.8
58	18791	Plat	Plasminogen activator, tissue	2.2	1.8	2.6
59	21354	Tap1	Transporter 1, ATP-binding cassette, subfamily B (MDR/TAP)	2.2	3.8	2.1
60	67775	Rtp4	Receptor transporter protein 4	2.1	2.9	1.6
61	230073	Ddx58	Dead (ASP-GLU-ALA-ASP) box polypeptide 58	2.1	3.2	1.6
62	16145	Irgp	Interferon gamma induced GTPase	2.1	3.6	1.6
63	18654	Pgf	Placental growth factor	2.1	3.1	2.0
64	20847	Stat2	Signal transducer and activator of transcription 2	2.0	3.2	1.7
65	73710	Tubb2b	Tubulin, beta 2B	2.0	3.3	2.9
66	24110	Usp18	Ubiquitin-specific peptidase 18	2.0	3.0	3.1
67	100048346	LOC100048346		2.0	3.0	2.7
68	54123	Irf7	Interferon regulatory factor 7	2.0	3.0	1.7
69	69453	1700027L20Rik	Riken cDNA 1700027L20 gene	2.0	4.7	1.3
70	15957	Ifit1	Interferon-induced protein with tetratricopeptide repeats 1	1.9	2.4	3.6
71	16336	Insl3	Insulin-like 3	1.9	3.2	2.1
72	16453	Jak3	Janus kinase 3	1.9	3.2	1.4
73	69550	Bst2	Bone marrow stromal cell antigen 2	1.9	3.0	2.4
74	19106	Eif2ak2	Eukaryotic translation initiation factor 2-alpha kinase 2	1.9	2.8	1.8
75	15040	H2-T23	Histocompatibility 2, T region locus 23	1.9	2.3	1.3
76	671535	Parp10	Poly (ADP-ribose) polymerase family, member 10	1.8	3.0	1.3
77	12262	C1qc	Complement component 1, Q subcomponent, C chain	1.7	1.6	1.3
78	16912	Psmb9	Proteasome (prosome, macropain) subunit, beta type 9 (large multifunctional peptidase 2)	1.7	2.4	1.1
79	16763	Lad1	Ladinin	1.7	2.5	1.6

(continued)

Table 79.2 (continued)

Nr.	Gene ID	Gene symbol	Gene name	FC 12 h BL	FC 24 h BL	FC 72 h BL
80	23962	Oasl2	2'-5' Oligoadenylate synthetase-like 2	1.7	2.2	1.8
81	83490	Pik3ap1	Phosphoinositide-3-kinase adaptor protein 1	1.6	2.4	1.9
82	13040	Ctss	Cathepsin S	1.6	1.7	-1.1
83	56847	Alah1a3	Aldehyde dehydrogenase family 1, subfamily a3	1.6	2.4	1.5
84	17069	Ly6e	Lymphocyte antigen 6 complex, locus E	1.5	1.9	3.3
85	60533	Cd274	CD274 antigen	1.3	2.2	1.9
86	15959	Ifit3	Interferon-induced protein with tetratricopeptide repeats 3	1.3	1.6	5.9
87	667370	I830012O16Rik		1.3	1.6	2.9
88	17084	Ly86	Lymphocyte antigen 86	1.3	1.6	1.7
89	17858	Mx2	Myxovirus (influenza virus) resistance 2	1.3	2.3	1.5
90	22169	Cmpk2	Thymidylate kinase family LPS-inducible member	1.1	1.4	1.8
91	11606	Agt	Angiotensinogen (serpin peptidase inhibitor, clade A, member 8)	1.1	-1.5	1.8
92	234311	Ddx60	Dead (ASP-GLU-ALA-ASP) box polypeptide 60	1.1	1.0	1.8
93	320756	9330155M09Rik		1.1	-1.3	3.5
94	229227	4932438A13Rik		1.0	-2.0	1.2
95	211673	Arfgef1	ADP-ribosylation factor guanine nucleotide-exchange factor 1 (brefeldin A-inhibited)	-1.2	-1.8	1.9
96	116847	Prelp	Proline/arginine-rich end leucine-rich repeat protein	-1.3	-1.2	1.4
97	71760	Agxt2l1	Alanine-glyoxylate aminotransferase 2-like 1	-1.4	-2.4	2.6
98	98363	Efhf1	EF-hand domain family, member D1	-1.5	-1.4	1.8
99	170788	Crb1	Crumbs homolog 1	-1.6	-1.7	1.6
100	73068	Fut11	Fucosyltransferase 11	-1.7	-2.8	1.5
101	14763	Gpr37	G protein-coupled receptor 37	-1.9	-1.8	1.2
102	19771	Rlbp1	Retinaldehyde-binding protein 1	-2.2	-2.8	2.6

FC fold change; BL blue light

Table 79.3 qPCR validation of selected transcripts in blue light-exposed retinas

Symbol	Name	FC 12 h BL	FC 24 h BL	FC 72 h BL
Upregulated				
Timp1	Tissue inhibitor of metalloprotease 1	30.5±0.6	172.7±11.9	7.5±0.5
Lcn2	Lipocalin 2	38.0±4.7	173.0±9.6	4.0±0.3
Steap 4	Six TM epithelial antigen of prostate 4	29.3±2.5	85.4±0.7	11.0±0.6
Serpina3n	Serine peptidase inhibitor a3n	37.6±4.7	56.6±0.5	8.7±0.5
Chi3l1	Chitinase 3 like 1	5.3±0.8	29.6±0.7	2.1±0.3
Irgm1	Immunity-related GTPase m1	2.4±0.5	26.1±0.8	6.5±0.3
Pgf	Placental growth factor	3.2±0.5	17.6±2.3	2.6±0.1
Parp10	Poly ADP Ribose family member 10	0.8±0.1	9.1±1.0	2.5±0.3
Crispld2	Cyst.-rich secr. prot. LCCL dom. cont. 2	6.7±0.8	9.1±0.8	1.7±0.1
Rfx2	Regulatory factor x2	5.0±0.2	8.6±1.6	1.8±0.3
IL33	Interleukin 33	5.0±0.1	7.0±0.8	1.3±0.2
Tm4sf1	Transmembrane 4 superfamily 1	8.5±0.9	5.2±0.1	1.3±0.1
Tmbim1	Transmembrane Bax inhibitor motif 1	2.8±0.1	4.5±0.2	1.3±0.1
Ch25h	Cholesterol 25 hydroxylase	3.7±0.2	2.4±0.1	2.1±0.1
Sprr1a	Small proline-rich protein 1a	3.0±0.2	1.9±0.1	1.6±0.1
Downregulated				
Fut11	Fucosyltransferase 11	-2.0±0.2	1.0±0.4	-1.1±0.2
Gpr37	G-protein-coupled receptor 37	-3.3±0.1	-1.6±0.2	1.4±0.1
Rlbp1	Retinaldehyde-binding protein 1	-5.0±0.1	-5.0±0.1	-1.1±0.2
Agxt2l1	Alanine glyoxylate aminotransferase 2l1	-1.4±0.4	-5.0±0.1	-1.1±0.2

Fold change (FC) values ±SD were normalized to the ATPase reference gene and were then calculated relative to dark-adapted control retinas. *n*=2 mice per time point in duplicate measurements

(*lipocalin 2*, *chitinase 3 like 1*, *immunity-related GTPase m1*, *regulatory factor x2*, *interleukin 33*), whereas reduced expression of *retinaldehyde-binding protein* and *G-protein-coupled receptor 37* likely reflects the retinal damage induced by blue light. The induction of *transmembrane bax inhibitor motif 1* and *small proline-rich protein 1a* may indicate antiapoptotic and regenerative mechanisms elicited by blue light.

79.4 Discussion

Previous experiments revealed activation of retinal microglia and bone marrow immigrants together with increased expression of proinflammatory cytokines and chemokines in blue light-exposed retinas (Joly et al. 2009). To follow up on these findings, we exposed MacGreen mice to blue light and analyzed microglial activation and transcriptomic changes. The histological investigations confirmed microglial migration to the blue light-induced lesion. The ONL of the healthy retina is normally devoid of microglia (Santos et al. 2008), but they invade this region after white light exposure (Ng and Streilein 2001; Harada et al. 2002; Zhang et al. 2005). White light-induced changes cause transformation of microglia into amoeboid cells, which do not return to their resting state after photodegeneration (Santos et al. 2010).

Microglial activity was also high several days after blue light exposure (Joly et al. 2009), indicating that persistently alerted microglia may be a hallmark of photo-induced retinal degenerations.

Our microarray data identified prominent changes in the blue light-exposed retinal transcriptome with more than 100 differentially expressed transcripts. A significant overlap exists with published data from white light-induced retinal damage (Chen et al. 2004; Rattner and Nathans 2005). Especially, genes associated with inflammation and apoptosis were induced in both conditions. Several blue light-induced transcripts like *lipocalin 2*, *serine peptidase inhibitor clade A member 3N*, *tissue inhibitor of metalloproteinase 1*, and *six-transmembrane epithelial antigen of protease 4* are related to immune response, matrix remodeling, and cell communication (Takamiya et al. 2001; Swiderski et al. 2007; Yang et al. 2007; Ramadoss et al. 2010). Thus, white light and blue light damage may share some mechanistic features.

We also detected several molecules dampening inflammation and markers associated with alternative activation of microglia. High expression of *Chi3l1*, *Crispld2*, and *Irgm1* may reflect an autoregulatory loop of microglial deactivation as previously shown for other inflammatory conditions (Bafica et al. 2007; Lee et al. 2009; Wang et al. 2009). Potentially, some of these molecules may be targets for limiting harmful microglial responses.

The transcriptomic data also revealed that endogenous rescue pathways were activated following blue light exposure. We identified upregulation of Lif/Jak/STAT signaling components in photoreceptors and Müller cells (*Lif*, *Stat3*, *Edn2*, *Fgf2*), which support photoreceptor survival (Joly et al. 2008; O'Driscoll et al. 2008). In addition, we noticed induction of the antiapoptotic transcript *Tmbim1* (Hu et al. 2009) and increased expression of the regeneration gene *Sprr1a* (Starkey et al. 2009).

Altered expression profiles of the AP-1 components c-jun and c-fos, S100 genes, or crystallins were not detected in the retinal transcriptome after blue light challenge, as previously reported for the retinal response to white light (Chen et al. 2004). Therefore, we hypothesize that blue light exposure triggers distinct molecular components of microglial activation, retinal apoptosis, and survival signaling, which are different from those previously reported for white light lesions.

Acknowledgments We thank David Hume for providing the MacGreen mice and Bernhard Weber for helpful comments. This study was supported by the Deutsche Forschungsgemeinschaft (FOR1074 TP4), the ProRetina foundation, and a RD2010 Young Investigator Award.

References

- Bafica A, Feng CG, Santiago HC et al (2007) The IFN-inducible GTPase LRG47 (*Irgm1*) negatively regulates TLR4-triggered proinflammatory cytokine production and prevents endotoxemia. *J Immunol* 179:5514–5522
- Brazma A, Hingamp P, Quackenbush J et al (2001) Minimum information about a microarray experiment (MIAME)-toward standards for microarray data. *Nat Genet* 29:365–371
- Chen L, Wu W, Dentchev T et al (2004) Light damage induced changes in mouse retinal gene expression. *Exp Eye Res* 79:239–247

- Ebert S, Weigelt K, Walczak Y et al (2009) Docosahexaenoic acid attenuates microglial activation and delays early retinal degeneration. *J Neurochem* 110:1863–1875
- Eichler GS, Huang S, Ingber DE (2003) Gene Expression Dynamics Inspector (GEDI): for integrative analysis of expression profiles. *Bioinformatics* 19:2321–2322
- Grimm C, Wenzel A, Williams T et al (2001) Rhodopsin-mediated blue-light damage to the rat retina: effect of photoreversal of bleaching. *Invest Ophthalmol Vis Sci* 42:497–505
- Harada T, Harada C, Kohsaka S et al (2002) Microglia-Muller glia cell interactions control neurotrophic factor production during light-induced retinal degeneration. *J Neurosci* 22:9228–9236
- Hu L, Smith TF, Goldberger G (2009) LFG: a candidate apoptosis regulatory gene family. *Apoptosis* 14:1255–1265
- Joly S, Lange C, Thiersch M et al (2008) Leukemia inhibitory factor extends the lifespan of injured photoreceptors in vivo. *J Neurosci* 28:13765–13774
- Joly S, Francke M, Ulbricht E et al (2009) Cooperative phagocytes: resident microglia and bone marrow immigrants remove dead photoreceptors in retinal lesions. *Am J Pathol* 174:2310–2323
- Lee CG, Hartl D, Lee GR et al (2009) Role of breast regression protein 39 (BRP-39)/chitinase 3-like-1 in Th2 and IL-13-induced tissue responses and apoptosis. *J Exp Med* 206:1149–1166
- Ng TF, Streilein JW (2001) Light-induced migration of retinal microglia into the subretinal space. *Invest Ophthalmol Vis Sci* 42:3301–3310
- Noell WK (1980) Possible mechanisms of photoreceptor damage by light in mammalian eyes. *Vision Res* 20:1163–1171
- O'Driscoll C, O'Connor J, O'Brien CJ et al (2008) Basic fibroblast growth factor-induced protection from light damage in the mouse retina in vivo. *J Neurochem* 105:524–536
- Ramados P, Chiappini F, Bilban M et al (2010) Regulation of hepatic six transmembrane epithelial antigen of prostate 4 (STEAP4) expression by STAT3 and CCAAT/enhancer-binding protein alpha. *J Biol Chem* 285:16453–16466
- Rattner A, Nathans J (2005) The Genomic Response to Retinal Disease and Injury: Evidence for Endothelin Signaling from Photoreceptors to Glia. *Neurobiology of Disease* 25:4540–4549
- Reme CE, Grimm C, Hafezi F et al (1998) Apoptotic cell death in retinal degenerations. *Prog Retin Eye Res* 17:443–464
- Santos AM, Calvente R, Tassi M et al (2008) Embryonic and postnatal development of microglial cells in the mouse retina. *J Comp Neurol* 506:224–239
- Santos AM, Martin-Oliva D, Ferrer-Martin RM et al (2010) Microglial response to light-induced photoreceptor degeneration in the mouse retina. *J Comp Neurol* 518:477–492
- Sasmono RT, Oceandy D, Pollard JW et al (2003) A macrophage colony-stimulating factor receptor-green fluorescent protein transgene is expressed throughout the mononuclear phagocyte system of the mouse. *Blood* 101:1155–1163
- Starkey ML, Davies M, Yip PK et al (2009) Expression of the regeneration-associated protein SPRR1A in primary sensory neurons and spinal cord of the adult mouse following peripheral and central injury. *J Comp Neurol* 513:51–68
- Suter M, Reme C, Grimm C et al (2000) Age-related macular degeneration. The lipofusion component N-retinyl-N-retinylidene ethanolamine detaches proapoptotic proteins from mitochondria and induces apoptosis in mammalian retinal pigment epithelial cells. *J Biol Chem* 275:39625–39630
- Swiderski RE, Nishimura DY, Mullins RF et al (2007) Gene expression analysis of photoreceptor cell loss in bbs4-knockout mice reveals an early stress gene response and photoreceptor cell damage. *Invest Ophthalmol Vis Sci* 48:3329–3340
- Takamiya A, Takeda M, Yoshida A et al (2001) Expression of serine protease inhibitor 3 in ocular tissues in endotoxin-induced uveitis in rat. *Invest Ophthalmol Vis Sci* 42:2427–2433
- Wang ZQ, Xing WM, Fan HH et al (2009) The novel lipopolysaccharide-binding protein CRISPLD2 is a critical serum protein to regulate endotoxin function. *J Immunol* 183:6646–6656
- Wenzel A, Grimm C, Samardzija M et al (2005) Molecular mechanisms of light-induced photoreceptor apoptosis and neuroprotection for retinal degeneration. *Prog Retin Eye Res* 24:275–306
- Wenzel A, Grimm C, Marti A et al (2000) c-fos controls the “private pathway” of light-induced apoptosis of retinal photoreceptors. *J Neurosci* 20:81–88

- Wenzel A, Grimm C, Seeliger MW et al (2001) Prevention of photoreceptor apoptosis by activation of the glucocorticoid receptor. *Invest Ophthalmol Vis Sci* 42:1653–1659
- Yang Z, Quigley HA, Pease ME et al (2007) Changes in gene expression in experimental glaucoma and optic nerve transection: the equilibrium between protective and detrimental mechanisms. *Invest Ophthalmol Vis Sci* 48:5539–5548
- Zhang C, Shen JK, Lam TT et al (2005) Activation of microglia and chemokines in light-induced retinal degeneration. *Mol Vis* 11:887–895

Chapter 80

Overexpression of ROM-1 in the Cone-Dominant Retina

Dibyendu Chakraborty, Shannon M. Conley, Zack Nash,
Xi-Qin Ding, and Muna I. Naash

Keywords ROM-1 • RDS • Cone • Mouse models • Nrl • Transgene

80.1 Introduction

Rod outer segment membrane protein-1 (ROM-1) is a nonglycosylated tetraspanin protein localized to the rim region of rod and cone outer segments (OSs). It shares many features with its glycosylated counterpart, RDS (Bascom et al. 1992; Moritz and Molday 1996). Both contain four transmembrane domains with short cytoplasmic N- and C-terminal regions and a large intradiscal loop (known as D2) of approximately 150 amino acids harboring seven highly conserved cysteine residues. ROM-1 and RDS interact noncovalently to form homo- and hetero-tetrameric complexes (Goldberg et al. 1995; Goldberg and Molday 1996). It is believed that RDS homo-tetrameric complexes are then linked together through intermolecular disulfide bonds to form octamers and higher-order homo-oligomers that are crucial for rim formation (Loewen and Molday 2000). This covalent oligomerization is mediated by a cysteine residue at position 150 in the D2 loop (Goldberg et al. 1998; Chakraborty et al. 2009). Although RDS is obligatory for OS formation, ROM-1 plays only a minor role in disc morphogenesis and is absent in lower vertebrates (Kedzierski et al. 1996; Li et al. 2003). Consistent with a secondary role in photoreceptor structural maintenance, in the absence of ROM-1 (*rom-1^{-/-}*), photoreceptors develop properly with only mildly abnormal OS morphology (Clarke et al. 2000). Cone OS ultrastructure is grossly normal in *rom1^{-/-}* mice (Clarke et al. 2000); however, it is difficult to study cones in the rod-dominant wild-type background which

D. Chakraborty • S.M. Conley • Z. Nash • X.-Q. Ding • M.I. Naash (✉)
Department of Cell Biology, University of Oklahoma Health Sciences Center,
940 Stanton L. Young Boulevard, BMS 781, Oklahoma City, OK 73104, USA
e-mail: muna-naash@ouhsc.edu

contains only 3–5% cones. In *rds*^{-/-}, ROM-1 is significantly reduced, suggesting that it is not stable in the absence of RDS or that its trafficking to the OS requires RDS (Nour et al. 2004).

The role of ROM-1 has not been well studied in cone photoreceptors. In the present study, we utilize transgenic mice overexpressing ROM-1 in the cone dominant background (*nrl*^{-/-}) to further our understanding of the role of ROM-1 in cone OS structure and function.

80.2 Materials and Methods

80.2.1 Generation of ROM-1 Transgenic Mice

The ROM-1 transgene consists of the ~1.1 kb full-length mouse ROM-1 cDNA, a ~1.3 kb fragment of the promoter region of the human interphotoreceptor retinoid-binding protein (IRBP) gene, and a ~0.9 kb SV-40 poly-A to stabilize the message. Generation and maintenance of transgenic lines were performed as described (Naash et al. 1993). Mice were bred into the *nrl*^{-/-} (generously shared by Dr. Anand Swaroop, NEI). Unfortunately, in June 2009 our animal colony suffered catastrophic damage as a result of infrastructure failures and all ROM-1 transgenic lines were lost. All experiments and animal protocols were approved by the local Institutional Animal Care and Use Committee (IACUC; University of Oklahoma Health Sciences Center, Oklahoma City, OK, USA) and conformed to the guidelines on the care and use of animals adopted by the Society for Neuroscience and the Association for Research in Vision and Ophthalmology (Rockville, MD, USA).

80.2.2 Gel Electrophoresis and Western Blot Analysis

Gel electrophoresis and western blot analysis were performed using polyclonal antibodies specific to the C-terminal region of ROM-1 (ROM-1-CT) and RDS (RDS-CT) (Ding et al. 2004; Chakraborty et al. 2009). Frozen retinas were analyzed (20 µg protein/lane) on reducing SDS-PAGE/western blot as previously described (Chakraborty et al. 2008).

80.2.3 Electroretinography (ERG)

Rod and cone electroretinography (ERG) was performed as previously described (Cheng et al. 1997; Farjo et al. 2006). For photopic recordings, animals were light adapted at an intensity of 29.03 cd/m² for 5 min and then exposed to 25 flashes at

79 cd s/m². These flashes were averaged and b-waves were measured from the trough of the a-wave to the crest of the b-wave. At least five animals per genotype were analyzed.

80.2.4 Electron Microscopy

The tissue collection, sectioning, and electron microscopy method was performed as described previously (Stricker et al. 2005). Two animals per genotype were analyzed.

80.3 Results

80.3.1 Expression of ROM-1 Protein in Transgenic Mice

To understand the role of ROM-1 in cone photoreceptors, we generated transgenic mice (ROM-T) wherein ROM-1 overexpression was driven by the photoreceptor-specific IRBP promoter. Five transgenic lines were examined and examination of these mice exposed no side effects of the transgene on animal weight or behavior. Founders were crossed with *rom-1*^{-/-} for evaluation of transgene expression. In this study, we present data from the highest expressing line.

To determine the level of ROM-1 protein generated by the transgene, western blot analysis was performed on retinal extract from ROM-T mice on *rom-1*^{-/-} background. Figure 80.1a shows reducing SDS-PAGE/western blots probed with anti-ROM-1, anti-RDS, and anti-actin antibodies. Expression from the transgene is lower than in the WT (Fig. 80.1a): densitometry indicates that ROM-1 levels from the transgene are approximately 7% of WT ROM-1 levels. RDS levels are grossly unaffected by either lack of ROM-1 or expression of the transgene. Previously, we have observed that the IRBP promoter does not express equally in rods and cones (Nour et al. 2004). We therefore analyzed ROM-1 levels in *nrl*^{-/-} and ROM-T/*nrl*^{-/-} retinas (Fig. 80.1b). Analysis indicates that ROM-1 levels are 20.2±8.2% (*n*=4) higher in ROM-T/*nrl*^{-/-} compared to *nrl*^{-/-} and that, as in the WT, RDS levels are not affected by expression of the ROM-T transgene.

80.3.2 Overexpression of ROM-1 Exerts Negative Effects on Cone Function and Structure

Ultrastructural analysis of ROM-T/*nrl*^{-/-} cone OSs at postnatal day (P) 30 (Fig. 80.2a, b) indicates that overexpression of ROM-1 leads to defects in cone OS structure; specifically to the formation and accumulation of open, vacuole-like structures

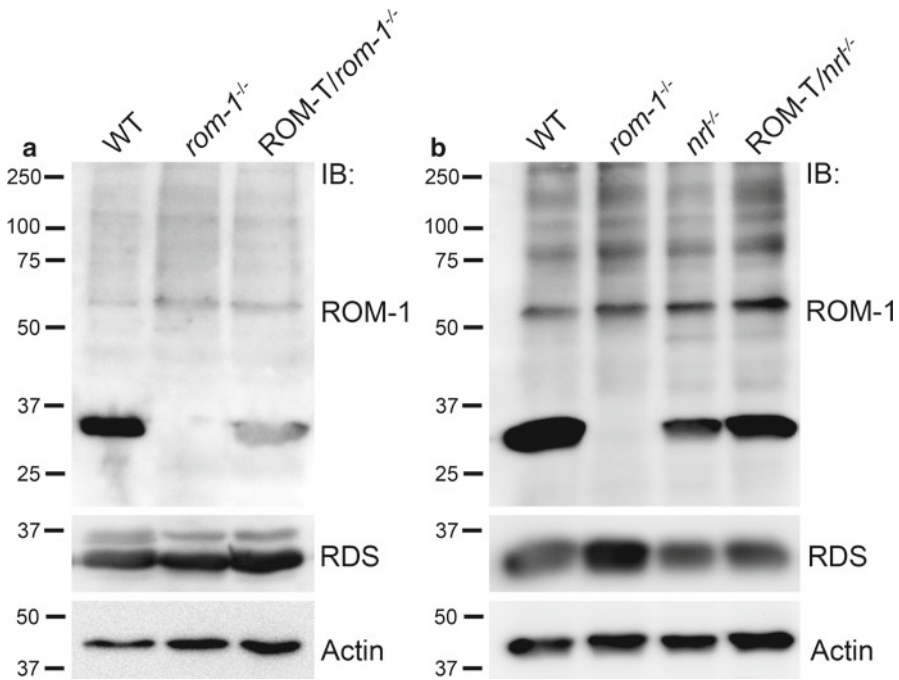


Fig. 80.1 Transgenic ROM-1 protein is stably expressed in the retina. Retinas were harvested from transgenic or nontransgenic animals as indicated at postnatal day (P) 30. Total retinal extracts were used for reducing SDS-PAGE followed by immunoblotting (IB) with the antibodies indicated. (a) ROM-1 protein is detected in transgenic retina in the *rom-1*^{-/-} background at ~7% of WT levels ($n=2$). (b) Representative western blot ($n=4$) showing ROM-1 levels in transgenic animals in the *nrl*^{-/-} background. ROM-1 levels in ROM-T/*nrl*^{-/-} mice are an average 120.2% (SD 8.2%) of levels in *nrl*^{-/-} controls

instead of normal flattened lamellae. To assess the affect of ROM-1 overexpression on cone-mediated vision, we recorded full-field photopic ERGs on ROM-T/*nrl*^{-/-} mice and nontransgenic controls (Fig. 80.2c). At P30, ROM-T/*nrl*^{-/-} photopic ERG amplitudes were reduced compared to *nrl*^{-/-} but not with significance. At P60 the degenerative trend was more pronounced and cone function was significantly decreased in ROM-T/*nrl*^{-/-} compared to *nrl*^{-/-} animals (* $P < 0.001$).

80.4 Discussion

ROM-1 function is closely tied to the structure and function of RDS and RDS complexes. Higher-order RDS homo-oligomers are required for disc rim formation and OS morphogenesis in rods and cones. Oligomerization-incompetent mutant RDS

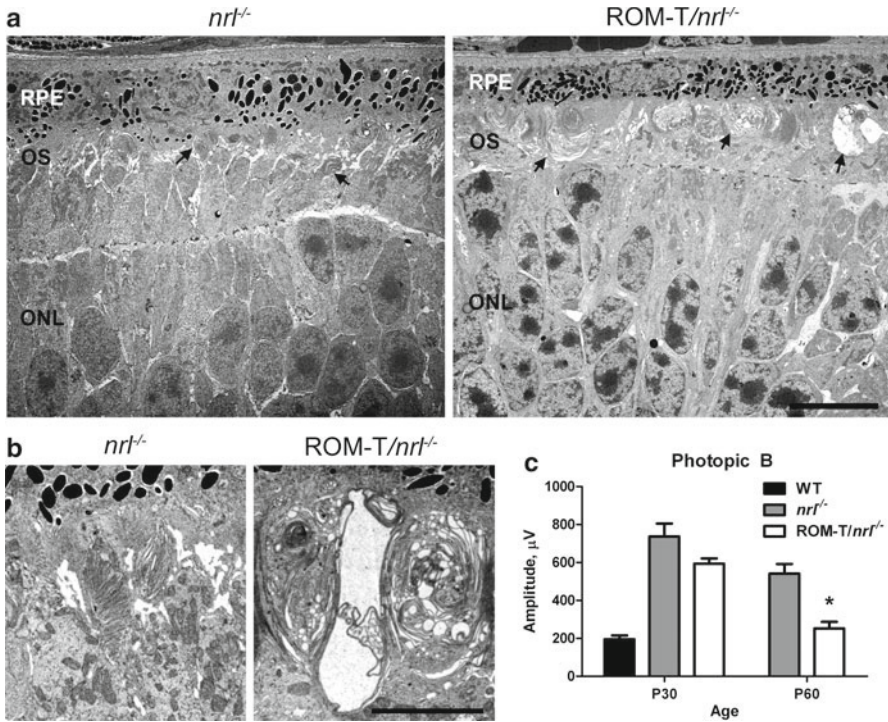


Fig. 80.2 Ultrastructural and functional analysis of ROM-T in cone photoreceptors. Eyes of the indicated genotypes were harvested from P30 transgenic and nontransgenic mice and processed for EM (**a, b**). Abnormal OSs were observed in ROM-T/*nrl*^{-/-} animals. Large, unpinched vacuoles were observed in cone OSs in contrast to the flattened lamellae in nontransgenic controls. Scale bar, 10 μ m (**a**), 5 μ m (**b**), ($N=2$ /genotype). (**c**) Photopic ERG from transgenic and nontransgenic animals is shown at P30 and P60. Significant decrease in photopic ERG amplitude was observed in transgenic animals at P60 in comparison to nontransgenic control ($P<0.001$ from student's *t*-test, $n\geq 5$ /genotype)

(C150S-RDS) cannot make proper rod or cone OSs in the *rd5*^{-/-} or *rd5*^{-/-}/*nrl*^{-/-} backgrounds (Chakraborty et al. 2009, 2010). When C150S-RDS is expressed in the presence of endogenous RDS, rods are unaffected while cones undergo rapid structural and functional degeneration (Chakraborty et al. 2009, 2010). These data suggest that cones are more sensitive to disruption of RDS complexes than rods. RDS forms hetero-tetramers and hetero-octamers with ROM-1 but higher-order oligomers are totally devoid of ROM-1 (Chakraborty et al. 2008). Consistent with this, formation of RDS higher-order oligomers is not affected by the absence of ROM-1 (Chakraborty et al. 2008). Although higher-order RDS homo-oligomers are obligatory for rim formation, little is known about the function of RDS/ROM-1 heteromeric complexes.

In the present study, we used transgenesis to overexpress ROM-1 protein by ~20% in the *nrl*^{-/-} retina. On the basis of prior data showing that RDS higher-order

oligomers are devoid of ROM-1, it was hypothesized that ROM-1 might be a negative regulator of RDS oligomerization (Loewen and Molday 2000). Our data provide some supporting evidence for this; we show that an excess of ROM-1 has a dominant-negative effect on cone OS ultrastructure and function. We hypothesize that altering the normal ROM-1/RDS ratio by overexpressing ROM-1 leads to a larger than normal quantity of ROM-1/RDS hetero-complexes or to an abnormal incorporation of ROM-1 into higher-order RDS oligomers and therefore to a reduction in the amount of proper RDS homo-oligomers. We have also noted that the ratio of ROM-1/RDS is less in cones than rods (unpublished data). That observation, coupled with the data presented here, and the prior studies of the *rom-1*^{-/-} mouse suggest that ROM-1 levels are tightly regulated and that an increase in the total amount of ROM-1 or in the ratio of ROM-1 to RDS can be detrimental to cones. Although the increase in ROM-1 levels in cones in our model is modest (~20%), we have previously demonstrated that expression of a mutant form of RDS (C150S) at even lower levels (<5% of WT) is capable of disrupting higher-order oligomers specifically in cones, resulting in a similar ultrastructural phenotype to that which we report here (Chakraborty et al. 2010).

Future studies will involve assessing the effects of overexpression of ROM-1 on rods. Based on previous studies, we predict that overexpression of ROM-1 in rods is likely to cause only slight abnormalities in comparison to the severe changes we observe in cones. Unfortunately, as a result of infrastructure failures in our animal housing facility, our mouse colony was catastrophically reduced and all ROM-1 transgenic lines were completely lost, so additional studies using these lines are not possible. In conclusion, we demonstrate that overexpression of ROM-1 and consequent alterations in the ROM-1/RDS ratio leads to negative effects on cone OS ultrastructure and function which furthers our understanding of the role of ROM-1 in cones.

References

- Bascom RA, Manara S, Collins L et al (1992) Cloning of the cDNA for a novel photoreceptor membrane protein (*rom-1*) identifies a disk rim protein family implicated in human retinopathies. *Neuron* 8:1171–1184
- Chakraborty D, Ding XQ, Fliesler SJ et al (2008) Outer segment oligomerization of rds: evidence from mouse models and subcellular fractionation. *Biochemistry* 47:1144–1156
- Chakraborty D, Conley SM, Stuck MW et al (2010) Differences in RDS trafficking, assembly, and function in cones vs. rods: Insights from studies of C150S-RDS. *Hum Mol Genet* 19:4799–4812
- Chakraborty D, Ding XQ, Conley SM et al (2009) Differential requirements for retinal degeneration slow intermolecular disulfide-linked oligomerization in rods versus cones. *Hum Mol Genet* 18:797–808
- Cheng T, Peachey NS, Li S et al (1997) The effect of peripherin/rds haploinsufficiency on rod and cone photoreceptors. *J Neurosci* 17:8118–8128
- Clarke G, Goldberg AF, Vidgen D et al (2000) Rom-1 is required for rod photoreceptor viability and the regulation of disk morphogenesis. *Nat Genet* 25:67–73

- Ding XQ, Nour M, Ritter LM et al (2004) The R172W mutation in peripherin/rds causes a cone-rod dystrophy in transgenic mice. *Hum Mol Genet* 13:2075–2087
- Farjo R, Skaggs JS, Nagel BA et al (2006) Retention of function without normal disc morphogenesis occurs in cone but not rod photoreceptors. *J Cell Biology* 173:59–68
- Goldberg AF, Molday RS (1996) Subunit composition of the peripherin/rds-rom-1 disk rim complex from rod photoreceptors: hydrodynamic evidence for a tetrameric quaternary structure. *Biochemistry* 35:6144–6149
- Goldberg AF, Moritz OL, Molday RS (1995) Heterologous expression of photoreceptor peripherin/rds and Rom-1 in COS-1 cells: assembly, interactions, and localization of multisubunit complexes. *Biochemistry* 34:14213–14219
- Goldberg AF, Loewen CJ, Molday RS (1998) Cysteine residues of photoreceptor peripherin/rds: role in subunit assembly and autosomal dominant retinitis pigmentosa. *Biochemistry* 37:680–685
- Kedziarski W, Moghrabi WN, Allen AC et al (1996) Three homologs of rds/peripherin in *Xenopus laevis* photoreceptors that exhibit covalent and non-covalent interactions. *J Cell Sci* 109 (Pt 10): 2551–2560
- Li C, Ding XQ, O'Brien J et al (2003) Molecular characterization of the skate peripherin/rds gene: relationship to its orthologues and paralogues. *Invest Ophthalmol Vis Sci* 44:2433–2441
- Loewen CJ, Molday RS (2000) Disulfide-mediated oligomerization of Peripherin/Rds and Rom-1 in photoreceptor disk membranes. Implications for photoreceptor outer segment morphogenesis and degeneration. *J Biol Chem* 275:5370–5378
- Moritz OL, Molday RS (1996) Molecular cloning, membrane topology, and localization of bovine rom-1 in rod and cone photoreceptor cells. *Invest Ophthalmol Vis Sci* 37:352–362
- Naash MI, Hollyfield JG, al-Ubaidi MR et al (1993) Simulation of human autosomal dominant retinitis pigmentosa in transgenic mice expressing a mutated murine opsin gene. *Proc Natl Acad Sci USA* 90:5499–5503
- Nour M, Ding XQ, Stricker H et al (2004) Modulating expression of peripherin/rds in transgenic mice: critical levels and the effect of overexpression. *Invest Ophthalmol Vis Sci* 45:2514–2521
- Stricker HM, Ding XQ, Quiambao A et al (2005) The Cys214 → Ser mutation in peripherin/rds causes a loss-of-function phenotype in transgenic mice. *Biochem J* 388:605–613

Chapter 81

Analysis of the RPE Sheet in the rd10 Retinal Degeneration Model

Micah A. Chrenek, Nupur Dalal, Christopher Gardner, Hans Grossniklaus, Yi Jiang, Jeffrey H. Boatright, and John M. Nickerson

Keywords Retinal pigment epithelium • RPE • Morphometrics • rd10 • Degeneration • Zona occludens 1

81.1 Introduction

We are interested in measuring changes in RPE cell morphology that occur in disease states. We hypothesized that changes in the local environment of the RPE cells as a result of retinal degeneration would result in changes in the morphology of RPE cells. To test this hypothesis, we examined the morphology of RPE cells in rd10 mice.

Rd10 mice have a missense mutation in phosphodiesterase 6B. PDE6B is the beta subunit of the phosphodiesterase that hydrolyzes cGMP in the phototransduction cascade. These mice are a model of autosomal recessive retinitis pigmentosa (RP) and have a retinal degeneration that begins at postnatal day 16 and is complete at 60 days old (Farber et al. 1988; Bowes et al. 1990; Chang et al. 2007).

The forces that organize RPE cell–cell contacts include adhesion, tension, and contraction. Tight junctions hold adjacent RPE cells together (Rizzolo 2007). A subcortical actin-myosin cytoskeleton contributes contractile forces that lead to regular polygonal (mostly hexagonal) shapes. One of the tight junction adhesion molecules that contribute to the characteristic RPE cell shape is zona occludens 1 (ZO-1), which also serves as a high quality marker of RPE cell borders. Trafficking

M.A. Chrenek • N. Dalal • C. Gardner • H. Grossniklaus • J.H. Boatright • J.M. Nickerson (✉)
Department of Ophthalmology, Emory University, 1365B Clifton Road NE,
TEC-B5602, Atlanta, GA 30322, USA
e-mail: litjn@emory.edu

Y. Jiang
Theoretical Division, Los Alamos National Laboratory, Los Alamos, NM 87545, USA

and movement of proteins that are part of the adhesion, tension, or contraction mechanism will lead to changes in force balance, which result in remodeling of cell shape and cell packing, and consequently measurable alteration or rearrangement of the patterns and tiling of the RPE sheet.

The physical description of patterning and tiling of endothelial cells in two dimensions is clinically useful in assessing pathology of corneal diseases. Here, we apply similar analyses to RPE sheets that may help predict disease stage, time course, and progression for retinal degeneration and AMD. Patterns and cell shape of the RPE sheet are evident in images from FAF and AO-cSLO, which are obtained non-invasively (de Bruin et al. 2008; Morgan et al. 2008; Geng et al. 2009; Schmitz-Valckenberg et al. 2010). Thus, analyses of these RPE patterns may become diagnostic and prognostic.

Here we begin to build a dynamic physical description of RPE sheet morphology and compare it to disease stage in the rd10 mouse, a genetic model of RP caused by a lesion in the PDE6B gene.

81.2 Methods

81.2.1 RPE Flatmount Technique

Mice were euthanized with CO₂ in accordance with Emory IACUC guidelines and the Association for Research in Vision and Ophthalmology guidelines for treatment of animals. Eyes were marked on the superior side with a blue sharpie and then enucleated, fixed for 10 min in 10% neutral buffered formalin, and then washed 3 times with PBS. Extra tissue was removed from the outside of the globe. Flatmounting was done by making four radial cuts from the center of the cornea back toward the optic nerve. A drop of PBS was placed on the eye to keep it moist. The flaps were peeled away from the lens and the lens removed. The iris and retina were removed using forceps. Tension from the sclera was relieved by making cuts halfway through each flap at the ciliary body/cornea margin and small cuts through the ciliary body.

81.2.2 ZO-1 Staining

The RPE flatmounts were blocked with HBSS + 0.01% Tween-20 and 1% BSA (antibody buffer) for 30 min. Immunostaining with a 1:100 dilution of rabbit anti-ZO-1 antibody (Invitrogen 61-7300) in antibody buffer was done for approximately 16 h at room temperature. The flatmounts were washed 5 times with HBSS + 0.01% Tween-20 (wash buffer) for 2 min and then stained for 1 h with Oregon Green conjugated goat anti-rabbit IgG secondary antibody (Invitrogen O11038) in antibody buffer and then washed 5 times with wash buffer. The flatmounts were mounted with Vectashield hardset (Vector Laboratories H-1400) and allowed to harden overnight.

81.2.3 Imaging

Imaging of the flatmounts was performed using a Nikon C1 confocal imaging system with Argon laser excitation at 488 nm. Confocal images were stitched together using Adobe Photoshop CS2. Cut boxes of equal size (181 × 266 pixels; 225 × 331 μm) were cropped from the merged flatmount image from areas devoid of dissection artifact. As many cut boxes as possible were taken from each image (45–60 cut boxes per image). Morphometric measurements including cell density, cell area, solidity, eccentricity, form factor, and number of neighbors were calculated using Cell Profiler (Lamprecht et al. 2007).

81.2.4 Statistics

Mean data from each flatmount were used for comparisons between genetic groups and time points. Experimental repeats were averaged and standard deviations of the averages between individual animals are represented as error bars in Fig. 81.2. Cochran's *t*-test for two sample sets with unequal variances was used to determine significance.

81.3 Results

Initially, we made RPE flatmounts from C57BL/6J (wildtype) and rd10 mice from 100, 180, and 330 days old mice and determined that there were massive changes in RPE cell morphology that occurred following retinal degeneration in the rd10 mice (data from 100-day old shown in Fig. 81.1). Figure 81.1 shows a superior portion of a 100-day old rd10 RPE flatmount with ciliary body at the top and the optic nerve at the bottom of the image. This image shows dramatic changes in RPE morphology from wildtype (see Fig. 81.2 for an example of wildtype morphology). Wildtype RPE cell morphology is mostly homogenous with an array of hexagonal cells (as shown in the top panel of Fig. 81.2) throughout the RPE sheet with a looser network of cells in the periphery at the margins of the ciliary body.

We decided to look at earlier time points to see if we could find changes in RPE morphology that precede the obvious changes that we see in Fig. 81.1. The top panel of Fig. 81.2 provides examples of the cut boxes that are used in Cell Profiler for analysis. Of the many analyses that can be run with Cell Profiler, we find that number of neighbors, eccentricity, and form factor are the most useful measures for RPE cell morphology.

The number of neighbors is very similar in all comparisons between wildtype and rd10. This is expected as at these time points there does not appear to be very much death of RPE cells. This indicates that from 30 to 60 days old, the changes in cell shape are not due to cells moving to fill in empty spots after cells have died.

Typically RPE cells have a regular hexagonal shape. Stretching or compression of the cells results in a distorted cell shape which can be measured as eccentricity.

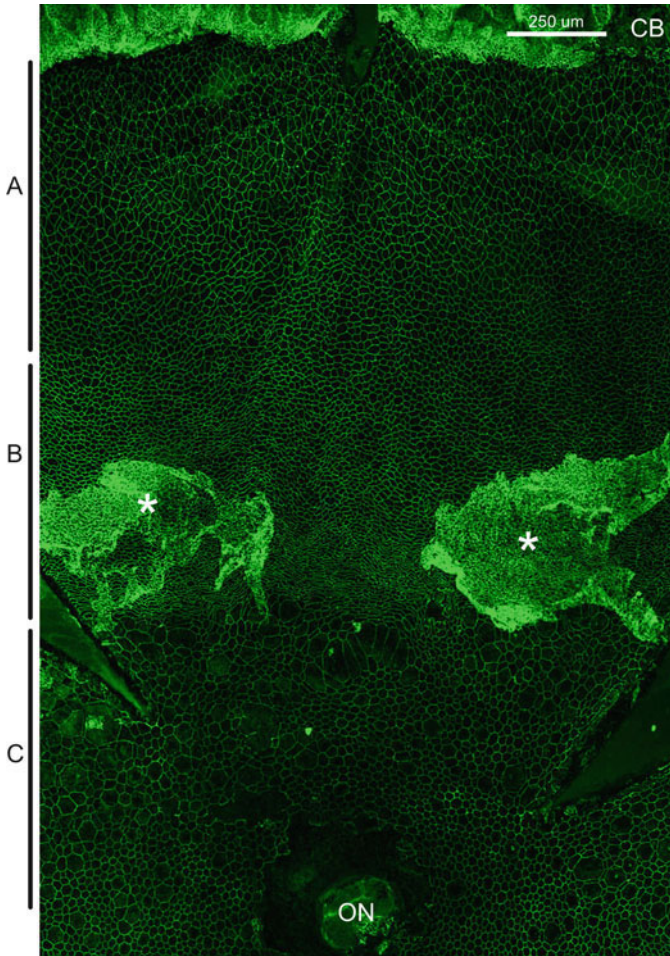
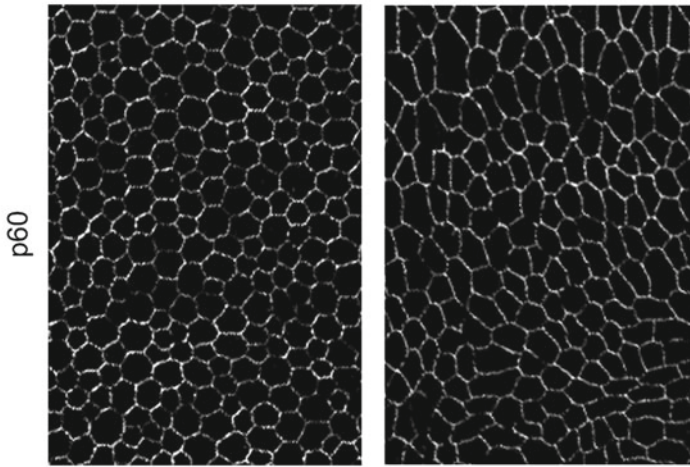


Fig. 81.1 Superior flap of an RPE flatmount stained with ZO-1 to outline RPE cells from a 100-day-old rd10 mouse. (a) Indicates the peripheral region, (b) indicates the mid periphery, and (c) indicates the posterior region of the RPE sheet. *CB* ciliary body; *ON* optic nerve, *asterisk* areas of RPE ingrowth away from Bruch's membrane. Size bar is 250 μm

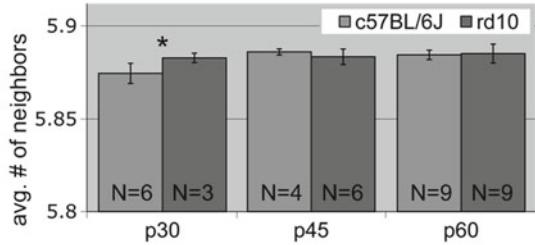
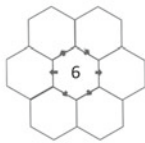
A typical circle has one focal point in the middle of the circle. As a circle is changed to an ellipse, the focal point splits into two foci that spread as the shape becomes more elliptical. The eccentricity measurement in Cell Profiler assigns two foci to each cell and provides the measurement between those foci. A larger number indicates more compressed/stretched cell morphology. We find that there is greater eccentricity in RPE cells from rd10 vs. wildtype as early as 30 days old.

Form factor is another measure of distortion from a circular shape: it measures the overall shape of the cell in terms of perimeter vs. cell area. This is calibrated to a circle of the same perimeter. As such, cell shape distortion from a normal hexagonal pattern

a example cutboxes used for Cell Profiler analysis
c57BL/6J rd10

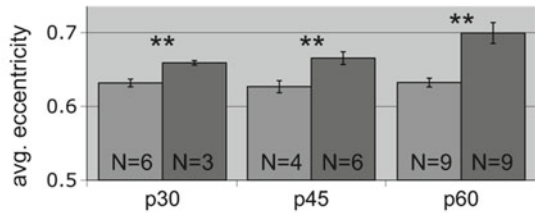
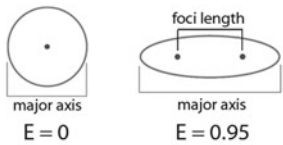


b number of neighbors



c eccentricity

foci length/major axis length



d form factor

area of a shape / area of a circle with the same perimeter

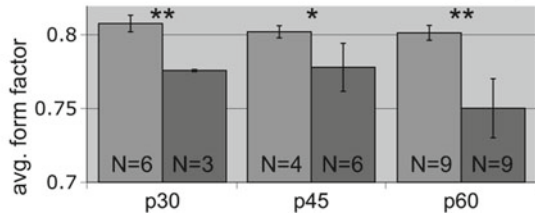
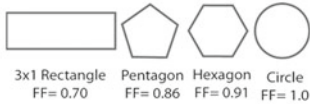


Fig. 81.2 Averaged RPE cell morphometrics. **(a)** Examples of cutboxes used for analysis, these were taken from all areas of the flatmount where there were no dissection artifacts. **(b)** Number of neighbors is consistent suggesting that there is no cell death at these time points. **(c, d)** Measures of cell shape are used to determine if we can detect RPE cell differences early in this degeneration. * $P < 0.05$, ** $P < 0.01$

reduces their similarity to a circle and generates a lower number in this measure. RPE cells from rd10 mice have a lower form factor than wildtype as early as 30 days old.

81.4 Discussion

There are major changes to the morphology of RPE cells following retinal degeneration in rd10 mice from 100 to 330 days old. In Fig. 81.1 we showed data from 100-day-old rd10 mice to demonstrate some of these disruptions. At later time points, the morphological changes spread to the whole retina and the patterning becomes more disorganized than what we see at 100 days old (data not shown).

The changes to cell morphology occur in three zones in a bullseye pattern around the optic nerve. In the posterior section of the RPE sheet around the optic nerve, there are many cells that are larger than normal with much variability in cell size. In the midperipheral region, cells have a compressed appearance and more tortuosity. In many samples from the 100-day-old rd10 mice, there is a ring of RPE ingrowth in this region. Parts of the RPE appear to be detached from Bruch's membrane and growing in multiple layers under the retina. In later time points, there are patches of this RPE ingrowth throughout the RPE sheet (data not shown). In the periphery near the ciliary body at 100 days old, RPE morphology looks quite similar to wildtype controls with a soft network of cells of uniform size. This area becomes disrupted later.

Having identified these qualitative differences in the RPE between wildtype and rd10 mice, we decided to use morphometric analysis software to quantify changes to RPE morphology at time points earlier than 100 days old. We analyzed RPE flatmounts from 30, 45, and 60 days old. Thirty days old is a point in the rd10 retinal degeneration when there are approximately 10% of photoreceptors remaining, and qualitatively there does not appear to be much effect on the RPE at this point. We theorized and have demonstrated that minute changes in the RPE morphology that are undetectable qualitatively by visual inspection can be detected quantitatively using computational analysis.

There are distinct changes that occur in the morphology of RPE cells in response to the retinal degeneration that occurs in rd10 mice (Fig. 81.2). These changes are detectable as early as 30 days old, well before the retina is completely degenerated. We have demonstrated that the use of morphometric analysis software can detect these early changes. With the improvements that are occurring in *in vivo* imaging technology, application of these morphometric measurements to human disease will be possible.

81.5 Conclusions

As rd10 is a model for retinitis pigmentosa, we predict that similar changes to RPE are occurring in RP patients, and there may be therapeutic complications with changes in RPE function. Understanding RPE cell morphology and how it pertains

to normal RPE cell function is also important for early AMD diagnosis and therapy. It may be possible to predict the progression of retinal disease by noninvasive imaging of RPE sheets using AO-cSLO, SD-OCT, or FAF imaging to determine the health of RPE cells.

Acknowledgments The authors would like to acknowledge the support from the following organizations: NIH R01EY014026, R01EY016470, NIH R24EY017045, NIH P30EY06360, Research to Prevent Blindness, and Foundation Fighting Blindness.

References

- Bowes C, Li T, Danciger M et al (1990) Retinal degeneration in the rd mouse is caused by a defect in the beta subunit of rod cGMP-phosphodiesterase. *Nature* 347:677–680
- Chang B, Hawes NL, Pardue MT et al (2007) Two mouse retinal degenerations caused by missense mutations in the beta-subunit of rod cGMP phosphodiesterase gene. *Vision Res* 47:624–633
- de Bruin DM, Burnes DL, Loewenstein J et al (2008) In vivo three-dimensional imaging of neovascular age-related macular degeneration using optical frequency domain imaging at 1050 nm. *Invest Ophthalmol Vis Sci* 49:4545–4552
- Farber DB, Park S, Yamashita C (1988) Cyclic GMP-phosphodiesterase of rd retina: biosynthesis and content. *Exp Eye Res* 46:363–374
- Geng Y, Greenberg KP, Wolfe R et al (2009) In vivo imaging of microscopic structures in the rat retina. *Invest Ophthalmol Vis Sci* 50:5872–5879
- Lamprecht MR, Sabatini DM, Carpenter AE (2007) CellProfiler: free, versatile software for automated biological image analysis. *Biotechniques* 42:71–75
- Morgan JJ, Hunter JJ, Masella B et al (2008) Light-induced retinal changes observed with high-resolution autofluorescence imaging of the retinal pigment epithelium. *Invest Ophthalmol Vis Sci* 49:3715–3729
- Rizzolo LJ (2007) Development and role of tight junctions in the retinal pigment epithelium. *Int Rev Cytol* 258:195–234
- Schmitz-Valckenberg S, Steinberg JS, Fleckenstein M et al (2010) Combined confocal scanning laser ophthalmoscopy and spectral-domain optical coherence tomography imaging of reticular drusen associated with age-related macular degeneration. *Ophthalmology* 117:1169–1176

Chapter 82

Networks Modulating the Retinal Response to Injury: Insights from Microarrays, Expression Genetics, and Bioinformatics

Félix R. Vázquez-Chona and Eldon E. Geisert

Keywords Retinal injury • Neuronal degeneration • Genetic networks • Crystallin • Glaucoma • Microarray • Lipin 1 • QTL analysis • Ganglion cell survival

82.1 Introduction

While our knowledge of the morphological and cellular changes of retinal wound healing is extensive, a select few of the phenotypic changes has been related to molecular makers and regulatory mechanisms. We used microarray technology to catalog gene expression changes after retinal injury and to relate the expression profiles to the biochemical and cellular context of retinal healing (Vazquez-Chona et al. 2004; Templeton et al. 2009).

82.2 Gene Expression After Retinal Injury

Our initial studies of retinal injury in adult rats revealed widespread changes at the site of injury and throughout the retina (Fig. 82.1a). From a technical aspect, we have shown that microarrays reliably predict the direction of mRNA and protein

F.R. Vázquez-Chona (✉)

Department of Ophthalmology, University of Utah, 65 Mario Capecchi Drive,
Salt Lake City, UT 84132, USA
e-mail: felix.vazquez@utah.edu

E.E. Geisert (✉)

Department of Ophthalmology, The Hamilton Eye Institute University of Tennessee Health
Science Center, 930 Madison Avenue, Suite 731, Memphis, TN 38163, USA
e-mail: egeisert@uthsc.edu

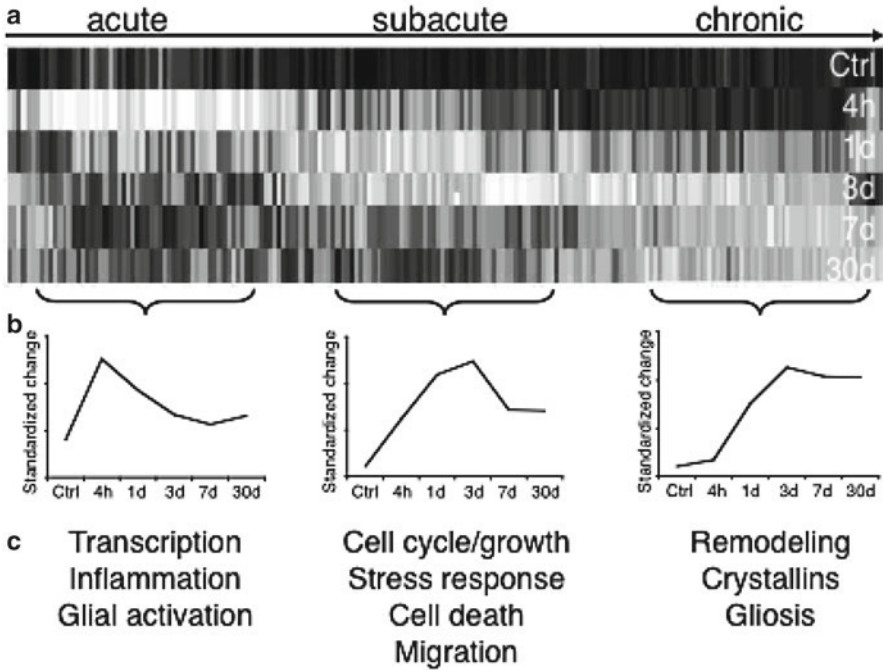


Fig. 82.1 Gene expression after retinal injury is highly regulated into distinct temporal groups and functionally related groups. (a) Heat map represents expression upregulation at 0 and 4 h, as well as 3, 7, and 30 days postinjury. *Dark hues* represent basal levels, whereas *bright hues* represent upregulation. Genes are listed in Fig. 82.3a. (b) Expression patterns after injury. (c) Genes within profiles are functionally related. Data adapted from Vázquez-Chona et al. (2004) (Copyright 2004 Association for Research in Vision and Ophthalmology, adapted and reproduced with permission)

changes, but provide qualitatively incomplete assessments of posttranscriptional and posttranslational modifications (Rogojina et al. 2003; Vazquez-Chona et al. 2004). Surprisingly, the large number of expression changes was highly regulated into three temporal patterns of expression – early acute (within hours), delayed subacute (within days), and late chronic phases (within weeks) (Fig. 82.1b). Genes within each phase are functionally related and reflect the sequelae of retinal wound healing (Fig. 82.1c). Of interest was the coordinated upregulation of crystallins α , β , and γ . Traditionally, crystallins were thought to function as structural lens components, but gene-sequence homology studies show that crystallins share homology with stress response genes such as heat-shock genes (Piatigorsky 1998; Horwitz 2003). Supporting their stress response function is the correlation of enhanced survival during degeneration with crystallin upregulation. For example, C57BL/6 mice express higher levels of crystallins and are more resistant to increased intraocular pressure than DBA/2J mice (Steele et al. 2006). The highly coordinated expression of crystallins and other functionally related groups suggested the presence of networks controlling the retinal response to injury.

82.3 Expression Genetics of Retinal Injury Genes

To discover the networks modulating gene expression, we used quantitative trait locus (QTL) analysis in mouse strains with known neurological differences (Vazquez-Chona et al. 2005, 2007). The C57BL/6 and DBA/2J strains differ in their response to increased intraocular pressure, optic nerve crush, neurotoxicity, audiogenic stress, and adult neurogenesis (Schauwecker and Steward 1997; Inman et al. 2002; John 2005; Templeton et al. 2009). To reveal the genetic networks modulating neurological phenotypes, members of our group combined expression profiling with linkage analysis in BXD recombinant inbred (RI) lines derived from the C57BL/6 (B) and DBA/2J (D) mouse strains (Chesler et al. 2005). Expression QTL (eQTL) analyses in BXD RI strains revealed that loci modulating expression phenotypes were also related to neurological phenotypes, and that distinct regulatory loci modulate functionally related genes (Chesler et al. 2005). Basal expression data from forebrain, striatum, and cerebellum as well as phenotypes and genetic linkage analyses for BXD RI strains are publicly available at www.GeneNetwork.org. We mined the expression genetics data at GeneNetwork to identify the eQTLs that modulate the expression of CNS wound-healing genes (Vazquez-Chona et al. 2005, 2007).

In BXD RI mouse forebrains, we found that the basal expression of acute phase genes is modulated by eQTLs on chromosomes 6, 12, and 14 (Fig. 82.2a) (Vazquez-Chona et al. 2005). Specificity and reliability were determined by comparing eQTLs across functional groups and tissues. For example, synaptic-related genes were also controlled by eQTLs on Chr. 6 and 14 in mouse forebrains, whereas wound-healing genes shared no eQTLs in analyses from hematopoietic stem cells (Vazquez-Chona et al. 2007). Thus the eQTL within the 10–30 Mb interval of Chr. 12 modulates acute phase genes known to be involved in CNS healing, neurogenesis, and cell death (Vazquez-Chona et al. 2007) (Fig. 82.3). BXD neurological phenotypes further support the role Chr. 12 network in the CNS response to degeneration (Fig. 82.2b). In BXD RI mouse strains, the DBA/2J allele for the Chr. 12 locus is one of the loci associated with susceptibility to noise-induced hearing loss and audiogenic seizures when exposed to intense auditory stimulation (Neumann and Collins 1991; Willott and Erway 1998). By contrast, the C57BL/6 allele is associated with enhanced neurogenesis and survival of new neurons and astrocytes in adult hippocampus (Kempermann and Gage 2002). Together BXD phenotypic and expression data suggest that a polymorphic gene within the Chr. 12 locus modulates the CNS response to degeneration (Vazquez-Chona et al. 2007).

82.4 Bioinformatics Can Predict Candidate Modulators

We used a suite of bioinformatic analyses and online databases (Table 82.1) to identify polymorphic genes with (a) expression variability correlating to their loci (*cis*-eQTLs), (b) single-nucleotide polymorphisms (SNPs) in motifs that can alter

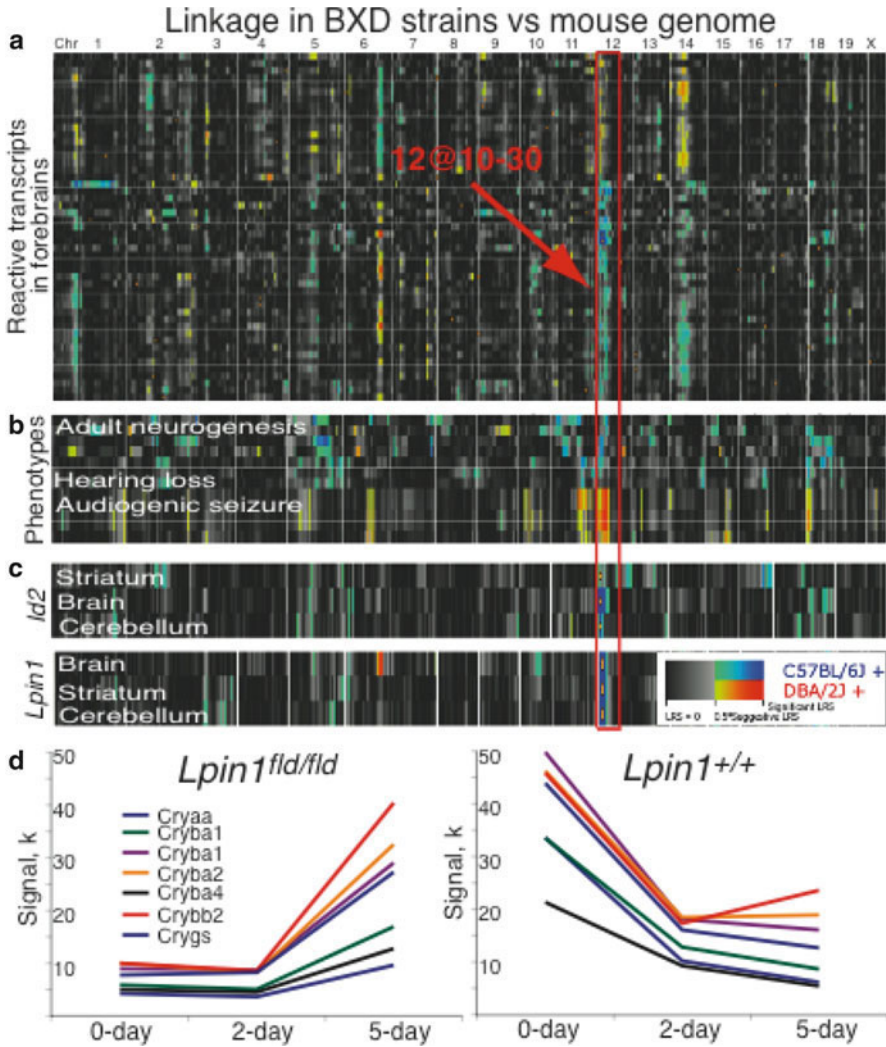


Fig. 8.2.2 Chromosome 12 locus modulates expression of wound-healing genes. **(a)** Quantitative trait locus (QTL) analysis maps the regulation of basal gene expression in BXD recombinant inbred (RI) strains. This regulation is based on the genetic correlation of expression (individual rows on the y-axis) to genomic markers across the mouse genome (x-axis). *Blue hues* represent correlations for elevated expression in mice with the C57BL/6 allele at a given locus, and *orange hues* represent correlations for elevated expression in mice with the DBA/2J allele. eQTLs on Chr. 6, 12, and 14 control basal expression of wound-healing genes in mouse forebrains. **(b)** Published data from phenotypes in BXD RI mouse strains further support that Chr. 12 locus associates with neurological phenotypes. **(c)** Linkage analyses for *Id2* and *Lpin1* expression across CNS tissues. **(d)** Gene expression changes in the crystallin family after optic nerve crush in *Lpin1^{fld/fld}* and *Lpin1^{+/+}* retina. *fld* (fat-liver dystrophy) mice express a nonfunctional Lipin 1 protein. Expression changes were measured using a full mouse Illumina microarray and represent averages from biological replicates. **(a–c)** Adapted from Vázquez-Chona et al. (2007), under the Creative Commons Attribution By License (<http://creativecommons.org/licenses/by/3.0/>)

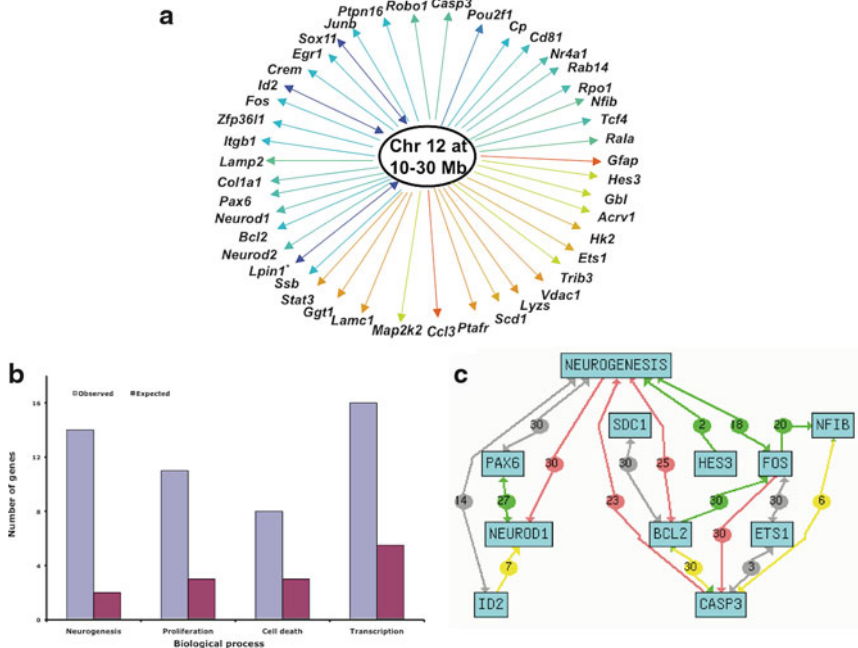


Fig. 82.3 Chromosome 12 locus modulates transcription, differentiation, proliferation, and apoptotic mechanisms. **(a)** Genetic networks were derived from transcripts sharing eQTLs as shown in Fig. 82.1. *Blue lines* connecting specific genes to the locus represent correlations for elevated gene expression in mice with the C57BL/6 allele, and *orange lines* represent correlation for elevated gene expression in mice with the DBA/2J allele. Genes located within the eQTLs (*cis*-eQTLs) are indicated with a *two-arrow line*. **(b)** The major functional themes described by the network’s gene functions are the regulation of transcription, differentiation, proliferation, and cell death. A non-biased, statistical approach to defining the function of the network ($n=44$ genes) is to compare the observed number of regulated genes as compared to the expected number in a population belonging to a particular functional category. For the chromosome 12 network, we observed 32% (14 out of 44 genes) of genes to be related to the regulation of neural development and differentiation. This percentage is higher than the percentage (7%) observed among the total population of retinal reactive transcripts and much higher than the percentage of expected genes in the entire genome. **(c)** We queried the biological literature using text-mining tools to illustrate networks within the transcripts grouped into the neurogenesis category (*Pax6*, *Neurod1*, *Neurod2*, *Id2*, *Nfib*, *Egr1*, *Hes3*, *Bcl2*, *Robo1*, *Ets1*, *Sox11*, *Casp3*, *Itgb1*, and *Sdc1*). The literature search documents the number of known molecular interactions of these genes, including activation and inhibition, that occur during neurogenesis. *Asterisk* probe set for *Lpin1* is not available in Affy U34 chip; however, post meta-analysis predicted and experimental models of gene expression confirmed the role of *Lpin1* as a wound-healing gene. Reproduced from Vázquez-Chona et al. (2007), under the Creative Commons Attribution By License. For further information go to <http://creativecommons.org/licenses/by/3.0/>

expression, and (c) biological significance to CNS wound healing (Vazquez-Chona et al. 2005, 2007). These analyses suggested that *Id2* and *Lpin1* were good candidate genes. Their expression variability in forebrain, cerebellum, and striatum of BXD RI mouse strains displayed highly significant *cis*-eQTLs (Fig. 82.2c). This means that a genetic variant (or variants) within or near the loci for *Id2* and *Lpin1*

Table 82.1 Bioinformatic analyses and online databases

Analysis	Database	Website
Gene expression		
Retinal development	Retina developmental gene expression Mouse retina SAGE library	www.scripps.edu/cb/friedlander/gene_expression http://bricweb.partners.org/cepko/default.asp
All tissues	Gene Expression Omnibus (GEO)	www.ncbi.nlm.nih.gov/geo
Expression QTL	GeneNetwork	www.genenetwork.org
Genes within QTLs	Genome browser Ensembl NCBI MapViewer	http://genome.ucsc.edu www.ensembl.org/Mus_musculus www.ncbi.nlm.nih.gov/mapview
Genes and loci causing retinal diseases	RetNet	www.sph.uth.tmc.edu/Retnet/
Loci associated with neurological phenotypes	BXD published phenotypes database	www.genenetwork.org
Single nucleotide polymorphisms (SNPs)	SNP browser Ensembl Mouse SNPView Entrez SNP databases	www.genenetwork.org/beta/snpBrowser.py? www.ensembl.org/Mus_musculus www.ncbi.nlm.nih.gov/SNP
Functional motifs		
Transcription factor binding sites	MOTIF	http://motif.genome.jp
Protein domains	Scansite	http://scansite.mit.edu
Cellular distribution of transcript		
Retina	Mouse Retina SAGE Library	http://bricweb.partners.org/cepko/default.asp
Brain	Gene Expression Nervous System Atlas (GENSAT)	www.ncbi.nlm.nih.gov/gensat
Gene ontology	WEB-based GEne SeT AnaLysis Toolkit (WebGestalt)	http://bioinfo.vanderbilt.edu/webgestalt/
Mining NCBI literature for interactions	Chilibot	www.chilibot.net

Table reproduced from Vázquez-Chona et al. (2007), under the Creative Commons Attribution By License

For further information go to <http://creativecommons.org/licenses/by/3.0/>

alters their expression. For example, our bioinformatic analyses of functional motifs showed that SNPs in *Id2* and *Lpin1* might affect transcription factor binding sites and splice variants, respectively (Vázquez-Chona et al. 2007). Publicly available microarray data also revealed that *Id2* and *Lpin1* are differentially displayed during retinal development and healing. Moreover, *Id2* and *Lpin1* were expressed in reactive glia of optic nerve heads and diabetic retinas (Vázquez-Chona et al. 2007). Together these bioinformatic analyses provided the rationale for focusing on transcription regulator *Id2* and the nuclear protein *Lpin1* as the best, current candidate genes.

82.5 Predicted Networks Require Validation

Evidence supporting the regulatory mechanism predicted by expression genetics and bioinformatics can include relevant cellular localization as well as relevant phenotypes from expression manipulation in cell and animal studies. For example, *Id2* is upregulated by reactive glia in brain, spinal cord, and optic nerve head (Vazquez-Chona et al. 2005). Moreover, our knockdown of *Id2* mRNA in cultured cerebellar astrocytes resulted in decreased migration and proliferation (Vazquez-Chona et al. 2007). Genetic studies show that ID2 deficiency enhances ocular metastasis and apoptotic rates in epithelial cells (Yokota and Mori 2002; Agapova et al. 2010). Currently, we are also measuring the wound-healing response in a mouse line expressing a nonfunctional Lipin 1 protein, the *fld* (fat-liver dystrophy) mouse (Peterfy et al. 2001). After optic nerve crush injury, *fld* mice displayed a 29% increase in surviving NeuN⁺ cells relative to wild-type mice ($p < 0.05$, student *t*-test). The enhanced survival of ganglion cells in *fld* mice correlated with the upregulation of the crystallin family; whereas in wild-type mice the increased cell death correlated with crystallin downregulation (Fig. 82.2d). Similarly, DBA/2J mice upregulated crystallins and is more resistant to optic nerve crushes than C57BL/6 mice (Templeton et al. 2009). These data suggest that the Crystallin Network is associated with increased survival of ganglion cells after optic nerve crush, and that Lipin 1 is an upstream modulator of the Crystallin Network and Chr. 12 network.

82.6 Conclusion

The present series of studies defined global changes that occur after ocular injury. They also defined a genetic network that modulates the retinal wound-healing response. Characterizing the interaction of Lipin 1 and the Crystallin Network may point to therapeutic strategies for enhancing ganglion cell survival. It may also lead to a genetic fingerprint or biomarker for predicting patients at higher risk of ganglion cell loss in blinding diseases such as glaucoma and ocular neuropathy. Our work is also moving microarray analyses from cataloging expression changes toward the discovery of expression networks and their modulators. During this process, we have developed approaches to define genetic networks by integrating gene expression profiling and higher-level bioinformatic analyses.

Acknowledgments EEG received support from PHS grant RO1EY017841, NIH/NEI Core Grant 5P30 EY13080-04S1, and unrestricted grant from Research to Prevent Blindness. FVC received support from Daniel L. Gerwin Fellowship, Fight For Sight fellowships SF04031 and PD07010, International Retinal Research Foundation (Charles D. Kelman, MD Postdoctoral Scholar award), NIH Training Grant 5T32 HD07491, and Knights Templar Eye Foundation.

References

- Agapova OA, Person E, Harbour JW (2010) Id2 deficiency promotes metastasis in a mouse model of ocular cancer. *Clin Exp Metastasis* 27:91–96
- Chesler EJ, Lu L, Shou S et al (2005) Complex trait analysis of gene expression uncovers polygenic and pleiotropic networks that modulate nervous system function. *Nat Genet* 37:233–242
- Horwitz J (2003) Alpha-crystallin. *Exp Eye Res* 76:145–153
- Inman D, Guth L, Steward O (2002) Genetic influences on secondary degeneration and wound healing following spinal cord injury in various strains of mice. *J Comp Neurol* 451:225–235
- John SW (2005) Mechanistic insights into glaucoma provided by experimental genetics the cogan lecture. *Invest Ophthalmol Vis Sci* 46:2649–2661
- Kempermann G, Gage FH (2002) Genetic influence on phenotypic differentiation in adult hippocampal neurogenesis. *Brain Res* 134:1–12
- Neumann PE, Collins RL (1991) Genetic dissection of susceptibility to audiogenic seizures in inbred mice. *Proc Natl Acad Sci USA* 88:5408–5412
- Peterfy M, Phan J, Xu P et al (2001) Lipodystrophy in the fld mouse results from mutation of a new gene encoding a nuclear protein, lipin. *Nat Genet* 27:121–124
- Piatigorsky J (1998) Multifunctional lens crystallins and corneal enzymes. More than meets the eye. *Annals N Y Acad Sci* 842:7–15
- Rogojina AT, Orr WE, Song BK et al (2003) Comparing the use of Affymetrix to spotted oligonucleotide microarrays using two retinal pigment epithelium cell lines. *Mol Vis* 9:482–496
- Schauwecker PE, Steward O (1997) Genetic determinants of susceptibility to excitotoxic cell death: implications for gene targeting approaches. *Proc Natl Acad Sci USA* 94:4103–4108
- Steele MR, Inman DM, Calkins DJ et al (2006) Microarray analysis of retinal gene expression in the DBA/2J model of glaucoma. *Invest Ophthalmol Vis Sci* 47:977–985
- Templeton JP, Nassr M, Vazquez-Chona F et al (2009) Differential response of C57BL/6J mouse and DBA/2J mouse to optic nerve crush. *BMC Neurosci* 10:90
- Vazquez-Chona F, Song BK, Geisert EE, Jr. (2004) Temporal changes in gene expression after injury in the rat retina. *Invest Ophthalmol Vis Sci* 45:2737–2746
- Vazquez-Chona FR, Lu L, Williams RW et al (2007) Genomic loci modulating the retinal transcriptome in wound healing. *Gene regulation and systems biology* : 1:327–348
- Vazquez-Chona FR, Khan AN, Chan CK et al (2005) Genetic networks controlling retinal injury. *Mol Vis* [electronic resource] 11:958–970
- Willott JF, Erway LC (1998) Genetics of age-related hearing loss in mice. IV. Cochlear pathology and hearing loss in 25 BXD recombinant inbred mouse strains. *Hearing Res* 119:27–36
- Yokota Y, Mori S (2002) Role of Id family proteins in growth control. *J Cell Physiol* 190:21–28

Chapter 83

Mislocalization of Oligomerization-Incompetent RDS is Associated with Mislocalization of Cone Opsins and Cone Transducin

Shannon M. Conley, Dibyendu Chakraborty, and Muna I. Naash

83.1 Introduction

Retinal degeneration slow (RDS) is a photoreceptor-specific member of the tetraspanin superfamily. Mutations in RDS cause many forms of retinal degeneration, ranging from rod-dominant retinitis pigmentosa to cone-dominant macular dystrophy and cone-rod dystrophy (<http://www.retina-international.com/sci-news/rdsmut.htm>). RDS is required for rod and cone outer segment (OS) biogenesis, but evidence suggests that the two cell types have divergent requirements for the protein. Rods without RDS (in the rod-dominant wild-type [WT] mouse) completely lack OSs and exhibit no rod-based electroretinogram (ERG) function (Sanyal and Jansen 1981). In contrast, cones lacking RDS (in the cone-dominant *nrl*^{-/-} background) form OSs and retain function (Farjo et al. 2006). The OSs of the *rds*^{-/-}/*nrl*^{-/-} are quite abnormal; they completely lack lamella and take the form of balloon-shaped membranous sacs.

More specifically, large oligomeric RDS complexes held together by C150-mediated disulfide bonds are required for the formation of the rim region of rod disks and cone lamellae. Transgenic mice expressing oligomerization-incompetent RDS (C150S-RDS) on the *rds*^{-/-} background do not form rod or cone OSs (Chakraborty et al. 2009; Chakraborty et al. 2010). In the presence of endogenous RDS, rods are not adversely affected by C150S-RDS, while cones exhibit a dramatic, dominant degeneration and aberrant rim formation.

In addition to causing dominant ultrastructural and functional degeneration, C150S-RDS produces defects in protein trafficking to the OS in cones but not in rods. In both the WT and *nrl*^{-/-} backgrounds, cones exhibit mislocalization of C150S-RDS protein (but not endogenous RDS) throughout the photoreceptor cell. Furthermore, mislocalization of C150S-RDS is accompanied by mislocalization of

S.M. Conley • D. Chakraborty • M.I. Naash (✉)
Department of Cell Biology, University of Oklahoma Health Sciences Center,
940 Stanton L. Young Boulevard. BMS 781, Oklahoma City, OK 73104, USA
e-mail: muna-naash@ouhsc.edu

cone opsins (Chakraborty et al. 2009). Here we ask whether other cone OS proteins are mislocalized in the presence of C150S-RDS to help understand the mechanism underlying this phenotype.

83.2 Materials and Methods

83.2.1 Construction of the Transgene

The COP-T-C150S-RDS transgenic mice were generated as described previously (Chakraborty et al. 2009; Chakraborty et al. 2010). Briefly, a 6.5 kb fragment of the human red/green opsin promoter (generously shared by Dr. Jeremy Nathans) was introduced in front of the full-length mouse Rds cDNA. In addition to the C150S mutation, the cDNA contained the P341Q modification to enable specific antibody recognition. Mice were bred into the cone-dominant *nrl*^{-/-} (generously shared by Dr. Anand Swaroop, NEI) background. All experiments and animal protocols were approved by the local Institutional Animal Care and Use Committee (IACUC; University of Oklahoma Health Sciences Center, Oklahoma City, OK, U.S.A.) and conformed to the guidelines on the care and use of animals adopted by the Society for Neuroscience and the Association for Research in Vision and Ophthalmology (Rockville, MD, U.S.A.).

83.2.2 Antibodies and Immunohistochemistry

Standard immunohistochemistry was performed as described previously (Chakraborty et al. 2009; Chakraborty et al. 2010) using frozen sections from mice at 30 days of age (P30). Eyes were collected mid-afternoon under room light. Images were captured with an Olympus BX-62 microscope equipped with a spinning disc confocal unit. Images were stored and deconvolved (no neighbors paradigm) using Slidebook® version 4.2 and are single slices of a confocal stack. The following antibodies were used in this study (1) mouse mAB 3B6 specifically recognizing transgenic but not endogenous RDS (generously shared by Dr. Robert Molday, University of British Columbia); (2) rabbit polyclonal antibodies against medium wavelength (M-) opsin and cone arrestin (M-opsin, mCAR, generously shared by Dr. Cheryl Craft, Keck School of Medicine, University of Southern California); (3) rabbit polyclonal antibody against the beta subunit of the cone cyclic nucleotide gated channel (CNGB3- generously shared by Dr. Xi-Qin Ding, University of Oklahoma Health Sciences Center); (4) rabbit polyclonal antibody against cone transducin (GNAT2-Santa Cruz Biotechnology, Santa Cruz, CA); (5) rabbit polyclonal antibody against short wavelength (S-) opsin, generated in house.

83.3 Results

83.3.1 OS Proteins are Normally Localized in COP-T/*nrl*^{-/-}

To enable study in a cone-dominant environment, mice expressing C150S-RDS under the control of the cone opsin promoter (COP-T) were crossed into the *nrl*^{-/-} background. As we have shown previously (Chakraborty et al. 2010), and here in Fig. 83.1a, transgenic mice exhibit mislocalization of COP-T protein (labeled with mAB 3B6) and mislocalization of M-opsin. To determine if this mislocalization was a general trend, or limited to opsin and COP-T, we investigated three other OS proteins. First, we examined the cone cyclic nucleotide gated channel (CNGB3), a membrane protein located exclusively on the cone OS plasma membrane, in contrast to cone opsin which is present in the plasma membrane and the lamella membrane. Second, we examined the membrane-associated protein cone transducin (GNAT2). Cone transducin is associated with cone opsin and is found in cone OSs. The third protein we examined is the cytosolic protein cone arrestin (CAR). In dark-adapted cones, CAR is found localized throughout the photoreceptor, while in the light, it is localized to the OS and synaptic region (with minimal staining of cell

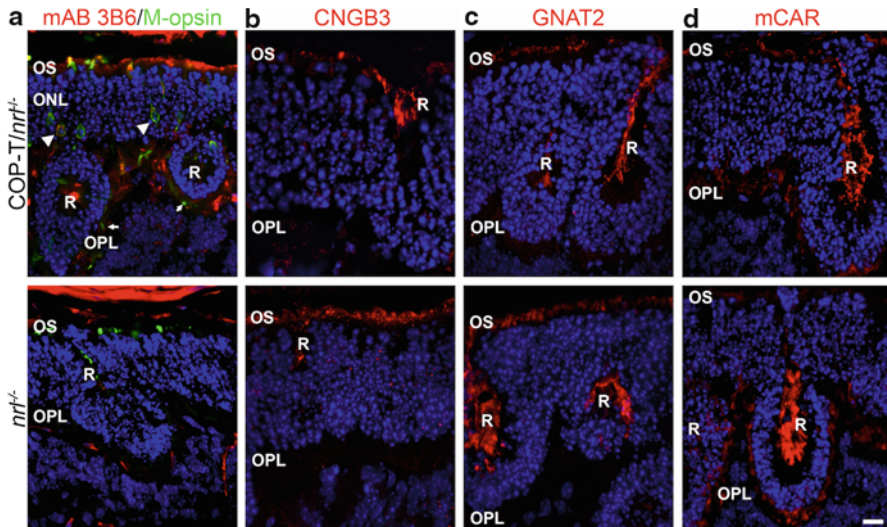


Fig. 83.1 M-opsin and COP-T but not other OS proteins are mislocalized in COP-T/*nrl*^{-/-} mice. P30 frozen sections were stained with (a) mAB 3B6 (to recognize COP-T-red) and M-opsin (green) (b) CNGB3-red (c) GNAT2-red (d) or mCAR-red. Nuclei were labeled with DAPI (blue). (a) M-opsin and COP-T are mislocalized throughout the photoreceptor in COP-T/*nrl*^{-/-} animals instead of being restricted to the OS as in the *nrl*^{-/-}. (b–d) CNGB3, GNAT2, and mCAR exhibit normal protein localization in the presence of the COP-T transgenic protein. Arrowheads-mislocalization in ONL, arrows mislocalization in the OPL. Scale bar 25 μ m, OS outer segment; ONL outer nuclear layer; OPL outer plexiform layer; R rosette

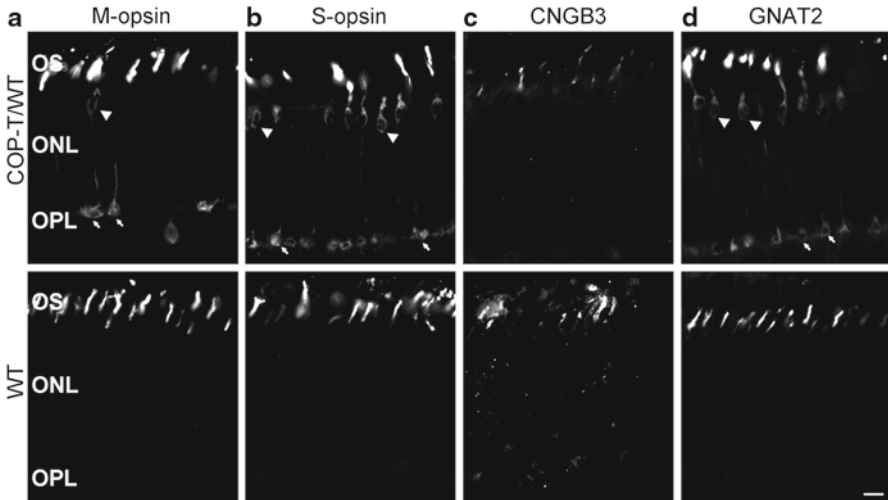


Fig. 83.2 GNAT2 is mislocalized with cone opsins in COP-T/WT mice. P30 frozen sections were stained with (a) M-opsin, (b) S-opsin, (c) CNGB3, and (d) GNAT2. M-opsin, S-opsin, and GNAT2 are mislocalized throughout the photoreceptor in COP-T/WT animals while CNGB3 is normally localized in the OS. *Arrowheads*-mislocalization in ONL, *arrows* mislocalization in the OPL. Scale bar 10 μ m, *OS* outer segment; *ONL* outer nuclear layer; *OPL* outer plexiform layer; *R* rosette

bodies and ISs) (Zhu et al. 2002). When we labeled P30, retinal sections (collected under room lighting) with antibodies against these three proteins (Fig. 83.1b–d), expression patterns in the COP-T/*nrl*^{-/-} are the same as *nrl*^{-/-}. We do not see any mislocalization reminiscent of the staining pattern of M-opsin or COP-T.

83.3.2 *GNAT2 is Mislocalized in COP-T/WT*

It has been documented that the cones of the *nrl*^{-/-} are similar to WT cones, but are shorter than normal cones, and undergo slow degeneration (Mears et al. 2001; Daniele et al. 2005). Previously, we have observed that the cone-dominant degenerative ERG phenotype associated with COP-T is less severe in *nrl*^{-/-} cones than in WT cones. Similarly, we observed that in WT cones, both M- and S-opsin are mislocalized, while in *nrl*^{-/-} cones, only M-opsin is mislocalized (Chakraborty et al. 2009; Chakraborty et al. 2010). We therefore decided to examine cone OS protein localization in WT cones expressing COP-T. As shown previously (Chakraborty et al. 2009) and in Fig. 83.2a b, both M- and S-opsin are mislocalized to the ONL and OPL in the COP-T/WT animals, but not in nontransgenic controls. As in the COP-T/*nrl*^{-/-}, CNG is properly localized to the OS in COP-T/WT animals (Fig. 83.2c). In contrast, GNAT2 exhibits marked mislocalization in the cones of the COP-T/WT (Fig. 83.2d). The pattern is identical to the opsin mislocalization we observe: some protein is found in the OS, with additional protein seen in the ONL (arrowheads) and the synaptic terminals (arrows).

83.4 Discussion

Although it is clear that higher-order, disulfide bonded RDS oligomers are required for OS formation, our observation that C150S-RDS is abnormally trafficked in cones but not in rods (Chakraborty et al. 2009; Chakraborty et al. 2010) suggests that assembly and packaging of RDS complexes in the IS may be different in rods vs. cones. In the rod IS, RDS assembles into noncovalently bound tetramers (Chakraborty et al. 2008). After trafficking to the rod OS, RDS homotetramers assemble into higher-order complexes that are held together by intermolecular disulfide bonds mediated by C150. While little is known about RDS assembly and trafficking in cones, our results from the COP-T mice suggest that normal RDS trafficking in cones may rely on formation of some covalently bound RDS complexes in the IS. In this case, oligomerization-incompetent RDS might be abnormally processed during the formation of trafficking vesicles at the trans Golgi.

Why abnormally packaged RDS (i.e. COP-T) should lead to cone opsin mislocalization is unclear. In a model of OS degeneration, it has been shown that in rods, RDS accumulates in cytoplasmic vesicles, while opsin accumulates on the plasma membrane of the IS, cell body, and synaptic terminal (Fariss et al. 1997). The authors suggest that this arises from differential targeting and trafficking of opsin and RDS vesicles to the OS. Similar evidence exists for cones: models which exhibit cone opsin mislocalization (such as *Kif3a*^{-/-} and *BBS4*^{-/-}), do not exhibit RDS mislocalization (Abd-El-Barr et al. 2007; Avasthi et al. 2009). These data are consistent with our previous publications from the COP-T model wherein endogenous RDS is not mislocalized even though opsin is, and suggest strongly that opsin and RDS do not traffic together. COP-T mislocalization mimics (and colocalizes) with the mislocalized cone opsin, in contrast to the pattern of RDS mislocalization seen by Fariss et al. (1997). This has led us to hypothesize that oligomerization-incompetent RDS is abnormally packaged into cone opsin-containing vesicles and interferes with normal OS targeting of those vesicles. If this hypothesis is correct, other proteins that traffic with cone opsin should also be mislocalized in COP-T cones.

A series of excellent publications has significantly enhanced our knowledge of normal cone and rod opsin trafficking, see (Karan et al. 2008). Based on results from multiple mouse models, it has been proposed that rod and cone opsin traffic in vesicles that also contain, among other proteins, rhodopsin kinase and either rod or cone transducin; while OS proteins such as RDS and the rod/cone CNGs traffic separately. In support of the hypothesis that COP-T is interrupting the normal trafficking of cone opsin-containing vesicles, we here demonstrate that GNAT2 but not CNG mislocalize in COP-T cones. Surprisingly, we do not see mislocalization of GNAT2 in the *nrl*^{-/-} background. In COP-T/*nrl*^{-/-} all cone transducin is found in the OS region. Similarly, we have observed that COP-T induces significant mislocalization of S-opsin in the WT background (see Fig. 83.2b and (Chakraborty et al. 2009)) with only minor mislocalization in the *nrl*^{-/-} (Chakraborty et al. 2010). These observations point to differences between the cones of the *nrl*^{-/-} and the cones of the WT. While the cones of the *nrl*^{-/-} exhibit cone-like morphological, ultrastructural, and electrophysiological features, they may also exhibit some rod-cone hybrid features.

In conclusion, the data we have presented here support the hypothesis that oligomerization-incompetent RDS is not packaged properly in the cone IS and may become abnormally packaged with cone opsin. Furthermore, this abnormality leads to aberrant trafficking of opsin-containing vesicles and may partially explain the cone-dominant degenerative phenotype we see in COP-T mice.

References

- Abd-El-Barr MM, Sykoudis K, Andrabi S et al (2007) Impaired photoreceptor protein transport and synaptic transmission in a mouse model of Bardet-Biedl syndrome. *Vision Res* 47: 3394–3407
- Avasthi P, Watt CB, Williams DS et al (2009) Trafficking of membrane proteins to cone but not rod outer segments is dependent on heterotrimeric kinesin-II. *J Neurosci* 29:14287–14298
- Chakraborty D, Ding XQ, Fliesler SJ et al (2008) Outer segment oligomerization of rds: evidence from mouse models and subcellular fractionation. *Biochemistry* 47:1144–1156
- Chakraborty D, Conley SM, Stuck MW et al (2010) Differences in RDS trafficking, assembly, and function in cones vs. rods: Insights from studies of C150S-RDS. *Hum Mol Genet* In Press
- Chakraborty D, Ding XQ, Conley SM et al (2009) Differential requirements for retinal degeneration slow intermolecular disulfide-linked oligomerization in rods versus cones. *Hum Mol Genet* 18:797–808
- Daniele LL, Lillo C, Lyubarsky AL et al (2005) Cone-like Morphological, Molecular, and Electrophysiological Features of the Photoreceptors of the Nrl Knockout Mouse. *Invest Ophthalmol Vis Sci* 46:2156–2167
- Fariss RN, Molday RS, Fisher SK et al (1997) Evidence from normal and degenerating photoreceptors that two outer segment integral membrane proteins have separate transport pathways. *J Comp Neurol* 387:148–156
- Farjo R, Skaggs JS, Nagel BA et al (2006) Retention of function without normal disc morphogenesis occurs in cone but not rod photoreceptors. *J Cell Biol* 173:59–68
- Karan S, Zhang H, Li S et al (2008) A model for transport of membrane-associated phototransduction polypeptides in rod and cone photoreceptor inner segments. *Vision Res* 48:442–452
- Mears AJ, Kondo M, Swain PK et al (2001) Nrl is required for rod photoreceptor development. *Nat Genet* 29:447–452
- Sanyal S, Jansen HG (1981) Absence of receptor outer segments in the retina of rds mutant mice. *Neurosci Lett* 21:23–26
- Zhu X, Li A, Brown B et al (2002) Mouse cone arrestin expression pattern: light induced translocation in cone photoreceptors. *Mol Vis* 8:462–471

Chapter 84

HSP70 Gene Expression in the Zebrafish Retina After Optic Nerve Injury: A Comparative Study Under Heat Shock Stresses

Chieko Fujikawa, Mikiko Nagashima, Kazuhiro Mawatari, and Satoru Kato

84.1 Introduction

Heat shock proteins (HSPs) are one of the molecular chaperones. HSPs play an important role for cell protection by various environmental stresses, such as heat, heavy metals, and reactive oxygen species (Beckmann et al. 1990; Chiang et al. 1989; Shi and Thomas 1992). Following stresses, HSPs are rapidly induced to control cell maintenance and survival. HSPs are transactivated Heat shock factor-1 (HSF-1) (Santoro 2000). HSF-1 normally exists in the cytoplasm, and is translocated to the nucleus with active phosphorylated form under stress conditions. Fish retinal ganglion cells (RGCs) can survive and regenerate their axons after optic nerve injury (ONI), which is the best model for CNS repair after injury (Sperry 1948; Attardi and Sperry 1963; Kato et al. 2007). Although many factors are involved in the fish optic nerve regeneration process, there is no report describing about HSPs and HSF-1 in the fish retina during nerve regeneration. In the present study, we compared the expression of HSP70 and HSF-1 in zebrafish retina after ONI and heat shock.

C. Fujikawa • K. Mawatari
Division of Health Sciences, Graduate School of Medicine,
Kanazawa University, 13-1 Takara-machi, Kanazawa, Ishikawa 920-8640, Japan

M. Nagashima
Department of Molecular Neurobiology, Division of Health Sciences, Graduate School
of Medicine, Kanazawa University, 13-1 Takara-machi, Kanazawa, Ishikawa 920-8640, Japan

S. Kato (✉)
Department of Molecular Neurobiology, Graduate School of Medicine, Kanazawa University,
13-1 Takara-machi, Kanazawa, Ishikawa 920-8640, Japan
e-mail: satoru@med.kanazawa-u.ac.jp

84.2 Materials and Methods

84.2.1 *Animals and Treatment*

Zebrafish (*Danio rerio*, body length 3–4 cm) were used throughout this study. Zebrafish were anesthetized with ice-cold water. The optic nerve was transected 1 mm away from the posterior of eyeball with scissors. After surgery, the fish were kept in water tank at 28°C for 0.5–72 h. Heat stress was performed at 37°C for 30 min.

84.2.2 *RNA Isolation and RT-PCR*

Total RNA was isolated from two eyes using Sepasol®-RNA I super (Nacalai Tesque). RT-PCR was performed using TaKaRa RNA PCR kit (AMV) Ver.3 (TaKaRa).

84.2.3 *Tissue Preparation*

At appropriate times, fish eyes were enucleated and fixed in 4% paraformaldehyde/5% sucrose in 0.1 M phosphate buffered saline at pH 7.4 (PBS) for overnight at 4°C. It was then immersed in ascending series of sucrose until final 20% sucrose/PBS overnight at 4°C. The tissue was immersed in OCT compound and frozen sectioned in 12 µm thickness and transferred to silane-coated coverslips and allowed to air dry before storing at –20°C.

84.2.4 *Immunohistochemistry*

Immunohistochemistry (IHC) was performed as described previously (Matsukawa et al. 2004). In brief, after autoclaved at 121°C for 20 min in 10 mM citrate buffer, tissue sections were washed and blocked for 30 min, and incubated with primary antibodies overnight at 4°C. The antibodies used in this study were anti-HSP70 (1:100, SANTA CRUZ BIOTECHNOLOGY, INC.) and anti-pHSF-1 (1:300, SANTA CRUZ BIOTECHNOLOGY, INC.). After washing, the sections were incubated with secondary antibodies, Alexa Fluor 488 antibody (Molecular probes) for 1 h at room temperature.

84.2.5 *In Situ Hybridization*

To investigate the localization HSP70 mRNA, in situ hybridization (ISH) was performed as described previously (Matsukawa et al. 2004). In brief, plasmids containing 436 bp of HSP70 cDNA were linearized, and antisense and sense cRNA

probes were generated with mixture of plasmid, T7 or SP6 RNA polymerase, and digoxigenin-labeled deoxy UTP. The retinal sections were prehybridized in hybridization buffer for 30 min at 42°C. Hybridization was performed with 500 ng of cRNA probes labeled with digoxigenin in 1 mL of hybridization solution overnight at 42°C. On the following day, the sections were washed and treated with 20 mg/mL RNase A at 37°C for 30 min. To detect the signals, the sections were incubated with an alkaline phosphatase-conjugated anti-digoxigenin antibody (Roche, Germany) overnight at 4°C, and visualization was performed using NBT/BCIP (Roche) as the substrate.

84.3 Results

84.3.1 *The Expression of HSP70 and HSF-1 in the Zebrafish Retina After ONI*

The expression of HSP70 and HSF-1 levels in the zebrafish retina after ONI were investigated using RT-PCR, ISH, and IHC. The levels of HSP70 mRNA (Figs. 84.1a and 84.1c–e) and protein (data not shown) were increased 2.2-folds at 0.5–24 h and then returned to the control level at 72 h after ONI. These increased expressions were limited to RGCs (Fig. 84.1c–e). The levels of HSF-1 mRNA were significantly increased in the zebrafish retina 2.2-folds at 0.5–24 h (Fig. 84.2a) and the phospho-HSF-1 protein was detected at 0.5 h in RGCs after ONI (data not shown).

84.3.2 *The Expression of HSP70 and HSF-1 in the Zebrafish Retina After Heat Shock*

The expression of HSP70 and HSF-1 levels in the zebrafish retina after heat shock were investigated using RT-PCR, ISH, and IHC. After heat shock at 37°C for 30 min, the levels of HSP70 mRNA was increased in the zebrafish retina 3.2-folds at 0.5–1 h, and then returned to the control level by 3 h (Fig. 84.1b). This increased expression was detected in all nuclear layers (Fig. 84.1f–h). Whereas the levels of HSF-1 mRNA were not changed in any time points (Fig. 84.2b), the phosphor-HSF-1 protein was detected at 0.5 h in all nuclear layers after heat shock (data not shown).

84.4 Discussion

We compared the expression change of HSP70 and HSF-1 in zebrafish retina after ONI and heat shock. The most noticeable difference between ONI and heat shock is the expression change of HSF-1 mRNA. After ONI, the continuous increase (0.5–72 h) of HSP70 mRNA was accompanied with the induction of HSF-1 mRNA and

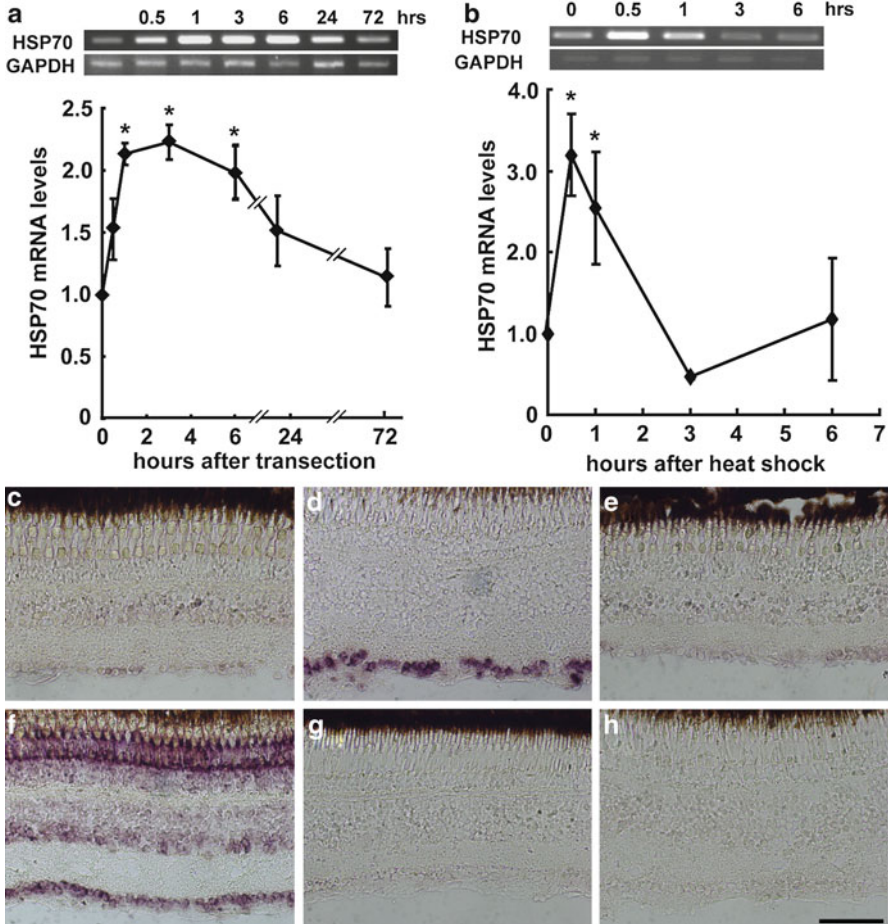


Fig. 84.1 Expression and localization of HSP70 mRNA in the zebrafish retina after optic nerve injury and heat shock stresses. **(a)** Expression of HSP70 mRNA in the zebrafish retina after optic nerve injury (ONI). * $p < 0.05$ vs. control $n = 3$ **(b)**: Expression of HSP70 mRNA in the zebrafish retina after heat shock. * $p < 0.05$ vs. control $n = 3$ **(c)**: Localization of HSP70 mRNA in the control (nontreatment) zebrafish retina. In control retina, weak signals of HSP70 mRNA were detected in all nuclear layers. **(d, e)**: Localization of HSP70 mRNA in the zebrafish retina after ONI. Strong signals of HSP70 mRNA were detected in RGCs 3 h after ONI **(d)**, and then the levels of HSP70 mRNA returned to the control value by 72 h **(e)**. **(f, g)**: Localization of HSP70 mRNA in the zebrafish retina after heat shock stresses. HSP70 mRNA was drastically increased in all nuclear layers 0.5 h after heat shock stresses **(f)**. The levels of HSP70 mRNA returned to the control value by 3 h **(g)**. **(h)** No positive signals could be seen in sense-probe. Scale bar equals to 50 μm . GCL: ganglion cell layer

pHSF-1 protein. In contrast, the transient increase (0.5–3 h) of HSP70 mRNA after heat shock was accompanied with the induction of pHSF-1 protein but not HSF-1 mRNA. These results indicate that the continuous induction of HSP70 mRNA by ONI is

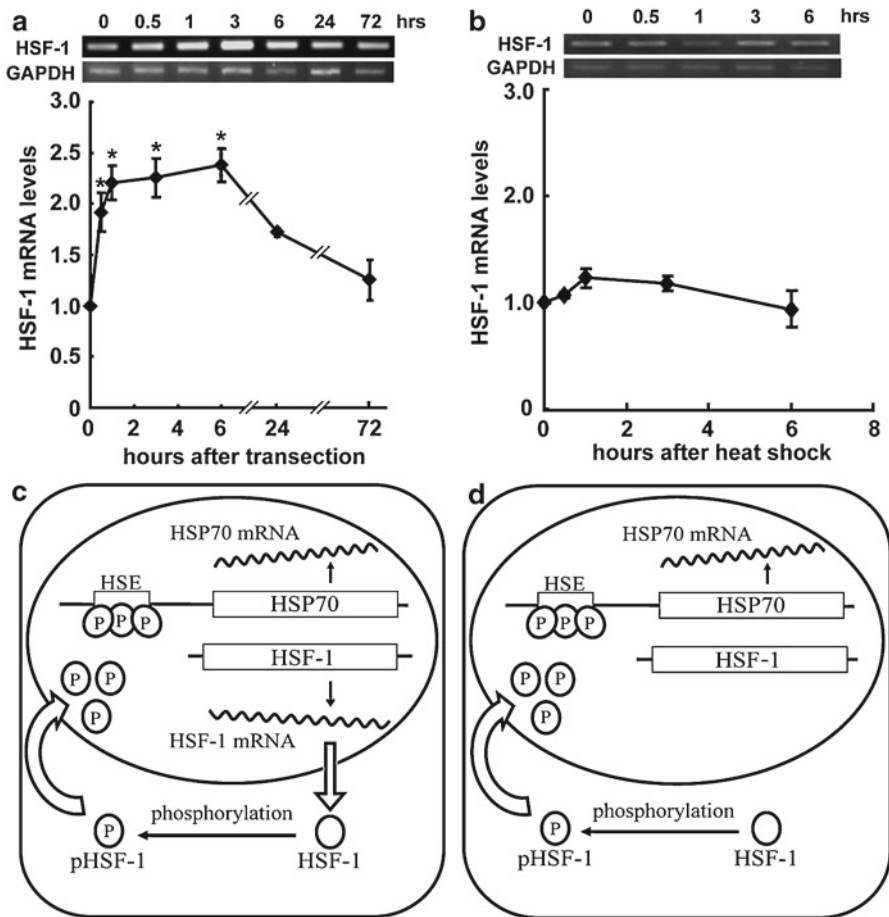


Fig. 84.2 Different induction mechanisms of HSP70 mRNA in the zebrafish retina after optic nerve injury and heat shock stresses. (a) Optic nerve injury condition. Levels of HSF-1 mRNA and phospho-HSF-1 protein both increased following HSP70 mRNA induction. * $p < 0.05$ vs. control $n = 3$ (b) Heat shock condition. Levels of phospho-HSF-1 protein were increased without transcriptional activation of HSF-1 mRNA. * $p < 0.05$ vs. control $n = 3$ (c) Schematic drawings of the HSP70 mRNA induction in the zebrafish retina after ONI. (d) Schematic drawings of the HSP70 mRNA induction in the zebrafish retina after heat shock

due to elevated translocation of pHSF-1 into the nucleus with transcriptional activation, whereas the transient induction of HSP70 mRNA by heat shock is due to elevated translocation of pHSF-1 into the nucleus without transcriptional activation.

In summary, Fig. [Error! Reference source not found.](#) a, b illustrate schematic drawings of the HSP70 induction after ONI (a) and heat shock stresses (b). After ONI, first, HSF-1 mRNA is transcribed from HSF-1 coding region. HSF-1 mRNA is translocated to the cytoplasm and translated to HSF-1 protein (nonactivated-form). HSF-1 protein in the cytoplasm is phosphorylated (pHSF-1) and then translocated

into the nucleus. pHSF-1 (activate form) translocated into the nucleus forms trimeric complexes and binds to Heat shock element (HSE) which exists upstream region of HSP70 promoter (Santoro 2000). Thereafter, HSP70 mRNA is transactivated under the regulation of trimeric pHSF-1. In contrast, after heat shock stresses, HSF-1 protein in the cytoplasm is phosphorylated and translocated into the nucleus and then pHSF-1 translocated into the nucleus after heat shock stresses transactivates HSP70 mRNA without transcriptional activation of HSF-1 mRNA.

Airaksinen et al. (2003) reported that HSF-1 mRNA in zebrafish embryonic fibroblast cell line did not induce even under heat shock stress for more than 30 min at 37°C. Such a distinct and continuous induction of HSF-1 mRNA after ONI might contribute signaling activation of successful optic nerve regeneration in zebrafish.

In the future, this work offers a clear to resolve the mammalian CNS regeneration.

Acknowledgments We thank to Ms Sachiko Higashi and Ms Tomoko Kano for secretarial and technical assistance.

References

- Airaksinen S, Jokilehto T, Råbergh CM et al (2003) Heat- and cold-inducible regulation of HSP70 expression in zebrafish ZF4 cells. *Comp Biochem Physiol B Biochem Mol Biol* 136:275–82
- Attardi DG, Sperry RW (1963) Preferential selection of central pathways by regenerating optic fibers. *Exp Neurol* 7:46–64
- Beckmann RP, Mizzen LE, Welch WJ (1990) Interaction of Hsp 70 with newly synthesized proteins: implications for protein folding and assembly. *Science* 248:850–854
- Chiang HL, Terlecky SR, Plant CP et al (1989) A role for a 70-kilodalton heat shock protein in lysosomal degradation of intracellular proteins. *Science* 246:382–385
- Kato S, Koriyama Y, Matukawa T et al (2007) Optic nerve regeneration in goldfish. In: Becker CG, Becker T (Eds) *Model Organisms in Spinal Cord Regeneration*. Weinheim 355–372
- Matsukawa T, Sugitani K, Mawatari K et al (2004) Role of purpurin as a retinol-binding protein in goldfish retina during the early stage of optic nerve regeneration: its priming action on neurite outgrowth. *J Neurosci* 24:8346–8353
- Santoro MG (2000) Heat shock factors and the control of the stress response. *Biochem Pharmacol* 59:55–63
- Shi Y, Thomas JO (1992) The transport of proteins into the nucleus requires the 70-kilodalton heat shock protein or its cytosolic cognate. *Mol Cell Biol* 12:2186–2192
- Sperry RW (1948) Patterning of central synapses in regeneration of the optic nerve in teleosts. *Physiol Zool* 21:351–361

Part IX
Retinal Development, Physiology, Cell and
Molecular Biology

Chapter 85

Restoration of Retinal Development in *Vsx2* Deficient Mice by Reduction of *Gdf11* Levels

Rosaysela Santos, Jeffry Wu, Jason A. Hamilton, Rita Pinter, Robert Hindges, and Anne L. Calof

Keywords TGF-beta • *Brn3b* • *Math5* • *Foxn4* • *Crx* • *Neurod1* • *Chx10* • *Fst* • Stem/progenitor cell • Micro-ophthalmia

85.1 Introduction

Null mutations in the *visual system homeobox 2* (*Vsx2*; a.k.a. *Chx10*) gene result in micro-ophthalmia and failed retinal development in man, mouse, and zebrafish (Burmeister et al. 1996; Barabino et al. 1997; Ferda Percin et al. 2000). *Vsx2^{or1/or1}* (*Chx10^{or}*, ocular retardation) mutant mice exhibit a 19-fold decrease in the number

R. Santos • A.L. Calof (✉)

Department of Anatomy & Neurobiology, Center for Complex Biological Systems,
University of California, Irvine, CA 92697-1275, USA
e-mail: alcalof@uci.edu

J. Wu

Department of Anatomy & Neurobiology, Center for Complex Biological Systems,
University of California, Irvine, CA 92697-1275, USA

BOOPT-School of Optometry, University of California, Berkeley, CA, 94720-2284, USA

J.A. Hamilton

Department of Anatomy & Neurobiology, Center for Complex Biological Systems,
University of California, Irvine, CA 92697-1275, USA

Department of Regenerative Medicine, Athersys Inc, 3021 Carnegie Ave.,
Cleveland, OH 44115-2634, USA

R. Pinter

MRC Centre for Developmental Neurobiology, Kings College, London, SE1 1UL, UK
Akron Molecules GmbH, Campus Vienna Biocenter 5, Vienna, 1030, Austria

R. Hindges

MRC Center for Developmental Neurobiology, Kings College, London, SE1 1UL, UK

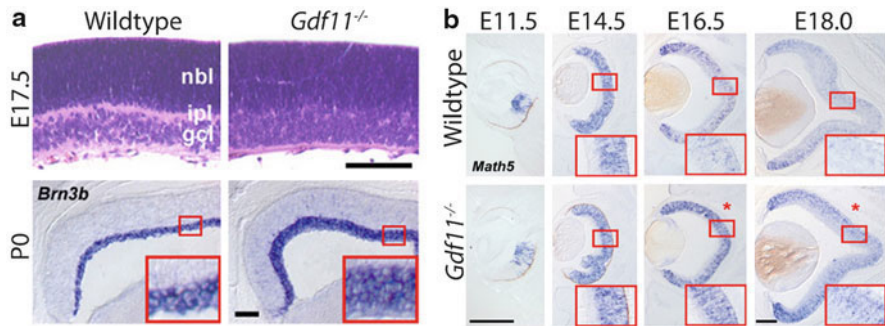


Fig. 85.1 GDF11 is a negative regulator of retinal neurogenesis. **(a)** H&E stain at E17.5 and *Brn3b* ISH at P0 show an increase in RGC, but no change in overall thickness of *Gdf11*^{-/-} retinas. **(b)** ISH showing prolonged expression of *Math5* in *Gdf11*^{-/-} retinas. Asterisks indicate reproducible *Math5* upregulation in *Gdf11*^{-/-} retina from wildtype controls. Scale bars: 100 μ m **(a)**, 200 μ m **(b)**. Adapted from (Kim et al. 2005)

of retinal cells, optic nerve aplasia, dramatic (if not complete) loss of bipolar interneurons, and the retinas lack a normal layered structure (Burmeister et al. 1996). Previous studies have shown that there are fewer proliferating cells in the retinas of *Vsx2*^{or/ord} mice during embryonic development, and that overproduction of retinal pigmented epithelium – in contrast to neural epithelium – is likely to be a major cause of the severe phenotypes observed in *Vsx2* mutant retinas (Burmeister et al. 1996; Rowan et al. 2004). These observations make the *Vsx2* mutant mouse a good model for understanding the onset, progression, and molecular etiology of development retinal dystrophies in man.

Growth and differentiation factor 11 (GDF11), a member of the TGF- β superfamily of signaling molecules, has been shown to be an autocrine negative regulator of neurogenesis, as well as an important regulator of stem/progenitor cell fate, in sensory epithelia (Wu et al. 2003; Kim et al. 2005; Lander et al. 2009). In the olfactory epithelium (OE), *Gdf11* negatively regulates neuronal cell number by causing cell-cycle arrest and/or differentiation of the progenitor cells that give rise to olfactory receptor neurons (ORNs), and as a result, the OE of *Gdf11*^{-/-} mice show an increased number of both neuronal progenitors and ORNs, and is thicker than that of wildtype mice (Wu et al. 2003; Lander et al. 2009). In the retina, absence of *Gdf11* results in an increase in the number of retinal ganglion cells (RGCs) (Fig. 85.1a), the earliest cell type to differentiate during retinal neurogenesis; however, this increase is at the expense of later-born cell types such as rod photoreceptors and amacrine cells (Kim et al. 2005). Multiple lines of evidence indicate that this effect is due to a change in the fate of retinal stem/progenitor cells, and is a consequence of prolonged expression of *Math5* (*Atoh7*, MGI), a transcription factor that confers competence to form RGCs, in *Gdf11*^{-/-} retina (Fig. 85.1b). GDF11 activity is required to downregulate expression of *Math5*, and in its absence, RGCs are produced for an extended period of time and accumulate in an aberrantly thick RGC layer (Fig. 85.1) and (Kim et al. 2005; Harada et al. 2007).

GDF11's role in modulating the activity of transcription factors that specify development of sensory epithelia and the cells within them has other consequences as well. For example, mice that lack the winged helix transcription factor FoxG1 lack an OE and have greatly reduced cerebral hemispheres (Xuan et al. 1995). We have found that the ability of FoxG1 to drive OE neurogenesis is due to its function as a negative regulator of GDF11 activity: Reduction of *Gdf11* levels rescues, to a significant extent, both the early developmental loss of neuronal progenitor cells in *Foxg1*^{-/-} OE, and the defects in nasal cavity and olfactory turbinate structure development seen in these mutants (Kawauchi et al. 2009). These effects are gene dose-dependent, with loss of even one allele of *Gdf11* restoring full histogenesis of the OE neuroepithelium in those regions of the nasal cavity that now develop (Kawauchi et al. 2009).

Given these diverse yet related developmental functions of GDF11, we speculated that reducing GDF11 levels might promote restoration of retinal development in the micro-ophthalmic *Vsx2*^{orJ/orJ} mouse. To test this idea, we used genetic manipulations to alter *Gdf11* levels in the retinas of *Vsx2*^{orJ/orJ} mouse, and examined retinal phenotypes at various developmental ages.

85.2 Materials and Methods

85.2.1 Animals

Gdf11^{+/-} mice (*Gdf11*^{tm2/+}) (Wu et al. 2003) maintained on a C57bl/6 background were bred with *Vsx2*^{orJ/orJ} mice to generate *Gdf11*^{+/-};*Vsx2*^{orJ/+} mice; these mice were intercrossed, or were bred with mice heterozygous for one gene only, to obtain animals of the various genotypes studied. Day of vaginal plug discovery was designated embryonic day (E) 0.5. The Institutional Animal Care and Use Committee of the University of California, Irvine, approved all protocols for animal use.

85.2.2 Histology and In Situ Hybridization

Tissues were fixed in 4% paraformaldehyde, cryoprotected, embedded, and cryosectioned at 20 μm as described (Murray et al. 2003). For in situ hybridization (ISH), cRNA probes for *Brn3b* (*POU4F2*), *Crx*, *Foxn4*, *Math5* (*Atoh7*), and *Neurod1* were synthesized and hybridized as described (Kim et al. 2005). Images were taken using a Zeiss Axiophot microscope equipped with AxioVision Software (Carl Zeiss, Thornwood, NY, USA).

85.3 Results

In a previous study, we noted that inactivation of one or two alleles of *Gdf11* progressively restores development of OE in *Foxg1*^{-/-} mice (Kawauchi et al. 2009). We performed a similar analysis by examining stained sections of retinas from *Gdf11*^{-/-};*Vsx2*^{orJ/orJ}, *Vsx2*^{orJ/orJ} and control (*Vsx2*^{orJ/+}) mice at various developmental stages, and measuring thickness of central retina in each case. Reduction of *Gdf11* levels rescues retinal thickness as early as day 14.5 of gestation (Table 85.1): The retina is about 20% thicker in *Gdf11*^{-/-};*Vsx2*^{orJ/orJ} retinas than in *Vsx2*^{orJ/orJ} retinas (although thickness is not restored to full control levels). Epithelial thicknesses and cell lamination were also noticeably rescued in *Gdf11*^{+/-};*Vsx2*^{orJ/orJ} retinas, implying a dose-dependence of this effect; this was most readily observed at later ages, as shown in Fig. 85.2.

Table 85.1 Rescued expression of developmental genes in *Vsx2*^{orJ/orJ} retinas

Gene	Gene Function	Age	Control	<i>Vsx2</i> ^{orJ/orJ}	<i>Gdf11</i> ^{-/-} ; <i>Vsx2</i> ^{orJ/orJ}
<i>Brn3b</i>	RGC development (Erkman et al. 1996)	E14.5	+++++	+/-	+++
<i>Neurod1</i>	Amacrine development (Harada et al. 2007)	E14.5	+++++	+/-	++
<i>Crx</i>	Photoreceptor development (Furukawa et al. 1999)	E14.5	+++++	+/-	+
<i>Foxn4</i>	Neuronal retina (Kelly et al. 2007)	E14.5	+++++	-	+++
<i>Math5</i>	Competence to make RGCs (Harada et al. 2007)	E14.5	+++++	+	++++
Thickness (increase relative to <i>Vsx2</i> ^{orJ/orJ})		E14.5	95%	(0%)	20%

Gene expression levels were scored from ISH and based on intensity and relative area of expression. “-” indicates no expression; “+/-” indicates low expression (<5 cells expressing); “+” indicates that expression was clearly observed. The strongest signal intensity with greatest expansion for each gene was scored as +++++. The scores of the various genes are compared to control retinas. Thickness of central retina was measured at E14.5



Fig. 85.2 Partial rescue of retinal lamination and thickness in *Vsx2*^{orJ/orJ} retina by inactivation of one allele of *Gdf11* at P7. Scale bar: 200 μ m

Expression of genes important for retinal development and neural cell differentiation show drastic reductions in their expression in *Vsx2*^{orJ/orJ} retinas (Rowan et al. 2004). We performed ISH to examine expression of *Brn3b*, *Neurod1*, *Crx*, *Foxn4*, and *Math5* in the retinas of *Vsx2* mutants, and in these mice when *Gdf11* levels were reduced. Absence of *Gdf11* resulted in increased expression of these genes (Table 85.1). For example, *Brn3b* is expressed in the presumptive ganglion cell layer (GCL) at E14.5 in control retinas. In contrast, *Vsx2*^{orJ/orJ} retinas exhibit a severe reduction in *Brn3b* expression, with only a few scattered cells expressing *Brn3b*. In *Gdf11*^{-/-};*Vsx2*^{orJ/orJ} retinas, *Brn3b* expression is increased in intensity, expanded in area, and is localized to a clearly-demarcated developing GCL. Similarly, *Foxn4* expression, normally expressed in stem/progenitor cells throughout the NBL, is absent in *Vsx2*^{orJ/orJ} retinas. Rescued retinas show an increase in ISH intensity and expanded *Foxn4* expression domain, restricted primarily to a demarcated NBL. Other retinal development genes show similar rescue of expression when *Gdf11* levels are reduced (Table 85.1).

85.4 Discussion

In the present study, we show that *Vsx2* mutant retinas can be rescued by reducing *Gdf11* activity and that this rescue is gene dosage dependent. Expression analysis shows that genes required for proper retina development are minimally expressed or absent in the central region of *Vsx2*^{orJ/orJ} retina. With loss of *Gdf11* (*Gdf11*^{-/-};*Vsx2*^{orJ/orJ} retinas), expression of these genes is expanded, and the retinal neuroepithelium displays a more-normal lamination pattern and is increased in thickness (Fig. 85.3). These observations indicate that cells within the *Vsx2* mutant retina retain the potential to produce differentiated neuronal cell types, and imply that this process is

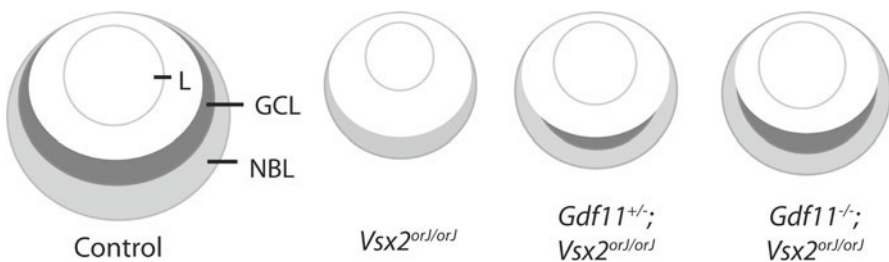


Fig. 85.3 Restoration of retinal development in *Vsx2*^{orJ/orJ} mice by reduction of *Gdf11* activity. Schematic model showing a section through a control eye at E14.5, with the developing ganglion cell layer (GCL) and neuroblastic layer (NBL) indicated. *Vsx2*^{orJ/orJ} eyes are smaller than controls, and have thinner retinas with no obvious lamination. *Gdf11*^{+/-};*Vsx2*^{orJ/orJ} eyes are larger and their retinas are thicker than *Vsx2*^{orJ/orJ} retinas and show some lamination, including partial development of the GCL. *Gdf11*^{-/-};*Vsx2*^{orJ/orJ} eyes and retinas are larger/thicker still, with clearly-visible GCL and NBL. L, lens

negatively regulated by the action of GDF11. Further support for this idea comes from the observation that reducing levels of follistatin (a high-affinity GDF11 antagonist expressed within neural retina; cf. (Kim et al. 2005)) in *Vsx2* mutants exacerbates the mutant phenotype (data not shown).

Interestingly, recent preliminary studies suggest that not only is developmental gene expression rescued by reducing *Gdf11* levels in *Vsx2^{orJ/orJ}* retinas; optic nerve development may be rescued as well: DiI tracing of RGC axons in perinatal *Gdf11^{-/-};Vsx2^{orJ/orJ}* mice indicates that a significant number of axons are present in an (aberrant) optic nerve, and that these axons extend as far as the optic chiasm (data not shown). These observations suggest that the rescue of retinal development seen in these animals may extend to a restoration of visual function.

Altogether, these studies show that manipulation of the GDF11 signaling pathway can strongly influence the severity of developmental retinal dystrophies, and suggest that pharmacological intervention with the GDF11 signaling pathway may be a potent means by which to treat retinal dystrophies. To this end, current studies are aimed at understanding the molecular mechanisms by which rescue is achieved.

Acknowledgements We thank T. Clevenger, R. Asperer, C. Yamanoglu, and M. Yazdi for technical assistance and K. Gokoffski, S. Kawauchi, and P. Hollenbeck for comments on the manuscript. This study was supported by grants from the Foundation Fighting Blindness (BR-CMM-0507-0380-UCI) and NIH (DC03583, GM076516) to ALC, and MRC G0601182 to RH. RS received the Young Investigator Travel Award by the National Eye Institute (NIH) to attend the XIVth International Symposium on Retinal Degeneration 2010.

References

- Barabino GA, Wise RJ, Woodbury VA et al (1997) Inhibition of sickle erythrocyte adhesion to immobilized thrombospondin by von Willebrand factor under dynamic flow conditions. *Blood* 89:2560–2567
- Burmeister M, Novak J, Liang MY et al (1996) Ocular retardation mouse caused by *Chx10* homeobox null allele: impaired retinal progenitor proliferation and bipolar cell differentiation. *Nat Genet* 12:376–384
- Erkman L, McEvelly RJ, Luo L et al (1996) Role of transcription factors *Brn-3.1* and *Brn-3.2* in auditory and visual system development. *Nature* 381:603–606
- Ferda Percin E, Ploder LA, Yu JJ et al (2000) Human microphthalmia associated with mutations in the retinal homeobox gene *CHX10*. *Nat Genet* 25:397–401
- Furukawa T, Morrow EM, Li T et al (1999) Retinopathy and attenuated circadian entrainment in *Crx*-deficient mice. *Nat Genet* 23:466–470
- Harada T, Harada C, Parada LF (2007) Molecular regulation of visual system development: more than meets the eye. *Genes Dev* 21:367–378
- Kawauchi S, Kim J, Santos R et al (2009) *Foxg1* promotes olfactory neurogenesis by antagonizing *Gdf11*. *Development* 136:1453–1464
- Kelly LE, Nekkalapudi S, El-Hodiri HM (2007) Expression of the forkhead transcription factor *FoxN4* in progenitor cells in the developing *Xenopus laevis* retina and brain. *Gene Expr Patterns* 7:233–238
- Kim J, Wu HH, Lander AD et al (2005) GDF11 controls the timing of progenitor cell competence in developing retina. *Science* 308:1927–1930

- Lander AD, Gokoffski KK, Wan FY et al (2009) Cell lineages and the logic of proliferative control. *PLoS Biol* 7:e15
- Murray RC, Navi D, Fesenko J et al (2003) Widespread defects in the primary olfactory pathway caused by loss of *Mash1* function. *J Neurosci* 23:1769–1780
- Rowan S, Chen CM, Young TL et al (2004) Transdifferentiation of the retina into pigmented cells in ocular retardation mice defines a new function of the homeodomain gene *Chx10*. *Development* 131:5139–5152
- Wu HH, Ivkovic S, Murray RC et al (2003) Autoregulation of neurogenesis by GDF11. *Neuron* 37:197–207
- Xuan S, Baptista CA, Balas G et al (1995) Winged helix transcription factor BF-1 is essential for the development of the cerebral hemispheres. *Neuron* 14:1141–1152

Chapter 86

The Different Functions of Norrin

Barbara M. Braunger and Ernst R. Tamm

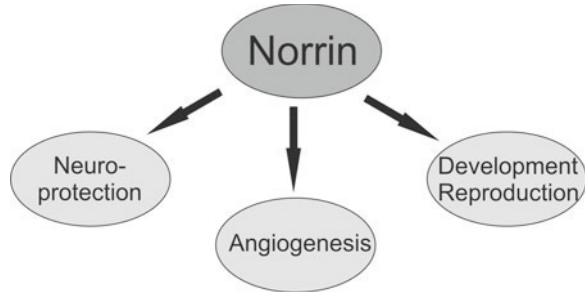
Keywords Norrin • Frizzled 4 • Wnt/ β -catenin signaling • Angiogenesis • Retinopathy of prematurity • Neuroprotection • Transgenic mice • Norrie disease

86.1 Introduction

Almost 20 years ago, mutations in the *NDP* (Norrie disease pseudoglioma) gene were identified as causative for Norrie disease. For a considerable number of following years, the available data on the functional role(s) of Norrin, the product of *NDP*, remained largely incomplete. Experimental studies were complicated by the fact that it turned out to be difficult to generate bioactive recombinant Norrin in larger amounts. In addition, the cells that secrete Norrin remained ill-defined, as the amounts of available mRNA and protein appeared to be very low in most tissues of the body. In the more recent years, this scenario has completely changed, as the signaling pathways of Norrin have been largely identified. Moreover, studies in animal (mouse) models have yielded important insights into a fundamental role of Norrin for capillary formation in retina and inner ear. Current data strongly indicate that Norrin has an additional neuroprotective role for retinal neurons, which appears to be largely independent from its role on the growth of retinal capillaries (Fig. 86.1).

B.M. Braunger • E.R. Tamm (✉)
Institute of Human Anatomy and Embryology, University of Regensburg,
Universitätsstr. 31, Regensburg D-93053, Germany
e-mail: ernst.tamm@vkl.uni-regensburg.de

Fig. 86.1 The multiple functions of Norrin



86.2 Norrie Disease

Norrie disease is a congenital X-linked recessive disease which is characterized by atrophic irides, corneal clouding, cataract, and retinal dysplasia with early vascular proliferation (pseudoglioma) followed by bulbar atrophy. In addition, affected patients show progressive sensorineural hearing loss, psychotic features, and in one third of the cases mental retardation (Warburg 1966; Berger 1998). By linkage analysis and positional cloning, mutations in *NDP* were identified as cause of Norrie disease (Berger et al. 1992; Meindl et al. 1992). In addition, the X-linked form of familial exudative vitreoretinopathy (FEVR) was found to be caused by missense mutations in Norrin (Chen et al. 1993; Fuchs et al. 1995; Meindl et al. 1995; Shastry et al. 1997a; Torrente et al. 1997; Shastry 1998), while autosomal-dominant familial exudative vitreoretinopathy was found to be caused by mutant frizzled-4, the ligand of Norrin (Robitaille et al. 2002). Mutations in *NDP* have also been identified in patients with Coat's disease (Black et al. 1999) and retinopathy of prematurity (Shastry et al. 1997b).

86.3 Norrin

Norrin is a secreted small protein which is characterized by a carboxyl-terminal cysteine-rich domain, which has been suggested to facilitate formation of a homodimer containing a cyteine-knot motif (Meitinger et al. 1993). Similar motifs have been observed in growth factors of the TGF- β superfamily. Recent studies using a knock-in mouse model have found a wide spread expression of Norrin in astrocytes of both forebrain and midbrain, in Bergmann glia of the cerebellum, and in Müller glia of the retina (Ye et al. 2011). During development, expression of Norrin has been observed in regions of the hindbrain and throughout the dorsal and mid-dorsal regions of the neural tube (Ye et al. 2011). Norrin activates the canonical Wnt/ β -catenin signaling pathway via specific binding to the frizzled (Fzd)4/low-density lipoprotein receptor-related protein (Lrp)5/6 receptor complex (Xu et al. 2004). Similar to the action of Wnt glycoproteins, binding of Norrin to the extracellular

cysteine rich domain of Fzd4 promotes oligomerization of Fzd4 with Lrp5/6 coreceptors to inactivate the β -catenin destruction complex causing an accumulation of intracellular β -catenin. As additional component of the Fzd4/Lrp5/6 receptor complex, TSPAN12 has been identified that multimerizes Fzd4 to form receptor clusters, and specifically promotes Norrin, but not Wnt-mediated β -catenin signaling (Junge et al. 2009). Strikingly, mutations in Norrin and Fzd4 result in very similar morphological phenotypes, both in mice and men (Xu et al. 2004; Smallwood et al. 2007; Ye et al. 2009).

86.4 Angiogenic Properties of Norrin

Ndp^{-/-} mutant mice with a targeted disruption of *Ndp* have been generated (Berger et al. 1996). The animals show complete absence of intraretinal capillaries and persistence of the hyaloid vasculature (Richter et al. 1998; Rehm et al. 2002; Luhmann et al. 2005b; Ohlmann et al. 2005). Comparable findings have been reported for the vessels within the stria vascularis of the cochlea (Rehm et al. 2002). β B1-crystallin-norrin transgenic mice with ocular overexpression of ectopic norrin under control of the lens-specific β B1-crystallin promoter have been developed and in mixed β B1-crystallin-norrin/*Ndp*^{-/-} mice, the vascular phenotype is completely rescued (Ohlmann et al. 2005). Recombinant Norrin induces proliferation, migration, and tube formation in retinal microvascular endothelial cells, effects that involve Wnt/ β -catenin signaling and induction of Sox17 and angiopoietin-2 (Ye et al. 2009; Ohlmann et al. 2010). Overall, there is considerable evidence that Norrin, Fzd-4, and Lrp5 constitute an essential signaling system that controls the formation of retinal capillaries during development (Ye et al., 2009). Norrin is not only required during the development of retinal capillaries, but substantially protects against vascular damage induced by high oxygen such as observed in retinopathy of prematurity (Ohlmann et al. 2010). In transgenic mice overexpressing norrin, vascular loss following oxygen exposure was significantly smaller as compared to wild-type littermates. In addition, the anatomical correct regrowth of vessels was significantly increased, while pathological neovascularization was suppressed.

86.5 Neuroprotective Properties of Norrin

Norrin-deficient mice show an early specific loss of retinal ganglion cells (RGC) suggesting a neuroprotective role of Norrin (Ohlmann et al. 2005). To analyze such a putative neuroprotective role of Norrin in more detail, RGC survival in mouse eyes was studied following damage after *N*-methyl-*D*-aspartate (NMDA) injection into the vitreous body (Seitz et al. 2010). After injection of NMDA, the numbers of optic nerve axons and of perikarya of surviving RGC were significantly higher in NMDA/Norrin injected eyes as compared to NMDA treated eyes, an effect that

could be blocked by adding dickkopf (DKK)-1, an inhibitor of the Wnt/ β -catenin signaling pathway. Comparable results were obtained by TUNEL labeling. Treatment of eyes with combined Norrin/NMDA activated Wnt/ β -catenin signaling and increased the retinal expression of leukemia inducible factor and endothelin-2, as well as that of neurotrophic growth factors such as fibroblast growth factor-2, brain-derived neurotrophic factor, lens epithelium-derived growth factor and ciliary neurotrophic factor. A similar activation of Wnt/ β -catenin signaling and an increased expression of neurotrophic factors were observed in cultured Müller cells after treatment with norrin, effects that again could be blocked by adding DKK-1. In addition, Norrin and conditioned cell culture medium of norrin-treated Müller cells increased survival of differentiated RGC-5 cells. Overall, norrin appears to have pronounced neurotrophic properties on retinal neurons with the distinct potential to decrease the damaging effects of NMDA-induced RGC loss. Norrin and the molecules involved in its signaling pathway appear to be promising targets to develop strategies that increase RGC survival not only in experimental animal models, but also in patients with RGC damage following ischemia or glaucoma. It is tempting to speculate that Norrin-induced activation of combined leukemia inducible factor, endothelin-2, fibroblast growth factor-2 and/or Wnt/ β -catenin signaling could also be neuroprotective for other types of retinal neurons.

86.6 The Role of Norrin in Reproduction and Development

Expression of Norrin has been observed in decidua and uteri of wild-type mice and in human placentae indicating a role for Norrin in reproduction. Indeed, there is impaired female fertility due to distinct reduction of decidualization in female *Ndp*^{-/-} mice. Deciduae are smaller and do not reach as deep into the endometrium as in wild-type mice. Fibrocytes of the deeper endometrial zone do not show transition to large roundish decidua cells, and are separated from each other by wide intercellular spaces (Luhmann et al. 2005a). Overall, Norrin appears to act on reproduction in two ways: by impairing vascularization of deciduae and by inducing malformation of endometrial fibrocytes.

References

- Berger W (1998) Molecular dissection of Norrie disease. *Acta Anat (Basel)* 162:95–100
- Berger W, van de PD, Bachner D et al (1996) An animal model for Norrie disease (ND): gene targeting of the mouse ND gene. *Hum Mol Genet* 5:51–59
- Berger W, van de PD, Warburg M et al (1992) Mutations in the candidate gene for Norrie disease. *Hum Mol Genet* 1:461–465
- Black GC, Perveen R, Bonshek R et al (1999) Coats' disease of the retina (unilateral retinal telangiectasis) caused by somatic mutation in the NDP gene: a role for norrin in retinal angiogenesis. *Hum Mol Genet* 8:2031–2035

- Chen ZY, Battinelli EM, Fielder A et al (1993) A mutation in the Norrie disease gene (NDP) associated with X-linked familial exudative vitreoretinopathy. *Nat Genet* 5:180–183
- Fuchs S, Kellner U, Wedemann H et al (1995) Missense mutation (Arg121Trp) in the Norrie disease gene associated with x-linked exudative vitreoretinopathy. *Hum Mutat* 6:257–259
- Junge HJ, Yang S, Burton JB et al (2009) TSPAN12 regulates retinal vascular development by promoting Norrin- but not Wnt-induced FZD4/beta-catenin signaling. *Cell* 139:299–311
- Luhmann UF, Meunier D, Shi W et al (2005a) Fetal loss in homozygous mutant Norrie disease mice: a new role of Norrin in reproduction. *Genesis* 42:253–262
- Luhmann UF, Lin J, Acar N et al (2005b) Role of the Norrie disease pseudoglioma gene in sprouting angiogenesis during development of the retinal vasculature. *Invest Ophthalmol Vis Sci* 46:3372–3382
- Meindl A, Lorenz B, Achatz H et al (1995) Missense mutations in the NDP gene in patients with a less severe course of Norrie disease. *Hum Mol Genet* 4:489–490
- Meindl A, Berger W, Meitinger T et al (1992) Norrie disease is caused by mutations in an extracellular protein resembling C-terminal globular domain of mucins. *Nat Genet* 2:139–143
- Meitinger T, Meindl A, Bork P et al (1993) Molecular modelling of the Norrie disease protein predicts a cystine knot growth factor tertiary structure. *Nat Genet* 5:376–380
- Ohlmann A, Seitz R, Braunger B et al (2010) Norrin promotes vascular regrowth after oxygen-induced retinal vessel loss and suppresses retinopathy in mice. *J Neurosci* 30:183–193
- Ohlmann A, Scholz M, Goldwisch A et al (2005) Ectopic norrin induces growth of ocular capillaries and restores normal retinal angiogenesis in Norrie disease mutant mice. *J Neurosci* 25:1701–1710
- Rehm HL, Zhang DS, Brown MC et al (2002) Vascular defects and sensorineural deafness in a mouse model of Norrie disease. *J Neurosci* 22:4286–4292
- Richter M, Gottanka J, May CA et al (1998) Retinal vasculature changes in Norrie disease mice. *Invest Ophthalmol Vis Sci* 39:2450–2457
- Robitaille J, MacDonald ML, Kaykas A et al (2002) Mutant frizzled-4 disrupts retinal angiogenesis in familial exudative vitreoretinopathy. *Nat Genet* 32:326–330
- Seitz R, Hackl S, Seibuchner T et al (2010) Norrin mediates neuroprotective effects on retinal ganglion cells via activation of the Wnt/beta-Catenin signaling pathway and the induction of neuroprotective growth factors in Müller cells. *J Neurosci* 30:5998–6010
- Shastry BS (1998) Identification of a recurrent missense mutation in the Norrie disease gene associated with a simplex case of exudative vitreoretinopathy. *Biochem Biophys Res Commun* 246:35–38
- Shastry BS, Hejtmancik JF, Trese MT (1997a) Identification of novel missense mutations in the Norrie disease gene associated with one X-linked and four sporadic cases of familial exudative vitreoretinopathy. *Hum Mutat* 9:396–401
- Shastry BS, Pendergast SD, Hartzler MK et al (1997b) Identification of missense mutations in the Norrie disease gene associated with advanced retinopathy of prematurity. *Arch Ophthalmol* 115:651–655
- Smallwood PM, Williams J, Xu Q et al (2007) Mutational analysis of Norrin-Frizzled4 recognition. *J Biol Chem* 282:4057–4068
- Torrente I, Mangino M, Gennarelli M et al (1997) Two new missense mutations (A105T and C110G) in the norrin gene in two Italian families with Norrie disease and familial exudative vitreoretinopathy. *Am J Med Genet* 72:242–244
- Warburg M (1966) Norrie disease: a congenital oculo-acoustico-cerebral degeneration. *Acta Ophthalmol* 89(suppl.):1–147
- Xu Q, Wang Y, Dabdoub A et al (2004) Vascular development in the retina and inner ear: control by Norrin and Frizzled-4, a high-affinity ligand-receptor pair. *Cell* 116:883–895
- Ye X, Smallwood P, Nathans J (2011) Expression of the Norrie disease gene (Ndp) in developing and adult mouse eye, ear, and brain. *Gene Expr Patterns* 11:151–155
- Ye X, Wang Y, Cahill H et al (2009) Norrin, frizzled-4, and Lrp5 signaling in endothelial cells controls a genetic program for retinal vascularization. *Cell* 139:285–298

Chapter 87

Roles of Homeobox Genes in Retinal Ganglion Cell Differentiation and Axonal Guidance

Qi Zhang and David D. Eisenstat

Keywords Retinal development • Retinal ganglion cell • Axonal guidance • Transcription factor • Homeobox gene

87.1 Introduction

Among the six major classes of retinal neurons, retinal ganglion cells (RGC) are the only projection neurons. RGCs differentiate in the mouse retina around E11.5 followed by horizontal, cone, and amacrine cells. The early generated RGC are located in the central inner retina, and the axons of these RGC commence their journey to central nervous system (CNS) targets immediately after terminal differentiation

Q. Zhang

Department of Human Anatomy and Cell Science, University of Manitoba,
Winnipeg, MB, Canada R3E 0V9

Manitoba Institute of Cell Biology, University of Manitoba,
Winnipeg, MB, Canada R3E 0V9

D.D. Eisenstat (✉)

Department of Human Anatomy and Cell Science, University of Manitoba,
Winnipeg, MB, Canada R3E 0V9

Department of Pediatrics and Child Health, University of Manitoba,
Winnipeg, MB, Canada R3E 0V9

Department of Biochemistry and Medical Genetics, University of Manitoba,
Winnipeg, MB, Canada R3E 0V9

Department of Ophthalmology, University of Manitoba,
Winnipeg, MB, Canada R3E 0V9

Manitoba Institute of Cell Biology, University of Manitoba,
Winnipeg, MB, Canada R3E 0V9
e-mail: eisensta@cc.umanitoba.ca

(Marquardt and Gruss 2002). Combinations of homeodomain (HD) and basic helix-loop-helix (bHLH) transcription factors (TF) play important roles in RGC cell fate specification and influence RGC axonal pathfinding choices *en route*. In this review, we will focus on the roles of HD transcription factors in these processes.

87.2 *Brn-3* Genes

The POU-domain is a bipartite DNA-binding protein domain, containing a POU-specific region and a POU-homeodomain region. The class IV POU-domain proteins, BRN3a, BRN3b, and BRN3c (*POU4f1*, *POU4f2*, and *POU4f3*, respectively) are the homologs of *Unc-86* in *C. elegans*. *Brn-3* genes are expressed in the embryonic and adult CNS, and are required for sensorineural development and survival.

All three *Brn-3* POU-homeodomain genes are expressed in the developing retina, specifically in postmitotic RGC. *Brn3b* expression is first detected in the earliest RGC at E11.5 in the central inner mouse retina, followed by *Brn3a* and *Brn3c* expression 2 days later (Xiang et al. 1995; Pan et al. 2005). Through E15.5 to the adult retina, *Brn3a* and *Brn3b* expression overlaps in 80% of RGC. However, *Brn3a* is the predominant gene expressed in P5 retinas, with few RGC expressing *Brn3b* (Quina et al. 2005). Only ~15% of RGC express *Brn3c* (Xiang et al. 1995).

The overlapping expression pattern and a similar specific DNA-binding site [(A/G)CTCATTA(T/C)] of these three BRN-3 proteins suggest their functional redundancy in retinogenesis. However, targeted mutations of *Brn-3* genes in mice show distinct defects, but only the *Brn3b*^{-/-} mouse shows an obvious retinal phenotype. In *Brn3b* null mice there is loss of 60–80% RGC in adult retinas, depending on the background genetic strain (Erkman et al. 1996; Gan et al. 1996). This RGC loss is due to enhanced apoptosis after E15.5, but not to defects of initial cell fate specification or migration. *Brn3b* is also required for RGC axon pathfinding and fasciculation (Erkman et al. 2000). *Brn3a* null mutants die at birth, with loss of dorsal root ganglion and trigeminal neurons (Erkman et al. 1996; Xiang et al. 1996). *Brn3c*^{-/-} mice display deficits in balance and complete deafness, attributed to loss of vestibular and auditory hair cells (Erkman et al. 1996; Xiang et al. 1997). Neither *Brn3a* nor *Brn3c* mutants show obvious defects in retinal development.

Brn3a and *Brn3c* are identified as downstream of *Brn3b* in retinogenesis, and there is reduced *Brn3a* expression in *Brn3b* mutants (Erkman et al. 1996). Despite the dominant roles of *Brn3b* in retinal development, several independent groups have reported that all three *Brn-3* genes are functionally equivalent in retinogenesis. Overexpression of *Brn3a*, *Brn3b*, or *Brn3c* in chick retinal progenitors exerts a similar effect in promoting RGC differentiation (Liu et al. 2000). Knocking-in the *Brn3a* coding sequence into a *Brn3b* null background mouse rescues RGC from apoptosis and restores RGC axonal pathfinding (Pan et al. 2005).

A recent study has shown that conditional deletion of *Brn3a* alters RGC dendritic stratification without influencing RGC axon central projections. However, the

conditional *Brn3b* knockout mice show reduced RGC numbers, loss of axonal projections to medial (MTN) and lateral terminal nuclei (LTN) and corresponding visual sensory defects (Badea et al. 2009).

87.3 *Dlx* Genes

Dlx genes are the vertebrate orthologs of *distal-less* (*Dll*). There are six *Dlx* genes identified in mice, which are arranged into three bigene clusters (*Dlx1/Dlx2*, *Dlx5/Dlx6*, and *Dlx3/Dlx7*), and are localized on mouse chromosomes 2, 6, and 11, respectively (Ghanem et al. 2003). Within the intergenic regions of *Dlx1/2* and *Dlx5/6*, several *cis*-acting regulators have been characterized, including *112a* and *112b* between the *Dlx1* and *Dlx2* genes, and *I56i* and *I56ii* separating *Dlx5* and *Dlx6* (Poitras et al. 2007). Two conserved enhancer elements, URE1 and URE2, have also been found in the 5' flanking region of *Dlx1* (Hamilton et al. 2005) (Du and Eisenstat, unpublished). These *cis*-acting elements are important for cross-regulatory interactions between the *Dlx* genes. One example is that DLX1 and DLX2 regulate *Dlx5/Dlx6* expression by acting on *I56i* (Zhou et al. 2004).

Dlx1 and *Dlx2* were first detected in the retinal neuroepithelium on E12.5 including mitotic cells adjacent to the ophthalmic ventricle (Eisenstat et al. 1999). Our recent study reported DLX2 immunostaining in E11.5 retina, with DLX2 expressed in a dorsal (high) to ventral (low) gradient (de Melo et al. 2008). At E13.5, both DLX1 and DLX2 are expressed throughout the retina, with boundaries in peripheral and central inner retina. Interestingly, some other "retinal" homeobox genes are expressed in a nearly complementary manner to DLX2 at this stage. At E13.5, the highest level of PAX6 expression is observed in the most peripheral retina and BRN3b is expressed in the inner central retina, where DLX2 is absent. By E18.5, DLX1 and DLX2 expressions are highly restricted to the ganglion cell layer (GCL) and inner part of the neuroblastic layer (NBL), where they are co-expressed with markers for RGC, amacrine, and horizontal cells. DLX1 expression resembles DLX2 in embryonic retina, but decreases dramatically after birth and cannot be detected in adult retina. However, DLX2 is robustly expressed in the GCL and inner nuclear layer (INL) throughout adulthood (de Melo et al. 2003).

Although the role of *Dlx* genes in forebrain development is well reported, very few studies have described *Dlx* gene function in retina development. Homozygous deletion of *Dlx1* and *Dlx2* is perinatally lethal, and leads to a 33% reduction of RGC number due to enhanced apoptosis of late-born RGCs (de Melo et al. 2005). *TrkB*, a receptor for brain derived neurotrophic factor (BDNF) mediated signalling, was identified as a DLX2 downstream target during mouse retinal development and may contribute to RGC survival (de Melo et al. 2008).

The role of *Dlx5* and *Dlx6* genes in retinogenesis is still not clear. *In situ* hybridization revealed *Dlx5* mRNA expression in retina by E16.5. In P0 and adult retina, *Dlx5* mRNA is co-expressed with DLX2 in the GCL and INL. The *Dlx5/Dlx6* intergenic

enhancer (*I56i*) is co-expressed with DLX5, DLX1, and DLX2 in RGC, amacrine, and horizontal cells (Zhou et al. 2004). There is no published report regarding the retinal phenotype of *Dlx5/Dlx6* knockout mice.

87.4 *Vax* Genes

Vax (Ventral anterior homeobox-containing) genes are a homeodomain gene subfamily, closely related to *Emx* genes, sharing sequence homology, similar chromosomal location, and expression patterns (Hallonet et al. 1998). In the mouse, *Vax1* mRNA is first detected at E8, in the anterior neural ridge and adjacent ectoderm. During embryogenesis, *Vax1* expression is restricted to the derivatives of these regions, including basal forebrain, ventral optic vesicle, optic disk, stalk, and chiasm (Hallonet et al. 1998). The targeted deletion of *Vax1* shows defects in RGC axonogenesis and axonal-glial associations, without influencing expression of *Pax2* and *BFI*. In addition, *Vax1*^{-/-} axons fail to fasciculate and do not extend toward the hypothalamic midline, leading to an absence of optic chiasm development. These RGC axon pathfinding defects are partially due to the loss of some important axon guidance cues, including *Netrin-1* and *EphB3*, but not *Slit1* (Bertuzzi et al. 1999). Another obvious phenotype of *Vax1* mutants is the failure of choroid fissure closure, known as coloboma. *Pax6* and *Rx* are ectopically expressed in the *Vax1* mutant optic nerve. However, *Pax2* expression remains unaffected in the mutants.

VAX2 shares an identical homeodomain with VAX1, and the *Vax2* gene is tightly linked with *Emx1* in mouse and human. By E9, *Vax2* transcripts are detected in the ventral optic vesicle, with lower expression in the optic nerve and stalk. *Vax1* and *Vax2* then share overlapping expression patterns in ventral retina and optic stalk. By E12, *Vax2* expression is restricted to the ventral neural retina in the whole retinal population. However, at later embryonic stages, *Vax2* is only detected in ventral RGC. *Vax2* is not expressed in the adult retina (Bertuzzi et al. 1999; Mui et al. 2002).

Consistent with its predominant ventral retinal expression pattern, *Vax2* plays a major role in ventralizing embryonic retina. Misexpression of *Vax2* in the dorsal retina is able to alter the expression of the putative dorsal-ventral marker genes, including upregulation of ventral retinal markers *EphB2/EphB3*, *Pax2*, and *Vax2* itself, and downregulation of the dorsally restricted TF, *Tbx5* (Barbieri et al. 1999). In addition, ectopic *Vax2* expression in dorsal retina is sufficient to induce profound axon pathfinding defects of dorsal RGC (Schulte et al. 1999). In agreement with these *Vax2* gain-of-function studies, the ventral RGC from *Vax2* null mice show complete dorsalization. The RGC axons from *Vax2*^{-/-} ventral retina aberrantly project to the lateral rostral edge of the superior colliculus (SC) together with all the dorsal RGC axons, instead of medial rostral SC, the destination of all the wild-type ventral RGC axons. The expression of *EphB2/EphB3* is absent in *Vax2*^{-/-} ventral retina.

87.5 Islet Genes

ISL1 and ISL2 are a subfamily of LIM homeodomain TF, characterized by two zinc-finger motifs (LIM domain) and a homeodomain. Both ISL1 and ISL2 play important roles in determining motor neuron subtype identity, axonal projections and peripheral innervations (Shirasaki and Pfaff 2002). Most of the work has been done in the spinal cord of vertebrate and invertebrate models. *Isl1* and *Isl2* are also expressed in the embryonic and postnatal retina.

Isl2 expression is first detected in the E13 retina, and by E17, almost all the *Isl2* positive cells are RGC (Pak et al. 2004). *Isl2* is expressed at high levels in the dorsal retina, with weak expression in the ventral-temporal region. By repressing *Zic2* and *EphB1*, *Isl2* specifies the contralateral projection of RGC axons. In comparison to the specific RGC expression of *Isl2*, *Isl1* expression shows different patterns from embryonic to postnatal retina. Prior to E15.5, *Isl1* is predominantly expressed in RGC. However, from E15.5 to the adulthood, *Isl1* expression is detected in RGC, amacrine cells, and bipolar cells (Elshatory et al. 2007). Recent work has shown that under the regulation of ATOH7 (formerly MATH5), *Isl1* defines a distinct but overlapping subpopulation of RGC with *Brn3b* (Mu et al. 2008; Pan et al. 2008)

87.6 Summary

In this review, we have described four major families of homeobox genes which play important roles in RGC differentiation as well as axonal pathfinding. The mechanism underlying how these HD TFs affect axonal pathfinding is not entirely known. One possibility is that the downstream targets directly regulated by these HD TF are responsible for axonal guidance. Examples of this are the repression of *EphB1* by *Isl2*, and *Vax1/Vax2* regulation of *EphB2/EphB3* expression. The roles of *Dlx* homeobox genes in RGC axonal guidance have not yet been reported. However, in the mouse telencephalon, *Dlx1* and *Dlx2* promote the tangential migration of GABAergic interneurons by repressing axonal growth (Cobos et al. 2007) and inhibiting Neuropilin-2 expression (Le et al. 2007). It is possible that the genetic program defining RGC identity also encodes a unique “sensory” network for their axons, determining how and where RGC axons respond to guidance cues *en route* to CNS targets.

References

- Badea TC, Cahill H, Ecker J et al (2009) Distinct roles of transcription factors brn3a and brn3b in controlling the development, morphology, and function of retinal ganglion cells. *Neuron* 61:852–864
- Barbieri AM, Lupo G, Bulfone A et al (1999) A homeobox gene, *vax2*, controls the patterning of the eye dorsoventral axis. *Proc Natl Acad Sci USA* 96:10729–10734

- Bertuzzi S, Hindges R, Mui SH et al (1999) The homeodomain protein *vax1* is required for axon guidance and major tract formation in the developing forebrain. *Genes Dev* 13:3092–3105
- Cobos I, Borello U, Rubenstein JL (2007) *Dlx* transcription factors promote migration through repression of axon and dendrite growth. *Neuron* 54:873–888
- de Melo J, Qiu X, Du G et al (2003) *Dlx1*, *Dlx2*, *Pax6*, *Brn3b*, and *Chx10* homeobox gene expression defines the retinal ganglion and inner nuclear layers of the developing and adult mouse retina. *J Comp Neurol* 461:187–204
- de Melo J, Du G, Fonseca M et al (2005) *Dlx1* and *Dlx2* function is necessary for terminal differentiation and survival of late-born retinal ganglion cells in the developing mouse retina. *Development* 132:311–322
- de Melo J, Zhou QP, Zhang Q et al (2008) *Dlx2* homeobox gene transcriptional regulation of *TrkB* neurotrophin receptor expression during mouse retinal development. *Nucleic Acids Res* 36:872–884
- Eisenstat DD, Liu JK, Mione M et al (1999) *DLX-1*, *DLX-2*, and *DLX-5* expression define distinct stages of basal forebrain differentiation. *J Comp Neurol* 414:217–237
- Elshatory Y, Deng M, Xie X et al (2007) Expression of the LIM-homeodomain protein *Isl1* in the developing and mature mouse retina. *J Comp Neurol* 503:182–197
- Erkman L, McEvelly RJ, Luo L et al (1996) Role of transcription factors *Brn-3.1* and *Brn-3.2* in auditory and visual system development. *Nature* 381:603–606
- Erkman L, Yates PA, McLaughlin T et al (2000) A POU domain transcription factor-dependent program regulates axon pathfinding in the vertebrate visual system. *Neuron* 28:779–792
- Gan L, Xiang M, Zhou L et al (1996) POU domain factor *Brn-3b* is required for the development of a large set of retinal ganglion cells. *Proc Natl Acad Sci USA* 93:3920–3925
- Ghanem N, Jarinova O, Amores A et al (2003) Regulatory roles of conserved intergenic domains in vertebrate *Dlx* bigene clusters. *Genome Res* 13:533–543
- Hallonet M, Hollemann T, Wehr R et al (1998) *Vax1* is a novel homeobox-containing gene expressed in the developing anterior ventral forebrain. *Development* 125:2599–2610
- Hamilton SP, Woo JM, Carlson EJ et al (2005) Analysis of four *DLX* homeobox genes in autistic probands. *BMC Genet* 6:52
- Le TN, Du G, Fonseca M et al (2007) *Dlx* homeobox genes promote cortical interneuron migration from the basal forebrain by direct repression of the semaphorin receptor neuropilin-2. *J Biol Chem* 282:19071–19081
- Liu W, Khare SL, Liang X et al (2000) All *Brn3* genes can promote retinal ganglion cell differentiation in the chick. *Development* 127:3237–3247
- Marquardt T, Gruss P (2002) Generating neuronal diversity in the retina: one for nearly all. *Trends Neurosci* 25:32–38
- Mu X, Fu X, Beremand PD et al (2008) Gene regulation logic in retinal ganglion cell development: *Isl1* defines a critical branch distinct from but overlapping with *Pou4f2*. *Proc Natl Acad Sci USA* 105:6942–6947
- Mui SH, Hindges R, O’Leary DD et al (2002) The homeodomain protein *Vax2* patterns the dorsoventral and nasotemporal axes of the eye. *Development* 129:797–804
- Pak W, Hindges R, Lim YS et al (2004) Magnitude of binocular vision controlled by *islet-2* repression of a genetic program that specifies laterality of retinal axon pathfinding. *Cell* 119:567–578
- Pan L, Yang Z, Feng L et al (2005) Functional equivalence of *Brn3* POU-domain transcription factors in mouse retinal neurogenesis. *Development* 132:703–712
- Pan L, Deng M, Xie X et al (2008) *ISL1* and *BRN3B* co-regulate the differentiation of murine retinal ganglion cells. *Development* 135:1981–1990
- Poitras L, Ghanem N, Hatch G et al (2007) The proneural determinant *MASH1* regulates forebrain *Dlx1/2* expression through the *I12b* intergenic enhancer. *Development* 134:1755–1765
- Quina LA, Pak W, Lanier J et al (2005) *Brn3a*-expressing retinal ganglion cells project specifically to thalamocortical and collicular visual pathways. *J Neurosci* 25:11595–11604
- Schulte D, Furukawa T, Peters MA et al (1999) Misexpression of the *Emx*-related homeobox genes *cVax* and *mVax2* ventralizes the retina and perturbs the retinotectal map. *Neuron* 24:541–553

- Shirasaki R, Pfaff SL (2002) Transcriptional codes and the control of neuronal identity. *Annu Rev Neurosci* 25:251–281
- Xiang M, Gan L, Zhou L et al (1996) Targeted deletion of the mouse POU domain gene Brn-3a causes selective loss of neurons in the brainstem and trigeminal ganglion, uncoordinated limb movement, and impaired suckling. *Proc Natl Acad Sci USA* 93:11950–11955
- Xiang M, Zhou L, Macke JP et al (1995) The Brn-3 family of POU-domain factors: primary structure, binding specificity, and expression in subsets of retinal ganglion cells and somatosensory neurons. *J Neurosci* 15:4762–4785
- Xiang M, Gan L, Li D et al (1997) Essential role of POU-domain factor Brn-3c in auditory and vestibular hair cell development. *Proc Natl Acad Sci USA* 94:9445–9450
- Zhou QP, Le TN, Qiu X et al (2004) Identification of a direct Dlx homeodomain target in the developing mouse forebrain and retina by optimization of chromatin immunoprecipitation. *Nucleic Acids Res* 32:884–892

Chapter 88

Unraveling the Molecular Mystery of Retinal Pigment Epithelium Phagocytosis

Nora B. Caberoy and Wei Li

Keywords Retinal pigment epithelium • Phagocytosis • Phagocytosis ligand • Tubby-like protein 1 • Tulp1 • MerTK • ORF phage display

88.1 Introduction

Photoreceptor outer segments (POS) in the retina are susceptible to photodamage. The clearance of damaged molecules and retinoid cycle require the shedding of POS at the tip of the outer segments in a diurnal rhythm, and the phagocytosis of shed POS by retinal pigment epithelium (RPE) cells (Strauss 2005). Defects in RPE phagocytosis signaling, such as MerTK phagocytic receptor, cause retinal degeneration. Our understanding of RPE phagocytosis is relatively limited. Only a handful of phagocytosis ligands and receptors of RPE cells were identified and characterized on case-by-case basis with daunting challenges. The barrier is how to identify unknown signaling molecules in an unbiased manner. Here we summarize a unique strategy of phagocytosis-based functional cloning for unbiased identification of phagocytosis ligands, which can be used as molecular probes to further delineate phagocytosis receptors, signaling cascades, and interactions with POS.

N.B. Caberoy • W. Li (✉)

Bascom Palmer Eye Institute, Department of Ophthalmology,
University of Miami Miller School of Medicine, 1638 NW 10th Avenue,
Miami, FL 33136, USA
e-mail: wli@med.miami.edu

88.2 Materials and Methods

88.2.1 *Open Reading Frame Phage Display*

Open reading frame (ORF) phage display cDNA library of adult mouse eyes was used for phagocytosis-based functional selection in ARPE19 cells, as described (Fig. 88.1a) (Caberoy et al. 2010a). After three rounds of phage selection, individual clones were randomly picked from plates of enriched phages and analyzed for their phagocytosis activity in the same cells. Positive clones were identified by DNA sequencing.

88.2.2 *RPE Phagocytosis Assay*

Membrane vesicles were prepared from the retina of wild-type or Tulp1^{-/-} mice, as described and labeled with CFSE (Caberoy et al. 2010a). Alternatively, membrane vesicles were prepared from Neuro-2a cells expressing membrane-targeted green fluorescent protein (mGFP). Vesicles were used for ARPE19 phagocytosis in the presence or absence of FLAG-tagged Tulp1, and phagocytosed fluorescence signals were analyzed by confocal microscopy (Caberoy et al. 2010a).

88.2.3 *MerTK Ligand Studies*

For co-immunoprecipitation (Co-IP) study, FLAG-tagged Tulp1 was expressed in HEK293 cells. Cell lysates were prepared and incubated with Mer-Fc (MerTK extracellular domain fused to human IgG1 Fc domain, R&D Systems) at 4°C, followed by protein A resin. The resin was washed and analyzed by Western blot using anti-FLAG mAb. For MerTK autophosphorylation, D407 RPE cells were stimulated with Tulp1 for 30 min at 37°C. The cells were lysed and analyzed by Western blot using anti-phospho-MerTK, as described previously (Caberoy et al. 2010c). For intracellular signaling study, ARPE19 cell phagocytosis of mGFP-labeled Neuro-2a vesicles was stimulated by Tulp1 in the presence or absence of excessive Mer-Fc. The cells were fixed, permeabilized, and incubated with antibodies against nonmuscle myosin II-A heavy chain (NMMII-A), followed by Texas Red-labeled secondary antibody and confocal microscopy analysis. For phagocytosis prey binding, Jurkat cells were induced for apoptosis by etoposide (40 µM) for 16 h and washed (Caberoy et al. 2010c). Healthy and apoptotic Jurkat cells were incubated with FLAG-tagged Tulp1, followed by FITC-labeled anti-FLAG antibody and flow cytometry analysis.

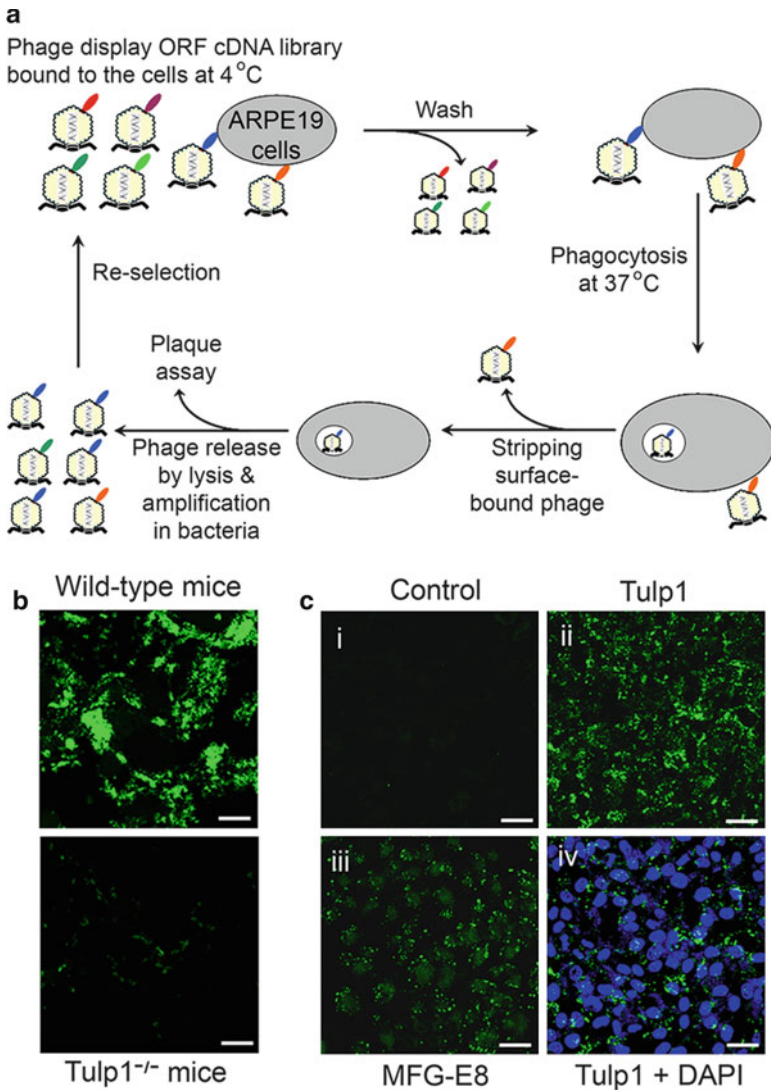


Fig. 88.1 Unbiased identification of phagocytosis ligands by ORF phage display. **(a)** The selection scheme of ORF phage display. **(b)** Membrane vesicles prepared from Tulp1^{-/-} mouse retina have reduced phagocytosis activity in ARPE19 cells. **(c)** FLAG-Tulp1 facilitates ARPE19 cell phagocytosis with membrane vesicles prepared from Neuro-2a cells. (Caberoy et al. 2010a with permission from *Exp. Cell Res.*)

88.3 Results

88.3.1 *Unbiased Identification of Tulp1 as a Phagocytosis Ligand*

We recently characterized the feasibility to enrich phagocytosis ligands by phage display (Caberoy et al. 2009). The question is whether this approach can be used for identification of unknown RPE phagocytosis ligands. Owing to uncontrollable protein reading frame, phage display with conventional cDNA library identified high percentage of non-ORF clones encoding short unnatural peptides (Li and Caberoy 2010), which have minimal implication in protein interaction networks. To address this problem, we constructed an ORF phage display cDNA library from adult mouse eye with minimal reading frame problem (Caberoy et al. 2010b). We designed a strategy of phagocytosis-based functional cloning for unbiased identification of RPE phagocytosis ligands (Fig. 88.1a) (Caberoy et al. 2010a). After three rounds of phage selection, functional analysis of enriched phage clones identified Tulp1 as a new ligand. Tulp1 as a ligand for RPE phagocytosis was independently validated by reduced phagocytosis with membrane vesicles prepared from Tulp1^{-/-} mouse retina (Fig. 88.1b). Recombinant FLAG-tagged Tulp1 was also capable of stimulating RPE phagocytosis (Fig. 88.1c). Tulp1 highly expressed in photoreceptor inner segments (Milam et al. 2000) has no classical signal peptide, but was characterized for its unconventional secretion (Caberoy and Li 2009), suggesting that it has the physiological access to its receptor on RPE surface.

88.3.2 *Characterization of MerTK as a Tulp1 Receptor*

To identify the receptor of Tulp1, we analyzed its binding to several known RPE phagocytosis receptors by Co-IP. The results showed that Tulp1 was a MerTK-binding protein (Fig. 88.2a). However, proteins with binding activity to a receptor may not always be real ligands, because proteins could bind to the receptor simply through nonligand binding sites without receptor activation and signaling cascade. A genuine ligand should be able to activate the cognate receptor and elicit receptor-specific signaling cascade. MerTK autophosphorylation has been widely used as a surrogate marker of its activation. The results showed that Tulp1 induced MerTK autophosphorylation in RPE cells (Fig. 88.2b). Moreover, Tulp1 induced rearrangement of NMMII-A (Fig. 88.2c), which was previously described as a MerTK-dependent signaling process (Strick et al. 2009). Excessive Mer-Fc blocked Tulp1-induced NMMII rearrangement (Fig. 88.2c).

Phagocytosis ligands, such as Gas6 and protein S of the only two unknown MerTK ligands, discriminatively bind to apoptotic cells, but not healthy cells, for selective phagocytic clearance of apoptotic cells. Likewise, these ligands in theory should specifically bind to shed POS vesicles, but not to unshed POS, so that only

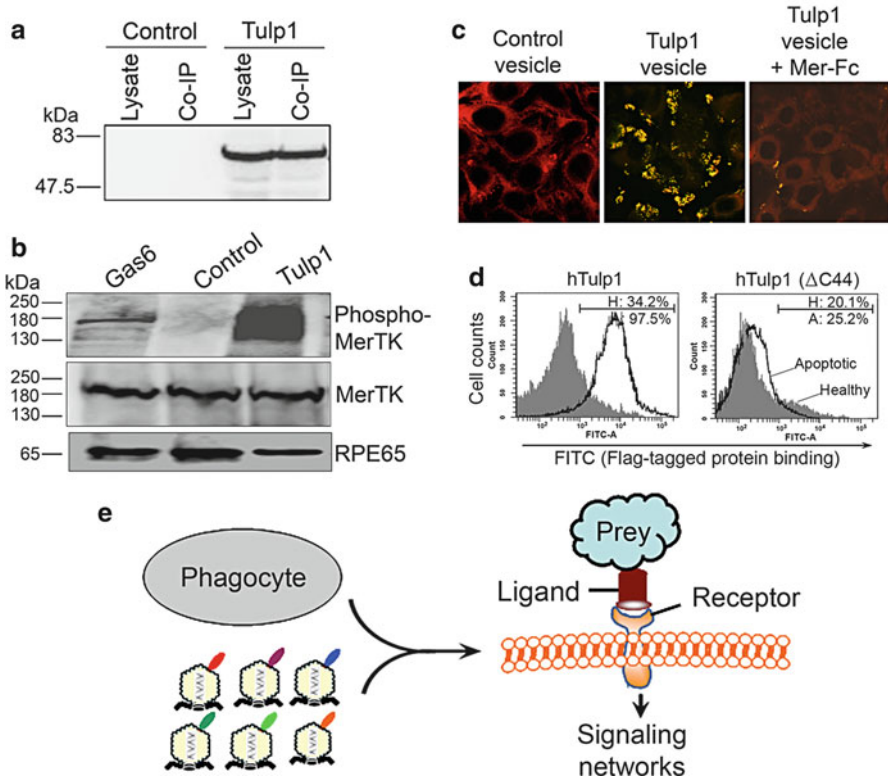


Fig. 88.2 Tulp1 as a new MerTK ligand. **(a)** Co-IP of Tulp1 and Mer-Fc. **(b)** MerTK autophosphorylation induced by Tulp1. Gas6 (50 nM) was included as a positive control. Western blots were analyzed using antibodies against phospho-MerTK, MerTK, or control RPE65 protein. **(c)** Tulp1-induced NMII-A rearrangement is blocked by excessive Mer-Fc. Red signal for NMII-A; green signal for GFP-labeled phagocytosed cargos; yellow signal, overlapping of the red and green signals. **(d)** Tulp1 binds to apoptotic cells, but not healthy cells. Deletion of C-terminal 44 amino acids abolished Tulp1 binding to apoptotic cells. (Caberoy et al. 2010c with permission from *EMBO J.* for a–d). **(e)** Unbiased mapping of phagocytosis ligands, receptors, intracellular signaling cascades and binding partners on preys by ORF phage display with phagocytosis-based functional selection

shed POS will be phagocytosed by RPE cells. However, it is technically difficult to prepare unshed POS for the analysis. Thus, we analyzed Tulp1 binding to apoptotic and healthy Jurkat cells. The results showed that Tulp1 selectively bound to apoptotic cells, but not healthy cells (Fig. 88.2d). Deletion of Tulp1 C-terminal end of 44 amino acids causes retinal degeneration with an unknown mechanism (Banerjee et al. 1998). This deletion also drastically reduced Tulp1 binding to apoptotic cells. Thus, these results indicated that the C-terminal domain of Tulp1 is essential for binding to phagocytosis preys.

88.4 Discussion

RPE phagocytosis is critical for the clearance of shed POS and the maintenance of the precise length of POS for its viability and photoexcitability. A handful of phagocytosis ligands, including Gas6, protein S, MFG-E8, were previously identified for a limited number of RPE phagocytosis receptors, such as MerTK, $\alpha_v\beta_5$ integrin and CD36. Most of these ligands and receptors were originally identified in macrophage phagocytosis on case-by-case basis with challenges and subsequently verified in RPE phagocytosis. The problem is that we really do not know the relative contribution of these ligands and receptors to RPE phagocytosis unless we thoroughly map and characterize all of them. However, identification of unknown signaling pathways for RPE phagocytosis is daunting in the absence of any molecular probe to begin with. By exploiting its unique functional character of phagocytosis, we identified Tulp1 as a new RPE ligand in the absence of receptor information by ORF phage display coupled with phagocytosis-based functional selection. This further led to identification of its receptor MerTK and characterization of the related intracellular signaling cascade. The C-terminal domain of Tulp1 with phagocytosis prey binding activity could be used as a bait to further identify its binding partners on apoptotic cells and POS vesicles in the future by yeast two hybrid system, mass spectrometry or even ORF phage display (Caberoy et al. 2010b). In summary, this study illustrated that the combination of ORF phage display and phagocytosis-based functional selection is capable of identifying phagocytosis ligands in the absence of receptor information (Fig. 88.2e). The intriguing part is that the heterogeneous ORF phage display cDNA library, when mixing with unknown heterogeneous receptors on phagocyte surface, is able to pull out new ligands with specific function. Identified ligands could be used as molecular probes to delineate their receptors, intracellular signaling cascades and binding partners on phagocytosis preys. By exploiting the only common functional characteristic of all phagocytes, this new strategy is able to unravel the mystery of molecular phagocyte biology in the absence of any molecular information. Conceivably, we should be able to thoroughly map all the ligands and receptors for RPE and other phagocytes by this new strategy to improve our capacity to modulate phagocytosis activity for disease therapy.

Acknowledgements We thank Dr. Douglas Graham for technical help with MerTK phosphorylation. This study was supported by NIH R01EY016211, R01EY016211-05S1, P30-EY014801, and an institutional grant from Research to Prevent Blindness.

References

- Banerjee P, Kleyn PW, Knowles JA et al (1998) TULP1 mutation in two extended Dominican kindreds with autosomal recessive retinitis pigmentosa. *Nat Genet* 18: 177–179
- Caberoy NB, Li W (2009) Unconventional secretion of tubby and tubby-like protein 1. *FEBS Lett* 583: 3057–3062

- Caberoy NB, Maiguel D, Kim Y, Li W (2010a) Identification of tubby and tubby-like protein 1 as eat-me signals by phage display. *Exp Cell Res* 316: 245–257
- Caberoy NB, Zhou Y, Jiang X et al (2010b) Efficient identification of tubby-binding proteins by an improved system of T7 phage display. *J Mol Recognit* 23: 74–83
- Caberoy NB, Zhou Y, Li W (2009) Can phage display be used as a tool to functionally identify endogenous eat-me signals in phagocytosis? *J Biomol Screen* 14: 653–661
- Caberoy NB, Zhou Y, Li W (2010c) Tubby and tubby-like protein 1 are new MerTK ligands for phagocytosis. *EMBO J (in press)*
- Li W, Caberoy NB (2010) New perspective for phage display as an efficient and versatile technology of functional proteomics. *Appl Microbiol Biotechnol* 85: 909–919
- Milam AH, Hendrickson AE, Xiao M et al (2000) Localization of tubby-like protein 1 in developing and adult human retinas. *Invest Ophthalmol Vis Sci* 41: 2352–2356
- Strauss O (2005) The retinal pigment epithelium in visual function. *Physiol Rev* 85: 845–881
- Strick DJ, Feng W, Vollrath D (2009) MerTK drives myosin II redistribution during retinal pigment epithelial phagocytosis. *Invest Ophthalmol Vis Sci* 50: 2427–2435

Chapter 89

Isolating Photoreceptor Compartment-Specific Protein Complexes for Subsequent Proteomic Analysis

Gregory H. Grossman, Gayle J.T. Pauer, George Hoppe,
and Stephanie A. Hagstrom

Keywords Photoreceptor • Retinal degeneration • Rhodopsin • Tulp1 • Mouse mutant • Trafficking

89.1 Introduction

Retinitis pigmentosa (RP) incorporates numerous genetically and phenotypically heterogeneous inherited retinal disorders, which affect over one million people worldwide (Boughman et al. 1980; Bunker et al. 1984). Mutations in *TULP1* cause an early onset form of autosomal recessive RP (Banerjee et al. 1998; Gu et al. 1998; Hagstrom et al. 1998; Paloma et al. 2000). Tulp1 is a photoreceptor-exclusive protein that is localized to the inner segment (IS), connecting cilium, perikarya, and synaptic terminals of the outer plexiform layer (OPL) (Hagstrom et al. 1999, 2001; Ikeda et al. 2000). *Tulp1*^{-/-} mice develop a rapid photoreceptor degeneration, in a manner similar to that in patients with RP due to *TULP1* mutations (Hagstrom et al. 1999). In these mice, the absence of Tulp1 results in distinct abnormalities that affect structure and function in separate photoreceptor compartments. Specifically, protein trafficking defects in the IS (Hagstrom et al. 1999, 2001) and a synaptic malformation (Xi et al. 2007; Grossman et al. 2009). This raises the question as to whether Tulp1 participates in separate, compartment-specific roles or if it functions

G.H. Grossman (✉) • G.J.T. Pauer • G. Hoppe
Department of Ophthalmic Research, Cole Eye Institute,
Cleveland Clinic, Cleveland, OH, USA
e-mail: grossmg@ccf.org

S.A. Hagstrom
Department of Ophthalmic Research, Cole Eye Institute, Cleveland Clinic,
9500 Euclid Avenue, Cleveland, OH 44195, USA

Department of Ophthalmology, Cleveland Clinic Lerner College of Medicine
of Case Western Reserve University, Cleveland, OH 44195, USA

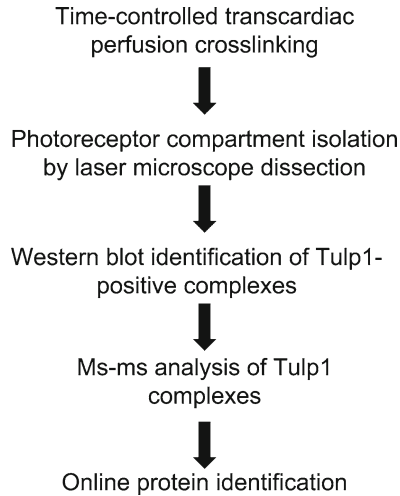


Fig. 89.1 The experimental design of the project, including the prospective use of tandem mass spectrometry (MS-MS) for identification of Tulp1 interactome constituents. First, time-controlled transcardiac perfusion (tcTPC) crosslinking with PFA is performed to maintain endogenous protein interactions. Second, laser microdissection (LMD) was performed to capture distinct compartments of the photoreceptor cells (IS and OPL), as well as a Tulp1-free control retinal sample (IPL). After the samples are pooled and homogenized, Western blot analysis using a Tulp1 antibody was conducted to identify Tulp1-containing complexes. Finally, protein constituents in the Tulp1-positive bands will be identified by MS-MS

in a generalized role necessary for multiple cellular processes. If Tulp1 performs two independent functions, we would expect two distinct compartment-specific interactomes rather than a singular set of interacting proteins. To address this question, we developed a method to separate photoreceptor compartments for downstream comparison of Tulp1-interacting proteins in the IS and the OPL. Our experimental design combined time-controlled transcardiac perfusion crosslinking (tcTPC) for capturing endogenous weak and/or transient interactions, laser microdissection (LMD) for isolating separate photoreceptor compartments, and Western blot analysis for detection of Tulp1-positive complexes (Fig. 89.1).

89.2 Materials and Methods

89.2.1 Animals

Tulp1^{-/-} mice were generated and genotyped as described previously (Hagstrom et al. 1999). All mice used in this study were postnatal day 16. All experiments on animals were approved by the Institutional Animal Care and Use Committee of the

Cleveland Clinic and were performed in compliance with the ARVO Statement for the Use of Animals in Ophthalmic and Visual Research.

89.2.2 Time-Controlled Transcardiac Perfusion Crosslinking (tcTPC)

TcTPC was carried out using a modified protocol that has previously been described (Schmitt-Ulms et al. 2004). Mice were anesthetized intraperitoneally with a mixture of ketamine (80 mg/kg) and xylazine (16 mg/kg). The thoracic cavity was opened and a 25-gauge $\times 3/4'' \times 12''$ Blood Collection Set (Becton Dickinson 367298) was inserted into the left ventricle. Prior to this insertion, a small cut was introduced into one of the lobes of the liver. A 4% paraformaldehyde (PFA) solution was prepared daily by diluting a 16% EM grade solution (Electron Microscopy Solutions; #15710-S) in 0.1 M PBS. The PFA solution was perfused for 8 min at a rate of 8 mL/min by a peristaltic pump (Fisher Scientific; #13-876-1) to covalently crosslink interacting proteins in vivo. A successful commencement of perfusion was indicated by an immediate color change of the heart and a lightening in the color of the liver within 30 s in the lobe that was cut. The inlet line was then switched to a solution of 2.6 M Tris pH 7.5 and perfused for 2 min to flush the PFA and stop crosslinking. A successful perfusion was indicated by a rigid neck and semiclear fluid after enucleation.

89.2.3 Preparation of Retinal Sections

After perfusion, the eyes were rapidly removed and placed into ice-cold Tris with Complete protease inhibitors (Fisher Scientific; #50-720-3977). The cornea and lens were removed, and the posterior pole was left in the Tris/complete solution on ice for 10 min. The poles were then transferred to ice-cold 0.1 M PBS for 5 min. The poles were embedded in OCT freezing medium, flash frozen on powdered dry ice, and transferred to -80°C . The frozen tissue was sectioned at 10 μm thickness with a cryostat (Leica, Wetzlar, Germany), and collected onto LMD slides (Leica, Wetzlar, Germany; Pet-membrane 1.4 μm #11505151). The sections were then lightly stained with hematoxylin and eosin for visualization of the retinal layers.

89.2.4 Laser Microdissection

All retinal compartment samples were isolated and collected using the Leica AS-LMD Laser Microdissection system with an automated stage and UV laser (Leica, Wetzlar, Germany). The laser was calibrated to the 20 \times objective lens as per the manufacturer's instructions. The following laser settings were used: aperture: 7, intensity: 45, speed: 5, bridge: fixed, offset: 26, and aperture difference: 6.

The compartments were dissected sequentially beginning with the apical OPL followed the IS and the inner plexiform layer (IPL). The dissected tissues were collected into separate centrifuge tubes and flash frozen. Digital images before and after laser dissection were archived to verify sampling location. It is important to note that one compartment was collected throughout the entire slide before moving onto the next compartment. This procedure along with the digital image capture after each extraction ensured that samples were not mixed. After the collection of all samples from an entire eye, the tubes collected from each compartment were pooled. The tissue was homogenized in 100 μ L of lysis buffer containing 50 mM Tris pH 8.0, 150 mM NaCl, 10% Glycerol, 0.5% Triton X-100, and 0.1% NP 40. The homogenate was vortexed gently, followed by rotation for 15 min at 4°C. The solution was centrifuged at 4,000 rpm for 10 min at 4°C, and the supernatant was stored at -80°C.

89.2.5 Retinal Homogenate

Following tcTPC, retinas from wt and *tulp1*^{-/-} mouse eyes were removed and homogenized under the same conditions as described above in the section immediately above.

89.2.6 Western Blotting Analysis

Western blot analysis was performed as previously described (Hagstrom et al. 2001; Xi et al. 2003, 2005, 2007). Briefly, proteins were separated on SDS-polyacrylamide gels and electroblotted to polyvinylidene difluoride membranes. The membranes were then incubated with a rabbit polyclonal M-tulp1N, diluted 1:1,000. This was followed by the hybridization of peroxidase-conjugated secondary antibodies and exposure to chemiluminescence.

89.3 Results

89.3.1 Isolation and Capture of Photoreceptor Compartments

Figure 89.2 shows photomicrographs of a mouse retinal section before and after LMD. In Fig. 89.2a, the IS, OPL, and IPL are clearly visible. In Fig. 89.2b, two separate white lines encircle the IS and the OPL. These cursor lines are drawn over the microscope image within the software and become the tracking path of the laser. Figure 89.2c shows the same retinal image after the laser cut. The clear areas are regions in which the tissue has been extracted. These images show that our

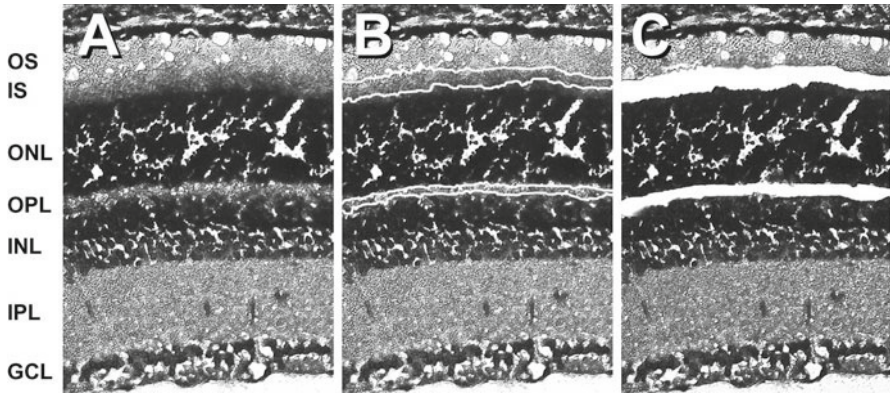


Fig. 89.2 This panel shows photomicrographs of a LMD experiment in a wt retinal section. (a) The IS and OPL are clearly visible. (b) The cursor line is drawn over the image and is the tracking path of the laser. (c) The image of the same retina taken after the laser cut through the tissue. The clear area is the region in which the tissue has been extracted

laser settings were powerful enough to cut through the fixed tissue sections yet optimal for extracting discrete cellular compartments without damaging other portions of the retina.

89.3.2 *Tulp1* Complexes in the Retina

We performed western blot analysis on native and crosslinked whole retinal homogenates from wt and *tulp1*^{-/-} animals. Results indicate a band at the correct predicted molecular weight of 78 kDa for Tulp1 in the crosslinked and native wt tissue, but not in the crosslinked or native *tulp1*^{-/-} tissue (data not shown). Furthermore, additional bands were detected above 150 kDa only in the wt-crosslinked homogenate. This data indicates that tcTPC is sufficient to crosslink proteins in retinal tissue, resulting in Tulp1 complexes.

89.3.3 *Tulp1* Compartment-Specific Complexes

Figure 89.3 shows a Western blot experiment of crosslinked retinal samples. In the whole retinal homogenate of one wt mouse eye, a band corresponding to Tulp1 is detected at ~78 kDa. This band is also present in the IS- and OPL-isolated samples. Importantly, this band is not detected in the IPL-isolated sample, as Tulp1 is not expressed in cells of this retinal layer. Two additional bands are seen at ~150 and

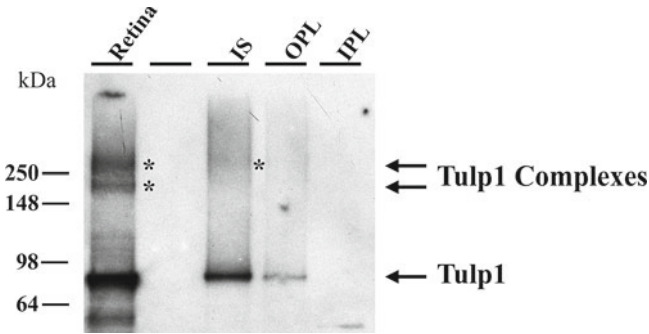


Fig. 89.3 This image shows the western blot analysis of cross-linked retinal samples using a Tulp1 antibody. In the crosslinked whole retinal homogenate, as well as in the IS- and OPL-isolated samples, a band corresponding to Tulp1 is detected at ~78 kDa. However, as expected, Tulp1 is not detected in the IPL-isolated sample. This indicates that our sampling method is contamination free. In the crosslinked whole retinal homogenate, two additional bands are detected at ~150 and ~280 kDa, indicating discrete Tulp1 complexes. In the IS sample, but not the OPL, a band matching the 280 kDa band in the retinal lysate is present, indicating a compartment-specific Tulp1 complex

~280 kDa (Fig. 89.3: double asterisk) in the whole retinal homogenate, indicating discrete Tulp1 complexes. Interestingly, a band matching the 280 kDa band (Fig. 89.3: single asterisk) seen in the wt retinal homogenate is present in the IS sample, but not the OPL sample.

89.4 Discussion

Herein, we report a strategy for the detection of Tulp1 complexes from separate photoreceptor compartments. Our overall goal is to reveal the mechanism(s) of action of Tulp1 in the photoreceptor by identifying Tulp1-interacting partners. It is now well understood that certain proteins have compartment-specific functions within a cell (Smalheiser 1996). Tulp1 is expressed in separate photoreceptor compartments, the IS and synapse. Therefore, we developed a strategy to compare Tulp1-interacting proteins between these two compartments. We combined two approaches to satisfy our criteria. First, we used tcTPC to conserve endogenous protein interactions, including the retention of low abundant and transient proteins (Schmitt-Ulms et al. 2004). Secondly, we used LMD to isolate and verify cellular compartments. The novel combination of these two techniques allowed us to identify several distinct Tulp1 complexes in the wt retina, which may indicate that Tulp1 forms multiple interactomes. Moreover, our results provide evidence that Tulp1 may have distinct compartment-specific interactomes. Proteomic analysis of the bands in these experiments should clarify the different roles that Tulp1 plays in the IS and OPL.

Acknowledgments This study was supported by National Institute of Health Grants EY16072 and EY15638 (SAH), Foundation Fighting Blindness (SAH), Fight for Sight (GHG), Research to Prevent Blindness (RPB) Center Grant, RPB Sybil B. Harrington Special Scholar Award (SAH), and Hope for Vision (SAH).

References

- Banerjee P, Kleyn PW, Knowles JA et al (1998) TULP1 mutation in two extended Dominican kindreds with autosomal recessive retinitis pigmentosa. *Nat Genet* 18:177–179
- Boughman JA, Conneally PM, Nance WE (1980) Population genetic studies of retinitis pigmentosa. *Am J Hum Genet* 32:223–235
- Bunker CH, Berson EL, Bromley WC et al (1984) Prevalence of retinitis pigmentosa in Maine. *Am J Ophthalmol* 97:357–365
- Grossman GH, Pauer GJ, Narendra U et al (2009) Early synaptic defects in *tulp1*^{-/-} mice. *Invest Ophthalmol Vis Sci* 50:3074–3083
- Gu S, Lennon A, Li Y et al (1998) Tubby-like protein-1 mutations in autosomal recessive retinitis pigmentosa. *Lancet* 351:1103–1104
- Hagstrom SA, Duyao M, North MA et al (1999) Retinal degeneration in *tulp1*^{-/-} mice: vesicular accumulation in the interphotoreceptor matrix. *Invest Ophthalmol Vis Sci* 40:2795–2802
- Hagstrom SA, North MA, Nishina PL et al (1998) Recessive mutations in the gene encoding the tubby-like protein TULP1 in patients with retinitis pigmentosa. *Nat Genet* 18:174–176
- Hagstrom SA, Adamian M, Scimeca M et al (2001) A role for the Tubby-like protein 1 in rhodopsin transport. *Invest Ophthalmol Vis Sci* 42:1955–1962
- Ikeda S, Shiva N, Ikeda A et al (2000) Retinal degeneration but not obesity is observed in null mutants of the tubby-like protein 1 gene. *Hum Mol Genet* 9:155–163
- Paloma E, Hjelmqvist L, Bayes M et al (2000) Novel mutations in the TULP1 gene causing autosomal recessive retinitis pigmentosa. *Invest Ophthalmol Vis Sci* 41:656–659
- Schmitt-Ulms G, Hansen K, Liu J et al (2004) Time-controlled transcardiac perfusion cross-linking for the study of protein interactions in complex tissues. *Nat Biotechnol* 22:724–731
- Smalheiser NR (1996) Proteins in unexpected locations. *Mol Biol Cell* 7:1003–1014
- Xi Q, Pauer GJ, West KA et al (2003) Retinal degeneration caused by mutations in TULP1. *Adv Exp Med Biol* 533:303–308
- Xi Q, Pauer GJ, Marmorstein AD et al (2005) Tubby-like protein 1 (TULP1) interacts with F-actin in photoreceptor cells. *Invest Ophthalmol Vis Sci* 46:4754–4761
- Xi Q, Pauer GJ, Ball SL et al (2007) Interaction between the photoreceptor-specific tubby-like protein 1 and the neuronal-specific GTPase dynamin-1. *Invest Ophthalmol Vis Sci* 48:2837–2844

Chapter 90

Expression of the Integrin Coreceptor Transglutaminase-2 in the RPE In Vivo and in Culture

Linda Ruggiero and Silvia C. Finnemann

Keywords Retinal pigment epithelium • Retina • Integrins • Transglutaminase 2 • Protein expression • Protein localization

90.1 Introduction

In the mammalian retina, rod photoreceptors shed the tips of their outer segments (POS) each morning following light onset (Young 1967). These POS are swiftly removed by the adjacent retinal pigment epithelium (RPE) via phagocytosis that involves coordinated activities of numerous membrane and cytoplasmic proteins (Young and Bok 1969). RPE cells in the healthy retina complete uptake and digestion of shed rod POS within a few hours after POS shedding. We previously found that RPE cells in culture fail to tether isolated POS for subsequent phagocytosis within about 12 h of a previous phagocytic challenge, although the principal tethering receptor for POS, $\alpha\text{v}\beta 5$ integrin, remains abundant at the apical, phagocytic surface of these RPE cells (Finnemann 2003b). These data suggest that RPE cells may increase or decrease their phagocytic competence by altering the activity of the POS-binding receptor $\alpha\text{v}\beta 5$ integrin. Indeed, RPE cells that lack $\alpha\text{v}\beta 5$ do not phagocytose shed POS in a diurnal rhythm, but exhibit constant levels of POS uptake at all times of day (Nandrot et al. 2004).

The molecular mechanism of particle recognition, tethering, and phagocytosis of RPE cells is similar to the molecular mechanisms used by bone marrow-derived macrophages and dendritic cells for removal of apoptotic cells. Like RPE cells, dendritic cells employ $\alpha\text{v}\beta 5$ integrin, while macrophages mainly use the related

L. Ruggiero • S.C. Finnemann (✉)

Department of Biological Sciences, Fordham University, Bronx, NY 10458, USA
e-mail: finnemann@fordham.edu

$\alpha\upsilon\beta 3$ but can be stimulated to use $\alpha\upsilon\beta 5$ as well (Finnemann et al. 1997; Albert et al. 1998; Finnemann and Rodriguez-Boulan 1999; Lucas et al. 2006). In all three cell types, the phagocytic particle binds to the integrin-tethering receptor indirectly via a soluble bridge protein, like the retina's MFG-E8, that contains both phosphatidylserine (PS) and integrin receptor-binding domains (Hanayama et al. 2002; Nandrot et al. 2007). Exposure of PS as an "eat me" signal by cells undergoing apoptosis has been studied extensively and is known to be sufficient for their engulfment by phagocytic cells (Schlegel and Williamson 2001). Notably, the specific molecular changes designating shedding POS tips in the retina remain poorly understood in comparison.

Little is known about the regulation of integrin receptor activity in preparation for or subsequent to phagocytic particle binding. The multifunctional soluble protein transglutaminase 2 (TG2) may act as coreceptor of $\beta 1$ or $\beta 3$ integrins (Akimov et al. 2000). Studies exploring TG2^{-/-} mice have recently shown that a complex of secreted TG2, MFG-E8, and $\alpha\upsilon\beta 3$ promotes clearance of apoptotic cells in macrophages (Toth et al. 2009). Interestingly, TG2 has been found to be associated with $\beta 5$ integrins on the surface of malignant melanoma cells, although its function in this system remains unknown (Fok et al. 2006). Depending on tissue and cell type, TG2 may localize intracellularly in the cytoplasm or nucleus, as well as extracellularly on the cell surface or in the extracellular matrix (Upchurch et al. 1991; Lesort et al. 1998; Verderio et al. 1998). Here, we report TG2 expression, localization, and relation to $\alpha\upsilon\beta 5$ integrin in murine retina and RPE.

90.2 Materials and Methods

90.2.1 *Animals and Tissue Collection*

Wild-type Long Evans rats, wild-type 129T2/SvEmsJ mice, and $\beta 5^{-/-}$ mice in the same background characterized previously (Nandrot et al. 2004, 2007) were housed under cyclic 12 h light: 12 h dark conditions and fed ad libitum. Three-month-old mice were sacrificed by CO₂ asphyxiation for tissue collection. Briefly, eyes were enucleated immediately postmortem. Following opening of cornea and removal of the lens, whole eyecups were either lysed or fixed as described below. Neural retina and eyecups with remaining RPE and choroid were isolated from whole eyecups by first incubating whole eyecups in Hanks buffer without Ca²⁺ and Mg²⁺ for 5 min before performing radial cuts toward the optic nerve, flattening eyecups in a dry petri dish, and removing the neural retina with a forceps with bent tip. Primary RPE was isolated from eyes of 10-day-old rat pups following a two-step protocol using hyaluronidase and trypsin described previously (Finnemann 2003a) and seeded on coverslips. All procedures were approved by the Fordham University Institutional Animal Care and Use Committee and adhered to the ARVO statement for the use of animals in ophthalmic and vision research.

90.2.2 Immunofluorescence Microscopy

Whole eyecups were incubated in 4% paraformaldehyde in 1X PBS for 10 min at RT. The lens was removed and the remaining retina and eyecup were incubated in 15% sucrose, 30% sucrose, and frozen in OCT. Primary rat RPE cells were fixed in ice-cold 95% ethanol, 5% acetic acid. 15 μ m-thick eyecup cross-sections or primary RPE were labeled with TG2 antibody (Santa Cruz Biotechnology) and secondary antibody conjugated to AlexaFluor488. Primary RPE was further labeled with β -catenin antibody (Sigma) and secondary antibody conjugated to AlexaFluor568. Nuclei were stained with DAPI. Mounted coverslips or sections were imaged on a Leica TSP5 confocal microscopy system.

90.2.3 Immunoblotting

Tissue samples were solubilized in 50 mM HEPES (pH 7.4), 150 mM NaCl, 10% glycerol, 1.5 mM MgCl₂, and 1% Triton X-100 with 1% of protease inhibitor cocktail (Sigma). Cleared lysates of whole mouse eyecups, isolated mouse neural retina, or eyecup without neural retina were separated on 10% SDS-polyacrylamide gels and electroblotted. Immunoblots were probed with primary antibodies to TG2, β 5 integrin (both Santa Cruz Biotechnology), or β -actin (Sigma), and processed for enhanced chemiluminescence detection.

90.3 Results

90.3.1 Comparison of TG2 Protein Levels of Wild-Type and β 5^{-/-} Mouse Eyecups

We first performed immunoblotting experiments to test if TG2 expression can be detected in the mouse eye. Figure 90.1 shows that TG2 antibody detects two bands in whole eyecup lysates migrating at ~80 kDa, the expected molecular size of mouse TG2, and an additional band at ~110 kDa that, to our knowledge, had not been reported previously. We subsequently incubated the same protein blots for β 5 integrin and for β -actin. These controls confirmed the genotype of our samples and that both samples had approximately the same total protein content. These results demonstrate equal levels of TG2 in whole eye lysates obtained from wild-type and β 5^{-/-} mice, indicating that loss of the integrin does not affect steady state levels of TG2.

Fig. 90.1 Comparison of TG2 levels in wild-type and $\beta 5^{-/-}$ eyecups. TG2 immunoblotting of whole eyecup samples from wild-type (wt) and $\beta 5^{-/-}$ yields two bands, at the expected molecular size of ~80 kDa (*arrow head*) and, unexpectedly, at ~110 kDa (*arrow*). Reprobing of the same blot for $\beta 5$ integrin and β -actin blotting confirmed genotype and equal load of samples (lanes as indicated)

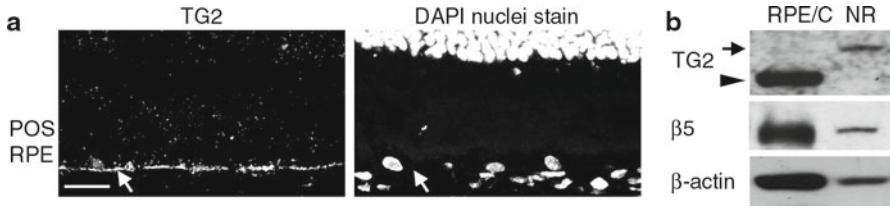
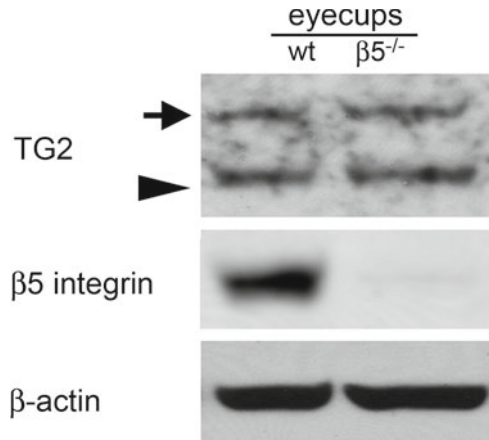


Fig. 90.2 Expression and localization of TG2 in mouse RPE in situ. (a) Image shows a representative cross-section of 3-month-old wild-type mouse retina labeled for TG2 (*left panel*) and counterstained with DAPI (*right panel*). Staining for TG2 is visible in the RPE (*arrow*), but not in the outer segment region. Scale bar equals 20 μ m. (b) Comparison of TG2 levels in wild-type mouse eyecup fractions containing either neural retina (NR) or RPE and choroid (RPE/C). TG2 of expected molecular size of 80 kDa is detected only in the RPE and choroid (*arrowhead*), while the unidentified band at 110 kDa is detected only in the NR (*arrow*)

90.3.2 Localization of TG2 in Wild-Type Mouse Retina

To determine the localization of TG2 in the mouse retina, we next performed TG2 immunofluorescence labeling of wild-type mouse eye cryosections. We observed TG2 at the basal aspect of the RPE (*arrow*), but did not detect it in the photoreceptor outer segment region (Fig. 90.2a). We did not observe TG2 staining in other regions of the neural retina either (data not shown). To confirm this result, we analyzed isolated neural retina and eyecups without neural retina, but containing RPE and choroid of wild-type mice by immunoblotting. We found that TG2 at the expected molecular size of 72 kDa (*arrow head*) is concentrated in the RPE/choroid containing eyecups and not detected in the neural retina fraction (Fig. 90.2b). The unexpected

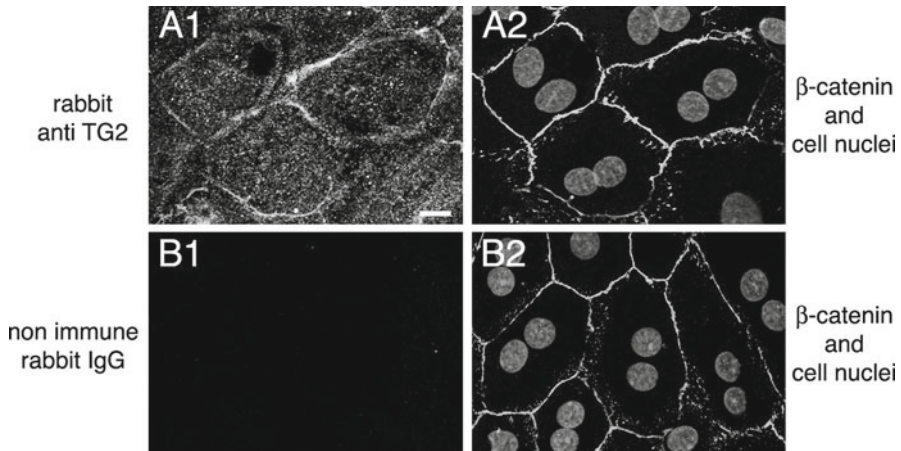


Fig. 90.3 Localization of TG2 in rat primary RPE. A1, A2: images show a representative field labeled with TG2 (A1) and β -catenin (adherens junctions) antibodies and DAPI (nuclei) (overlay of both in A2). Scale bar equals 10 μ m. B1, B2: images show a representative field labeled with nonimmune rabbit IgG (B1), β -catenin antibody, and DAPI (overlay of both in B2) demonstrating specificity of the TG2 signal in A1

110 kDa band of the TG2 blot (arrow) was detected only in the neural retina fraction. Whether or not this band represents a form of TG2 remains unknown. Taken together, immunofluorescence microscopy and tissue fractionation experiments suggest that TG2 in the mouse eyecup is mostly expressed by the RPE.

90.3.3 Localization of TG2 in Wild-Type Rat RPE in Primary Culture

RPE cells in primary culture may differ from RPE cells in the eye with respect to protein expression or subcellular localization. To determine if this was the case for TG2, we seeded isolated patches of wild-type rat RPE on coverslips and studied their TG2 expression using immunofluorescence microscopy. Figure 90.3A1 shows cytoplasmic TG2 protein distribution in primary RPE that is markedly enriched at lateral membranes. There, TG2 partially overlaps with the cytoplasmic protein β -catenin that is part of the lateral adherens junction complex (compare Fig. 90.3A1 with Fig. 90.3A2). TG2 staining was specific as incubation of fixed cells with secondary antibody alone did not produce labeling (Fig. 90.3B1).

90.4 Discussion

The association of TG2 with β integrins and their ligands and its role in the phagocytosis of apoptotic cells by macrophages led us to speculate that TG2 may also play a role in the $\alpha\text{v}\beta 5$ integrin-dependent phagocytosis of POS by RPE cells. Here, we determined TG2 expression in whole eyecup lysates from $\beta 5^{-/-}$ mice and found that they do not differ from wild-type mouse eyecups in TG2 expression levels. Furthermore, we examined TG2 expression in the mouse eye by immunohistochemistry and by immunoblotting and found that TG2 is present in the RPE but is absent from its apical, phagocytic surface and from photoreceptor outer segments. Finally, RPE cells in primary culture, which possess apical $\alpha\text{v}\beta 5$ integrin and vigorous phagocytic activity toward experimental particles, retain basolateral TG2 expression. Taken together, these results suggest that TG2 is unlikely to form a direct complex with the phagocytic machinery. Rather, TG2 may participate in processes specific to the basolateral aspect of the RPE. TG2 has been shown to regulate adhesion to fibronectin by acting as coreceptor of $\alpha 3$ and $\alpha 1$ integrins in fibroblasts (Akimov et al. 2000). RPE cells possess a number of basolateral integrins that mediate adhesion to Bruch's membrane components (Finnemann et al. 1997). It is thus possible that TG2 regulates RPE interactions with its extracellular matrix. Alternately, TG2 in the RPE may function independently of integrins.

Acknowledgments These studies were supported by NIH grant EY-13295 to S.C.F.

References

- Akimov SS, Krylov D, Fleischman LF et al (2000) Tissue transglutaminase is an integrin-binding adhesion coreceptor for fibronectin. *J Cell Biol* 148:825–838
- Albert ML, Pearce SFA, Francisco LM et al (1998) Immature dendritic cells phagocytose apoptotic cells via $\alpha\text{v}\beta 5$ and CD36, and cross-present antigens to cytotoxic T lymphocytes. *J Exp Med* 188:1359–1368
- Finnemann SC (2003a) Focal adhesion kinase signaling promotes phagocytosis of integrin-bound photoreceptors. *EMBO J* 22:4143–4154
- Finnemann SC (2003b) Role of $\alpha\text{v}\beta 5$ integrin in regulating phagocytosis by the retinal pigment epithelium. *Adv Exp Med Biol* 533:337–342
- Finnemann SC, Rodriguez-Boulan E (1999) Macrophage and retinal pigment epithelium phagocytosis: apoptotic cells and photoreceptors compete for $\alpha\text{v}\beta 3$ and $\alpha\text{v}\beta 5$ integrins, and protein kinase C regulates $\alpha\text{v}\beta 5$ binding and cytoskeletal linkage. *J Exp Med* 190:861–874
- Finnemann SC, Bonilha VL, Marmorstein AD et al (1997) Phagocytosis of rod outer segments by retinal pigment epithelial cells requires $\alpha\text{v}\beta 5$ integrin for binding but not for internalization. *Proc Natl Acad Sci USA* 94:12932–12937
- Fok JY, Ekmekcioglu S, Mehta K (2006) Implications of tissue transglutaminase expression in malignant melanoma. *Mol Cancer Ther* 5:1493–1503
- Hanayama R, Tanaka M, Miwa K et al (2002) Identification of a factor that links apoptotic cells to phagocytes. *Nature* 417:182–187
- Lesort M, Attanavanich K, Zhang J et al (1998) Distinct nuclear localization and activity of tissue transglutaminase. *J Biol Chem* 273:11991–11994

- Lucas M, Stuart LM, Zhang A et al (2006) Requirements for apoptotic cell contact in regulation of macrophage responses. *J Immunol* 177:4047–4054
- Nandrot EF, Kim Y, Brodie SE et al (2004) Loss of synchronized retinal phagocytosis and age-related blindness in mice lacking $\alpha 5$ integrin. *J Exp Med* 200:1539–1545
- Nandrot EF, Anand M, Almeida D et al (2007) Essential role for MFG-E8 as ligand for $\alpha 5$ integrin in diurnal retinal phagocytosis. *Proc Natl Acad Sci USA* 104:12005–12010
- Schlegel RA, Williamson P (2001) Phosphatidylserine, a death knell. *Cell Death Differ* 8:551–563
- Toth B, Garabuczi E, Sarang Z et al (2009) Transglutaminase 2 is needed for the formation of an efficient phagocyte portal in macrophages engulfing apoptotic cells. *J Immunol* 182:2084–2092
- Upchurch HF, Conway E, Patterson MK, Jr. et al (1991) Localization of cellular transglutaminase on the extracellular matrix after wounding: characteristics of the matrix bound enzyme. *J Cell Physiol* 149:375–382
- Verderio E, Nicholas B, Gross S et al (1998) Regulated expression of tissue transglutaminase in Swiss 3 T3 fibroblasts: effects on the processing of fibronectin, cell attachment, and cell death. *Exp Cell Res* 239:119–138
- Young RW (1967) The renewal of photoreceptor cell outer segments. *J Cell Biol* 33:61–72
- Young RW, Bok D (1969) Participation of the retinal pigment epithelium in the rod outer segment renewal process. *J Cell Biol* 42:392–403

Chapter 91

On Your Marks... Get Bound... Internalize!

Ah-Lai Law and Emeline F. Nandrot

Keywords Retinal pigment epithelium • Photoreceptor outer segments • Phagocytosis • Daily rhythm • $\alpha v \beta 5$ integrin • MFG-E8 • FAK • MerTK • Annexin 2

91.1 Introduction

Membranous disks of photoreceptor outer segments (POS) containing photopigments are constantly being produced and shed from the distal end of photoreceptors (PR). Elimination of these aged POS by the retinal pigment epithelium (RPE) is indispensable for the proper functioning of both rod and cone PRs. This internalization process allows the degradation of accumulated photo-oxidative compounds and maintains constant PR length and the delicate balance of proteins, lipids, and metabolites in both PR and RPE cells. This chapter is a short review of the molecules known to be involved in the three steps required for rod PR phagocytosis: particle recognition, binding, and internalization.

A.-L. Law • E.F. Nandrot (✉)
INSERM, U968, Paris 75012, France

Genetics Department, UPMC Univ Paris 06, UMR_S 968,
Institut de la Vision, Paris 75012, France

CNRS, UMR_7210, 17 rue Moreau, Paris 75012, France
e-mail: emeline.nandrot@inserm.fr

91.2 On Your Marks...

Circadian rhythms play an important role in regulating PR turnover: rods shed their distal POS tips at the onset of light (LaVail 1976), followed by a burst of phagocytosis by RPE cells to clear shed POS tips (Young and Bok 1969) (Fig. 91.1a). Components of the RPE phagocytic machinery must recognize “eat me” signals displayed on POS tips to stimulate the timely engulfment that follows POS shedding. The best studied “eat me” signal is the exposure of phosphatidylserine (PS) on the external membrane leaflet of apoptotic cells. Similar to apoptotic cells, POS disk membranes were shown to contain PS (Boesze-Battaglia and Albert 1992), and normal RPE cells specifically bind and/or internalize PS-containing liposomes (Ryeom et al. 1996a).

In recent years, animal models helped us identify several key molecules that compose this machinery. $\alpha v\beta 5$ integrin receptors, uniquely expressed on the apical surface of polarized RPE cells, are required for the synchronized peak of phagocytosis observed about two hours after light onset (Nandrot et al. 2004). Mice deficient in $\beta 5$ integrin resulted in loss of the phagocytic rhythm, age-related accumulation of lipofuscin, and blindness, as well as an overall decrease in retinal adhesion (Nandrot et al. 2006).

$\alpha v\beta 5$ integrin binding to shed POS is mediated by its ligand milk fat globule-EGF-factor 8 (MFG-E8), which is secreted by RPE cells (Nandrot et al. 2007), by recognition of $\alpha v\beta 5$ RGD motifs (Finnemann et al. 1997). In wild-type RPE

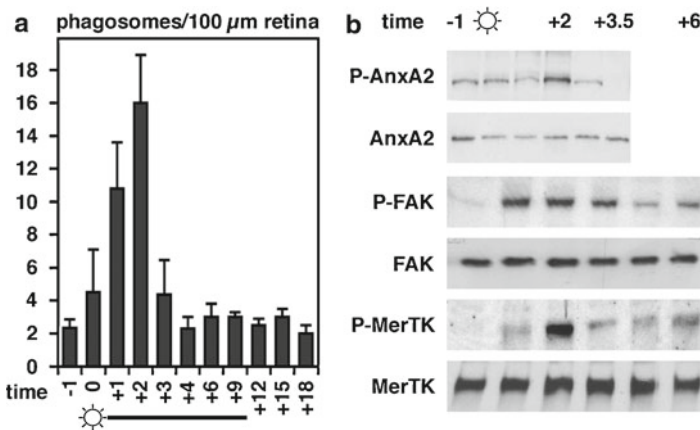


Fig. 91.1 Molecules of the RPE phagocytic machinery are sequentially activated. (a, b) We harvested eyecups from wild-type mice at different time-points during the day. (a) Number of phagosomes present in RPE cells were counted on retinal sections and peak 2 h after light onset. (b) Protein lysates were analyzed by SDS-PAGE and immunoblotted for total and tyrosine-phosphorylated proteins as indicated. Modified from © Nandrot et al. (2004) and Law et al. (2009). Originally published in *The Journal of Experimental Medicine*. doi: 10.1084/jem.20041447 and in *Molecular Biology of the Cell* doi: 10.1091/mbc.E08-12-1204

supplemented with MFG-E8, POS binding was significantly increased while there was no effect on RPE lacking $\alpha\beta 5$. The phenotype exhibited by MFG-E8^{-/-} mice mirrors those of $\beta 5$ ^{-/-} mice with loss of the synchronized peak of phagocytosis while maintaining steady-state levels of uptake, although absence of MFG-E8 results in a negligible decrease in retinal adhesion and animals do not develop age-related blindness (Nandrot et al. 2007).

MFG-E8 secreted from macrophages has also been shown to link PS on apoptotic cells to $\alpha\beta 3$ integrin receptors (Hanayama et al. 2002). In addition, POS quantitatively compete with apoptotic cells for binding to $\alpha\beta 5$, indicating that POS and apoptotic cells expose surface signals that are recognized by both $\alpha\beta 3$ and $\alpha\beta 5$ integrins (Finnemann and Rodriguez-Boulan 1999).

91.3 Get Bound...

Following POS engagement, focal adhesion kinase (FAK) colocalization with $\alpha\beta 5$ on the RPE apical surface increases and FAK is activated through tyrosine-phosphorylation (Finnemann 2003). In vivo rhythmic phosphorylation of FAK is followed by phosphorylation of the mer tyrosine kinase (MerTK) internalization receptor, both receptor activities increasing promptly after light onset (Nandrot et al. 2004) (Fig. 91.1b). Subsequent internalization of POS coincides with the dissociation of activated FAK from $\alpha\beta 5$. Inhibition of FAK signaling did not affect $\alpha\beta 5$ -dependant binding, but blocked internalization. Inhibition of FAK signaling also diminished MerTK phosphorylation, which suggests that MerTK activation is, either directly or indirectly, mediated by FAK and thus provides a critical link between POS binding and internalization (Finnemann 2003).

A naturally occurring gene deletion in the Royal College of Surgeons (RCS) rat results in a nonfunctional truncated MerTK protein (Nandrot et al. 2000; D'Cruz et al. 2000). RPE cells from RCS rats are able to bind POS but cannot internalize them (Chaitin and Hall 1983), leading to an accumulation of shed POS in the sub-retinal space and rapid PR loss, resulting in blindness (LaVail et al. 1981). This defect is rescued when wild-type MerTK is expressed in both cultured RCS RPE cells and RCS rat retina, demonstrating that MerTK is a necessary component of POS phagocytosis (Vollrath et al. 2001).

Although rhythmic activation of MerTK is mediated by $\alpha\beta 5$ in vivo, activation of MerTK during POS phagocytosis could also be stimulated in vitro by its own ligands: growth arrest-specific gene 6 (Gas6) and protein S (ProS). Both proteins are able to interact with negatively charged PS (Hall et al. 2002) and bind directly to the TAM family of tyrosine kinase receptors that include MerTK (Nyberg et al. 1997). Gas6 was long thought to be the cognate ligand for MerTK and binding of Gas6 to POS was shown to stimulate POS phagocytosis in vitro (Hall et al. 2001). However, Gas6 knockout mice do not display any phagocytic defect or PR degeneration as opposed to Mer kinase-dead (Mer^{KD}) mice (Prasad et al. 2006). In contrast, there has been substantial evidence to support a role for ProS as a ligand for

MerTK: ProS greatly stimulates POS internalization in vitro, its depletion inhibits internalization, and it is expressed in the retina, suggesting that ProS could also be a regulator of RPE phagocytosis (Hall et al. 2005; Prasad et al. 2006).

More recently, the CD81 tetraspanin receptor was found to contribute to POS binding by interacting with $\alpha\beta 5$ as a coreceptor to facilitate POS internalization (Chang and Finnemann 2007). Overexpression of CD81 in RPE cells increased $\alpha\beta 5$ expression levels and POS binding. Another receptor from the scavenger family, CD36, may also be involved in POS binding: experiments using CD36 antibodies to block receptor function decreased binding of 1. PS-containing liposomes to RPE cells (Ryeom et al. 1996a), and 2. POS to RPE cells and their internalization (Ryeom et al. 1996b). A later study showed that CD36 specifically affects the rate of POS internalization and its downstream signaling seems independent of $\alpha\beta 5$ (Finnemann and Silverstein 2001).

91.4 Internalize

The signaling steps discussed above are essential for MerTK activation and POS internalization. Intracellular signals downstream of MerTK are likely to involve second messenger molecules, such as intracellular inositol 1,4,5-trisphosphate (InsP_3) that rises following POS binding only in cells with intact MerTK (Heth and Marescalchi 1994). MerTK activation and its ability to mediate cytoskeletal changes may govern its obligatory role in particle internalization observed in both macrophages and RPE cells. It is still not clear how MerTK function promotes particle engulfment, but one can envisage that MerTK activation ultimately leads to cytoskeletal reorganization, including actin-mediated extension of pseudopods, essential for particle engulfment.

Annexin 2 (anxA2), a regulator of actin dynamics, was recently identified to have a role in RPE phagocytosis (Law et al. 2009). Indeed, anxA2 is recruited to early phagosomes and dissociates away once they are internalized. In wild-type animals, anxA2 is tyrosine-phosphorylated before light onset (Fig. 91.1b), followed by FAK and c-Src phosphorylation. *ANX A2*^{-/-} mice show an accumulation of phagosomes in RPE apical processes, and FAK and c-Src activation were delayed. These data suggest that the role of anxA2 lies upstream of FAK, and that the recruitment of anxA2 to forming phagosomes is important for the synchronized activation of FAK and phagosome internalization. AnxA2 phosphorylation reaches its maximum at the same time as MerTK (Fig. 91.1b). Thus, activation of MerTK may be important in generating second messengers required for completion of anxA2 activity at the forming phagosomes. AnxA2 binds directly to phosphatidylinositol 4,5-bisphosphate ($\text{PtdIns}4,5\text{P}_2$) at the cell membrane following micromolar increases of calcium (Hayes et al. 2004). AnxA2 is then phosphorylated and stimulates actin nucleation and polymerization in vitro (Hayes et al. 2006; Hayes and Moss 2009; de Graauw et al. 2008) and is thus well placed to mediate the connection between phagosome membrane and actin cytoskeleton during phagocytosis.

While the formation of pseudopods requires significant membrane and actin dynamics, a contractile force must also be generated to mediate constriction of the pseudopod for phagosome closure. There is growing evidence that motor proteins of the myosin family have an important role in phagocytosis. First, myosin II has been reported to be directly linked to MerTK in RPE cells (Strick et al. 2009). These authors showed that while absence of MerTK does not affect recruitment of actin to the phagocytic cup, it disrupts myosin II localization on phagosomes and inhibits phagocytosis by wild-type RPE cells. Second, Shaker 1 mice that are mutated in the myosin VIIa (*MYO7A*) gene, a model of Type 1B Usher Syndrome (USH1B), are deaf, have abnormal electroretinograms, their melanosomes are absent from RPE apical processes, and PRs have a slower rate of disk renewal (Gibbs et al. 2003). Moreover, phagosomes accumulate in the apical region of RPE cells, resulting in slower phagosome degradation.

91.5 Perspectives

RPE cells and macrophages share many components of their respective phagocytic machinery. The RPE system is unique in that POS and RPE cells are in permanent contact and phagocytosis follows a rhythmic profile, whereas macrophages are activated when they encounter apoptotic cells. This is fascinating and suggests that the timely recognition of “eat me” signals on POS by RPE cells and increased activity of downstream proteins are highly regulated at the molecular level. Pieces of this intricate puzzle are still missing and are needed to fully understand RPE phagocytosis.

References

- Boesze-Battaglia K, Albert AD (1992) Phospholipid distribution among bovine rod outer segment plasma membrane and disk membranes. *Exp Eye Res* 54:821–823
- Chaitin MH, Hall MO (1983) Defective ingestion of rod outer segments by cultured dystrophic rat pigment epithelial cells. *Invest Ophthalmol Vis Sci* 24:812–820
- Chang Y, Finnemann SC (2007) Tetraspanin CD81 is required for the alpha v beta5-integrin-dependent particle-binding step of RPE phagocytosis. *J Cell Sci* 120:3053–3063
- D’Cruz PM, Yasumura D, Weir J et al (2000) Mutation of the receptor tyrosine kinase gene *Mertk* in the retinal dystrophic RCS rat. *Hum Mol Genet* 9:645–651
- Finnemann SC, Bonilha VL, Marmorstein AD et al (1997) Phagocytosis of rod outer segments by retinal pigment epithelial cells requires alpha(v)beta5 integrin for binding but not for internalization. *Proc Natl Acad Sci USA* 94:12932–12937
- Finnemann SC, Rodriguez-Boulan E (1999) Macrophage and retinal pigment epithelium phagocytosis: apoptotic cells and photoreceptors compete for alphavbeta3 and alphavbeta5 integrins, and protein kinase C regulates alphavbeta5 binding and cytoskeletal linkage. *J Exp Med* 190: 861–874
- Finnemann SC, Silverstein RL (2001) Differential roles of CD36 and alphavbeta5 integrin in photoreceptor phagocytosis by the retinal pigment epithelium. *J Exp Med* 194:1289–1298
- Finnemann SC (2003) Focal adhesion kinase signaling promotes phagocytosis of integrin-bound photoreceptors. *EMBO J* 22:4143–4154

- Gibbs D, Kitamoto J, Williams DS (2003) Abnormal phagocytosis by retinal pigmented epithelium that lacks myosin VIIa, the Usher syndrome 1B protein. *Proc Natl Acad Sci USA* 100: 6481–6486
- de Graauw M, Tijdens I, Smeets MB et al (2008) Annexin A2 phosphorylation mediates cell scattering and branching morphogenesis via cofilin Activation. *Mol Cell Biol* 28:1029–1040
- Hall MO, Prieto AL, Obin MS et al (2001) Outer segment phagocytosis by cultured retinal pigment epithelial cells requires Gas6. *Exp Eye Res* 73:509–520
- Hall MO, Obin MS, Heeb MJ et al (2005) Both protein S and Gas6 stimulate outer segment phagocytosis by cultured rat retinal pigment epithelial cells. *Exp Eye Res* 81:581–591
- Hall MO, Obin MS, Prieto AL et al (2002) Gas6 binding to photoreceptor outer segments requires gamma-carboxyglutamic acid (Gla) and Ca(2+) and is required for OS phagocytosis by RPE cells in vitro. *Exp Eye Res* 75:391–400
- Hanayama R, Tanaka M, Miwa K et al (2002) Identification of a factor that links apoptotic cells to phagocytes. *Nature* 417:182–187
- Hayes MJ, Merrifield CJ, Shao D et al (2004) Annexin 2 binding to phosphatidylinositol 4,5-bisphosphate on endocytic vesicles is regulated by the stress response pathway. *J Biol Chem* 279:14157–14164
- Hayes MJ, Moss SE (2009) Annexin 2 has a dual role as regulator and effector of v-Src in cell transformation. *J Biol Chem* 284:10202–10210
- Hayes MJ, Shao D, Bailly M, Moss SE (2006) Regulation of actin dynamics by annexin 2. *EMBO J* 25:1816–1826
- Heth CA, Marescalchi PA (1994) Inositol triphosphate generation in cultured rat retinal pigment epithelium. *Invest Ophthalmol Vis Sci* 35:409–416
- LaVail MM, Pinto LH, Yasumura D (1981) The interphotoreceptor matrix in rats with inherited retinal dystrophy. *Invest Ophthalmol Vis Sci* 21:658–668
- LaVail M (1976) Rod outer segment disk shedding in rat retina: relationship to cyclic lighting. *Science* 194:1071–1074
- Law A, Ling Q, Hajjar KA et al (2009) Annexin A2 regulates phagocytosis of photoreceptor outer segments in the mouse retina. *Mol Biol Cell* 20:3896–3904
- Nandrot E, Dufour EM, Provost AC et al (2000) Homozygous deletion in the coding sequence of the c-mer gene in RCS rats unravels general mechanisms of physiological cell adhesion and apoptosis. *Neurobiol Dis* 7:586–599
- Nandrot EF, Anand M, Almeida D et al (2007) Essential role for MFG-E8 as ligand for alphavbeta5 integrin in diurnal retinal phagocytosis. *Proc Natl Acad Sci USA* 104:12005–12010
- Nandrot EF, Anand M, Sircar M et al (2006) Novel role for alphavbeta5-integrin in retinal adhesion and its diurnal peak. *Am J Physiol Cell Physiol* 290:C1256–1262
- Nandrot EF, Kim Y, Brodie SE et al (2004) Loss of synchronized retinal phagocytosis and age-related blindness in mice lacking alphavbeta5 integrin. *J Exp Med* 200:1539–1545
- Nyberg P, He X, Hårdig Y et al (1997) Stimulation of Sky tyrosine phosphorylation by bovine protein S--domains involved in the receptor-ligand interaction. *Eur J Biochem* 246:147–154
- Prasad D, Rothlin CV, Burrola P et al (2006) TAM receptor function in the retinal pigment epithelium. *Mol Cell Neurosci* 33:96–108
- Ryeom SW, Silverstein RL, Scotto A et al (1996a) Binding of anionic phospholipids to retinal pigment epithelium may be mediated by the scavenger receptor CD36. *J Biol Chem* 271: 20536–20539
- Ryeom SW, Sparrow JR, Silverstein RL (1996b) CD36 participates in the phagocytosis of rod outer segments by retinal pigment epithelium. *J Cell Sci* 109 (Pt 2):387–395
- Strick DJ, Feng W, Vollrath D (2009) MerTK drives myosin II redistribution during retinal pigment epithelial phagocytosis. *Invest Ophthalmol Vis Sci* 50:2427–2435
- Vollrath D, Feng W, Duncan JL et al (2001) Correction of the retinal dystrophy phenotype of the RCS rat by viral gene transfer of MerTK. *Proc Natl Acad Sci USA* 98:12584–12589
- Young RW, Bok D (1969) Participation of the retinal pigment epithelium in the rod outer segment renewal process. *J Cell Biol* 42:392–403

Chapter 92

Endo-Lysosome Function in the Retinal Pigment Epithelium in Health and Disease

Aparna Lakkaraju

Keywords Retinal pigment epithelium • Age-related macular degeneration • Lipofuscin • A2E • Late endosome • Lysosome • Cholesterol • Protein lipid trafficking • Niemann–Pick C1 • Apolipoprotein

92.1 Introduction

The eukaryotic cell has numerous membrane-bound organelles, each with distinct structure, composition, and function. The endosomal network, which transports proteins and lipids in the biosynthetic and endocytic routes, is a key regulator of cellular homeostasis (Rodriguez-Boulan et al. 2005; Lakkaraju and Rodriguez-Boulan 2008). Endosomes are classified as early, recycling, or late based on their hierarchy in the endocytic route and lysosomes are the terminal degradative compartments of the cell (Fig. 92.1). Conventional wisdom has long held that proteins or lipids shunted into late endosomes cannot escape lysosomal degradation. A growing body of work however suggests that late endosomes and lysosomes are important platforms for protein–lipid sorting, cholesterol trafficking, and signaling (van der Goot and Gruenberg 2006). The complexity of the endosomal network increases in polarized cells such as the retinal pigment epithelium (RPE) because these cells communicate with different extracellular environments at their apical and basolateral surfaces (Fig. 92.1b). RPE cells are also postmitotic, which places additional pressure on their endo-lysosomal system because these organelles have to perform efficiently for the entire lifespan of the organism. Several independent lines of evidence now indicate that a decline in endo-lysosomal function could contribute to retinal degenerative diseases.

A. Lakkaraju (✉)

Department of Ophthalmology and Visual Sciences, School of Medicine and Public Health, University of Wisconsin-Madison, 1300 University Ave, MSC 3385, Madison, WI 53706, USA
e-mail: lakkaraju@wisc.edu

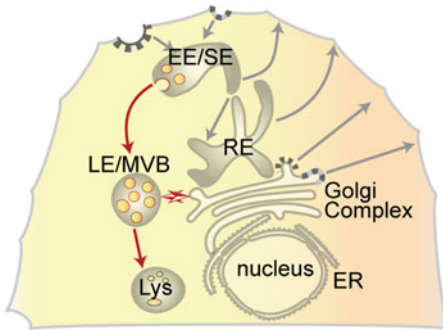
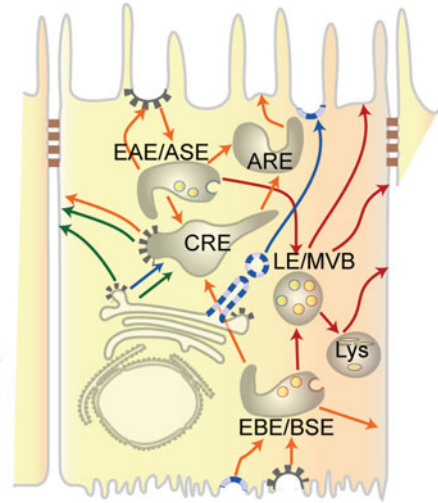
a Non-polarized cell**b Polarized epithelial cell**

Fig. 92.1 The endo-lysosomal network. Endosomes lie at the intersection of the biosynthetic and endocytic routes in the cell. Polarized cells (**b**), such as retinal pigment epithelial cells, have more complex endo-lysosomal systems than nonpolarized cells (**a**), such as fibroblasts. Newly synthesized proteins are transported from the trans-Golgi network (TGN) to the plasma membrane either directly or via endosomal intermediates. (**a**) Endocytosed cargo is recycled back to the cell surface by early or sorting endosomes (EE/SE) and recycling endosomes (RE). Cargo to be degraded is sorted into membrane invaginations of EE/SE, which eventually mature into late endosomes or multivesicular bodies (LE/MVB) and lysosomes (Lys). (**b**) Epithelial cells have distinct apical and basolateral domains demarcated by tight junctions, and the endosomal network plays a key role in the establishment and maintenance of polarity. Cargo is first internalized at apical and basolateral surfaces into early apical or basolateral sorting endosomes (EAE/ASE or EBE/BSE). Recycling cargo is transported to common recycling endosomes (CRE) and then sorted into apical or basolateral recycling routes. The apical recycling route includes the apical recycling endosomes (ARE), which is similar to the RE in nonpolarized cells. Although apical and basolateral endocytic pathways intersect at the level of late endosomes, little is known about late endosome/lysosome biogenesis and function in epithelial cells

92.2 Late Endosomes and Lysosomes: Function and Dysfunction

The biogenesis of late endosomes and lysosomes requires the concerted actions of both the biosynthetic and endocytic pathways in the cell. Newly synthesized lysosomal hydrolases and membrane proteins are delivered to late endosomes and lysosomes from the *trans*-Golgi network. Cargo endocytosed at the plasma membrane passes through several endosomal intermediates that undergo multiple fusions and constant remodeling, resulting in the formation of late endosomes with intraluminal vesicles (ILVs) formed by the inward budding of the endosomal limiting membrane (van Meel and Klumperman 2008; Saftig and Klumperman 2009). However, not all

ILVs are created equal: fusion of the limiting membrane with the plasma membrane releases ILVs as exosomes into the extracellular space, whereas ILVs containing ubiquitinated signaling receptors and other proteins are segregated into domains that eventually mature into lysosomes (van der Goot and Gruenberg 2006; Lakkaraju and Rodriguez-Boulan 2008).

Mutations in genes coding for lysosomal hydrolases or membrane proteins cause a heterogeneous group of ~50 disorders known as lysosomal storage diseases (LSDs). In LSDs, unmetabolized substrates accumulate in lysosomes and activate pathogenic cascades resulting in oxidative stress, inflammation, autophagy, and eventually, cell death (Vitner et al. 2010). Examples of LSDs include Tay–Sachs disease, Fabry disease, and Niemann–Pick disease Type A, B, and C. Apart from these genetic disorders, chronic dysfunction of the endo-lysosomal system in post-mitotic cells plays a causal role in the pathogenesis of several age-related diseases such as Alzheimer’s and Parkinson’s diseases (Nixon et al. 2008). Dystrophic neurites filled with autophagosomes, autolysosomes, and lysosomal dense bodies, indicative of widespread endo-lysosomal abnormalities, have been reported in Alzheimer’s disease brains (Nixon et al. 2005).

92.3 Late Endosomes and Lysosomes in the RPE

The RPE is a monolayer of epithelial cells that lies between photoreceptors and choriocapillaries. Tight junctions between RPE cells form the outer blood–retinal barrier and RPE cells perform many functions indispensable for photoreceptor health and vision: they metabolize and recycle retinoids, secrete growth factors for photoreceptors and choriocapillaries, and control the transport of nutrients into, and metabolites out of, the retina (Bok 1993; Strauss 2005). Perhaps the most important function performed by the RPE is the daily phagocytosis and degradation of shed photoreceptor outer segments (Bok 2005). In fact, RPE cells are the most phagocytically active cells in the body. Since RPE cells are postmitotic and each RPE cell is responsible for 30–40 photoreceptors in humans, this is an enormous metabolic challenge for RPE endo-lysosomal system. Over time, autofluorescent lipid–protein aggregates called lipofuscin accumulate in RPE lysosomes (Fig. 92.2) (Feeney-Burns and Eldred 1983). Lipofuscin also accumulates in other postmitotic cells such as neurons and cardiac myocytes, suggesting a gradual decline in lysosomal function with age. A major fluorophore of RPE lipofuscin is A2E, a retinoid by-product of the visual cycle that progressively accumulates throughout life. A2E-induced RPE dysfunction has been implicated in both inherited (Stargardt’s and Best’s diseases) and age-related macular dystrophies. Although several hypotheses have been put forth to explain how A2E could damage the RPE (reviewed in (Sparrow and Boulton 2005)), true mechanistic insight into this complex phenomenon is still elusive.

Accumulations of drusen, extracellular deposits in the Bruch’s membrane beneath the RPE, are also a characteristic feature of aging and age-related macular

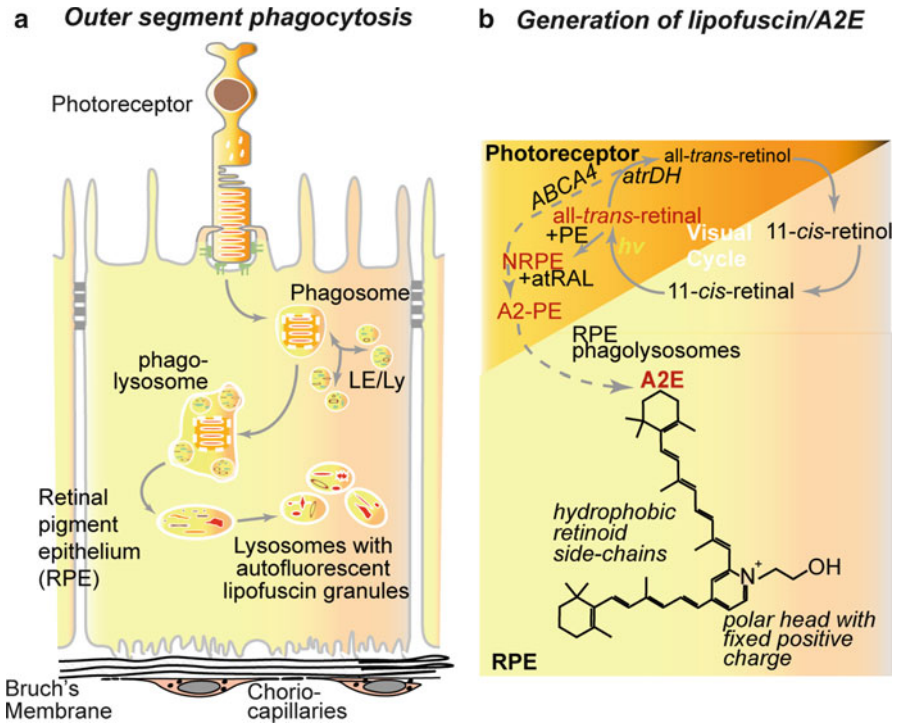


Fig. 92.2 Phagocytosis of outer segment discs (**a**) and lipofuscin formation (**b**). After phagocytosis, phagosomes containing outer segment discs fuse with late endosomes and lysosomes (LE/Ly) to form phagolysosomes. Lysosomal hydrolases in phagolysosomes are responsible for metabolizing phagocytosed discs. Over time, undegraded lipids and proteins accumulate in secondary lysosomes in the form of autofluorescent lipofuscin granules. One component of RPE lipofuscin that has been structurally characterized is the bis-retinoid A2E. See Sparrow and Boulton (2005) and Travis et al. (2007) for details on the mechanism of A2E formation. A2E is a wedge-shaped hydrophobic molecule with a fixed positive charge. It is primarily composed of carbon-carbon double bonds and cannot be degraded by any known lysosomal enzymes

degeneration (AMD). Histopathological analyses of eyes with AMD showed that cholesterol and apolipoproteins are major components of drusen (Anderson et al. 2001; Curcio et al. 2010). Cholesterol in the retina is essential for disc biogenesis and for modulating rhodopsin activity (Boesze-Battaglia and Albert 1990). RPE cells ingest significant amounts of free and esterified cholesterol from phagocytosed outer segment discs and from lipoproteins via the chorioid circulation. Cholesterol is then metabolized in RPE late endosomes and lysosomes and transported to various intracellular destinations or to the plasma membrane for efflux. Epidemiological and genetic data have implicated serum cholesterol levels and genes involved in cholesterol metabolism and transport, such as apolipoprotein E, ATP-binding cassette protein A1 (ABCA1), cholesterol ester transfer protein, and lipoprotein lipase, as risk factors for AMD (Zarepari et al. 2005; Chen et al. 2010; Klein et al. 2010; Neale et al. 2010).

92.4 RPE Late Endosome–Lysosome Dysfunction, Impaired Cholesterol Trafficking, and Retinal Degenerations

Emerging research indicates that AMD shares common pathogenic features with other chronic age-related diseases like atherosclerosis, Alzheimer’s disease, and Parkinson’s disease at the level of cholesterol homeostasis (Cassery and Topol 2004; Liu et al. 2010). Pertinently, aberrant cholesterol metabolism interferes with endo-lysosomal function (Wenk 2005) because membrane cholesterol levels control organelle motility by modulating vesicle budding, activation of rab GTPases, and association with molecular motors (Simons and Gruenberg 2000; van der Goot and Gruenberg 2006). As stated in Sect. 92.2, another characteristic of many age-related diseases is abnormal endo-lysosomal function, supporting a link between cholesterol homeostasis, endo-lysosome dynamics, lipofuscin accumulation, and disease pathogenesis (Fig. 92.3).

RPE late endosomes and lysosomes are central to retinal function because they are the sites of outer segment disc metabolism, lipofuscin/A2E generation, and cholesterol metabolism. We previously demonstrated that A2E specifically causes cholesterol accumulation in RPE late endosomes and lysosomes (Lakkaraju et al. 2007). Both A2E and cholesterol are cone-shaped lipids that compete for space under

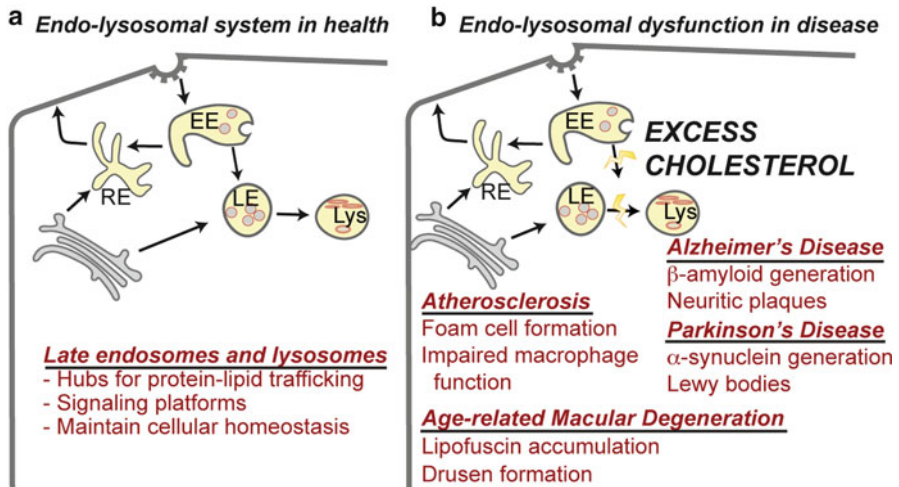


Fig. 92.3 The endo-lysosomal system in health (a) and disease (b). In normal cells, late endosomes and lysosomes play essential roles in maintaining cellular homeostasis. Chronic endo-lysosomal dysfunction has been implicated in age-related diseases such as atherosclerosis, AMD, and Alzheimer’s and Parkinson’s diseases. Cholesterol accumulation in the endo-lysosomal pathway is another common link between these diseases. Membrane cholesterol levels control organelle motility by modulating vesicle budding, activation of rabGTPases, and association with molecular motors. Consequently, excess cholesterol within the cell interferes with protein–lipid sorting and lysosome function, resulting in the accumulation of undegraded protein–lipid aggregates which play causal roles in disease pathogenesis

the phospholipid umbrella in the membrane to minimize unfavorable interactions with the aqueous phase (Huang and Feigenson 1999). As a consequence, cholesterol is displaced from the membrane by A2E and gets trapped within the late endosomal lumen where it accumulates. Importantly, drugs that transcriptionally activate cholesterol transporters restore cholesterol homeostasis in RPE cells (Lakkaraju et al. 2007).

Impaired cholesterol trafficking in the RPE increases lipofuscin production, possibly by interfering with late endosomal motility and lysosomal function. Loss of the Niemann–Pick C1 protein, a cholesterol transporter present on late endosomes, results in the accumulation of both cholesterol and lipofuscin in the RPE, progressive photoreceptor degeneration, and loss of visual function in mice and fruit flies (Phillips et al. 2008; Claudepierre et al. 2010). In the neural retina, mutant rhodopsin accumulates in late endosomes and triggers light-dependent photoreceptor degeneration (Chinchore et al. 2009; Midorikawa et al. 2010), underscoring the role of the endo-lysosomal system in maintaining retinal health.

92.5 Conclusions

There is strong experimental, epidemiological, and histopathological support for an association between a slow, progressive decline in RPE endo-lysosomal function, lipofuscin accumulation, and disturbed cholesterol homeostasis, resulting in a feed-forward cycle that could eventually lead to retinal degeneration. Ongoing research in our laboratory is focused on unraveling the cellular and molecular mechanisms underlying these processes. Understanding how endosomes and lysosomes in the RPE respond to aging and cellular stress could help identify novel drug targets that modulate endo-lysosomal function, which may be beneficial in age-related retinal disease.

Acknowledgments Supported by grants from the American Health Assistance Foundation (M2009093) and the Karl Kirchgessner Foundation and a career development award from Research to Prevent Blindness

References

- Anderson DH, Ozaki S, Nealon M et al (2001) Local cellular sources of apolipoprotein E in the human retina and retinal pigmented epithelium: Implications for the process of drusen formation. *Am J Ophthalmol* 131:767–781
- Boesze-Battaglia K, Albert AD (1990) Cholesterol modulation of photoreceptor function in bovine retinal rod outer segments. *J Biol Chem* 265:20727–20730
- Bok D (1993) The retinal pigment epithelium: a versatile partner in vision. *J Cell Sci Suppl* 17:189–195
- Bok D (2005) Evidence for an inflammatory process in age-related macular degeneration gains new support. *Proc Natl Acad Sci USA* 102:7053–7054

- Cassery I, Topol E (2004) Convergence of atherosclerosis and Alzheimer's disease: inflammation, cholesterol, and misfolded proteins. *Lancet* 363:1139–1146
- Chen W, Stambolian D, Edwards AO et al (2010) Genetic variants near TIMP3 and high-density lipoprotein-associated loci influence susceptibility to age-related macular degeneration. *Proc Natl Acad Sci USA* 107:7401–7406
- Chinchore Y, Mitra A, Dolph PJ (2009) Accumulation of Rhodopsin in Late Endosomes Triggers Photoreceptor Cell Degeneration. *Plos Genetics* 5: e1000377
- Claudepierre T, Paques M, Simonutti M et al (2010) Lack of Niemann-Pick type C1 induces age-related degeneration in the mouse retina. *Mol Cell Neurosci* 43:164–176
- Curcio CA, Johnson M, Huang JD et al (2010) Apolipoprotein B-containing lipoproteins in retinal aging and age-related macular degeneration. *J Lipid Res* 51:451–467
- Feeney-Burns L, Eldred GE (1983) The fate of the phagosome: conversion to 'age pigment' and impact in human retinal pigment epithelium. *Trans Ophthalmol Soc UK* 103 (Pt 4):416–421
- Huang J, Feigenson GW (1999) A microscopic interaction model of maximum solubility of cholesterol in lipid bilayers. *Biophys J* 76:2142–2157
- Klein R, Cruickshanks KJ, Nash SD et al (2010) The prevalence of age-related macular degeneration and associated risk factors. *Arch Ophthalmol-Chic* 128:750–758
- Lakkaraju A, Rodriguez-Boulan E (2008) Itinerant exosomes: Emerging roles in cell and tissue polarity. *Trends Cell Biol* 18:199–209
- Lakkaraju A, Finnemann SC, Rodriguez-Boulan E (2007) The lipofuscin fluorophore A2E perturbs cholesterol metabolism in retinal pigment epithelial cells. *Proc Natl Acad Sci USA* 104:11026–11031
- Liu JP, Tang Y, Zhou SF et al (2010) Cholesterol involvement in the pathogenesis of neurodegenerative diseases. *Mol Cell Neurosci* 43:33–42
- Midorikawa R, Yamamoto-Hino M, Awano W et al (2010) Autophagy-dependent rhodopsin degradation prevents retinal degeneration in drosophila. *J Neurosci* 30:10703–10719
- Neale BM, Fagerness J, Reynolds R et al (2010) Genome-wide association study of advanced age-related macular degeneration identifies a role of the hepatic lipase gene (LIPC). *Proc Natl Acad Sci USA* 107:7395–7400
- Nixon RA, Yang DS, Lee JH (2008) Neurodegenerative lysosomal disorders: a continuum from development to late age. *Autophagy* 4:590–599
- Nixon RA, Wegiel J, Kumar A et al (2005) Extensive involvement of autophagy in Alzheimer disease: an immuno-electron microscopy study. *J Neuropathol Exp Neurol* 64:113–122
- Phillips SE, Woodruff EA, 3rd, Liang P et al (2008) Neuronal loss of Drosophila NPC1a causes cholesterol aggregation and age-progressive neurodegeneration. *J Neurosci* 28:6569–6582
- Rodriguez-Boulan E, Kreitzer G, Musch A (2005) Organization of vesicular trafficking in epithelia. *Nat Rev Mol Cell Biol* 6:233–247
- Saftig P, Klumperman J (2009) Lysosome biogenesis and lysosomal membrane proteins: trafficking meets function. *Nat Rev Mol Cell Biol* 10:623–635
- Simons K, Gruenberg J (2000) Jamming the endosomal system: lipid rafts and lysosomal storage diseases. *Trends Cell Biol* 10:459–462
- Sparrow JR, Boulton M (2005) RPE lipofuscin and its role in retinal pathobiology. *Exp Eye Res* 80:595–606
- Strauss O (2005) The retinal pigment epithelium in visual function. *Physiol Rev* 85:845–881
- van der Goot FG, Gruenberg J (2006) Intra-endosomal membrane traffic. *Trends Cell Biol* 16: 514–521
- van Meel E, Klumperman J (2008) Imaging and imagination: understanding the endo-lysosomal system. *Histochem Cell Biol* 129:253–266
- Vitner EB, Platt FM, Futerman AH (2010) Common and uncommon pathogenic cascades in lysosomal storage diseases. *J Biol Chem* 285:20423–20427
- Wenk MR (2005) The emerging field of lipidomics. *Nat Rev Drug Discov* 4:594–610
- Zarepari S, Buraczynska M, Branham KE et al (2005) Toll-like receptor 4 variant D299G is associated with susceptibility to age-related macular degeneration. *Hum Mol Genet* 14:1449–1455

Chapter 93

$\alpha\text{v}\beta\text{5}$ Integrin-Dependent Diurnal Phagocytosis of Shed Photoreceptor Outer Segments by RPE Cells Is Independent of the Integrin Coreceptor Transglutaminase-2

Linda Ruggiero, Zsolt Sarang, Zsuzsa Szondy, and Silvia C. Finnemann

Keywords Photoreceptor outer segment renewal • Retinal pigment epithelium • Phagocytosis • Integrins • Transglutaminase 2 • Knockout mice • Retina

93.1 Introduction

In mammals, diurnal phagocytosis of shed photoreceptor outer segments (POS) by the retinal pigment epithelium (RPE) is important for retinal function. This process is under circadian regulation with a burst of rod shedding and RPE phagocytic activity occurring each morning. We previously showed that RPE cells use the integrin family adhesion receptor $\alpha\text{v}\beta\text{5}$ and its ligand MFG-E8, a secreted glycoprotein, to bind POS and stimulate their engulfment (Finnemann et al. 1997; Nandrot et al. 2004, 2007). Mice lacking either $\alpha\text{v}\beta\text{5}$ integrin or MFG-E8 lose the diurnal peak of phagocytosis and display similar numbers of POS phagosomes at all times of day. By contrast, wild-type RPE cells carry POS phagosomes only for a short period of time after light onset (LaVail 1976).

Like RPE cells, macrophages and dendritic cells rely on integrin receptors and secreted ligands including MFG-E8 for the recognition and phagocytosis of apoptotic cells (Savill et al. 2002). Studies of bone marrow-derived macrophages and dendritic cells in cell culture have shown that these cells express both $\alpha\text{v}\beta\text{5}$ integrin

L. Ruggiero • S.C. Finnemann (✉)
Department of Biological Sciences, Fordham University, Bronx, NY 10458, USA
e-mail: finnemann@fordham.edu

Z. Sarang • Z. Szondy
Department of Biochemistry and Molecular Biology, Apoptosis
and Genomics Research Group, Hungarian Academy of Sciences,
University of Debrecen, Debrecen, Hungary

and the closely related $\alpha v\beta 3$ integrin. However, while macrophages use dominantly $\alpha v\beta 3$ for clearance phagocytosis (Finnemann and Rodriguez-Boulan 1999; Lucas et al. 2006), dendritic cells rely on $\alpha v\beta 5$ (Albert et al. 1998). Much evidence suggests that these integrin/ligand complexes are essential for efficient phagocytosis and often assemble larger complexes in which additional proteins functionally interact (Chang and Finnemann 2007).

Transglutaminase 2 (TG2) is a multifunctional enzyme that is found intracellularly, in the cytoplasm and/or in the nucleus, as well as extracellularly associated with the cell surface and/or in the extracellular matrix (reviewed by Zemskov et al. 2006). In vitro and immunoprecipitation studies show that secreted TG2 binds to fibronectin with high affinity and mediates cell adhesion by forming complexes with $\beta 1$ and $\beta 3$ integrins that are present on the cell surface (Akimov et al. 2000; Akimov and Belkin 2001). TG2 has been found associated with the surface of macrophages, where it specifically forms a complex with $\beta 3$ integrin and MFG-E8 (Toth et al. 2009a). The TG2/integrin complex has been implicated in the phagocytosis of apoptotic cells by macrophages because macrophages harvested from TG2^{-/-} mice exhibit defective phagocytosis of apoptotic cells compared to wild-type cells. In this experimental system, lack of extracellular TG2 prevents $\alpha v\beta 3$ integrin clustering likely causing the phagocytic defect (Toth et al. 2009a, b). TG2^{-/-} mice generated by deleting the catalytic domain of TG2 are viable, fertile, and develop normally with no gross phenotypic abnormalities (De Laurenzi and Melino 2001). However, close examination found evidence for defective clearance phagocytosis in TG2^{-/-} liver and thymus (Szondy et al. 2003).

The role of TG2 in phagocytosis by macrophages and its association with β integrins and MFG-E8 led us to investigate its potential role in the phagocytic activity of RPE cells. We hypothesized that TG2^{-/-} retina may exhibit abnormalities as a consequence of impaired phagocytosis of POS by the RPE. Hence, we examined retinal structure and diurnal phagocytosis of POS by the RPE in TG2^{-/-} mice to directly test this hypothesis.

93.2 Materials and Methods

93.2.1 Animals and Tissue Collection

TG2^{-/-} mice were originally generated and characterized by De Laurenzi and Melino (2001). Mice were housed under cyclic 12:12 h light/dark-light conditions and fed *ad libitum*. Two- and twelve-month-old animals were sacrificed at 1 and 8 h after light onset by CO₂ asphyxiation. Eyecups were enucleated and immediately fixed by immersion in formaldehyde/ethanol/acetic acid and embedded in paraffin. All procedures were approved by the local institutional animal care and use committees and adhered to the ARVO statement for the use of animals in ophthalmic and vision research.

93.2.2 Histology

Eight micrometer cross-sections of paraffin-embedded eyecups from TG2^{-/-} mice were preheated to 50°C for 20 min and paraffin was removed using citrus clearing solvent (Richard-Allan Scientific) followed by rehydration with decreasing ethanol concentrations. To examine retinal layers, sections were stained with Hematoxylin followed by Eosin and subsequent dehydration by ethanol. Slides were coverslipped with Vectashield and imaged by brightfield microscopy.

93.2.3 Quantification of POS Phagosomes in the RPE

Opsin-positive inclusions in the RPE were quantified in 8 μm cross-sections from TG2^{-/-} mice as a measure of RPE phagocytic activity (Nandrot et al. 2007). Paraffin was removed from sections as described above, and the tissue was bleached with 1% sodium borohydrate and labeled with rhodopsin antibody B6-30 (a kind gift by P. Hargrave, University of Florida, Gainesville), antimouse IgG-AlexaFluor 488 (Invitrogen), and DAPI. Sections were mounted in Vectashield, and x-y image stacks were acquired at 0.24- μm intervals on a Leica TSP5 confocal microscopy system. Opsin-labeled phagosomes in the RPE were counted on maximal projections of 5- μm -thick stacks. Phagosome counts were normalized to length of retina and averaged (for details please see Nandrot et al. 2007).

93.3 Results

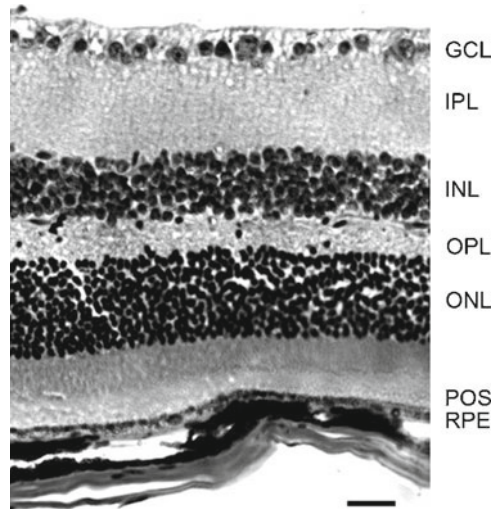
93.3.1 TG2^{-/-} Mice Display Normal Retinal Architecture

We examined cross-sections of eyecups taken from TG2^{-/-} mice and stained by H&E for obvious alterations in morphology of the neural retina or the RPE. We found that all retinal layers, namely the POS, photoreceptor outer nuclear layer (ONL), outer plexiform layer (OPL), inner nuclear layer (INL), inner plexiform layer (IPL), ganglion cell layer (GCL), as well as the RPE, were present and intact, with no obvious disruption (Fig. 93.1). Appearance of the RPE was normal as well. This was true for young adult mice at 2 months of age (not shown) and for aged mice at 1 year of age (Fig. 93.1).

93.3.2 The RPE in TG2^{-/-} Mice Displays a Normal Diurnal Peak of Rod POS Phagocytosis

Phagocytosis of POS by the vertebrate RPE is synchronized to the light/dark cycle in wild-type animals, with a daily burst of phagocytosis of shed rod POS shortly

Fig. 93.1 Analysis of morphology of TG2^{-/-} retinal tissue. Representative H&E stained cross-section of an eyecup from a 1-year-old TG2^{-/-} mouse showing intact RPE, photoreceptor outer segments (POS), outer nuclear layer (ONL), outer plexiform layer (OPL), inner nuclear layer (INL), inner plexiform layer (IPL), and ganglion cell layer (GCL). Scale bar equals 25 μm



after the onset of light. To examine whether lack of TG2 alters rod POS phagocytosis by the RPE, we counted rhodopsin-labeled phagosomes that were present in the RPE of TG2^{-/-} mice at the expected peak and off peak times of phagocytosis. Phagosomes were highly abundant in the RPE of TG2^{-/-} mice 1 h after light onset (Fig. 93.2a). As characteristic for wild-type mouse RPE, TG2^{-/-} mouse RPE carries a significantly higher number of phagosomes in the morning (1 h after light onset), and a decline in phagosome number later in the day (8 h after light onset). This was true of both young adult and aged mice (Fig. 93.2b).

93.4 Discussion

The experimental results presented here demonstrate that complete and constitutive absence of TG2 does not affect the overall retinal architecture in either young or aged mice as TG2^{-/-} mice exhibit the presence and normal morphology of all retinal layers. Based on the lack of any obvious difference in morphology of TG2^{-/-} and wild-type retina, we decided not to expand the characterization of the TG2^{-/-} retina to assess whether it is functionally normal, e.g., by recording electroretinograms. We can thus not exclude that lack of TG2 may cause subtle changes in retinal neuronal or RPE functions that our postmortem tissue analysis failed to detect. Additionally, loss of TG2 does not affect the diurnal pattern of phagocytosis of POS by the RPE since TG2^{-/-} mice exhibit the expected burst of phagosome number shortly after light onset and a decline 8 h later. Given that TG2 in the mouse eye is mainly expressed by the RPE (cf. Ruggiero and Finnemann in this issue) our data strongly suggest that TG2 expression is not essential for the development or maintenance of any retinal cell type or retinal cell interactions.

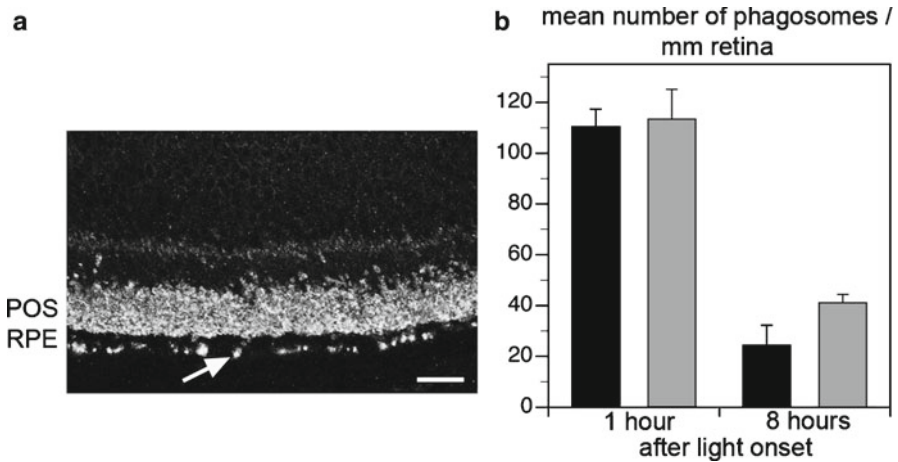


Fig. 93.2 Analysis of RPE phagocytosis of POS in $\text{TG2}^{-/-}$ mouse retina. **(a)** Representative image of a rhodopsin-labeled retinal cross-section indicating the presence of numerous phagosome inclusions (*arrow* shows example) in the RPE layer of a 1-year-old $\text{TG2}^{-/-}$ mouse at 1 h after light onset. Scale bar equals 20 μm . **(b)** Average number of phagosomes detected in RPE of 2-month-old (*black bars*) and 1-year-old (*gray bars*) $\text{TG2}^{-/-}$ mice sacrificed 1 or 8 h after light onset as indicated. *Bars* represent mean \pm s. e. m, $n=4$

Synchronized diurnal phagocytosis of rod POS by the RPE requires the ligand receptor pair $\alpha\text{v}\beta\text{5}$ integrin and MFG-E8. Mice lacking $\alpha\text{v}\beta\text{5}$ integrin or MFG-E8 lose the peak of phagocytosis that occurs at the onset of light in wild-type mice. In this study, we examined the potential role of TG2 in phagocytosis of POS by RPE by quantifying phagosome accumulation in the RPE at light onset and 8 h later in $\text{TG2}^{-/-}$ mice. If TG2 was a necessary component for the recognition and engulfment of POS by RPE through interactions with $\alpha\text{v}\beta\text{5}$ integrin and/or MFG-E8, we would expect similar numbers of phagosomes in $\text{TG2}^{-/-}$ RPE at both time points, like in $\beta\text{5}^{-/-}$ and $\text{MFG-E8}^{-/-}$ RPE. Instead, we found a pronounced diurnal rhythm of rod POS phagocytosis in $\text{TG2}^{-/-}$ mice similar to the rhythm in wild-type mice. We conclude that the $\alpha\text{v}\beta\text{5}$ integrin-MFG-E8-dependent pathway does not require TG2 to function suggesting that it may utilize a different cofactor with similar functions as TG2 that remains to be identified.

Macrophages and RPE cells share expression of many proteins involved in clearance phagocytosis. All proteins known thus far to be involved in RPE phagocytosis have also been implicated in macrophage phagocytosis at least in *in vitro* settings. This study shows that RPE cells do not necessarily utilize the same proteins for phagocytosis as macrophages even if they express them. Macrophages use $\alpha\text{v}\beta\text{3}$ to dispose of apoptotic cells *in vitro*, and TG2 has been shown to be functionally related only to $\alpha\text{v}\beta\text{3}$ in this process. Dendritic cells and RPE cells, on the other hand, rely on $\alpha\text{v}\beta\text{5}$. Although dendritic cells also express high amounts of TG2 on their cell surface (Hodrea et al. 2010), we found that their phagocytosis is also independent of TG2 (our unpublished observation). These data indicate that while $\alpha\text{v}\beta\text{3}$

requires TG2 as a coreceptor for its function in the phagocytosis of apoptotic cells, $\alpha\text{v}\beta 5$ does not. These observations are in agreement with the findings that TG2 acts as a coreceptor for $\beta 1$ and $\beta 3$, but not for all β integrins (Akimov et al. 2000). RPE cells also express $\alpha\text{v}\beta 3$ integrin but they are unable to employ this alternate recognition receptor for POS uptake because $\alpha\text{v}\beta 3$ is restricted to the basolateral surface in the RPE where it likely mediates specific interactions with Bruch's membrane proteins. Thus, the highly polarized phenotype of the RPE may limit their repertoire of proteins available for phagocytosis. Whether TG2 physically or functionally interacts with $\alpha\text{v}\beta 3$ in RPE cells will require further investigation.

Acknowledgments These studies were supported by NIH grant EY-13295 to S.C.F. and Hungarian Research Fund OTKA 77587 to Z.S.

References

- Akimov SS, Krylov D, Fleischman LF et al (2000) Tissue transglutaminase is an integrin-binding adhesion coreceptor for fibronectin. *J Cell Biol* 148:825–838
- Akimov SS, Belkin AM (2001) Cell-surface transglutaminase promotes fibronectin assembly via interaction with the gelatin-binding domain of fibronectin: a role in TGF β -dependent matrix deposition. *J Cell Sci* 114:2989–3000
- Albert M, Pearce SFA, Francisco LM et al (1998) Immature dendritic cells phagocytose apoptotic cells via $\alpha\text{v}\beta 5$ and CD36, and cross-present antigens to cytotoxic T lymphocytes. *J Exp Med* 188:1359–1368
- Chang Y, Finnemann SC (2007) Tetraspanin CD81 is required for the $\alpha\text{v}\beta 5$ integrin-dependent particle-binding step of RPE phagocytosis. *J Cell Sci* 120:3053–3063
- De Laurenzi V, Melino G (2001) Gene disruption of tissue transglutaminase. *Mol Cell Biol* 21: 148–155
- Finnemann SC, Rodriguez-Boulan E (1999) Macrophage and retinal pigment epithelium phagocytosis: apoptotic cells and photoreceptors compete for $\alpha\text{v}\beta 3$ and $\alpha\text{v}\beta 5$ integrins, and protein kinase C regulates $\alpha\text{v}\beta 5$ binding and cytoskeletal linkage. *J Exp Med* 190:861–874
- Finnemann SC, Bonilha VL, Marmorstein AD et al (1997) Phagocytosis of rod outer segments by retinal pigment epithelial cells requires $\alpha\text{v}\beta 5$ integrin for binding but not for internalization. *Proc Natl Acad Sci USA* 94:12932–12937
- Hodrea J, Demyen MA, Majai G et al (2010) Transglutaminase 2 is expressed and active on the surface of human monocyte-derived dendritic cells and macrophages. *Immunol Lett* 130:74–81
- LaVail MM (1976) Rod outer segment disk shedding in rat retina: relationship to cyclic lighting. *Science* 194:1071–1074
- Lucas M, Stuart LM, Zhang A et al (2006) Requirements for apoptotic cell contact in regulation of macrophage responses. *J Immunol* 177:4047–4054
- Nandrot EF, Kim Y, Brodie SE et al (2004) Loss of synchronized retinal phagocytosis and age-related blindness in mice lacking $\alpha\text{v}\beta 5$ integrin. *J Exp Med* 200:1539–1545
- Nandrot EF, Anand M, Almeida D et al (2007) Essential role for MFG-E8 as ligand for $\alpha\text{v}\beta 5$ integrin in diurnal retinal phagocytosis. *Proc Natl Acad Sci USA* 104:12005–12010
- Savill J, Dransfield I, Gregory C et al (2002) A blast from the past: clearance of apoptotic cells regulates immune responses. *Nat Rev Immunol* 2:965–975
- Szondy Z, Sarang Z, Molnar P et al (2003) Transglutaminase 2^{-/-} mice reveal a phagocytosis-associated crosstalk between macrophages and apoptotic cells. *Proc Natl Acad Sci USA* 100: 7812–7817

- Toth B, Garabuczi E, Sarang Z et al (2009a) Transglutaminase 2 is needed for the formation of an efficient phagocyte portal in macrophages engulfing apoptotic cells. *J Immunol* 182:2084–2092
- Toth B, Sarang Z, Vereb G et al (2009b) Over-expression of integrin $\beta 3$ can partially overcome the defect of integrin $\beta 3$ signaling in transglutaminase 2 null macrophages. *Immunol Lett* 126: 22–28
- Zemskov EA, Janiak A, Hang J et al (2006) The role of tissue transglutaminase in cell-matrix interactions. *Front Biosci* 11:1057–1076

Chapter 94

Trafficking of Presynaptic PMCA Signaling Complexes in Mouse Photoreceptors Requires Cav1.4 α_1 Subunits

Wei Xing, Abram Akopian, and David Krizaj

Keywords Calcium extrusion • Nob2 • Photoreceptor • *Cacna1f* • Voltage-operated • PMCA • PMCA1 • Ribbon synapse • Retina

94.1 Introduction

The Cav1.4 α_1 subunit gates sustained neurotransmitter release at mammalian retinal ribbon synapses. Gain and/or loss of function mutations in the *Cacna1f* gene that encodes Cav1.4 result in enhanced or suppressed voltage-operated Ca^{2+} influx in heterologously expressing cells (Hemara-Wahanui et al. 2005; Hoda et al. 2006; Peloquin et al. 2007). In vivo, *Cacna1f* mutations cause night blindness in mice and humans (Strom et al. 1998; Bech-Hansen et al. 1998; Lodha et al. 2010) by compromising Ca^{2+} -dependent exocytosis in terminals of rod and cone photoreceptors. Accordingly, CSNB2 patients are typically diagnosed by abnormal ERG b-waves and can exhibit reduced acuity, impaired night vision, refractive disorders,

W. Xing

Department of Ophthalmology and Visual Sciences, Moran Eye Center,
University of Utah School of Medicine, Salt Lake City, UT 84132, USA

A. Akopian

Department of Physiology and Neuroscience, New York University
Medical Center, New York, NY 10016, USA

D. Krizaj (✉)

Department of Ophthalmology and Visual Sciences, Moran Eye Center, University
of Utah School of Medicine, Salt Lake City, UT 84132, USA

Department of Physiology, University of Utah School of Medicine,
Salt Lake City, UT 84132, USA

e-mail: david.krizaj@hsc.utah.edu

strabismus, and nystagmus (Miyake et al. 1986). The *Cacna1fnob2* (*nob2*) mouse model of CSNB2, which lacks ~90% of Cav1.4 transcripts, shows an absence of the b-wave but an essentially normal photopic optokinetic acuity (Doering et al. 2008). In contrast, Cav1.4 knockout (KO; *Cacna1fG305*) mice created by excision of the floxed exon 7 exhibit neither b-waves nor optokinetic responses (Mansergh et al. 2005). Both KO and *nob2* retinas are characterized by “floating” presynaptic ribbons and by extensive outgrowth of postsynaptic bipolar and horizontal dendritic processes into the outer retina (Bayley and Morgans 2007; Specht et al. 2009; Baehr and Frederick 2009). It is unclear, however, whether compromised Ca^{2+} influx in *nob2* rods is associated with impaired development of photoreceptor synapses and/or reorganization of presynaptic Ca^{2+} homeostatic mechanisms. We have therefore investigated the function of Cav 1.4 subunits in organization of the photoreceptor perisynaptic complex that regulates steady-state $[\text{Ca}^{2+}]_i$ and sustained glutamate release in rods and cones. Plasma membrane Ca^{2+} ATPases (PMCAs) represent a high-affinity Ca^{2+} clearance mechanism that balances sustained influx via L-type channels located in photoreceptor terminals (Križaj and Copenhagen 1998; Križaj et al. 2002) and controls the kinetics of the postsynaptic light response by regulating the rate of clearance of residual $[\text{Ca}^{2+}]_i$ within photoreceptor terminals (Duncan et al. 2006). We report here that PMCA transporters and RIBEYE proteins exhibit a profound mislocalization in photoreceptors from *nob2* retinas. This result suggests that steric interactions mediated through the Cav1.4 peptide and/or Ca^{2+} fluxes gated by the α_{1F} pore are essential for proper trafficking of PMCAs to the synapse and for organization of the active zone in synaptic terminals of mouse photoreceptors.

94.2 Materials and Methods

94.2.1 Animals

C57BL6 wild type and AXB-6/PgnJ animals homozygous for *Cacna1fnob2* were purchased from Jackson laboratories (Bar Harbor, MN). *Basoon* KO mice were a kind gift from Dr. Yong Wang (University of Utah). Animals were maintained in the University animal quarters on a 12 h:12 h light:dark cycle. Animal handling and anesthetic procedures were approved by University Institutional Animal Care committees and conform to NIH guidelines.

94.2.2 Immunohistochemistry

Immunostaining procedures were performed as described previously (Križaj et al. 2002; Mizuno et al. 2010). Polyclonal pan PMCA (used at 1:100), PMCA1

(1:350–1:500), and PMCA2 (1:350) antibodies were purchased from Affinity Bioreagents (Golden, CO). The secondary antibodies utilized were goat antimouse or goat antirabbit IgG (H+L) conjugated to fluorophores (Alexa 488 and Alexa 594 conjugates, Invitrogen), diluted 1:500 or 1:1,000 or goat antimouse Cy3 from Jackson ImmunoResearch at 1:1,000.

94.3 Results

94.3.1 *Nob2 Mutation of Cav1.4 Is Associated with Mislocalization of PMCA1 but not PMCA2*

Steady-state $[Ca^{2+}]_i$ in rod and cone terminals is maintained by PMCA1 transporters whereas PMCA2 is mainly localized to rods (Križaj et al. 2002; Duncan et al. 2006). To determine whether compromised expression of L-type channels affects localization of PMCA transporters, we immunostained *nob2* retinas with the 5F10 pan-PMCA antibody that recognizes all four PMCA isoforms (Križaj and Copenhagen 1998) and with PMCA1 and PMCA2-selective antibodies that had been validated in previous studies of the rodent retina (Križaj et al. 2002; Rentería et al. 2005). As shown in Fig. 94.1c, pan PMCA-immunoreactive (ir) puncta were displaced from the outer plexiform layer (OPL) to irregularly spaced juxtannuclear locations across the outer nuclear layer (ONL). Regions of displaced PMCA-ir were typically shadowed by disorganized OPL underneath. Similar displacement into ONL was observed with the PMCA1 antibody (Fig. 94.1g) whereas PMCA2-ir in *nob2* retinas showed no changes from controls (Fig. 94.1k). Few obvious changes were evident in inner retinal expression of *nob2* PMCA1 (Fig. 94.1b, f). While the PMCA1 transporter antibody stained the expected two IPL bands corresponding to b3/b7 cone bipolar cells (e.g., Križaj et al. 2002), PMCA1-ir in *nob2* preparations was not displaced into the inner nuclear layer (INL). Dislocation of PMCA1-ir was paralleled by severe disorganization of RIBEYE-ir (Fig. 94.1n). These results suggest that the Cav1.4 subunit is required for proper expression, sorting, and/or targeting of PMCA1 to photoreceptor, but not bipolar, synapses. Moreover, PMCA1 but not PMCA2 localization is compromised by the loss of Cav1.4 protein.

Bassoon is a large cytomatrix protein (420 kDa) located at the base of photoreceptor synapses where it may anchor the filamentous network associated with the active zone to the ribbon and the plasma membrane (tom Dick et al. 2003). To determine whether PMCA1 is tethered to the perisynaptic region through bassoon, we analyzed PMCA1 expression in bassoon KO mice. Elimination of Bassoon induced a PMCA1 localization phenotype that was indistinguishable from the improper expression observed in *nob2* retinas. This data suggests that PMCA1 forms the arciform complex together with Cav1.4 and Bassoon.

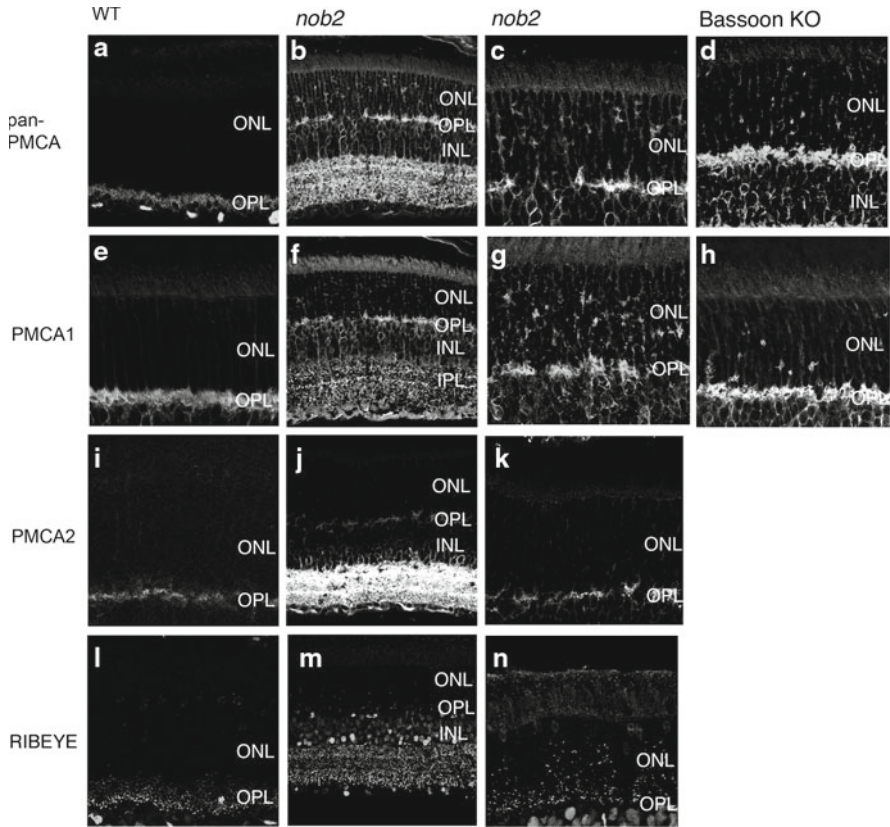


Fig. 94.1 PMCA1 is mislocalized following ablation of Cav1.4 and Bassoon. (a–d) pan-PMCA-ir in wild type, *nob2*, and Bassoon KO retinas shows prominent displacement into the ONL. (e–f) PMCA1-ir. (i–k) PMCA2-ir. (l–n) RIBEYE-ir in *nob2* retinas

94.4 Discussion

The data presented in this study shows that proper targeting of synaptic proteins and PMCA to photoreceptor terminals requires adequate expression of the Cav1.4 subunit. Loss of Cav1.4 resulted in selective dislocation of the presynaptic machinery at photoreceptor, but not bipolar, ribbon synapses.

It has been suggested that the CSNB2-like phenotype of the *Cacna1f^{nob2}* mouse is caused by diminished production of full-length protein as well as failed targeting of the mutant protein to the plasma membrane (Doering et al. 2008). Our data is consistent with this hypothesis. Displacement of RIBEYE in *nob2* retinas was accompanied by partial, but not complete, dislocation of the key PMCA Ca²⁺ clearance protein from OPL into ONL. Mislocalization of PMCA1-ir into “aggresome-like” puncta to juxtannuclear positions within the *nob2* ONL rods suggests that Cav1.4 subunits are required for tethering the housekeeping PMCA1 mechanism

into a multimeric complex, possibly in association with MPP4 and PSD-95 MAGUK proteins that interact with the full-length “b” splice variant of PMCA1 (Križaj et al. 2002; Yang et al. 2007; Aartsen et al. 2009).

It is not clear whether continuous Ca^{2+} influx through “resting” release from ER stores, store-operated, and/or TRP channel conductances (Križaj et al. 2009; Szikra et al. 2009) can partially compensate for the loss of voltage-operated Ca^{2+} influx at *nob2* rod synapses. Although RIBEYE signals also showed prominent dislocation into the *nob2* ONL, the displacement of the ribbon complex in itself was not sufficient to block asynchronous exocytosis in bipolar and hair cells of Bassoon KO mice (Khimich et al. 2005; Midorikawa et al. 2007). In addition to improper targeting and/or anchoring of PMCA1 (Fig. 94.1), *Bassoon*-null retinas exhibit many of the same morphological and physiological features as *Cacna1f* and *Cabp4* mutant/KO retinas, including decreased amplitudes and increased implicit times of the b-wave (Dick et al. 2003; Haeseleer 2008). If Bassoon tethers both Ca^{2+} channels and PMCA transporters into the arciform complex, synchronous vesicle release at photoreceptor ribbon synapses is likely to be governed by local Ca^{2+} microdomains rather than average $[\text{Ca}^{2+}]_i$ levels that are typically measured with fluorescent indicator dyes. Other presynaptic components required for sustained signaling at rod synapses were observed to be displaced in *nob2* retinas in parallel with PMCAs (D.K. and W.X. in preparation), raising the question of whether such protein agglomerates within the distal ONL represent release-competent proto-synapses. In summary, our study shows that the Cav1.4 α_1 subunit is required for proper targeting of the presynaptic PMCA complex and for tethering of PMCA1 transporters and the Ca^{2+} clearance mechanism into a multimeric presynaptic arciform complex.

Acknowledgments The work was supported by The National Institutes of Health (EY13870, P30EY014800, EY 12497), The Foundation Fighting Blindness, and the Moran TIGER award. The research was also supported by an unrestricted award from Research to Prevent Blindness to the Moran Eye Institute at the University of Utah.

References

- Aartsen WM, Arsanto JP, Chauvin JP et al (2009) PSD95 β regulates plasma membrane Ca^{2+} pump localization at the photoreceptor synapse. *Mol Cell Neurosci* 41:156–165
- Baehr W, Frederick JM (2009) Naturally occurring animal models with outer retina phenotypes. *Vision Res* 49:2636–2652
- Bayley PR, Morgans CW (2007) Rod bipolar cells and horizontal cells form displaced synaptic contacts with rods in the outer nuclear layer of the *nob2* retina. *J Comp Neurol* 500:286–298
- Bech-Hansen NT, Naylor MJ, Maybaum TA et al (1998) Loss-of-function mutations in a calcium-channel α_1 -subunit gene in Xp11.23 cause incomplete X-linked congenital stationary night blindness. *Nat Genet* 19:264–267
- Dick O, tom Dieck S, Altrock WD et al (2003) The presynaptic active zone protein bassoon is essential for photoreceptor ribbon synapse formation in the retina. *Neuron* 37:775–786
- Doering CJ, Rehak R, Bonfield S et al (2008). Modified Ca^{2+} expression in the *Cacna1f*(*nob2*) mouse due to alternative splicing of an ETn inserted in exon 2. *PLoS One* 3:e2538

- Duncan JL, Yang H, Doan T et al (2006) Scotopic visual signaling in the mouse retina is modulated by high-affinity plasma membrane calcium extrusion. *J Neurosci* 26:7201–7211
- Grossman GH, Pauer GJ, Narendra U et al (2010) Tubby-like protein 1 (tulp1) is required for normal photoreceptor synaptic development. *Adv Exp Med Biol* 664:89–96
- Haeseleer F (2008) Interaction and colocalization of CaBP4 and Unc119 (MRG4) in photoreceptors. *Invest Ophthalmol Vis Sci* 49:2366–2375
- Hemara-Wahanui A, Berjukow S, Hope CI et al (2005) A CACNA1F mutation identified in an X-linked retinal disorder shifts the voltage dependence of Cav1.4 channel activation. *Proc Natl Acad Sci USA* 102:7553–7558
- Hoda JC, Zaghetto F, Singh A et al (2006) Effects of congenital stationary night blindness type 2 mutations R508Q and L1364H on Cav1.4 L-type Ca²⁺ channel function and expression. *J Neurochem* 96:1648–1658
- Khimich D, Nouvian R, Pujol R et al (2005) Hair cell synaptic ribbons are essential for synchronous auditory signalling. *Nature* 434:889–894
- Križaj D, Copenhagen DR (1998) Compartmentalization of calcium extrusion mechanisms in the outer and inner segments of photoreceptors. *Neuron* 21:249–256
- Križaj D, Demarco SJ, Johnson J et al (2002) Cell-specific expression of plasma membrane calcium ATPase isoforms in retinal neurons. *J Comp Neurol* 451:1–21
- Križaj D, Huang H, Zou J et al (2009) Localization and function of TRPC1 channels in the mammalian retina. *IOVS Abstr* 5177a, Ft. Lauderdale, FL
- Lodha N, Bonfield S, Orton NC et al (2010) Congenital stationary night blindness in mice - a tale of two *cacnal1f* mutants. *Adv Exp Med Biol* 664:549–558
- Mansergh F, Orton NC, Vessey JP et al (2005) Mutation of the calcium channel gene *Cacna1f* disrupts calcium signaling, synaptic transmission and cellular organization in mouse retina. *Hum Mol Genet* 14:3035–3046
- Midorikawa M, Tsukamoto Y, Berglund K et al (2007) Different roles of ribbon-associated and ribbon-free active zones in retinal bipolar cells. *Nat Neurosci* 10:1268–1276
- Miyake Y, Yagasaki K, Horiguchi M et al (1986) Congenital stationary night blindness with negative electroretinogram. A new classification. *Arch Ophthalmol* 104:1013–1020
- Mizuno F, Barabas P, Rajadhyaksha AM, et al (2010) Internalization of Cav1.3 L-type Ca channels control glutamate-induced deregulation of Ca homeostasis in vertebrate retinal neurons. *Journal of Physiology* 588:953–966
- Peloquin JB, Rehak R, Doering CJ et al (2007) Functional analysis of congenital stationary night blindness type-2 CACNA1F mutations F742C, G1007R, and R1049W. *Neuroscience* 150:335–345
- Rentería RC, Strehler EE, Copenhagen DR et al (2005) Ontogeny of plasma membrane Ca²⁺ ATPase isoforms in the neural retina of the postnatal rat. *Vis Neurosci* 22:263–274
- Specht D, Wu SB, Turner P et al (2009) Effects of presynaptic mutations on a postsynaptic *Cacna1c* calcium channel colocalized with mGluR6 at mouse photoreceptor ribbon synapses. *Invest Ophthalmol Vis Sci* 50:505–515
- Szikra T, Barabas P, Bartoletti TM et al (2009) Calcium homeostasis and cone signaling are regulated by interactions between calcium stores and plasma membrane ion channels. *PLoS One* 4:e6723
- Strom TM, Nyakatura G, Apfelstedt-Sylla E et al (1998) An L-type calcium-channel gene mutated in incomplete X-linked congenital stationary night blindness. *Nat Genet* 19:260–263
- Yang J, Pawlyk B, Wen XH et al (2007) *Mpp4* is required for proper localization of plasma membrane calcium ATPases and maintenance of calcium homeostasis at the rod photoreceptor synaptic terminals. *Hum Mol Genet* 16:1017–29

Chapter 95

Roles for AMP-Activated Protein Kinase in RPE Cell Function

Suofu Qin

Keywords AMPK • Barrier function • Inflammation • Phagocytosis • RPE • Survival

95.1 Introduction

The retinal pigment epithelium (RPE) is a monolayer of cuboidal cells located between the underlying choroidal vasculature and the outer segments of retinal photoreceptor cells (Strauss 2005). The major functions of RPE cells include: supporting the survival and normal functioning of photoreceptors by acting as part of the outer blood-retinal barrier to control exchange of nutrients and waste products; shuttling of retinoids required for visual pigment synthesis to photoreceptors; and phagocytizing shed photoreceptor outer segments (POS) membrane discs for photoreceptor renewal (Strauss 2005). RPE cells also produce immunological factors necessary for establishing immune privilege of the eye (Streilein et al. 2002). Failure in performing these functions may contribute to the retinal degeneration observed in age-related macular degeneration (AMD), an idiopathic retinal degenerative disease that predominates among the elderly in the Western world as a cause of irreversible, profound vision loss (Qin 2007). The pathogenic mechanisms that contribute to the development of AMD remain elusive. However, growing evidence indicates that oxidative stress-induced injury to the RPE plays an important role in the drusen biogenesis and the pathogenesis of AMD (Hageman et al. 2001). Lipid peroxidation, oxygen consumption, and daily phagocytosis of shed POS generate reactive oxygen species (ROS), putting RPE cells under chronic oxidative stress. Via reacting with proteins, DNA, and phospholipids, these ROS exhibit many biological

S. Qin (✉)

Department of Biological Sciences, Retinal Disease Research, Allergan, Inc., 2525 Dupont Drive, Irvine, CA 92612-1599, USA
e-mail: qin_suofu@allergan.com

effects that cause selective modification of cell signaling as well as cell toxicity. However, minimal mechanistic data are available about how oxidative stress affect physiological and pathophysiological functions of RPE cells.

AMP-activated protein kinase (AMPK) is a Ser/Thr kinase, consisting of α , β , and γ subunits, each of which has two or more isoforms that are encoded by distinct genes and are differentially expressed in various tissues (Carling 2004; Fogarty and Hardie 2010). The catalytic subunit of AMPK α has two major isoforms $\alpha 1$ and $\alpha 2$. The $\alpha 1$ isoform is primarily cytoplasmic, whereas $\alpha 2$ is predominantly nuclear and plays a role in transcriptional regulation (da Silva Xavier et al. 2000). AMPK activation results in up-regulation of ATP-producing catabolic pathways such as the metabolism of fatty acids and glucose, while ATP-consuming anabolic pathways such as the synthesis of fatty acids and proteins are downregulated. In addition to being a key regulator of physiological energy dynamics, AMPK has been demonstrated to play roles in regulating various cellular processes such as proliferation, apoptosis (Okoshi et al. 2008; Liu et al. 2010), inflammation and immune responses (Giri et al. 2004), and cell polarity and permeability (Scharl et al. 2009). In this review, the role of AMPK α in regulating RPE cell monolayer integrity, phagocytosis, cytokine production, and survival is discussed.

95.2 Mechanistic Regulation of AMPK Activity

95.2.1 *Allosterical Activation of AMPK*

AMPK is activated by increases in the concentration of AMP, arising from metabolic and environmental stresses that consume or deplete ATP. AMP binds to the γ subunit, which allosterically activates AMPK by inducing a conformational change that prevents the pseudosubstrate domain from interacting with the α subunit kinase domain (Carling 2004; Fogarty and Hardie 2010). The conformational change induced by AMP binding to AMPK also reduces the affinity of AMPK as a substrate for Thr¹⁷² dephosphorylation by inactivating phosphatases such as protein phosphatase 2C (PP2C) (Fogarty and Hardie 2010). A-769662, a synthetic AMPK agonist, works in a similar way as AMP to allosterically activate AMPK, but by binding to the β rather than the γ subunit (Fogarty and Hardie 2010).

95.2.2 *Activation of AMPK via Thr¹⁷²Pphosphorylation by AMPK Kinase*

Conformational change exposes the activation T loop of the α subunit kinase domain to AMPK kinases, which activate AMPK via Thr¹⁷² phosphorylation. Thr¹⁷² phosphorylation is essential and sufficient for AMPK activation (Carling 2004; Fogarty

and Hardie 2010). LKB1, a tumor suppressor, is the major AMPKK in many cell types (Carling 2004). Recent work reveals that the calcium/calmodulin-dependent protein kinase kinase β (CaMKK β) and the transforming growth factor β -activated kinase 1 are also AMPKKs in some cell systems (Fogarty and Hardie 2010). The fact that CaMKK β acts as a AMPKK suggests that AMPK can be activated in the absence of an increase in AMP. Increase in cytosolic Ca²⁺ often causes ATP-consuming processes such as ATP-driven membrane pumps to pump Ca²⁺ back. In this case, AMPK activation could be a mechanism to anticipate the upcoming high demand for ATP.

95.2.3 AMPK Inactivation

Effect of AMP on AMPK activation is antagonized by ATP (Fogarty and Hardie 2010), thus AMPK is sensitive to the change in ratio of AMP to ATP. Alternately, AMPK is inactivated via dephosphorylation of Thr¹⁷² by protein phosphatases, in particular, PP2C (Fogarty and Hardie 2010). In certain circumstances, AMPK activity can be inhibited by ubiquitin-dependent proteasome degradation of AMPK protein (Qi et al. 2008) or by LKB1 inactivation via the formation of covalent adduct through Cys²¹⁰ modification with chemically reactive lipids (Wagner et al. 2006).

95.3 AMPK and RPE Cell Barrier Function

Tight junctions enable the RPE to form the outer retinal-blood barrier by joining neighboring cells together that controls the exchange of nutrients and waste products, and that helps establish cell polarity and maintain different protein compositions of the apical and basolateral membranes. AMPK has recently emerged as a regulator of cell polarity in epithelial cells. Activation of AMPK is required for repolarization of Madin-Darby canine cells in responses to depletion of extracellular calcium (Zhang et al. 2006). ATP depletion-dependent activation of AMPK induces polarization in an intestinal epithelial cell line (Lee et al. 2007). Thus, as maintenance of the permeability barrier provided by epithelia is critical, AMPK activation is diverting what limited energy is available to a crucial survival function. The human RPE cell line, ARPE19, develops a relatively leaky monolayer *in vitro* that has a transepithelial electrical resistance reading of around 40~50 Ω /cm². ARPE19 cells express both AMPK α 1 and AMPK α 2 with a more predominant expression of AMPK α 1 (Qin and De Vries 2008). Knockdown of AMPK α by siRNA reveals that AMPK α is not required for, but only delays the assembly of tight junctions. This delay is exclusively attributed to deletion of AMPK α 2. Consistent with this observation, AMPK α has been reported not to be involved in regulating cell polarity in the retina of *Drosophila* eye (Amin et al. 2009).

AMPK α is required for the maintenance of epithelial cell polarity under energetic stress (Mirouse et al. 2007). Oxidative stress often causes ATP depletion and

RPE cells are under chronic oxidative stress *in vivo*. Oxidative stress induced by hydrogen peroxide activates AMPK α in human RPE cells, but AMPK α appears to have no role in hydrogen peroxide-induced breakdown of RPE cell monolayer (Qin and De Vries 2008). Interestingly, the lipid peroxidation product, 4-hydroxy-2-nonenal (4-HNE), inhibits AMPK α and causes an increase in RPE cell monolayer permeability (Qin and Rodrigues 2010). Knockout of AMPK α 2 but not AMPK α 1 mostly restores the integrity of RPE monolayer damaged by 4-HNE, raising a possibility that AMPK α 2 regulates 4-HNE-induced disassembly of tight junctions in an energy-independent manner. AMPK effects seem to depend on cell type, cell status (cancer vs. normal), inducer, and AMPK α activity. Therefore, caution should be used when interpreting experimental results in a particular cell type.

95.4 AMPK and RPE Cell Phagocytosis

RPE cells maintain survival and normal functions of photoreceptors via phagocytizing shed POS. The clearance of POS is also important for the maintenance of RPE monolayer integrity and function. Under normal conditions, knockdown of AMPK α inhibits the ability of RPE cells to phagocytize POS by 40%. Moreover, knockdown of AMPK α 2 inhibits phagocytosis of POS to a similar extent as knockdown of AMPK α , whereas there is no effect with knockdown of AMPK α 1, revealing that RPE cell phagocytosis depends, at least in part, on AMPK α 2 but not AMPK α 1 (Qin and De Vries 2008). Under stress conditions, sublethal concentrations of hydrogen peroxide activate AMPK α that then inhibits RPE cell phagocytosis. Similar results are observed when AMPK α is activated by the AMP analog, AICAR. Again, AMPK α 2, but not AMPK α 1, mediates the effects of oxidative stress-induced inhibition of RPE cell phagocytosis. AMPK α 2 rather than AMPK α 1 knockout causes a dramatic decrease in oxidative stress-induced AMPK signaling (Qin and De Vries 2008). Currently, it is unclear why oxidative stress-induced inhibition of RPE cell phagocytosis is selectively regulated by AMPK α 2. One possible explanation could be that the differential localization of the α 1 (cytosol) and α 2 (nuclear) isoforms of AMPK contributes to the isoform-selective regulation of RPE cell phagocytosis in response to oxidative stress. What is the significance of reduced phagocytosis of cells undergoing oxidative stress? Continued RPE phagocytosis of POS may add a further insult to the already stressed RPE cells. Reduction of RPE cell phagocytosis by AMPK α 2 activation could protect oxidative stressed-RPE cells from further damage by decreasing phototoxicity caused by the oxidized POS.

95.5 AMPK and RPE Cell Inflammatory Responses

RPE cells play a role in creation and maintenance of the immune privilege of the subretinal space by providing the outer blood-retinal barrier and by expressing cell surface molecules and secreting soluble mediators that influence the immune system (Streilein et al. 2002). RPE cell inflammatory responses are involved in retinal

inflammation and in the pathogenesis of AMD (Hageman et al. 2001; Qin and Rodrigues 2008). Suppression of AMPK α 1 selectively enhances IL-6 production by ~3 fold, whereas AMPK α 2 knockdown stimulates IL-8 production by ~4 fold. These effects appear to be isoform-specific since combined knockdown of both α 1 and α 2 does not further elevate the levels of IL-6 and IL-8 (Qin et al. 2008). Thus, AMPK might contribute to establish subretinal immune privilege by limiting production of inflammatory cytokines. In response to TNF α - or IL-1 β , AMPK appears to have no role in the production of IL-6, IL-8, and MCP-1 by RPE cells (Qin et al. 2008). Furthermore, dys-regulation of IL-8 and MCP-1 by 4-HNE in RPE cells is not associated with AMPK inhibition (Qin and Rodrigues 2010). However, this does not exclude the possibility that production of other cytokines and/or induction of cytokine production by other agonists is controlled by AMPK in activated RPE cells.

95.6 AMPK and RPE Cell Survival

AMPK maintains energy homeostasis by controlling a number of energetic processes through the augmentation of energy producing pathways such as fatty acid oxidation and glucose uptake, concomitant with the suppression of energetically consuming pathways of fatty acid synthesis and gluconeogenesis (Fogarty and Hardie 2010). AMPK activation has been reported to enhance cell death (Okoshi et al. 2008) or protect cells from injury (Liu et al. 2010). In actively dividing cancer cells, inhibition of ATP-consuming processes by AMPK may be less compatible with their survival, whereas in nondividing cells, where the protective effects of AMPK have been observed under acute stress, the shutdown of ATP-consuming pathways may show a protective effect. In RPE cells, knockdown of AMPK α 1 results in a modest increase in cell growth, while knockdown of AMPK α 2 does not affect RPE cell viability in untreated cells. Oxidative stress induced by hydrogen peroxide activates AMPK α , but activated AMPK α has no role in hydrogen peroxide-induced RPE cell death (Qin and De Vries 2008). However, oxidative stress induced by 4-HNE inhibits AMPK α and triggers RPE cell death. Inhibition of AMPK α with a general AMPK α inhibitor also triggers RPE cell death. Intriguingly, when challenged with 4-HNE, a specific knockdown of AMPK α 2 expression protects RPE cells, while knockdown of AMPK α 1 is found to sensitize RPE cells to 4-HNE toxicity (Qin and Rodrigues 2010). The fact that inhibition of AMPK α 1 promotes RPE cell death is consistent with the reported role of AMPK α 1 in mediating expression of antioxidant genes (Liu et al. 2010). The molecular mechanism by which knockdown of AMPK α 2 protects RPE cells from 4-HNE is not clear at present.

95.7 Perspectives

The role of AMPK in the regulation of RPE cell function and pathological responses is a relatively new area of investigation. It is evident that AMPK is an important modulator of a number of RPE cell functions; however, characterization of the

signaling cascades regulated by AMPK has yet to be elucidated in the context of AMPK activation or inhibition. Furthermore, why should a signaling system that evolves to respond to energy deficiency also have a crucial role in tight junction and immune regulation? Understanding AMPK-dependent signaling pathways will shed light on how AMPK modulates diverse processes such as energy balance, cell survival, immunity, tight junction, and cell polarity. The development of isoform-selective inhibitors of AMPK will aid in the discovery of these pathways and may provide novel therapeutic targets for retinal diseases.

References

- Amin N, Khan A, St Johnston D et al (2009) LKB1 regulates polarity remodeling and adherens junction formation in the *Drosophila* eye. *Proc Natl Acad Sci USA* 106:8941–8946
- Carling D (2004) The AMP-activated protein kinase cascade—a unifying system for energy control. *Trends Biochem Sci* 29:18–24
- da Silva Xavier G, Leclerc I, Salt IP et al (2000) Role of AMP-activated protein kinase in the regulation by glucose of islet β cell gene expression. *Proc Natl Acad Sci USA* 97:4023–4028
- Fogarty S, Hardie DG (2010) Development of protein kinase activators: AMPK as a target in metabolic disorders and cancer. *Biochim Biophys Acta* 1804:581–591
- Giri S, Nath N, Smith B et al (2004) 5-aminoimidazole-4-carboxamide-1- β -D-ribofuranoside inhibits proinflammatory response in glial cells: a possible role of AMP-activated protein kinase. *J Neurosci* 24:479–487
- Hageman GS, Luthert PJ, Victor Chong NH et al (2001) An integrated hypothesis that considers drusen as biomarkers of immune-mediated processes at the RPE-Bruch's membrane interface in aging and age-related macular degeneration. *Prog Retin Eye Res* 20:705–732
- Lee JH, Koh H, Kim M et al (2007) Energy-dependent regulation of cell structure by AMP-activated protein kinase. *Nature* 447:1017–1020
- Liu C, Liang B, Wang Q et al (2010) Activation of AMP-activated protein kinase α 1 alleviates endothelial cell apoptosis by increasing the expression of anti-apoptotic proteins Bcl-2 and survivin. *J Biol Chem* 285:15346–15355
- Mirouse V, Swick LL, Kazgan N et al (2007) LKB1 and AMPK maintain epithelial cell polarity under energetic stress. *J Cell Biol* 177:387–392
- Okoshi R, Ozaki T, Yamamoto H et al (2008) Activation of AMP-activated protein kinase induces p53-dependent apoptotic cell death in response to energetic stress. *J Biol Chem* 283:3979–3987
- Qi J, Gong J, Zhao T et al (2008) Downregulation of AMP-activated protein kinase by Cidea-mediated ubiquitination and degradation in brown adipose tissue. *EMBO J* 27:1537–1548
- Qin S (2007) Oxidative damage of retinal pigment epithelial cells and age-related macular degeneration. *Drug Dev Res* 68:213–225
- Qin S, De Vries GW (2008) α 2 But not α 1 AMP-activated protein kinase mediates oxidative stress-induced inhibition of retinal pigment epithelium cell phagocytosis of photoreceptor outer segments. *J Biol Chem* 283:6744–6751
- Qin S, Ni M, De Vries GW (2008) Implication of S-adenosylhomocysteine hydrolase in inhibition of TNF- α - and IL-1 β -induced expression of inflammatory mediators by AICAR in RPE cells. *Invest Ophthalmol Vis Sci* 49:1274–1281
- Qin S, Rodrigues GA (2008) Progress and perspectives on the role of RPE cell inflammatory responses in the development of age-related macular degeneration. *J Inflamm Res* 1:49–65
- Qin S, Rodrigues GA (2010) Differential roles of AMPK α 1 and AMPK α 2 in regulating 4-HNE-induced RPE cell death and permeability. *Exp Eye Res* 91:818–824
- Scharl M, Paul G, Barrett KE et al (2009) AMP-activated protein kinase mediates the interferon- γ -induced decrease in intestinal epithelial barrier function. *J Biol Chem* 284:27952–27963

- Strauss O (2005) The retinal pigment epithelium in visual function. *Physiol Rev* 85:845–881
- Streilein JW, Ma N, Wenkel H et al (2002) Immunobiology and privilege of neuronal retina and pigment epithelium transplants. *Vision Res* 42:487–495
- Wagner TM, Mullally JE, Fitzpatrick FA (2006) Reactive lipid species from cyclooxygenase-2 inactivate tumor suppressor LKB1/STK11: cyclopentenone prostaglandins and 4-hydroxy-2-nonenal covalently modify and inhibit the AMP-kinase kinase that modulates cellular energy homeostasis and protein translation. *J Biol Chem* 281:2598–2604
- Zhang L, Li J, Young LH et al (2006) AMP-activated protein kinase regulates the assembly of epithelial tight junctions. *Proc Natl Acad Sci USA* 103:17272–17277

Chapter 96

Genome-Wide Occupancy Analysis by ChIP-chip and ChIP-Seq

Hong Hao

Keywords ChIP-chip • ChIP-Seq • Chromatin signature • Transcription • Enhancer • Histone • Transcription regulatory network • Photoreceptor • Development

96.1 Introduction

Transcription regulatory network establishes and maintains gene expression programs, which lie at the center of development, physiology, and disease. Transcription factors regulate expression level, spatiotemporal pattern of their target genes by binding to *cis* DNA regulatory elements that are located within promoters close to transcription start site (TSS), or distal enhancers (Maston et al. 2006). One primary function of transcription factor is to recruit cofactors that perform chromatin-remodeling activities or can directly interact with the basal transcriptional machinery (Lemon and Tjian 2000). Transcription factors, in some cases, mediate long-range chromosome looping that brings distal enhancers in close proximity to promoters, and hence, assist in the assembly of basal transcriptional machinery at the promoters (Miele and Dekker 2008). Specific histone modifications have been associated with open vs. close chromatin conformation, thereby leading to gene activation or repression (Heintzman and Ren 2007). To achieve tight control of gene regulation in a spatiotemporal-specific manner, multiple transcription factors within a transcription regulatory network collaborate to regulate common target genes (Heintzman and Ren 2007). The current understanding of transcription regulation was largely developed from characterization of individual genes, and genome-wide studies are needed to re-examine these principles. Identification of genome-scale occupancy of

H. Hao (✉)

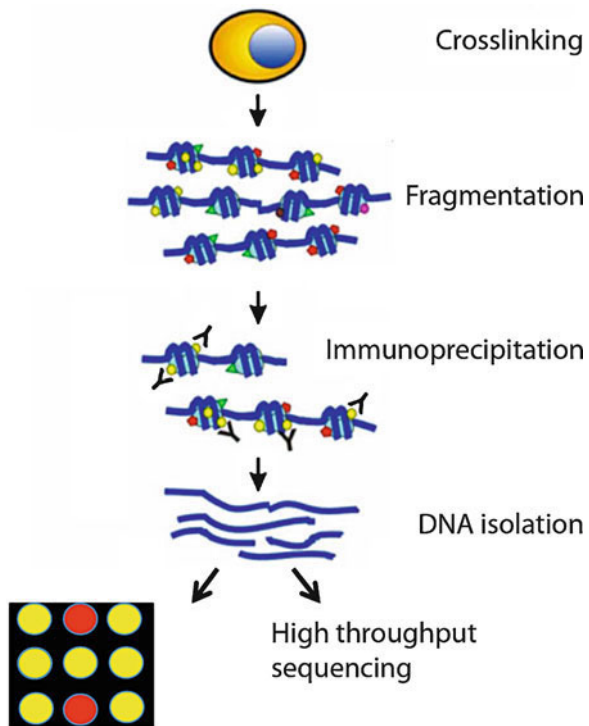
Neurobiology-Neurodegeneration and Repair Laboratory, National Eye Institute,
National Institutes of Health, Bethesda, MD 20892, USA
e-mail: haoh@mail.nih.gov

transcription factors, components of basal transcription machinery, and modified histones constitute the first steps to uncover mechanism of global transcription regulation and should provide insight into development and disease.

96.2 ChIP-chip and ChIP-Seq by Illumina and ABI/SOLiD

Chromatin immunoprecipitation (ChIP) allows isolation and identification of genomic fragments occupied *in vivo* by proteins such as transcription factors and histones (Kirmizis and Farnham 2004). For ChIP, *in vivo* protein-DNA interactions are cross-linked by treatment of cells with formaldehyde and chromatin is fragmented by sonication or enzyme digestion. An antibody that recognizes protein of interest is used to immunoprecipitate the chromatin fragments that are cross-linked with the protein. A normal IgG is used as an immunoprecipitation control. After decross-linking, RNase treatment, and protein digestion, the chromatin is purified either by phenol chloroform extraction and ethanol precipitation or using Qiagen kit. Particular candidate genes can be analyzed by PCR using primers flanking putative binding sites, whereas unbiased genome-wide analysis can be performed by microarray (ChIP-chip) or high-throughput sequencing (ChIP-Seq) (Fig. 96.1).

Fig. 96.1 Chromatin immunoprecipitation (ChIP)-chip and ChIP-Seq. Retina cells are treated with formaldehyde to cross-link *in vivo* protein-DNA interaction. Cells are lysed and chromatin is fragmented by sonication. Protein-DNA complexes are immunoprecipitated by an antibody that recognizes the protein of interest. A normal IgG is used as an immunoprecipitation control. After decross-linking and removal of RNA and protein, DNA is isolated and purified. The DNA can be analyzed by either hybridization to a chip (ChIP-chip) or by high-throughput sequencing (ChIP-Seq)



For ChIP-chip, ChIPed DNA and input DNA, as a control, are blunt-ended by T4 DNA polymerase to allow ligation with a universal oligonucleotide linker, and then are amplified in an unbiased fashion (Kim and Ren 2006). The ChIPed DNA and input control are labeled with fluorescent dyes and hybridized to microarrays (Kim and Ren 2006). Significantly higher fluorescent intensity with ChIPed DNA than with input control indicates enriched binding of protein of interest with the genomic fragment, the identity of which is revealed by the corresponding probes on the microarray. ChIP-chip was used successfully in yeast (Ren et al. 2000); however, studies in higher eukaryotic genomes that are larger and more repetitive are a challenge to the technology. CpG island microarrays and promoter arrays focusing on certain genomic area were used in early studies (Ren et al. 2002; Weinmann et al. 2002). Later, tiling microarrays utilizing short regularly spaced oligonucleotide probes to cover whole genomes were developed. Because the probes are designed to cover nonrepetitive area of the genome, ChIP-chip coverage is less complete than that achieved by direct sequencing. Applications of ChIP-chip are reviewed elsewhere (Zecchini and Mills 2009).

For ChIP-Seq, ChIPed DNA is used to generate a library that is analyzed using high-throughput next-generation sequencing (NGS) platforms such as 454 (now Roche), Solexa (now Illumina), and ABI/SOLiD (now Life Technologies). To construct a ChIP-Seq library for Illumina platform, the ChIPed DNA using either an antibody specific to the protein of interest or a normal IgG control are blunt-ended using DNA polymerase I and phosphorylated using T4 kinase. After adding adenine using Taq polymerase, ChIPed DNA is ligated to a universal adaptor that allows for automatic creation of an asymmetric PCR template. The resulting ChIP-Seq library undergoes linear amplification in a small cycle number PCR, and then is hybridized a flowcell to generate clusters in a PCR-like process. The clusters are linearized and sequenced in a sequencing-by-synthesis process. We conducted parallel ChIP assays to identify genome-wide occupancy of rod-specific transcription factor NRL and generated ChIP-Seq libraries for both Illumina and ABI NGS platforms. The procedures for libraries construction are similar between two platforms and we acquired highly comparable results (unpublished data). False enrichment in ChIP-Seq can be a result of preferred fragmentation of “open” chromatin, nonspecific immunoprecipitation, or PCR preference (Barski and Zhao 2009). It is important to include an IgG control library to distinguish these areas from true binding sites. In our study, sequencing of NRL antibody library detected 7011 binding sites, whereas 5040 was validated as true binding sites by comparing with result from IgG library (unpublished data).

ChIP-Seq offers numerous advantages over ChIP-chip (Park 2009). First, ChIP-Seq offers higher resolution that is determined by the size of chromatin fragments used for ChIP and the depth of sequencing. We fragmented the chromatin to 150–200 bp and achieved good results. The resolution of ChIP-chip is determined by the size of chromatin fragments used for ChIP and is largely limited by the probe density. Second, ChIP-Seq offers better sensitivity without having to suffer the noise generated in the hybridization step in ChIP-chip. Third, ChIP-Seq offers genome-wide coverage that is not limited by the repertoire of probes available on the chip. Finally, ChIP-Seq requires significantly less ChIPed DNA than ChIP-chip.

We used 12 and 25 ng of ChIPed DNA for ChIP-Seq analysis using Illumina and ABI NGS platforms, respectively, whereas 2 μ g of ChIPed DNA was required for a ChIP-chip experiment using the mouse genome-tiling array (Affymetrix). A major limiting factor in ChIP-Seq study is computational analysis of the large amount of data, which is reviewed elsewhere (Park 2009).

96.3 Insights from Genome-Wide Occupancy Studies

96.3.1 Location of Transcription Factor Occupancy

ChIP-chip or ChIP-Seq analyses reveal genome-wide occupancies of transcription factors, relative to TSS, which provide insight into the mechanisms by which transcription factors regulate transcription. Some factors including E2F transcription factor family members and basal transcription factors such as RNA polymerase II (RNAPII) bind almost exclusively to the proximal promoters (Farnham 2009). However, most other analyzed factors bind to diverse regions of the genome, including extragenic regions distant from the TSS and intragenic regions including introns and exons (Farnham 2009). It poses a challenge to identify target genes when the transcription factor-binding site is distant from proximal promoters. Chromosome conformation capture (3C) assay that allows detection of long-range chromosome looping may be of assistance to detect such loopings between distant binding sites (also termed enhancers) with promoters (Simonis et al. 2007).

Biotin ChIP-chip analysis determined promoter-binding targets for 9 transcription factors within the mouse ES transcription network. A striking association was found between the number of factors bound to a promoter region and the chance of target gene expression in undifferentiated ES cells. The target gene promoter bound by multiple factors is more likely to be expressed rather than turned off in ES cells. It is not known whether multiple factor binding was limited only to promoter regions because the study used promoter arrays instead of genome arrays. ChIP-seq analysis of 13 transcription factors that are implicated in maintaining pluripotency of mouse embryonic stem (ES) cells showed that specific distal genomic regions are bound by several factors in close proximity (Chen et al. 2008). A subset of these regions showed strong enhancer activities in transfected ES cells (Chen et al. 2008). This finding supports the notion that transcription factors can bind at distal enhancers to regulate transcription cooperatively. ChIP-Seq analyses of more transcription factors are needed for understanding the transcription regulatory networks underlying development, physiology, and disease.

96.3.2 Chromatin Signatures

Chromatin, composed of histone and DNA, contains information in the form of covalent modifications to histones that indicates the function and activity of the

underlying DNA sequences (Heintzman et al. 2007). ChIP-chip and ChIP-Seq studies of various histone modifications enabled use of chromatin signatures to enumerate novel functional sequences and gene regulation in mammalian genomes (Barski and Zhao 2009; Hon et al. 2009). For details on chromatin signatures composed of distinct sets of histone modifications marking active promoters, repressed promoters, enhancers, and transcribed regions, see reviews elsewhere (Barski and Zhao 2009; Hon et al. 2009). Mikkelsen et al. found that chromatin signature changes during mouse ES cell differentiation reflecting changes in gene expression patterns between pluripotent ES cells and lineage-committed cells (Mikkelsen et al. 2007). Heintzman et al. discovered that H3K4me1 is specifically enriched at enhancers and can be used to identify functionally active enhancers (Heintzman et al. 2009). ChIP-Seq analyses identified a large number of binding events for transcription factors; however, only a portion of these sites are proved to be functional. H3K4me1 ChIP-Seq can be used to narrow down the functional binding events identified by ChIP-Seq analysis of transcription factors.

96.4 Applications of ChIP-chip and ChIP-Seq to the Study of Photoreceptor

Rod and cone photoreceptors, being terminally differentiated neurons with high metabolic rates, are prone to genetic and environmental insults and photoreceptor cell death is a major cause of blindness in developed countries (Wright et al. 2010). Rod and cone photoreceptors along with other retinal cell types are differentiated from multipotent retinal progenitor cells in a conserved order of birth (Livesey and Cepko 2001; Marquardt and Gruss 2002). Transcription factors (ROR β , OTX2, NRL, CRX, NR2E3, and TR β 2) play important roles in photoreceptor cell fate determination and development (Swaroop et al. 2010). OTX2 is essential but not sufficient to induce photoreceptor cell fate. Downstream of OTX2, CRX regulates photoreceptor terminal differentiation, whereas NRL determines rod vs. cone photoreceptor cell fate. NR2E3, a direct transcriptional target of NRL, primarily represses the expression of cone photoreceptor-specific genes. Mutations in human CRX, NRL, and NR2E3 genes have been found in human patients with retinopathies (Swaroop et al. 2010). Transcription regulatory networks composed of transcription factors, cofactors, and target genes remain largely uncharacterized during photoreceptor development and homeostasis.

Combining NRL ChIP-Seq and transcription profiling, we identified 333 direct NRL target genes in adult mouse retina (unpublished data). In vivo knockdown of NRL target genes identified retinal candidate disease genes (unpublished data). Corbo et al. performed CRX ChIP-Seq and identified thousands of in vivo binding events in adult mouse retina (Corbo et al. 2010), suggesting that CRX plays an important regulatory role in maintaining homeostasis of mature photoreceptors. It would be interesting to combine this information with transcription profiling data to identify direct CRX target genes. ChIP-chip analysis of tagged Cyclin D1 knock-in mouse retina revealed that Cyclin D1 regulates Notch1 gene during

development (Bienvenu et al. 2010). Mitton et al. performed ChIP-chip analysis of RNA polymerase II (Pol-II) and detected activation of over 800 additional genes that were undetected by previous microarray analysis during photoreceptor maturation (Tummala et al. 2010). High-resolution mapping of Pol-II, without complications from mRNA degradation in microarray analysis, provided a new resource for correlation to expression data (Tummala et al. 2010). In an effort to define chromatin signatures in developing and mature retina, Barstable et al. performed ChIP-Seq analysis of multiple histone modifications using retina from wild-type mouse and control retina from mutant mouse with photoreceptor degeneration (unpublished data). This study provided the first chromatin state analysis in developing and mature retinas. Transgenic mice that express GFP under the control of 2.5 kb *Nrl* promoter allow isolating photoreceptors at various development stages by flow sorting (Akimoto et al. 2006). It would be interesting to compare chromatin signatures between retinal progenitor cells and individual differentiating retinal cell types including purified photoreceptors at various developmental stages.

96.5 Conclusions and Perspectives

Genome-wide occupancy analyses of transcription factors and modified histones are the first steps toward understanding transcription regulation networks underlying development, physiology, and disease. It is important to expand the analysis to more transcription factors at different developmental stages. It is also important to characterize chromatin signatures of purified retinal cell types at various stages of development. Finally, to elucidate the transcription regulatory network in retina development and disease, the approaches must be multipronged and combine the genome-wide occupancy analysis with global expression profiling and *in vivo* functional analysis.

Acknowledgments I am grateful to Dr. Anand Swaroop for advice. This work was supported by intramural funds of the National Eye Institute.

References

- Akimoto M, Cheng H, Zhu D et al (2006) Targeting of GFP to newborn rods by *Nrl* promoter and temporal expression profiling of flow-sorted photoreceptors. *Proc Natl Acad Sci USA* 103: 3890–3895
- Barski A, Zhao K (2009) Genomic location analysis by ChIP-seq. *J Cell Biochem* 107:11–18
- Bienvenu F, Jirawatnotai S, Elias JE et al (2010) Transcriptional role of cyclin D1 in development revealed by a genetic-proteomic screen. *Nature* 463:374–378
- Chen X et al (2008) Integration of external signaling pathways with the core transcriptional network in embryonic stem cells. *Cell* 133:1106–1117
- Corbo JC, Lawrence KA, Karlstetter M et al (2010) CRX ChIP-seq reveals the cis-regulatory architecture of mouse photoreceptors. *Genome Res* 20:1512–1525

- Farnham PJ (2009) Insights from genomic profiling of transcription factors. *Nat Rev Genet* 10: 605–616
- Heintzman ND, Ren B (2007) The gateway to transcription: identifying, characterizing and understanding promoters in the eukaryotic genome. *Cell Mol Life Sci* 64:386–400
- Heintzman ND, Stuart RK, Hon G et al (2007) Distinct and predictive chromatin signatures of transcriptional promoters and enhancers in the human genome. *Nat Genet* 39:311–318
- Heintzman ND et al (2009) Histone modifications at human enhancers reflect global cell-type-specific gene expression. *Nature* 459:108–112
- Hon GC, Hawkins RD, Ren B (2009) Predictive chromatin signatures in the mammalian genome. *Hum Mol Genet* 18:R195–201
- Kim TH, Ren B (2006) Genome-wide analysis of protein-DNA interactions. *Annu Rev Genomics Hum Genet* 7:81–102
- Kirmizis A, Farnham PJ (2004) Genomic approaches that aid in the identification of transcription factor target genes. *Exp Biol Med (Maywood)* 229:705–721
- Lemon B, Tjian R (2000) Orchestrated response: a symphony of transcription factors for gene control. *Genes Dev* 14:2551–2569
- Livesey FJ, Cepko CL (2001) Vertebrate neural cell-fate determination: lessons from the retina. *Nat Rev Neurosci* 2:109–118
- Marquardt T, Gruss P (2002) Generating neuronal diversity in the retina: one for nearly all. *Trends Neurosci* 25:32–38
- Maston GA, Evans SK, Green MR (2006) Transcriptional regulatory elements in the human genome. *Annu Rev Genomics Hum Genet* 7:29–59
- Miele A, Dekker J (2008) Long-range chromosomal interactions and gene regulation. *Mol Biosyst* 4:1046–1057
- Mikkelsen TS et al (2007) Genome-wide maps of chromatin state in pluripotent and lineage-committed cells. *Nature* 448:553–560
- Park PJ (2009) ChIP-seq: advantages and challenges of a maturing technology. *Nat Rev Genet* 10:669–680
- Ren B, Cam H, Takahashi Y et al (2002) E2F integrates cell cycle progression with DNA repair, replication, and G(2)/M checkpoints. *Genes Dev* 16:245–256
- Ren B, Robert F, Wyrick JJ et al (2000) Genome-wide location and function of DNA binding proteins. *Science* 290:2306–2309
- Simonis M, Kooren J, de Laat W (2007) An evaluation of 3C-based methods to capture DNA interactions. *Nat Methods* 4:895–901
- Swaroop A, Kim D, Forrest D (2010) Transcriptional regulation of photoreceptor development and homeostasis in the mammalian retina. *Nat Rev Neurosci* 11:563–576
- Tummala P, Mali RS, Guzman E, Zhang X, Mitton KP (2010) Temporal ChIP-on-Chip of RNA-Polymerase-II to detect novel gene activation events during photoreceptor maturation. *Mol Vis* 16:252–271
- Weinmann AS, Yan PS, Oberley MJ, Huang TH, Farnham PJ (2002) Isolating human transcription factor targets by coupling chromatin immunoprecipitation and CpG island microarray analysis. *Genes Dev* 16:235–244
- Wright AF, Chakarova CF, Abd El-Aziz MM, Bhattacharya SS (2010) Photoreceptor degeneration: genetic and mechanistic dissection of a complex trait. *Nat Rev Genet* 11:273–284
- Zecchini V, Mills IG (2009) Putting chromatin immunoprecipitation into context. *J Cell Biochem* 107:19–29

Chapter 97

The Bisretinoids of RPE Lipofuscin: A Complex Mixture

Janet R. Sparrow and Kazunori Yamamoto

Keywords Bisretinoids • Retinal pigment epithelium • Lipofuscin • Photooxidation • Vitamin A aldehyde • Macular degeneration • ABCA4 • ELOVL-4

97.1 RPE Lipofuscin Is Unique in Its Origin

Ageing cells, particularly those cell types that are nondividing, are often marked by nondegradable proteins and organelles that accumulate as lipofuscin (Yin 1996; Cuervo and Dice 2000; Sparrow and Boulton 2005). The retinal pigment epithelial (RPE) cells of the eye carry an additional burden; However, these cells also amass fluorescent compounds that are acquired by the RPE due to its role in phagocytosing photoreceptor outer segment membrane (Katz et al. 1986; Sparrow 2007). All of the RPE lipofuscin pigments isolated to date are bisretinoid compounds and we have proposed biosynthetic pathways by which they form (Sakai et al. 1996; Parish et al. 1998; Ben-Shabat et al. 2002b; Fishkin et al. 2005; Kim et al. 2007; Wu et al. 2009) (Fig. 97.1). As expected, the lipofuscin of RPE is housed within organelles of the lysosomal compartment; these bodies are often referred to as lipofuscin granules (Feeney-Burns and Eldred 1983; Boulton et al. 1990; Clancy et al. 2000; Haralampus-Grynaviski et al. 2003). Amino acid analysis of lipofuscin granules purified from

J.R. Sparrow (✉)

Department of Ophthalmology, Columbia University, New York, NY 10032, USA

Department of Pathology and Cell Biology, Columbia University, New York, NY 10032, USA

e-mail: jrs88@columbia.edu

K. Yamamoto

Department of Ophthalmology, Columbia University, New York, NY 10032, USA

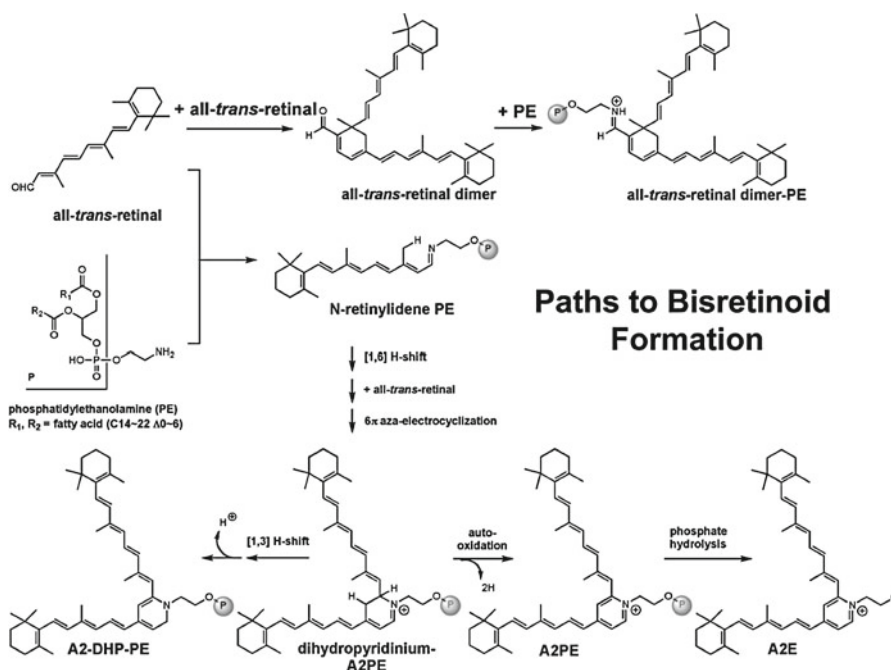


Fig. 97.1 Biosynthetic pathways by which RPE bisretinoids form in photoreceptor outer segments. Condensation reactions between phosphatidylethanolamine (PE) and all-*trans*-retinal generate *N*-retinylidene-PE. The multistep pathway proceeds through intermediates that include an unstable phosphatidyl-dihydropyridinium compound (dihydropyridinium-A2PE). Elimination of one hydrogen from the central ring would lead to the formation of the stable compound A2-dihydropyridine-phosphatidylethanolamine (A2-DHP-PE) while loss of two hydrogens would produce the phosphatidyl-pyridinium bisretinoid A2PE. Alternatively, two molecules of all-*trans*-retinal can condense to form an aldehyde-bearing dimer (all-*trans*-retinal dimer) that then through a Schiff base linkage with phosphatidylethanolamine forms all-*trans*-retinal dimer-PE. Phosphate hydrolysis of A2PE releases A2E. This cleavage occurs in RPE cell lysosomes via phospholipase D. Similarly, phosphate hydrolysis of A2-DHP-PE and all-*trans*-retinal dimer-phosphatidylethanolamine generates A2-DHP-ethanolamine and all-*trans*-retinal dimer-ethanolamine, respectively (not shown)

human RPE revealed very little protein (approximately 2%) (Ng et al. 2008). On the other hand there is abundant evidence that the formation of lipofuscin bisretinoids, in one way or another, involves reactions with phosphatidylethanolamine sitting in the outer segment membrane. Once the bisretinoids are deposited in RPE lysosomes, these compounds can undergo an initial phosphate cleavage to varying extents (discussed below). Further degradation of A2E does not occur, however, probably because the unusual structure of this pigment makes it unrecognizable by the various lysosomal enzymes.

97.2 A2E, Isomers, and Precursors

A prominent component of RPE lipofuscin is the di-retinal conjugate A2E (Sakai et al. 1996; Parish et al. 1998). The polar head of A2E consists of an aromatic ring carrying a positive charge conferred by a quaternary amine nitrogen. Two side-arms extend from the ring, each arm being derived from a molecule of all-*trans*-retinal (Sakai et al. 1996). The alternating double and single bonds that extend the length of the long arm and into the pyridine and ionone rings of A2E provide the extended conjugation system that imparts absorbance at wavelengths in the visible range of the spectrum (~440 nm). The absorbance at ~340 nm is generated within the short arm.

The double bonds along the side-arms of A2E are all in the *trans* (*E*) position, a lower energy configuration. However, photoisomerization of A2E generates several *cis*-isomers the most abundant of which is iso-A2E, wherein the double bond at the C13-14 position assumes the *cis* (*Z*) configuration (Parish et al. 1998). Other *cis*-isomers having *Z*-olefins at the C9/9'-10/10' and C11/11'-12/12' positions are also detected in eye extracts (Ben-Shabat et al. 2002b). For all of these photoisomers of A2E, absorbance spectra are slightly blue shifted relative to A2E (e.g., A2E: λ_{\max} 338, 439; iso-A2E: λ_{\max} 337, 428).

97.3 The All-*Trans*-Retinal Dimer Series of Lipofuscin Fluorophores

While A2E absorbs in the visible spectrum at about 440 nm (the blue region), at least two compounds in RPE lipofuscin have ~510 nm absorbance. One of these, the pigment all-*trans*-retinal dimer-phosphatidylethanolamine (all-*trans*-retinal dimer-PE) is produced when two molecules of all-*trans*-retinal condense to form an aldehyde-bearing dimer (all-*trans*-retinal dimer) that can proceed to form a conjugate with phosphatidylethanolamine via a Schiff base linkage that exhibits pH-dependent protonation (Fishkin et al. 2005; Kim et al. 2007). The second ~510 nm absorbing species all-*trans*-retinal dimer-E can be generated subsequently by phosphate cleavage of all-*trans*-retinal dimer-PE. Moreover, with deprotonation and Schiff base hydrolysis of all-*trans*-retinal dimer-PE and -E, unconjugated all-*trans*-retinal dimer can re-form. We detect the protonated (all-*trans*-retinal dimer-PE and -E) and unprotonated unconjugated (all-*trans*-retinal dimer) forms of this group of compounds in extracts of RPE lipofuscin from humans and mice (Fishkin et al. 2005; Kim et al. 2007).

As with the other lipofuscin pigments, the all-*trans*-retinal dimer series of compounds are housed in lysosomes (pH~5). Conditions in the lysosome appear to support both protonated and unprotonated forms; nevertheless the relative levels of these three pigments are pH dependent. We observed pH modulation of all-*trans*-retinal dimer/all-*trans*-retinal dimer-PE when we exposed posterior eyecups of *Abca4*^{-/-} mice to chloroquine, a weak base amine that in its neutral form enters lysosomes

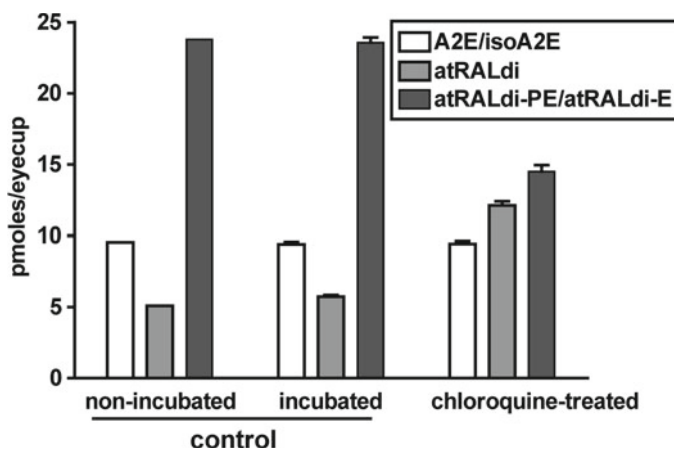


Fig. 97.2 An increase in lysosomal pH changes the relative levels of all-*trans*-retinal dimer vs. all-*trans*-retinal dimer-PE. Eyecups of *Abca4*^{-/-} mice (age 2 months; pigmented Rpe65 Met450; 4 eyecups/sample) were incubated with chloroquine (100 μ M in HEPES-buffered DMEM; 37°C, 20 min)

where it becomes protonated, accumulates, and increases the pH of these acidic organelles, Chloroquine-induced alkalinization of lysosomes shifted the balance toward deprotonation and hydrolysis of all-*trans*-retinal dimer-PE, resulting in lower levels of the latter along with higher levels of unconjugated all-*trans*-retinal dimer. The detection of pH-sensitive lipofuscin compounds that protonate–deprotonate is of additional interest because this is a property that has often been erroneously attributed to A2E. However, A2E/isoA2E are pyridinium salts containing a quaternary amine nitrogen that confers a permanent positive charge on the head group; A2E cannot deprotonate or reprotonate (Parish et al. 1998).

The pigments all-*trans*-retinal dimer-PE and all-*trans*-retinal dimer-E are composed of long (seven double-bond conjugations) and short (four conjugations) polyene arms extending from a cyclohexadiene ring. The relatively long wavelength absorbance of all-*trans*-retinal dimer-PE and all-*trans*-retinal dimer-E (all-*trans*-retinal dimer-PE, $\lambda_{\max} \sim 290, 510$ nm) is attributable to protonation of the Schiff base linkage in these compounds. The absorbance spectrum of unconjugated all-*trans*-retinal dimer exhibits maxima at ~ 290 and 432 nm.

97.4 The Bisretinoid A2-DHP-PE

Yet another RPE bisretinoid A2-dihydropyridine-phosphatidylethanolamine (A2-DHP-PE) has been isolated from RPE lipofuscin extracted from human, mouse, and bovine eyes (Wu et al. 2009). It is notable that, unlike A2E, A2-DHP-PE presents with a noncharged dihydropyridinium ring. Nevertheless, like A2E, its emission

maximum is approximately 600 nm (golden yellow autofluorescence) although it has an excitation maximum of 490 nm (Sparrow et al. 2010). In normal human RPE, the ratio of A2E to A2-DHP-PE is approximately 1:1; the same ratio is observed in wild-type mouse eyes (Wu et al. 2009). As with the other phosphatidyl-bisretinoids (A2PE and all-*trans*-retinal dimer-PE) that form in photoreceptor outer segments, A2-DHP-PE is subject to phosphate hydrolysis in the lysosomes of RPE; the cleavage product A2-DHP-E is detected, although at low levels (Wu et al. 2009). Our experiments indicate that while A2PE is readily cleaved (to A2E) in RPE lysosomes, A2-DHP-PE and all-*trans*-retinal dimer-PE undergo phosphate hydrolysis less readily (Sparrow et al. 2008; Wu et al. 2009). The resistance of A2-DHP-PE to phosphate cleavage explains why A2-DHP-PE is a substantial peak in RPE extracts, although the reason for this is not known.

97.5 Photooxidized Forms of Bisretinoid Pigments in RPE Lipofuscin

The complex mixture of lipofuscin pigments in the RPE includes several photooxidized species of bisretinoid (Jang et al. 2005; Kim et al. 2007). For instance, A2E and all-*trans*-retinal dimer when irradiated at an excitation maximum in the blue region of the spectrum serve as photosensitizers generating various reactive forms of oxygen with singlet oxygen adding to these bisretinoids at carbon-carbon double bonds (Sparrow et al. 2000, 2002; Ben-Shabat et al. 2002a; Jang et al. 2005; Kim et al. 2008). The reactive species generated within photooxidized A2E include endoperoxides, epoxides, and furanoid moieties and these oxidized forms of bisretinoid have been identified in hydrophobic extracts of human RPE and *Abca4*^{-/-} mouse eyecups (Jang et al. 2005; Kim et al. 2007). Importantly, the photodegradation of bisretinoid that follows from photooxidation releases methylglyoxal (MG), a dicarbonyl that is known for mediating advanced glycation end product (AGE) modification of proteins (Wu et al. 2010b). Thus, photodegradation of bisretinoid is likely a source of the AGE detected in aging Bruch's membrane and drusen (Handa et al. 1999; Crabb et al. 2002).

97.6 Discussion

The fluorescent bisretinoids that accumulate as lipofuscin in RPE cells form when all-*trans*-retinal escapes reduction to all-*trans*-retinol and instead undergoes reaction. Notable behaviors of these bisretinoids include a photosensitivity to visible light and an interplay between these compounds and lysosomal functioning. The extensive systems of conjugated double bonds that occupy the side-arms and that in some cases also extend into the central rings are responsible for the ability of these compounds to absorb light in the visible spectrum. The fluorescence emissions of

these pigments are similar and peak at approximately 600 nm. The bisretinoids of RPE are increased several-fold in the *Abca4* null mutant mouse, a model of recessive Stargardt macular degeneration (Weng et al. 1999; Mata et al. 2000, 2001; Kim et al. 2004; Maiti et al. 2006; Wu et al. 2009), and the enhanced formation of these bisretinoids is associated with photoreceptor cell degeneration that is readily detectable at 8–9 months of age (Wu et al. 2010a). Less pronounced increases in A2E are also observed in *Elovl4* 5-bp deletion knock-in mice (Vasireddy et al. 2009) and in transgenic mice carrying the mutated human ELOVL4 gene under control of the interphotoreceptor retinoid-binding protein (Kunys et al. 2010).

Acknowledgments This work was supported by National Institutes of Health Grant EY12951 (to JRS) and a grant from Research to Prevent Blindness to the Department of Ophthalmology. JRS is the recipient of a Research to Prevent Blindness Senior Investigator Award.

References

- Ben-Shabat S, Itagaki Y, Jockusch S et al (2002a) Formation of a nona-oxirane from A2E, a lipofuscin fluorophore related to macular degeneration, and evidence of singlet oxygen involvement. *Angew Chem Int Ed* 41:814–817
- Ben-Shabat S, Parish CA, Vollmer HR et al (2002b) Biosynthetic studies of A2E, a major fluorophore of RPE lipofuscin. *J Biol Chem* 277:7183–7190
- Boulton M, Docchio F, Dayhaw-Barker P et al (1990) Age-related changes in the morphology, absorption and fluorescence of melanosomes and lipofuscin granules of the retinal pigment epithelium. *Vision Res* 30:1291–1303
- Clancy CMR, Krogmeier JR, Pawlak A et al (2000) Atomic force microscopy and near-field scanning optical microscopy measurements of single human retinal lipofuscin granules. *J Phys Chem B* 104:12098–12101
- Crabb JW, Miyagi M, Gu X et al (2002) Drusen proteome analysis: an approach to the etiology of age-related macular degeneration. *Proc Natl Acad Sci USA* 99:14682–14687
- Cuervo AM, Dice JR (2000) When lysosomes get old. *Exp Gerontol* 35:119–131
- Feeney-Burns L, Eldred GE (1983) The fate of the phagosome: conversion to ‘age pigment’ and impact in human retinal pigment epithelium. *Trans Ophthalmol Soc UK* 103:416–421
- Fishkin N, Sparrow JR, Allikmets R et al (2005) Isolation and characterization of a retinal pigment epithelial cell fluorophore: an all-trans-retinal dimer conjugate. *Proc Natl Acad Sci USA* 102:7091–7096
- Handa JT, Verzijl N, Matsunaga H et al (1999) Increase in advanced glycation end product pentosidine in Bruch’s membrane with age. *Invest Ophthalmol Vis Sci* 40:775–779
- Haralampus-Grynaviski NM, Lamb LE, Clancy CMR et al (2003) Spectroscopic and morphological studies of human retinal lipofuscin granules. *Proc Natl Acad Sci USA* 100:3179–3184
- Jang YP, Matsuda H, Itagaki Y et al (2005) Characterization of peroxy-A2E and furan-A2E photooxidation products and detection in human and mouse retinal pigment epithelial cells lipofuscin. *J Biol Chem* 280:39732–39739
- Katz ML, Drea CM, Eldred GE et al (1986) Influence of early photoreceptor degeneration on lipofuscin in the retinal pigment epithelium. *Exp Eye Res* 43:561–573
- Kim SR, Jockusch S, Itagaki Y et al (2008) Mechanisms involved in A2E oxidation. *Exp Eye Res* 86:975–982
- Kim SR, Fishkin N, Kong J et al (2004) The Rpe65 Leu450Met variant is associated with reduced levels of the RPE lipofuscin fluorophores A2E and iso-A2E. *Proc Natl Acad Sci USA* 101:11668–11672

- Kim SR, Jang YP, Jockusch S et al (2007) The all-trans-retinal dimer series of lipofuscin pigments in retinal pigment epithelial cells in a recessive Stargardt disease model. *Proc Natl Acad Sci USA* 104:19273–19278
- Kuny S, Gaillard F, Mema SC et al (2010) Inner Retina Remodeling in a Mouse Model of Stargardt-like Macular Dystrophy (STGD3). *Invest Ophthalmol Vis Sci* 51:2248–2262
- Maiti P, Kong J, Kim SR et al (2006) Small molecule RPE65 antagonists limit the visual cycle and prevent lipofuscin formation. *Biochem* 45:852–860
- Mata NL, Weng J, Travis GH (2000) Biosynthesis of a major lipofuscin fluorophore in mice and humans with ABCR-mediated retinal and macular degeneration. *Proc Natl Acad Sci USA* 97:7154–7159
- Mata NL, Tzekov RT, Liu X et al (2001) Delayed dark adaptation and lipofuscin accumulation in *abcr*+/- mice: implications for involvement of *ABCR* in age-related macular degeneration. *Invest Ophthalmol Vis Sci* 42:1685–1690
- Ng KP, Gugiu BG, Renganathan K et al (2008) Retinal pigment epithelium lipofuscin proteomics. *Mol Cell Proteomics* 7:1397–1405
- Parish CA, Hashimoto M, Nakanishi K et al (1998) Isolation and one-step preparation of A2E and iso-A2E, fluorophores from human retinal pigment epithelium. *Proc Natl Acad Sci USA* 95:14609–14613
- Sakai N, Decatur J, Nakanishi K et al (1996) Ocular age pigment “A2E”: An unprecedented pyridinium bisretinoid. *J Am Chem Soc* 118:1559–1560
- Sparrow JR (2007) RPE lipofuscin: formation, properties and relevance to retinal degeneration. In: Tombran-Tink J, Barnstable CJ (eds) *Retinal Degenerations: Biology, Diagnostics and Therapeutics*. Humana Press, Totowa, NJ
- Sparrow JR, Boulton M (2005) RPE lipofuscin and its role in retinal photobiology. *Exp Eye Res* 80:595–606
- Sparrow JR, Nakanishi K, Parish CA (2000) The lipofuscin fluorophore A2E mediates blue light-induced damage to retinal pigmented epithelial cells. *Invest Ophthalmol Vis Sci* 41:1981–1989
- Sparrow JR, Kim SR, Cuervo AM et al (2008) A2E, a pigment of RPE lipofuscin is generated from the precursor A2PE by a lysosomal enzyme activity. *Adv Exp Med and Biol* 613:393–398
- Sparrow JR, Zhou J, Ben-Shabat S et al (2002) Involvement of oxidative mechanisms in blue light induced damage to A2E-laden RPE. *Invest Ophthalmol Vis Sci* 43:1222–1227
- Sparrow JR, Wu Y, Nagasaki T et al (2010) Fundus autofluorescence and the bisretinoids of retina. *Photochem Photobiol Sci* 9:1480–1489
- Vasireddy V, Jablonski MM, Khan NW et al (2009) Elov14 5-bp deletion knock-in mouse model for Stargardt-like macular degeneration demonstrates accumulation of ELOVL4 and lipofuscin. *Exp Eye Res* 89:905–912
- Weng J, Mata NL, Azarian SM et al (1999) Insights into the function of Rim protein in photoreceptors and etiology of Stargardt’s disease from the phenotype in *abcr* knockout mice. *Cell* 98:13–23
- Wu L, Nagasaki T, Sparrow JR (2010a) Photoreceptor cell degeneration in *Abcr*^{-/-} mice. *Adv Exp Med Biol* 664:533–539
- Wu Y, Fishkin NE, Pande A et al (2009) Novel lipofuscin bisretinoids prominent in human retina and in a model of recessive Stargardt disease. *J Biol Chem* 284:20155–20166
- Wu Y, Yanase E, Feng X et al (2010b) Structural characterization of bisretinoid A2E photocleavage products and implications for age-related macular degeneration. *Proc Natl Acad Sci USA* 107:7275–7280
- Yin D (1996) Biochemical basis of lipofuscin, ceroid, and age pigment-like fluorophores. *Free Rad Biol Med* 21:871–888

Chapter 98

Biochemical Characterization of Cone Cyclic Nucleotide-Gated (CNG) Channel Using the Infrared Fluorescence Detection System

Xi-Qin Ding, Alexander Matveev, Anil Singh, Naoka Komori,
and Hiroyuki Matsumoto

Keywords Retina • Photoreceptor • Cone • CNG channel • Achromatopsia

98.1 Introduction

Photoreceptor cyclic nucleotide-gated (CNG) channels play a pivotal role in phototransduction (Kaupp and Seifert 2002). Structurally, CNG channels belong to the superfamily of voltage-gated ion channels. The channel comprises two structurally related subunit types, the A and B subunits. Rod CNG channel is composed of CNGA1 and CNGB1 while cone CNG channel is composed of CNGA3 and CNGB3. It is known that the proper subunit interaction and complex formation are critical for the channel function (Trudeau and Zagotta 2002). The structure of the native rod CNG channel has been well studied using bovine retina, showing a stoichiometry of three CNGA1 and one CNGB1 (Weitz et al. 2002; Zhong et al. 2002). In contrast, our understanding of the cone CNG channel structure is quite limited. This is due to the difficulty of studying cone-specific protein in a rod-dominant retina and the structural feature of the cone CNG channel subunits. The molecular masses of CNGA3 and CNGB3 are similar to each other (72 vs. 80 kDa), which

X.-Q. Ding (✉) • A. Matveev
Department of Cell Biology, University of Oklahoma Health Sciences Center,
Oklahoma City, OK 73104, USA
e-mail: xi-qin-ding@ouhsc.edu

A. Singh • N. Komori • H. Matsumoto
Department of Biochemistry and Molecular Biology, University of Oklahoma
Health Sciences Center, Oklahoma City, OK 73104, USA

makes the study of composition and stoichiometry of cone CNG channel quite challenging using the conventional approaches. We have shown that the cone-dominant *Nrl*^{-/-} retina is a valuable tool to study cone CNG channel (Matveev et al. 2008). This work examined the complex structure of cone CNG channel prepared from *Nrl*^{-/-} retina using the infrared fluorescence Western detection combined with chemical cross-linking and blue native-PAGE and the findings improved our understandings of the cone CNG channel structure.

98.2 Materials and Methods

98.2.1 *Infrared Fluorescence Western Detection of Cone CNG Channel*

Mouse retinal membrane protein extracts were prepared as described previously (Ding et al. 2009). The membrane proteins were separated by 10% SDS-PAGE, followed by transferring onto polyvinylidene fluoride (PVDF) membrane for infrared fluorescence Western Detection. The rabbit anti-CNGA3 and anti-CNGB3 were labeled with the IRDye-800CW and IRDye-680 fluorescence dyes (LI-COR Biosciences UK Ltd). The Odyssey[®] Infrared Imaging System (LI-COR Biosciences UK Ltd) was used for the imaging quantitative analysis. Peptide competition experiments were performed as described previously (Matveev et al. 2008).

98.2.2 *Chemical Cross-Linking*

Chemical cross-linking experiments were performed using *Nrl*^{-/-} retinal membrane preparations as described previously (Matveev et al. 2008). The amino-specific cross-linker BS³ at varying concentrations was used; the cross-linking reactions were terminated by addition of 5.0 mM DTT; and cross-linking products were resolved onto 3–8% Nu-PAGE, followed by infrared fluorescence detection.

98.2.3 *Blue Native-PAGE*

Blue native-PAGE was performed as described by Wittig et al. (2006). Several types of detergents, including digitonin, Brij 96, Triton X100, and dodecylmaltoside (DDM), were tested to solubilize the membranes, and DDM was shown to produce an optimal solubilization and was used in this study.

98.3 Results

98.3.1 Simultaneous Detection of CNGA3 and CNGB3 in the Mouse Retina by Infrared Fluorescence Western Detection

CNGA3 and CNGB3 in the mouse retina were detected by the respective antibodies labeled with both IRDye-800CW (green) and IRDye-680 (red) dyes with a linear range ($r^2 \geq 0.97$) (Fig. 98.1a). Simultaneous detection of CNGA3 and CNGB3 on

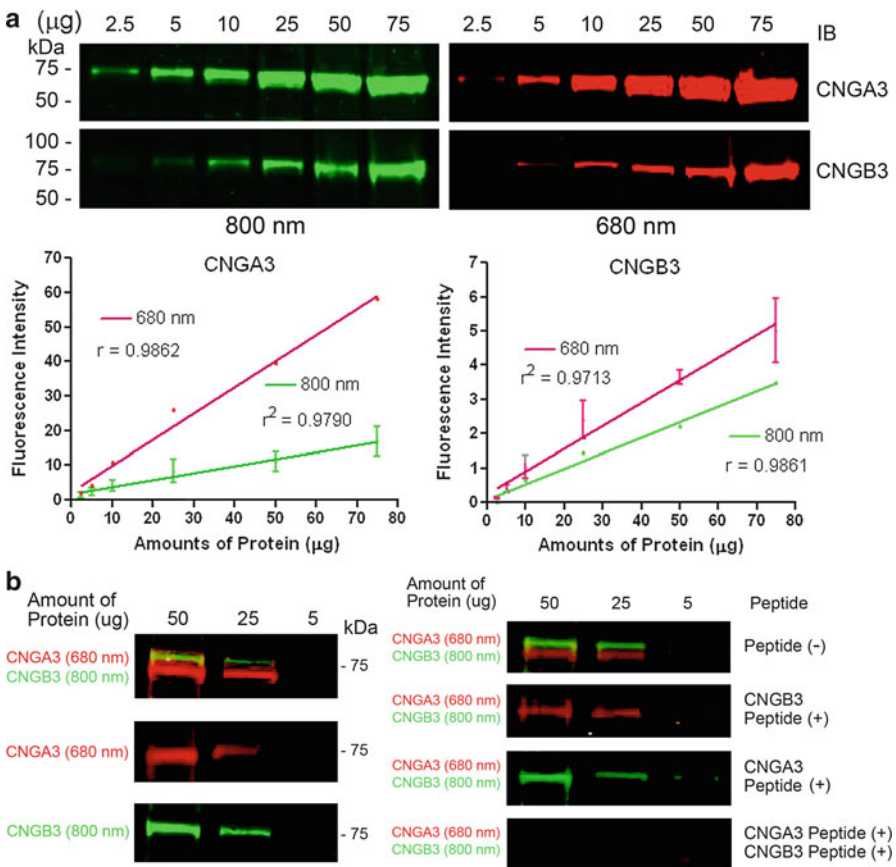


Fig. 98.1 Simultaneous detection of CNGA3 and CNGB3 in the mouse retina by infrared fluorescence Western detection. Increasing amounts (2.5–75 μg) of Nrl^{-/-} retinal membranes were resolved by 10% SDS-PAGE, followed by immunoblotting using anti-CNGA3 and anti-CNGB3 labeled with IRDye-680 and IRDye-800CW. **(a)** Quantitative detection of CNGA3 and CNGB3 in the mouse retina. **(b) Left panel**, simultaneous detection of CNGA3 and CNGB3 in the mouse retina using infrared fluorescence detection. **Right panel**, peptide competition experiments showed specificity of the detection. The blots were incubated with antibodies in the absence and presence of the specific peptides (150 μg/mL) followed by fluorescence scanning and imaging

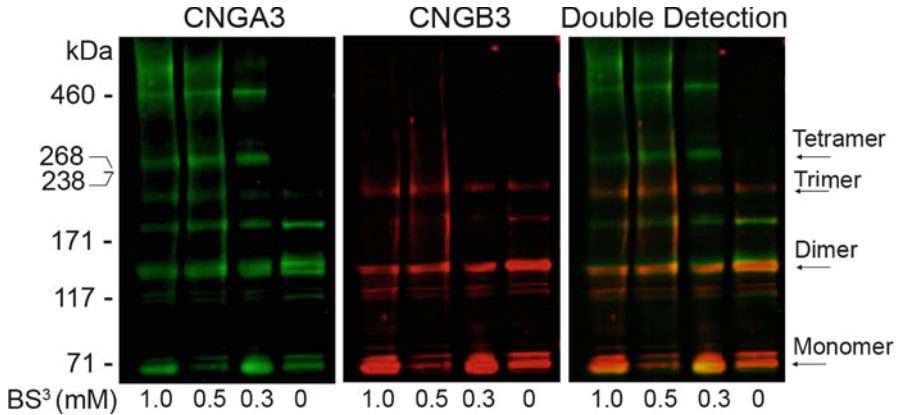


Fig. 98.2 Analysis of cone CNG channel complexes using chemical cross-linking and infrared fluorescence detection. The reactions were performed using *Nrl*^{-/-} retinal membranes and the amino-specific cross-linker BS³ at varying concentrations as indicated at room temperature for 30 min. The cross-linking products were separated by 3–8% Nu-PAGE, followed by infrared fluorescence Western detection

the same blots was achieved (Fig. 98.1b, left panel), and the specific detection was shown by peptide competition experiments (Fig. 98.1b, right panel).

98.3.2 *Analysis of Cone CNG Channel Complexes Using Chemical Cross-Linking and Infrared Fluorescence Detection*

Chemical cross-linking is a useful approach to evaluate the composition of a protein complex and the spatial proximity between two or more macromolecules (Matveev et al. 2008; Schwarzer et al. 2000). We analyzed the cone CNG channel complexes by chemical cross-linking combined with infrared fluorescence detection. Figure 98.2 shows a typical gel separation of the cross-linked products with varying concentrations of BS³, analyzed by infrared fluorescence detection. The cross-linked products equivalent to the dimer (~150 kDa), trimer (~240 kDa), and tetramer (~320 kDa) of the channel complexes, respectively, were detected by both anti-CNGA3 and anti-CNGB3 antibodies. The overlay image shows the co-detections of CNGA3 and CNGB3 subunits at varying sizes of the complexes. The relative signals of CNGB3 were more abundant in the dimeric and trimeric complexes but less abundant in the tetrameric complexes. Quantification of the fluorescence intensities of the tetrameric complexes shows that the CNGA3 signal was nearly threefold higher than the CNGB3 signal.

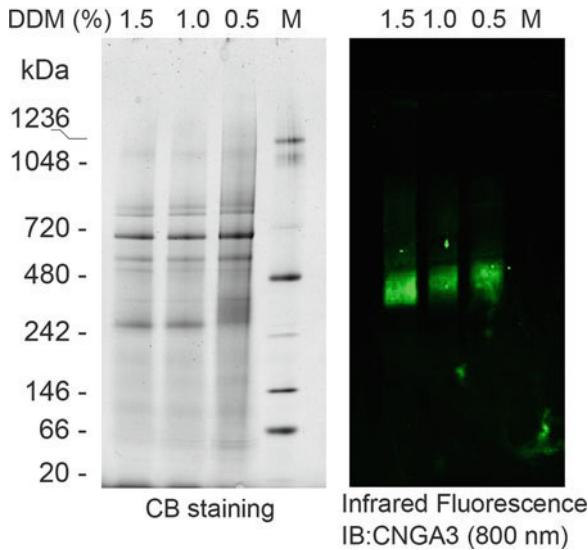


Fig. 98.3 Analysis of cone CNG channel by blue native-PAGE. (a) Blue native-PAGE separation of *Nrl*^{-/-} retinal membranes solubilized by various concentrations of DDM. The membrane proteins were resolved by 3–12% native gel using a blue native gel electrophoresis system. *CB* Coomassie blue. (b) Proteins resolved on blue native gel were transferred onto PVDF membranes, followed by infrared fluorescence Western detection using anti-CNGA3 labeled with IRDye-800CW

98.3.3 Analysis of Cone CNG Channel by Blue Native-PAGE

Blue native-PAGE has been widely used to study the structure of a protein complex (Chavan et al. 2006; Pyndiah et al. 2007). We applied this technique to evaluate the structure of cone CNG channel under native conditions. Figure 98.3 shows a typical blue native-PAGE separation of *Nrl*^{-/-} retinal membranes visualized by Coomassie blue staining (Fig. 98.3a) and by infrared fluorescence Western detection (Fig. 98.3b). The channel complexes migrated to an area between 300 and 480 kDa, which is close to the results obtained from the chemical cross-linking experiments.

98.4 Discussion

Unlike that of the rod CNG channel our understanding of the cone CNG channel structure is quite limited. Two reports so far have described the stoichiometry of cone CNG channel using heterologous expression systems. The study by Zhong et al. proposed a three CNGA3 and one CNGB3 stoichiometry based on the identification

of a C-terminal leucine zipper homology domain in all the A subunits of CNG channel (Zhong et al. 2002). In contrast, a 2A:2B stoichiometry was proposed by Peng et al. based on their electrophysiological recordings and biochemical studies using a *Xenopus oocytes* expression system (Peng et al. 2004). With co-immunoprecipitation and chemical cross-linking, we have shown that the native cone CNG channel is a heterotetrameric complex. This work utilizes the advantages of infrared fluorescence detection to analyze the complex structure of the native cone CNG channel. The infrared fluorescence Western detection has been shown to provide a valuable tool for quantitative, two-color detection of proteins and analysis of components of a protein complex (Yashiro et al. 2005). This especially gives advantages in detecting proteins that migrate on a gel at a similar position. By using this technique combined with chemical cross-linking, we detected more abundant CNGA3 in the tetrameric complex. Taken together with the findings of the specific interactions between CNGA3 and CNGB3 and between two CNGA3 but not between two CNGB3 (Matveev et al. 2010), this work provided experimental evidence supporting three CNGA3 and one CNGB3 stoichiometry.

We also analyzed the channel complexes that were resolved under native conditions using blue native-PAGE. This technique permits a high-resolution separation of multiprotein complexes under native conditions and is specially designed for membrane proteins. We successfully resolved the channel complexes on a blue native-PAGE. Combined with a subsequent SDS-PAGE in the second dimension, protein complexes separated by blue native-PAGE can be dissected into their subunits. Success in the blue native-PAGE enables us to further analyze the channel complexes with a blue native-PAGE/SDS-PAGE 2D system.

In summary, we analyzed native cone CNG channel complexes using infrared fluorescence detection combined with chemical cross-linking and blue native-PAGE. The experimental results suggest that the cone CNG channel is a heterotetrameric complex likely at a stoichiometry of three CNGA3 and one CNGB3.

Acknowledgments This work was supported by grants from the National Center for Research Resources (P20RR017703), the National Eye Institute (P30EY12190, R01EY019490, and R21EY17888), the American Health Assistance Foundation, and the Oklahoma Center for the Advancement of Science & Technology (OCAST). We thank Micaela J. Langevin for technical assistance.

References

- Chavan M, Chen Z, Li G et al (2006) Dimeric organization of the yeast oligosaccharyl transferase complex. *Proc Natl Acad Sci USA* 103:8947–52
- Ding XQ, Harry S, Umino Y et al (2009) Impaired cone function and cone degeneration resulting from CNGB3 deficiency: down-regulation of CNGA3 biosynthesis as a potential mechanism. *Hum Mol Genet* 18:4770–80
- Kaup UB and Seifert R (2002) Cyclic nucleotide-gated ion channels. *Physiol Rev* 82:769–824
- Matveev AV, Fitzgerald JB, Xu JH et al (2010) The disease-causing mutations in the carboxyl terminus of the cone cyclic nucleotide-gated channel CNGA3 subunit alter the local secondary structure and interfere with the channel active conformational change. *Biochemistry* 49:1628–39

- Matveev AV, Quiambao AB, Browning Fitzgerald J et al (2008) Native cone photoreceptor cyclic nucleotide-gated channel is a heterotetrameric complex comprising both CNGA3 and CNGB3: a study using the cone-dominant retina of *Nrl*^{-/-} mice. *J Neurochem* 106:2042–55
- Peng C, Rich ED, Varnum MD (2004) Subunit configuration of heteromeric cone cyclic nucleotide-gated channels. *Neuron* 42:401–10
- Pyndiah S, Lasserre JP, Menard A et al (2007) Two-dimensional blue native/SDS gel electrophoresis of multiprotein complexes from *Helicobacter pylori*. *Mol Cell Proteomics* 6:193–206
- Schwarzer A, Schauf H, Bauer PJ (2000) Binding of the cGMP-gated channel to the Na/Ca-K exchanger in rod photoreceptors. *J Biol Chem* 275:13448–54
- Trudeau MC and Zagotta WN (2002) An intersubunit interaction regulates trafficking of rod cyclic nucleotide-gated channels and is disrupted in an inherited form of blindness. *Neuron* 34:197–207
- Weitz D, Ficek N, Kremmer E et al (2002) Subunit stoichiometry of the CNG channel of rod photoreceptors. *Neuron* 36:881–9
- Wittig I, Braun HP, Schagger H (2006) Blue native PAGE. *Nat Protoc* 1:418–28
- Yashiro K, Corlew R, Philpot BD (2005) Visual deprivation modifies both presynaptic glutamate release and the composition of perisynaptic/extrasynaptic NMDA receptors in adult visual cortex. *J Neurosci* 25:11684–92
- Zhong H, Molday LL, Molday RS et al (2002) The heteromeric cyclic nucleotide-gated channel adopts a 3A:1B stoichiometry. *Nature* 420:193–8

Chapter 99

Ras-Associating Domain Proteins: A New Class of Cyclic Nucleotide-Gated Channel Modulators

Vivek K. Gupta, Ammaji Rajala, and Raju V.S. Rajala

Keywords Cyclic nucleotide-gated channel • Ras-associating domain • Growth factor receptor bound protein-14 • Photoreceptor • PHLPP1 • PHLPP2

99.1 Introduction

Like almost all major biological processes, phototransduction is achieved by the interaction of proteins, leading to manifold functional outcomes. Cyclic nucleotide-gated (CNG) channels comprise an indispensable element in phototransduction and as such are apt and inclined to play a regulatory role. CNG channels play important roles in visual and olfactory transduction (Yau and Baylor 1989; Biel et al. 1999; Kaupp and Seifert 2002; Yau and Hardie 2009; Gerstner et al. 2000). In the visual system, a cyclic guanosine monophosphate (cGMP)-gated channel is found in the outer membrane of retinal photoreceptor cells. The cGMP-sensitive cation channel is the sensor of the changes in cytoplasmic cGMP concentration brought about by light (Yau and Baylor 1989). CNG channels comprise two structurally related subunit types: A and B (Kaupp and Seifert 2002). The rod channel consists of CNGB1 and CNGA1 subunits, whereas the cone channel contains CNGA3 and CNGB3 subunits. Heterologous expression studies have shown that the A subunits are responsible for the ion-conducting activity of the channel, whereas the B subunits function as modulators (Gerstner et al. 2000). The CNG channel sensitivity toward cGMP has been studied extensively and has been shown to depend on and regulated by

V.K. Gupta • A. Rajala

Department of Ophthalmology, Dean A. McGee Eye Institute, University of Oklahoma Health Sciences Center, 608 Stanton L. Young Blvd, Oklahoma City, OK 73104, USA

R.V.S. Rajala (✉)

Departments of Ophthalmology and Cell Biology, Dean A. McGee Eye Institute, University of Oklahoma Health Sciences Center, 608 Stanton L. Young Blvd, Oklahoma City, OK 73104, USA

e-mail: raju-rajala@ouhsc.edu

several other factors prominent of which are $\text{Ca}^{2+}/\text{CaM}$, divalent ions, diacylglycerol, phospholipids, and phosphorylation state (reviewed in Kaupp and Seifert 2002). These channels have an N-terminal and a C-terminal cytoplasmic region, which are freely available in the cytoplasm for a multitude of factors to interact with. We recently reported that Ras-associating domain of growth factor receptor-bound protein 14 (Grb14) binds to the C-terminal region of rod CNGA1 subunit and modulates its activity in vivo (Gupta et al. 2010). Studies from several laboratories have shown that RA/RBD domain-containing proteins are expressed in the retina which include c-Raf (Pimentel et al. 2000), Pi3k (Rajala et al. 2002), AF-6 (Kanai-Azuma et al. 2000), Tiam1 (Tanaka et al. 2004), PHLPP1 and 2 (Kanan et al. 2010), Grb14 (Rajala et al. 2005), and EPAC (Ivins et al. 2004), however, no information is available on their effect on channel. PHLPP1 and PHLPP2 (PH domain and Leucine-rich repeat Protein Phosphatases) (Gao et al. 2005) are the two putative RA domain-containing proteins which play an important role in IR signaling (Kanan et al. 2010). In this study, we have investigated the effect of RA domain-containing proteins, PHLPP1 and PHLPP2, on rod CNG channel sensitivity.

99.2 Materials and Methods

99.2.1 Cell Culture Studies and Vectors

HEK293T cells (2.5×10^5) were seeded in each dish 12–18 h before transfection and transfected with the cDNA constructs (Wigler et al. 1978). The generation of CNGA1, Grb14 (Myc), PHLPP1, and PHLPP2 (FLAG) vectors has been described previously (Gupta et al. 2010; Kanan et al. 2010; Rajala et al. 2009). The fluorescent indicator Indo-1/AM was used to quantify Ca^{2+} influx through CNGA1 channels in HEK293T cell suspensions (Gupta et al. 2010).

99.2.2 Sequence Alignment and Domain Assessment

The RA domain of Grb14 (106–192; Uniprot id. Q6ZVD8) was used to align with the human PHLPP2 (Uniprot id. Q14449) sequence using multiple sequence alignment portals (Corpet 1988). Having ascertained the span of RA domain in PHLPP2, this sequence was further aligned with the human PHLPP1 (β) (Uniprot id. Q14449) and the exact position of PHLPP1 (β) RA domain determined.

99.2.3 Statistical Methods

Data were analyzed using Graphpad Prism software (GraphPad Software, San Diego, CA), expressed as the mean \pm S.D., and compared the differences by Student's *t* test. The critical level of significance was set at $p < 0.05$.

99.3 Results

99.3.1 Assessment of RA Domains in PHLPP1 and PHLPP2

We have reported recently that Grb14 inhibits CNGA1 channel activity through its RA domain (Gupta et al. 2010). Both PHLPP1 (β) and 2 have been speculated to possess a putative RA domain (Gao et al. 2009). Primary structural analysis indicates that both PHLPP1 (β) and PHLPP2 possess a discernible RA domain followed by a PH domain like the Grb14 family members (Fig. 99.1). The domain organization of both PHLPP1 (β) and PHLPP2 are shown in Fig. 99.1. The RA domain-like sequence was assigned to regions 430–515 and 44–129 in human PHLPP1 and PHLPP2 isoforms based on the primary structure comparison with human Grb14 RA domain (106–192). No such sequence was observed in PHLPP1 (α) isoform. A similarity of 20–25% was observed at the primary structural level (with what). Both of these isoforms were observed to be present in retina; however, PHLPP2 is highly expressed in rod photoreceptors (Kanan et al. 2010). The sequence comparison indicates that RA domain in the two families of proteins is not highly homologous further highlighting the structural and functional heterogeneity among the RA

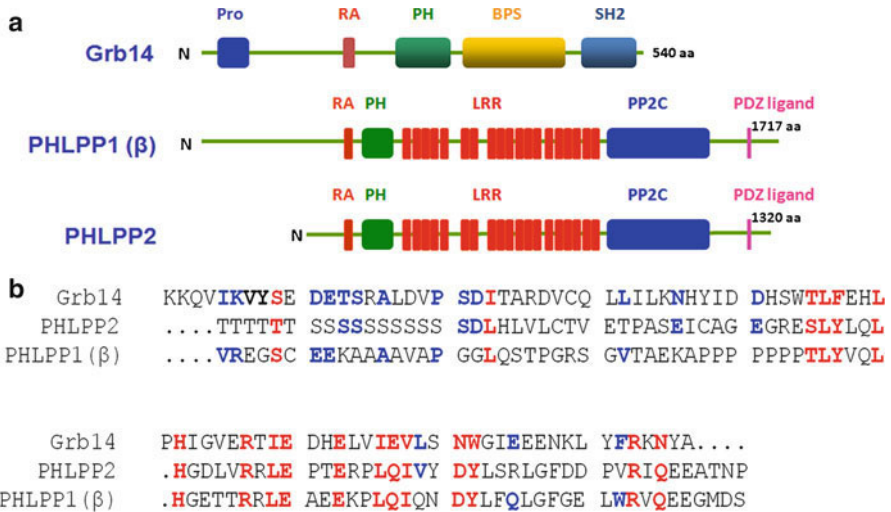


Fig. 99.1 Comparative domain analysis of the Grb14 with PHLPP1 (β) and PHLPP2. (a) The primary structure analysis of the PHLPP1 (β) and PHLPP2 shows that these proteins contain RA and PH domain in a pattern similar to the Grb14 family. Various domains of the proteins are shown diagrammatically. (b) The primary structural homology between RA domains of these proteins was established by multiple sequence alignment. The similarity consensus is 90% (red: Grb14 and PHLPP1 (β) and 2; blue: Grb14 and either PHLPP1 (β) or PHLPP2). *Pro* proline-rich region; *RA* Ras-associating; *PH* pleckstrin homology; *BPS* between PH and SH2; *SH2* Src-homology-2 region; *LRR* leucine-rich repeat; *PP2C* protein phosphatase 2C; *PDZ* postsynaptic density protein (PSD95); *drosophila* disc large tumor suppressor (DlgA), and zonula occludens-1 protein (zo-1)

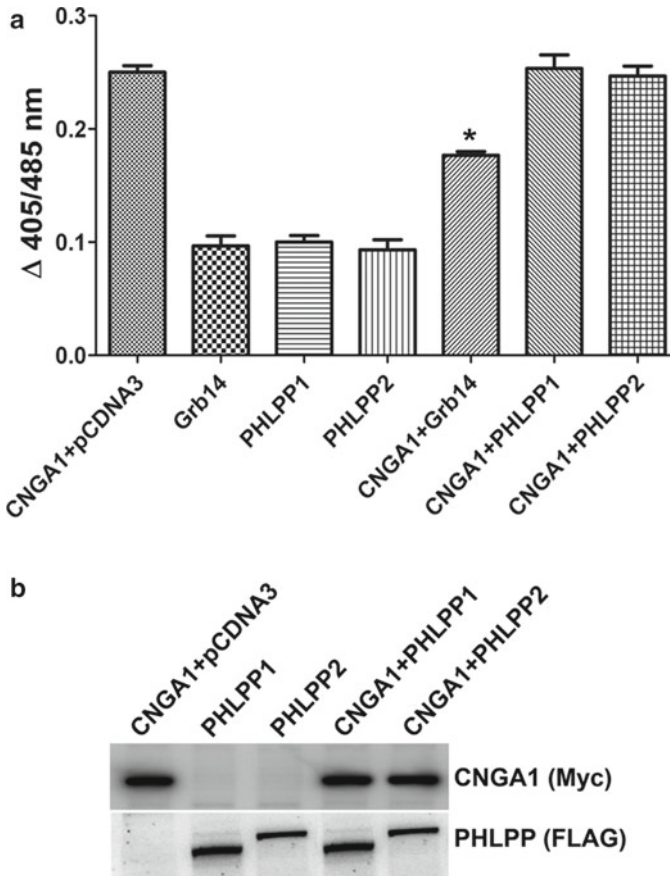


Fig. 99.2 Effect of PHLPP1 and PHLPP2 on CNG channel activity. (a) Myc-CNGA1 was transiently coexpressed with myc-Grb14, FLAG-PHLPP1, or FLAG-PHLPP2 and examined for their effect on channel activity. Cells transfected with Grb14, PHLPP1 (β), or PHLPP2 alone were used to measure the nonchannel-mediated Ca^{2+} permeability. CNGA1 cotransfected with empty plasmid was used as control. (b) Lysates were subjected to immunoblot analysis with anti-Myc antibodies for CNGA1 and anti-FLAG antibodies for PHLPP1 and PHLPP2, respectively. Data mean \pm SD, $n=3$; $p<0.05$

domains, although a phylogenetic convergence cannot be ruled out. A similar structural organization of the PHLPP (1, 2) isoforms with Grb14 protein suggests that PHLPP1 and PHLPP2 isoforms may also modulate the CNG channel activity.

99.3.2 *PHLPP1 and 2 Do Not Have Channel Modulatory Properties*

PHLPP1 and 2 are present in the retina and their activity is known to be regulated by the Akt which in turn gets activated upon activation of IR pathway (Kanan et al. 2010).

The effect of each of the PHLPP1 (β) and PHLPP2 was investigated on CNGA1 channel function upon overexpression in HEK293 cells, and it was observed that none of these proteins is capable of modulating CNG channel function (Fig. 99.2a). Grb14 coexpression with CNGA1 was used as a control (Gupta et al. 2010). CNGA1 coexpression with empty plasmid was used as a positive control. The lack of modulation was not due to lack of the protein expression as each of these proteins was expressed to comparable levels (Fig. 99.2b). The individual protein expression of Grb14, PHLPP1 (β), and PHLPP2 was used to subtract the nonspecific effect of autofluorescence and Indo-1AM/ Ca^{2+} bleeding through membranes (Fig. 99.2a).

99.4 Discussion

cGMP-gated channels play a pivotal role in phototransduction and light adaptation through maintenance of photoreceptor homeostasis. Mutations in the rod CNG channel are found in patients with *retinitis pigmentosa* (Driyja et al. 1995) whereas mutations in the cone CNG channel are associated with achromatopsia, progressive cone dystrophy, and early-onset macular degeneration (Kohl et al. 2000, 2005; Nishiguchi et al. 2005; Wissinger et al. 2001). This necessitates a thorough understanding of the physiological role and regulation of these channels for eventual therapeutic intervention. We recently reported that the RA domain of Grb14 is self-sufficient to promote the channel to be in an *off* state (Gupta et al. 2010). This opens up myriad possibilities that the other RA domain-containing proteins may have analogous role in modulating CNG channel function. Even though PHLPP1 and 2 are RA domain proteins, they failed to inhibit the channel activity. Our data suggest that not all RA domain proteins are modulators of CNG channel, suggesting the existence of heterogeneity among several RA domains. Interestingly, several RA domain-containing proteins also contain PH domains (Raaijmakers and Bos 2009), which help these proteins to localize to the plasma membrane through their interaction with phosphoinositides (PIs). Grb14 also contains a PH domain; however, we did not observe any channel modulatory property associated with this domain (Gupta et al. 2010). Proper localization of RA domain proteins through PH–PI interaction on CNG channel modulation cannot be ruled out. This study also opens up numerous possibilities for looking up other RA domain proteins as modulators of CNG channel in photoreceptors, and perhaps these domains may be used as therapeutic agents to treat retinal degenerations.

One of the biggest future challenges is to understand the RA/RBD-containing protein interactions with Ras or Ras-like domain-containing proteins in a quantitative manner in their three-dimensional orientations and study the underlying energetics. This study however makes it clear that effect of RA domain-containing proteins is discriminatory and that RA domains cannot be considered as rigid bodies.

Acknowledgments This work was supported by grants from the NIH (EY016507; EY00871; EY12190). Vivek K. Gupta received a travel award to attend the XIVth International Symposium on Retinal Degeneration held at Mont-Tremblant, Quebec, Canada, 2010.

References

- Biel M, Zong X, Ludwig A et al (1999) Structure and function of cyclic nucleotide-gated channels. *Rev Physiol Biochem Pharmacol* 135:151–71
- Corpet, F (1988) Multiple sequence alignment with hierarchical clustering. *Nucl. Acids Res.* 16: 10881–10890
- Dryja TP, Finn JT, Peng YW et al (1995) Mutations in the gene encoding the alpha subunit of the rod cGMP-gated channel in autosomal recessive retinitis pigmentosa. *Proc. Natl. Acad. Sci. USA.* 92:10177–10181
- Gao T, Furnari F, Newton AC (2005) PHLPP: A Phosphatase that Directly Dephosphorylates Akt, Promotes Apoptosis, and Suppresses Tumor Growth. *Mol Cell* 18:13–24
- Gao MH, Miyanojara A, Feramisco JR et al (2009) Activation of PH-domain Leucine-Rich Protein Phosphatase 2 (PHLPP2) by Agonist Stimulation in Cardiac Myocytes Expressing Adenyl Cyclase Type 6. *Biochem Biophys Res Commun* 26:193–198
- Gerstner A, Zong X, Hofmann F et al (2000) Molecular cloning and functional characterization of a new modulatory cyclic nucleotide-gated channel subunit from mouse retina. *J Neurosci* 20:1324–32
- Gupta VK, Rajala A, Daly RJ et al (2010) Growth factor receptor-bound protein 14: a new modulator of photoreceptor-specific cyclic-nucleotide-gated channel. *EMBO Rep.* 11:861–867
- Ivins JK, Parry MK, Long DA (2004) A Novel cAMP-Dependent Pathway Activates Neuronal integrin Function in Retinal Neurons. *The Journal of Neuroscience* 24:1212–1216
- Kaupp UB and Seifert R (2002) Cyclic nucleotide-gated ion channels. *Physiol Rev* 82:769–824
- Kanai-Azuma M, Mattick JS, Kaibuchi K et al (2000) Co-localization of FAM and AF-6, the mammalian homologues of *Drosophila faf* and *canoe*, in mouse eye development. *Mechanisms of Development* 91:2383–386
- Kanan Y, Matsumoto H, Song H et al (2010) Serine/threonine kinase akt activation regulates the activity of retinal serine/threonine phosphatases, PHLPP and PHLPL. *J Neurochem* 113:477–488
- Kohl S, Baumann B, Broghammer M et al (2000) Mutations in the CNGB3 gene encoding the beta-subunit of the cone photoreceptor cGMP-gated channel are responsible for achromatopsia (ACHM3) linked to chromosome 8q21. *Hum Mol Genet* 9:2107–16
- Kohl S, Varsanyi B, Antunes GA et al (2005) CNGB3 mutations account for 50% of all cases with autosomal recessive achromatopsia. *Eur J Hum Genet* 13:302–8
- Nishiguchi KM, Sandberg MA, Gorji N et al (2005) Cone cGMP-gated channel mutations and clinical findings in patients with achromatopsia, macular degeneration, and other hereditary cone diseases. *Hum Mutat* 25:248–58
- Pimentel B, Sanz C, Varela-Nieto I et al (2000) c-Raf regulates cell survival and retinal ganglion cell morphogenesis during neurogenesis. *J Neurosci* 20:3254–3262
- Rajala RVS, McClellan ME, Ash JD et al (2002) *In Vivo* Regulation of Phosphoinositide 3-Kinase in Retina through Light-induced Tyrosine Phosphorylation of the Insulin Receptor β -Subunit. *J Biol Chem* 277:43319–43326
- Rajala RVS, Chan MD, Rajala A (2005) Lipid-Protein Interactions of Growth Factor Receptor-Bound Protein 14 in Insulin Receptor Signaling. *Biochemistry* 44:15461–15471
- Rajala A, Daly RJ, Tanito M et al (2009) Growth factor receptor-bound protein 14 undergoes light-dependent intracellular translocation in rod photoreceptors: functional role in retinal insulin receptor activation. *Biochemistry* 48:5563–72
- Raaijmakers JH, Bos JL (2009) Specificity in Ras and rap signaling. *J Biol Chem* 284: 10995–10999
- Tanaka M, Ohashi R, Nakamura R et al (2004) Tiam1 mediates neurite outgrowth induced by ephrin-B1 and EphA2. *EMBO J* 10:1075–1088
- Yau KW, Hardie RC (2009) Phototransduction motifs and variations. *Cell* 139:246–64
- Yau KW, Baylor DA (1989) Cyclic GMP-activated conductance of retinal photoreceptor cells. *Annu Rev Neurosci* 12:289–327
- Wigler M, Pellicer A, Silverstein S, Axel R (1978) Biochemical transfer of single-copy eucaryotic genes using total cellular DNA as donor. *Cell* 14:725–731
- Wissinger B, Gamer D, Jagle H et al (2001) CNGB3 mutations in hereditary cone photoreceptor disorders. *Am J Hum Genet* 69:722–37

Chapter 100

Tulp1 Is Involved in Specific Photoreceptor Protein Transport Pathways

Stephanie A. Hagstrom, Rao F. Watson, Gayle J.T. Pauer,
and Gregory H. Grossman

Keywords Photoreceptor • Retinal degeneration • Tulp1 • Mouse mutant • Protein transport

100.1 Introduction

Retinitis pigmentosa (RP) refers to a large number of genetically and phenotypically heterogeneous inherited retinal disorders that affect over one million people worldwide (Boughman et al. 1980; Bunker et al. 1984). RP is characterized by photoreceptor degeneration, with the initial development of night blindness leading to the eventual loss of all useful vision (Berson 1993). Mutations in the gene *TULP1* have been shown to be the underlying cause of an early onset form of autosomal recessive RP (Hagstrom et al. 1998; Banerjee et al. 1998; Gu et al. 1998; Paloma et al. 2000; Mataftsi et al. 2007; Abbasi et al. 2008). TULP1 is a member of the Tubby-like protein family which includes TULP2, TULP3, and TUB (North et al. 1997). While TUB and TULP3 are widely dispersed throughout the central nervous system, the expression of TULP1 and TULP2 is largely restricted to photoreceptor cells and testis, respectively (North et al. 1997; Kleyn et al. 1996; Nishina et al. 1998; Sahly et al. 1998; Ikeda et al. 1999; He et al. 2000). Though the role of TULPs remains unclear, TULP proteins are important in neuronal function.

S.A. Hagstrom (✉)

Department of Ophthalmic Research, Cole Eye Institute, Cleveland Clinic,
9500 Euclid Avenue, Cleveland, OH 44195, USA

Department of Ophthalmology, Cleveland Clinic Lerner College of Medicine
of Case Western Reserve University, Cleveland, OH 44195, USA
e-mail: hagstrs@ccf.org

R.F. Watson • G.J.T. Pauer • G.H. Grossman

Department of Ophthalmic Research, Cole Eye Institute, Cleveland Clinic,
9500 Euclid Avenue, Cleveland, OH 44195, USA

This is emphasized by the association of *TUB* and *TULP1* mutations with neurosensory disease phenotypes.

To investigate Tulp1, we generated a mouse model that mimics the rapid photoreceptor degeneration described in patients (Hagstrom et al. 1999). Our model has provided evidence that Tulp1 plays a key role in protein trafficking in the photoreceptor inner segment (IS) (Hagstrom et al. 1999, 2001; Xi et al. 2005, 2007; Grossman et al. 2009). Tulp1 is expressed exclusively in photoreceptors and is localized to the IS, connecting cilium (CC) and synaptic terminals (Hagstrom et al. 1999, 2001; Ikeda et al. 2000). In *tulp1*^{-/-} mice, retinal function declines in parallel with photoreceptor degeneration. At an early age prior to photoreceptor degeneration, rhodopsin is mislocalized, and rhodopsin-bearing vesicles accumulate around the ellipsoid region of the IS (Hagstrom et al. 1999). However, other outer segment (OS) proteins are not mislocalized in the *tulp1*^{-/-} retina. These defects initiated the hypothesis that Tulp1 may be involved in vectorial protein transport from the IS to the OS (Hagstrom et al. 1999, 2001; Xi et al. 2005, 2007; Grossman et al. 2009).

Our understanding of the molecular processes that regulate protein trafficking in photoreceptors is limited. This is of particular importance in light of the highly polarized and compartmentalized structure of photoreceptors and the large amounts of proteins that are synthesized in the IS and delivered to the OS on a daily basis. It is clear that this process involves the sorting of proteins into vesicles at the trans-Golgi network (TGN), the directional translocation of these vesicles through the IS, and the delivery of vesicles to the synaptic terminal or the apical IS plasma membrane where they dock and fuse for incorporation into the OS (Deretic 2006). The role of Tulp1 in this process and the mechanism by which *TULP1* mutations lead to RP remain undefined.

Proposed OS protein transport pathways have been deduced from the study of a handful of mutant mouse models (Yang et al. 1999; Baehr et al. 2007; Zhang et al. 2007; Karan et al. 2008). Therefore, it is critical to study additional mouse mutants which present phenotypes showing OS protein transport defects. To define the protein transport pathways which are affected in the Tulp1 mutant mouse, we analyzed the localization of several categories of OS resident proteins and chaperone proteins known to be critical in the transport of OS proteins in *tulp1*^{-/-} retinas as compared to wild-type (wt) retinas. These results reveal that OS proteins are affected differently in *tulp1*^{-/-} mice, providing evidence that Tulp1 functions in selective OS transport pathways.

100.2 Materials and Methods

100.2.1 Animals

Tulp1^{-/-} mice were generated and genotyped as described previously (Hagstrom et al. 1999). Mice were euthanized by CO₂ inhalation followed by cervical dislocation. All experiments on animals were approved by the Institutional Animal Care

and Use Committee of the Cleveland Clinic and were performed in compliance with the ARVO Statement for the Use of Animals in Ophthalmic and Visual Research.

100.2.2 Immunofluorescent Staining of Retinal Sections

Mouse eyes were prepared as previously described (Xi et al. 2007). Briefly, after removal of the cornea and lens, the posterior poles were fixed in 4% paraformaldehyde, immersed through a graded series of sucrose solutions, embedded in OCT freezing medium, flash frozen on powdered dry ice, and immediately transferred to -80°C . The tissue was sectioned at 10- μm thickness using a cryostat at -30°C . Retinal sections were blocked before incubation with primary antibodies overnight at 4°C . Primary and secondary antibodies and dilutions were used as previously described (Grossman et al. 2011). Sections were imaged using an Olympus BX-61 fluorescent microscope equipped with a CCD monochrome camera.

100.3 Results

We have previously shown that *tulp1*^{-/-} photoreceptors exhibit an aberrant localization of rhodopsin but not of peripherin/RDS (Hagstrom et al. 1999). Therefore, we sought to determine whether additional OS proteins rely on the presence of Tulp1 for their transport to the OS compartment. To this end, we surveyed a panel of OS resident proteins in the *tulp1*^{-/-} retina as compared to the wt retina. Table 100.1 presents the results of the immunolocalization of several well-studied phototransduction and structural OS proteins. All studies were conducted at P16, an age at which photoreceptor development is complete in wt mice, but precedes photoreceptor degeneration in *tulp1*^{-/-} mice (Hagstrom et al. 1999; Grossman et al. 2009).

Table 100.1 Localization of OS proteins in the *tulp1*^{-/-} retina

OS protein	Outer segment	Inner segment	Soma	Synapse
Peripherin/rds	✓			
ROM1	✓			
GRK1	✓			
PDE6- β	✓			
CNGB1	✓			
GC1	✓	✓		
GCAP1	✓	✓	✓	✓
GCAP2	✓	✓	✓	✓
Blue cone opsin	✓	✓	✓	✓
Rhodopsin	✓	✓	✓	✓

This table summarizes the results of our immunolocalization studies of the OS proteins in *tulp1*^{-/-} mice at P16. A check mark denotes the presence of immunoreactivity in the specific photoreceptor compartment, while an empty box denotes a lack of signal

We identified several proteins that retain their normal localization in the *tulp1*^{-/-} retina. These proteins include ROM1, GRK1, PDE6, and CNGB1. However, in addition to rhodopsin, four additional OS resident proteins are mislocalized to other photoreceptor compartments. Although staining of GCAP1 and 2, GC1 and blue cone opsin is still apparent in the OS, all four proteins are mislocalized to additional compartments.

Next we analyzed whether photoreceptor proteins that exhibit light-dependent movement in and out of the OS are affected in the *tulp1*^{-/-} retina. Transducin and arrestin are two signal transduction proteins that translocate in response to lighting conditions (Calvert et al. 2006; Slepak and Hurley 2008). Immunolocalization reveals that in response to light, transducin is able to translocate properly in the *tulp1*^{-/-} retina, whereas arrestin is not.

Next we compared the distribution of chaperone proteins that regulate the trafficking of OS proteins (Deretic 2006; Norton et al. 2005). Our results show that three of the chaperone proteins that are involved in the transport of rhodopsin are severely mislocalized in the *tulp1*^{-/-} retina. These are Rab6, Rab8, and Rab11. By contrast, one of the chaperones implicated in the transport of peripheral membrane-associated proteins (PMAPs), PrBP/ δ , is not mislocalized.

100.4 Discussion

In this study, we surveyed the localization of several OS proteins in the *tulp1*^{-/-} retina as compared to the wt retina to define Tulp1-dependent OS transport pathways. Representative OS proteins of different functional classes (i.e., phototransduction and structural) and different membrane affiliations (i.e., integral membrane, peripheral membrane-associated, and cytosolic) were analyzed. In addition, we also evaluated several IS proteins that function as OS protein chaperones in an attempt to pinpoint the defective transport step.

Our results indicate that the trafficking of several PMAPs, including PDE, GRK1, and transducin, do not appear to be affected in the *tulp1*^{-/-} retinas. These proteins are posttranslationally processed solely in the ER and involve protein transfer to vesicular carriers. As expected, the chaperone protein known to interact with the prenyl chains of GRK1 and PDE, PrBP/ δ , is correctly localized in *tulp1*^{-/-} retinas. GCAP1 is a PMAP that is mislocalized in the *tulp1*^{-/-} retina; however, this mislocalization may be due to a secondary effect. It has been postulated that nontransmembrane proteins are transported in vesicles with their integral membrane protein (IMPs) partners (Karan et al. 2008). Thus, the mislocalization of GCAP1 may be the result of traveling in vesicles with its integral membrane-binding partner GC1. This hypothesis is supported by our current results showing that GC1 is mislocalized in Tulp1's absence. In addition, the cytosolic protein GCAP2 was also mistrafficked in Tulp1's absence. IMPs are posttranslationally processed in the Golgi and bud from vesicles derived from the TGN surface. Although two OS-specific IMPs, rhodopsin and GC1, are mistargeted in Tulp1's absence, there are other OS IMPs

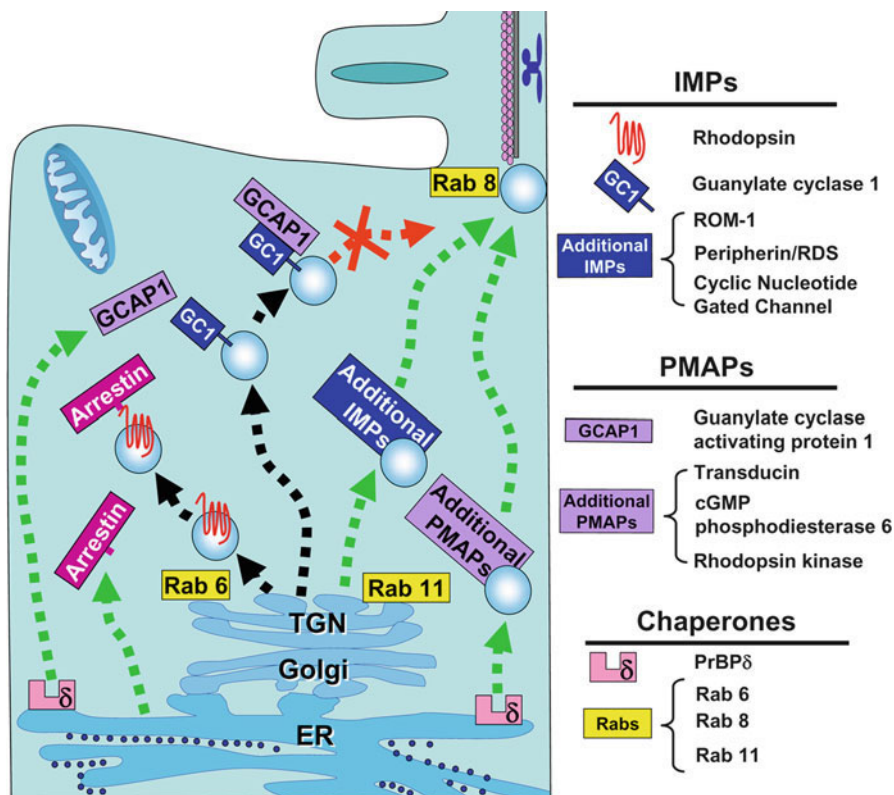


Fig. 100.1 A proposed model of OS protein transport in photoreceptors. Lack of Tulp1 affects selective TGN-associated transport pathways (black dashed lines) but not others (green dashed lines)

that are able to localize properly without Tulp1, specifically peripherin/rds and ROM-1. Therefore, Tulp1 appears to be involved in the transport of specific IMPs and the proteins that cotransport with them.

In sum, Tulp1 is involved in the trafficking of selective IMPs, as well as their binding partners with which they cotransport in post-Golgi vesicles (Fig. 100.1). Tulp1 participates in two separate OS protein transport pathways; one that transports GC1 along with its binding partner GCAP1 and another that transports rhodopsin and its associated protein arrestin. Alternative pathways that transport other IMPs, such as ROM1, peripherin, and CNGB1, are not Tulp1 dependent. Tulp1 does not appear to be involved with the transport of PMAPs.

Acknowledgments National Institute of Health Grants EY16072 and EY15638 (SAH), Foundation Fighting Blindness (SAH), Prevent Blindness Ohio (RFW), Fight For Sight (GHG), Research to Prevent Blindness (RPB) Center Grant, RPB Sybil B. Harrington Special Scholar Award (SAH), and Hope for Vision (SAH).

References

- Abbasi AH, Garzosi HJ, Ben-Yosef T (2008) A novel splice-site mutation of TULP1 underlies severe early-onset retinitis pigmentosa in a consanguineous Israeli Muslim Arab family. *Mol Vis* 14:675–682
- Banerjee P, Kleyn PW, Knowles JA et al (1998) TULP1 mutation in two extended Dominican kindreds with autosomal recessive retinitis pigmentosa. *Nat Genet* 18:177–179
- Baehr W, Karan S, Maeda T et al (2007) The function of guanylate cyclase 1 and guanylate cyclase 2 in rod and cone photoreceptors. *J Biol Chem* 282:8837–8847
- Berson EL (1993) Retinitis pigmentosa. The Friedenwald Lecture. *Inves Ophthalmol Vis Sci* 34:1659–1676
- Boughman JA, Conneally PM, Nance WE (1980) Population genetic studies of retinitis pigmentosa. *Am J Hum Genet* 32:223–235
- Bunker CH, Berson EL, Bromley WC et al (1984) Prevalence of retinitis pigmentosa in Maine. *Am J Ophthalmol* 97:357–365
- Calvert PD, Strissel KJ, Schiesser WE et al (2006) Light-driven translocation of signaling proteins in vertebrate photoreceptors. *Trends Cell Biol* 16:560–568
- Deretic D (2006) A role for rhodopsin in a signal transduction cascade that regulates membrane trafficking and photoreceptor polarity. *Vision Res* 46:4427–4433
- Grossman GH, Pauer GJ, Narendra U et al (2009) Early synaptic defects in *tulp1*^{-/-} mice. *Invest Ophthalmol Vis Sci* 50:3074–3083
- Grossman GH, Watson RF, Pauer GJT et al (2011) Tulp1-dependent Outer Segment Protein Transport Pathways in Photoreceptor Cells. *Exp Eye Res Aug. 16* (Epub ahead of print)
- Gu S, Lennon A, Li Y et al (1998) Tubby-like protein-1 mutations in autosomal recessive retinitis pigmentosa. *Lancet* 351:1103–1104
- Hagstrom SA, North MA, Nishina PL et al (1998) Recessive mutations in the gene encoding the tubby-like protein TULP1 in patients with retinitis pigmentosa. *Nat Genet* 18:174–176
- Hagstrom SA, Duyao M, North MA et al (1999) Retinal degeneration in *tulp1*^{-/-} mice: vesicular accumulation in the interphotoreceptor matrix. *Invest Ophthalmol Vis Sci* 40:2795–2802
- Hagstrom SA, Adamian M, Scimeca M et al (2001) A role for the Tubby-like protein 1 in rhodopsin transport. *Invest Ophthalmol Vis Sci* 42:1955–1962
- He W, Ikeda S, Bronson RT et al (2000) GFP-tagged expression and immunohistochemical studies to determine the subcellular localization of the tubby gene family members. *Brain Res Mol Brain Res* 81:109–117
- Ikeda S, He W, Ikeda A et al (1999) Cell-specific expression of tubby gene family members (tub, Tulp1, 2, and 3) in the retina. *Invest Ophthalmol Vis Sci* 40:2706–2712
- Ikeda S, Shiva N, Ikeda A et al (2000) Retinal degeneration but not obesity is observed in null mutants of the tubby-like protein 1 gene. *Hum Mol Genet* 9:155–163
- Karan S, Zhang H, Li S et al (2008) A model for transport of membrane-associated phototransduction polypeptides in rod and cone photoreceptor inner segments. *Vision Res* 48:442–452
- Kleyn PW, Fan W, Kovats SG et al (1996) Identification and characterization of the mouse obesity gene *tubby*: a member of a novel gene family. *Cell* 85:281–290
- Mataftsi A, Schorderet DF, Chachoua L et al (2007) Novel TULP1 mutation causing leber congenital amaurosis or early onset retinal degeneration. *Invest Ophthalmol Vis Sci* 48:5160–5167
- Nishina PM, North MA, Ikeda A et al (1998) Molecular characterization of a novel tubby gene family member, TULP3, in mouse and humans. *Genomics* 54:215–220
- North MA, Naggert JK, Yan Y et al (1997) Molecular characterization of TUB, TULP1, and TULP2, members of the novel tubby gene family and their possible relation to ocular diseases. *Proc Natl Acad Sci USA* 94:3128–3133
- Norton AW, Hosier S, Terew JM et al (2005) Evaluation of the 17-kDa prenyl-binding protein as a regulatory protein for phototransduction in retinal photoreceptors. *J Biol Chem* 280:1248–1256

- Paloma E, Hjelmqvist L, Bayes M et al (2000) Novel mutations in the TULP1 gene causing autosomal recessive retinitis pigmentosa. *Invest Ophthalmol Vis Sci* 41:656–659
- Sahly I, Gogat K, Kobetz A et al (1998) Prominent neuronal-specific tub gene expression in cellular targets of tubby mice mutation. *Hum Mol Genet* 7:1437–1447
- Slepek VZ, Hurley JB (2008). Mechanism of light-induced translocation of arrestin and transducin in photoreceptors: interaction-restricted diffusion. *IUBMB Life* 60:2–9
- Xi Q, Pauer GJ, Marmorstein AD et al (2005) Tubby-like protein 1 (TULP1) interacts with F-actin in photoreceptor cells. *Invest Ophthalmol Vis Sci* 46:4754–4761
- Xi Q, Pauer GJ, Ball SL et al (2007) Interaction between the photoreceptor-specific tubby-like protein 1 and the neuronal-specific GTPase dynamin-1. *Invest Ophthalmol Vis Sci* 48:2837–2844
- Yang RB, Robinson SW, Xiong WH et al (1999) Disruption of a retinal guanylyl cyclase gene leads to cone-specific dystrophy and paradoxical rod behavior. *J Neurosci* 19:5889–5897
- Zhang H, Li S, Dhoan T et al (2007) Deletion of PrBP/delta impedes transport of GRK1 and PDE6 catalytic subunits to photoreceptor outer segments. *Proc Natl Acad Sci USA* 104:8857–8862

Chapter 101

Potential Cellular Functions of *N*-Ethylmaleimide Sensitive Factor in the Photoreceptor

Shun-Ping Huang and Cheryl M. Craft

Keywords Arrestin 1 • *N*-ethylmaleimide sensitive factor • Retinitis pigmentosa protein 2 • Phototransduction • Oguchi disease • NSF attachment proteins receptor • Retinitis pigmentosa • Synapses • ATPase • Protein trafficking

101.1 Introduction

Vesicle traffic and fusion are essential, not only for cellular homeostasis but also for neuronal signal transmission across the synaptic junction of nerves, cell growth, and membrane repair. The basic fusion process is mediated by vesicle (v)-soluble *N*-ethylmaleimide sensitive factor attachment proteins receptors

S.-P. Huang

Mary D. Allen Laboratory for Vision Research, Doheny Eye Institute,
Keck School of Medicine of the University of Southern California,
Los Angeles, CA 90033-9224, USA

Department of Ophthalmology, Keck School of Medicine of the University
of Southern California, Los Angeles, CA 90033-9224, USA

C.M. Craft (✉)

Mary D. Allen Laboratory for Vision Research, Doheny Eye Institute,
Keck School of Medicine of the University of Southern California,
Los Angeles, CA 90033-9224, USA

Department of Ophthalmology, Keck School of Medicine of the University
of Southern California, Los Angeles, CA 90033-9224, USA

Department of Cell and Neurobiology, Keck School of Medicine of the University
of Southern California, Los Angeles, CA 90033-9224, USA
e-mail: ccraft@usc.edu

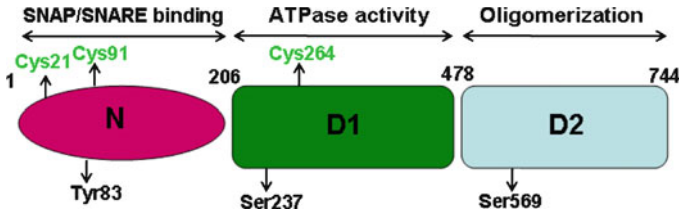


Fig. 101.1 Structure of NSF domains. Each NSF monomer is comprised of three domains: an N-terminal domain (amino acid 1–205) that is responsible for the interaction with a-SNAP and SNAREs; and two homologous ATP-binding domains, D1 (amino acids 206–477), in which the hydrolytic activity is associated with NSF-driven SNARE complex disassembly, and D2 (amino acids 478–744), which is responsible for hexamer formation. Critical residues involved in post-translational processing include Cys21, 91 and 264, Tyr83, Ser237, and Ser569

(SNAP receptors; SNAREs) on the secretory vesicle with their cognate target (t)-SNAREs on the target membrane (Sollner et al. 1993), which assemble in trans-configuration into four-helix bundle complexes, bringing the membranes into close proximity (Jahn and Scheller 2006; Rizo and Rosenmund 2008; Martens and McMahon 2008), which then directly or indirectly leads to fusion. After membrane fusion, all SNAREs constituting one complex are anchored in a relaxed *cis*-configuration to one membrane. Disassembly of these SNAREs complexes for subsequent vesicle transport and recycling is achieved by the concerted action of α -SNAP and NSF.

N-ethylmaleimide sensitive factor (NSF) is a homo-hexameric member of the ATPase-associated family with various cellular activities protein (AAA) family, required for intracellular membrane fusion. NSF functions as a SNAP receptor (SNARE) chaperone that binds through soluble NSF attachment proteins (SNAPs) to SNARE complexes and utilizes the energy of ATP hydrolysis to dissociate SNARE complexes after membrane fusion, thus facilitating SNAREs recycling.

Each NSF protomer contains an N-terminal domain (NSF-N) and two AAA-domains: a catalytic NSF-D1 and a structural NSF-D2 (Fig. 101.1). The amino acid residues 1–205 in the NSF-N domain are required for SNAP–SNARE binding; residues 206–477 in the NSF-D1 domain are responsible for the majority of the ATP hydrolysis, while the carboxy-terminal residues 478–744 in the NSF-D2 domain are required for hexamerization (Tagaya et al. 1993; Nagiec et al. 1995). Within the N-terminal subdomain of both NSF-D1 and NSF-D2, there is a highly conserved region called Second Region of Homology (SRH), which is highly conserved in AAA proteins (Hanson and Whiteheart 2005). By using detailed mutagenesis analysis, Zhao and collaborators (Zhao et al. 2010) showed that a positively charged surface on NSF-N, bounded by R67 and K105, and the conserved central

pore motifs in NSF-D1 (Y296 and G298) are involved in SNAP–SNARE binding but not basal ATP hydrolysis. Sensor 1 is at the N-terminus of the SRH and is important for basal ATPase activity and nucleotide binding. At its carboxy-terminus are two arginine residues, termed Arginine Fingers, which are critical for ATP hydrolysis by the NSF hexamer. Sensor 2 comes from C-terminal helical subdomain and plays a role in ATP- and SNAP-dependent SNARE complex binding and disassembly.

NSF binds to SNARE complexes via its adaptor protein, α -SNAP, only in the presence of ATP (Nagiec et al. 1995). The intrinsic ATPase activity of NSF is low (Tagaya et al. 1993). NSF binding to immobilized α -SNAP stimulates the ATPase activity (Morgan et al. 1994), and maximal stimulation of ATPase activity is achieved when both α -SNAP and SNARE complexes are included (Matveeva and Whiteheart 1998).

101.2 NSF in Photoreceptor Synaptic Regulation

In the G-protein-coupled receptor (GPCR) phototransduction cascade, visual Arrestin1 (Arr1) binds to and deactivates phosphorylated, light-activated opsins, a process that is critical for effective recovery and normal vision. We discovered a novel synaptic protein–protein interaction between Arr1 and NSF that is enhanced in a dark environment when photoreceptors are depolarized and the rate of exocytosis is elevated compared to a light environment (Huang et al. 2010; Huang 2010) (Fig. 101.2a, b). In Figs. 101.2 and 101.3, representative images of sections from either dark- or light-adapted retinas highlight differences in immunohistochemical retinal dual localization in mouse of Arr1 and NSF, respectively (Figs. 101.2a–d and 101.3a–d). We also provided convincing *in vitro* evidence supporting the interaction of Arr1 with NSF to modulate its ATPase activity and to drive disassembly of the SNARE complex. Furthermore, we observed with *in vivo* studies using FM-143 imaging that synaptic vesicle recycling in photoreceptors is dramatically decreased with depolarization and photopic electroretinogram (ERG) b-wave analysis in *Arr1*^{-/-} compared to control mice is defective in light adaptation (Brown et al. 2010). Not only does Arr1 bind to the junction of NSF N-terminal and the first ATPase domains in an ATP-dependent manner, but Arr1 also enhances both NSF ATPase and NSF disassembly activities. In mouse retinas with no Arr1 expression, the expression levels of NSF and other synapse-enriched genes are markedly reduced and lead to a substantial decrease in the exocytosis rate. These cumulative findings demonstrate that normal photoreceptor synaptic function involves the ability of Arr1 to regulate and to enhance the dark-associated activity of NSF in the photoreceptor synapse.

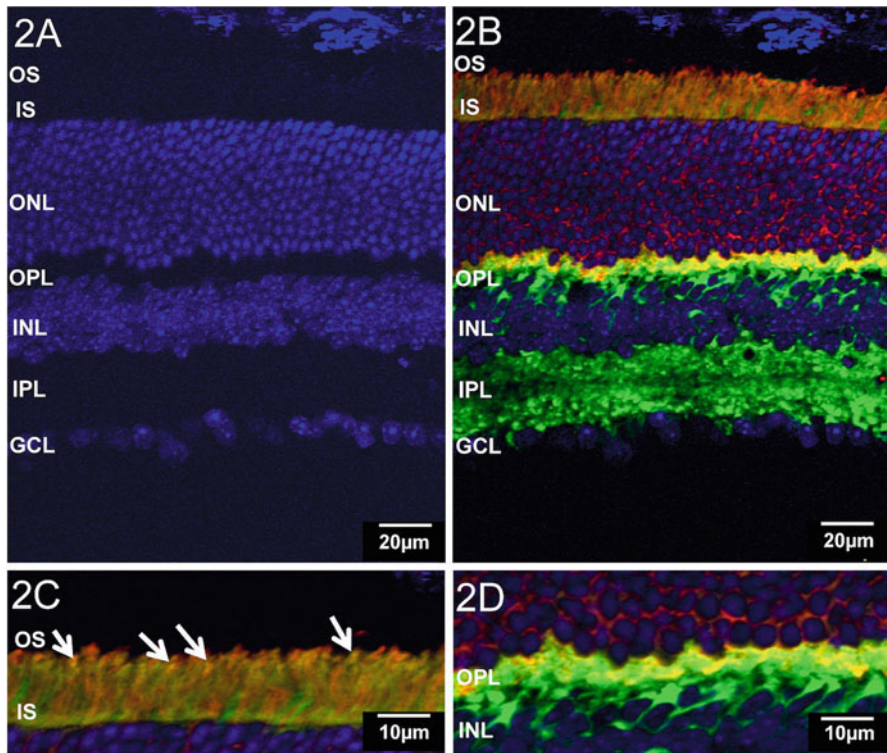


Fig. 101.2 NSF and Arr1 localization in dark-adapted retinas. Immunohistochemical fluorescent labeling of retinal sections with dual localization of NSF and Arr1 staining in the WT mice dark-adapted (DA) overnight and killed in the dark. Adult WT mouse retina frozen sections were triple labeled fluorescently with the antimouse Arr1 MAb D9F2 (red, 1:20,000), antirabbit NSF PAB (green, 1:2,500, Abcam), and secondary antibodies conjugated to Alexa Fluor 488 or 568, respectively (1:500, invitrogen), and DAPI for the nuclei (blue, (a, b)). NSF immunoreactive staining pattern of NSF is mainly in the OPL and IPL in dark-adapted retinas (c, d). Arr1 immunoreactive pattern is predominantly in the inner segment, perinuclear area and a fraction in the photoreceptor terminal in DA retinas ((c), higher magnification; large arrows). OS outer segment; IS inner segments; ONL outer nuclear layer; OPL outer plexiform layer; INL inner nuclear layer; IPL inner plexiform layer; GLC ganglion cell layer. Scale bar, 20 μ m in upper panels; 10 μ m in lower panels

101.3 NSF in Photoreceptor Membrane Protein Trafficking

While the major function of NSF is involved in vesicle transport and recycling, it also interacts with other proteins such as the AMPA receptor subunit (Osten et al. 1998), β -arrestin1 (McDonald et al. 1999), GluR2 (Nishimune et al. 1998), and β 2-AR (Cong et al. 2001) and is thought to affect their trafficking pattern. More evidence suggests that NSF may be regulated by transient posttranslational modifications such as phosphorylation and nitrosylation. These modifications are ideal mechanisms for reversible regulation of membrane trafficking.

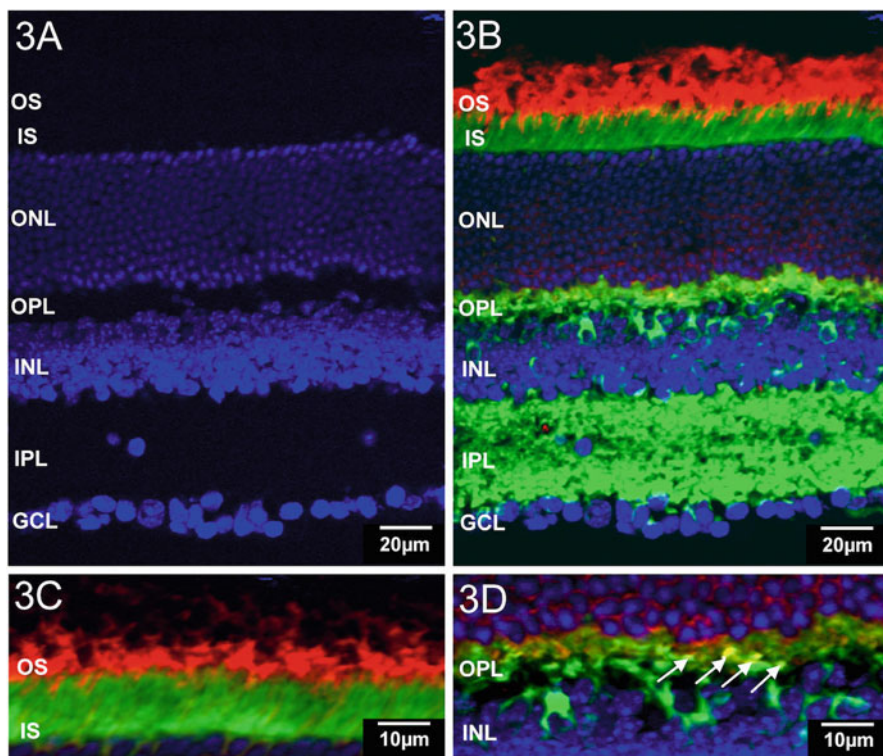


Fig. 101.3 NSF and Arr1 localization in light-adapted retinas. Immunohistochemical fluorescent labeling of NSF and Arr1 in retinal sections from WT mouse exposed to light for 2 h prior to killing (light-adapted [LA]). Adult WT mouse retina frozen sections were triple labeled fluorescently as in Fig. 101.2 ((a, b) DAPI stains nuclei blue). NSF immunoreactive staining pattern of NSF is mainly in the OPL and IPL in light-adapted retinas (c, d). Arr1 immunoreactive pattern is translocated to the outer segment in LA retinas. Arr1 immunoreactivity is extensively dual localized with NSF immunological staining and limited punctate dual staining in the OPL in LA retina ((d) higher magnification; *smaller arrows*). Abbreviations are listed in Fig. 101.2. Scale bar, 20 μm in *upper* panels; 10 μm in *lower* panels

Recently, Molday and his collaborators observed that NSF specifically interacts with RP2 in the retina (Holopainen et al. 2010), which is a ubiquitously expressed protein encoded by a gene associated with X-linked retinitis pigmentosa (Breuer et al. 2002; Miano et al. 2001; Schwahn et al. 1998; Sharon et al. 2003). RP2 is known to bind to the GTP-bound form of ADP ribosylation factor like 3 (Arl3), a member of the Arl subfamily of Ras-related GTP-binding proteins (Bartolini et al. 2002; Kuhnel et al. 2006; Veltel et al. 2008) and acts as an efficient GTPase-activating protein (GAP) for Arl3 (Veltel et al. 2008). NSF and RP2 was shown to colocalize in the ciliary region, inner segment, outer nuclear layer, and synaptic region in the photoreceptor. Furthermore, RP2 binds to the N-terminal domain of NSF and this binding is abolished for the E138G and Δ I137 mutation of RP2 known

to cause X-linked retinitis pigmentosa. These data may indicate RP2 binding to NSF, and Arl3 may play a crucial role in the vesicle trafficking of proteins to the photoreceptor ciliary region as well as in the photoreceptor synapse.

101.4 Summary

Recent work has established potential new functional roles for NSF in the photoreceptor. First, the interaction of Arr1 and NSF is ATP-dependent, and the N-terminal domain of Arr1 interacts with the N and D1 junctional domains of NSF. The Arr1–NSF interactions are greater in the photoreceptor synaptic terminal in the dark. Furthermore, Arr1 enhances the NSF ATPase activity and increases the NSF disassembly activities, which are critical for NSF functions in sustaining a higher rate of exocytosis in the photoreceptor synapses and the compensatory endocytosis to retrieve vesicle membrane and vesicle proteins for vesicle recycling. These data demonstrate the Arr1 and NSF interaction are necessary for both maintenance and modulation of normal photoreceptor synaptic regulation. Second, NSF colocalizes and specifically binds to RP2, especially in the ciliary and synaptic region of the photoreceptor, and NSF–RP2 interaction may play an important role in membrane protein trafficking in the photoreceptor.

Inherited retinal degeneration affects about 1 in 2,000–3,000 individuals in the world and is the leading cause of visual loss in young people and accounts for a large proportion of blindness in adult life. These studies accelerate our ability to gain insight into the diverse roles of the NSF in the photoreceptor cells and enable us to understand more precisely the molecular mechanisms underlying night blindness associated with clinically diagnosed Oguchi disease or other forms of retinitis pigmentosa.

Acknowledgments We thank members of the Mary D. Allen Laboratory for scientific discussions, Bruce M. Brown for his technical expertise, Lawrence Rife for ERG analysis, Ernesto Barron for preparation of figures, and Jeannie Chen for the *Arr1*^{-/-} mice. CMC is the Mary D. Allen Chair in Vision Research, DEI, and a Research to Prevent Blindness (RPB) Senior Scientific Investigator. This work was supported, in part, by NIH Grant EY015851 (CMC), EY03040 (DEI), RPB (DEI & CMC), Dorie Miller, Tony Gray Foundation, Mary D. Allen Foundation (Dr. Richard Newton Lolley Memorial Scholarship [SPH]), and a RD2010 Travel Award (SPH).

References

- Bartolini F, Bhamidipati A, Thomas S et al (2002) Functional overlap between retinitis pigmentosa 2 protein and the tubulin-specific chaperone cofactor C. *J Biol Chem* 277:14629–14634
- Breuer DK, Yashar BM, Filippova E et al (2002) A comprehensive mutation analysis of RP2 and RPGR in a North American cohort of families with X-linked retinitis pigmentosa. *Am J Hum Genet* 70:1545–1554
- Brown BM, Ramirez T, Rife, L et al (2010) Visual arrestin 1 contributes to cone photoreceptor survival and light adaptation. *Invest Ophthalmol Vis Sci* 51:2372–2380

- Cong M, Perry SJ, Hu LA et al (2001) Binding of the beta2 adrenergic receptor to N-ethylmaleimide-sensitive factor regulates receptor recycling. *J Biol Chem* 276:45145–45152
- Hanson PI, Whiteheart SW (2005) AAA+ proteins: have engine, will work. *Nat Rev Mol Cell Biol* 6:519–529
- Holopainen JM, Cheng CL, Molday LL et al (2010) Interaction and Localization of the Retinitis Pigmentosa Protein RP2 and NSF in Retinal Photoreceptor Cells. *Biochemistry* 49:7439–7447
- Huang SP (2010) Exploring Alternative Roles of Visual Arrestin 1 in Photoreceptor Synaptic Regulation and Deciphering the Molecular Pathway of Retinal Degeneration Using Mouse Knockout Technology. Ph.D. dissertation. University of Southern California
- Huang SP, Brown BM, Craft CM (2010) Visual Arrestin 1 acts as a modulator for N-ethylmaleimide-sensitive factor in the photoreceptor synapse. *J Neurosci* 30:9381–9391
- Jahn R, Scheller RH (2006) SNAREs--engines for membrane fusion. *Nat Rev Mol Cell Biol* 7:631–643
- Kuhnel K, Veltel S, Schlichting I, Wittinghofer A (2006) Crystal structure of the human retinitis pigmentosa 2 protein and its interaction with Arl3. *Structure* 14:367–378
- Martens S, McMahon HT (2008) Mechanisms of membrane fusion: disparate players and common principles. *Nat Rev Mol Cell Biol* 9:543–556
- Matveeva E, Whiteheart SW (1998) The effects of SNAP/SNARE complexes on the ATPase of NSF. *FEBS Lett* 435:211–214
- McDonald PH, Cote NL, Lin FT et al (1999) Identification of NSF as a beta-arrestin1-binding protein. Implications for beta2-adrenergic receptor regulation. *J Biol Chem* 274:10677–10680
- Miano MG, Testa F, Filippini F et al (2001) Identification of novel RP2 mutations in a subset of X-linked retinitis pigmentosa families and prediction of new domains. *Hum Mutat* 18:109–119
- Morgan A, Dimaline R, Burgoyne RD (1994) The ATPase activity of N-ethylmaleimide-sensitive fusion protein (NSF) is regulated by soluble NSF attachment proteins. *J Biol Chem* 269:29347–29350
- Nagiec EE, Bernstein A, Whiteheart SW (1995) Each domain of the N-ethylmaleimide-sensitive fusion protein contributes to its transport activity. *J Biol Chem* 270:29182–29188
- Nishimune A, Isaac JT, Molnar E et al (1998) NSF binding to GluR2 regulates synaptic transmission. *Neuron* 21:87–97
- Osten P, Srivastava S, Inman GJ et al (1998) The AMPA receptor GluR2 C terminus can mediate a reversible, ATP-dependent interaction with NSF and alpha- and beta-SNAPs. *Neuron* 21:99–110
- Rizo J, Rosenmund C (2008) Synaptic vesicle fusion. *Nat Struct Mol Biol* 15:665–674
- Schwahn U, Lenzner S, Dong J et al (1998) Positional cloning of the gene for X-linked retinitis pigmentosa 2. *Nat Genet* 19:327–332
- Sharon D, Sandberg MA, Rabe VW et al (2003) RP2 and RPGR mutations and clinical correlations in patients with X-linked retinitis pigmentosa. *Am J Hum Genet* 73:1131–1146
- Sollner T, Bennett MK, Whiteheart SW et al (1993) A protein assembly-disassembly pathway in vitro that may correspond to sequential steps of synaptic vesicle docking, activation, and fusion. *Cell* 75:409–418
- Tagaya M, Wilson DW, Brunner M et al (1993) Domain structure of an N-ethylmaleimide-sensitive fusion protein involved in vesicular transport. *J Biol Chem* 268:2662–2666
- Veltel S, Gasper R, Eisenacher E et al (2008) The retinitis pigmentosa 2 gene product is a GTPase-activating protein for Arf-like 3. *Nat Struct Mol Biol* 15:373–380
- Zhao C, Matveeva EA, Ren Q et al (2010) Dissecting the N-ethylmaleimide-sensitive factor: required elements of the N and D1 domains. *J Biol Chem* 285:761–772

Chapter 102

Identification of Pigment Epithelium-Derived Factor Receptor (PEDF-R) Antibody Epitopes

Preeti Subramanian, Matthew Rapp, and S. Patricia Becerra

Keywords PEDF-R antibody • Epitope • PEDF • Phospholipase A₂ • PNPLA2

102.1 Introduction

PEDF-R is a PNPLA2 protein with demonstrable triglyceride lipase, triacylglycerol transacylase, and phospholipase activities. It has an N-terminal acyltransferase/lysophospholipase domain (human amino acid sequence numbers 3–178) and a patatin domain (human amino acid sequence numbers 10–179). PEDF-R is also known as TTS-2.2, iPLA₂ζ, ATGL and desnutrin (Notari et al. 2006). Among human, rat, and mouse species, PEDF-R is highly conserved (87% identity for both human/mouse and for human/rat and 96% for mouse/rat).

The gene of PEDF-R (*pnpla2*) has been identified in the retina (Notari et al. 2006). Although *PEDF-R* transcripts are abundantly identified in adipose tissues, the ARPE-19 cell line and the retina precursor R28 and RGC-5 cell lines also express PEDF-R transcripts (Notari et al. 2006). In the native retina, the PEDF-R protein is distributed in the RPE and in the inner segments of the photoreceptors, and at lower levels, in the inner nuclear and retinal ganglion cell layer (Notari et al. 2006). Several lines of evidence point to the subcellular localization of PEDF-R to plasma membranes having four transmembrane domains, two extracellular loops, one intracellular loop, and intracellular N-end and C-end tails (Notari et al. 2006).

P. Subramanian (✉) • S.P. Becerra
National Eye Institute, National Institutes of Health, Building 6, Room 134,
6 Center Drive, MSC 0608, Bethesda, MD 20892-0608, USA
e-mail: subramanianp@nei.nih.gov

M. Rapp
University of Maryland Baltimore County, Baltimore, MD 21250, USA

PEDF-R is an enzyme with phospholipase A activity that hydrolyzes phospholipids into fatty acids and lysophospholipids. In particular, phospholipase A₂ can specifically hydrolyze the sn-2 acyl bond of phospholipids releasing fatty acid, like arachidonic acid or docosahexaenoic acid. These products can act as lipid second messengers and cause further downstream signaling. Thus, regulation of this enzyme can result in important downstream biological events. In this regard, we have demonstrated that PEDF-R has high affinity binding for PEDF (Notari et al. 2006), a multifunctional protein involved in retinal neuronal survival and differentiation, and in preventing angiogenesis and the growth and invasion of tumor cells and has anti-inflammatory properties (Crawford et al. 2001; Bouck 2002; Wang et al. 2003; Barnstable and Tombran-Tink 2004; Garcia et al. 2004). More interestingly, PEDF can stimulate the in vitro PLA activity of PEDF-R (Notari et al. 2006) and it can enhance the liberation of a DHA derivative termed neuroprotectin D1 (Bazan et al. 2005), which is a neuronal survival and anti-inflammatory agent (Bazan 2005) like PEDF. Therefore, it has been proposed that the signaling activated by PEDF is mediated by the interactions between PEDF and PEDF-R to enhance retina cell survival.

Given that understanding the interactions between PEDF-R and PEDF are of interest to elucidate mechanisms of action of PEDF, it is important to have well-characterized tools for studying PEDF-R. In this study, we have characterized an antibody for PEDF-R available through commercial source (R&D systems) that can be used to detect PEDF-R in samples from human, mouse, and rat. We have explored the antibody-binding site(s) on PEDF-R using recombinant PEDF-R polypeptides and peptides. We have also used rat retina R28 cells as native source, because recent studies have shown that PEDF is a survival factor for R28 cells in response to serum starvation (Notari et al. 2005; Murakami et al. 2008). We provide information for an epitope and blocking peptides for the anti-PEDF-R as tools for further PEDF-R studies.

102.2 Materials and Methods

102.2.1 Peptides, Proteins, and Antibodies

Peptides were designed from exons 4, 5, 6, 7, and 8 of human PEDF-R and were chemically synthesized by a commercial source (Aves labs). Expression vectors for PEDF-R and PEDF-R4 were constructed into pEXP1-DEST vector with N-terminal epitope-tags (Xpress and His) as described (Notari et al. 2006). Recombinant proteins were expressed by cell-free in vitro protein synthesis using the pEXP-based vectors and *Escherichia coli* extracts from IVPS™ (Invitrogen). Recombinant proteins were purified using His tag affinity column chromatography with Ni-NTA resin (Invitrogen). Sheep polyclonal anti-PEDF-R was from R&D systems (Cat# AF5365); Secondary antibody HRP-conjugated donkey anti-sheep IgG was from SIGMA.

102.2.2 Slot Blot

Solutions of synthetic peptides (1 μg) were applied to wells in a manifold (Life Technologies) containing a nitrocellulose membrane (Bio-rad, Cat# 162-0116, 0.45 μm) presoaked in transfer buffer (Tris/Glycine/methanol). Peptides were transferred to membranes using vacuum as a driving force and the membrane subjected to immuno-blot.

102.2.3 Membrane Fractionation

R28 cells (kind gift of Dr. Gail Seigel, University of Buffalo) were cultured in DMEM media with 10% of fetal calf serum (FCS) and 1% of Penicillin/Streptomycin (P/S) at 37°C with 5% CO_2 . Confluent cells (90%) were harvested and separation of cytosolic and membrane fraction was obtained by centrifugation at 80,000 $\times g$ as described previously (Notari et al.). Protein concentration was determined with Protein Assay (Bio-Rad).

102.2.4 Polyacrylamide Gel Electrophoresis

Protein samples were resolved using NuPAGE 4–12% polyacrylamide gel in Bis-Tris buffer with NuPAGE MOPS-SDS as running buffer (Invitrogen). After electrophoresis, proteins from gel were then transferred to nitrocellulose membranes using the iBlot Gel Transfer system (Invitrogen) for immuno-blot. Prestained markers were from Bio-Rad (Cat# 161-0305).

102.2.5 Immuno-Blot

The membrane was incubated in blocking solution (1% BSA in Tris buffered saline plus 0.1% Tween-20, TBS-T) for 1 h at room temperature. The primary antibody was 0.25 mg/mL anti-PEDF-R in 1% BSA/TBS-T, and the secondary was HRP-conjugated donkey anti-sheep IgG (diluted 1:20,000 in 1% BSA/TBS-T). To block the binding of anti-PEDF-R, the antibody was preincubated with E4a and E4b peptides (at 1 mg/mL each) for 1 h at room temperature, followed by 16 h at 4°C before addition to the blot. Washes between primary and secondary antibody incubations were with TBS-T for 5 min each and 3 times. For immunodetection, SuperSignal West Dura Extended Duration Substrate (Pierce) was used following the manufacturer's protocol. The blot was exposed to an X-ray film to visualize the immunoreactive signal by chemiluminescence.

102.3 Results

102.3.1 Immunoreactivity to Recombinant PEDF-R Polypeptide Fragments

We tested the immunoreactivity of anti-PEDF-R to recombinant PEDF-R polypeptide fragments fused to Xpress and His tags. We expressed full-length PEDF-R and PEDF-R4, a C-terminal truncated version that is derived from the first four exons of PEDF-R. Given that these recombinant polypeptides have the Xpress tag, we used anti-Xpress antibody to confirm their expression (Fig. 102.1a). The PEDF-R antibody recognized both recombinant proteins of apparent molecular weights ~81 kDa for the full-length PEDF-R and ~40 kDa for the truncated PEDF-R4 version (Fig. 102.1b). The results suggest that the antibody recognition site does not require the C-terminal half of PEDF-R, and it could be located within the first four exons 1–4.

102.3.2 Immunoreactivity to Synthetic PEDF-R Peptides

Ten peptides spanning exons 4, 5, 6, 7, and 8 (Fig. 102.2) were generated synthetically. With equal amounts of each peptide transferred onto the membrane immunoreactions with anti-PEDF-R antibody revealed that only three peptides E4a, E4b, and P1 were detected (Fig. 102.3). Anti-PEDF-R bound with highest affinity to E4a followed by E4b and then P1. The results demonstrate that the exon 4 region contains the epitope for anti-PEDF-R, the E4a region being more antigenic than E4b.

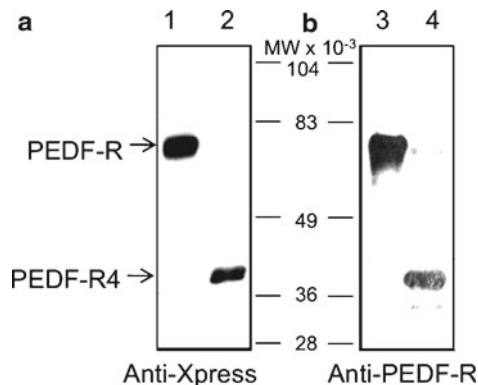


Fig. 102.1 Western blot of recombinant PEDF-R polypeptides. Full-length PEDF-R and C-terminal truncated PEDF-R4 were expressed using in vitro cell-free *Escherichia coli* expression system. Purified proteins were resolved by SDS-PAGE and electrotransferred to a membrane for immunostaining. Photographs of blots immunostained with anti-Xpress (a) and anti-PEDF-R (b) are shown. Lanes 1 and 3 were PEDF-R, lanes 2 and 4 were PEDF-R4. Migration positions of PEDF-R and PEDF-R4 are indicated with *arrows*, and of molecular weight markers are in between the two blots

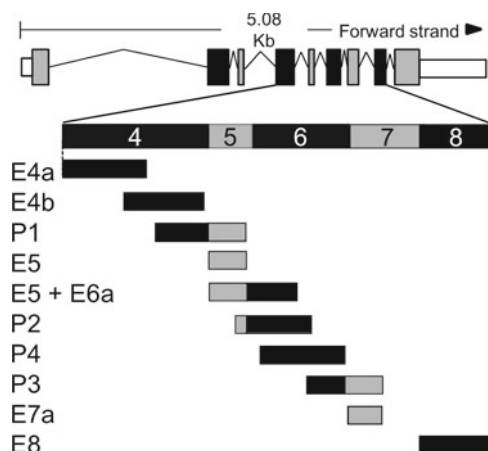


Fig. 102.2 Schematic of rat PEDF-R transcript. Transcript summary information for rat PEDF-R was obtained from <http://www.ensembl.org> for ENSRN00000025319. Exons are illustrated by *boxes*; coding regions are *black* and *gray*; introns are the *lines* flanking the boxes. Expanded region illustrates the design of synthetic peptides

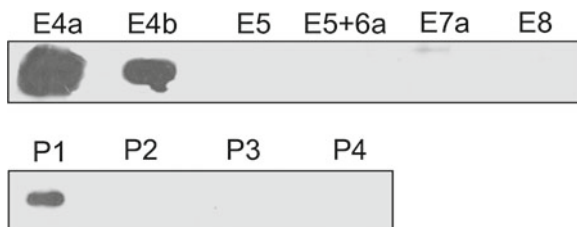


Fig. 102.3 Slot blot of PEDF-R peptides. Peptides (1 mg) were applied to a nitrocellulose membrane using a slot-blot technique and immunostained with anti-PEDF-R. Peptides are indicated to the *top* of the photograph

102.3.3 Immunoreactivity to Native Rat PEDF-R

Western blots of R28 cell membrane proteins with anti-PEDF-R antibody revealed three distinct immunoreactive protein bands (Fig. 102.4). The molecular sizes for these proteins were estimated to be 81, 70, and 65 kDa, relative to the migration pattern of the prestained markers. The signal for the three bands decreased when anti-PEDF-R was preincubated with a mixture of E4a and E4b peptides (Fig. 102.4), indicating that the immunoreactivity was blocked with E4, the antibody-binding region. This demonstrated that these three rat R28 proteins were specifically recognized by anti-PEDF-R.

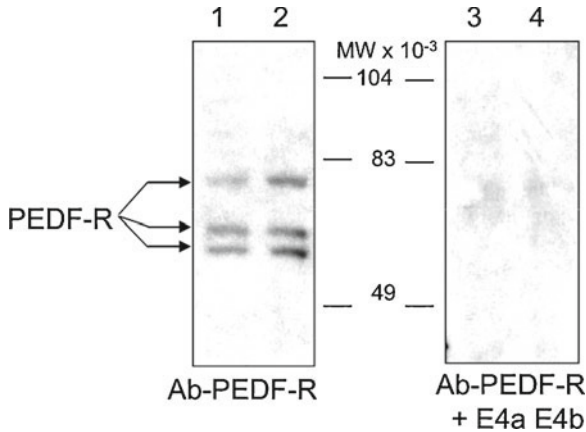


Fig. 102.4 Western blot of native PEDF-R from retina R28 cells. Membrane fractions obtained from R28 cells were resolved by SDS-PAGE. Total protein loaded in lanes 1–4 was 6 μ g each. Lanes 1 and 2, and lanes 3 and 4 were replicates. Immunoreactions with anti-PEDF-R were for lanes 1 and 2, and with anti-PEDF-R preincubated with peptides E4a and E4b were for lanes 3 and 4. Migration positions of PEDF-R isoforms are indicated with *arrows*, and molecular weight markers are in the *center*

102.4 Discussion

In this study, we have identified the epitope of the antibody that detects PEDF-R. We have mapped the epitope to the coding region of exon 4 of PEDF-R. Antibody anti-PEDF-R recognizes native rat PEDF-R, full-length recombinant human PEDF-R and the C-terminal-truncated PEDF-R4. PEDF-R4 terminates after exon 4, thereby retaining the antibody epitope. Given that the intensity of PEDF-R immunoreactivity decreased in this order E4a > E4b > P1, and that peptide E5 is not immunostained with anti-PEDF-R, the signal with P1 was most likely due to detection of its overlap with the E4b region. The antibody did not recognize any other region of PEDF-R. These results lead us to conclude that the epitope is located on the coding region of exon 4 of PEDF-R.

The rat *PEDF-R* gene contains nine exons with a coding capacity of 478 amino acids, in contrast to the 504 amino acid for the human product. Immunoreactions of rat R28 cell membrane fractions with anti-PEDF-R revealed three proteins with apparent molecular weights of 81, 70, and 65 kDa that contain the E4 region of PEDF-R. These proteins were specifically recognized to be PEDF-R as they were blocked upon preincubation of the antibody with the peptides E4a and E4b. While the 81-kDa protein corresponds to the full-length PEDF-R, the smaller proteins may result from alternative splice transcripts of PEDF-R. Ensembl reveals a splice variant lacking exon 6 in rat *PEDF-R*, thus resulting in a shorter polypeptide. R&D Systems reports three alternative splice mouse mRNAs with coding regions for three polypeptides of

molecular weights similar to those in the present study. Another possibility is that the 70- and 65-kDa protein versions result after posttranslational modifications. Previous studies demonstrated a single PEDF-R immunoreactive band of ~83-kDa protein in R28 cells with an antibody to RA peptide derived from the N-terminal half of E4b (Subramanian et al. 2010). This suggests that the RA region might be missing in the 71- and 65-kDa PEDF-R proteins. More importantly, our results demonstrate that R28 cells contain PEDF-R protein versions with the E4 region, which contains the PEDF-binding region (Locatelli-Hoops et al. 2008) important for stimulating the PLA activity of PEDF-R.

In summary, the antibody for PEDF-R used in this study is a useful tool to identify PEDF-R protein, and the E4a and E4b peptides are excellent blocking peptides for this antibody, which will prove useful in characterization of PEDF-R isoforms.

References

- Barnstable CJ, Tombran-Tink J (2004) Neuroprotective and antiangiogenic actions of PEDF in the eye: molecular targets and therapeutic potential. *Prog Retin Eye Res* 23:561–577
- Bazan NG (2005) Neuroprotectin D1 (NPD1): a DHA-derived mediator that protects brain and retina against cell injury-induced oxidative stress. *Brain Pathol* 15:159–166
- Bazan NG, Marcheselli VL, Hu J et al (2005) Pigment epithelium-derived growth factor (PEDF) selectively up-regulates NPD1 synthesis and release through the apical side of human RPE cells in primary cultures. *Invest Ophthalmol Vis Sci* 46:167
- Bouck N (2002) PEDF: anti-angiogenic guardian of ocular function. *Trends Mol Med* 8:330–334
- Crawford SE, Stellmach V, Ranalli M et al (2001) Pigment epithelium-derived factor (PEDF) in neuroblastoma: a multifunctional mediator of Schwann cell antitumor activity. *J Cell Sci* 114:4421–4428
- Garcia M, Fernandez-Garcia NI, Rivas V et al (2004) Inhibition of xenografted human melanoma growth and prevention of metastasis development by dual antiangiogenic/antitumor activities of pigment epithelium-derived factor. *Cancer Res* 64:5632–5642
- Murakami Y, Ikeda Y, Yonemitsu Y et al (2008) Inhibition of nuclear translocation of apoptosis-inducing factor is an essential mechanism of the neuroprotective activity of pigment epithelium-derived factor in a rat model of retinal degeneration. *Am J Pathol* 173:1326–1338
- Notari L, Baladron V, Aroca-Aguilar JD, Balko N et al (2006) Identification of a lipase-linked cell membrane receptor for pigment epithelium-derived factor. *J Biol Chem* 281:38022–38037
- Notari L, Miller A, Martinez A et al (2005) Pigment epithelium-derived factor is a substrate for matrix metalloproteinase type 2 and type 9: implications for downregulation in hypoxia. *Invest Ophthalmol Vis Sci* 46:2736–2747
- Subramanian P, Notario PM, Becerra SP (2010) Pigment Epithelium-derived Factor Receptor (PEDF-R): A Plasma Membrane-linked Phospholipase with PEDF Binding Affinity. *Adv Exp Med Biol* 664:29–37
- Wang L, Schmitz V, Perez-Mediavilla A et al (2003) Suppression of angiogenesis and tumor growth by adenoviral-mediated gene transfer of pigment epithelium-derived factor. *Mol Ther* 8:72–79
- Locatelli-Hoops S, Notari L, Becerra SP (2008) Identification of Structural Determinants on PEDF-R Responsible for Binding PEDF. ARVO Meeting Abstracts. *Invest Ophthalmol Vis Sci* 49:5768

Chapter 103

HCN1 Channels Significantly Shape Retinal Photoresponses

Naoyuki Tanimoto, Arne Brombas, Frank Müller, and Mathias W. Seeliger

Keywords Photoreceptors • HCN1 channels • Electroretinography • Knockout mice • Retinal signal processing • Flicker ERG

103.1 Introduction

In mammals, there are four genes encoding hyperpolarization-activated and cyclic nucleotide-gated (HCN) channels (HCN1-4) which are expressed in the heart and the nervous system including the retina (Moosmang et al. 2001; Müller et al. 2003). Among the four HCN channel isoforms, HCN1 has the fastest kinetics and is strongly voltage-dependent; therefore, HCN1 channels were considered to be important for the shaping and shortening of photoreceptor voltage responses (Demontis et al. 1999; Fain et al. 1978). In the mammalian retina, particularly strong expression of HCN1 channels is detected in the membrane of the photoreceptor inner segments (Knop et al. 2008; Müller et al. 2003). It has been found that a knockout of HCN1 in mice (Nolan et al. 2003) leads to exaggerated, prolonged rod responses in the ERG, together with a reduced flicker fusion frequency (Knop et al. 2008). In this chapter, the functional properties of HCN1 channels in the mouse retina are described by comparing single-flash and flicker ERG responses between HCN1 knockout and control wild-type animals.

N. Tanimoto (✉) • M.W. Seeliger
Division of Ocular Neurodegeneration, Centre for Ophthalmology,
Institute for Ophthalmic Research, University of Tübingen, Schleichstr. 4/3,
Tübingen, Germany
e-mail: naoyuki.tanimoto@med.uni-tuebingen.de

A. Brombas • F. Müller
Institut für Strukturbiologie und Biophysik (ISB-1), Forschungszentrum Jülich,
Jülich, Germany

103.2 Mechanism of HCN1 Channel Activity in Normal Photoreceptor

A flash of light activates phototransduction, which leads to the closure of cyclic nucleotide-gated channels in the outer segments. This diminishes the dark current resulting in a hyperpolarization of the plasma membrane. The hyperpolarizing voltage change induces the opening of HCN1 channels in the inner segments after a delay of about 30 ms in mammalian rods at body temperature. An inward current through the open HCN1 channels reduces the level of the hyperpolarization, i.e., the membrane potential is shifted back toward the resting state, making the light response transient.

103.3 Altered Single-Flash ERG Responses in HCN1^{-/-} Mice

The murine Ganzfeld ERG is a measure of overall retinal function. ERGs were recorded according to procedures previously described (Seeliger et al. 2001; Tanimoto et al. 2009). Single-flash ERG recordings were performed under dark-adapted (scotopic) conditions with different stimulus intensities (Fig. 103.1). HCN1^{-/-} mice and wild-type (wt) littermates were 6 weeks old. Typical normal ERG responses are seen at middle to high stimulus intensities under scotopic conditions (the *left column* in Fig. 103.1a). Typically, an ERG response begins with a negative deflection initiated by photoreceptors which is called a-wave. The large positive deflection reflects the activity of ON bipolar cells, which is called b-wave. The amplitude of the b-wave is usually much larger than that of the a-wave in mice. The small oscillations on top of the b-wave, which are called oscillatory potentials, involve inner retinal circuitry with different origins. Under scotopic conditions, the responses at low stimulus intensities are composed of a b-wave only. The responses were comparable between HCN1^{-/-} and wt mice up to the stimulus intensity of $-3.0 \log cd^*s/m^2$ (the top two overlays in Fig. 103.1b), showing that deletion of HCN1 has no effect on the sensitivity of the light responses. At the stimulus intensity of $-2.0 \log cd^*s/m^2$, the response onset and the activation phase of the b-wave did not differ between the two mouse lines; however, the trailing edge of the b-wave became larger in HCN1^{-/-} mice. The difference between wt and HCN1^{-/-} grew more prominent at the intensity of $-1.5 \log cd^*s/m^2$ (*arrows* in Fig. 103.1b). This intensity dependency of the HCN1 channel effect is supported by pharmacological studies (Demontis et al. 1999; Fain et al. 1978). At the stimulus intensity of $-1.5 \log cd^*s/m^2$ and above, no difference was observed in the a-wave between both mouse lines, in agreement with HCN1 channels being expressed in the inner segment of photoreceptors, but not in the outer segment. It has been also demonstrated that the loss of HCN1 channels does not affect photoreceptor outer segment currents using the paired-flash ERG protocol (Knop et al. 2008). The initial part of the b-wave was not altered in HCN1^{-/-} mice, because HCN1 channels are not involved in the onset of

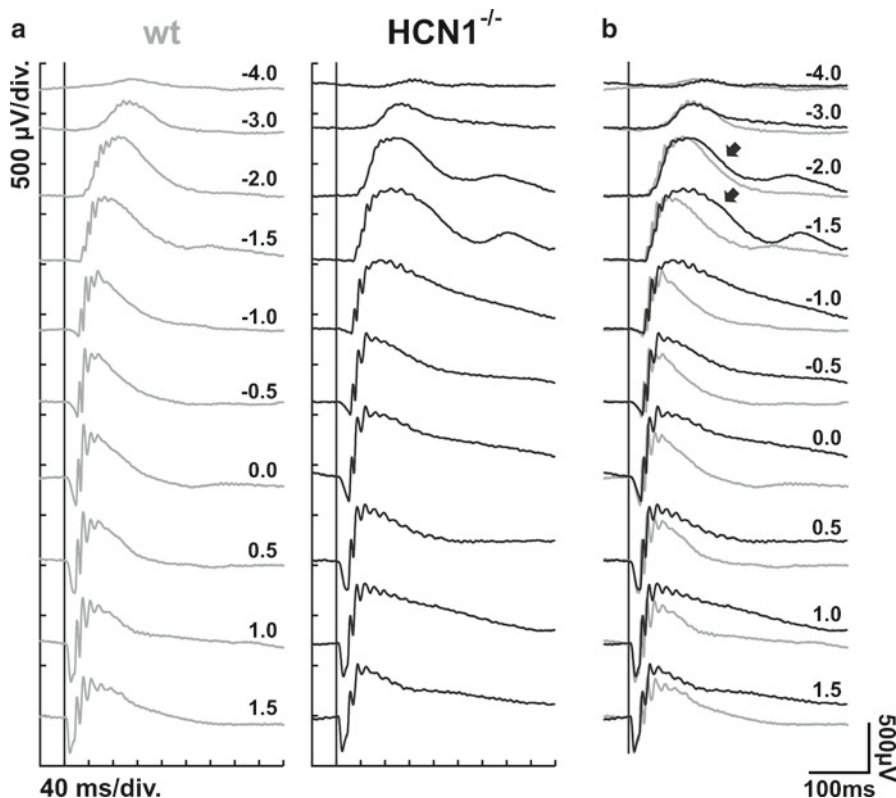


Fig. 103.1 Prolonged retinal photoresponses in $HCN1^{-/-}$ mice. **(a)** Representative single-flash electroretinograms (ERGs) recorded under dark-adapted (scotopic) conditions from a wild-type (*wt*, *left*) and a $HCN1^{-/-}$ mouse (*right*). Flash intensities are indicated in ($\log(cd^*s/m^2)$). The vertical line indicates the timing of the light flash. **(b)** Overlay of the single-flash ERG responses shown in **(a)**. There was no evidence for differences in b-wave amplitude or waveform between the two mouse lines in the low-intensity range up to $-3.0 \log cd^*s/m^2$ under scotopic conditions. A waveform difference between $HCN1^{-/-}$ and *wt* mice became manifest at and above $-2.0 \log cd^*s/m^2$ (arrows in **(b)**). In the higher intensities, the b-wave was noticeably prolonged in $HCN1^{-/-}$ animals, which led to a delayed return of the light-evoked responses to baseline. The a-wave and the initial portion of the b-wave were not altered in $HCN1^{-/-}$ mice

the light response. The shape of the trailing edge of the b-wave was concave in *wt* mice, whereas its concavity almost disappeared in $HCN1^{-/-}$ mice. As a result, the light-evoked responses in $HCN1^{-/-}$ mice returned to baseline much more slowly than those in *wt* mice. In $HCN1^{-/-}$ mice, the prolonged photoreceptor response induces a sustained decrease of glutamate release to ON-bipolar cells upon stimulation with bright light; therefore, bipolar cell responses become prolonged, which was observed as a prolonged ERG b-wave.

103.4 Reduction in Scotopic ERG Flicker Fusion Frequency in HCN1^{-/-} Mice

The ability to respond to train of flashes (flicker) was tested in order to investigate the influence of prolonged single-flash ERG responses. Responses to repetitive flashes for a fixed intensity (-2.0 or $-0.5 \log cd^*s/m^2$) with varying frequency (0.5, 1, 2, 3, 5, 7, 10, 12, 15, and 30 Hz) were recorded under dark-adapted conditions (Fig. 103.2). Flicker responses were averaged either 20 times (for 0.5, 1, 2, and 3 Hz) or 30 times (for 5 Hz and above), i.e., steady-state flicker responses were analyzed. At the intensity of $-2.0 \log cd^*s/m^2$, the effect of HCN1 channel knockout on b-wave configuration was very small (Fig. 103.1b), most probably because the hyperpolarization of the photoreceptors at the given light intensity was too small to substantially activate HCN1 channels. The phenotype of HCN1 knockout detected at 0.5 Hz in the flicker ERG was similar to that observed in single-flash ERG, e.g., normal onset and normal activation phase of the b-wave analogue, and mild prolongation of the trailing edge of the b-wave analogue. With increasing stimulus frequency, a regular amplitude decline was observed up to 12 Hz in wt and in HCN1^{-/-} mice (Fig. 103.2a, c). At 30 Hz, neither the wt nor the HCN1^{-/-} retina could resolve the flickering stimulus. By contrast, at the intensity of $-0.5 \log cd^*s/m^2$, the flicker response in HCN1^{-/-} mice showed manifest prolongation of the b-wave analogue at the stimulus frequency of 0.5 Hz (Fig. 103.2b, d), which is quite similar to the prolongation of the b-wave that was clearly seen in the scotopic single-flash ERG (Fig. 103.1b). As seen in the scotopic single-flash ERGs, the a-wave analogue and the initial part of the b-wave analogue were comparable between wt and HCN1^{-/-} mice. With increasing stimulus frequency, amplitudes decreased dramatically in HCN1^{-/-} mice, and no responses were detectable above 7 Hz, whereas wt mice showed flicker responses in the higher frequency range up to 12 Hz. This demonstrated a remarkable reduction of the ability to follow higher-frequency flicker in the HCN1^{-/-} animals above threshold of HCN1 channel activation.

103.5 Summary and Perspective

In this chapter, the impact of HCN1 channels on the retinal functional properties was presented. HCN1 channel loss led to an intensity-dependent prolongation of the rod system response, in agreement with the threshold mechanism of activation of the channel. Rod outer segment functionality was not altered, supporting the main site of action in the inner segment. Fixed-intensity variable frequency flicker series showed a regular amplitude decline near threshold and a reduced flicker fusion frequency above threshold due to increased waveform width. It was suggested that shortening and shaping of light responses by activation of HCN1 is an important step at least in the scotopic pathways. The retina of HCN1 knockout animals

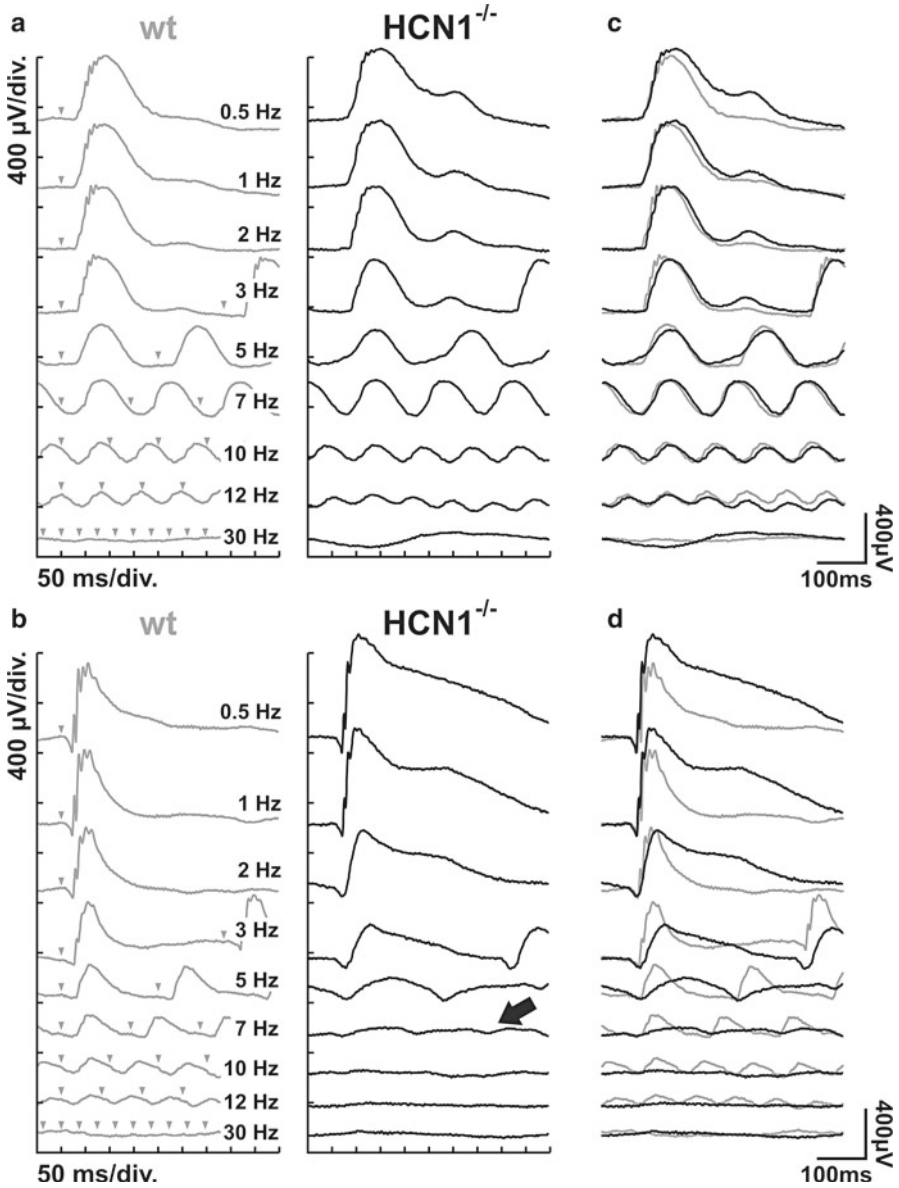


Fig. 103.2 Effect of lack of HCN1 channels on flicker fusion frequency. **(a, b)** Representative records of scotopic flicker frequency series at the intensity of $-2.0 \log cd^*s/m^2$ **(a)** and $-0.5 \log cd^*s/m^2$ **(b)** from a wt (*left*) and a HCN1^{-/-} mouse (*right*). The *arrowheads* indicate the timing of the light stimuli. **(c, d)** Overlay of the flicker responses shown in **(a)** and **(b)** **(c)**; $-2.0 \log cd^*s/m^2$, **(d)**; $-0.5 \log cd^*s/m^2$). At high stimulus intensities such as $-0.5 \log cd^*s/m^2$ **(b, d)**, the remarkable prolongation of the waveform in the absence of HCN1 led to a reduced flicker fusion frequency (at around 7 Hz, *arrow* in **(b)**), whereas due to a mild prolongation of the waveform at $-2.0 \log cd^*s/m^2$ **(a, c)**, response amplitudes do not differ significantly between wt and HCN1^{-/-} mice

provides a valuable system with which to study the role of HCN1 in the shaping and processing of retinal light responses especially to repetitive stimulation.

Acknowledgments We thank Dr. Eric Kandel (Columbia University, USA) for providing the HCN1 knockout line. This work was supported by the Deutsche Forschungsgemeinschaft (DFG, grants Se837/5-2, and 6-1) to M.W.S., the Kerstan Foundation to N.T., and the European Union (grant LSHG-CT-2005-512036) to A.B. and F.M.

References

- Demontis GC, Longoni B, Barcaro U et al (1999) Properties and functional roles of hyperpolarization-gated currents in guinea-pig retinal rods. *J Physiol* 515:813–828
- Fain GL, Quandt FN, Bastian BL et al (1978) Contribution of a caesium-sensitive conductance increase to the rod photoresponse. *Nature* 272:467–469
- Knop GC, Seeliger MW, Thiel F et al (2008) Light responses in the mouse retina are prolonged upon targeted deletion of the HCN1 channel gene. *Eur J Neurosci* 28:2221–2230
- Moosmang S, Stieber J, Zong X et al (2001) Cellular expression and functional characterization of four hyperpolarization-activated pacemaker channels in cardiac and neuronal tissues. *Eur J Biochem* 268:1646–1652
- Müller F, Scholten A, Ivanova E et al (2003) HCN channels are expressed differentially in retinal bipolar cells and concentrated at synaptic terminals. *Eur J Neurosci* 17:2084–2096
- Nolan MF, Malleret G, Lee KH et al (2003) The hyperpolarization-activated HCN1 channel is important for motor learning and neuronal integration by cerebellar Purkinje cells. *Cell* 115:551–564
- Seeliger MW, Grimm C, Ståhlberg F et al (2001) New views on RPE65 deficiency: the rod system is the source of vision in a mouse model of Leber congenital amaurosis. *Nat Genet* 29:70–74
- Tanimoto N, Muehlfriedel RL, Fischer MD et al (2009) Vision tests in the mouse: functional phenotyping with electroretinography. *Front Biosci* 14:2730–2737

Chapter 104

The Role of the P2X7 Receptor in the Retina: Cell Signalling and Dysfunction

Kirstan A. Vessey, Andrew I. Jobling, Ursula Greferath, and Erica L. Fletcher

Keywords Adenosine 5'-triphosphate (ATP) • Purine receptor • P2X7 receptor • Retina • Photoreceptors • Ganglion cells • Müller cells • Microglia

104.1 Introduction

104.1.1 ATP and Purinergic Receptors

Adenosine 5'-triphosphate (ATP) has long been known for its role in energy metabolism within the cell; however, in the last 40 years, the role of extracellular ATP as a signalling molecule has been the subject of intense research (Abbracchio et al. 2009 for review). ATP and its breakdown products adenosine and ADP, and other related purines such as UDP and UTP, have been found to act as transmitters at a wide range of purine receptors. The purinergic signalling system is expressed throughout both the central and peripheral nervous system and is not limited to traditional exocytotic neurotransmission (Abbracchio et al. 2009). In the retina, the purinergic system plays a role in signalling between all cell types: neurons, endothelial cells (blood vessels) and glia, including Müller cells, astrocytes, and microglia (Housley et al. 2009).

K.A. Vessey (✉) • A.I. Jobling • U. Greferath • E.L. Fletcher
Department of Anatomy and Cell Biology, The University of Melbourne,
Level 7, Medical Building, Grattan Street, Melbourne, VIC 3010, Australia
e-mail: k.vessey@unimelb.edu.au

104.1.2 ATP Storage, Release and Degradation

There are multiple mechanisms for the storage and release of ATP (Abbracchio et al. 2009). The traditional mechanism of vesicular storage and exocytotic release of ATP has been shown to occur in both the peripheral and central nervous systems. In the retina, ATP may be co-released with other transmitters in an exocytotic manner from both inhibitory (e.g. GABAergic) and excitatory neurons (e.g. Cholinergic). Other non-traditional mechanisms for ATP release have also been proposed. These include ATP release from astrocytes by lysosome exocytosis and release from pannexin and/or connexin hemi-channels. In the retina, there is evidence for hemi-channel release of ATP from the retinal pigment epithelium (RPE) (Pearson et al. 2005) and mechanical stimulation-induced ATP release from glia (Newman 2001). ATP release from dying neurons has also been suggested to be a potential signal in propagating cytotoxic response mechanisms and further cell death in the surrounding cells.

Once released into the extracellular space, ATP is rapidly degraded by ectonucleotidases to ADP and/or AMP and then further degraded to adenosine (Corriden and Insel 2010). Ectonucleoside triphosphate diphosphohydrolases (E-NTPDases) hydrolyse nucleotide triphosphates and diphosphates to monophosphates. Ecto-5'-nucleotidases then further hydrolyse AMP to adenosine (Corriden and Insel 2010). In the retina, there is evidence for ectonucleotidase degradation of ATP at synaptic terminals (Puthussery et al. 2006) and both NTPDases 1 and 2 have been found to be expressed (Ricatti et al. 2009). This suggests that ATP, ADP and adenosine are present as bioactive ligands in the retina.

104.1.3 Purine Receptors

There are two main classes of purine receptors, P1 and P2 (Abbracchio et al. 2009). The P1 receptors are activated by adenosine and four subclasses have been identified so far. The P2 receptors can be further divided into two general classes, the P2X and P2Y-receptors. The P2X-receptors are ligand-gated ion channels that are activated primarily by ATP. There are seven subclasses of P2X-receptors, P2X1-7. The P2Y-receptors are seven transmembrane, G-protein-coupled receptors. At least eight subclasses have currently been identified which may be activated by ATP, ADP, UTP and/or UDP, depending on the receptor subclass. All classes of purine receptors have been found to be expressed in the retina. Furthermore, all cell types in the retina, neurons, glia and microglia express some complement of purine receptors (Ward et al. 2010 for review). The remainder of the current review will focus specifically on the role of the P2X7 receptor in the retina with regard to cell signalling and neuronal degeneration.

104.2 The P2X7 Receptor

The P2X7 receptor was first cloned in 1996 from the rat brain and was allocated to the class of P2X receptors based on comparable sequence homology (Surprenant et al. 1996). However, P2X7 receptors are unique when compared with the other P2X receptors. While they are permeable to sodium, calcium, and potassium, causing cell membrane depolarisation, they are relatively insensitive to ATP (Surprenant et al. 1996). Moreover, the P2X7 receptor has a long intracellular C-terminus which is critical for ion channel function, but also allows the receptor to form a pore in the plasma membrane allowing molecules of up 900 kDa into the cell following prolonged stimulation with ATP. Indeed, the involvement of the P2X7 receptor pore in mediating cell apoptosis had caused the receptor to initially be labelled the P2Z “death” receptor (Ferrari et al. 1999). Thus, the P2X7 receptor has the dual capacity to act in modulating cell signalling and also in modulating responses in pathological situations.

104.2.1 *Role of the P2X7 Receptor in Neuronal Modulation in the Retina*

P2X7 receptor mRNA and protein have been detected in neuronal cells within the rodent and primate retina (Wheeler-Schilling et al. 2001; Ishii et al. 2003; Puthussery and Fletcher 2004; Puthussery et al. 2006). Specific labelling has been detected on rods near the ribbon synapses, and on horizontal cells, amacrine cells and ganglion cells. In the inner retina, P2X7 receptors were found to be expressed in amacrine cell synapses presynaptic to rod bipolar cell terminals, close to the dyad synapses. This suggests that the P2X7 receptor may modulate signal transmission within the rod pathway (Puthussery and Fletcher 2004). In line with this finding, administration of benzoyl ATP (Bz-ATP), a P2X receptor agonist selective for P2X7, has been found to alter the function of the rod and cone pathways in the rat (Puthussery et al. 2006). This implicates a role for the P2X7 receptor in neuronal transmission within the retina.

104.2.2 *Role of the P2X7 Receptor in Neuronal Degeneration in the Retina*

In addition to a putative functional role of the P2X7 receptor in modulating retinal output, the receptor has also been implicated in mediating direct neurotoxicity in the brain and retina. Pathological increases in the expression of P2X7 receptor mRNA occur in many models of neurodegeneration such as Alzheimer’s disease, Parkinson’s disease, cerebral ischemia and spinal cord injury (Monif et al. 2010 for review).

In the retina, P2X7 receptor mRNA is upregulated in a mouse model of retinitis pigmentosa during the period of photoreceptor degeneration (Franke et al. 2005). Indeed, excess stimulation of P2 receptors by injection of ATP into the vitreous of the adult rat eye has been shown to induce photoreceptor cell death and deficits in photoreceptor function, likely via the direct activation of P2X7 receptors on photoreceptors (Puthussery and Fletcher 2009). Puthussery and Fletcher (2009) suggest that an increase in P2X7 receptor expression during retinal degeneration may increase the sensitivity of the photoreceptors to ATP, predisposing them to calcium-induced neurotoxicity and apoptosis due to excessive stimulation. In line with this proposal, photoreceptor degeneration can be slowed in the rd1 mouse model of retinitis pigmentosa by intravitreal administration of a P2X receptor antagonist; however, further work is required to confirm the specific involvement of the P2X7 receptor in this process (Puthussery and Fletcher 2009).

The P2X7 receptor has also been implicated in ganglion cell death in glaucoma (Zhang et al. 2005; Resta et al. 2007; Hu et al. 2010). The levels of ATP are increased in the aqueous humour of human patients with acute glaucoma (Zhang et al. 2007) and in rat eyes with experimentally induced pressure damage (Resta et al. 2007). Stimulation of P2X7 receptors on ganglion cells using the agonist Bz-ATP causes a rise in intracellular calcium levels and cell death in vitro (Zhang et al. 2005). Also in vivo, intravitreal administration of BzATP has been shown to induce ganglion cell death in neonatal rats (P14-P28). This effect can be blocked by the relatively selective P2X7 receptor blockers brilliant blue G and MRS 2540, suggesting that excess stimulation of P2X7-receptors on ganglion cells may induce their death (Hu et al. 2010). In line with this theory, administration of brilliant blue G has been shown to reduce the occurrence of ganglion cell trauma and death in retina from rats with experimentally induced pressure damage (Resta et al. 2007). Given these findings, P2X7 receptor antagonists may provide a potential therapy for slowing or preventing neuronal cell loss in diseases such as retinitis pigmentosa and glaucoma.

104.2.3 Role of the P2X7 Receptor in Müller Cells

Müller cells along with astrocytes represent the macroglia of the retina. In particular, Müller cells, which are radial glia that span the thickness of retina, are important for providing support for neighbouring neurons in the form of neurotransmitter recycling, provision of energy and ion homeostasis (Bringmann et al. 2006). There is currently debate in the literature regarding the expression of P2X7 receptors in Müller cells. It has been suggested that Müller cells do not express P2X7 receptor mRNA (Jabs et al. 2000) nor protein (Ishii et al. 2003). However, other studies suggest that they do produce P2X7 receptor mRNA and protein, and these studies provide additional functional evidence for P2X7 receptor-mediated calcium currents in Müller cells induced by BzATP (Bringmann et al. 2001). These studies have shown that P2X7 receptors in Müller cells may modulate gliosis in retinal disease. P2X7 receptor-mediated currents in Müller cells are upregulated in proliferative

vitreoretinopathy (Bringmann et al. 2001) and in proliferative diabetic retinopathy (Bringmann et al. 2002), causing Müller cell dysfunction such as alterations in potassium conductance, hypertrophy and proliferation. Further research is required to determine if blockade of the P2X7 receptor-induced currents restores Müller cell function in these diseases.

104.2.4 Role of the P2X7 Receptor in Retinal Microglial Cells

Microglia are the resident macrophages of the central nervous system (Monif et al. 2010). In development, they are involved in pruning neuronal synapses and removing apoptotic cells. Following injury, microglia migrate to the source of damage, release neuroinflammatory mediators and phagocytose dying cells (Monif et al. 2010). In pathological situations, excessive extracellular ATP not only activates the P2X7 receptor ion channel on microglia, but also stimulates formation of the receptor pore (Monif et al. 2009). This activation of P2X7-receptors causes the microglia to alter from their quiescent, ramified state to become amoeboid or activated and to proliferate. Once activated, microglia release chemokines for recruitment of other microglia and also bioactive factors including cytokines that can be neuroprotective or neurotoxic (Monif et al. 2010). In particular, microglia are prone to exacerbating a chronic inflammatory response inducing further neuronal trauma in response to injury and some of this effect can be blocked by inhibition of the P2X7 receptor.

Although this pathway has been studied extensively in other regions of the central nervous system, very few studies have investigated the role of the P2X7 receptor in modulating microglial activity in the retina or in retinal disease. Stimulation of the P2X7 receptor with BzATP has been shown to cause pore formation in microglia only and not other cells in the intact rat retina, even though many neuronal populations have been shown to express P2X7 receptors (Innocenti et al. 2004). This suggests that P2X7 receptor pore formation may be microglia-specific in the retina and that this plays a role in microglial activation in inflammation. In addition, BzATP stimulation of the P2X7 receptor on cultured retinal microglia has been shown to cause release of inflammatory cytokines such as interleukin 1 β and tumour necrosis factor α (Morigiwa et al. 2000). These data suggest that activation of P2X7 receptors may play an important role in microglial responses in the retina; however, further research is required to elucidate the role of the P2X7 receptor in microglia in retinal disease.

104.3 Conclusion

The purinergic system plays a role in signalling between all cell classes in the retina including neurons and glia. In particular, the P2X7 receptor has an unusual role. Under physiological conditions, it is involved in modulation of neuronal signalling in

the rod and cone pathway, Müller cell membrane conductance and microglial activity. Under pathological conditions, it plays a role in neuronal and Müller cell dysfunction and in the activation of microglia in response to injury. Understanding the mechanisms that regulate the physiological vs. pathological roles of the P2X7 receptor in the retina may provide a target for therapy of a variety of retinal diseases.

References

- Abbracchio MP, Burnstock G, Verkhratsky A et al (2009) Purinergic signalling in the nervous system: an overview. *Trends Neurosci* 32:19–29
- Bringmann A, Pannicke T, Uhlmann S et al (2002) Membrane conductance of Müller glial cells in proliferative diabetic retinopathy. *Can J Ophthalmol* 37:221–227
- Bringmann A, Pannicke T, Moll V et al (2001) Upregulation of P2X(7) receptor currents in Müller glial cells during proliferative vitreoretinopathy. *Invest Ophthalmol Vis Sci* 42:860–867
- Bringmann A, Pannicke T, Grosche J et al (2006) Müller cells in the healthy and diseased retina. *Prog Retin Eye Res* 25:397–424
- Corriden R, Insel PA (2010) Basal release of ATP: an autocrine-paracrine mechanism for cell regulation. *Sci Signal* 3:re1
- Ferrari D, Los M, Bauer MK et al (1999) P2Z purinoreceptor ligation induces activation of caspases with distinct roles in apoptotic and necrotic alterations of cell death. *FEBS Lett* 447:71–75
- Franke H, Klimke K, Brinckmann U et al (2005) P2X(7) receptor-mRNA and -protein in the mouse retina; changes during retinal degeneration in BALB/Crds mice. *Neurochem Int* 47:235–242
- Housley GD, Bringmann A, Reichenbach A (2009) Purinergic signaling in special senses. *Trends Neurosci* 32:128–141
- Hu H, Lu W, Zhang M et al (2010) Stimulation of the P2X7 receptor kills rat retinal ganglion cells in vivo. *Exp Eye Res* 91:425–432
- Innocenti B, Pfeiffer S, Zrenner E et al (2004) ATP-induced non-neuronal cell permeabilization in the rat inner retina. *J Neurosci* 24:8577–8583
- Ishii K, Kaneda M, Li H et al (2003) Neuron-specific distribution of P2X7 purinergic receptors in the monkey retina. *J Comp Neurol* 459:267–277
- Jabs R, Guenther E, Marquardt K et al (2000) Evidence for P2X(3), P2X(4), P2X(5) but not for P2X(7) containing purinergic receptors in Müller cells of the rat retina. *Brain Res Mol Brain Res* 76:205–210
- Jo YH, Schlichter R (1999) Synaptic corelease of ATP and GABA in cultured spinal neurons. *Nat Neurosci* 2:241–245
- Jo YH, Role LW (2002) Coordinate release of ATP and GABA at in vitro synapses of lateral hypothalamic neurons. *J Neurosci* 22:4794–4804
- Monif M, Burnstock G, Williams DA (2010) Microglia: proliferation and activation driven by the P2X7 receptor. *Int J Biochem Cell Biol* 42:1753–1756
- Monif M, Reid CA, Powell KL et al (2009) The P2X7 receptor drives microglial activation and proliferation: a trophic role for P2X7R pore. *J Neurosci* 29:3781–3791
- Morigiwa K, Quan M, Murakami M et al (2000) P2 Purinoceptor expression and functional changes of hypoxia-activated cultured rat retinal microglia. *Neurosci Lett* 282:153–156
- Newman EA (2001) Propagation of intercellular calcium waves in retinal astrocytes and Müller cells. *J Neurosci* 21:2215–2223
- Pearson RA, Dale N, Llaudet E et al (2005) ATP released via gap junction hemichannels from the pigment epithelium regulates neural retinal progenitor proliferation. *Neuron* 46:731–744
- Puthussery T, Fletcher EL (2004) Synaptic localization of P2X7 receptors in the rat retina. *J Comp Neurol* 472:13–23

- Puthussery T, Fletcher EL (2009) Extracellular ATP induces retinal photoreceptor apoptosis through activation of purinoceptors in rodents. *J Comp Neurol* 513:430–440
- Puthussery T, Yee P, Vingrys AJ et al (2006) Evidence for the involvement of purinergic P2X receptors in outer retinal processing. *Eur J Neurosci* 24:7–19
- Resta V, Novelli E, Vozzi G et al (2007) Acute retinal ganglion cell injury caused by intraocular pressure spikes is mediated by endogenous extracellular ATP. *Eur J Neurosci* 25:2741–2754
- Ricatti MJ, Alfie LD, Lavoie EG et al (2009) Immunocytochemical localization of NTPDases 1 and 2 in the neural retina of mouse and zebrafish. *Synapse* 63:291–307
- Surprenant A, Rassendren F, Kawashima E et al (1996) The cytolytic P2Z receptor for extracellular ATP identified as a P2X receptor (P2X7). *Science* 272:735–738
- Ward MM, Puthussery T, Vessey KA et al (2010) The role of purinergic receptors in retinal function and disease. *Adv Exp Med Biol* 664:385–391
- Wheeler-Schilling TH, Marquardt K, Kohler K et al (2001) Identification of purinergic receptors in retinal ganglion cells. *Brain Res Mol Brain Res* 92:177–180
- Zhang X, Zhang M, Laties AM et al (2005) Stimulation of P2X7 receptors elevates Ca²⁺ and kills retinal ganglion cells. *Invest Ophthalmol Vis Sci* 46:2183–2191
- Zhang Z, Chen G, Zhou W et al (2007) Regulated ATP release from astrocytes through lysosome exocytosis. *Nat Cell Biol* 9:945–953

Chapter 105

A Tale of Two Kinases in Rods and Cones

Shoji Osawa and Ellen R. Weiss

Keywords GRK • Rod • Kinase • Cone • Photoreceptor • PKA • Recoverin • Opsin • Rhodopsin • cAMP

105.1 Introduction

The G protein-coupled receptor kinase (GRK) family of serine/threonine kinases contains seven members with varying tissue localization in vertebrates. Rhodopsin kinase (GRK1) was the first member of the family identified and was shown to limit the lifetime of its substrate, rhodopsin, via phosphorylation followed by arrestin binding (Wilden and Kühn 1982; Kühn and Wilden 1987). A central role for GRK1 in retinopathies was identified when Oguchi disease, a form of stationary night blindness, was found to be due to an inactivating mutation in GRK1. Although the vision of patients with this disease is fairly normal in bright light, they have difficulty seeing in dim light. Later, individuals with similar visual problems were identified with mutations that interfere with the function of arrestin. Defects in either of these genes cause patients to suffer from an inability to properly deactivate rhodopsin, leading to problems with recovery and dark adaptation (Dryja 2000).

S. Osawa

Department of Cell and Developmental Biology, The University of North Carolina at Chapel Hill, CB# 7090, 108 Taylor Hall, Chapel Hill, NC 27599, USA

E.R. Weiss (✉)

Department of Cell and Developmental Biology, The University of North Carolina at Chapel Hill, CB# 7090, 108 Taylor Hall, Chapel Hill, NC 27599, USA

Lineberger Comprehensive Cancer Center, The University of North Carolina at Chapel Hill, Chapel Hill, NC 27599-7090, USA
e-mail: erweiss@med.unc.edu

Table 105.1 Distribution of GRK1 and GRK7 in vertebrate photoreceptor cells

	Rods	Cones
Human	1	1, 7
Monkey	1	1, 7
Xenopus	1	1, 7
Chicken	1	1, 7 ^a
Zebrafish	1A	1B, 7
Carp	1A	1B, 7
Pig	1	7
Dog	1	7
Medaka	1-1, 1-2	7
Mouse	1	1

^aExpression of chicken GRK7 is speculative

One question that arose from studying patients with Oguchi disease was, if GRK1 is the only GRK involved in phototransduction in rods and cones, why do Oguchi patients exhibit relatively mild defects in cone recovery (Cideciyan et al. 1998)? In contrast, mice null for GRK1 (GRK1^{-/-} mice) do exhibit severe defects in cone recovery (Chen et al. 1999; Lyubarsky et al. 2000). A potential explanation would be that human cones express a second GRK that also phosphorylates the cone opsins. In 1998, the full-length cloning of GRK7 from medaka fish (Hisatomi et al. 1998) and the 13-lined ground squirrel, a cone-dominant mammal (Weiss et al. 1998), was reported. Ultimately, GRK7 was also cloned from a number of rod dominant mammals, such as human, pig, and cow, as well as additional species of fish and frog (Chen et al. 2001; Weiss et al. 2001; Shimauchi-Matsukawa et al. 2005; Wada et al. 2006; Osawa et al. 2008). These discoveries explain why Oguchi patients have only a mild defect in cone recovery; humans express both GRK1 and GRK7 in cones and when GRK1 is missing, there is partial compensation by GRK7 (Cideciyan et al. 2003).

These genetic studies reveal an interesting heterogeneity in the expression of GRK1 and GRK7 (Table 105.1) that spans 400 million years of vertebrate evolution (Futuyama 1998). All vertebrates examined to date express GRK1 in rods. On the other hand, some vertebrates express only GRK7 in cones and others (including primates) express both GRK1 and GRK7 (Zhao et al. 1999; Weiss et al. 2001; Shimauchi-Matsukawa et al. 2005; Wada et al. 2006; Imanishi et al. 2007). Surprisingly, mice and rats have lost the gene for GRK7 and express only GRK1 in cones (Weiss et al. 2001; Caenepeel et al. 2004), also explaining why GRK1^{-/-} mice have more severely impaired vision under photopic conditions than Oguchi patients (Lyubarsky et al. 2000).

105.2 The Function of GRK7

Because cones function under a larger dynamic range of light than rods, they undergo different kinetics of deactivation and recovery (Baylor 1987; Knox and Solessio 2006). Differences in the structure, protein profile, and ionic balance

between rods and cones may play a role in the distinct properties of these cells, as described in an excellent recent review by Kawamura and Tachibanaki (2008). How GRK7 might contribute to the unique properties of cones is an area of active research in several laboratories. Our laboratory determined that GRK7 phosphorylates the cone opsins in mammals (Liu et al. 2005) and Rinner et al. (2005) provided direct evidence that GRK7 is required for cone recovery in zebrafish. Information on the relative roles of GRK1 and GRK7 in humans may be derived from comparative studies of individuals with different retinopathies. For example, the visual properties of individuals with normal vision were compared with Oguchi disease patients lacking functional GRK1 and patients with Enhanced S Cone Syndrome (ESCS), whose retinas have large numbers of S cones expressing no GRK and L/M cones lacking GRK7 (Cideciyan et al. 2003). Electroretinographic studies indicate that cones lacking either GRK1 or GRK7 exhibit a reduction in normal deactivation after light exposure, but not as severe as those lacking both GRKs (Cideciyan et al. 2003). Therefore, GRK1 and GRK7 can partially compensate for each other if either one of them is missing.

The activities of GRK1 and GRK7 have been compared in several model systems. Using rods and cones isolated from carp retina, Kawamura and colleagues evaluated the rates of rod (rhodopsin) and cone opsin phosphorylation by their endogenous GRKs. They reported that GRK7 is 10 times more abundant in cones than GRK1 in rods and that the catalytic activity of GRK7 is 10 times higher than GRK1 (Tachibanaki et al. 2005). Although the absolute values were different, Fukada and coworkers came to a similar conclusion regarding the higher intrinsic activity of zebrafish GRK7 compared to GRK1 (Wada et al. 2006). In contrast, work by Horner et al. (2005) using FLAG-tagged human GRK1 and GRK7 indicated that the K_m and V_{max} values of human GRK1 and GRK7 for rhodopsin and ATP were fairly similar *in vitro*. Additional studies of these two kinases *in vivo* may further clarify their distinct or overlapping roles in cone visual signaling.

105.3 Regulation of GRK1 and GRK7 Activity Under Changing Light Conditions

GRK1 activity has been studied extensively in mammalian rods (Maeda et al. 2003) and was the first GRK family member found to be allosterically regulated by its substrate, rhodopsin, such that the light-activated form of the rhodopsin activates the kinase (Fowles et al. 1988; Palczewski et al. 1991). This has also been shown for GRK2 (Chen et al. 1993) and is likely to be true for all other GRKs (Huang et al. 2009). GRK1 is also regulated by the Ca^{2+} -sensor protein, recoverin (Kawamura 1993; Chen et al. 1995; Klenchin et al. 1995). In dim light, when Ca^{2+} levels are high, inhibition of rhodopsin phosphorylation by recoverin prolongs the lifetime of the photoreceptor (Makino et al. 2004; Chen et al. 2010). Arinobu et al. (2010) compared the effect of recoverin on GRK1 activity with the effect of visinin (a cone-specific paralog of recoverin in lower vertebrates) on GRK7 activity using rod and cone membranes prepared from carp retina. They reported that the K_D

values for recoverin and visinin are similar for GRK1 and GRK7. However, cone opsin phosphorylation by GRK7 is inhibited by visinin to a greater extent than rhodopsin phosphorylation by GRK1 inhibited by recoverin. The authors propose that these results are due to structural differences whereby GRK7 is more sterically constrained in the binding of its substrate than GRK1.

Although cGMP is clearly the critical second messenger for phototransduction, there is evidence of a role for cAMP in photoreceptor physiology. Cyclic AMP levels are high in the dark and low in the light in photoreceptor cells (Farber et al. 1981; Cohen et al. 1992) and regulate a variety of physiological processes in a circadian fashion that involve a feedback loop between dopamine, synthesized in amacrine/interplexiform cells, and melatonin, synthesized primarily in photoreceptors (Tosini et al. 2008; Wiechmann and Summers 2008). Several substrates for cAMP-dependent protein kinase (PKA) have been identified in photoreceptors, including phosphducin, arylalkylamine N-acetyltransferase (AANAT; a key enzyme in melatonin synthesis), the γ subunit of cGMP-phosphodiesterase, and several transcription factors (Bauer et al. 1992; Lee et al. 1992; Xu et al. 1998; Ganguly et al. 2001; Liu and Green 2002; Ivanova and Iuvone 2003; Yu et al. 2007). Our laboratory identified sites in the amino terminus of GRK1 and GRK7 (Ser21 and Ser36, respectively) that are phosphorylated by PKA *in vitro* (Horner et al. 2005). We also observed that phosphorylation by PKA reduces the ability of these kinases to phosphorylate rhodopsin. Using phospho-specific antibodies, we have determined that GRK1 and GRK7 are phosphorylated *in vivo*. Phosphorylation by PKA is high in the dark and low in the light, consistent with the light-dependent changes in cAMP levels (Osawa et al. 2008; Weiss et al. 2008). These experiments introduce the possibility of a novel mechanism for regulating the lifetime of rhodopsin and the cone opsins via light-dependent changes in GRK activity, resulting in higher sensitivity of the visual response under dim light and reduced sensitivity under more intense light.

It is clear from recent studies that at least one GRK is essential to deactivate the photoresponse in cones (Cideciyan et al. 1998, 2003; Lyubarsky et al. 2000), but why do many vertebrates, including humans, express two GRKs in cones? There are several possibilities: the expression of two GRKs may simply have an additive effect. This may provide a quantitative advantage for survival in specific environments where quick signal termination by higher levels of GRKs may improve visual acuity in animals that are active in daylight. Alternatively, these two kinases may have distinct biochemical properties that may differentiate their roles in cones. A better understanding of the function of these two kinases in cones will advance our knowledge of how the retina adapts to a broad range of light intensities in the natural environment.

Acknowledgments The authors would like to acknowledge financial support from the NEI (EY072224 and EY019758) and from the NIH Core Grant for Vision Research (EY5722; Duke University).

References

- Arinobu D, Tachibanaki S, Kawamura S (2010) Larger inhibition of visual pigment kinase in cones than in rods. *J Neurochem* 115:259–268
- Bauer PH, Müller S, Puzicha M et al (1992) Phosducin is a protein kinase A-regulated G-protein regulator. *Nature* 358:73–76
- Baylor DA (1987) Photoreceptor signals and vision. The Proctor lecture. *Invest Ophthalmol Vis Sci* 28:34–49
- Caenepeel S, Charyczak G, Sudarsanam S et al (2004) The mouse kinome: discovery and comparative genomics of all mouse protein kinases. *Proc Natl Acad Sci USA* 101:11707–11712
- Chen CK, Burns ME, Spencer M et al (1999) Abnormal photoresponses and light-induced apoptosis in rods lacking rhodopsin kinase. *Proc Natl Acad Sci USA* 96:3718–3722
- Chen CK, Inglese J, Lefkowitz RJ et al (1995) Ca²⁺-dependent interaction of recoverin with rhodopsin kinase. *J Biol Chem* 270:18060–18066
- Chen CK, Woodruff ML, Chen FS et al (2010) Background light produces a recoverin-dependent modulation of activated-rhodopsin lifetime in mouse rods. *J Neurosci* 30:1213–1220
- Chen CK, Zhang K, Church-Kopish J et al (2001) Characterization of human GRK7 as a potential cone opsin kinase. *Mol Vis* 7:305–313
- Chen CY, Dion SB, Kim CM et al (1993) Beta-adrenergic receptor kinase. Agonist-dependent receptor binding promotes kinase activation. *J Biol Chem* 268:7825–7831
- Cideciyan AV, Jacobson SG, Gupta N et al (2003) G-protein-coupled receptor kinase 1 (GRK1) and GRK7 expression and cone deactivation kinetics in enhanced S-cone syndrome (ESCS) caused by mutations in NR2E3. *Invest Ophthalmol Vis Sci* 44:1268–1274
- Cideciyan AV, Zhao X, Nielsen L et al (1998) Null mutation in the rhodopsin kinase gene slows recovery kinetics of rod and cone phototransduction in man. *Proc Natl Acad Sci USA* 95:328–333
- Cohen AI, Todd RD, Harmon S et al (1992) Photoreceptors of mouse retinas possess D₄ receptors coupled to adenylate cyclase. *Proc Natl Acad Sci USA* 89:12093–12097
- Dryja TP (2000) Molecular genetics of Oguchi disease, fundus albipunctatus, and other forms of stationary night blindness: LVII Edward Jackson Memorial Lecture. *Am J Ophthalmol* 130:547–563
- Farber DB, Souza DW, Chase DG et al (1981) Cyclic nucleotides of cone-dominant retinas. Reduction of cyclic AMP levels by light and by cone degeneration. *Invest Ophthalmol Vis Sci* 20:24–31
- Fowles C, Sharma R, Akhtar M (1988) Mechanistic studies on the phosphorylation of photorexited rhodopsin. *FEBS Lett* 238:56–60
- Futuyama DJ (1998) *Evolutionary Biology*, 3rd Edition. Sunderland, MA: Sinauer Associates, Inc.
- Ganguly S, Gastel JA, Weller JL et al (2001) Role of a pineal cAMP-operated arylalkylamine N-acetyltransferase/14–3–3-binding switch in melatonin synthesis. *Proc Natl Acad Sci USA* 98:8083–8088
- Hisatomi O, Matsuda S, Satoh T et al (1998) A novel subtype of G-protein-coupled receptor kinase, GRK7, in teleost cone photoreceptors. *FEBS Lett* 424:159–164
- Horner TJ, Osawa S, Schaller MD et al (2005) Phosphorylation of GRK1 and GRK7 by cAMP-dependent protein kinase attenuates their enzymatic activities. *J Biol Chem* 280:28241–28250
- Huang CC, Yoshino-Koh K, Tesmer JJ (2009) A surface of the kinase domain critical for the allosteric activation of G protein-coupled receptor kinases. *J Biol Chem* 284:17206–17215
- Imanishi Y, Hisatomi O, Yamamoto S et al (2007) A third photoreceptor-specific GRK found in the retina of *Oryzias latipes* (Japanese killifish). *Zool Sci* 24:87–93
- Ivanova TN, Iuvone PM (2003) Circadian rhythm and photic control of cAMP level in chick retinal cell cultures: a mechanism for coupling the circadian oscillator to the melatonin-synthesizing enzyme, arylalkylamine N-acetyltransferase, in photoreceptor cells. *Brain Res* 991:96–103

- Kawamura S (1993) Rhodopsin phosphorylation as a mechanism of cyclic GMP phosphodiesterase regulation by S-modulin. *Nature* 362:855–857
- Kawamura S, Tachibanaki S (2008) Rod and cone photoreceptors: molecular basis of the difference in their physiology. *Comp Biochem Physiol A Mol Integr Physiol* 150:369–377
- Klenchin VA, Calvert PD, Bownds MD (1995) Inhibition of rhodopsin kinase by recoverin. Further evidence for a negative feedback system in phototransduction. *J Biol Chem* 270:16147–16152
- Knox BE, Solessio E (2006) Shedding light on cones. *J Gen Physiol* 127:355–358
- Kühn H, Wilden U (1987) Deactivation of photoactivated rhodopsin by rhodopsin-kinase and arrestin. *J Recept Res* 7:283–298
- Lee RH, Ting TD, Lieberman BS et al (1992) Regulation of retinal cGMP cascade by phosducin in bovine rod photoreceptor cells. Interaction of phosducin and transducin. *J Biol Chem* 267:25104–25112
- Liu P, Osawa S, Weiss ER (2005) M opsin phosphorylation in intact mammalian retinas. *J Neurochem* 93:135–144
- Liu X, Green CB (2002) Circadian regulation of nocturnin transcription by phosphorylated CREB in *Xenopus* retinal photoreceptor cells. *Mol Cell Biol* 22:7501–7511
- Lyubarsky AL, Chen C-K, Simon MI et al (2000) Mice lacking G-protein receptor kinase 1 have profoundly slowed recovery of cone-driven retinal responses. *J Neurosci* 20:2209–2217
- Maeda T, Imanishi Y, Palczewski K (2003) Rhodopsin phosphorylation: 30 years later. *Prog Ret Eye Res* 22:417–434
- Makino CL, Dodd RL, Chen J et al (2004) Recoverin regulates light-dependent phosphodiesterase activity in retinal rods. *J Gen Physiol* 123:729–741
- Osawa S, Jo R, Weiss ER (2008) Phosphorylation of GRK7 by PKA in cone photoreceptor cells is regulated by light. *J Neurochem* 107:1314–1324
- Palczewski K, Buczylo J, Kaplan MW et al (1991) Mechanism of rhodopsin kinase activation. *J Biol Chem* 266:12949–12955
- Rinner O, Makhankov YV, Biehlmaier O et al (2005) Knockdown of cone-specific kinase GRK7 in larval zebrafish leads to impaired cone response recovery and delayed dark adaptation. *Neuron* 47:231–242
- Shimauchi-Matsukawa Y, Aman Y, Tachibanaki S et al (2005) Isolation and characterization of visual pigment kinase-related genes in carp retina: polyphyly in GRK1 subtypes, GRK1A and 1B. *Mol Vis* 11:1220–1228
- Tachibanaki S, Arinobu D, Shimauchi-Matsukawa Y et al (2005) Highly effective phosphorylation by G protein-coupled receptor kinase 7 of light-activated visual pigment in cones. *Proc Natl Acad Sci USA* 102:9329–9334
- Tosini G, Pozdeyev N, Sakamoto K et al (2008) The circadian clock system in the mammalian retina. *Bioessays* 30:624–633
- Wada Y, Sugiyama J, Okano T et al (2006) GRK1 and GRK7: unique cellular distribution and widely different activities of opsin phosphorylation in the zebrafish rods and cones. *J Neurochem* 98:824–837
- Weiss ER, Ducceschi MH, Horner TJ et al (2001) Species-specific differences in expression of G-protein-coupled receptor kinase (GRK) 7 and GRK1 in mammalian cone photoreceptor cells: implications for cone cell phototransduction. *J Neurosci* 21:9175–9184
- Weiss ER, Jo R, Osawa S (2008) GRK1 Is Phosphorylated in Dark-Adapted Mice in vivo. *ARVO Meeting Abstracts* 49:1668
- Weiss ER, Raman D, Shirakawa S et al (1998) The cloning of GRK7, a candidate cone opsin kinase, from cone- and rod-dominant mammalian retinas. *Mol Vis* 4, 27:<<http://www.molvis.org/molvis/v4/p27>>
- Wiechmann AF, Summers JA (2008) Circadian rhythms in the eye: the physiological significance of melatonin receptors in ocular tissues. *Prog Ret Eye Res* 27:137–160
- Wilden U, Kühn H (1982) Light-dependent phosphorylation of rhodopsin: the number of phosphorylation sites. *Biochemistry* 21:3014–3022

- Xu LX, Tanaka Y, Bonderenko VA et al (1998) Phosphorylation of the gamma subunit of the retinal photoreceptor cGMP phosphodiesterase by the cAMP-dependent protein kinase and its effect on the gamma subunit interaction with other proteins. *Biochemistry* 37:6205–6213
- Yu CJ, Gao Y, Willis CL et al (2007) Mitogen-associated protein kinase- and protein kinase A-dependent regulation of rhodopsin promoter expression in zebrafish rod photoreceptor cells. *J Neurosci Res* 85:488–496
- Zhao X, Yokoyama K, Whitten ME et al (1999) A novel form of rhodopsin kinase from chicken retina and pineal gland. *FEBS Lett* 454:115–121

Chapter 106

Protein Tyrosine Phosphatase 1B: A Novel Molecular Target for Retinal Degenerative Diseases

Devaraj K. Basavarajappa, Vivek K. Gupta, and Raju V.S. Rajala

Keywords Insulin receptor • Protein tyrosine phosphatase-1B • Retinal degeneration • Rhodopsin • Neuroprotection

106.1 Introduction

The activity of receptor tyrosine kinases (RTKs) is regulated by the extent of phosphorylated tyrosine residues that dictate their signaling output. Protein tyrosine phosphatases (PTPs) are the major negative regulators of RTKs and their downstream effector signaling (Ostman and Böhmer 2001). PTP1B is a prototypical member of the PTP family, considered as a direct negative regulator of several receptor and receptor-associated tyrosine kinases (Tonks 2003; Haj et al. 2003; Stuible and Tremblay 2010). PTP1B is widely expressed nonreceptor PTP that is associated with the endoplasmic reticulum (ER) and other intracellular membranes via a hydrophobic interaction of its C-terminal targeting signal (Frangioni et al. 1992; Haj et al. 2002). Full-length PTP1B contains 435 amino acids and the catalytic domain is constituted by N-terminal residues 30–278, while the 35 C-terminal residue sequence targets the enzyme to cytosolic face of the endoplasmic reticulum

D.K. Basavarajappa • V.K. Gupta
Department of Ophthalmology, Dean A. McGee Eye Institute, University of Oklahoma Health Sciences Center, 608 Stanton L. Young Boulevard, Oklahoma City, OK 73104, USA

R.V.S. Rajala (✉)
Departments of Ophthalmology and Cell Biology, Dean A. McGee Eye Institute, University of Oklahoma Health Sciences Center, 608 Stanton L. Young Boulevard, Oklahoma City, OK 73104, USA
e-mail: raju-rajala@ouhsc.edu

(Frangioni et al. 1992; Barford et al. 1994). PTP1B dephosphorylates and inactivates several membrane receptors tyrosine kinases (RTKs) such as the epidermal growth factor receptor (EGFR) (Flint et al. 1997), the platelet-derived growth factor receptor (PDGFR) (Haj et al. 2003), the insulin receptor (IR) (Salmeen et al. 2000, and the insulin-like growth factor-1 receptor (IGF-1R) (Buckley et al. 2002). PTP1B is also involved in down-regulation of JAK/STAT pathway (Cook and Unger 2002; Myers et al. 2001; Gu et al. 2003). Dysregulation of PTP1B activity has been shown to contribute towards the pathogenesis of several human diseases including cancer, diabetes, obesity, and immune disorders (Zhang and Zhang 2007; Combs 2010). The importance of PTP1B in diverse pathophysiological conditions has made PTP1B as the focus of intense interest for drug targeting.

106.2 Importance of Insulin Receptor Signaling in Retina

Insulin receptor (IR) signaling in retina has received a considerable attention due to its importance in photoreceptor survival. Retinal neurons contain high affinity receptors for insulin (Reiter et al. 2003; Rajala et al. 2008). The IR signaling has been demonstrated as an important pathway for retinal development, physiology, and survival (Rajala et al. 2008; Song et al. 2003; Barber et al. 2001). The IR activation provides a trophic signaling for retinal neurons via phosphatidylinositol 3-kinase (PI3K)/Akt pathway (Rajala et al. 2002; Barber et al. 2001). IR/PI3K/Akt signaling pathway has been shown to protect retinal neurons from anti-apoptotic mechanisms, primarily by Akt-mediated phosphorylation and inhibition of many proapoptotic targets (Dudek et al. 1997; Datta et al. 1999). IR signaling is also involved in 17 β -estradiol-mediated neuroprotection in the retina (Yu et al. 2004). A growing body of evidence suggests that diabetic retinopathy is characterized by early onset of retinal neuronal cell death (Barber et al. 1998). Several studies have demonstrated that diabetes progressively impairs the retinal IR signaling pathway and that the loss of this survival pathway may contribute to the initial stages of diabetic retinopathy (Barber et al. 1998; Reiter et al. 2006; Rajala et al. 2009). *Retinitis pigmentosa* is an inherited retinal degenerative disease that leads to blindness and studies have shown that stimulation of insulin/mTOR pathway delays cone cell death in *retinitis pigmentosa* mouse model (Punzo et al. 2009). Studies from our laboratory for the past decade clearly show that IR and its downstream effect signaling is functionally important for both the rod and cone photoreceptor survival (Rajala et al. 2008; Ivanovic et al. 2009).

106.3 Interaction Between PTP1B and IR

PTP1B has been implicated as a major negative regulator of insulin receptor signaling by dephosphorylating IR and its effector proteins (Byon et al. 1998; Goldstein et al. 1998; Dadke et al. 2000; Calera et al. 2000). The ability of PTP1B to regulate insulin-receptor kinase activity has been established at the molecular level by examining

the crystal structure of PTP1B in complex with the triphosphorylated insulin-receptor kinase activation loop (Salmeen et al. 2000). The overexpression of PTP1B results in the inhibition of IR signaling and the introduction of anti-PTP1B antibodies into cells enhances IR signaling (Ahmad et al. 1995). A number of systemic and tissue-specific mouse models of PTP1B deficiency have confirmed its physiological effect on insulin sensitivity and high fat diet-induced weight gain (Elchebly et al. 1999; Klamann et al. 2000; Bence et al. 2006; Delibegovic et al. 2009). Neuronal PTP1B has also been shown to regulate body weight, adiposity, and leptin action (Bence et al. 2006). The expression, activity, and functional role of PTP1B activity in the retina have been well documented (Rajala et al. 2009, 2010). Interestingly, the photoreceptor-specific deletion of PTP1B resulted in enhanced IR survival signaling. These studies indicate that the IR activation in photoreceptor cells is regulated by PTP1B activity (Rajala et al. 2010).

106.4 Implication of PTP1B Activity in Retinal Diseases

In retina, the PTP1B activity is regulated in a light-dependent manner through photobleaching of rhodopsin (Rajala et al. 2010). One of the important issues in the retina research is how the mutations in human rhodopsin gene slowly disable and eventually disrupt the photoreceptor function and survival. Defects in the photobleaching of rhodopsin and mutations in the rhodopsin gene enhance the activity of PTP1B. This enhanced PTP1B activity may contribute to the progression of retinal degenerations. Further, the PTP1B activity is also elevated in *Rpe65^{-/-}* mice, a mouse model of leber congenital amaurosis (LCA-type 2) (Rajala et al. 2010). *Retinitis pigmentosa* (RP) is one of the most common forms of inherited retinal degeneration and an elevated PTP1B activity in RP models has also been observed (Rajala et al. 2010). Decreased retinal IR signaling has been observed in the diabetes (Barber et al. 1998; Reiter et al. 2006; Rajala et al. 2009). This reduction of IR signaling is associated with the increased PTP1B activity in diabetes (Rajala et al. 2009). In addition, PTP1B is known to act as negative regulator of JAK/STAT pathway (Myers et al. 2001; Gu et al. 2003). This pathway has also been demonstrated as neuroprotective signal in light stress-induced degeneration models (Samardzija et al. 2006; Ueki et al. 2009). The dysregulation of PTP1B activity may contribute to the death of retinal neurons and ultimately lead to retinal degeneration.

106.5 PTP1B as a Therapeutic Target

PTP1B has been considered as a suitable target in the resolution of several disease pathologies. It is a preferred target for diabetes and obesity treatments (Zhang and Zhang 2007; Combs 2010). In order to effectively target this protein in alleviation of retinal pathologies mediated through its high activity, it is essential to have a thorough understanding of the structure, physiological mechanism of action, and regulatory control of this enzyme. It is essential that the drug used specifically

discriminates between the PTP1B and other phosphatases, most of which act by similar catalytic mechanisms and exhibit a striking similarity in their active sites and structures. The resolution of crystal structures in complex with IR (Salmeen et al. 2000) and EGFR (Jia et al. 2001) has enabled in understanding its mechanism of action to a great extent. The requisite inhibitor(s) should be targeted to both active site and the secondary binding regions in such a way that it achieves a unique selectivity among the tyrosine phosphatases but without significantly compromising their potency (Combs 2010). The postmitotic nature of the retina and the presence of blood retinal barrier necessitate that the potential drug has minimal toxicity and high pharmacodynamic turnover rate in eye. Genetic engineering to promote the expression of physiological inhibitors of PTP1B may be the best strategy, but considering the practical limitations and lack of complete knowledge of retinal physiology, administering a selective potential PTP1B peptide mimetic inhibitor or antisense oligonucleotides may be a step forward to rescue or delay the photoreceptor cell death in retinal degenerative diseases. Consistent with this idea, we recently reported that intravenous injection of an allosteric inhibitor of PTP1B protects the rats against light stress-induced retinal degeneration through the protection of IR phosphorylation (Rajala et al. 2010).

106.6 Conclusions

PTP1B has emerged as the best-validated drug target for diabetes and obesity. PTP1B is considered as a major negative regulator of IR and JAK/STAT signaling, which have been demonstrated as neuroprotective pathways in retina. The emerging understanding of retinal physiology indicates that phototransduction is integrated with the RTK survival signaling. Defects in phototransduction can either manifest their effects or their effects might be aggravated through the key players in RTK signaling. This is coupled with the fact that enhanced PTP1B activity has been associated with several retinal degenerative diseases. All these observations steer us to an understanding that PTP1B is an extremely important regulatory valve whose malfunction can lead to severe degenerative phenotypes and the key role of this enzyme provides an opportunity to manipulate its *in vivo* properties and thereby regulate several phenotypes, which are mediated through its malfunction.

Acknowledgments This work was supported by grants from the NIH (EY016507-05; EY00871).

References

- Ahmad F, Li PM, Meyerovitch J et al (1995) Osmotic loading of neutralizing antibodies demonstrates a role for protein-tyrosine phosphatase 1B in negative regulation of the insulin action pathway. *J Biol Chem* 270:20503–20508
- Barber AJ, Lieth E, Khin SA et al (1998) Neural apoptosis in the retina during experimental and human diabetes: early onset and effect of insulin. *J Clin Invest* 102:783–791

- Barber AJ, Nakamura M, Wolpert EB et al (2001) Insulin rescues retinal neurons from apoptosis by a phosphatidylinositol 3-kinase/Akt-mediated mechanism that reduces the activation of caspase-3. *J Biol Chem* 276:32814–32821
- Barford D, Flint AJ, Tonks NK (1994) Crystal structure of human protein tyrosine phosphatase 1B. *Science* 263:1397–1404
- Bence KK, Delibegovic M, Xue B et al (2006) Neuronal PTP1B regulates body weight, adiposity and leptin action. *Nat Med* 12:917–924
- Buckley DA, Cheng A, Kiely PA et al (2002) Regulation of insulin-like growth factor type I (IGF-I) receptor kinase activity by protein tyrosine phosphatase 1B (PTP-1B) and enhanced IGF-I-mediated suppression of apoptosis and motility in PTP-1B-deficient fibroblasts. *Mol Cell Biol* 22:1998–2010
- Byon JC, Kusari AB, Kusari J (1998) Protein-tyrosine phosphatase-1B acts as a negative regulator of insulin signal transduction. *Mol Cell Biochem* 182:101–108
- Calera, M.R., Vallega G, Pilch PF (2000) Dynamics of protein-tyrosine phosphatases in rat adipocytes. *J Biol Chem* 275:6308–6312
- Combs AP (2010) Recent advances in the discovery of competitive protein tyrosine phosphatase 1B inhibitors for the treatment of diabetes, obesity, and cancer. *J Med Chem* 53:2333–2344
- Cook WS and Unger RH (2002) Protein tyrosine phosphatase 1B: a potential leptin resistance factor of obesity. *Dev Cell* 2:385–387
- Dadke S, Kusari J, Chernoff J (2000) Down-regulation of insulin signalling by protein-tyrosine phosphatase 1B is mediated by an N-terminal binding region. *J Biol Chem* 275:23642–23647
- Datta SR, Brunet A, Greenberg ME (1999) Cellular survival: a play in three Akts. *Genes Dev* 13:2905–2927
- Delibegovic M, Zimmer D, Kauffman C et al (2009) Liver-specific deletion of protein-tyrosine phosphatase 1B (PTP1B) improves metabolic syndrome and attenuates diet-induced endoplasmic reticulum stress. *Diabetes* 58:590–599
- Dudek H, Datta SR, Franke TF, et al (1997) Regulation of neuronal survival by the serine-threonine protein kinase Akt. *Science* 275:661–665
- Elchebly M, Payette P, Michaliszyn E et al (1999) Increased insulin sensitivity and obesity resistance in mice lacking the protein tyrosine phosphatase-1B gene. *Science* 283:1544–1548
- Flint AJ, Tiganis T, Barford D, Tonks NK (1997) Development of “substrate-trapping” mutants to identify physiological substrates of protein tyrosine phosphatases. *Proc Natl Acad Sci USA* 94:1680–1685
- Frangioni JV, Beahm PH, Shifrin V et al (1992) The nontransmembrane tyrosine phosphatase PTP-1B localizes to the endoplasmic reticulum via its 35 amino acid C-terminal sequence. *Cell* 68:545–560
- Goldstein BJ, Ahmad F, Ding W et al (1998) Regulation of the insulin signalling pathway by cellular protein-tyrosine phosphatases. *Mol Cell Biochem* 182:91–99
- Gu F, Dube N, Kim JW et al (2003) Protein tyrosine phosphatase 1B attenuates growth-hormone-mediated JAK2-STAT signaling. *Mol Cell Biol* 23:3753–3762
- Haj FG, Markova B, Klamann LD et al (2003) Regulation of receptor tyrosine kinase signaling by protein tyrosine phosphatase-1B. *J Biol Chem* 278:739–744
- Haj FG, Verveer PJ, Squire A et al (2002) Imaging sites of receptor dephosphorylation by PTP1B on the surface of the endoplasmic reticulum. *Science* 295:1708–1711
- Ivanovic I, Le YZ, Anderson RE, Rajala RV (2009) Deletion of the p85 regulatory subunit of phosphoinositide 3-kinase in cone photoreceptor cells results in cone photoreceptor degeneration. *ARVO abstract A389*
- Jia Z, Barford D, Flint AJ et al (2001) Structural basis for phosphotyrosine peptide recognition by protein tyrosine phosphatase-1B. *Science* 268:1754–1758
- Klamann LD, Boss O, Peroni OD et al (2000) Increased energy expenditure, decreased adiposity, and tissue-specific insulin sensitivity in protein-tyrosine phosphatase1B-deficient mice. *Mol Cell Biol* 20:5479–5489
- Myers MP, Anderson NJ, Cheng A et al (2001) TYK2 and JAK2 are substrates of protein tyrosine phosphatase 1B. *J Biol Chem* 276:47771–47774

- Ostman A and Böhmer FD (2001) Regulation of receptor tyrosine kinase signaling by protein tyrosine phosphatases. *Trends Cell Biol* 11:258–266
- Punzo C, Kornacker K, Cepko CL (2009) Stimulation of the insulin/mTOR pathway delays cone death in a mouse model of retinitis pigmentosa. *Nat Neurosci* 12:44–52
- Rajala A, Tanito M, Le YZ et al (2008) Loss of neuroprotective survival signal in mice lacking insulin receptor gene in rod photoreceptor cells. *J Biol Chem* 283:19781–19792
- Rajala RV, McClellan ME, Ash JD, et al (2002) In vivo regulation of phosphoinositide 3-kinase in retina through light-induced tyrosine phosphorylation of the insulin receptor beta-subunit. *J Biol Chem* 277:43319–43326
- Rajala RV, Tanito M, Neel BG et al (2010) Enhanced retinal insulin receptor-activated neuroprotective survival signal in mice lacking the protein-tyrosine phosphatase-1B gene. *J Biol Chem* 285:8894–8904
- Rajala RV, Wiskur B, Tanito M (2009) Diabetes reduces autophosphorylation of retinal insulin receptor and increases protein-tyrosine phosphatase-1B activity. *Invest Ophthalmol Vis Sci* 50:1033–1040
- Reiter CE, Sandirasegarane L, Wolpert EB et al (2003) Characterization of insulin signaling in rat retina in vivo and ex vivo. *Am J Physiol* 285:E763-E774
- Reiter CE, Wu X, Sandirasegarane L (2006) Diabetes reduces basal retinal insulin receptor signaling: reversal with systemic and local insulin. *Diabetes* 55:1148–1156
- Salmeen A, Andersen JN, Myers MP et al (2000) Molecular basis for recognition and dephosphorylation of the activation segment of the insulin receptor by protein tyrosine phosphatase 1B. *Mol Cell* 6:1401–1412
- Salmeen A, Andersen JN, Myers MP, Tonks NK, Barford D (2001) Molecular basis for the dephosphorylation of the activation segment of the insulin receptor by protein tyrosine phosphatase 1B. *Mol Cell* 6:1401–1412
- Samardzija M, Wenzel A, Aufenberg S, et al (2006) Differential role of Jak-STAT signaling in retinal degenerations. *FASEB J* 20:E1790–E1801
- Song J, Wu L, Chen Z (2003) Axons guided by insulin receptor in *Drosophila* visual system. *Science* 300:502–505
- Stuible M and Tremblay ML (2010) In control at the ER: PTP1B and the down-regulation of RTKs by dephosphorylation and endocytosis. *Trends Cell Biol* 20: 672–679
- Tonks NK (2003) PTP1B:from the sidelines to the front lines! *FEBS Lett* 546:140–148
- Ueki Y, Le YZ, Chollangi S et al (2009) Preconditioning-induced protection of photoreceptors requires activation of the signal-transducing receptor gp130 in photoreceptors. *Proc Natl Acad Sci USA* 106:21389–21394
- Yu X, Rajala RV, McGinnis JF et al (2004) Involvement of insulin/phosphoinositide 3-kinase/Akt signal pathway in 17 beta-estradiol-mediated neuroprotection. *J Biol Chem* 279:13086–13094
- Zhang S and Zhang ZY (2007) PTP1B as a drug target: recent developments in PTP1B inhibitor discovery. *Drug Discov Today* 12:373–81

Chapter 107

Protein Tyrosine-*O*-Sulfation in Bovine Ocular Tissues

Yogita Kanan, Robert A. Hamilton, Kevin L. Moore,
and Muayyad R. Al-Ubaidi

Keywords Protein tyrosine-*O*-sulfation • Tyrosylprotein sulfotransferase • Soluble interphotoreceptor matrix • Insoluble interphotoreceptor matrix • Soluble interretinal pigment epithelium matrix • Insoluble interretinal pigment epithelium matrix • Sulfation

107.1 Introduction

Protein tyrosine-*O*-sulfation (henceforth, will be referred to as sulfation) is a post-translational modification that involves the addition of a sulfate group from the universal sulfate donor 3'-phosphoadenosine 5'-phosphosulfate (PAPS) onto a tyrosine residue of a protein. The reaction occurs in the trans-Golgi network and is catalyzed by two enzymes, tyrosylprotein sulfotransferase 1 and 2 (TPST 1 and 2, EC 2.8.2.20) (Lee and Huttner 1983). These enzymes are type II transmembrane proteins with their catalytic activity directed towards the lumen (Lee and Huttner 1985). So far, it has been observed that only proteins that traverse the Golgi network (secretory and transmembrane proteins) are sulfated by TPSTs. Sulfation is a constitutive post-translational modification and so far no enzyme has been detected that removes the sulfate group from the tyrosine residues.

Sulfation has been observed in every multicellular eukaryote examined from plants (Komori et al. 2009) to humans (Moore 2009). Prokaryotes and unicellular

Y. Kanan • R.A. Hamilton • M.R. Al-Ubaidi (✉)
Department of Cell Biology, University of Oklahoma Health Sciences Center,
940 Stanton L. Young Boulevard, BMSB 781, Oklahoma City, OK 73104, USA
e-mail: Muayyad-Al-ubaidi@ouhsc.edu

K.L. Moore
Cardiovascular Biology Research Program, Oklahoma Medical Research
Foundation, Oklahoma City, OK 73104, USA

eukaryotes are incapable of sulfation. Therefore, sulfation is a posttranslational modification that occurs only in multicellular eukaryotes.

Sulfation can modulate a protein's function by influencing the interaction of the protein with its partner(s). Studies have shown that sulfation of chemokine receptors enhances the affinity to their cognate receptors (Fong et al. 2002; Farzan et al. 2002; Veldkamp et al. 2006). Sulfation of the leukocyte protein PSGL-1 is required for the high-affinity interaction with P-selectin on endothelial cells (Wilkins et al. 1995). Also, sulfation of the human coagulation factor VIII is required for the optimum binding to von Willebrand factor, which acts as a carrier for factor VIII in the plasma (Leyte et al. 1991). Deficient sulfation of Factor VIII disrupts this binding and causes mild-to-moderate hemophilia in patients (Higuchi et al. 1990).

It was recently reported that sulfated proteins are present in the retina and retinal pigment epithelium (RPE) of a wide variety of species including human and mouse (Kanan et al. 2009a). It was also shown that sulfation is important for vision since in its absence electroretinographic (ERG) response for rods and cones was drastically reduced (Sherry et al. 2010). To further understand the functional significance of sulfation, the current report examines the distribution of sulfated proteins in various ocular tissues from the bovine eye with an intention to ultimately identify the sulfated proteins from these tissues and determine their role in vision.

107.2 Materials and Methods

107.2.1 Isolation of Tissues from Bovine Eyes

Bovine eyes were collected from a slaughter house (Country Home Meats Co., Edmond, Oklahoma). The cornea, aqueous humor, lens, iris, vitreous humor, retina, RPE, and sclera were harvested directly into Urea/Thiourea buffer (7M Urea, 2M Thiourea, 2% CHAPS) to efficiently solubilize all proteins including those that are membrane-bound. In addition, to identify secreted proteins from the retina and RPE, soluble interphotoreceptor matrix (S-IPM) was isolated by incubating retina and RPE in cold PBS containing protease inhibitors (Halt Protease Inhibitor Cocktail, Pierce, Rockford, IL) for 10 min, followed by centrifugation at low speed to pellet out the retina and RPE tissue. The supernatant from the retina contained the soluble interphotoreceptor matrix (S-IPM) components and that from the RPE contained the soluble interretinal pigment epithelium matrix (S-IRPEM) components. The precipitant contained insoluble part of the matrix and the membrane-bound proteins and is designated IS-IPM for the retina and IS-IRPEM for the RPE.

107.2.2 Western Blot of Tissue Lysates

About 15 μ g of total protein lysates from different parts of the bovine eye were run on a 10% SDS polyacrylamide gel (SDS-PAGE) and transferred to nitrocellulose

membranes (Bio-Rad, Hercules, CA) and probed with the PSG2 antibody (Hoffhines et al. 2006a). The blots were imaged using a Kodak Imager (Rochester, New York).

107.3 Results

When the membrane containing total lysates from different bovine ocular tissues was probed with the PSG2 antibody, all samples showed the presence of multiple sulfated proteins (Fig. 107.1a). However, the lane containing lens extracts shows two protein bands (asterisks in Fig. 107.1a) that were identified by PSG2. However,

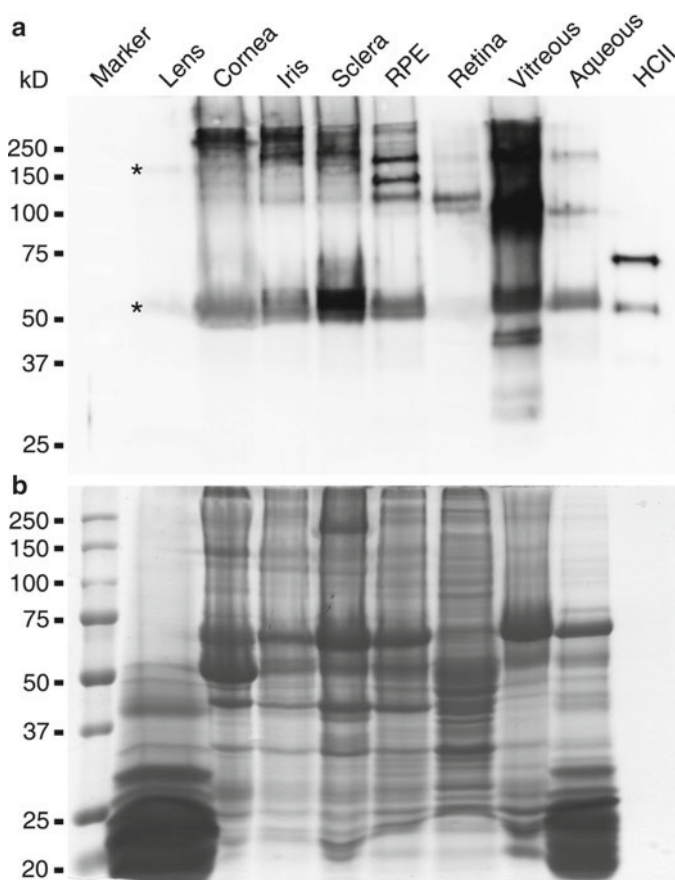


Fig. 107.1 (a) Western blot analysis of tyrosine-*O*-sulfated proteins in bovine ocular tissues. About 15 μ g of total protein lysates from lens, cornea, iris, sclera, RPE, retina, vitreous humor, and aqueous humor were run on a 10% SDS-PAGE and transferred to nitrocellulose membrane and probed with PSG2 antibody to reveal tyrosine-*O*-sulfated proteins. HCII was used as positive control for sulfation. (b) A sister gel to the one presented in (a) was stained with coomassie blue to demonstrate equivalent amounts of proteins loaded

these two bands are present in very small amounts suggesting that sulfation is not highly utilized in the lens.

Bovine cornea (Fig. 107.1a) harbors several distinct sulfated proteins with sizes between 50 and >250 kDa. Bovine aqueous humor expresses three separate sulfated proteins with a major band at 60 kDa. The iris lanes exhibited several bands of sulfated proteins of sizes between 50 and >250 kDa. The vitreous humor appears to be the richest source of sulfated proteins with bands detected with PSG2 between 30 and >250 kDa. Bovine retina expresses a single prominent band at 140 kDa and several minor species of sulfated proteins. The RPE expresses at least six sulfated proteins of sizes between 50 and >250 kDa. The sclera exhibited a pattern close to that observed for the iris. HCII, a 75 kDa protein (human heparin cofactor II), is a known sulfated protein and therefore served as a positive control for the PSG2 antibody in the blot. To show that equal amounts of different samples were loaded on the SDS-PAGE, coomassie blue-stained gel is shown (Fig. 107.1b).

Since sulfated proteins are secreted and either compose the soluble fraction of the extracellular matrix (ECM), or the insoluble fraction of the ECM including those that are membrane-bound, S-IPM, IS-IPM, S-IRPEM, and IS-IRPEM were isolated and run on SDS-PAGE and probed with PSG2 (Fig. 107.2a). Comparing the pattern obtained with S-IPM and IS-IPM shows that the 140 kDa band is prominent only in the IS-IPM, while a 60 kDa band is prominent in the S-IPM. This band was barely obvious in total retinal extracts (Fig. 107.1a).

Comparing the S-IRPEM to IS-IRPEM shows that there are multiple sulfated proteins of sizes between 37 and 200 kDa in the S-IRPEM with a band at ~60 kDa as the most prominent (Fig. 107.2a). However, the higher molecular weight sulfated bands seem to be retained in the IS-IRPEM. To demonstrate that equivalent amounts of proteins were loaded on SDS-PAGE, coomassie blue-stained gel is shown (Fig. 107.2b).

107.4 Discussion

Protein sulfation is a posttranslational modification that was discovered more than half a century ago; however, its role in the eye was not studied until recently (Kanan et al. 2009b; Sherry et al. 2010). Its importance to vision was evaluated by studying animal models that lack both tyrosine sulfating enzymes TPST-1 and TPST-2. These animals show reduced rod and cone ERGs, and abnormalities in photoreceptor outer segments and synaptic termini, providing evidence that sulfated proteins are important for vision (Sherry et al. 2010).

To further understand the role of sulfated proteins in the eye, the current study was undertaken. The goal was to identify sulfated proteins in ocular tissues other than the retina and RPE.

Western blotting and probing with the PSG2 antibody (Hoffhines et al. 2006a) were utilized. This antibody was generated using phage display technology and can detect sulfotyrosine residues within proteins (Hoffhines et al. 2006b). This antibody has also been used to isolate sulfated proteins from mouse epididymis by

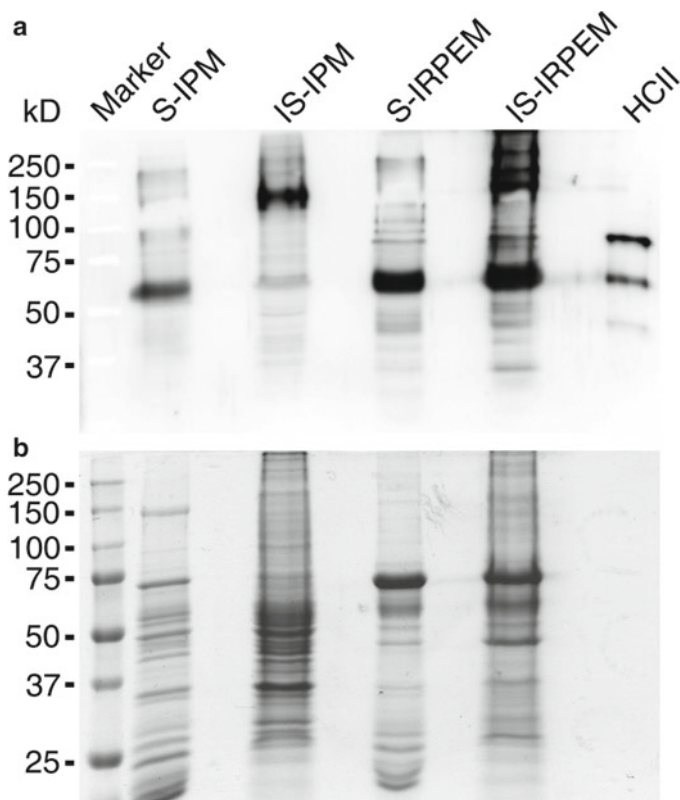


Fig. 107.2 (a) Western blot analysis of tyrosine-*O*-sulfated proteins in the soluble interphotoreceptor matrix (S-IPM) and soluble interretinal pigment epithelium matrix (S-IRPEM) vs. insoluble interphotoreceptor matrix (IS-IPM) and insoluble interretinal pigment epithelium matrix (IS-IRPEM) in bovine eye. About 15 μ g protein samples from bovine ocular tissues and 50 ng of HCF II (positive control) were run on a 10% SDS-PAGE and blotted onto nitrocellulose and then probed with the PSG2 antibody to reveal tyrosine-*O*-sulfated proteins. (b) A sister gel to the one presented in (a) was stained with coomassie blue to show that equivalent amounts of proteins were loaded in each lane

immunoaffinity purification (Hoffhines et al. 2009), and therefore, is an excellent tool for detecting sulfated proteins in tissues. A notable finding in this study is that the lens expresses very low levels of sulfated proteins. Among the other tissues tested, the vitreous humor was the richest source of sulfated proteins. Another notable finding is the observation of a band at 60 kDa that was common to all ocular tissues and therefore could be the same protein that is expressed in different parts of the eye or may be expressed and secreted from a single ocular tissue. Interestingly, this band is present in S-IPM as well as in the IS-IPM in the retina and similarly in the RPE. If this band is of the same protein, then the commonality of this protein to all ocular tissues may point to the functional significance of this sulfated protein. However, it is yet to be shown whether this protein is unique to ocular tissues or is

an important component of all ECMs. The presence of proteins of similar sizes is not limited to the 60 kDa band, but other protein bands of similar sizes were observed in different tissues. That does not preclude the possibility that the same protein may exist in different ocular tissues.

Future plans include identification of the sulfated proteins in different ocular tissues. This can be accomplished by subjecting extracts from tissues to immunoaffinity purification with PSG2 antibody. Once these proteins are identified, their sulfation status will be further confirmed by immunoprecipitation with antigen-specific antibodies and immunoblotting with the PSG2 antibody. Then the sulfated tyrosine will be determined by site-directed mutagenesis followed by immunoprecipitation with antigen-specific antibodies and immunoblotting with PSG2 antibody. The role of sulfation in the overall function of the protein in vision will be studied using gene “knock-in” mice that have the sulfotyrosine mutated to phenylalanine followed by ERG and other means of assessments of visual function.

Acknowledgments This study was partly supported by grants from the National Center For Research Resources (P20RR017703), the National Eye Institute P30EY12190, Oklahoma Center for the Advancement of Science and Technology (OCAST) (YK), R01 EY14052 and R01 EY018137 (MRA), FFB (MRA), Hope For Vision, NY (MRA), and the Reynolds Oklahoma Center on Aging (MRA).

References

- Farzan M, Babcock GJ, Vasilieva N et al (2002) The role of post-translational modifications of the CXCR4 amino terminus in stromal-derived factor 1 alpha association and HIV-1 entry. *J Biol Chem* 277:29484–29489
- Fong AM, Alam SM, Imai T et al (2002) CX3CR1 tyrosine sulfation enhances fractalkine-induced cell adhesion. *J Biol Chem* 277:19418–19423
- Higuchi M, Wong C, Kochhan L et al (1990) Characterization of mutations in the factor VIII gene by direct sequencing of amplified genomic DNA. *Genomics* 6:65–71
- Hoffhines AJ, Damoc E, Bridges KG et al (2006a) Detection and purification of tyrosine-sulfated proteins using a novel anti-sulfotyrosine monoclonal antibody. *J Biol Chem* 281:37877–37887
- Hoffhines AJ, Damoc E, Bridges KG et al (2006b) Detection and purification of tyrosine-sulfated proteins using a novel anti-sulfotyrosine monoclonal antibody. *J Biol Chem* 281:37877–37887
- Hoffhines AJ, Jen CH, Leary JA et al (2009) Tyrosylprotein sulfotransferase-2 expression is required for sulfation of RNase 9 and Mfge8 in vivo. *J Biol Chem* 284:3096–3105
- Kanan Y, Hoffhines A, Rauhauser A et al (2009a) Protein tyrosine-O-sulfation in the retina. *Exp Eye Res* 89:559–567
- Kanan Y, Hoffhines A, Rauhauser A et al (2009b) Protein tyrosine-O-sulfation in the retina. *Exp Eye Res* 89:559–567
- Komori R, Amano Y, Ogawa-Ohnishi M et al (2009) Identification of tyrosylprotein sulfotransferase in Arabidopsis. *Proc Natl Acad Sci USA* 106:15067–15072
- Lee RW, Huttner WB (1983) Tyrosine-O-sulfated proteins of PC12 pheochromocytoma cells and their sulfation by a tyrosylprotein sulfotransferase. *J Biol Chem* 258:11326–11334
- Lee RW, Huttner WB (1985) (Glu62, Ala30, Tyr8)_n serves as high-affinity substrate for tyrosylprotein sulfotransferase: a Golgi enzyme. *Proc Natl Acad Sci USA* 82:6143–6147
- Leyte A, van Schijndel HB, Niehrs C et al (1991) Sulfation of Tyr1680 of human blood coagulation factor VIII is essential for the interaction of factor VIII with von Willebrand factor. *J Biol Chem* 266:740–746

- Moore KL (2009) Protein tyrosine sulfation: a critical posttranslation modification in plants and animals. *Proc Natl Acad Sci USA* 106:14741–14742
- Sherry DM, Murray AR, Kanan Y et al (2010) Lack of protein-tyrosine sulfation disrupts photoreceptor outer segment morphogenesis, retinal function and retinal anatomy. *Eur J Neurosci* 32: 1461–1472
- Veldkamp CT, Seibert C, Peterson FC et al (2006) Recognition of a CXCR4 sulfotyrosine by the chemokine stromal cell-derived factor-1alpha (SDF-1alpha/CXCL12). *J Mol Biol* 359: 1400–1409
- Wilkins PP, Moore KL, McEver RP et al (1995) Tyrosine sulfation of P-selectin glycoprotein ligand-1 is required for high affinity binding to P-selectin. *J Biol Chem* 270:22677–22680

ERRATUM TO

Chapter 103 HCN1 Channels Significantly Shape Retinal Photoresponses

Naoyuki Tanimoto, Arne Brombas, Frank Müller, and Mathias W. Seeliger

M.M. LaVail et al. (eds.), *Retinal Degenerative Diseases*, Advances in Experimental Medicine and Biology 723, DOI 10.1007/978-1-4614-0631-0, pp. 807–812
© Springer Science+Business Media, LLC 2012

DOI 10.1007/978-1-4614-0631-0_108

In the original version, the affiliations and addresses are incorrect. The correct affiliations and full addresses are as follows:

N. Tanimoto • M.W. Seeliger
Division of Ocular Neurodegeneration, Centre for Ophthalmology,
Institute for Ophthalmic Research, University of Tübingen, Schleichstr. 4/3,
D-72076 Tübingen, Germany
e-mail: naoyuki.tanimoto@med.uni-tuebingen.de

A. Brombas • F. Müller
Institute of Complex Systems, Cellular Biophysics (ICS-4),
Forschungszentrum Jülich, D-52425 Jülich, Germany

A. Brombas (current address)
Queensland Brain Institute, The University of Queensland, Upland Road,
St Lucia, Queensland 4072, Australia

Index

A

- AAV. *See* Adeno-associated virus (AAV)
- ABCA4* gene, 408–409
- ABCA4*^{-/-} mouse eyecups, 763–764
- Abe, T., 305
- ABI/SOLiD platform, 755
- Ablonczy, Z., 75
- Achromatopsia (ACHM), 183. *See also* Cyclic nucleotide-gated (CNG) channels
- Adamowicz, M., 573
- Adaptive optics (AO) imaging
 - analysis and interpretation, 451–452
 - bull's eye maculopathy, 454–455
 - clinical examination, 452
 - dominant drusen, 452–454
 - retinal atrophy and visual loss, 454–456
- Adeno-associated virus (AAV), 180
 - rescued retinal function, 202–203
 - retinal structure integrity, 201–202
 - RHO301* gene expression, 201
 - usher syndrome type 1B, 239
 - XIAP protein, 211–212
- Adenosine 5'-triphosphate (ATP), 813
 - degradation, 814
 - and purinergic receptors, 813
 - storage and release of, 814
- A2-dihydropyridine-phosphatidylethanolamine (A2-DHP-PE), 764–765
- ADRP. *See* Autosomal dominant retinitis pigmentosa (ADRP)
- Advanced glycation end product (AGE), 765
- A2E, 725, 763
- AFF. *See* Autofluorescent foci (AFF)
- Age-related macular degeneration (AMD), 62, 64, 65, 67–68
 - angiogenic response, 273
 - ARMS2*, 369–370
 - chronic age-related disease, 727
 - diagnostic tools, 274
 - histopathological analysis, 726
 - HTRA1*, 370
 - neovascular ocular diseases, 246
 - retina, 272
 - retina autophagy (*see* Autophagy)
 - retinal neovascular disorders, 255
 - risk factors, 726
 - therapeutic approaches, 270
 - VEGF levels, 272
- Aguayo, 161
- Aguirre, G.D., 321, 353, 611
- Ahern, K., 553
- AIF. *See* Apoptosis-inducing factor (AIF)
- Airaksinen, S., 668
- Akopian, A., 739
- Albarracin, R.S., 121
- Ali, R.R., 17, 177
- Allikmets, R., 368
- All-*trans*-retinal dimer phosphatidylethanolamine, 763–764
- Al-Ubaidi, M.R., 835
- Ambati, J., 3
- AMD. *See* Age-related macular degeneration (AMD)
- AMP-activated protein kinase (AMPK)
 - cellular process, role in, 746
 - and RPE cell function
 - allosterical activation, 746
 - cell barrier function, 747–748
 - cell inflammatory response, 748–749
 - cell survival, 749
 - phagocytosis, 748
 - via Thr¹⁷²Pphosphorylation, 746–747

- AMP-activated protein kinase
(AMPK) (*cont.*)
Ser/Thr kinase, 746
subunit, 746
- Amyloid- β role
AMD, 67–68
cytotoxic, neural retina, 69–70
drusen component, 68
proinflammatory retina, 70–71
RPE cell structure and function, 68–69
- Amyloid precursor protein (APP), 68
- Anand-Apte, B., 261, 293
- Anderson, R.E., 129
- Angiogenesis, 681
- Animal model
rd 10 mice, RPE sheet analysis (*see* Rd10 mice, retinal degeneration model)
ROM-1 overexpression
electron microscopy, 635
electroretinography, 634–635
gel electrophoresis, 634
transgenic mice, 634
western blot analysis, 634
- Annear, M.J., 177
- Annexin 2 (anxA2), 720
- Apolipoprotein, 726
- Apoptosis, 207
- Apoptosis-inducing factor (AIF), 210
- Apoptotic cell death, 554
- Aranesp/AMG114, 138, 139
- Arinobu, D., 823
- Aron, L., 415
- Arrestin 1 (Arr1)
dark-or light-adapted retinas, 793–795
protein–protein interaction, 793
- Arylalkylamine N-acetyltransferase
(AANAT), 824
- Aryl hydrocarbon receptor (AhR)
AMD pathogenesis, 55–56
cellular oxidative stress response, 54
cigarette smoke, 52
genetic linkage and genome-wide association study, 51–52
molecular and biological mechanism, 51
proteosomal degradation, 54–55
RPE cellular response, oxidant injury, 52–53
- Association for Research in Vision and Ophthalmology, 642
- Autofluorescent foci (AFF), 464
- Autoimmune biomarkers
“after-the-fact” phenomenon, 14
AMD pathogenesis, 12–13
immunomics, 15
inflammation and immune system, 12
proinflammatory factors, 14
protein modification, 11
role of autoimmunity, 13–14
- Autophagy, 208
AMD, 87–88
molecular events, 84–85
neural retina, 85–86
RPE, 86–87
signaling mechanisms, 85
- Autophagy-related proteins (Atg), 84
- Autosomal dominant cone and cone-rod dystrophy
characterisation, 337
genetic analyses, 338
hereditary retinal dystrophies, 337
mutation spectrum, 338–340
patients and clinical examinations, 338
- Autosomal dominant retinitis pigmentosa (ADRP), 191, 215, 500–502, 573
AAV gene delivery
rescued retinal function, 202–203
retinal structure integrity, 201–202
RHO301 gene expression, 201
animal models, 200
electroretinography, 200–201
outer nuclear layer, 201
RHO301 gene cloning, 200
- Axonal guidance. *See* Homeobox genes
- Ayyagari, R., 225
- B**
- Bachor, T.P., 101
- Bagheri, N., 479
- Bai, L., 183
- Bainbridge, J.W., 177
- Bai, Y., 299
- Balaggan, K.S., 271
- Balb-c male mice, 102
- Bandyopadhyay, M., 23
- Bardet–Biedl syndrome (BBS), 533
- Barker, S.E., 177, 180
- Barrier modulation
characteristics, 157–158
Claudin-5, 156
IMPDH1 gene, 156, 157
potential benefits, 156, 157
RPE, 157
- Barstable, 758
- Bartoe, J.T., 177
- Basavarajappa, D.K., 829
- Basic helix–loop–helix (bHLH), 686
- Bassoon KO mice, 740, 741

- β -carotene monooxygenase 1 (BCMO1), 168
 BCM. *See* Blue cone monochromacy (BCM)
 Beaulieu, C., 371
 Becerra, S.P., 799
 Bech-Hansen, N.T., 371
 Becirovic, E., 183
 Beck, S.C., 183
 Bell, B.A., 459, 479
 Beltran, W.A., 353
 Bennett, J., 129
 Bernd, A., 471
 Best corrected visual acuity (BCVA), 472
 Best disease, 604
 BEST1 missense mutations
 anion channel malfunction, 612
 BVMD, 611, 616
 canine bestrophin-1 topology, 613–614
 cellular homeostasis, 616
 comparative protein modeling, 613–615
 membrane protein, 616
 protein structure, 613
 topological model, 612–613
 Bestrophin-1. *See also* BEST1 missense mutations
 anion conductance loss, 604
 cytoplasmic function, 607–609
 function, 604
 localization, 604–606
 retinal degeneration, 603
 vitelliforme macular dystrophy, 604
 Best vitelliform macular dystrophy (BVMD), 604, 611, 616
 Betacellulin (BTC)
 angiogenesis, 295
 biological functions, 294
 future aspects, 296
 role, retina, 295
 structure and expression, 294
 Bian, Q., 43
 Biel, M., 183
 Birch, D.G., 313, 497
 Bis-retinoid precursors, 75
 Bisretinoids, RPE lipofuscin
 A2-DHP-PE, 764–765
 all-*trans*-retinal dimer vs.all-*trans*-retinal dimer PE, 763–764
 biosynthetic pathways, 761–762
 photooxidation, 765
 Blacque, O.E., 433
 Blanks, J., 269
 Blast-like alignment tool (BLAT), 522, 523
 Blood-retinal barrier (BRB)
 Claudin-5 siRNA, 156–157
 iBRB modulation, 158–159
 IMPDH1 gene, 156, 157
 potential benefits, 158
 RPE, 157
 tight junctions, 155–156
 Blue cone monochromacy (BCM), 599
 Blue light damage
 apoptosis, 619
 cryosection, 623
 DNA microarray, 620
 histological investigation, 629
 MacGreen mice, 620
 microglia accumulation, 622–623
 quantitative real-time PCR, 620–621
 retinal cross sections and whole mounts, 620
 retinal degeneration, 619
 RNA isolation and reverse transcription, 620
 transcriptomic changes
 DNA microarray analysis, 623, 624
 expression, 625–628
 microarrays algorithm, 624
 qPCR validation, 629
 Blue native-PAGE
 analysis of, 773
 detergents, 770
 protein complex separation, 774
 Boatright, J.H., 641
 Bonilha, V.L., 479
 Bothnia-type retinal dystrophy
 11-*cis*-retinal
 illumination, 590
 photoisomerization, 592–593
 CRALBP WT and R234W
 expression, purification,
 crystallization, 590
 ligand-binding cavity, 592
 structure determination, 590–592
 crystallographic statistics, 593
 RLBP1 gene, 589
 Boulton, M.E., 83, 726
 Bovine ocular tissues
 isolation of, 836
 PSG2 antibody, 838–839
 SDS-PAGE, 836–837
 S-IRPEM vs. IS-IRPEM, 838, 839
 Western blot analysis, 837–838
 Bowles, K.E., 505
 Bowne, S.J., 313
 Braunger, B.M., 679
 Bredberg, D.L., 590
 Bright-field macroscopic imaging, 480
 Brij 96, 770
Brn-3 genes, 686–687
 Brombas, A., 807
 Bruban, J., 67

- Bruch's membrane (BM), 12, 725, 765
 Brush, R.S., 553
 BTC. *See* Betacellulin (BTC)
 Bulls' eye maculopathy, 454, 455
 Büning, H., 183
 Butler, M.C., 145
 BVMD. *See* Best vitelliform macular dystrophy (BVMD)
- C**
 Caberoy, N.B., 693
Cacnalf gene, 739
Caenorhabditis elegans, BBS proteins
 cellular functions, 534
 IFT transport, 534–535
 nephronophthisis, 534
 photoreceptor degeneration, 536–537
 phototransduction, 536
 pleiotropic disorder, 533
 primary cilium, 534
 RPE cells, 535
 Cai, J., 83
 Cai, X., 245
 Calof, A.L., 671
 Calpain and photoreceptor apoptosis
 age-related macular degeneration, 547
 barrier modulation, 551
 blood retina barrier, 549
 calpain activation, 548–549
 calpain inhibitors, 549
 caspase 8, 548
 transgenic mouse models, 549
 Campbell, M., 155, 547, 567
 Canine-specific TaqMan assay, 361
 Carboxy-ethyl-pyrrole (CEP), 13
 Carroll, J., 451
 Caspase 8, 548
 Caspase-dependent apoptosis, 5
 Castañeda, M.M., 101
 Cav1.4 α 1 subunit
 Cacnalf gene, 739
 knockout mice, 740
 loss of, 742
 Cdc42, 583
 Cell death
 autophagosome, 208
 characterisation, 207
 future aspects, 212
 inherited retinal dystrophies, 209–210
 macroautophagy, 208
 mammalian autophagy, 208
 pathway blockage, 211–212
 retinal damage models, 210–211
 TOR kinase, 208
 Cellular homeostasis, 83
 Cellular retinaldehyde-binding protein (CRALBP)
 11-*cis*-retinal
 illumination, 590
 photoisomerization, 592–593
 expression, purification, crystallization, 590
 ligand-binding cavity, 592
 structure determination, 590–592
 Ceramide kinase like (CERKL) gene, 555
 Ceramide signaling
 apoptotic cell death, 554
 bioactive sphingolipids, 553
 Cer production, 554
 photoreceptor apoptosis, 554–556
 RPE cell death, 556
 Cerebral neurodegenerative disease, 65
 Cer-induced RPE apoptosis, 556
 CFF. *See* Critical flicker frequency
 Chakraborty, D., 633, 657
 Chalmers, K.J., 367
 Chang, B., 130
 Chavali, V.R.M., 225
 Cheetham, M.E., 527, 595
 Chemical cross-linking
 amino-specific cross-linker BS³, 770
 with infrared fluorescence detection, 772, 774
 Nrl-/-retina membrane, 770
 protein complex evaluation, 772
 Chemical mutagenesis, 400
 Chemotactic cytokines, 39
 Chen, H., 553
 Chiang, W.-C., 559
 Choroidal neovascularization (CNV), 4, 254
 CCR3
 animals and subretinal Matrigel injection, 280
 antagonist SB328437 effects, 281–283
 blood vessels and measurement, 280
 Matrigel model, 280–281
 role of, 279
 constitutive vs. regulated expression, 270–271
 endostatin effectiveness, 273–274
 hypoxia-regulated expression, 272–273
 RPE-specific promoters, 271–272
 Choroidal vascular development
 animal experiments, 300
 choroidal vessels, 303
 quantification, 300–301
 retinal integrity, 301
 RPE-produced VEGF, 301

- Choroideremia (CHM)
 affected family members, 383
 clinical characteristics, 383
 confocal microscopy, 382–383
E. coli particles, 383
 FACS analysis, 382–383
 gene replacement, 386
 lysosome-mediated degradation, 386
 patient population, 382
 proteolytic degradation, 385
 trafficking defects, 386
- Chow, A.Y., 115
- Chrenek, M.A., 641
- Chromatin immunoprecipitation (ChIP), 754
- Chromatin signatures, 756–757
- Chromosome 10q26 susceptibility
ARMS2, 369–370
 genetic association, 368–369
- Ciavatta, V.T., 115
- Ciliary neurotrophic factor (CNTF)
 adaptive optics scanning laser
 ophthalmoscopy, 98
 cone degeneration, 94
 COS regeneration, 96–97
 light-sensing function, 97
 loss of cones, 95
 loss of COS progress, 94–95
 PNA-negative areas, 96
 retinal degeneration, 94
 S334ter rats, 94
- Ciliopathy, 318
- Circadian rhythms, 718
- cmr2* mutant, 613, 614
- CNGA3
 achromatopsia, 183
 electrophysiological analysis, 184
 ERG measurements, 186
 ganglion cells activation, 187
 immunohistochemistry, 185
 mouse expression, 185
 photoreceptor function, 185–186
 rAAV vectors and injection, 184
 retinal cone-mediated signaling,
 187–188
 water habituation, 185
- CNV. *See* Choroidal neovascularization
 (CNV)
- Coat's disease, 680
- Cochran's *t*-test, 643
- Colley, N.J., 407
- Collin, R.W.J., 345
- Cone dystrophy. *See* *OPN1LW* and *OPN1MW*
 cone opsin gene
- Cone opsin promoter (COP-T), 659
- Cone photoreceptors
 ROM-1 protein
 electron microscopy, 635
 electroretinography, 634–635
 gel electrophoresis and western blot
 analysis, 634
 ROM-1 overexpression, cone function
 and structure, 635–637
 ROM-1 protein expression, transgenic
 mice, 635, 636
 transgenic mice generation, 634
- Cone-rod dystrophy (CRD), 321, 497
- Congenital stationary night blindness
 clinical phenotype, 377
 clinical variability, 375–376
 ERG features, 377
 genetic analysis, 372
 CACNA1F mutations, 373
 GRM6 mutations, 374
 NYX mutations, 374
 TRMP1 mutations, 374
 X-linked CSNB, 375
 negative bright flash ERG, 377
 nystagmus, 377
 statistical Analysis, 372
 strabismus, 377
 subjects, 372
- Conley, S.M., 633, 657
- Connor, T.B. Jr., 451
- Coomassie blue staining, 773
- Corbo, J.C., 757
- Cotter, T.G., 549
- C1q tumor necrosis factor-5 (*CIQTNF5*/
CTRP5), 225, 226
- Craft, C.M., 253, 791
- CRALBP. *See* Cellular retinaldehyde-binding
 protein (CRALBP)
- Cremers, F.P.M., 345
- Critical flicker frequency (CFF)
 ERG protocol, 506–507
 ISCEV standard tests, 506
 photopic, 508–510
 scotopic, 507–508
- Cronin, T., 129
- Crouch, R.K., 75
- CRX
 photoreceptor terminal
 determination, 757
 retinal development, *vsx2*, 675
- Cubilla, M.A., 101
- Cutler, A., 293
- Cyclic guanosine monophosphate (cGMP)
 channel
 light adaptation, 781

- Cyclic guanosine monophosphate (cGMP) channel (*cont.*)
 N-terminal and C-terminal region, 778
 phototransduction, 781
 subunits, 777
- Cyclic nucleotide-gated (CNG) channels
 cell culture studies and vectors, 778
 cone
 blue native-PAGE, 770
 chemical cross-linking, 770, 772
 infrared fluorescence Western detection, 770
 stoichiometry of, 773–774
 subunits, 769
 PHLPP1 and PHLPP2
 modulatory properties, lack of, 780–781
 RA domain assessment, 779–780
 RA/RBD domain-containing proteins, 778
 rods, 769
 sequence alignment and domain assessment, 778
 statistical methods, 778
 visual and olfactory transduction, 777–778
- Cytosolic protein cone arrestin (CAR), 659
- D**
- Dahrouj, M., 23
 Daiger, S.P., 313
 Dalal, N., 641
 Dark-adapted rod electroretinogram, 497
 Dark-rearing *rd10* mouse
 candidate retinal genes, 132
 C57Bl/6J, 130
 electroretinogram, 130–131
 immunohistochemical analysis, 132
 immunolabeling, 131
 LR-*rd10* mice, 133, 134
 phosphodiesterase 6b mutation, 129
 P23H-3 transgenic mouse, 133
 PNM3, 131–132
 QrtPCR analysis, 131
 retinal gene expression, 135
 rod function, 134
 RTPCR, 129
- Dean, M., 368
 De Laurenzi, V., 732
 Dendritic cells (DCs), 12
 den Hollander, A.I., 345
 Desiderio, D.M., 11
 Devery, S., 595
 Dexamethasone (DEX), 101, 105
 Dhubhghaill, S.N., 155
- Diabetes, betacellulin, 295
 Diabetic retinopathy, 293
 neovascular ocular diseases, 246
 pericyte injury, 285
 retinal neovascular disorders, 254
- Dickkopf (DKK)-1, inhibitor, 681
 Dinet, V., 67
 Ding, X.-Q., 633, 769
Dlx genes, 687–688
 DNA microarray, 620
 Dodecylmaltoside (DDM), 770
 Donovan, M., 549
 Dorey, C.K., 269
 Double-stranded RNA (dsRNA), 4
Drosophila photoreceptor degeneration, 556
 Dryja, T.P., 411
 Dunn, W.A. Jr., 83
 Dwyer, M., 51
- E**
- Ebenezer, E.D., 595
 Ebert, S., 619
 Ectonucleoside triphosphate diphosphohydrolases (E-NTPDases), 814
 Eisenstat, D.D., 685
 Elastokines, 64
 Electroretinogram (ERG), 506–510, 823
Arr1^{-/-} mice, 793
 autosomal dominant retinitis pigmentosa, 200–201
 photopic CFF, 508–510
 protocol, 506–507
 retinal photoresponses, *HCN1*^{-/-} mice, 809
 ROM-1 overexpression, 634–635
 scotopic CFF, 507–508
 small interfering RNA, 217
 standard ISCEV flicker test, 506, 510
 translational vision research models program, 392
- Endogenously expressed bestrophin-1, 605
 Endoplasmic reticulum, 289, 290, 607, 608
 Endoplasmic reticulum-associated degradation (ERAD)
 cytosolic events, 561–562
 dislocation, 560–561
 glucosidase activation, 559
 misfolded proteins recognition, 560
 P23H rhodopsin, 562–563
 protein-folding cycle, 560
 quality control, 559
- Endostatin, 273–274
 Endotoxin-induced autoimmune uveitis (EAU), 20

- Enhanced S cone syndrome (ESCS), 823
 ENU mutagenesis. *See* *N*-ethyl-*N*-nitrosourea (ENU) mutagenesis
 Epidermal growth factor (EGF), 294
 Epidermal growth factor receptor (EGFR), 830
 Epitope-tagged PEDF-R expression, 800
 ERG. *See* Electroretinogram (ERG)
 Erythropoietin (Epo), 138
 glycosylation analogs, 141
 overexpression, 140
 retinal protection, 140
 External limiting membrane (ELM), 454
 Extracellular matrix (ECM), 370, 838
 Eye development, 399–400
- F**
 Factor XIIIa, Goldfish
 cDNA clone, 449
 cloning, 446
 gene expression change, 447–448
 induced neurite outgrowth, 448
 transglutaminase (TG), 445
fad mutant, 441
 Fahim, A.T., 313
 Fahl, E., 183
 Familial exudative vitreoretinopathy (FEVR), 680
 Familial (Mendelian) maculopathies, 62
 Fariss, R.N., 661
 Farkas, M.H., 519
 Farrar, G.J., 567
 Fat-liver dystrophy (*fld*) mouse, 655
 Faulkner, A.E, 115
 Fenretinide
 amine analog, 172
 BCMO1 inhibitor, 169–170
 BSG1 enzyme, 168
 cancer treatment, 167
 catalytic activation, 170, 172
 constructs, 168
 HPLC analysis, retinoid and carotenoids, 168
 molecular docking, 169
 noncompetitive inhibition behavior, 170, 171
 protein expression and enzyme assay, 168
 RBP4, 167
 synthesis, 168–169
 tertiary structure modeling, 169
 Fibroblast growth factors (FGFs), 302
 Finnemann, S.C., 709, 731
 Fischer, M.D., 183, 491
 Flatmount technique, 642
 Fletcher, E.L., 813, 816
 Focal adhesion kinase (FAK), 719
 Fong, W.G., 207
 Fourier transforms (FFTs), 507
 Fritsche, L.G., 369
 Frizzled 4 (Fzd-4), 681
 Fujikawa, C., 663
 Fukada, 823
- G**
 Ganglion cell functions, 476
 Ganglion cell layer (GCL), 675, 687
 Gardner, C., 641
 Gardner, J.C., 595
 Geisert, E.E., 649
 Gel electrophoresis, 634
 Gene expression, retinal injury
 in adult rats, 649
 bioinformatic analyses, 651, 653–654
 in *fld* mice, 655
 network modulation, 651–653
 online databases, 651, 653–654
 patterns of, 650
 Gene therapy
 AAV-mediated gene therapy, 239
 AMD, 270
 HRE, 272
 lentivirus-mediated gene therapy, 237–239
 RDS/peripherin disease., 216
 Genini, S., 353
 Genome-wide occupancy analysis
 ChIP-chip and ChIP-Seq
 ChIPed DNA, 755
 NGS platforms, 755–756
 in vivo protein-DNA interactions, 754
 transcription regulatory network
 histone modifications, 756–757
 transcription factor, 756
 Gentleman, S., 167
 Gerling, I.C., 11
 Glaucoma, 655, 816
 Glucocorticoid-dependent mechanisms
 balb-c male mice, 102
 caspase-3 activation, 103–104
 DEX, 101, 105
 GR α immunoreactivity, 104
 light-exposed retinas, 102–103
 mifepristone, 101, 105
 mineralocorticoid receptor, 105
 OS damage, 105
 rhodopsin, 103
 Gobbo, O.L., 155
 Godara, P., 451
 Gollisch, T., 183
 González-Duarte, R., 329

- Gorbatyuk, M.S., 191, 199, 569
 Gorbatyuk, O.S., 191
 G-protein-coupled receptor (GPCR), 18, 793
 G protein-coupled receptor kinase (GRK)
 in changing light conditions, regulation of,
 823–824
 expression of, 822
 function of, 822–823
 photoreceptor, distribution in, 822
 retinopathy, role in, 821
 Grant, G.R., 519
 Grant, M.B., 83
 Graphpad Prism software, 778
 Greferath, U., 813
 Gregory-Evans, C.Y., 399
 Grey, A.C., 75
 Griciuc, A., 415
 Grimm, C., 491, 581
 Grossman, G.H., 293, 701, 783
 Grossniklaus, H., 641
 Growth and differentiation factor 11 (GDF11)
 olfactory epithelium (OE), 672
 retinal ganglion cells, 672
 retinal neurogenesis, negative regulator
 of, 672
 signaling molecule, 672
 transcription factor, role in, 673
 Vsx2^{ort/ort} mouse retina
 animal model, 673
 epithelial thickness and cell
 lamination, 674
 gene expression, 675
 histology and in situ hybridization, 673
 rescued expression, 674
 retinal development, restoration of, 675
 Growth factor receptor-bound protein 14
 (Grb14), 778
 Gubin, A., 167
 Gu, J., 15
 Guo, D.C., 315
 Gupta, V.K., 777, 829
 Gutierrez, D.B., 75
 Guziewicz, K.E., 611
- H**
 Hagstrom, S.A., 701, 783
 Hamilton, J.A., 671
 Hamilton, R.A., 835
 Hammerhead ribozyme (hhRz), 147
 Hanrahan, F., 155
 Hao, H., 753
 Hardcastle, A.J., 527, 595
 Hauswirth, W.W., 191, 199, 215
- HCN1 channels
 HCN1^{-/-} mice, retina
 flicker fusion frequency, 810, 811
 single-flash ERG response, 808–809
 knockout mice, 807
 photoreceptor
 mechanism in, 808
 shaping and shortening, 807
 HDAC I/II inhibitors, 109
 HDAC inhibition, *Rd1* mouse
 C3H wild-type mice, 108
 HDAC assay, 108
 histone modifications, 107
 molecular cell death pathways, 112
 PARP activity, 109–110
 photoreceptor cell death, 108
 rd1 photoreceptors, 111
 rd1 retina, 109
 rhodopsin, 111
 TUNEL and immunostaining, 109
 in vitro retinal explant cultures, 108
 Heat shock proteins (HSPs), 567
 heat shock factor-1, 663
 role, 663
 Hedstrom, L., 539
 Heintzman, N.D., 757
 Héon, E., 533
 Hereditary retinal degeneration, 93
 He, X., 589
 Heynen, S.R., 581
 Hicks, W., 391
 Hindges, R., 671
 Holder, G.E., 595
 Hollyfield, J.G., 459, 479
 Homeobox genes
 Brn-3 genes, 686–687
 Dlx genes, 687–688
 islet genes, 689
 Vax genes, 688
 Homeodomain (HD), 686
 Homozygosity mapping
 autosomal recessive disease, 346
 consanguineous vs. nonconsanguineous
 families
 ABCA4 mutation, 348
 arCRD cohorts, 349
 arRP genes, 348
 retinal dystrophy genes, 349
 schematic representation, 347
 future aspects, 350
 population composition, 349
 single nucleotide polymorphisms, 346
 strengths and limitations, 350
 Hood, D.C., 497

- Hoppe, G., 701
 Horner, T.J., 823
 Huang, D., 93, 279
 Huang, S.-P., 791
 Huber, G., 183, 491
 Human bestrophinopathy, 615
 Human postmortem eyes
 AMD retina, 483–485
 bright-field macroscopic imaging, 480
 macular hole, 482, 483
 normal retina, 481–482
 OCT, 481, 487
 RPE detachment, 482–484
 RP retina, 484–486
 SLO, 480–481
 tissue preparation, 480
 in vivo imaging, 485–487
 Human retinal gene (HRG), 529
 Human retinal pericytes
 activating transcription factor 4, 287–289
 C/EBP homologous protein, 287–289
 cell culture, 286
 ER stress inhibition, 289, 290
 glucose fluctuation, 285
 glucose regulated protein (GRP78), 287
 macrophage chemoattractant protein 1,
 285, 287
 materials, 286
 statistical analysis, 287
 western blot analysis, 286
 Humphries, M.M., 155, 547, 567
 Humphries, P., 155, 491, 547, 567
 Hyde, D.R., 427
 Hydroquinone (HQ), 27
 4-Hydroxy(phenyl) retinamide (4-HPR). *See*
 Fenretinide
 Hyperoxia, 33–34
 Hypoxia-regulated expression, 272–273
 Hypoxia-response elements (HREs), 272
- I**
 Iannaccone, A., 11
 IFT. *See* Intraflagellar transport (IFT)
 Illumina platform, 755
 Immunomics, 15
 Induced pluripotent stem (iPS) cells, 523
 Infrared fluorescence Western detection
 cone CNG channel
 advantages of, 774
 blue native-PAGE, analysis by, 773
 chemical cross-linking, 772–773
 CNGA3 and CNGB3, simultaneous
 detection of, 771
 mouse retinal membrane protein, 770
 Nrl^{-/-}retina, 770
 Ingenuity pathway analysis (IPA), 360
 Inner blood retina barrier (iBRB), 550
 Inner plexiform layer (IPL), 704
 Inosine 5 ϵ -monophosphate dehydrogenase
 (IMPDH1), 539
 Inositol 1,4,5-triphosphate (InsP₃), 720
 Institutional Animal Care and Use Committee
 of the Cleveland Clinic, 702
 Insulin receptor (IR) signaling
 and PTP1B
 in diabetes, 831
 interaction between, 830–831
 in retina, 830
 Intracellular trafficking genes
 intraflagellar transport, 438–439
 membrane transport, 440
 microtubule-dependent molecular motor, 439
 Intraflagellar transport (IFT), 438–439, 529
 IRDye-680 fluorescence dye, 770
 Ishikawa, Y., 305
 Islet genes, 689
- J**
 Jiang, Y., 641
 Jin, H., 535
 Jobling, A.I., 813
- K**
 Kanan, Y., 835
 Kanda, A., 369
 Kang, M.J., 420
 Kanuga, N., 595
 Kato, S., 161, 445, 663
 Kaul, C., 459
 Kauper, K., 93
 Kawamura, S., 823
 Keaney, J., 567
 Kenna, P.F., 155, 547, 567
 Kennedy, B.N., 433
 Kiang, A.-S., 155, 547, 567
 Kim, M.K., 115
 Kitiratschky, V., 337
 Kleinman, M.E., 3
 Knockdown technology, 401
 Knockout mouse models, 516
 Koch, S., 183
 Kohl, S., 337
 Kolniak, T.A., 145
 Komori, N., 769
 Koriyama, Y., 161

- Kortvely, E., 61, 369
 Kraft, T.W., 503, 505
 Krishnamoorthy, V., 183
 Krishnamurthy, P., 11
 Krizaj, D., 739
 Kroeger, H., 559
 Kumasaka, N., 305
 Kunchithapautham, K., 23
 Kurtenbach, A., 471
 Kuznetsova, T., 321
- L**
- Laird, J., 167
 Lakkaraju, A., 723
 Langmann, T., 619
 Laser microdissection (LMD), 703–704
 Late endosome–lysosome
 cholesterol trafficking, 723
 function and dysfunction, 724–725
 health and disease, 727–728
 protein–lipid sorting, 723
 in RPE, 725–726
 signaling, 723
 Laties, A.M., 93
 LaVail, M.M., 93, 191, 215, 553
 Law, A.-L., 717, 718
 LDL receptor-related protein (Lrp), 680
 Leber congenital amaurosis (LCA), 177, 540
 Lechtreck, K.F., 535
 Lenchik, N.I., 11
 Lentivirus-mediated gene therapy, 237–239
 Lewin, A.S., 191, 199, 215
 Le, Y.Z., 299
 Li, F., 129
 Light-damaged zebrafish retina
 induction of Müller glial proliferation, 429
 regeneration, 428–429
 Light-induced retinal degeneration, 34, 102–103
 apoptotic cell death, 122
 cone opsin gene regulation, 125
 cone photoreceptor function, 122
 emerging therapeutic modality, 126
 gap and *fgf* genes, 122
 histopathological changes, 126
 opn1mw gene expression, 127
 OS, photic injury, 123–125
 photoreceptor cell death, 123
 postcon retinas, 127
 retinal dystrophies, 121
 retinal function, photic injury, 125–126
 Lin, J.H., 191, 559
 Lipid storage disease, 555
 Lipofuscin (LF), 24, 75–76, 80, 85, 88
 accumulation, 86
 late endo-lysosome, RPE, 725
 in RPE
 amino acid analysis, 761–762
 bisretinoids (*see* Bisretinoids, RPE
 lipofuscin)
 Littink, K.W., 345
 Liu, J., 536
 Li, W., 693
 Li, Y., 93, 279
 Lobsiger, J., 589
 Local vs. systemic mononuclear phagocytes
 CCR2 and CX3CR1 signalling, 19–20
 cellular innate immune system, 21
 chemokine mouse model, 20
 chemokine receptor CX3CR1, 19
 CNV, 17
 geographic atrophy, 17
 microenvironment signals, 18
 myeloid cells, 19
 reticular drusen, 21
 systemic and local innate immune cells, 18
 Locke, K.G., 497
 Lodha, N., 371
 Lohr, H.R., 210
 Lopes, V.S., 235
 Loucks, C.M., 371
 Luhmann, U.F.O., 17
 Luibl, V., 68, 69
 Luo, L., 93, 279
 Lutein/zeaxanthin supplementation
 ARPE-19 cells, 45
 C57BL mice, 47–48
 cell culture and treatment, 45
 dietary supplementation, 48
 experiments with animals, 44–45
 immunoglobulin accumulation, 44
 light-induced photoreceptor death, 44
 materials, 44
 oxidative stress, 43
 primary macrophage culture, 46–47
 pro-inflammatory cytokines, 49
 RPE, 45–46
 visual loss protection, 43
 Lysosomes, 85
 Lyubarsky, A., 129, 131
- M**
- MacDonald, I.M., 381
 Macroautophagy, 83, 208
 Macrophage chemoattractant protein 1
 (MCP-1), 285
 Macula lutea, 61

- Macular drusen, 452
 Macular edema, 61
 Macular hole, 482, 483
 Maculopathy
 extracellular matrix role, 65
 macula lutea, 61
 pathomechanisms, 64
 risk factors, 64–65
 shared protein networks, 62–63
 Madin–Darby canine kidney (MDCK) cells
 cell culture, 354, 359
 cellular viability assessment, 359
 Maher, A.R., 595
 Malek, G., 51
 Mandal, M.N.A., 553
 Mao, H., 199
 Marfany, G., 329
 Mascarelli, F., 67
 Matrix-assisted laser desorption/ionization (MALDI), 76
 Matsukawa, T., 161
 Matsumoto, H., 769
 Matthes, M.T., 215, 553
 Matveev, A., 769
 Ma, W., 37
 Mawatari, K., 663
 MBT. *See* Mushroom bodies tiny (MBT)
 McDonnell, D., 51
 McGinnis, J.F., 245
 McGrew, D.A., 539
 Medaka fish, 822
 Melanosomes, 238
 Melino, G., 732
 Membrane-associated protein cone transducin (GNAT2), 659
 Mer tyrosine kinase (MerTK), 694
 characterization of, 696–697
 ligand study, phagocytosis RPE, 694
 POS engagement, 719–720
 retinal degeneration, 693
 Michaelides, M., 595
 Michalakakis, S., 183
 Microglia
 cellular interaction, 40
 inflammatory mediators and neurotrophic agents, 37
 legal blindness, 37
 maladaptive inflammatory response, 38
 P2X7 receptor, retina, 817
 retinohoroidal interface, 38–39
 RPE interaction, 39–40
 Micro-ophthalmia, 671
 Microphotodiode arrays (MPA), 115–120
 Mifepristone (MFP), 103, 105
 Mikkelsen, T.S., 757
 Milenkovic, V.M., 603, 611, 616
 Milewicz, D.M., 315
 Milk fat globule EGF-factor (MFG-E8), 718–719
 Mitter, S.K., 83
 Mitton, K.P., 758
 Mok, C.A., 533
 Molday, L.L., 795
 Molecule-specific imaging and quantitation
 A2E generation, 80
 A2E oxidation sites, 78–79
 bis-retinoid precursors, 75
 LC-MS/MS-based technique, 80
 lipofuscin accumulation, 75, 80
 MALDI imaging, 76
 murine RPE, 77
 quantitation A2E, 77–78
 RPE tissue preparation, 76
 Moore, A.T., 595
 Moore, K.L., 835
 Morphometrics analysis software, 646
 Mowat, F.M., 177
 Mühlfriedel, R., 183
 Müller, C., 603
 Müller cells, P2X7 receptor, 816–817
 Müller, F., 807
 Müller glia, 429, 430
 Murine macrophages, 46–47
 Mushroom bodies tiny (MBT), 582–583
 Mutation in gene encoding, zebrafish
 intracellular trafficking genes (*see* Intracellular trafficking genes)
 phototransduction protein, 435, 438
 structural factor, 440
 structural protein, 440
 N
 Naash, M.I., 633, 657
 Nagai, N., 305
 Nagashima, M., 663
 Naggert, J.K., 391
 Nakashima, H., 445
 Nandrot, E.F., 717, 718
 Nanoceria, 250
 Nash, Z., 633
 Natoli, R., 31
 Neeli, I., 11
 Nelson, C.M., 427
 Neovascular ocular diseases
 age-related macular degeneration, 246
 animal models

- Neovascular ocular diseases (*cont.*)
- Akimba (*Ins2 Akita VEGF+/-*) mouse, 248
 - Akita (*Ins2 Akita+/-*) mouse, 248
 - choroidal neovascularization, 247
 - vascular endothelial growth factor, 247
 - Vldlr* gene, 247
 - diabetic retinopathy, 246
 - oxygen induced retinopathy, 248
 - retinopathy of prematurity, 246
 - therapeutic treatment
 - angiogenic pathways, 248–249
 - nanomedicine, 249–250
 - regenerative medicine, 250–251
 - targeting pathology, 248–249
- Nepriylsin (NEP), 68
- N*-ethylmaleimide sensitive factor (NSF), 529
- ATPase activity, 793
 - domain structure, 792
 - homo-hexameric member, 792
 - photoreceptor
 - and Arrestin 1 (Arr1) (*see* Arrestin 1 (Arr1))
 - protein trafficking, 794–796
 - SNAP–SNARE binding, 792–793
- N*-ethyl-*N*-nitrosourea (ENU) mutagenesis, 391, 400
- Neural retina, 69–70, 85–86
- Neuronal progenitor cell proliferation, 429–430
- Neuroprotective dose response, RCS rats
- ERG testing, 119
 - light dosing, 116–117
 - microphotodiodes, 115
 - MPA device, 120
 - MPAs implantation, 116
 - photoreceptor numbers, 117
 - photoreceptor survival, 118
 - retinal function, 117–118
 - retinal function testing, 117
 - retinal preservation, 119
 - subretinal electrical stimulation, 116
 - xenon flashes, 119
- Neurotrophic growth factors, 681
- Neussert, R., 603
- Next generation sequencing (NGS), 350, 755
- bioinformatic analysis, 522–523
 - RNA-seq analyses, 523
- Nguyen, A.T.H., 155, 547
- Nickerson, J.M., 641
- Niemann–Pick C1 protein, 728
- Nishina, P.M., 391
- N*-methyl-*D*-aspartate (NMDA) injection, 681
- Noninvasive optical-biopsy, 479
- Norrin
- carboxyl-terminal cysteine-rich domain, 680
 - disease
 - congenital X-linked recessive disease, 680
 - missense mutations, 680
 - NDP* gene, 679
 - symptoms, 680
 - functions of, 682
 - in knock-in mouse model, 680
 - properties
 - angiogenic, 681
 - neuroprotective, 681–682
 - reproduction and development, role in, 682
- O**
- OCT. *See* Optical coherence tomography (OCT)
- Odyssey® Infrared Imaging System, 770
- Oguchi disease
- GRK1 retinopathy, 821, 822
 - in photoreceptor, NSF role, 796
- Ogun, O., 595
- Ogunshola, O.O., 581
- Oka, C., 370
- Oligomerization-incompetent RDS
- C150S-RDS protein, mislocalization of, 657–658
 - rods and cones
 - antibody and immunohistochemistry, 658
 - GNAT2 mislocalization, COP-T/WT, 660
 - M-opsin and COP-T mislocalization, COP-T/nrl^{-/-}, 659–660
 - transgenic mice, 658
 - transgenic mice, 657
- Onami, H., 305
- Oogai, K., 445
- OPNILW* and *OPNIMW* cone opsin gene
- cone dystrophy, 599
 - heterogeneous disorder, 595
 - immunoblotting and immunocytochemistry, 596–597
 - missense mutation, 599
 - molecular genetic analysis
 - array, 598
 - gene-specific primer, 596
 - P23H treatment, 599
 - RPGR* mutation, 597
 - W177R mutation, 598–599
 - ophthalmic assessment, 596
 - phenotype, 597

- polymorphism, 600
 - retinitis pigmentosa, 599
 - Opn1mw* gene expression, 127
 - Optical coherence tomography (OCT), 462–464, 466, 467, 479, 481
 - Optic nerve injury (ONI), 663
 - Optic nerve regeneration, gold fish
 - animal care, 446
 - factor XIIIa
 - cDNA clone, 449
 - cloning, 446
 - gene expression change, 447–448
 - induced neurite outgrowth, 448
 - transglutaminase (TG), 445
 - optic nerve transection, 449
 - retinal explant culture, 447
 - in situ hybridization, 446
 - wound healing, 445
 - Optic nerve repair
 - apoptosis, 165
 - IGF-I, 162
 - mammalian CNS injury, 165
 - neurite outgrowth-promoting factors, 162
 - nNOS, 163
 - optic nerve regeneration process
 - stages, 161
 - purpurin, 163–164
 - TG, 163
 - O’Riordan, C., 573
 - Osawa, S., 821
 - Ou, G., 534
 - Outer nuclear layer (ONL), 140, 142, 201
 - Outer plexiform layer (OPL), 701
 - Outer segment (OS) protein, 784
 - Oxidative stress, 747–748
 - Oxygen induced retinopathy, 248
- P**
- Papke, M., 337
 - Paquet-Durand, F., 107, 491
 - Parboosingh, J.S., 371
 - Pardue, M.T., 115
 - Pauer, G.J.T., 701, 783
 - pax6a* gene, 430
 - Peanut agglutinin (PNA), 94
 - PEDF. *See* Pigment epithelium-derived factor receptor (PEDF-R)
 - Penfold, P.L., 12
 - Peng, C., 774
 - Petersen-Jones, S.M., 177
 - Petr-Silva, H., 215
 - Phagocytosis, retinal pigment epithelium, 429
 - functional character of, 698
 - MerTK ligand study, 694
 - ORF phage, 694, 695
 - signaling, 693
 - Tulp1*^{-/-} mice, 694
 - Phosphatidylethanolamine (PE), 762
 - 3’-Phosphoadenosine 5’-phosphosulfate (PAPS), 835
 - Phosphodiesterase 6B (PDE6B), 641
 - Phosphoinositol (PI) signaling, 416
 - Phospholipase A₂ (PNPLA2), 800
 - Photic injury
 - OS, 123–125
 - retinal function, 125–126
 - Photopic critical flicker frequency, 508–510
 - Photoreceptor
 - apoptosis, 494, 554–556
 - cAMP-dependent protein kinase, 824
 - cell death, 123
 - cells, 237
 - ChIP-chip and ChIP-Seq, applications of, 757–758
 - CNG channel (*see* Cyclic nucleotide-gated (CNG) channels)
 - cyclic AMP, 824
 - cytoskeleton, 583–584
 - degeneration and survival, 584
 - GRK1 and GRK7 (*see* G protein-coupled receptor kinase (GRK))
 - HCN1 channel, mechanism of, 808
 - N*-ethylmaleimide sensitive factor (*see* *N*-ethylmaleimide sensitive factor (NSF))
 - OS protein transport, *tulp1*^{-/-} retina
 - animal model, 784–785
 - immunofluorescent staining, 785
 - localization, 785
 - trafficking, 786–787
 - survival, glucocorticoid-dependent mechanisms (*see* Glucocorticoid-dependent mechanisms)
 - Tulp1* complexes
 - crosslinked retinal samples, 705–706
 - homogenization, 704
 - in IS and OPL, 702
 - isolation and capture of, 704–705
 - laser microdissection, 703–704
 - retinal section preparation, 703
 - tcTPC, 703
 - Tulp1*^{-/-} mice, 702–703
 - Western blot analysis, 704, 705
 - zebrafish
 - morphogenesis, 434–435
 - significance, 433–434
 - vertebrate, 433

- Photoreceptor degeneration
Caenorhabditis elegans, 536–537
 HDAC inhibition (*see* HDAC inhibition, *Rdl* mouse)
- Photoreceptor mosaic imaging. *See* Adaptive optics (AO) imaging
- Photoreceptor neurons (PNs), 415
- Photoreceptor outer segment (POS), 693, 717, 731, 745
- Photoreceptor perisynaptic complex
 Cav1.4 α 1 subunit function, 740
 PMCA transporter and RIBEYE protein animal model, 740
 immunostaining, 740–741
 PMCA1 mislocalization, 741–742
- Phototransduction, 409–410
 cyclic nucleotide-gated channel, 769
 defects in, 832
 GPCR, 793
 GRK, 822
 protein interaction, 777
- P23H rhodopsin (RHO) photoreceptors
 BiP/Grp78 protein, 196–197
 control-injected eyes, 193
 ERG, 193
 gene therapy, 196
 genetic modifications, 191
 homozygous transgenic animals, 192
 HSF1 expression, 195–196
 human BiP/Grp78 expression, 193–194
 immunohistochemistry, 192
 mouse RHO 301 expression, 194
 retinal integrity, 194
 trafficking, 195
 transgenic rat, 196
- Pierce, E.A., 519
- Pigment epithelium-derived factor (PEDF), 69
- Pigment epithelium-derived factor receptor (PEDF-R)
 antibody, 800
 blocking peptides, 804–805
 immuno-blot, 801
 immunoreactivity
 rat retina R28 cell, as native, 803–804
 recombinant PEDF-R polypeptide, 802
 synthetic peptides, 802–803
 membrane fractionation, 801
 and PEDF interaction, 800
 peptides and proteins, 800
 phospholipase A activity, 800
 polyacrylamide gel electrophoresis, 801
 retina
 distribution, 799
pnpla2 gene, 799
 RPE and photoreceptor, 799
 slot blot, 801
- Pinealocytes, 514
- Pinter, R., 671
- Plasma membrane Ca²⁺ ATPases (PMCAs), 740
- Platelet-derived growth factor receptor (PDGFR), 830
- PNPLA2. *See* Phospholipase A₂ (PNPLA2)
- Poliakov, E., 167
- Poly-ADP-ribosylated proteins (PAR), 110
- Polyvinylidene fluoride (PVDF), 770
- Pomares, E., 329
- Prentice, H., 269
- Programmed cell death (PCD). *See* Cell death
- Proinflammatory cytokines, 40
- Protein misfolding
 beta-sheet breakers, 569
 chaperone activation, 569–570
 gene therapy, 570
 loss-of-function, 568
 mediating factors cell toxicity, 570
 nonproductive intermediates, 567
 photoreceptor cells, 568–569
 RDS-peripherin, 568
 rhodopsin, 569
 therapeutic strategies, toxicity, 569
- Protein tyrosine-*O*-sulfation. *See* Sulfation
- Protein tyrosine phosphate-1B (PTP1B)
 insulin receptor signaling
 interaction between, 830–831
 in retina, 830
 nonreceptor PTP, 829
 retinal disease, activity in, 831
- RTK
 dephosphorylation and inactivation, 830
 JAK/STAT pathway, 830
 negative regulator, 829
 structure, 829
 therapeutic target, 831–832
- Provis, J., 31
- PTGS agents
 development, 146–147
 expression and animal testing, 151
 hammerhead ribozyme, 147
 lead candidate identification, 151
 lead candidate optimization, 150–151
 siRNA, 148
- Purpurin, 163–164
- Puthussery, T., 816

Q

- Qin, S., 745
 Qin, T., 43
 Qi, X., 83
 Quantitative reverse transcription-PCR (qRT-PCR)
 canine-specific TaqMan assay, 354–358
 experimental conditions, 361
 MDCK cell
 cell culture, 354, 359
 cellular viability assessment, 359
 Quantitative trait locus (QTL) analysis, 651

R

- RAC1, 582–584
 Radic, M.Z., 11
 RA domain-containing protein
 cell culture, 778
 domain assessment, 778
 Grb14, 781
 IR signaling, role in, 778
 PHLPP1 and PHLPP2
 assessment of, 779
 on CNG channel activity, effect of, 780–781
 sequence alignment, 778
 statistical methods, 778
 vectors, 778
 Rahman, A.K., 553
 Rajala, A., 777
 Rajala, R.V.S., 777, 829
 Ranchon-Cole, I., 140
 Rao, H.V., 83
 Rapamycin, 27, 280
 Rapp, M., 799
 Rayborn, M.E., 459
 RCS rats implantation
 photoreceptor survival, 119
 retinal function, 117–118
 Rd10 mice, retinal degeneration model
 autosomal recessive RP, 641
 cell shape, 643–642, 646
 dramatic changes in, 643, 644
 flatmount technique, 642
 mean data, 643, 644
 missense mutation, PDE6B, 641
 morphometrics, 643, 645
 Nikon C1 confocal imaging system, 643
 ZO-1 staining, 642
 Receptor tyrosine kinase (RTK), PTP1B
 dephosphorylation and inactivation, 830
 JAK/STAT pathway, 830
 negative regulator, 829
 Recombinant adeno-associated virus (rAAV)
 vector, 216, 218–219
 Redmond, M., 76
 Redmond, T.M., 167, 491
 Remé, C., 619
 Ren, Z., 43
 Retina
 ATP (*see* Adenosine 5'-triphosphate (ATP))
 cholesterol, 726
 function, 731
 HNC1 channels (*see* HCN1 channels)
 insulin receptor signaling in, 830
 photoreceptor outer segments, 693
 purine receptors, 814
 purinergic system, 813
 P2X7 receptor, role of
 microglial cells, 817
 Müller cell, 816–817
 neuronal degeneration, 815–816
 neuronal modulation, 815
 vs. P2X receptor, 815
 Retinal abnormalities, mice
 abnormal pathology, 468
 AFF, 464
 animal model, 460–461
 histology, 462
 imaging procedures, 462
 noninvasive ocular imaging, 467
 retinal arteriole-venous malformation, 463
 retinal morphology, 460
 RPE, 462–463
 SLO & OCT images, 464–467
 superior-temporal abnormality, 463
 visible fundus photography, 467
 Retinal atrophy and visual loss, 454–456
 Retinal cone-mediated signaling, 187–188
 Retinal degeneration, 138
 amyloid- β role (*see* Amyloid- β role)
 anticomplement strategy, 34
 apoptotic cells, 34
 ceramide signaling (*see* Ceramide signaling)
 Drosophila melanogaster
 ABCA4 gene, 408–409
 compound eye, 409–410
 genetic screening, 411
 phototransduction, 409–410
 red-eyed *Vs.* white-eyed, 408
 retinitis pigmentosa, 409

- Retinal degeneration (*cont.*)
- spontaneous mutation, 407
 - enzymatic cleavages, 31
 - gene association study, 32
 - in human, 411–412
 - hyperoxia, 33–34
 - MerTK phagocytic receptor, 693
 - pathogenic complement activation, 32
 - photoreceptor injury, 33
 - P23H-3 rodent, 33, 35
 - PTP1B activity, 831
 - Sprague Dawley (SD) rats, 32
 - zebrafish
 - drug discovery, 403
 - embryogenesis, 399
 - functional assessment, 401–402
 - genetic resources, 400–401
 - morphological and embryological features, 399–400
- Retinal degeneration slow (RDS)
- mutation in, 657
 - rod and cone outer segment biogenesis, 657
 - rods and cones
 - C150S-RDS expression, 636–637
 - disc rim formation, 636
 - OS morphogenesis, 636
 - and ROM-1 protein, 633, 636–638 (*see also* Rod outer segment membrane protein-1)
- Retinal degenerative disease (RDD)
- clinical examinations, 498
 - dark-adapted rod amplitude, 500–502
 - gene therapy, 152
 - human clinical translation, 151
 - lead candidate identification, 150
 - lead candidate optimization, 150–151
 - mRNA expression, 148
 - mRNA structure determinations, 148–149
 - pair-flash ERG results, 498
 - PTGS agents, 147–148
 - PTGS development, 146–147
 - PTGS expression and animal testing, 151
 - rod inactivation kinetics evaluation, 498–499
 - rod photoresponse recovery kinetics, 499–500
 - T_{sat} correlation, 500–502
- Retinal dystrophies, 519
- Bothnia-type (*see* Bothnia-type retinal dystrophy)
 - direct molecular diagnosis
 - mutation screening chips, 330, 331
 - next-generation sequencing, 332
 - resequencing chips, 330, 332
 - future aspects, 334
 - homozygosity mapping
 - autosomal recessive disease, 346
 - consanguineous vs. nonconsanguineous families, 347–349
 - future aspects, 350
 - population composition, 349
 - single nucleotide polymorphisms, 346
 - strengths and limitations, 350
 - indirect molecular diagnosis
 - cosegregation SNP-Chips, 333
 - homozygosity mapping, 332–333
 - optimized cost-effective multitiered strategy, 333–334
- Retinal ganglion cell (RGC), 161, 471
- growth and differentiation factor 11, 672
 - norrin-deficient mice, 681
 - transcription factors, 686
 - Brn-3* genes, 686–687
 - Dlx* genes, 687–688
 - islet genes, 689
 - Vax* genes, 688
- Retinal gene expression, 135
- Retinal injury
- in adult rats, 649
 - bioinformatic analyses, 651, 653–654
 - in *fld* mice, 655
 - network modulation, 651–653
 - online databases, 651, 653–654
 - patterns of, 650
- Retinal ischemia, 211
- Retinal light damage
- anemia, 138
 - aranesp/AMG114, 138, 139
 - Epo expression, 140, 141
 - Epo glycosylation analogs, 141
 - ERG amplitudes, 140, 141
 - intravitreal injections, 139
 - light-induced cell death, 138
 - nonhematopoietic cells, 141
 - ONL thickness, 140, 142
 - outer nuclear layer thickness, 140
 - retinal degenerations, 138
- Retinal neovascular disorders (RNV)
- age-related macular degeneration, 255
 - neovascularization
 - genetic mouse models, 255–256
 - nongenetic models, 256–257
 - preclinical drug testing, 257
 - proliferative diabetic retinopathy, 254
 - retinopathy of prematurity, 254
- Retinal nerve fibre layer (RNFL), 474
- Retinal pigment epithelial (RPE) cells, 452, 454, 462–463, 520–521, 535, 604–606
- antimycin A treatment, 27

- ARPE-19, 24–25
- bevacizumab, 28
- blood vessel growth, 27
- CD55 and CD59 inhibitors, 25, 26
- cell-cell contact, 641
- CNV, 24
- dendritic cell, 731, 735
- endo-lysosome network, 723–724
- FAK and MerTK, receptor activities, 719–720
- glycoprotein secretion, 731
- internalization, 720–721
- late endosome–lysosome (*see* Late endosome–lysosome)
- macrophages, 731, 735
- macula, 23
- melanosomes, 237
- morphometrics, 643, 645
- MYO7A* gene, 236
- oxidative stress, 24
- pattern and cell shape of, 642, 643
- phagocytosis
 - functional character of, 698
 - MerTK ligand study, 694
 - ORF phage, 694, 695
 - signaling, 693
 - Tulp1*^{-/-} mice, 694
- PR phagocytic machinery, molecules of
 - animal models, 718
 - “eat me” signal, 718
 - milk fat globule EGF-factor, 718–719
 - phosphatidylserine, 718
- ranibizumab, 28
- rapamycin, 27
- rd 10 mice
 - autosomal recessive RP, 641
 - flatmount technique, 642
 - mean data, 643, 644
 - missense mutation, PDE6B, 641
 - Nikon C1 confocal imaging system, 643
 - ZO-1 staining, 642
- RPE layer, 38
- shed POS, 709
- synchronized diurnal phagocytosis, rod POS, 735
- transglutaminase-2
 - animal and tissue collection, 710, 732
 - histology, 733
 - immunoblotting, 711
 - immunofluorescence microscopy, 711
 - localization and expression, 712–713
 - POS phagosome quantification, 733
 - TG2*^{-/-} mice (*see* Transglutaminase-2 (TG2))
 - wild type vs. $\beta 5$ -/- eye cups, 711–712
 - vascular endothelial cell expression, 25
 - VEGF-R2 receptor, 26
 - zona occludens 1, tight junction molecule, 641
- Retinal pigment epithelial (RPE) cells
 - autophagy, 86–87
- Retinal pigment epithelium (RPE)
 - AMPK
 - allosterical activation, 746
 - cell barrier function, 747–748
 - cell inflammatory response, 748–749
 - cell survival, 749
 - cellular process, role in, 746
 - inactivation, 747
 - phagocytosis, 748
 - Ser/Thr kinase, 746
 - subunit, 746
 - via Thr¹⁷²P phosphorylation, 746–747
 - cell signaling modification, 745–746
 - chronic oxidative stress, 745
 - drusen biogenesis and AMD pathogenesis, 745
 - functions, 745
 - location of, 745
- Retinal pigment epithelium (RPE) lipofuscin
 - A2E, 763
 - bisretinoid
 - A2-DHP-PE, 764–765
 - all-*trans*-retinal dimer vs. all-*trans*-retinal dimer PE, 763–764
 - biosynthetic pathways, 761–762
 - photooxidation, 765
- Retinal vascular permeability. *See* Betacellulin (BTC)
- Retinitis pigmentosa (RP), 107, 209, 409, 497, 584, 599, 781
 - adRP, 519
 - BCVA, 472
 - characteristics, 783
 - cohort study, 474
 - electrophysiological recordings, 472–473
 - ERAD, 562–563
 - ganglion cell functions, 476
 - heterogeneous inherited retinal disorder, 701
 - IMPDH1-linked
 - characterization, 539
 - enzymatic properties, 540
 - IMPDH and retina, 540
 - IMPDH structure and function, 540–541
 - retinal splice variants, 541–542
 - rhodopsin mutations, 539
 - translation regulation, 542–543

- Retinitis pigmentosa (RP) (*cont.*)
 inner retina structure-function relation, 475
 next-generation sequencing (NGS)
 bioinformatic analysis, 522–523
 RNA-seq analyses, 523
 pathophysiological processes, 477
 in photoreceptor, NSF role, 796
 photoreceptors death, 477
 pre mRNA processing factor mutation, 520
Prpf31-knockout animals, 520
 rd 10, autosomal recessive model, 641
 retinal disorder, 783
 retinal nerve fibre layer imaging, 474
 RGC morphology, 471
 RNA splicing factor mutant mice, 523
 RP diagnosis, 472
 RPE degeneration, 520, 521
 SMA, 520
SMN1 mutations, 521
- Retinitis pigmentosa GTPase regulator (RPGR)
 candidate modifier genes, 314, 315
 clinical diversity, 314
 data analysis, 315–316
 modifier SNPs, 316–317
 phenotypic heterogeneity, 316
 protein transport, 314
- Retinitis pigmentosa protein (RP2)
Chlamydomonas protein, 528
 cilia localisation and function, 528–529
 interaction partners, 529–530
 mutations, 527
 TBCC, 527–528
Trypanosome protein, 528
 UNC119, 529
 vesicle traffic, 528
- Retinol-binding protein (RBP4), 167
- Retinopathy of prematurity (ROP)
NDP mutations, 680
 neovascular ocular diseases, 246
 retinal neovascular disorders, 254
- Retinoschisis (RS1)
 clinical pathology, 515–516
 gene therapy, 516–517
 molecular pathology, 516
RS1 gene and protein, 514
 X-linked retinoschisis mutations, 515
- Reverse tetracycline transactivator (rtTA), 255
- Rex, T.S., 140
- Reynolds, A.L., 433
- Rha, J., 451
- RHO. *See* Rhodopsin (RHO)
- Rhodopsin (RHO), 103
 AAV gene delivery, 201–203
 animal models, 200
 electroretinography, 200–201
 pathologies, *Drosophila*
 abnormalities in phototransduction, 418
 maturation, trafficking and proteasomal clearance, 419–420
 mutations, 416–417
 PNs, 415
 programmed cell death, 420
 Rh1 endocytosis and autophagy, 418–419
 PTP1B activity, 831
RHO301 gene cloning, 200
 translational vision research models program, 395–396
- Rho GTPases
 activation, 581–582
 overlapping function, 582
 photoreceptor
 cytoskeleton, 583–584
 degeneration and survival, 584
 retinal development, 582–583
- Ribbon synapses, 739
- Rinner, O., 823
- Ripamonti, C., 595
- Ritter, M.R., 251
- Rivera, A., 368
- RNV. *See* Retinal neovascular disorders (RNV)
- Robson, A.G., 595
- Rod inactivation kinetics evaluation, 498–499
- Rod ON-bipolar cells (RBCs), 130
- Rod opsin retinitis pigmentosa
 autophagy, 577–579
 characteristics, 573
 gene expression analysis, 574–575
 immunofluorescence, 574
 intracellular trafficking, 575
 P23H rhodopsin, 576, 577
 protein misfolding disease, 573
 TUNEL assay detection, 574
 UPR activation, 575
 vectors expression, 574
 western blotting, 574
 wild-type opsin, 577–578
- Rod outer segment membrane protein-1 (ROM-1)
 electron microscopy, 635
 electroretinography, 634–635
 gel electrophoresis and western blot analysis, 634
 ROM-1 overexpression, cone function and structure, 635–637
 ROM-1 protein expression, transgenic mice, 635, 636
 transgenic mice generation, 634

- Rohrer, B., 23, 34
 Rotstein, N.P., 557
 RPE. *See* Retinal pigment epithelium (RPE)
 Rpe65-deficiency
 AAV, 180
 Briard dogs, 177–178
 eye treatment, 180
 gene therapy
 phase I/II clinical trials, 179–180
 proof-of-principle trials, 179
 LCA, 177
 photoreceptor/cone degeneration, 178
 therapeutic intervention, 179
 treatment safety and efficacy, 180
RPGRIPI
 cilia assembly, 323–324
 cilia protein network, 322
 ciliogenesis, 324
 cytoskeleton dynamic regulation, 324
 expression, 322
 Ins44 mutation, 325–326
 knockout studies, 322
 molecular network components, 325
 retina, 322
 Ruggiero, L., 709, 731
 Rutar, M., 31
 Ryoo, H.D., 420
- S**
 Saadi, A., 553
 Saari, J.C., 590
 Salomon, R.G., 167
 Sancho-Pelluz, J., 107
 Santos, R., 671
 Sarang, Z., 731
 Sato, Y., 305
 Sauer, A., 337
 Scanning laser ophthalmoscopy (SLO),
 462–466, 479, 480
 Scaria, A., 573
 Schaich, S., 337
 Schey, K.L., 75
 Schmidt, J., 183
 Schwarz, N., 527
 Scotopic critical flicker frequency, 507–508
 SD-OCT. *See* Spectral domain optical
 coherence tomography
 SDS polyacrylamide gel (SDS-PAGE)
 R28 cell, membrane fractions, 804
 tissue lysate, Western blot of, 836
 Seeliger, M.W., 183, 491, 807
 Sezate, S.A., 245
 SFD. *See* Sorsby fundus dystrophy (SFD)
- Shang, F., 43
 Shared protein networks, maculopathy, 62–63
 Shi, L.Y., 391
 Sieving, P.A., 513
 Silvin, C., 381
 Singh, A., 769
 siRNA. *See* Small interfering ribonucleic acid
 (siRNA)
 Sliesoraityte, I., 471
 SLO. *See* Scanning laser ophthalmoscopy (SLO)
 Small interfering ribonucleic acid (siRNA)
 cell culture, 226–227
 CTRP5/*Ctrp5* expression, 230–231
 design, 226
 ELOVL4 mRNA
 ELOVL4-GFP fusion protein, 228
 protein expression, 227–228
 quantitative RT-PCR analysis, 229
 STGD3, 229
 wild-type ELOVL4 allele, 229
 rds expression
 AAV production, 217
 cell transfection, 216–217
 combination therapy, 220–222
 construction, 220
 electroretinogram, 217
 HEK-293 cells, 218
 rAAV-5 vector, 218–219
 RNA isolation, 217
 semiquantitative real-time PCR, 217
 statistical analysis, 218
 subretinal injection, 217
 transfection, 226–227
 transfection Cos-7 cells, 227
 Smith, A.J., 177
 Smith, G.W., 269
 Soluble interphotoreceptor matrix
 (S-IPM), 836
 Soluble interretinal pigment epithelium matrix
 (S-IRPEM), 836
 Song, A., 573
 Sonoda, H., 305
 Sorsby, A., 261
 Sorsby fundus dystrophy (SFD), 62
 angiogenesis molecular mechanism,
 264–265
 animal models, 264
 clinical manifestations, 262
 therapeutic intervention, 262
TIMP3
 AMD, 265
 molecular characteristics, 262
 mutation spectrum, 262
 Sparrow, J.R., 726, 761

- Spectral domain optical coherence tomography (SD-OCT)
 advantages, 491–492
 C57BL/6 wild-type mice, 494–495
 focal light damage, 493
 histological analysis, 492–493
 photoreceptor apoptosis, 495
 rapid degenerative process, 493
 retinal imaging, 492
 retinal structure, dynamic changes, 495
 rod outer segments, 493
- Spinal muscular atrophy (SMA), 520
- Sporadic maculopathy, 62
- Stabila, P., 93
- Stanton, C.M., 367
- Stargardt disease, 76, 167, 502
- Stargardt-like macular degeneration (STGD3), 229, 232
- Stat3 protein, 430
- Staurosporin, 359, 360
- Stepien, K.E., 451
- Stocker, A., 589
- Stockman, A., 595
- Stöhr, H., 261
- Strauß, O., 603
- Strunnikova, N., 381
- Subramanian, P., 799
- Suburo, A.M., 101
- Sugimoto, M., 293
- Sugitani, K., 161, 445
- Sugrue, A., 83
- Sulfation
 bovine ocular tissues
 isolation of, 836
 PSG2 antibody, 838–839
 SDS-PAGE, 836–837
 S-IRPEM *vs.* IS-IRPEM, 838, 839
 Western blot analysis, 837–838
 human coagulation factor VIII, 836
 in multicellular eukaryotes, 835–836
 posttranslational modification, 835
 protein function, modification of, 835
 in retina and RPE, 836
 significance of, 836
- Sullivan, J.M., 145
- Sullivan, L.S., 313
- Suzuki, M., 155
- Szondy, Z., 731
- T**
- Tachibanaki, S., 823
- Taggart, R.T., 145
- Takahashi, K., 270
- Tam, L.C.S., 155, 547, 567
- Tamm, E.R., 679
- Tanimoto, N., 183, 807
- Tanito, M., 129
- Tao, W., 93
- Target of rapamycin (TOR) kinase, 208
- Thurman, J.M., 23
- Time-controlled transcardiac perfusion crosslinking (tcTPC), 702
- Timmers, A., 200, 217
- Toll-like receptor (TLR)-mediated cell response
 age-related macular degeneration (AMD)
 caspase-dependent apoptosis, 5
 CNV, 4
 L412F gene, 4, 6
 photoreceptor arrays, 5
 retinal pigment epithelium (RPE), 5–6
 VEGF-A polymorphism, 6
 neuroimmunity, 3–4
 short interfering RNA (siRNA)-based drugs, 6–7
- Tran, J.-T.A., 553
- Transcription factor (TF)
 ChIP-chip and ChIP-Seq analysis, 756
 chromatin-remodeling activity, 753
 distal enhancer, 753
 photoreceptor, role in, 757–758
 RGC cell, role in (*see* Retinal ganglion cell (RGC))
- Transferase dUTP nick end labeling (TUNEL), 109
- Transgenic mice
 β B1-crystallin norrin, 681
 ROM-1, cone photoreceptors, 634
- Transglutaminase-2 (TG2)
 animal and tissue collection, 710
 α v β 5 integrin-dependent phagocytosis, 714
 β 1 or β 3 coreceptor, 710
 immunoblotting, 711
 immunofluorescence microscopy, 711
 TG2^{-/-} mice display morphology of, 733, 734
 rod POS phagocytosis, 733–735
 in vivo and immunoprecipitation studies, 732
 wild-type, localization
 mouse retina, 712–713
 rat RPE, primary culture, 713
 wild type *vs.* β 5^{-/-}-eyecups, 711–712
- Transient receptor potential (TRP), 409–410
- Translational vision research models program
 chemically induced mutants, 391

- clinical evaluation and electroretinography, 392
- genetic mapping, 392
- histological analysis, 393
- mice origins and husbandry, 392
- mutational analysis, 392
- Pde6a* alleles, 393
- rhodopsin mutation, 395–396
- tubby-like protein 1, 393–395
- Travis, G., 76, 726
- Triton X100, 770
- Troeger, E., 471
- TRP. *See* Transient receptor potential (TRP)
- Tsilfidis, C., 207
- Tubby-like protein 1 (Tulp1), 393–395
- C-terminal domain, 698
- expression of, 783
- location, 701
- membrane vesicle preparation, 694, 695
- mutation in, 701
- neuronal function, 783
- phagocytosis ligand, 696
- photoreceptor compartment
- crosslinked retinal samples, 705–706
- homogenization, 704
- in IS and OPL, 702
- isolation and capture of, 704–705
- laser microdissection, 703–704
- retinal section preparation, 703
- tTPC, 703
- Tulp1*^{-/-} mice, 702–703
- Wester blot analysis, 704, 705
- receptor, 696–697
- role, 784
- Tulp1^{-/-} mice, animal model
- CO₂ inhalation, 784
- immunofluorescent staining, 785
- Tubulin cofactor C (TBCC), 527
- Tyrosylprotein sulfotransferase (TPST), 835
- U**
- Ueffing, M., 61, 415
- Unfolded protein response (UPR), 573
- Usher syndrome type 1B
- AAV-mediated gene therapy, 239
- characterisation, 235
- lentivirus-mediated gene therapy, 237–239
- MYO7A* gene, 236
- Myo7a*-mutant mice, 237, 238
- strategies, 240
- V**
- Valter, K., 31, 121
- Vascular endothelial growth factor (VEGF), 254, 279, 307
- Vasireddy, V., 225
- Vasohibin-1
- corneal and retinal neovascularization, 309
- expression, 307
- mRNA extraction, 306–307
- real-time polymerase chain reaction, 306–307
- RPE
- dynamics and proliferation, 307–309
- preparation, 306
- real-time RPE impedance analysis, 306
- vascular maturation processes, 309
- western blot analysis, 307
- Vázquez-Chona, F.R., 349, 650, 652–654
- Vessey, K.A., 813
- Vijayasathy, C., 513
- Vinores, S.A., 272
- Visual system homeobox 2 (Vsx2)* gene
- failed retinal development, 671
- GDF11 levels (*see* Growth and differentiation factor 11 (GDF11))
- micro-ophthalmia, 671
- mutant mouse, 671–672
- W**
- Wadsworth, S., 573
- Wagner-Schuman, M., 451
- Wakusawa, R., 305
- Walczak, Y., 619
- Walker, T.A., 115
- Wang, G., 369
- Wang, J.J., 285, 391
- Wang, T., 88
- Wang, Z., 279
- Wan, H., 11
- Watson, R.F., 783
- Webb, K.D., 313
- Webb, T.R., 595
- Weiss, E.R., 821
- Wen, R., 93, 279
- Wen, Y., 497
- Western blot analysis
- ROM-1 overexpression, 634
- sulfation, bovine ocular tissues, 837–838
- Tulp1, photoreceptor compartment, 704
- Wheaton, D.K., 313
- Wild type (WT), 148
- Williams, D.S., 235
- Williams, J.T., 313
- Wissinger, B., 337

- Wittig, I., 770
 Wnt/ β -catenin signaling pathway
 DKK-1, inhibitor of, 681
 neurotropic growth factors, 681
 Wong, W.T., 37
 Won, J., 391
 Wright, A.F., 367
 Wright, G.A., 595
 Wu, D., 43
 Wu, J., 671
- X**
 Xia, X., 279
 Xing, W., 739
 X-linked cone dystrophy (XLCOD5). *See*
 OPN1LW and OPN1MW cone
 opsin gene
 X-linked inhibitor of apoptosis (XIAP)
 protein, 211–212
 X-linked juvenile retinoschisis (XLRS), 514
 X-linked progressive retinal atrophy 2
 (XLPRA2), 354
 X-linked retinitis pigmentosa, 314–315
- Y**
 Yamamoto, K., 761
 Yang, H., 553
 Yasumura, D., 215, 553
 Yau, E.H., 145
 Yetemian, R.M., 253
 Yu, M., 553
- Z**
 Zangerl, B., 321, 611
 Zebrafish
 light-damaged retina model, 427
 induction of Müller glial proliferation,
 429
 regeneration, 428–429
 mutation in genes encoding
 intracellular trafficking genes (*see*
 Intracellular trafficking genes)
 phototransduction protein, 435, 438
 screening, 435
 structural factor, 440
 structural protein, 440
 neuronal progenitor cell proliferation,
 429–430
 photoreceptor outer segment
 morphogenesis, 434–435
 significance, 433–434
 vertebrate photoreceptors, 433
 retina, HSP70 and HSF-1
 animal model, 664
 expression and localization, after ONI
 and heat shock, 665–667
 immunohistochemistry, 664
 mRNA mechanism, 665, 666
 in situ hybridization, 664–665
 tissue preparation, 664
 treatment, 664
 retinal degeneration
 drug discovery, 403
 embryogenesis, 399
 functional assessment, 401–402
 mitochondrial vertebrate, 400
 morphological and embryological
 features, 399–400
 mutant strain repository, 401
 screen, 400–401
 ZGC, 400
 retinal stem cell mutants, 441
 transcription factors for Müller
 glia, 430
 Zebrafish Gene Collection (ZGC), 400
 Zein, W.M., 381
 Zhang, C., 272
 Zhang, Q., 685
 Zhang, S.X., 285
 Zhao, C., 792
 Zhao, L., 37
 Zheng, L., 299
 Zhong, H., 773
 Zhong, Y., 285
 Zhu, M., 299
 Ziccardi, L., 513
 Zolotukhin, S., 217
 Zong, X., 183
 Zrenner, E., 471